Advances in Science, Technology & Engineering Systems Journal

Editorial

Advances in Science, Technology and Engineering Systems Journal (ASTESJ) is an online-only journal dedicated to publishing significant advances covering all aspects of technology relevant to the physical science and engineering communities. The journal regularly publishes articles covering specific topics of interest.

Current Issue features key papers related to multidisciplinary domains involving complex system stemming from numerous disciplines; this is exactly how this journal differs from other interdisciplinary and multidisciplinary engineering journals. This issue contains 46 accepted papers related to electrical engineering domain.

Editor-in-chief
Prof. Passerini Kazmersk

CONTENTS

ASTES

The Implementation of Straw Mulch Experiments to Increase Tomato (Lycopersicum esculentum Mill.) Production in Horticulture Learning

Dewa Nyoman Oka[1,*], I Gede Sudirgayasa[1], Ni Nyoman Serma Adi[1], Noor Ridha Yanti[2]

[1]Departement of Biology Education, IKIP Saraswati, Tabanan-Bali, 82113, Indonesia

[2]Department of Public Health, University of Cahaya Bangsa, Banjar, 70122, Indonesia

A R T I C L E   I N F O

A B S T R A C T

The increasingly rapid development of science and technology, as well as the influence of globalization has contributed to updates in educational so that one method taken by apply experiments in horticulture learning activities. This study aims to determine the effect of rice straw mulch on tomato production and the effectiveness of the implementation of this experiment in the horticultural learning process. This research experimental used144 of tomatoes plants that were divided into four groups. First group is the control group with the thickness of the straw 0%, second group with a thickness of mulch 5%, third group with mulch thickness 10% and fourth group with mulch thickness 15%. The results show there is a significant difference from the average weight of tomatoes after being given various mulch thickness treatments that was continued with the Least Significant Difference test with significant differences seen group 15% straw thickness where group had the highest tomato fruit weight with the average tomato fruit weight per plants 1426.72 g. This experiment is quite effective in implementing horticulture learning because this experiment takes only 116 days and can increase activity, motivation, creativity, foster students' rational and scientific thinking.

1. Introduction

Tomato (*Lycopersicum esculentum* Mill.) is one type of vegetable that is popular with people because of its good nutritional content. In 100 g tomatoes there are substances that are useful for the human body, including 1 g of protein, 4.2 grams of carbohydrates, 0.3 g of fat, 5 mg of calcium, 27 mg of phosphorus, 0.5 mg of iron, 1500 SI of vitamin A, 60 mg of vitamin B and 40 mg of vitamin C. Tomatoes were found to have the increased variability of lycopene, in 1 kg tomatoes contains 104.699 mg [1]. Tomatoes have many benefits including preventing canker sores, eliminating acne, preventing cancer, preventing digestive disorders, and so on. Researchers from the Rowett Research Institute in Aberdeen, Scotland, managed to find other benefits of tomatoes, so the yellow gel that covers the tomato seeds can prevent blood thickening and blood clots that can cause heart disease and stroke [2]. Tomatoes (*Lycopersicum esculentum* Mill.) are the most popular vegetables with high nutritional value and a good source of Potassium and Vitamins A and C [3]. Tomato

(*Lycopersicum esculentum* Mill.) is a type of shrub and belongs to the Solanaceae family.

Tomatoes are an important component in the composition of the daily menu, including being used as table fruit, a mixture of vegetables, chili sauce [4]. Along with the development and improvement of public health, the consumption of tomatoes as a source of vitamins is increasingly in demand for most Indonesians so that the need for tomatoes continues to increase, both as fresh food, vegetables, and as an ingredient in the food industry. In Europe (EU), Italy and Spain are the largest EU fresh tomatoes producers. panish fresh tomatoes are traded to Northern Europe, mainly toward France, United Kingdom, Germany, and Netherlands. In some cases imports from Spain cover a large share of total import of destination countries [5]. Tomato is a widely cultivated horticultural plant. The level of people's need for tomatoes is quite high, because tomatoes are consumed almost every day. The high demand for tomatoes causes tomato cultivation to require serious handling, so that production and fruit quality are always maintained [6].

---

*Corresponding Author: Dewa Nyoman Oka, Email: dewanyomanoka99@gmail.com

Tomato plants need environmental conditions in the form of temperature and soil moisture that can ensure optimum plant growth and production. To be able to optimize the growth of tomato plants, it is necessary to modify the growing environmental conditions in the form of soil temperature and soil moisture by using the right plant cultivation technology, one of which is by giving plant residues in the form of organic mulch. Mulch is defined as a material or mineral that is deliberately spread on the surface of the soil or agricultural land. One of the organic mulches which is an agricultural waste material is rice straw. The use of organic mulch in the form of straw mulch is the right alternative choice because it can improve soil structure, soil fertility and indirectly maintain soil aggregation and porosity, which means, it will maintain soil capacity to hold water after composition. Straw mulch can maintain soil moisture and suppress the growth of weeds and diseases so that it is expected to make tomato plants grow well and optimally.

Ecological assets that play an important role for the sustainability of ASEAN countries, namely agricultural for arable land. The role of humans is very important for the environment because various human activities can have a positive impact on the environment and the economy of a country and have a negative impact, namely a decrease in environmental degradation so that it can affect ecological assets for sustainability of ASEAN countries [7].

Organic farming can support sustainable food security and food availability [8] like organic mulches. Organic mulches such as straw, hay, grass or leaves can provide many benefits for organic farming. The use of organic mulch such as straw can reduce soil temperature and produce higher soil moisture compared to using black plastic mulch [9]. Organic mulch can limit weed growth, protect the soil from drought and reduce nutrient leaching, so that it has a positive impact on the yield of cultivated crops and improves their quality [10]. Surface mulching either with synthetic plastic sheets (or films) or natural organic waste materials is now used to protect plants from root-borne diseases and for water conservation. Organic mulch contains sawdust, dry grass (grass clippings), corn cobs, rice and wheat straw, water hyacinth, etc. It is very effective for vegetable growth and yield through increased soil moisture content, heat energy and the addition of some organic nitrogen and other minerals to improve soil nutrient status [3]. The use of various types of mulch on tomato plants is expected to be able to create a suitable microclimate for plants, improve soil physical properties including soil organic material, permeability, soil porosity and growth rate, facilitate nutrient cycling in soil, water, plant systems and improve nutrient availability for plants [11].

There are many factors that influence the progress of a nation, one of which is the condition of education that occurs in the country, so to achieve it, it requires a renewal in the field of education. Updates in education are an effort to improve the quality of national education, including by updating learning methods. In general, learning methods in schools tend to be teacher oriented, i.e. teacher-centered learning. The teacher oriented tradition is still widely used by educators so that it does not empower students. This condition results in low levels of success in students. Updates in the field of education position teachers to have a big role to contribute to the improvement of education

quality in schools. Thus, the learning system must have good planning. According to Sugiyono [12] with the increasingly rapid development of science and technology, as well as the influence of globalization that has contributed to almost all aspects of human life at this time, the demands for schools are growing as well because the school's function has long been used as "*agent of change"* and *"agent of modernization*" by community. This implies demands for teachers to continuously develop teaching materials and teaching methods in order to meet the demands of the developing community. Biology learning basically involves students directly in obtaining knowledge so that curiosity arises. To explore students' curiosity, one method taken is by applying experiments in learning activities. Experiments are able not only to foster students' curiosity, but also to encourage rational and scientific ways of thinking so that the results of experiments can be accepted as scientific products while the steps in its implementation are dealing with scientific processes.

According to the constructivism view, learning that is currently applied must be oriented towards building the knowledge of students independently. Students are trained to find independent learning information and actively create cognitive structures in interaction with their environment so that student-centered learning is realized. One good learning strategy that is in line with the nature of constructivism is the application of a practicum-based learning model. In practicum-based learning, students are more directed at experimental learning (learning based on concrete experiences), discussions with friends, which will then get new ideas and concepts. Therefore, learning is seen as a process of compiling knowledge from concrete experiences, collaborative activities, and reflection and interpretation [13].

Experimental learning is very suitable for learning biology, because it can provide learning conditions that develop optimal thinking and creativity skills. Students are given the opportunity to compose their own concepts in their cognitive structures, which can then be applied in their lives. The use of this experimental method has the aim of making students capable or competent and finding their own answers or problems which are faced by conducting their own experiments. In addition, students can be trained in scientific ways of thinking, by experimenting with students finding evidence of the truth and theory of something that is being studied [14].

From the description above, the research purpose to determine the effect of rice straw mulch on increasing tomato plant production and the effectiveness of the implementation of this experiment in the horticultural learning process.

2. Methods

2.1. Materials

The population of this study was all tomato plants in the nursery with length, width and height (150 x 40 x 10) cm. After 10 days, the tomato plants are transferred to new media in a small 5 cm diameter plastic bag that has been prepared previously. At three weeks of age, the seedlings were transferred from the plastic bag media to the plot of the study area, where each plot was filled with six plants. In one block where the research was located there were four plots according to the number of experimental groups, namely (1) the control group with the thickness of the straw (0%); (2) the

group with the thickness of the mulch (5%); (3) the group with the thickness of the mulch (10%) and (4) the group with the thickness of the mulch (15%). There are six blocks according to the number of repetitions. The total tomato plants used in the sample in this study were 6 x 4 x 6 tomato plants, equal to 144 tomato plants.

2.2. Data Analysis

This type of research is experimental, using a completely randomized design. The obtained data were the weight of ripe tomatoes which were picked three times, starting from 96 days to 116 days. The results of weighing the tomato fruit were then recapitulated, the results of the recapitulation were tested for normality and homogeneity using the SPSS software version 22. The normality test was performed using the *Kolmogorov-Smirnov* and *Shapiro-Wilk* statistics with SPSS software version 22. Meanwhile, the homogeneity test was carried out with the *Levene* test. Significance level (α) was set at 0.05.

The criteria used for the normality and homogeneity test was if the significance number (sig.) was greater than the significance level (α) then the statistical numbers obtained were not significant, meaning that the sample data came from a normally distributed population, vice versa. If the requirements for normality and homogeneity have been met, then a parametric analysis is carried out using the ANOVA test. If there were significant differences, it was necessary to carry out further tests to determine which treatment groups were significantly different. Further tests were carried out with the Least Significant Difference (LSD) test. Student learning outcomes using experiment-based learning methods were evaluated using normative assessments.

3. Result

After the tomatoes reached 96 days from the nursery, the ripe fruit picking was carried out to calculate the weight of the tomatoes produced per plants, the fruit picking was done three times until the tomatoes were 116 days old. The results of weighing the tomato fruit were then recapitulated, the results of the recapitulation can be seen in Table 1.

Based on table 1 above, it can be described the average weight of tomatoes (g) plants at various thicknesses of straw mulch, as shown in Figure 2.
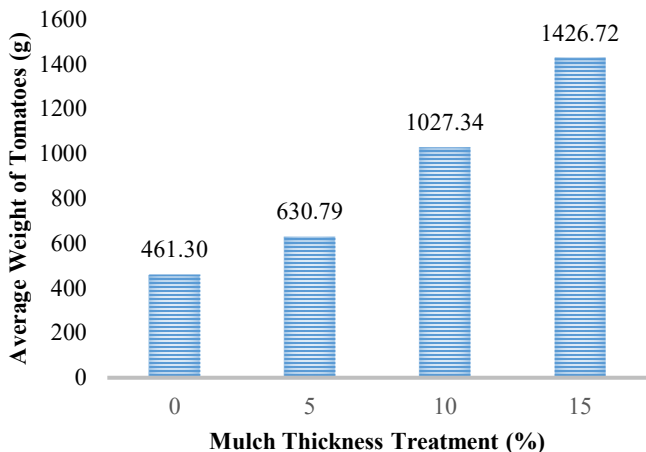
Figure 1. Average Tomato Fruit Weight (g) plants at various thicknesses of mulch

Table 1: Average Tomato Fruit Weight (g) plants at various thicknesses of straw mulch

TREATMENT		BLOCK					
Symbol	Straw Thickness	I	II	III	IV	V	VI
(1)	0%	917,50	690,83	1095,00	683,33	658,33	608,35
(2)	5%	1010,35	1176,00	1334,33	846,66	116,66	977,17
(3)	10%	1514,17	1183,83	1790,33	1825,83	1789,50	1475,50
(4)	15%	1878,30	2216,50	2303,35	2091,00	2121,83	2140,00
Total		5320,32	5266,66	6523,01	5446,82	5686,32	5201,02
Average		1330,08	1316,67	1630,75	1631,71	1421,58	1300,26

3.1. Prerequisite Test

Before conducting the Anova test, a prerequisite test was carried out in the form of a normality test and a homogeneity test. Based on the results of the normality test with SPSS software version 22, data is obtained as in Table 2.

Table 2: Summary of Normality Test

Straw Thickness(%)	Kolmogorov-Smirnov[a]			Shapiro-Wilk		
	Statistic	Df	Sig.	Statistic	Df	Sig.
0	0.339	6	0.030	.831	6	0.110
5	0.274	6	0.180	.858	6	0.183
10	0.277	6	0.165	.865	6	0.208
15	0.239	6	0.200[*]	.939	6	0.651

Based on the results of the Shapiro-Wilk normality test, all treatments obtained Sig. above the predetermined significance value of 0.05. This means that the data is normally distributed so that Anova testing can be done.

The next test is the homogeneity test which is also carried out with the help of SPSS. The results of the homogeneity test are shown in Table 3.

Table 3: Homogeneity Test Results

Levene Statistic	df1	df2	Sig.
1.401	3	20	0.272

Based on the results of the homogeneity test with the Levene test, the Sig. equal to 0.272. This value is much greater than the predetermined significance value of 0.05. Thus it can be said that the fourth variant of the mulch thickness treatment is homogeneous, so that anova testing can be carried out.

3.2. One Way Anova Test

Based on the one-way ANOVA test that has been carried out with the help of SPSS software version 22 can be seen in Table 4.

Table 4: Summary of One Way Anova Test Results

	Sum of Squares	Df	Mean Square	F	Sig.
Between Groups	7110075.329	3	2370025.110	31.593	0.000
Within Groups	1500343.171	20	75017.159		
Total	8610418.500	23			

Based on the table above, it is known that the F value is 31.593 with a Sig. amounting to 0.000. This means that there is a significant difference from the average weight of tomatoes after being given various mulch thickness treatments. Because there is a significant difference, it is necessary to carry out further tests to find out which treatment pairs are significantly different. Further tests were carried out with the LSD test, the results of which can be seen in Table 5.

Table 5: Summary of LSD Test Results

(I) Straw Thickness (%)	(J) Straw Thickness (%)	Mean Difference (I-J)	Std. Error	Sig.	95% Confidence Interval	
					Lower Bound	Upper Bound
0	5	-134.63833	158.13197	0.405	-464.4958	195.2192
	10	-820.88667*	158.13197	0.000	-1150.7442	-491.0292
	15	-1349.60667*	158.13197	0.000	-1679.4642	-1019.7492
5	0	134.63833	158.13197	0.405	-195.2192	464.4958
	10	-686.24833*	158.13197	0.000	-1016.1058	-356.3908
	15	-1214.96833*	158.13197	0.000	-1544.8258	-885.1108
10	0	820.88667*	158.13197	0.000	491.0292	1150.7442
	5	686.24833*	158.13197	0.000	356.3908	1016.1058
	15	-528.72000*	158.13197	0.003	-858.5775	-198.8625
15	0	1349.60667*	158.13197	0.000	1019.7492	1679.4642
	5	1214.96833*	158.13197	0.000	885.1108	1544.8258
	10	528.72000*	158.13197	0.003	198.8625	858.5775

*. The mean difference is significant at the 0.05 level.

Based on the LSD further test with the help of SPSS, it was found that all pairs of mulch thickness treatments were significantly different except for pairs of 0% and 5% thickness of mulch. That is, the mulch treatment with a thickness of 0% and 5% has no difference in affecting the average weight of tomatoes. Or there is a significant difference between group (3) with 10% straw thickness and group (4) 15% straw thickness where group (4) has the highest tomato fruit weight.

3.3. Evaluation of learning outcomes

Evaluation of the learning outcomes of students who participated in this experiment showed that: (1) there was an increase in activity, creativity, motivation and involvement of students in the learning process; (2) students gained real experience that was able to strengthen their understanding of theoretical concepts; (3) It helped students to foster their rational and scientific thinking; (4) students can hone cognitive, psychomotor and affective skills in identifying problems, and developing problems and finding effective solutions to solve problems; (5) students can cultivate collaboration and acquire leadership skills.

4. Discussion

Based on the results of the one-way ANOVA analysis, it is known that the F value is 31.593 with a Sig. amounting to 0.000. This means that there is a significant difference from the average weight of tomatoes after being given various mulch thickness treatments. This is because organic mulch is able to suppress weeds, regulate soil moisture and soil surface temperature. Organic mulch can improve overall soil quality by increasing soil organic matter, soil porosity, water holding capacity while stimulating life in the soil and increasing nutrient availability [10]. Organic mulch is very effective for vegetable growth and yield through increasing soil moisture content, heat energy and adding some organic nitrogen and other minerals to improve soil nutrient

status [3]. The use of various types of mulch on tomato plants is expected to be able to create a suitable microclimate for plants, improve soil physical properties including soil organic matter, permeability, soil porosity and growth rate, facilitate nutrient cycling in soil, water, plant systems and improve nutrient availability for plants [11]. From the above quotations we can conclude that rice straw mulch can (1) reduce the growth of weeds, (2) reduce water evaporation so as to maintain soil moisture content and soil temperature; (3) preventing the appearance of soil scales so that the soil remains loose and soil aeration is maintained; and (4) rotting straw mulch will increase soil nutrients, especially organic nitrogen and other minerals.

Based on the LSD further test with the help of SPSS, it was found that all pairs of mulch thickness treatments were significantly different except for pairs of 0% and 5% thickness of mulch. This means that mulch treatment with a thickness of 0% and 5% does not differ significantly in influencing the average weight production of tomatoes. Meanwhile, mulch treatment with a thickness of 10% and 15% had a significantly different effect on the average weight production of tomatoes, where mulch treatment with a thickness of 15% had a better effect than mulch treatment with a thickness of 10% [11].

Why does mulch treatment with a thickness of 10% and 15% have a significant different effect on the average weight production of tomatoes and mulch treatment with a thickness of 15% is a better effect than mulch treatment with a thickness of 10%? Because in the mulch treatment with a thickness of 15% weeds cannot grow at all, so there are absolutely no disturbing plants, consequently water and the elements present in the soil are only used by tomato plants. The impact is better tomato growth and is able to produce fruit more optimally.

Hay weeds, especially weeds with a thickness of 15%, evaporate less than treatment with a thickness of 10% straw, so that the soil moisture content and soil temperature are better preserved in the treatment with a thickness of 15% straw. Water has a vital function for living things, including plants. This is closely related as the basic material to be used in the photosynthesis process, which is a plant physiological process for the formation of carbohydrates [15]. Water is one of the environmental factors that has a big influence on the decrease in the production of a plant and from an ecological point of view, it is the main limitation in the terrestrial environment or in the aquatic environment is water.

Straw mulch, especially mulch with a thickness of 15%, is better able to prevent the appearance of soil scales so that the soil is more loose and soil aeration is more maintained than the straw mulch with a thickness of 10%. This is very important for maintaining the progress of the metabolic processes that take place in the root cells, especially the respiration of root cells, which greatly affects root growth and transport of soil nutrients from the soil to the leaves. With good aeration will affect crown growth and ultimately will increase the production of tomato plants. For tomatoes with a straw mulch thickness of 15%, the amount of straw is clearly higher than that of 10% straw mulch, so that the addition of organic nitrogen in the treatment with a straw thickness of 15% is more than tomatoes with a thickness of 10% mulch. Since organic nitrogen is obtained from rotting straw mulch. This organic nitrogen is indispensable for growth, especially in the

vegetative phase, namely the growth of branches, leaves and stems. Nitrogen is also useful in the process of forming green leaves or chlorophyll. Chlorophyll is very useful to help the photosynthesis process. In addition, nitrogen is useful in the formation of proteins, fats and various other organic compounds. Lack of nitrogen can cause abnormal or stunted plant growth. The leaves will turn yellow and then dry out. If a lot of nitrogen deficiency (severe) can cause plant tissue to dry out and die. Fruits that lack nitrogen have imperfect growth, ripen quickly and have low protein content. So the increase in tomato weight in straw mulch with a thickness of 10% and 15% occurs because straw mulch can add adequate organic nitrogen elements to the soil. This optimal organic nitrogen makes tomato fruit growth perfect and its protein content increases [8].

The use of technology in the suitability of peatlands for cultivation in a certain area is optimally carried out using methods based on of the Food and Agriculture Organization (FAO) guidelines. The system test results showed an accuracy rate of 92.86% with the application of land suitability evaluation for planting other types of plants besides lowland rice. Based on the results of future land suitability evaluations, farmers can develop horticultural crops, namely cultivating tomatoes on peatlands [16].

Evaluation of the learning outcomes of students who participated in this experiment showed that: (1) there was an increase in activity, creativity, motivation and involvement of students in the learning process; (2) students gained real experience that enabled them to strengthen their understanding of theoretical concepts; (3) it helped students to foster their rational and scientific thinking; (4) students can hone cognitive, psychomotor and affective skills in identifying problems, and developing problems and finding effective solutions to solve problems; (5) students can cultivate collaboration and acquire leadership skills. This happens because students were involved directly in obtaining knowledge so that curiosity arose. Experiments are able not only to foster students' curiosity, but also to encourage rational and scientific ways of thinking so that the results of experiments can be accepted as scientific products while the steps in its implementation are as scientific processes. Experimental learning is able to provide learning conditions that develop optimal thinking and creativity skills. Students are given the opportunity to compose their own concepts in their cognitive structures, which can then be applied in their lives. The use of this experimental method has a goal that students are able to find their own answers or problems by conducting their own experiments. In addition, students can be trained in a scientific way of thinking, by experimenting with students finding evidence of the truth and the theory of something being studied [14].

Biology being the center of scientific learning is needed in studying advanced domains such as medicine, genetics, zoology, etc. For successful dissemination of biological science, integration of high-tech communication practices in teaching of biology is applied in education, teachers familiarize themselves with the pedagogical principles and management strategies used in classroom instruction [17].

This is in line with what was stated by [18] which stated that good learning is learning that requires student activity and meaning *(meaningful discovery learning)*. In active learning *(discovery learning)*, students are no longer placed in a passive position as recipients of teaching materials given by teachers / lecturers, but as subjects who are active in thinking processes, seeking, processing, unraveling, combining, concluding, and solving problems. Education is a lifelong process of cultivating and empowering students, where in this process there must be educators who provide role models and are able to build will, and develop the potential and creativity of students. This principle causes a paradigm shift in the educational process, from the teaching paradigm to the learning paradigm. Teaching paradigm which emphasizes more on the role of educators in transforming knowledge to their students has shifted to learning paradigm which gives more roles to students to develop their potential and creativity. In the learning process, the ability for creativity is obtained through: Observing, Questioning, Associating, Experimenting, and Networking.

Therefore, teachers/ lecturers need to design a learning process that prioritizes personal experience through the process of observing, asking questions, reasoning, and trying [observation based learning] to increase the creativity of students. In addition, it is accustomed for students to work in a network through collaborative learning.

5. Conclusions

Based on the research results and the description above, it can be concluded that: (1) straw mulch affects tomato production; (2) straw mulch with a thickness of 5% gave no significant difference, while straw mulch with a thickness of 10% and 15% had a significantly different effect, where straw mulch with a thickness of 15% had a higher yield of tomatoes than mulch straw with a thickness of 10%; and (3) This experiment is quite effective in implementing horticultural learning because this experiment takes only 116 days, it can increase activity, motivation, creativity, rational and scientific thinking of students. Besides, this experiment also involves students in the learning process, provides real experience, improves cognitive, psychomotor, affective abilities, and fosters collaboration and leadership skills.

Conflict of Interest

The authors declare no conflict of interest.

References

[1] T. Suwanaruang, "Analyzing Lycopene Content in Fruits," Agriculture and Agricultural Science Procedia, **11**, 46–48, 2016, doi: 10.1016/j.aaspro.2016.12.008.

[2] E. Fitriani, "Untung Berlipat Budidaya Tomat Di Berbagai Media Tanam," Penerbit Pustaka Baru Press. Yogyakarta, **221**, 2012.

[3] S.S. Al-Ismaily, R.A. Al-Yahyai, S.A. Al-Rawahy, "Mixed Fertilizer can Improve Fruit Yield and Quality of Field-Grown Tomatoes Irrigated with Saline Water," Journal of Plant Nutrition, **37**(12), 1981–1996, 2014, doi:10.1080/01904167.2014.920364.

[4] V. Sidhu, D. Nandwani, L. Wang, Y. Wu, "A Study on Organic Tomatoes: Effect of a Biostimulator on Phytochemical and Antioxidant Activities," Journal of Food Quality, **2017**, 5020742, 2017, doi:10.1155/2017/5020742.

[5] F.G. Santeramo, "Price Transmission in the European Tomatoes and Cauliflowers Sectors," Agribusiness, **31**(3), 399–413, 2015, doi: 10.1002/agr.21421.

[6] V. Novitasari, R. Agustrina, B. Irawan, Y. Yulianty, "Pertumbuhan Vegetatif Tanaman Tomat (Lycopersicum esculentum Mill.) dari Benih Lama yang Diinduksi Kuat Medan Magnet 0, 1 mT, 0, 2 mT, dan 0, 3 mT," Jurnal Biologi Indonesia, **15**(2), 2020.

[7] A. Yunani, J. Dalle, Miar, S. Maulida, "Can Life Quality Dimensions Alter

Ecological Footprint For Sustainability Of Asean Countries? Role Of Per Capita Income, Happiness And Human Development," Journal of Security and Sustainability Issues, **10**, 242–252, 2020, doi:10.9770/jssi.2020.10.Oct(18).

[8] T. Adiprasetyo, S. Sukisno, N. Setyowati, S. Ginting, M. Handajaningsih, "The Prospect of Horticultural Organic Farming as Sustainable Agricultural Practice for Reducing Poverty: The Case in Bengkulu City, Indonesia," International Journal on Advanced Science, Engineering and Information Technology, **5**, 402, 2015, doi:10.18517/ijaseit.5.6.595.

[9] S. Biswas, M. Akanda, M. Rahman, M.A. Hossain, "Effect of drip irrigation and mulching on yield, water-use efficiency and economics of tomato," Plant, Soil and Environment, **61**, 97–102, 2015, doi:10.17221/804/2014-PSE.

[10] E. Kosterna, "The effect of soil mulching with straw on the yield and selected components of nutritive value in broccoli and tomatoes," Folia Horticulturae, **26**, 2014, doi:10.2478/fhort-2014-0003.

[11] I.K.D.A. Saputra, I.W. Tika, N.L. Yulianti, "Pengaruh Penggunaan Beberapa Jenis Mulsa terhadap Sifat Fisik Tanah dan Laju Pertumbuhan Tanaman Tomat (Lycopersicum Esculentum L)," Jurnal BETA (Biosistem Dan Teknik Pertanian); Vol 9 No 1 (2021): IN PRESS, 2021.

[12] Sugiyono, Metode penelitian pendidikan:(pendekatan kuantitatif, kualitatif dan R & D), Alfabeta, 2008.

[13] M.S. Hayat, "Pembelajaran Berbasis Praktikum Pada Konsep Invertebrata Untuk Pengembangan Sikap Ilmiah Siswa," Bioma, (Vol 1, No 2, Oktober (2011): Bioma), 2011.

[14] M. Mulyani, "Penggunaan Metode Eksperimen Untuk Meningkatkan Hasil Belajar Tentang Rangkaian Listrik Seri Dan Paralel Pelajaran Ipa Pada Siswa Kelas Vi Sd Negeri 3 Karanggandu Kecamatan Watulimo Kabupaten Trenggalek," Jurnal Pendidikan Profesional, **4**(3), 2016.

[15] K. Amaru, E. Suryadi, N. Bafdal, F.P. Asih, "Kajian Kelembaban Tanah dan Kebutuhan Air Beberapa Varietas Hibrida DR UNPAD," Jurnal Keteknikan Pertanian, **1**(1), 2013.

[16] J. Dalle, D. Hastuti, F. Akmal, "Evaluation of Peatland Suitability for Rice Cultivation using Matching Method," Polish Journal of Environmental Studies, **30**(3), 2041–2047, 2021, doi:10.15244/pjoes/127420.

[17] A. Putra, A. Akrim, J. Dalle, "Integration of High-Tech Communication Practices in Teaching of Biology in Indonesian Higher Education Institutions," International Journal of Education and Practice, **8**, 746–758, 2020, doi:10.18488/journal.61.2020.84.746.758.

[18] N. Hanafiah, C. Suhana, "Konsep strategi pembelajaran," Bandung: Refika Aditama, 2009.

ASTES

Development of Electric Power Availability Recorder for Accurate Energy Billing of Unmetered Facilities

Chibuzo Victor Ikwuagwu[1,2], Ikechukwu Emmanuel Okoh[1], Stephen Aroh Ajah[3], Cosmas Uchenna Ogbuka[2,4,*], Godwin Ogechi Unachukwu[1,2], Emenike Chinedozi Ejiogu[2,4]

[1]*Department of Mechanical Engineering, University of Nigeria, Nsukka, 410001, Nigeria*

[2]*Africa Centre of Excellence for Sustainable Power and Energy Development (ACE-SPED), University of Nigeria, Nsukka, 410001, Nigeria*

[3]*Department of Mechanical Engineering, Alex Ekwueme Federal University, Ndufu-Alike, Nigeria*

[4]*Department of Electrical Engineering, University of Nigeria, Nsukka, 410001, Nigeria*

A B S T R A C T

The design, fabrication and testing of a power availability recorder (PAR) to track the duration of electricity supply in facilities is presented. The design was executed with C-Language encoded in a microcontroller which served as the central processing unit of the device. Proteus software was, subsequently, used to simulate the real-life practicability of the device before the prototype was constructed. This device is designed to record power availability in seconds which can be converted to hours while energy consumption is recorded in kWh. Thereafter, the device was functionally tested and installed in a customers' premises for a period of three (3) months. Energy Consumed was plotted against Availability using GraphPad Prism Software and it could be seen that Availability and Energy Consumption are directly proportional to each other. This forms a sound basis for discrediting the outrageous bills issued by the utility companies for months when there were few hours or no power availability. It follows therefore that if installed in unmetered households, this device could go a long way in curbing the excesses and checking the inefficiency of the utility companies in terms of unjustifiable estimated bills issued to their customers.

1. Introduction

Energy remains the major driving force for industrial, social and economic development of any country. It is also a key consideration in the sustainable management of the environment [1, 2]. Electricity is one of the cleanest and most versatile forms of energy, with high utilization efficiencies. Most energy resources are usually converted to electricity as their terminal useful energy form [3]. Consequently, electricity has become the energy form with the greatest utility in household, industrial and commercial activities in both developed and developing countries [3]. Nigeria, which is a lower middle-income country with a per capita income of $2790/yr and a poverty rate of 53%, ranks among the 10 largest oil exporting countries in the world [4]. Yet, according to the International Energy Agency, the annual per capita electricity

consumption was only 140 kWh/cap/yr in 2015, when the population was 181 million [5]. This may be compared to 12,000 kW/cap/yr for the USA, a high-income country with a population of approximately 321 million [6]. The low value for Nigeria portrays a low level of development of her electricity supply subsector. Nigeria's population is projected to rise to 266 million by 2030 [7]. Thus, substantial improvements in power generation and supply are very critical if the country is to adequately meet her future electricity needs. A growth rate of 567 GWh/yr in total generation was projected in [8], while [9] suggest that in the near future, a generating capacity of 85 TWh should be installed to meet the expected demand. This situation has led to a renewed call for diversification of energy sources with emphasis on renewables to serve the needs of off-grid rural communities [10-12].

To achieve the electricity supply objective, the country commenced a restructuring of the Electricity Supply Industry, ESI,

from a government monopoly to a competitive private sector driven industry in 2001 [13, 14]. Even after successful completion of this restructuring, the ESI still manifests low power availability where access exists, frequent blackouts, estimated billing of millions of unmetered customers, difficulty in balancing supply and demand, and lack of disaggregated consumption data by economic sector, geopolitical division, facilities and homes [15]. For progress to the next and fully competitive stage, full and reliable metering of the electricity being traded among operators and between operators and consumers, among other improvements, is essential. As of 2017 only 45.3% of electricity customers on the grid were metered [16] and about 50% of the meters were either faulty or obsolete [17]. This means that a large percentage of customers, especially in the rural areas, were and still are subjected to estimated billing [18]. A supposed balance between total generation and metered sales is then arbitrarily shared among unmetered customers. The practice is thus open to abuse by the supply companies and promotes inefficient use of power by the consumers. According to [15], a large number of Nigerian electricity customers were willing to adopt the pre-paid metering, PPM, system principally due to frustration with the unjust billing by the supply companies. In contrast, in countries which have full metering and 24-hour power supply, availability is not an issue, bills accurately reflect consumption and customers are happy to pay for electricity consumed [19]. Authentic and balanced billing reduces rancor and disputes between suppliers and customers, supports business growth and economic progress and positively influences facility management and efficient use of energy. Countries with similar problems to Nigeria's cannot enjoy these benefits. Until the country attains full metering of its customers, estimated billing of customers will be inevitable. A more equitable method must be found for making these estimates and as will be shown in this work, one such method uses the power availability value. This makes the Power Availability Recorder, PAR, a useful device in end consumer electricity trading. Other approaches have been proposed for determining estimated monthly consumption and bill. One of such is the use of the Artificial Neural Network model as was applied to residential customers by [20]. An optimized web-based billing meter, using C# programming language with MySQL for backend data base was presented by [21]. The meter measures and transmits consumed units of a customer at the end of a month, through a dedicated network.

As noted in [22], facilities resource metering is very vital for robust building energy management. Constant monitoring of an installation gives facility and property managers the information they need to improve usage and behaviour, lower electricity consumption, reduce capital expenditure and cut energy costs [23]. In countries where 24-hour/day power supply is not assured, especially if further complicated by limited metering coverage, energy management analysis of the type envisage above will need data on the power availability profiles in the regions or facilities of interest, in addition to data on energy consumption and power demand. A means of accounting for the periods of power outage needs to be incorporated into the power metering and accounting system. This calls for a device, or timer, that records electricity availability to a building or facility [22]. Several studies have been conducted on electricity consumption all over the world [24-25] but in Nigeria, it is observed that electricity consumption is strongly dependent on power availability.

In this study, a Power Availability Recorder (PAR) was developed, functionally tested and installed in four selected customers' premises. Power availability data was taken from the device at 6am and at 6pm daily for a period of three (3) months. This further proved the device to be durable.

2. Formulation of the PAR

Codes in C-Language were written into the microcontroller of the device which serves as the central processing unit of the device. After that, Proteus software was used to simulate the real-life workability of the device. This was followed by fabrication the prototype and testing [26].

2.1. Design Considerations

The design method follows a top-down design and a bottom-up implementation approach. The design is based on a pic microcontroller and integrated circuit (IC) with other peripherals. A firm was developed in embedded C language to run in the microcontroller and coordinate and execute some task. The device is sub divided into the following integral modules: The timing module, Power sensing module, Data logging module, Display module, Power supply module.

- *The Timing Module*

The system incorporates a precision timer for taking record of time of power availability in seconds. In this design, a 16-bit built-in timer in the microcontroller was used. The timing is formatted as follows: DD: HH: MM: SS (Days: Hours: Minutes: Seconds).

- *Power Sensing Module*

This part of the circuit senses when power is available and sends a signal to the microcontroller to start timing. The circuit include a voltage buffer to eliminate loading effect from the DC source and a Zener regulator to ensure a constant voltage level.

- *Data Logging Module*

This module computes the duration for which power was available in real time and saves it in memory. The status of the power source is checked every seconds. Here, an LC256 EEPROM (Electrically Erasable Programmable Read Only Memory) chip is used. This EEPROM can hold up to 256kb of data which is just enough for this research.

- *Display Module*

This is the interface through which the user can interact with the device. The display module and the input buttons (delete and reset buttons) make up the user interface. Here we use a 16X2 alphanumeric LCD (Liquid Crystal Display) module. The duration of power availability is displayed on the LCD module. The user can read recorded data from the display screen or delete data in memory or reset device through this interface.

- *Power Supply module*

The device is designed to be powered from 220/240 AC mains when it is available and will be powered by a 9V battery when the ac mains is not available. The power supply circuit transforms the 220/240 AC source voltage to a clean regulated 5V DC. This is the required voltage for powering the various discrete components in the circuit.

The power supply circuit is design to supply up to 1A, hence the max dc power supplied to the device is:

$$P_{max} = I_{max} * V_{DC} \qquad (1)$$

From the design parameters in this device, the output maximum power recorded in the device was calculated as:

$$P_{max} = 1 * 5 = 5W$$

If this device operated for certain period of time (*t*), the total energy used can be calculate as:

$$E_{max} = P_{max} * t \qquad (2)$$

An off the shelve 7805 linear regulator IC was used to provide a constant DC supply. The power supply also includes an auxiliary source (battery) for powering up the device and reading out logged data and performing other user operations when mains power is unavailable. The power supply is designed to smartly switch to battery mode whenever mains power is off. The block diagram of the power supply circuit is shown in the Figure 1.

2.2. The System Block Diagram

The block diagram of the device indicating the interconnection of the various components is shown in Figure 2.

2.3. The device firmware

The device firmware was developed in embedded C-language and compiled to a Hex file with the CCS PICC compiler. The program algorithm is illustrated in the flowchart of Figure 3.

3. Simulation Studies

Proteus ISIS CAD software was used to simulate the circuit and perform virtual testing. The simulation shows proof of concept. The power sensor circuit is to output a logic '1' when power is available and a logic '0' when power is unavailable. The CPU reset and memory clear/timer reset circuits will also output either a logic '1' or '0' as the case may be when clicked.

Consequently, we modeled the power sensor circuit, CPU reset circuit and memory clear/timer reset circuit with a PROTEUS momentary logic state source. The momentary logic state source is a component in PROTEUS, it can be configured to output a logic '1' or '0' when clicked. In the simulation, the color red represents logic '1' while blue represents logic '0'.
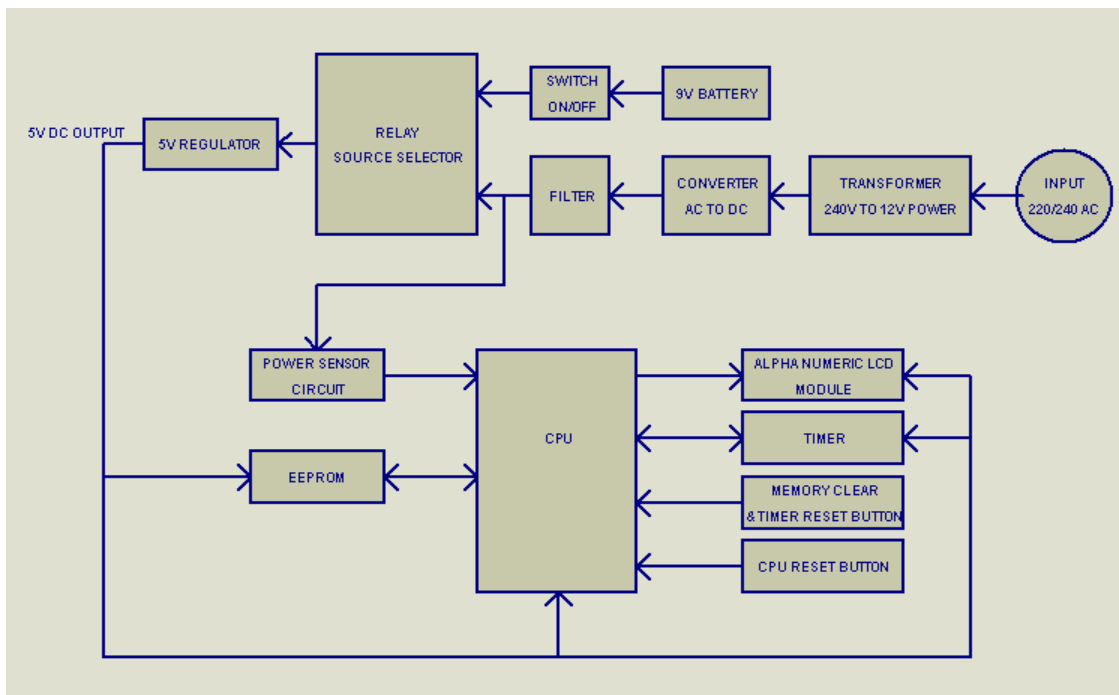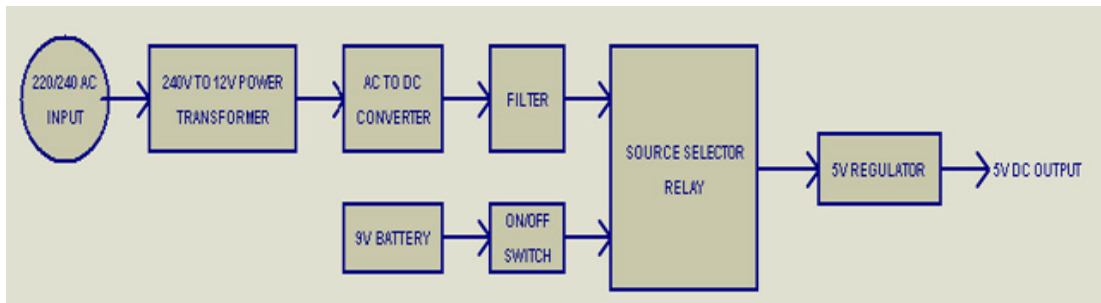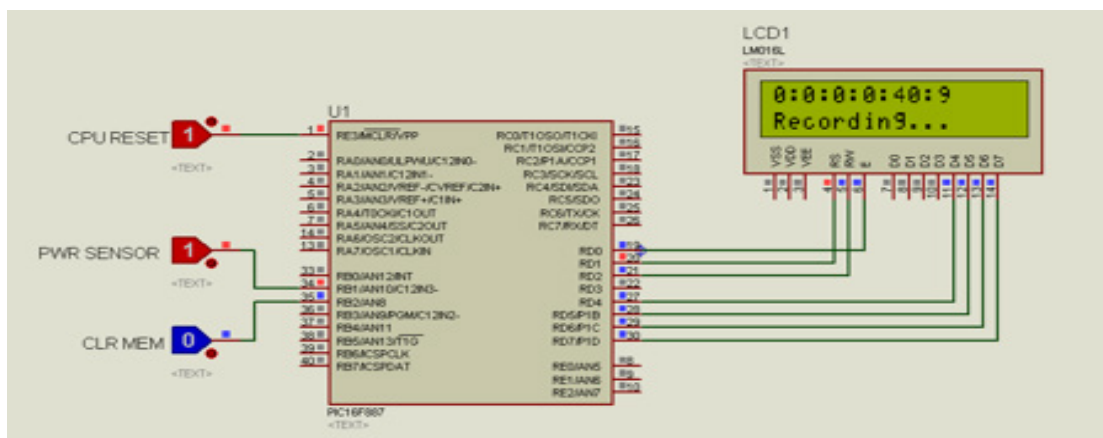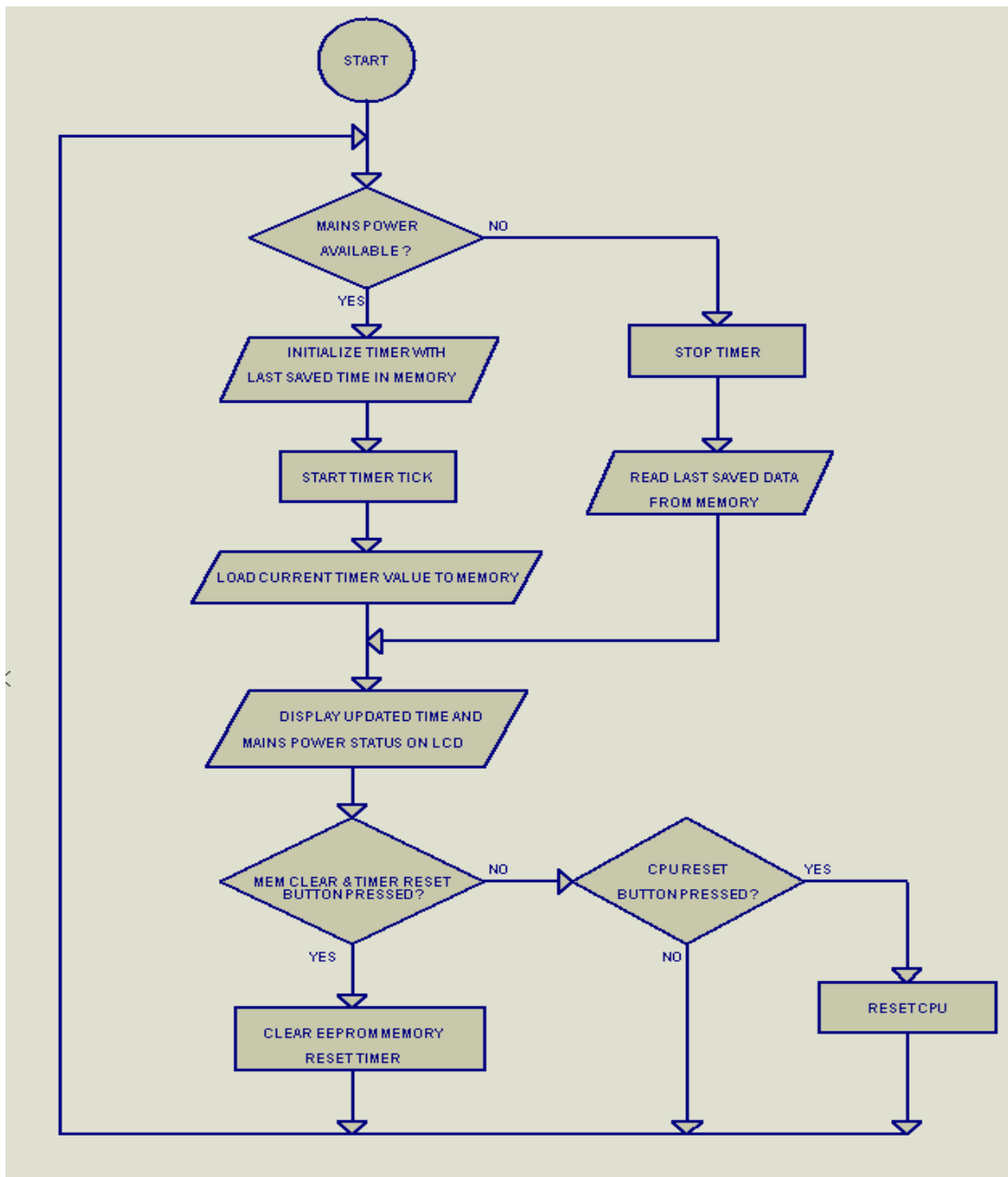
3.1. Simulation of Power Duration Logging

Figure 4 is the simulation of the device logging the power duration. The power sensor in this case is red, which implies that power is available and the device is logging. The time duration is display on the alphanumeric LCD as shown in Figure 4. The CPU reset pin is active low which implies that a logic '0' signal is required to activate the CPU reset operation. Therefore, the pin is normally set to logic '1'.

3.2. Simulation of "No power" Condition

Use SI (MKS) as primary units. (SI units are encouraged.) English units may be used as secondary units (in parentheses). An

exception would be the use of English units as identifiers in trade, such as

3.3. Simulation of Memory Clear and Timer Reset Operation

In figure 6, the CLR MEM (memory clear and timer reset) circuit is red (logic '1') indicating CLR MEM signal has been sent to the CPU. The CPU then activates the function which deletes all logged data in the memory and resets the timer to zero.

3.4. Power Supply Circuit Simulation

This shows the sinusoidal nature of the current and voltage display of the device during operation.
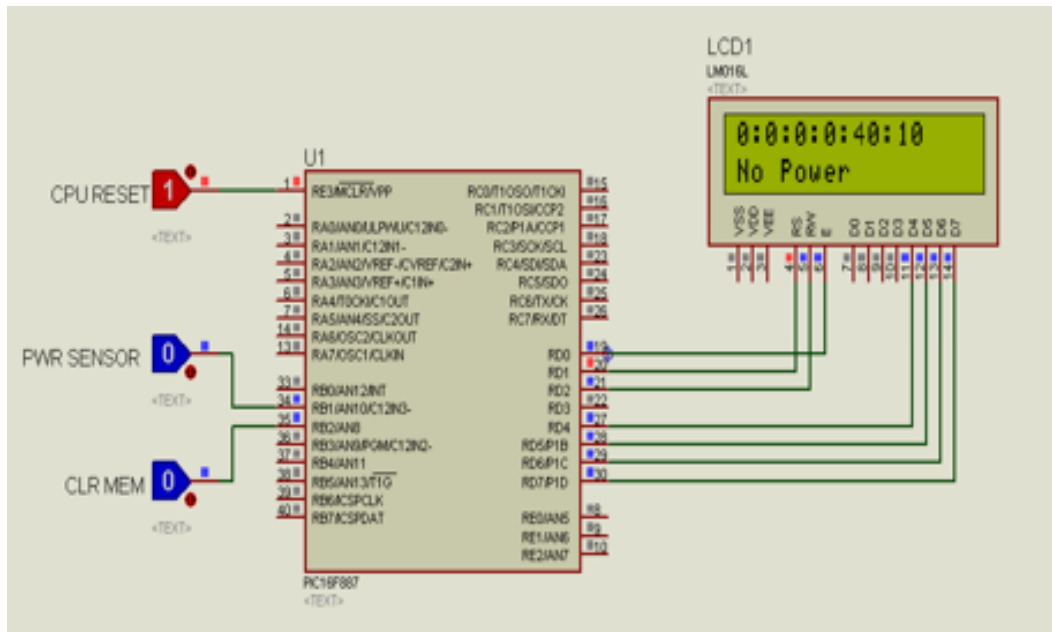
Figure 5: "No Power" Condition Simulation
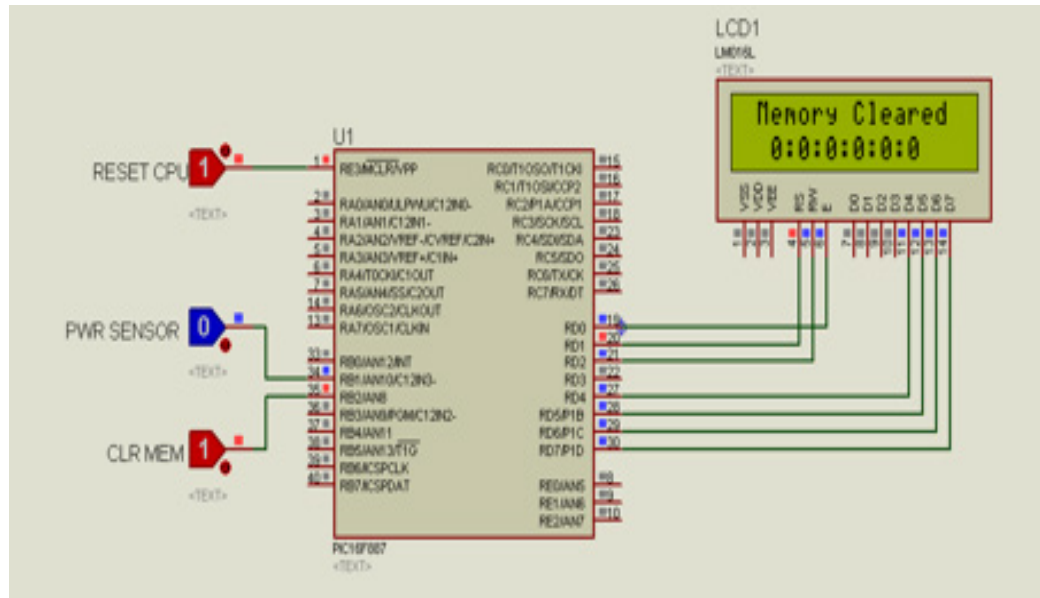
Figure 6: Memory Clear and Timer Reset Simulation
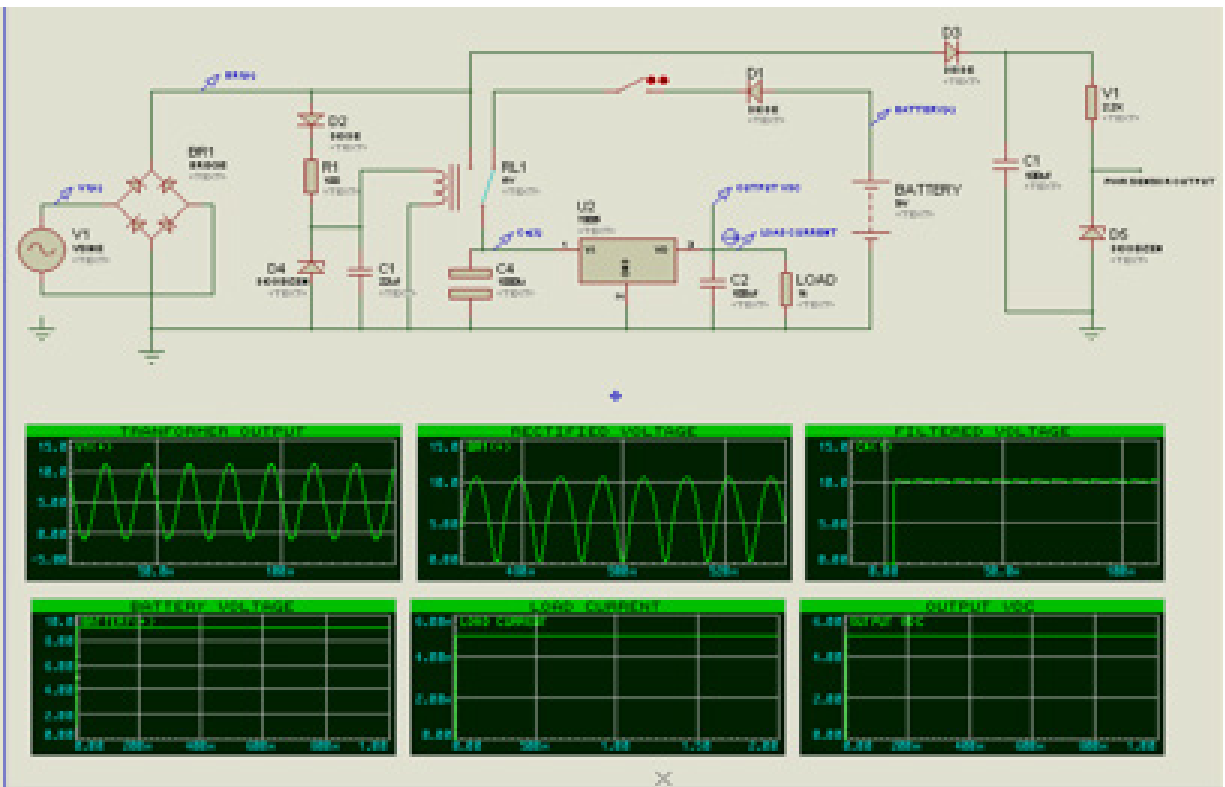
Figure 7: Power Supply Circuit Simulation

$$Y = 18.49*X - 0.0$$
(a) Month of March

$$Y = 16.57*X - 0.0$$
(b) Month of April

$$Y = 20.15*X - 0.0$$

(c) Month of May

$$Y = 18.41*X - 0.0$$

(d) All Three Months
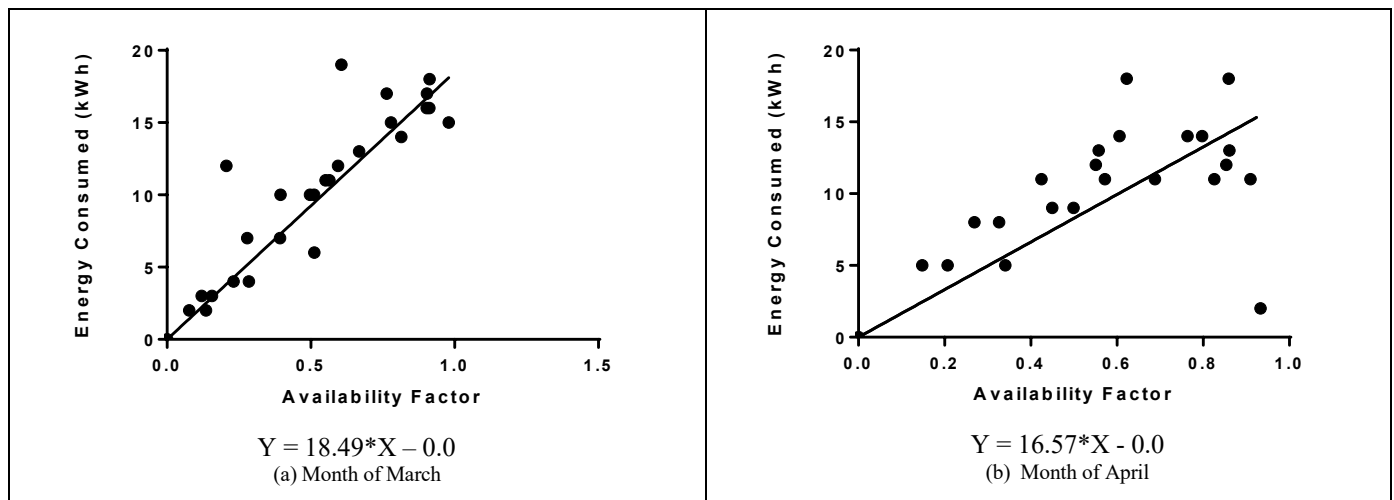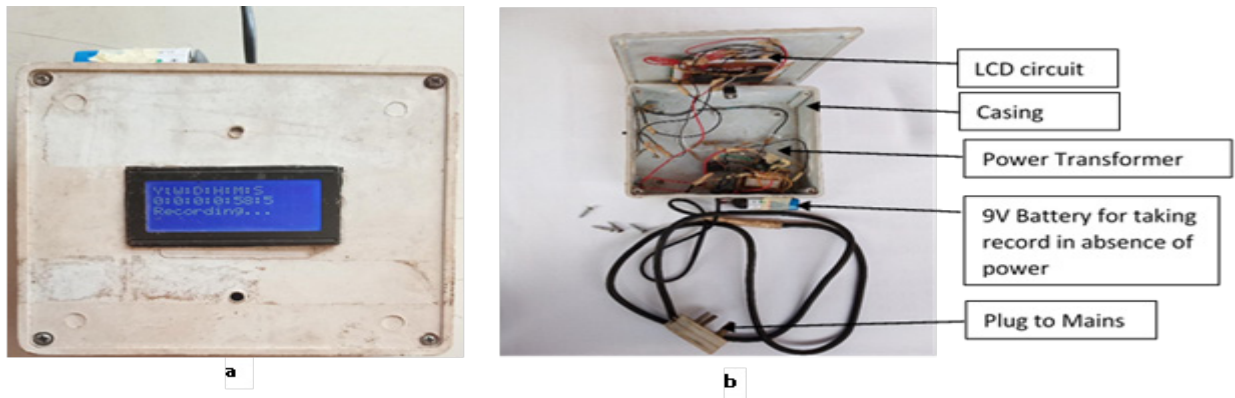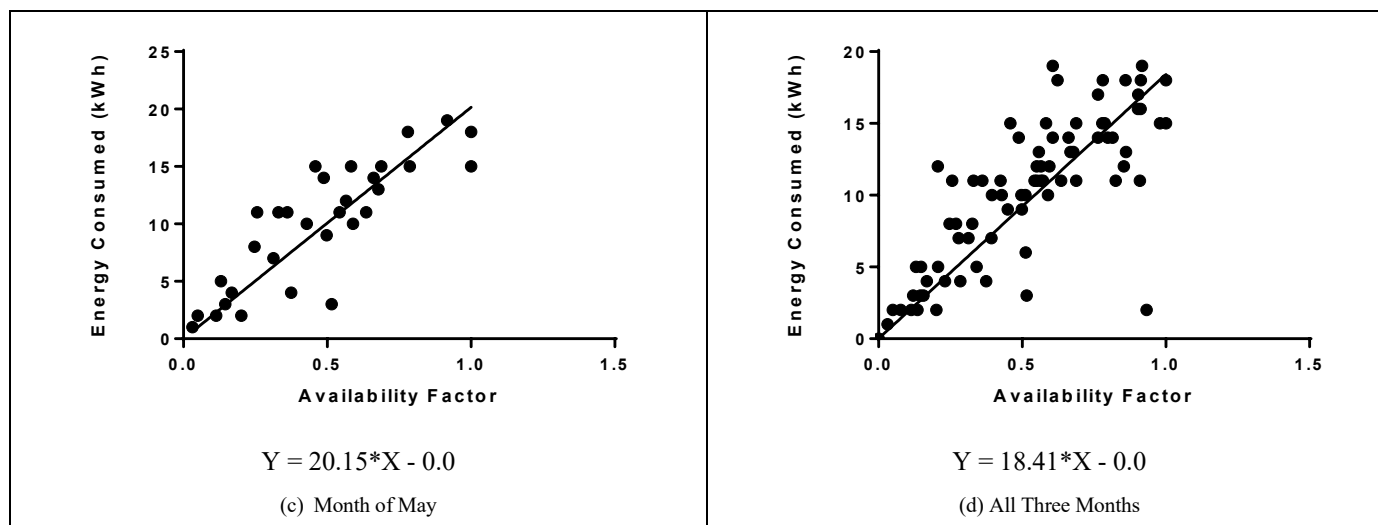
Figure 9: Daily energy consumed versus daily availability factor for March – May 2020 for No. 3 Zik's Drive, University of Nigeria, Nsukka

4. Operational Testing of the Power Availability Recorder

After the design and construction of the PAR, it was tested to ascertain its functionality and operability. The device was seen to be very efficient in recording power availability over a period of Three (3) months and also shows to be highly durable since no fault was recorded throughout the period in which it was under use. Figure 8 shows the prototype of the PAR after it was fabricated. The device worked as intended. It was installed and used to collect power availability data for a length of three (3) months in a residential building inside University of Nigeria, Nsukka without encountering any hitch. The power availability data obtained from the device was used to plot Energy consumption against Availability Factor using GraphPad Prism Software for each month and then for the three (3) months combined together as shown in figure 9.

Figure 9 shows the variation of Energy consumed in a facility with Power Availability. It is evident that increase in availability yields corresponding increase in Energy consumed. The graphs show that this is true for the three months when availability was recorded in a residential building inside the University Community used as test a case for this research work. The slope of the relationship shows that there exists a strong positive relationship between the two. This is an experimental evidence that availability currently controls consumption and in fact limits it, given the very low power availability in the country at this time. The daily availability factor is calculated using equation 3 where Total Hours is taken to be 24 hours of the day.

$$Availability\ Factor = \frac{Hours\ Available}{Total\ Hours} \quad (3)$$

5. Discussions

From the graphs in Figure 9 it is evident that electrical energy consumed in a facility or building changes with Availability. It is evident from this figure that increase in availability yields corresponding increase in Energy consumed in a building. All the graphs show that this is true for a household inside the University of Nigeria, Nsukka used as a test case for this research work for at least a period of three months. The slope of the relationship shows that there exist a strong positive relationship between the

two. This is an experimental evidence that availability currently controls consumption and in fact limits it, given the very low power availability in the country at this time.

6. Conclusion

Improvement of the existing electrical energy measurement devices had been done in terms of accurate stable power measurements. The instrument for the measurement of power availability in facilities, PAR has been successfully designed, constructed and tested. This newly developed device is able to record and store the amount of energy supply and used within the time of the power availability. During the recording period, the PAR shuts down by itself when the supplied power is below a certain regulated value which is not able to power devices in the customers` residence. The PAR works as was conceived before embarking on the project and hence can be produced massively if adequately funded by relevant agencies. It is therefore recommended that the utilities install the availability recorder in each phase of a transformer feeding a community so as to keep track of the actual figure of availability in a community and to obtain the community's availability factor. Energy meters should be installed in a statistically significant number of households in the community which can work together with the availability data in obtaining the load use factor for the rural communities. An extensive project should be undertaken to determine the availability factors and load use factors for communities, zones or regions of a particular country. These may be used for improved determination of the actual bills for unmetered customers and in any regional or national energy modeling and planning activities. Some other researches and inclusions are in progress to see how an energy meter can be designed and incorporated into the device.

Conflict of Interest

Development (ACE-SPED), University of Nigeria, Nsukka that enabled the timely completion of this research.

References

[1] F. I. Abam, B. N. Nwankwojike, "Energy resource structure and on-going sustainable development policy in Nigeria: a review," International Journal of Energy and Environmental Engineering, **5**(102), 1–16, 2014.doi: 10.1007/s40095-014-0102-8.

[2] P. Bajpai, V. Dash, "Hybrid renewable energy systems for power generation in stand-alone applications: A review," Renewable and Sustainable Energy Reviews, **16**(5),2926–2939, 2012, DOI: 10.1016/j.rser.2012.02.009.

[3] Y. Liu, Y.Gao, Y. Hao, H. Liao, "The Relationship between residential electricity consumption and income: a piecewise linear model. Energies", 9, 1–11, 2016, doi.org/10.3390/en9100831.

[4] S. O. Oyedepo, O. P. Babalola, S. C. Nwanya, O. Kilanko, A. O. Abidakun, O. L. Agberegha, "Towards a sustainable electricity supply in Nigeria: the role of decentralized renewable energy system," European Journal of Sustainable Development Research, **2**(4), 2018, DOI: 10.20897/ejosdr/3908

[5] J. E. Payne, "A survey of the electricity consumption-growth literature," Applied Energy, **87**(3), 723–731, 2010, DOI: 10.1016/j.apenergy.2009.06.034

[6] C. W. Factbook, "Energy consumption per capital and population of countries,"https://photius.com/rankings/2015/energy/electricity_consumption_per_capita_2015_1.html (accessed on 02 07 2020)

[7] F. I. Kazeem, "On mathematical projection of Nigeria population using numerical techniques," FULafia Journal of Science & Technology, **5**(2),176–182, 2019.

[8] O. Y. Usman, F. Polytechnic, K. Abdullah, U. Tun, H. Onn, "Modeling and forecast of residential electricity consumption in Nigeria advanced research in energy and engineering modeling and forecast of residential electricity consumption in Nigeria," Advanced Research in Energy and Engineering, **1**(2), 1–7, 2020.

[9] O. Bode, M. Kipngetich, A. Fisayo, T. Amara, O. Idowu, T. Senjyu, "Challenges and prospects of Nigeria's sustainable energy transition with lessons from other countries' experiences," Energy Reports, **6**, 993–1009, 2020, 10.1016/j.egyr.2020.04.022

[10] I.M. Chinaeke-Ogbuka, C. U. Ogbuka, C.A. Nwosu, T.C. Madueme "A renewed call for renewable energy exploitation for sustainable national development" The Fourth Electrical Engineering National Conference, Energy Sources for Power Generation (ES4PG), University of Nigeria, Nsukka 21st-23rd July, 2013, 162-168, 2013.

[11] C.A. Nwosu, G.C. Asomba, C.U. Ogbuka, "Community-based independent power plant: a case for renewable energy resources". Pacific Journal of Science and Technology. **9**(2), 452-460, 2008.

[12] D.D. Agwu, I.M. Chinaeke-Ogbuka, C.U. Ogbuka, "Toward effective harnessing of wind energy for power generation in nigeria" The Fourth Electrical Engineering National Conference, Energy Sources for Power Generation (ES4PG) UNN, Nsukka 21st-23rd July, 2013, 97-102, 2013

[13] Federal Government of Nigeria and A. Ministry of Power, Electric Power Sector Reform Act (EPSRA) 2005. 2005.

[14] Federal government of Nigeria, "National Electric Power Policy, 2001" Ministry of Power, Abuja," 2001.

[15] M. O. Oseni, "Assessing the consumers' willingness to adopt a prepayment metering system in Nigeria," Energy Policy, **86**, 154–165, 2015,DOI: 10.1016/j.enpol.2015.06.038

[16] National electricity regulatory commission, "Bridging the Metering Gap as reported in www.pwc.com/ng," 2017.

[17] Bridging the Metering Gap: Strategies for Success (Part 1)", Pricewaterhouse Coopers Ltd, Advisory Outlook, www.pwc.com/ng. 2018.

[18] A. A. E. Audu, S. O. Paul, "Privatization of power sector and poverty of power supply in Nigeria: A policy analysis," International Journal of Development and Sustainability, **6**(10) 1218–1231, 2017.

[19] N. Kambule, K. Yessoufou, N. Nwulu, C. Mbohwa, "Exploring the driving factors of prepaid electricity meter rejection in the largest township of South Africa," Energy Policy, **124**(9), 199–205, 2019, DOI: 10.1016/j.enpol.2018.09.041

[20] A. M. Orimogunje, "Development of an ANN-based Estimated Electricity Billing System," 2018 IEEE PES/IAS PowerAfrica, 96–101, 2018. DOI: 10.1109/PowerAfrica.2018.8521004

[21] D. E. Ebem, U. Arinze, "An optimized web-based energy billing system for electricity consumers in Nigeria," Advances in Multidisciplinary and Scientific Research, **4**(3), 53–64, 2018.DOI: 10.22624/AIMS/V4N3P7

[22] Metering installation requirements. https://www.bia.gov/sites/bia.gov/files/assets/public/pdf/idc037760.pdf (accessed on 14 05 2020)

[23] J. Genet and C. Schubert, "Designing a metering system for small and medium-sized buildings," in Schneider Electirc, 2–14, 2018.

[24] A. Oyetunji, E. Odugboye, T. A. Arimoro, "Analysis of electricity billing system in corporate buildings in Lagos, Nigeria.," J. Manag. Econ. Stud., **1**(6), 1–22, 2019, DOI: 10.26677/TR1010.2019.150

[25] M. Zaman, F. Shaheen, A. Haider, S. Qamar, "Examining relationship between electricity consumption and its major determinants in Pakistan,"International Journal of Energy Economics and Policy, **5**(4), 998–1009, 2015.

[26] C. V. Ikwuagwu, "Development and testing of a power availability recorder for buildings and facilities", M.Eng thesis, Mechanical Engineering, University of Nigeria, Nsukka, 2017.

14

Environmental Acoustics Modelling Techniques for Forest Monitoring

Svetlana Segarceanu[*,1], George Suciu[1], Inge Gavăt[2]

[1]*Beia Consult International, Bucharest, 041386, Romania*

[2]*University Politehnica of Bucharest, Applied Electronics Department, Bucharest, 060042, Romania*

A B S T R A C T

Environmental sounds detection plays an increasing role in computer science and robotics as it simulates the human faculty of hearing. It is applied in environment research, monitoring and protection, by allowing investigation of natural reserves, and showing potential risks of damage that can be deduced from the environmental acoustic. The research presented in this paper is related to the development of an intelligent forest environment monitoring solution, which applies signal analysis algorithm to detect endangering sounds. Environmental sounds are processed using some modelling algorithms based on which the acoustic forest events can be classified into one of the categories: chainsaw, vehicle, genuine forest background noise. The article will explore and compare several methodologies for environmental sound classification, among which the dominant Deep Neural Networks, the Long Short-Term Memory, and the classical Gaussian Mixtures Modelling and Dynamic Time Warping.

1. Introduction

Environmental sound recognition (AESR) is a relatively new discipline of computer science destined to extend the field of speech-based applications, or the study of music sounds, by exploring the vast range of environmental non-speech sounds.

This paper is an extension of work originally presented in the 43rd International Conference on Telecommunications and Signal Processing, held in Milan in July 2020 [1]. It investigates several sound modelling and classification paradigms, in the context of a forest monitoring system.

The new research area of AESR is intended to simulate the important function of human hearing, and possibly, to overpower human perception. This is motivated by the fact that hearing is the human second most important sense after vision and should not be disregarded when trying to build a computer that simulates human behaviour and senses. Consequently, AESR recently became an essential field of computer science [2]-[4].

By environmental sounds we mean everyday sounds, natural or artificial, other than speech. Natural sounds may be leaves rustling, animal noise, birds chirping, water ripple, wind blowing through trees, waves crashing onto the shore, thunder. Artificial sounds include sounds produced by diverse engines like cars, cranes, ATVs, snowmobile, lawnmower, pneumatic hammer, chainsaw, etc., but also creaky doors or creaky floors, gunshots, crowd in a club, breaking glass, vehicle tyres or brake noise. The environments where this discipline is applied are also very diverse, falling into two broad categories:

- Natural environment like forest environment, ecological units, seashore environment; however, the degree of naturalness is variable, and purely natural environments are very rare as one may intercept voices, vehicle sounds, chainsaw in forests or even jungle.

- Built environment, also called human made environment, like the urban environment, the household, maybe agricultural environment, harbours; obviously in any of these environments, natural acoustic events, like thunder, rain falling, wind blowing may also happen.

In reality there are no purely natural or artificial sounds, neither purely speech nor non-speech acoustic events. Most of the application investigate mixed environments where natural and artificial, speech or non-speech acoustic events are equally possible.

The applicability of AESR is related to the advent of Internet of Things (IoT). IoT devices have sensors, possibly acoustic,

[*]Corresponding Author Svetlana Segărceanu, Email:
svetlana.segarceanu@beia.ro

and software that enable the collection and exchange of data through the Internet. Automatic recognition of the surrounding environment allows devices to switch between tasks with minimum user interference [5]. For a robot, audio recordings may provide important information about location and direction of a moving vehicle, or environmental information, such as speed of wind.

AESR has an important role in security, environment protection or environment research. Among possible applications are the identification of deforestation threats and illegal logging activities, through automatic detection of specific sounds like several engines, chainsaws, or vehicles. Detecting other illegal activities like hunting in forest or ecological reserves, by spotting gun shots, or human voices would be a useful application [6]-[9]. In recent times, solutions based on environmental sound recognition are applied in early wildfire detection [10].

Another type of applications concerns scientific monitoring of the environment. Such applications are intended for instance, to detect species, by discrimination between different animals or birds' sounds [11], [12].

Computational Auditory Scene Analysis (CASA), is a very complex field of AESR, aimed to the recognition mixtures of sound sources by simulating human listening perception using computational means. It mainly addresses two important tasks, Environmental Audio Scene Recognition (EASR) and Sound Event Recognition (SER) and has a huge importance in environment audio observation and surveillance. EASR refers to recognition of indoor or outdoor acoustic scenes (e.g., cafes/restaurants, home, vehicle or metro stations, supermarkets, versus crowded or silent streets, forest landscape, countryside, beaches, gym halls, swimming pools). SER is intended to the investigation of specific acoustic events in the audio environments, like dog barking, gunshots, sudden brake sounds, or human non-speech events, like coughing, whistling, screaming, child crying, snoring, sneezing [13].

An emerging field is the investigation and detection of acoustic emissions, used in monitoring landslide phenomena [14]. Acoustic emissions (AE) are elastic waves generated by movement at particle-to-particle contacts and between soil particles and structural elements. They are not perceived by the human ear, are super audible, and therefore their frequencies are very high, expected to range between 15kHz and 40 kHz. The devices used to acquire these waves should ensure a sampling frequency of over 80 kHz. AE monitoring is an active area, not very well developed due to low energy levels of these waves, which make it challenging to detect and quantify [15], [16].

Likewise, recent studies have shown that moving avalanches emit a detectable sub-audible sound signature in the low frequency infrasonic spectrum [17].

The study of underwater acoustic infrasonic emissions, provided by hydrophones, is another field of AESR research [18].

Our paper explores forest acoustics aiming to find the suitable sound modelling and classification approaches. The focus of our research is the detection of logging risk by identification of specific classes of sounds: chainsaw, vehicles, or possibly speech. We extend an earlier research on acoustic signal processing, by

exploring the dominant paradigm in data modelling and, the deep neural networks (DNN). We investigate two types of DNNs, the Deep Feed Forward Neural Networks (FFNN) and a popular version of Recurrent Neural Networks (RNNs), the Long Short-Term Memory (LSTM). The two neural networks will be run on two types of feature spaces: the Mel-cepstral and the Fourier log-power spectrum feature spaces. We will compare their results with the former performance obtained using the Gaussian Mixtures Modelling (GMM) and the Dynamic Time Warping (DTW) in the context of a closed-set identification system. One main goal is to stress the importance of feeding as input to DNN less processed features, like log-power spectrum, as compared to the more elaborate sets of features, e.g., Mel-frequency cepstral features. Another purpose of the paper is to clarify some issues concerning signal pre-processing framework, like length of the analysis window and the underlying frequency domain to be used in spectral analysis.

The paper is structured as follows: the next section describes the state-of-the-art in environmental sound recognition; the third section details our approach, the signal feature extraction and modelling methods we applied in sound recognition; the fourth section presents the setup of the experiments and evaluates the proposed methods; the last part presents the conclusions of the paper.

2. State-of-the-art

Early attempts [2], [19] to assess speech typical methods in the context of non-speech acoustics, analyse classical methods like Artificial Neural Networks (ANN), or Learning Vector Quantization (LVQ), on Fourier, or Linear Predictive Coding (LPC) feature spaces.

In [20], the authors make an overall investigation of recognition methodologies for different categories of sounds. The environmental sounds are classified as stationary and non-stationary. The framework used for stationary acoustic signals coincides to a great extent with the one used in voice-based applications (speech or speaker recognition) in what concerns the specific features and feature space modelling methods. For feature extraction, the spectral features, like those derived from Mel analysis – Mel Frequency Cepstral Coefficients (MFCCs), LPC, Code Excited Linear Prediction (CELP), or techniques based on signal autocorrelation, prevail. The modelling approaches are also shared with voice-based applications: GMM, k-Nearest Neighbours (k-NN), Learning Vector Quantisation (LVQ), DTW, Hidden Markov Models (HMM), Support Vector Machine (SVM), Neural Networks, and deep learning. Concerning non-stationary signals, some successful techniques are based on sparse representations like the Matching Pursuit (MP) and MP-Gabor features. Alternative approaches use fusion of MFCC and other parameters to boost the performance.

In [5], the authors review the current methodologies used in AESR and evaluate their performance, efficiency, and computational cost. The leading approaches of the moment are GMM, SVM and DNN or Recurrent Neural Networks (RNN) The paper describes open-set identification experiments on two types of acoustic events, baby cries and smoke alarm, and a very large range of complementary environment acoustic events. as impostor data. In this respect GMM, using the Universal Background Model

(GMM-UBM) and two neural network architectures were compared. The Deep Feed Forward Neural Network yielded the best identification rate, while the best computational cost is made by GMM. SVM has an intermediate identification rate, yet at a high computational cost, assessed accounting for four basic operations: addition, comparison, multiplication, and lookup table retrieval (LUT). The computational cost is a critical feature in the context of IoT, where sound analysis applications are required to run on embedded platforms with hard constraints on the available computing power.

In [13], the authors make a thorough and extensive investigation of the most recent achievements and tendencies in AESR, more precisely in EASR and SER fields of CASA. from the perspective of acoustic feature extraction, the modelling methodology, performance, available acoustic databases. Besides the conventional approaches, new classes of features were applied lately by several implementations. Such characteristics are the auditory image-based features, basically regarding the time-frequency spectrograms as bidimensional images. where the frequency is not necessarily in the linear domain, but possibly adapted to a perceptual scale. Besides the log-power spectrum, Mel or Bark-frequency log-scale spectrograms, Spectrogram Image Features (SIF) [21], such characteristics as Mel scale with Constant-Q-Transform [22], wavelet coefficients [23] are referred.

Another class of features are generated by learning approaches with the goal to provide lower and enhanced representations. Such features are obtained applying techniques like quantization, i-vector, non-negative matrix factorization (NMF) [24], sparse coding, Convolutional Neural Network–Label Tree Embeddings (CNN-LTE) [25], etc.

Concerning the experimented methodologies, the deep learning methods are predominant, with Feed-Forward Neural Networks and Convolutional Neural Networks (CNN) in the leading position. Many strategies are currently operating CNNs in conjunction with a variety of features, among which log-scaled mel-spectrograms [26]-[28], CNN-LTE [25] or in hybrid approaches [29]. These implementations outperformed the other attempts to approach EASR and SER tasks.

Avalanche or landslide monitoring applications use methodologies based on thresholds for acoustic emissions energy, depending on the hazard risk level.

Concerning the general framework applied in AESR, we draw on the ideas presented in [20]. The usual pre-processing of the acoustic signal, applied in AESR includes a framing step, possibly followed by sub-framing or sequential processing. In the "framing" stage the signal is processed continuously, frame by frame. A classification decision is made for each frame and successive frames may belong to different classes. This is illustrated in figure 1, where a chainsaw is detected in a forest environment. Framing can enhance the acoustic signal classification by structuring the stream into more homogeneous blocks to better catch the acoustic event. Yet, there is no way of setting an optimal frame length, as for stationary events a length of 3s is a reasonable choice, while for acoustic events like thunder or gunshots, a 3s window length might be too large, and contain other acoustic events, so they could be associated to inappropriate classes. Due to the latest advances in instrumentation, different

frame lengths are used to streamline energy consumption during a monitoring process, based on detecting energy levels of environmental sounds.
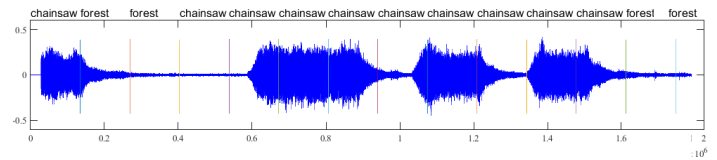
Figure 1: Framing process of a real-life sound and classification of each frame
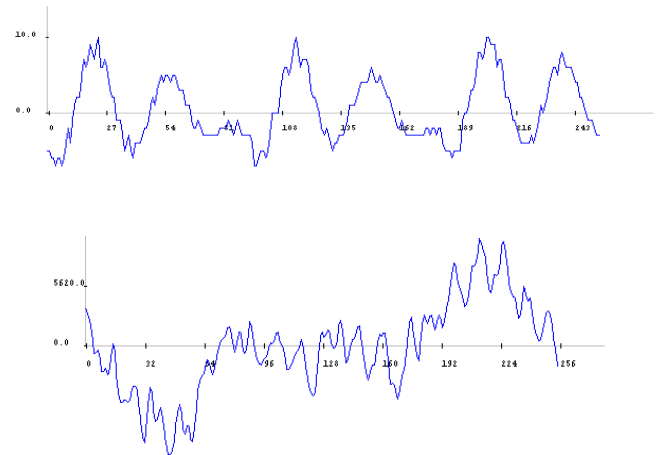
Figure 3: 22ms of chainsaw sound
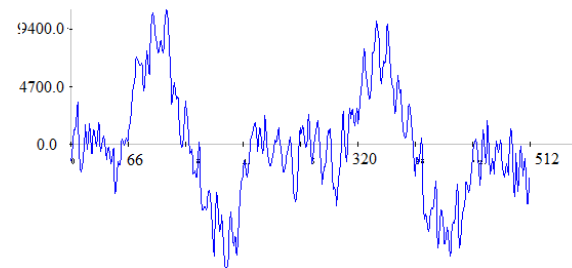
Figure 4: 44ms of chainsaw sound

Next, a sub-framing process is applied, by dividing the frame into usually overlapping, analysis subframes. The length of a subframe is explicitly set in [20] to 20-30ms. This length is suited for speech analysis, as it ensures a good resolution in time and frequency. Figure 2 presents 22ms of male speech which includes three fundamental periods of the respective voice. Whereas figure 4 represents 44ms of chainsaw sound which contains two periods of the chainsaw sound. However, we cannot infer anything about the signal periodicity from the segment of 22ms of chainsaw sound, represented in figure 3. Therefore, considering sub-frames of 44ms is a reasonable choice for chainsaw detection. However, a realistic setup must consider a value convenient to all sounds in the acoustic environment.

The further processing applied on the analysis frames is the same with that applied in speech signal analysis and its final goal is to extract characteristic features. The largely applied features are somehow derived from the Fourier features, and called spectral features. Non-spectral features are, for instance, energy, Zero-Crossing Rate (ZCR), Spectral Flatness (SF), all calculated in time domain. Concerning spectral analysis, the relevant frequency

interval for a signal sampling frequency of 44.1 kHz is not the whole frequency domain furnished by the Fourier transform, [0, 22.05] kHz, but a shorter range, as shown in figures 5,6. By setting the appropriate analysis frequency interval, we may improve the performance as accuracy and speed of execution, as another benefit of shortening the frequency interval is the decrease of the number of spectrum samples to be processed.
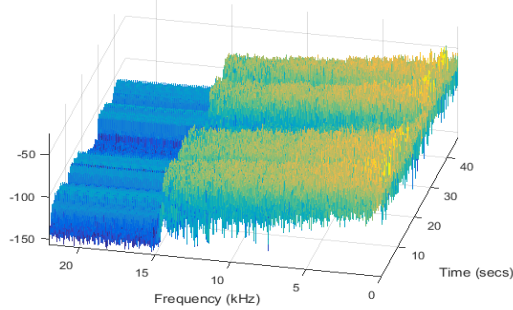
Figure 5: Power spectrum of a chainsaw sound
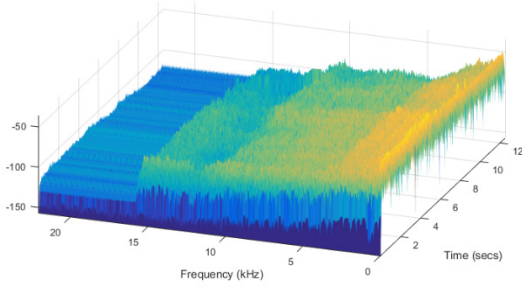
Figure 6: Power spectrum of a snowmobile sound

When choosing the spectral analysis, the usual pre-processing on the analysis frame involves (Hamming) windowing and pre-emphasis.

3. The Method

We have applied the framework mentioned above. At framing we divided the audio signal recordings into intervals of 3 seconds. We have used analysis frames of lengths of 22, 44 and 88ms with the usual pre-processing scheme as in speech-based applications. The modelling methods we have evaluated are GMM, DTW and FFNN. As baseline for the feature space, we used the Fourier spectrum coefficients and MFCCs. The set of MFCC parameters was possibly increased with Zero Crossing Rate (ZCR) or/and Spectral Flatness (SF). We have applied GMM on the MFCC feature space, and called this approach MFCC-GMM, DTW on the spectral features space, and FFNN on both the MFCC and spectral features spaces.

3.1. MFCC-GMM

GMM provides probabilistic weighted clustering that generates a coverage of the data space rather than a partition [30], [31]. Each cluster is modelled by a Gaussian distribution, usually called component, defined by the mean μ and the standard deviation Σ of cluster data, along with a weight w of the component inside the mixture. A data set belonging to the same class C, can be modelled by one or more Gaussian components, and the parameters of each component are calculated using the Estimation-Maximization

algorithm, resulting in a model $\lambda_C = ((w_k, \mu_k, \Sigma_k), k = 1..., K)$, where K is the number of components. A key step of the algorithm is the initialization where initial values of the parameters (means, variances and weights) are defined. Poor initialization entails bad quality of classification or even impossibility to define the Gaussian parameters. We used at initialization a hierarchical algorithm, Pairwise Nearest Neighbour (PNN) [32] to ensure balanced data clustering, although other hierarchical algorithms such as Complete Linkage Clustering, or Average Linkage Clustering also provide good performance. We have evaluated different distance measures between hierarchy branches: Minkowski (Euclidean distance when square powers are considered), Chebyshev, Euclidian standardised distance. GMM modelling was applied on a feature space consisting of MFCCs and/or Spectral Flatness and ZCR, to generate models for C (C=3) classes of sounds. To classify a sequence of d dimensional features $X = \{x_1, x_2,...,x_T\}$ into one of the classes its likelihood to belong to each class c is evaluated as

$$log(X, \lambda_c) = \sum_{t=1}^{T} p(x_t/\lambda_c) \tag{1}$$

where

$$p(x_t/\lambda) = \sum_{k=1}^{K} w_k \frac{1}{(2\pi)^{\frac{d}{2}}|\Sigma_k|^{\frac{1}{2}}} e^{-\frac{1}{2}(x_t-\mu_k)^T \Sigma_k^{-1}(x_t-\mu_k)} \tag{2}$$

and the class with the maximum likelihood is selected:

$$\lambda_{best} = \underset{\lambda \in \{\lambda_1, \lambda_2,..,\lambda_C\}}{\operatorname{argmax}} (log(X, \lambda)) \tag{3}$$

Mel frequency analysis [33] [34] is a perceptual approach to signal analysis based on human sensing of the frequency domain. We applied the MATLAB implementations of the Mel-scale frequency:

$$f_{mel}(f) = 1127 \ln(1 + f/700) \tag{4}$$

and bank of triangular filters for linear frequencies $f \in [f_{low}, f_{high}]$:

$$H_m[k] = \begin{cases} 0 & k < f[m-1] \text{ or } k \geq f[m+1] \\ \frac{k-f[m-1]}{(f[m]-f[m-1])} & f[m-1] \leq k < f[m] \\ \frac{f[m+1]-k}{(f[m+1]-f[m])} & f[m] \leq k < f[m+1] \end{cases} \tag{5}$$

The power spectrum calculated on an analysis frame, is passed through the bank filter in (5), and the Mel Frequency Cepstral Coefficients (MFFCs) are derived by applying the Discrete Cosine Transform to the logarithm of the filtered spectrum [33].

Spectral Flatness (tonal coefficient) is meant to highlight noise from tonal sound and is calculated as ratio of geometrical and arithmetical means of spectral coefficients on analysis frames.

A zero crossing arises when two neighbouring samples have opposite signs, and its value on an analysis frame is:

$$Z_n = \sum_{m=-\infty}^{\infty} |sgn(x(m)) - sgn(x(m-1))| * w(n-m) \tag{6}$$

3.2. Spectra Alignment using Dynamic Time Warping

Dynamic Time Warping (DTW) measures the similarity of two, usually time-varying, sequences, by optimally aligning them using a recurrent algorithm [35], complying with specific constraints, concerning boundary conditions, monotony, and continuity of the similarity function, and building an optimal path. One of the issues raised by the DTW algorithm is the long execution time, the main reason for which is the full calculus of DTW matrices, usually defined by distances between the elements of the sequences. This can be contained by restraining the calculus to a low number of elements, the most likely to participate in the definition of the optimal path by applying an adjusting window as in figure 4, where the popular Sakoe-Chiba band [36] is applied. Figure 7 presents the graphical rendering of a DTW matrix for two sequences *s(t)* and *r(t)*, the Sakoe-Chiba band, in grey, highlighting the optimal path, which does not lie entirely inside the band. When applying the Sakoe-Chiba band, the optimal path should lie inside the band and is figured in red in the image, accompanying only inside the band the real optimal path figured in black, thick where it lies within the band.
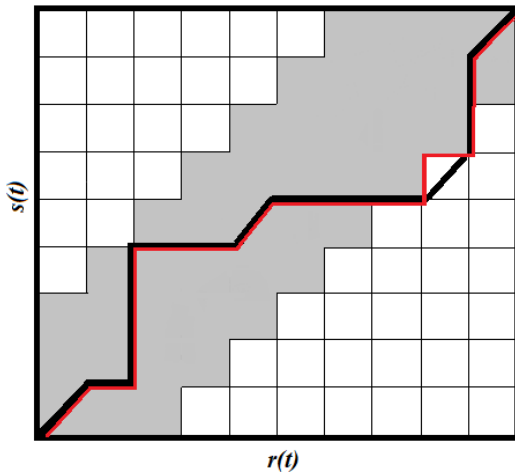
Figure 7: Alignment of sequences *r, s*, using the Sakoe- Chiba band, and the two optimal paths, the real one (black) and the one lying inside the band, which generally coincide.

The DTW algorithm was applied on power spectra of the signal. The power spectrum on an analysis window is calculated as sum of squared Fourier coefficients. One argument for using DTW to align spectral series is the fact that the acoustic signals received from devices of the same type share the same characteristics, such as sampling frequency, so, the generated spectra have the same lengths. Another premise is the fact that the interesting domain for this type of application is under 15 kHz, or even 10 kHz, which is demonstrated by figures 5, 6. This fact is used to align equal length spectra by the DTW algorithm. In the experiments the sampling frequency of the available audio files is equal to 44.1 kHz, the Fourier spectrum covers the domain [0, 22.05] kHz, but if the useful frequency domain is restricted to [0, 7.4] kHz and the analysis frame is of 22ms, the number of features is 171 instead of 512.

Classification of a sequence of feature vectors using the DTW algorithm consists in calculating the distortion between these vectors and the template (training) sequences, and to select the class whose templates show the smallest distortion with respect to the given feature sequence. The calculation involved in this process is based on the distances between individual vectors in the two sets to be compared. The distance may be evaluated in different ways. We have applied two distance measures in the calculus of the distortion measure, the Euclidian norm, and the 1-norm (sum of absolute values).

3.3. Deep feedforward networks (FFNN)

The artificial neural networks (ANNs) were intended to simulate human associative memory. They learn by processing known input examples, and corresponding expected results, creating weighted associations between them, stored within the network data structure. Deep feedforward networks or multilayer perceptrons (MLPs), are the quintessential deep learning models [37]. The basic unit of a FFNN is the artificial neuron, which expresses the biological concept of neuron [38]. They receive input data, combine the input through internal processing elements like weights and bias terms, and apply an optional threshold using an activation (transfer) function, as shown in figure 8. Transfer functions are applied to provide a smooth, differentiable transition as input values change. They are used to model the output to lie between 'yes' and 'no', mapping the output values between 0 to 1 or -1 to 1, etc. Transfer function are basically divided into linear and non-linear activation functions. Non-linear transfer functions are "S" – shaped functions like *arctg*, hyperbolic tangent, logistic functions as in (7):

$$f(x) = \sigma(x) = \frac{1}{1+e^{-x}} \tag{7}$$
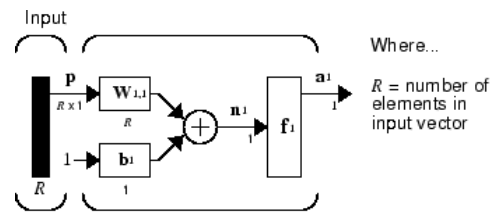
Figure 8: Structure of a neuron

The goal of a feedforward network for modelling and classification is to define a mapping $y = f(x, \theta)$ and learn the value of parameters θ to ensure the best approximation of the expected value y by the output of f, given the input x and parameters θ. FFNNs have one or more hidden layers of sigmoid neurons followed by an output layer of linear neurons. A layer of neurons brings together the weight vectors and biases corresponding to its neurons, so it can be expressed by a matrix of weights and bias vectors, as in figure 9, 10. The transfer function is supposed to be the same for each neuron in the layer. The general diagram of a network is shown in figure 11, where the parameters to be tuned are the weight matrices and bias terms applied at the level of each layer, so that the output of the overall system would be close to expected values. These networks are called feedforward because the information flows in one direction through intermediate computations and there is no feedback connection. The number of neurons does not necessarily decrease with the layer level as presented in figure 10, but usually the goal is to reduce the dimensionality of the input layer, a process similar to feature extraction. The computation corresponding to figure 12 can be expressed by :

$$a^k = f^k(W_k a^{k-1} + b_k) =$$
$$f^k\big(W_k\big(f^{k-1}(W_{k-1}a^{k-2} + b_{k-1})\big) + b_k\big) = \quad (8)$$
$$f^k\big(W_k\big(f^{k-1}(W_{k-1}(f^{k-2}(W_{k-2}a^{k-3} + b_{k-2})) + b_{k-1})\big) + b_k\big) = \cdots$$
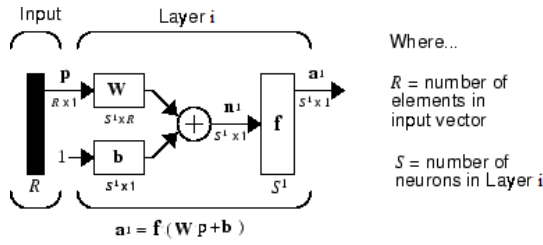
Figure 9: Structure of a layer of neurons
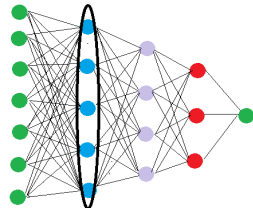
Figure 10: A Feed Forward Neural Network with three highlighted layers
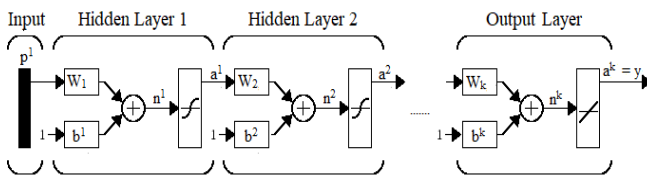
Figure 11: Flow of data in a feedforward network

In equations (8) the known information is

- The input parameters p, which might be measurements from sensors (wind speed, temperature, humidity), parameters coming from images (matrices of colours, or grey hues), or parameters coming from acoustic signals (Fourier spectrum on an analysis window, or more complicated parameters like cepstral, linear prediction coefficients),

- The expected output: for instance, to solve a three classes problem the output corresponding to each class input might be defined as either unidimensional (a scalar value for each class): (-1, 0, 1) or (0, 1. 2) or multidimensional (a vector for each class):((1, 0, 0), (0, 1, 0), (0, 0, 1)),

- The neural network architecture: number of hidden layers, number of neurons on each layer, etc.

Unknown parameters are:

- weights at layer k: W_k,

- bias terms at layer k: b_k.

Learning the unknown parameters is performed during the training process. Training of a FFNN can be made in batch mode or in incremental mode [38]. In batch mode, weights and biases are updated after all the inputs and targets are presented. Incremental networks receive the inputs one by one and adapt the weights according to each input. Usually, batch training is used. Equations (8) have as unknowns, the weight matrices and the bias terms, and

a much more numerous training known data (all the input data and the corresponding expected values). This implicates the realistic conclusion that there will not be any solution of the equation system, so the training process looks for the values of the parameters, weights and biases, that make the error between the output value and expected output, minimal:

$$e(W, b) = \sum_{i=1}^{N}(y_i - a_i^k(p, W, b))^2 \quad (9)$$

where N is the number of (input, output) pair samples.

To minimize the least mean square (LMS) expression in (8) several schemes based on LMS algorithm using variants of the steepest descent procedure, are used. MATLAB has implemented and supports a range of network training algorithms among which: Levenberg-Marquardt Algorithm (LMA), Bayesian Regularization (BR), BFGS Quasi-Newton, Resilient Backpropagation, Scaled Conjugate Gradient, One Step Secant, etc. To start minimization of (9) using any of these algorithms, the user should provide an initial guess for the parameter vector θ=(W, b). The performance of the system depends on this initial guess. Most of the above algorithms try to optimize this process.

At the end of the training process, we get a FFNN model:

$$net = (W_k, b_k), \qquad k= 1,2...K. \quad (10)$$

where K is the number of layers in the network. To classify a vector of data $x = \{x_1, x_2, ..., x_d\}$, we "feed" it at the input of the network, perform all the operations applying the weights and biases to the input data, as in figure 11, and evaluate the output:

$$score = net (x) \quad (11)$$

If we code the output classes $y = \{y_1, y_2, ..., y_C\}$, C the number of classes, we compare the obtained output score to these values and if score is closest to y_c the input vector x will belong to class c.

We have applied the feedforward algorithm by feeding at input two types of features: power spectrum features and MFCCs.

3.4. Long Short-Time Memory (LSTM)

LSTM [39] is an artificial Recurrent Neural Network, and as any RNN is designed to handle sequences of events that occur in succession, with the understanding of each event based on information from previous events. They are able to handle tasks such as stock prediction or enhanced speech detection. One significant challenge for RNNs performance is that of the vanishing gradient which impacts RNNs long-term memory capabilities, restricted to only remembering a few sequences at a time. LSTMs proposes an architecture to overcome this drawback and allow to retain information for longer periods compared to traditional RNNs. Unlike standard feedforward neural networks, LSTM has feedback connections. It is capable of learning long-term dependencies, useful for certain types of prediction requiring the network to retain information over longer time periods, can process entire sequences of data (such as speech or video). It has been introduced in 1997 by the German researchers, Hochreiter and Schmidhuber.

The architecture of a LSTM Neural Network includes the cell (the memory part of the LSTM unit) and three "regulators", called gates, of the flow of information inside the LSTM unit:

- input gate to control the extent to which new values flow into the cell

- output gate to control the extent to which a value remains in the cell

- forget gate to control to what extent the value in the cell is used to compute the output activation of the LSTM unit

The LSTM is able to remove or add information to the cell state, through these gates. Some variations of the LSTM, like the Peephole LSTM or the Convolutional LSTM, ignore one or more of these gates.

The cell is responsible for keeping track of the dependencies between the elements in the input sequence. The activation function of LSTM gates is often the logistic sigmoid function. The connections to and from the LSTM gates, some recurrent, are weighted. The weights are learned during training, they determine how the gates operate. The diagram of a cell is presented in Figure 1(https://en.wikipedia.org/wiki/Long_short-term_memory#/media/File:The_LSTM_cell.png) and the LSTM flow is shown in figure 13 (Understanding LSTM Networks -- colah's blog) .
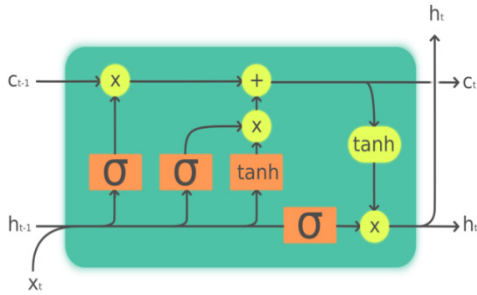
Figure 12: Structure of a LSTM cell
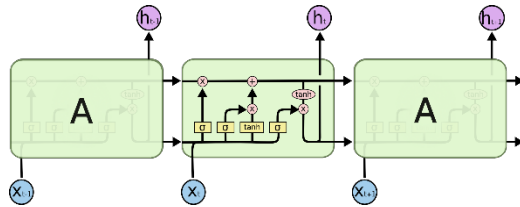
Figure 13: LSTM chain

The calculations that solve the LSTM paradigm are [39]:

$$f_t = \sigma_g(W_f x_t + U_f h_{t-1} + b_f)$$
$$i_t = \sigma_g(W_i x_t + U_i h_{t-1} + b_i)$$
$$o_t = \sigma_g(W_o x_t + U_o h_{t-1} + b_o) \qquad (12)$$
$$\widetilde{c}_t = \sigma_c(W_c x_t + U_c h_{t-1} + b_c)$$
$$c_t = f_t \cdot c_{t-1} + i_t \cdot \widetilde{c}_t$$
$$h_t = o_t \cdot \sigma_h(c_t)$$

where the known data are:

- $x_t \in R^d$ - input vector to the LSTM unit,

- d and h - number of input features and number of hidden units, respectively,

Unknowns :

- $f_t \in R^h$ - forget gate's activation vector

- $i_t \in R^h$ - input/update gate's activation vector

- $o_t \in R^h$ - output gate's activation vector

- $h_t \in R^h$ - hidden state vector (output vector of the LSTM unit)

- $\widetilde{c}_t \in R^h$ - cell input activation vector

- $c_t \in R_h$ - cell state vector

- $W \in R^{hxd}$, $U \in R^{hxd}$, $b \in R^h$ - weight matrices and bias vector parameters which need to be learned during training

Activation functions are:

- σ_g - sigmoid function

- σ_c - hyperbolic tangent function

- σ_h - hyperbolic tangent function or, linear function

The LSTM training is made in a supervised mode by a set of algorithms like gradient descent, combined with backpropagation through time to compute the gradients needed during the optimization process, in order to change each weight of the LSTM network in proportion to the derivative of the error (at the output layer of the LSTM network) with respect to corresponding weight. With LSTM units, when error values are backpropagated from the output layer, the error remains in the LSTM unit's cell. This allows to avoid the problem with standard RNNs where error gradients vanish exponentially with the size of the time lag between important events. The system is trained using the equations (6).

4. Experimental results

The goal of the experiments was to evaluate the four methodologies and find the optimal configuration for each one. The experiments considered only three classes of sounds which could exhaust the specific sounds in the forest environment susceptible to illegal deforestation. They are chainsaw, vehicle, and genuine forest sounds. The identification process was closed set. Segments of 3s were considered and each segment was evaluated individually. We have assessed several lengths of subframes (analysis frames), based on an above remark (see figures 2-4). So, the analysis frames lengths considered are mainly 22ms, 44ms, 88ms. Concerning the frequency interval length, [f_{low}, f_{high}], we have investigated lengths of 3.7, 7.4, 10 and 12 kHz. We have conducted these experiments using the MATLAB framework.

The acoustic material contains 99 recordings of the three classes of sounds, in average about 15s each, 39 were used for training and 60 for testing. The testing set resulted in 685 segments of three seconds. The performance of each of the approaches we tested is presented subsequently. The performance was evaluated in terms of Identification rate, the ratio of numbers of correctly identified segments and the evaluated segments.

4.1. MFCC-GMM

We have applied GMM on the feature space consisting of Mel-cepstral features, accompanied or not by ZCR and Spectral

Flatness. We have tested several hierarchical clustering initialization methods, using different distance measures between branches, varied the number of Gaussian components, the number of the cepstral coefficients, the values of the frequency interval [f_{low}, f_{high}], and the length of the analysis frame. On the given acoustic material, the performance obtained with the PNN initialization, using the Euclidian Standardized distance, were slightly better than when using the other hierarchical methods. The MATLAB settings for analysis frame, 25ms, f_{low} =300 Hz, f_{high}=3.7 kHz are the most beneficial. Moreover, adding ZCR and SF improved the results. 12-13 GMM components and 13-14 MFCCs seemed to be the best configuration. Some results are presented in Table 1. We have chosen to assign an identical number of Gaussian components, as our acoustic material is currently quite scarce, and the investigated problem is less complex than, for instance, the task of an audio scene recognition. A more rigorous approach should consider the structure of the underlying acoustic feature space, as shown in [40], to assign the number of components to each category of sound.

Table 1: Performance of AESR using the MFCC-GMM approach, with additional ZCR and SF features, different values of f_{low} and f_{high} expressed in kHz, number of Gaussian components, number of Mel-cepstral coefficients

	f_{low}	f_{high}	Components	Coeficients	Identification Rate			
					Chainsaw	Forest	Vehicle	General
Euclidia	0.3	3.7	14	13	66.47	77.16	61.07	68.07
	0.3	4	13	13	61.85	76.72	59.92	66.27
	0	3.7	14	13	67.63	79.31	56.87	67.47
Standard	0.3	3.7	14	13	62.43	80.17	62.21	**68.52**
	0.3	3.7	15	13	60.69	80.17	62.21	68.07
	0.3	3.7	15	12	67.63	76.29	61.83	68.37

4.2. Spectra Alignment using Dynamic Time Warping

On applying DTW we have aligned Fourier Power Spectra. More precisely, we have aligned segments of these spectra defined on frequency intervals [f_{low}, f_{high}]. The frequency domain was restricted to some intervals included in [0, 7400] Hz. The length of the analysis window was set to 22ms. For analysis frames of 22ms the number of samples per frame, given the sampling frequency of 44.1 kHz, is 970, and the length of the Fourier Transform is the closest power of 2 greater than the number of signal samples, that means 1024. For shorter frequency intervals the corresponding Fourier subset involves less samples, less data to be processed, and a shorter execution time:

- [0, 7400] Hz - 171 samples;
- [0, 3700] Hz - 86 samples;
- [300, 3700] Hz - 80 samples;
- [300, 7400] Hz - 165 samples.

For this reason, the length of the analysis frame was set to 22ms. A 25ms frame would have meant a 2048 long Discrete Fourier Transform, and hence, power spectrum.

We have compared the performance of the DTW alignment for several lengths of the frequency interval [f_{low}, f_{high}], different lengths of the Sakoe- Chiba band, and the two distance measures in the calculus of the distortion measure, the Euclidian norm, and the 1-norm (sum of absolute values). The best results for analysis frames of 22ms, f_{low}=0, f_{high}=7.4 kHz, for the largest applied Sakoe- Chiba band, and the 1-norm. Some of the results can be viewed in the table 2.

Table 2: AESR Performance Using Dynamic Alignment of Power Spectra intervals of various lengths and applying Saloe-Chiba windows endowed with different widths

distance	Sakoe band	f_{low}	f_{high}	Identification Rate			
				Chainsaw	Forest	Vehicle	General
Norm1	15	0	7.4	69.57	74.14	67.94	70.44
		0	3.7	57.39	81.9	67.94	69.06
	20	0	11	50.43	76.72	67.94	65.19
		0	7.4	68.7	75.86	67.94	70.72
		0	3.7	57.39	83.62	67.94	69.61
	25	0	3.7	57.39	84.48	67.94	69.89
		0	7.4	68.7	76.72	67.94	70.99
	30	0	7.4	69.57	76.72	67.94	71.27
		0	3.7	57.39	86.21	67.94	70.44
Standardised	20	0	3.7	58.26	86.21	66.41	70.17
		0	7.4	68.7	76.72	67.18	70.72
	25	0	3.7	58.26	87.07	66.41	70.44
		0.3	7.4	66.09	77.59	67.18	70.17
		0	7.4	68.7	77.59	67.18	70.99
	30	0	7.4	68.7	77.59	67.18	70.99

4.3. Experiments using the FFNN

We have applied FFNN methodology in two hypostases: the first by feeding at input Mel-cepstral features (coming with or without Spectral Flatness, and/or ZCR) and the second, by feeding Fourier power spectrum features. In the first case we have extracted 12 to 20 Mel-cepstral coefficients, on an analysis window, using different frequency intervals [f_{low}, f_{high}], and different analysis window lengths. In the second case the number of coefficients depended on the length of the frequency interval.

At training we fed the information at the of sample level, each sample being associated with the expected outputs 1, 0 or -1, depending on the nature of the sound sample (chainsaw, genuine forest, vehicle engines). A sample in this case means a feature vector (of Mel-cepstral coefficients or Fourier spectrum coefficients, etc., calculated on an analysis window).

We applied the batch training and evaluated the BR, and LMA training algorithms. At classification, when training by feeding vectors of features, we evaluated each 3s segment by assessing each sample in the segment and finally the whole segment. A sample belongs to a certain class if its output *score* in (11) is closest to the respective class expected output, 1, 0 or -1. The overall decision on the 3s level is taken by applying one of the rules:

- Majority voting (the segment is associated with the class for which most of the samples of the segment belong to the respective class);

- Average output: the average output score of the samples on the segment is closest to the expected output of a certain class.

Concerning the network architecture, we have tested several configurations of FFNNs, 2 to 4 layers, with 6 to 10 neurons on each layer. As the performance of the test depends on the initialization of the training process, we provided 5 tests for each configuration. Because of the great choice of parameters, such as the length of the analysis window, or f_{low}, f_{high}, and configurations to be investigated, we could not exhaust all the possible combinations. The tables 3 and 4 present some relevant results.

Table 3: FFNN – MFCC -results of 5 tests using networks of 4 layers, with 9, 8, 7, 6 neurons respectively 88ms analysis windows, , [f_{low}, f_{high}] =[0, 7.4] kHz, 18 Mel-coefficients, and Spectral flatness. Training was accomplished by Bayesian Regularization, and classification using the majority voting rule

	Chainsaw	Forest	Vehicle	General
test1	52.36	93.10	62.69	70.13
test2	51.83	75.86	62.69	64.13
test3	48.69	89.66	60.00	66.91
test4	50.26	81.90	68.46	67.94
test5	58.64	93.10	61.92	71.60

Table 3 shows one the best performance, identification rates expressed in percent, obtained using Mel-cepstral features as input, using a 4 layers FFNN, with 9, 8, 7, 6 neurons on each layer, 88ms analysis windows, [0, 7.4] kHz, frequency interval for which the coefficients were computed. 18 Mel-coefficients were extracted, and Spectral flatness and ZCR added on each analysis frame. Training was accomplished by Bayesian Regularization, the default in MATLAB, and classification using the majority voting rule. The average performance was 68.14%. Similar results were obtained using other configurations, for instance an identification rate of 67.43% was achieved with a 3-layer network, 88ms analysis frame, [f_{low}, f_{high}] =[0, 10] kHz, 17 Mel cepstral coefficients, with SF added. However, all the tests provided a low identification rate for the "chainsaw" class. This performance is lower, or comparable to the ones obtained applying the classical GMM and DTW approaches.

Table 4 presents the results of 5 tests using FFNN of 4 layers, with 9, 8, 7, 6 neurons respectively, with Power Spectrum coefficients as input, 88ms analysis windows, [0, 7400] Hz frequency interval for spectral features. At training we applied the Bayesian Regularization algorithm and at classification the majority voting rule. The average performance was 78.82%.

Table 4: FFNN – Power Spectrum – results of 5 tests using networks of 4 layers, with 9, 8, 7, 6 neurons respectively, 88ms analysis windows, [f_{low}, f_{high}] =[0, 7.4] kHz, training models obtained by Bayesian Regularization and classification using the majority voting rule

	Chainsaw	Forest	Vehicle	General
test1	74.86	92.24	74.61	80.67
test2	65.96	91.37	78.46	79.35
test3	78.01	87.06	77.69	80.96
test4	67.53	80.17	78.46	75.98
test5	75.39	77.58	78.07	77.16

Tables 5 and 6 present some relevant results obtained using the LMA algorithm at training.

Table 5 presents the identification rate (in percent) of 5 tests using a 4-layernetwork, an analysis frame of 88ms, [f_{low}, f_{high}] =[0, 10] kHz, 18 Mel cepstral coefficients, without adding extra parameters. At classification, the majority voting rule was applied. The average achieved performance was 69.54%.

Table 5: FFNN – MFCC -results of 5 tests using networks of 4 layers, with 9, 8, 7, 6 neurons respectively 88ms analysis windows, , [f_{low}, f_{high}] =[0, 10] kHz, 18 Mel-coefficients. Training was accomplished using LMA, and classification using the majority voting rule

	Chainsaw	Forest	Vehicle	General
test1	58.12	90.52	70.77	73.94
test2	52.36	85.35	65.39	68.52
test3	44.50	87.07	75.00	70.57
test4	40.31	76.72	67.31	62.96
test5	49.74	87.93	72.31	71.30

Table 6 presents the results of 5 tests using networks of 3 layers, with 9, 8, 7 neurons respectively, 88ms analysis windows, and the frequency interval [0, 3700] Hz, applying LMA training and classification using the majority voting rule. The average recognition rate was 79.17%.

Table 6: FFNN applied on Power Spectra results of 5 tests using networks of 3 layers, with 9, 8, 7 neurons respectively, 88ms analysis windows, , [f_{low}, f_{high}] = [0, 3700] Hz, training models obtained by LMA and classification using the majority voting rule

	Chainsaw	Forest	Vehicle	General
test1	72.77	84.48	77.69	78.62
test2	75.39	79.31	85.76	80.67
test3	69.11	89.65	69.23	76.13
test4	69/63	90.08	79.61	80.38
test5	64.92	87.93	84.23	80.08

Table 7: FFNN applied on Power Spectrum results of 5 tests using networks of 4 layers, with 10, 9, 8, 7 neurons respectively, 88ms analysis windows, [f_{low}, f_{high}] = [0, 3700] Hz, training using LMA and classification and the average score on the 3s frames

	Chainsaw	Forest	Vehicle	General
test1	50.26	92.24	65.769	70.42
test2	61.25	95.69	70.769	76.57
test3	43.97	94.82	65.00	69.25
test4	53.40	93.10	70/38	73.35
test5	57.59	98.27	62.30	73.20

Table 8: Average Identification rates obtained using FFNN applied on Power Spectra, with 3 layers with 9, 8, 7 neurons, respectively, using different values for f_{high} and lengths of the analysis frame, training with Bayesian Regularization and majority vote classification.

		analysis frame lengths		
		22ms	44ms	88ms
Frequency interval (Hz)	[0, 3700]	71.04	76.31	78.83
	[0, 7400]	74.98	76.02	77.22
	[0, 10000]	69.64	74.76	76.02
	[0, 12000]	72.61	75.17	74.00

Table 7 contains the results of 5 tests applying FFNN to spectral coefficients, calculated on the frequency domain [0, 3.7] kHz, using a 88ms analysis windows, and applying the LMA training on 4-layer networks with 10, 9, 8, 7 neurons. The classification algorithm used the average score on 3s frames. The average performance was 72.56%.
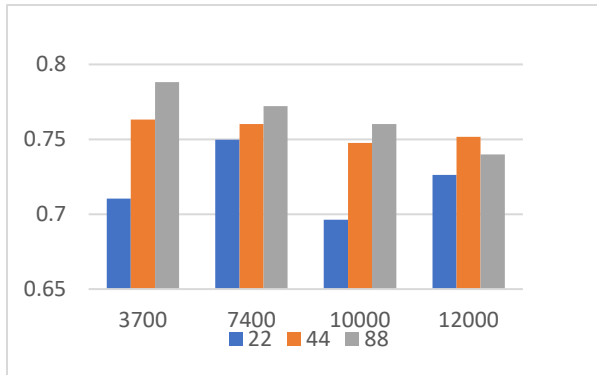
Figure 14: Average Identification rates for different values of f_{high} and length of the analysis frame

As an overall conclusion of the results, the Fourier spectrum as input to FFNN yielded very good results when applying the classification majority vote rule. The average score rule produced poorer results, with a low performance for the "chainsaw" class, but they are still better than using Mel-cepstral analysis or the GMM and DTW approaches. The BR and LMA produced comparable results, maybe LMA results were more balanced among the 5 tests (the standard deviation among the identification rates is lower). Concerning the network architecture for the Fourier spectrum variants of 2, 3 or 4 layers produce comparable results, especially when using the majority voting rule. The LMA training resulted in performance quite similar results as those obtained using the BR, for many configurations besides the one illustrated in Table 6, and the results are well balanced among the three classes of sounds. Perhaps the identification rates for the "chainsaw" class are a bit lower. In what concerns the average score classification, the 3 layers FFNN seemed to work better than 4-layer nets.

Concerning the analysis window, the results are better in all the cases for lengths of 44ms or 88ms. Table 8 and Figure 14 present the average overall identification rates for the FFNN applied on power spectra using the BR training, and majority voting at classification, several analysis window lengths and frequency intervals. The best average score is obtained for the spectrum restricted to [0, 3700]Hz, and an analysis window of 88ms, but in fact the results are very close among the frequency intervals. Among the 5 tests for each configuration there were many identification rates above 80%.

With regard to the results obtained using the Mel-cepstral coefficients as input, the conclusion concerning the optimum analysis window length is that window lengths greater than 44ms produced better performance. The frequency intervals [0, 7.4] kHz and [0, 10] kHz yielded better results. The general conclusion is that adding Spectral flatness and sometimes ZCR helped to increase the performance, although the example of Table 5 is an exception.

4.4. Experiments using the LSTM

In the experiments using LSTM we used the same input as in the FFNN experiments. The number of hidden units was set to 100 and each cell configured with 5 layers, the default MATLAB configuration. Table 9 presents the best results obtained so far by applying LSTM. We have fed as input 18 dimensional sheer Mel-cepstral vectors, calculated on 44ms analysis window and filtering the frequency domain to [0, 12] kHz. The average performance among the 5 tests is 64.85%. As can be seen the identification rates are unbalanced among the three classes. In any other configurations the results were even worse.

Table 9: Results of 5 tests using LSTM applied on an input set of Mel-cepstral 18-dimensional vectors, calculated on 44ms analysis windows, and the frequency interval of [0, 12] kHz

	Chainsaw	Forest	Vehicle	General
test1	48.69	86.20	47.69	61.05
test2	37.69	93.10	56.92	63.83
test3	42.40	97.41	45	62.07
test4	67.53	90.51	47.69	67.78
test5	62.82	93.10	53.46	69.54

Concerning the experiments using as input the Fourier spectrum we failed to obtain interesting results, as the network did not behave well at training Figures 15, 16 present the estimation of the achieved accuracy during the training process for LSTM applied to Mel-cepstral input and power spectra respectively. While the first process achieves maximum accuracy in less than 100 iterations the LSTM applied to power spectra achieves less than 80% in more than 300 iterations.
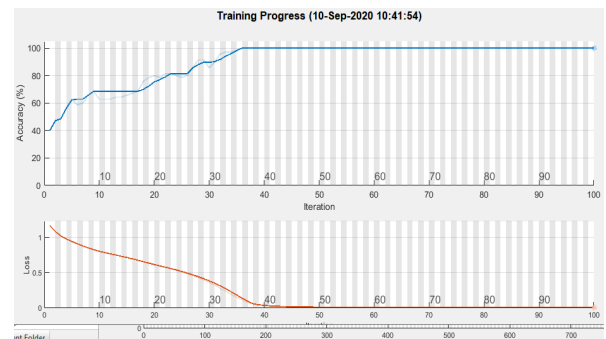
Figure 15: Accuracy estimation during training for a LSTM - MFCC process
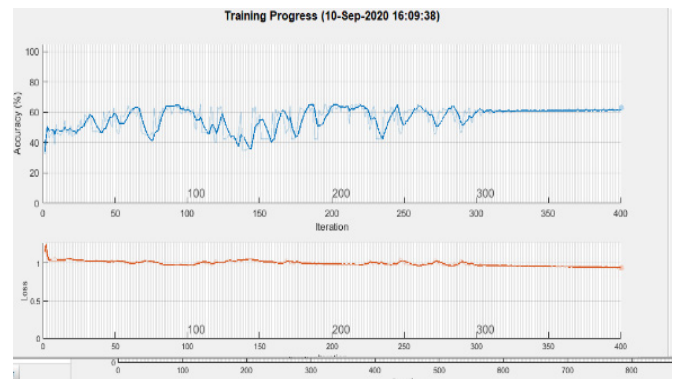
Figure 16: Accuracy estimation during training for a LSTM applied on Fourier power spectra.

Regarding the experiments using as input the Fourier spectrum we failed to obtain interesting results, as the network did not behave well at training Figures 15, 16 present the estimation of the achieved accuracy during the training process for LSTM applied to Mel-cepstral input and power spectra respectively. While the first process achieves maximum accuracy in less than 100 iterations the LSTM applied to power spectra achieves less than 80% in more than 300 iterations.

5. Conclusions and future work

The goal of this study was to test some state-of-the-art methodologies applied in AESR, Gaussian Mixtures Modelling, Dynamic Time Warping, and two types of Deep Neural Networks, in the context of forest acoustics. Another specific objective was to evaluate the behaviour of these techniques, in several configurations, such as different lengths of the analysis window, or find the frequency intervals on which the Fourier spectrum is more relevant for such type of applications.

We have succeeded to achieve significantly better performances using Feed Forward Neural Networks, in a certain setup, compared to the classical methods, GMM, and DTW. We used two types of networks (Deep Feedforward Neural Network and LSTM) and have fed as inputs two types of data, Mel-cepstral and Fourier power spectral coefficients. In this context we tested two training methods, the Levenberg-Marquardt Algorithm, and the Bayesian Regularization, and two different classification approaches.

Deep Feed Forward Neural Networks experiments output the best results when using the sheer spectral features, and especially when using the majority voting rule, with an average identification rate of over 78%, with about 10% higher than other methods performance. This fact suggests that FFNN, based on Fourier spectral features, using a less complex processing sequence, is able to produce more valuable features than the elaborate Mel cepstral analysis. A difference is in the number of features at input, while the Mel features are fewer than 20, the spectrum on [0, 7400] Hz frequency interval means about 170 coefficients.
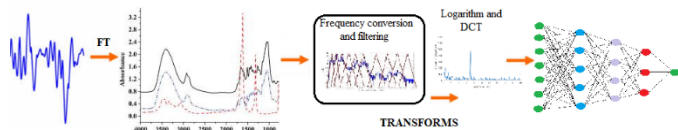
Figure 17: FFNN using Mel cepstral input applies a range of transforms (frequency conversion. spectrum filtering, logarithm, Discrete Cosinus Transform) on the Fourier spectrum and feeds the result to the network
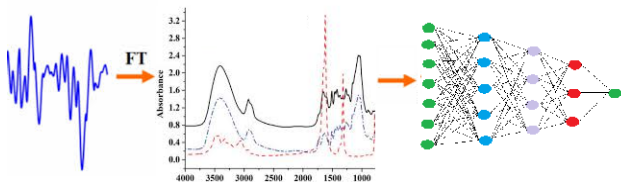
Figure 18: FFNN using Fourier Spectrum coefficients as has a simpler schema, and probably devises more valuable features through the layers of the network

Figures 17, 18 summarize this idea. Figure 17 presents the more complex row of operations to be accomplished on the power spectrum when the input to the FFNN involves Mel-cepstral analysis. Figure 18 presents the straightforward processing of

spectrum by the FFNN, when just spectral coefficients are fed to the network.

The disappointing results using the LSTM network may have several reasons. One of them may be the unproper use of the LSTM MATLAB tool. A second reason may reside in the fact that this type of network might be not suited to the kind of problem we want to solve.

Another advantage of using FFNN is the fact that it is easy to implement in programming environments other than MATLAB. While the models can be generated in MATLAB, the classification part can be implemented in other programming languages, like C++, Java, etc. using the parameters established at training.

Concerning the length of the analysis window the experimental results have shown that its length must be set above 44ms or higher. We have chosen the length of the analysis window somehow empirically, therefore the use of an analytical approach, e.g., [41], to establish the proper length of the frame would be a future direction of research.

We could not draw a well-founded conclusion about the optimal frequency interval, as for 3.7 kHz to 10 kHz, the results do not vary too much.

Although the neural networks have apparently the advantage of training jointly several classes of data, this did not result in better results in comparison with the classical methods.

As future work we intend to extend our research by including the CNN framework.

Another important objective would be investigation of methods to merge decision of several sources, possibly by using a probabilistic logic.

Another important objective is to extend the field of research to other AESR applications, in the field of scientific environment monitoring (e.g., detect bird or species), or early detection of disasters such as land sliding or avalanches, where acoustic emissions are among the data used as input.

Conflict of Interest

The authors declare no conflict of interest.

Acknowledgment

References

[1] S. Segarceanu, E. Olteanu, G. Suciu, "Forest Monitoring Using Forest Sound Identification," in 2020 International Conference on Telecommunications and Signal Processing (TSP-2020), 346-349 2020, doi: 10.1109/TSP49548.2020.9163433.

[2] S. Cowling, M. Cowling, R. Sitte, "Recognition of Environmental Sounds Using Speech Recognition Techniques," Advanced Signal Processing for Communication Systems, 31-46, 2006,. doi : 10.1007/0-306-47791-2_3.

[3] X. Guo, Y. Toyoda, H. Li, J. Huang, S. Ding, Y. Liu, "Environmental Sound Recognition Using Time-Frequency Intersection Patterns," Applied Computational Intelligence and Soft Computing, vol. 2012, 6 pages, 2012, https://doi.org/10.1155/2012/650818.

[4] S. Sivasankaran, K.M.M. Prabhu, "Robust features for Environmental Sound,"

in 2013 IEEE Conference on Electronics, Computing and Communication Technologies (CONECCT), 1-6, 2013, doi:10.1109/CONECCT.2013.6469297.

[5] S. Sigtia, A. Stark, S. Krstulovic, M. Plumbley, "Automatic environmental sound recognition: Performance versus computational cost," IEEE/ACM Transactions on Audio, Speech, and Language Processing, **24**(11). 2096-2107, 2016, doi: 10.1109/TASLP.2016.2592698.

[6] M. Babiš, M. Ďuríček, V. Harvanová, M. Vojtko, "Forest Guardian – Monitoring System for Detecting Logging Activities Based on Sound Recognition," in 2011 7th Student Research Conference in Informatics and Information Technologies, **2**, 354-359, 2011.

[7] J. Papán, M. Jurecka, J. Púchyová, "WSN for Forest Monitoring to Prevent Illegal Logging," in 2012 IEEE Proceedings of the Federated Conference on Computer Science and Information Systems, 809-812, 2012.

[8] R. Buhuș, L. Grama, C. Rusu, 2017, "Several Classifiers for Intruder Detection Applications," in 2017 9th International Conference on Speech Technology and Human-Computer Dialogue (SpeD), 2017, doi: 10.1109/SPED.2017.7990432.

[9] L. Grama, C.Rusu, "Audio Signal Classification Using Linear Predictive Coding And Random Forest," in 2017 9th International Conference on Speech Technology and Human-Computer Dialogue (SpeD), 1-9, 2017, doi: 10.1109/SPED.2017.7990431.

[10] S. Zhang, D. Gao, H. Lin, Q. Sun, "Wildfire Detection Using Sound Spectrum Analysis Based on the Internet of Things," in 2019 Sensors, **19**(23), 2019, doi: 10.3390/s19235093.

[11] L. A.Venier, M. J. Mazerolle, A. Rodgers, K. A. McIlwrick, S. Holmes, D. Thompson, "Comparison of semiautomated bird song recognition with manual detection of recorded bird song samples," Avian Conservation and Ecology, **12**(2), 2017, doi:10.5751/ ACE-01029-120202.

[12] D. Mitrovic, M. Zeppelzauer, C. Breiteneder, "Discrimination and Retrieval of Animal Sounds," in 2006 12th International Multi-Media Modelling Conference. IEEE, 2006, doi: 10.1109/MMMC.2006.1651344.

[13] S.Chandrakala, S. Jayalakshmi, "Environmental Audio Scene and Sound Event Recognition for Autonomous Surveillance: A Survey and Comparative Studies," ACM Computing Surveys, **52**(3), 1-34, 2019, doi: 10.1145/3322240.

[14] N. Dixon A., Smith, J. A. Flint, R. Khanna, B. Clark, M. Andjelkovic, "An acoustic emission landslide early warning system for communities in low-income and middle-income countries," Landslides, **15**, 1631–1644, 2018, doi:10.1007/s10346-018-0977-1.

[15] Z. M. Hafizi, C.K.E. Nizwan, M.F.A. Reza & M.A.A. Johari, "High Frequency Acoustic Signal Analysis for Internal Surface Pipe Roughness Classification," Applied Mechanics and Materials, **83**, 249-254, 2011, doi:10.4028/www.scientific.net/AMM.83.249.

[16] V. Gibiat, E. Plaza, P. De Guibert, "Acoustic emission before avalanches in granular media," The Journal of the Acoustical Society of America, **123**(5), 3270, 2008,doi: 10.1121/1.2933600 .

[17] T. Thüring, M. Schoch, A. van Herwijnen, J. Schweizer, "Robust snow avalanche detection using supervised machine learning with infrasonic sensor arrays," Cold Reg. Sci. Technol., **111**, 60–66, 2015. doi: 10.1016/j.coldregions.2014.12.014

[18] L. G. Evers, D. Brown, K. D. Heaney, J. D. Assink, P. S.M. Smets, M.Snellen, "Infrasound from underwater sources," The Journal of the Acoustical Society of America, **137**(4), 2372-2372, 2015, doi: 10.1121/1.4920617.

[19] M. Cowling, R Sitte, T. Wysock, "Analysis of Speech Recognition Techniques for use in a Non-Speech Sound Recognition System," Advanced Signal Processing for Communication Systems. Springer, 2002.

[20] S. Chachada, C.-C. Jay Kuo , "Environmental Sound Recognition: A Survey," APSIPA Transactions on Signal and Information Processing, **3**, 2014, doi: 10.1109/APSIPA.2013.6694338.

[21] I. V. McLoughlin, Hao-min Zhang, Zhi-Peng Xie, Yan Song, Wei Xiao, "Robust Sound Event Classification using Deep Neural Networks. Audio, Speech, and Language Processing," IEEE/ACM Transactions on Audio, Speech and Language Processing, **23** (3). 540-552, 2015, doi:10.1109/TASLP.2015.2389618) (KAR id:51341.

[22] T. Lidy, A. Schindler, "CQT-based convolutional neural networks for audio scene classification," in 2016 Proceedings of the Detection and Classification of Acoustic Scenes and Events Workshop (DCASE'16), **90,** 1032-1048. doi: 10.1145/3322240.

[23] A. Rabaoui, M. Davy, S. Rossignol, N. Ellouze, "Using one-class SVMs and wavelets for audio surveillance," IEEE Trans. on Information Forensic and Security, **3**(4), 763–775, 2008, doi: 10.1109/TIFS.2008.2008216.

[24] D. Stowell, D. Clayton., "Acoustic event detection for multiple overlapping similar sources," in 2015 Proceedings of the IEEE Workshop on Applications of Signal Processing to Audio and Acoustics (WASPAA'15).

1–5, 2015, doi: 10.1109/WASPAA.2015.7336885.

[25] H. Phan, P. Koch, L. Hertel, M. Maass, R. Mazur, A. Mertins, "CNN-LTE: A class of 1-X pooling convolutional neural networks on label tree embeddings for audio scene classification," in 2017 Proceedings of the International Conference on Acoustics, Speech, and Signal Processing (ICASSP'17), 136-140, 2017, doi: 10.1109/ICASSP.2017.7952133.

[26] Karol J. Piczak, "Environmental sound classification with convolutional neural networks," in *2*015 IEEE 25th International Workshop on Machin*e* Learning for Signal Processing (MLSP), 1–6, 2015, doi: 10.1109/MLSP.2015.7324337.

[27] Y. Han, K. Lee, "Convolutional neural network with multiple-width frequency-delta data augmentation for acoustic scene classification," in 2016 Proceedings of the IEEE AASP Challenge on Detection and Classification of Acoustic Scenes and Events, 2017.

[28] R. Ahmed, T. I. Robin, A. A. Shafin, "Automatic Environmental Sound Recognition (AESR) Using Convolutional Neural Network," International Journal of Modern Education and Computer Science, **12**(5), 41-54, 2020, doi: 10.5815/ijmecs.2020.05.04.

[29] H. Eghbal-zadeh, B. Lehner, M. Dorfer, G. Widmer, "A hybrid approach with multichannel i-vectors and convolutional neural networks for acoustic scene classification," in 2017 25th European Signal Processing Conference (EUSIPCO), 2749-2753, 2017, doi: 10.23919/EUSIPCO.2017.8081711.

[30] D. Reynolds, "Gaussian mixture models," Encyclopedia of Biometrics, 659–663, 2009, doi:10.1007/978-0-387-73003-5_196.

[31] X. Huang, A. Acero, H. Hon, Spoken Language Processing:A Guide to Theory, Algorithm, and System Development, Prentice Hall, 2001.

[32] O.Virmajoki, P. Fränti, "Fast pairwise nearest neighbor based algorithm for multilevel thresholding," Journal of Electronic Imaging, **12**(**4**), 648-659, 2003, doi: 10.1117/1.1604396.

[33] S. B. Davis, P. Mermelstein, "Comparison of parametric representations for monosyllabic word recognition in continuously spoken sentences," IEEE Trans. on ASSP, **28**, 357–366, 1980, doi: 10.1109/TASSP.1980.1163420.

[34] S. Furui, "Cepstral analysis technique for automatic speaker verification," IEEE Transactions on Acoustics, Speech, and Signal Processing, **29**, 254–272, 1981, doi: 10.1109/TASSP.1981.1163530.

[35] P. Senin,"Dynamic Time Warping Algorithm Review," Technical Report Information and Computer Science Departament University of Hawaii, 2008.

[36] H. Sakoe, S. Chiba, "Dynamic programming algorithm optimization for spoken word recognition," Trans. Acoustics, Speech, and Signal Proc., **26**, 43-49, 1978, doi:10.1109/TASSP.1978.1163055.

[37] V. Zacharias, AI for Data Science Artificial Intelligence Frameworks and Functionality for Deep Learning, Optimization, and Beyond, Technics Publications, 2018.

[38] M. H. Beale, M. T.Hagan, H. B. Demuth, Neural Network Toolbox™ User's Guide, The MathWorks, Inc., Natick, Mass., 2010.

[39] H. Sak, A. Senior, F. Beaufays, "Long short-term memory recurrent neural network architectures for large scale acoustic modeling," in 2014, Fifteenth annual conference of the international speech communication association (INTERSPEECH-2014), 338-342, 2014.

[40] M. Kuropatwiński, "Estimation of Quantities Related to the Multinomial Distribution with Unknown Number of Categories," in 2019 Signal Processing Symposium (SPSympo), 277–281, 2019, doi:10.1109/sps.2019.8881992.

[41] E. Punskaya, C. Andrieu, A. Doucet, W. Fitzgerald, "Bayesian curve fitting using MCMC with applications to signal segmentation," IEEE Transactions on signal processing, **50**(3), 747-758, 2002, doi**:** 10.1109/78.984776.

Electroencephalogram Based Medical Biometrics using Machine Learning: Assessment of Different Color Stimuli

Md Mahmudul Hasan[1,*], Nafiul Hasan[2], Dil Afroz[3], Ferdaus Anam Jibon[4], Md. Arman Hossen[2], Md. Shahrier Parvage[2], Jakaria Sulaiman Aongkon[5]

[1]*Centre for Accident Research and Road Safety- Queensland, Queensland University of Technology, Brisbane, QLD 4059, Australia*

[2]*Department of Electrical and Electronic Engineering, Bangladesh Army University of Engineering and Technology, Qadirabad, 6431, Bangladesh*

[3]*Department of Computer Science and Engineering, Bangladesh Army University of Engineering and Technology, Qadirabad, 6431, Bangladesh*

[4]*Department of Computer Science and Engineering, Sheikh Fazilatunnesa Mujib University, Jamalpur, 2000, Bangladesh*

[5]*Department of Electrical and Electronic Engineering, Shahjalal University of Science and Technology, Sylhet, 3100, Bangladesh*

A R T I C L E   I N F O

A B S T R A C T

A methodology of medical signal-based biometrics has been proposed in this paper for implementing a human identification system controlled by electroencephalogram in respect of different color stimuli. The advantage of biosignal based biometrics is that they provide more efficient operation in simple experimental condition to ensure accurate identification. Red, Green, Blue (primary colors) and Yellow (secondary color) were chosen as the color stimuli for making more comfortable EEG regenerating environment. Four supervised classification models, namely, Logistic Regression (LR), K- Nearest Neighbor (KNN), Support Vector Machine (SVM) and Random Forest Classifier (RFC) were trained and tested for assessing the performance of the EEG based biometric identification, with five-fold cross-validation. Four different measures (sensitivity, specificity, accuracy and area under the receiver operating characteristic curve) were used to evaluate the overall performance. The results suggested that Blue color stimuli perform the best among all the color stimulus with an accuracy ranging from (77.2-88.9%). The classifiers identify each of the subjects with any color having an accuracy ranged from (70.9-88.9%), and the RFC shows the best accuracy which is 88.9% in the case of blue color stimuli.

1. Introduction

This paper is an extension of work originally presented in 1st International Conference on Advances in Science, Engineering and Robotics Technology 2019 [1]. The presented paper utilized electroencephalogram (EEG) for medical biometrics using color stimuli using only one classifier (artificial neural networks) where the current article is expanded further to validate the EEG based biometrics using multiple machine learning models. Also, this paper examines the utility of the different color stimulus on the EEG based human identification system.

Biometrics refers to the process of identifying and authenticating a person based on a unique identifier. By utilizing a person's unique feature, the human identification system is built for different security applications. Existing biometric systems use knowledge or possession-based features like passcode, PIN, fingerprint, voice which are extensively being used for device security and other security purposes [2]. There are some limitations in the existing authentication technologies, for example, the fingerprints can be replicated, and facial detection can be fooled [3]. The Boston Marathon bombing incident has shown the failure of the so-called advanced facial identification system [3]. Furthermore, with the development in hacking

techniques such as replication of fingerprints has resulted in reduced reliability of the conventional biometric identification systems [3, 4].

In the given circumstances, unique electroencephalogram remains the only choice due to its non-biasing nature [3-6]. For this reason, physiological signal based biometrics such as EEG uses neurons activity is becoming research of interest due to its person to person variability characteristics [7]. To utilize the medical signals for biometric identification, a study was performed [3], where the authors have tried to develop an EEG-based approach in order to make an efficient human identification. In [3], the authors found the beta band as the most influential rhythm of EEG for human identification.

However, generating similar EEG signal frequently is tough and can't be declared as a standard method. The main issue with the EEG is that it is variable and needs a specific environment to reproduce the similar patterned brainwave [3, 4]. To simplify this experimental condition, the use of color stimuli is the right choice. Every color has a unique effect on the brainwaves, which was observed by statistical analysis of the signal as per the previous studies [8]. In [4], the authors explained that frequency domain shows better performance than time domain, and the value of power spectrum density varies a lot among individuals while varies a little within an individual. It is also observed that the use of both time and frequency domain feature comes out with the best performance for human identification system [4]. A study developed an EEG based architecture for identifying the individuals based on the brainwaves using color stimulus based experiment, which was performed on three participants in a laboratory-based work [9]. The authors used three fundamental colors (Red, Green and Blue) [10] and one secondary color Yellow color stimulus for human identification purpose. The results suggested that the blue color is the most sensitive to the human identification, whereas the secondary color Yellow gave the worst performance in identification. The study showed promising results but utilized only one classifier (ANN) for the classification approach and only one performance measure (mean square error) for the assessment of the system [1]. However, considering the sensitivity and specificity metrics are most important for an EEG based detection system. As higher sensitivity with lower specificity leads to the higher false alarm, and the opposite trend causes the missing of a lot of positive states, a compromise between the two metrics is crucial. Though there are very limited works on the field of biometric identification using brainwaves, these systems are worth for the IoT devices and cyber security with the application of AI.

In this study, the data was recorded using the BIOPAC® data acquisition unit, the pre-processing and feature extraction was done using the Acqknowledge 4.1® software [11]. Most importantly, four supervised classification models, namely Logistic Regression, K- Nearest Neighbor (KNN), Support Vector Machine (SVM) and Random Forest Classifier (RFC) were trained and tested for evaluating the performance of each of the EEG rhythm, with five-fold cross-validation. Moreover, four different performance measures (sensitivity, specificity, accuracy and area under the receiver operating characteristic curve-AUROC) were utilized to examine the performance of the human identification system.

The following part of this paper is organized as follows- a brief methodology, including experimental design and tools, then the result section with the findings. Last, the paper was concluded with as short summary, followed by a discussion on the outcomes, research implications and future works.

2. Methodology

2.1 Experimental Design

The experiment was conducted in the laboratory-based environment. The different steps for developing the electroencephalogram based human identification system by color stimuli is shown in Figure 1. With the given experimental conditions, EEG were obtained by the BIOPAC® system from the selected participants. The next step is removing the noise and artifact due to eye blinking and body movement. Then FIR band pass filter was utilized to separate bands in Acqknowledge 4.1 software. Afterwards, eight features were extracted for each band, and the selected features were supplied towards the machine learning tools. Four different supervised learning techniques, namely K-nearest neighbors (KNN), support vector machines (SVM), logistic regression (LR) and random forest classifier (RFC) were developed in python 3.6.9 platform, and models were applied for human identification. The best classifier was evaluated by comparing their performance metrics.
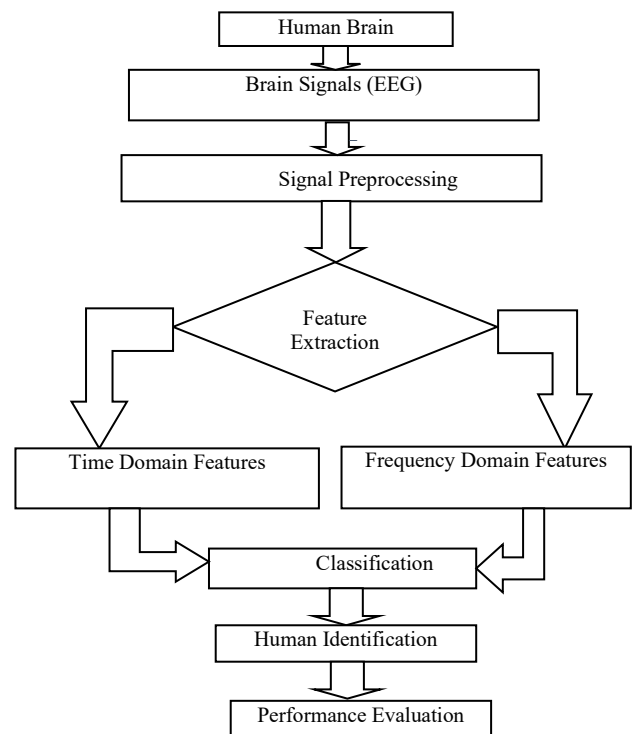
Figure 1: Block diagram of the proposed EEG based human identification system

2.2. Experimental Equipment

2.2.1. Hardware tool

For the signal acquisition, a BIOPAC® MP 36 system [11] was used at the Biomedical Engineering Lab, Khulna University of Engineering and Technology (KUET), Bangladesh. This is a wired data acquisition system which has a signal acquisition and a processing unit to interface with the computer.

2.2.2. Pre-processing software tool

As a software tool, BIOPAC student Lab Pro® was used to record the physiological signals. Acqknowledge 4.1® software was used for the feature extraction purpose [11,12]. Machine learning based classification models were developed and applied in the python 3.6.9 version in Google Colab platform, which is research based online environment affiliated by Google .

2.3. Participants

For participation in this experiment, recruitment was done with online advertisement on Facebook, Twitter and LinkedIn. In total, three subjects participated in the experiment who were male, healthy and not suffering from any color blindness or psychological illness. The color blindness was tested using the Ishihara 38 Plates CVD Test [13] upfront after they arrive in the laboratory to check their vision and to ensure they are not suffering from difficulties in choosing colors, especially the deuteranopic vision (red-green color blindness). Then, color stimulus were shown in a computer monitor (21.5" with a 1920 ×1080 resolution) while they were instructed to focus on indefinite color for 15 minutes long, with their normal blinking. In total, twenty trials were taken for each color (red, green, blue and yellow). The electrodes were placed on the right central (C4), and the right occipital (O2) position.

Figure 2: Experimental environment in BME, KUET

2.4. Experimental Procedure

2.4.1. Signal Preprocessing

The recorded signal contains artefacts due to muscle movement, eye blinking, hand movement and the background effect behind the color stimulus, the primarily obtained EEG signals could have contained noise. Additionally, the line frequency was 50 Hz, which also adds noise to the data. To pre-process raw EEG was gone through band-pass finite impulse response (FIR) filter with a range of 0.5 to 44 Hz, as it removes the non-linear trends of the signals. Later, the signals was further smoothed, taking a moving average over a short period of the signal. The pre-processing makes the signal viable for extracting different time and frequency domain features.

2.4.2. Feature Extraction

Feature extraction is one of the major steps of biosignal processing and analysis, which contains valuable information from the time-series signal. Several features were extracted in time and frequency domain, including maximum value (Emax), standard deviation (STDDEV), skew (sk), kurtosis (k), power spectrum density (PSD) mean, PSD max, Fast Fourier Transform (FFT) mean, FFT max (total eight feature) were extracted for different subjects using the Acknowledge 4.1® software. The feature were tabulated in the excel sheet for the future stages.

2.4.3. Feature Scaling

Machine learning models work on different strategies, and thus the range of the feature values is an essential factor. The features extracted from time and frequency domains have a different range in their magnitude. Since different machine learning models works with different features putting them in a same matrix, it is necessary to put all the features in a same range, which is referred to as feature scaling. Two common types of feature scaling is done in preliminary data: standardization and normalization [14]. As a part of the normalization process, MinMaxScaling was performed in this study in python platform. Using the MinMaxscaler() function from sklearn library. Here the data is shrunk within a range between [-1,1].

$$x_{new} = \frac{x - x_{min}}{x_{max} - x_{min}} \qquad (1)$$

If x_{new} is symbolized as the the normalized value of a feature point x, within a range x_{min} and x_{max}, then the normalization formula can be given by the equation (1) [14].

2.5. Classification

The ultimate goal of the study is to identify the individual by means of the EEG features, applying the machine learning techniques. Machine learning is a hot topic nowadays, which is referred to as the application of artificial intelligence, which provides a system capable of learning nature of a given dataset. Basically, there are three categories of Machine Learning models and application, supervised learning, unsupervised learning and reinforcement learning. Supervised learning is extensively used for the classification and regression problem [15]. Previous studies worked with EEG have used supervised learnings, especially KNN [16], SVM [17], RFC [18] and LR [19]. Based on the previous studies, these four classifiers were chosen for the data classification in this research. Moreover, these models works on different algorithms of learning from the given data points, which might be worthful to see which one perform the best for the human identification purpose.

2.5.1. Logistic Regression

The simplest way to classify data points was linear regression, and the disadvantages of the linear regression models were overcome by the logistic regression models. Logistic regression is a supervised learning model, which works based on the linear method, and the predictions are made using a logistic or sigmoid function σ(t). The sigmoid function is an 'S' patterned curve that takes a real number and maps within a range between 0 and 1, which is given by equation (2).

$$\sigma(t) = \frac{e^t}{e^t + 1} = \frac{1}{1 + e^{-t}} \qquad (2)$$

Contemplating the two types of variables, dependent and independent, Logistic regression predict dependant variable basing on the independent variable. The 'C parameter was tuned here in the Logistic Regression model to lessen the overfitting problem, which could produce over-optimistic results [20].

2.5.2. K-nearest neighbours (KNN)

One of the simplest supervised learning models is KNN, which is a non-parametric method where k nearest training examples in the feature space is taken as input and neighbours vote do the classification generally used for classification and regression. At the very starting point, KNN read the value of K, type of distance D and test data; then it finds the K nearest neighbours D to the test data and thus sets the maximum label class of K to test data. The same processes are gone through an iterative process named looping. In details, its algorithm initializes the value of K from 1 (setting as initial iteration value). After loading data, iteration from initial K =1 (generally) to the total number of training data point. Then, distances specifically Euclidean distance between test data and each row of training data is measured and sorted in ascending order to get topmost K rows from the sorted array and the most frequent class is returned as the predicted class [21]. The value of K was tuned, and the K for best efficiency was chosen in the classifier model in this research to reduce overfitting. With the chosen 'K' value the model was further developed, trained and tested with the given data.

2.5.3. Support Vector Machines (SVM)

One of the most popular supervised learning approaches, SVM aims to obtain a hyperplane which classifies the data point (data points can be at any side of hyperplane) in feature dimensional space while depending on both linear and non-linear regression. Data points distance across to hyperplane are called support vector whose detection can exchange hyper plane's location [21]. The model used a Gaussian kernel for SVM classifier in this research due to the non-linear trend of the dataset. Two parameters- 'C' and 'gamma' was adjusted within a set of values using the grid search algorithm to reduce the overfitting problem, which could cause a non-generalized model.

2.5.4. Random Forest Classifier (RFC)

In addition to the binary logic or decision tree-based classifiers, ensemble-based models are now getting popularity due to their robustness. Random forests are made of individual decision trees with a logic of group of weak learners to finally make a strong learner while the decision trees operate as divided or conquer. A class is predicted from every decision tree and a final class is predicted by model depending on their vote [21]. Two parameters were tuned in the RFC models, namely, 'n_estimate', which implies the number of trees in the forest and 'max-depth' which signifies the depth of each tree. With the tuned parameters, the model was further developed, trained and tested to find out the performance measures.

2.6. Performance Measures

2.6.1. Sensitivity or True Positive Rate (TPR)

True positive rate or Sensitivity is the proportion of the true positives (desired factor), which is correctly identified from the given test set [22]. The definition of sensitivity can be provided by equation (3), where, TP = True Positive and FN = False Negative. In this study, sensitivity is the measure of the proportion of successfully identifying a specific person.

$$\text{Sensitivity} = \frac{TP}{TP+FN} \qquad (3)$$

2.6.2. Specificity or True Negative Rate (TNR)

True negative rate or Specificity is the proportion of true negative (undesired factor) in which was correctly excluded from the given test sets [22]. The definition of specificity can be provided by equation (4), where, TN = True Negative and FP = False Positive. In the case of this study, specificity is the measure of not correctly identifying a specific person.

$$\text{Specificity} = \frac{TN}{TN+FP} \qquad (4)$$

2.6.3. Accuracy

The accuracy is the proportion of true results, in an experiment, being either true positive or true negative [22]. The definition of accuracy can be provided by equation (5), given that TP = True positive, TN= True Negative, FP= False Positive and FN = False Negative. In this study, accuracy is the proportion of the successful identification, either a specific person or not being that person.

$$\text{Accuracy} = \frac{TP+TN}{TP+TN+FP+FN} \qquad (5)$$

2.6.4. Area under the receiver operating characteristic (ROC) curve (AUC)

A system having a higher discrepancy between sensitivity can cause false alarm or missing positive states (in this case, identification of a specific individual). Therefore, it is essential to find out the best compromise between them. As a part of this step, ROC is performed, which is a plot of the sensitivity (true positive rate) against the (1- specificity) or false positive rate. Here all the possible combination of TPR and FPR are plotted, showing the trade-off between them [23].

Validation of the performance of the models is an important step towards evaluation of a model. Five-fold cross-validation was done in this study while evaluating the performance measures. The mean value and the standard deviation (SD) were noted, considering the five experimental validations. As the classification is a four-class problem, one vs. all method was used in all the classification approach, splitting the four-class problem in binary class. Thus, the mean sensitivity, specificity and AUC was calculated from the obtained confusion matrix, which was used for further analysis.

3. Results

3.1. Data visualization

Visualizing the data is one of the main steps to understand the data points, and thus it helps to take the further decisions in the machine learning approach. The data points found from the selected features were plotted in box and violin plots to observe the range of each of the features. The following Figure 3 shows that the time and frequency domain features are having a versatile variation in the range. Range of the difference features varies

among themselves either in the time domain or in the frequency domain. Thus, feature scaling was done on the given dataset, and the scale features were supplied to the learning models.
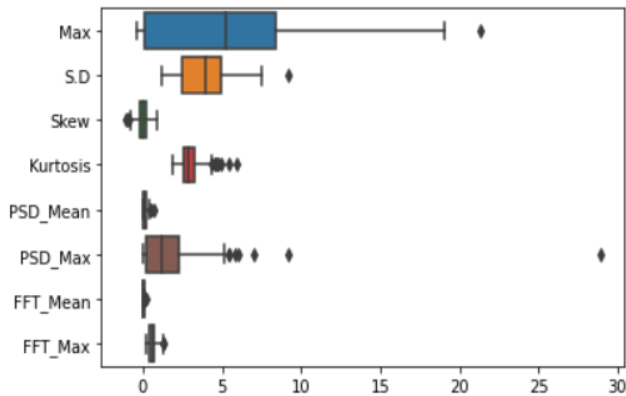
Figure 3: Boxplot of part of the EEG data showing the varying magnitude of different features

3.2. Classification Performance

Finalizing the feature scaling, the scaled features were supplied towards the machine learning models after necessary parameter tuning. Four different performance measures were evaluated, namely, sensitivity or true positive rate (TPR), specificity or True negative rate (TNR), accuracy and area under the receiver operating characteristic (ROC) curve (AUC). The obtained results are listed below in Table 1, which visualizes the performance metrics with respect to the classification models.

Table 1: Performance measures (mean value) for EEG biometrics using four different classifiers, using a five-fold cross-validation

		LR	KNN	SVM	RFC
Red Stimuli	Sensitivity	75.4	70.6	77.1	74.8
	Specificity	72.5	70.7	76.6	81
	Accuracy	79.1	74.1	78.3	79.8
	AUC	74.1	80.3	69	83.7
Blue Stimuli	Sensitivity	89.8	90.9	84.1	93.3
	Specificity	89.8	80.8	81.9	90.6
	Accuracy	**82.8**	**81.7**	**77.2**	**88.9**
	AUC	75.6	84.1	77.3	90
Green Stimuli	Sensitivity	76.6	72.9	68.6	83.3
	Specificity	75.8	77.4	71.8	76.3
	Accuracy	75	70.9	81	83.6
	AUC	78.6	80.6	70.4	83.8
Yellow Stimuli	Sensitivity	76.4	76.11	73.3	84.1
	Specificity	81.6	75.63	73.5	84.4
	Accuracy	75.5	74.69	76.5	86
	AUC	76.9	72.83	79.5	84

3.2.1. Scenario-1: HID using Red Color stimuli

While using the red color stimuli for human identification, the performance measures (mean ± SD) obtained from the human identification from four different classifiers, namely logistic regression (LR), K-nearest Neighbours (KNN), Support Vector Machine (SVM) and Random Forest Classifier (RFC) are shown in the Figure 4. The plots show that the gap between sensitivity and specificity is highest in RFC (6.1%) and lowest in the case of KNN (0.1%). RFC shows the highest gap between sensitivity and specificity (6.1%). Overall, considering the accuracy and ROC, RFC gives the best performance with an accuracy of 79.8%.
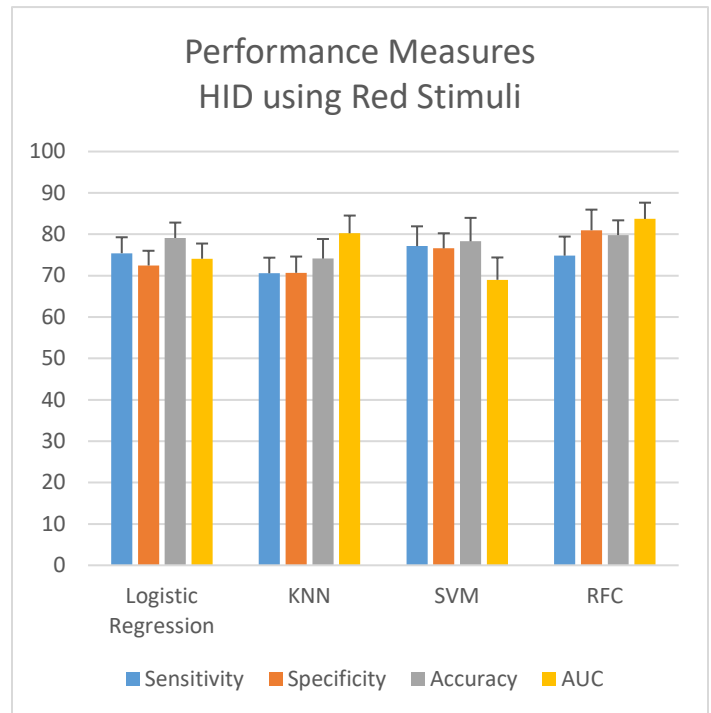
Figure 4: Performance measurement of red stimuli
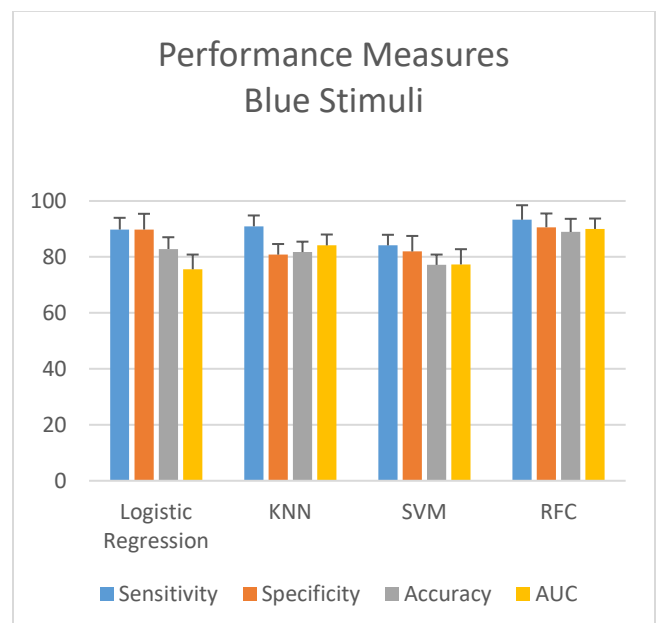
Figure 5: Performance measurement of blue stimuli

3.2.2. Scenario-2: HID using Blue Color stimuli

While using the blue color stimuli for human identification, the performance measures (mean ± SD) obtained from the human identification from four different classifiers are shown in the Figure 5. Here, KNN shows the highest gap (10.1%) between sensitivity and specificity, and LR shows a zero gap between the two metrics. Overall, RFC gives an accuracy of 88.9%, which performs the best.

3.2.3. Scenario-3: HID using Green Color stimuli

While using the green color stimuli for human identification, the performance measures (mean ± SD) obtained from the human identification from four different classifiers are shown in the Figure 6. The plots show that the gap between sensitivity and specificity is highest in RFC (7.03%) and lowest in the case of LR (0.85%). Overall, RFC gives an accuracy of 83.6%, which performs the best.
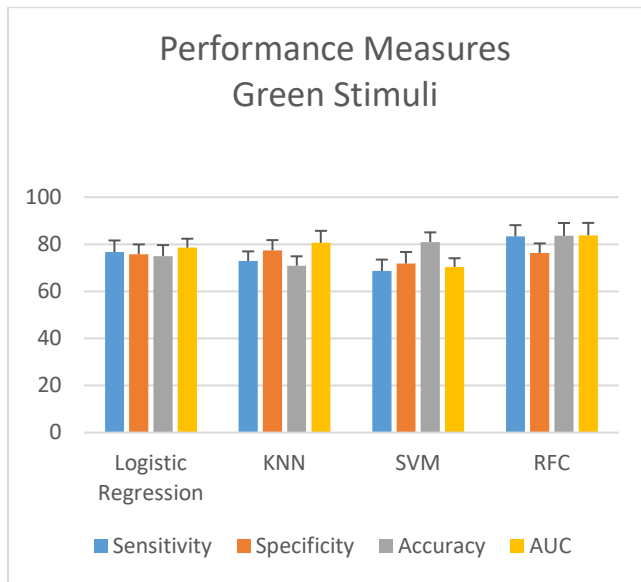
Figure 6: Performance measurement of green stimuli
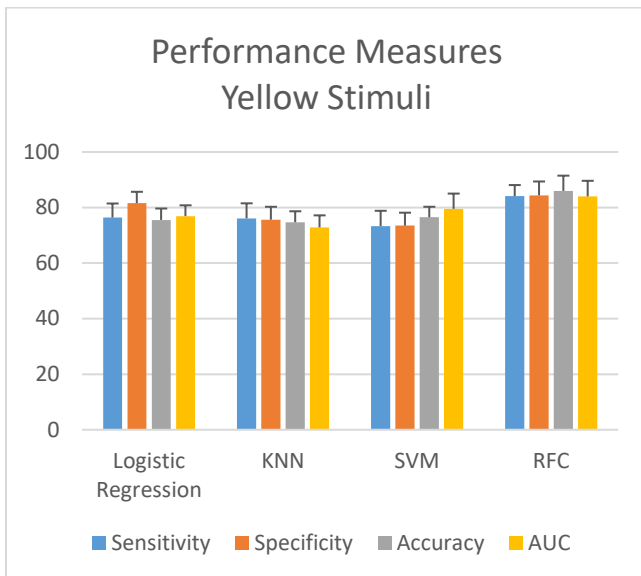
Figure 7: Performance measurement of yellow stimuli

3.2.4. Scenario-4: HID using Yellow Color stimuli

While using the yellow color stimuli for human identification, the performance measures (mean ± SD) obtained from the human identification from four different classifiers are shown in the Figure 7. The plots show that the gap between sensitivity and specificity is highest in LR (5.2%) and lowest in the case of SVM (0.2%). LR shows the highest gap between sensitivity and specificity. Overall, RFC gives an accuracy of 86%, which performs the best.

3.3. Choosing the best scenario/best performance in subject identification

In order to find out the best color stimuli for human identification, the accuracy and AUC measures was selected as two reference metrics as it is difficult to compare different classifiers using several factors. The plots of the accuracy for four different classifiers corresponding to the four color are shown in Figure 8 below. From the figure, it is evident that the accuracy for blue stimuli is better than any other colors for all the four classifiers. Overall, it is evident that all the classifiers identify subjects by using blue color more accurately. So, in the rest of the papers, the performance for the blue color will be considered.
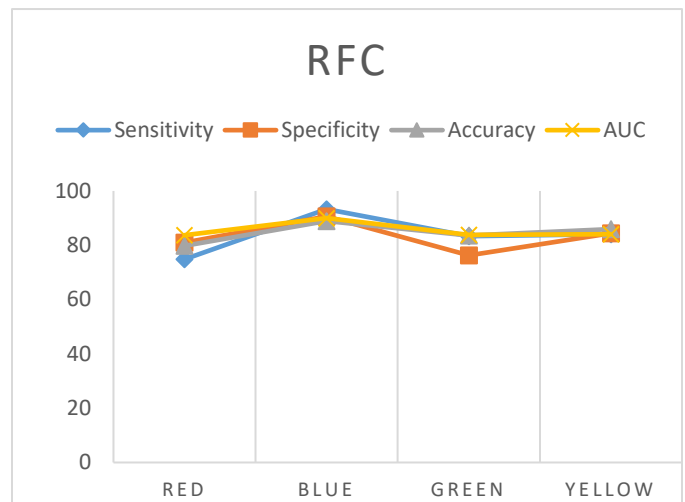
Figure 8: performance measurement of RFC
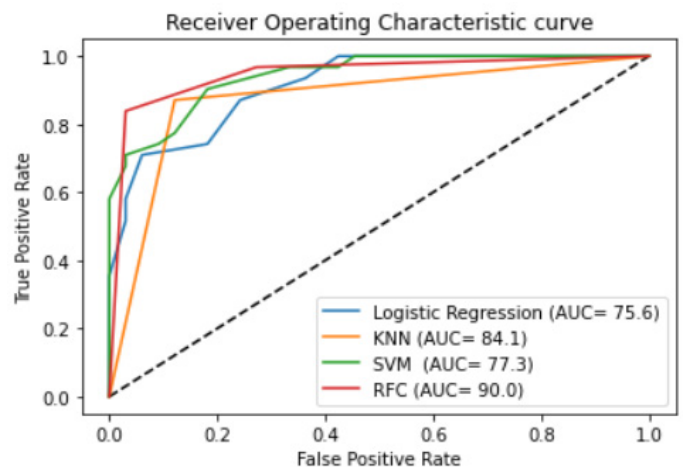
Figure 9: Comparison of AUC for four different classifiers for blue color based HID

3.4. Choosing the best Classifier

Considering the blue color for human identification, the plots for the area under the ROC curve for the classifiers are shown in the Figure 9. The figure illustrates that the RFC classifier show the best compromise between sensitivity and specificity, with covering the highest area under the ROC curve (AUC= 0.90%). Thus, the next part the paper will compare the performance of the color stmuli considering RFC. Overall, all the plots show that RFC performs the best on EEG based human identification for blue color stimuli.
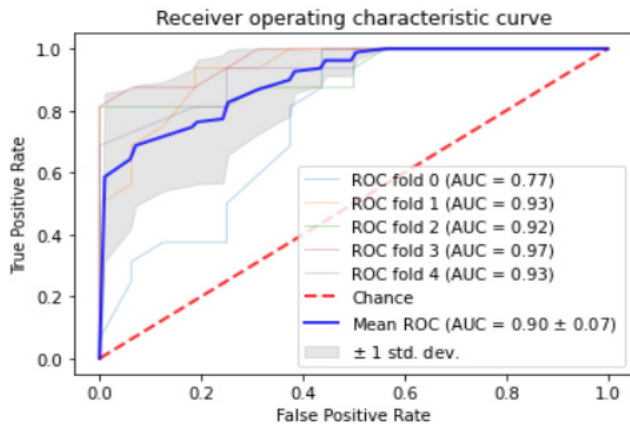
Figure 10: ROC Plots for Blue Stimuli based RFC model with 5 fold CV

As the RFC performs the best, the Area under the AUC curve plots for this model with blue color stimuli in 5 different experiments is given in Figure 10 for five-fold cross-validation. The AUC for the blue color stimuli ranged from (0.77-0.93), with a mean of 0.90 and 0.07 standard deviation. This signifies that, the blue color shows an excellent performance than the other colors while using RFC classifier in order to make EEG based medical biometric system.

4. Discussion

Four different color stimulus were used in this study for assessing the performance of the EEG rhythms for medical biometrics. The results revealed that Blue stimuli perform the best among the other colors. It also revealed that the maximum performance was obtained using the RFC Classifier, with a sensitivity, specificity and accuracy of 93.3%, 90.6% and 88.9%. Moreover, RFC based model with blue stimuli based dataset shows promising AUC (0.90), which is a good compromise between sensitivity and specificity. The finding of this study is consistent with the previous study [1], where the authors found the Blue stimuli as the best performing rhythm, though they have used only one classifier (ANN) and one performance metrics (mean square error). The possible reason behind the best performance of ANN in that study could be the backpropagatipon algorithm, which is strong enough to learn the inherent features and complex structure of the data. Nonetheless, the random forest algorithm works on the majority voting of the multiple decision trees, thus it provides very precise performance, and it is less prone to overfitting. Thus, achieving the similar outcome validates the use of the blue color stimuli for medical biometrics. On the other hand, while using the random forest classifier, the red stimuli perform the worst (RFC accuracy= 79.8%).

However, the scope of the paper is not out of limitations. The background effect is one of the main challenges while using the color stimulus. Inter-individual difference among participants is another factor, which is needed to be considered. As the paper represented a novel methodology of EEG based medical biometrics system using four different colours in a laboratory-based condition, more research is required to find out the feasibility in real-world condition as well.

5. Conclusion

In order to develop an EEG based medical biometrics system using this proposed model, an analysis was done in this study to find out the feasibility of the time and frequency domain EEG features, with respect to different color stimuli. Here efficiency is obtained after applying several steps- feature scaling, tuning of classifiers and finally with five-fold cross-validation of the developed models. The analysis of the results show that the blue color based biometrics system shows the best accuracy than the other color stimuli and the accuracy profiles are promising, i.e. LR (82.8.3%), KNN (81.7%), SVM (77.2%), RFC (88.9%). The further research investigation found that the blue color stimuli with RFC classifier showed the best accuracy while the red color stimuli showed the most insufficient accuracy. However, the experiment could be done on more number of participants to validate the model based on leave one participant out approach. Also, efficiency will increase with the addition of more EEG channels which can be considered for future work. Using a deep-learning framework would be more appropriate, which will reduce the time for handcrafted feature extraction.

Conflict of Interest

The authors declare no conflict of interest.

References

[1] M.M. Hasan, N. Hasan, M.M. Islam, M. Suhi, "Human identification based on color stimuli," in 2019 1st International Conference on Advances in Science, Engineering and Robotics Technology (ICASERT), IEEE: 1–4, 2019. DOI: 10.1109/ICASERT.2019.8934893

[2] F.F.I.E. Council, "Authentication in an internet banking environment," FFIEC Gencies (August 2001 Guidance), 2005.

[3] M.M. Hasan, M.H.A. Sohag, M.E. Ali, M. Ahmad, "Estimation of the most effective rhythm for human identification using EEG signal," in 2016 9th International Conference on Electrical and Computer Engineering (ICECE), IEEE: 90–93, 2016, doi:10.1109/ICECE.2016.7853863.

[4] M.M. Hasan, M.H.A. Sohag, M. Ahmad, "EEG biometrics based on small intra-individual and large inter-individual difference of extracted features," in 2016 2nd International Conference on Electrical, Computer & Telecommunication Engineering (ICECTE), IEEE: 1–4, 2016. DOI: 10.1109/ICECTE.2016.8934893

[5] A. Riera, A. Soria-Frisch, M. Caparrini, C. Grau, G. Ruffini, "Unobtrusive biometric system based on electroencephalogram analysis," EURASIP Journal on Advances in Signal Processing, **2008**(1), 143728, 2007.

[6] C.R. Hema, M.P. Paulraj, H. Kaur, "Brain signatures: A modality for biometric authentication," in 2008 International Conference on Electronic Design, IEEE: 1–4, 2008. DOI: 10.1109/ICED.2008.8934893

[7] Q. Gui, Z. Jin, W. Xu, "Exploring EEG-based biometrics for user identification and authentication," in 2014 IEEE Signal Processing in Medicine and Biology Symposium (SPMB), IEEE: 1–6, 2014.

[8] D. Zakzewski, I. Jouny, Y.C. Yu, "Statistical features of EEG responses to

color stimuli," in 2014 40th Annual Northeast Bioengineering Conference (NEBEC), IEEE: 1–2, 2014.

[9] M.M. Hasan, N. Hasan, A. Rahman, M.M. Rahman, "Effect of Smoking in EEG Pattern and Time-Frequency Domain Analysis for Smoker and Non-Smoker," in 2019 International Conference on Computer, Communication, Chemical, Materials and Electronic Engineering (IC4ME2), IEEE: 1–4, 2019. DOI: 10.1109/IC4ME247184.2019.9036492

[10] D.Q. Utama, T.L.R. Mengko, R. Mengko, M.N. Aulia, "Color blind test quantification using RGB primary color cluster," in 2016 International Conference on Information Technology Systems and Innovation (ICITSI), IEEE: 1–4, 2016.

[11] D. Acquisition, Analysis with BIOPAC MP Systems, AcqKnowledge 4 Software Guide. pdf, Biopac Systems, Inc. ISO 9001: 2008.

[12] M.M. Hasan, M. AshfaqulIslam, S.A. Imtiyaz, M. MahbubHasan, "Presumption method for detecting and analyzing human mental behavior by employing EEG signal," in 2018 4th International Conference on Electrical Engineering and Information & Communication Technology (iCEEiCT), IEEE: 519–523, 2018. DOI: 10.1109/ICME247184.2018.9036492

[13] D. Flück, "Ishihara 38 Plates CVD Test| Colblindor," Colblindor. Wordpress. Nd Web, 7–11, 2016.

[14] C. Colantuoni, G. Henry, S. Zeger, J. Pevsner, "SNOMAD (Standardization and NOrmalization of MicroArray Data): web-accessible gene expression data analysis," Bioinformatics, **18**(11), 1540–1541, 2002, doi:https://doi.org/10.1093/bioinformatics/18.11.1540.

[15] F. Pedregosa, G. Varoquaux, A. Gramfort, V. Michel, B. Thirion, O. Grisel, M. Blondel, P. Prettenhofer, R. Weiss, V. Dubourg, "Scikit-learn: Machine learning in Python," The Journal of Machine Learning Research, **12**, 2825–2830, 2011.

[16] S. Bhattacharyya, A. Khasnobish, S. Chatterjee, A. Konar, D.N. Tibarewala, "Performance analysis of LDA, QDA and KNN algorithms in left-right limb movement classification from EEG data," in 2010 International conference on systems in medicine and biology, IEEE: 126–131, 2010.

[17] H. Lee, S. Choi, "Pca+ hmm+ svm for eeg pattern classification," in Seventh International Symposium on Signal Processing and Its Applications, 2003. Proceedings., IEEE: 541–544, 2003.

[18] L. Fraiwan, K. Lweesy, N. Khasawneh, H. Wenz, H. Dickhaus, "Automated sleep stage identification system based on time–frequency analysis of a single EEG channel and random forest classifier," Computer Methods and Programs in Biomedicine, **108**(1), 10–19, 2012, doi:https://doi.org/10.1016/j.cmpb.2011.11.005.

[19] J. Kim, J. Lee, C. Lee, E. Park, J. Kim, H. Kim, J. Lee, H. Jeong, "Optimal feature selection for pedestrian detection based on logistic regression analysis," in 2013 IEEE International Conference on Systems, Man, and Cybernetics, IEEE: 239–242, 2013.

[20] H. Rajaguru, S.K. Prabhakar, "Non linear ICA and logistic regression for classification of epilepsy from EEG signals," in 2017 international conference of electronics, communication and aerospace technology (ICECA), IEEE: 577–580, 2017.

[21] K. AlSharabi, S. Ibrahim, R. Djemal, A. Alsuwailem, "A DWT-entropy-ANN based architecture for epilepsy diagnosis using EEG signals," in 2016 2nd International Conference on Advanced Technologies for Signal and Image Processing (ATSIP), IEEE: 288–291, 2016, doi:10.1109/ATSIP.2016.7523093.

[22] W. Zhu, N. Zeng, N. Wang, "Sensitivity, specificity, accuracy, associated confidence interval and ROC analysis with practical SAS implementations," NESUG Proceedings: Health Care and Life Sciences, Baltimore, Maryland, **19**, 67, 2010.

[23] D. Justin, R.S. Concepcion, A.A. Bandala, E.P. Dadios, "Performance Comparison of Classification Algorithms for Diagnosing Chronic Kidney Disease," in 2019 IEEE 11th International Conference on Humanoid, Nanotechnology, Information Technology, Communication and Control, Environment, and Management (HNICEM), IEEE: 1–7, doi:10.1109/HNICEM48295.2019.9073568.

Mechanical Characterization of Recycled Aggregates Concrete Based on its Compressive Strength

Khaoula Naouaoui[*], Toufik Cherradi

Mohammadia School of engineers, Mohamed V University Agdal, Rabat, 10000, Morocco

A R T I C L E I N F O	A B S T R A C T
	The construction industry has undergone several changes in recent years linked to new laws and international conventions aimed at protecting the environment and combating pollution. Construction industry alone produces tons of waste annually due to debris produced either during construction or during deconstruction. To combat this, companies are forced to control their debris either by reusing it on site or by sending it to specialized landfills. Thus, new materials appear constantly based on the recycled materials. Recycled aggregate concrete was thus born. It is a concrete based on the use of recycled aggregates retrieved from the demolished structures to replace natural aggregates. Characteristics of this type of concrete depends of the chosen replacement percentage of natural aggregates specially the mechanical properties. This article is part of my research studies done in the civil laboratory of the Mohammadia School of engineers. The study is based on the identification of the recycled aggregates, the determination of physicals and mechanical characteristics of the aggregates, the determination of the effect of the use of recycled aggregates on the concrete characteristics and finally the improve of the quality of the concrete to prove so that it can replace ordinary concrete. The test results described in this article show that the increase of the replacement by recycled aggregates decreases the mechanical properties especially when it is up to 25-30%. The results also prove that the ad of additives especially plasticizer with 1% replacement of cement improves the compressive strength of concrete and allows us to use up to 50% of replacement.

1. Introduction

The field of construction knows a radical undergoing and innovative changes in the designs proposed, the types of materials used and the domains of their use. Concrete, as the main construction material, is now at the center of several studies, researches, innovations and improvements. Several types of new concrete are proposed for their quality, compliance with environmental and / or technical requirements, design and special needs. One of the concrete types proposed for their environmental value, their support for sustainable development is the recycled aggregates concrete.

The comparison of its properties with those of concrete based on naturel aggregates. A summary of the comparison between the two concretes is detailed below:

Related to the compressive strength, the majority of studies confirm that up to [20-30] percentage replacement of natural aggregates by recycled ones, the compressive strength is almost

the same but beyond this replacement level, it decreases considerably. Main recent studies results are as folow.

Many experimental studies match our synthesis that up to 25% the compressive strength is the same and that the decrease's max is 20% for 100 % replacement level [1]. Others conducted a synthesis of several researches and works in his article. He concluded that in case compressive strength values of the original concrete, of which recycled aggregate is manufactured, and targeted values were approximately equal. The strength values of recycled aggregate concrete was 5 to 10% lower than those of the comparable naturel aggregate concrete were [2].

For the modulus of elasticity, the experimental studies prove that its values have almost the same trend as compressive strength results. The increase in insignificant for percentage level up to 75 % (9 %) and it reaches 18% for 100% replacement of natural aggregates by recycled ones [1]. In another study, they found a reduction of 34.8% when the replacement level is 100 % compared to the control concrete [3]. Meanwhile, other researchers found 45 % of reduction for the same replacement level. [4]

[*]Corresponding Author: Khaoula Naouaoui, naouaoui.khaoula@gmail.com

Studies done on durability properties as open porosity, sorptivity, chloride permeability confirm that they decrease with the increase of RCA content. The study also concluded that the rate of deterioration is higher compared to mechanical characteristics.

For example, for 100% replacement level, the resistance to chloride permeability decrease by 9.5% [5], the water absorption is lower by 7.37% [3] and the open porosity by 20% [6].

2. Experimental Protocol

This section is related to the description of the experimental protocol done to determinate the mechanical properties of concrete based on the restitution of the natural aggregates by recycled one.

2.1. Concrete formulation to determinate the constituents

The main of our study is to determine the possibility of replacing naturel concrete by recycled aggregates concrete in the majority of types of building, thus the concrete chosen to study have the following characteristics:

- Basic concrete, ordinary, used in all types of based constructions.

- F_{c28} = 25MPA.

- Slump: Average of 7cm.

To formulate this concrete, the constituents chosen are:

For aggregates, we have chosen two aggregate, the first are natural ones and the second recycled aggregates based on a crushed building. For the two of them we used two dimensions: [5-12.5] and [12.5-31.5]

The result of the granulometric test of the two aggregates is presented in the figure 1:
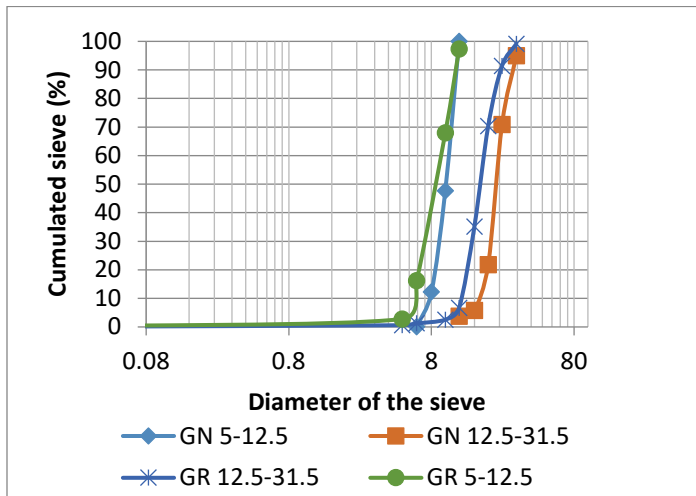
Figure 1: Granometric curve for natural and recycled aggregates used in experimental study (GN : Naturel gravel / GR : recycled gravel).

The quantities of materials used based on the dreux gorisse method [7] are, as follows:

- Water : 0.19 m^3 / 190 kg

- Cement : 0.29 m^3 / 350 kg

- Sand : 0.29 m^3 / 472.85 kg

- Gravillon G1 : 0.15 m^3 / 376.14 kg

- Gravillon G2 : 0.2 m^3 / 537.3 kg

2.2. Concrete mixtures

The aim of the study is to detect the effect of the replacement percentage of natural aggregates by recycled aggregates in the compressive strength of concrete and the effect of different types of additives in improving the mechanical characterisation of theses concretes.

The replacement ratio studied are 0% - 20% -50% -75% - 100%.

For the mixture with additives, we used three product from SIKA- MAROC:

- Plasticizer/ water reducer: BV40

- Superplasticizer/ high water reducer: ViscoCrete Tempo 10 M

- New generation superplasticizer: SikaFluid R.

The first step of experimental study was as explained before, the effect of the replacement of naturel aggregates by recycled ones. The quantity of component used for every mixture in detailed in the table.

Table 1: Quantity used in the compressive strength test (kg)

Component		0 % GR	20 % GR	30 % GR	50 % GR	75 % GR	100 % GR
Cement		350					
Water		193					
Sand		473					
GN	5-12.5	402	321,6	281,4	201	100,5	0
	12.5-31.5	512	409,6	358,4	256	128	0
GR	5-12.5	0	80,4	120,6	201	301,5	402
	12.5-31.5	0	102,4	153,6	256	384	512

The second step of study was to determinate the effect of additives in improving the concrete quality. To do this, we used three types of adjuvants with different percentages. The experimental protocol is as details below:

The test aims to view the effect of the ad of superplasticizer on the comparison between different replacement levels by calculating the compressive strength for various replacement levels with the superplasticizer. The component is similar to the previous one; it is based on using different percentages of replacement of natural aggregates by recycled one. The only difference is the use of superplasticizer.

Second part of the study is to determinate the Compressive strength with different adjuvants. For this comparative test, we

used a concrete based on 50% of recycled aggregates and 50% of natural aggregates. We, then, added the three types of adjuvant with 1% of replacement of cement with means 3.5 kg/m³ of concrete.

The last step of comparison is the Compressive strength with different percentages of the adjuvant. For this comparative test, we used different percentage of the Tempo 10M (0.5%, 1% and 1.5%) as a partial replacement of cement. The concrete used is based on 50% of recycled aggregates and 50% of natural aggregates.

3. Experimental results and discussions

3.1. Physical characterization of recycled aggregates

The physical characterization of aggregates from the demolition of an old building can be summarized as detailed below.

Table 2: Summarize of the physical characterization tests

	Recycled aggregates 5-12.5	Recycled aggregates 12.5-31.5
Absolute Density	2480 kg/m³	
Water content	1.49%	4.32%
Water absorption	11.11%	9.4%

The absolute density is 2.48t/m³ approximatively 2.5t/m³ wich is the absolute density of reinforced concrete.

The comparison between two recycled aggregates of two different classes GR1 (5-12.5) and GR2 (12.5-31.5) showed that the water content is greater for large aggregates. This is justified by the presence of several pores which disappear during fine crushing of the aggregates.

The comparison has also shown that the water absorption rate is higher for small aggregates. This is justified by the superiority of the contact surface.

3.2. Compressive strength without additives

The aim was to determinate the effect of the replacement percentage on the compressive strength, so we made mixtures with 0, 20, 30, 50 75 and 100 % replacement percentage.

The results of compressive strength in 7, 21, 28 and 90 days are detailed in Table 3.

Table 3: Compressive strength results for concrete without additives (MPA)

	0% RA	20% RA	30% RA	50% RA	75% RA	100% RA
7j	16,5	14,65	16,75	13,55	14,05	14,5
21j	23,4	19,9	14,8	14,3	19	14,7
28j	24,8	23,55	23,5	18,05	17,7	15
90j	26,3	25,35	23,55	20,25	19,4	17,8

In order to make the comparison easier and more remarkable, a j-day compression graph for all replacement percentages was established. (figure2)
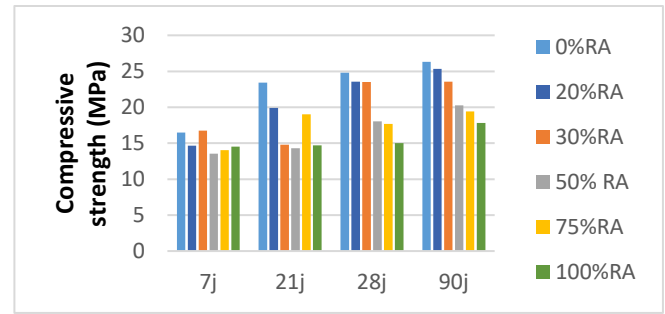
Figure 2: Compressive strength test results representation

At early age, 7 and 28 days, the resistance to compression cannot be decisive because the inter-component reactions are still in progress, so we can notice that the evolution of the resistance for mixtures with 0 or 20% restitution is greater than the others. For concrete containing 30% natural aggregates, it is noted that the compression at 7 days is greater than that of 21 days. This is probably due to poor sampling and that not reflects a real decrease in compression.

28 days is considered to be the reference for resistance in the short and medium term because the compression reaches 90% of its maximum value. The results at 28 days in our study are similar to the majority of researchers. The compressive strength decreases with increasing replacement rate.

After compression tests on recycled aggregate concrete with different percentages, it has been found that beyond 50%, an improvement in quality is required to adopt this type of concrete.

The first proposal to improve this is to add an additive that reduces the water requirement of the aggregates and thus improves the quality of the concrete.

In order to determine the best combination (type of adjuvant and percentage of addition), a series of mixtures are proposed:

- Concrete with 50% recycled aggregates and 1% added admixture with different types of admixture.

- Concrete with 50% recycled aggregates and one type of adjuvant with different percentage of adjuvant added.

- Concrete with several recycled aggregate's percentage and one type and percentage chosen for adjuvant.

3.3. Compressive strength with different adjuvants

The purpose of this step is to compare the effect of several types of adjuvants with a percentage of 1%.

These adjuvants are of several types:

- Plasticizer: BV 40

- Superplasticizer: Tempo 10 m

- New generation superplasticizer: SFR

The choosen percentage of recycled aggregates for this test is 50% as replacement of natural aggregates.

Compression tests are done at 7 and 28 days. The results are detailed in table 6.

Table 4: Compressive strength results for concrete with various additives (MPa)

Type of adjuvant	Compressive strength at 7 days	Compressive strength at 28 days
BV40	19,87	22,63
SFR	11,50	16,65
Tempo 10 M	17,47	21,45

From the results of these tests, it is noted that:

-      The new generation superplasticizer gives the lowest result. This can be interpreted as a bad interaction between the aggregates and their cement paste attached with the additive.

-   The plasticizer gives the best resistance

-   The superplasticizer also gives a good result, better than without additives.

3.4. Compressive strength with different percentages of the adjuvant

These tests aim at the optimal choice of the percentage of the adjuvant in the mixture.

The results of these tests demonstrate that beyond 1%, compression decreases considerably.

Then, for our next mixes, the chosen percentage is 1%.

Table 5: Compressive strength results for concrete with different percentage of additive (MPa)

Type of adjuvant	Percentage of adjuvant	Compressive strength at 7 days	Compressive strength at 28 days
Tempo 10 M	0,5%	14,35	19,90
	1,0%	17,47	21,45
	1,5%	12,87	16,03

3.5. Compressive strength for various replacement levels with the superplasticizer

The purpose of this part of the tests is to see the result of the combination of the adjuvant tempo10M - percentage 1% with various percentages of recycled aggregates.

Table 6: Compressive strength results for concrete with additive (MPa)

percentage of RA	Compressive strength at 7 days	Compressive strength at 28 days
25	18,33	24,3
50	17,47	21,45
75	14,5	20,47
100	14,3	19,65

We conclude that these tests adhere to the results of concrete without additives where compression decreases with increasing percentage of recycled aggregates.

3.6. Conclusion

The plasticizer (BV40) as well as this superplasticizer (Tempo 10 M) with a percentage of 1% improves the compressive strength: 18.05 for concrete with 50% recycled aggregates without addition, 22.63 with addition of BV40 and 21.45 with addition of Tempo 10 M.

4.   Conclusion and Perspectives

Our article summarizes the results of experimental works conducted as part of a PhD research on the characterization of recycled aggregates.

The tests focus on the mechanical characterization and essentially the compression test, considered essential in any concrete study.

It was split in four steps: Test on ordinary concrete with various percentages of natural aggregates with and without adjuvant, tests on concrete with 50% recycled aggregates with different additives and with different percentages of admixtures.

The results show that:

•   Compression decreases with increasing percentage of recycled.

•   Up to 30% replacement of natural by recycled aggregates, the concrete is acceptable from a mechanical characterization point of view

•   The addition of plasticizer and superplasticizer has improved the quality of the concrete. This can be explained by the fact that recycled aggregates require more water and these additives reduce this need.

•   The optimum percentage of addition of the plasticizer is 1%

A review of the literature shows that one of the main methods to improve the quality of concrete is to improve the quality of aggregates by removing the adhered mortar, causing higher water absorption and chemical interaction with other concrete components as used with a customized low-cost simple treatment method [8]

To conclude, a concrete based on recycled aggregates could be used with a maximum release rate of 25-30% without addition and 50% with the addition of superplasticizer additives.

This study focused on mechanical characterization, the goal being an ordinary building plan under current conditions.

For more complicated projects and more developed concretes, more in-depth studies must be established based on:

•   The quality of the aggregates to be used

•   The aggregate / cement interaction

•   The results of the mechanical tests

- The results of durability tests; these tests are essential for buildings with a lifespan of more than 50 years or buildings in environments liable to attack concrete.

Conflict of Interest

The authors declare no conflict of interest.

References

[1] M.R. Riaz, R.Hameed, M.Ilyas, A.Akram, Z.A. Siddiqi , "Mechanical Characterization of Recycled Aggregate Concrete" , Pakistan. Journal of Engineering & Applied Sciences. **16**, 25–32,2015.

[2] M. Malešev, V.Radonjanin, G.Broćeta, "properties of recycled aggregate concrete, Contemporary Materials", **2** , 239-249 ,2014, doi: 10.7251/COMEN1402239M .

[3] M. Chakradhara Rao, S.K. Bhattacharyya, S.V. Barai , "Influence of field recycled coarse aggregate on properties of concrete", Materials and Structures, **44**, 205-220, 2011, doi:10.1617/s11527-010-9620-x.

[4] J. Xiao,W. Li , Y.Fan, X. Huang , A, "overview of study on recycled aggregate concrete in China (1996-2011)", Construction and Building Materials, 31, 364-383 , 2012 , doi:10.1016/j.conbuildmat.2011.12.074.

[5] S.C. Kou, C.S.Poon, "Long-term mechanical and durability properties of recycled aggregate concrete prepared with the incorporation of fly ash", Cement and Concrete Composites, **37,** 12-19, 2013, doi:10.1016/j.cemconcomp.2012.12.011.

[6] C. Thomas, J.Setién, J.A.Polanco, P.Alaejos, M.Sanchez De Juan, "Durability of recycled aggregate concrete", Construction Building Materials, **40**, 1054-1065 ,2013, doi: 10.1016/j.conbuildmat.2012.11.106.

[7] H. Chbani, B. Saadouki, M. Boudlal, M. Barakat, "Formulation of Ordinary Concrete using the Dreux-Gorisse Method", Procedia Structural Integrity, **28**, 430-439, ,2020 doi: 10.1016/j.prostr.2020.10.050

[8] G. Dimitrou, P.Savva, M.F.Petrou , "Enhancing mechanical and durability properties of recycled aggregate concrete", Construction Building Materials, **158**, 228-235 , 2018, doi: 10.1016/j.conbuildmat.2017.09.13 .

Plummeting Makespan by Proficient Workflow Scheduling in Cloud Environment

Juhi Singh, Shalini Agarwal*

Department of Computer Science, Shri Ramswaroop Memorial University, Lucknow, 225003, India

A R T I C L E I N F O	A B S T R A C T
	Cloud is an Internet-based computing technology in which on-demand shared resources such as software, platforms, repositories, and information are delivered to customers. In the emerging era of computing cloud environment provide the use of resources with the concept of virtualization. Workflow of the tasks has vital role for the improvement of computing performance which leads to improved quality of service. As per the demand of user's number of tasks are scheduled in such a way so that better performance is computed using partial deadline of the workflow. In this paper we have introduced with the workflow concepts, further we aim to diminish makespan for the proposed workflow scheduling algorithm. Here makespan refers to overall time duration taken for the sequence of tasks, by the resources so as to complete the execution of each and every task.

1. Introduction

Every day, everyone is connected in one way or another to this digital world, and this is because the field of information technology is escalating. User-friendly environment is the main factor of internet, so that diverse groups of individuals like students, researchers and business people complete their work by providing numerous opportunities to accomplish their goals. Many users connect to the Internet and use their IT infrastructure to meet their daily needs. As the demand for the internet increases, the services provided over the internet such as software, platforms, database services, storage services, etc. are also escalating. Here the imperative term cloud computing comes into existence. It provides countless diverse services to its users over a network. Because of concept "Pay as you Go", end user can get the most out of using this service at a lower cost.

1.1. Workflow

The increasing demand and heterogeneity of cloud computing is gaining recognition among the scientific commune to leverage cloud services to implement large-scale electronic applications. These applications are in the form of a set of tasks representing workflow. Computations performed considering task dependencies are regarded as Workflows. It allows users to straightforwardly elucidate multifaceted multi-step calculation tasks. Workflow tasks are associated to the mechanization of procedures where tasks, information or documents are delivered between partakers in accordance with a specific policy set and allow the formation of different

applications in Directed Acyclic Graph. Each and every in DAG is represented as task and each edge symbolizes the dependencies [1], [2].

A mechanism to manage various workflows on cloud, is known as Workflow Management System (WMS). Figure 1 depicts some significant constituents of WMS. Workflow can be categorized as:

- Single workflow - It includes one or more instances using the same architecture
- Multiple workflow – It can take into account manifold cases of diverse structures of workflow.

Figure 1: Components of Workflow Management System

1.2. Workflow Design

Figure 2 portrays the workflow design mechanism. It is concerned with how to delineate and configure constituent of a

*Corresponding Author: Juhi Singh, Department of Computer Science, SRMU, Lucknow, India, 225003, juhisingh.srmcem@gmail.com

workflow. The workflow portrays the relationship and dependencies between workflows. DAG and Non-DAG [3] are two categories of workflow design. Directed Acyclic Graph is further characterized as Selection, Sequence and Parallel, while Non-DAG can be classified as Repeat, Parallel and Selection. In sequence architecture, the tasks are executed in a sequence, whereas in a parallel architecture, the workflows can be executed synchronously.

In a selection structure, workflows can run in sequence or in parallel. The recurrence pattern structure performs tasks iteratively [4]. Another is the workflow model, which is a constituent of workflow design, delineates the workflow at both the task and structure levels in both abstract and concrete workflows. Abstract workflows are characterized as a nonfigurative template with no commit to cloud resources to carry out the tasks, while concrete workflows are called actionable workflows. The workflow configuration permits users to coalesce diverse components through user-oriented and stand-alone systems.
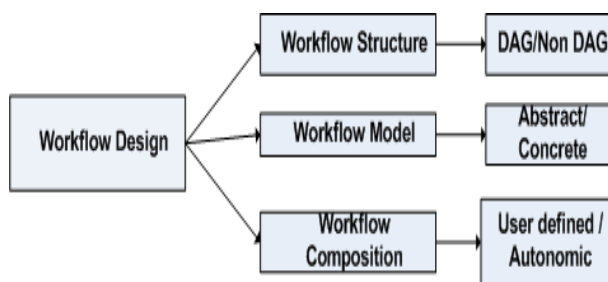
Figure 2: Workflow Design Components

1.3. Workflow Scheduling

The workflow scheduler is necessity for the arrangement of workflows task on the cloud resources that are utilized to implement the workflow. The components that must be delineated to schedule a workflow are revealed below in Figure 3:
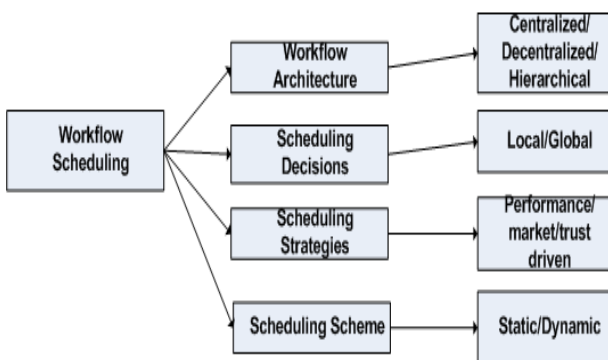
Figure 3: Workflow Scheduling Components

1.4. Fault Tolerance in Workflow

Fault tolerance is linked to tackle errors that can take place during the scheduling and execution phase of workflow tasks for various reasons such as unavailability of resources, resource breakdown, task malfunction, resource overload, network collapse, out of memory, etc

2. Literature Review

Arrangement of tasks can affect cloud system performance, so numerous workflow techniques as well as scheduling

algorithms for scientific workflows have been studied and discussed below:

- Enhanced Scheduling of Resources: In [5], the author introduced a scheduling algorithm to attain optimization or more precise to sub-optimization for scheduling tasks. The authors exploited IGA (Improved Genetic Automated Scheduling Policy) to produce better results.
- Transaction Exhaustive Cost Restraint: In [6], author introduced an algorithm for scheduling tasks that took into account time and cost. Their simulation showed that this algorithm diminishes costs while adhering to deadlines.
- In [7], a superior algorithm based on cost was proposed by author. This algorithm capably assigns tasks to available resources in the cloud. Resource cost, computing performance, convalescing computing connectivity ratio is evaluated in this algorithm.
- In [8], author introduced a new cost scheduling algorithm based on deadlines. It took into account the features of cloud computing to hold cost-concentrated and limited workflows. It diminishes execution time and cost while enabling consumer input instantly.
- Inferences based on PSO for programming workflow applications: In [9], author introduced computation and data communication for applications that include the cost for both and provided a guideline based on Particle Clustering Optimization (PSO). This algorithm can be utilised for workflow applications that have dissimilar computing and communication overheads. Experiential results showed that PSO can attain cost savings and well distribute workloads to cloud resources. Also in [10], authors expanded PSO to provide deadline-based resource scheduling and provisioning. However, these authors did not explain resource failures or extreme dependence on essential tasks.
- Market-oriented hierarchical scheduling technique was proposed by author in [11], which includes both the levels of scheduling that is task-level scheduling and service-level scheduling, where task-level scheduling concept copes with optimizing device allocation from a task to a VM on cloud data centers and service-level scheduling concept copes with task assigned to service.
- Stretchy workflow scheduling: In [12], author proposed SHEFT workflow scheduling algorithm which is a stretchy workflow scheduling in cloud environment. Investigational upshots showed that this algorithm performs better than various other workflow scheduling algorithms. This algorithm perks up workflow uptime, as well as it also facilitates resources to flexibly measure uptime.
- Multi-workflow Multi-QoS (MQMW) constrained scheduling strategy: In [13], research work author introduced a scheme for workflows with multiple QoS. Authors boosted the rate of access to scheduling and also diminished the duration and outlay of workflows for the cloud platform, so improved Quality of Service was proposed for multiple workflows using constrained scheduling strategy.
- In [14], research work author suggested SA to schedule all the tasks on platform with the aspire of plummeting execution time, but they did not analyse malfunctioning.

3. Proposed Workflow Scheduling Approach

The literature survey on various workflow algorithms is done one different aspect. The proposed workflow scheduling

algorithm generates planned scheme of tasks which reduces the entire cost of implementing a workflow which meets a deadline defined by user. The algorithm consists of two chief stages:

- Deadline allocation
- Scheduling.

Deadline allocation doles out the time limit for the overall workflow between individual tasks. Scheduling arranges every task with the economical service that is able to run the task earlier than its deadline.

The proposed algorithm focuses on the two concepts of task start times, which is Earliest Begin Time (EBT) and Actual Begin Time (ABT). EBT is calculated prior to schedule of workflow while the ABT is calculated when the tasks are arranged. The EBT of each non-arranged task t_i, EBT (t_i), is delineated as follows:

$$EBT(t_{entry})=0 \qquad (1)$$

$$EBT(t_i) = \max_{t_p \in t_i's \ parents} \left\{ EBT(t_p) + LET(t_p) + TT(e_{p,i}) \right\} \qquad (2)$$

where

LET(t_i): Least Execution Time of a task t_i, on service $s_j \in S$ with the least ET (t_i, s_j) between all available services.

TT($e_{p,i}$) is the transmission time from parent node to task t_i.

$$LET(t_{entry}) = LET(t_{exit}) = 0. \qquad (3)$$

As a result, the Earliest Completion Time (ECT) of an unscheduled task t_i, ECT (t_i), can be delineated as follows:

$$ECT(t_i) = EBT(t_i) + LET(t_i) \qquad (4)$$

In addition, we delineate Latest Completion Time (LCT) of task that are unscheduled t_i, LCT (t_i), refers the latest time for t_i which can terminate its execution such that the deadline D of the entire workflow is reduced.

It can be calculated as follows:

$$LCT(t_{exit})=D \qquad (5)$$

$$LCT(t_i) = \min_{t_c \in t_i's \ children} \left\{ LCT(t_c) + LET(t_c) + TT(e_{p,c}) \right\} \qquad (6)$$

The Service that is selected for every arranged task t_i, SS $(t_i) = s_{j,k}$, is delineated as the selected service for executing t_i while scheduling process, where $s_{j,k}$ is the k_{th} occurrence of service s_j.

The Decisive Parent of a node t_i refers to the not assigned parent of t_i that has the newest arrival time of data at t_i. It is taken as the parent t_p of t_i for which ECT (t_p)+ TT $(e_{p,i})$ which has maximal value.

The partial Decisive Path (PDP) of a node t_i is:

- Blank if t_i does not have some unassigned parents.
- Composed of Decisive Parent t_p of t_i and the PDP of t_p if has any unassigned parents.

Algorithm 1 : Scheduling Algorithm

procedure Schedule_Workflow (G (T, E), D)

Step 1: verify existing computation services

Step 2: add t_{entry} , t_{exit} and their corresponding dependencies to G

Step 3: calculate EBT (t_i), ECT (t_i) and LCT(t_i) for each task in G

Step 4: ABT(t_{entry}) ← 0, ABT(t_{exit}) ← D

Step 5: mark t_{entry} and t_{exit} as assigned

Step 6: call Assign_Parents(t_{exit})
}

Algorithm 2 : Algorithm for Parents Assignment (Step 6)

procedure Assign_Parents (t)
{
   while (t has any unassigned parent)
   {
     PDP = null , t_i = t

     While (t_i has any unassigned parent)
     {
       add Decisive_Parent (t_i) at the start of   PDP

       t_i = Decisive_Parent (t_i)
     }

     Step 7: call Assign_Path(PDP)

     for each t_i ∈ PDP
     {
     update EBT and ECT for every successor of t_i

     update LCT for every predecessor of t_i

     Step 6: call Assign_Parents(t_i)
     }
   }
}

Algorithm 3 : Algorithm for Path Assignment (Step 7)

procedure Assign_Path(P)
 {
   $s_{i,j}$ = the cheapest applicable existing instance for P
     if ($s_{i,j}$ = null)
     {
      launch a new instance $s_{i,j}$ of the cheapest service s_i
      which can finish each task of P before its LCT
     }

   Schedule P on $s_{i,j}$ and set SS (t_i), ABT (t_i) for each t_i ∈ P
   Set all tasks of P as assigned
}

4. **Performance Evaluation**

To appraise the proposed algorithm, we need to measure its performance in some workflow models. One of the structures

we used in this article is the Montage. Figure 4 depicts the approximate structure format of this workflow:
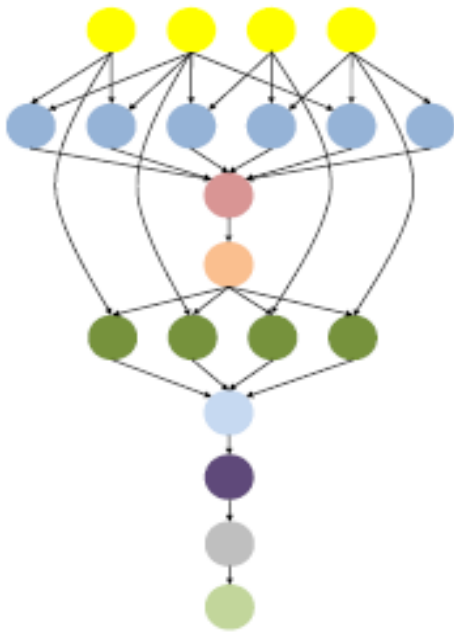
Figure 4: Structure of Montage workflow
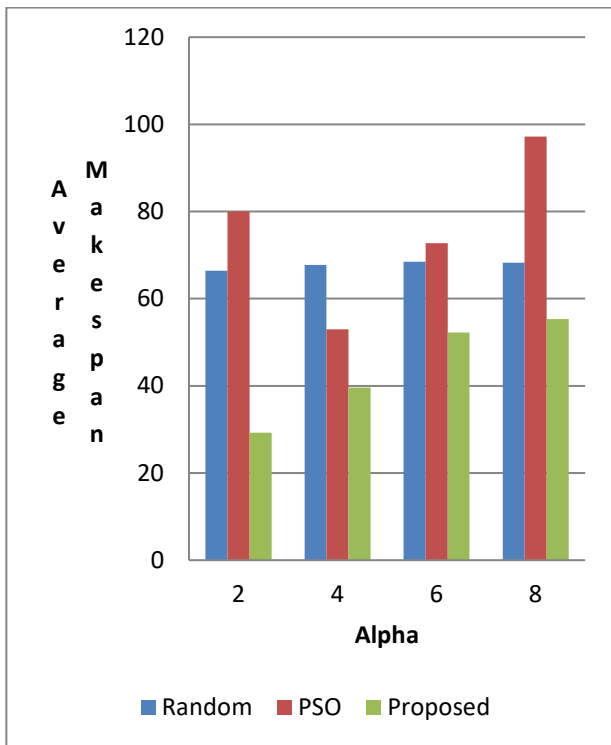
Figure 5: Comparison of average makespan for proposed algorithm

For calculation of the effectiveness of the proposed algorithm, we use makespan as a parameter. Makespan is the total time taken for resources to complete the overall execution of the tasks.

For evaluation of our proposed algorithm, we set a deadline for each workflow. We first delineate the fastest schedule. MF indicates the makespan that is fastest program in a workflow. It is only a least duration for that workflow to execute, so to establish time limit for every workflow, we delineate the deadline with factor α and delineate the new deadline of the workflow with its arrival plus α * MF. Since there is no

elucidation for α = 1, we take the range of α from 2 to 8 in our experiment.

Below is a comparison of the proposed approach with the stochastic approach and the PSO [9]. The graph is plotted for the parameter value of average makespan and alpha factor as deadline of the workflow.

Table 1: Comparison of average makespan for proposed algorithm

Alpha Value	Algorithm	Average Makespan
Alpha Factor =2	Random	68
	PSO	80
	Proposed	30
Alpha Factor =4	Random	68
	PSO	52
	Proposed	40
Alpha Factor =6	Random	68
	PSO	72
	Proposed	54
Alpha Factor =8	Random	68
	PSO	97
	Proposed	56

5. Conclusion

In this research paper, we aimed to design an algorithm that takes an approach to schedule workflow in one phase. The approach is intended to schedule each and every partial decisive path into a one occurrence of a computation service. The time complexity of algorithms is $O(n^2)$, where n indicates the number of tasks in the workflow. The complexity of polynomial time makes it appropriate for bulky workflows. We assess our algorithm by measuring its recital in Montage synthetic workflow. The results show that the proposed algorithm works better than other approaches.

References

[1] X. Zhou, G. Zhang, J. Sun, J. Zhou, T. Wei, S. Hu, "Minimizing cost and makespan for workflow scheduling in cloud using fuzzy dominance sort based HEFT," Future Generation Computer Systems, **93**, 278–289, 2019, doi:10.1016/j.future.2018.10.046.

[2] J. Yu, R. Buyya, "Scheduling Scientific Workflow Applications with Deadline and Budget Constraints Using Genetic Algorithms," Scientific Programming, **14**, 217–230, 2006, doi:10.1155/2006/271608.

[3] J. Yu, R. Buyya, "A Budget Constrained Scheduling of Workflow Applications on Utility Grids using Genetic Algorithms," Workshop on Workflows in Support of Large-Scale Science, 2006, doi:10.1109/WORKS.2006.5282330.

[4] J. Yu, R. Buyya, "A Taxonomy of Workflow Management Systems for Grid Computing," Journal of Grid Computing, **3**(3), 171–200, 2005, doi:10.1007/s10723-005-9010-8.

[5] H. Zhong, K. Tao, X. Zhang, An Approach to Optimized Resource Scheduling Algorithm for Open-Source Cloud Systems, 2010, doi:10.1109/ChinaGrid.2010.37.

[6] Y. Yang, K. Liu, J. Chen, X. Liu, D. Yuan, H. Jin, An Algorithm in SwinDeW-C for Scheduling Transaction-Intensive Cost-Constrained Cloud Workflows, 2008, doi:10.1109/eScience.2008.93.

[7] S. Selvarani, S. Sadhasivam, "Improved cost-based algorithm for task scheduling in cloud computing," Computational Intelligence and Computing Research (ICCIC), 2010, doi:10.1109/ICCIC.2010.5705847.

[8] K. Liu, H. Jin, J. Chen, X. Liu, D. Yuan, Y. Yang, "A Compromised-Time-Cost Scheduling Algorithm in SwinDeW-C for Instance-Intensive Cost-Constrained Workflows on a Cloud Computing Platform," IJHPCA, **24**, 445–456, 2010, doi:10.1177/1094342010369114.

[9] S. Pandey, L. Wu, S. Guru, R. Buyya, A Particle Swarm Optimization-Based Heuristic for Scheduling Workflow Applications in Cloud Computing Environments, 2010, doi:10.1109/AINA.2010.31.

[10] M.A. Rodriguez, R. Buyya, "Deadline Based Resource Provisioningand Scheduling Algorithm for Scientific Workflows on Clouds," IEEE

Transactions on Cloud Computing, **2**(2), 222–235, 2014, doi:10.1109/TCC.2014.2314655.

[11] Z. Wu, X. Liu, Z. Ni, D. Yuan, Y. Yang, "A market-oriented hierarchical scheduling strategy in cloud workflow systems," The Journal of Supercomputing, **63**(1), 256–293, 2013, doi:10.1007/s11227-011-0578-4.

[12] C. Lin, S. Lu, Scheduling Scientific Workflows Elastically for Cloud Computing, 2011, doi:10.1109/CLOUD.2011.110.

[13] M. Xu, L. Cui, H. Wang, Y. Bi, "A Multiple QoS Constrained Scheduling Strategy of Multiple Workflows for Cloud Computing," in 2009 IEEE International Symposium on Parallel and Distributed Processing with Applications, 629–634, 2009, doi:10.1109/ISPA.2009.95.

[14] M. Kaid, M. Othman, "Simulated Annealing Approach To Cost-Based Multi-QoS Job Scheduling in Cloud Computing Enviroment," American Journal of Applied Sciences, **11**, 872–877, 2014, doi:10.3844/ajassp.2014.872.877.

Numeric Simulation of Artificial Antigravity upon General Theory of Relativity

Yoshio Matsuki[1,*], Petro Ivanovich Bidyuk[2]

[1]*National University of Ukraine "Kyiv-Mohyla Academy", Kyiv 04070, Ukraine*

[2] *Educational and Scientific Complex "Institute for Applied System Analysis" of the National Technical University of Ukraine "Igor Sikorsky Kyiv Polytechnic Institute", Kyiv 03056, Ukraine*

A R T I C L E I N F O	A B S T R A C T
	This paper is an extended version of the work presented at a conference held in Kyiv, Ukraine, in October 2020, which reported the result of the numeric simulation on the artificial antigravity. This paper further describes the derivation of the idea of the artificial antigravity, and adds the simulation of angular momentum that is needed to describe the antigravity. Also, because the angular momentum is the perpendicular movement to a three-dimensional curved surface in a four-dimensional space-time, this paper challenges the limit of applying the curvature tensor in quantum mechanics; while, current quantum mechanics has been established on the flat surface. The artificial rotation of a hypothetical object is simulated, in which the gravity is so strong that the time-space can be distorted. The spherical polar coordinate system is selected to describe the curvature of the space, and the curvature tensor is formulated. Then the tensor is multiplied by the Euler's rotation matrix to make the inner product for the gravitational energy and the outer cross-product for the angular momentum of the rotation. To simulate the distorted time-space, two cases are selected: the linear distortion and the non-linear distortion upon the distance from the center of the strong gravity; also, the speed of the rotation is set in two options: the slower and the faster. Then the equation of motion is set by the curvature tensor to calculate the coefficient of the gravitational energy on the surface of the sphere in the spherical polar coordinates, and to calculate the coefficient of the angular momentum in the perpendicular direction to the sphere. The result shows that the antigravity can be produced by rotating the object, and the angular momentum can show the opposite directions by the selection of the rotation speed.

1. Introduction

This paper (hereinafter the "extended paper") is an extension of the report presented at the 2020 IEEE 2nd International Conference on System Analysis_Intelligent Computing (SAIC) held in Kyiv, Ukraine, in October 2020 [1] (hereinafter the "conference paper"). The conference paper was a byproduct, on a sideline, of the other series of our research [2–7], which was aimed at finding the origin of the global climate change.

At the beginning of the research [2-5], we assumed that Moon's gravity could be related to the increase of the global temperature, then we calculated the coefficients of several variables such as the distance between Moon and Earth, the global temperature, the emitted carbon dioxide, with the method of econometrics, regarding the distance between Moon and Earth as the surrogate for the energy of the Moon's gravitational field and gravitational

waves. Then we reached an assumption that there should be anti-gravitational waves as the antimatter of graviton (gravitational waves) similar to positron as the antimatter of electron; and, we derived the equation of motion of anti-gravitational waves, upon the equation of motion for gravitational waves [8] that was predicted in the flat surface in the rectilinear coordinate system, approximating the special theory of relativity. Then we reported the result of our analysis in a paper [6]. The geometrical relation between the positive and negative flows of gravitational waves (gravitational and anti-gravitational waves) that we made for [6] is shown in Figure 1.

The next question was "How can both positive and negative flows be created?" Then we reviewed the general theory of relativity [8] that explained the gravitational field by the following equations:

*Corresponding Author: Khaoula Naouaoui, naouaoui.khaoula@gmail.com
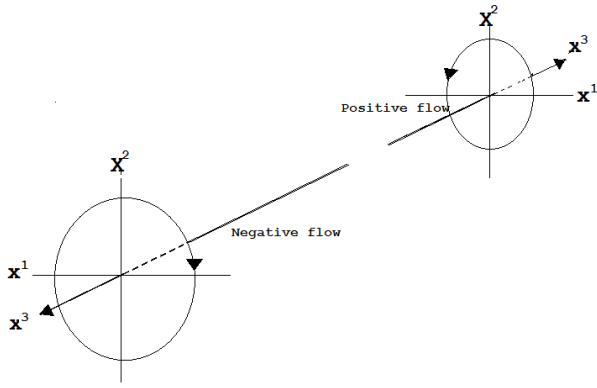
Figure 1: Geometrical relation between positive and negative flows of gravitational waves [6]

$$R_{\mu\nu} = \Gamma^{\alpha}_{\mu\alpha,\nu} - \Gamma^{\alpha}_{\mu\nu,\alpha} - \Gamma^{\alpha}_{\mu\nu}\Gamma^{\beta}_{\alpha\beta} + \Gamma^{\alpha}_{\mu\beta}\Gamma^{\beta}_{\nu\alpha} \tag{1}$$

$$\Gamma^{\alpha}_{\mu\nu} = g^{\alpha\alpha}\Gamma_{\alpha\mu\nu} = \frac{1}{2}g^{\alpha\alpha}(g_{\alpha\mu,\nu} + g_{\alpha\nu,\mu} - g_{\mu\nu,\alpha}) \tag{2}$$

$R_{\mu\nu}$ is called the Ricci tensor, which is a variation of the curvature tensor, and $\Gamma^{\alpha}_{\mu\nu}$ is called a Christoffel symbol. Also, $g^{\mu\nu}$ is called the fundamental tensor that makes the Christoffell symbol. The equation (3) shows how the fundamental tensor describes a four-dimensional space-time. Here, the notation for the differential of the tensor is given by $F_{,\mu} = \dfrac{\partial}{\partial x^{\mu}}F$, where F is any function such as $\Gamma^{\alpha}_{\mu\nu}$ and/or $g_{\mu\nu}$, and x^{μ} is the $\mu-th$ variable (vector) in the given coordinate system.

$$g^{\mu\nu} = \begin{bmatrix} g^{00} & g^{01} & g^{02} & g^{03} \\ g^{10} & g^{11} & g^{12} & g^{13} \\ g^{20} & g^{21} & g^{22} & g^{23} \\ g^{30} & g^{31} & g^{32} & g^{33} \end{bmatrix} = \begin{bmatrix} 1-\dfrac{2m}{r} & 0 & 0 & 0 \\ 0 & -(1-\dfrac{2m}{r})^{-1} & 0 & 0 \\ 0 & 0 & -r^2 & 0 \\ 0 & 0 & 0 & -r^2\sin^2\theta \end{bmatrix} \tag{3}$$

The fundamental tensor also makes a geodesic, a path of extremal distance, as shown below.

$$ds^2 = g^{00}dt^2 + g^{11}dr^2 + g^{22}d\theta^2 + g^{33}d\phi^2 \tag{4}$$

In the equation (4), t is time, m is the mass of a planet, r is the distance from the planet, θ is the angle from the axis of r, and ϕ is the angle of the rotation around the axis of r in the spherical polar coordinate system. In (3), there is a singularity at $r = 2m$: therefore, the space is divided into two regions, $r < 2m$ and $r > 2m$. In the region of $r < 2m$, the mass of the planet must be very dense and heavier and it can be a black hole. To connect these two regions, a different coordinate system was invented [8], which makes the distorted time, τ, and the distorted distance, ρ, by the following equations:

$$\tau = t + f(r) \tag{5}$$

$$\rho = t + g(r) \tag{6}$$

The section *2.2.* describes how this idea is taken into account in the numeric simulation.

Then the equation (3) was transformed to the equation (7).

$$g^{\mu\nu} = \begin{bmatrix} 1 & 0 & 0 & 0 \\ 0 & -\dfrac{2m}{\mu(\rho-\tau)^{\frac{2}{3}}} & 0 & 0 \\ 0 & 0 & -\mu^2(\rho-\tau)^{\frac{4}{3}} & 0 \\ 0 & 0 & 0 & -\mu^2(\rho-\tau)^{\frac{4}{3}}\sin^2\theta \end{bmatrix} \tag{7}$$

Then the geodesic was also transformed from (4) to (8).

$$ds^2 = g^{00}d\tau^2 + g^{11}d\rho^2 + g^{22}d\theta^2 + g^{33}d\varphi^2 \tag{8}$$

The followings show how to make (1) and (2) by the fundamental tensor:

For example, if $\mu = \nu = 1$,

$$g^{11} = -\frac{2m}{\mu(\rho-\tau)^{\frac{2}{3}}} \tag{9}$$

$$g_{11} = -\frac{\mu(\rho-\tau)^{\frac{2}{3}}}{2m} \tag{10}$$

$$g_{11,\rho} = \frac{\partial}{\partial\rho}(-\frac{\mu}{2m}(\rho-\tau)^{\frac{2}{3}}) \tag{11}$$

According to [8], in the empty space where only the gravitational field of a planet exists, $R_{\mu\nu}$ becomes zero as shown in (12); then (13) is the equation of motion of a particle.

$$R_{\mu\nu} = 0 \tag{12}$$

$$g^{\mu\nu}(g_{\alpha\mu,\nu} - \frac{1}{2}g_{\mu\nu,\alpha}) = 0 \tag{13}$$

Then in order to describe gravitational waves moving in the gravitational field, the equation of motion is differentiated once again as shown below.

$$\frac{d}{dx^{\beta}}g^{\mu\nu}(g_{\alpha\mu,\nu} - \frac{1}{2}g_{\mu\nu,\alpha}) = g^{\mu\nu}_{,\beta}(g_{\alpha\mu,\nu} - \frac{1}{2}g_{\mu\nu,\alpha}) + g^{\mu\nu}(g_{\mu\alpha,\nu\beta} - \frac{1}{2}g_{\mu\nu,\alpha\beta})$$

$$= g^{\mu\nu}(g_{\mu\alpha,\nu\beta} - \frac{1}{2}g_{\mu\nu,\alpha\beta}) = 0 \tag{14}$$

This equation leads to the equation (15), and this is the equation of motion for gravitational waves, according to [8].

$$g^{\mu\nu}g_{\alpha\beta,\mu\nu} = 0 \tag{15}$$

The notation for the secondary differential of $g_{\mu\nu}$, for example by the vectors, x^{α} and x^{β}, is $g_{\mu\nu,\alpha\beta} = \dfrac{\partial^2}{\partial x^{\alpha}\partial x^{\beta}}g_{\mu\nu}$.

Here, we show this equation only for describing how the gravitational field is related to the creation of gravitational waves; although, this extended paper doesn't include the simulation of gravitational waves.

Then we made the numeric simulation [7] on the curved space, deriving the mathematical forms of the components of the Ricci tensor (1). The following equation is an example of the Ricci tensor in case of $\mu = \nu = 0$, $\alpha = 2$, $\beta = 1$:

$$R_{00} = \Gamma_{02,0}^2 - \Gamma_{00,2}^2 - \Gamma_{00}^2 \Gamma_{21}^1 + \Gamma_{01}^2 \Gamma_{02}^1$$
$$= g^{22}\Gamma_{202,0} - g^{22}\Gamma_{200,2} - g^{22}\Gamma_{200}g^{11}\Gamma_{121} + g^{22}\Gamma_{201}g^{11}\Gamma_{102}$$

$$= \frac{1}{2}\{-\mu^2(\rho-\tau)^{\frac{4}{3}}\}\{-\frac{4}{3}(-1)(\rho-\tau)^{-\frac{7}{3}}\}_{,\tau} = \{\frac{-2}{3(\rho-\tau)}\}_{,\tau} = \frac{2}{3(\rho-\tau)^2} \quad (16)$$

Then we calculated the coefficient of each component of the tensor, for $\mu = 0$, 1, 2, 3, $\nu = 0$, 1, 2, 3, $\alpha = 0$, 1, 2, 3, and $\beta = 0$, 1, 2, 3, using a personal computer. The algorithm to calculate the coefficients is described in the section *2.3*.

After making the numeric simulation [7] with the curvature tensor, there was still a need to confirm the negative flow of gravitational waves that are to be created by some movement of a strong gravity; however, we could not find any suitable physical object that could be referred to. Therefore, we invented an idea of the hypothetical rotation of an artificial object shown in Figure 2 as a possibility of the movement of a strong gravity. Then we reported the result of the simulation in the conference paper [1] as the "theory and simulation of artificial antigravity".

While the conference paper [1] has reported the result of the simulation on the gravitational energy made by rotating the very strong gravity, this extended paper reports one more feature, the angular momentum, by which we attempt to examine whether there is a consistent explanation of anti-gravitational waves shown in Figure 1, or not.
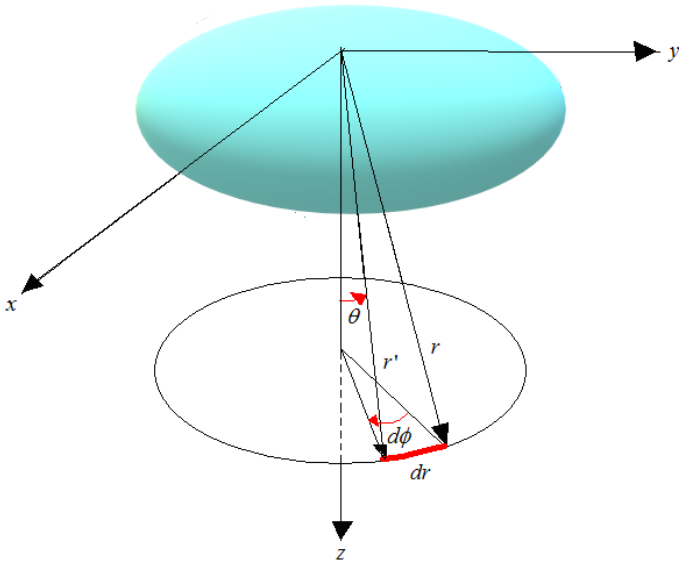
Figure 2: Rotation of an object

It is noted that there is no data taken out from any experiments in laboratories or observations in the cosmos, but this research is made solely on the mathematical model taken out from the general theory of relativity [8] as well as the classical mechanics [9].

For the numeric simulation, we used a personal computer's software, which was developed for the econometrics of geometry [10]. The algorithm of this software was originally developed in the rectilinear coordinate system; but, we used it for calculating the coefficients of the equation of motion in the spherical polar coordinate system as a special case of the curved space. In other words, we used the function of the orthogonal transformation of the matrix algebra as the surrogate for the tensor algebra needed in the general theory of relativity.

2. Method

2.1. Curvature Tensor before the Rotation

For the simulation of this extended paper, we used the same curvature tensor shown in (17) that we used for our previous research for the conference paper [1]. This tensor is for simulating the gravitational field before the rotation. From it, we took the components of R_{11}, R_{22} and R_{33} for simulating the spatial movement of the object, but excluded R_{00} from the simulation because it is for the distorted time coordinate, which is beyond the scope of this research.

$$R_{\mu\nu} = \begin{bmatrix} R_{00} & 0 & 0 & 0 \\ 0 & R_{11} & 0 & 0 \\ 0 & 0 & R_{22} & 0 \\ 0 & 0 & 0 & R_{33} \end{bmatrix} \quad (17)$$

The diagonal components of $R_{\mu\nu}$ are shown in the equations from (18) to (21), which are taken from our previous research [7].

$$R_{00} = \frac{5}{9(\rho-\tau)^2} \quad (18)$$

$$R_{11} = \frac{20}{3(\rho-\tau)^2} + \frac{11\mu}{18m(\rho-\tau)^{\frac{4}{3}}} \quad (19)$$

$$R_{22} = \frac{28}{9\mu^2(\rho-\tau)^{\frac{10}{3}}} + \frac{140m}{9\mu^2(\rho-\tau)^4} + \frac{4}{\sin^2\theta} + \cot^2\theta \quad (20)$$

$$R_{33} = \frac{-28}{9\mu^2(\rho-\tau)^{\frac{10}{3}}\sin^2\theta} + \frac{140m}{9\mu^3(\rho-\tau)^4\sin^2\theta} + \frac{4}{\sin^2\theta} + \frac{11\cot^2\theta}{\sin^2\theta} \quad (21)$$

μ is given by the following equation with the mass of a planet, m:

$$\mu = (\frac{3}{2}\sqrt{2m})^{\frac{2}{3}} \quad (22)$$

2.2. Distortion of time and space in strong gravity

We used the same assumption of our previous research [1] for simulating the distortion of time and space, as shown in Figure 3 and Figure 4. In these figures, r is the distance from the center of the strong gravity, t is the time to travel for the distance, τ is the distorted time (5), which expands and shrinks depending on the distance r and the time t; and, ρ is the distorted distance (6), which expands and shrinks depending on the time t and the distance r.

For the simulation, we created two models, Case-1 (non-linear model) and Case-2 (linear model) as shown in Table 1, which assign the functions of $f(r)$ in the equation (5) and $g(r)$ in the equation (6).

Table 1: Two models for simulating the distorted time-space

	Case-1 (Non-linear model)	Case-2 (Linear model)
$f(r)$	$\log \cdot r$	$1/r$
$g(r)$	e^r	r

Then we made the distributions of r and t, following the description of [8], "Any signal, even a light signal, would take an infinite time to cross the boundary of a black hole". However, we could not set the infinite values for the simulation; therefore, instead we set 24 discrete finite values in order to mock "It takes more time to travel closer to the center of the black hole". The values of r and t are assigned to make input vectors for the numeric simulation with a personal computer.
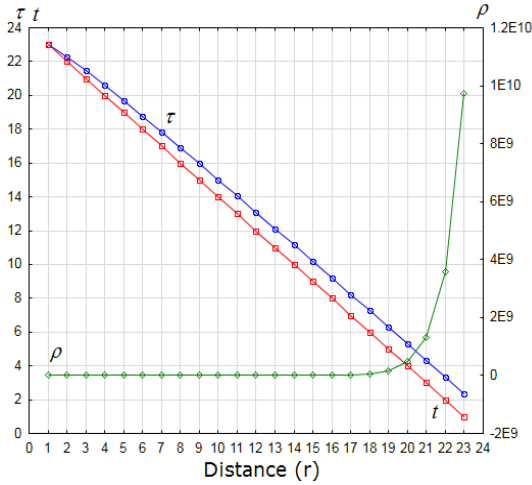
Figure 3: Time and distance from the center of the gravity, Case-1 (non-linear distortion): $f(r) = \log r$ and $g(r) = e^r$
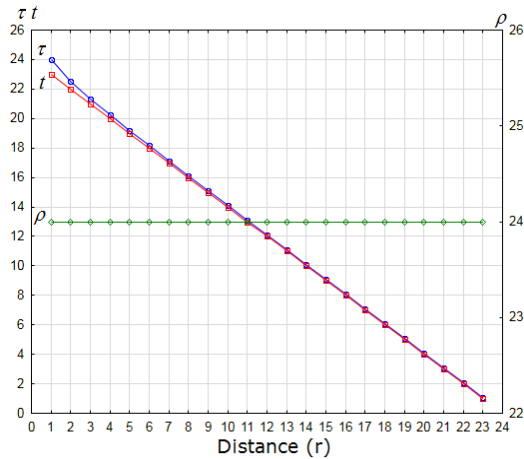
Figure 4: Time and distance from the center of the gravity, Case-2 (linear distortion): $f(r) = \dfrac{1}{r}$ and $g(r) = r$

2.3. Algorithm for the gravitational energy with no rotation

We used the same algorithm that we used for our previous research [1] to calculate the relative intensity of the gravitational energy with the curvature tensor, which was to be reflected by the stress-energy tensor placed at the end of the distance Υ in Figure 3 and 4.

The Einstein's equation that rules the motion of particles in the gravitational field is shown below.

$$(R^{\mu\nu} - \frac{1}{2} g^{\mu\nu} R)_{,\nu} = 0 \tag{23}$$

Then we took the idea of the stress energy tensor from the classical mechanics [9] and set the equation (24), where T is the stress energy tensor and k is a constant.

$$R_{\mu\nu} - \frac{1}{2} g_{\mu\nu} R = kT \tag{24}$$

In order to calculate the coefficients of the tensor, we made the equation shown below, where c_1, c_2 and c_3 are the coefficients that make a column vector, c.

$$H = kT - R_{\mu\nu} = kT - (c_1 X_1 + c_2 X_2 + c_3 X_3) \tag{25}$$

For calculating c, we formed a 3×3 matrix, X, by three vectors, X_1, X_2 and X_3, as shown in (26) for making the projected image of the gravitational energy on the surface of the sphere in the spherical polar coordinate system.

$$X = [X_1 \quad X_2 \quad X_3] = [R_{11} \quad R_{22} \quad R_{33}] \tag{26}$$

Then we formed H with matrix algebra, as shown below.

$$H = kT - Xc \tag{27}$$

To solve this equation, we set the constraint (28), where X' is the transposed matrix of X.

$$X'H = X'(kT - Xc) = 0 \tag{28}$$

The matrix algebra continues as shown in (29) and (30) to calculate the values of c.

$$X'Xc = X'kT \tag{29}$$

$$c = (X'X)^{-1} X'kT \tag{30}$$

The standard errors of the coefficients are also calculated by (31), where $V(c)$ is the variance of the c.

$$\sqrt{V(c)} = \sqrt{\hat{\sigma}^2 (X'X)^{-1}} \tag{31}$$

$\hat{\sigma}^2$ is calculated by the equations from (32) to (34).

$$\hat{\sigma}^2 = e'e/(n-l) \tag{32}$$

$$e = M \cdot kT \tag{33}$$

$$M = I - X(X'X)^{-1} X' \tag{34}$$

n is the number of rows of each column of X, while in this simulation the value of n is 23 as shown in Figure 3 and 4. l is the number of columns of X, and I is a 23×23 unit matrix that holds 1 (unity) in all diagonal components and 0 in the other components. $(X'X)^{-1}$ is the inverse matrix of $X'X$, and e' is the transposed vector of e.

2.4. Algorithm for the gravitational energy with rotation

If the object rotates as shown in Figure 2, its coordinate system is transformed by the transformation matrix D of the Euler's angles [9] shown below.

$$D = \begin{bmatrix} \cos\phi & \sin\phi & 0 \\ -\sin\phi & \cos\phi & 0 \\ 0 & 0 & 1 \end{bmatrix} \tag{35}$$

For the rotation of the object around one axis of ϕ, the tensor of the object's coordinate system, $R_{\mu\nu}$, is multiplied by D; then it is transformed as shown below.

$$D \cdot R_{\mu\nu} = \begin{bmatrix} \cos\phi & \sin\phi & 0 \\ -\sin\phi & \cos\phi & 0 \\ 0 & 0 & 1 \end{bmatrix} \cdot \begin{bmatrix} R_{11} & 0 & 0 \\ 0 & R_{22} & 0 \\ 0 & 0 & R_{33} \end{bmatrix}$$

$$= \begin{bmatrix} \cos\phi \cdot R_{11} & \sin\phi \cdot R_{22} & 0 \\ -\sin\phi \cdot R_{11} & \cos\phi \cdot R_{22} & 0 \\ 0 & 0 & R_{33} \end{bmatrix} \tag{36}$$

The components, $\sin\phi \cdot R_{22}$ and $-\sin\phi \cdot R_{11}$ are anti-symmetrical, which are perpendicular to the rotation axis, z for ϕ of Figure 2. From the above transformed tensor after the rotation, $D \cdot R_{\mu\nu}$, we took out its diagonal components and formed (37), to calculate the relative intensity of the principal moment of the rotation.

$$\begin{bmatrix} dR_{11} & 0 & 0 \\ 0 & dR_{22} & 0 \\ 0 & 0 & R_{33} \end{bmatrix} = \begin{bmatrix} \cos\phi \cdot R_{11} & 0 & 0 \\ 0 & \cos\phi \cdot R_{22} & 0 \\ 0 & 0 & R_{33} \end{bmatrix} \tag{37}$$

Then we formed H as shown below to calculate the coefficients of the diagonal components.

$$H = kT - (c_1 \cdot dR_{11} + c_2 \cdot dR_{22} + c_3 \cdot R_{33}) \tag{38}$$

Henceforth we followed the same procedure explained in the section *2.3.*, but with the matrix shown below.

$$X = \begin{bmatrix} \cos\phi \cdot R_{11} & \cos\phi \cdot R_{22} & R_{33} \end{bmatrix} \tag{39}$$

2.5. Algorithm for the angular momentum of the rotation

We formed a matrix shown in (40), by taking out the anti-symmetrical components of $D \cdot R_{\mu\nu}$ from (36); then formed a column vector shown in (41).

$$\begin{bmatrix} 0 & \sin\phi \cdot R_{22} & 0 \\ -\sin\phi \cdot R_{11} & 0 & 0 \\ 0 & 0 & 0 \end{bmatrix} = \begin{bmatrix} 0 & R_{22} \cdot d\Omega_3 & 0 \\ -R_{11} \cdot d\Omega_3 & 0 & 0 \\ 0 & 0 & 0 \end{bmatrix} \tag{40}$$

$$\begin{bmatrix} dR_{11} \\ dR_{22} \\ dR_{33} \end{bmatrix} = \begin{bmatrix} R_{22} \cdot d\Omega_3 \\ -R_{11} \cdot d\Omega_3 \\ 0 \end{bmatrix} \tag{41}$$

With the above column vector, we formed H shown below, for calculating the coefficients of the vector's components.

$$H = kT - (c_1 \cdot R_{22} \cdot d\Omega_3 - c_2 \cdot R_{11} \cdot d\Omega_3) \tag{42}$$

Then we followed the same procedure as explained above, but with the matrix shown in (43) of the anti-symmetrical components. It is to simulate the angular momentum that is to be projected on the imaginary flat surface, which is perpendicular to the spherical surface.

$$X = \begin{bmatrix} \sin\phi \cdot R_{22} & -\sin\phi \cdot R_{11} \end{bmatrix} = \begin{bmatrix} R_{22} \cdot d\Omega_3 & -R_{11} \cdot d\Omega_3 \end{bmatrix} \tag{43}$$

here a little explanation is needed about $d\Omega_3$ of (43). At first, ε of (44) is an infinitesimal rotation operator. But, in general it has a form of (45) according to the Reference [9]. Then a rotated vector as the cross-product of $R_{\mu\nu}$ and $d\Omega$ makes (46).

$$\varepsilon = \begin{bmatrix} 0 & d\Omega_3 & 0 \\ -d\Omega_3 & 0 & 0 \\ 0 & 0 & 0 \end{bmatrix} \tag{44}$$

$$\varepsilon = \begin{bmatrix} 0 & d\Omega_3 & -d\Omega_2 \\ -d\Omega_3 & 0 & d\Omega_1 \\ d\Omega_2 & -d\Omega_1 & 0 \end{bmatrix} \tag{45}$$

$$\begin{bmatrix} dR_{11} \\ dR_{22} \\ dR_{33} \end{bmatrix} = R_{\nu\nu} \times d\Omega = \begin{bmatrix} R_{11} \\ R_{22} \\ R_{33} \end{bmatrix} \times \begin{bmatrix} d\Omega_1 \\ d\Omega_2 \\ d\Omega_3 \end{bmatrix} = \begin{bmatrix} R_{22}d\Omega_3 - R_{33}d\Omega_2 \\ R_{33}d\Omega_1 - R_{11}d\Omega_3 \\ R_{11}d\Omega_2 - R_{22}d\Omega_1 \end{bmatrix} \tag{46}$$

However, in this simulation, we assumed (47) and (48), which make (41) instead of (46).

$$d\Omega_1 = d\Omega_2 = 0 \tag{47}$$

$$d\Omega_3 = \sin\phi \tag{48}$$

2.6. Input data

The time t and the distance r are set as shown in Figure 3 for Case-1 and in Figure 4 for Case-2. For simulating the spatial expansion of the gravitational field, we assumed as if θ would become larger in far distance as shown in Figure 5. For simulating the rotation of the object, we set two cases, assuming ϕ_1 (the rotation 1) and ϕ_2 (the rotation 2) also as shown in Figure 5. With these settings, $\sin\theta$, $\cos\theta$, $\cot\theta$, $\sin\phi_1$, $\sin\phi_2$, $\cos\phi_1$ and $\cos\phi_2$ behave as shown in Figure 6.
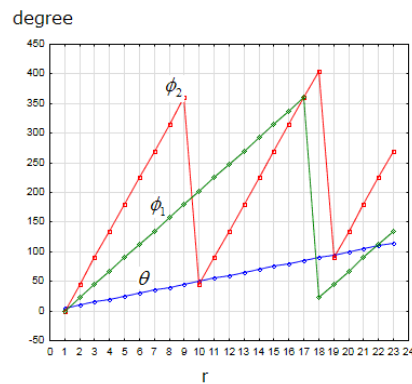
Figure 5: Angles, θ, ϕ_1 and ϕ_2, for the simulation

In addition, we set the stress-energy tensor as 1; because, the purpose of this simulation is to measure the relative intensity of each component of the tensors.
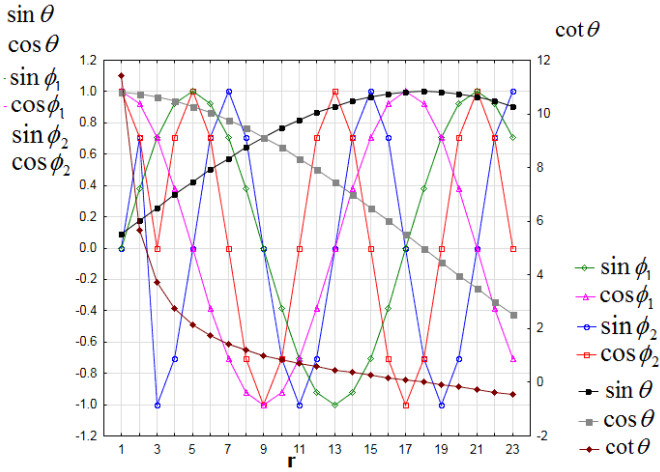
Figure 6: $\sin\theta$, $\cos\theta$, $\cot\theta$, $\sin\phi_1$, $\sin\phi_2$, $\cos\phi_1$ and $\cos\phi_2$

3. Result

3.1. Gravitational energy and angular momentum: overview

Figure 7 (Table 2) shows the relative intensity of the gravitational energy of the object, which is projected on the surface of the sphere of the curved space, and the angular momentum of the perpendicular vector to the surface. In Case-1 (non-linear distortion of the time and space), the gravitational energy (on curved surface) is negative (gravity) before the rotation, but it changes to positive (antigravity) in the rotation 1, and then to negative (gravity) again in the rotation 2. It means that the antigravity appears, depending on the speed of the rotation of the object. The sign of the angular momentum (on perpendicular vector) changes from positive to negative when the rotation becomes faster (from the rotation 1 to the rotation 2). It means that the direction of the angular momentum changes, depending on the speed of the rotation. In Case-2 (linear distortion of time and space), the gravitational energy is positive with no rotation (but smaller than in Case-1 and closer to zero) in Figure 7; while, the gravitational energy (negative) becomes larger when the object rotates faster. The angular momentum of Case-2 changes as it changes in Case-1.
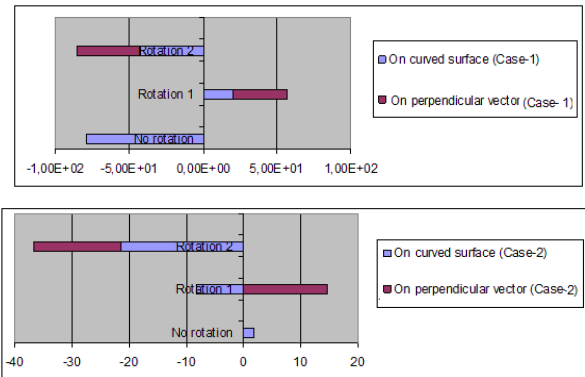
Figure 7: Gravitational energy on curved surface and angular momentum on perpendicular direction to the surface

Note: In Figure 7, "On curved surface" means the gravitational energy, which is the sum of the calculated coefficients in the equation of (25) for the no rotation and the sum of the calculated coefficients in the equation of (38) for each of the rotation 1 and the rotation 2. "On perpendicular vector" means the angular momentum, which is the sum of the calculated coefficients of (42) for each of the rotation 1 and the rotation 2.

Table 2: Intensities of gravitational energy and angular momentum: overview

	Case-1		Case-2	
	On curved surface	On perpendicular vector	On curved surface	On perpendicular vector
No rotation	-78.55	---	1.770	---
Rotation 1	20.00	36.90	-8.178	14.77
Rotation 2	-41.96	-43.00	-21.31	-15.29

3.2. Gravitational energy in three directions

Figure 8 (Table 3) and Figure 9 (Table 4) show the intensities of the gravitational energy, projected on the spherical curved surface in the components of R_{11}, R_{22} and R_{33} with no rotation, and in the components of $\cos\phi \cdot R_{11}$, $\cos\phi \cdot R_{22}$ and R_{33} with the rotation 1 and the rotation 2.

In Figure 8 for Case-1, only the component of R_{11} appears on the surface with no rotation, and only the component of $\cos\phi \cdot R_{11}$ appears with the rotation 1 and the rotation 2. The rotation 1 shows the antigravity (positive).

In Figure 9 for Case-2, the component of $\cos\phi \cdot R_{22}$ also appears in addition to the component of $\cos\phi \cdot R_{11}$ when the object rotates, and they become positive (antigravity) with the rotation 1 and the rotation 2. Here, it is noted that the components of $\cos\phi \cdot R_{22}$ and R_{33} don't appear in Case-1 of Figure 8, but their calculated values are shown in Table 3; and, in Case-2 the component of R_{33} doesn't appear in Figure 9, but its calculated values are shown in Table 4.
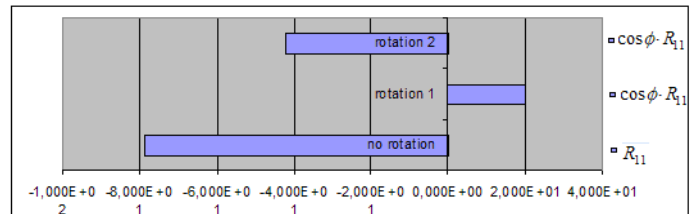
Figure 8: Projection of the gravitational energy in 3 directions on the surface of the curvature, Case-1
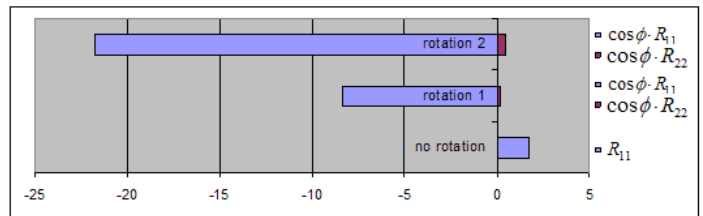
Figure 9: Projection of the gravitational energy in 3 directions on the surface of the curvature, Case-2

Table 3: Intensity of gravitational energy in 3 components, Case-1

Diagonal components of $R_{\mu\nu}$	c and $\sqrt{V(c)}$ of $R_{\mu\nu}$ before the rotation	Diagonal components of rotated $R_{\mu\nu}$	c and $\sqrt{V(c)}$ (Rotation 1)	c and $\sqrt{V(c)}$ (Rotation 2)
R_{11}	-78.68 (26.49)	$\cos\phi \cdot R_{11}$	20.01 (58.22)	-42.05 (52.30)
R_{22}	0.1307 (0.03369)	$\cos\phi \cdot R_{22}$	-5.516×10^{-3} (0.0803)	0.08903 (0.06829)
R_{33}	-6.803×10^{-5} (2.557×10^{-4})	R_{33}	-3.290×10^{-4} (3.869×10^{-4})	-2.990×10^{-4} (5.403×10^{-4})

Note: The value without the bracket is the coefficient c; and, the value in the bracket is the standard error of the coefficient $\sqrt{V(c)}$. By econometrics [10], briefly the calculated coefficient is more significant if its standard error of the coefficient is smaller than the value of the coefficient.

Table 4: Intensity of gravitational energy in 3 components, Case-2

Diagonal components of $R_{\mu\nu}$	c and $\sqrt{V(c)}$ of $R_{\mu\nu}$ before the rotation	Diagonal components of rotated $R_{\mu\nu}$	c and $\sqrt{V(c)}$ (Rotation 1)	c and $\sqrt{V(c)}$ (Rotation 2)
R_{11}	1.767 (7.364)	$\cos\phi \cdot R_{11}$	-8.368 (11.85)	-21.79 (16.36)
R_{22}	2.862×10^{-3} (0.1469)	$\cos\phi \cdot R_{22}$	0.1924 (0.2427)	0.4849 (0.3369)
R_{33}	1.110×10^{-5} (2.224×10^{-3})	R_{33}	-2.854×10^{-3} (3.673×10^{-3})	-7.281×10^{-3} (5.099×10^{-3})

3.3. Angular momentum in two directions

Figure 10 (Table 5) and Figure 11 (Table 6) show the intensities of the rotation's angular momentum in two directions, $\sin\phi \cdot R_{22}$ and $-\sin\phi \cdot R_{11}$, which are perpendicular to the rotation axis, ϕ. In Figure 10 for Case-1, only the vector's component of $-\sin\phi \cdot R_{11}$ appears for the rotation 1. For the rotation 2, the component of $-\sin\phi \cdot R_{11}$ appears, and $\sin\phi \cdot R_{22}$ is very slightly visible in this figure.
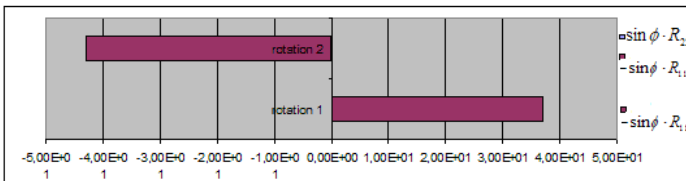
Figure 10: Angular momentum of the rotating object in 2 directions, case-1
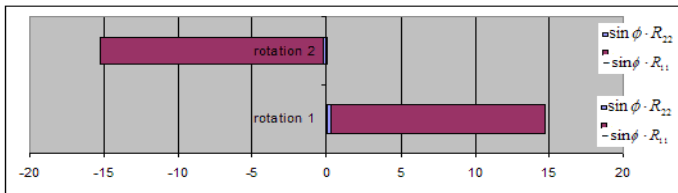
Figure 11: Angular momentum of the rotating object in 2 directions, case-2

In Figure 11 for Case-2, the vector's component of $\sin\phi \cdot R_{22}$ also appears. In both Case-1 and Case-2, when the speed of the

rotation increases from the rotation 1 to the rotation 2, the sign of the angular momentum changes from plus to minus. It means that the direction of the angular momentum reverses when the speed of the rotation of the object changes.

This result suggests a consistency with our previous report on the direction of the spin momentum of gravitational waves [6] shown in Figure 1; however, because gravitational waves are beyond the scope of this extended paper, further discussion on the similarity between the direction of the angular momentum of the antigravity and the direction of the spin momentum of anti-gravitational waves should be postponed to the other research.

Table 5: Intensity of the rotation's angular momentum, Case-1

	c and $\sqrt{V(c)}$ (Rotation 1)	c and $\sqrt{V(c)}$ (Rotation 2)
$dx_1 = R_{22} \cdot d\Omega_3 = \sin\phi \cdot R_{22}$	9.077×10^{-2} (5.072×10^{-2})	-4.816×10^{-2} (5.931×10^{-2})
$dx_2 = -R_{11} \cdot d\Omega_3 = -\sin\phi \cdot R_{11}$	36.83 (46.33)	-42.94 (45.44)

Table 6: Intensity of the rotation's angular momentum, Case-2

	c and $\sqrt{V(c)}$ (Rotation 1)	c and $\sqrt{V(c)}$ (Rotation 2)
$dx_1 = R_{22} \cdot d\Omega_3 = \sin\phi \cdot R_{22}$	0.2821 (0.2621)	-0.2285 (0.2597)
$dx_2 = -R_{11} \cdot d\Omega_3 = -\sin\phi \cdot R_{11}$	14.48 (16.65)	-15.06 (16.69)

3.4. Physical meaning of the results

When the idea of quantum mechanics was developed in the early 20th century, there was a discussion [11] to select the coordinate system for quantum mechanics from Einstein's special theory of relativity or his general theory of relativity. He compared two types of the coordinate systems: one was on the flat space-like surface (Figure 12), and another on the curved space-like surface (Figure 13). In each figure, three-dimensional surfaces, S1, S2, S3, S1' in Figure 12 and S in Figure 13, are placed in four-dimensional time-space, where X_0 is for the time, and X_1, X_2, X_3 for the space. The special theory of relativity is explained in Figure 12, while the general theory of relativity is in Figure 13. Figure 13 represents a three-dimensional curved surface in a four-dimensional space-time, which has the property of being everywhere space-like, and the perpendicular vector to the surface has to be in the light-cone of Figure 13, according to [11].
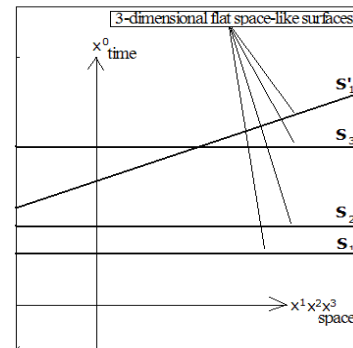
Figure 12: Flat space-like surface (remade from [11]
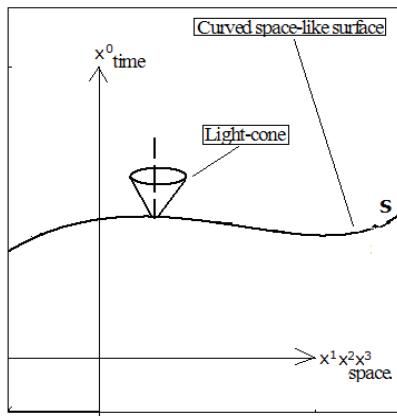
Figure 13: Curved space-like surface (remade from [11]

Then it was predicted by [11] that this perpendicular movement to the curved space must have a physical meaning. However, it was found that the curvature tensor could not satisfy the condition for solving the equation of motion in such a perpendicular direction to the curved surface. Henceforward the theory of quantum mechanics was not developed on the curved surface of Figure 13, but on the flat surface of Figure 12.

In our previous research for the conference paper [1], we made a simulation on the energy of the gravitational field, which was the projection on the spherical surface; but, not the movements of the vectors perpendicular to the spherical surface. However, in this extended paper, we also report the result of the simulation of the angular momentum, which is the perpendicular component of the movement of the curved surface. This part challenges the decision to use the flat surface for quantum mechanics in the early 20th century.

For solving the equation of motion in a three-dimensional curved surface in a four-dimensional space-time, the curvature tensor is needed. But, in our research we used the spherical polar coordinate system as a surrogate of the curved surface so that we could still use the orthogonal transformation of the matrix algebra, which was available originally for the flat space.

The vector components of the spherical surface are the projections of the gravitational energy; and, the movements of these vectors are the movements of the curved surface itself. It looks like Figure 14.
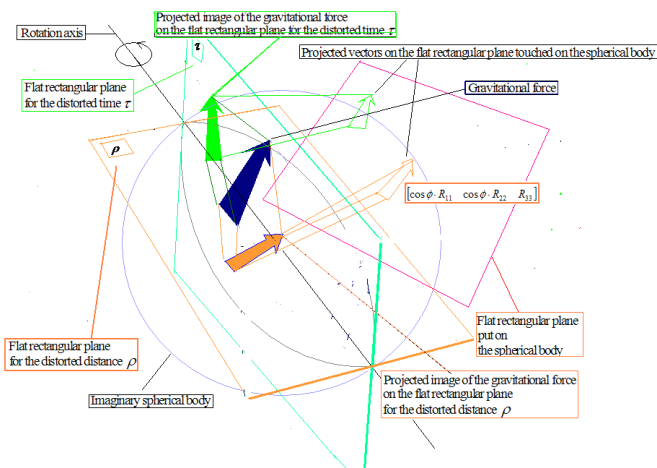
Figure 14: The vector projected on the spherical surface

In Figure 14, a flat rectangular plane is put on the surface of an imaginary spherical body. And, inside of the spherical body, there is one arrow that represents the gravitational force. The rotating object, which is not shown in this figure, is assumed to be located in the center of the spherical body. Also one rotation axis is shown in this figure. On this axis, there are two flat rectangular planes: one is for the distorted time, τ; and, another is for the distorted distance, ρ. First, the arrow of the gravitational force inside of the imaginary spherical body is projected to each of these two flat planes that are with the signs of τ and ρ. Then each of these two arrows is further projected to the flat rectangular plane that touches the surface of the spherical body. Here three vectors of (39) must be on this rectangular plane on the surface, and the calculated coefficients of (38) represent the intensities of the gravitational energy, shown in Figure 8 (Table 3) and Figure 9 (Table 4). If the speed changes in the rotation of the object, the direction of the rotation of the object doesn't change, but the direction of the projected image of the arrow on the rectangular plane of Figure 14 changes. Here it is noted that we didn't include τ in the simulation for this extended paper.

For simulating the vectors of the angular momentum, we used the cross product of anti-symmetrical vectors as the projection of the momentum vector in the perpendicular direction to the curved surface. It looks like Figure 15. The vectors of (43) are projected on the perpendicular plane with the sign of ρ in this figure. The calculated coefficients of (42) are the intensities of the angular momentum, shown in Figure 10 (Table 5) and Figure 11 (Table 6). If the speed changes in the rotation of the object, the direction of the rotation of the object doesn't change; but, the direction of the projected image of the arrow changes on the perpendicular plane for ρ of Figure 15.
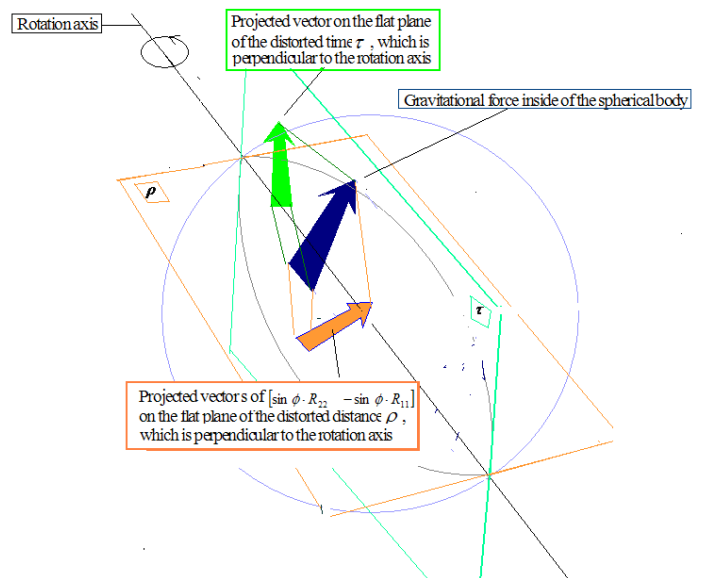
Figure 15: The vectors projected on the perpendicular components of the spherical surface

It is noted that we replaced the generally curved surface of Figure 13 by the spherical polar coordinate system as a surrogate for the simulation. And, we mocked the general movement of the curved surface by the rotation of the curved sphere as shown in Figure 15. In Figure 13, the perpendicular movement of the

generally curved surface is the movement in the light cone, and it is not necessarily the angular momentum. On the other hand, in Figure 15, the perpendicular movement of the spherical polar coordinate system appears as the angular momentum, only when the system rotates.

4. Conclusions and Recommendations

In this research, we investigated how the intensity and the direction change upon the gravitational energy and the angular momentum when the speed of the rotation of the artificial object changes, using Euler's rotation matrix by calculating the coefficients of the equation of motion, which is made of the curvature tensor with the component on the curved surface and the perpendicular component to the surface. The result of the simulation shows that the rotating object, in which time and space are nonlinearly distorted by the strong gravity, can produce the antigravity as the projected image on the curved surface, and change the direction of its angular momentum on the projected perpendicular image to the curves surface.

The change of the direction of the angular momentum upon the emerged antigravity implies our previous prediction [6] on the direction of the spin of anti-gravitational waves, in which anti-gravitational waves have the clockwise spin, while gravitational waves have the anti-clockwise spin. However, the conclusion has not been made on this issue because the analysis we described in [6] was made on the flat space, while we made the simulation in the spherical polar coordinate system for this extended paper. In addition, the discussion about gravitational waves is beyond the scope of this extended paper and it should be deferred to the other research; although, the similarity between the antigravity and the anti-gravitational waves may have been implied by the equation of gravitational waves, which is to be derived as the secondary differential of the equation for the gravitational field.

In addition, our simulation has challenged the limit of the general theory of relativity in its application to quantum mechanics, which is: the perpendicular movement to the generally curved surface could not satisfy the condition to solve the equation of motion. Henceforward the curved space was not used for setting quantum mechanics. However, we challenged this limit, by using the spherical polar coordinate system with the tensor algebra that makes the cross product of anti-symmetrical vectors for simulating the projection of the angular momentum in the perpendicular direction to the spherical surface.

In this research, we used the system of spherical polar coordinates as the surrogate of the generally curved surface; however, in the near future, the developed computer technologies must increase the possibility of simulating the generally curved surface of the Einstein's equations also for solving the equation of motion of quantum particles.

References

[1] Y. Matsuki, P.I. Bidyuk, "Theory and Simulation of Artificial Antigravity," 2020 IEEE 2nd International Conference on System Analysis Intelligent Computing, 2020, doi: 10.1109/SAIC51296.2020.9239195.

[2] Y. Matsuki, P.I. Bidyuk, "Empirical Analysis of Moon's Gravitational Wave and Earth's Global Warming," System Research & Information Technology, N1, 107-118, 2018, doi: 10.20535/SRIT.2308.8893.2018.1.09.

[3] Y. Matsuki, P.I. Bidyuk, "Analysis of Moon's Gravitational-Wave and Earth's Global Temperature: Influence of Time-Trend and Cyclic Change of Distance from Moon," System Research & Information Technology, N3, 19-30, 2018, doi: 10.20535/SRIT.2308.8893.2018.3.02.

[4] Y. Matsuki, P.I. Bidyuk, "Empirical Investigation on Influence of Moon's Gravitational-Field to Earth's Global Temperature," System Research & Information Technology, N2, 18-24, 2019, doi: 10.20535/SRIT.2308.8893.2019.2.02.

[5] Y. Matsuki, P.I. Bidyuk, "Calculating Energy Density and Spin Momentum Density of Moon's Gravitational-Waves in Rectilinear Coordinates," System Research & Information Technology, N3, 7-17, 2019, doi: 10.20535/SRIT.2308.8893.2019.3.01.

[6] Y. Matsuki, P.I. Bidyuk, "Analysis of Negative Flow of Gravitational Waves," System Research & Information Technology, N4, 7-18, 2019, doi: 10.20535/SRIT.2308.8893.2019.4.01.

[7] Y. Matsuki, P.I. Bidyuk, "Numerical Simulation of Gravitational Waves from a Black Hole, using Curvature Tensors," System Research & Information Technology, N1, 54-67, 2020, doi: 10.20535/SRIT.2308.8893.2020.1.05.

[8] P.A.M. Dirac, "General Theory of Relativity", New York: Florida University, A Wiley Inter-science Publication, John Wiley & Sons, 1975.

[9] H. Goldstein, C.P. Poole, J.L. Safko, Classical Mechanics, 3rd Edition published by Pearson Education. Inc., 2002.

[10] A.S. Goldberger, A Course in Econometrics, Harvard University Press, Cambridge, Massachusetts, USA, 1991.

[11] P.A.M. Dirac, Lectures on quantum mechanics, originally published by the Belfer Graduate School of Science, Yeshiva University, New York, 1964.

ASTES

Power Converters and EMS for Fuel Cells CCHP Applications: A Structural and Extended Review

Nganyang Paul Bayendang*, Mohamed Tariq Kahn, Vipin Balyan

Department of Electrical, Electronic and Computer Engineering (DEECE), Cape Peninsula University of Technology (CPUT), Bellville, Cape Town, 7535, South Africa

A B S T R A C T

Fuel Cells (FCs) and Combined Cooling, Heating and Power (CCHP) systems are becoming very popular due to their environmental friendliness and immense applications. This extended review paper commenced by introducing the rampant South Africa's electricity crisis as the basis for the study, followed by some structural analyses of up to forty-four miscellaneous power electronics converters case studies applicable to fuel cells including at least sixteen FCs energy management systems (EMS) applicable case studies. The review rationale is to determine innovative best practices that can be applied to devise an efficient power converter and EMS for an energy efficient FC CCHP system. From these analyses, it is realized that each power converter and EMS scheme has its merits and demerits depending on the targeted applications and most importantly the research project objectives − that is, whether the goals are to reduce costs, enhance efficiency, reduce size, boost performance, simplicity, durability, reliability, safety etc. Therefore, the conclusion drawn is, there is no "one size fits all" approach, as all the various reviewed case studies reported relatively good results based on their chosen schemes for their targeted applications. Notwithstanding, this review highlights are, i) the interleaved boost converter and variants as well as ii) the maximum power point tracking (MPPT) technique; are the most widely used schemes, as they are reasonably effective and simple to implement. The contributions brought forward are i) an apt single reference study that presents a quick topological insight and synopsis of assorted FCs power converters as well as EMS and ii) our proffered FC CCHP system undergoing research to offer an innovative energy efficient solution for basic household energy needs such as electricity, heating, cooling and lighting.

1. Introduction

Compounded with re-occurring electrical energy and power problems in South Africa and at large Africa; this extended article to [1], extensively investigates with emphasis on fuel cells (FCs), some assorted research on power converters and energy management systems / storage (EMSs) techniques. Currently, there's up to 2 hours of daily electricity rolling blackouts in South Africa (RSA), due to RSA national energy utility company (ESKOM) inability to generate enough energy to meet its local electricity demands. This is due to the legacy apartheid energy system being over-stretched with more underprivileged areas / users now having access to electricity, old energy infrastructures being upgraded, poorly designed and in-efficient new energy infrastructures, poor technical maintenance, inadequate technical abilities, corruption as well as illicit business and political reasons.

Thus, various optional renewable energy sources, especially solar and wind powers are being commissioned to augment and or stabilize RSA national grid supply and also for personal use. Alternative energy sources such as i) FCs − which produce power and heat as well as water when fueled with H_2 and O_2 and ii) thermo-electricity − which simply generates a) electricity based-on Seebeck effect and b) heat / cold based-on Peltier effect, are of interests. In this regard, our research focuses on FCs and thermo-electricity; however, these clean energy sources need supporting technologies and techniques to operate well. In light of this, we review applicable best practices that can be developed to execute an energy efficient fuel cell alternative power / energy system for domestic and commercial combined cooling, heating and power (CCHP) applications − since electricity, heat / cold and light are the most commonly used forms of energy in most homes in RSA. FCs CCHP systems are versatile, clean and becoming very trendy;

*Corresponding Author: NP Bayendang, CPUT DEECE, +27765404896, bayendangn@cput.ac.za

thus, discussed next are miscellaneous power converters and EMS research applicable to FCs and by extension FC CCHP systems.

A fuel cell stack closed-circuit voltage is a function of the FC activation, concentration and Ohmic losses governed by the Nernst equation. This FC loaded condition draws more current resulting to a voltage dip/drop as a result of delay of Hydrogen / Oxygen flow and this phenomenon is called the fuel cell fuel starvation. This voltage drop and the load current together with other FC parameters, establish the degree and duration of the problem. This issue is tackled diversely as analyzed briefly in [1].

In [1]-[36], DC-DC power converters are paramount to either boost and or reduce DC power sources (e.g FCs) and then sustain a consistent power thereafter. FCs typically produce low DC voltage but high current, which combined with the possibility to fluctuate when connected to a load, demands power regulations to the DC bus and ultimately to the different DC and or AC loads.

In DC-DC power converters, with the exception of linear regulators, the fundamental three switching kinds are the step-down, step-up and step-up / step-down − from which various and or improved versions are derived to give isolated derivatives with one or multiple switches including the soft-switching versions.

The voltage output from step-down DC-DC power converters, is always lesser than its voltage input. Contrarily, the voltage output from a step-up DC-DC converter is always more than its voltage input. The step-down / step-up power converter based-on its duty cycle value; can respectively either lower (duty cycle < 0.5) or increment (duty cycle > 0.5) the converter voltage output.

As per [37]-[70], EMSs are essential to manage the power converters to ensure maximum power is transferred to the load, the bus is stable and the energy / power supply system is efficient.

2. Power Converters

Power converters are required to buck, boost and provide regulated voltage to the DC bus. In what follows and summarized in Table 1, are miscellaneous case studies that structurally analyzed in brief details, some power converters for use with FCs.

2.1. DC-DC Power Converters Architectures for Fuel Cells Applications

As presented in [23], power sources based on fuel cells are now trendy devices. They offer reliability, flexibility as well as efficiency through multi-stack topologies. To access the market requires simplifying further the FCs design and its supporting components, which among others include the power converters which ensure the output voltage is regulated. Their research thus focused on DC-DC power converters by giving an inclusive outline on the interfaces of power converters for use in aircraft, railways, automotive and small static areas such as households.

The significance of selecting the correct power converters topology and the related technology is crucial, as its facets allow thermal compatibility with various methods for integrating the DC-DC power converters to the fuel cells. These topological and technological features that have been examined and displayed in Figures 1a -1f with highlights in Figures 1e -1f, are some popular

power converters topologies. In their study, they indicated how connecting a fuel cell stack / DC-DC power converters in parallel and in series increase the current and voltage outputs respectively.
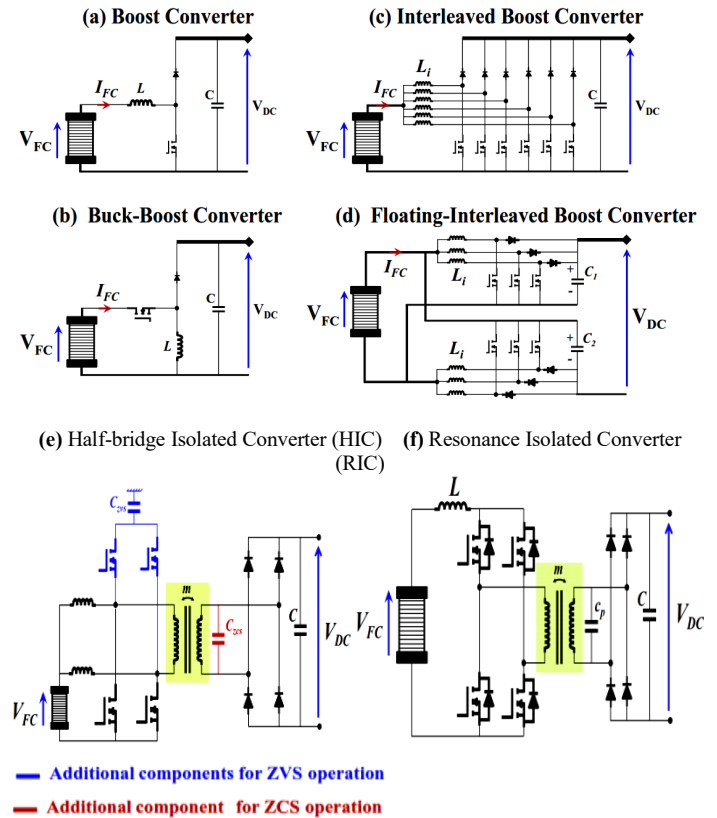
Figure 1: DC-DC Power Converters Architectures for Fuel Cells Applications (adapted from [23])

Explained in their research and portrayed in Figures 1c and 1d, are non-isolated multi-phase boost converters, which are mainly appropriate for applications that require low DC bus voltage. The interleaved topologies shown, meet the prerequisite for curbing low FC ripple currents. The depicted standard interleaved boost converter (IBC) shown in Figure 1c and the floating interleaved converter (FIC) in Figure 1d, show similar merits. Z-sources inverters (ZSI) were also articulated, in which their features and merits make them suitable choices for 3-phase electric drives − for instance automotive / railway applications. Furthermore, the study indicated that the isolated converters based-on high frequency planar transformer (which according to [23], only one quantity was left in the market in 2014), is beneficial in high DC link voltage applications such as railway. Contrarily, the isolated converters give a low efficiency for medium power applications. However, the soft-switching function enables the enhancement of the converter efficiency but at the cost of using supplementary components in the converter configurations. These improvements are shown in Figures 1e and 1f − whereby the half-bridge isolated converter (HIC) and the current-fed full-bridge resonant isolated converter (RIC), respectively illustrate the zero-voltage switching (ZVS) and zero current switching (ZCS) operations, in which both increase the efficiency by reducing the devices switching losses. The technological review on the other hand focused on the new wideband-gap semiconductor materials and the utilization of Silicon Carbide (SiC) and Gallium Nitride (GaN) devices with low

on-resistance, high power densities and high speed switching with less losses, which could transcend to major improvements in the power converters performance. Nowadays, GaN devices are suited for low/mid power applications, whereas SiC technology is more desirable for designing high power FCs DC-DC converters.

2.2. State-of-the-Art Fuel Cells DC-DC Converters

According to [13], fuel cells are current intensive sources that have become popular. The study presented various suitable topologies of DC-DC power converters for FCs output voltage conditioning. The goal of the main DC-DC power converter between the FC and DC bus was emphasized, which demands the power converter be designed/operated using high efficiency, high voltage ratio and high density with low-cost. As a result, their paper highlighted some tips in this regard as well as the positives and negatives. Some of the schemes are shown in Figures 2a - 2c.
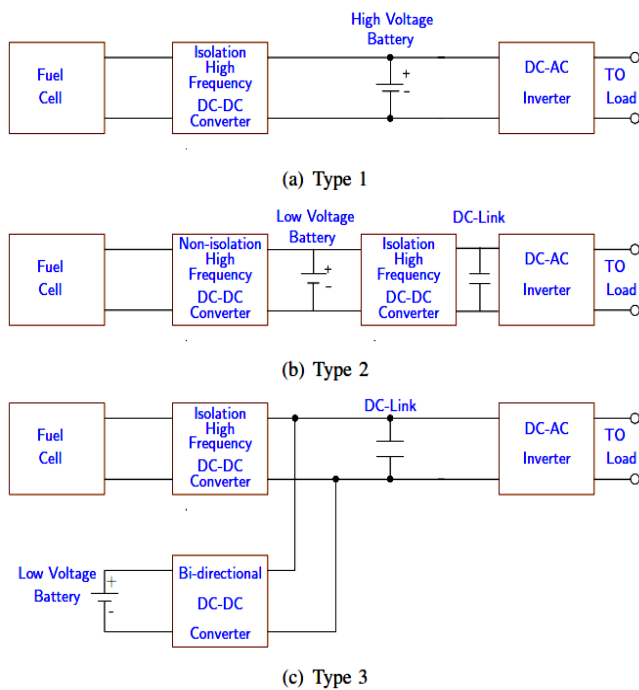
Figure 2: Fuel Cells DC-DC Power Converters (adapted from [13])

2.3. A Soft Switched Push-pull Current-fed Converter for FC Applications

Examined in [14], a zero-voltage switching (ZVS) current-fed push pull DC–DC converter is suggested for fuel cells power generation system as pictured in Figure 3. In the study, the auxiliary circuit in this converter supplies ZVS condition for all converter switches which reduces switching losses and further absorbs at turnoff instances, the voltage surge across the switches.

This merit, enhances the converter efficiency and reduces the size and converter weight – which henceforth enables the implementation of a very simple control circuit based on pulse width modulation (PWM). This setup was then used to analyse and validate the operation of the converter using a lab prototype. The projected DC-DC power converter experimental results, the various operating modes as well as their corresponding timing waveforms, are presented in detailed in their published paper.
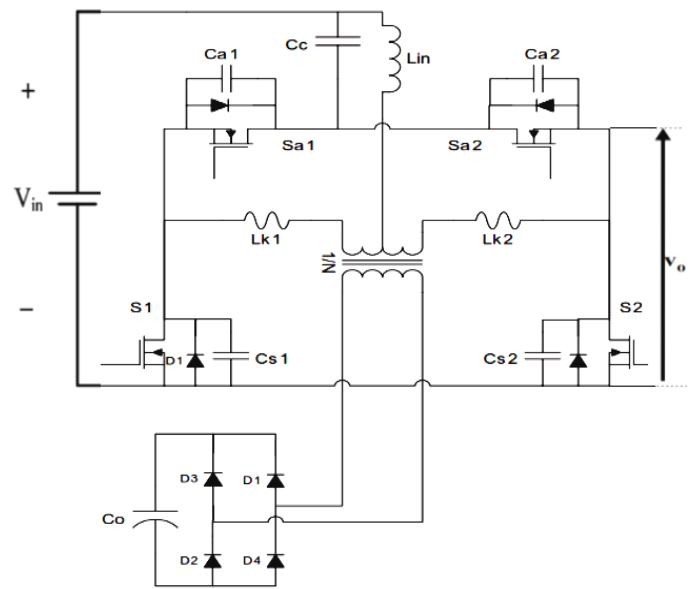
Figure 3: The Proposed Soft Switched Push-pull Current-fed Converter (adapted from [14])

2.4. Topology of FC Hybrid Power Source for Efficient Operation and High Reliability

Proposed in [15], is a fuel cell hybrid power source (HPS) topology with the attribute to curb the ripple current of the FC inverter system. The ripple current usually occurs at the DC port of the FC HPS when operating the inverter system − which is connected to the grid or which supplies AC motors in vehicular applications. As a result, if the alleviation measures are not implemented, this ripple current is propagated back to the FC stack. The suggested FC HPS has other good performance features; such as the maximum power point tracking (MPPT), high steadfastness in operation during transient power pulses and finally improved energy efficiency in peak power applications.
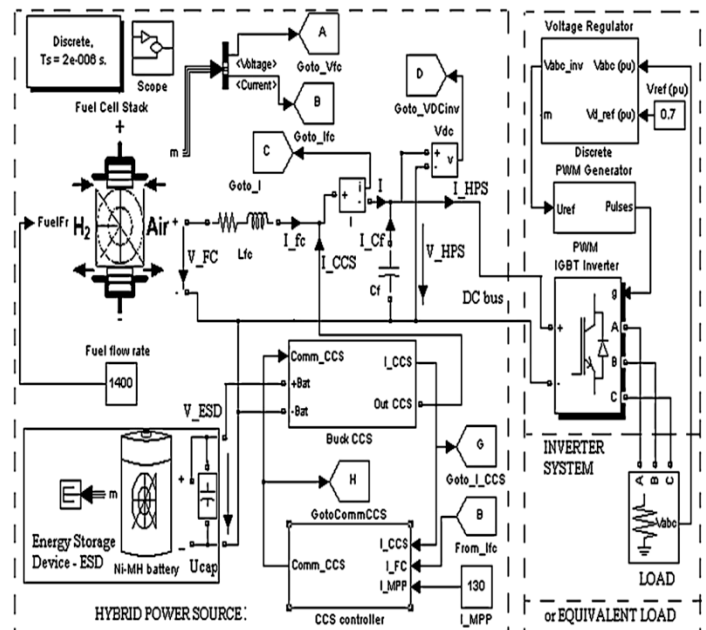
Figure 4: The Proposed Hybrid Power Source Topology (adapted from [15])

To mitigate the ripple, this approach made use of an inverter system powered directly from the FC stack with a controlled buck current source that was used as the low power source. The low frequency (LF) ripple reduction is rooted in active control, whereby the anti-ripple current is injected in HPS output node and this has the LF power spectrum similar to the inverter ripple. In light of this, the fuel cell ripple current was curbed by the designed active control. Indicators defined to evaluate the mitigation ratio of the LF harmonics were used to assess the ripple current alleviation performances. The relatively good performances shown were attained with the use of a hysteresis current control, but better if a devoted nonlinear controller is used, which can be designed in two ways as follows i) simulation trials that assist to draw the attributes of ripple mitigation ratio verse fuel cell ripple current and ii) fuzzy logic controller (FLC). The ripple factor was ~ 1% in both cases. Figure 4 depicts the study.

2.5. Power Flow Control Methods for Ultra-capacitor Bidirectional Converter in DC Micro-grid

Postulated in [16], distributed generation (DG) in the form of DC micro-grids depicted in Figure 5a, has recently attracted increasing research interests. A bidirectional DC-DC converter (BDC) shown in Figure 5b, is required to incorporate renewable energy resources and energy storage devices such as an ultra-capacitor (UC) to the DC bus of a DC micro-grid to sustain the charging and discharging states of the ultra-capacitor. For the quick dynamic response of the ultra-capacitor, a bidirectional voltage-fed setup is suitable, though for a broad input voltage fluctuation of the ultra-capacitor, this setup manifests a greater circulating power flow and greater conduction losses in the end. Presented in this study are a comprehensive overview on the numerous modulation schemes that are employed to manage the power flow of the bidirectional voltage-fed DC-DC converter for the ultra-capacitor applications. An in-depth analysis of the bidirectional converter investigating the impact of the circulating power flow interval was developed and analytical methods such as the conventional phase-shift control (CPC) modulation were applied to develop alternative modulation schemes to advance the efficiency and performance of the bidirectional power converter.
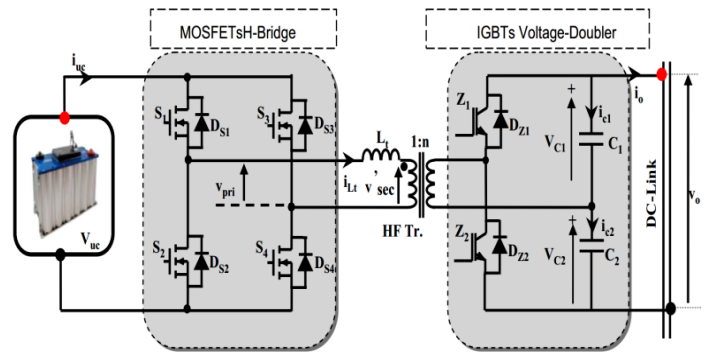
Figure 5 (b): BDC Power Flow Control Methods for Ultra-capacitor in DC Micro-grid (adapted from [16])

2.6. Fuel Cell and Power Converter Models in MatLab / Simulink

Studied in [19], MatLab and Simulink were employed to model a power converter and PEM FC. Depicted in Figure 6, the first section of the research discussed the methodology for an accurate model for the fuel cell stack, as well as its static and dynamic behaviors − which form a crucial aspect in the design of electrical power generation founded on fuel cells. The technique applied was simulated annealing (SA) optimization algorithm, which justifies its customization to meet the goal of a speedy convergence to institute the correct values for the fuel cell parameters. The correlation between the simulation and the experimental results proved that the suggested model provided an accurate depiction of the static and dynamic behaviors for the PEM FC. The second section of the study engaged on feasible architectures that can be tailored for the DC-DC power converter.

The preferred topology must be suitable to take control and optimize the operation point of the fuel cell; as a result, the soft switching attests to be particularly fitting, especially the series resonant topology converters − because it reduces the switching losses and consequently increasing the efficiency. This converter execution can be explained as follows: the supplied voltage by the stack, which is normally low (29V - 42V), is changed to a constant and high amplitude, in this case, a 400VDC bus is used to generate power to the grid via an inverter. The high frequency (HF) transformer is a boost voltage transformer, which is as well used to offer galvanic isolation between the low and high voltage levels of the circuits. In the primary side of the transformer, the resonant converter with its inductor-capacitor (LC) series resonant circuit, provides the sinusoidal waveforms of voltage and current. The circuit resonant frequency is determined by choosing suitable values for the L and C elements, from which the FC DC voltage is initially inverted to AC in the primary side of the HF transformer and then rectified to DC on the secondary side. The PEM FC is protected from the ripple voltage and current the converter produces by the LC filter in the primary side, which as well stores the DC bus energy. The secondary side LC filter reduces the ripple voltage and current to the load. In conclusion, the simulation results were correlated using actual data acquired from a commercial system. As a result, it was justified that, the hybridization of a suitable power converter using a well-defined controller in conjunction with a well-optimized FC stack model, makes FC good for power generation.
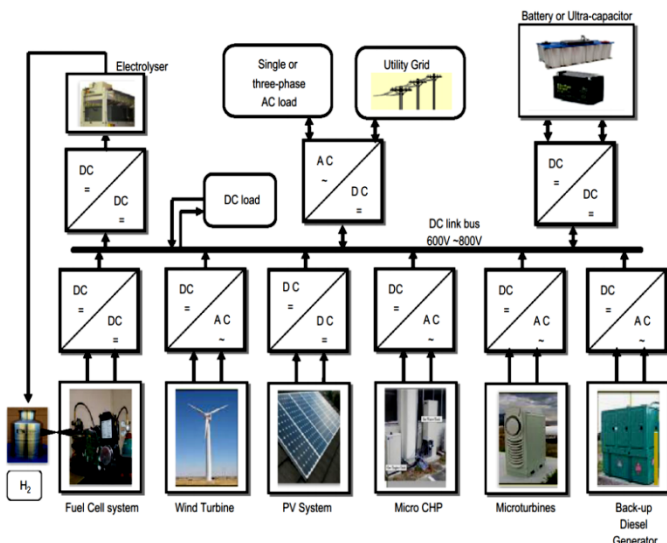
Figure 5 (a): DC Micro-grid Distributed Generation (adapted from [16])
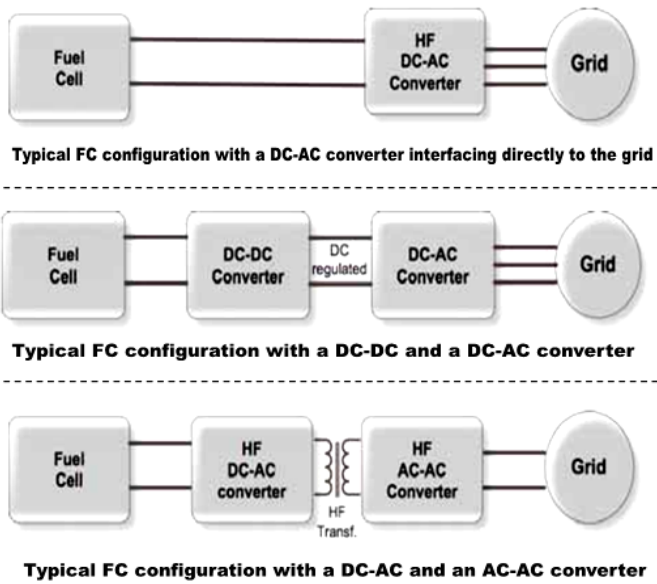
Figure 6: FC Power Converter Models in MatLab / Simulink (adapted from [19])

2.7. High Voltage DC-DC Boost Converter Suitable for Varying DC Voltage Sources

Researched in [11], is a high voltage step-up converter appropriate for varying voltage sources such as photovoltaic (PV) and by extension fuel cells as well as thermo-electric generators (TEGs). Different varying voltage boost sources were assessed to institutes their limits, from which a multi-phase tapped-coupled inductor DC-DC boost converter that can attain high voltage boost ratios from a variable power supply (PV in this case) and without adversely compromising the performance, was then postulated as pictured in Figure 7. The suggested converter achieved minimal voltage and current ripples at both the input and output as well as exhibited reasonable performance at high power levels making it preferred for high power applications. The simulated and practical results correlated to confirm the research.
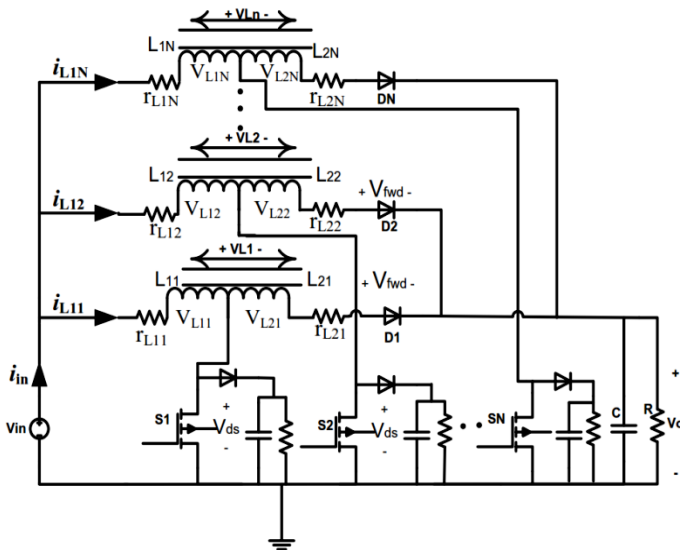
Figure 7: High Voltage DC-DC Boost Converter Suitable for Varying Voltage Sources (adapted from [11])

2.8. High Power Efficient DC-DC Buck Converter Suitable for Varying Voltage Sources

According to [10], in a varying power generation source such as wind (likewise solar-cells and TEGs as well as fuel cells), the power converter efficiency is one of the crucial aspects for the performance of the system. In such systems, the DC-DC step-down converter is usually used for high power systems. Taking into account the cost and efficiency of a converter, their research focus was mainly on the devise of enhanced buck converter topologies with interest on the (inductor, capacitor and diode) LCD converter depicted in Figure 8a – which is to be used for a peak power standalone wind power generation system. A (resistor, capacitor and diode) RCD and an improved RCD buck converter could also remove the voltage spikes; however, it unfortunately further depletes the stored voltage amplitude when the power is switched-off − this is because C_1 discharges the voltage stored through R_1. Therefore, the need for a LCD version.
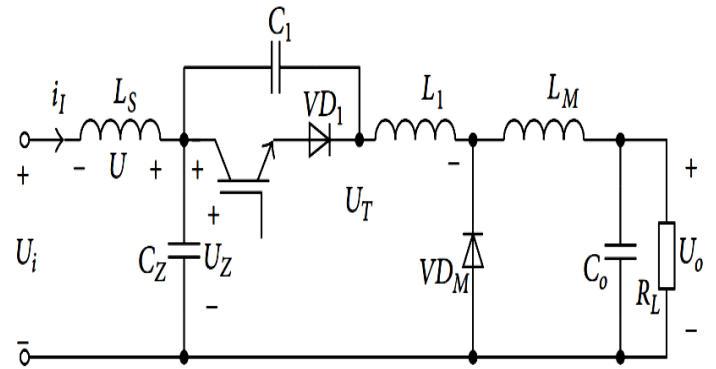
Figure 8 (a): High Power Efficiency DC-DC Buck Converter Suitable for Varying Voltage Sources (adapted from [10])
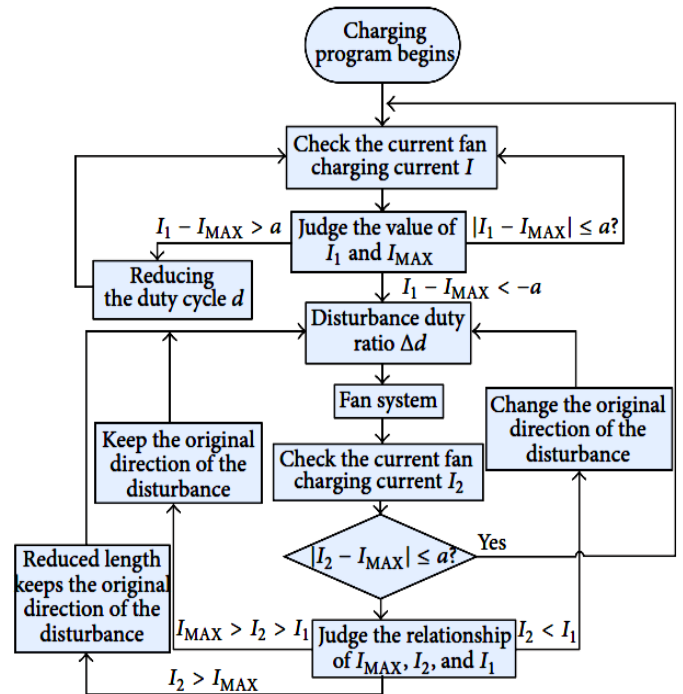
Figure 8 (b): DC-DC Buck Converter Climbing Mountain MTTP Algorithm Flowchart for Varying Voltage Sources (adapted from [10])

This issue was addressed by using a better improved LCD buck converter as shown in Figure 8a. This version does not have any resistor but an inductor with negligible energy loss as displayed in the test result. This LCD architecture is also known as zero-voltage switching (ZVS). At resonance, L_1 and C_1 cancel out, reducing the voltage spike and increasing the switching speed. The practical designed LCD converter is based-on Figure 8a and instead of IGBTs, it uses multi-MOSFETs in parallel to boost the current and the switching speed of the converter. By employing MPPT, the practical utmost efficiency of the designed 2kW DC - DC step-down converter was approximately 96%.

MPPT algorithm ensures the maximum power generated stays constant by monitoring the desired reference output with the generated output and adjusting the duty cycle or PWM signal to the active switch(es) of the power converter. The common MPPT techniques according to [10], includes i) optimum tip speed ratio, ii) power curve control and iii) climbing mountain – the latter was used in the study and its flowchart is illustrated in Figure 8 b.

2.9. High Gain IBC for Fuel Cells Applications

As researched by [9], distributed generation most capable technologies is fuel cell and to design a high efficiency power system using fuel cell, a fitting DC-DC converter is necessary. Among the different DC-DC converters, interleaved converters with switched capacitor are considered a preferred topology for FC systems because of reduced ripple currents in the input and output circuits, quicker transient reaction, small electromagnetic emissions, enhanced efficiency and reliability. This improved conversion efficiency is attained by dividing the output current into 'n' parts, to significantly eliminate I^2R losses and inductor losses. The research aim was to devise and implement a high gain interleaved boost converter based-on switched capacitors (to improve converter voltage gain) for fuel cell systems. In the interleaved converter proposed, the front-end inductors are magnetically cross-coupled to enhance the electrical performance and reduce the weight and size. By using switched capacitors interfaced with FCs, MatLab and Simulink were used to simulate an interleaved converter, from which a prototype was developed to validate the simulation results. Figure 9 depicts the IBC.
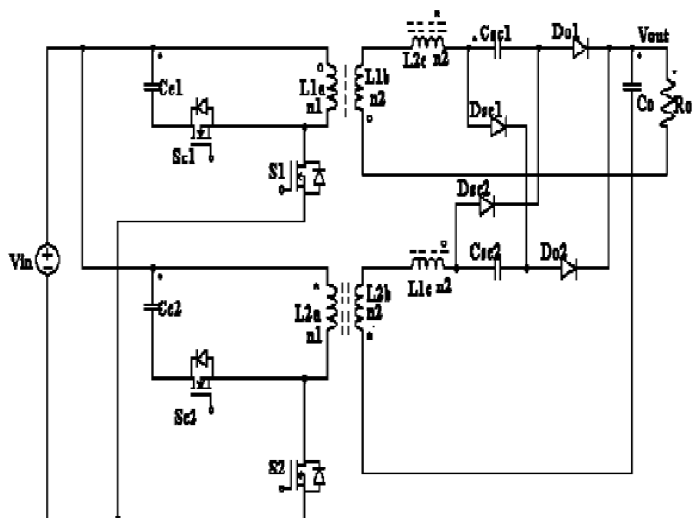
Figure 9: High Gain IBC for Fuel Cells Applications (adapted from [9])

2.10. High Efficiency Isolated Boost Converters for High-Power Low-Voltage FC Uses

As investigated in [8], fuel cells power systems, as portrayed in Figure 10a, show significant output impedance which reduces the output voltage with increased in the output power; as a result, system peak power is attained at converter smallest input voltage. In light of this, a new low-leakage inductance low-resistance to low-voltage high-power isolated boost converter design technique, was presented as shown in Figure 10b. By optimizing the transformer design and circuit lay-out, very low levels of parasitic circuit inductance were attained. Power MOSFETs fully rated for recurring avalanche, were used to eliminate primary side voltage clamp circuits and switch on-state losses. Furthermore, extensive interleaving of the primary and secondary transformer windings, reduced the transformer proximity effect losses.

Silicon Carbide rectifying diodes are not prone to reverse recovery and therefore allow fast diode turn-off, hence were used to further reduce losses. As illustrated in the study, test results from a 1.5kW full-bridge step-up converter confirmed theoretical analysis and demonstrated a very high efficiency. The maximum efficiency was up to 98% whereas the worst-case efficiency with maximum power and at minimum input voltage was ~ 96.8%.
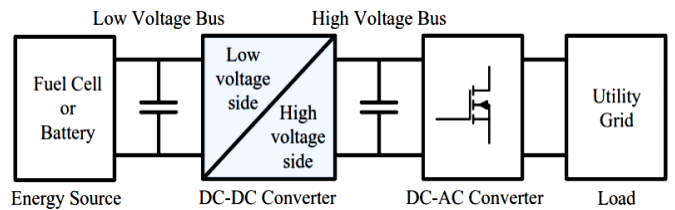
Figure 10 (a): Fuel Cell Power Supply System (adapted from [8])
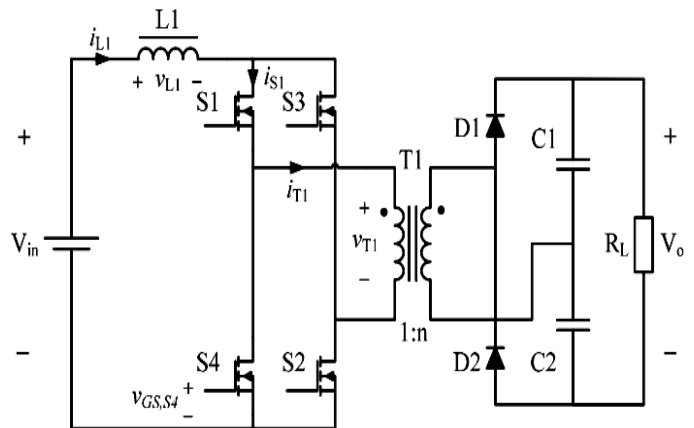
Figure 10 (b): FC High-Power Low-Voltage High Efficiency Isolated Boost Converters (adapted from [8])

2.11. High Power Buck-Boost DC-DC Converters: Automotive Power-train Applications

Investigated in [12], is a high-power buck-boost DC-DC converter for use in the power-trains of hybrid cars as shown in Figures 11a and 11b. To enable smooth transitions between both energy transfer directions, a special digital control strategy was implemented. Equipped with this feature, the converter can obtain the energy management in the electric power-train.

The digital control provides full protection against over-voltage, over-current and over-temperature. Two efficient prototypes of 24kW and 70kW bidirectional (buck-boost) DC-DC converters were developed and evaluated. The presented measurements show that higher voltages for the power-train and storage battery assure higher efficiency due to lower current losses by the use of IGBTs. Using integrated liquid cooling of up to 85°C with very low losses, a high-power density of up to 5W/cm³ was achieved. Characterization data of the converter and measurements in the target application (a hybrid fuel cell car) with test parameters and values of passive components used, are shown in the study as well as what happens when the converter transits from boost to buck mode. Finally, presented in the full manuscript are voltage and current dynamics as well as the efficiencies and output power in the various operation modes.
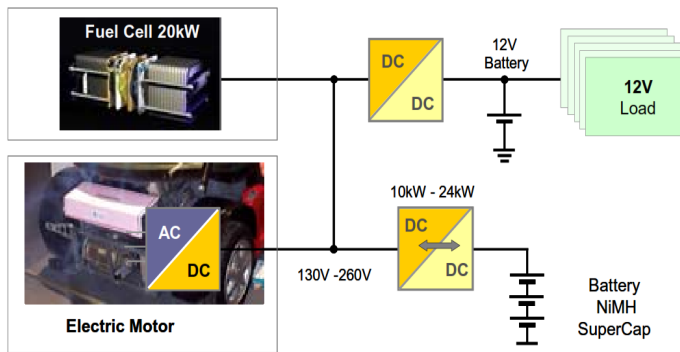
Figure 11 (a): Concept Overview (adapted from [12])
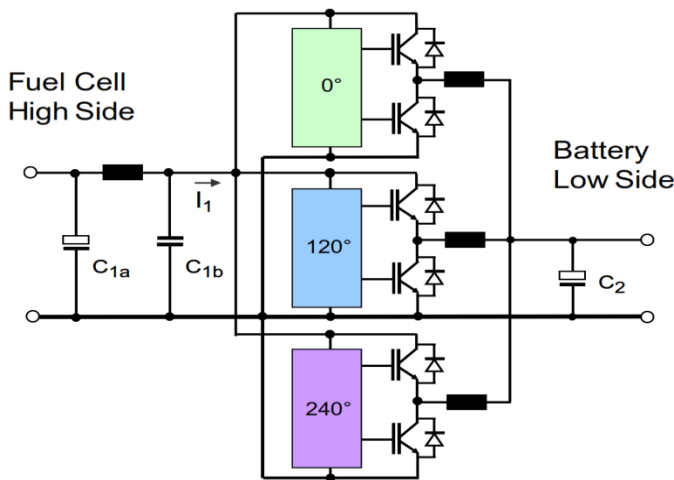
Figure 11 (b): High Power Buck-Boost DC-DC Converters: Automotive Power-train Applications (adapted from [12])

2.12. PEM FC System with DC-DC Boost Converter: Design, Modelling and Simulation

Indicated in [3], fuel cells as exemplified in Figure 12a, are regarded as one of the most proficient devices for standalone and grid connected distributed generations (DGs), due to their environmental friendliness, modularity and high energy potential capability. The drawbacks in the extensive use of FCs are their i) sluggish dynamic response to abrupt load changes and ii) costly installation. Their research focused on the simulation of dynamic behaviour of a Nexa 1.2kW PEM FC using DC-DC step-up converter, which was correlated with cascaded 2-stack FC model.

The performance of the basic DC-DC boost converter as power converter for the Nexa TM 1.2kW PEM FC model was analyzed for changing loads to manage the power flow for improved performance. As the FC pressure or temperature rises, the power density of the FC stack also increases for rising loads; therefore, to analyse this dynamic behaviour for changes against temperature, an advanced parametric model based on circuit simulator PSpice for a class of PEM FC was also developed in addition to the fuel cell models based on thermodynamics and electrochemical equations. The fuel cell performance is governed by its electrical and thermal efficiencies − the electrical efficiency of the fuel cell relies on the fuel cell activation and concentration losses besides the natural Joule heating (Ohmic loss), whereas the thermodynamic efficiency relies on the fuel cell fuel processing, water management and the fuel cell system's temperature control.
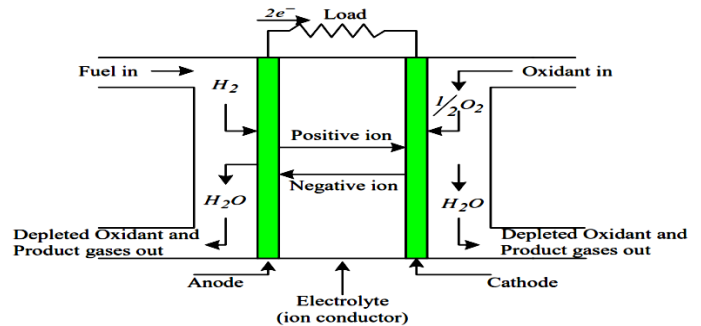
Figure 12 (a): Fuel Cell Overview (adapted from [3])
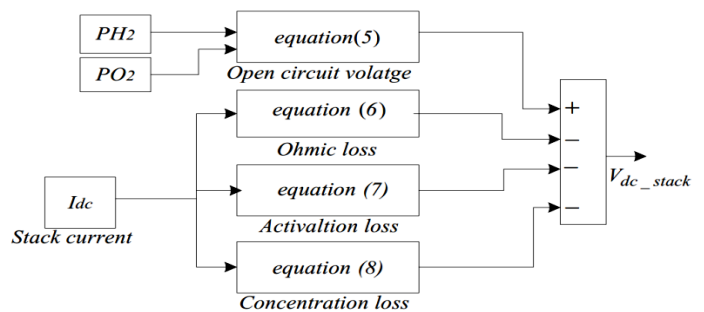
Figure 12 (b): PEM FC System with DC-DC Boost Converter: Design, Modeling and Simulation (adapted from [3])

All these factors were taken into consideration when the design was done using Matlab / Simulink as in Figure 12b. It was noticed that for instantaneous loads variation from 0.6 - 1.1kW, the fuel cell current and voltage took about 50 - 70ms to attain a new steady state. This delay is known as the fuel cell fuel starvation phenomenon – this makes the fuel cells non-linear and should not be operated, because the electrolyte membrane of the FC can be destroyed. The FCs must be operated only in its linear region. The DC-DC converter used was a basic boost converter with PI controller, which gave better performance for load variations without using any storage devices. A constant bus voltage of 80V was maintained in the converter output, regardless of changes in the load and fuel cell terminal voltages. Steady state error was reduced to zero by the PI controller. In their conclusion, operating fuel cells with a basic step-up converter using PI controller, can give better performance for standalone / grid connected low power applications. This claim is evident in the measured and simulated results shown in their full research paper.

2.13. Methodology to Design FC Based Systems Power Converters: A Resonant Approach

Presented in [6], is the evaluation, devise and implementation of a fuel cell-based power generation scheme, which necessitates suitable selection of i) the FC model and ii) the power electronics converters shown in Figure 13a. The fuel cell model used is semi-empirical based on PEM FC Mark 1020 with static and dynamic properties as well as the FC limited current and voltage supply ratings − irrespective of the converter used. The power converter employed a resonant technique that provides high frequency operation, minimal component stresses, soft switching etc.

The power converter controller was split into two functions, namely: i) the voltage controller − which stabilizes the converter output voltage during loading fluctuations and ii) the PEM controller − which enhances the performance by maintaining the PEM FC in its optimal point of operation. The outcome confirmed that the researched converter is a good choice to enhance the efficiency of a PEM FC, because it permits a sufficient control of the power delivered by the fuel cell while sustaining the requirements dictated by the load to maximize the gains with soft-switching control. The FC DC is converted either to DC then to AC (DC-DC-AC) or FC DC to direct AC or FC DC to DC and AC-AC isolated by a transformer. The operation mode of the DC power conversion can be divided into i) linear, ii) switching and iii) soft-switching or resonant. The four non-isolation buck, boost, buck-boost and Cuk converters can be respectively converted to forward, boost, flyback and Cuk; by adding isolation transformer and when the isolation converters use more than a switch; it could be a push-pull, half bridge or full bridge as portrayed in Figure 13b. The results showed that the chosen power converter is suitable to improve the PEM FC efficiency, as it allows proper control of the power delivered by the FC, by satisfying the criteria enforced by the load regulation with minimal losses as a result of adopting soft switching.

Figure 13 (a): DC-DC Converters Overview (adapted from [6])
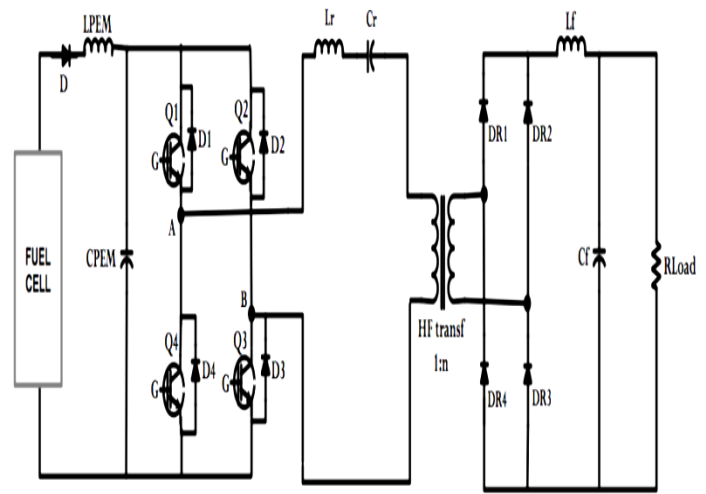
Figure 13 (b): Methodology to Design FC Based Power Converters Systems: A Resonant Approach (adapted from [6])

2.14. Design and Control of a 6-phase IBC Based-on SiC Semiconductors with EIS Functionality for Fuel Cell Electric Vehicle

Researched by [20] indicates that, in today's FC Electric Vehicle (FCEV), DC-DC converter is paramount to step-up the PEM FC output voltage to a high level (400 - 700V). As a result, the research aim was to design a 6-phase IBC based on SiC semiconductors and inverse coupled inductors of cyclic cascade structure having high compactness, high efficiency and high voltage gain ratio. The reliability and durability have to be enhanced to advance the consumption and commercialization of FC technologies. Electrochemical Impedance Spectroscopy (EIS) is typically used for PEM FC's diagnosis. To eliminate additional equipment and sensor, the on-line EIS detection functionality incorporated with the control technique of the suggested PEM FC linked to the DC-DC step-up converter was also investigated. The interleaved topology helped decreased the FC current ripple to ensure an extended FC lifespan. Furthermore, the multi-phase topology shared the high input current, hence reducing Joule heating, which allays the electrical stress of the power switches; thus, this redundancy ensures the reliability and robustness of the converter. The magnetic core design is also critical, as it controls the amount of ripple; as a result, the three types Uncoupled (UC)-IBC, Direct Coupled (DC)-IBC, and Inverse Coupled (IC)-IBC were experimented. The SiC-based semiconductors increased the switching frequency and decreased power losses. The on-line EIS detection functionality was integrated with sliding mode control (SMC) of the postulated DC-DC step-up converter. Fuel cells most common problems of membrane drying and flooding were estimated based on PEM FC's equivalent electric circuit model. The real-time hardware-in-the-loop (HIL) validation of the proposed converter was achieved. MicroLabBox (embedded real-time processor with (Field Programmable Gate Array (FPGA)), was used as the real-time platform for prototyping. In all, a 21kW PEM FC's voltage model was developed as the power source and the HIL framework provided in real-time − a benefit to monitor the converter's dynamic working process that was not viable with the offline simulation. Figures 14a-14c summarize the study.
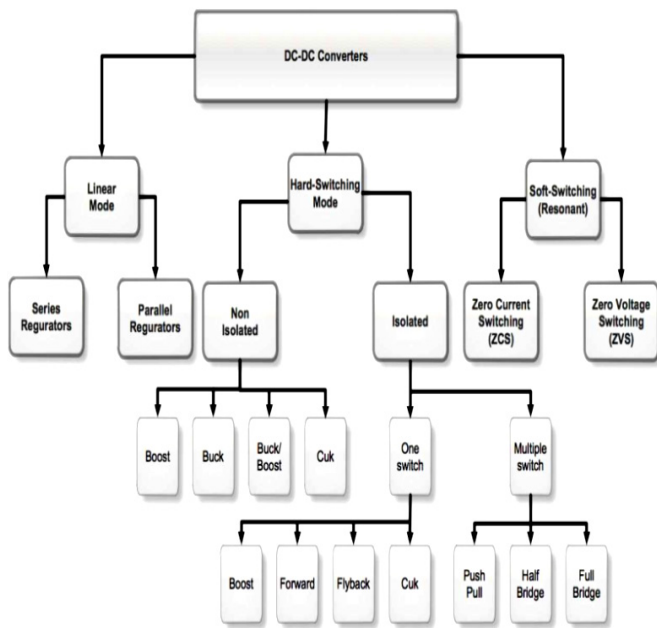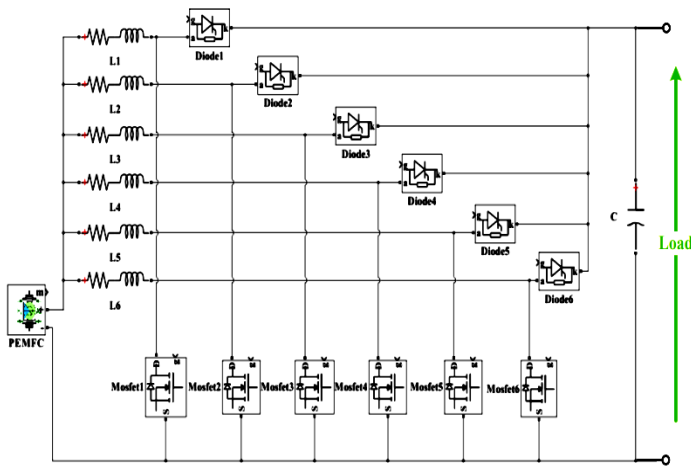
(a). 6-phase IBC (UC-IBC)
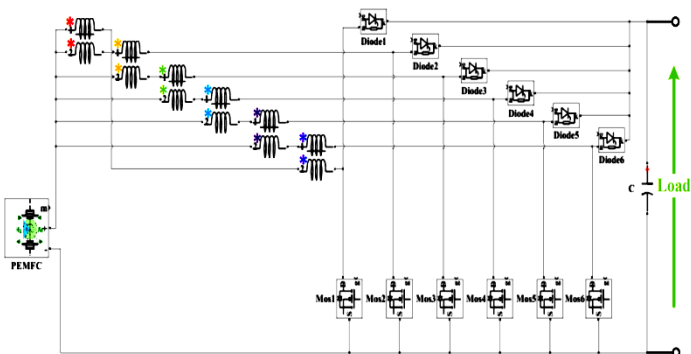
(b). 6-hase IBC based on direct coupled inductor of cyclic cascade structure (DC-IBC)
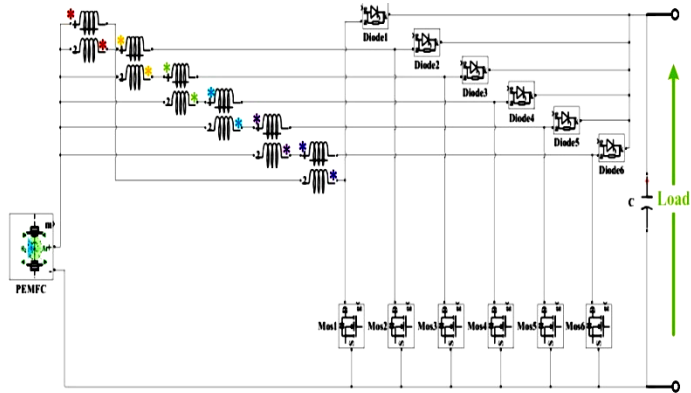
(c). 6-hase IBC based on inverse coupled inductor of cyclic cascade structure (IC-IBC)

Figure 14: Six-phase IBC Based on SiC Semiconductors with EIS (adapted from [20])

2.15. Design Considerations for DC-DC Converters in Fuel Cells Systems

As examined in [4], the development of alternative energy sources, has been improved by the fast increase of fossil fuel costs along with a rise in environmental education – which include but unlimited to FCs, wind, solar and ocean tidal-wave power. Among them, FCs due to their high modularity, efficiency and basic design have received increased interests in recent years. However,

their low voltage output and wide variation from unloaded to fully loaded, demands the need of a power converter to interface the FC to its loads. In light of this, their research was undertaken, in which design considerations were attained analytically and experimentally verified to enable an efficient and stable fuel cell as well as power converter system. Further to the design guidelines, investigated also were new power converter layouts that do not need the use of transformers to accomplish a large voltage gain. The general outcomes are means of i) mathematical analysis and ii) experimental prototypes, that contributed to the lessening of the cost and size of the power converter as well as to raise the efficiency of the system. It was discovered that when the FC load current is not purely DC, the Hydrogen usage of the stack increased and the power output of the FC decreased. This effect importance is a function of the ripple current frequency as demonstrated in their full research.
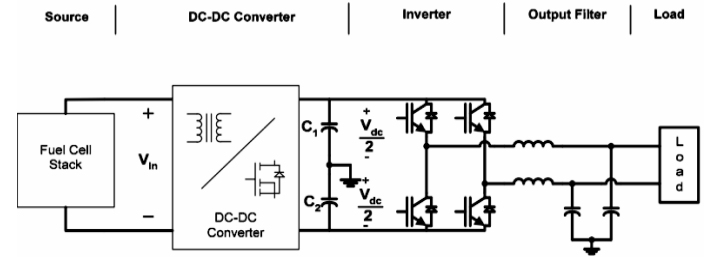
(a) Typical fuel cell power conversion system for residential applications
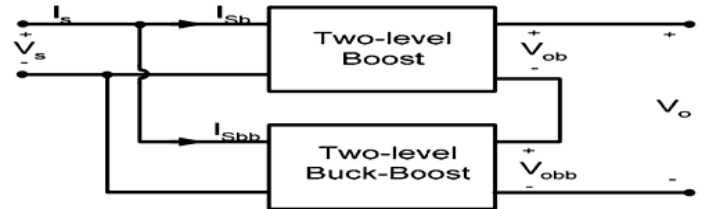
(b) Block diagram of the proposed DC-DC converter
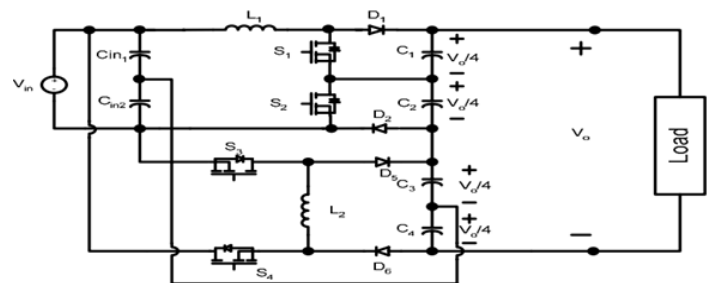
(c) Circuit schematic of the proposed two level boost and buck-boost converter
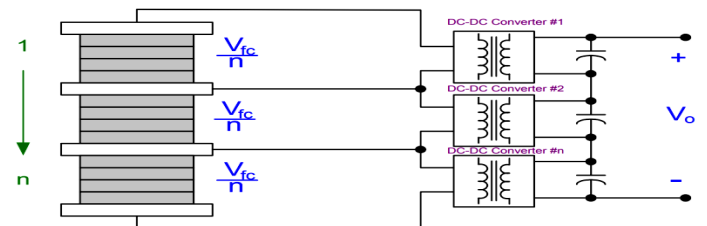
(d) Proposed sectioned / taped FC stacked with modular DC-DC converter

Figure 15: Design Considerations for DC-DC Converters in FCs Systems (adapted from [4])

Furthermore, by using analytical and experimental methods, it was demonstrated that for load currents with low frequency ripple (<1kHz), the Hydrogen usage increased up to 7% whereas the power output of the FC decreased up to 30%. In addition, if the frequency of the ripple current is high, >20kHz, the Hydrogen utilized by the FC also increased in the range from 1 - 3%, whereas its power output dropped by 5%. It was further realized that the FC thermal performance was not rigorously affected by high frequency ripple currents presence – due to discontinuous operation mode. It was also found that the FC internal impedance can considerably affect the dynamics of the DC-DC converter. Also, the diminished power left during purging of the FC stack has been shown to be another possible cause for instability. To allay these problems, super-capacitors were connected in parallel to the FCs and a method to compute the value of the super-capacitor to attain stability was derived. A 30W boost converter system experimental results confirmed the validity of the suggested solution. Finally, good dynamic behaviour and stability were proven to be feasible with the use of super-capacitors connected to the output of the FCs. To lessen the cost and volume of the system, a high gain transformer-less DC-DC converter was researched – it employed a two level boost and a two level buck-boost converter in cascade to achieve a high voltage gain and low input ripple current, which contributed to lower electromagnetic interference (EMI). Experimental results demonstrated the viability of the DC-DC converter and showed a possible voltage gain of 5. Normally, FCs are constructed by stacking many cells which limit the generated power to the weakest cell in the stack. In addition, if one or more FCs fail, the entire system must be overhauled. To address these shortcomings, a new modular FC stack and DC-DC converter were pioneered – the FC stack was partitioned into different sections with autonomous operations. This has increased system reliability at a reduced output power should a section failed. Additionally, the generated power from the system was optimized by adjusting the drawn current from each section based on the voltage they produced, which resulted in a 10-14% extra power generation. Common mode noise due to transients was also noticed and was resolved by using shielded transformers. Figures 15a - 15d exposit the highlights of the study.

2.16. An Overview of Various Fuel Cell DC-DC Converters

According to [24], fuel cells are now becoming the preferred alternative renewable energy source, as their power production process is not affected by fluctuating environmental factors, contrary to solar cells and wind power plants. However, fuel cells produce low DC output voltage which requires stepping-up and interfacing them to the DC bus. Thus, the need for DC-DC boost power converters, which could be interleaving to help minimize the power ripples as well as bidirectional to charge storage devices such as a battery. In this regard, their paper discussed various interleaved (2, 3, 4 and 6 phases) and bidirectional (non-isolated and isolated) DC-DC boost converters architectures. The non-isolated BDC DC-DC boost converters covered include i) buck-boost converter, ii) cascaded buck-boost converter, iii) CUK converter, iv) SEPIC-ZETA converter and v) switched capacitor. The isolated BDC DC-DC boost converters covered include i) dual half bridge (DHB) and ii) dual active full bridge (DAFB). Figure 16 illustrates the research overview and the conclusion

drawn is interleaved boost converters improve power ripples and the more the interleaving, the better the ripple reduction; however, the more costly and bulky it becomes due to the many components used. BDC can additionally charge storage devices and furthermore, the isolated types can offer galvanic protection in high power applications; however, their large size due to the extra isolating transformer, makes them unsuitable for portable and or compact applications.
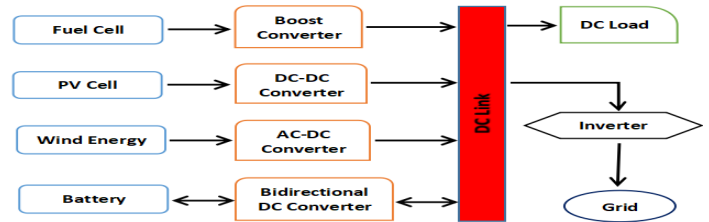
Figure 16: An Overview of Various Fuel Cell DC-DC Converters (redrawn from [24])

2.17. Challenges and Developments of Automotive Fuel Cell Hybrid Power System and Control

As assessed in [25], fuel cells are the future replacement for internal combustion engine in vehicles, though the current costs and Hydrogen supply infrastructure are the limiting factors. In their analysis, they noted that FCs in hybrid power systems have energy control, inertia, power, model and optimization problems which were summarized briefly with emphasis on the electro-chemical reactions, dynamics and the core parameters affecting FCs efficiency and durability. Their review concludes by highlighting that fuel cells have various challenges and the best solution is one that is inclusive by incorporating various hardware and software solutions to optimize fuel cells costs, performance and longevity. Figure 17a exemplifies a typical FC system and Figure 17b illustrates a simplified FCEV architecture.
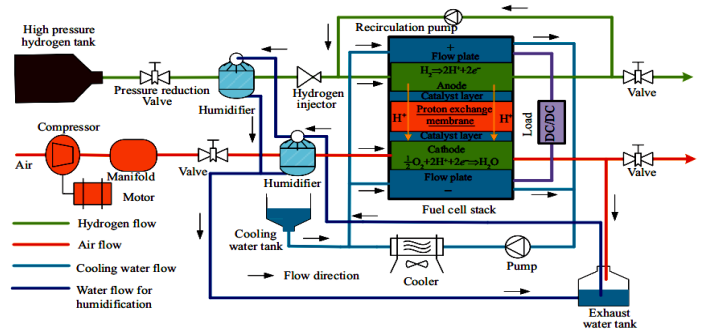
(a) Typical fuel cell system
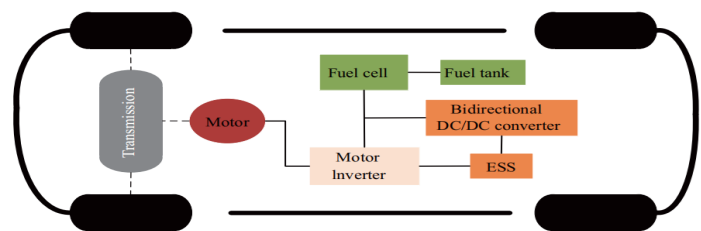
(b) Fuel cell electric vehicle power-train

Figure 17: Fuel Cell System and FCEV Power-train (adapted from [25])

2.18. Experimental Study and Performance Analysis on High Power Fuel Cell System

In [26], it's affirmed that PEM fuel cell for use in vehicles requires high power density — normally during starting-up and accelerating. As a result, their study presented an experimental research of a 100kW fuel cell power supply system with focus on measuring the system parameters such as voltage, current, temperature, pressure and hydrogen consumption. Two test set-ups were used; a i) rated and ii) cycle working condition tests. In the former, the system operates for an hour at a rated point with constant working conditions and the outcomes revealed stable operations when working constantly at the rated output power. In the latter, the test is conducted based-on their specified national standard, in which the fuel cell voltage is regulated to be a fixed value and the output current is varied with the working conditions. The conclusion arrived at is the researched fuel cell power engine reached 80kW at rated power with peak power exceeding 100kW. Figures 18a and 18b exemplify the researched FC power schemes.

Figure 19a illustrates the concept design and Figures 19b and 19c, portray the DC-DC converter with a full bridge and voltage doubler outputs respectively. Normally, the primary side of the high-frequency transformer (HF-X) windings constitutes a two-phase current-fed high-frequency resonant inverter with complementary Q1 / Q2 as the active switches and L1 / L2 as the coupled inductors. HF-X leakage (Lr) and magnetizing inductances (Lm) produce the multi-resonant transitions with Cp, to generate the high voltage boost ratio and quasi-resonant sub-interval for soft commutations. The leakage inductance operates as a snubber inductor to reduce the high di/dt rate at Q1 and Q2 switched-on transitions. For a higher boost ratio, the full bridge rectifier output can be substituted with a voltage doubler rectifier. Their findings showed that the postulated power converter can attain a snubber-less ZCS commutations, a greater voltage boost ratio and low power ripple; making it suited for smart homes use.

(a)

(a) Concept overview

Figure 18: (a) The Power System Overview and (b) Fuel Cell Power Engine (adapted from [26])

2.19. Coupled Inductor-assisted Current-Fed Snubber-less Zero-Current-Soft Switching High Step-Up DC-DC Converter for Fuel Cell Power Interface

Presented in [27], is a ZCS current-fed isolated DC-DC boost converter for a fuel cell smart home power system. To avoid ripple current from damaging the fuel cell electrodes and to ensure good boost voltage ratio, their design incorporated a magnetically coupled interleaved inductors with a 180° phase shift and a small number of passive components. A 50/60W 1MHz prototype based on 600V GaN-HFETs, was performance tested focusing on the design efficiency, ripple and voltage ratio.

(b) High step-up dc-dc converter with full-bridge rectifier
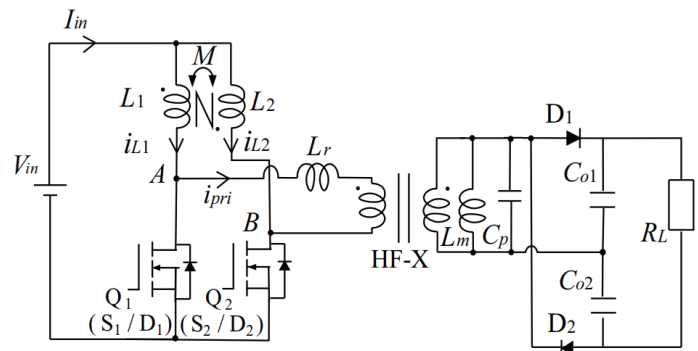
(c) High step-up dc-dc converter with voltage doubler rectifier

Figure 19: System Concept Design and High Step-up DC-DC Converter Types (adapted from [27])

2.20. Survey of DC-DC Non-Isolated Topologies for Unidirectional Power Flow in Fuel Cell Vehicles

Investigated in [28], is an outstanding research on fuel cells power-trains and power converters. Its extensively discussed in details the theoretical and architectural frameworks of fuel cells. Figures 20a and 20b respectively portray in totality a summary of fuel cell types and power electronics converters classifications.
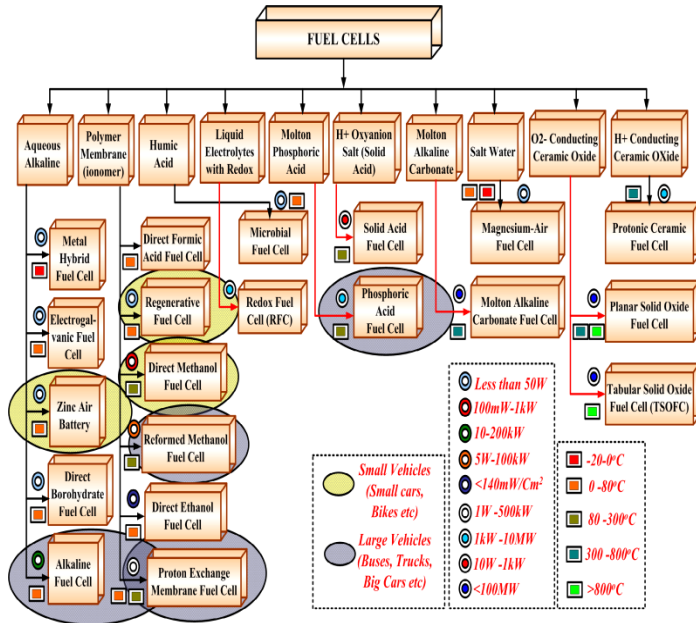
(a) Fuel cells classification

(b) Power converters classification

Figure 20: Fuel Cells and Power Converters Classifications (adapted from [28])
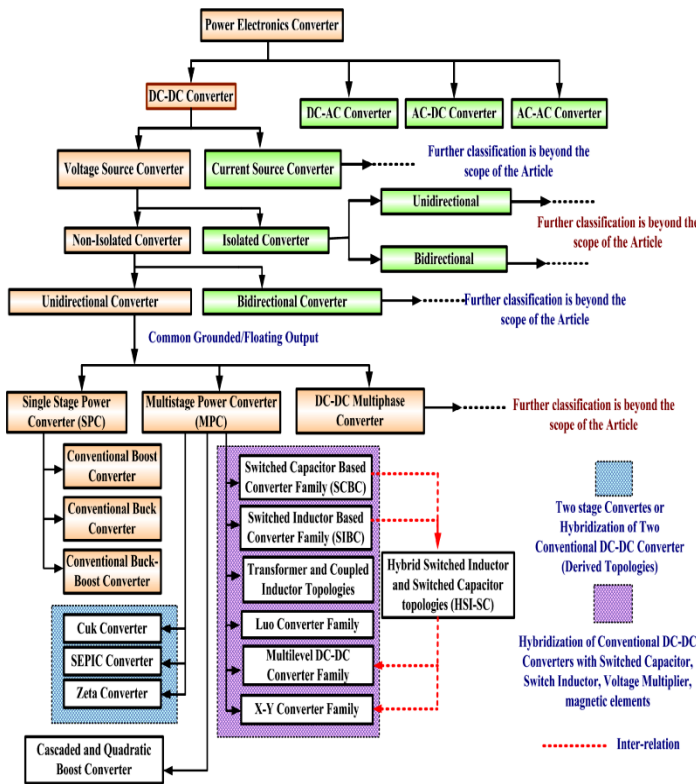
2.21. Performance Analysis of PV and Fuel Cell-based Grid Integrated Power System

Studied in [29], is a smart grid power generation system constituting solar cells and solid oxide fuel cells (SOFC) hybrid system as shown in Figure 21a. The SOFC augments the PV system during power outages due to fault and non-sunny periods. Alternative to SOFC; biomass and wind power systems can be used by integrating them with phase lock loop (PLL) to maintain a constant output supply. The power electronics made used of a DC-DC converter, a three phase DC-AC inverter for interfacing to the electrical grid and AC loads. In addition, is a LC filter to eliminate unwanted signals in the power system. The energy management techniques used include P&O MPPT as well as reference frame theory and PLL to enable a reliable power supply. Figures 21b - 21c respectively show the PV and SOFC schemes.
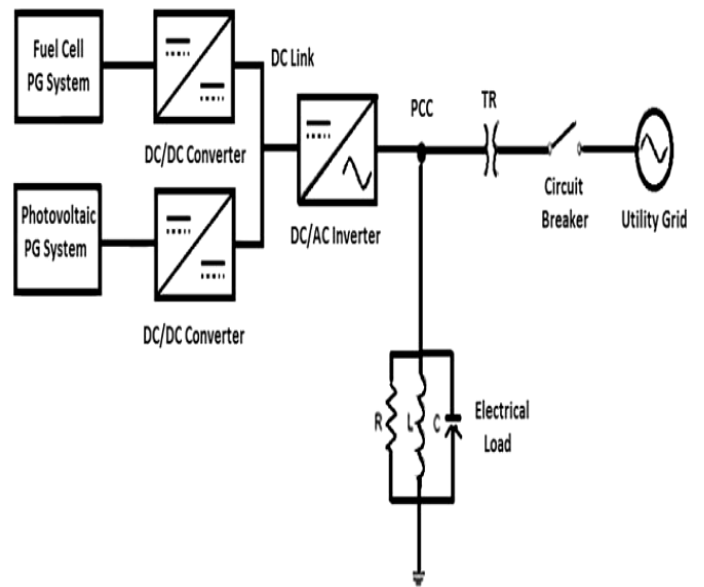
(a) Concept overview
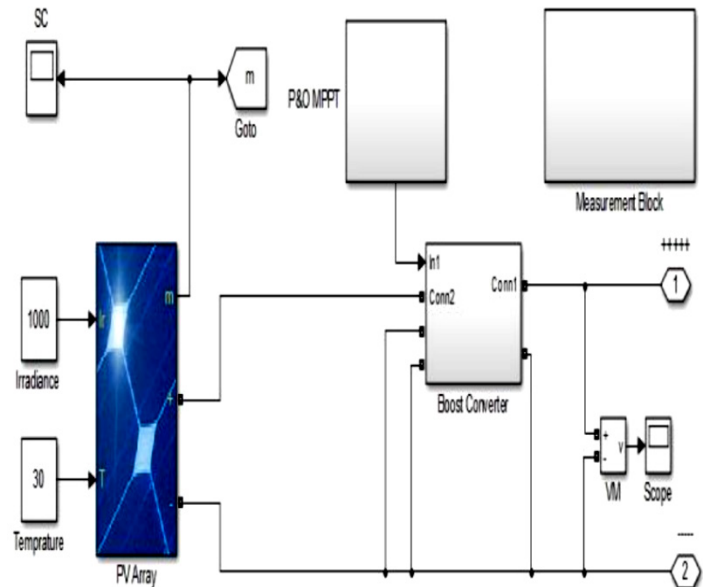
(b) Solar cell power system modeled with Matlab

(c) Fuel cell power system modeled with Matlab

Figure 21: System Concept Design, PV and Fuel Cell Power Systems Depictions
(adapted from [29])

2.22. Modeling and Simulation of DC-DC Converters for Fuel Cell Systems

Affirmed in [30], FC is the future renewable energy source, especially for portable applications. Fuel cells as a result of their low output voltage, require highly efficient power converters; thus, their research using MatLab, focused on the modeling and simulations of four types of DC-DC converters, namely i) boost, ii) SEPIC, iii) LUO and iv) ZETA. Their study was tested using the same fuel cell output voltage of 12V, connected to each converter input with each converter output voltage set at 48V. It was found that the ZETA topology offers the best total harmonic distortion (THD), followed by LUO, SEPIC and Boost with respective THD of 31.22%, 53.83 %, 65.38 % and 80.22 %. It was furthermore concluded that the ZETA topology THD performance can be improved with the addition of more filtering components. Figures 22a - 22c exemplified the SEPIC, LUO and ZETA DC-DC power converters modeled using Matlab Simulink.

(b) Fuel cell with LUO DC-DC converter simulation model
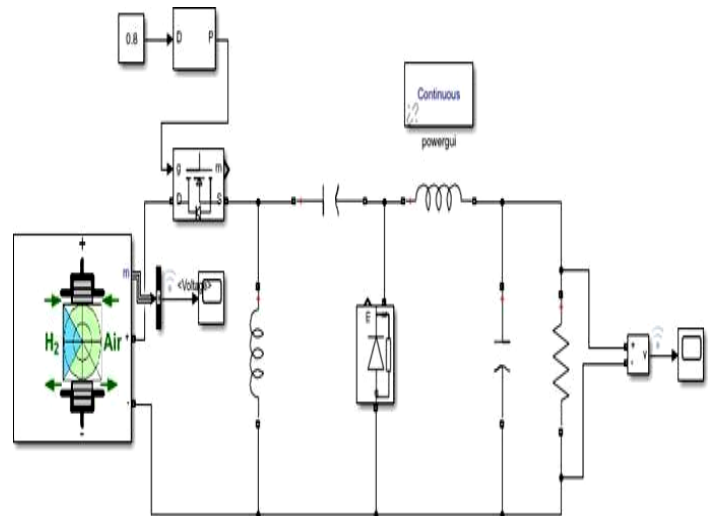
(c) Fuel cell with ZETA DC-DC converter simulation model

Figure 22: Simulink Model of FC with SEPIC, LUO and ZETA DC-DC Power
Converters Topology (adapted from [30])

2.23. Smart Fuel Cell Module (6.5 kW) for a Range Extender Application

Researched in [31] using SolidWorks, is a 6.5kW fuel cell model with a mechanically integrated 6-phase interleaved DC-DC boost converter for electric vehicles applications. The design constraints were such that the power converter was mounted on the fuel cell terminal plates and cooled using the same FC cooling system as shown in Figures 23a and 23b. The choice of the power converter topology was driven by the simplicity of its design, since the converter must fit on the FC terminals as well as the fuel cell configuration. As a result, the classic boost converter was chosen, as it employed the minimal components count and furthermore the phase inductors and switching devices can be respectively connected directly on the FC positive and negative plates as pictured in Figure 23b. Continuous conduction mode was chosen for the converter and the ripple was minimal.

(a) Fuel cell with SEPIC DC-DC converter simulation model

To conclude their study, the measured converter efficiency was >95% for a minimum output power of 1.5kW and output voltage of 240V. Future work for an aircraft use was considered.
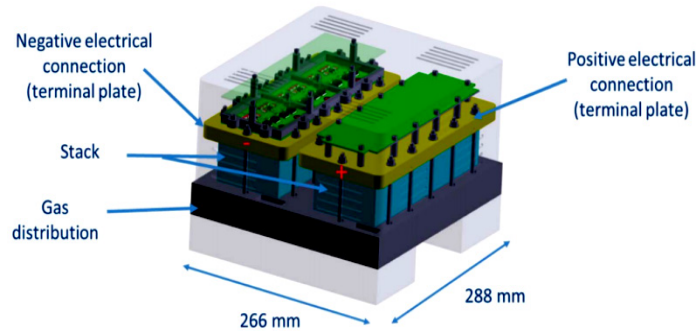
(a) Fuel cell concept design modeled with SolidWorks
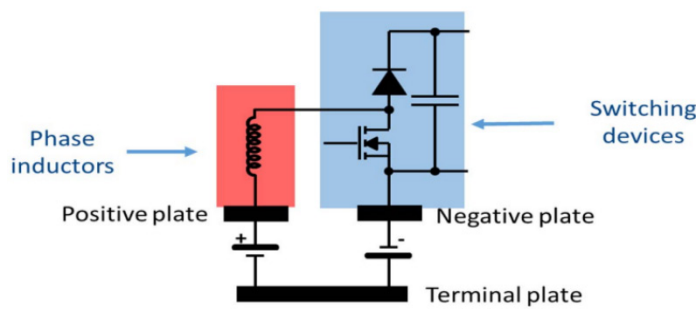
(b) Integration of the power converter on the fuel cell plates

Figure 23: SolidWorks Model of the FC with Integrated Power Converter (adapted from [31])

2.24. Power Converter Topology for Conditioning a Fuel Cell Battery Voltage

Stated in [32], their research conditioned the output voltage of a FC battery using DC-DC boost converter. The main novelty was to substitute the classic boost converter inductor (L) with a inductor-capacitor-inductor (LCL) filter topology as shown in Figure 24. The output voltage was then controlled using a sliding mode strategy including a load impedance observer. The simulated results showed good performance with varying loads.
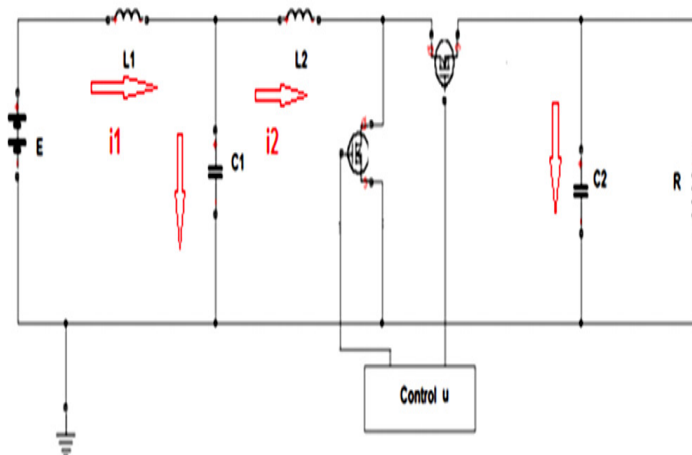
Figure 24: LCL Boost DC-DC Power Converter (adapted from [32])

2.25. Modeling and Simulation of an Aerodrome Electrical Power Source Based-on Fuel Cells

Examined in [33], reducing fuel usage and emissions such as NO_x, is aviation present challenge. As a result, there is the need to develop latest power sources using non-polluting sources such as Hydrogen fuel cells. Their work presented the modeling and simulation of a potential configuration for a hybrid aerodrome fuel cell power source. Their postulated architecture consists of a fuel cell stack, DC to DC set-up converter, super-capacitor and a buck-boost converter. The fuel cell and super-capacitor are respectively connected to a boost and buck-boost converter as correspondingly shown in Figures 25a and 25b. With this set-up, the fuel cell with slower power dynamics, supplies the bulk of the power during steady state operation, whereas the super-capacitor with a faster power dynamics, assist the fuel cell during peak power transient demand as well as stores power from the DC bus. The suggested configurations were simulated using MatLab, Simulink and Simscape Power Systems and it can be summed that the hybrid power aerodrome source shown in Figure 25c, can work efficiently, enabling its use for such long-term applications.
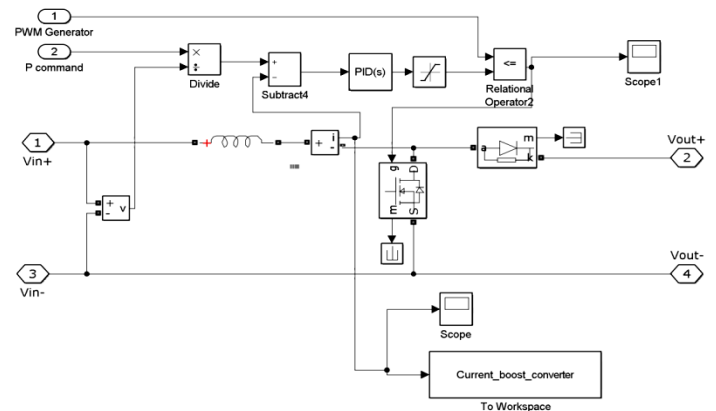
(a) Fuel cell with boost DC-DC converter
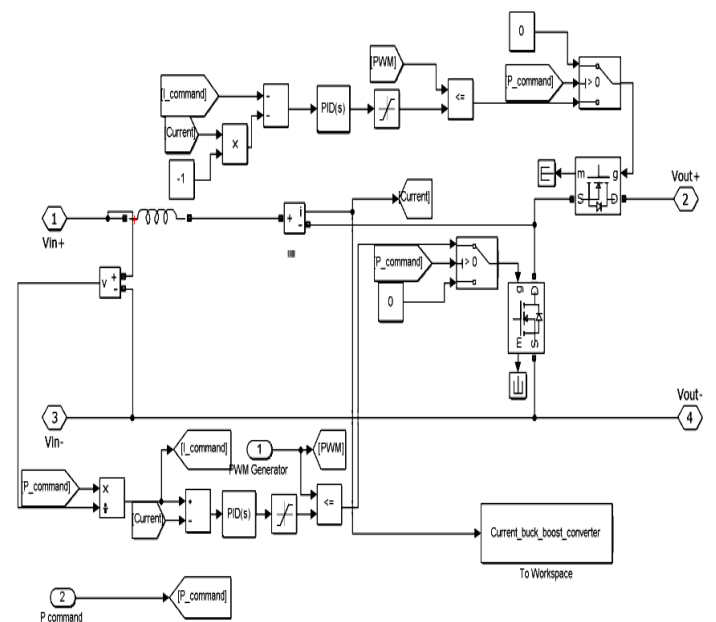
(b) Super-capacitor with buck-boost DC-DC converter
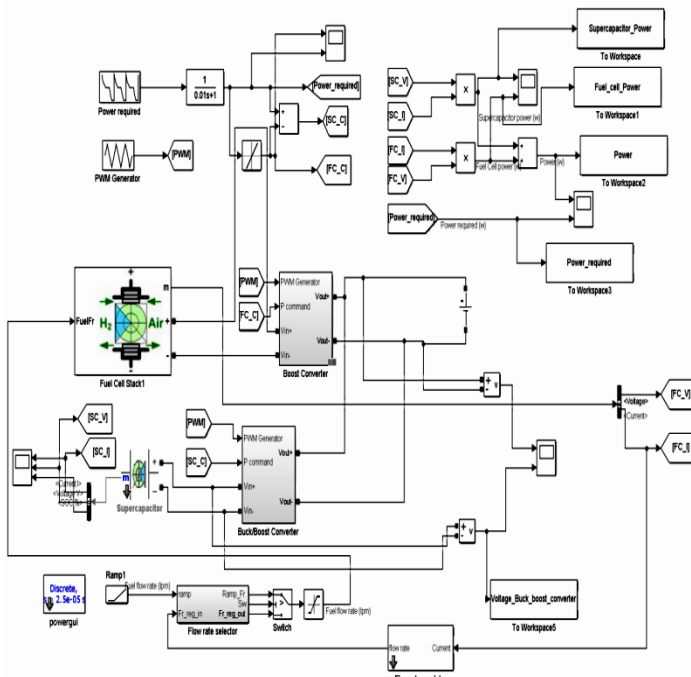
(c) Fuel cell and super-capacitor with boost and buck-boost DC-DC converters

Figure 25: Hybrid Fuel Cell and Super-capcitor Power System with Respective Boost and Buck-boost DC-DC Converters (adapted from [33])

2.26. Current-fed Modular Multilevel Converter (CMMC) for Fuel Cell and Photovoltaic Integration

Indicated in [34], is a CMMC single-stage solution to interface a low voltage photovoltaic and fuel cells DC power supplies to a higher voltage AC load and or grid. Usually, power conditioning stage (PCS) in the form of modular multilevel converters, have been used in various low to high voltage applications with good results; however, their two-stage configuration makes them bulky, hence the need for CMMC — whereby the boosting capability is integrated within the inversion, making it a single-stage DC-AC converter / inverter with additional redundancy and modularity. This enables it use in low voltage applications, where low voltage MOSFETs with low ON-state resistance can be used to increase the power conversion efficiency. A 10kW three-phase CMMC using PLECS, was simulated to verify its functionality. Figures 26a and 26b depict the traditional two-stage DC-AC using (a) a boost converter before the inversion and (b) a step-up transformer after the inversion. Figure 26c exemplifies the single-stage CMMC.

(a) Two-stage DC-AC with boost converter before the inversion
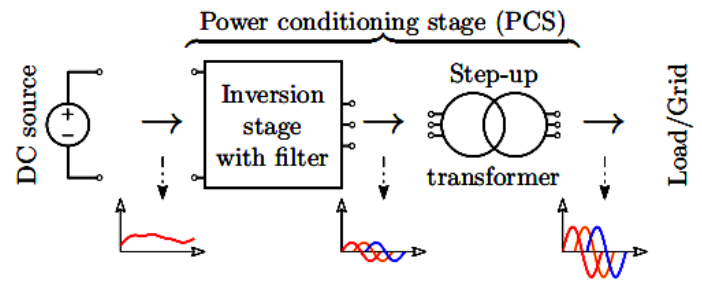
(b) Two-stage DC-AC with step-up transformer after the inversion
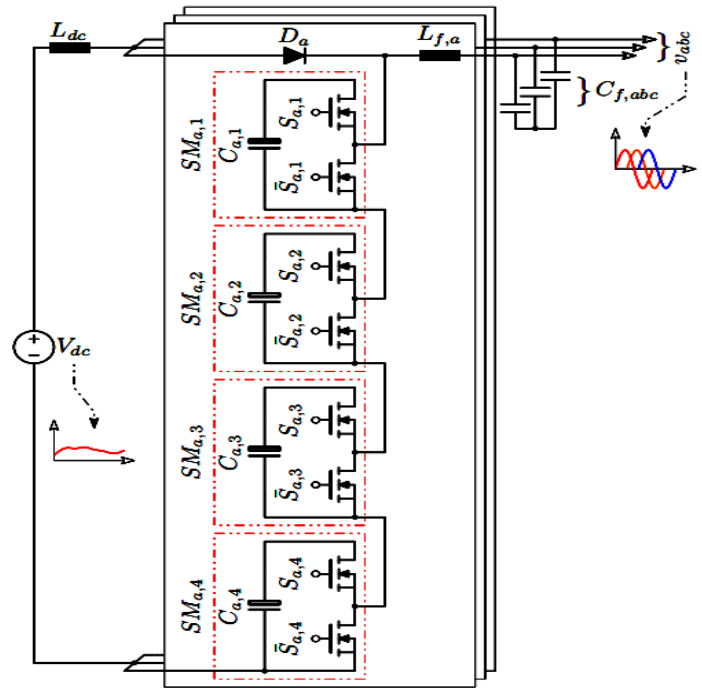
(c) Single-stage DC-AC three-phase CMMC with four sub-modules per phase

Figure 26: Two-stage Traditional and Single-stage CMMC DC-AC Inverters (adapted from [34])

2.27. Novel Four-Port DC–DC Converter for Interfacing Solar PV–Fuel Cell Hybrid Sources with Low-Voltage Bipolar DC Micro-grids

Presented in [35] is a bipolar DC micro-grid (BDCMG) power supply system based on a novel 4-port dual-input dual-output DC-DC converter to interface fuel cells, PV and wind power sources to a low voltage BDCMG. Usually, a BDCMG requires several traditional DC-DC power converters to supply power to the BDCMG poles; however, their researched model in addition to being reliable and efficient, is also compact and unidirectional. It can also function as a single-input dual-output converter as well as with two degrees of freedom using its two switches. Furthermore, the duty cycle changes has no effects on the converter dynamic model; thus, the converter can be controlled with just one controller in different modes, making it less complex. By deriving a small signal model for each operating mode, the converter control system was designed. MPPT was used to track the PV voltage and inductor current without needing an extra PV sensor. Its steady and dynamic states operations were validated using close and open loops results.   In-lined with both simulations and

theoretical analyses, they observed that the 24V pole voltage and the photovoltaic power are maintained under different conditions (such as during solar irradiation fluctuations and transient load power demands); thus, validating the converter design performance and reliability. The converter was found to have a 93% peak efficiency and ~87% rated power efficiency. Figure 27a exemplifies the proposed BDCMG power scheme and Figure 27b depicts the converter topology whereas Figure 27c shows a different load configuration.
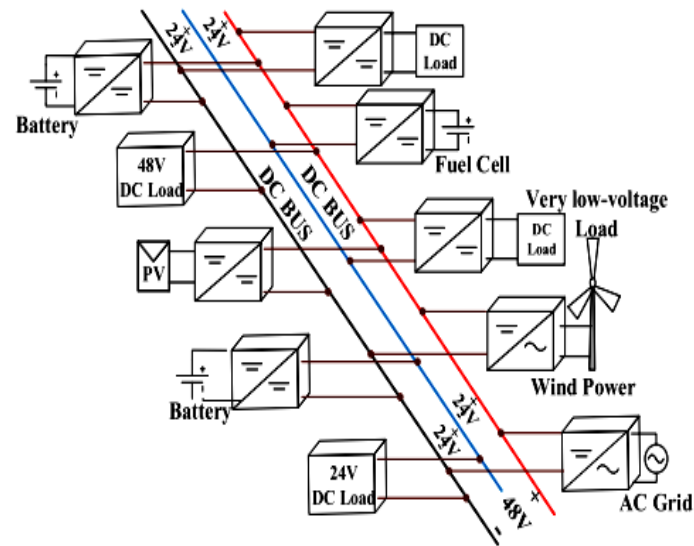
(a) Low-voltage (48-V) BDCMG system.
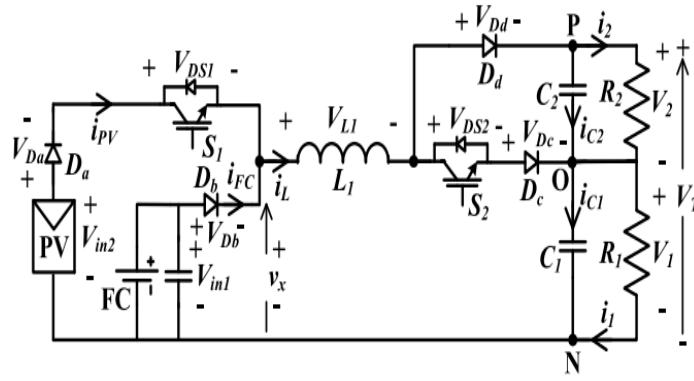
(b) Converter topology
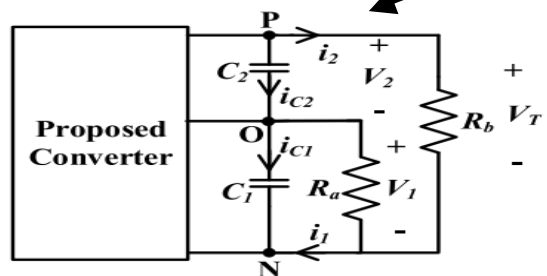
(c) Converter topology with alternative load representation

Figure 27: BDCMG System and Converter Topologies (adapted from [35])

2.28. Study on Boost Converters with High Power-Density for Hydrogen-Fuel-Cell Hybrid Railway System

Investigated in [36] is a high power hybrid hydrogen fuel cell railway system portrayed in Figure 28a − with focus on designing an efficient and high power density DC-DC converter, since fuel cells are normally low DC power sources and can not supply the needed 1500V to drive the inverter input needed for the railway traction AC motors. Therefore, two DC-DC power converters, namely the interleaved boost converter shown in Figure 28b and the three-level boost converter depicted in Figure 28c, were researched to determine the most suitable DC-DC boost power converter architecture. Taking into considerations and also using optimal design methods were the boost inductor, output capacitor and power semiconductor devices performances with respect to the hybrid railway specifications. Both power converters designs were verified with a 600V input and 1200V / 20kW output setup and the results concluded that the three-level boost converter performed better in-terms of the efficiency, power density and dynamic current response. As a result, it was chosen as the most suitable topology for the hybrid hydrogen fuel cell rail system.
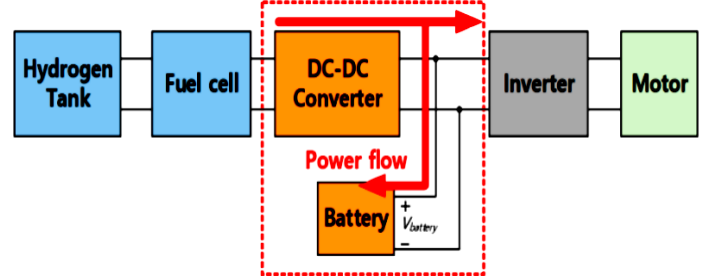
(a) Propulsion system for hybrid hydrogen-fuel-cell railway system
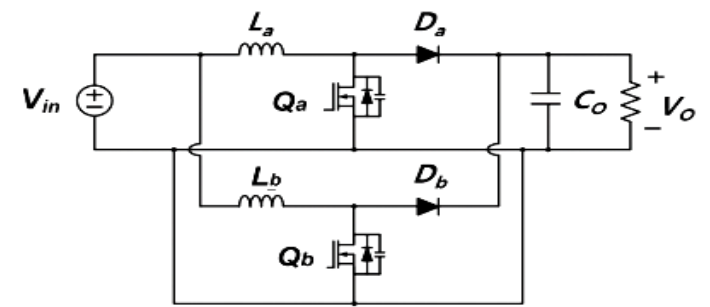
(b) High step-up DC-DC interleaved boost converter (IBC)
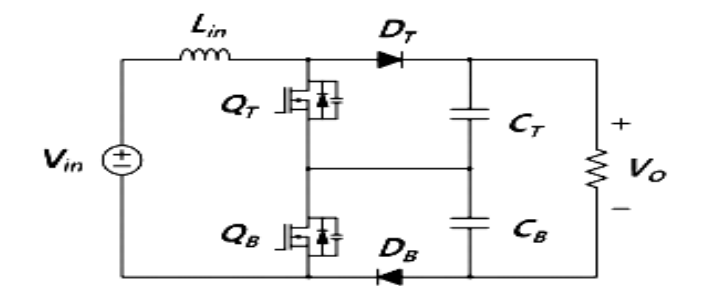
(c) High step-up DC-DC three-level boost converter

Figure 28: Concept Design with High Step-up DC-DC IBC and Three-level Boost Converter (adapted from [36])

Table 1 summarizes the fuel cells power converters studies reviewed − in which the major highlights, advantages and disadvantages of each where applicable, are briefly recapitulated.

Table 1: Power Converters Studies Examined Summary (adapted from [1])

Power Converters	Highlights, Merits and Demerits
Study 2.1 (A. Kolli *et al*, 2015) [23]	Various FCs DC-DC power converters setups. Emphasis on different types of interleaved converters for high, medium and low power uses. FCs in parallel /series raise output power.
Study 2.2 (M. Kabalo *et al*, 2010) [13]	FC vehicles cutting edge DC-DC converters. High voltage ratio, compactness and efficiency with affordability, should be used to implement power converters. Presented different schemes.
Study 2.3 (M. Delshad & H. Farzanehfard, 2011) [14]	ZVS current fed push-pull DC-DC converter. When power is off, voltage surge across the switch is absorbed. This improve its efficiency and compactness to enable basic PWM control.
Study 2.4 (N. Bizon, 2011) [15]	A new architecture of FC HPS for efficient functioning and better steadfastness. HPS with active MPPT and hysteretic current controls were used to minimize ripple current from FC.
Study 2.5 (O.A. Ahmed & J.A.M. Bleijs, 2013) [16]	For an UC in DC micro-grids, a bidirectional voltage-fed setup is preferred for quick dynamic response, though for a broad input voltage instability at the UC, there is greater circulating power flow and conduction losses.
Study 2.6 (A. Carvalho *et al*, 2011) [19]	Modeled a PEM FC using MatLab. Noted the preferred model must take control and optimise the FC operation points. Soft switching based on series resonant and SA was used, as it reduces switching losses and boost efficiency.
Study 2.7 (F.M. Mwaniki, 2014) [11]	Multi-phase tapped-coupled inductor suited for varying high power DC-DC converter uses. Showed minimal input & output power ripples.
Study 2.8 (Y. Huangfu *et al*, 2015) [10]	High power efficiency step-down converter for discrete wind power supply scheme, akin PV. Achieved a 2kW supply with 96% efficiency with step-down ZVS/LCD scheme with MPPT.
Study 2.9 (R. Seyezhai *et al*, 2013) [9]	Interleaved converters with switched capacitor are considered the suitable topology for FC systems, because of reduced ripple power in the input and output, quicker transient reaction, small EMI, enhanced efficiency and reliability.
Study 2.10 (M. Nymand & M.A.E. Andersen, 2008) [8]	A new low-leakage inductance low-resistance design approach to low-voltage high-power isolated boost converters. Poorest efficiency at minimum input voltage with maximum power was ~97%. The maximal efficiency was ~98%.
Study 2.11 (B. Eckardt *et al*, 2005) [12]	FC automotive power-train application using high current buck-boost DC-DC converter with digital control to render apt protection against over-current, over-voltage & over-temperature.
Study 2.12 (A. Kirubakaran *et al*, 2009) [3]	PEM FC setup with DC-DC step-up converter: Design, modeling and simulation. For instant load fluctuation from 0.6 – 1.1kW, the FC current and voltage took ~50 - 70ms (fuel starvation) to attain a new steady state. The altering voltage was tracked with PI controller.
Study 2.13 (M.T. Outeiro & A. Carvalho, 2013) [6]	A method to devise power converters for fuel cell rooted schemes using resonant technique. Independent voltage and PEMFC controllers. Enhanced FC efficiency by managing FC *P_out*.
Study 2.14 (H. Wang, 2019) [20]	Devise and management of a 6-phase IBC rooted in SiC with EIS functionality for FC HEV. IBC dynamic model with HIL real-time.
Study 2.15 (L.M.P. Fanjul, 2006) [4]	Design deliberations for DC-DC converters in FC schemes. Used analytical and experimental schemes to achieve a steady and efficient FC & power converter system. A modular FC stack and DC-DC converter were pioneered by dividing it into autonomous optimal sections.
Study 2.16 (D. Ravi *et al*, 2018) [24]	IBC and BDC were researched. IBC improves power ripples. The more the interleaving, the better the ripple reduction; though, the more costly. BDC can charge storage devices and furthermore, the isolated types offer galvanic protection in high power uses; however, their large size makes them unfit for portable uses.
Study 2.17 (J. Gao *et al*, 2019) [25]	FCs have various challenges and the best solution is one that is inclusive with various hardware and software solutions to optimize better FCs costs, performance and longevity.
Study 2.18 (H. Liu *et al*, 2020) [26]	Investigated a high power fuel cell system. Two test setups were used; a i) rated and ii) cycle working condition tests and found that fuel cell power engine reached 80kW at rated power with the peak power exceeding 100kW.
Study 2.19 (R. Miyazaki *et al*, 2020) [27]	A current-fed snubber-less ZCS FC high step-up DC-DC converter was studied. It achieved a greater voltage boost ratio and low power ripple, making it suitable for smart homes use.
Study 2.20 (M.S. Bhaskar *et al*, 2020) [28]	Reviewed extensively and comprehensively in theory and topologically, the different types of fuel cells with focus on the use of fuel cells in FCEV power-trains. Miscellaneous types of power converters were also assessed in details.
Study 2.21 (K.S. Rathode *et al*, 2019) [29]	Researched a hybrid PV and FC system. The power electronics used a DC-DC converter, a three phase DC-AC inverter for interfacing to the electrical grid and AC loads with P&O MPPT as well as reference frame theory and PLL to enable a reliable power supply system.
Study 2.22 (S. Kavyapriya & R.K. Kumar, 2020) [30]	Modeled and simulated four step-up power converters schemes. Found that the ZETA topology offers the best THD, followed by LUO, SEPIC and Boost with THD of 31.22%, 53.83 %, 65.38 % and 80.22 % respectively.
Study 2.23 (P. Bazin *et al*, 2020) [31]	Implemented a smart FC with built-in DC-DC power converter. The classic boost converter with 6-phase interleaving was chosen, as it fitted well, efficient & offered least parts used. The efficiency was >95% for a nominal output power of ~1.5kW and output voltage of 240V.
Study 2.24 (A. Gonnet *et al*, 2019) [32]	Studied power converter topology for FC battery voltage conditioning. The classic boost converter inductor was replaced with a LCL filter. Gave good performance at varying loads.
Study 2.25 (J. Corcau *et al*, 2019) [33]	Modeled & simulated a hybrid aerodrome FC power source consisting of a FC stack, a boost and buck-boost DC to DC converters as well as super-capacitor to provide clean, stable, peak power and energy dynamics during transients.
Study 2.26 (A. Abdelhakim & F. Blaabjerg, 2020) [34]	Proposed a CMMC single-stage solution to interface a low voltage PV and fuel cells DC power supplies to a higher voltage AC load or grid. This offers better performance and is less bulky, contrary to a two-stage boost converter.
Study 2.27 (P. Prabhakaran & V. Agarwal, 2020) [35]	Presented a BDCMG power supply system based on a novel 4-port dual-input dual-output DC-DC converter to interface fuel cells, PV and wind power sources to a low voltage BDCMG. The converter was reliable, compact, versatile and unidirectional with a 93% peak efficiency and a ~87% rated power efficiency.
Study 2.28 (H.S. Youn *et al*, 2020) [36]	Investigated a high power hybrid hydrogen FC railway system with focus on designing an efficient and high power density DC-DC converter. Two DC-DC power converters, namely the IBC and three-level boost converter were researched to determine the most suitable DC-DC boost power converter architecture. The three-level boost converter out performed the IBC in terms of efficiency, power density and dynamic current response and was chosen.

3. Energy Management Systems / Storage (EMSs)

In [37]-[70], EMS simply deals with the partial or overall management / control of a device, a section or the entire system – that is, from when, where and how the energy / power is generated, used, processed, converted and or stored. Furthermore, some housekeeping such as thermal management is carried-out as well. The management performed could be i) on-demand (upon users requests or executions as per system dynamics dictates), ii) on-schedule (pre-programmed to do certain routine tasks at a particular time) and iii) artificial intelligence (based-on machine learning). Usually, a dedicated microcontroller and or power management chip or an adequate computing platform is used to optimally process and execute advanced control algorithms that i) manages power generation devices (fuel cells, solar-cells, wind-farms, TEGs, etc) and supporting systems (water pumps or fans), ii) manages power conversion switching devices (switch ON and Off or pulsing the power ICs or MOSFETs or IGBTs etc as required), iii) monitoring energy storage devices (batteries, super-capacitors / ultra-capacitors etc), iv) controlling the end user applications (e.g. HEV) and finally v) housekeeping (temperature monitoring, timestamp etc) and interacting with the system processes optimally to ensure the closed loop power generation / energy conversion and storage processes are efficient, affordable, quicker, safer and reliable. Examined in what follows are some case studies on power and energy conversions management schemes applicable to FCs and suitable for FC CCHP systems.

3.1. MIL, SIL and PIL Tests for MPPT Algorithm

Investigated by [37], a boost converter is necessary to convert DC voltage to another DC voltage (DC-DC). In their research, solar energy was harvested by PV array and tracked for continuous power generation using model based MPPT technique. The converter contained a MOSFET as the converter switch, which is managed by PWM signal. Once the MOSFET switch is ON, the energy from the PV module is stored in the inductor and the reverse biased diode disengages the output from the PV generator while the output capacitor supplies current to the load. Conversely, when the MOSFET switch is OFF, the inductor is in a discharge state and forward biases the diode to engage the output to the PV generator. The PV panel voltage and inductor voltage (discharging state) combine to give the output voltage, which is always more than input voltage, hence boost conversion. The study was systematically performed in three stages as follows i) model-in-the-loop (MIL), ii) software-in-the-loop (SIL) and iii) processor-in-the-loop (PIL) as depicted in Figure 29 – in which an algorithm with customized variable step was modeled and connected to a simulated PV panel and a boost converter. The MPPT model was simulated first using Simulink and the process is called MIL as shown in Figure 29. The result acquired using MIL test under STC was asserted in the study and as presented in the steady state, the PV power is equal to 60.54W which is the highest power of the Solarex MSX-60 panel under STC (1,000W/m² and 25°C). The study first demonstrated the MIL test result when the irradiance was raised from 500 to 1000 W/m², then reduced to 800W/m² and finally to 600W/m² − the tailored algorithm gave quicker response during irradiance changes and the steady-state oscillations were almost negligible.

The algorithm was changed from MIL format to SIL and the same irradiance test pattern repeated again to test the MPPT tracking and the same result was achieved similar to that of MIL.

Finally, the code was changed to PIL format and the same irradiance test pattern repeated again to test the MPPT tracking using hardware-in-the-loop as illustrated in Figure 29, which also gave the same result. This concludes that the implemented MPPT algorithm is accurate, as all the three algorithm formats gave the same outcomes. This approach can be applicable also to fuel cells.
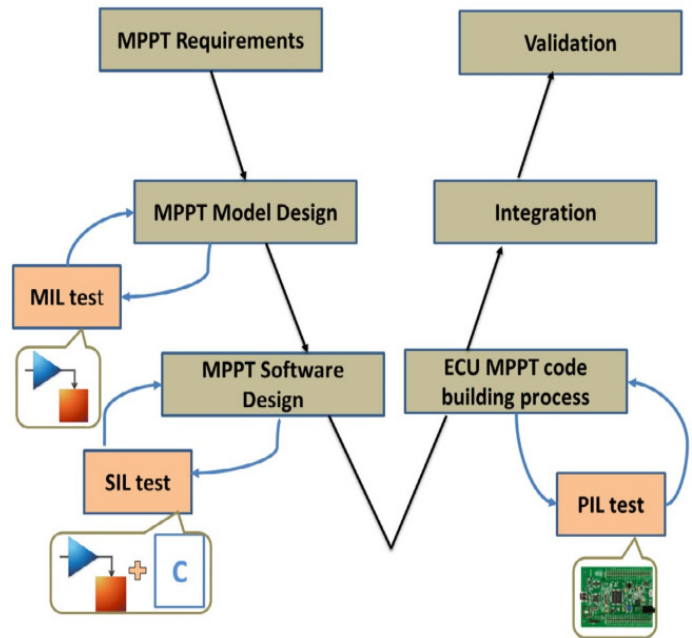
Figure 29: MIL, SIL and PIL Tests for MPPT Algorithm (adapted from [37])

3.2. Review on EMS for FCs Hybrid Electric Vehicle: Issues and Challenges

According to [38], different ways of using a battery to supplement a fuel cell to reliably supply power without experiencing the fuel cell fuel starvation phenomenon were investigated. The basic rationale in the literature was to formulate various types of power converters and energy management systems / storage (EMS) governed by different control strategies − which include but not limited to the followings techniques a) fuzzy logic [39], b) power frequency splitting [40], c) space dynamic equation, d) deterministic dynamic programming [41], e) neural network optimization algorithm [42], etc.

Furthermore in [38], super-capacitor (SC) instead of a battery, was used to supplement a fuel cell. Super-capacitors are known to have very high power density (relative to a battery or FC), enabling it to react faster in transient conditions of brief high current demand. This method requires as well various topologies of power converters and EMS governed by different control techniques, which include but unlimited to the following methods a) differential flatness controls [43], b) polynomial control technique [44], c) wavelet-based load-sharing algorithm [45], d) fuzzy logic [46], e) wavelet adaptive linear neuron (WADALINE) [47], f) adaptive optimal control algorithm (AOCA) [48], etc.
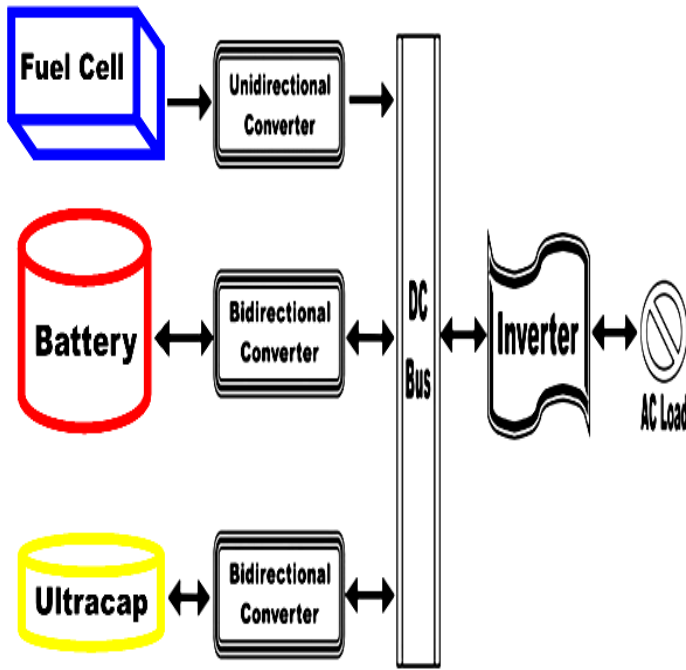
Figure 30: Fuel Cell, Battery and Ultra-capacitor Hybrid Power System (redrawn from [38])

Figure 31: Hybrid Fuel Cell, Battery and Super-cap with EMS (adapted from [57])

Finally, the third setup as stated in [38], involves all three – the FC, battery and finally the super-capacitor all connected in parallel. This setup requires as well various topologies of power conversion and EMS governed by different control methods, which include but unlimited to the following approaches a) proportional integral (PI) regulator [49], b) fuzzy logic [50], c) various FC, battery and SC configurations [51], d) traction control method [52], e) flatness control technique [53], f) PWM control [54], state machine strategy [55] PI and nonlinear sliding mode controllers [56] etc. The fuel cell, battery and super-capacitor technique is the most effective and widely used, as it provides both high energy and high power densities, as well as storage when needed. Figure 30 summarily depicts this technique.

3.3. A Comparative Study of EMS Schemes for a FC Hybrid Emergency Power System of More-Electric Aircraft (MEA)

Researched in [57], an articulation of assorted EMS for a fuel cell-based emergency power system of a More-electric aircraft was presented. Akin to Figure 30, the fuel cell hybrid system comprises of a FC, Li-ion battery and super-capacitor, together with DC-DC converters and DC-AC inverter as shown in Figure 31. The EMS techniques comparatively studied include those used in FC vehicle applications such as the proportional integral (PI), the state machine, the fuzzy logic /frequency decoupling, the equivalent consumption minimization and the rule-based fuzzy logic strategies. The main metrics used to compare the various EMS strategies performance are the i) the H_2 consumption, ii) state of charge of the batteries / super-capacitors and iii) general system efficiency. Lastly, a novel technique using the wavelet transform of their instantaneous power, was used to measure the tensions on each energy source to determine the impact on their life cycle. Simulation models as well as an experimental test setup were developed to simulate and practically verify the study.
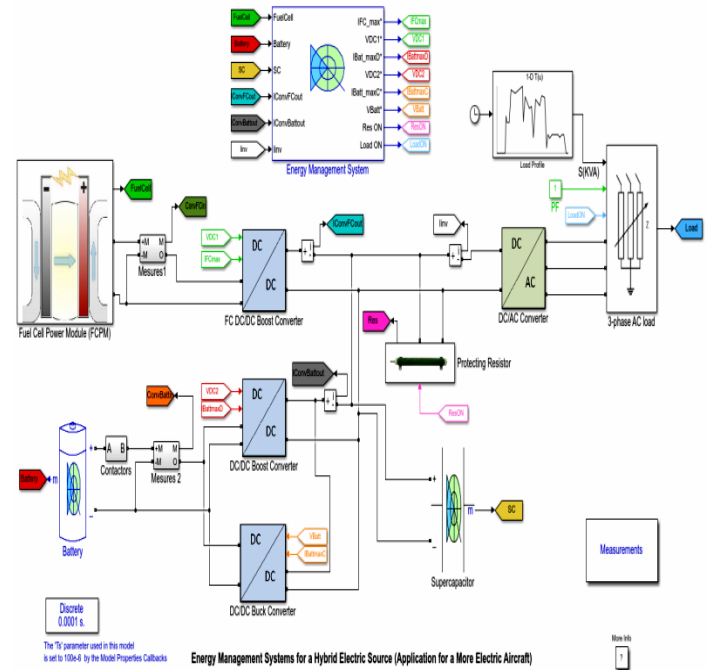
3.4. Model-Free Control of Multi-phase IBC for FC / Reformer Power Generation

Fuel cells require power converters to boost their low DC output voltage, as well as a control mechanism to optimize its operation. According to [58], the regulation parameters are set using a linear method to assess the convergence problem; as a result, they developed further a model free control (MFC) to manage the fuel cell power for DC micro-grid applications. In their approach, a 2-phase interleaved boost converter was implemented to address the non-linear control problem. Relative to PI and flatness control techniques, a MFC is simple and don't need precise info of the DC micro-grid parameters, though MFC still needs to know the power converter inductances value. The simulated design was done using dSPACE MicroLabBox and practically tested using a 50V 2.5kW PEMFC with two 2.5kW converters connected in parallel to the FC output and both tests correlated with excellent performance. Figure 32a depicts the FC power plant overview and Figures 32b and 32c respectively represent the IBC architecture and a two-phase MFC technique.
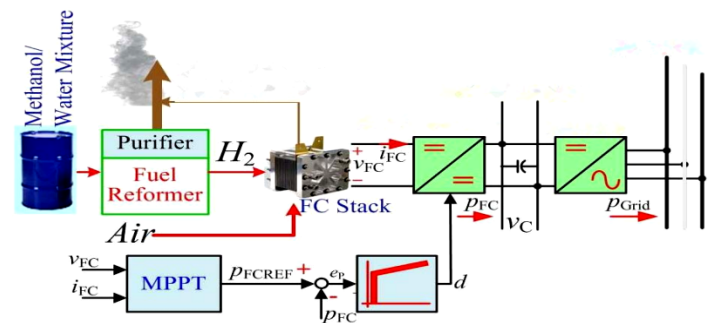
(a) FC / reformer power plant for grid connected applications
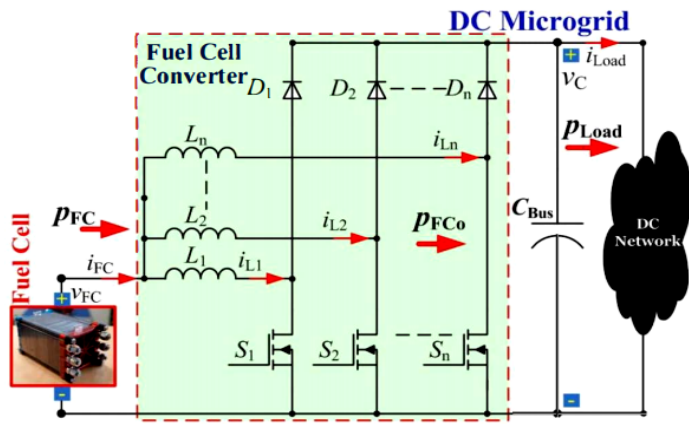
(b) Multi-phase parallel IBC for FC applications
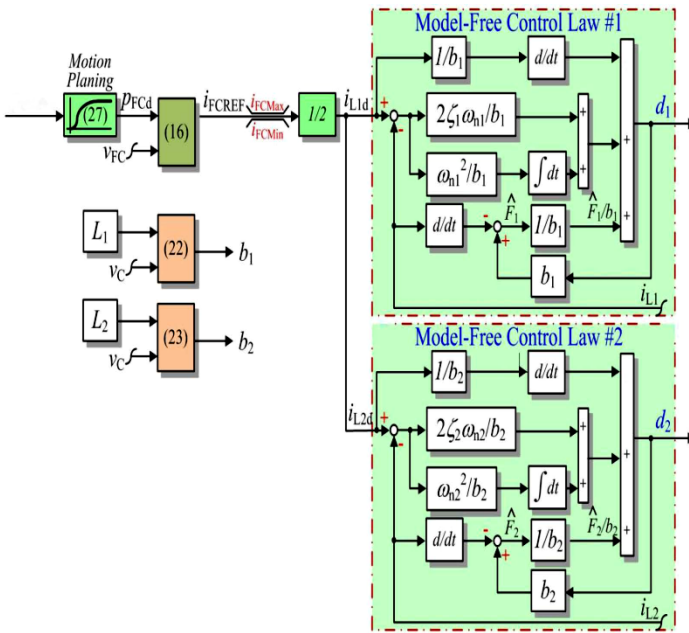
(c) Suggested MFC of the FC power for the multi-phase FC power converter

Figure 32: FC Power Plant, Power Converter and MFC (adapted from [58])

3.5. Control and Grid Connection of a FC Power System

As now known, FC is gaining traction in micro-grids and other applications due to their environmental friendliness. Studied in [59] is 900 cells (0.7V per cell) 625V PEMFC stack connected to a 3-phase electrical network using a 700V DC-DC conventional boost converter and a 420V voltage source converter (VSC) DC-AC inverter. PI linear controllers are used in the power converter to monitor the voltage/current and to regulate the electrical dynamics needed to reliably supply power to the grid. The VSC regulates autonomously the active and reactive powers injected to the grid, using two linear control loops PI(1) and PI(2) and a sinusoidal pulsed width modulation (SPWM) scheme. MatLab / Simulink was used to model and simulate the design and the PI controller could reach steady state within 50ms. The VSC inverter controller was able to reach steady state within 30ms when the active and reactive powers were doubled. Figure 33a illustrates the FC electrical network and Figures 33b and 33c, respectively denote the PI and VSC controllers strategy.
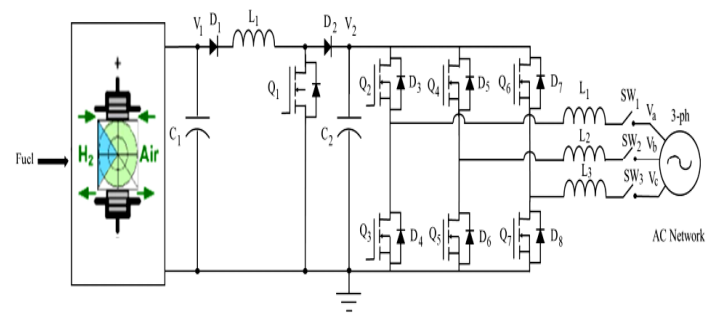
(a) The fuel cell stack, power converter and 3-phase grid
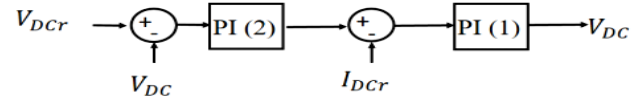
(b) The boost converter PI controller sketch
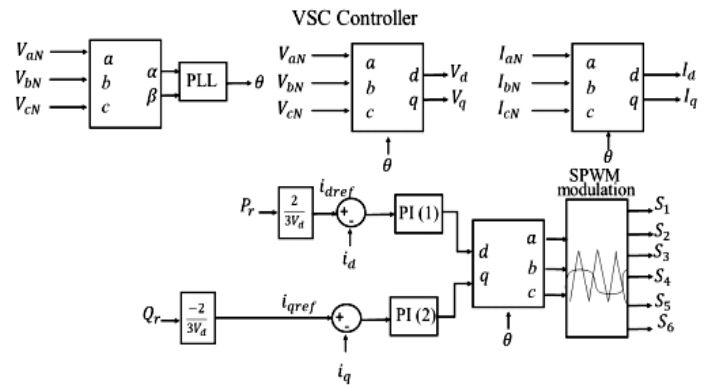
(c) The VSC control and modulation strategy

Figure 33: The FC, Power Converter and Electrical Grid with PI and VSC Controllers Schemes (adapted from [59])

3.6. A Novel Control Scheme for High Efficiency FC Power Systems in Parallel Structure

Discussed in [60] is a basic control technique for greater efficiency power converters of a FC distributed generation (DG) system shown in Figures 34a-34c. Usually, multiple FCs and power converters are connected in parallel to meet the power rating required for a FC DG systems. However, power systems have three main losses; namely core, switching and conduction losses − the switching and core losses are insensitive to load fluctuations, whereas the conduction loss is proportional to power output. Therefore, when power systems work under light-load conditions, the switching and the core losses can significantly contribute to the total losses, as the conduction loss will be small. As a result, the traditional paralleling approach entails the power system operates the same irrespective of the load size, making the power system in-efficient at light-load (small current) conditions, due to the predominantly switching and core losses. Therefore, the parallel system efficiency under light-load is enhanced by changing accordingly the quantity of parallel power units to meet just the light-load demand − doing so substantially reduce the switching and core losses, as less power units will be operating and more can be added under heavy-load. Three 300W units were paralleled to achieve a 900W FC DG efficient system.
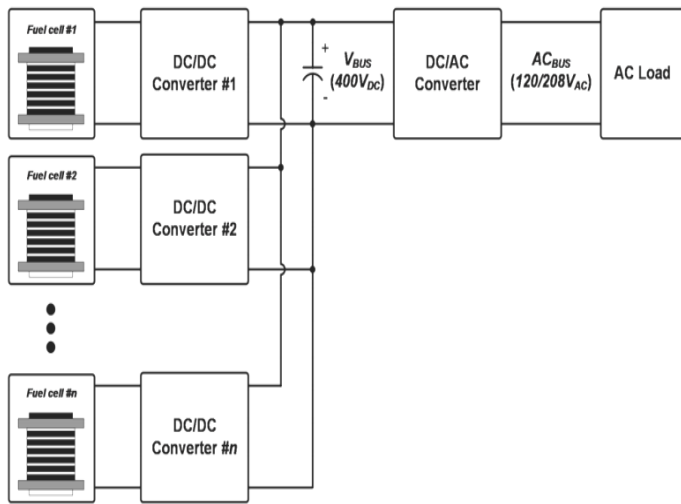
(a) Parallel FC DG system
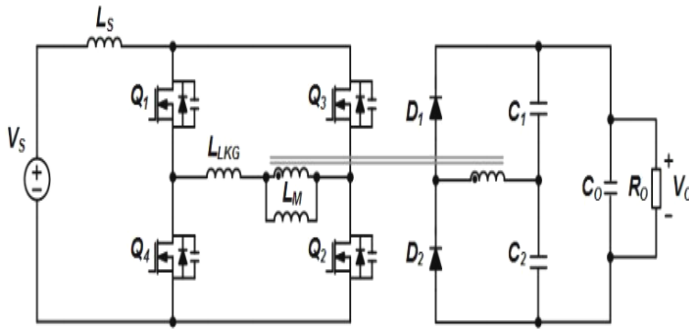
(b) Current-fed isolated full-bridge power converter
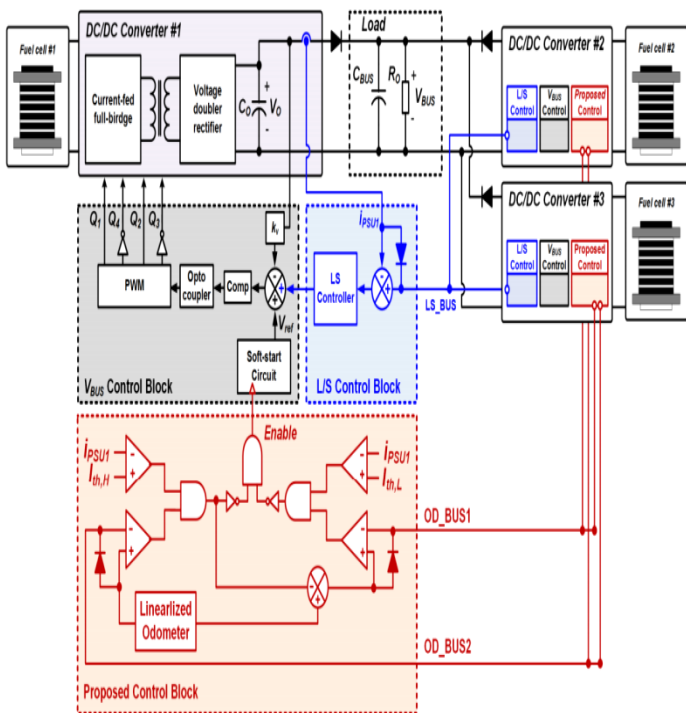
(c) Proposed control scheme block diagram

Figure 34: The Proposed FC System, Power Converter and Controller Scheme
(adapted from [60])

3.7. An EMS Strategy Based-on State Machine with Power Compensation for PV-PEMFC-Li-ion Battery Power System

Investigated in [61] is a hybrid power supply system constituting a PEMFC, PV and auxiliary Li-ion battery for electric vehicles as exemplified in Figure 35a. A conventional FC and solar cell DC-DC boost converters are used and for a Li-ion battery, a boost-buck power converter is employed. To efficiently coordinate the different power / energy sources and stabilize the DC bus voltage, a state machine EMS control technique with power compensation was employed. The rationale is to minimize the frequency of the PEM FC power output variations and ensuring the Li-ion battery charges and discharges within the ideal intervals. Figure 35b illustrates the state machine EMS used to adjust the FC voltage and Li-ion SoC to attain optimal results.
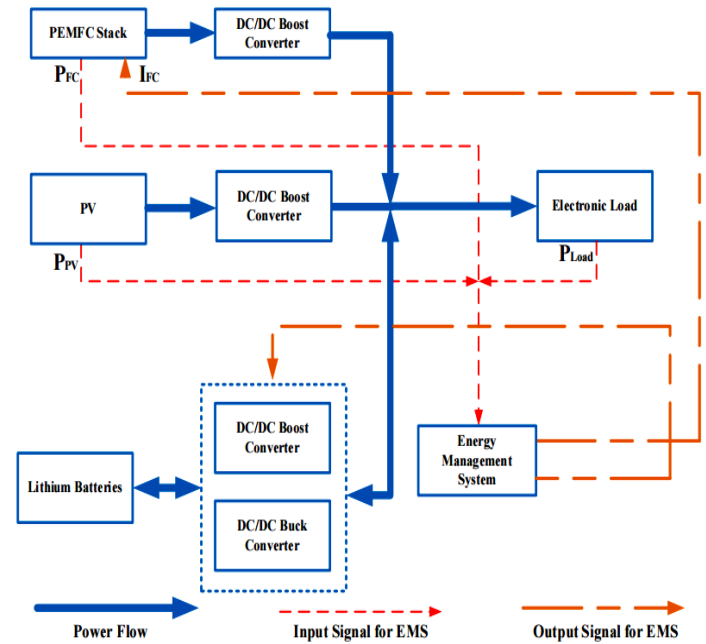
(a) FC, TV and Li-ion Power System Overview
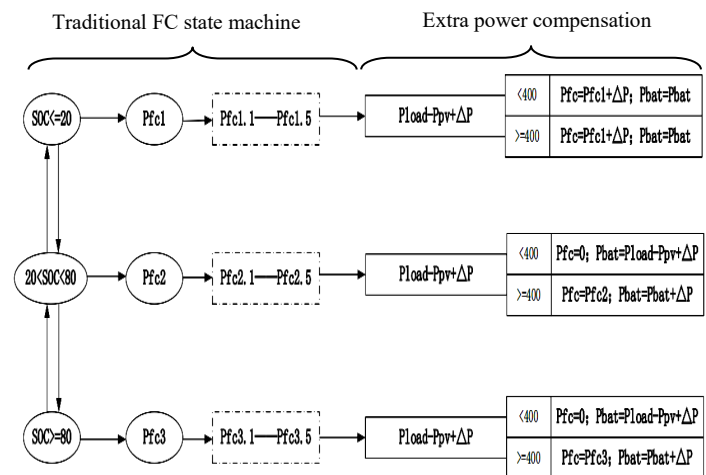
(b) Optimized FC state machine EMS with power compensation

Figure 35: Proposed Power System and State Machine EMS (adapted from [61])

3.8. Development of a Fuzzy-Logic-Based EMS for a Multi-port Multi-operation Mode Residential Smart Micro-grid

Demonstrated in [62] is an advanced grid-tied residential smart micro-grid composing of a fuel cell, solar cell and battery bank to supply the local loads using both electric and magnetic buses. Typically, an electric bus comprising of multiple converter based micro-grids is used; however, this setup is costly and bulky with numerous and large conversion stages; thus, the addition of a common magnetic bus with multi-port converters circumvent these shortcomings and furthermore isolate the conversion ports. Their hybrid architecture with EMS translates to a centralized quicker and versatile system. The suggested micro-grid was capable of working in multiple grid-tied and off-grid modes using a fuzzy logic energy management unit (EMU) controller to choose the proper mode of operation − taking into cognizance short and long-term energy generation and usage. The micro-grid operation performance was enhanced using synchronized bus-voltage balance control technique. The executions of the micro-grid and EMU were experimentally tested for three different cases of the residential load in grid-connected and off-grid modes. The energy distribution and cost analyses for each case show the merits of the EMU for both the grid and user. The various control schemes for each of the power converters/inverters is detailed in the full text. Figure 36 exemplifies and summarizes the research.
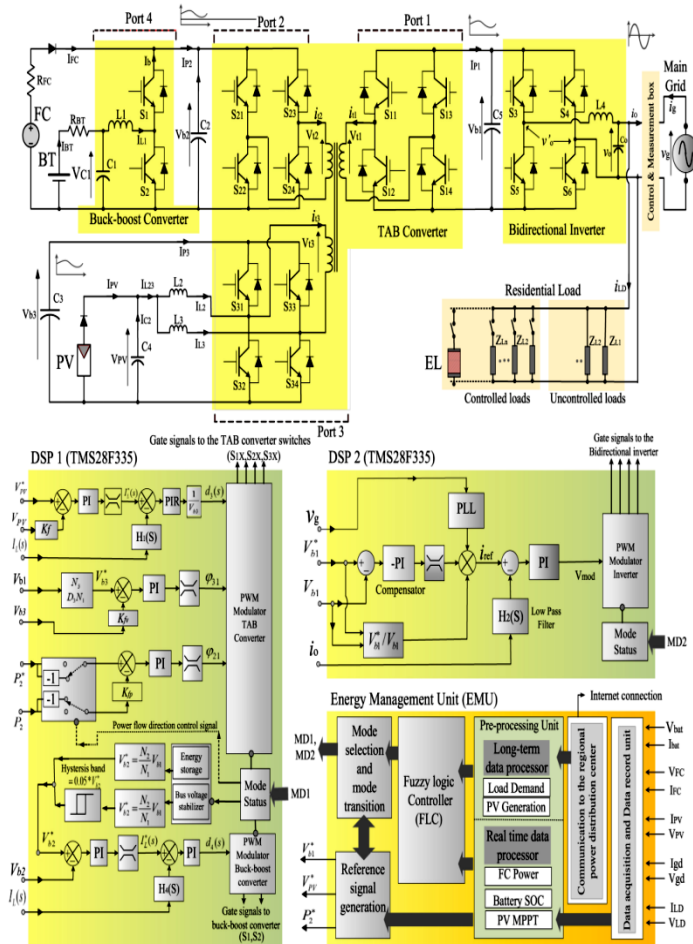
Figure 36: Proposed Smart Micro-grid including Converters, Controllers and EMU (adapted from [62])

3.9. Frequency Separation-based Power Management Strategy for a FC-Powered Drone

Studied in [63] is a hybrid FC and super-capacitor with a DC-DC boost converter power system for drones depicted in Figure 37a. The EMS control technique exploited is routed-in frequency separation-based technique whereby the required power is shared between the energy sources − in this case, the FC and super-capacitor. Depicted in Figures 37b and 37c, the drone flight load profile is divided into low and high frequency components, in which the FC connected to the DC-DC boost converter is controlled to handle the low frequency dynamics whereas the supercapacitor handles the high frequency dynamics during peak power demands as expatiated in Figure 37c. The system was simulated using a real power profile from a small hexacopter experimental flight test and the results justify the EMS was capable of minimizing the fuel cell power variations with the supercapacitor handling all of the transient / peak power demands, consequently prolonging the FC lifetime and drone flight periods.
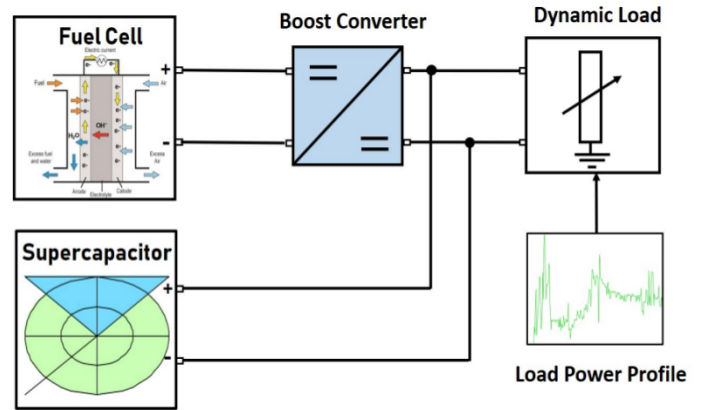
(a) Drone FC and super-capacitor power system overview
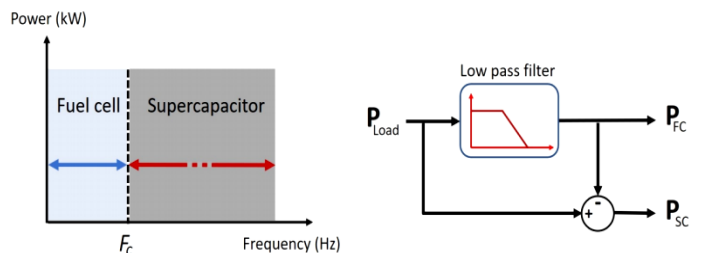
(b) Frequency power sharing concept
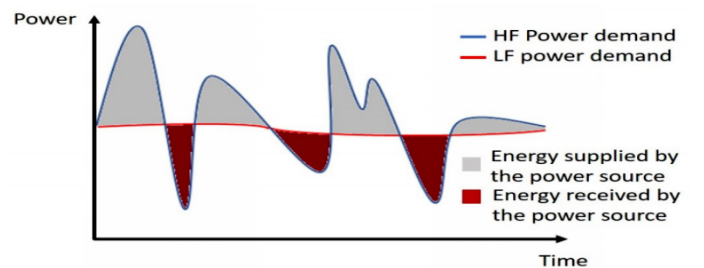
(c) Power frequency sharing

Figure 37: Proposed Drone Hybrid Power System and Frequency Separation EMS (adapted from [63])

3.10.   MPPT Control of an IBC for a PEM FC Applications

Stated in [64] is simply how FC power can be stepped-up using a four-phase IBC and controlled efficiently using a MPPT P&O EMS. The IBC further reduced the FC voltage and current ripples whereas the MPPT ensured max power is extracted from the fuel cell. Figures 38a-38c summarize the implementation.
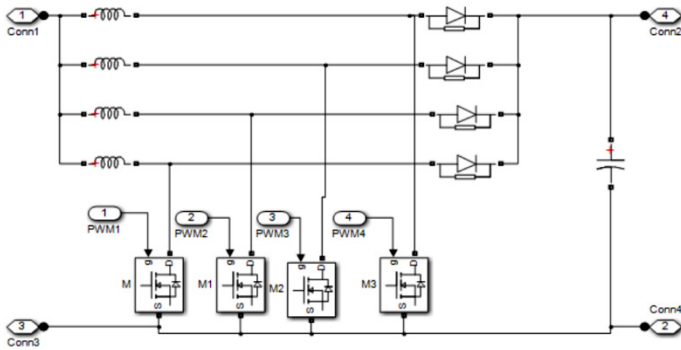
(a) Four-phase IBC Simulink model
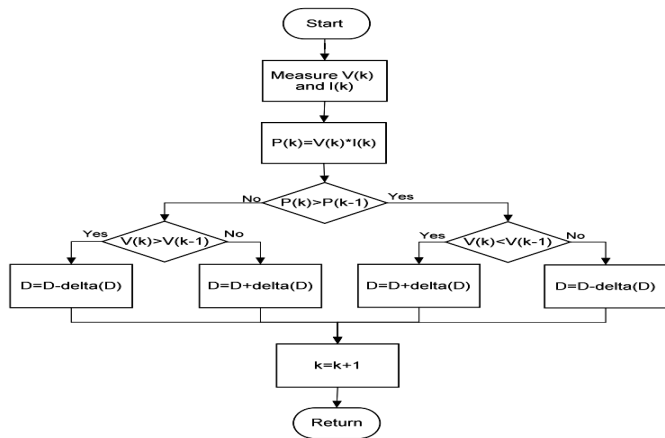
(b) Perturb and Observe MPPT
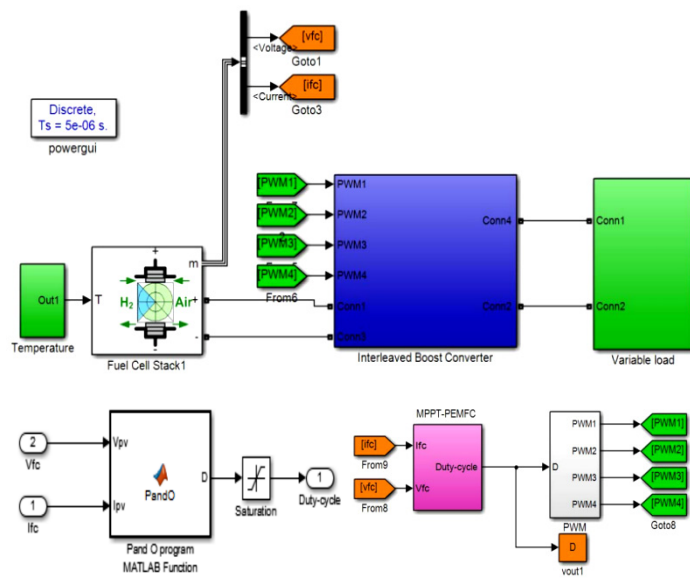
(c) IBC with MPPT Simulink model

Figure 38: FC and Four-phase IBC with MPPT P&O EMS (adapted from [64])

3.11.   Power Flow Control via Differential Power Processing to Enhance Reliability in Hybrid Systems based on PEM FC

Presented in [65] is an interesting study on interconnecting fuel cells to obtain maximum output power. Two interconnection techniques; namely, i) modular integrated converter (MIC) and ii) differential power processing (DPP) including their power converters (synchronous switching bidirectional buck-boost) and EMS technique (MPPT P&O / Hill Climbing (HC)) were modeled using Matlab and discussed in details. As depicted in Figure 39a, the MIC topology has each FC connected in parallel to its own separate converter and each converter is in turn connected in series. This allows several converter topologies and control schemes to be implemented independently. However, the main disadvantages are the number of converters used, the cost involved and poor conversion efficiency − as 100% of the power produced by each FC sub-module is processed. As displayed in Figure 39b, the DPP architecture simply has two FCs connected in parallel with a single buck-boost converter, thereby reducing the total number of power converters by one. Further advantages include simplicity, speed, affordability and improved efficiency − since only a fraction of the FC sub-module generated power is processed. However, the main disadvantage is the complexity in the control technique implementation, since the active balance needs to communicate with each FC sub-module to apply MPPT.

(a) MIC topology showing FCs and converters interconnections

Using Matlab / Simulink, MPPT P&O algorithm illustrated in Figure 39c was implemented on the DPP converter to achieve a fast control loop. The simulation verified the merits of the DPP topology and the MPPT P&O algorithm convergence technique.

3.12. EMS in a Multi-source System using Isolated DC-DC Resonant Converters

Described in [66] is a hybrid FC and super-capacitor with PI controller power system. The research purpose was to develop a control mechanism for the fuel cell and super-capacitor DC-DC resonant power converters to share the system power according to their dynamic responses. Usually, the FC has a slower power dynamic relative to the super-capacitor; therefore, initially the super-capacitor will handle the instant peak power demands whereas the FC provides the bulk of the power during steady state. The isolated LLC resonant converter connects the FC to the DC bus, whereas the super-capacitor connects to the DC bus via the bidirectional resonant converter which charges and discharges the super-capacitor. The modeling and simulations were done using Matlab / Simulink with PLECS and the findings affirm the merits of using resonant converters − which also offer isolation and reduced switching losses. Portrayed in Figure 40a is the FC and super-capacitor hybrid power system and Figures 40b and 40c respectively lucubrate FC and super-capacitor PI controllers.

(b) DPP topology showing FCs and converters interconnections
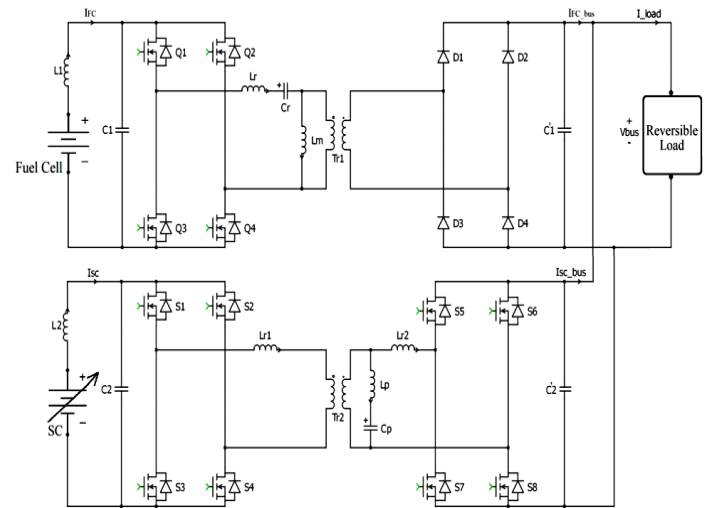
(a) FC and super-capacitor hybrid system

(c) HC / P&O MPPT control algorithm
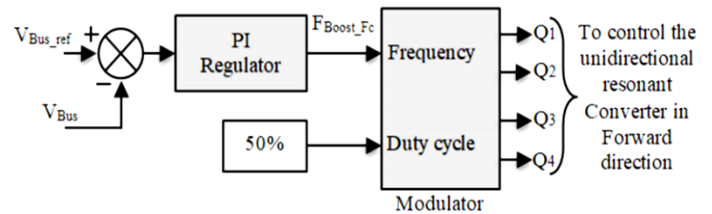
(b) Fuel cell voltage control loop
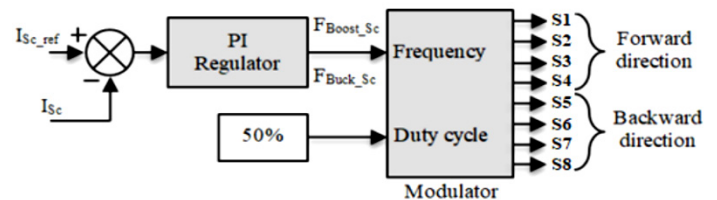
(c) Super-capacitor's bidirectional control loop

Figure 39: MIC, DPP and MPPT P&O Techniques (adapted from [65])

Figure 40: FC, Super-capacitor Hybrid Power System with PI Controller (adapted from [66])

3.13. EMS Optimization for a FC Hybrid Vehicle based on Power Losses Minimization

Indicated in [67], fuel cells hybrid vehicle is a suitable alternative to internal combustion engine vehicles, as they are environmentally friendly. Their research thus proposed an energy management optimization technique for the power distribution system, to increase the driving range of fuel cell hybrid vehicles. The hybrid energy system constitutes a FC connected to a power converter which in turns connects concurrently to a battery and a DC load as represented in Figure 41a. The suggested control optimization algorithm is based on minimizing the energy losses in the system. Using Simulink / PSIM; the losses, costs, size and mass were evaluated, in which it was found that lower FC power and higher battery capacity offer low energy losses and low consumption; whereas maximum fuel cell power and lowest battery capacity provide minimum costs, mass and size. The results correlated other studies in the literature. Figures 41b and 41c depict the basic FC and battery models respectively and Figure 41d shows the optimization algorithm high level overview.
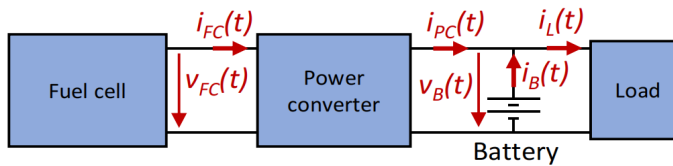
(a) Fuel cell, power converter and battery hybrid power overview

$$v_{FC}(t) = v_{FCoc} - R_{FCc} \cdot i_{FC}(t) - R_{FCv}(i_{FC}) \cdot i_{FC}(t) \qquad (1)$$
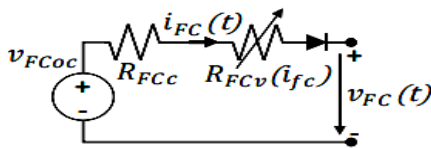
(b) Super-capacitor simplified model

$$v_B(t) = v_{Boc}(SoC) - R_B \cdot i_B(t) \qquad (2)$$
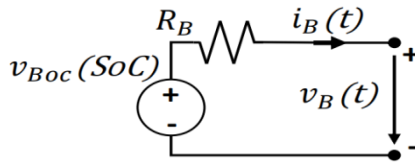
(c) Battery basic model
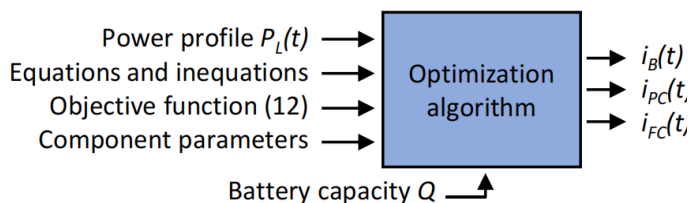
(d) Optimization algorithm input and output data

Figure 41: System Overview, Fuel Cell and Battery Models and Optimization Algorithm Overview (adapted from [67])

3.14. Dynamic Modeling and Closed-loop Control of Hybrid Grid-connected Renewable Energy System with Multi-input Multi-output Controller

Proposed in [68] and summarized in Figure 42a, is the use of multi-input multi-output (MIMO) technique to dynamically model and closed-loop control a hybrid grid-tied renewable energy system. The system constitutes a solar cell and FC each respectively connected to their boost converters which are in turn connected in parallel to a single-phase H-bridge inverter to supply an AC load. The system employed the traditional MPPT and PI control techniques compensated by the MIMO network detailed in Figure 42b. Using the system transfer functions frequency response, the MIMO controller gains are tuned. MatLab and Simulink were used to simulate and analyse the designed MIMO controller accuracy and effectiveness and from the results, MIMO is quick and stable at various functional points, having a negligible steady-state error as well as with a grid THD of ~1.48% in accordance with standards of distribution networks.
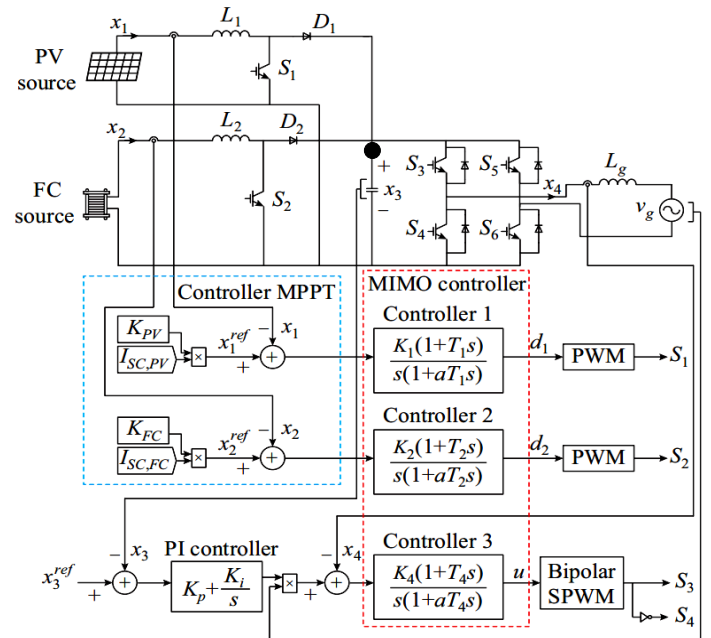
(a) Suggested control structure for grid-connected PV/FC hybrid energy system
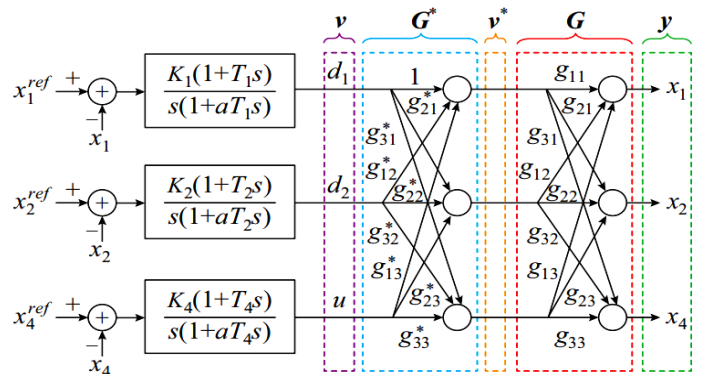
(b) Compensation network

Figure 42: Proposed FC and PV Hybrid Energy System and Compensation Network (adapted from [68])

3.15. FCEVs — A Brief Review of Current Topologies and EMS Strategies

Articulated in [69], advancement in technology and new international policies on electric / hybrid electric vehicles are becoming trendy. In light of this, their research focused on fuel cells and energy storage devices as well as power converters and EMS techniques to sustain hybrid electric vehicle dynamic power demands. Different fuel cell energy / power configurations and power converters topologies were assessed and the highlights are presented in Figures 43a and 43b − respectively a fuel cell with storage devices and dual-input high step-up isolated converter. Furthermore, miscellaneous EMS strategies were examined with focus on energy efficiency, usage of hydrogen and sub-systems decay involved. The pros and cons of rule-based, learning-based and optimisation-based EMS strategies were discussed and the conclusion is to hybridize modern and existing strategies to eliminate the uncertainties regarding EMS techniques robustness.

3.16. A Review and Research on FCEVs: Topologies, Power Electronic Converters, EMS Methods, Technical Challenges, Marketing and Future Aspects

Analyzed extensively in [70], fuel cells are the future especially for FCEV as shown in Figure 44a. In this respect, a comprehensive study of types of FCs with electric motors are explained with focus on their areas of applications, diagnostic properties and working environments. Furthermore, power converters which boost the FC voltages to drive different motor topologies used in FCEVs, are elaborated based on their structural frequency of use, their architecture and difficulty. Summarized in Figure 44b, assorted FCEVs power converters EMS schemes and technical challenges were examined and the final closing remarks highlighted the present status and future prospects using significant number of marketing and target data.

(a) FC, battery and ultra-capacitor hybrid electric vehicle configuration
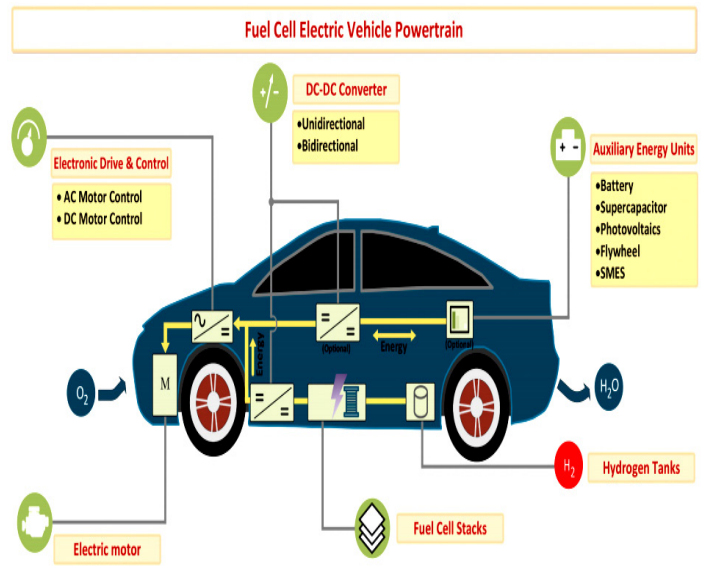
(a) FCEV power transmission system with auxiliary power supplies

(b) Dual-Input High Step-Up Isolated Converter (DHSIC)

Figure 43: FC Hybrid Electric Vehicle and DHSIC Scheme (adapted from [69])
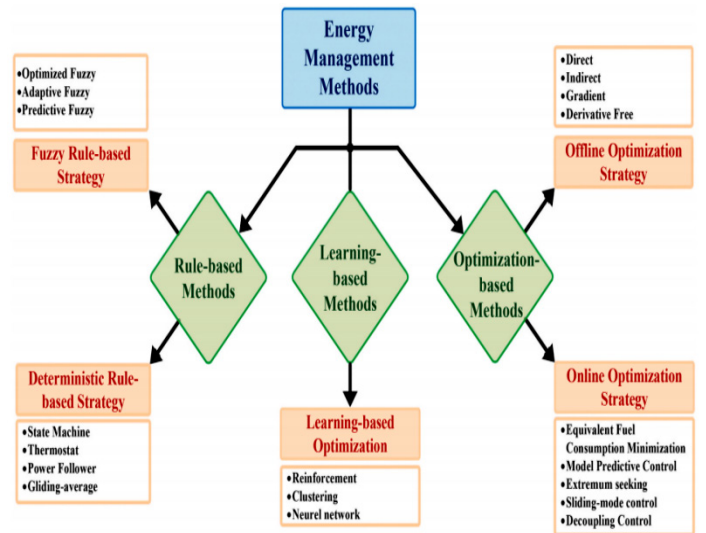
(b) FCEVs EMS classification of technical challenges and system problems

Figure 44: FCEV Power Transmission System and EMS Schemes and Challenges (adapted from [70])

Table 2: EMS Case Studies Examined Summary

EMS Research	Highlights, Merits and Demerits
Study 3.1 (S. Motahhir *et al*, 2017) [37]	MIL, SIL and PIL tests for MPPT algorithm. Implemented MPPT algorithm on each and all three formats reasonably gave similar results.
Study 3.2 (N. Sulaiman *et al*, 2015) [38]	Extensive analysis on FC fuel starvation and EMS schemes for FC HEV: In-depth FC issues, challenges & solutions were presented.
Study 3.3 (S.N. Motapon *et al*, 2014) [57]	Implemented simulated and experimental test frameworks for relative analyses of various EMS methods for a FC hybrid power system.
Study 3.4 (P. Mungporn *et al*, 2019) [58]	Developed further a model free control (MFC) to manage the fuel cell power for DC micro-grid applications. In their approach, a 2-phase interleaved boost converter was implemented to address the non-linear control problem and the simulated and practical results correlated.
Study 3.5 (G.G. Suárez-Velázquez *et al*, 2020) [59]	Used VSC to autonomously regulate the active and reactive powers injected to the grid, via a sinusoidal SPWM strategy and two linear control loops PI(1) and PI(2). The VSC was able to reach steady state within 30ms when the active and reactive powers were doubled.
Study 3.6 (Y. Jeong *et al*, 2019) [60]	The efficiency of parallel FC systems under light-load is enhanced by changing accordingly the quantity of parallel power units to meet the light-load demand and substantially reduce the switching / core losses. Three 300W units were paralleled to achieve a 900W efficient system.
Study 3.7 (Y. Zhang *et al*, 2019) [61]	A state machine EMS control technique with power compensation was employed to curb the frequency of the PEM fuel cell power output variations and ensuring the Li-ion battery charges & discharges within the ideal periods.
Study 3.8 (M. Jafari *et al*, 2019) [62]	Demonstrated an advanced grid-tied household smart micro-grid consisting of a fuel cell, solar cell and battery bank to provide the local loads using both electric and magnetic buses. The magnetic bus with the multi-port converters augments the electric bus and further isolates the conversion ports. The EMU controller was tested for three distinct scenarios of the home load and the distribution of energy and cost analyses for each case, show the EMU merits.
Study 3.9 (M.N. Boukoberine *et al*, 2020) [63]	The EMS method used is routed-in frequency separation-based scheme, whereby the required power is shared between the energy sources.
Study 3.10 (E.M. Barhoumi *et al*, 2020) [64]	FC power can be stepped-up using a four-phase IBC and controlled efficiently using a MPPT EMS scheme to reduce power ripples.
Study 3.11 (K.S. Artal-Sevil *et al*, 2020) [65]	Presented MIC and DPP connections of FCs with power converters. MPPT was used on the DPP converter to achieve a fast control loop.
Study 3.12 (M. Arazi *et al*, 2020) [66]	Developed a mechanism for FCs and SCs DC-DC resonant power converters to share the system power using their dynamic responses.
Study 3.13 (A. Martin-Lozano *et al*, 2020) [67]	Proposed an EMS optimization technique for the power distribution system to increase the driving range of fuel cell hybrid vehicles. The results correlated other studies in the literature.
Study 3.14 (M. Salimi *et al*, 2021) [68]	Suggested the used of MIMO technique to dynamically model and closed-loop control a FC hybrid grid-tied renewable energy system.
Study 3.15 (I.S. Sorlei *et al*, 2021) [69]	Used FCs and energy storage devices as well as power converters and EMS techniques to sustain hybrid electric vehicle dynamic power.
Study 3.16 (M. İnci *et al*, 2021) [70]	Reviewed extensively FC types with electric motors with focus on their uses, diagnostic properties and finally working environments.

Table 2 summarizes the reviewed EMS FC applicable studies.

4. Conclusion

Energy insecurity and electrical energy in particular, is a progressive pressing societal crisis in South Africa and Africa. In this regard, this article articulated a structural review of forty four different power converters and EMS research case studies to reasonably choose and develop a suitable FC power converter and EMS scheme for a hybrid FC CCHP system for households / commercial applications. From the review, it was observed that the power converters based on IBC / variants and as well isolated boost converters were of interests. IBC are simple, more robust, good for ripples reduction and peak power applications. However, the fundamental IBC topology is not isolated and adding isolation transformers offers protection but increases the costs and size. Likewise, EMS techniques can be grouped under rule-based, learning-based and optimization-based but the most popular EMS strategy used with power converters are the MPPT and PI controller. Furthermore, FCs can also be modularized with each FC sub-module having its own power converters and EMS scheme to increase the system efficiency. In sum, there is no method that is flawless − choosing a particular approach and trading-off different features depend on the targeted applications and the research objectives; whether to maximize efficiency, robustness, safety, performance etc and minimize costs, size, noise, complexity etc. For our research project, power converters based-on IBC variants and BDC with EMS based on MPPT and or PID controller for use with FC, Li-ion battery, ultra-capacitor and thermo-electric devices are considered to investigate further the CCHP system postulated in Figure 45 to conclude the study.

Figure 45: Postulated Fuel Cell CCHP System Undergoing Research

Glossary

AC	Alternating Current
AOCA	Adaptive Optimal Control Algorithm
BDC	Bidirectional DC-DC Converter
BDCMG	Bipolar DC Micro-grid
CCHP	Combined Cooling, Heating and Power
CMMC	Current-fed Modular Multilevel Converter
CPC	Conventional Phase-shift Control
CPUT	Cape Peninsula University of Technology
DAFB	Dual Active Full Bridge
DC	Direct Current
DC-IBC	Direct Coupled-Interleaved Boost Converters
DG	Distributed Generation
DHB	Dual Half Bridge
DHSIC	Dual-Input High Step-Up Isolated Converter
DPP	Differential Power Processing
EGS	Energy Generation System
EIS	Electrochemical Impedance Spectroscopy
EMI	Electro Magnetic Interference
EMS	Energy Management Systems / Energy Management & Storage
EMU	Energy Management Unit
FC	Fuel Cell
FCEV	Fuel Cell Electric Vehicle
FCS	Fuel Cell Stack
FIC	Full-bridge Isolated Converter
FLC	Fuzzy Logic Controller
FPGA	Field Programmable Gate Array
GaN	Gallium Nitride
HC	Hill Climbing
HF	High Frequency
HIC	Half-bridge Isolated Converter
HIL	Hardware In the Loop
HPS	Hybrid Power Source
IBC	Interleaved Boost Converters
IC-IBC	Inverse Coupled-Interleaved Boost Converters

LF	Low Frequency
MFC	Model Free Control
MIC	Modular-Integrated Converter
MIL	Model In the Loop
MIMO	Multi-Input Multi-Output
MPPT	Maximum Power Point Tracking
PCS	Power Conditioning Stage
PEM	Proton Exchange Membrane or Polymer Electrolyte Membrane
PI	Proportional Integral
PIL	Processor In the Loop
PLL	Phase Lock Loop
PV	Photovoltaic
PWM	Pulse Width Modulation
RIC	Resonance Isolated Converter
SA	Simulated Annealing
SC	Super-capacitor
SiC	Silicon Carbide
SIL	Software In the Loop
SOC	State of Charge
SMC	Sliding Mode Control
SPWM	Sinusoidal Pulsed Width Modulation
TEG	Thermoelectric Generator
THD	Total Harmonic Distortion
UC	Ultra-capacitor
UC-IBC	UnCoupled-Interleaved Boost Converters
VSC	Voltage Source Converter
WADALINE	Wavelet Adaptive Linear Neuron
ZCS	Zero Current Switching
ZSI	Z-Source Inverter
ZVS	Zero Voltage Switching

Conflict of Interest

The authors declare no conflict of interest.

References

[1] N.P. Bayendang, M.T. Kahn, V. Balyan, I. Draganov, "CCHP Systems Analysis with Emphasis on Fuel Cells, Thermoelectricity and Power

Converters," 2020 5th International Conference on Smart and Sustainable Technologies, SpliTech 2020, 2020, doi:10.23919/SpliTech49282.2020.9243720.

[2] S. Vigneshwaran, R. Vijayalakshmi, "High efficiency DC/DC buck-boost converters for high power DC system using adaptive control," American-Eurasian Journal of Scientific Research, **11**(5), 381-389, 2016. doi: 10.5829/idosi.aejsr.2016.11.5.22957.

[3] A. Kirubakaran, J. Shailendra, R.K. Nema, "The PEM fuel cell system with DC/DC boost converter: Design, modeling and simulation," International Journal of Recent Trends in Engineering, **1**(3), 2009, doi: 01.ijepe.01.01.05.

[4] L.M.P. Fanjul, Design Considerations for DC-DC Converters in Fuel-cell Systems, PhD Thesis, Texas A&M University, 2006.

[5] M. Grotsch, M. Mangold, A. Kienle, "Analysis of the coupling behaviour of PEM fuel cells and DC-DC converters", Energies, **2**, 71-96, 2009, doi: 10.3390/en2010071.

[6] M.T. Outeiro, A. Carvalho, Methodology of Designing Power Converters for Fuel-cell Based Systems: A Resonant Approach, New Developments in Renewable Energy, 2013, http://dx.doi.org/10.5772/54674.

[7] K. Suh and A.G. Stefanopoulou, "Coordination of Converter and Fuel Cell Controllers," in Proceedings of the 2005 IEEE International Symposium on, Mediterrean Conference on Control and Automation Intelligent Control, Limassol, Cyprus, 2005, doi: 10.1109/.2005.1467076.

[8] M. Nymand, M.A.E. Andersen, "A New Approach to High Efficiency in Isolated Boost Converters for High-Power Low-Voltage Fuel Cell Applications," in 2008 13th Power Electronics and Motion Control Conference, Poznan, Poland, 2008, 127-131, https://doi.org/10.1109/EPEPEMC.2008.4635255.

[9] R. Seyezhai, R. Anitha, S. Mahalakshmi, M. Bhavani, "High gain interleaved boost converter for fuel cell applications," Bulletin of Electrical Engineering and Informatics, **2**(4), 2013, 265-271, doi: https://doi.org/10.11591/eei.v2i4.192.

[10] Y. Huangfu, R. Ma, B. Liang, Y. Li. "High power efficiency buck converter design for standalone wind generation system," International Journal of Antennas and Propagation, Volume 2015, Special Issue: Recent Advances in Theory and Applications of Electromagnetic Metamaterials, http://dx.doi.org/10.1155/2015/751830.

[11] F.M. Mwaniki, High voltage boost DC-DC converter suitable for variable voltage sources and high power photovoltaic application, MEng Dissertation, University of Pretoria, 2014, http://hdl.handle.net/2263/37320.

[12] B. Eckardt, M. März, A. Hofmann, M. Gräf and J. Ungethüm, "High Power Buck-Boost DC/DC Converter for Automotive Power-train Application," in 2005 Official Proceedings of the International Conference of Power Electronics, Intelligent Motion, Power Quality: PCIM 2005 Europe, Nürnberg, Germany, 2005, 685, http://publica.fraunhofer.de/documents/N-46644.html.

[13] M. Kabalo, B. Blunier, D. Bouquain, A. Miraoui, "State-of-the-Art of DC-DC Converters for Fuel Cell Vehicles," in 2010 IEEE Vehicle Power and Propulsion Conference, Lille, France, 2010, doi: 10.1109/VPPC.2010.5729051.

[14] M. Delshad, H. Farzanehfard, "A new soft switched push pull current fed converter for fuel cell applications," Energy Conversion and Management, **52**(2), 917–923, 2011, https://doi.org/10.1016/j.enconman.2010.08.019.

[15] N. Bizon, "A new topology of fuel cell hybrid power source for efficient operation and high reliability," Journal of Power Sources, **196**(6), 3260–3270, 2011, doi: 10.1016/j.jpowsour.2010.11.049.

[16] O.A. Ahmed, J.A.M. Bleijs, "Power flow control methods for an ultra-capacitor bidirectional converter in DC micro-grids – a comparative Study," Renewable and Sustainable Energy Reviews, **26**, 727–738, 2013, https://doi.org/10.1016/j.rser.2013.06.021.

[17] A. Kolli, A. Gaillard, A. De Bernardinis, O. Bethoux, D. Hissel, Z. Khatir, "Design and Control of a High Frequency Six-phase Interleaved DC/DC Converter based on SiC Power MOSFETs for a PEMFC," in 2015 6th International Conference on Fundamentals and Development of Fuel Cells (FDFC 2015), Toulouse, France, 2015.

[18] A. Kolli, A. De-Bernardinis, Z. Khatir, A. Gaillard, O. Béthoux and D. Hissel, "Part-load Control Strategy of a 20kW SiC Power Converter for Embedded PEMFC Multi-stack Architectures," IECON 2015 - 41st Annual Conference of the IEEE Industrial Electronics Society, Yokohama, Japan, 2015, 4627-4632, doi: 10.1109/IECON.2015.7392821.

[19] A. Carvalho, M.T. Outeiro, MatLab in Model-Based Design for Power Electronics Systems, Engineering Education and Research Using MatLab, 2011, doi: 10.5772/21144.

[20] H. Wang, Design and Control of a 6-phase Interleaved Boost Converter based on SiC semiconductors with EIS Functionality for Fuel Cell Electric Vehicle. PhD Thesis, UBFC and UTBM, Belfort, France, 2019.

[21] J.W. Pratt, L.E. Klebanoff, K. Munoz-Ramos, A.A. Akhil, D.B. Curgus, B.L. Schenkman, Proton Exchange Membrane Fuel Cells for Electrical Power Generation On-Board Commercial Airplanes, SAND2011-3119 Unlimited Release Printed, 2011.

[22] J.L. Casteleiro-Roca, A.J. Barragán, F. Segura, J.L. Calvo-Rolle, J.M. Andújar, "Fuel cell output current Prediction with a hybrid intelligent system," Complexity, Volume 2019, Special Issue: Advanced Controls in Complex Clean Energy Devices, Subsystems, and Processes, https://doi.org/10.1155/2019/6317270.

[23] A. Kolli, A. Gaillard, A. De Bernardinis, O. Bethoux, D. Hissel, Z. Khatir, "A review on DC/DC converter architectures for power fuel cell applications," Energy Conversion and Management, **105**, 716-730, 2015, https://doi.org/10.1016/j.enconman.2015.07.060.

[24] D. Ravi, S.S. Letha, P. Samuel, B.M. Reddy, "An Overview of Various DC-DC Converter Techniques used for Fuel Cell based Applications," 2018 International Conference on Power Energy, Environment and Intelligent Control (PEEIC), Greater Noida, India, 2018, 16-21, doi: 10.1109/PEEIC.2018.8665465.

[25] J. Gao, M. Li, Y. Hu, H. Chen, Y. Ma, "Challenges and developments of automotive fuel cell hybrid power system and control," Science China Information Sciences, **62**(5), 2019, doi: https://doi.org/10.1007/s11432-018-9690-y.

[26] H. Liu, L. Xu, Z. Hu, J. Li, H. Jiang, M. Ouyang, "Experimental Study and Performance Analysis on High Power Fuel Cell System," IECON 2020 The 46th Annual Conference of the IEEE Industrial Electronics Society, Singapore, 2020, 2031-2035, doi: 10.1109/IECON43393.2020.9254802.

[27] R. Miyazaki, T. Mishima, C.M. Lai, "Coupled Inductor-assisted Current-Fed Snubber-less Zero-Current-Soft Switching High Step-Up DC-DC Converter for Fuel Cell Power Interface," 2020 IEEE 9th Global Conference on Consumer Electronics (GCCE), Kobe, Japan, 2020, 797-801, doi: 10.1109/GCCE50665.2020.9291776.

[28] M.S. Bhaskar, V.K. Ramachandaramurthy, S. Padmanaban, F. Blaabjerg, D.M. Ionel, M. Mitolo, D. Almakhles, "Survey of DC-DC Non-Isolated Topologies for Unidirectional Power Flow in Fuel Cell Vehicles," in IEEE Access, 8, 178130-178166, 2020, doi: 10.1109/ACCESS.2020.3027041.

[29] K.S. Rathode, S.K. Sharma, S. Shringi, "Performance Analysis of PV & Fuel cell based Grid Integrated Power System," 2019 International Conference on Communication and Electronics Systems (ICCES), Coimbatore, India, 2019, 970-975, doi: 10.1109/ICCES45898.2019.9002090.

[30] S. Kavyapriya, R.K. Kumar, "Modeling and Simulation of DC-DC Converters for Fuel Cell System," International Journal of Engineering and Advanced Technology (IJEAT), **9**(3), 2020, doi: 10.35940/ijeat.C5754.029320.

[31] P. Bazin, B. Beranger, J. Ecrabey, L. Garnier, S. Mercier, "Smart fuel cell module (6.5 kW) for a range extender application," 2020 22nd European Conference on Power Electronics and Applications (EPE'20 ECCE Europe), Lyon, France, 2020, 1-8, doi: 10.23919/EPE20ECCEEurope43536.2020.9215856.

[32] A. Gonnet, S.G. Jorge, C. Busada, J. Solsona, "Power converter topology for conditioning a fuel cells battery voltage," 2019 Argentine Conference on Electronics (CAE), Mar del Plata, Argentina, 2019, 9-14, doi: 10.1109/CAE.2019.8709157.

[33] J. Corcau, L. Dinca, I. Adochiei, T. L. Grigorie, "Modeling and Simulation of an Aerodrome Electrical Power Source Based on Fuel Cells," 2019 E-Health and Bioengineering Conference (EHB), Iasi, Romania, 2019, 1-4, doi: 10.1109/EHB47216.2019.8969870.

[34] A. Abdelhakim, F. Blaabjerg, "Current-fed Modular Multilevel Converter (CMMC) for Fuel Cell and Photovoltaic Integration," 2020 IEEE 21st Workshop on Control and Modeling for Power Electronics (COMPEL), Aalborg, Denmark, 2020, 1-6, doi: 10.1109/COMPEL49091.2020.9265695.

[35] P. Prabhakaran, V. Agarwal, "Novel Four-Port DC–DC Converter for Interfacing Solar PV–Fuel Cell Hybrid Sources With Low-Voltage Bipolar DC Microgrids," in IEEE Journal of Emerging and Selected Topics in Power Electronics, **8**(2), 1330-1340, 2020, doi: 10.1109/JESTPE.2018.2885613.

[36] H.S. Youn, D.H. Yun, W.S. Lee, I.O. Lee, "Study on Boost Converters with High Power-Density for Hydrogen-Fuel-Cell Hybrid Railway System", Electronics, **9**(5), 771, 2020, doi: https://doi.org/10.3390/electronics9050771.

[37] S. Motahhir, E.G. Abdelaziz, A. Derouich, "MIL and SIL and PIL tests for MPPT algorithm," Cogent Engineering, **4**(1), 2017, https://doi.org/10.1080/23311916.2017.1378475.

[38] N. Sulaiman, M.A. Hannan, A. Mohamed, E.H. Majlan, W.R. Wan Daud, "Review on energy management system for fuel cell hybrid electric vehicle: Issues and challenges," Renewable and Sustainable Energy Reviews, **52**, 802–814, 2015, https://doi.org/10.1016/j.rser.2015.07.132.

[39] D. Xiao, Q. Wang, "The Research of Energy Management Strategy for Fuel Cell Hybrid Vehicle," in 2012 International Conference on Industrial Control and Electronics Engineering, Xi'an, China, 2012, 931–934, doi: 10.1109/ICICEE.2012.247.

[40] N. Ouddah, M. Boukhnifer, A. Raisemche, "Two Control Energy Management Schemes for Electrical Hybrid Vehicle," in 2013 Proceedings of the 10th International Multi-conference on Systems, Signals & Devices (SSD13), Hammamet, Tunisia, doi: 10.1109/SSD.2013.6564135.

[41] O. Sundstrom, A. Stefanopoulou, "Optimal Power Split in Fuel Cell Hybrid Electric Vehicle with Different Battery Sizes, Drive Cycles and Objectives," in 2006 IEEE Conference on Computer Aided Control System Design, 2006 IEEE International Conference on Control Applications, 2006 IEEE International Symposium on Intelligent Control, Munich, Germany, 1681–1688, doi: 10.1109/CACSD-CCA-ISIC.2006.4776894.

[42] C.J. Xie, S.H. Quan, Q.H. Chen, "Multiple Model Control for Hybrid Power System of Fuel Cell Electric Vehicle," in 2008 IEEE Vehicle Power and Propulsion Conference, Harbin, China, 2008, doi: 10.1109/VPPC.2008.4677527.

[43] P. Thounthong, S. Pierfederici, J.P. Martin, M. Hinaje, B. Davat, "Modelling and control of fuel-cell super-capacitor hybrid source based on differential flatness control," IEEE Transaction on Vehicle Technology, **59** (6), 2700–2710, 2010, doi: 10.1109/TVT.2010.2046759.

[44] A. Tani, M.B. Camara, B. Dakyo, Y. Azzouz, "DC/DC and DC/ACconverters control for hybrid electric vehicles energy management ultra-capacitors and fuel cell," IEEE Transactions on Industrial Informatics, 9(2), 686–696, 2013, doi: 10.1109/TII.2012.2225632.

[45] M. Uzunoglu, M.S. Alam, "Modelling and analysis of an FC/UC Hybrid vehicular power system using a novel-wavelet-based load sharing algorithm," IEEE Transaction on Energy Conversion, **23**(1), 263–272, 2008, doi: 10.1109/TEC.2007.908366.

[45] D.S. Efstathiou, A.K. Petrou, P. Spanoudakis, N.C. Tsourveloudis, K.P. Valavanis, "Recent Advances on the Energy Management of a Hybrid Electric Vehicle," in 2012 20th Mediterranean Conference on Control & Automation (MED), Barcelona, Spain, 2012, 896–901, doi: 10.1109/MED.2012.6265752.

[47] Y. Ates, M. Uzunoglu, O. Erdinc, B. Vural, "A Wavelet-ADALINE Network based Load Sharing and Control Algorithm for a FC/UC Hybrid Vehicular Power System," in Proceedings of the 2009 International Conference on Clean Electrical Power, Capri, Italy, 2009, 591–94, doi: 10.1109/ICCEP.2009.5211976.

[48] C.H. Zheng, C.M. Lee, Y.C. Huang, W.S. Lin, "Adaptive Optimal Control Algorithm for Maturing Energy Management Strategy in Fuel–cell/Li-ion/Super-Capacitor Hybrid Electric Vehicles," in 2013 9th Asian control conference, Istanbul, Italy, 2013, 1–7, doi: 10.1109/ASCC.2013.6606091.

[49] M.A. Hannan, F.A. Azidin, A. Mohamed, "Multi-sources model and control algorithm of an energy management system for light electric vehicles," Energy Converters Management, 62, 123–30, 2012, https://doi.org/10.1016/j.enconman.2012.04.001.

[50] J.S. Martinez, D. Hissel, M.C. Pera, M. Amiet, "Practical control structure and energy management of a test bed hybrid electric vehicle." IEEE Transactions on Vehicular Technology, **60**(9), 4139–4152, 2011, doi: 10.1109/TVT.2011.2169821.

[51] E. Schaltz, P.O. Rasmussen, "Design and Comparison of Power Systems for a Fuel Cell Hybrid Electric Vehicle," in IEEE Industry Applications Society Annual Meeting," Edmonton, AB, Canada, 2008, 1–8, doi: 10.1109/08IAS.2008.184.

[52] V. Paladini, T. Donateo, A. De Risi, D. Laforgia, "Super-capacitors fuel-cell hybrid electric vehicle optimization & control strategy development," Energy Conversion and Management, **48**(11), 3001-3008, 2007, https://doi.org/10.1016/j.enconman.2007.07.014.

[53] M. Zandi, A. Payman, J.P. Martin, S. Pierfederici, B. Davat, F. Meibody-Tabar, "Energy management of a fuel cell/super-capacitor/battery power source for electric vehicular applications," IEEE Transactions on Vehicular Technology, **60**(2), 433–443, 2011, doi: 10.1109/TVT.2010.2091433.

[54] H. Fathabadi, "Novel fuel cell/battery/super-capacitor hybrid power source for fuel-cell hybrid electric vehicles," Energy, 143, 467 – 477, 2018, https://doi.org/10.1016/j.energy.2017.10.107.

[55] Q. Li, H. Yang, Y. Han, M. Li, W. Chen, "A state machine strategy based on droop control for an energy management system of PEMFC-battery, super-capacitor hybrid tramway," International Journal of Hydrogen Energy, **41**(36), 16148 – 16159, 2016, https://doi.org/10.1016/j.ijhydene.2016.04.254.

[56] O. Kraa, H. Ghodbane, R. Saadi, M.Y. Ayad, M. Becherif, A. Aboubou, M. Bahri, "Energy Management of Fuel Cell/ Super-capacitor Hybrid Source Based on Linear and Sliding Mode Control," in the International Conference on Technologies and Materials for Renewable Energy, Environment and Sustainability, TMREES15, Energy Procedia, 2015, 74, 1258 – 1264, https://doi.org/10.1016/j.egypro.2015.07.770.

[57] S.N. Motapon, L. Dessaint, K. Al-Haddad, "A comparative study of energy management schemes for a fuel-cell hybrid emergency power system of More-Electric Aircraft," IEEE Transactions on Industrial Electronics, **61**(3),1320-1334, 2014, doi: 10.1109/TIE.2013.2257152.

[58] P. Mungporn, B. Yodwong, P. Thounthong, B. Nahid-Mobarakeh, N. Takorabet, D. Guilbert, N. Bizon, P. Kumam, C. Kaewprapha, "Model-Free Control of Multiphase Interleaved Boost Converter for Fuel Cell/Reformer Power Generation," 2019 Research, Invention, and Innovation Congress (RI2C), Bangkok, Thailand, 2019, 1-6, doi: 10.1109/RI2C48728.2019.8999919.

[59] G.G. Suárez-Velázquez, G.E. Mejia-Ruiz, P.M. García-Vite, "Control and Grid Connection of Fuel Cell Power System," 2020 IEEE International Autumn Meeting on Power, Electronics and Computing (ROPEC), Ixtapa, Mexico, 2020, 1-5, doi: 10.1109/ROPEC50909.2020.9258729.

[60] Y. Jeong, R.A.L. Rorrer, B. Lee, J. Park, "A Novel Control Scheme for High Efficiency Fuel Cell Power Systems in Parallel Structure," 2019 IEEE Energy Conversion Congress and Exposition (ECCE), Baltimore, MD, USA, 2019, 940-946, doi: 10.1109/ECCE.2019.8912856.

[61] Y. Zhang, Y. Huangfu, W. Liu, L. Guo, "An energy management strategy based on state machine with power compensation for photovoltaic-PEMFC-lithium battery power system," 2019 IEEE International Conference on Industrial Technology (ICIT), Melbourne, VIC, Australia, 2019, 1675-1680, doi: 10.1109/ICIT.2019.8843696.

[62] M. Jafari, Z. Malekjamshidi, D.D. Lu, J. Zhu, "Development of a Fuzzy-Logic-Based Energy Management System for a Multiport Multioperation Mode Residential Smart Microgrid," in IEEE Transactions on Power Electronics, 34(4), 3283-3301, 2019, doi: 10.1109/TPEL.2018.2850852.

[63] M.N. Boukoberine, Z. Zhou, M. Benbouzid, T. Donateo, "Frequency Separation-based Power Management Strategy for a Fuel Cell-Powered Drone," 2020 2nd International Conference on Smart Power & Internet Energy Systems (SPIES), Bangkok, Thailand, 2020, 209-214, doi: 10.1109/SPIES48661.2020.9242975.

[64] E.M. Barhoumi, P. Chukwuleke Okonkwo, I. B. Belgacem, M. Zghaibeh, "MPPT Control of an Interleaved Boost Converter for a Polymer Electrolyte Membrane Fuel Cell Applications," 2020 International Conference on Electrical and Information Technologies (ICEIT), Rabat, Morocco, 2020, 1-5, doi: 10.1109/ICEIT48248.2020.9113228.

[65] J.S. Artal-Sevil, J.A. Domínguez-Navarro, C. Bernal-Ruiz, A. Coronado-Mendoza, "Power Flow Control through Differential Power Processing to improve reliability in hybrid systems based on PEM-Fuel Cell," 2020 Fifteenth International Conference on Ecological Vehicles and Renewable Energies (EVER), Monte-Carlo, Monaco, 2020, 1-12, doi: 10.1109/EVER48776.2020.9243125.

[66] M. Arazi, A. Payman, M. B. Camara, B. Dakyo, "Energy management in a Multi-source System using isolated DC-DC resonant converters," 2020 22nd European Conference on Power Electronics and Applications (EPE'20 ECCE Europe), Lyon, France, 2020, 1-7, doi: 10.23919/EPE20ECCEEurope43536.2020.9215662.

[67] A. Martin-Lozano, A. Barrado, A. Rodriguez-Lorente, A. Lázaro, C. Fernández, "Energy Management System Optimization for a Fuel Cell Hybrid Vehicle based on Power Losses Minimization," 2020 IEEE 14th International Conference on Compatibility, Power Electronics and Power Engineering (CPE-POWERENG), Setubal, Portugal, 2020, 402-408, doi: 10.1109/CPE-POWERENG48600.2020.9161482.

[68] M. Salimi, F. Radmand, M. H. Firouz, "Dynamic Modeling and Closed-loop Control of Hybrid Grid-connected Renewable Energy System with Multi-input Multi-output Controller," in Journal of Modern Power Systems and Clean Energy, **9**(1), 94-103, 2021, doi: 10.35833/MPCE.2018.000353.

[69] I.S. Sorlei, N. Bizon, P. Thounthong, M. Varlam, E. Carcadea, M. Culcer, M. Iliescu, M. Raceanu, "Fuel Cell Electric Vehicles — A Brief Review of Current Topologies and Energy Management Strategies", Energies, **14**(1), 252, 2021, doi: https://doi.org/10.3390/en14010252.

[70] M. İnci, M. Büyük, M.H. Demir, G. İlbey, "A review and research on fuel cell electric vehicles: Topologies, power electronic converters, energy management methods, technical challenges, marketing and future aspects," Renewable and Sustainable Energy Reviews, **137**, 2021, doi: https://doi.org/10.1016/j.rser.2020.110648.

SLIP-SL: Walking Control Based on an Extended SLIP Model with Swing Leg Dynamics

Junho Chang, Mustafa Melih Pelit[*], Masaki Yamakita

Tokyo Institute of Technology, Systems and Control Engineering Department, 152-8552, Japan

ARTICLE INFO

ABSTRACT

This paper details an extension to the SLIP model named spring loaded inverted pendulum model with swing legs (SLIP-SL). SLIP-SL extends the SLIP model by introducing swing leg dynamics while keeping its passive nature. This way, reference trajectories for the center of mass and swing foot trajectories can be simultaneously obtained which was not possible with the SLIP. This makes implementation easier and can increase tracking performance. We show how a variety of feasible two-phased walking trajectories can be obtained for this template model using direct collocation optimization methods. It is also shown through simulation studies that reference SLIP-SL trajectories can be used to control a fully actuated bipedal robot with the proposed feedback linearization controller to reach a stable cyclic gait.

1 Introduction

This paper is an extension of the work originally presented at *IEEE/ASME International Conference on Advanced Intelligent Mechatronics (AIM). IEEE, 2020* [1].

All the environments that we live and work in are designed to be traversed by humans who have a bipedal gait. This makes the bipedal robots advantageous since they would easily adapt to these environments. Bipedal robots can move in discontinuous terrains (ex. stairs) and turn in narrow spots. These and many other reasons have driven researchers to study the bipedal gait as a locomotion method for robots.

There is a variety of methods that researchers can choose to control the gait of a bipedal robot. Using an inverted pendulum model as a template in conjunction with the zero moment point (ZMP) criterion has been used extensively [2], [3]. An up and coming method is obtaining optimal trajectories and inputs through various optimization methods and using them as a reference [4], [5]. Another popular method is to use simple models that can recreate certain fundamental aspects of human or animal gait, as template models for bipedal robots. A template model that is commonly used for this purpose is called the bipedal spring loaded inverted pendulum (SLIP) model [6], [7].

Bipedal SLIP model consists of two complaint legs and a point mass (Figure 2). This model is passive, i.e. there are no external inputs, and its motion is determined by the mechanical parameters and initial conditions. By choosing these carefully, a range of trajec-

tories can be obtained that converge to a limit-cycle. Humans walk in a two phased manner and Bipedal SLIP model can mimic this gait. Human gait is explained with great detail in [8]. These two phases are called single stance phase and double stance phase. In the single stance phase, only one leg is in contact with the ground and the other leg is "swinging". And in the double stance phase, both feet are on the ground. However, SLIP model has one big assumption that differs substantially from a human gait: in the single stance phase, swing leg is assumed to move instantaneously to the proper
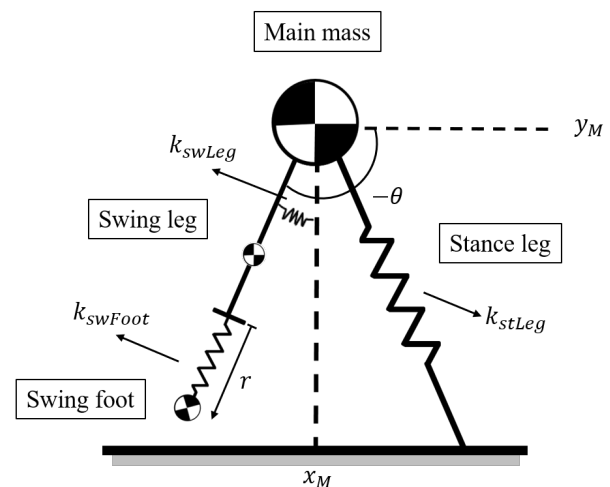
Figure 1: SLIP-SL Model in the single stance phase

*Corresponding Author: Mustafa Melih Pelit, Meguro-ku, Ookayama 2-12-1, South 5 Building, 305C, Tokyo, Japan. Email: pelit@ac.sc.e.titech.ac.jp

touch-down position. This means that when the bipedal SLIP is chosen as the template model for the controller of a bipedal robot, desired trajectories for the swing foot can not be obtained from it. Additional steps are necessary to achieve the swinging motion. [9] proposes a conceptual model where SLIP model is combined with a segmented leg so that the effects of swinging can be studied but reference trajectories and a controller is necessary to achieve the desired motion. In this paper, an extended SLIP model will be proposed so that reference center of mass trajectories and swing foot trajectories can be obtained simultaneously. This model will be called spring loaded inverted pendulum model with swing leg (SLIP-SL) which is shown in Figure 1.

SLIP-SL also has a two-phased gait and in the double stance phase, it is the same as the bipedal SLIP model. The difference is in the single stance phase where the model consists of three massed elements. The model also has three springs to facilitate the movement of these components. SLIP-SL model doesn't have any inputs, so it keeps the passive nature of the bipedal SLIP. The passive nature necessitates that proper spring parameters and initial conditions are chosen so that feasible trajectories can be realized. In this paper, direct collocation methods [10] were used to conduct simultaneous parameter and trajectory optimization for finding the suitable parameters. Then, a feedback linearization controller is proposed to track the obtained SLIP-SL trajectories with a 5-link fully actuated bipedal robot model. Effectiveness of the proposed controller and SLIP-SL's ability to be used as a template for walking are investigated through simulation studies.

This paper is organized as follows: Section 2 describes the dynamics of SLIP-SL and the bipedal robot model, Section 3 details the optimization work that is needed for finding feasible SLIP-SL trajectories, Section 4 introduces the proposed feedback linearization controller and in Section 5 simulation results are presented and discussed.

2 Systems and Modeling

This section will begin by introducing the bipedal SLIP model which is followed by the extended SLIP model named SLIP-SL and finally the model for the bipedal robot will be introduced. Explanation of the SLIP model will be brief since there are many works such as [6] that do an excellent job and going in depth on the matter. This paper will focus on the extended model and fully covers it but it is recommended to have a basic knowledge of the SLIP.

2.1 Bipedal SLIP Model

Bipedal SLIP Model can be seen in Figure 2. It consists of a point mass and two massless legs made out of springs. This model can mimic the two phased walking of humans, namely the single and the double stance phase. In the double stance phase, both feet are on the ground and both spring-like legs are pushing the mass. Then, a lift-off event happens where the foot in the back leaves the ground and the model goes into the single stance phase. This phase continues until the touch down event (when the swing foot touches the ground, depending on the angle of attack α and the free length of the spring L_0) at which point it goes back to the double stance

phase. This continues in a cycle and walking motion is achieved. The springs are always in contraction and they are always pushing since an actual leg can not pull us towards the ground.

This system is passive so its motion is determined by its parameters such as such as spring stiffness, angle of attack and the initial conditions such as initial the velocity. Different types of gaits can be achieved with this model by changing the parameters and initial conditions so that a stable human-like gait with double peaked ground reaction forces can be achieved. This model has been very popular among researchers because of its simple nature and it has been extensively used to generate reference trajectories for center of mass (CoM) position. However, it has one significant assumption which is that the swing leg is assumed to move instantaneously to the proper position required for touch-down. This is possible since the springs are assumed to be massless. However, this is not the case for actual robots which must perform the swinging motion with actual massed legs so that they can walk. So, when the SLIP model is used as a reference, additional steps are necessary to generate the swing leg motion. Also, since SLIP model ignores the swinging motion, adding it later on might prove to be difficult and will act as a disturbance to the CoM trajectory. That is the advantage of the SLIP-SL model which we will introduce. It is an extension to the SLIP model to include swing leg dynamics in the single stance phase.
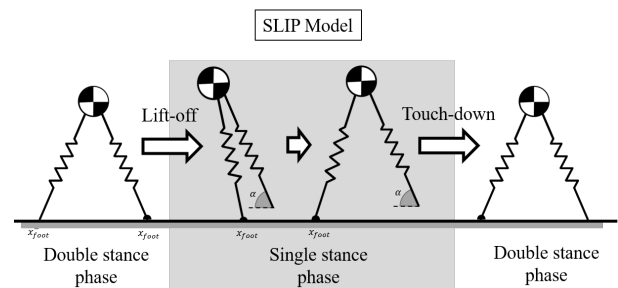
Figure 2: Bipedal SLIP Model

2.2 SLIP-SL model

Spring loaded inverted pendulum model with swing leg (SLIP-SL) can be seen in Figure 1 and its motion throughout a full step is represented in Figure 3. This model also walks in two phases, like its predecessor. In the double stance phase, SLIP-SL and SLIP are identical. What makes SLIP-SL different from the SLIP model is the addition of swing leg dynamics in the single stance phase. In the single stance phase, SLIP-SL consists of 3 massed elements which are the main mass 'M', a massed swing leg and a point mass representing the swing foot and 3 springs which are the linear spring that connects 'M' to the ground, the torsional spring that is connected between the point mass and the swing leg and the linear spring which connects the swing foot and the swing leg. After the touch-down event, SLIP-SL goes to the double stance phase, the swing elements disappear and the model becomes the same as the SLIP model in the respective phase. SLIP-SL consists of a point mass and two massless springs in the double stance phase.

In the single stance phase, equation of motion for the SLIP-SL model can be written as:

$$\tilde{M}(\tilde{q})\ddot{\tilde{q}} + \tilde{C}(\tilde{q}, \dot{\tilde{q}}) + \tilde{G}(\tilde{q}) = \tilde{S}\tilde{\tau} \tag{1}$$
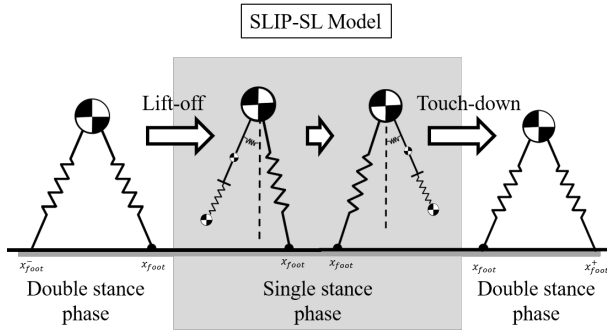
Figure 3: SLIP-SL Model

where $\tilde{q} = [x_M, y_M, \theta, r]^T$ are the generalized coordinates, $\tilde{M}(\tilde{q}) \in \mathbb{R}^{4\times4}$ is an inertia matrix, $\tilde{C}(\tilde{q}, \dot{\tilde{q}}) \in \mathbb{R}^4$ is a Coriolis and centrifugal terms vector, $\tilde{G}(\tilde{q}) \in \mathbb{R}^4$ is the gravity term, $\tilde{\tau} \in \mathbb{R}^3$ are the resultant forces and torques due to springs and $\tilde{S} \in \mathbb{R}^{4\times3}$ is the appropriate mapping matrix for them. The resultant forces can be calculated as:

$$\tilde{\tau} = \begin{bmatrix} k_{0,\text{ss}}(L_{0,ss} - L_{st,ss}) \\ k_{\text{swLeg}}(\theta_0 - \theta) \\ k_{\text{swFoot}}(r_0 - r) \end{bmatrix}, \tag{2}$$

where $k_{0,\text{ss}}$, k_{swLeg} and k_{swFoot} are the stiffness values for the stance leg spring, the torsional spring at the "hip" and the linear spring connecting the swing foot with the swing leg, respectively and $L_{0,\text{ss}}$, θ_0 and r_0 are the free positions of those springs where subscript "ss" indicates the single stance phase. L_{st} is the length of the stance leg. x_M and y_M respectively represent horizontal and vertical positions of the main mass, θ represents the angle of the swing leg with respect to the vertical axis and r represents the distance between the end of the swing leg and swing foot point which are represented in Figure 1.

In the double stance phase, dynamics of the SLIP-SL model can be written as:

$$m\begin{bmatrix} \ddot{x}_{\text{CoM}} \\ \ddot{y}_{\text{CoM}} \end{bmatrix} = F_{\text{sw}} + F_{\text{st}} + mg, \tag{3}$$

where

$$m = m_M + m_{\text{swLeg}} + m_{\text{swFoot}}, \tag{4}$$

indicates the total mass of the system, x_{CoM} and y_{CoM} are the horizontal and vertical positions of the center of mass and $g = [0, -9.81]^T$ is the gravitational acceleration. Forces generated by the stance and swing leg springs can be calculated as:

$$F_{st} = k_{0,\text{ds}}\left(\frac{L_{0,\text{ds}}}{L_{st}} - 1\right)\left(\begin{bmatrix} x_{\text{CoM}} \\ y_{\text{CoM}} \end{bmatrix} - \begin{bmatrix} x_{foot} \\ 0 \end{bmatrix}\right), \tag{5}$$

$$F_{sw} = k_{0,\text{ds}}\left(\frac{L_{0,\text{ds}}}{L_{sw}} - 1\right)\left(\begin{bmatrix} x_{\text{CoM}} \\ y_{\text{CoM}} \end{bmatrix} - \begin{bmatrix} x^-_{foot} \\ 0 \end{bmatrix}\right), \tag{6}$$

where subscript "ds" indicates the double stance phase. Definitions of x_{foot} can be seen in Figure 3.

2.3 Bipedal Robot Model

In this part, the dynamics of the 5 linked bipedal robot will be introduced. This model consists of 5 links which are connected to each other with revolute joints and it moves in the sagittal plane. The model is fully actuated and has an ankle torque.

Dynamics of the bipedal robot in the single stance phase can be written as:

$$M(q)\ddot{q} + C(q, \dot{q})\dot{q} + G(q) = Su, \tag{7}$$

where $q = [\theta_1, \theta_2, \theta_3, \theta_4, \theta_5]^T \in \mathbb{R}^5$ are the generalized coordinates, $M(q) \in \mathbb{R}^{5\times5}$ is an inertia matrix, $C(q, \dot{q}) \in \mathbb{R}^{5\times5}$ is a Coriolis and centrifugal terms matrix, $G(q) \in \mathbb{R}^5$ is the gravity term, $S \in \mathbb{R}^{5\times5}$ is the distribution matrix of actuation torques and $u \in \mathbb{R}^5$ are the input torques. This model can be seen in Figure 4 with the description of generalized coordinates and input torques (indicated with the red arrows).

Like the SLIP-SL model, bipedal robot model also has a two phased walking pattern. In the single stance phase, only one foot is on the ground and other is doing the swinging motion. Single stance phase ends and the system goes into the double stance phase when the swing foot touches the ground.

When the swing foot contacts the ground, a collision occurs where the generalized momentum of the system changes discontinuously. This can be modeled by assuming that an impulse force acts on the system to change the velocities while position is kept the same. This can be expressed as:

$$M(q)\Delta\dot{q} = J_c^T \lambda_{\text{impact}}, \tag{8}$$

where $J_c \in \mathbb{R}^{2\times5}$ is a constraint Jacobian matrix that maps the joint velocities to the swing foot velocity in horizontal and vertical directions. The generalized reaction forces in x and y directions are indicated as $\lambda_{\text{impact}} = [\lambda^x_{\text{impact}}, \lambda^y_{\text{impact}}]^T \in \mathbb{R}^2$. Assuming that the impact is inelastic, velocity of the swing foot touching the ground
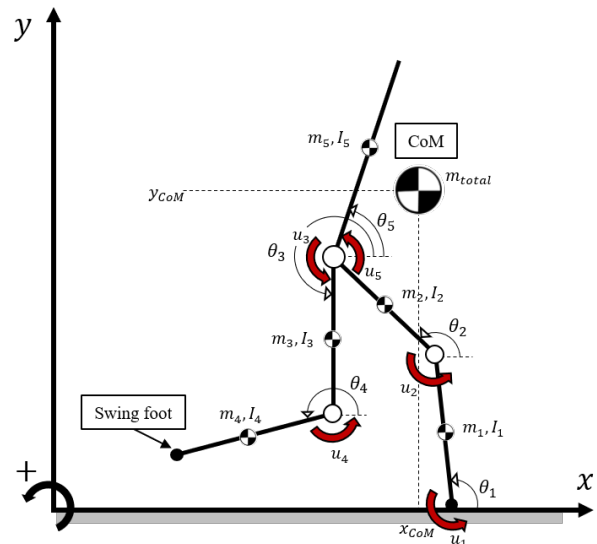
Figure 4: 5 link fully actuated robot model

will become zero after the impact which can be written as:

$$\boldsymbol{J}_c(\boldsymbol{q})\dot{\boldsymbol{q}}^+ = 0 \Leftrightarrow \boldsymbol{J}_c(\boldsymbol{q})\Delta\dot{\boldsymbol{q}} = -\boldsymbol{J}_c(\boldsymbol{q})\dot{\boldsymbol{q}}^-, \tag{9}$$

where $^-$ superscript indicates the moment just before the impact and $^+$ just after the impact. By solving (8) and (9) for λ_{impact} the following expression can be derived:

$$\lambda_{\text{impact}} = -(\boldsymbol{J}_c\boldsymbol{M}^{-1}\boldsymbol{J}_c^T)^{-1}\boldsymbol{J}_c\dot{\boldsymbol{q}}^-. \tag{10}$$

By inserting λ_{impact} into (8), we can obtain:

$$\dot{\boldsymbol{q}}^+ = (\boldsymbol{I} - \boldsymbol{M}^{-1}\boldsymbol{J}_c^T(\boldsymbol{J}_c\boldsymbol{M}^{-1}\boldsymbol{J}_c^T)^{-1}\boldsymbol{J}_c)\dot{\boldsymbol{q}}^-, \tag{11}$$

which are the generalized velocities just after the impact. At the moment of impact, definitions of the legs are also switched (swing leg becomes the stance leg and vice versa).

The system is now in the double stance phase where both feet are in contact with the ground. To model this, a constraint force $\lambda_{\text{ds}} = [\lambda_{\text{ds}}^x, \lambda_{\text{ds}}^y]^T \in \mathbb{R}^2$ is added to keep the swing foot on the ground. In the vertical direction, this constraint force can only push the robot ($\lambda_{ds}^y > 0$). With the non-slip assumption, double stance phase dynamics can be modeled by introducing the following constraint:

$$\boldsymbol{J}_c(\boldsymbol{q})\dot{\boldsymbol{q}} = 0. \tag{12}$$

Using this constraint, dynamical equation of the double stance phase can be written as:

$$\boldsymbol{M}(\boldsymbol{q})\ddot{\boldsymbol{q}} + \boldsymbol{C}(\boldsymbol{q},\dot{\boldsymbol{q}})\dot{\boldsymbol{q}} + \boldsymbol{G}(\boldsymbol{q}) = \boldsymbol{S}\boldsymbol{u} + \boldsymbol{J}_c^T\lambda_{\text{ds}}. \tag{13}$$

The constraint force λ_{ds} can be obtained by taking time derivative of equation (12) as:

$$\boldsymbol{J}_c\ddot{\boldsymbol{q}} + \dot{\boldsymbol{J}}_c\dot{\boldsymbol{q}} = 0, \tag{14}$$

and inserting it into (13) as follows:

$$\lambda_{\text{ds}} = -(\boldsymbol{J}_c\boldsymbol{M}^{-1}\boldsymbol{J}_c^T)^{-1}(\boldsymbol{J}_c\boldsymbol{M}^{-1}(\boldsymbol{S}\boldsymbol{u} - \boldsymbol{C}\dot{\boldsymbol{q}} - \boldsymbol{G}) + \dot{\boldsymbol{J}}_c\dot{\boldsymbol{q}}). \tag{15}$$

3 Direct Collocation Optimization

In this section, the optimization conducted to find periodic trajectories for SLIP-SL will be described. SLIP-SL is a passive model which means its gait solely depends on its mechanical parameters and initial conditions. In order to find the proper value, Direct Collocation Methods [10] were used in this study. These methods tackle the trajectory optimization problem by discretizing and converting it into a form which can be handled by nonlinear programming (NLP) solvers. There are many commercially available NLP solvers and in this study OpenOCL [11] will be used which can handle the multi-phase and simultaneous trajectory and parameter optimization problem. Finding the global minimum is not guaranteed when using the direct collocation methods. Global minimum is not easily found in a nonlinear problem with constraints such as 16. The advantage of direct collocation over other optimization methods such as genetic algorithms or learning based algorithms is that dynamics of the system can be embedded as constraints to the optimization problem painlessly.

The optimization can be formulated as:

$$\min_{\boldsymbol{x}_i,\boldsymbol{p},T_i} \quad \sum_{i=1}^{2}\left(\int_{T_{i-1}}^{T_i} J_i(\boldsymbol{x}_i(t),\boldsymbol{p})dt\right) \text{for } i \in \{1,2\}$$
$$\text{s.t.} \quad \dot{\boldsymbol{x}}_i = \boldsymbol{f}_i(\boldsymbol{x}_i(t),\boldsymbol{p}) \tag{16}$$
$$\boldsymbol{r}_{i,k}(\boldsymbol{x}_i(\mu_{i,k}),\boldsymbol{p}) \le 0,$$

where $t \in [0, T_i]$ is the time, T_i is the end time of the respective phase, $\boldsymbol{x}_i(t)$ is the state trajectory, $\boldsymbol{p}$ are the parameters, $J_i(x, p)$ are the path cost functions, $\boldsymbol{f}_i(\boldsymbol{x}, \boldsymbol{p})$ are the system dynamics (described in Section 2.2) and $\boldsymbol{r}_{i,k}(\boldsymbol{x}_i, \boldsymbol{p})$ are the grid-constraints. $i = 1$ represents the single stance phase and $i = 2$ represents the double stance phase for SLIP-SL (T_1 is when the touch-down happens at the end of "ss" and T_2 is when the lift-off happens at the end of "ds"). In this paper, the Cost of Transport (CoT) [6] and a cost function to keep the swing foot low was used. CoT is an indicator of the walking efficiency.

Path, boundary and stage transition constraints are needed so that the solver can find feasible walking trajectories. Path constraints are:

- Bounds were set for the parameters to be optimized:

$$15000 \le k_{0,i} \le 16000 \ [N/m], i \in \{ss, ds\}$$
$$1 \le L_{0,\text{ss}} \le 1.2 \ [m]$$
$$0 \le k_{\text{swFoot}} \le 20000 \ [N/m]$$
$$0 \le k_{\text{swLeg}} \le 15000 \ [Nm/rad] \tag{17}$$
$$0 \le \theta_0 \le 2\pi \ [rad]$$
$$-10 \le r_0 \le 10 \ [m]$$

- Stance leg spring in the single stance phase and both legs' springs in the double stance phase are always under contraction: $L_{st,ss} \le L_{0,ss}, L_{st,ds} \le L_{0,ds}, L_{sw,ds} \le L_{0,ds}$

- Constraining the vertical position of CoM: $0 \ [m] \le y_{\text{CoM}} \le 0.85 \ [m]$

- Swing foot is always above the ground during the single stance phase: $y_{\text{swFoot}} \ge 0$

- Elliptic virtual obstacle must be avoided by the swing foot during the single stance phase:

$$\left(\frac{x_{\text{swFoot}} - d_{obs}}{w_{obs}}\right)^2 + \left(\frac{y_{\text{swFoot}}}{h_{obs}}\right)^2 \ge 1, \tag{18}$$

where $d_{obs} = x_{\text{swFoot}} = 0 \ [m]$ is the horizontal position of the ellipse obstacle, $w_{obs} = 0.2 \ [m]$ and $h_{obs} = 0.04 \ [m]$ are width and height of the ellipse.

- Swing foot vertical velocity must be greater or equal to zero: $\dot{x}_{\text{swFoot}} \ge 0$

- Vertical acceleration of CoM should be negative in the single stance phase so that system doesn't try to lift the CoM up when there is only one leg on the ground: $\ddot{y}_{\text{CoM,ss}} \le 0 \ [m/s^2]$
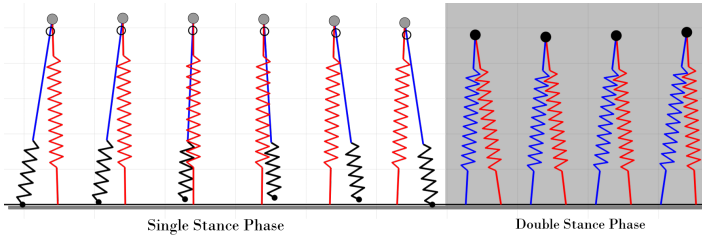
Figure 5: Snapshots of SLIP-SL's one step where gray dot in the single stance phase indicates the position of the point mass 'M' and the circle indicates the position of CoM

Boundary constraints:

- Swing foot starts on the ground from a stationary position in the beginning of the single stance phase and touches the ground at the end of the single stance phase: $y_{\text{swFoot}}(0) = 0$, $\dot{x}_{\text{swFoot}}(0) = 0$, $\dot{y}_{\text{swFoot}}(0) = 0$, $y_{\text{swFoot}}(T_1) = 0$

- Initial step length and the final step length should be same (for cyclic walking): $x_{\text{foot}} - x_{\text{foot}}^- = x_{\text{foot}}^+ - x_{\text{foot}}$

- The initial position of the main mass relative to the stance foot should be the same as the final one (for cyclic walking): $x_{stFoot,0} - x_M(0) = x_{stFoot}(T_2) - x_M(T_2)$

- Constraints for cyclic walking: $y_{\text{CoM}}(0) = y_{\text{CoM}}(T_2)$, $\dot{x}_{\text{CoM}}(0) = \dot{x}_{\text{CoM}}(T_2)$, $\dot{y}_{\text{CoM}}(0) = \dot{y}_{\text{CoM}}(T_2)$

- At the stage transition, CoM position and velocity were constrained to be continuous.

- At the end of the double stance phase, swing leg should be ready to lift off, i.e. swing leg spring should be at its free length: $L_{\text{sw,ds}}(T_2) = L_{0,\text{ds}}$

Parameters to be optimized are spring stiffness values $k_{0,ss}$, $k_{0,ds}$, k_{swFoot}, k_{swLeg}, their respective free positions $L_{0,ss}$, $L_{0,ds}$, r_0, θ_0 and the initial conditions.

The optimization was conducted on MATLAB 2019b software by using 10 collocation points for each stage. Resulting spring parameters can be seen in Figure 6 for various trajectories and a snapshot of SLIP-SL's one step can be seen in Figure 5 for a sample trajectory. Trajectory 'A' from Figure 6 will be used as the reference in Section 5 where the step size was also constrained to 0.25 [m] to avoid large ankle torques. The constant mechanical parameters of SLIP-SL are given in Table 1.

Table 1: SLIP-SL's constant mechanical parameters

m_M : 70 [kg]	m_{swLeg} : 7 [kg]
m_{swFoot} : 3 [kg]	L_{thigh} : 0.7 [m]
$I_{\text{swLeg}} = m_{\text{swLeg}} l_{\text{thigh}}^2 / 12 \ [kg \cdot m^2]$	$I_{\text{swFoot}} = m_{\text{swFoot}} L_{\text{thigh}}^2$

4 Feedback Linearization Control

In this section, the proposed controller will be introduced so that 5 linked bipedal robot model can track the reference SLIP-SL trajectories. The controller uses the feedback linearization notion,

in a similar manner to [12] where a total energy control approach was used with the bipedal SLIP model. However, in this paper, a trajectory tracking approach will be used.

4.1 Single Stance Phase

For the control of the robot in the single stance phase, there are three main tasks: tracking CoM trajectory $\boldsymbol{x}_G \in \mathbb{R}^2$, tracking swing foot trajectory $\boldsymbol{\xi} \in \mathbb{R}^2$, controlling the trunk orientation $\theta_5 \in \mathbb{R}$. The velocities related to these tasks can be calculated as:

$$\dot{\boldsymbol{x}}_{t,\text{ss}} = \boldsymbol{J}_{t,\text{ss}}(\boldsymbol{q})\dot{\boldsymbol{q}}, \tag{19}$$

where $\dot{\boldsymbol{x}}_{t,\text{ss}} = [\dot{\boldsymbol{x}}_G, \dot{\boldsymbol{\xi}}, \dot{\theta}_5]^T$ is the velocity in the task space where subscript "ss" indicates the single stance phase and $\boldsymbol{J}_{t,\text{ss}}(\boldsymbol{q}) = [\boldsymbol{J}_G, \boldsymbol{J}_\xi, \boldsymbol{J}_{\theta_5}]^T$ are the combination of Jacobian matrices. $\boldsymbol{J}_G$ maps generalized velocities to the velocity of the center of mass, $\boldsymbol{J}_\xi$ maps generalized velocities to swing foot velocities and $\boldsymbol{J}_{\theta_5}$ maps generalized velocity to the trunk's angular velocity. By taking the time derivative of Equation (19) and inserting the obtained $\ddot{\boldsymbol{q}}$ into Equation (7) we can get:

$$\ddot{\boldsymbol{x}}_t = \boldsymbol{J}_{t,\text{ss}} \boldsymbol{M}^{-1}(\boldsymbol{S}\boldsymbol{u} - \boldsymbol{C}\dot{\boldsymbol{q}} - \boldsymbol{G}) + \dot{\boldsymbol{J}}_{t,\text{ss}}\dot{\boldsymbol{q}}. \tag{20}$$

Inputs should be chosen as:

$$\boldsymbol{u} = \boldsymbol{S}^{-1}\left(\boldsymbol{M}\boldsymbol{J}_{t,\text{ss}}^{-1}(\ddot{\boldsymbol{x}}_{t_d,ss} - \dot{\boldsymbol{J}}_{t,\text{ss}}\dot{\boldsymbol{q}}) + \boldsymbol{C}\dot{\boldsymbol{q}} + \boldsymbol{G}\right), \tag{21}$$

to get $\ddot{\boldsymbol{x}}_t = \ddot{\boldsymbol{x}}_{t_d,\text{ss}}$. By choosing:

$$\ddot{\boldsymbol{x}}_{t_d,\text{ss}} = \begin{bmatrix} K_{P_G}(x_{\text{CoM,des}} - x_{\text{CoM}}) + K_{D_G}(\dot{x}_{\text{CoM,des}} - \dot{x}_{\text{CoM}}) \\ K_{P_G}(y_{\text{CoM,des}} - y_{\text{CoM}}) + K_{D_G}(\dot{y}_{\text{CoM,des}} - \dot{y}_{\text{CoM}}) \\ K_{P_{\text{sw}}}(x_{\text{sw,des}} - x_{\text{sw}}) + K_{D_{\text{sw}}}(\dot{x}_{\text{sw,des}} - \dot{x}_{\text{sw}}) \\ K_{P_{\text{sw}}}(y_{\text{sw,des}} - y_{\text{sw}}) + K_{D_{\text{sw}}}(\dot{y}_{\text{sw,des}} - \dot{y}_{\text{sw}}) \\ K_{P_T}(\theta_{5,\text{des}} - \theta_5) + K_{D_T}(-\dot{\theta}_5) \end{bmatrix} \tag{22}$$

where K_P and K_D are the proportional and derivative gains for the controller and $\theta_{5,des}$ is the desired trunk angle, desired trajectories can be tracked. Desired trajectories will be chosen as the SLIP-SL trajectories that were obtained in Section 3. In this study, the desired trunk angle was chosen as $\theta_{5,\text{des}} = \pi$ [rad].

4.2 Double Stance Phase

During the double stance phase, swing foot remains on the ground which means there is one less task to be carried out. This means that some modifications should be made to the single stance phase controller so that it can be used in the double stance phase. The task space for the double stance phase then becomes:

$$\dot{\boldsymbol{x}}_{t,ds} = \begin{bmatrix} \dot{\boldsymbol{x}}_G \\ \dot{\theta}_5 \end{bmatrix} \in \mathbb{R}^3. \tag{23}$$

This reduction in dimension of the task space is somewhat problematic since we need to determine 5 separate inputs but the dimension of $\dot{\boldsymbol{x}}_{t,ds}$ is 3 which means there is more than one correct way to allocate the inputs. To calculate the proper inputs, the following equation can be used:

$$\dot{\boldsymbol{q}}_{\text{hip}} = \boldsymbol{J}_{\text{hip,sw}}(\boldsymbol{q}_{\text{sw}})\dot{\boldsymbol{q}}_{\text{sw}} = \boldsymbol{J}_{\text{hip,st}}(\boldsymbol{q}_{\text{st}})\dot{\boldsymbol{q}}_{\text{st}}, \tag{24}$$
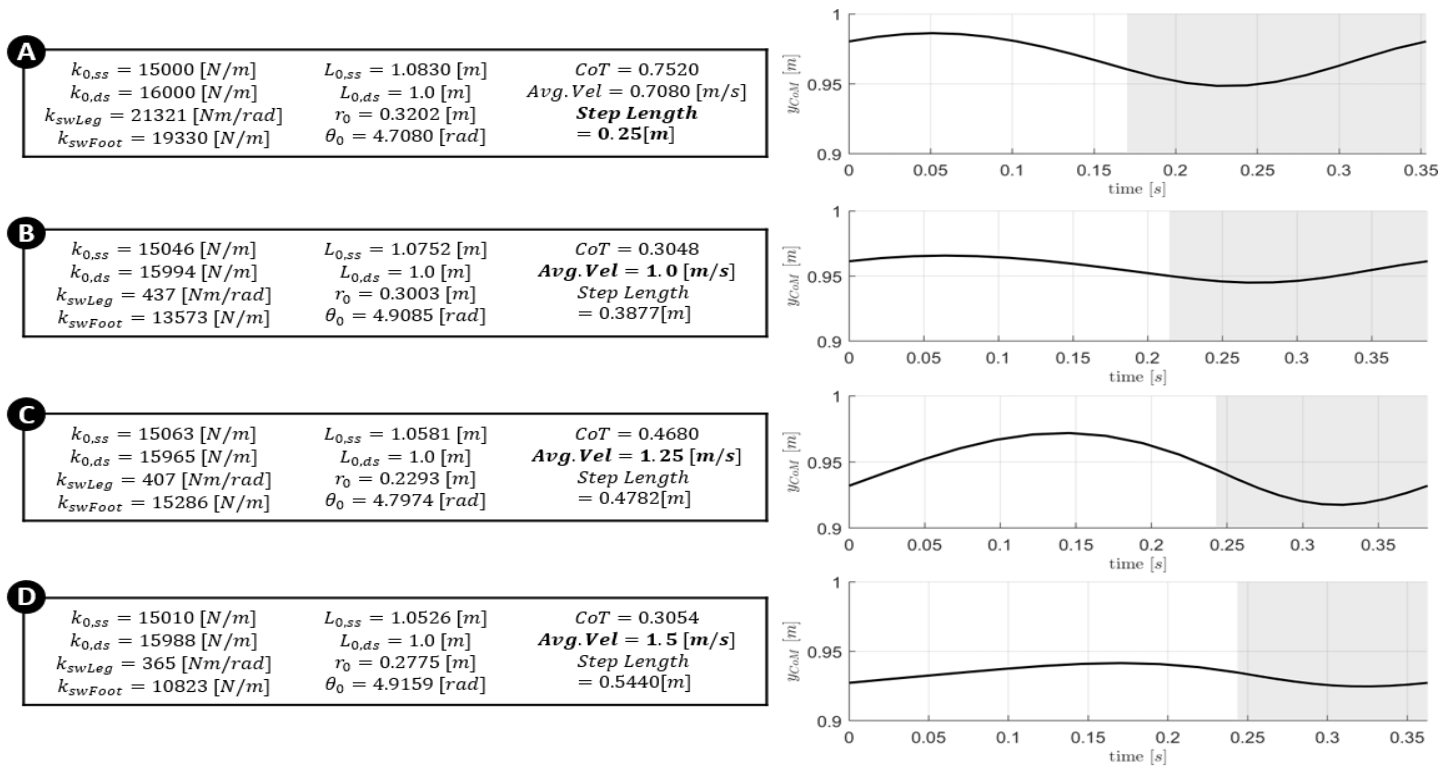
Figure 6: Optimization results for various SLIP-SL trajectories. For the trajectory A, step length was constrained to 0.25 [m] to get better ankle torques and this trajectory is the one that was used as reference in Section 4. For B, C and D trajectories, average velocity constraints were added. In this figure, resulting mechanical parameters, costs of transport and step length are given as well as the SLIP-SL's y_{CoM} trajectory. In the plots on the right, gray background means that the SLIP-SL is in double stance phase.

where $J_{\text{hip}, i}(q_i)$ is the jacobian matrix that maps the corresponding legs angular velocities, $\dot{q}_{\text{st}} = [\dot{\theta}_1, \dot{\theta}_2]^T$ and $\dot{q}_{\text{sw}} = [\dot{\theta}_3, \dot{\theta}_4]^T$, to the velocity of the hip. This holds since both foot are on the ground during the double stance phase. From equation (24),

$$\dot{q}_{\text{st}} = J_{\text{hip,st}}^{-1}(q_{\text{st}})J_{\text{hip,sw}}(q_{\text{sw}})\dot{q}_{\text{sw}}, \qquad (25)$$

can be obtained to get:

$$\dot{q} = \underbrace{\begin{bmatrix} J_{\text{hip,st}}^{-1}J_{\text{hip,sw}} & 0_{2\times1} \\ I_{2\times2} & 0_{2\times1} \\ 0_{1\times2} & 1 \end{bmatrix}}_{\Gamma(q)} \underbrace{\begin{bmatrix} \dot{q}_{\text{sw}} \\ \dot{\theta}_5 \end{bmatrix}}_{\dot{q}_a}. \qquad (26)$$

After taking the time derivative of (26), then substituting the $\ddot{q}$ and $\dot{q}$ terms from (26) into (7) and multiplying with Γ^T from left, following can be obtained:

$$M_a(q)\ddot{q}_a + C_a(q,\dot{q})\dot{q}_a + G_a(q) = u_a, \qquad (27)$$

where

$$\begin{cases} M_a = \Gamma^T M \Gamma \\ C_a = \Gamma^T (C\Gamma + M\dot{\Gamma}) \\ G_a = \Gamma^T G \\ u_a = \Gamma^T S u \end{cases} \qquad (28)$$

Using a similar technique that was used for deriving (21):

$$u_a = M_a J_{t,\text{ds}}^{-1}(\ddot{x}_{t_d,\text{ds}} - \dot{J}_{t,\text{ds}}\dot{q}_a) + C_a\dot{q}_a + G_a, \qquad (29)$$

can be found where $\ddot{x}_{t_d,\text{ds}}$ should be chosen as:

$$\ddot{x}_{t_d,\text{ds}} = \begin{bmatrix} K_{P_G}(x_{\text{CoM, des}} - x_{\text{CoM}}) + K_{D_G}(\dot{x}_{\text{CoM}} - \dot{x}_{\text{CoM}}) \\ K_{P_G}(y_{\text{CoM, des}} - y_{\text{CoM}}) + K_{D_G}(\dot{y}_{\text{CoM, slipsl}} - \dot{y}_{\text{CoM}}) \\ K_{P_T}(\theta_{5,\text{des}} - \theta_5) + K_{D_T}(-\dot{\theta}_5) \end{bmatrix}. \qquad (30)$$

However, only $u_a \in \mathbb{R}^3$ can be obtained in this way which only has dimension 3. What we need to control the robot is $u \in \mathbb{R}^5$. One way to calculate u is by using the relation $u_a = \Gamma^T S u$ given in (28) as:

$$u = S^{-1}\left(\underbrace{W^{-1}\Gamma(\Gamma^T W^{-1}\Gamma)^{-1}}_{(\Gamma^T)^{+W}} u_a\right), \qquad (31)$$

where $(\Gamma^T)^{+W}$ is the weighted matrix inverse operation. $W \in \mathbb{R}^{5\times5}$ matrix can be used to penalize high input torques such as the ankle torque but we selected it as identity matrix for this paper.

Controllers for the single and double stance phases are thus derived. Another important aspect of the controller in tracking the SLIP-SL trajectories is the switching of phases at the correct moments. When the biped robot is in the double stance phase and the tracked trajectory goes into single stance phase, controller switches to the single stance phase controller and commands the robot to lift its foot so it too can switch to the proper phase.

5 Simulation Results and Discussion

In the following simulation study, the designed controller's ability to track the reference SLIP-SL trajectories and the suitability of the SLIP-SL as a template model for walking will be tested. Table 3 shows the mechanical parameters of the 5 link robot and Table 2 shows the chosen gain values for the controller and the torque limits on the motors were set at 200 [Nm]. Gain values are chosen with the help of a particle swarm optimization algorithm (PSO) [13]. We were able to find controller parameters that resulted in stable gaits easily by hand-tuning but with the help of PSO we were able get results with better walking efficiency.

Table 2: Control Parameters

K_{P_G} : 54	K_{D_G} : 9
$K_{P_{sw}}$: 82	$K_{D_{sw}}$: 8
K_{P_T} : 36	K_{D_T} : 4

The simulations were implemented in MATLAB 2020b's Simulink environment with ode45 solver and variable step settings (absolute tolerance was set to 1e-8).

Figure 7 shows the resulting CoM trajectory and trunk orientation the controlled system when the proposed controller is used. Figure 8 shows the swing foot trajectories for the same system. It can be seen that the proposed controller does a good job in tracking the reference trajectories of the SLIP-SL template, which were obtained in Section 3. The reference SLIP-SL trajectories for the swing foot would not be available if a template such as the popular SLIP was used.

Table 3: 5 Link Model Parameters

$l_1 = l_4$: 0.48 [m]	$l_2 = l_3$: 0.48 [m]	l_5 : 0.48 [m]
$m_1 = m_4$: 5 [kg]	$m_2 = m_3$: 5 [kg]	m_5 : 60 [kg]
$I_i = m_i l_i^2 / 12$ [$kg \cdot m^2$], $i = 1, 2, 3, 4, 5$		

It can be seen in Table 2 that relatively low gains were chosen for this study. Tracking performance can be increased by using larger gains but since this model is fully actuated and has an ankle torque, zero moment point (ZMP) condition must also be checked. ZMP criterion states that if the center of pressure moves to the toe (or to the "outside" of the foot), foot would rotate and system would be under actuated [14]. For this trajectory, center of pressure stays within a 30 [cm] foot.

Figure 9 shows snapshots of one step of the 5 link models gait. to check the stability of the gait, Poincaré map approach was considered [12]. The dimensions of the Poincaré map were selected as the $\theta_P = \text{atan2}(\dot{y}_{CoM}, \dot{x}_{CoM})$, y_{CoM} and total energy of the 5 link model E at the vertical leg orientation (VLO). VLO happens when CoM of the 5 link model is at the same horizontal position as the stance foot. VLO was chosen as the Poincaré section because the horizontal position doesn't need to be considered at this point. Poincaré stability criterion indicates that if the return map converges to a fixed point, a hybrid system with impact effects can be considered periodic [12]. Poincare Map for the controlled 5 link model is shown in Figure 10. It can be seen that the gait converges to a stable point in the section after a couple of steps which indicates stability.
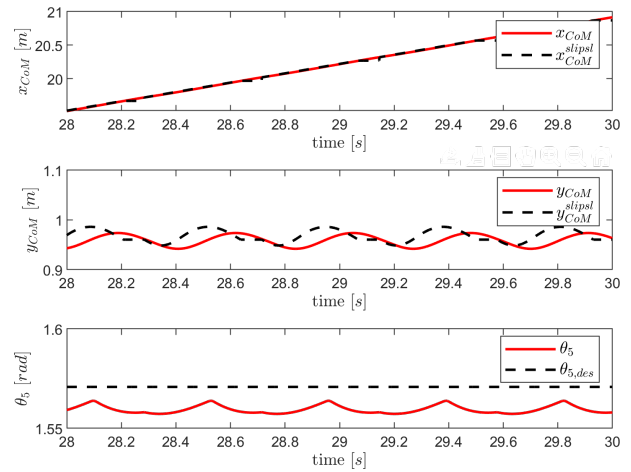
Figure 7: Trajectory tracking results for CoM horizontal position, vertical position and trunk orientation

The CoT value for the reference SLIP-SL trajectory was 0.7520 and this value is 0.7745 for the controlled 5 link robot. Also, the average velocity of the SLIP-SL trajectory was 0.7080 [m/s] and this value was 0.6974 [m/s] for the controlled system. These values being very similar between the reference and the controlled model also indicates the validity of the proposed controller. Cost of transport being slightly higher is expected because the 5 linked model needs to keep its body upright but SLIP-SL doesn't have this issue.

In this paper, it was also shown that by using direct collocation optimization, various SLIP-SL trajectories can be obtained (Figure 6) that resemble the walking gait. Cost of transport tended to decrease when the average velocity of the gait was increased and step length was not constrained but this kind of trajectories can be more demanding on the inputs and they sometimes resulted in large ankle torques which was troubling for the ZMP criterion. Also stiffness of the legs were limited to 15000 [Nm] $\leq k_{0,i} \leq$ 16000 [Nm], $i \in \{ds, ss\}$ to keep the CoM height within a certain range.

This stiffness limits was chosen to have a similar height trends with [12] and [6] where k_0 was 15696 [Nm]. It can be seen that $k_{0,ss} \neq k_{0,ds}$ for the given trajectories but it was possible to find feasible trajectories with $k_{0,ss} = k_{0,ds}$, even with $k_{0,ss} = k_{0,ds} =$
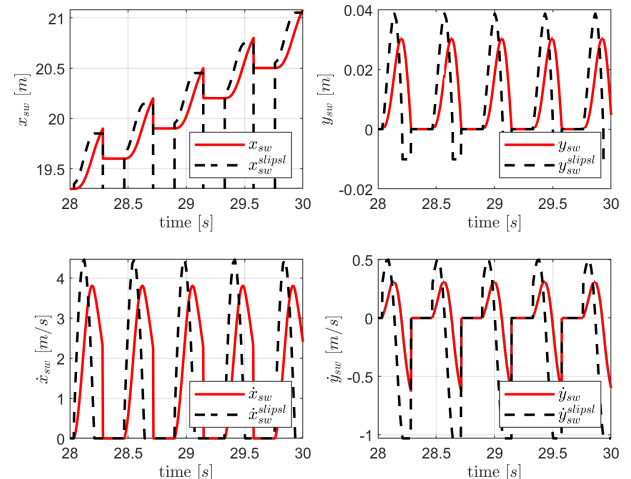
Figure 8: Trajectory tracking results for the swing foot
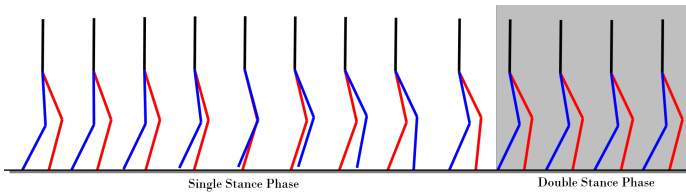
Figure 9: Snapshots from a step of the 5 Link model

15696 [Nm] but this doesn't really mean that linear leg springs were the same in single and double stance phase since $L_{0,ss} \neq L_{0,ds}$. The free length of the springs in the double stance phase was set to 1 [m] to be the same with [12] but $L_{0,ss}$ needs to be larger than this value to keep the CoM high enough. If $L_{0,ss}$ was 1.0 [m], CoM would sag further than desired range in the single stance phase.

6   Conclusion

In this paper, a template model called SLIP-SL was proposed which is an extension to the popular SLIP model. SLIP model can generate the reference CoM trajectories that can mimic the two-phased walking but it doesn't have the swing leg dynamics. Thus, when this template model is used, additional steps are necessary for obtaining the swing foot trajectory so that the actual robot can be controlled. Since the swinging motion is a huge part of the walking gait that needs to be taken into account, SLIP-SL adds this dynamics while keeping the passiveness of the SLIP model.

Since the SLIP-SL is passive, proper mechanical parameters and initial conditions needs to be determined to get feasible walking trajectories. It was demonstrated that direct collocation methods can be used to find the proper parameters for the passive SLIP-SL model. This step was crucial since there are many parameters that needs to be decided and other more exhaustive search methods might not work. It was shown that a variety of trajectories with different average velocities, CoM behaviors etc. can be obtained using the same basic principles. Then, a controller was introduced to track the
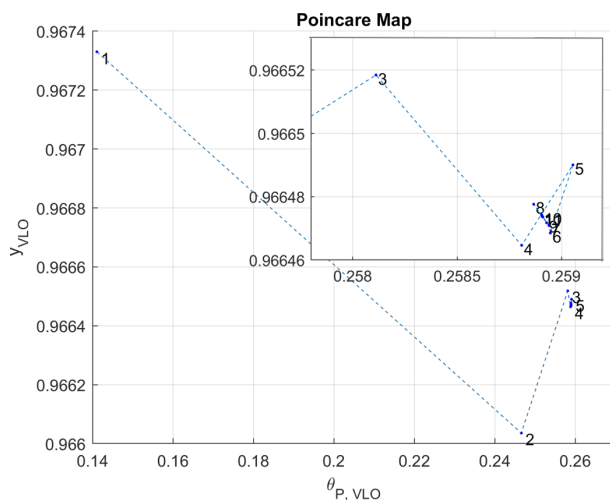
Figure 10: 2D section of the Poincaré Map where the numbers indicate the step number (zoomed in version is shown in the right upper corner of the figure)

obtained reference trajectories and it was shown that it can satisfactorily track the reference SLIP-SL trajectories to reach a stable

gait while also satisfying the ZMP criterion. These results also confirmed that SLIP-SL can be used as a template model for walking robots.

In the future, we would like to introduce robustness to this passive system by making the springs variable ones and controlling them to reject disturbances. Another area we would like to explore is achieving a variable speed gait with the bipedal model. We want to achieve this by smoothly switching between different reference SLIP-SL trajectories.

References

[1] M. M. Pelit, J. Chang, R. Takano, M. Yamakita, "Bipedal Walking Based on Improved Spring Loaded Inverted Pendulum Model with Swing Leg (SLIP-SL)," in 2020 IEEE/ASME International Conference on Advanced Intelligent Mechatronics (AIM), 72–77, IEEE, 2020, doi:10.1109/aim43001.2020.9158883.

[2] S. Kajita, F. Kanehiro, K. Kaneko, K. Fujiwara, K. Harada, K. Yokoi, H. Hirukawa, "Biped walking pattern generation by using preview control of zero-moment point," in 2003 IEEE International Conference on Robotics and Automation (Cat. No. 03CH37422), volume 2, 1620–1626, IEEE, 2003, doi:10.1109/robot.2003.1241826.

[3] R. Takano, M. Yamakita, "Sequential-contact bipedal running based on SLIP model through zero moment point control," in 2017 IEEE International Conference on Advanced Intelligent Mechatronics (AIM), 1477–1482, IEEE, 2017, doi:10.1109/aim.2017.8014227.

[4] H. Yano, J. Chang, R. Takano, M. Yamakita, "Simultaneous Optimization of Trajectory and Parameter for Biped Robot with Series Elastic Actuators," IFAC-PapersOnLine, **52**(22), 7–12, 2019, doi:10.1016/j.ifacol.2019.11.039.

[5] A. Patel, S. L. Shield, S. Kazi, A. M. Johnson, L. T. Biegler, "Contact-implicit trajectory optimization using orthogonal collocation," IEEE Robotics and Automation Letters, **4**(2), 2242–2249, 2019, doi:10.1109/lra.2019.2900840.

[6] J. Rummel, Y. Blum, A. Seyfarth, "Robust and efficient walking with spring-like legs," Bioinspiration & biomimetics, **5**(4), 046004, 2010, doi:10.1088/1748-3182/5/4/046004.

[7] H. Geyer, A. Seyfarth, R. Blickhan, "Compliant leg behaviour explains basic dynamics of walking and running," Proceedings of the Royal Society B: Biological Sciences, **273**(1603), 2861–2867, 2006, doi:10.1098/rspb.2006.3637.

[8] J. S. Park, C. M. Lee, S.-M. Koo, C. H. Kim, "Gait phase detection using force sensing resistors," IEEE Sensors Journal, **20**(12), 6516–6523, 2020, doi:10.1109/jsen.2020.2975790.

[9] M. A. Sharbafi, A. M. N. Rashty, C. Rode, A. Seyfarth, "Reconstruction of human swing leg motion with passive biarticular muscle models," Human movement science, **52**, 96–107, 2017, doi:10.1016/j.humov.2017.01.008.

[10] M. Kelly, "An introduction to trajectory optimization: How to do your own direct collocation," SIAM Review, **59**(4), 849–904, 2017, doi:10.1137/16m1062569.

[11] J. Koenemann, G. Licitra, M. Alp, M. Diehl, "OpenOCL–Open Optimal Control Library," 2017, doi:10.1137/16m1062569.

[12] G. Garofalo, C. Ott, A. Albu-Schäffer, "Walking control of fully actuated robots based on the bipedal slip model," in 2012 IEEE International Conference on Robotics and Automation, 1456–1463, IEEE, 2012, doi:10.1109/icra.2012.6225272.

[13] J. Kennedy, R. Eberhart, "Particle swarm optimization," in Proceedings of ICNN'95-international conference on neural networks, volume 4, 1942–1948, IEEE, 1995, doi:10.5772/6754.

[14] E. R. Westervelt, J. W. Grizzle, C. Chevallereau, J. H. Choi, B. Morris, Feedback control of dynamic bipedal robot locomotion, CRC press, 2018, doi:10.1201/9781420053739.

Real Time and Post-Processing Flight Inspection by Drone: A Review

Sékou Togola, Sountongnoma Martial Anicet Kiemde*, Ahmed Dooguy Kora

e-Inov laboratory, Ecole Supérieure Multinationale des Télécommunications de Dakar, Dakar, 10000, Sénégal

ARTICLE INFO	ABSTRACT
	Air Navigation Aids (NAVAIDs) whether implemented on the ground or in space and the Precision Approach Path Indicator (PAPI) system need to be checked in flight to ensure compliance with the standards set by International Civil Aviation Organization (ICAO). This activity has been carried out for decades by conventional aircraft and is usually done at low altitude around airports. This makes the task very dangerous and costly in terms of human lives. The use of Unmanned Aerial Vehicle (UAVs) or Drone to provide flight inspection and to progressively replace conventional aircraft through two measurement methods are described in this paper. We also propose an improved real-time trajectography system based on a Satellite Based Augmentation System (SBAS) correction, a comparative cost study between aircraft and UAV, while proposing levers for reducing flight inspection time and thus reducing costs. Study of environmental impact of flight inspection is discussed and strategies for using drones to reduce flight inspection costs are also discussed. From this study we draw the conclusions that flight inspection by drone allows first of all the risk of accident reduction for the navigation personnel on board and therefore a completely safe conduct of flight inspection; also it is cheaper for the air navigation services to use drones in addition to the fact that they are ecological solutions as they produces less greenhouse gases unlike the aircraft.

1. Introduction

Flight inspection [1], which consists in a periodical flight check of NAVAIDs like VHF Omni Range (VOR), Instrument Landing System (ILS), Distance Measurement Equipment (DME), etc., is an International Civil Aviation Organization (ICAO) [2] requirement for Air Navigation Service Providers (ANSP) and airport managers. For many years, flight inspection has been performed with aircraft. Today, technological advances and minuaturisation have given rise to Remotely Piloted Aircraft (RPA) called Drones or UAV. Applications for civil Drones are many and varied. In several applications, the use of civil drones is a better quality, price and environmental cost option. One of these applications could also be to carry out flight inspection of NAVAIDs using a Drone [3]. In this paper, we propose two architectures for drone's flight inspection. Moreover, this paper is an extended version of our first paper proposing the two architectures mentioned above [4]. This extended version also studies the economic, ecological and life protection aspects of drone flight inspection team members compared to the classical

method by plane. And to do so, the paper has been divided into six sections. Section II is devoted to an overview of the state of the art of flight inspection , section III proposes a real-time and post-processing architecture for drone-based flight inspection and the improvement over the trajectography system, section IV discusses cost analysis, section V examines environnemental and safety impact, and section VI provides discussion, while identifying the innovation proposed by our solution and strategy for the use of drones to reduce the costs of flight inspection.

2. State of art

In [5], the authors describe the standard volumes of the instrument landing system, the analyses of the instrument landing system after the flight inspection itself and the restrictions resulting from non-standard values of the inspected instrument landing system parameter and present the standard profiles flown during the flight inspection. In [6], the authors present the architecture of a new flight inspection system based on the use of unmanned aircraft. The proposed architecture is remotely operated and has flight inspection capabilities using radio signal sensors: It also has

*Corresponding Author: Sountongnoma Kiemde, kiemde.anicet97@gmail.com

an accurate positioning system, based on the Global Navigation Satellite System, and uses a low-bandwidth, long-range and redundant data link [6]. In [7], the authors focus on the identification and definition of different types of interference and their classification according to their nature, while they try to methodically describe the measurement procedure, listing the technical equipment needed to carry out the task of identifying and measuring the source of interference of the GNSS signal. In [8], the authors use a drone equipped with the necessary instruments to measure Glide Path-Localizer navigation systems and PAPI lights to ensure the accuracy of the data transmission of these NAVAIDs and to make the required adjustments if necessary, for any changes prior performing the Flight Inspection.

In [9], the authors study (The feasibility, difficulties, benefits and risks) mainly a new method of flight inspection based on an unmanned aerial vehicle (UAV). They show that the general trend is to use UAVs for in-flight inspections in the future. In [10], the authors present an Unmanned Aerial System (UAS), called position information by GPS and coded overlay navigation signals (PIGEONS). The system uses a lightweight hexacopter, with a wingspan of 55 cm, that performs autonomous flight and uses an on-board Software Defined Radio (SDR) that measures instrument landing systems (ILS) and VHF omnidirectional range (VOR) [10]. The ILS system was tested at the DAB airport in Daytona Beach, FL and the VOR was tested at the OMN airport in Ormond Beach, FL [10]. In [11], the authors present a software defined radio (SDR) platform-based unmanned aerial system (UAS) and radio navigation receiver for preliminary validation of radio navigation aids prior to a real flight inspection.

3. Drone based flight inspection architectures

Procedures for the flight verification and validation of air navigation aids are defined in ICAO Document 8071 [1] and for flight validation of Performance Based Navigation (PBN) procedures in ICAO Document 9906 [12]. These procedures apply to the different types of flight inspection, of which there are three.

- Flight inspection of the commissioning of a NAVAID or PAPI: this is a comprehensive flight inspection that establishes the validity of the radio signals around the service area. It is only after commissioning that the equipment obtains authorization from the National Aeronautical Authorities to transmit.
- Periodic flight inspection : verify that the radio signals of the navigational aid are always transmitted in accordance with the regulations. To do this, periodic inspections steal some of the profiles from the commissioning inspection and compare the results with previous results. The interval is generally 6 months for ILS/DME ; and 12 months for VOR/DME and PAPI.
- Special flight inspection : Special flight inspections are required at the request of personnal maintenance or due to an incident or accident investigation. In such inspection, only problematic flight procedures are tested. After any

modification to a navigational aid, the periods for periodic inspections are also shortened.

The general concept of the UAV flight inspection operation has been presented in [4]. In this section, we will present successively the real time and post-processing measurement methods, the architecture of the equipment on board the Drone and the improvement over the trajectography system.

3.1. Real time flight inspection

In the case of the conventional aircraft, the flight inspector measures and displays the curves directly in real time on the on-board laboratory. Here, since it is a remote flight inspection, the activation of the measurement functions and the plotting of the curves are done remotely on the ground station which acts as a data processing computer. The parameters of the controlled stations (VOR for example) and the Differential Global Positionning System (DGPS) parameters of the UAV are captured by the receivers on board the UAV (see figure 2) and transmitted through a low latency wireless link [4]. There are two possible scenarios. For measurements within the airport, the measured data is transmitted directly from the UAV to the ground station. For distant measurements, e.g. 25 Nm from the airport, the FAR-RELAY [13]. Drone system is deployed to transmit both the measured parameters and the telemetry data from the Drone.

In the event of non-compliance with the standards observed during the measurements, the flight inspector will report this deviation to the CNS technicians who will make the appropriate adjustments. The drone then repeats the measurements until the deviation is corrected. For the accuracy of the flight profiles, the flight inspection bench (in-flight inspection station here) generates the precise trajectory to be followed to carry out the various measurements (pilot guidance or assistance) and sends it to the UAV control station. The flight inspector communicates to the UAV pilot via an intercom (in the case of aircraft) or radio the different types of flight profiles to be followed (e.g. level flight, normal approach, left/right offset approach, etc.) in order to perform the measurements.

3.2. Post-processing flight inspection

As the UAV can be programmed, it offers flexibility to make measurements at specific points. Here, the method consists of recording the parameters of the equipment to be calibrated and the precise positioning information (DGPS) of the UAV (see figure 3). The mission module on board the drone also provides the time-stamping function by automatically linking the measured VOR / ILS parameters to the DGPS positioning data signal. The data processing will be done afterwards on the ground station once the drone is recovered. For measurements made within the airport and long distances, the data is recorded on a device on board the UAV. Within the airport, the telemetry data of the UAV are sent directly to the UAV control station while the FAR RELAY system is used to transmit these data from the UAV for long distances.

As in the case of the paragraph above (paragraph 3.1), the measurements are repeated until the measured parameters for a given station are in standard.

3.3. Flight inspection Drone payload (On-board equipment)

In this diagram (see figure 4), the data from the different receivers (VOR, ILS, DME and DGPS) are multiplexed and sent on a VHF or UHF datalink through the telemetry, with a RAVEON M7 transmitter/receiver. On the ground, the data is recovered and demultiplexed then sent to the treatment station that will calculate the differences between the reference signal (DGPS) and the measured beacon signal of positioning. This station is equipped with flight inspection software used for this purpose and a database of the airport facilities where is located equipment to be check. The coordinates of the phase center of LOCALIZER's antenna for example and WGS84 coordinates of the runway thresholds are used. The receivers are switched on remotely (telecontrol) for the realization of the flight inspection of a given equipment (VOR, ILS or DME).

All the receivers on board the Drone and the ground calculations station are synchronized in time with the GPS. At the end of the flight check, different curves and reports are printed with a printer.

3.4. Improvement of the trajectography system

The current trajectory system used for flight inspection is based on the Differential Global Positioning System (DGPS) and has the disadvantage of dragging GPS boxes from site to site. The use of the OMNISTAR SBAS solution [14], which gives an equivalent or a better accuracy than conventional DGPS, is an efficient way of performing this task. The DGPS system used have an accuracy of 10 cm x 10 cm x 20 cm in 3-D.

The OMNISTAR constellation HP and G2, (see figure 1) has a worldwide coverage allowing flight inspection almost everywhere in the world [14].

Figure 1: OmniSTAR XP and G2 satellite coverage[14]

This solution is also applicable to conventional flight inspection aircraft. This makes it possible to dispense with landing to put the trajectography equipment on the ground. Briefings with the Control Tower and ATSEPs are done by radio. It also makes it possible to limit to only one integration of antenna to the aircraft instead of two antennas respectively above and below the aircraft cabin. Figure 4 (see below) gives an illustration of the use of the two trajectography solutions : DGPS and OMNISTAR HP or G2.

4. Cost analysis

Table 1 gives a classification of UAVs considering endurance, wingspan, range and cost, ranging from the cheapest (miniature UAV) to the most expensive (HALE UAV). The UAV that we propose and that allows us to carry out all the measurement for both periodic flight inspection and commissioning is the SKY-Y UAV or equivalent [4], [15] which is a MALE UAV. Table 4 gives the hourly costs of flight inspection by type of vector. The cost per hour of flight inspection depends on the type of aircraft and the flight inspection unit. The costs shown in this table are average values. Table 5 compares the acquisition cost of each aircraft and the cost of flight inspection bench.

So far, no study has shown that the use of civilian drones is more economical than flight inspection by aircraft. Nevertheless in [6], resented the drone solution as being less expensive. The cost analysis mainly considers the cost of flight hours, the purchase price of the aircraft or drone, the fees of the on-board personnel, the purchase price of the measurement equipment. Differences in the number of units and the year of the contract may also have an impact on costs that we do not consider. Some are variable costs that depend on the number of hours flown, while others are fixed costs that are independent of the number of hours flown. For example, crew and fuel costs are mostly variable, while insurance, aircraft depreciation, overhead and maintenance are mostly fixed. Included in the costs already listed are costs related to crew costs or fees for flight inspection staff and equipment for the flight inspection. The advantage with drone flight inspection is the absence of many of the costs mentioned above. This is a considerable financial gain for the flight inspection operators.

For example, remote operation by drone avoids the costs of personnel deployment, dangerous flight and salary costs. In addition, travel time is saved and can be spent on increasing the number of inspections per day.

5. Environmental and Safety Impact

The world is currently dealing with the growing ozone hole. To reverse this trend, and reduce the use of greenhouse gases, states around the world have signed a treaty called the "Paris Climate Accord". All areas of industry are concerned by this commitment. Civil aviation, particularly flight inspection, has a major role to play, hence the interest of our study.

Tables 2 and 3 show the amount of carbon emission due to fuel combustion according to the type of flight inspection. From these tables, we clearly see that, beyond the choice of the aircraft to be used for flight inspection, the drone emits less carbon than the aircraft. For example, among the aircraft used for flight inspection in our study, Beechcraft King Air 200 emits 300 kg of carbon per hour compared to the SKY Y drone with 15kg of carbon per hour. Although the civil drone SKY-Y is not necessarily the most polluting drone, we think that the drones proposed by some companies are much less polluting than the SKY-Y drone. The carbon production of the drone depends on the size of the drone [8]. Drones can also help us to reduce our carbon dioxide CO_2 footprint. Drones generally consume less energy per kilometer.

Table 1: Drone classification

Drone Type	Altitude	Endurance	Weight	Speed	Envergure	Range of action
Miniature	very low	20 min	< 2 kg	50 km/h	50cm	15 km
Tactics	200 to 5000 m	2 to 8h	< 1 ton	150 to 700 km/h	A few meters	30 to 500 km
MALE (Medium Altitude Long Endurance)	5000 to 12000 m	12 to 24 h	< 3.5 tons	220 to 360 km/h	10 to 20m	1000 km
HALE (High-Altitude Long-Endurance)	Up to 20000 m	12 to 48 h	Up to 15 tons	220 to 650 km/h	20 to 40 m	>=10000 km

Table 2: Flight hours by aircraft type and by type of NAVAIDs for periodic flight inspection

N°	Type of in-flight calibration vector	Cal. VOR/DME [16]	Cal. ILS/DME[16]	Cal. PAPI [16]	Fuel cons. (in liter/hour of flight)²	Observations
1	ATR 42-300	01 h 00	3 h 00	01 h 00	641 [17]	510 kg/h
2	BEECH King Air 200	01 h 00	3 h 00	01 h 00	378 [18]	300 kg/h
3	CESSNA Sovereign Plus	01 h 00	3 h 00	01 h 00	725 [19]	576 kg/h
4	DA42MPP	01h 00	3 h 00	01h 00	326 [20]	259 kg/h
5	Drone SKY-Y Finmeccanica	01 h 00	3 h 00	01 h 00	21 [21]	15 kg/h

Note: The quantities of fuel consumed per flight hour are averages taking into account the fact that fuel consumption is not uniform during all phases of a flight. For example, at take-off, it is higher than during the other phases of a flight (cruise and descent).

For the calculation of CO_2 emissions, we use the data provided by [22] and [23].These documents give CO_2 equivalents produced by 1 kg of fuel oil or kerosene. Our basis of calculation is then 3.15 kg of CO_2 produced for each kg of kerosene burnt, hence the table below.

Table 3: CO_2 emissions by aircraft type during periodic flight inspection

N°	Type of in-flight calibration vector	CO_2 release for NAVAIDS in kg (during Periodic Flight Calibration)			Total CO_2 emissions for NAVAIDs & PAPI (in kg)
		VOR/DME	ILS/DME	PAPI	
1	ATR 42 -300	1606.5	4819.5	1607	8033
2	BEECH King Air 200	945	2835	945	4725
3	CESSNA Soverign Plus	1814.4	4611.5	1537	7962.2
4	DA42MPP	815.85	2447.55	815.85	4078.65
5	Drone SKY-Y Finmeccanica	47.25	141.5	47.25	236

Table 4: Cost per flight hour by aircraft type

N°	Type of in-flight calibration vector	Cal. VOR/DME	Cal. ILS/DME	Cal. PAPI	Cost /flight hour (in Euros)	Total cost (ILS+VOR/DME+PAPI in Euro)
1	ATR 42-300	01 h 00	3 h 00	01 h 00	5 000	25 000
2	BEECH King Air 200	01 h 00	3 h 00	01 h 00	5 000	25 000
3	CESSNA Soverign Plus	01 h 00	3 h 00	01 h 00	5 000	25 000
4	DA42MPP	01 h 00	3 h 00	01 h 00	2 000	10 000
5	Drone SKY-Y Finmeccanica	01 h 00	3 h 00	01 h 00	1 500	7 500

Table 5: Acquisition cost of flight inspection bench

N°	Type of in-flight calibration vector	Cost of acquisition (in millions of US $)	Price Calibration bench (in millions of US $)
1	ATR 42 -300	22	2- 3
2	BEECH King Air 200	8	2- 3
3	CESSNA Soverign Plus	30	2 -3
4	DA42MPP	2-3	2 - 3
5	Drone SKY-Y Finmeccanica	1.5 - 2	0.2
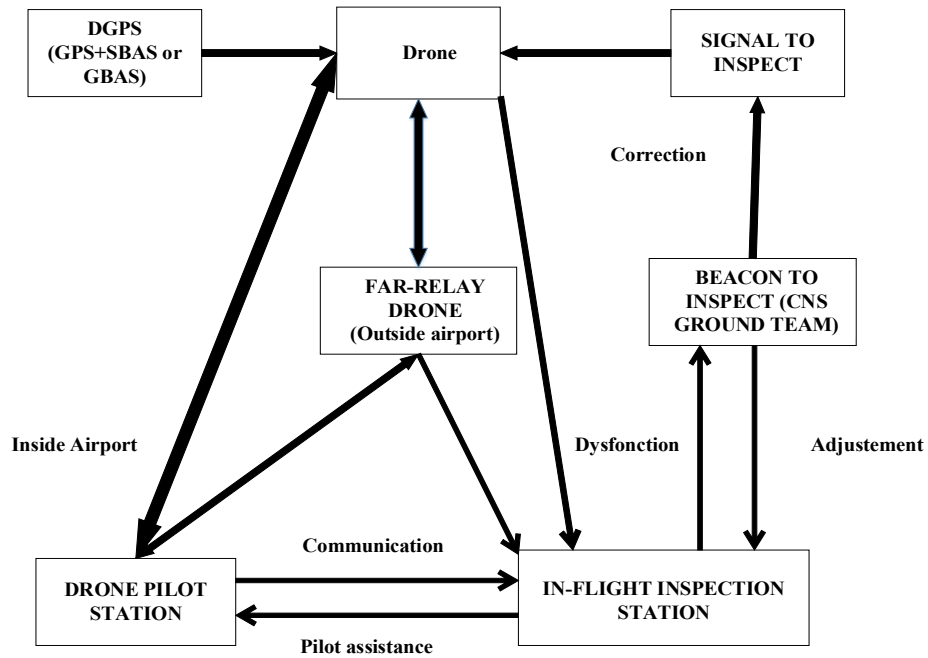
Figure 2: Schematic of real time measurement [4]
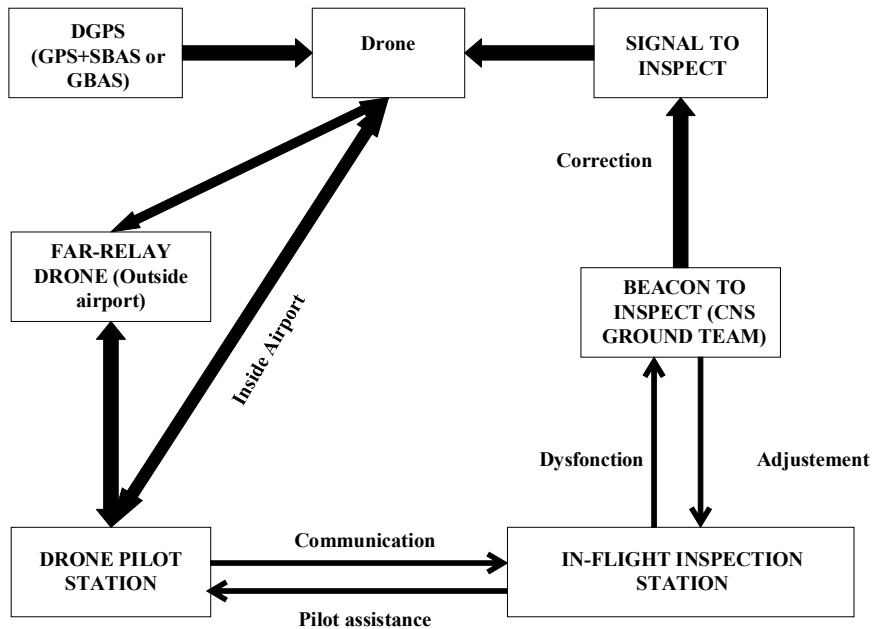
Figure 3: Schematic of post-processing measurement [4]
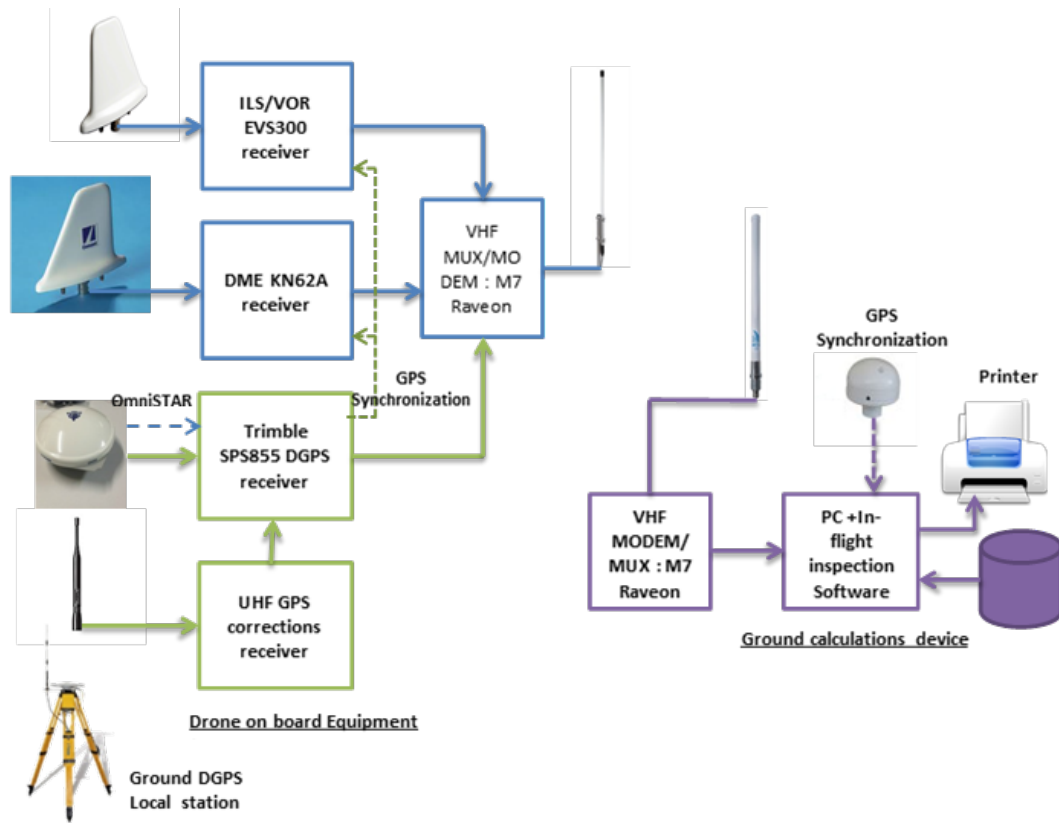
Figure 4: Drone on-board equipment

Drone flight inspection changes the energy consumption and Greenhouse Gases (GHG) emissions of the main aircraft fuels used for inspection, namely diesel and gasoline. Drones still contribute to pollution from natural gas to electricity sources that vary from region to region used to charge the drones.

Nevertheless, drones are not without consequences for the environment. For example, we have impacts from the manufacturing and extraction of raw materials for lithium-ion batteries for most civilian drones. Battery-powered drones remain a major challenge.

As mentioned at the beginning of this article, airborne inspection takes place at very low altitudes and most crashes of airborne inspection aircraft are like Controlled Flight In to Terrain (CFIT). UAVs (e.g. multi-rotor) allow extended observations at low altitudes without any risk to the flight inspection personnel.

Therefore, in addition to reducing the cost, the drone also reduces the safety risk for the inspection personnel in flight because they are all on the ground, unlike the conventional aircraft.

6. Discussion

The Drone used by [8] allows the extension of the measurements made on the ground by measuring the Glide Path slope and the LOC axis as well as the slope of the PAPI and is limited around airport. A flight inspection drone is proposed by [9] for ILS/DME and PAPI measurements but at less than 50 km with a ground-based GPS augmentation system. The hexacopter, a small UAV proposed by [10], allows measurements for ILS and

VOR within the airport with a ground DGPS system. A MALE drone with an autonomy of 10 flight hours is proposed by [24], but the solution is based on a ground augmentation system (DGPS). The drone proposed by [25] allows certain measurements to be taken for flight inspection of the ILS/DME, VOR/DME and PAPI. But this system has a range limited to 10 km. The above solutions offer flight inspection services of Communication Navigation and Surveillance (CNS) equipment and PAPI with short range UAVs. This makes it impossible to perform several measurements such as ILS/DME coverage at 50 km. Therefore, when designing VOR/DME based arrival and departure procedures, it is necessary to ensure that there is good radiation (coverage measurement) from these devices at 50 km around them. These coverage measurements must be made by flying an uninterrupted distance of 314 km by the UAV [4]. The FAR drone system that we have proposed allows for long distance measurements using these drones but does not allow for measurements over 314 km. The UAV solution SKY- Y or equivalent and the architecture we have proposed allow for these different measurements to be made in both real and delayed time. The above solutions all use a ground station as a trajectory system to reinforce the GPS and obtain centimetric accuracy. This requires the installation of an additional receiver on board the UAV to receive the correction data. The solution we have proposed (OMNISTAR HP or G2) allows direct reception of corrections from geostationary satellites and therefore no additional receiver for the UAV. This reduces the drone's payload.

Today some companies propose multi-rotor drones for flight inspection. These drones cost much less than the one we used for

our study. Despite the existence of all these solutions proposed by the companies, we notice the absence of a favorable regulatory framework for the use or adoption of civil drones for flight inspection. Most countries have not yet authorized the use of drones [26] and ICAO document 8071 only mentions aircraft for flight inspection [1]. Also, the evolution of regulations is necessary for a true integration of drones in air traffic. Indeed, every country does not have its own flight inspection unit. The forty or so available inspection organizations [27] pool their resources to satisfy the entire world. For example, in the ASECNA (Agency for Air Navigation Safety in Africa and Madagascar) zone, 17 African countries pool a Flight Control Unit. Another aspect that we did not consider in our study and which is important is the time saving obtained by air navigation personnel. This time saving could be used by staff to improve quality or to increase the time spent on data collection or analysis.

The data in Table 2 relates to the periodic flight inspection. For commissioning type in-flight inspections, these values are multiplied by 2 for ILS/DME and PAPI while it is of order 3 for VOR/DME. Thus, the quantities of CO_2 emitted are doubled for some and tripled for others (Table 3). The costs are also multiplied in this order. Rigorous ground maintenance makes it possible to extend the periodic flight control interval of NAVAIDs and PAPIs on the one hand, and the use of small electrically powered drones [8], [9] and [10] on the other hand. This will reduce the carbon footprint for ILS/DME and PAPI by half by moving from a regulatory periodicity of 6 months for ILS/DME to 12 months. And for PAPI from 12 months to 18 months. It is the same for flight inspection of the commissioning type where certain measurements could be made by these so-called Drones. This will also reduce the cost of annual flight inspections by half. In the case of the VOR/DME, for the commissioning flight inspection, this consists of flying a drone at 100 meters (circle of radius 100 m) to preset the centering curve and the modulation rate parameters 9960 Hz and 30 Hz of the VOR. For the ILS, the most demanding measurement during commissioning is the measurement of the nulls of the three Glide Path antennas and the adjustment of the Localizer beam [5]. These measurements can also be performed by a drone. This will reduce the flight time of a commissioning inspection to that of a periodic flight inspection.

Most flight inspection software has measurement coupling functions. For example, the measurement of the axis of the Localizer can be coupled with the measurement of the Glide slope. This saves about 30 minutes on the usual 03 hours of time. A good training of CNS experts on the ground and the availability of an experienced Air Traffic Controller (ATCO) on the day of the flight inspection also reduces the turnaround time of flight inspection aircraft without compromising safety. These levers can be leveraged to reduce the costs and environmental impact of flight inspection. Finally, the use of a SKY-Y [21] or equivalent drone for inspection will certainly reduce flight inspection costs by half and the environmental impact will also be largely limited.

7. Conclusion

Flight inspection is a very technical operation, very expensive, with environmental costs and a danger for flight inspection staff if it is only carried out by transport aircraft. This paper proposed

two architectures for using civil drones for flight inspection. Both architectures allow long-distance data collection using drone relay systems or MALE drone. In addition, the paper carried out a comparative financial and environmental study of the use of Drones compared to transport aircraft. The regulatory aspect of drones was also discussed and strategies for the use of electric UAVs to reduce the costs of flight inspection especially during Navaid commissioning. The use of drones for flight inspection appears to be more economical, environmentally friendly and safer for the lives of the flight inspection team members. Nevertheless, both architectures could be improved in future studies. In this study we were not able to carry out a quantitative study of the subject matter, but this may be the subject of another article. Also, flight inspection of RNAV GNSS procedures has not been addressed. The proposed architectures in this article are the basis for different types of flight inspections, so they can be used for the case of RNAV GNSS procedures.

Conflict of Interest

The authors declare no conflict of interest.

Acknowledgment

References

[1] I.C.A.O. (ICAO), Manual on testing of Radio Navigation Aids Volume I - Testing of Ground-based Radio Navigation Systems 4 th Edition, 2000.

[2] I.C.A.O. (ICAO), Annex 10, aeronautical telecommunications, volume II communication procedures including those with PANS status., 7thedition ed., 2016.

[3] S. Togola, Feasibility study of NAVAIDs or PAPI in-flight inspection by Drone: Case of ASECNA, ENAC, Toulouse France, 2016.

[4] A.D.K. Sékou TOGOLA, Sountongnoma Martial Anicet KIEMDE, "Real Time and Post-Processing Flight Inspection by Drone: A Survey," in 2020 43rd International Conference on Telecommunications and Signal Processing (TSP), Milan, Italy: 399–402, 2020.

[5] A. Novák, J. Pitor, "Flight inspection of instrument landing system," in 2011 IEEE Forum on Integrated and Sustainable Transportation Systems, 329–332, 2011.

[6] E.P. Cristina Barrado, J. Ramírez, Marc Pérez-Batlle, Eduard Santamaria, Xavier Prats, "Remote Flight Inspection Using Unmanned Aircraft," Journal of Aircraft, 50(1), 38–46, 2013, doi:10.2514/1.C031450.

[7] K.H.M.B. Andrej Novák, "Measurement of GNSS signal interference by a flight laboratory," in Transportation Research Procedia, 271–278, 2018, doi:10.1016/j.trpro.2018.12.011.

[8] K.P. Ebrahim Rahnama, Mostafa AsaadiIran, "PRE-flight checks of navigation systems and PAPI lights using a UAV," in 2018 Integrated Communications, Navigation, Surveillance Conference, 2018.

[9] S.Z. Xinqiao Liu, "Research on Flight Inspection Using Unmanned Aircraft," Journal of Physics Conference Series, (1237:042053), 2019.

[10] D. Sommer; A. Sarath Chandra Reddy Irigireddy; Justin Parkhurst; Kevin Pepin; Eduardo-Rojas Nastrucci, "UAV-Based Measuring System for Terrestrial Navigation and Landing Aid Signals," in 2020 AIAA/IEEE 39th Digital Avionics Systems Conference (DASC), 1–7, 2020, doi:10.1109/DASC50938.2020.9256447.

[11] K. Horapong et al. "Design and use of 'Drone' to support the radio navigation aids flight inspection," in IEEE/AIAA 36th Digital Avionics Systems Conference (DASC), 2017, doi:10.1109/DASC.2017.8102114.

[12] 9906 Doc ICAO, "Quality Assurance Manual for Flight Procedure Design Volume 5 Validation of Instrument Flight Procedures."

[13] C.V. Prodromos-Vasileios Mekikis, Elli Kartsakli, Luis Alonso, "Flexible

Aerial Relay Nodes for Communication Recovery and D2D Relaying," in IEEE 5th Global Conference on Consumer Electronics, 2016.

[14] Trimble Navigation Limited, OmniSTAR HP, 2014.

[15] A. Aeronautica, Medium Altitude Long Endurance (MALE), 2017.

[16] ASECNA, MANUEL DES SPECIFICATIONS DE CALIBRATION EN VOL, Dakar-Sénégal, 2015.

[17] ATR-42-3XX, Consommation fuel.

[18] Beechcraft King Air 200, Consommation fuel.

[19] CESSNA Citation Soverign I/SP, Consommation fuel.

[20] DA42MPP, Consommation fuel.

[21] Mark Rutherford, The Italian stylings of the Sky-Y aerial drone, Https://Www.Cnet.Com/News/the-Italian-Stylings-of-the-Sky-y-Aerial-Drone/, 2007.

[22] IATA, CO2 calculation, 2020.

[23] C.N. Jardine, Calculating The Carbon Dioxide Emissions Of Flights, 2009.

[24] Airfield Technology, "IFIS2016PROCEEDINGS," Belgrade, Serbia.

[25] Cursir, Cursir Drone.

[26] Global Drone Regulations Database, Interactive map of drone legislation around the world.

[27] M. Rodera, Flight Inspection Service Providers, 2018.

Integration Information Systems Design of Material Planning in the Manufacturing Industry using Service Oriented Architecture

Dimas Sirin Madefanny[1,*], Suharjito[2]

[1]*Department of Computer Sciences, BINUS Graduate Program Master of Computer Sciences Bina Nusantara University, Jakarta, 11480, Indonesia*

[2]*Department of Computer Sciences, BINUS Online Learning Bina Nusantara University, Jakarta, 11480, Indonesia*

A R T I C L E   I N F O

A B S T R A C T

PT XYZ has an Enterprise Resource Planning application that is used by the Planning Department to view stocks and plan production materials. Currently calculation of production materials takes more than 30 seconds just to export to Excel then a few minutes to adjust the data format to the planning form and the data used is not real-time. Each item needs to be calculated one by one per period, then the size of the Excel file used varies according to the time period and requires more storage. To support real-time integration and process efficiency planning and storage reduction, an integration between Enterprise Resource Planning application and web applications has been made using a Service Oriented Architecture approach. The Web service uses RESTful and has been tested using Quality of Service and the Vulnerability Test. Based on the test results using the Jmeter simulation with 10 users, it is obtained Latency 1.2 seconds and Load Time 1.2 seconds with an average amount of data sent 1280.73 bytes. The test results using OWASP ZAP show vulnerability to the web service header made from the web server version used by PHP version 5.6.40. With the results of these tests, the web service is able to replace the export and import process as well as create real-time data connectivity and replace storage media with databases, thereby reducing the time needed for planning activities.

1. Introduction

A manufacturing company in Indonesia which is engaged in automotive industry, which has a Core Business in manufacturing car air conditioning components and other commodities in refrigeration spare parts for storage equipment. In a manufacturing company, accuracy and speed in planning and shipping finished goods are the benchmarks for the success of the automotive company business. In article [1], an ERP (Enterprise Resource Planning) information system designed to integrate all departments as a data center that becomes an information center for all parts of the company.

Based on article [2], using SOA approach on ERP will make would make the implementation on business process integration much better and easier. From the paper [3], the combination of

ERP and SOA in software development will reducing the gap of support system and business processes.

Systems which not integrated and manual systems are weaknesses from implementation ERP system carried out by Manufacturing Company In material planning production at Manufacturing Company needs to perform processing Task using the Excel application prior to entry into the ERP system. In addition to processing data using Excel, you still need to export data from ERP by Copy-Paste Inventory into Excel format. The model has been proposed by [4], all personnel from various departments must work together for producing up-to-date and accurate reports. From the description, there are several problems that will be discussed in this research: (a) How to design a system that can increase the effectiveness of planning for production with SOA?; (b) How to design a service that can integrate several systems used in material planning?. The objective of the case study as follows: (a) To design a system that can improve the

*Corresponding Author: Dimas Sirin Madefanny, Email:
dimas.madefanny@binus.ac.id

effectiveness of production material planning; (b) To design a system that can be used in Service-based material planning.

The benefits obtained from implementing a System Oriented Architecture in this case study are: (a) Increase efficiency and effectiveness in application development by reusing components / services [5]; (b) Bridging information systems with different platforms within the Manufacturing Company; (c) Provide flexibility to business opportunities; (d) Provide real-time information; (e) Improve application usage efficiency.

2. Literature Review

2.1. ERP Architecture

Article [6] proposed a modern ERP system architecture which has two physical architecture of ERP systems: Two-tier ERP architecture, Three-tier ERP architecture. There are many advantages in applying the three-tier architecture of ERP systems for the organizations over the traditional client-server architecture. For any type of ERP implementation strategy, whether it is to buy full out-of-the-box ERP products or to design and develop a custom ERP solution, the organization's ERP project managers and specialists need to acquire a good knowledge of ERP software architecture.

2.2. Service Oriented Architecture RESTful

In article [7], the author proposed Service Oriented Architecture (SOA) for software integration, because it has become one of the reference patterns using a more concise SOA architecture based on the RESTful style for industrial process design and modeling. The objective of this research is to improve interoperability and flexibility in today's manufacturing industry. In the evaluation phase, a simple Restful prototype and several industrial device scenarios were presented using two different methods: HTTP and Constrained Application Protocol (CoAP). From the research results, it is concluded that the performance of SOA architecture with the REST method in the manufacturing industry is able to answer today's needs.

The application of IoT in article [8], the environments on different industrial require data services, processing, and big data integration for supporting the analysis platforms to strengthening unstructured big data storage capacity. The big data analysis will be processed through the relevant interface using the client and web server in HTTP transactions hosted by HTTP messages, and complete HTTP messages are usually plain text. The service is developed using the REST-based ASP.NET Web API on the Cloud server. Services that are able to provide reliable services for operational monitoring, asset management, and data visualization. Service separation occurs in the background between the front-end and back-end which increases the intelligence and accuracy of distribution management.

SOAP/WSDL has standard registry as described in research [9], where producer can register service specification and consumer can discover service endpoint using UDDI. Recently RESTful web service gained momentum in development of distributed application and research community already started discussion about RESTful based Service Oriented Architecture (SOA) but there is no standard central repository. The XML REST registry based services studied based on their dynamic nature as well as the

quality of web-based services RESTful for complex scenarios such as travel scheduling..

The proprietary and widely used industrial project in [10], SOA methodology IBM RUP/SOMA supports the middle SOA analysis & design strategy, covering all SOA analysis & design activities. It also has the best prescription rates, as it provides a description of the activities, steps, inputs and outputs for each phase. It adopts existing techniques and notations such as BPM, UML, BPEL, WSDL, WS-BPEL

The benefits experienced in organizations of SOA implementation on article [11], can be divided into two subcategories: improved business agility and lowered costs. All twelve of the organizations in their researchexperienced improved business agility and lower costs as a result of SOA implementation.

The author proposed the security architecture on constructed adaptive way in article [12],. Enterprise application integration (EAI) is a well-known, industry-recognized architectural principle built on a loosely coupled application architecture. SOA web service has become the choice due to its simplicity in internet protocol. A new architectural paradigm appears in SOA, Representational State Transfer (REST) which has a security deficiency where it relies on network / transport layer security on Web 2.0 technology. In the research mentioned, the RESTful web service security vulnerability check was carried out using the OWASP rating methodology view and analysis of existing security solutions. Thus, the security architecture design is built in a way that is adaptive friendly Internet-of-Things (IoT) in an advanced way consisting of three cycle parts: learn, predict, and prevent.

The implementation Web Service on Laravel PHP framework in article [13], using RESTful API which become the mainstream after SOAP. This article explained how to effectively build a RESTful API. Micro services architecture become the standard of web services, and why RESTFUL API has become a major Web service development paradigm due to lightweight, scalability.

In article [14] explained the usage of the web services is expected to provide independency and fast integration. Article [15] presented the platform validates the incoming request from different consumers without any relation to the operating system or the programming language that the consumer uses. Since it uses http RESTful services then the approach will function correctly. As well, the provided framework requires the NodeJs to be installed and as known, the NodeJs is available for most used operating systems.

Advantages of a RESTful architecture described by [16], include a) communication advantages, such as reduced communication overhead and the possibility to introduce layers of caching, and b) system design advantages including stable service interfaces across applications and use of a resource-oriented information model in cyber-physical systems.

Implementation concept of ERP in Winmentor Enterprise using Extended Web RESTful services in [17]. The commercial documents for payment process were generated as PDF files by email to customers, linked with the central database via the REST services.

Integration application in large companies commonly using Service Oriented Architecture (SOA) related to article [18]. SOA-based solutions for enterprises have behaviors such as: loosely-couple, reusable, autonomy, composable, making SOA can be implemented in any business process entity flexibly, as long as the company has a business design. SOA provides better alignment between IT and Business processes, reduces IT burden, increases vendor diversity, and can support new technologies. Although IT adoption in SMEs and Large Enterprises is different, SMEs can also experience these benefits, with a good understanding of the characteristics of SMEs and a suitable SOA approach.

The SOA perspective in article [3], concludes that the question is not about SOA or ERP but rather to provide an ERP designed by SOA. By looking at ERP as a service, it is clear that the combination of ERP and SOA is one way forward when designing IS that aims to bridge the gap between IS and business, for example processes, and, enable businesses to fuse with IS to form a serviceable SOA-based ERP.

The communication problem that arose in [19], between ERP and automated transfer protocols was no standard, complicated configuration and this process was only done by experts. WETMAPS as an intermediary software, implements a web service called REST to provide solutions in data exchange between ERP and AGV systems. An ERP system sends information to an intermediary system and stores it in a database. For each robot sends status information to the AGV system, and is forwarded to an intermediate system then it is updated into the database to provide REST web services. The proposed system increases the work process functionality of the AGV system, without adding the latest versions and robots.

The integration methods proposed in [20], for Cloud ERP API and Internet of Things (IoT) basically in the form of SOAP or RESTful according to the semantic methods. The concept of integrating ERP services with IoT across the cloud can simplify mapping and enable new mappings and transformations when new services are created or API changes. From the proposed method, temperature data can be stored in the ERP database which can then be used as material for analysis or new action requests in ERP.

2.3. QOS Web Service

The rapid growth of web services become the key aspect for authors to demonstrates the functionality of web services invocation from distributed and heterogeneous environment [21]. The research not concentrated on issues like chance of service failure, response time etc. It is proposing a paradigm to create a new web service based on existing services called as Hybrid approach to enhance the performance of a web service.

The description on Quality of Service (QoS) on web service in article [22], are measured against functional metrics and non-functional metrics, namely the quality aspects of Web Service metrics. The Quality Attribute is what distinguishes Web Services. The International Tele Communication Union (ITU) defines Quality as "the totality of the characteristics of an entity that bears its ability to meet stated and implied needs" and technology giant Microsoft defines the Quality Attribute as "The factors that influence run-time behavior, system design, and user experience "

Table 1: Table Research Comparisons

Method	Result
SOA, REST	A prototype of the lightweight RESTful Framework and several scenarios of industrial devices are presented and response times are measured using two different RESTful protocols: HTTP and CoAP. From the results obtained it can be concluded that the performance of SOA with REST in industrial environments is suitable for current needs.
REST	Web application developer Bay RESTful web API, which is potential in improving the Intelligence and Management precision of distribution grid
SOA, SOA analysis, SOA design, SOMA, SOAF	The most defining SOA methodology is the IBM RUP / SOMA which is a proprietary and widely used industrial project. It supports the middle SOA analysis & design strategy, covering all SOA analysis & design activities.
SOA	Benefits from SOA implementation can be divided into two subcategories: improved business agility and lowered costs
SOA, Web Services, REST	Examine the security vulnerabilities of RESTful web services in the view of popular OWASP rating methodologies and analyze the gaps in the existing security solutions, predicts the potential attacks on SOA based on obtained results by the developed theoretical security model, and the written algorithms as part of security solution prevent the SOA attacks.
SOA, RESTful	The Micro Service architecture is already the de facto industry standard for web services, and Restful Web Services has become the preferred technology model for Micro services applications due to its lightness, scalability, and HTTP protocol compatibility.

The difference with the previous research and studies lies in the background of the case which point to the material being studied to extend the ERP for planning material. The conceptual architecture used for this research was RESTful web service because of the successful research conducted [17] could provide uniform interface, addressability, statelessness, and connectedness.

3. Methodology

The first step, search the literature about SOA then determine the background study and topic of research. Then do some analysis from the background problem and do some observation, data acquisition on the existing system that had been deployed. The next step was designing system architecture with the method selected for this topic research and do some testing afterwards

based on quality of services had been created. The last step to evaluate and write the article based on the results.
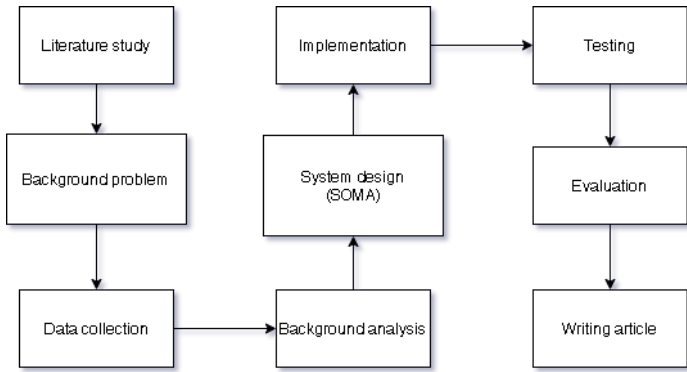
Figure 1: Research Method

3.1. Identification

This research was conducted against the background of the material planning process at Manufacturing Company which was not adopted on ERP implementation. The material planning process taken Place outside the ERP System using worksheets application. The data retrieval and calculation processes need several steps and applications used to produce production material planning.
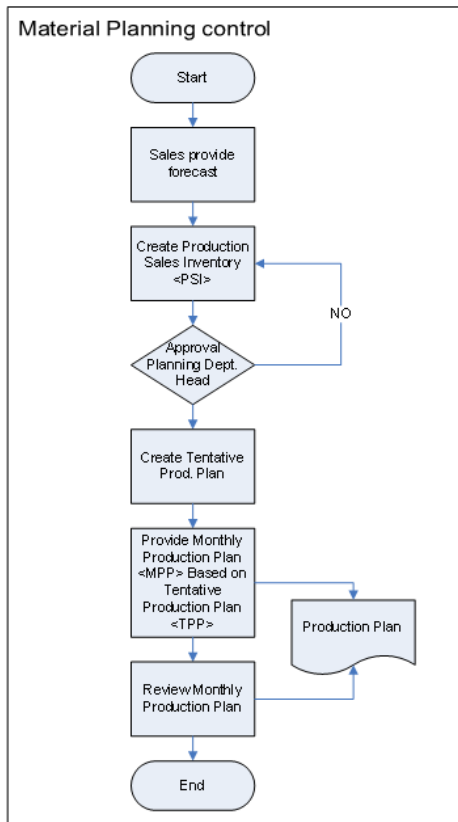
Figure 2: Flowchart material planning

3.2. Data Collection

One of the methods in collecting data by the author is interviews and observations to related sections that have

contributed to the making of material planning. After obtaining sufficient information, the problem is formulated in accordance with the current conditions (according to the time of observation). Then the SOA architecture literature review is carried out as a reference in providing solutions to the problems found and the SOMA (Service Oriented Modelling Architecture)[23] design method for the solution approach.

3.3. Current Condition

Figure 2 show the Business process from creating forecast and used by PPIC (Production Planning and Inventory Control) to create an MRP (Material Requirement Planning) document. Starting from Marketing which makes Sales Forecast which is used as the basis for making PSI (Production Sales and Inventory), then continues to make TPP (Tentative Production Plan) and MPP (Monthly Production Plan) before being approved as MRP (Material Requirement Planning).

3.4. Analysis

The analysis and system design are carried out in accordance with the reference literature used in the SOMA methodology. Then for this proposed design a descriptive justification is also carried out to test whether the proposed design has answered the problems that have been previously formulated. From the results of the descriptive justification conclusions and suggestions are drawn.
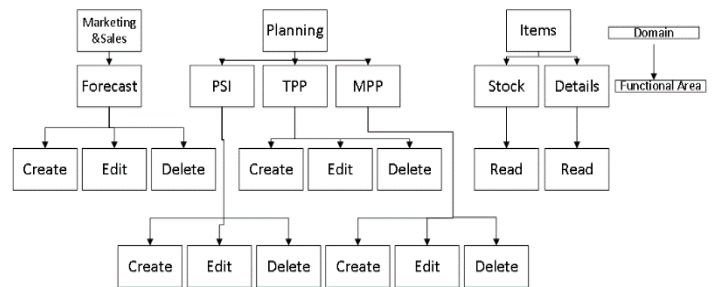
Figure 3: Decomposition Domain
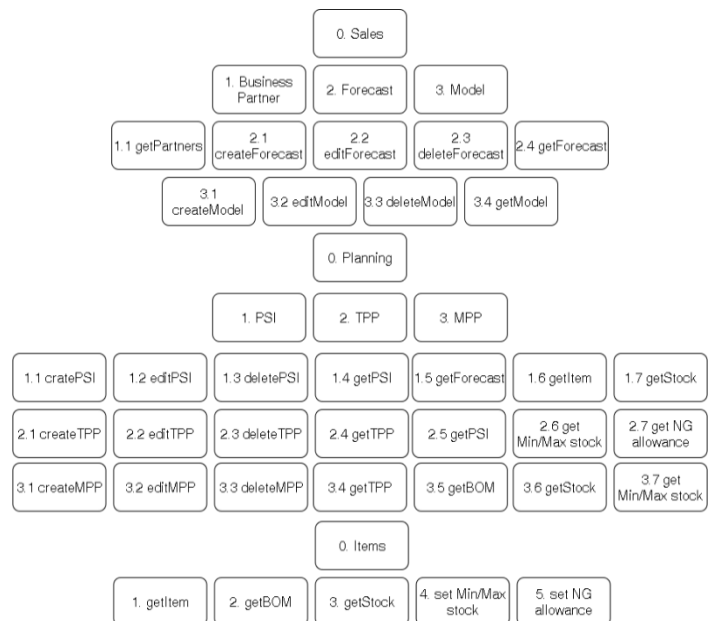
Figure 4: Service decomposition

In Figure 3 shows the domain decomposition process from marketing, planning and warehouse, each domain has several processes. Sub process of marketing is making Forecast, create Forecast, delete Forecast, get Customer, get Project, get Order Quantity. Each business process will be decomposed in order to produce Service components.

Figure 4 showing the creation of Service Layers made of modules/function that being used as a service, the module Group are sales, planning and item and the PSI (Production Sales and Inventory), TPP (Tentative Production Plan), and MPP (Monthly Production Plan) act as a Service layer.

After identifying the service by defining the domain and function area, then developing in more detail into detailed services in Figure 3, the results are used as a service layer which will be used as SOA Solution.
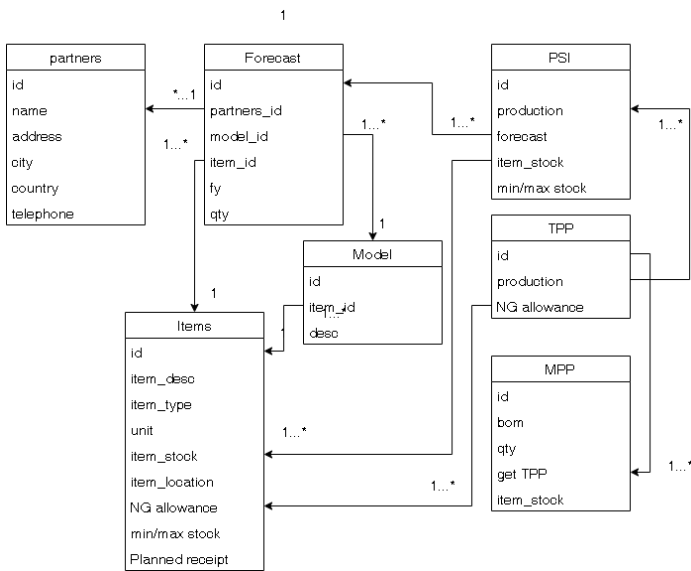
Figure 5: Domain model
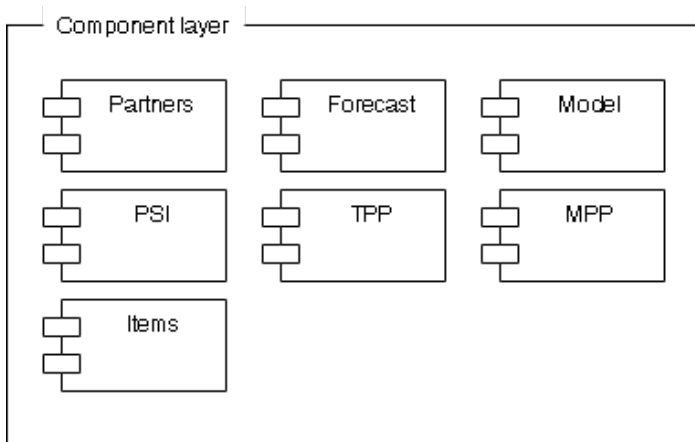
Figure 6: Component layer

At the Specification stage, a service component design is carried out which is obtained from the identification results in the previous process. The results of this stage include the services used to achieve the Goal Service Modeling and SOA architectural design. This stage is divided into 2 main stages, namely the Figure

5 Domain Model for mapping the content of object services and Component Specifications for mapping components in each of the main applications and the use of services by these components.

Figure 6, this stage is the final stage of the specification in which the services will be connected according to the component in more detail based on the specification stage that has been done previously

At this stage, Figure 6 is the final stage of the specification to define the components that will be used in connection with the service layer and business process layer to form a unified relationship starting from the Operational process layer, component layer, and also the service layer.
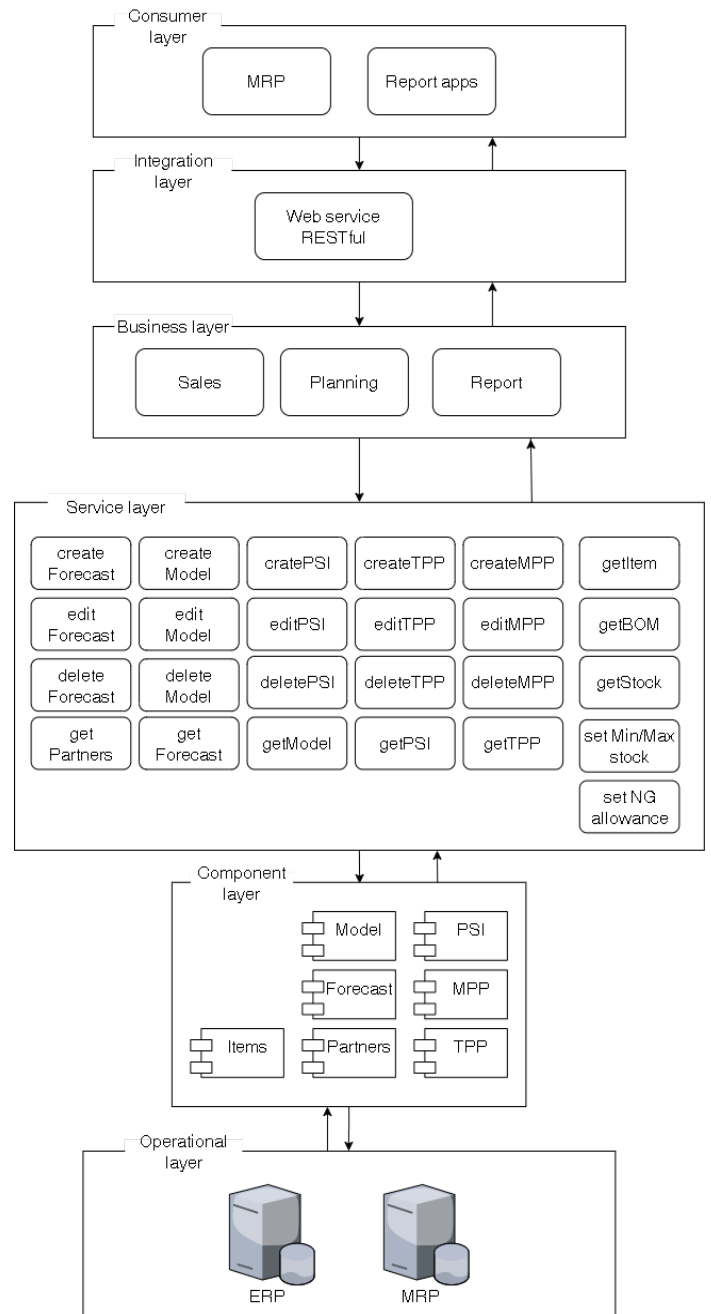
Figure 7: SOA Reference Architecture

3.5. Implementation

From the detailed component results, generated the SOA Reference Architecture that will be implemented for integrating ERP application and MRP application using RESTful method built on web app framework MVC (Model View Controller)[24] Codeigniter which creating output in Json format and the Development using Visual Code.

Figure 7 was the process in creating the web Services accordance to SOA reference architecture.

4. Using the Template

For the evaluation phase in testing the web service, the Quality of Service reference is used and the tool used is Apache JMeter [25] and OWASP ZAP. Apache Jmeter serves to test web apps, but also designed to load test functional behavior and perform measurement while OWASP ZAP serves as an application vulnerability tool to find security flaws in web applications.

As measurement of web Services using JMeter[25] with a simulation of 50 user, and the measurement detail as follows:

Table 2: Throughput category[26]

Throughput category	Throughput (Bps)	Indeks
Very Good	100	4
Good	75	3
Normal	50	2
Bad	<25	1

Table 2 throughput is the effective data transfer rate, measured in bps. Throughput is the total number of successful packet arrivals observed at the destination during the time interval, assessment formula Throughput = data received / delivery time.

Table 3: Latency category[26]

Latency category	Delay (Ms)	Indeks
Very Good	<150ms	4
Good	150ms – 300 ms	3
Normal	300ms – 450 ms	2
Bad	<450ms	1

Table 3 Latency is the time it takes for data to travel the distance from origin to destination. Delay can be affected by distance, physical media, congestion or long processing time.

The web service was tested using JMeter with a total quantity of process simulation of 50 users.

Table 4: Testing results using Jmeter

Service	Latency	Throughput	Result
bom_get	743.3	33.63348416	Normal
details_get	1150.94	51.38125	Good
forecasts_get	727.84	32.34844444	Normal
forecasts_post	857.08	21.2674938	Bad
forecastsCountAll_get	785.36	36.52837209	Normal
inventory_put	2537.46	85.43636364	Very good
models_get	794.74	35.7990991	Normal
models_post	879.08	27.73123028	Normal
modelsCountAll_get	803.3	37.89150943	Normal
name_get	839.68	37.82342342	Normal
partners_get	873.72	41.80478469	Normal
partnersDesc_get	669.3	26.45454545	Normal
psi_get	943.72	42.31928251	Normal
stock_get	775.86	34.79192825	Normal

From the test results Table 4, shows the number of sample data used as many as 50 processes, the throughput assessment results category may varies, relatively normal throughput depending on the amount of data pulled from the database. The best result get from the details_get service for pulling material item description only. The forecasts_post included in the insufficient category because getting all information for the first tme of the business process.

Figure 8: ZAP vulnerability test

Figure 8 shows a web service testing project that has been created using OWASP ZAP, as a whole the web service shows that there are no bugs in the application but has a vulnerability in the Header-Rest Service which is in the RESTful server library.

5. Conclusion

The information system that has been created can be integrated with an ERP system that has a database platform and a programming language that is different from the SOA approach. Where the required business functions can be converted into services using the RESTful concept. With SOMA will help reducing the complexity of the architecture, these can be reused by other applications with different specifications.

Calling the services can be done easily because it uses the HTTP protocol, thereby increasing flexibility in the development of the next application that does not depend on the database and the same programming language.

Recommendation for the next development would be increase the performance and security of the services. Periodically evaluation needed to improve the system integration with deployment and development newer version of ERP.

References

[1] E.F. Monk, Ellen F.; Wagner, Bret J.; and Monk, "Concepts in Enterprise Resource Planning," 493, 2001.

[2] N. Holmberg, B. Johansson, R.A. De Carvalho, "How to gain synchronization between business processes and enterprise resource planning systems: A SOA based perspective on ERP implementation," in CONFENIS 2013 - 7th International Conference on Research and Practical Issues of Enterprise Information Systems, 2013.

[3] N. Holmberg, "A Service Oriented Perspective of Enterprise Resource Planning Systems," Journal of Systems Integration, **8**(2), 14–24, 2017, doi:10.20470/jsi.v8i2.304.

[4] H.F. Erdiyana, Suharjito, "ERP System Integration with Mobile Applications Using Service Oriented Architecture," in Proceedings of 2019 International Conference on Information Management and Technology,

ICIMTech 2019, 2019, doi:10.1109/ICIMTech.2019.8843745.

[5] Muhardany, Suharjito, A.A. Sukmadhani, E. Gunawan, "Development of E-commerce approach to service oriented architecture using SOMA methodology," in Proceedings of 2020 International Conference on Information Management and Technology, ICIMTech 2020, 2020, doi:10.1109/ICIMTech50083.2020.9211161.

[6] M. Amini Valashani, A.M. Abukari, "ERP SYSTEMS ARCHITECTURE FOR THE MODERN AGE: A REVIEW OF THE STATE OF THE ART TECHNOLOGIES," 2020, doi:10.22034/JAISIS.2020.103704.

[7] J. V. Espí-Beltrán, V. Gilart-Iglesias, D. Ruiz-Fernández, "Enabling distributed manufacturing resources through SOA: The REST approach," Robotics and Computer-Integrated Manufacturing, **46**, 156–165, 2017, doi:10.1016/j.rcim.2016.09.007.

[8] Y. Zhu, J. Li, J. Chen, H. Wei, "A framework research of power distribution equipment condition monitoring cloud platform based on RESTful web service," in 2017 IEEE Conference on Energy Internet and Energy System Integration, EI2 2017 - Proceedings, Institute of Electrical and Electronics Engineers Inc.: 1–6, 2017, doi:10.1109/EI2.2017.8245318.

[9] D. Rathod, "Registry for RESTful Web Service: REST Registry," International Journal of Research -GRANTHAALAYAH, **5**(7), 128–135, 2017, doi:10.29121/granthaalayah.v5.i7.2017.2114.

[10] S. Svanidzaite, "A comparison of SOA methodologies analysis & design phases," in CEUR Workshop Proceedings, 2012.

[11] T. Yoon, B.K. Jeong, "Service Oriented Architecture (SOA) Implementation: Success Factors and Realized Benefits," International Journal of Information Systems in the Service Sector, 2018, doi:10.4018/IJISSS.2018040101.

[12] M.I. Beer, M.F. Hassan, "Adaptive security architecture for protecting RESTful web services in enterprise computing environment," Service Oriented Computing and Applications, 2018, doi:10.1007/s11761-017-0221-1.

[13] X. Chen, Z. Ji, Y. Fan, Y. Zhan, "Restful API Architecture Based on Laravel Framework," in Journal of Physics: Conference Series, 2017, doi:10.1088/1742-6596/910/1/012016.

[14] S. Widiyanto, A.B. Setyawan, A. Tarigan, H. Sussanto, "The developing one door licensing service system based on RESTful oriented services and MVC framework," in AIP Conference Proceedings, American Institute of Physics Inc., 2016, doi:10.1063/1.4940297.

[15] M. Wael, Encapsulation of MES Functionalities as RESTful Web Services for Knowledge-Driven Manufacturing Systems, 2017.

[16] S. Grüner, J. Pfrommer, F. Palm, "RESTful Industrial Communication with OPC UA," IEEE Transactions on Industrial Informatics, 2016, doi:10.1109/TII.2016.2530404.

[17] L. Rusu, E. Gerőcs-Szász, "EXTENDED ERP USING RESTFUL WEB SERVICES CASE STUDY: WINMENTOR ENTERPRISE ®," JOURNAL OF INFORMATION SYSTEMS & OPERATIONS MANAGEMENT, 2018.

[18] P. Albertus Kusuma Seta, A.A. Arman, "General service oriented architecture (SOA) for Small Medium Enterprise (SME)," in 2014 International Conference on ICT For Smart Society (ICISS), IEEE: 217–221, 2014, doi:10.1109/ICTSS.2014.7013176.

[19] I. Draganov, S. Stefanova, "A solution for optimizing the integration of AGV systems in enterprises which are using ERP systems," in HORA 2020 - 2nd International Congress on Human-Computer Interaction, Optimization and Robotic Applications, Proceedings, 2020, doi:10.1109/HORA49412.2020.9152869.

[20] D. Andročec, R. Picek, M. Mijač, "The ontologically based model for the integration of the IoT and Cloud ERP services," in CLOSER 2018 - Proceedings of the 8th International Conference on Cloud Computing and Services Science, 2018, doi:10.5220/0006763104810488.

[21] R.R. Reddy, C. R. M., & Rao, "QOS of Web Service : Survey on Performance and Scalability," Computer Science and Information Technology, **3**(9), 65–73, 2013, doi:10.5121/csit.2013.3907.

[22] A. Negi, P. Kaur, "A Systematic Literature Review on QoS for SOA-based Web Services," Article in INTERNATIONAL JOURNAL OF COMPUTER SCIENCES AND ENGINEERING, 2018, doi:10.26438/ijcse/v6i7.735444.

[23] A. Arsanjani, S. Ghosh, A. Allam, T. Abdollah, S. Ganapathy, K. Holley, "SOMA: A method for developing service-oriented solutions," IBM Systems Journal, 2008, doi:10.1147/sj.473.0377.

[24] W. Warkim, D.I. Sensuse, "System Integration Model with Service Oriented Architecture Method Approach and Model View Controller at the Research Center for Science and Technology Development of the Indonesian Institute of Sciences," Jurnal Teknik Informatika Dan Sistem Informasi, **3**(1), 2017, doi:10.28932/jutisi.v3i1.572.

[25] S. Matam, J. Jain, JMeter Recipes, Apress, Berkeley, CA: 221–242, 2017, doi:10.1007/978-1-4842-2961-3_10.

[26] Y.A. Pranata, I. Fibriani, S.B. Utomo, "Analysis of Quality Of Service Performance Optimization In Data Communication Services Using Ns-2 At PT. PLN (Persero) Jember," Sinergi, **20**(2), 149, 2016, doi:10.22441/sinergi.2016.2.009.

A Theory on How Strings Responds to Gravitation by Refraction in Curved Spacetime

Sung Hoon Baek[*]

Department of Computer Engineering, Jungwon University, Goesan-gun, 28024, South Korea

A R T I C L E   I N F O

A B S T R A C T

General relativity and its modified theories are unable to account for quantum mechanics and cannot explain dark matter or the origin of the gravitation. This paper presents a theory that describes how Newtonian gravitation originates at the level of the particle, and how particles induce gravitation and respond to the source of gravitation. This paper provides a deeper understanding of gravitation and a complete derivation of Newtonian gravitation from the level of particles; and shows how some particles can act like being massless and does not follow the Newtonian gravitation. In addition, This paper provides a new method, which determines a steep spacetime curvature and provides a new aspect of the galactic center. Past measurements of light-bending during total eclipses are consistent with the proposed theory.

1   Introduction

According to general relativity, the observed gravitational effect results from the curvature of spacetime [1]. In 1919, the deflection of light was measured and found to be as predicted by general relativity: gravitation from stars bends the paths of light rays. A tiny shift in light rays around the Sun was observed during a total solar eclipse [2].

In 1959, Pound and Rebka reported the first successful measurement of the gravitational redshift, which is a phenomenon in which the wavelength of a photon shifts to a longer wavelength when the photon moves upward against a gravitational field [3, 4]. These and other experimental results have confirmed the existence of gravitational time dilation. Many experiments verified the existence of gravitational time dilation and gravitational light-bending.

General relativity describes gravitational spacetime using tensors. Between about 1960 and the mid-1980s a variety of modifications to special relativity have been proposed, including scalartensor theories [5], vector-tensor theories [6], and tensor-vector-scalar theories [7]. A number of physicists have invented alternative theories, such as the Dickie framework and the parameterized post-Newtonian formalism [5, 8, 9].

Recently, string theory has established a connection between the microscopic world of high-energy particles and the large-scale world of gravitation [2]. Physicists have also proposed a number of models to describe mass [10]–[15].

Instead of using tensors, this paper utilizes the refraction prin-

ciple of Snell-Descartes to investigate gravitation from the particle level to the cosmic scale.

The refractional trajectory of light is the shortest path that is equivalent to the geodesic in a curved space. These two methods describe the same thing, but the former uses calculus, and the latter uses tensor calculus.

A ray of light changes its direction when it passes from one to another medium because the speed of the light changes in different media. This phenomenon is called refraction [16]. In gravitational time dilation, the distance that light travels changes across gradually changing spacetime. This change also results in refraction by gravitation.

Several works [17, 18] have described light-bending around a mass using the refraction mechanism, but this paper extends it to a complete derivation of Newtonian gravitation from the level of the particle using the refraction principle.

The presented derivation provides us a clear understanding of where the gravitation originated, how particles participate in creating gravitation and respond to gravitation, why all composite bodies in a gravitational field have the same acceleration, and why a particle acts like being massless.

Classical physics is applicable only to a flat space. Modern physics has extended the space and time into a spacetime curvature during a century. However, general relativity makes the mistake of including a part of classical physics, and fails to describe a steep curvature of spacetime. The Section 3.3 describes this in detail. To avoid this mistake, this paper simply utilizes only the refraction

[*]Corresponding Author: Sung Hoon Baek, Email: shbaek@jwu.ac.kr

principle, Lorentz invariance, and two proposed postulates. This paper presents a new metric to describe a steep spacetime curvature, and compares it with the prior one.

2 Overview

In string theory, particles consist of one-dimensional objects called strings. We assume the following: (Postulate 1) The photon is a straight open string as a particle. All strings flow with the speed of light like the photon does, but the strings of the other particles flow within their geometric space. The strings flow in various directions depending on their geometry.

When multiple particles are chained together to comprise a nucleus, their geometric orientations are restrained, and they flow to various directions in their restrained space. When particles are linked with each other to form a nucleus, statistically a set of strings flow in every direction. Newtonian gravitation is obtained from the statistically omnidirectional flows of strings.

There is no specific boson for gravitation. All of the particles consist of strings and participate in creating gravitation, and respond to gravitation. Hence, all composite bodies in a gravitational field have the same acceleration [19]. However, a free and stationary particle can exhibit imperfect omnidirectional movement, taking a preferred orientation to minimize gravitational force, and in this case it has a different acceleration that described by Newtonian gravitation. In addition, a specific shape of particle can act like being massless.

Figure 1 shows the omnidirectional flows of a string across spacetime layers. The lower space layer has greater time dilation than the upper one according to the gravitational time dilation. The velocity of the string is constant across space layers, according to the Lorentz invariance, but time is slower in the lower space. Thus, the distance traveled in the lower space layer is shorter than in the upper one for the same coordinate time.

Strings experience refraction like a ray of light as it passes from one medium to another medium, changing its direction. Refraction was experimentally and theoretically established by the Snell-Descartes law four hundred years ago.
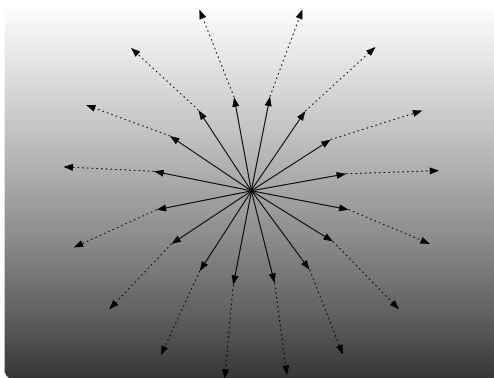
Figure 1: Omnidirectional movements and their refraction across space layers with different time dilations.

The speed of light is slower in water than in air, thus the distance traveled is shorter in water. In a similar way, time is slower in the lower space thus the distance traveled is shorter in the lower space. The re-fractional trajectory of light is the shortest path that is equivalent to the geodesic in a curved space.

Kinetic energy and thermal energy can also refracted by gravitation, because the trajectory of movement depends on the shortest path.

Refractions are illustrated as dotted lines in Figure 1. At the first time, the central velocity of the particle is zero. A short time later, the particle experiences refraction and the sum of the changes of the vertical distance for every direction heads for the center of gravitation. This refraction results in the gravitational acceleration.

This paper presents a derivation of Newtonian gravitation from the refractions of omnidirectional flows across gradually changing spacetime.

3 Derivation

This section shows the process for deriving for Newtonian gravitation from refraction by gravitational time dilation.

3.1 Refraction

This section derives the changed altitude of an inclined string (a ray of light) by refraction during a short time Δt. We have to consider two different cases, where the string heads downward and upward. Then, we take into account all possible directions.

Let $T(r)$ be the time ratio between the time at a distance r and the time at infinity. The distance r is the coordinate distance from the center of gravitation. The relationship between the elapsed time at a distance r, $\Delta t(r)$, and the elapsed time at infinity, $\Delta t(\infty)$, is given by

$$\Delta t(r) = T(r)\Delta t(\infty). \tag{1}$$

Let $T_r(r')$ be the relative time at the distance r' from the viewpoint of an object that is at the distance r, then $T_r(r')$ is defined by

$$T_r(r') = T(r')/T(r) \tag{2}$$

The relative time at the distance $r + \Delta r$ from the viewpoint of the object that is at the distance r, $T_r(r + \Delta r)$, is

$$T_r(r + \Delta r) = T(r + \Delta r)/T(r) \tag{3}$$

We define $s_r(r)$ as the slope of the relative time from the viewpoint of the object that is at the distance r with respect to the coordinate distance.

$$
\begin{aligned}
s_r(r) &= \lim_{\Delta r \to 0} \frac{T_r(r + \Delta r) - T_r(r)}{\Delta r} \\
&= \lim_{\Delta r \to 0} \frac{T(r + \Delta r)/T(r) - T(r)/T(r)}{\Delta r} \\
&= \lim_{\Delta r \to 0} \left(\frac{T(r + \Delta r)}{T(r)} - 1 \right) \frac{1}{\Delta r}.
\end{aligned}
\tag{4}
$$

The amount of refraction depends on the relative time (see Eq. (10)). (Postulate 2) Hence, we assume that the slope of the relative time $s_r(r)$ determine the gravitational acceleration and follow the divergence theorem. This means that $s_r(r)$ is proportional to the mass of the gravitational source and the inverse square of coordinate distance, as in the following equation.

$$s_r(r) = \frac{aM}{r^2}, \tag{5}$$

where a is a coefficient, and M is the mass of the gravitational source.

We define R as the following equation,

$$R \equiv aM. \tag{6}$$

We call R the gravitational radius. It is similar to the Schwarzschild radius but it is little different from that.

By combining Eqs. (4), (5), and (6), we get

$$\left(\frac{T(r + \Delta r)}{T(r)} - 1 \right) \frac{1}{\Delta r} = \frac{R}{r^2}, \tag{7}$$

$$\frac{T(r + \Delta r)}{T(r)} = 1 + \frac{R}{r^2} \Delta r. \tag{8}$$

This equation is used to find the gravitational acceleration in the next section.

3.1.1 Downward

This section derives the vertical acceleration for a string with an inclined angle.

Δr is the small change in vertical distance that a string flows during a small time Δt.

In Figure 2, time is slower in the lower space than in the upper space that is illustrated with a brighter rectangle. We have to be aware of that the time dilation across spaces is continuous even though Figure 2 makes it appear to be discontinuous.
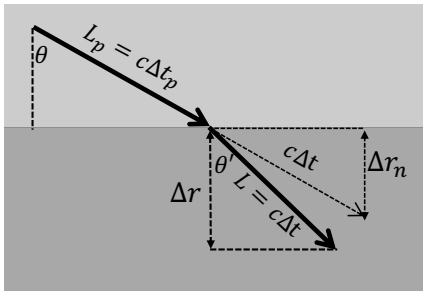
Figure 2: Refraction when an inclined string travels downward.

Accordingly, it takes Δt in the lower space while it takes Δt_p in the upper space. The former is less than the latter ($\Delta t < \Delta t_p$). The length that a string travels is L in the lower space while it is L_p in the upper space during the same coordinate time. L is $c\Delta t$ and L_p is $c\Delta t_p$, where c is the speed of light in vacuum. The difference in the distances traveled in the different spaces causes refraction.

When an inclined string makes an incident angle θ with the vertical line, the incident angle changes into θ' after a short time Δt. The refraction index n describes the relationship between the incident angle θ and the refraction angle θ' is given by Snell's law [16].

$$\frac{1}{n} = \frac{\sin \theta'}{\sin \theta} = \frac{L}{L_p} = \frac{c\Delta t}{c\Delta t_p} = \frac{\Delta t}{\Delta t_p}, \tag{9}$$

Using Eqs. (1) and (9), we obtain

$$\frac{1}{n} = \frac{T(r + \Delta r)}{T(r)}, \tag{10}$$

From Eqs. (8) and (10), we obtain

$$\frac{1}{n} = 1 + \frac{R}{r^2} \Delta r. \tag{11}$$

Using the geometry shown in Figure 2 and Eqs. (9) to (11), the vertical distance that a string with the refraction angle θ' travels for a short time Δt, Δr, is given by

$$
\begin{aligned}
\Delta r &= -c\Delta t \cos \theta' \\
&= -c\Delta t \sqrt{1 - (\sin \theta')^2} \\
&= -c\Delta t \sqrt{1 - \left(\frac{1}{n} \sin \theta \right)^2} \\
&= -c\Delta t \sqrt{1 - \left(\left(1 + \frac{R\Delta r}{r^2} \right) \sin \theta \right)^2}.
\end{aligned}
\tag{12}
$$

From Eq. (12), we obtain a quadratic function for Δr as the following.

$$\left(\frac{1}{(c\Delta t)^2} + \frac{s^2 R^2}{r^4} \right)(\Delta r)^2 + \frac{2 * R s^2}{r^2} \Delta r + s^2 - 1 = 0, \tag{13}$$

where $\sin \theta$ is substituted with s to simplify the equation. Using the quadratic formula, the change in vertical distance, Δr, is given by

$$
\begin{aligned}
\Delta r &= \frac{-R s^2 / r^2 \pm \sqrt{s^2 R^2 / r^4 + (1 - s^2)/(c\Delta t)^2}}{1/(c\Delta t)^2 + s^2 R^2 / r^4} \\
&= \frac{-\frac{R s^2 (c\Delta t)^2}{r^2} \pm \sqrt{\frac{s^2 R^2 (c\Delta t)^4}{r^4} + (1 - s^2)(c\Delta t)^2}}{1 + \frac{s^2 R^2 (c\Delta t)^2}{r^4}}.
\end{aligned}
\tag{14}
$$

Let Δr_d be the change in vertical distance when a string heads downward; then it is always negative. Hence, Δr_d is chosen as the negative version of the two solutions of Eq. (14).

$$\Delta r_d(\theta) = \frac{-\frac{R s^2 (c\Delta t)^2}{r^2} - \sqrt{\frac{s^2 R^2 (c\Delta t)^4}{r^4} + (1 - s^2)(c\Delta t)^2}}{1 + \frac{s^2 R^2 (c\Delta t)^2}{r^4}}, \tag{15}$$

where $s = \sin \theta$ and $0 \le \theta < \pi/2$.

When a string is parallel to the horizontal plane ($\theta = \pi/2$), there might be no gravitational acceleration. Hence, $\pi/2$ is excluded in Eq. (15). This special case is discussed in Section 5.

Let $\Delta r_n(\theta)$ be the vertical distance traveled if it is not affected by refraction, as shown in Figure 2. Then the small change of the

downward velocity is given by

$$
\begin{aligned}
dv_d &= \lim_{\Delta t \to 0} \frac{\Delta r_d(\theta)}{\Delta t} - \frac{\Delta r_n(\theta)}{\Delta t} \\
&= \lim_{\Delta t \to 0} \frac{\Delta r_d(\theta)}{\Delta t} - \left(-\frac{c\Delta t \cos\theta}{\Delta t}\right) \\
&= \lim_{\Delta t \to 0} \frac{-\frac{Rs^2 c^2 \Delta t}{r^2} - \sqrt{0 + (1 - s^2)c^2}}{1 + 0} + c\cos\theta \quad (16) \\
&= \frac{-Rc^2 dt \sin^2\theta}{r^2} - c\cos\theta + c\cos\theta \\
&= -\frac{c^2 R \sin^2\theta}{r^2} dt.
\end{aligned}
$$

The refractional acceleration with a downward angle is obtained by

$$
a_d(\theta) = \frac{dv_d}{dt} = -\frac{c^2 R \sin^2\theta}{r^2}, \quad (17)
$$

where $0 \le \theta < \pi/2$.

The gravitational acceleration is determined by the incident angle θ of the string. Acceleration is minimized when the incident angle is perpendicular to the horizontal plane of the gravitation. However, Newtonian gravitation is statistically composed of various incident angles. This is described in the Section 'Every Direction'.

3.1.2 Upward

Here, let's consider a case where a string flows upward, as shown in Figure 3. The incident angle of a string, θ, is greater than $\pi/2$ and less than π. let $\phi = \pi - \theta$. We get the same equation as for the refraction index, Eq. (9).
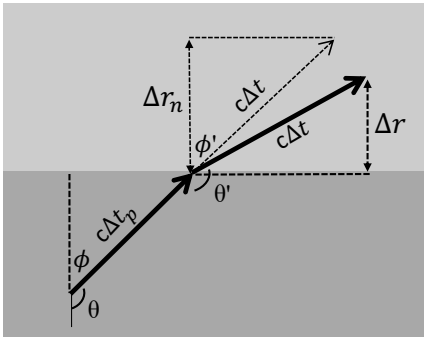
Figure 3: a refraction when an inclined string travels upward.

$$
\frac{1}{n} = \frac{\sin\phi'}{\sin\phi} = \frac{\sin(\pi - \theta')}{\sin(\pi - \theta)} = \frac{\sin\theta'}{\sin\theta}.
$$

The vertical distance Δr, is a positive value, it is hence given by

$$
\begin{aligned}
\Delta r &= c\Delta t \cos\phi' \quad (18) \\
&= c\Delta t \sqrt{1 - \left(\left(1 + \frac{R\Delta r}{r^2}\right)\sin\theta\right)^2}. \quad (19)
\end{aligned}
$$

It has a different sign than Eq. (12). However, this equation (19) results in the same quadratic equation as Eq. (13).

Let Δr_u be the change in distance when a string heads upward. Δr_u is chosen as the positive version of the two solutions of Eq. (14).

$$
\Delta r_u(\theta) = \frac{-\frac{Rs^2(c\Delta t)^2}{r^2} + \sqrt{\frac{s^2 R^2 (c\Delta t)^4}{r^4} + (1 - s^2)(c\Delta t)^2}}{1 + \frac{s^2 R^2 (c\Delta t)^2}{r^4}}, \quad (20)
$$

where $s = \sin\theta$ and $\pi/2 < \theta \le \pi$.

The small change in upward velocity is given by

$$
\begin{aligned}
dv_u &= \lim_{\Delta t \to 0} \frac{\Delta r_u(\theta)}{\Delta t} - \frac{c\Delta t \cos\theta}{\Delta t} \\
&= \frac{-Rc^2 dt \sin^2\theta}{r^2} + c\cos\theta - c\cos\theta \quad (21) \\
&= -\frac{c^2 R \sin^2\theta}{r^2} dt.
\end{aligned}
$$

dv_u is the same as dv_d, thus the refractional acceleration with an upward angle is the same as Eq. (17). We obtain

$$
a_u(\theta) = \frac{dv_u}{dt} = -\frac{c^2 R \sin^2\theta}{r^2}, \quad (22)
$$

where $s = \sin\theta$ and $\pi/2 < \theta \le \pi$.

3.1.3 Every Direction

If we remember the first postulate, the strings comprising a particle flow in several directions depending on its geometry with the speed of light inside its particle space. Multiple particles that are combined with each other make statistically omnidirectional flows, which is regulated by Newtonian gravitation. Hence, we consider all incident angles.
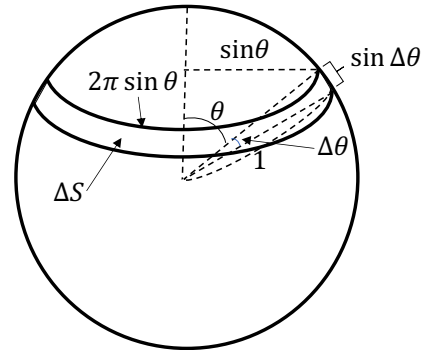
Figure 4: Each incident angle has different amount of area in the three-dimensional space.

The flow directions are evenly distributed in a sphere. Each different incident angle makes a different ring area ΔS in the sphere as shown in Figure 4. The number of flows with the incident angle θ is proportional to the ring area $\Delta S(\theta)$, which is given by

$$
\Delta S(\theta) = 2\pi \sin\theta \sin\Delta\theta = 2\pi \sin\theta \Delta\theta. \quad (23)
$$

We can obtain the statistical acceleration for all directions from Eqs. (17), (22), and (23). The acceleration created by gravitational

time dilation is given by.

$$
\begin{aligned}
a &= \lim_{\Delta\theta\to 0} \frac{\sum_0^{\pi/2} \Delta S(\theta) a_d(\theta) + \sum_{\pi/2}^{\pi} \Delta S(\theta) a_u(\theta)}{\sum_0^{\pi} \Delta S(\theta)} \\
&= \lim_{\Delta\theta\to 0} \frac{\sum_0^{\pi} -2\pi \frac{c^2 R}{r^2} \sin^3\theta \Delta\theta}{\sum_0^{\pi} 2\pi \sin\theta \Delta\theta} \\
&= \frac{\int_0^{\pi} -\frac{c^2 R}{r^2} \sin^3\theta d\theta}{\int_0^{\pi} \sin\theta d\theta} \\
&= -\frac{c^2 R}{2r^2} \left(\frac{1}{3}\cos^3\theta - \cos\theta\right)\Big|_0^{\pi} \\
&= -\frac{2c^2 R}{3r^2}.
\end{aligned}
\tag{24}
$$

3.2 Newtonian Gravitation

All particles consist of strings and participate in creating gravitation and respond to gravitation. An object that moves with high-speed experiences both time dilation and Lorentz contraction according to the Lorentz transformations. The string flows at the speed of light. Hence, we can expect not only gravitational time dilation but also gravitational spatial contraction around strings. Gravitational spatial contraction corresponds to the curved space of general relativity.

The acceleration created by gravitational spatial contraction is the same as that produced by gravitational time dilation. So, the total refractional acceleration created by both time and space is doubled from Eq. (17) and described by the formula

$$
g(\theta) = \frac{2c^2 R \sin^2\theta}{r^2}.
\tag{25}
$$

The Newtonian acceleration that is created by both space and time is doubled from Eq. (24). Finally, it is written using the formula

$$
g = -\frac{4c^2 R}{3r^2}.
\tag{26}
$$

We can compare Eq. (26) with the equation for Newtonian gravitation as the following equation:

$$
\frac{GM}{r^2} = \frac{4c^2 R}{3r^2},
\tag{27}
$$

where M is the mass of the gravitational source, and G is the gravitational constant.

The gravitational radius R is written

$$
R = \frac{3GM}{4c^2}.
\tag{28}
$$

3.3 Gravitational Time Dilation Function

3.3.1 Proposed function

This section shows a derivation of this gravitational time dilation function $T(r)$.

We go back to Eq. (1). The gravitational time dilation function $T(r)$ is used to obtain a locally measured (proper) time $d\tau$ from the

coordinate time dt, which is the time measured by a stationary clock at infinity.

$$
d\tau = T(r)dt.
\tag{29}
$$

We combine Eqs. (10) and (11) into the following equation:

$$
\begin{aligned}
1 + \frac{R}{r^2}dr &= \frac{T(r+dr) - T(r) + T(r)}{T(r)} \\
&= 1 + \frac{T(r+dr) - T(r)}{T(r)}.
\end{aligned}
\tag{30}
$$

Using Eq. (30), the differential equation for the gravitational time dilation function is given by

$$
\frac{dT(r)}{dr} = \frac{R}{r^2}T(r).
\tag{31}
$$

By solving this differential equation, the gravitational time dilation function is given by

$$
T(r) = t_1 e^{-\frac{R}{r}},
\tag{32}
$$

where t_1 is a constant.

If $T(\infty) = 1$, we get

$$
T(r) = e^{-\frac{R}{r}}.
\tag{33}
$$

Finally, from Eqs. (29) and (33), we get the relationship between t and τ.

$$
d\tau = e^{-\frac{R}{r}}dt.
\tag{34}
$$

3.3.2 Prior work

Here, we compare the proposed solution with the prior solution of general relativity. The Schwarzschild metric as a solution to the Einstein field equations is

$$
\begin{aligned}
ds^2 &= -c^2(1 - \frac{2GM}{c^2 r})dt^2 + (1 + \frac{2GM}{c^2 r})dr^2 \\
&\quad + r^2(d\theta^2 + \sin^2\theta d\psi^2).
\end{aligned}
\tag{35}
$$

The Schwarzschild metric includes the counterpart of $T(r)$ as in the following equation:

$$
d\tau = \sqrt{1 - \frac{2GM}{c^2 r}}dt.
\tag{36}
$$

Eq. (36) is different from Eq. (34) because it is derived using the following classical equation of potential energy :

$$
P = -\frac{GMm}{r}.
\tag{37}
$$

This potential energy is for a flat spacetime where dl can be replaced by dr. l is the locally measured (proper) length. r is the coordinate length measured at infinity.

Here, this paper proposes a new potential energy for a curved spacetime. The gravitational potential energy at a local position l is

$$
P = \int_{\infty}^{l} \frac{GMm}{r^2}dl.
\tag{38}
$$

We can get the the classical equation (37), if dl are replaced by dr in Eq. (38). However, the energy is the product of the force and the length that is locally measured at the viewpoint of the object. The local displacement dl is longer than the coordinate displacement dr in a curved spacetime. Hence, we should not use dl instead of dr, and the classical potential energy cannot be used in a curved spacetime.

3.3.3 Comparison with the prior work

If $R/r \ll 1$ (sluggish spacetime), the proposed equation $T(r)$ has a form similar to the Schwarzschild metric. The Taylor series of the proposed time dilation function can be written

$$T(r)^2 = 1 - \frac{2R}{r} + (\frac{2R}{r})^2 \frac{1}{2!} + \cdots. \tag{39}$$

If $R/r \ll 1$, we can take only the first and the second terms of the series. We obtain a form similar to the Schwarzschild metric as the following:

$$T(r) \quad \simeq \quad \sqrt{1 - \frac{2R}{r}} = \sqrt{1 - \frac{3GM}{2c^2 r}}, \tag{40}$$

$$d\tau \quad \simeq \quad \sqrt{1 - \frac{3GM}{2c^2 r}} dt, \tag{41}$$

where it is valid for a sluggish spacetime.

Eq. (41) has a form similar to Eq. (36), but Eq. (41) has 3/2 instead of 2 in Eq. (36). The reason for this difference is that the straight string (photon) has different gravitational acceleration than composite bodies with multi-directional flows, but the general relativity assumes that the straight string and composite bodies are equivalent.

3.4 Gravitational Spatial Contraction

Let $S(r)$ be the gravitational spatial contraction function. $S(r)$ determines how much space at the coordinate distance r is contracted. Spatial contraction is reciprocal to time dilation according to the Lorentz transformation. So, the spatial contraction function is

$$S(r) = \frac{1}{T(r)} = e^{\frac{R}{r}}. \tag{42}$$

Let l be the locally measured (proper) length. Let r be the coordinate length measured at infinity. The relationship between the two lengths can be expressed by

$$dl = S(r)dr = e^{\frac{R}{r}} dr. \tag{43}$$

The Schwarzschild metric includes the counterpart of the spatial contraction function as the following equation:

$$dl = \sqrt{1 + \frac{2GM}{c^2 r}} dr. \tag{44}$$

Eqs. (43) and (44) are different for the reason explained in the previous section.

Figure 5 compares the two equations. Eq. (43) can produces a much greater space for blackholes than Eq. (44). This may give us a new clue for dark matter.
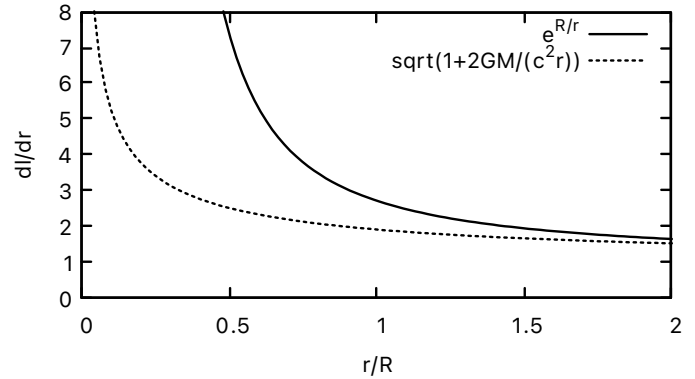
Figure 5: Comparison of the space ratio (dl/dr) using the proposed metric ($e^{R/r}$) and general relativity ($\sqrt{1 + 2GM/(c^2 r)}$).
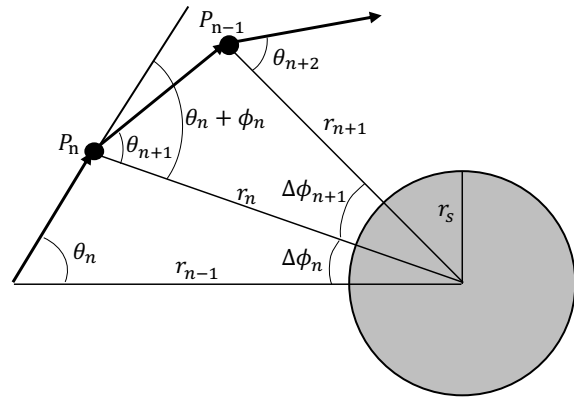
Figure 6: The trajectory of light bended by a star.

4 Gravitational Lens

When a ray of light travels around a star, we can determine the light trajectory if the incident angle, the distance from the star, and the mass of the star are given.

4.1 Numerical Method

This section describes a numerical method that finds the light trajectory around a star. It is useful even if R/r is not small. The next section introduces an analytical method that is valid when $R/r \ll 1$.

As shown in Figure 6, the stellar radius is r_s. The given distance from the center of the star is r_n. The given incident angle of light is θ_n. The next distance from the star, r_{n+1}, after a short time Δt, is

$$r_n = \sqrt{(c\Delta t \sin \theta_n)^2 + (r_{n-1} - c\Delta t \cos \theta_n)^2}. \tag{45}$$

For the short time Δt, the angle made by the previous position, the center of the star, and the next position of light, $\Delta\phi_n$, is obtained

by

$$\Delta\phi_n = \sin^{-1}\frac{c\Delta t \sin\theta_n}{r_n}. \tag{46}$$

The change in distance is defined by

$$\Delta r = r_n - r_{n-1}. \tag{47}$$

The incident angle θ_i is

$$\theta_i = \theta_n + \Delta\phi_n. \tag{48}$$

The refraction index is obtained from the time ratio (Eq. (9)) and the space ratio because the total refraction is caused by both space and time.

$$\begin{aligned}\frac{1}{n} &= \frac{\sin\theta_{n+1}}{\sin(\theta_i)}\\ &= \frac{T(r_n + \Delta r)}{T(r_n)} \Big/ \frac{S(r_n + \Delta r)}{S(r_n)}\\ &\simeq 1 + \frac{2R\Delta r}{r^2},\end{aligned} \tag{49}$$

where Δr is infinitesimally small.

From Eq. (49), we get the next angle,

$$\theta_{n+1} = \begin{cases} \sin^{-1}\left(\frac{1}{n}\sin\theta_i\right), & \text{if } \theta_i < \pi/2;\\ \pi - \sin^{-1}\left(\frac{1}{n}\sin\theta_i\right), & \text{otherwise.} \end{cases} \tag{50}$$

We can iterate the sequences of Eqs. (45) to (50) to get the light trajectory using a computer program.

4.2 Analytical Method

4.2.1 The prior method

The amount of light-bending seen from the Earth can be obtained by a geodesic in a curved spacetime which is introduced in general relativity. In 1911, Einstein obtained a deflection angle of

$$\alpha = \frac{2GM_{sun}}{c^2 r}[radians] = \frac{0.87}{r}[arcsec], \tag{51}$$

where r is the visual distance in solar radii from the center of the Sun.

In 1915, he modified the above equation by adding the effect of curved space thus doubling the bending angle in the following equation:

$$\alpha = \frac{4GM_{sun}}{c^2 r}[radians] = \frac{1.75}{r}[arcsec]. \tag{52}$$

The derivation of this equation is described in prior articles [20].

This derivation is obtained from the velocity of light in a gravitational field. Using Eqs. (36) and (44), we obtain the velocity of light

$$v = \frac{dr}{dt} = \frac{\sqrt{1 + 2GM/c^2 r}\,dl}{\sqrt{1 - 2GM/c^2 r}\,d\tau} \simeq \sqrt{1 + \frac{4GM}{c^2 r}}\,c, \tag{53}$$

where $GM/(c^2 r) \ll 1$.

The full derivation of light-bending is too long to contain in this paper.

4.2.2 Proposed method

From Eqs. (28), (34), and (43), our counterpart of Eq. (53) can be written as

$$\begin{aligned}v = \frac{dr}{dt} &= \frac{S(r)dl}{T(r)d\tau} = e^{\frac{3GM}{2c^2 r}}c\\ &= \sqrt{e^{\frac{3GM}{c^2 r}}}\,c \simeq \sqrt{1 + \frac{3GM}{c^2 r}}\,c,\end{aligned} \tag{54}$$

where $GM/(c^2 r) \ll 1$.

To get the angle of light-bending using the proposed method, we can substitute Eq. (53) with Eq. (54). Finally, the angle of light-bending is obtained by substituting 4 of Eq. (52) with 3.

$$\alpha = \frac{3GM_{sun}}{c^2 r}[radians] = \frac{1.31}{r}[arcsec]. \tag{55}$$

4.3 The Expeditions: Gravitational Refraction and Solar Atmospheric Refraction

Over the last century, there have been many expeditions to measure light-bending during a total eclipse. Goldoni and Stefanini summarized these observational results [21].

In 1919, two expeditions obtained the values 1.61 ± 0.30 and 1.98 ± 0.16 arcsec, where $1/r$ is omitted. In 1922, the obtained mean values ranged from 1.42 arcsec to 2.16 arcsec. Freunclich et al. obtained an average value of 2.24 ± 0.1 arcsec in 1929. Japanese astronomers gave the average deflection value of 1.71 arcsec in 1936, but their plates were quite unreliable. Subsequent expeditions obtained 2.01 ± 0.27, 1.70 ± 0.10, 1.66 ± 0.18, and 1.75 ± 0.06 arcsec, in 1947, 1952, 1973, and 2017, respectively. Even in the latest result, the most critical item is that the plate scale is only 2 arcsec per pixel [22]. This low resolution makes it hard to obtain an accurate result.

The major factors that can bend light are the atmospheric refraction of the Earth, the solar gravitational refraction (deflection), and the solar atmospheric refraction. Prior measurements considered the atmospheric refraction of the Earth but excluded that of the Sun.

NASA revealed that the solar atmosphere, called the corona, is much larger than previously observed [23]. Its radius is 12 solar radii, and the solar atmosphere is sparsely filled with solar particles, which can slow down the speed of light and causes solar atmospheric refraction. The past observations for light bending are measured within the solar atmosphere.

The particle density in the solar atmosphere can also vary. This may be one of the reasons why the observational results were various. Unfortunately, we don't have enough information to know how much the solar atmosphere can refract light.

Due to the solar atmospheric refraction, observations should be greater than the proposed expectation of 1.31. Past measurements have ranged from 1.42 to 2.24, which are consistent with the proposed theory.

5 Quantum Gravity

The small change in vertical distance with the incident angle of $\pi/2$, $\Delta r_u(\pi/2)$, is zero in Eq. (20). This means that there is no gravitational force to circular strings that are parallel to the horizontal plane of gravitation. The gravitational acceleration for the incident angle of $\pi/2$, $a_u(\pi/2)$, is nonzero in Eq. (22). However, if Δt is finite like the Planck time. the quantum gravitational acceleration with the parallel angle is obtained as zero from Eq. (21) according to the following equation.

$$
\begin{aligned}
a_q(\pi/2) &= \frac{\Delta v_u(\pi/2)}{\Delta t} \\
&= \frac{1}{\Delta t}\left(\frac{\Delta r_u(\pi/2)}{\Delta t} - 0\right) \\
&= \frac{1}{\Delta t}\left(\frac{0}{\Delta t} - 0\right) \\
&= 0.
\end{aligned}
\tag{56}
$$

In other words, the gravitational acceleration with the incident angle of $\pi/2$ is zero, because the smallest length and the smallest time are finite according to the quantum mechanics.

A lonely and stationary string with a circular shape can rotate like a gyroscope, maintaining its rotational axis perpendicular to the gravitational horizontal plane. When its incident angle become $\pi/2$ by gyroscopic rotation, there is no gravitational force to this string. This explains how neutrinos have elusive mass [24] and how the gluon acts like being massless.

A massive particle and a set of combined particles may create nearly omnidirectional flows, which would regulate them to Newtonian gravitation. However, a free, stable, and lonely particle can also have imperfect omnidirectional flows, which will result in a preferred orientation, to minimize gravitational force.

The gravitation is created by the strings. The strings interact with the gravitation. Therefore, the gravitation in the microscopic world depends on quantum mechanical geometric shapes of the strings. This proposed theory is an entirely alternate theory of quantum gravity. However, this may provide a clue for quantum gravity [25, 26], supergravity [27, 28], and loop quantum gravity [29, 30, 31].

Quantum gravity describes gravity according to quantum mechanics. Supergravity assumes the graviton has a superpartner. Quantum gravity and supergravity postulate that the graviton is a messenger particle of gravity. In these theories, the photon and the gluon as force carriers for the electromagnetic interaction and the strong interaction are massless. According to the proposed theory, without the postulate of graviton, we can explain the gravitation is created by all kinds of particles and some particles act like being massless.

Loop quantum gravity (LQG) is a theory that merges quantum mechanics and general relativity. LQG postulates that the structure of space is composed of loops woven into an extremely fine network with a scale on the order of a Planck length. Particles consist of certain patterns of braiding of open and closed strings [13], which can be modeled as the loop network. According to the proposed theory, the source of gravitation is the strings, so the gravitation can be modeled with quantum loops of open and closed strings.

The Compton Scattering experiment shows that photons have momentum [32]. The several studies proposed and measured that the photon consists of a positive charge and a negative charge [33, 34]. The photon is made out of the electromagnetic wave. This means that the electromagnetic wave can create momentum and charges. In addition, it can create gravitation and respond to gravitation.

6 Summary

This paper includes a complete derivation of the equation of Newtonian gravitation from gravitational time dilation using the refraction principle. All particles participate in creating gravitation and respond to gravitation.

The gravitational acceleration depends on the incident angle, which explains why Newtonian gravitation is not regulated at the level of particles. However, a set of multiple restrained particles will result in nearly omnidirectional flows and can be regulated to Newtonian gravitation.

Gravitation is caused by not only curved space but also curved time. Composite bodies have less gravitational acceleration than a photon with an incident angle of $\pi/2$ by 2/3.

The gravitational time dilation is an inverse exponential function, whose exponent is proportional to the mass and the inverse of separation from the gravitational source. This is different than the Schwarzschild metric, but it has a form similar to that in a sluggish spacetime because the general relativity mistakenly uses a part of classical physics (potential energy) which is suitable for a flat spacetime.

Conflict of Interest   The author declares no conflict of interest.

References

[1] J. B. Hartle, Gravity: An introduction to Einstein's general relativity, American Association of Physics Teachers, 2003, doi:10.1119/1.1604390.

[2] C. M. Will, Theory and experiment in gravitational physics, Cambridge university press, 2018.

[3] R. V. Pound, G. A. Rebka Jr, "Gravitational red-shift in nuclear resonance," Physical Review Letters, **3**(9), 439, 1959, doi:10.1103/PhysRevLett.3.439.

[4] R. V. Pound, J. L. Snider, "Effect of gravity on gamma radiation," Physical Review, **140**(3B), B788, 1965, doi:10.1103/PhysRev.140.B788.

[5] C. Brans, R. H. Dicke, "Mach's principle and a relativistic theory of gravitation," Physical review, **124**(3), 925, 1961, doi:10.1103/PhysRev.124.925.

[6] M. Gasperini, "Singularity prevention and broken Lorentz symmetry," Classical and Quantum Gravity, **4**(2), 485, 1987, doi:10.1088/0264-9381/4/2/026.

[7] J. D. Bekenstein, "Relativistic gravitation theory for the modified Newtonian dynamics paradigm," Physical Review D, **70**(8), 083509, 2004, doi: 10.1103/PhysRevD.70.083509.

[8] K. Nordtvedt Jr, "Equivalence principle for massive bodies. I. Phenomenology," Physical Review, **169**(5), 1014, 1968, doi:10.1103/PhysRev.169.1014.

[9] C. M. Will, K. Nordtvedt Jr, "Conservation laws and preferred frames in relativistic gravity. I. Preferred-frame theories and an extended PPN formalism," The Astrophysical Journal, **177**, 757, 1972.

[10] M. Pawłowski, R. Raczka, "A unified conformal model for fundamental interactions without dynamical Higgs field," Foundations of Physics, **24**(9), 1305–1327, 1994, doi:10.1007/BF02148570.

[11] C. Csaki, C. Grojean, L. Pilo, J. Terning, "Towards a realistic model of Higgsless electroweak symmetry breaking," Physical review letters, **92**(10), 101802, 2004, doi:10.1103/PhysRevLett.92.101802.

[12] C. Csaki, C. Grojean, H. Murayama, L. Pilo, J. Terning, "Gauge theories on an interval: Unitarity without a Higgs boson," Physical Review D, **69**(5), 055006, 2004, doi:10.1103/PhysRevD.69.055006.

[13] S. O. Bilson-Thompson, F. Markopoulou, L. Smolin, "Quantum gravity and the standard model," Classical and Quantum Gravity, **24**(16), 3975, 2007, doi:10.1088/0264-9381/24/16/002.

[14] X. Calmeta, N. Deshpandeb, X. Hec, S. Hsub, "Invisible Higgs boson, continuous mass fields and unHiggs mechanism," arXiv preprint arXiv:0810.2155, 2008, doi:10.1103/PhysRevD.79.055021.

[15] M. Carena, H. E. Haber, "Higgs boson theory and phenomenology," Progress in Particle and Nuclear Physics, **50**(1), 63–152, 2003, doi:10.1016/S0146-6410(02)00177-1.

[16] M. Born, E. Wolf, Principles of optics: electromagnetic theory of propagation, interference and diffraction of light, Elsevier, 2013.

[17] R. Gupta, A. Pradhan, S. Gupta, "Refraction-Based Alternative Explanation for: Bending of Light Near a Star, Gravitational Red/Blue Shift and Black-Hole," arXiv preprint arXiv:1004.1467, 2010.

[18] X.-H. Ye, Q. Lin, "Gravitational lensing analysed by the graded refractive index of a vacuum," Journal of Optics A: Pure and Applied Optics, **10**(7), 075001, 2008, doi:10.1088/1464-4258/10/7/075001.

[19] P. S. Wesson, Five-dimensional physics: classical and quantum consequences of Kaluza-Klein cosmology, World Scientific, 2006.

[20] T. Yarman, A. Kholmetskii, M. Arik, "Bending of light caused by gravitation: the same result via totally different philosophies," arXiv preprint arXiv:1401.3110, 2014.

[21] E. Goldoni, L. Stefanini, "A century of light-bending measurements: bringing solar eclipses into the classroom," Physics Education, **55**(4), 045009, 2020, doi:10.1088/1361-6552/ab8778.

[22] D. G. Bruns, "Gravitational starlight deflection measurements during the 21 August 2017 total solar eclipse," Classical and Quantum Gravity, **35**(7), 075009, 2018, doi:10.1088/1361-6382/aaaf2a.

[23] K. C. Fox, "NASA's STEREO Maps Much Larger Solar Atmosphere Than Previously Observed," https://www.nasa.gov/content/goddard/nasas-stereo-maps-much-larger-solar-atmosphere-than- previously-observed/, June 25, 2014.

[24] M. Aker, K. Altenmüller, M. Arenz, M. Babutzka, J. Barrett, S. Bauer, M. Beck, A. Beglarian, J. Behrens, T. Bergmann, et al., "Improved upper limit on the neutrino mass from a direct kinematic method by KATRIN," Physical review letters, **123**(22), 221802, 2019, doi:10.1103/PhysRevLett.123.221802.

[25] P. K. Townsend, "Four lectures on M-theory," arXiv preprint hep-th/9612121, 1996.

[26] M. J. Duff, "M theory (The Theory formerly known as strings)," International Journal of Modern Physics A, **11**(32), 5623–5641, 1996, doi:10.1142/S0217751X96002583.

[27] C. V. Johnson, "Jackiw-Teitelboim supergravity, minimal strings, and matrix models," Physical Review D, **103**(4), 046012, 2021, doi:10.1103/PhysRevD.103.046012.

[28] D. Stanford, E. Witten, "JT gravity and the ensembles of random matrix theory," arXiv preprint arXiv:1907.03363, 2019.

[29] P. A. M. Casares, "A review on Loop Quantum Gravity," arXiv preprint arXiv:1808.01252, 2018.

[30] T. Thiemann, "Loop quantum gravity: an inside view," in Approaches to fundamental physics, 185–263, Springer, 2007, doi:10.1007/978-3-540-71117-9_10.

[31] C. Rovelli, "Loop Quantum Gravity Living Reviews in relativity http://www.livingreviews.org/Articles," Volume1/1998-1rovelli, 1998.

[32] A. H. Compton, "A quantum theory of the scattering of X-rays by light elements," Physical review, **21**(5), 483, 1923, doi:10.1103/PhysRev.21.483.

[33] A. Hankins, C. Rackson, W. Kim, "Photon charge experiment," American Journal of Physics, **81**(6), 436–441, 2013, doi:10.1119/1.4793593.

[34] H. W. Giertz, "The photon consists of a positive and a negative charge, measuring gravity waves reveals the nature of photons," 2013.

A Novel Approach for Estimating the Service Lifetime of Transformers within Distributed Solar Photovoltaic (DSPV) Systems

Bonginkosi Allen Thango*, Jacobus Andries Jordaan, Agha Francis Nnachi

Department of Electrical Engineering, Tshwane University of Technology, Emalahleni, 1034, South Africa

ABSTRACT

The rapid transformation of the energy sector in South Africa towards renewable energy (RE) production calls for the management of assets to keep pace with the ongoing developments in a reliable manner. Aging assets, increasing energy needs and reliable supply of energy without load shedding are some of the challenges utilities are facing in South Africa. In resolving these challenge, imaginative solutions are required to maintain the installed assets and determining the viability of refurbishment, replacement or upgrading. In the current work, an extension of the author's previous work, a novel approach for estimating the service lifetime of transformers within Distributed Solar Photovoltaic (DSPV) Systems in South Africa is introduced. This experiential form has been derived by extensive experimental trials. The proposed approach is initially employed to evaluate the Degree of polymerization (DP) of cellulose insulation based on measured furan (2FAL) contents of 9 case scenarios. The calculated DP is then used to evaluate the service lifetime of these units. In efforts to authenticate the proposed approach, a comparative study is conducted against 5 other models. Finally, the proposed approach is compared with the results of the measured DP. It is observed that the proposed approach produce accurate estimates with an approximation not exceeding 1% and 2.2% from the measured DP and service lifetime respectively.

1. Introduction

Oil-immersed Distributed Solar Photovoltaic (DSPV) system transformers are commonly designed for a service lifetime of about 30 years [1], [2]. During service, the cellulose insulation degrades under the interactive effects emanating from electrical, thermal and chemical components. The mechanism of degradation of cellulose insulation (DCI) is reliant on the conditions such as harmonics, distorted load cycle and excessive heating that the transformer may be subjected to during their designed service lifetime. There are four underlying factors that elevate the DCI viz. moisture, oxygen, acid and excessive temperature. The oil-cellulose insulation system in DSPV transformers is prevalent on account of its cost-effectiveness and capacity to withstand severe electrical and thermal stresses [3], [4]. Due to the costly exercise of replacing field transformers, the utility owners will keep the units in service while performing periodical online monitoring and routine testing of the insulation system. Therefore, diagnostic techniques suchlike Dissolved Gas Analysis (DGA) and Furan Analysis (FA) are increasingly being recognized as efficacious and irrefutable procedures to evaluate the reliability of oil-cellulose insulation system.

The chemical structure of cellulose insulation is composed of strings of anhydroglucoses linked via glycosidic bonds [5] – [7]. These bonds have relatively low temperature resistance in relation to hydrocarbon bonds prevailing in DSPV transformer oil [8]. This degradation phenomenon triggers depolymerisation which leads to degraded forms of glucose as shown in Figure 1 [9]. The formation of glucose will further degrade to forge furans, water and combustible gases [9 – 11].
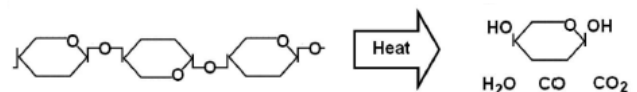
Figure 1: Thermal degradation of cellulose insulation

The generation of Furan compounds (FCs) is distinctly on the cellulose insulation and seemed to be kind of stable at elevated

temperatures reaching 140°C within the transformer oil [12]. The existence of FCs remains in oil-immersed transformers even at elevated temperatures geared towards providing a divulgence to the condition of the cellulose insulation.

The FCs 2-FAL, 5-hydroxymethyl-2-furaldehyde, 2-acetylfuran, 5-methyl-2-furaldehyde, and 2-furfurolare are the most widely known in the transformer manufacturing industry. The FC 2-FAL is most widely-used in the industry relating its content to the cellulose degree of polymerization (DP) which is the number of monomeric units in the cellulose polymer [13] – [14]. Furans are a constituent of the products of degradation of the transformer cellulose insulation. During service, they are moderately dissolvable in the transformer oil. The relationship between the transformer state and the concentration of the furan content in the oil is as shown in Table below.

Table 1: 2FAL concentration criterion

Status	Concentration [in ppm]
Healthy	2FAL < 0.5
Satisfactory	$0.5 \leq 2FAL \leq 1$
Warning	$1.1 \leq 2FAL \leq 1.5$
Poor	$1.6 \leq 2FAL \leq 2$
Extremely poor	$2FAL \geq 2.1$

In the current work, an extension of the author's previous work [14], a novel approach for estimating the service lifetime of transformers within DSPV Systems in South Africa is introduced. This experiential form has been derived by extensive experimental trials. The proposed approach is initially employed to evaluate the DP of cellulose insulation based on measured 2FAL contents on a fleet of selected case scenarios. The calculated DP is then used to evaluate the service lifetime of these units. In efforts to authenticate the proposed approach, a comparative study is conducted against 5 other models. Finally, the proposed approach is compared with the results of the measured DP. It is observed that the proposed approach produce accurate estimates with an approximation not exceeding 1% and 2.2% from the measured DP and service lifetime respectively.

2. DP Models

In this day and age, the aging condition of transformers can be established by mathematical modelling which launch the relationship between furan concentrations, DP, and transformer service lifetime.

2.1. Existing DP models

Several authors in [15] - [19] have established mathematical formulae which relate the furan concentrations and the measure of the DP of the insulation material. An illustration of this relationship based upon this methods is presented in Figure 2. A Further in [20], mathematical formulae has been developed to describe the relationship between DP and the service lifetime. In order to attain a thread that binds the furan concentrations and the DP of the cellulose insulation (CI), the DP methods are compared at different furan contents. The comparison indicate that the methods can evaluate the DP ranging from 1 to 14.
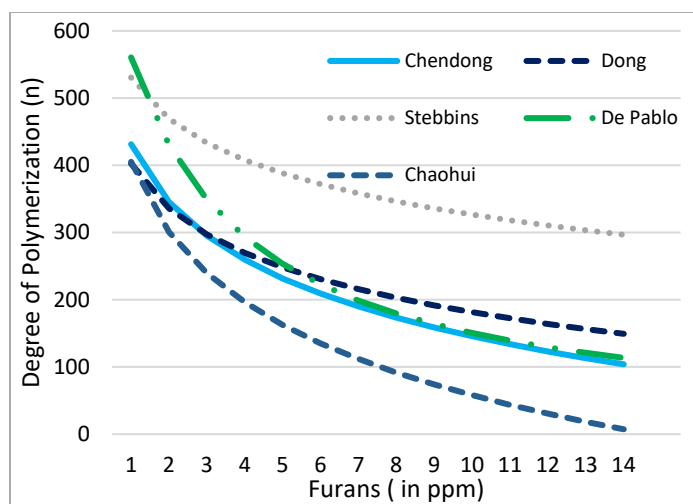
Figure 2: Correlation between the DP and Furans (2FAL)

The development, identification and behaviour of furan compounds has been described by [21], [22] and [23]. In the next sub-section a comprehensive description of the model proposed in this work is presented.

2.2. Proposed model

Based upon observational data, a fleet of mineral oil samples were analysed to develop a novel DP model for transformers serving exclusively in distributed solar photovoltaic systems. The proposed model can be applied to ascertain the DP of cellulose insulation with accuracy following 2-FAL measurement in the oil. The proposed model is as shown in Eq. (1) below.

$$DP = 763.67 - 584.23x + 398x^2 - 135.52x^3 + 17.14x^4 \quad (1)$$

Here,

$x -$ 2-FAL

The concentration (in ppm) of the furan content 2-FAL can be easily substituted in the formulae to obtain the DP of a transformer.

2.3. Transformer Service Lifetime

The transformer age can be obtained by applying Eq. (2) and Eq. (3) below [20]. With the knowledge of the DP of the transformer, the service lifetime can be ascertained.

$$Service\ lifetime (in\ years) = 20.5\ ln\left(\frac{1100}{DP}\right) \quad (2)$$

$$\%Life\ used = \frac{log_{10}(DP) - 2.903}{-0.006021} \quad (3)$$

3. Case Scenario

In this section, the 2FAL results of 9 mineral-oil immersed DSPV transformers are considered. The gas concentrations are obtained from oil samples collected from various DSPV facilities. The studied transformers range from 100kVA to 20 000 kVA as shown in Table 2.

Table 2: Case Studies

Case	Rating (kVA)	Voltage (kV)	2FAL
A	1500	6.6/0.5	1.778
B	1500	6.6/0.5	2.377
C	100	0.525/0.4	3.00
D	150	0.525/0.4	1.601
E	20 000	6.6/0.5	0.676
F	20 000	6.6/0.5	0.231
G	20 000	88/6.6	0.143
H	4000	6.6/0.5	1.513
I	2000	6.6/0.5	1.563

The 2-FAL contents were measured during the routine maintenance of the transformers.

3.1. Degree of Polymerization

In order to determine the accuracy of the formulae presented by the authors in [15] – [19] and the proposed formula in the current work, the DP for the studied cases are evaluated and tabulated as a shown in Table 3 below. Stebbins [18] results are observed to yield a significantly protruding DP values compared to all the other methods.

Table 3: DP of studied transformers using furan compounds (2FAL)

Case	2FAL	Chendong [15]	De Pablo [16]	Dong [17]	Stebbins [18]	Chaohui [19]	Proposed
A	1,778	360	454	347	480	318	393
B	2,377	324	396	319	454	275	351
C	3	295	349	297	433	240	322
D	1,601	373	474	357	489	334	405
E	0,676	480	622	440	565	464	512
F	0,231	613	731	543	660	626	648
G	0,143	673	757	589	703	699	688
H	1,513	380	485	363	494	343	411
I	1,563	376	479	360	491	338	408

These DP values are a measure of the realistic aging of the cellulose insulation, which governs the transformer's service lifetime. And so, it is possible to evaluate the service lifetime of a transformer and make comparison with real life by means of furan concentration within the oil. The latter improves the assessment of the reliability of service transformers.

3.2. Transformer Service Lifetime

Further to previous sub-section, the remaining service lifetime of the studied cases is determined using the DP results as presented in Table 4 for all models.

Table 4: Remaining service lifetime estimation

Case	2FAL	Chendong [15]	De Pablo [16]	Dong [17]	Stebbins [18]	Chaohui [19]	Proposed
A	1,778	22,90	18,16	23,64	17,02	25,41	21,12
B	2,377	25,06	20,97	25,35	18,15	28,44	23,43

Case	2FAL	Chendong [15]	De Pablo [16]	Dong [17]	Stebbins [18]	Chaohui [19]	Proposed
C	3	26,97	23,53	26,84	19,10	31,25	25,18
D	1,601	22,17	17,25	23,05	16,62	24,42	20,49
E	0,676	17,00	11,70	18,78	13,65	17,68	15,66
F	0,231	11,98	8,38	14,47	10,46	11,55	10,84
G	0,143	10,08	7,65	12,80	9,18	9,31	9,62
H	1,513	21,79	16,78	22,74	16,41	23,90	20,17
I	1,563	22,01	17,05	22,92	16,53	24,20	20,35

The relationship between the DP and the service lifetime is illustrated by Figure 3 below.
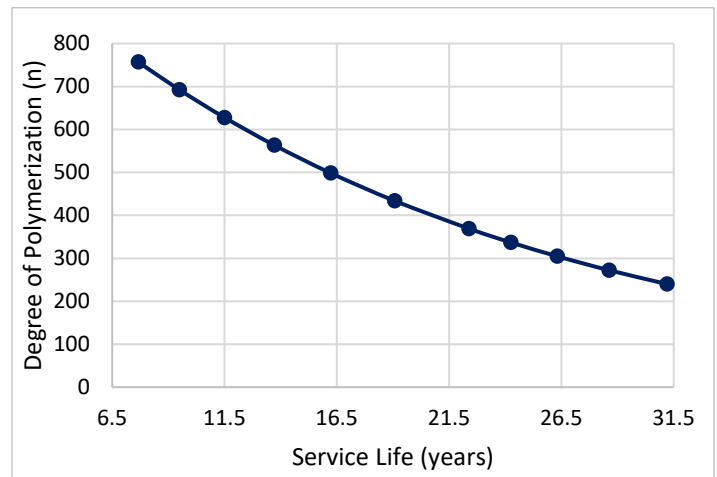
Figure 3: Correlation between the DCI and Furans (2FAL)
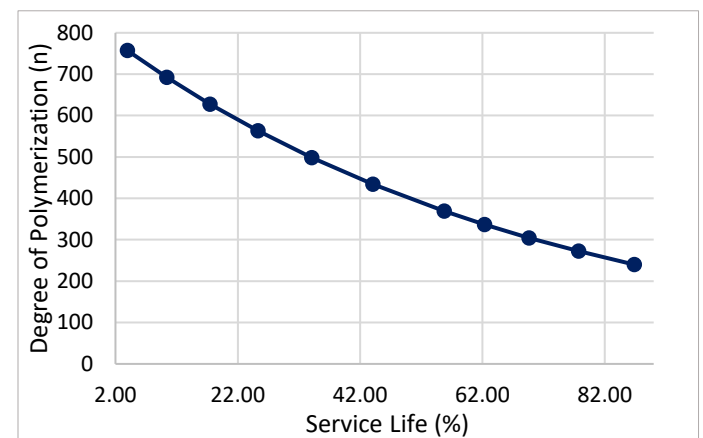
Figure 4: Correlation between the DP and %Service lifetime

It can be observed that as the transformer life is service is longer, the DP decreases. In Table 5, the percentage of the service lifetime for all cases is presented.

Table 5: Percentage of transformer service lifetime

Case	2FAL	Chendong [15]	De Pablo [16]	Dong [17]	Stebbins [18]	Chaohui [19]	Proposed
A	1,778	57,58	40,90	60,18	36,89	66,42	51,32
B	2,377	65,18	50,79	66,21	40,87	77,09	59,46
C	3	71,92	59,81	71,44	44,22	86,95	65,61

Case	2FAL	Chend ong [15]	De Pablo [16]	Dong [17]	Stebb ins [18]	Chao hui [19]	Prop osed
D	1,601	55,02	37,70	58,12	35,51	62,93	49,10
E	0,676	36,83	18,18	43,10	25,03	39,23	32,13
F	0,231	19,16	6,50	27,93	13,81	17,65	15,15
G	0,143	12,48	3,94	22,07	9,31	9,77	10,88
H	1,513	53,67	36,06	57,03	34,77	61,11	47,98
I	1,563	54,44	37,00	57,66	35,19	62,15	48,62

The percentage of service lifetime is observed to correlate with the data presented in Table 4. The correlation between the DP and the percentage service lifetime is illustrated by Figure 4.

It is observed that the DP decreases with respect to the aging of the transformer.

3.3. Practical Results

In this subsection, the values of the measured DP and 2FAL of the nine studied transformers that operate in various DSPV systems are presented in Table 6.

Table 6: Percentage of service lifetime

Case	2FAL	Measured DP	Service Life	% Service Lifetime
A	1,778	389	21,30	51,96
B	2,377	352	23,35	59,16
C	3	322	25,20	65,67
D	1,601	404	20,56	49,35
E	0,676	515	15,57	31,78
F	0,231	641	11,08	15,99
G	0,143	694	9,46	10,29
H	1,513	412	20,15	47,92
I	1,563	411	20,20	48,10

3.4. Results comparison

The error of estimation for DP, service lifetime and percentage service lifetime against the measured results are presented in this subsection for the studied DSPV transformers. In Table 7, it can be observed that the proposed formula gives an accurate estimation of the DP in comparison to the other models across all nine cases.

Table 7: Error of estimation: DP

Case	Chend ong [15]	De Pablo [16]	Dong [17]	Stebbi ns [18]	Chaohui [19]	Propos ed
A	7,5%	16,6%	10,8%	23,2%	18,2%	0,88%
B	8,0%	12,3%	9,3%	28,9%	22,0%	0,42%
C	8,3%	8,5%	7,7%	34,6%	25,5%	0,09%
D	7,6%	17,5%	11,4%	21,2%	17,2%	0,36%
E	6,8%	20,8%	14,5%	9,8%	9,8%	0,48%
F	4,3%	14,1%	15,3%	3,1%	2,3%	1,17%
G	3,0%	9,2%	15,1%	1,4%	0,7%	0,81%
H	7,7%	17,9%	11,9%	20,0%	16,7%	0,09%
I	8,4%	16,6%	12,4%	19,6%	17,7%	0,72%

It is observed that the proposed formula produces accurate estimates with an approximation not exceeding 1% from the

measured DP. As a result, it is evident that the proposed formula achieves a higher accuracy. In Table 8, the error of estimation of the calculated and measured results of the service lifetime is presented.

Table 8: Error of estimation: Service Life

Case	Chendo ng [15]	De Pablo [16]	Dong [17]	Stebbin s [18]	Chaoh ui [19]	Propos ed
A	7,5%	14,7%	11,0%	20,1%	19,3%	0,85%
B	7,3%	10,2%	8,6%	22,3%	21,8%	0,37%
C	7,0%	6,6%	6,5%	24,2%	24,0%	0,07%
D	7,8%	16,1%	12,1%	19,1%	18,8%	0,35%
E	9,2%	24,8%	20,7%	12,3%	13,6%	0,64%
F	8,1%	24,4%	30,6%	5,6%	4,3%	2,16%
G	6,6%	19,1%	35,4%	2,9%	1,6%	1,77%
H	8,1%	16,7%	12,9%	18,5%	18,6%	0,09%
I	8,9%	15,6%	13,5%	18,2%	19,8%	0,74%

It is observed that the proposed formula produce accurate estimates with an approximation not exceeding 2.2% from the measured service lifetime.

Table 9: Error of estimation: % of transformer service life

Case	Chendo ng [15]	De Pablo [16]	Dong [17]	Stebbin s [18]	Chaoh ui [19]	Propos ed
A	10,8%	21,3%	15,8%	29,0%	27,8%	1,22%
B	10,2%	14,2%	11,9%	30,9%	30,3%	0,51%
C	9,5%	8,9%	8,8%	32,7%	32,4%	0,10%
D	11,5%	23,6%	17,8%	28,1%	27,5%	0,52%
E	15,9%	42,8%	35,6%	21,2%	23,4%	1,10%
F	19,8%	59,4%	74,7%	13,7%	10,4%	5,27%
G	21,3%	61,7%	114,5%	9,5%	5,1%	5,71%
H	12,0%	24,8%	19,0%	27,4%	27,5%	0,13%
I	13,2%	23,1%	19,9%	26,8%	29,2%	1,09%

It is observed that the proposed formula produce accurate estimates with an approximation not exceeding 5.8% from the measured percentage service lifetime.

At large, the overall assessment of the proposed formula presented in this work presented the highest precision in the estimation of the DP of the cellulose insulation in comparison to the other 5 models.

4. Conclusion

The knowledge of the transformer service lifetime and the specific point in time that is suitable to replace transformers is critical for utility owners. These determinations are dependent upon the condition of the cellulose and liquid insulation. In practical terms, knowledge on the condition of insulation is crucial to undertake adequate life cycle and reliability management of transformers in the facility. In the transformer industry, the physical chemistry of oil is prevalent in the evaluation of the transformer life cycle considering that oil samples can easily be extracted at site to the laboratory for analysis.

In the current work, an extension of the author's previous work [14], a novel approach for estimating the service lifetime of transformers within DSPV Systems in South Africa was introduced. This experiential form has been derived by extensive experimental trials. The proposed approach was initially employed to evaluate the DP of cellulose insulation based on measured 2-FAL contents (in ppm) of 9 case scenarios. The calculated DP was then used to evaluate the service lifetime of these units. In efforts to authenticate the proposed approach, a comparative study was conducted against 5 other models. Finally, the proposed approach was compared with the results of the measured DP. It was observed that the proposed approach produce accurate estimates with an approximation not exceeding 1% and 2.2% from the measured DP and service lifetime respectively.

In future work, the authors will test the proposed formula with other different transformers. Further, the authors will carry out work related to the reliability analysis of DPSV transformers based upon their operating hours in service by apply the Weibull distribution technique and support vector machine to classify their reliability.

Conflict of Interest

The authors declare no conflict of interest.

References

[1] P. Mann, "Determination of transformer life expectancy," in Electrical Engineering, **82** (8), 512-514, 1963, doi: 10.1109/EE.1963.6540988.

[2] D. Martin, Y. Cui, T. Saha, N. Lelekakis and J. Wijaya, "Life estimation techniques for transformer insulation," 2013 Australasian Universities Power Engineering Conference (AUPEC), Hobart, TAS, 1-6, 2013, doi: 10.1109/AUPEC.2013.6725457.

[3] T. A. Prevost and T. V. Oommen, "Cellulose insulation in oil-filled power transformers: Part I - history and development," in IEEE Electrical Insulation Magazine, **22** (1), 28-35, 2006, doi: 10.1109/MEI.2006.1618969.

[4] B. A. Thango, J. A. Jordaan and A. F. nnachi, "Stray Gassing of Transformer Oil in Distributed Solar Photovoltaic (DSPV) Systems," 2020 6th IEEE International Energy Conference (ENERGYCon), Gammarth, Tunis, Tunisia, 484-488, 2020, doi: 10.1109/ENERGYCon48941.2020.9236522.

[5] L. Cheim, D. Platts, T. Prevost and S. Xu, "Furan analysis for liquid power transformers," in IEEE Electrical Insulation Magazine, **28** (2), no. 2, 8-21, 2012, doi: 10.1109/MEI.2012.6159177.

[6] J. R. Sans, K. M. Bilgin and J. J. Kelly, "Large-scale survey of furanic compounds in operating transformers and implications for estimating service life," Conference Record of the 1998 IEEE International Symposium on Electrical Insulation (Cat. No.98CH36239), Arlington, VA, USA, **2**, 543-553, 1998 doi: 10.1109/ELINSL.1998.694852.

[7] M. T. Imani, K. Homeier, P. Werle and G. Dräger, "How Far are Furan Compounds Reliable Indicators for Thermal Aging of Oil Impregnated Cellulose Insulation?," 2018 IEEE Conference on Electrical Insulation and Dielectric Phenomena (CEIDP), Cancun, 438-441, 2018 doi: 10.1109/CEIDP.2018.8544859.

[8] C. Zhang and J. M. K. Macalpine, "Furfural Concentration in Transformer Oil as an Indicator of Paper Ageing, Part 1: A Review," 2006 IEEE PES Power Systems Conference and Exposition, Atlanta, GA, 1088-1091, 2006, doi: 10.1109/PSCE.2006.296461.

[9] G. Xia and G. Wu, "Study on the impact of initial moisture contents on ageing characteristics of transformer oil-paper insulation," 2016 IEEE International Conference on High Voltage Engineering and Application (ICHVE), Chengdu, 1-4, 2016, doi: 10.1109/ICHVE.2016.7800632.

[10] D. Suksawat, K. Atthaphotpong, K. Takboontam, K. Satirapattanakiat, C. Raphephat and N. Pattanadech, "Furan Analysis of Oil Impregnated Paper Aged by Chemical Stress," 2020 8th International Conference on Condition Monitoring and Diagnosis (CMD), Phuket, 422-425, 2020, doi: 10.1109/CMD48350.2020.9287264.

[11] A. Akshatha, R. Kumar A, S. Rajan J and H. Ramachandra, "Studies on chemical and dielectric phenomena in paper - oil insulation due to sulphur compounds in mineral oil," 2014 IEEE Electrical Insulation Conference (EIC), Philadelphia, PA, 281-285, 2014, doi: 10.1109/EIC.2014.6869392.

[12] "IEEE Guide for Evaluation and Reconditioning of Liquid Immersed Power Transformers," in IEEE Std C57.140-2017 (Revision of IEEE Std. C57.140-2006), 1-88, 2017, doi: 10.1109/IEEESTD.2017.8106924.

[13] "IEEE Standard Test Procedure for Thermal Evaluation of Insulation Systems for Liquid-Immersed Distribution and Power Transformers," in IEEE Std C57.100-2011 (Revision of IEEE Std C57.100-1999) , 1-37, 2012, doi: 10.1109/IEEESTD.2012.6143968.

[14] B. A. Thango, J. A. Jordaan and A. F. Nnachi, "Service Life Estimation of Photovoltaic Plant Transformers Under Non-Linear Loads," 2020 IEEE PES/IAS PowerAfrica, Nairobi, Kenya, 1-5, 2020, doi: 10.1109/PowerAfrica49420.2020.9219912.

[15] X. Chendong, Monitoring Paper Insulation Ageing by measuring Furfural Contents in Oil, 7th International Symposium on High Voltage Engineering, 26 - 30, 1991.

[16] A. De Pablo, Interpretation of Furanic Compounds Analysis - Degradation Models, CIGRE WG D1.01.03, former WG 15-01, Task Force 03, 1997.

[17] M. Dong, Z. Yan and G. J. Zhang, "Comprehensive diagnostic and aging assessment method of solid insulation in transformer," 2003 Annual Report Conference on Electrical Insulation and Dielectric Phenomena, Albuquerque, NM, USA, 137-140, 2003, doi: 10.1109/CEIDP.2003.1254813.

[18] R. D. Stebbins, D. S. Myers and A. B. Shkolnik, "Furanic compounds in dielectric liquid samples: review and update of diagnostic interpretation and estimation of insulation ageing," Proceedings of the 7th International Conference on Properties and Applications of Dielectric Materials (Cat. No.03CH37417), Nagoya, Japan, **3**, 921-926, 2003, doi: 10.1109/ICPADM.2003.1218572.

[19] C. Lin et al., "The Aging Diagnosis of Solid Insulation for Oil-Immersed Power Transformers and Its Remaining Life Prediction", 2010 Asia-Pacific Power and Energy Engineering Conference, DOI:10.1109/APPEEC.2010.5449486.

[20] M. K. Pradhan and T. S. Ramu, "On the estimation of elapsed life of oil-immersed power transformers," in IEEE Transactions on Power Delivery, **20** (3), 1962-1969, 2005, doi: 10.1109/TPWRD.2005.848663.

[21] WG. D1.01, "Furanic Compounds for diagnosis", cigré, Electra, 4, 2012, doi: ELT_261_06-furanic-compounds-for-diagnosis.

[22] R. A. Abd El-Aal, K. Helal, A. M. M. Hassan and S. S. Dessouky, "Prediction of Transformers Conditions and Lifetime Using Furan Compounds Analysis," in IEEE Access, **7**, 102264-102273, 2019, doi: 10.1109/ACCESS.2019.2931422.

[23] H. Shertukde, Distributed Photovoltaic (DPV)-Grid Transformer Applications, CRC Press, 2017, doi: Distributed-Photovoltaic-Grid-Transformers/Shertukde/p/book/9781138073845.

Peculiar Stray Gassing Occurrences in Solar Photovoltaic Transformers during Service

Bonginkosi Thango[*], Jacobus Jordaan, Agha Nnachi

Deptartment of Electrical Engineering, Tshwane University of Technology, Emalahleni, 1034, South Africa

A R T I C L E   I N F O

A B S T R A C T

Distributed Solar Photovoltaic (DSP) Plants are one of the fastest growing renewable energy systems in South Africa. The primary components forming an integral part of the point of common coupling (PCC) are, the inverter used to convert dc voltage to ac voltage and step-up transformers which step-up low voltage input to the desired output level. However, DSP plant step-up transformers are considered to be one of the most sensitive equipment on the plant. These transformers are challenged with various electrical problems including abnormal levels of harmonics. The presence of harmonics in these transformers results in higher service losses thereby raising the hotspot (HS) temperature, in which, consequently introduce the stray gassing phenomena of the insulating oils. This calls for understanding of the nature of the problem and possible remediation to ensure enhanced power quality. Present work, an extension of previous work, investigate a reported case of peculiar stray gassing of transformer insulation oils during service. Initially, the harmonic spectrum of the DSP plant is presented and the related service losses at fundamental and under harmonic conditions are computed. Furthermore, the thermal performance of the transformer under these conditions is investigated. Lastly, the Dissolved Gas Analysis (DGA) results of the oil samples are presented. Novelty, findings of this work indicate that the generation of hydrogen arising from stray gassing may stem from severely hydro-treated mineral oil, but is also strenuously affected by transformer thermal aging of polymers, choice of core steel grade, zinc tank walls and vanishes. The production surplus of methane and ethane are also witnessed in the first years of service and reaches substantial concentration levels. Potentially, these occurrences also arises from the thermal aging of polymers. The authors make some recommendations to utility owners to make a distinction of stray gassing from transformer fault by means of routine inspection aside from DGA value basis withal to the increase in gas diffusion rate. Further, the authors make some significant contribution by further recommending procedures that can be employed as remedies during the design phase and manufacturing processes. Lastly, the authors highlight the need to establish standards that will provide support for transformers intended to operate in DSP applications.

1. Introduction

In line with the objectives of solving South Africa's power generation constraints, the Government's Integrated Resource Plan enacted in 2010 (IRP2010) [1] revealed the determination to produce 17.8 GW generation capacity from renewable energy resources by the year 2030. The additional electrical energy fed by the Independent Power Producers (IPPs) into the national grid has provided sustainable and supplemental solution to the heavy load shedding suffered by many South Africans. Despite this unquestionable success, the substantial growth in the South African renewable energy market including DSP plants is associated with many technical challenges. One of the foremost challenges is the irregular penetration of high voltage and current harmonics on the step-up transformers connected to the PCC. This phenomenon is a result of the switching action caused by inverters, nonlinear loads and resonances generated when the DSP plant is connected to the medium voltage (MV) network.

As a result, the inclined operational cost of the DSP plant due to high energy cost per kilowatt is incurred by the increase of the harmonic no-load and load losses in the step-up transformer. During service, the no-load losses are steady losses and are independent of the loading of the transformer [2]-[7]. The

magnetizing current necessary to energize the transformer core generate the no-load losses. In harmonic rich environments, no-load losses are impelled by voltage harmonics which increase hysteresis and eddy current losses in the core laminations. The last-mentioned problem initiate core vibrations, core saturation and electrical stresses in the insulation materials. The current harmonics predominantly affect the load losses of the DSP plant transformer. The load losses are dependent on the transformer loading profile and are widespread upon the copper conductors which then affect the alternating current (AC) resistance of the windings and other metallic parts [2], [3]. As a result, the winding temperature is increased and spread into the tank walls, flitch plates, core clamps and other metallic components of the active part. The hottest spot on the winding, which is generally located in the area nearby the top of the DSP plant transformer, restricts the loading capacity of the transformer. Furthermore, it determines the insulation service life and the probable risk of emancipating gas bubbles during extreme loading conditions [8]-[10]. Over time, excessive HS temperature brings upon thermal aging and the degradation of the cellulose insulation which determines the end of transformer service life.

Authors in [11]-[13] expressed the view that emancipation of gas bubbles or stray gassing in the service lifetime of the transformer is dependent on the insulating oils. For several years, DGA has been regarded as the most crucial procedure for assessing health condition of oil-immersed transformers. Drawn up on the basis regular inspection and characteristics of dissolved gases mined from transformer oil samples, an evaluation can be made on the transformer internal anomalies and severity thereof. Many authors have investigated the insulating oils status based on the DGA [14], [15] and [16]. In the past ten years, with the rise in the deployment of DSP plants in South Africa, empirical experience has indicated that dissolved gases can also materialize at relatively lower temperature (90–200°C) in the absence of anomalies or transformer fault. It should be noted that this gassing should not be misconstrued with gassing patterns of insulating oils by means of Partial discharges (PD) or catalysed reactions for case in a point of core steel grade zinc tank wall surface and coating. The DGA-evaluation tools also take into account this thermal stray gassing occurrences to permit clearer distinction between permissible stray gassing and peculiar gassing on account of PD and generation of HS temperatures in various active part components [14]-[16].

This work, an extension of previous work [16] presents the results of stray gassing results that were carried out on a 2500kV, mineral-oil filled transformer. Particularly, solution oriented on the impact of harmonic currents on the service losses and thermal performance of the studied DSP the plant transformer. Moreover, the observed stray gassing occurrences of the unit as a result of (1) the generation of HS temperatures in the active part components; and (2) the core steel grade, zinc tank wall surface and coating. The authors make a significant contribution by further recommending procedures that can be employed as remedies during the design phase and manufacturing processes.

2. Case Scenario

In this section, a harmonic study is carried out on a 2500kVA, mineral-oil filled DSP plant transformer to evaluate the no-load losses and load losses. The detailed classification of these losses

are detailed by the authors in [17] and [18]. The advancement of computational power has enabled the development of tools capable of simulating complex geometries, mapping of electromagnetic fields and accurate evaluation of these transformer losses. A software tool embedding analytical methods with Finite Element Method (FEM) is used to estimate the transformer losses. The tool is automated to simulate complete transformer model geometries, magnetic field quantities and computation of eddy current losses in tank walls, flitch plate, core clamps, bus-bar's and windings. Figure 1 shows the complete model of the transformer 2-D geometry with the main parts that are susceptible to the leakage flux.
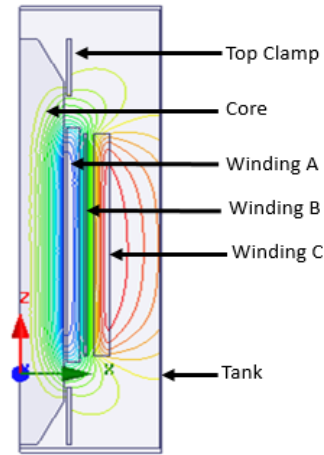
Figure 1: 2D geometry of the DSP plant transformer

2.1. Design based on the International Electrotechnical Commission (IEC) harmonic spectrum

The no-load losses and stray losses in windings and structural parts evaluated at nominal tap position are tabulated in Table 1. In order to compute these losses to account for the presence of harmonics it is necessary to obtain the values of the harmonic loss factors using the IEC 519-2014 [19] standard. Generally, from a manufactures perspective, the case of considering the harmonic spectrum proposed by this standard for a transformer intended to operate in a DSP plant is when there is no full harmonic spectrum supplied by the IPP. The harmonic spectrum recommended by IEC is shown in Figure 2.
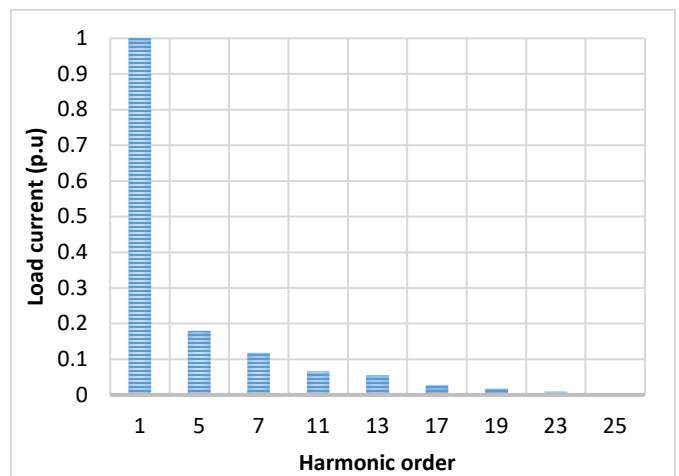
Figure 2: IEC 519-2014 Harmonic spectrum [2]

To estimate the service losses due to this harmonic spectrum, the transformer is initially designed at fundamental frequency to produce the rated losses as shown in Table 1. Thereafter, a harmonic loss factor is computed based on the supplied harmonic spectrum. The authors have presented a detailed computation of the harmonic loss factor in [17] and [18]. The Harmonic factor is in essence intended to predict the increase in the transformer losses under harmonics condition. The resultant service losses that will occur in transformer is as tabulated below.

Table 1: Tabulated loss computation under a harmonic spectrum

Type of loss	Rated losses (W)	Harmonic factor	Service losses (W)
No-load	0.180	1	0.180
I^2R	11.041	1.055	11.654
Winding Eddy	0.213	3.986	0.921
Other stray	1.194	1.252	1.495
Tank-HV side	0.249	1.252	0.312
Tank-LV side	0.494	1.252	0.619
Bus-Bar	0.013	1.252	0.129
Top yoke Clamp	0.029	1.252	0.036
Bottom yoke Clamp	0.046	1.252	0.058
Flitch plate	0.02	1.252	0.003

From both the fundamental and harmonic losses above, it can be noticed that the loss percentage error is higher for winding stray losses. Additionally, the core losses are observed to be constant, indicating that the no-load losses are independent of the harmonic currents. The minimum winding stray losses as a result of axial and radial leakage fields are computed by optimizing the selection of conductor dimensions while maintaining the permissible flux and current density of the winding [20] and [21]. The transformer winding subject to harmonic distortion is designed using continuously transposed cable epoxy (CTCE) with minimum axial and radial dimensions of each conductor to reduce the eddy losses [20] and [21]. The tank is designed using mild steel which hold a nonlinear permeability. The quantity of the magnetic field in the tank walls is evaluated by eliminating the impact of nonlinearity. Thereafter, the losses in the LV and HV tank walls are computed taking into account the effect of nonlinearity through repetitive estimation. The flitch plates are also mild steel type and contain slots at the upper and lower positions. While their loss quantity is low compared to winding eddies and tank losses under harmonic effects, the magnetic field quantity is high which results in the flitch plate being more susceptible to HS temperature.

2.2. Design based on the harmonic studies

The harmonic current level at the PCC is presented in Figure 3. The results are obtained by modelling the DSP plant in DigSILENT Power Factory as a single line diagram which is composed of the DSP plant passive components. The highest harmonic current order corresponds with the measured harmonic

data. Notably, this high harmonic order exceeds the recommended IEEE spectrum presented in the last section.
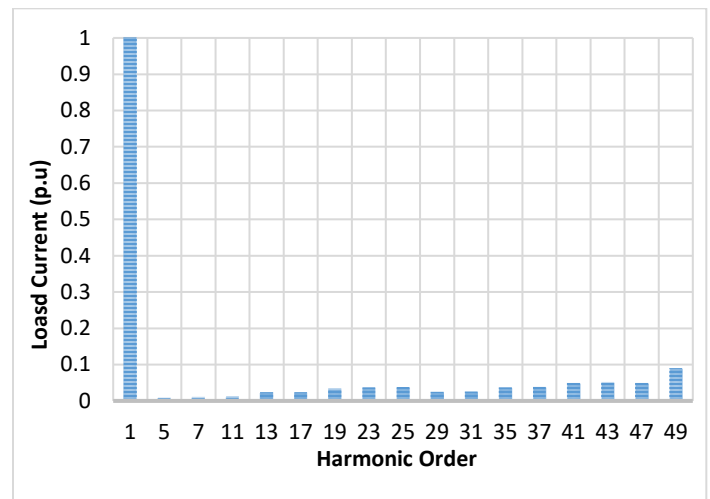
Figure 3: Simulated transformer harmonic spectrum at the PCC

The corresponding results when the design philosophy is tailored with the simulated harmonic spectrum are shown in Table 2. There are extreme differences in the percentage error between fundamental losses and the services losses. The transformer losses are observed to be even more extremely sensitive towards the simulated harmonic spectrum compared to the previous case. At large, these results outline the obligation for IPP's to conduct harmonic studies in order to provide technical information to manufactures which reflect the actual harmonic distortions that will be realised by the transformer and to design transformers suitable for such extreme conditions.

Table 2: Transformer losses based on actual DSP plant harmonic spectrum

Type of loss	Rated losses (W)	Harmonic factor	Service losses (W)
No-load	0.180	1	0.180
I^2R	11.041	1.055	11.654
Winding Eddy	0.213	3.986	0.921
Other stray	1.194	1.252	1.495
Tank-HV side	0.249	1.252	0.312
Tank-LV side	0.494	1.252	0.619
Bus-Bar	0.013	1.252	0.129
Top yoke Clamp	0.029	1.252	0.036
Bottom yoke Clamp	0.046	1.252	0.058
Flitch plate	0.02	1.252	0.003

To analyse the complete transformer harmonic response (THR), Figure 4 shows the results of the predicted transformer losses by IEC harmonic spectrum and compares them with the simulated harmonic spectrum the transformer is subjected to while in service. The transformer under inspection was designed without

the provision of a full harmonic study from the IPP, and judging from the results, the indication is that it was under-designed for the environment it was intended to operate, which would explain the reported high temperature rise and oil gassing patterns. Subsequently, this knowledge gap led to insufficient design of the winding conductor sizes and cooling system for this application.
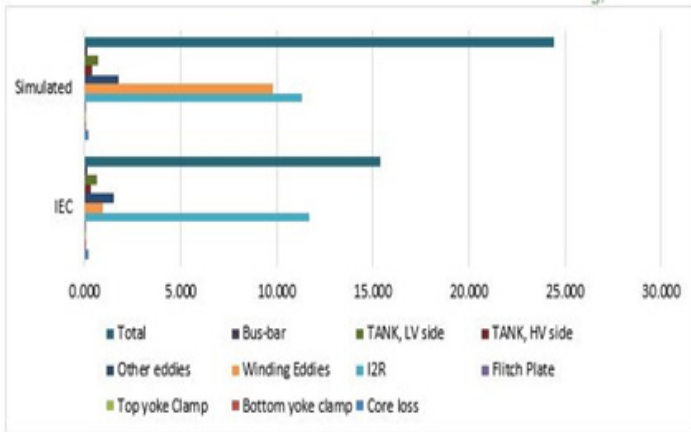
Figure 4: Loss comparison (IEC vs. Simulated Harmonic Spectrum)

In the next section, the temperature rise due to the increase in service losses is presented.

3. Thermal design

At tender stage, the transformer technical specifications supplied by IPP's to the manufacture generally include information about the permissible top oil, mean winding and HS temperatures. Electrical designers are then challenged to optimize transformer designs such that they adhere to the IEC 60076-2 [22] and IEEE C57.91-1995 [23] standards and to design the thermal and cooling requirements at an ambient temperature. During the manufacturing stage, as part of the Factory Acceptance Tests (FAT's) for newly manufactured transformers, the temperature rise test is conducted with the intent to demonstrate these temperatures, at full load and specified ambient temperature. The loading capability of the transformer is predominantly regulated by the HS temperature. In accordance with the IEC, the HS temperature is described as the mean winding temperature rise over the mean oil temperature multiply by a HS factor [22] and [23].
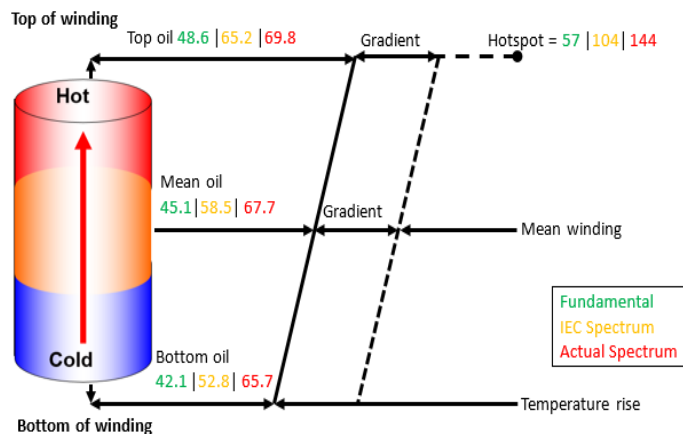
Figure 5: Simulated transformer harmonic spectrum at the PCC

A simplified thermal model of the transformer at fundamental frequency, IEC spectrum and simulated spectrum are shown in Figure 5. In this case, an IEC factor of 1.1 for DSP plant transformers is used in the calculation of the HS temperature. In Figure 5, the temperature rise within the windings is observed to increase linearly from the winding bottom to the top. A constant temperature difference between the oil duct and winding conductor along the winding is also observed. Moreover, the HS temperature is greater than the winding temperature rise as a result of the transformer losses.

The maximum error for the hot spot temperature between the fundamental values against the actual spectrum is 153%. That is 70% more than the HS temperature it was designed for under the IEC spectrum. This outcome clearly indicate that the transformer oil pumped through the winding conductors to execute the required cooling is not sufficient for transformer loading of actual harmonic spectrum. For the cooling system, the transformer oil viscosity and density vary with temperature rise, as such heat affects the fluid-flow sequence. Moreover, the quantity of the thermal fields resulting in such high HS temperature is derived from joule losses as a result of current flow in the windings and increased electromagnetic fields under harmonic conditions.

4. Stray gassing patterns

This section present findings of oil samples taken from the oil-filled hermetic DSP plant transformer under study for laboratory tests. The transformer was suspected to have oil gassing as indicated by the installed Oil Temperature Indicator (OTI). The results of Dissolved Gas Analysis (DGA) are given in Table 3. These results were taken after the transformer was in operation for about 4% of the predicted service life based on the design philosophy considering the IEC 519-2014 [19] to compute the losses, thermal and cooling requirements.

Table 3: DGA oil sample results (ppm)

Type of gas	Limits	Gas concentration
H_2	<100	1478
O_2	-	28899
N_2	-	72484
CO	<1000	28
CO_2	<15 000	860
CH_4	<80	438
C_2H_4	<150	36
C_2H_6	<35	561
C_2H_2	<7000	18
TCG	<720	2541

The adverse effect for under-designing this transformer for requirements such as suitable conductor choice and size, and cooling system can be observed from the gas concentration exceeding the permissible IEC limits as shown in red in Table 3. Due to the excessive nature and production rates of hydrogen, a possible solution would be to replace the oil in all the affected units in case there were contaminants in the oil that resulted in the production of the abnormal gassing patterns. If the observed gassing patterns persist after the oil replacement, then a redesign of the transformer units might be needed. A proper harmonic study of the DSP plant as well as the loading conditions should be conducted in order to design for the DSP conditions. For the above

case, the oil in the transformer was replaced to counter the abnormal gassing phenomena. As can be seen from Table 4, replacing the oil had a positive impact on the gases in that new DGA results showed that all of the gasses were within the specified limits. This then proved the suspected oil degeneration.

Table 4: DGA oil sample results after oil replacement (ppm)

Gasses	Limits [23]	Gas concentration
H_2	<100	150
O_2	-	19455
N_2	-	90800
CO	<1000	89
CO_2	<15 000	2291
CH_4	<80	84
C_2H_4	<150	0
C_2H_6	<35	222
C_2H_2	<7000	0
TCG	<720	545

Air and moisture are generally the main determinants of gas pressure in the transformer oil. The progression of these components are determined by the transformer tank design and loading profile. The above irregular gas bubbling patterns are observed at hot spot temperature [22] far beyond the maximum permissible temperature of 78°C by the IEC. These patterns instigate rapid ageing of oil and cellulose insulation.

5. Findings and possible remedies for stray gassing

Novelty, remedial measures proposed on the current work from a transformer manufacture perspective in addressing stray gassing problems are summarised. These measures are based on collated data from many case studies conducted in the factory. During transformer service, these studies have been found to be linked up to the generation of hydrogen arising from stray gassing, in which stems from severely hydro-treated mineral oil, but is also strenuously affected by transformer thermal aging of polymers, choice of core steel grade, zinc tank walls and vanishes.

5.1. Harmonic spectrum

It was observed that an underestimation of the harmonic spectrum may affect the application of adequate winding design to account for the actual harmonics. Moreover, an improper cooling system is designed for the reduction of the HS temperatures in the windings and structural parts. In addressing these shortcoming, during the design stage, a complete harmonic spectrum of a DSP plant must be provided as it is critical for electrical designers in the computation of transformer load losses. The authors, recommends collaboration between the IPP and the manufactures to carry out in depth harmonic studies. The latter will enable adequate winding design and sufficient cooling system for the generated hotspot temperatures.

The main problems linked up to the tank walls include apertures, bubbling, orange peel and fissures. During the transformer manufacturing assembly line, these problems arises during processes linking up the tanking and painting phase.

5.2. Gummy tracks on the transformer tank walls: After drying out

Gummy tracks on the transformer tank walls arises from the addition of a sluggish drying dissolvent resulting to poor dissipation of the dissolvent and an insufficient hardening agent to the tank walls coating. The gaps among layers have been observed to be deficient when the coating is extremely dense and the coating layer is still wet. Additionally, the gummy tracks on the tank walls has been found to be due to contaminated tanks walls prior to coating.

5.3. Apertures in transformer tank walls

Apertures in tank walls during the assembly line may arise when the tank steel sheets are not cautiously handled. This phenomena has been observed as voids of diameter of about 0.1mm. Additionally, if the coating has not been settled for a certain period, the coating viscosity will be high and potentially the air bubbles have not been cleared. Additionally, prior to the tank welding, shot blasting must not be carried for the spare parts.

An adequate drying dissolvent and hardening agent must be designated and moderately added. The manufacture must also maintain the coated tank walls pollution-free. A best practice might be coating of the top-coat after the undercoating has completely dried out. When the climate is inimical during the assembly line, then the manufacture must ascertain excellent airing. The coating must not be carried out at high temperature and moisture.

6. Conclusion

This work, presents the results of stray gassing results that were carried out on a 2500kV, mineral-oil filled transformer. Particularly, solution oriented on the impact of harmonic currents on the service losses and thermal performance of the studied DSP the plant transformer. Moreover, the observed stray gassing occurrences of the unit as a result of (1) the generation of HS temperatures in the active part components; and (2) the core steel grade, zinc tank wall surface and coating.

In the case of an IPP who is not well informed about the actual harmonic levels occurring in the DSP plant, the authors recommend that manufactures make provision of the harmonic spectrum simulation prior to the electrical design process. In any case if the IEC harmonic spectrum meet the needs of the IPP, there should be a clear written agreement between the IPP and the manufacturer regarding the maximum permissible harmonics being in accordance with the IEC spectrum.

Novelty, findings of this work indicate that the generation of hydrogen arising from stray gassing may stem from severely hydro-treated mineral oil, but is also strenuously affected by transformer thermal aging of polymers, choice of core steel material and tank walls vanishes. The production surplus of methane and ethane are also witnessed in the first years of service and reaches substantial concentration levels. Potentially, these occurrences also arises from the thermal aging of polymers. The authors make some recommendations to utility owners to make a distinction of stray gassing from transformer fault by means of routine inspection aside from DGA value basis withal to the increase in gas diffusion rate. Finally, the authors highlight the need to establish standards that will provide support for transformers intended to operate in DSP applications. At large this work identifies the shortcomings of the design considerations for

transformers intended to operate in DSP applications and recommend corrective measures to address these challenges.

The authors make a significant contribution by further recommending procedures that can be employed as remedies during the design phase and manufacturing processes.

Conflict of Interest

The authors declare no conflict of interest.

References

[1] Government Gazette," Integrated Energy Plan (IEP)", The National Energy Regulator Act, **34**, 2008, doi: wp-content/uploads/2017/04/IEP-IRP-gW-ELA-Comment-310317.pdf.

[2] B. A Thango, D.B Nyandeni, P.M Molepo, "Solar Power Plant Transformer Loss Computation under Harmonic Currents using Finite Element Method", in 9th CIGRE Southern Africa Regional Conference, 1 – 4, 2019.

[3] E. Arslan, S. Sakar, M. E. Balci," On the no-load loss of power transformers under voltages with sub-harmonics", in IEEE International Energy Conference (ENERGYCON), 228-233, 2014, doi: doi: 10.1109/ENERGYCON.2014.6850433.

[4] S.V. Kulkarni, S.A. Khaparde," Stray loss evaluation in power transformers-a review", IEEE Power Engineering Society Winter Meeting. Conference Proceedings, **3**, 2269-2274, 2000, doi: 10.1109/PESW.2000.847708.

[5] T. D. Kefalas and A. G. Kladas, "Harmonic Impact on Distribution Transformer No-Load Loss," in IEEE Transactions on Industrial Electronics, **57** (1), 193-200, 2010, doi: 10.1109/TIE.2009.2030207.

[6] E. So, R. Arseneau and E. Hanique, "No-load loss measurements of power transformers under distorted supply voltage waveform conditions," in IEEE Transactions on Instrumentation and Measurement, **52**(2), 429-432, 2003, doi: 10.1109/TIM.2003.809910.

[7] B.A. Thango, J. A. Jordaan and A.F. Nnachi, "Service Life Estimation of Photovoltaic Plant Transformers under Non-Linear Loads", 2020 IEEE PES/IAS PowerAfrica Conference, 1-5, 2020 doi: doi: 10.1109/PowerAfrica49420.2020.9219912.

[8] A. Elmoudi, M. Lehtonen and H. Nordman, "Effect of harmonics on transformers loss of life," Conference Record of the 2006 IEEE International Symposium on Electrical Insulation, Toronto, Ont., 408-411, 2006, doi: 10.1109/ELINSL.2006.1665344.

[9] K. Dursun and N. Rahmanov, "Harmonic load losses in power transformer windings using Finite Element methods," Eurocon 2013, 1526-1530, 2013, doi: 10.1109/EUROCON.2013.6625180.

[10] D. M. Said and K. M. Nor, "Effects of harmonics on distribution transformers," in 2008 Australasian Universities Power Engineering Conference, 1-5, 2008.

[11] J. Weesmaa, M. Sterner, B. Pahlavanpour, L. Bergeld, J. Nunes and K. Sundkvist, "Study of stray gassing measurements by different methods," 2013 Annual Report Conference on Electrical Insulation and Dielectric Phenomena, Shenzhen, 184-189, 2013, doi: 10.1109/CEIDP.2013.6748192.

[12] I. Hohlein, "Unusual cases of gassing in transformers in service," in IEEE Electrical Insulation Magazine, **22** (1), 24-27, 2006, doi: 10.1109/MEI.2006.1618968.

[13] D. Martin, N. Lelekakis, J. Wijaya, M. Duval and T. Saha, "Investigations Into the Stray Gassing of Oils in the Fault Diagnosis of Transformers," in IEEE Transactions on Power Delivery, **29** (5), 2369-2374, 2014, doi: 10.1109/TPWRD.2014.2316501.

[14] F. Jakob, P. Noble and J. J. Dukarm, "A Thermodynamic Approach to Evaluation of the Severity of Transformer Faults," in IEEE Transactions on Power Delivery, **27** (2), 554-559, 2012, doi: 10.1109/TPWRD.2011.2175950.

[15] M. Phoshoko, "Predictive maintenance of transformers through stray gassing studies", 66th AMEU Convention, 2017, doi: wp-content/uploads/2017/11/Pages-from-AMEU-2017_-46-51.pdf.

[16] B. A. Thango, J. A. Jordaan and A. F. Nnachi, "Stray Gassing of Transformer Oil in Distributed Solar Photovoltaic (DSPV) Systems," 2020 6th IEEE International Energy Conference (ENERGYCon), Gammarth, Tunis, Tunisia, 484-488, 2020,doi: 10.1109/ENERGYCon48941.2020.9236522.

[17] B.A. Thango, J. A. Jordaan, A.F. Nnachi, "Effects of Current Harmonics on Maximum Loading Capability for Solar Power Plant Transformers", 2020 International SAUPEC/RobMech/PRASA Conference, 1-5, 2020, doi: 10.1109/SAUPEC/RobMech/PRASA48453.2020.9041101.

[18] B.A. Thango, J.A. Jordaan, A.F. Nnachi, "Step-Up Transformers for PV Plants: Load Loss Estimation under Harmonic Conditions", 19th International Conference on Harmonics and Quality of Power (ICHQP), 1-5, 2020, doi: 10.1109/ICHQP46026.2020.9177938.

[19] IEEE 519: 2014, "Recommended practices and requirements for harmonic control in electrical power systems", 1-29, 2014, doi: 10.1109/IEEESTD.2014.6826459.

[20] T.V. Oommen, S.R Lindgren," Bubble evolution from transformer overload", IEEE/PES Transmission and Distribution Conference and Exposition. Developing New Perspectives (Cat. No.01CH37294), **1**, 137-142, 2001, doi: 10.1109/TDC.2001.971223.

[21] M.C. Hlatshwayo, The computation of winding eddy losses in power transformers using analytical and numerical methods, Masters Thsis, 2013.

[22] IEC 60076-7, "Power transformers – Part 7: Loading guide for mineral-oil-immersed power transformers", 2005.

[23] "IEEE Guide for Loading Mineral-Oil-Immersed Transformers," in IEEE Std C57.91-1995 , 1-112, 1995, doi: 10.1109/IEEESTD.1995.8684643.

A Review on TAM and TOE Framework Progression and How These Models Integrate

Julies David Bryan[*], Tranos Zuva

School of Applied and Computer Science, Department of ICT, Vaal University of Technology, Vanderbijlpark, 1911, South Africa

ARTICLE INFO	ABSTRACT
	The TAM is a model that is widely used to understand IT adoption and usage process accordingly and the reason for its popularity is that the model clarifies variances like behavioral intention (BI) relevant to IT appropriation and use over a broad range of settings. The model's main factors for system use is perceived usefulness (PU) and perceived ease of use (PEOU). Likewise, the T-O-E framework is a popular framework for three stimuli that influence organizational adoption namely technology, organization, and environment. Much literature has dealt with the use of TAM and T-O-E frameworks together with their derivatives without looking at the shortfall of these models. This paper reviewed one hundred and seventeen papers that used or reviewed TAM or TOE models. The contribution of this paper is the address of the usefulness, limitations, and criticism of the two models and also how the TAM and the T-O-E frameworks can be integrated into a hybrid model using a generic framework. In conclusion these models can be used separately or as a hybrid depending on the situation at hand. In future it important to harmonize the so many factors of the models that have been suggested and used in literature.

1. Introduction

Research studies on IT adoption have rapidly evolved over the last three decades. A diverse number of theoretical models have been created such as Innovation Diffusion Theory (IDT), Theory of Planned Behavior (TBP), Diffusion of innovations (DOI), Electronic Data Interchange model (EDI), etc. Two of the most valued research studies that contribute to IT adoption are Technology Acceptance Model (TAM) and Technology-Organization-Environment (T-O-E).

In the 1970s, anticipating system growth became a niche of attraction to many researchers due to the growing technology demand and system adoption failure that goes with it [1]. According to [2] the vast majority of studies neglected to deliver solid estimates that could clarify framework acknowledgment or dismissal and recommended Technology Acceptance Model in 1985 [1]. Davis proposed that the user interaction with any system is a reaction that can be interpreted and foreseen by user inspirations, shaped by foreign catalyst [1]. As per [1] user inspirations are shaped through a foreign catalyst that abides system's features and capabilities. Davis, who counted on preceding work done by [3] continue amend his model and

propose the Technology Acceptance Model in which he advises that user motivation can be driven by three factors:

- Perceived Ease of Use (PEOU)
- Perceived Usefulness (PU)
- Attitude towards using the system. (A)

According to [1] Davis's thesis on user's attitude towards a system is a major factor that determents if a user will use or reject a system. A user's attitude is leverage by perceived usefulness and perceived ease of use.

Broad literature on Information Technology (IT) appropriation demonstrates that there are a few investigations at the individual level [4]. Numerous theories and models uses IT adoption at the individual level such as Technology Acceptance Model (TAM) [1,2,4], Theory of Planned Behaviour (TPB) [3], TAM 2 [5] Unified Theory of Acceptance and Use of Technology (UTAUT) [5]. However, studies show that there is less investigation at organisational level.

According to [6] the whole process is an innovation from development by engineers and business people to the adoption and execution of those advancements by clients inside the context of

an organization. As per [7] the T-O-E framework performs the process of how the organisation impacts the appropriation and execution of innovations. As per [7] the T-O-E framework is an association hypothesis which clarifies three unique components association's setting impact reception choices. The components are technology, organisational and environmental context, and each of the three is set to impact technological innovation. [6] built up a structure for hierarchical reception dependent on the Contingency Theory of Organisations. According to [3] the strength of a organisation is determined by both internal and external elements which can be described as environment, organisation size, and organisation strategy. Upon decision making three key elements environmental, organisational and technological needs to be factored in, and organizational adoption is based on technology, organisation, and environment [4].

The contribution of this paper is to determine and understand usage and modifications, progression, limitations, and criticisms of the Technology Acceptance Model (TAM) and Technology-Organisation-Environment (T-O-E). The paper also looks at how these two models can be integrated to complement one another.

2. Technology Acceptance Model (TAM) Overview

As per [8], [2] established the Technology Acceptance Model (TAM) by assuming that users will perceive usefulness to technology through ease to use as they become willing to use the technology. When employees realize that the new technology will make their life easier and more productive the greater the odds are for them to use and accept it [8].

As per [1], with the rapid technological growth in the 1970s, many organizations struggled to adapt to system failure. Due to the increasing system failures, numerous researchers started to study the area of predicting systems [9]. The TAM was then proposed by [10] in 1985 during his studies at MIT Sloan School of Management [1]. According to [1], Davis proposed that system usage is a human behavior that is user motivation driven and directly influenced by external stimulation like system's components and efficiency. This can be seen in the Figure1 below.
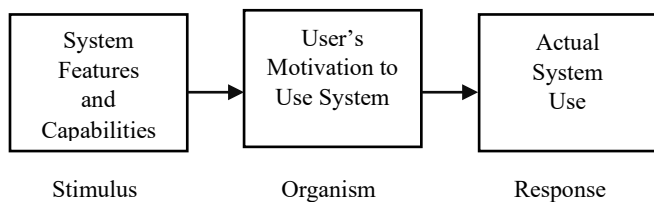
Figure 1: Model for technology acceptance [22].

Davis then continued with his research by relying on prior work done by [11] on the Theory of Reasoned Action. The refined model of Davis can be seen in Figure 2.

In Figure 2, [11] propose that user motivation can be described by three factors: Perceived Ease of Use, Perceived Usefulness, and Attitude Towards Using the systems [1]. As per the [9] Davis model, TAM hypothesized that attitude towards the system is a considerable factor whether used or rejected by the user. User's attitude is influenced by two primary convictions namely perceived usefulness and perceived ease of use.
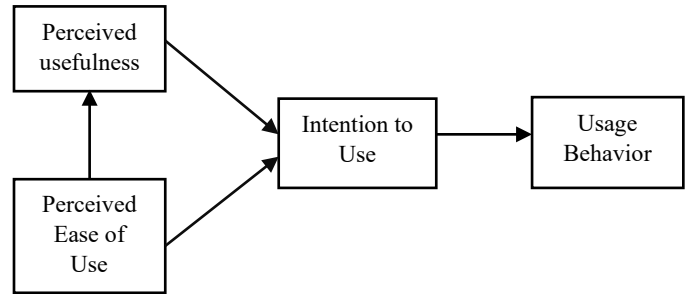
Figure 2: Original TAM [11].

According to [12] on the contrary, states that the TAM theory is based on social behavior by someone's attitude which is predicted to use an information system. [3] argue that when it comes to personal use of technology, social influences like friends and colleague is a major factor. However, when it comes to the organisations, the work climate cannot be controlled by follow workers but the organisation regulate direct the conduct of the workers as there is rule-administered conduct at organisations for utilizing a system. [8] states that TAM is simple and easy to understand and is mention by [13] to be the most popular means of measuring the scale of acceptance of technology by users.

TAM studies the individual relationship of technology acceptance, adoption, and BI to use [6,14]. As per [13] and [14], the main factors for system use with TAM is PU and PEOU. PU can be described as "the prospective user's subjective probability that using a specific application system that will increase his or her job performance within an organisational context," and PEOU is defined as "the degree to which the prospective user expects the target system to be free of effort" [2]. As per [15], PEOU influences PU because of its ease of use making TAM a popular model. It has been proven by numerous research studies that these two variables are frequently used for testing and [14] stated that these PU and PEOU variables are mentioned 40 percent for people's goal to utilize (admission) and resulting execution (transformation) of technology. TAM hasn't only been developed to predict user adoption, but it was also designed to predict user behavior after the individual has interacted with the system [16]. The TAM model is supported as a goal-based model which specifies that the goal to embrace innovation is a decent indicator of its genuine use [16]. Henceforth, it very well may be reasoned that the TAM model got solid ramifications for technology endorsements from conceptual and theoretical perspectives. [6]. [17] declares the primary reason why TAM was developed was to model user consent for IT with the desire to explain the BI system usage that was a footing for IT dealing with BIs and usage of IT [17]. [6] states that to have a better overview on IT adoption and acceptance, the primitive framework (i.e. TAM2 and TAM3) had to be extended and includes PU and PEOU categories. There were four modifications that assisted with the TAM evolution, these can be named as adjusting outer precursors; changing prescient factors; controlling mediator factors, and shifting outcome measures [13] and [18]. The underlying center segment basic to all alterations of TAM comprises of three builds: PU, PEOU, and BI [13,18] and in the centre part, BI is influenced by PU and PEOU, PU is affected by PEOU. It is concluded by [18] and [3] PU and PEOU are two

centre develops that shape client perspectives and aims in adopting a technology system.

In summary, the TAM model is widely used to understand IT adoption and usage process according to [6]. The reason for its popularity as per [16] is that the model clarifies variance like behavioural intention (BI) applicable to IT adoption of use overbroad contexts. Another reason why TAM is so famous is that it foresees an owner's IT consent by the user and the job usage [14]. [1] on the contrary, states that the reason why it is widely used is that TAM explains the determinants of user acceptance of a wide range of end-user computing technologies.

3. Limitations and Criticism of TAM

Even though TAM is popularly used, it does come with limitations and these are found in moderating and external variables [13]. TAM looks at future behaviour and not on actual behaviour [15, 18] as this also aids to its limitations. [13] confesses that TAM is known for its restricted chance of clarification and expectation, detail and absence of common-sense worth.

A crucial extension to TAM by [19] was to introduce TAM2 as TAM had some limitations in illustrating reason for a person to perceive system usefulness. For this reason, additional variables were added to the perceive usefulness variable in TAM [9]. A second important alteration to TAM by [19] was identifying the decedent to the perceived ease of use variable in the TAM model. For this reason, two new decedents namely anchors and adjustments were added. As per [9] anchors were thought-about personal computers and the usage of it, well adjustment was thought-about as direct involvement with the target system. Other limitations stated by [9] has been flagged by numerous researcher and has grouped the criticism into three categories:

3.1. Limitations in the methodology used for testing the TAM model

The biggest criticism of TAM is the model makes use of self-report use data instead of measuring against real system data. According to [20] self-report data is abstract and inaccurate when measuring system usage. Even so, many studies still make use of self-report use data. As per [21] the TAM model makes use of students as participants in a controlled environment to obtain test results and for this reason, these test results cannot be generalized to the outside world as studies have distinctive intentions like obtaining grades, rewards, etc. [20, 22].

3.2. TAM model variable and relationship limitations.

According to [23] attitude is an important factor for system usage and TAM needs to review it. The TAM model was clone in 1998, but the attitude variables were not removed as proposed by [21], instead, two additional attitude variables, affective and cognitive were added. [21]. A survey by [23] requested participants to rate their usage of spreadsheet applications. The outcome of the survey shows that the effective attitude variable did not portray the statistical connotation to anticipate system use however the results on the cognitive attitude were very significant.

3.3. TAM model theoretical foundation limitations.

According to [24], the poor hypothetical relationship was defined among the various builds detailed in TAM. He scrutinized the hypothetical quality of the goal real use connect, and saw that conduct couldn't be considered as a terminal objective. [24] claims that conduct should be treated as a way to a more terminal intention and behavior should be a fundamental target. Besides, he clarified that the aim may not hold delegate enough of real use, because the time-frame among goal and appropriation could be full vulnerabilities and different elements, that may impact a person's choice to embrace innovation. In [24], likewise scrutinized the chance of deciding conduct by including measures for perceived usefulness and perceived ease of use.

"There is a scope of investigating the role of certain other variables such as technological influences, the role of firm size in the technology make/buy decisions, the innovativeness of the firm, a firm's level of technology readiness, security, trust, marketing effort and also on evaluating the consequences of technology usage on performance such as responsiveness and financial performance" [15, 18, 25]. It must be noted by [26] that the TAM has been used in almost every IT research adoption theory and because of its frequent use, the quality of TAM could be at risk, as this could lead to degreed in the research field. Another limitation mentioned by [20] shows that TAM experimental investigations don't deliver predictable or clear outcomes and proves that demonstrates the TAM model needs to be incorporated with other IT reception models and hypotheses.

4. Technology Acceptance Model (TAM) progression

As per [13, 27, 28] the TAM is a principal adoption theory in the IT sector. TAM discloses how external variables can have an impact on adoption decision making on fundamental financial, functional, and beliefs and therefore recommends PU and PEOU as the central reason for adoption in IT [9]. An individual's goal to exploit an application is interpreted and forecast by his view of the innovation's handiness and its straightforwardness. According to [19] perceived usefulness can be determined by both perceived ease of use and predict attitudes. Over the years TAM has shown great acceptance, utilization, and reproduction but the model failed to give essential data on the user's assumption for only PU and PEOU. Based on this limitation it was necessary for the model by expanding or integrating with other IT acceptance models [9]. The integration of TAM with different models enhanced TAM by including utilization and putting premiums in explicit settings and outside factors that impact an innovation's appropriation procedure [9].

According to [7] many studies have been made to the original TAM model the causes the model to evolve. TAM-TBP was a new model introduced by [16] to integrate TAM and the theory of planned behaviour (TBP). In 2000, TAM2 was developed by [19] that extended new variables to the existing model. In 2003, the Unified Theory of Acceptance and the Use of Technology (UTAUT) model was proposed. There have been numerous studies made by scholars to alter the TAM by adding new variables. The Construct of Compatibility variable was added in 1998 by [13].

New playful factors were added by [29] to examine the acceptance of the Internet. Variables like "experience", "self-efficacy", "perceived risk", and "social influence" were added to the TAM model by [30]. An additional study made by [17] helped to extend cognitive absorption, playfulness, and self-efficacy. In 1996 two types of perceived usefulness namely near-term and

long-term were added [2]. In 2000, two new constructs were added to TAM namely perceived entertainment value and perceived presentation attractiveness, [11] was the scholar for this addition. Peer influence was then combined with TAM in 2002 by [3, 7].
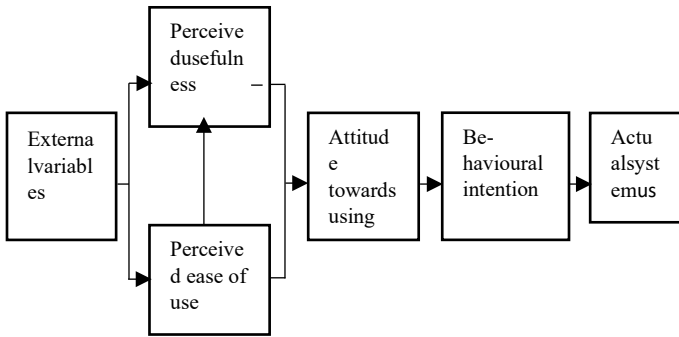
Figure 3: Technology Acceptance Model [30].

TAM has been used by scholars around the globe to perceive the acceptance of completely different sorts of information systems. A newly developed model by [6] based TAM named the shopping acceptance model (OSAM) was created to study online shopping behaviour. In 2003, in [31], the author developed an e-commerce model based on TAM with new variables trust and perceived risk.

5. Technology-Organization- Environment (T-O-E) Overview

As per [4], T-O-E Framework was developed by [6] for organisational adoption based on the Contingency Theory of Organisations. Well, it is claimed by [9] that [6] expect a nonexclusive arrangement of components to anticipate the probability of adoption. The framework proposes that an organisation should be consistent with its surroundings and environmental needs and its strength is determined by both internal and external factors like environment, organisation size, and organisation strategy [3]. Three key determinants were distinguished that influence organisational adoption: technology, organisation, and environment. It is imperative when one is making a decision, three factors of influence need to be looked into namely technology development [80] organisational conditions, business and organisational re-configuration [2], and industry environment [27].

Within the T-O-E framework, technological development presents the technologies accessible to an organisation. The organisation context outline the organisation characteristics well the environment context outlines the business field that consists of industry, competitors, regulations, and relationships with the government. As per [6], these are external factors that can have restraints and opportunities for technological innovations. The drawback of T-O-E is the assumption that the model will apply to large organisations, where customers make certain of congruity and fewer grievances, than to SMEs [9].

According to [6] there are three contexts that leverage technology innovation adoption and implementation process and these contexts of the T-O-E framework can be listed as follows.
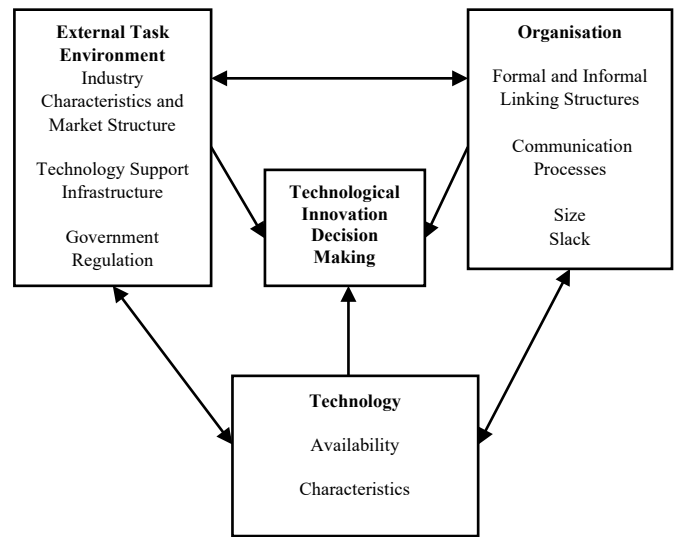
Figure 4: The technology–organization–environment framework [7].
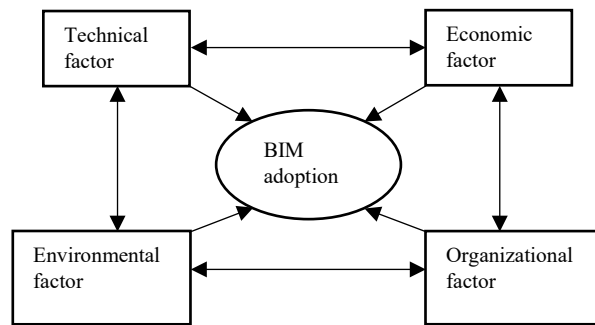
Figure 5: The derivative of T-O-E framework of BIM technology [30].

5.1. Technology context

In [2] and [16], the author defines that the technology context consisting of variables that has an impact on an individual, an organisation, and an industry's adoption of innovations and comprises of five innovation attributes as per [32] and [16] and also other attributes. Aside from innovation variables, other significant variables like system absorption, digestion, trail ability, intricacy, seen direct advantages, seen backhanded advantages and normalization has been included by several research studies while observability is found insignificant [1, 2, 9, 12, 18, 22, 32–34].

5.2. Organisation context

Adoption aptitude is impacted by explicit and spontaneous intra-hierarchical components for correspondence and supervision; along with resources and creativity of the organisation [32]. In [4], the author states that organisational context comprises of organisation scope, organisation size, and legislative belief. As per [1–3, 9, 12, 18, 22, 32, 33, 35] the most important variables of organisational context includes "financial resources, firm structure, organisational slack, innovation capacity, knowledge capability, operational capability, strategic use of technology, trust, technological resources, top management support, support for innovation, quality of human capital, organisational knowledge accumulation, expertise and infrastructure, and organisational

readiness while financial capacity and technology competence are identified as insignificant". The clarification explained by the makers is, relationship of all sizes have perceived the fundamental meaning of development for the achievement of their associations, consequently are glad to contribute enthusiastically to progressions to improve their high grounds. [12, 32, 34]; states that the role of top management is not the same and differs in context. As per [2] some inter-organisational variables context are on EDI that identifies the power of partners, an expectation in the partner and tie responsibility with a partner and dependency of the partner.

5.3. Environmental context

Environmental context is an area where the company targets business operations like government incentives and regulations [4]. The environmental context consists of variables like rivalry, relations with buyers and suppliers, and areas of the industry life cycle [2, 4, 6, 9,12, 18, 22, 24, 32-34] says the environmental context variables covers client order, serious weight, outer weight, inside weight, exchanging accomplice pressure, merchant uphold, business reliance, ecological vulnerability, data power and organisation force.

In summary, T-O-E has materialized to be a widespread framework used for theoretical perspective on IT adoption [24]. Consideration of technological, organisational, and environmental variables has made the T-O-E frame invaluable over other selection models in contemplating innovation appropriation, innovation use, and worth creation from innovation development [2, 8, 9, 32, 36].

6. Limitations and Criticism of T-O-E framework

As per [32] the T-O-E framework limitation as glossary of variables that is not well integrated or well developed and needs more research study on organisational adoption. [1] likewise featured that T-O-E system has no significant develops in the model and the factors in every unique circumstance [33] states that there lack in power of technology and adoption variance is unexplained. On the contrary [12] declares that the major constructs and the variables in the T-O-E framework are not concise and differ from context to context. For this reason as by [9,35] and [3, 12, 24, 32, 36] other variables like sociological variables, cognitive variables, technology readiness, ability to leverage IT investment through different channels professionals' experience and skills, managerial capabilities of change management, security concerns, government promotion and factors salient to the country context such as government policy/regulation, technology infrastructure, and culture is needed to refine the T-O-E framework.

7. Technology-Organisation-Environment (T-O-E) progression

According to [37], the T-O-E framework lack change for different reasons from original development. This lack of evolution can be described as follows. Firstly, as per [24], T-O-E characterizes as a universal theory as T-O-E is used as a framework in which a large group of different elements can be set. For this reason, researchers and scholars saw little need to change or refine the T-O-E framework. Second, the T-O-E structure may have seen generally little advancement because it has been seen as lined up

with other adoption model theories. For this reason, pressure has been seen by the T-O-E framework and other theories for the T-O-E framework to assimilate in contesting innovations. As per [38], it can be seen that the T-O-E framework has been persistent with the theory of the diffusion on innovation (DOI). For example, DOI adoption on individual leader characteristics and internal characteristics of organisational structure is equally yok to T-O-E's organisation context element. Another consistency can be seen with DOI's external characteristics of the organisation with T-O-E's environmental context. Lastly, consistency can be seen in the technological characteristics of the innovation with T-O-E's technological context [39, 40]. Since these theories are portrayed as notably comparable, the T-O-E system has not been adjusted because of DOI [37].

As per [9] several research studies explains the essence of the T-O-E framework which can be explained as e-commerce Enterprise Resource Planning, e-business, , open systems, Knowledge Management Systems, Electronic Data Interchange etc. in Table 1.

Table 1: Organisational Adoption of Information Technologies

Author(s)	Domain
[22]	"Internet/E-Business"
[21]	"HRIS"
[2]	"Green IT Initialization"
[67]	"E-Business"
[3]	"KMS"
[32]	"Enterprise Systems"
[37]	"Mobile Commerce"
[18]	"E-Business"
[16]	"ERP"
[2]	"Web Site"
[6]	"E-Commerce"
[41]	"IT"
[32]	"E-Signature"
[3]	"E-Commerce"
[37]	"E-Business"
[2,25]	"E-Business"
[6]	"Internet"
[6]	"E-Business"
[32]	"E-Commerce"
[27]	"IT"
[2]	"Open System"

Over the past 30 years, the T-O-E framework has exhibit influence across many technological, industrial, and national/cultural contexts [7]. The T-O-E framework has been used across various industries to explain the adoption of inter-organisational systems [2, 42]. E-business [2, 6, 7, 15], electronic data interchange (EDI) [42], open systems[2], enterprise systems [32] and a broad spectrum of general IS applications [2]. The T-O-E model has been used to clarify the selection of advancements in a large group of ventures, including manufacturing [2, 15] health care [34] retail, wholesale, and financial services [15]. According to [2, 7, 15] and [6] the T-O-E model has been approved in European, American, and Asian contexts, as well as in both

developed as well as developing countries. In every one of the experimental investigations that test the T-O-E system, analysts have utilized somewhat various elements for technological, organisational, and environmental contexts. [7] claims that researchers agree with [6] that the three T-O-E contexts affect adoption, however, they have speculated that for every particular innovation or setting that is being contemplated, there is a special arrangement of components or measures. [6] argues that one relevant factor in technological context that influences the adoption of e-business is " technology readiness." [6] also states that "firm size", global scope" and "financial resources are the appropriate elements that ought to be concentrated to see how organisational context influences the adoption of e-business. When looking at environmental context influences, "regulatory environment" and "competition intensity" are suitable in the adoption of e-business.

8. Integration of TAM and T-O-E framework

As per [30] the creation of TAM by [2] was in light of the Theory of Reasoned Action (TRA) in 1989. [2] perceived that a person's behavioural intention to use a newly created system is associated with their perceived usefulness and ease of use. Meanwhile, the perceived ease of use influences perceived usefulness, and the perceived usefulness and ease of use are influenced by foreign variables.

As per [43] the T-O-E framework persuades models of technological, organisational, and environmental backgrounds to adopt and achieve technological innovations. he goes on to say the technological context indicates internal and external technologies by firms, organisational context refers to company size, organisational structure, and human resource, well environmental context looks at components like competition, partners, and industry environment that out-side the control of a firm [30].

The Technology Acceptance Model and Technology Organisation Environment System have been generally applied in I.T. and data innovation across various research studies [30]. The two models complement each other as TAM is flexible with external variables and can abduct a person's acceptance behaviours while on the other side of the coin T-O-E acknowledges the technical, environmental and organisational elements that have an effect on technology acceptance and adoption at organizational level. Many research studies where TAM and T-O-E are integrated can be found. [24] has integrated TAM and T-O-E to illustrate cloud adoption at organisational level. Another study by [34] evaluates system factors in the adoption of ERP in manufacturing companies. Lastly, [28] set up the UTAUT-T-O-E technology acceptance model framework and investigated the components influencing IT selection [30]. Figure 6 illustrates the integration of TOE External variables to TAM.

Joining the TAM in Figure 3 with the TOE structure in Figure 5, an incorporated TAM-TOE model for BIM innovation was created as seen in Figure 7.

The impact scale of each factor on different variables are determined through their logical relationship in the system to shape the immediate impact network, at that point the reason and focus level of each factor is determined to decide the circumstances and end-result between the elements. This strategy can visually demonstrate the logical relationships between factors through determinant analytics and can disentangle complex issues.

External variables
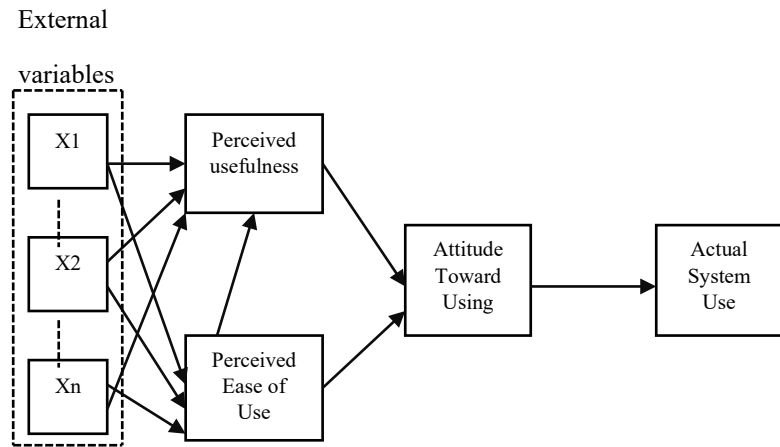
Figure 6: TAM-TOE derivative integration model [30].

External variables
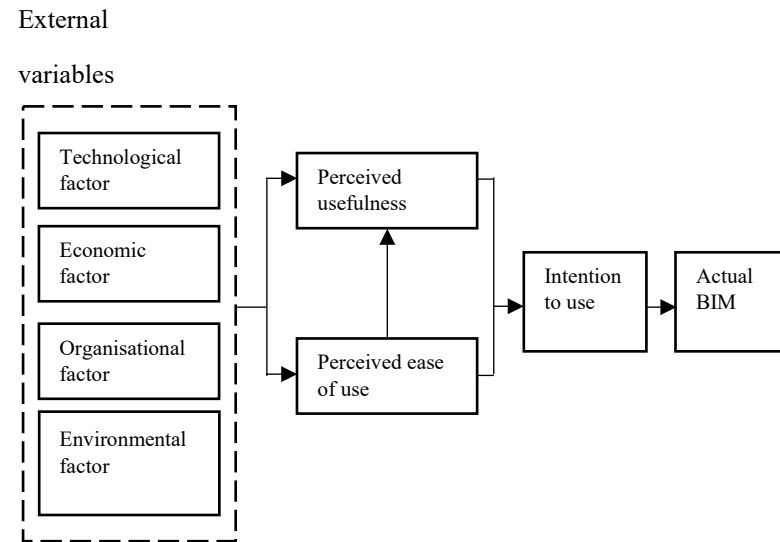
Figure 7: The derivative integrated TAM-T-O-E model of BIM technology [30].

8.1. Technical factors

According to [30] technical factors can be classified into three past research studies, namely localization, standardization, and compatibility.

- Localization: Localization as per [13], Building Information Modelling (BIM) consists of software operating environment, the adaption of ventures, and management process.
- Standardization: Specifies milestones, deliverables, and objectives to accomplish.
- Compatibility: This describes the strength and challenges of different application software from a different corporation, their integration, and are compatibility with each other.

8.2. Economic factors

According to [30] there two economic factors: cost and return in investment.

- Cost: Cost normally consist of hardware, software, training and consulting fee for professionals [59].
- Return on investment: Refers is a new technology that would have the potential and opportunities for new revenue income.

Table 2: A summary of the literature on external variables in the Building Information Modelling (BIM) TAM-T-O-E model.

Category	Code	External Variables	References																					sum
			A	B	C	D	E	F	G	H	I	J	K	L	M	N	O	P	Q	R	S	T	U	
Technological Context	EV1	Localization of BIM				●										●	●	●	●	●			●	7
	EV2	Standardization of BIM	●	●	●		●	●	●	●	●	●	●	●	●	●	●		●	●	●	●	●	19
	EV3	Compatibility of BIM	●		●	●	●		●	●	●	●	●	●	●	●	●	●	●	●	●	●	●	19
Economic Context	EV4	Cost of using BIM	●	●	●		●	●	●		●	●	●			●	●		●	●	●			15
	EV5	Return on investment		●			●	●	●			●							●				●	7
Organisational Context	EV6	Organisational pattern and workflow	●	●	●		●	●		●	●			●	●	●	●		●	●			●	15
	EV7	Traditional thinking mode	●	●			●	●	●	●	●	●		●		●			●	●			●	13
	EV8	Executive support	●		●	●	●	●		●		●	●	●		●	●	●	●			●	●	15
	EV9	Number of BIM experts and technical staff	●	●	●		●		●			●	●			●	●		●	●	●		●	13
Environmental Context	EV10	Requirement from in the industry		●	●		●	●							●		●	●		●	●	●			10
	EV11	Popularity of BIM in the industry		●	●	●		●	●			●		●	●			●		●	●	●			12
	EV12	Competitions from other companies			●	●			●					●	●		●	●				●		8

Notes. A = [44] B = [19] C = [77]; D = [45]; E = [6]; F = [18] G = [26]; H = [46]; I = [24] J = [23]; K = [34]; L = [34]; M = [47]; N = [72]; O = [59]; P = [23]; Q = [24]; R = [48]; S = [8]; T = [26]; U = [22].

8.3. Organisational factors

As per [30], the four organisational factors can be listed as organisational mode and workflow, traditional thinking mode, support from senior management, and several experts and technicians.

- Organisational model and Workflow: It is normally fixed and is difficult to change the organisational model and workflow. Roles and responsibilities and work context frustrate application extension to a degree [30].
- Traditional Thinking mode: People are hesitant to change and handle issues in the same way [30], [24].

- Top Management Support: top management duty is one of the significant achievement factors for receiving BIM innovations [33].
- A number of BIM experts and technicians: The requirement of professionals with related technical experience and insights.

8.4. Environmental factors.

As per [30], environmental factors are shown at national, industrial, and enterprise levels for perceptions and attitudes in adoption and have been classified as national policy requirements, popularity in the BIM industry, and competition from other companies.

- National policy requirements: As per [15], national policies is crucial to the development of information technology. For instance, the British government has assumed a significant part in advancing the application and the improvement of BIM [18].
- Popularity in the BIM industry: With greater acceptance, BIM adoption is becoming more popular.
- Competition from other companies: Completion can be clarified in two ways of competition namely, cost and differentiation.

The study merges TAM and TOE and proposes a Building Information Modelling (BIM) TAM-TOE model that consists of 12 external variables. An informative questionnaire was derived from the 12 external variables and 3 internal variables. A span number DEMATEL strategy was utilized to figure the impact degree, affected degree, centrality degree, and causal level of every factor. By ascertaining the centrality and reason for each factor, the key components influencing the selection of BIM are acquired, an 'impact and cause chart' was made dependent on the absolute relations between factors.

The study significant discoveries can be summed up as:

Firstly, the Requirement from public arrangements (EV10) is the most grounded driving variable, followed by Traditional thinking modes (EV7), Standardization of BIM (EV2), Compatibility of BIM (EV3), Competitions from other companies (EV12), Popularity of BIM in the industry (EV11), Localization of BIM and Return on investment (EV5).

Secondly, the re-enactments and emphases of the eight propulsive variables affirm that the objective variable Intention to use (IV3) fluctuated essentially and is responsive with changes of firstly, The Requirement from national policies (EV10), and then the Standardization of BIM (EV2).

9. Conclusion

TAM is a powerful adoption theory in the IT sector and has been used by numerous research studies. The model looks at an individual's goal when utilizing a system or application and recommend PU and PEOU as the central reason for IT adoption. Over the years TAM has shown great acceptance, utilization, and reproduction but the model failed to give essential data on the user's assumption to only PU and PEOU. Based on this limitation it was necessary for the model by expanding or integrating with other IT acceptance models [9]. The T-O-E framework proposed a generic set of factors of technology adoption. The T-O-E framework looks at three contexts namely Technology, Organisation, and Environmental. TAM and its all-encompassing forms have a high ability to clarify the innovation reception while the meaning of the T-O-E system is likewise perceived in clarifying technology adoption. The marriage of these two models brings a new and unique developed redesign that takes TAM and T-O-E models to a more extensive level to advance and encourage improved informative and prescient focal points of IT adoption.

The TAM and T-O-E framework can be used separately or as a hybrid depending on the situation at hand. In future it important to harmonize the so many factors of the models that have been suggested and used in literature.

This review paper doesn't overrule the acknowledgment of other reception models, yet it investigates the writing to create a selection model for study comparable data advances as referenced before.

Acknowledgment

References

[1] C. Low, Y. Chen, M. Wu, "Understanding the determinants of cloud computing adoption," Industrial Management and Data Systems, **111**(7), 1006–1023, 2011, doi:10.1108/02635571111161262.

[2] K. Zhu, K. Kraemer, S. Xu, "Electronic business adoption by European firms: A cross-country assessment of the facilitators and inhibitors," European Journal of Information Systems, **12**(4), 251–268, 2003, doi:10.1057/palgrave.ejis.3000475.

[3] T.S.H. Teo, S. Lin, K. hung Lai, "Adopters and non-adopters of e-procurement in Singapore: An empirical study," Omega, **37**(5), 972–987, 2009, doi:10.1016/j.omega.2008.11.001.

[4] M.I. Salwani, G. Marthandan, M.D. Norzaidi, S.C. Chong, "E-commerce usage and business performance in the Malaysian tourism sector: Empirical analysis," Information Management and Computer Security, **17**(2), 66–185, 2009, doi:10.1108/09685220910964027.

[5] V. Venkatesh, F.D. Davis, M.G. Morris, "Dead or alive? The development, trajectory and future of technology adoption research," Journal of the Association for Information Systems, **8**(4), 267–286, 2007, doi:10.17705/1jais.00120.

[6] S. Xu, K. Zhu, J. Gibbs, "Global Technology, Local Adoption: A Cross-Country Investigation of Internet Adoption by Companies in the United States and China," Electronic Markets, **14**(1), 13–24, 2004, doi:10.1080/1019678042000175261.

[7] K. Zhu, K.L. Kraemer, V. Gurbaxani, S.X. Xu, Migration to open-standard interorganizational systems: Network effects, switching costs, and path dependency, MIS Quarterly: Management Information Systems, 2006, doi:10.2307/25148771.

[8] J. Xu, "Research on Application of BIM 5D Technology in Central Grand Project," in Procedia Engineering, 174 600-610, 2017, doi:10.1016/j.proeng.2017.01.194.

[9] H. Okorie Awa, O. Ukoha, B. Emecheta, "Integrating TAM and TOE Frameworks and Expanding their Characteristic Constructs for E-Commerce Adoption by SMEs," in Proceedings of the 2012 InSITE Conference, 571–588, 2012, doi:10.28945/1676.

[10] C. Carnaghan, K. Klassen, "Exploring the determinants of web-based E-business evolution in Canada," in Association for Information Systems - 13th Americas Conference on Information Systems, AMCIS 2007: Reaching New Heights, 5 3532-3543, 2007.

[11] S. Alwahaishi, V. Snášel, "Modeling the Determinants Affecting Consumers' Acceptance and Use of Information and Communications Technology," International Journal of E-Adoption, **5**(2), 25–39, 2013, doi:10.4018/jea.2013040103.

[12] Y.M. Wang, Y.S. Wang, Y.F. Yang, "Understanding the determinants of RFID adoption in the manufacturing industry," Technological Forecasting and Social Change, **77**(5), 803–815, 2010, doi:10.1016/j.techfore.2010.03.006.

[13] Y.H. Li, "An empirical investigation on the determinants of E-procurement adoption in Chinese manufacturing enterprises," in 2008 International Conference on Management Science and Engineering 15th Annual Conference Proceedings, ICMSE, 32–37, 2008, doi:10.1109/ICMSE.2008.4668890.

[14] Y. a Au, H. Zafar, A Multi-Country Assessment of Mobile Payment Adoption, 2008, doi:10.1111/1467-8616.00112.

[15] N. Schillewaert, M.J. Ahearne, R.T. Frambach, R.K. Moenaert, "The adoption of information technology in the sales force," Industrial Marketing Management, **34**(2), 323–336, 2005, doi:10.1016/j.indmarman.2004.09.013.

[16] M.J. Pan, W.Y. Jang, "Determinants of the adoption of enterprise resource planning within the technology-organization-environment framework: Taiwan's communications industry," Journal of Computer Information Systems, **48**(3), 94–102, 2008, doi:10.1080/08874417.2008.11646025.

[17] K. Amoako-Gyampah, A.F. Salam, "An extension of the technology acceptance model in an ERP implementation environment," Information and Management, **41**(6), 731–745, 2004, doi:10.1016/j.im.2003.08.010.

[18] W.W. Wu, "Developing an explorative model for SaaS adoption," Expert Systems with Applications, **38**(12), 15057–15064, 2011, doi:10.1016/j.eswa.2011.05.039.

[19] V. Venkatesh, M.G. Morris, G.B. Davis, F.D. Davis, "User acceptance of information technology: Toward a unified view," MIS Quarterly: Management Information Systems, **27**(3), 425–478, 2003, doi:10.2307/30036540.

[20] O. Ukoha, H.O. Awa, C.A. Nwuche, I.F. Asiegbu, "Analysis of explanatory and predictive architectures and the relevance in explaining the adoption of IT in SMEs," Interdisciplinary Journal of Information, Knowledge, and Management, (6), 217–230, 2011, doi:10.28945/1431.

[21] I. Troshani, C. Jerram, H.S. Rao, "Industrial Management & Data Systems Exploring the public sector adoption of HRIS," Industrial Management & Data Systems Personnel Review International Journal of Productivity and Performance Management Iss Kirstie S. Ball Personnel Review, **111**(3), 470–488, 2011.

[22] S.Y. Yousafzai, G.R. Foxall, J.G. Pallister, Technology acceptance: a meta-analysis of the TAM: Part 1, Journal of Modelling in Management, 2007, doi:10.1108/17465660710834453.

[23] H.D. Yang, Y. Yoo, "It's all about attitude: Revisiting the technology acceptance model," Decision Support Systems, **38**(1), 19–31, 2004, doi:10.1016/S0167-9236(03)00062-9.

[24] K. Zhu, K.L. Kraemer, S. Xu, "The Process of E-Business Assimilation in Organizations : A Technology Diffusion Perspective," Journal of the Institute for Operations Research and Management Sciences, 2005.

[25] L. Raymond, F. Bergeron, S. Blili, "The Assimilation of E-business in Manufacturing SMEs: Determinants and Effects on Growth and Internationalization," Electronic Markets, 2005, doi:10.1080/10196780500083761.

[26] M.D. Williams, Y.K. Dwivedi, B. Lal, A. Schwarz, "Contemporary trends and issues in IT adoption and diffusion research," Journal of Information Technology, **24**(1), 1–10, 2009, doi:10.1057/jit.2008.30.

[27] I. Arpaci, O. Turetken, Y.C. Yardimci, S. Ozkan, "Organizational Adoption of Information Technologies: A Literature Review Telework View project Sentiment Analysis View project ORGANIZATIONAL ADOPTION OF INFORMATION TECHNOLOGIES: A LITERATURE REVIEW," INTERNATIONAL JOURNAL OF EBUSINESS AND EGOVERNMENT STUDIES, **4**(2), 731–745, 2012.

[28] L. Silva, Post-positivist review of Technology Acceptance Model, Journal of the Association for Information Systems, 2007, doi:10.17705/1jais.00121.

[29] J.W. Moon, Y.G. Kim, "Extending the TAM for a World-Wide-Web context," Information and Management, **38**(4), 217–230, 2001, doi:10.1016/S0378-7206(00)00061-6.

[30] X. Qin, Y. Shi, K. Lyu, Y. Mo, "USING A TAM-TOE MODEL TO EXPLORE FACTORS OF BUILDING INFORMATION MODELLING (BIM) ADOPTION IN THE CONSTRUCTION INDUSTRY," JOURNAL OF CIVIL ENGINEERING AND MANAGEMENT, **26**(3), 463–468, 2020, doi:10.3846/jcem.2020.12176.

[31] P.A. Pavlou, "Consumer acceptance of electronic commerce: Integrating trust and risk with the technology acceptance model," International Journal of Electronic Commerce, **7**(3), 101–134, 2003, doi:10.1080/10864415.2003.11044275.

[32] B. Ramdani, P. Kawalek, O. Lorenzo, "Predicting SMEs' adoption of enterprise systems," Journal of Enterprise Information Management, (22), 10–24, 2009, doi:10.1108/17410390910922796.

[33] M.S. Musawa, E. Wahab, "The adoption of electronic data interchange (EDI) technology by Nigerian SMEs: A conceptual framework," Journal of Business Management and Economics, 2012.

[34] H. Xu, J. Feng, S. Li, "Users-orientated evaluation of building information model in the Chinese construction industry," Automation in Construction, (39), 32-46, 2014, doi:10.1016/j.autcon.2013.12.004.

[35] K.W. Wen, Y. Chen, "E-business value creation in Small and Medium Enterprises: a US study using the TOE framework," International Journal of Electronic Business, **8**(1), 80, 2010, doi:10.1504/ijeb.2010.030717.

[36] T. Oliveira, M.F. Martins, U.N. De Lisboa, "Literature Review of Information Technology Adoption Models at Firm Level," Review of Economics Studies, 2011.

[37] L. Da Chen, J. Tan, "Technology adaptation in E-commerce: Key determinants of virtual stores acceptance," European Management Journal, **22**(1), 74–86, 2004, doi:10.1016/j.emj.2003.11.014.

[38] S. Priyanka, "Technology Acceptance Model: A Survey of Literature," International Journal of Business and Social Research (IJBSR), 2015.

[39] A.Y.L. Chong, B. Lin, K.B. Ooi, M. Raman, "Factors affecting the adoption level of c-commerce: An empirical study," Journal of Computer Information Systems, **50**(2), 13–22, 2009, doi:10.1080/08874417.2009.11645380.

[40] W. Hong, K. Zhu, "Migrating to internet-based e-commerce: Factors affecting e-commerce adoption and migration at the firm level," Information and Management, **43**(3), 204–221, 2006, doi:10.1016/j.im.2005.06.003.

[41] C. Zhang, L. Cui, L. Huang, C. Zhang, "Exploring the role of government in information technology diffusion: An empirical study of IT usage in Shanghai firms," in IFIP International Federation for Information Processing, 393–407, 2007, doi:10.1007/978-0-387-72804-9_26.

[42] A.N. Mishra, P. Konana, A. Barua, "Antecedents and consequences of Internet use in procurement: An empirical investigation of U.S. manufacturing firms," Information Systems Research, **18**(1), 103–120, 2007, doi:10.1287/isre.1070.0115.

[43] N. Rao Kowtha, T. Whai Ip Choon, "Determinants of website development: A study of electronic commerce in Singapore," Information and Management, **39**(3), 227–242, 2001, doi:10.1016/S0378-7206(01)00092-1.

[44] D. Mehran, "Exploring the Adoption of BIM in the UAE Construction Industry for AEC Firms," in Procedia Engineering, 2016, doi:10.1016/j.proeng.2016.04.144.

[45] L. Zhou, L. Dai, D. Zhang, "ONLINE SHOPPING ACCEPTANCE MODEL-A CRITICAL SURVEY OF CONSUMER FACTORS IN ONLINE SHOPPING（自己构造的模型，列表写出了已存在的文献中用于衡量online shopping acceptance的factors，分为两方面：online和shopping）," Journal of Electronic Commerce Research, 2007.

[46] Z. Zakaria, N. Mohamed Ali, A.T. Haron, A.M. Ponting, Z. Abd. Hamid, "Exploring the barriers and driving factors in implementing Building Information Modeling (BIM) in the Malaysian Construction Industry: A Preliminary Study," The Journal of The Institution of Engineers, Malaysia, **58**(12), 7250–7257, 2014.

[47] J. Won, G. Lee, C. Dossick, J. Messner, "Where to Focus for Successful Adoption of Building Information Modeling within Organization," Journal of Construction Engineering and Management, **139**(11), 04013014, 2013, doi:10.1061/(asce)co.1943-7862.0000731.

[48] R. Bose, X. Luo, "Integrative framework for assessing firms' potential to undertake Green IT initiatives via virtualization - A theoretical perspective," Journal of Strategic Information Systems, **110**(2), 269–283, 2011, doi:10.1016/j.jsis.2011.01.003.

Synchronization in a Class of Fractional-order Chaotic Systems via Feedback Controllers: a Comparative Study

Juan Luis Mata-Machuca[*]

Instituto Politecnico Nacional, UPIITA, Department of Advanced Technologies, Mexico City, 07340, Mexico

A R T I C L E   I N F O

A B S T R A C T

In this paper a synchronization methodology of two fractional-order chaotic oscillators under the framework of identical synchronization and master-slave configuration is introduced. The proposed methodology is based on a fractional-order feedback control design under the frame of control theory, the feedback controllers provide synchronization convergence. A comparative study between a proportional control, a nonlinear fractional-order proportional-integral control and an active control is presented. The above is showed via an analysis of the dynamic of the called synchronization error. Numerical experiments using the mathematical model of the fractional-order unified chaotic system and its equivalent electronic circuit corroborate the satisfactory results of the proposed schemes.

1   Introduction

A significant development of chaos occurred after the publication by Lorenz [1] of a work related with the existence of non-periodic solutions in a model formed by nonlinear differential equations. Lorenz's contribution provided the interest in studying deterministic systems that generate dynamic trajectories strongly influenced by sensitivity to initial conditions. However, it was until 1975 when the term chaos was introduced [2], since then chaotic systems have been studied intensively, and this is one important area of current research in physics, mathematics, and engineering. The analysis of nonlinear complex dynamic behaviors has led to important technological application. In particular the analysis of chaotic oscillators has had important advances in process engineering, cryptography of images, secure data transmission, life science, and information processing, between others [3]–[5].

There are several definitions about chaotic systems. However, in general terms, a chaotic system is a deterministic dynamic system that exhibits irregular behavior, similar to random behavior [6, 7]. A very important aspect in relation to chaos theory is the synchronization of chaotic systems. Since Pecora and Carrol [8] showed

that two seemingly random and unpredictable chaotic behaviors can converge in a single trajectory, new expectations arose around chaos theory, trying to solve its control, understanding and prediction.

The synchronization of chaotic systems consists of coupling two or more chaotic systems, after a transitory time, they exhibit identical chaotic oscillations. Synchronization can be solved from the point of view of control theory, designing a slave system which follows the variables of the master system. In the open literature has been presented a lot of important contributions for the design of control schemes for synchronization purposes in chaotic oscillators [9]–[11], observer based controllers [12, 13], adaptive algorithms [14, 15], optimal controllers [16, 17] and so on [18]–[20].

From the above, control theory has been looking for advanced techniques in order to reach a high performance in the operation of processes, in particular with dynamic systems with complex behavior, such as the nonlinear fractional-order systems [21]–[23]. The fractional calculus for the study of dynamic systems with chaotic behavior has emerged as an alternative framework, since it has been proved that it is possible that a class of systems exhibits chaos despite its order is fractional [24]–[27]. Generally, nonlinear systems display complex dynamic behavior as steady state multiplicity, in-

[*]Corresponding Author: Juan Luis Mata-Machuca, Email: jmatam@ipn.mx

stabilities, complex oscillations and so on under different initial conditions, external disturbances and time-varying parameters, leading to chaotic dynamic behaviors. However, besides of the scientific interest on the study and analysis of nonlinear system with exotic dynamic behaviors, the applications for engineering purposes have been growing importantly [28]–[31].

There are many engineering applications based on dynamical systems with fractional operators, for instance: fractional modelling of the human arm dynamics [32], modelling and identification of viscoelastic mechanical systems [33], modelling of electrical systems [34], analysis and control of economics and financial systems [35, 36], vibration and acoustics phenomena [37], modeling of friction in electric machines [38], problems in electrochemistry, biophysics and bioengineering [39]–[41], methods for signal and image processing [42, 43], applications in automatic control, mechatronics and robotics [44]–[46], among others [47]–[51]. However, there are a few practical applications in this field to prove the feasibility of the physical realization of the proposed techniques [52]–[54]. Some works deal with the master-slave synchronization of fractional-order systems via unidirectional linear coupling [55]–[58], where the proposed methods are applied in the synchronization of fractional-order Rössler, Chua, Chen, unified systems and so on.

The main contribution of this work is to achieve the synchronization of a class of fractional-order systems and its verification via the equivalent electronic circuit by means of a proportional control, a nonlinear fractional-order proportional-integral control and an active control. The synchronization implies that all trajectories of the slave system tend to follow all trajectories of the master system. In this sense, the main problem is to find a control input such that the synchronization is possible. The suitable conditions for the synchronization are obtained by solving the dynamical equation of the synchronization error. Furthermore, to verify the effectiveness of the suggested approach we have implemented an electronic circuit using Matlab-Simulink's Simscape library to obtain the synchronization regime between two fractional-order unified chaotic systems for the same order.

2 Fractional-order feedback controllers

The master system of fractional order α can be represented by,

$$D^\alpha x_i = f_i(x_1, x_2, \ldots, x_n), \tag{1}$$

with $x_i(0) = x_{i0}$, $i = 1, 2, \ldots, n$, $x = [x_1, x_2, \ldots, x_n]^T \in \Omega \subset \mathbb{R}^n$ is the state vector, and $f : \Omega \to \mathbb{R}^n$ is a nonlinear continuous function.

In (1), the fractional derivative of x_i is defined as [?],

$$
\begin{aligned}
D^\alpha x_i = {}_{t_0}D_t^\alpha x_i(t) &= \frac{d^\alpha x_i(t)}{dt^\alpha} \\
&= \frac{1}{\Gamma(m-\alpha)} \int_{t_0}^t \frac{d^m x_i(\tau)}{d\tau^m} (t-\tau)^{m-\alpha-1}\, d\tau,
\end{aligned} \tag{2}
$$

where: $\alpha \in \mathbb{R}^+$, $m-1 \le \alpha < m$, $m \in \mathbb{N}$, $\frac{d^m x_i(\tau)}{d\tau^m}$ is the m-th time derivative of x_i and Γ is the gamma function.

2.1 Proportional control

Let us propose the controlled slave system of fractional order α as follows,

$$
\begin{aligned}
D^\alpha z_i &= f_i(z_1, z_2, \ldots, z_n) + u_i \tag{3} \\
u_i &= k_i(x_i - z_i) \tag{4}
\end{aligned}
$$

with $z_i(0) = z_{i0}$, $i = 1, 2, \ldots, n$, $z = [z_1, z_2, \ldots, z_n]^T \in \Omega \subset \mathbb{R}^n$ is the state vector of the slave system, and k_i is the proportional gain.

Let us define the synchronization error as,

$$\varepsilon_i = x_i - z_i. \tag{5}$$

The synchronization performance is obtained by means of the analysis of the dynamics of the synchronization error.

First, we take the time derivative of order α of (5),

$$D^\alpha \varepsilon_i = D^\alpha x_i - D^\alpha z_i \tag{6}$$

Now, replacing the fractional dynamics of equations (1) and (3) into (6),

$$D^\alpha \varepsilon_i + k_i \varepsilon_i = f_i(x) - f_i(z) \tag{7}$$

Then, the solution of (7) is given by,

$$
\begin{aligned}
\varepsilon_i(t) = {}&\varepsilon_{i0} E_\alpha(-k_i t^\alpha) + \\
&+ \int_0^t (t-\tau)^{\alpha-1} E_{\alpha,\alpha}(k_i(t-\tau)^\alpha)\left[f_i(x) - f_i(z)\right] d\tau
\end{aligned} \tag{8}
$$

where $\varepsilon_{i0} = x_{i0} - z_{i0}$.

In (8), the Mittag-Leffler function is defined as [?],

$$E_\alpha(q) = \sum_{j=0}^\infty \frac{q^j}{\Gamma(\alpha j + 1)}, \quad q \in \mathbb{C},\ \mathbb{R}e(\alpha) > 0 \tag{9}$$

$$E_{\alpha,\alpha}(q) = \sum_{j=0}^\infty \frac{q^i}{\Gamma(\alpha j + \alpha)}, \quad q,\ \alpha \in \mathbb{C},\ \mathbb{R}e(\alpha) > 0 \tag{10}$$

To guarantee the convergence of the synchronization error in (8), Assumption 1 and 2 are introduced,

Assumption 1 $|f_i(x) - f_i(z)| \le L_i < \infty$

Assumption 2 *The proportional gain is positive.*

Applying Assumption 1 in (8) we have,

$$
\begin{aligned}
|\varepsilon_i(t)| \le {}&|\varepsilon_{i0} E_\alpha(-k_i t^\alpha)| + \\
&+ L_i \int_0^t |(t-\tau)^{\alpha-1} E_{\alpha,\alpha}(-k_i(t-\tau)^\alpha)| d\tau
\end{aligned}
$$

Finally, by Assumption 2,

$$\lim_{t\to\infty} |\varepsilon_i(t)| \le \frac{L_i}{k_i} \tag{11}$$

From the previous analysis, the following proposition is established.

Proposition 1 *If Assumptions 1 and 2 are fulfilled, then the synchronization of the master system (1) and the controlled slave system (3)-(4) is achieved, where, the trajectories of ε_i belongs to a closed ball with radius proportional to L_i/k_i.* □

2.2 Nonlinear fractional-order PI control

Let us consider (1) as the master system. In this case, the slave system is described by,

$$
\begin{align}
D^\alpha z_i &= f_i(z_1, z_2, \ldots, z_n) + u_i, \quad i = 1, 2, \ldots, n \tag{12} \\
u_i &= f_i(x) - f_i(z) + k_i \varepsilon_i + K_{I_i} e_i \tag{13} \\
D^\alpha e_i &= \varepsilon_i \tag{14}
\end{align}
$$

where, $\varepsilon_i = x_i - z_i$, k_i is the proportional gain and K_{I_i} is the integral gain.

Property 1 (see [59]) *Let I^α be the fractional integral of order α. Then,*

$$
I^\alpha(D^\alpha e_i) = e_i \tag{15}
$$

Applying Property 1 in both sides of (14),

$$
e_i = I^\alpha(D^\alpha e_i) = I^\alpha \varepsilon_i \tag{16}
$$

We analyze the dynamics of the synchronization error,

$$
\begin{align}
D^\alpha \varepsilon_i &= f_i(x_1, x_2, \ldots, x_n) - f_i(z_1, z_2, \ldots, z_n) - u_i \tag{17} \\
u_i &= f_i(x) - f_i(z) + k_i \varepsilon_i + K_{I_i} e_i \tag{18} \\
D^\alpha e_i &= \varepsilon_i \tag{19}
\end{align}
$$

Proposition 2 *Let P be a matrix defined by,*

$$
P = \begin{bmatrix} -k_i & -k_{I_i} \\ 1 & 0 \end{bmatrix}
$$

For $0 < \alpha < 1$, the interconnected system (17)-(19) is asymptotically stable if,

$$
|arg(eig(P))| > \frac{\alpha \pi}{2} \tag{20}
$$

where, $eig(P)$ are the eigenvalues of P.

Proof. The closed-loop system could be expressed as,

$$
\begin{bmatrix} D^\alpha \varepsilon_i \\ D^\alpha e_i \end{bmatrix} = \underbrace{\begin{bmatrix} -k_i & -k_{I_i} \\ 1 & 0 \end{bmatrix}}_{P} \begin{bmatrix} \varepsilon_i \\ e_i \end{bmatrix} \tag{21}
$$

The eigenvalues of P are obtained in terms of proportional and integral gains,

$$
eig(P) = \frac{-k_i \pm \sqrt{k_i^2 - 4K_{I_i}}}{2}
$$

Hence, (21) is asymptotically stable if $|arg(eig(P))| > \frac{\alpha \pi}{2}$. $\square$

2.3 Active control

Let us represent the master system (1) as,

$$
D^\alpha x = Ax + g(x), \tag{22}
$$

In (22), $g : \Omega \to \mathbb{R}^n$ is a nonlinear continuous function and the matrix $A \in \mathbb{R}^{n \times n}$ is defined by,

$$
A = \begin{bmatrix} a_{11} & a_{12} & \cdots & a_{1n} \\ a_{21} & a_{22} & \cdots & a_{2n} \\ \vdots & \vdots & & \vdots \\ a_{n1} & a_{n2} & \ldots & a_{nn} \end{bmatrix} = \begin{bmatrix} A_1 \\ A_2 \\ \vdots \\ A_n \end{bmatrix} \tag{23}
$$

where, a_{ij} are constant coefficients and $A_i = \begin{bmatrix} a_{i1} & a_{i2} & \cdots & a_{in} \end{bmatrix}$ denotes the i-th row of matrix A, for $i = 1, 2, \ldots, n$.

Then, master system (22) can be rewritten as,

$$
\begin{align}
D^\alpha x_i &= A_i x + g_i(x) \\
&= \sum_{j=1}^n a_{ij} x_j + g_i(x), \quad i = 1, 2, \ldots, n \tag{24}
\end{align}
$$

The corresponding slave system is proposed as,

$$
D^\alpha z_i = \sum_{j=1}^n a_{ij} z_j + g_i(z) + u_i, \quad i = 1, 2, \ldots, n \tag{25}
$$

Then, the dynamics of the synchronization error is obtained by (24) and (25),

$$
D^\alpha \varepsilon_i = \sum_{j=1}^n a_{ij} \varepsilon_j + g_i(x) - g_i(z) - u_i, \quad i = 1, 2, \ldots, n \tag{26}
$$

Proposition 3 *Equation (26) is asymptotically stable if the signal u_i is active,*

$$
u_i = \sum_{j=1, \ j \neq i}^n a_{ij} \varepsilon_j + g_i(x) - g_i(z) + k_i \varepsilon_i, \quad i = 1, 2, \ldots, n \tag{27}
$$

and the following condition is satisfied,

$$
k_i > a_{ii} \tag{28}
$$

Proof. Substituting 27 into (26),

$$
D^\alpha \varepsilon_i = (-k_i + a_{ii}) \varepsilon_j, \quad i = 1, 2, \ldots, n \tag{29}
$$

or, in matrix form

$$
D^\alpha \varepsilon = \underbrace{\begin{bmatrix} -k_1 + a_{11} & 0 & \ldots & 0 \\ 0 & -k_2 + a_{22} & & \vdots \\ \vdots & & \ddots & 0 \\ 0 & \ldots & 0 & -k_n + a_{nn} \end{bmatrix}}_{\bar{A}} \varepsilon \tag{30}
$$

Matrix $\bar{A}$ is Hurwitz stable if $k_i > a_{ii}$, $i = 1, 2, \ldots, n$. Then (30) is asymptotically stable. $\square$

3 The fractional-order unified chaotic system

Consider the fractional-order master system [54],

$$
\begin{aligned}
D^\alpha x_1 &= (25\beta + 10)(x_2 - x_1) \\
D^\alpha x_2 &= 28x_1 - x_2 + 29\beta x_2 - 35\beta x_1 - 10x_1 x_3 \\
D^\alpha x_3 &= 10x_1 x_2 - \frac{\beta + 8}{3} x_3
\end{aligned}
\tag{31}
$$

With $\beta = 1$ and $\alpha = 0.9$ system (31) exhibits chaotic behaviour, in the sense of Definition 1.

Definition 1 ([6]) *An attractor is said to be chaotic if it is bounded and all the trajectories starting form it are Lyapunov unstable. Then, a dynamic system is chaotic if it has at least one chaotic attractor.*

System (31) is simulated through the Matlab-Simulink diagram shown in Figure 1, where blocks F1, F2 and F3 correspond to the approximation of the integral operator with order $\alpha = 0.9$.


```
function Dx = fcn(X)
beta=1;

Dx1=(25*beta+10)*(X(2)-X(1));
Dx2=28*X(1)-X(2)+29*beta*X(2)-35*beta*X(1)-10*X(1)*X(3);
Dx3=10*X(1)*X(2)-((beta+8)/3)*X(3);
Dx=[Dx1;Dx2;Dx3];
```
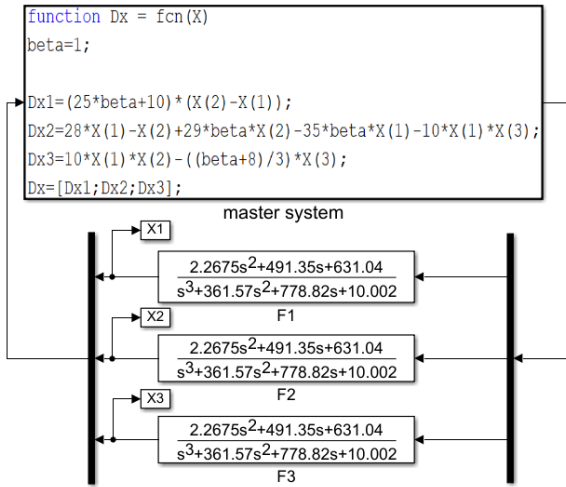
Figure 1: Simulation of system (31) using Matlab-Simulink

For simulation purposes, initial condition of block F1, was set to -0.001. Figure 2 shows the numerical simulation of system (31) via the phase portraits.

Now, in order to illustrate the behavior of system (31), we change the weight parameters (α, β). The simulation results are given in Figure 3 with parameters: (a) $\alpha = 0.9$, $\beta = 0$, (b) $\alpha = 0.9$, $\beta = -1$, (c) $\alpha = 0.8$, $\beta = 0.5$ and (d) $\alpha = 0.7$, $\beta = 1$. Clearly, system (31) is not chaotic with these set of parameters, where the integral operator with orders $\alpha = 0.8$ and $\alpha = 0.7$ is defined by [24],

$$
\frac{1}{s^{0.8}} \approx \frac{5.235s^3 + 1453s^2 + 5306s + 254.9}{s^4 + 658.1s^3 + 5700s^2 + 658.2s + 1}
\tag{32}
$$

and

$$
\frac{1}{s^{0.7}} \approx \frac{5.406s^4 + 177.6s^3 + 209.6s^2 + 9.197s + 0.01450}{s^5 + 88.12s^4 + 279.2s^3 + 33.30s^2 + 1.927s + 0.0002276}
\tag{33}
$$
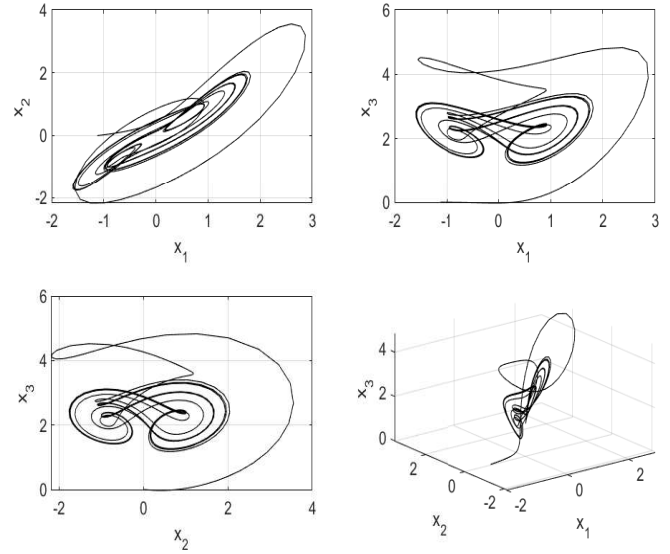
Figure 2: Simulation results of system (31), $\beta = 1$ and $\alpha = 0.9$.
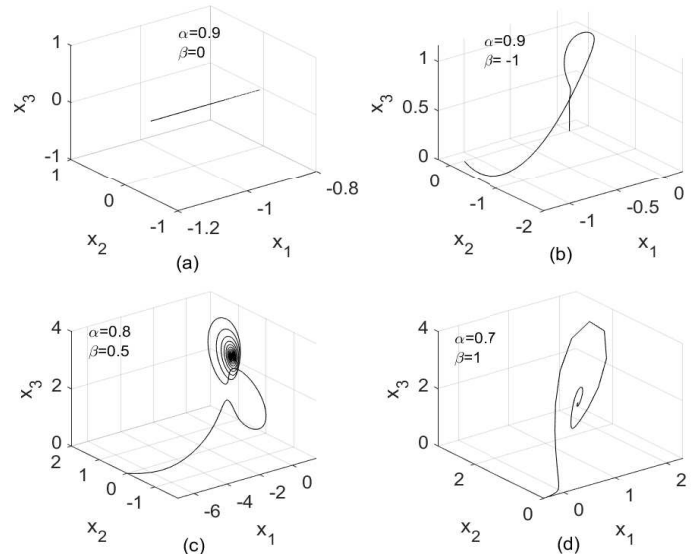
Figure 3: Phase portraits of system (31) with different values of (α, β)..

4 Synchronization results and discussion

The fractional-order slave system that synchronizes with system (31) is represented as,

$$
\begin{aligned}
D^\alpha z_1 &= (25\beta + 10)(z_2 - z_1) + u_1 \\
D^\alpha z_2 &= 28z_1 - z_2 + 29\beta z_2 - 35\beta z_1 - 10z_1 z_3 + u_2 \\
D^\alpha z_3 &= 10z_1 z_2 - \frac{\beta + 8}{3} z_3 + u_3
\end{aligned}
\tag{34}
$$

where $\beta = 1$, $\alpha = 0.9$ and u_1, u_2 and u_3 are the control signals.

It is necessary to calculate the control gains values. First, for the proportional control, we obtain the constants L_i over the bounded set $\Omega = \{x \in \mathbb{R}^n \mid |x_i| \leq M_i\}$,

$$L_i = \max_{1 \leq i \leq n} \|f_i'(x)\| \tag{35}$$

where $f_i'(x)$ is the Jacobian matrix.

Then, considering that $M_1 \approx 2$, $M_2 \approx 3$ and $M_3 \approx 4$, we have that $L_1 = 35$, $L_2 = 47$, and $L_3 = 30$.

According to Proposition 1, the maximum synchronization errors are defined as

$$\varepsilon_{i_{max}} = \frac{L_i}{k_i} = 0.05 \tag{36}$$

In Equation (36) we consider the synchronization errors are bounded by 0.05, they are acceptable for complete practical synchronization. Equation (36) yields to $k_1 = 700$, $k_2 = 940$, and $k_3 = 600$.

For the nonlinear PI controller, the gain values are obtained in order to guarantee a settling time of 0.02s and an overshoot of 1% in the three coordinates, then $ki = 400$ and $K_{I_i} = 58613$, for $i = 1, 2, 3$. And for the active controller we have the following conditions,

$$k_1 > -25\beta + 10 \tag{37}$$

$$k_2 > 29\beta - 1 \tag{38}$$

$$k_3 > -\frac{\beta + 8}{3} \tag{39}$$

In this case, we choose $k_1 = 200$, $k_2 = 100$ and $k3 = 100$.

Figure 4 shows the phase portraits of the master and slave systems when the control signals are off, clearly all systems are unsynchronized due to the initial conditions are different. However, when the feedback controllers are activated the synchronization is achieved since the trajectories of the controlled slave system tend to follow the trajectories of the master system.
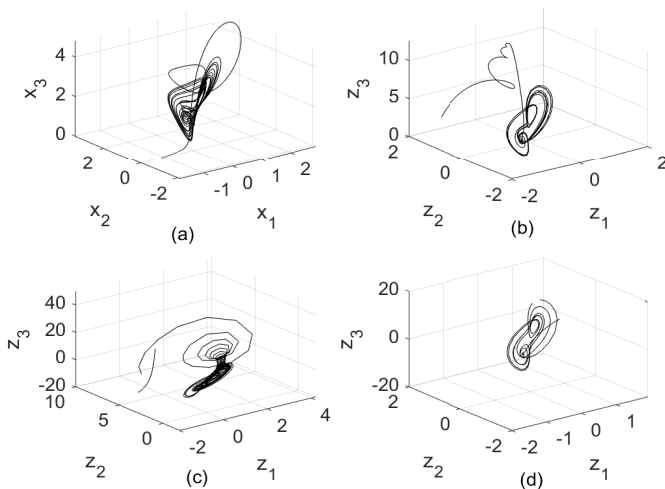
Figure 4: Unsynchronized systems.

In Figure 5 the synchronization performance is verified via the synchronization errors. We observe that the synchronization errors converge to zero when the feedback control is activated. As we can note, the corresponding slave trajectory reach almost immediately the master trajectory for the proportional control, also, when the nonlinear PI control acts, the corresponding trajectory has a higher oscillatory overshoot and a settling time of 0.02s, and for the active control, the synchronization errors converge exponentially to zero at 0.02 s.
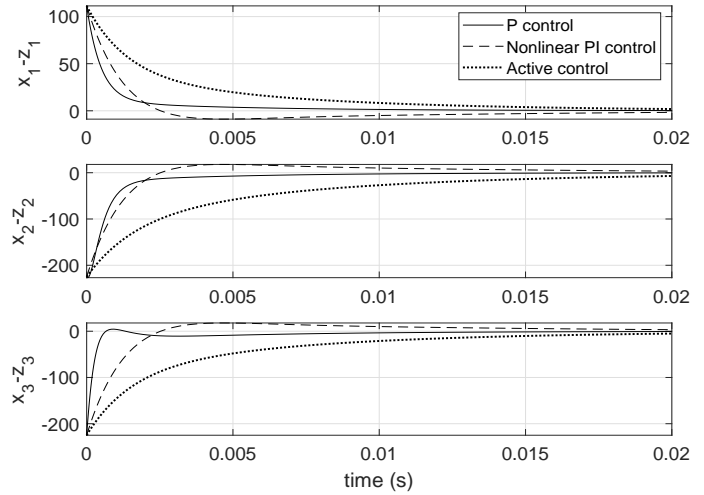
Figure 5: Synchronization errors.

The above-mentioned behaviors for the state variables under feedback controllers can be explained for the performance of the three controllers under comparison. Figure 6 is related to the control effort performance, it can be observed that the control effort for the proportional controller is very high due to the magnitude presented at the startup and transient condition. On the other hand, PI and active controllers show a smooth behavior, leading the trajectory to the controlled slave system to the required master trajectory in a larger settling time.
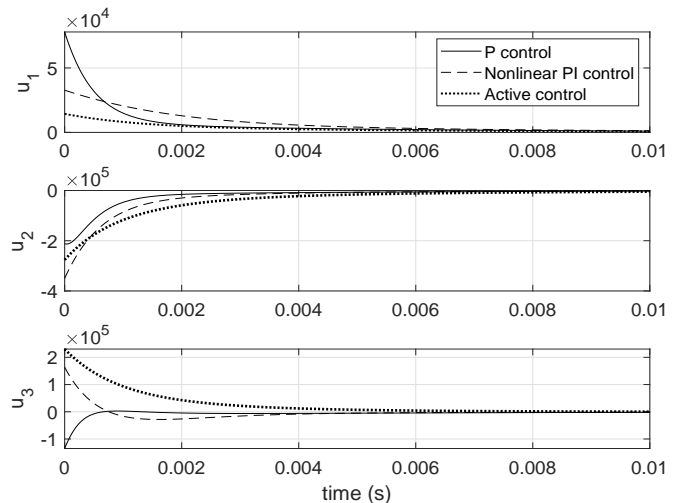
Figure 6: Control signals.

5   Equivalent electronic circuit

System (31) is translated to the electric circuit shown in Figure 7.
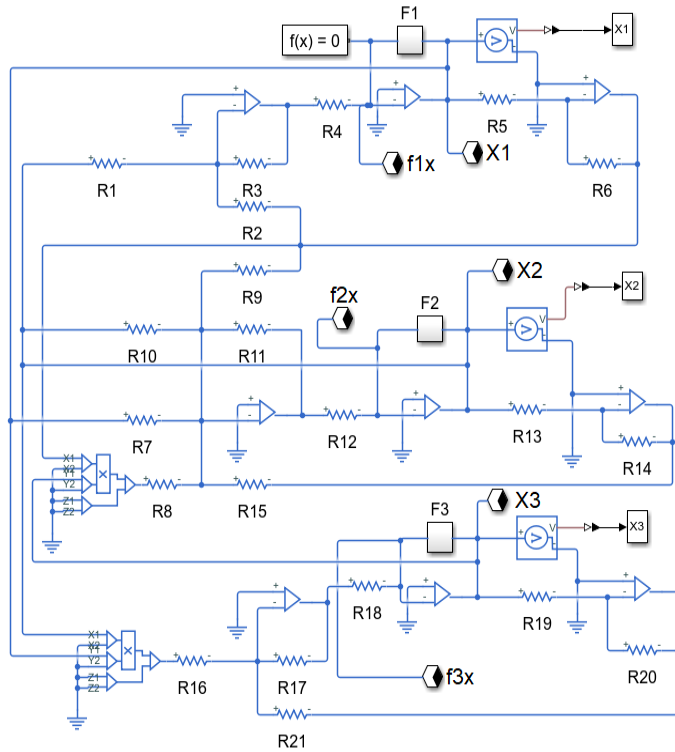
Figure 7: Electrical model of master system (31) using Simulink's Simscape library.

Component values are taken as: $R_4 = R_{13} = R_{18} = 100\,k\Omega$, $R_1 = R_5 = R_7 = R_8 = R_{10} = R_{14} = R_{16} = R_{20} = 10\,k\Omega$, $R_2 = R_3 = R_6 = R_{21} = 33\,k\Omega$, $R_9 = R_{11} = R_{15} = 27\,k\Omega$ and $R_{12} = R_{17} = R_{19} = 100\,k\Omega$.

Fractional integrators blocks F1, F2 and F3 are represented as $\frac{1}{s^{0.9}}$. Figure 8 shows the approximation of $\frac{1}{s^{0.9}}$ as an electric circuit using the Simscape libraries.
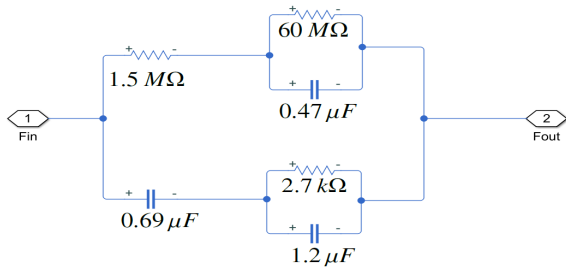
Figure 8: Integrator blocks F1, F2,..., F12.

6   Verification of the master-slave synchronization

The synchronization is verified via the equivalent electronic circuits of master and slave systems. The controlled slave electronic circuit is given in Figure 9, where u_1, u_2 and u_3 are the control inputs

introduced in Section 2. In order to obtain $-z_1$, $-z_2$ and $-z_3$, in this circuit, for each signal z_1, z_2 and z_3 is added an inverting operational amplifier with unity gain, the value of R is equal to 10kΩ. To avoid the crossing of physical lines we employ connection labels. The label block ◑ makes connections between two blocks without using lines.
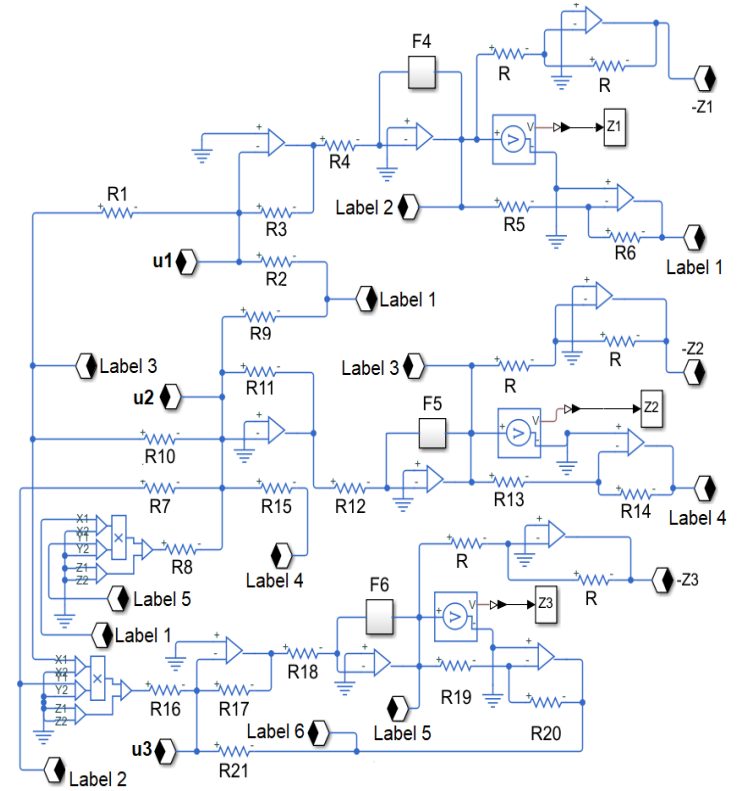
Figure 9: Electrical circuit schematic for the slave system (34).

Master circuit of Figure 7 and slave circuit of Figure 9 are coupled since the control inputs require information signals from both circuits.

The equivalent circuit for the proportional control (4) is shown in Figure 10. Resistors R_{P1}, R_{P2} and R_{P3} are related with the control gains of Section 4 as follows,

$$R_{P1} = 10\frac{R_3}{k_1} = 471\ \Omega \tag{40}$$

$$R_{P2} = 10\frac{R_{11}}{k_2} = 287\ \Omega \tag{41}$$

$$R_{P3} = 10\frac{R_{17}}{k_3} = 1.67\ k\Omega \tag{42}$$
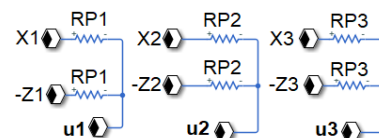
Figure 10: Proportional control.

The nonlinear fractional-order PI control (13)-(14) is proposed by means of the circuit of Figure 11.

where, $F_i(x) = \sum\limits_{j=1,\ j\neq i}^{n} a_{ij}x_j + g_i(x)$ and $F_i(z) = \sum\limits_{j=1,\ j\neq i}^{n} a_{ij}z_j + g_i(z)$.
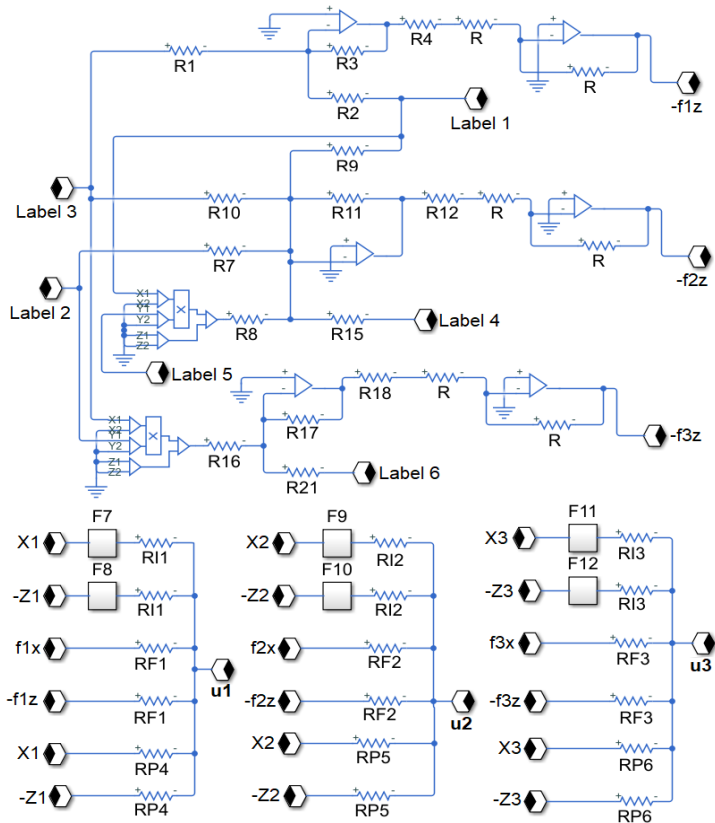
Figure 11: Nonlinear fractional-order PI control.
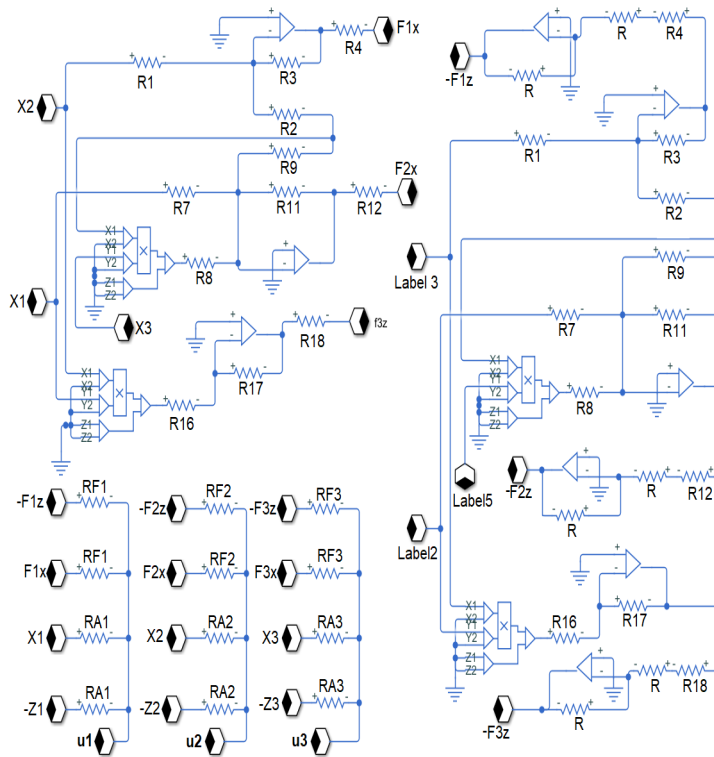
Figure 12: Active control.

The parameter values are obtained as,

$$R_{P4} = 10\frac{R_3}{k_1} = 825\ \Omega \tag{43}$$

$$R_{P5} = 10\frac{R_{11}}{k_2} = 675\ \Omega \tag{44}$$

$$R_{P6} = 10\frac{R_{17}}{k_3} = 250\ \Omega \tag{45}$$

$$R_{I1} = 10\frac{R_3}{K_{I_1}} = 5.63\ \Omega \tag{46}$$

$$R_{I2} = 10\frac{R_{11}}{K_{I_2}} = 4.6\ \Omega \tag{47}$$

$$R_{I3} = 10\frac{R_{17}}{K_{I_3}} = 17\ \Omega \tag{48}$$

$$R_{F1} = 10\ R_3 = 330\ \text{k}\Omega \tag{49}$$

$$R_{F2} = 10\ R_{11} = 270\ \text{k}\Omega \tag{50}$$

$$R_{F3} = 10\ R_{17} = 1\ \text{M}\Omega \tag{51}$$

Finally, the equivalent circuit for the active control (27) is given by Figure 12. The active control (27) has been rewritten as,

$$u_i = F_i(x) - F_i(z) + k_i\varepsilon_i, \quad i = 1, 2, \ldots, n \tag{52}$$

The corresponding parameter values are: $R_{F1} = 330$ kΩ, $R_{F2} = 270$ kΩ, $R_{F3} = 10\ R_{17} = 1$ MΩ and,

$$R_{A1} = 10\frac{R_3}{k_1} = 1.65\ \text{k}\Omega \tag{53}$$

$$R_{A2} = 10\frac{R_{11}}{k_2} = 2.7\ \text{k}\Omega \tag{54}$$

$$R_{A3} = 10\frac{R_{17}}{k_3} = 10\ \text{k}\Omega \tag{55}$$

Figure 13 shows the phase portraits of the master-slave synchronization obtained by means of the equivalent electronic circuits given by Figures 7 and 9 along with the control inputs of Figures 10, 11 and 12. For all simulations, initial voltage on capacitor of $0.69\,\mu F$ takes several arbitrary values: 1 V (block F1), -2 V (block F4), 1 V (block F5), 1 V (block F6), while the rest of capacitors remain at 0 V. Notably, the whole phase portrait of the controlled slave system is synchronized with the corresponding phase portrait of the master system using the proposed controllers, for arbitrary initial conditions. However, an important characteristic is that the nonlinear fractional-order PI control and the active control lead to complex circuit structures.
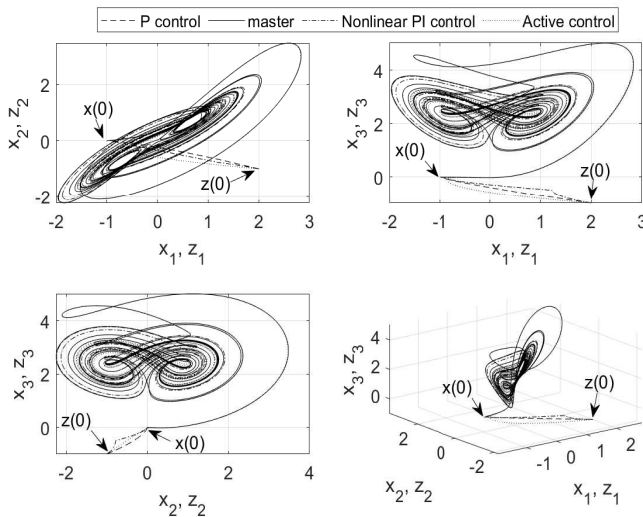
Figure 13: Master-slave synchronization.

7 Conclusions

This work studied the master-slave synchronization in a class of chaotic systems with fractional-order via feedback control. First, the feedback controllers were designed. In this sense, a proportional control was proposed, it guarantees that the synchronization error is bounded, as well as, a nonlinear fractional-order PI control and an active control were introduced, where the stability of the closed-loop system depends on the control gains, here for both controllers the synchronization error is asymptotically stable. Next, as application example, the fractional-order unified chaotic system was considered as master system. In fact, a set of numerical simulations based on the mathematical models of master and slave system showed that the synchronization is fulfilled by means of the proposed feedback controllers. It is important to mention that the proportional control exhibited the higher control effort, which could be a restriction in another class of systems, for instance, in those involving actuators. On other hand, in the transient condition, the active control is slower than the other ones. Finally, the synchronization was verified with success using the equivalent electronic circuits. As can be noticed, the proportional control has a simple circuit structure.

Conflict of interest   The author declares no conflict of interest.

References

[1] E. N. Lorenz, "Deterministic Nonperiodic Flow," Journal of the Atmospheric Sciences, **20**, 1963, doi:10.1175/1520-0469(1963)020⟨0130:dnf⟩2.0.co;2.

[2] T.-Y. Li, J. A. Yorke, "Period Three Implies Chaos," The American Mathematical Monthly, **82**, 1975, doi:10.2307/2318254.

[3] G. Li, B. Zhang, "A Novel Weak Signal Detection Method via Chaotic Synchronization Using Chua's Circuit," IEEE Transactions on Industrial Electronics, **64**, 2017, doi:10.1109/TIE.2016.2620103.

[4] M. H. Abd, F. R. Tahir, G. A. Al-Suhail, V. T. Pham, "An adaptive observer synchronization using chaotic time-delay system for secure communication," Nonlinear Dynamics, **90**, 2017, doi:10.1007/s11071-017-3825-2.

[5] H. Li, X. Liao, M. Luo, "A novel non-equilibrium fractional-order chaotic system and its complete synchronization by circuit implementation," Nonlinear Dynamics, **68**, 2012, doi:10.1007/s11071-011-0210-4.

[6] A. L. Fradkov, Cybernetical Physics, From Control of Chaos to Quantum Control, 2007.

[7] R. Femat, G. Solis-Perales, "Robust synchronization of chaotic systems via feedback," 2008, doi:10.1007/978-3-540-69307-9.

[8] L. M. Pecora, T. L. Carroll, "Synchronization in chaotic systems," Physical Review Letters, **64**, 1990, doi:10.1103/PhysRevLett.64.821.

[9] S. Boccaletti, J. Kurths, G. Osipov, D. Valladares, C. Zhou, "The synchronization of chaotic systems," Physics reports, **366**(1-2), 1–101, 2002.

[10] L. Huang, R. Feng, M. Wang, "Synchronization of chaotic systems via nonlinear control," Physics Letters, Section A: General, Atomic and Solid State Physics, **320**, 2004, doi:10.1016/j.physleta.2003.11.027.

[11] L. M. Pecora, T. L. Carroll, "Synchronization of chaotic systems," Chaos: An Interdisciplinary Journal of Nonlinear Science, **25**(9), 097611, 2015.

[12] Y. Zhao, W. Zhang, H. Su, J. Yang, "Observer-Based Synchronization of Chaotic Systems Satisfying Incremental Quadratic Constraints and Its Application in Secure Communication," IEEE Transactions on Systems, Man, and Cybernetics: Systems, **50**(12), 5221–5232, 2020, doi:10.1109/TSMC.2018.2868482.

[13] S. Mohammadpour, T. Binazadeh, "Observer-based synchronization of uncertain chaotic systems subject to input saturation," Transactions of the Institute of Measurement and Control, **40**, 2018, doi:10.1177/0142331217705435.

[14] A. Das, F. L. Lewis, "Distributed adaptive control for synchronization of unknown nonlinear networked systems," Automatica, **46**, 2010, doi:10.1016/j.automatica.2010.08.008.

[15] S. Wen, Z. Zeng, T. Huang, "Adaptive synchronization of memristor-based Chua's circuits," Physics Letters, Section A: General, Atomic and Solid State Physics, **376**, 2012, doi:10.1016/j.physleta.2012.08.021.

[16] B. Naderi, H. Kheiri, A. Heydari, R. Mahini, "Optimal Synchronization of Complex Chaotic T-Systems and Its Application in Secure Communication," Journal of Control, Automation and Electrical Systems, **27**, 2016, doi:10.1007/s40313-016-0245-3.

[17] W. D. Chang, "PID control for chaotic synchronization using particle swarm optimization," Chaos, Solitons and Fractals, **39**, 2009, doi:10.1016/j.chaos.2007.01.064.

[18] Z. Liu, "Design of nonlinear optimal control for chaotic synchronization of coupled stochastic neural networks via Hamilton–Jacobi–Bellman equation," Neural Networks, **99**, 2018, doi:10.1016/j.neunet.2018.01.003.

[19] C. Huang, J. Cao, "Active control strategy for synchronization and anti-synchronization of a fractional chaotic financial system," Physica A: Statistical Mechanics and its Applications, **473**, 2017, doi:10.1016/j.physa.2017.01.009.

[20] R. Martínez-Guerra, J. L. Mata-Machuca, "Fractional generalized synchronization in a class of nonlinear fractional order systems," Nonlinear Dynamics, **77**(4), 1237–1244, 2014.

[21] X. J. Wen, Z. M. Wu, J. G. Lu, "Stability analysis of a class of nonlinear fractional-order systems," IEEE Transactions on Circuits and Systems II: Express Briefs, **55**, 2008, doi:10.1109/TCSII.2008.2002571.

[22] Y. Li, Y. Q. Chen, I. Podlubny, "Mittag-Leffler stability of fractional order nonlinear dynamic systems," Automatica, **45**, 2009, doi:10.1016/j.automatica.2009.04.003.

[23] S. Liu, S. Jiang, X. Li, X. F. Zhou, "Lyapunov stability analysis of fractional nonlinear systems," Applied Mathematics Letters, **51**, 2016, doi:10.1016/j.aml.2015.06.018.

[24] T. T. Hartley, C. F. Lorenzo, H. K. Qammer, "Chaos in a Fractional Order Chua's System," IEEE Transactions on Circuits and Systems I: Fundamental Theory and Applications, **42**, 1995, doi:10.1109/81.404062.

[25] C. Li, G. Peng, "Chaos in Chen's system with a fractional order," Chaos, Solitons and Fractals, **22**, 2004, doi:10.1016/j.chaos.2004.02.013.

[26] V. Daftardar-Gejji, S. Bhalekar, "Chaos in fractional ordered Liu system," Computers and Mathematics with Applications, **59**, 2010, doi:10.1016/j.camwa.2009.07.003.

[27] Z. Wang, X. Huang, G. Shi, "Analysis of nonlinear dynamics and chaos in a fractional order financial system with time delay," Computers and Mathematics with Applications, **62**, 2011, doi:10.1016/j.camwa.2011.04.057.

[28] H. G. Sun, Y. Zhang, D. Baleanu, W. Chen, Y. Q. Chen, "A new collection of real world applications of fractional calculus in science and engineering," Communications in Nonlinear Science and Numerical Simulation, **64**, 2018, doi:10.1016/j.cnsns.2018.04.019.

[29] J. A. T. MacHado, M. F. Silva, R. S. Barbosa, I. S. Jesus, C. M. Reis, M. G. Marcos, A. F. Galhano, "Some applications of fractional calculus in engineering," Mathematical Problems in Engineering, **2010**, 2010, doi:10.1155/2010/639801.

[30] J. Zarei, M. Tabatabaei, "Fractional order unknown input filter design for fault detection of discrete fractional order linear systems," Transactions of the Institute of Measurement and Control, **40**, 2018, doi:10.1177/0142331217746493.

[31] G. C. Wu, Z. G. Deng, D. Baleanu, D. Q. Zeng, "New variable-order fractional chaotic systems for fast image encryption," Chaos, **29**, 2019, doi:10.1063/1.5096645.

[32] I. Tejado, D. Valério, P. Pires, J. Martins, "Fractional order human arm dynamics with variability analyses," Mechatronics, **23**, 2013, doi:10.1016/j.mechatronics.2013.05.003.

[33] J. J. D. Espíndola, J. M. D. S. Neto, E. M. Lopes, "A generalised fractional derivative approach to viscoelastic material properties measurement," volume 164, 2005, doi:10.1016/j.amc.2004.06.099.

[34] J. Sabatier, O. P. Agrawal, J. A. T. Machado, Advances in fractional calculus: Theoretical developments and applications in physics and engineering, 2007, doi:10.1007/978-1-4020-6042-7.

[35] W.-C. Chen, "Nonlinear dynamics and chaos in a fractional-order financial system," Chaos, Solitons and Fractals, **36**(5), 1305–1314, 2008, doi:https://doi.org/10.1016/j.chaos.2006.07.051.

[36] S. Dadras, H. R. Momeni, "Control of a fractional-order economical system via sliding mode," Physica A: Statistical Mechanics and its Applications, **389**, 2010, doi:10.1016/j.physa.2010.02.025.

[37] D. Klatt, R. L. Magin, F. Mainardi, T. J. Royston, N. C. Perkins, I. Y. Shen, "Special section: Fractional calculus in vibration and acoustics," 2014, doi:10.1115/1.4027482.

[38] R. Cipin, C. Ondrusek, R. Huzlík, "Fractional-order model of DC motor," 2014, doi:10.1007/978-3-319-02294-9_46.

[39] R. L. Magin, "Fractional calculus in bioengineering," 2004, doi:10.1615/CritRevBiomedEng.v32.10.

[40] K. B. Oldham, "Fractional differential equations in electrochemistry," Advances in Engineering Software, **41**, 2010, doi:10.1016/j.advengsoft.2008.12.012.

[41] R. L. Magin, "Fractional calculus models of complex dynamics in biological tissues," Computers and Mathematics with Applications, **59**, 2010, doi:10.1016/j.camwa.2009.08.039.

[42] P. Ghamisi, M. S. Couceiro, J. A. Benediktsson, N. M. Ferreira, "An efficient method for segmentation of images based on fractional calculus and natural selection," Expert Systems with Applications, **39**, 2012, doi:10.1016/j.eswa.2012.04.078.

[43] H. Sheng, Y. Chen, T. Qiu, Fractional processes and fractional-order signal processing: techniques and applications, Springer Science & Business Media, 2011.

[44] S. Ghasemi, A. Tabesh, J. Askari-Marnani, "Application of fractional calculus theory to robust controller design for wind turbine generators," IEEE Transactions on Energy Conversion, **29**, 2014, doi:10.1109/TEC.2014.2321792.

[45] R. E. Gutiérrez-Carvajal, L. F. D. Melo, J. M. Rosário, J. A. MacHado, "Condition-based diagnosis of mechatronic systems using a fractional calculus approach," International Journal of Systems Science, **47**, 2016, doi:10.1080/00207721.2014.978833.

[46] L. B. G. Bozzini, "Fractional-order derivatives and their application to the position control of robots," International Journal of Mechanics and Control, 39, 2009.

[47] C. Li, G. Chen, "Chaos and hyperchaos in the fractional-order Rössler equations," Physica A: Statistical Mechanics and its Applications, **341**, 2004, doi:10.1016/j.physa.2004.04.113.

[48] W. H. Deng, C. P. Li, "Chaos synchronization of the fractional Lü system," Physica A: Statistical Mechanics and its Applications, **353**, 2005, doi:10.1016/j.physa.2005.01.021.

[49] C. Li, X. Liao, J. Yu, "Synchronization of fractional order chaotic systems," Physical Review E - Statistical Physics, Plasmas, Fluids, and Related Interdisciplinary Topics, **68**, 2003, doi:10.1103/PhysRevE.68.067203.

[50] R. Martínez-Martínez, J. Mata-Machuca, R. Martínez-Guerra, J. León, G. Fernández-Anaya, "Synchronization of nonlinear fractional order systems," Applied Mathematics and Computation, **218**, 2011, doi:10.1016/j.amc.2011.08.075.

[51] J. D. Gabano, T. Poinot, "Fractional modelling and identification of thermal systems," Signal Processing, **91**, 2011, doi:10.1016/j.sigpro.2010.02.005.

[52] M. F. Tolba, A. M. AbdelAty, N. S. Soliman, L. A. Said, A. H. Madian, A. T. Azar, A. G. Radwan, "FPGA implementation of two fractional order chaotic systems," AEU - International Journal of Electronics and Communications, **78**, 2017, doi:10.1016/j.aeue.2017.04.028.

[53] K. Rajagopal, A. Karthikeyan, A. K. Srinivasan, "FPGA implementation of novel fractional-order chaotic systems with two equilibriums and no equilibrium and its adaptive sliding mode synchronization," Nonlinear Dynamics, **87**, 2017, doi:10.1007/s11071-016-3189-z.

[54] X. R. Chen, C. X. Liu, F. Q. Wang, "Circuit realization of the fractional-order unified chaotic system," Chinese Physics B, **17**, 2008, doi:10.1088/1674-1056/17/5/022.

[55] L. G. Yuan, Q. G. Yang, "Parameter identification and synchronization of fractional-order chaotic systems," Communications in Nonlinear Science and Numerical Simulation, **17**, 2012, doi:10.1016/j.cnsns.2011.04.005.

[56] J. G. Lu, "Chaotic dynamics of the fractional-order Lü system and its synchronization," Physics Letters, Section A: General, Atomic and Solid State Physics, **354**, 2006, doi:10.1016/j.physleta.2006.01.068.

[57] P. Zhou, "Chaotic synchronization for a class of fractional-order chaotic systems," Chinese Physics, **16**, 2007, doi:10.1088/1009-1963/16/5/016.

[58] X. Wu, J. Li, G. Chen, "Chaos in the fractional order unified system and its synchronization," Journal of the Franklin Institute, **345**, 2008, doi:10.1016/j.jfranklin.2007.11.003.

[59] E. Demirci, N. Ozalp, "A method for solving differential equations of fractional order," Journal of Computational and Applied Mathematics, **236**, 2012, doi:10.1016/j.cam.2012.01.005.

Realization and Energy Optimization of a Recharging Station for Electric Vehicles with Fixed Storage and Photovoltaic Panels

David Roszczypala[*], Christophe Batard, Nicolas Ginot, Frédéric Poitiers

Communicating Systems team, I.E.T.R, Polytech, rue Christian Pauc Nantes, 44300, France

A R T I C L E   I N F O

A B S T R A C T

During the past years, a lot of research work have been done on the topic of smart grids and more specifically on the charging of electric vehicles (EVs), which will become an essential aspect in the coming years. The various works carried out on these themes have allowed the development of efficient tools to organize energy exchanges within these networks and to make this energy available to electric vehicles on certain time intervals. However, the problems related to the compatibility between the different elements of these networks seem to be largely underestimated. The collaborative work between IETR and Dropbird highlights the technological challenges that significantly hinder the deployment of relevant charging algorithms and experiments with dynamic programming-based algorithms to circumvent these obstacles.

1 Introduction

The advent of many electric vehicles implies some environmental changes, however, the conversion of a number of motorists to electric vehicles implies a growth in electricity demand and adds additional constraints on the power grid. Figure 1 shows the growth (estimated by the french grid operator) in the number of EVs and their demand for electricity on the French electrical grid in the coming years

Year	2010	2016	2030
Number of EVs	a few thousands	100 000	5 millions
Cumul. power demand (3.7kW)	a few MW	400 MW	20 GW
Cumul. power demand (50kW)	100 MW	5 GW	250 GW
Needed energy per year	a few GWh	a few 100 GWh	10 TWh
Cumul. storage capacity	a few 10 MWh	2.5 GWh	125 GWh

Figure 1: Evolution of EV energy needs (France)

The need for electricity corresponds to the virtual demand (in the scenario where all electric vehicles charge simultaneously), the calculation of the annual energy needed is based on a scenario of 15kWh/100 km and 13,000 km/year (source: ENT2008, datas in perpetual variation) and on a storage possibility of 20kWh of on-board batteries (again, these data are constantly changing). On the basis

of these elements, we note that the energy required to recharge the vehicle is always moderate compared to the total annual electricity consumption (consumption of electric vehicles in 2030: 10 TWh, -total grid consumption in 2016: 470 TWh), while the electricity needs can be very large (several tens to several hundreds of GW, compared to the total installed power in 2016 of 130 GW). The development of EVs seems feasible without significantly increasing electricity production, but the punctual need for energy can be problematic if judicious recharging methods are not planned. A research work carried out in Spain in 2011 [1], shows the interest of smart charging planning methods. In this work, a simple decrease in the concurrency factor can decrease the additional costs of EVs by 60-70%. On the other hand, the application of strategies that allow charging during off-peak hours could also avoid up to 35% of the necessary additional expenses. In conjunction with this limited increase in electricity consumption, it is important to highlight the storage opportunities that several million EVs will provide, and the new possibilities for controlling an increasingly intermittent electricity grid. In this paper, we will develop the implementation of a smart parking with renewable energy generation and fixed storage taking into account the constraints of the grid, while showing the difficulties encountered due to interoperability issues. The load management of an EV fleet is a subject that is widely covered in the literature, around five main axes: bi-directional charging [2], decentralised [3], mobility management [4], [5], integration of renewable energies [6], adding ancillary services to the grid [7].

Many algorithms based on different methods have been devel-

---

[*]Corresponding Author: David Roszczypala, Email: david.roszczypala@univ-nantes.fr

oped and tested in simulation for the intelligent management of energy flows in a network with multiple sources and loads. Multi-agent systems (MAS) allow the decentralisation of the energy management system based on the collaboration of different actors. Initially designed to model the collective behaviour of groups of individuals evolving together while being able to make their own choices, MAS are today frequently used for energy management systems in micro-grids with several sources [8]. The energy management of a system is usually carried out by an EMS (Energy Management System) with centralised control. The use of multi-agent systems is tantamount to decentralising energy control by giving decision-making power to different actors. Another application example is given by Taesic Kim et al. in their paper [9]. It is an application on a micro-grid composed of a set of dwellings, each with production, storage and load devices (domestic, electric car ...). An SMA solution is proposed to optimise the energy flows within the network in order to minimise peak load, reduce the energy costs of the inhabitants and maximise the energy efficiency of the storage system. Despite their wide use, the use of SMAs is controversial in the scientific community, as the results of the interaction between agents are sometimes unpredictable, therefore predicting the behaviour of the overall system from these constituent entities can become very complex.

Fuzzy logic is an extension of classical logic which allows the imprecision of data to be taken into account and thus seeks to come closer (to some extent) to the flexibility of human reasoning. It is based on Lotfi Zadeh's mathematical theory of fuzzy sets, which presents an extension of classical set theory to imprecisely defined sets. As opposed to Boolean logic, fuzzy logic allows to add a degree of truth to a condition, which allows this condition to be in a state different from true or false. In their paper [10], Kyriakarakos et al. give an example of the use of fuzzy logic for energy management in a microgrid with multi-source power supply for remote areas. The network in question consists of an AC bus on which are connected production elements : PV panels with their inverter, wind generator, hydrogen fuel cell, loads : seawater desalination module, various domestic loads, an electrolyser to create hydrogen from water, and an electrochemical storage battery connected through an AC/DC converter. Simulations have shown that the use of fuzzy logic for energy control makes it possible to respect the constraints imposed for a much smaller system dimensioning and therefore to save a lot of energy and money. Another example of fuzzy logic energy management including intelligent load management of electric vehicles is given in [11]. The performance of the algorithm is evaluated from the point of view of peak consumption and charging cost. Fuzzy logic makes it possible to implement inference systems with seamless, flexible and non-linear decision making, closer to human behaviour than conventional logic. Moreover, the rules are expressed in natural language. This has many advantages, such as including the knowledge of a non-computer expert at the heart of a decision-making system or even modelling certain aspects of natural language more finely. However, fuzzy logic has some drawbacks, such as not being able to predict that the system will behave optimally. Performance will therefore have to be measured a posteriori and adjustments will be made by trial and error. For these reasons, fuzzy logic hasn't been chosen for this specific experimentation.

Artificial neural networks (ANN) are a family of bio-inspired

algorithms : their principle is borrowed from the functioning of biological neurons (in a simplistic way). They are designed to reproduce certain characteristics of biological memories by the fact that they are parallel, capable of learning, able to store information in the connections between neurons, able to process incomplete information. An example of the use of neural networks for the control of a generator in a micro-grid is given in [12]. The system is a micro-grid for the production of energy and drinking water for regions isolated from the power grid; it is composed of solar photovoltaic panels, a diesel generator, an electrochemical storage battery, a desalination unit, and conventional domestic loads. A neural network is used to control the diesel generator (On/Off and intensity) in order to minimise dependence on the generator, greenhouse gas emissions and engine wear due to incomplete combustion. Another example is given in [13], where the design and validation of an innovative control system based on an artificial neural network for a hybrid micro-grid is proposed. The use of neural networks for energy flow management is however complex to implement and may require a large computing capacity.

In this paper, we will develop a supervision method for the intelligent charging of electric vehicles based on dynamic programming. This optimization method, developed by Richard Bellman in 1957, consists in solving a global problem by breaking it down into sub-problems, each with its own solution. After presenting the concept of the microgrid, this method will be developed in section III of this paper. The results obtained will be presented and analysed
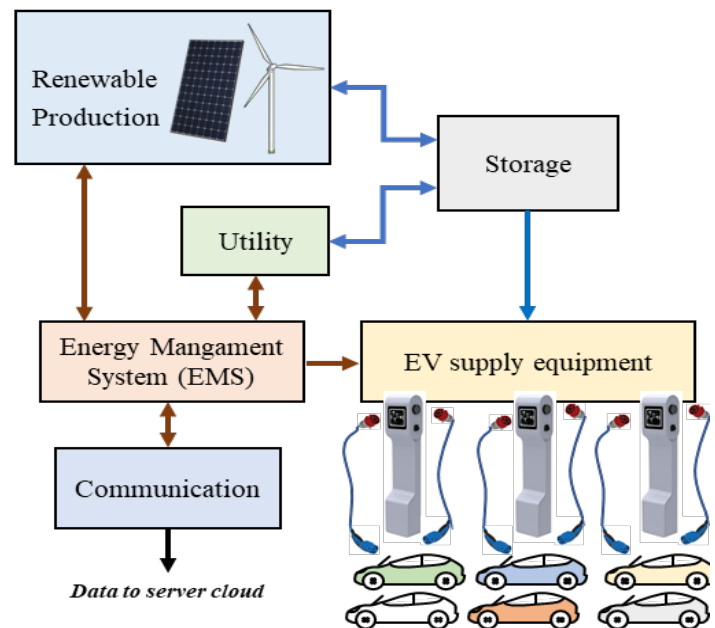
Figure 2: Experimental bench structure

2 Context and Experimental Bench

Dropbird is working on EV charging station management solutions and also on a planned charging organization in order to improve the performance of charging sites. The objective is to ensure max-

imum access to energy for EV users and to reduce the negative consequences for parking lot/network managers. This objective can manifest itself in two ways: with a given set of constraints, ensure that a maximum number of EVs can be charged or, with a given amount of EVs, minimize the strain on the power grid.

In order to carry out our studies, a flexible experimental environment has been created. It consists of an energy management system connected to multiple elements: EVSEs, DN, ESS, PV, remote control as shown in figure 2. Despite the fact that the environment is experimental, the users are various real local workers so the user satisfaction has to be respected the owned data is limited. The only data gathered on the PEV is the vehicle characteristics (battery capacity) and the initial SoC. Communication is also allowed between the EMS and the DN to receive requests of load demand response.
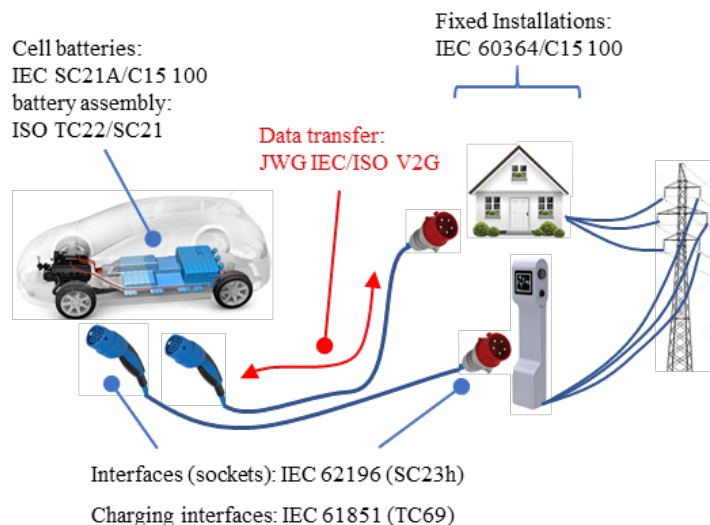
Figure 3: Normative context
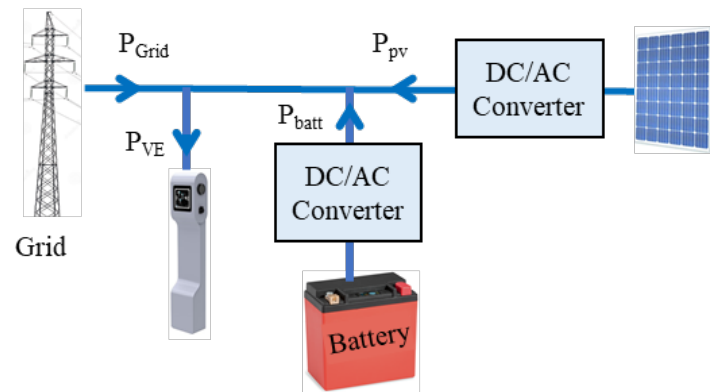
Figure 4: Energy flow within the experimental micro-grid

The development of such an experimental platform requires to meet normative constraints and standards. The main international standards associated to EV charging can be seen in figure 3.

Figure 4 sums up the energy flows exchanged by the different equipments connected to the micro-grid.

3 Algorithm structure

The energy management algorithms developed here are primarily EV recharge control algorithms; however, they are intended to control not only the EVSEs but also all elements of the system. We can speak of an EMS (energy management system) that will interact with the different elements described in figure 2: the EMS communicates with the EVSEs of course, but also with the inverter of the solar production, the fixed storage system, the distribution grid manager. The figure 5 shows the exchanges of measurements or control between the EMS and the other elements: an instantaneous measurement of the photovoltaic production, of the battery state of charge, of the charge power of each connected EV is transmitted to the EMS at each time step of the algorithm.
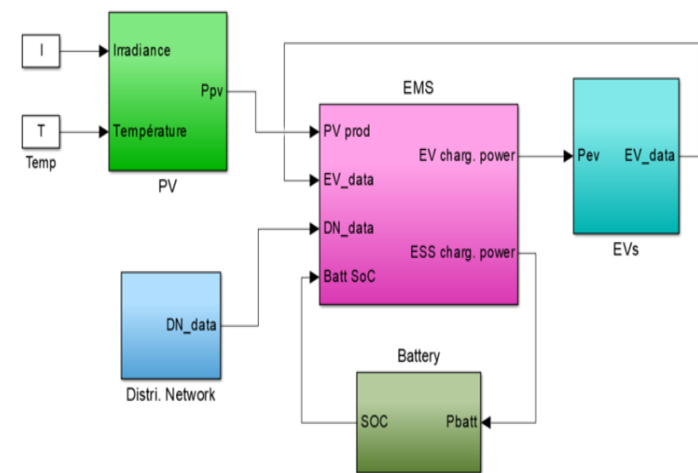
Figure 5: Information and control links

4 Dynamic Programming

Energy management in a parking lot with renewable energy sources consists in making a sequence of decisions spread over a day. The behavior of the users not being modeled, a simulation on an indeterminate day (working week or weekend) is rational. The concepts of artificial intelligence and more particularly of decision support are perfectly adapted to our problem. Enumeration (the simplest principle) is used [14].

4.1 Choosing the right energy management tool

In order to develop an independent intelligent energy management system, different strategies based on artificial intelligence were analyzed in simulation: multi-agent systems, fuzzy logic, artificial neural networks and dynamic programming.

4.2 Energy management uses

The method, defined by Bellman and used for sequential optimization problems, was developed in the 1980s to manage water reservoirs in hydroelectric installations [15]. Since the beginning of the

2000s, it has been used for the optimized use of energy in electric vehicles (such as the simultaneous management of several motors) [16]–[17], and, recently, for the management of electric energy storage from wind power and the management of a fleet of electric vehicles in [18], [19].

4.3 Principle

Bellman's principle of optimality forms the basis of the concept of dynamic programming. This principle states that "every optimal policy is composed of optimal sub-policies". The simplest (and most time-consuming) way to construct an optimal decision-making scenario is to list all possible choices at each step time and determine the least costly path. The number of possible paths can be considerably reduced using Bellman's principle by considering only the optimal subpaths at each computational step. As we elaborate the different possible paths, at each time step k, we keep only the best path that allows us to reach this state at this time: x(k). To use this method, it is necessary to discretize the time in time steps k, with 1¡k¡N, as well as each of the state variables x_1, x_2, x_3, x_4, x_5.

Dynamic programming is both a mathematical optimization method and a computer programming method. It is an algorithmic method for solving optimization problems.
Dynamic programming is used in particular for problems requiring a sequential decision-making sequence. It allows to determine the optimal trajectory by considering the problem as an optimal path to compute, and by decomposing it into sub-paths.

For example, if you want to solve the following optimization problem :

$$\min_{u_0,\ldots,u_{T-1}} \sum_{t=0}^{T-1} C_t(x_t, u_t) + K(x_T) \qquad (1)$$

$$x_{t+1} = f_t(x_t, u_t), \text{ for } x_0 \text{ given} \qquad (2)$$

$$u_t \in U_t(x_t)$$

where

- $C_t(x, u)$ is the cost to go from t to $t + 1$ starting from the state x by applying the u command;

- $K(x)$ is the final cost for the final state x;

- f_t is the dynamic function of the system;

- $U_t(x_t)$ is the set of possible commands at time t starting from state x.

Problem can be written as follows :

$$\min_{u_0,\ldots,u_{T-1}} \left\{ L_0(x_0, u_0) + \min_{u_1,\ldots,u_{T-1}} \sum_{t=1}^{T-1} C_t(x_t, u_t) + K(x_T) \right\} \qquad (3)$$

$$x_{t+1} = f_t(x_t, u_t) \qquad (4)$$

$$x_1 = f_0(x_0, u_0) \qquad (5)$$

$$u_t \in U_t(x_t)$$

Or again :

$$\min_{u_0} C_0(x_0, u_0) + V_1(f_0(x_0, u_0)) \qquad (6)$$

Where $V_1(x)$ is the value for the problem starting from the state $x_1 = x$ at time $t = 1$.

The optimal value $V_{t_0}(x)$ starting from the state x at time step t can thus be written :

$$V_{t_0}(x) = \min_{u_0,\ldots,u_{T-1}} \sum_{t=t_0}^{T-1} C_t(x_t, u_t) + K(x_T) \qquad (7)$$

$$\text{with} \quad x_{t+1} = f_t(x_t, u_t), x_{t_0} = x$$

$$u_t \in U_t(x_t)$$

The Bellman equation appears:

$$V_T(x) = K(x) \qquad \forall x \in \mathbb{X}_T \qquad (8)$$

$$V_t(x) = \min_{u_0,\ldots,u_{T-1}} C_t(x_t, u_t) + V_{t+1} \circ \underbrace{f_t(x, u_t)}_{x_{t+1}} \qquad \forall x \in \mathbb{X}_T \qquad (9)$$

And the optimal strategy is given by :

$$\pi_t^*(x) \in arg\ min \left\{ C_t(x_t, u_t) + V_{t+1} \circ \underbrace{f_t(x_t, u_t)}_{x_{t+1}} \right\} \forall x \in \mathbb{X}_T \qquad (10)$$

5 Simulations and Results

5.1 Validation of the operation of the dynamic programming algorithm

Before carrying out complex simulations using dynamic programming algorithms, a first series of tests was performed on a simple case that is easy to grasp in order to verify the behavior of the system controlled by the dynamic programming algorithms, and to validate that its behavior seems intuitively coherent. For this purpose, a simulation with a single EV (always connected) and a fixed battery was carried out, with the parameter to minimize the cost of charging. The simulation does not take into account photovoltaic production. The electricity tariff is variable depending on the time of day and defined so that the EV is not able to charge 100% while the cost is at its lowest (consistent with the values of nominal charging power and battery capacity). Thus, to enable the EV to charge at minimum cost, the system must necessarily be controlled so that the storage battery also charges during the low cost period, and provides the EV with this low-cost energy purchased from the EV outside the off-peak period. The state of charge of the battery must also be the same at the beginning and end of the simulation.
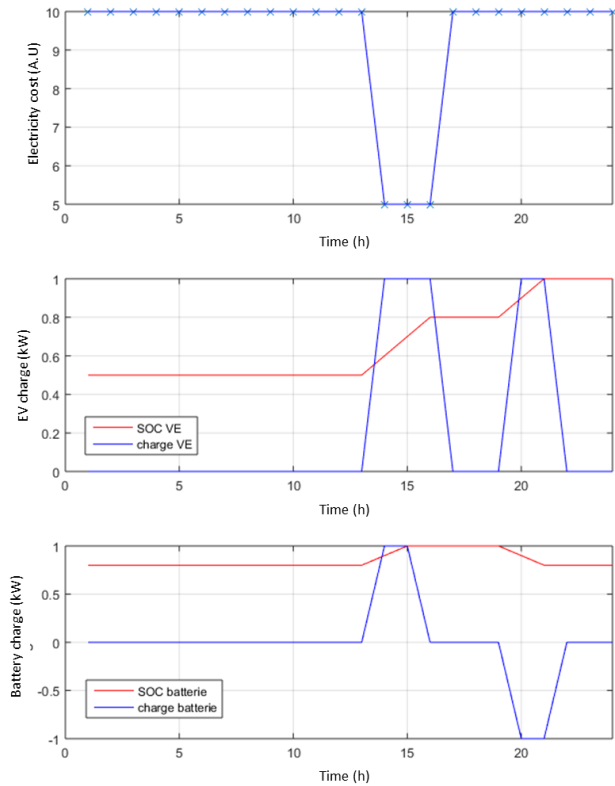
Figure 6: Test of the dynamic algorithm : after DP algorithm has been implemented, a simple intuitive case has been used to check its correct behaviour. The figure shows the battery is charged when electricity price is low according to cost function as long as it is possible

The results of the simulation are given in figure 6. The first graph describes the variation of the hourly rate of electricity for our simulation, the second graph represents the charge of the electric vehicle in blue (1 for *in charge* and 0 for *no charge*) and the variations of the state of charge of its internal battery in red. The third graph represents the charge and the variation of the state of charge for the fixed storage battery. It is immediately apparent that the algorithm controlled the system logically: the EV was charged when energy was cheapest (cost function to be minimized: total price of recharge). Since this was not enough time for the EV to receive enough energy to fully charge, the fixed battery was used well: it was also recharged when electricity was cheap, so that enough energy was stored to complete the charge of the EV outside the period of low price, and end the day with exactly the same level of charge as at the beginning. The timing of the energy delivery is random, from a cost minimization point of view, so it makes no difference whether the EV is charged with battery energy before or after the off-peak period, since the battery starts the day with a fairly high state of charge (70 percent), and no setpoint has been implemented for this action. This result allows to validate this first test of consistency of the dynamic programming algorithms.

In this paper, a simulation based on elementary rules makes it possible to judge the efficiency of the dynamic programming algorithms implemented: cases 1 and 2 are designed by implementing

simply-expressed rules to control the system.

- 1. In case 1, the EV is always charged at nominal power as long as the demand exists (presence of EV and SoC less than 1), the power taken from the grid corresponds to the difference between the demand and what can be produced by the solar panels.

- 2. In case 2, the EV is also charged at constant nominal power, the fixed batteries tend to compensate for solar production (they produce if the power demanded Pve is higher than the power of the solar panels Ppv and are charged otherwise). The energy in the fixed batteries must be the same at the beginning and end of the day (battery state of charge at 70%) to justify the consistency of the simulation, and to compare with the case without fixed storage.

- 3. In the third case, a decision-making process is based on a single decision at each time step: charging EVs at rated power or not charging, which allows the cost matrix to be filled quickly (no use of the fixed battery). The cost function chosen is to minimize the total energy consumed by the network, as modeled by equation14.

$$minJ = min \sum_{k=1}^{N-1} P_{grid}(k) * cost(k) \quad (11)$$

$$= min \sum_{k=1}^{N-1} (P_{EV}(k) - P_{PV}(k)) * cost(k) \quad (12)$$

- 4. A fourth case is also added for comparison purposes, similar to case 3, but this time to minimize the cost of energy over a day, as modeled by equation12.

$$minJ = min \sum_{k=1}^{N-1} P_{grid}(k) \quad (13)$$

$$= min \sum_{k=1}^{N-1} P_{EV}(k) - P_{PV}(k) \quad (14)$$

5.2 Simply-expressed rules (cases 1 and 2)

For the first case, the results are given in the figure 7 : in blue, the photovoltaic production over the day, in cyan the hourly energy pricing, which was defined in collaboration with the distribution network manager in order to limit the consumption of the EVs over 3 periods corresponding to morning, midday, and evening peaks. All the electric vehicles arrive at 6:00 am and are automatically charged without planning as soon as they arrive (red curve on the figure). The charging is not optimized and does not take into account the pricing or the photovoltaic production.

For the second case, the fixed storage battery is added, allowing to store the energy produced by the solar panels in order to increase the self-consumption of renewable energy. The first graph of the figure 8 shows the use of the battery (in red, the power supplied by

the battery, and in green the state of charge). On the second graph, we find the behavior of case 1, since it is still a simulation without load planning intelligence.
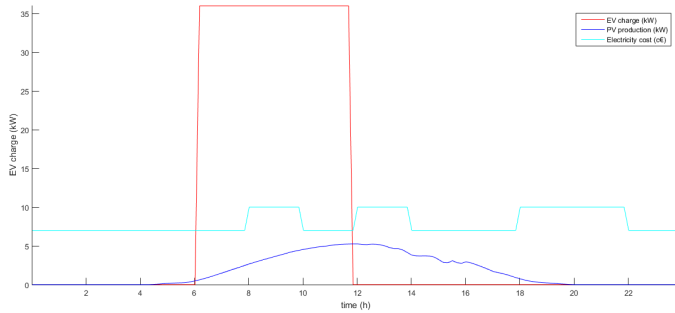
Figure 7: Reference case 1 : without battery
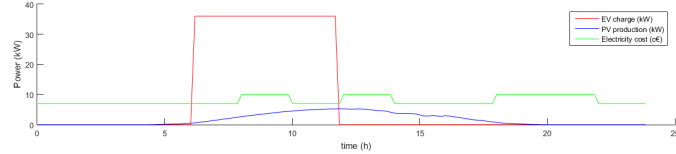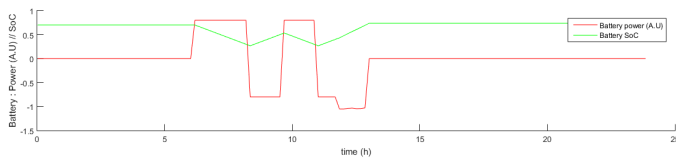
Figure 8: Reference case 2 : with battery

5.3 *Minimizing energy consumption*

We have now integrated the dynamic scheduling algorithm to plan the charging in an intelligent way. In the figure 9, we can see on the top graph the hourly charging, and on the bottom one, we find in green the PV production, in blue the charging power, and in red, the state of charge of the EV batteries. In this case, the algorithm is designed to minimize energy consumption, so EV charging is favored during the time slots when renewable production is at its maximum.
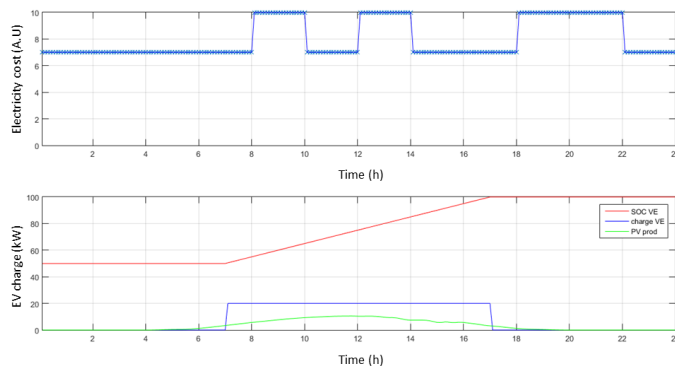
Figure 9: Results for minimal energy consumption

5.4 *Minimizing charging cost*

For the last case, the cost function to minimize is the total cost. Thus, we can see on the figure 10 that EV charging is planned on periods when electricity is cheaper and renewable generation is also available.
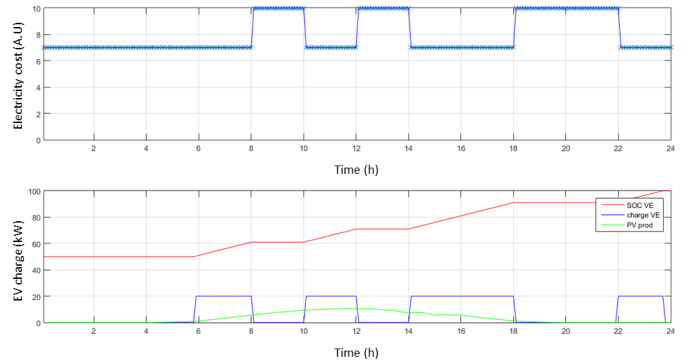
Figure 10: Results for minimal charging cost

5.5 *Experimental test*

The developed dynamic programming algorithm has been implemented and tested for minimizing charging cost in a real parking lot with 22kW AC EVSEs, which is illustrated on figure 11. The experimentation environment has been created and developed on the experimental site of the French distribution network operator. We also developed a supervision interface to remotely monitor the system and energy supply strategies. Figure 12 shows the web monitoring interface. Experimental data is confidential but the first experimental results are consistent with the simulations.

Figure 11: Experimental environment : part of the EVs, EVSEs and PV panels used for our study
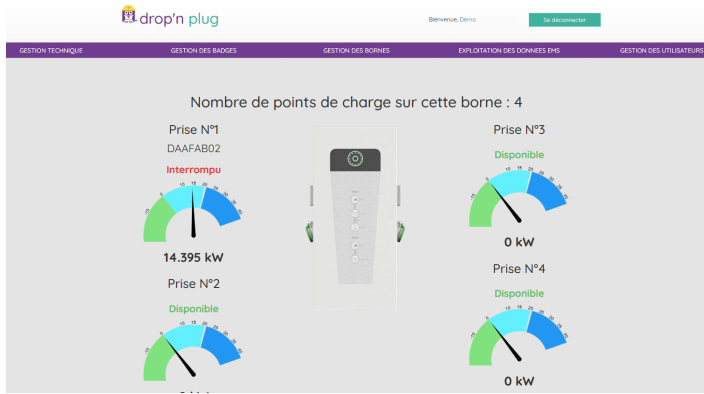
Figure 12: Screen capture of the web monitoring interface used for experimental data

6 Limits of deterministic model

Difficulties in using a deterministic model for inconsistencies with reality and planning is due to a lack of access to system data. Unlike the EV driver, the operator responsible for managing the charging stations is unable to easily visualize the SoC visible on the dashboard. Data exchanges between the EV and the EV charging infrastructure (IRVE) are governed by the IEC 61851 standard (and soon by the IEC 15118 standard). However, the access to the SoC through the EVSE will not be facilitated by EV manufacturers. This decision, political and commercial above all, limits the development of smart charging stations. The relevance of the criteria to be used for efficient load planning is discussed in [20]. The need to have access to certain data (arrival / departure of VE, SoC, etc.) for robust management algorithms is also mentioned. The unpredictable behaviour of people using ESVEs is considered a non-deterministic aspect.

6.1 Data gathering

In order to compensate for the lack of information described above, a system for collecting data from users can be set up. In the case of a fleet of electric vehicles of a company or that of people having a subscription to a public or private parking, the collaboration of the people in charge of the recharging of the electric vehicles and their agreement to provide the data necessary for the correct sequencing of the algorithm is the main drawback of this method. One solution to retrieve the data is that each user declares the EV's expected departure time, model and state of charge. Without going through a declarative process, an experiment was carried out to recover useful data for recharging EVs. The company Dropbird was tested a communication system between the EV and the EVSE through on-board diagnostics (OBD). The first tests carried out seem very promising.

6.2 Users behaviour modelling

Modelling user behavior is a key issue, whether access to the SoC is available or not. So far, all users have been modelled as arriving at the same time to charge their EV. This particular case is not realistic. Also, an optimization taking into account more realistic user behaviour was carried out. An optimized management law for a family of random cases (in the sense of "average") is preferred over the search for a list of optimal choices for a given case. An identification of the recurring behaviours of the users will be carried out from real behaviour data, which will make it possible to create a matrix of transitions between the different possible states. Each transition will be associated with a probability of passing from one state to another (present/absent) depending on the arrival time, presence time and/or state of charge.
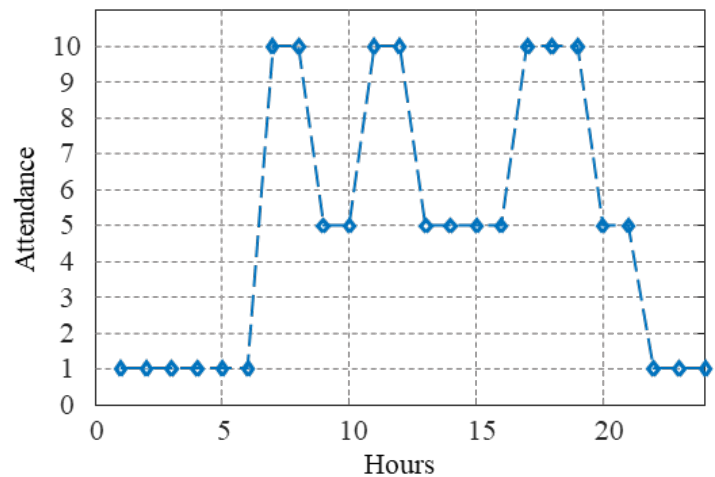
Figure 13: Attendance factor added to model to take into account the probability of a new incoming vehicle to the parking, depending on the time of the day

6.3 Users behaviour quick approximation

A study of fictitious cases was carried out with the aim of making a first approximation of user behavior. Fictitious users whose behaviour is modelled by several random variables (initial state of charge, battery capacity, arrival time) were simulated.

Fictitious users whose behaviour is modelled by several random variables were simulated: initial state of charge, battery capacity, arrival time. These variables are initialized for each EV when it arrives by picking a random value from a range of realistic values. An "attendance" variable was defined on the basis of our observations. This variable gives the probability that an EV will arrive to recharge, depending on the time of day, as illustrated to the Figure 13.

In order to observe the impact of user behaviour on the load planning and to compare the planning in cases where access to the state of charge is possible or not, a simulation was carried out on a parking lot. not having renewable energies. Figure 14 shows, for different scenarios, the distribution of the final state of charge and the final energy on board for all the electric vehicles that have used the parking lot during the day. For the same user behaviour but with different management methods, 3 simulations were performed. In Fig. 14a), the state of charge of the incoming vehicles is unknown to the parking manager, the energy is allocated first to the earliest arrived EV.
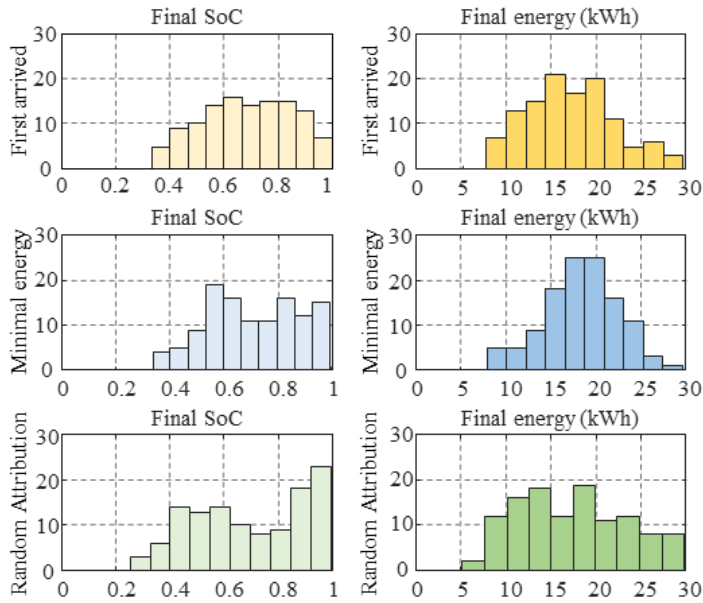
Figure 14: Number of EVs for each value of final energy and final SOC at departure time, for three different strategies of allocation of available energy : first come first served (a), minimum energy (b), random (c)
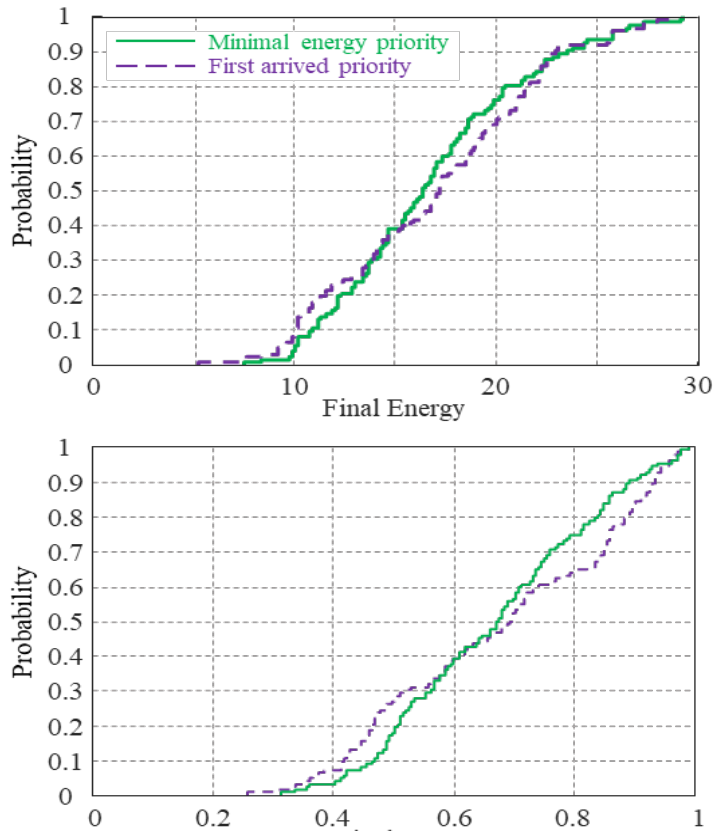
Figure 15: Cumulative probability of EV final Energy / final SOC at departure time. Cumulative distribution is given for 2 strategies : priority to first arrived or priority to lowest energy

In Figure 14 (b), it is considered that the SoC and the battery

capacity of each EV are accessible. The energy is then allocated to the EV with the lowest autonomy, that is to say to the EV with the minimum stored energy. In Fig. 14c), the SoC of the incoming vehicles is unknown. Energy is assigned to the EV when it comes to connect. To allow another waiting EV to start charging, we must wait for an EV to reach full charge or for an EV start. The choice is made randomly if several EVs are on standby. The simulation of figure 14b) shows that it is possible to significantly reduce the number of EVs with final energy less than 15 kWh (the distribution is shifted to the right). Figure 15 compares more explicitly the cases illustrated in Figures 14 (a and b).

In figure 13, the criterion used is the energy available in the EVs from the car park (at the end of charging). The distribution of this data is used to qualify our load planning algorithm. This distribution is given for 2 planning algorithms: in red for the case where the energy allocation is given to the EV with the minimum energy (the SoC is accessible) and in blue for the case where the energy allocation is given on first arrival (the SoC is not accessible). A criterion corresponding to a range of approximately 100 km is set, i.e. approximately a minimum energy at the end of charging of 15kWh. For the case without access to the SoC, this value is guaranteed for 60% of the EVs, while for the case with access to the Soc, this value is guaranteed for 70% of the EVs. To ensure a minimum energy level for each EV at the end of charging, knowledge of SoC is essential.

7 Conclusion and perspectives

In this paper, the optimization of energy flows within a network of micro-parking lots with EV charging stations and energy production was carried out using dynamic programming algorithms. Their proper functioning has been first validated in simulation by considering a predetermined use. The implementation of the algorithms in a real experimental demonstrator has been made. The first results obtained validate the effectiveness of the algorithms. This is the first step in a long process, the final objective of which is the creation of an energy management system. The final objective is to propose an optimal management law for all types of car parks equipped with recharging infrastructures, taking into account their specificity. Among the work to be developed, we can cite the increasing complexity of dynamic simulation by adding degrees of freedom, but also the strengthening of the study of user behavior in order to define random cases based on reality.

References

[1] L. Pieltain Fernandez, T. Gomez San Roman, R. Cossent, C. Mateo Domingo, P. Frias, "Assessment of the Impact of Plug-in Electric Vehicles on Distribution Networks," **26**(1), 206–213, doi:10.1109/TPWRS.2010.2049133.

[2] G. B. Shrestha, B. C. Chew, "Study on the optimization of charge-discharge cycle of electric vehicle batteries in the context of Singapore," 1–7, IEEE, 2007, doi:10.1109/AUPEC.2007.4548023.

[3] Z. Ma, D. Callaway, I. Hiskens, "Decentralized charging control for large populations of plug-in electric vehicles: Application of the Nash certainty equivalence principle," 191–195, IEEE, 2010, doi:10.1109/CCA.2010.5611184.

[4] S. Deilami, A. S. Masoum, P. S. Moses, M. A. S. Masoum, "Real-Time Coordination of Plug-In Electric Vehicle Charging in Smart Grids to Minimize Power Losses and Improve Voltage Profile," **2**(3), 456–467, doi: 10.1109/TSG.2011.2159816.

[5] D. Dallinger, D. Krampe, M. Wietschel, "Vehicle-to-Grid Regulation Reserves Based on a Dynamic Simulation of Mobility Behavior," IEEE Transactions on Smart Grid, **2**(2), 302–313, 2011, doi:10.1109/TSG.2011.2131692.

[6] A. Y. Saber, G. K. Venayagamoorthy, "Resource Scheduling Under Uncertainty in a Smart Grid With Renewables and Plug-in Vehicles," **6**(1), 103–109, doi:10.1109/JSYST.2011.2163012.

[7] E. Sortomme, M. A. El-Sharkawi, "Optimal Scheduling of Vehicle-to-Grid Energy and Ancillary Services," IEEE Transactions on Smart Grid, **3**(1), 351–359, 2012, doi:10.1109/TSG.2011.2164099.

[8] J. Lagorse, D. Paire, A. Miraoui, "A multi-agent system for energy management of distributed power sources," **35**(1), 174–182, doi:10.1016/j.renene.2009.02.029.

[9] T. Kim, J. Yun, W. Qiao, "A multiagent system for residential DC microgrids," in 2015 IEEE Power & Energy Society General Meeting, 1–5, IEEE.

[10] G. Kyriakarakos, A. I. Dounis, K. G. Arvanitis, G. Papadakis, "A fuzzy logic energy management system for polygeneration microgrids," **41**, 315–327, doi: 10.1016/j.renene.2011.11.019.

[11] N. J. Schouten, M. A. Salman, N. A. Kheir, "Energy management strategies for parallel hybrid vehicles using fuzzy logic," **11**(2), 171–177.

[12] A. Al-Alawi, S. M Al-Alawi, S. M Islam, "Predictive control of an integrated PV-diesel water and power supply system using an artificial neural network," **32**(8), 1426–1439, doi:10.1016/j.renene.2006.05.003.

[13] Y. Ates, O. Erdinc, M. Uzunoglu, B. Vural, "Energy management of an FC-UC hybrid vehicular power system using a combined neural network-wavelet transform based strategy," **35**(2), 774–783, doi:10.1016/j.ijhydene.2009.11.021.

[14] Louis Frecon, Manuel d'intelligence artificielle, presses polytechniques et universitaires romandes edition, 2009.

[15] Yakowitz, Dynamic programming applications in water resources ≫. Water Resources Research, water resources research edition, 1982.

[16] X. Zeng, J. Wang, "A Parallel Hybrid Electric Vehicle Energy Management Strategy Using Stochastic Model Predictive Control With Road Grade Preview," IEEE Transactions on Control Systems Technology, **23**(6), 2416–2423, 2015, doi:10.1109/TCST.2015.2409235.

[17] D. Scaradozzi, M. Fanesi, "Advanced Control Strategies to Improve Nonlinear Automotive Dynamical Systems Consumption," Axioms, **8**, 123, 2019, doi:10.3390/axioms8040123.

[18] P. Haessig, Dimensionnement et gestion d'un stockage d'énergie pour l'atténuation des incertitudes de production éolienne, Ph.D. thesis, École normale supérieure de Cachan-ENS Cachan, 2014.

[19] R. L. G. Latimier, Gestion et dimensionnement d'une flotte de véhicules électriques associée à une centrale photovoltaïque: co-optimisation stochastique et distribuée, Ph.D. thesis, Université Paris-Saclay, 2016.

[20] K. N. Kumar, B. Sivaneasan, P. L. So, "Impact of Priority Criteria on Electric Vehicle Charge Scheduling," **1**(3), 200–210, doi:10.1109/TTE.2015.2465293.

Hiding Information in DNA Sequence Data using Open Reading Frame Guided Splicing

Amal Khalifa[*]

Computer Science Department, Purdue University Fort Wayne, Fort Wayne, IN- 46814, USA

A R T I C L E I N F O	A B S T R A C T
	Encouraged by the huge publicly available genomic databases, research in the field of steganography was recently extended to utilize DNA sequence data to conceal secret information. As an extension of the work presented earlier by the author, this paper proposes an approach for a secure data communication channel between two parties. At one side of the communication, the sender starts the hiding process by encrypting the secret message using a bio-inspired 8x8 play-fair ciphering algorithm. Next, the secret sequence is randomly spliced and merged into the cover sequence replacing its non-coding regions. Using the secret key shared in advance, the receiver, on the other side of communication, can extract and concatenate the segments of the encrypted message and reveals the original message after deciphering. The method was proven to be robust to brute-force attacks while providing a hiding capacity up to two bit-per-nucleotide. A comparison with some existing techniques showed that the proposed method outperforms most of them not only in terms of the hiding capacity but also for the feature of blind extraction.

1. Introduction

Despite the proven efficiency of cryptography in protecting the security of information during communication, this protection is not guaranteed after the sent information is received and decrypted. On the other hand, Steganography introduced innovative ways to hide the existence of the secret information into innocent looking cover media in such a way that the resultant stego-media is hardly distinguishable from the original one. This makes it almost impossible to discover the concealed information or even suspect its existence. The first use of steganography dates back to the fifth century BC as documented in "Histories" of Herodotus [1]. The story happened during the conflict between Persia and Greece when Demaratus sent a secret message to warn the Spartans about the surprise attack planned by Xerxes, the tyrant king of Persia. The message was carved on a wooden tablet and covered with wax. Being apparently blank, the tablet was not intercepted by the Persian guards along the road. When the tablet reached its destination, the message was revealed after scrapping the wax off. With the element of surprise lost, the Persian fleet was lured in the harbor and damaged in less than a day. A modern model for a steganographic system was formulated by Simmons in terms of a prisoner's problem [2]. It assumes that Alice and Bob are trying to prepare an escape plan and need to exchange messages without drawing the attention of the warden. So, they embed their secret messages some cover-object using a secret key. Only using the same key, the message can be extracted from the transmitted stego-object.

In the digital era, modern steganographic techniques use a variety of digital media for the purpose of data hiding. Examples of such media include: images [3], audio tracks [4], video files [5], 3D Objects [6], and even file systems [7]. Recently, researchers attempted to use Deoxyribonucleic Acid (DNA) sequence data as a cover medium. In 1999, a paper published in Nature [8] presented one of the earliest methods for using biological DNA as a cover for the purpose of information hiding. The authors used a synthesized a DNA strand to encode the secret data that was then copied and camouflaged within an enormous number of similarly sized fragments of human DNA. Later, a small amount of the resultant DNA-containing solution was printed as a dot on a period in a typed letter. When mailed, the recipient of the letter was able to successfully recover the secret message after laboratory analysis. Another interesting example is live data storage, where digital data can be stored in the genome of a living organism; preserved for thousands of years and protected even from nuclear explosions [9]. The authors of [10] proposed a watermarking technique for RNA sequences in such a way the functionality of the organism remains intact. The main application for such a technique is protecting genetic discoveries such as gene therapy, transgenic crops, and tissue cloning. A similar approach was

[*]Corresponding Author: Amal Khalifa, Email: khalifaa@pfw.edu

proposed in [11] where the message is encrypted before hiding and block-sum checking is used to detect errors in mutations.

Another category of DNA-based steganographic methods was motivated by the huge publicly available genomic databases that store DNA sequence data on digital files following a simple format. In [12], the authors proposed that both the sender, and the receiver should agree or share a reference sequence before the communication takes place. The secret message can then be embedded into the reference sequence using one of three different methods. With the help of the reference sequence, the reverse of the hiding process can be performed by the rreceiver to extract the hidden message. However, communicating a sequence twice can draw suspicion and may affect the security of the steganographic channel itself. Secondly, the reference sequence is randomly modified without any consideration to the biological functionality of the DNA sequence. Addressing this later point, the authors of [13] introduced a hiding method that exploits the codon redundancy feature of DNA to hide data into sequence data without affecting the type nor the structure of protein it encodes for. Reversible hiding techniques, on the other hand, works in a way such that the cover sequence can be recovered from the stego-DNA sequence. an example of such technique was proposed in [14] where the cover sequence is coded into symbols that have integer values and the hiding process is then implemented using multilevel histogram shifting. Other methods added the power of encryption to provide more security to the hidden messages [15]. Some of these ciphers are actually bio-inspired and can be used to represent the message into a DNA sequence such as [16], [17] and [18]. A more recent research investigated using DNA steganography and PCR technology for the purpose of quantum key distribution (QKD) [19]. The authors of [20] provide a more comprehensive review on recent DNA-based steganographic methods.

In this paper, we present a method for securely hiding information into DNA sequences. The method is an extension of the work published by the author in [21]. The original research hides a secret message into a reference DNA sequence where both the message and the reference sequences are divided into random-length splices that are eventually merged to form the setgo-sequence. Before embedding, the binary message is encrypted and encoded into a DNA sequence using an 8x8 playfair cipher. In order to perform the extraction process correctly, it was proposed to add a header section before the embedded message to store the length of the hidden message. In this research, however, we propose a novel splicing technique based on the genes detected in the cover sequence. Therefore, the need for the message-size header information is eliminated. Finally, since the message splices are replacing the non-coding regions of the cover, the resultant stego-sequence is shorter. Although the aforementioned modifications don't increase the hiding capacity but it enhances both applicability and security of the method. The rest of the paper is organized as follows: section 2 provides a brief overview on some useful characteristics of DNA sequence data. Section 3 describes the details of the hiding and the extraction modules of the proposed method. In section 4, the performance of the proposed approach is measured, analyzed, and compared with some other techniques. Finally, section 5 concludes the paper.

2. DNA Sequence Data

The genetic information of all living organisms, as well as viruses, is stored in DeoxyriboNucleic Acid (DNA) molecules. A DNA molecule consists of two polynucleotide strands coiled around each other in the form of double helix structure. Each individual strand of DNA is made up with 4 different types of nucleotides. Nucleotides can contain either a purine base : adenine (A) and guanine (G) or pyrimidine base: thymine (T) and cytosine (C). In nature, A pairs only with T and G pairs only with C [22]. As a data medium, DNA can be represented as string of characters over the alphabet {A, C, G, T}. Using some coding rule, a DNA string can be converted into a string of binary digits where each base is mapped into two bits. Figure 1 shows an example of such coding rule along with a sample sequence encoded using this rule.

Base	bits
A	00
C	01
G	10
T	11

AGTAGTCATCAT

001011001011010011100011
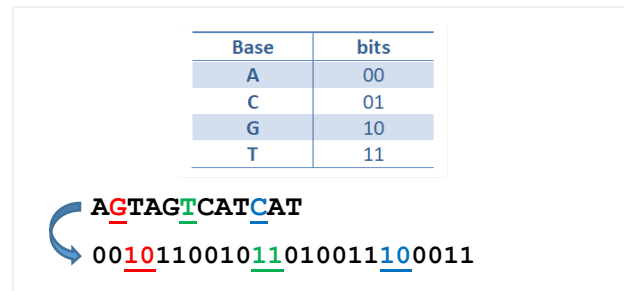
Figure 1: An example digital coding of DNA sequence data

The information stored in the DNA molecule plays a vital role in controlling all aspects of cell functionality. Through the complicated process of Central Dogma, the DNA sequence is read, copied, and eventually translated into a chain of amino acids that forms a protein [23]. Although the reading and the copying process is made one base at a time, the translation process reads the sequence into units of three adjacent nucleotides; called codons. With only 4 possible bases; there are 64 (4^3) distinctive ways to form 3-base long codons. As shown in figure 2, a three-letter abbreviation designates the type of amino acid molecule as in "Phe" and "Leu". Notice that some codons code for more than one amino acid. This is a feature called codon degeneracy [22]. Furthermore, three of the codons; indicated as STOP, identifies the end of the protein chain and doesn't actually code for any amino acid.
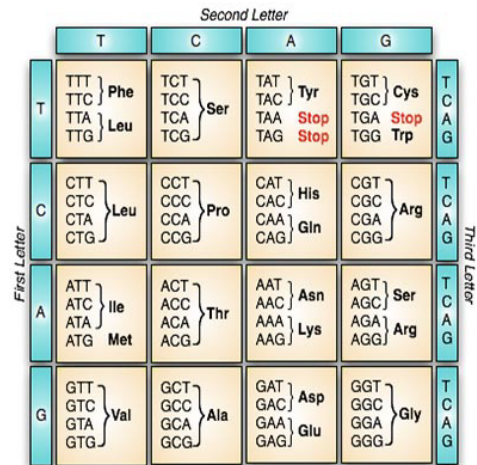
Figure 2: The genetic code table

In fact, not all parts of the DNA sequence code for proteins. That segment of the DNA that code for a protein is called a gene and hence other segments are referred to as non-coding regions. Genes can be identified by searching the DNA sequence for open reading frames (ORF). An ORF is a long stretch of codons that is preceded by a start codon (ATG) and will be uninterrupted by stop codons (TGA, TAG or TAA) [24]. This searching process proceeds by dividing the DNA sequence into a set of consecutive, non-overlapping triplets. This can start at the first, the second, or the third base in the sequence resulting in three different reading frames in that direction. The reading frame that has the potential to be translated into protein is identified as an ORF. Since DNA is double stranded and either strand could include a gene, there is a total of six reading frames: three in forward direction and three in the reverse complement direction. Figure3 shows an example of a sample a sample sequence and the three reading frames in its forward direction. The potential ORFs found in each frame are highlighted well. Notice that this sequence has three potential genes, one in each reading frame. The gene identified in frame 2 for instance consists of exactly three codons in between the start and the stop codons.
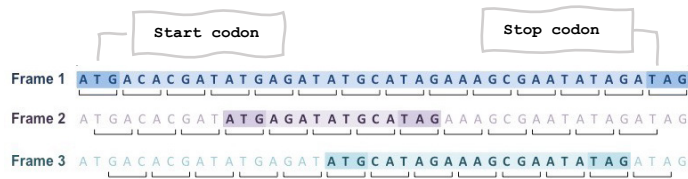
Figure 3: An example of Open Reading Frames (ORF) for gene identification

3. The Steganographic method

A steganographic communication channel consists of two main processes: hiding and extraction. Whereas the hiding process is normally carried out by the sender, the extraction process is performed by the receiver to reveal the secret message. As shown in figure 6, the proposed hiding process starts with ciphering the message and encoding it into a DNA sequence. Next, the cover sequence is spliced to identify the ORFs. The embedding process then moves forward by infusing the message sequence into the cover sequence splices. On the other side of the communication, the receiver extracts the secret message from the stego-sequence simply by reversing the hiding steps. Here we assume that both of the sender and the receiver share a secret key in advance. This key is used in different steps of the hiding process to make sure that only the intended recipient will be able to retrieve the hidden message.

3.1. The Hiding Process

The detailed steps of the hiding process are listed in Algorithm 1. It starts with an encryption step that utilizes a DNA-inspired implementation of Playfair cipher [17]. The classical Playfair cipher uses a 5 by 5 table to substitute a pair of letters (digraph) and with another one following a few simple rules. This implementation was originally proposed to work plaintext consisting only of alphabets without punctuation, or even numerical values. The cipher also requires a preprocessing step in order to remove spaces and handle double-letter digraphs. However, in [17], the author proposed using a randomly constructed 8x8 matrix representing the 64 different DNA codons.

This technique is capable of ciphering any type of digital data not only text. In addition, the preprocessing step is no longer required since the digraphs are represented over the DNA not English alphabet. The final output of this cipher can be coded back into characters or left in its DNA data representation. In this research, we decided to use the cipher proposed in [17] to encrypt the secret message and use its intermediate DNA representation of the cipher-text. The encrypted message sequence is then infused into the cover sequence following a structured splicing methodology.

The splicing process is performed on both the cover and the message sequences. However, the splicing is carried out differently on each one of them. First, the cover sequence (C) is divided into coding and non-coding regions through an ORF analysis. Guided by the ORF result, the coding genes (C_g) are identified, and the cover sequence is spliced out at those specific locations. On the other hand, the message sequence (M) is randomly spliced into random-length segments (m_i) similar to the insertion method proposed in [12]. Finally, the message splices and the cover genes are merged to form the stego-sequence (S). The merging process is done in a very special way. As shown in figure 4, the merging process starts with a message segment followed by the first cover gene and then another message segment that is followed by the second cover gene and so on.

In fact, the base composition of message sequence can vary depending on several factors such as the message content, the secret key, and binary coding rule. Therefore, and like any random sequence, a message sequence will comprise of coding and non-coding regions as well. This may introduce a challenge in the extraction process on how to distinguish between a cover gene and a message gene. Therefore, we suggest adding a separator codon at the end of each message segment to uniquely identify the start of a cover gene.
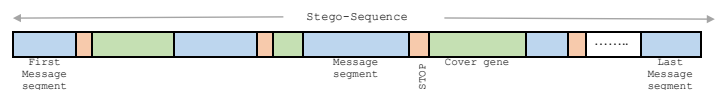
: Merging message splices with cover genes.

Theoretically, this codon can be any of the 63 codons (except the start codon). However, we suggest using one of the three stop codons (STOP) to avoid forming new genes in the message sequence that may overlap with the cover genes causing issues during the extraction process. Figure 6 shows an example of such a situation. The figure shows four ORFs (highlighted in blue). The first two of them are part of the message sequence, while the other two are cover genes since they are proceeded with the stop codon (TAA in this case).

Figure 5: An example of a ORFs formed in message splices.

3.2. The Extraction Process

The extraction is obviously the reverse process of hiding. As listed in Algorithm 2, the message retrieval starts with sequence splitting based on the specified reading frame. The locations of the start and the stop codons of the genes can then be identified. It is expected to find more genes in the stego-sequence than those used from the cover during the hiding process. As mentioned above, depending on the message contents and the randomness of the encryption algorithm, the message sequence can form new genes. Therefore, the proposed algorithm checks, for every detected gene, the codon that proceeds its start codon. If it is the specified STOP codon utilized during the hiding process, the gene will be skipped and the message segment that follows will be extracted. Otherwise, this detected gene actually belongs to the message sequence.

Figure 7 uses the same stego-sequence example shown in figure 6. Here only the highlighted segments belong to the message sequence. Notice how the first message segment spans the range of bases from 1 to 357 but when extracted, it will be concatenated from four different segments because of the two ORFs formed in its content. Furthermore, since the third and the fourth detected ORFs are cover genes, the segment following each one of them is extracted and appended to the message sequence extracted so far. Once all ORFs are processed, all segments of the message will be extracted, concatenated, and deciphered. Thus, there is no need to embed any header information to store the length of the hidden message as required in [21]. It is important to mention that, the extraction process here is done blindly without the need to reference the reference cover sequence.

Algorithm 1: Message Hiding

Input: C : A reference DNA sequence, used as a cover
 Msg : a secret message
 Key : a secret key-word
Result: S : A Stego-DNA sequence

1. Message Ciphering
 1.1 Encode Msg into Msg_{DNA} using a DNA binary coding rule
 1.2 Build an 8x8 codon matrix
 1.3 Shuffle the matrix based on the Key
 1.4 **for each** pair of codons in Msg_{DNA} **do**
    if the pair appears on the same row of the matrix, replace each codon with its immediate right with wrap around
    else if the pair appears on the same column of the matrix, replace each codon with its immediate below with wrap around.
    else replace the pair with the pair at the corners of the rectangle defined by the original pair.
    end
  end
 1.5 Build a column-wise square matrix filled with bases in Msg_{DNA} in reverse order
 1.6 **for each** column and row in sequence matrix **do**
   1.6.1 Rotate circular upward on the column
   1.6.2 Rotate circular left on the row
   end
 1.7 Rearrange encrypted message into a linear sequence Msg_{cph}

2. Cover Splicing
 2.1 Locate genes in C considering one of the ORFs.
 2.2 Let (C_1 , C_2 , C_3 , ... C_{t_c}) be the detected cover genes.

3. Message Splicing:
 3.1 Let i be a value derived from Key
 3.2 Generate a sequence of random numbers (i_1 , i_2 , i_3 ...) using i as the seed
 3.3 Find the smallest integer t_m such that :
   $\sum_{k=1}^{tm} i_k > | Msg_{cph} |$
 3.4 **if** $t_m < t_c$
   Divide Msg_{cph} into t_m -1 segments (M_1 , M_2 , M_3 , ... M_{t_m-1}) with lengths (i_1 , i_2 , i_3 , ... i_{t_m-1}) respectively and keep the residual part of Msg_{cph} in M_{t_m}
   else
    return.
   end

4. Segment merging:
 4.1 Initialize S as an empty sequence
 4.2 **for each** $k = 1$ to t_m -1 **do**
   Append M_k to S
   Append $STOP$ to S
   Append C_k to S
 4.3 Append M_{t_m} to S
5. return S

end

Algorithm 2: Message retrieval

Input: S : A Stego-DNA sequence
 Key : a secret key-word
Result: Msg : the embedded secret message

1. ORF Splicing
 1.1 find location of genes in S for the specified ORF
 1.2 Let (S_1 , S_2 , S_3 , ... S_t) be the detected cover genes
 1.3 Let $start(S_i)$ return the location of the start codon for the gene S_i
 1.4 Let $stop(S_i)$ return the location of the stop codon for the gene S_i

2. Message extraction:
 2.1 Initialize Msg_{cph} as an empty sequence
 2.2 let k = 1
 2.3 **for** $k = 1$ to t -1
   if $start(S_k)$ is proceeded by STOP
    extend Msg_{cph} by adding the bases from $stop(S_k)$ to $start(S_{k+1})$
   else
    extend Msg_{cph} by adding the bases from $start(S_k)$ to $start(S_{k+1})$
   end

  end
 2.4 Append the bases following $stop(S_t)$ to Msg_{cph}

3. Message Deciphering:
 3.1 Build an 8x8 codon matrix
 3.2 Shuffle the matrix based on the Key
 3.3 **for each** pair of codons in Msg_{DNA} **do**
    if the pair appears on the same row of the matrix, replace each codon with its immediate right with wrap around
    else if the pair appears on the same column of the matrix, replace each codon with its immediate below with wrap around.
    else replace the pair with the other pair at corners of the rectangle defined by the original pair.
    end

  end
 3.4 Build a column-wise square matrix filled with bases in Msg_{DNA} in reverse order
 3.5 **for each** column and row in sequence matrix
    Rotate circular upward on the column
    Rotate circular left on the row
   end
 3.6 Rearrange deciphered message into a linear sequence Msg_{DNA}
 3.7 Convert Msg_{DNA} into Msg using the specified coding rule

4. return Msg

end

```
000001  CCTCTTACATTCGGCTTGCCTTATGAAAGTTGGGTCAGCTGTAACGCACCTGCATTTCAGTCCT
000065  GATCGATCAGTGCTCCCCGTTTGTATGTTATGTTAGGAAGATTTGTCTCATCTTATGATTCCAC
000129  CGACAGTACCGTCCGCGCTGAAGGGCTGCGTGCAGACAACGGTCTTAAATTTGTTGTCCGATTC
000193  GGAGTGTTCCGCGCTCTTACATTCGGCTTGCCTTATGAAAGTTGGGTCAGCTGTAACGCACCTG
000257  CATTTCAGTCCTGATCGATCAGTGCTCCCCGTTTGTATGTTATGTTAGGAAGATTTGTCTCATC
000321  TTATGATTCCACCGACAGTACCGTCCGCGCTGAGAGGTAAATGCATAATTTTCTAAGAGAAAGC
000385  AGATTTCAAAAATAGCTGCGTGCAGACAACGGTCTTAAATTTGTTGTCCGATTCGGGAGTGTAAA
000449  TGGAAGCTGCTGTGTGTTGTCATATCCAAGGGCGATTTCTCAGCAAGGGGAGCTGGTTAGTGCT
000513  CAGGAATACAGACAGATGATTCCGCGCTCTTACATTCGGCTTGCCTTATGAAAGTTGGGTCAGG
```

Figure 7: An example of detecting and extracting message splices.

4.   Performance Analysis

4.1. Hiding Capacity

Usually, the hiding capacity of a steganographic technique is measured by the maximum number of bits that can be hidden into the cover media. For DNA data, this capacity is measured in bit-per-nucleotide (*bpn*) which reflects how many bits can be hidden for each nucleotide in the cover sequence. Since the proposed algorithm requires only that the number of message segments should be less than or equal to the number of genes in the cover sequence, this doesn't impose any restrictions on the length of message. Theoretically, fine tuning the embedding parameters would allow us to hide a message sequence that is as long as the cover sequence itself. Furthermore, since each encoded nucleotide in a message sequence represents 2 bits, the hiding capacity of the proposed method can be expressed as follows:

$$Capacity = \frac{size\ of\ message\ in\ bits}{size\ of\ cover\ in\ bases}$$

$$= \frac{2*|C|}{|C|} = 2\ bpn \tag{1}$$

where C represents the cover sequence and |C| refers to the length of C in base pairs (bp).

4.2. Security

Generally speaking, the harder for an attacker to crack the implementation of a steganographic method, the more secure this approach is. Therefore, the proposed method was designed in way that the details of the hiding process are based on several parameters the attacker needs to guess correctly in order to extract the hidden message. Beside the value of the secret key, the attacker needs to know: the binary rule used to encode the DNA nucleotides, the random number generator used during the message splicing, the ORF selected for cover splicing, and the stop codon used to separate between message and cover segments.

First, given the fact that there are only 4 nucleotides, there are 4! = 24 possible binary coding rules. So, the probability of a successful guess on this parameter is 1/24 . Similarly, there are 6 different ORFs and 3 different stop codons. This makes the probability of predicting each one of them to be 1/6 and 1/3 respectively. More importantly, to find the sequence of numbers generated to randomly slice the message sequence, an attacker may need to make a number of guesses [12] up to the value computed in (2). Where *n* represents the length of the message sequence and $\binom{n}{k}$ is the set of all *k*-combinations of *n*.

$$\binom{n}{n-1} + \binom{n}{n-2} + \binom{n}{n-3} + \dots + \binom{n}{0}$$

$$= \sum_{k=0}^{n-1} \binom{n}{n-1-k} = 2^n - 1 \tag{2}$$

Since the summations of the *k*'s can be as long as the cover sequence, the probability of a successful guess for this parameter can reach $\frac{1}{(2^{|C|}-1)}$, where C represents the cover sequence and |C| refers to the length of C in base pairs (*bp*). In conclusion, the probability of cracking the hiding process of the proposed method can be estimated as follows:

$$P_{bf} \frac{1}{(2^{|C|}-1)} \times \frac{1}{24} \times \frac{1}{6} \times \frac{1}{3} \tag{3}$$

Considering the fact that |C| may reach hundreds of thousands bases, it is almost impossible for an attacker to retrieve the hidden message based on a successful guess. In addition, the message itself is protected by a powerful cipher that adds another layer of security to the hidden message in case the steganographic method fails.

5.   Results and Discussions

In this section, the proposed method is tested using 10 different cover sequences. The discussion is then followed by a comparison with some existing methods based on different performance measures.

5.1. Experimental results

The sequence data was drawn from the Genbank database on the National Center for Biotechnology Information (NCBI) website using their unique accession numbers. The downloaded files in the FASTA format which is a text-based format that starts with a single-line description followed by lines of sequence data using the {A, C, T, G} alphabet. Furthermore, in this set of experiments, we choose to randomly generate 30KB of textual data and use it as a sample secret message. However, this should not limit the applicability of the proposed algorithm to hide any type of digital data as long as it is encoded using a rule similar to the one given in Fig. 1.

Table 1 summarizes the experimental results for 10 sequences using the secret key "12345". It lists the lengths of the cover- and stego- sequences as well as the number of ORFs detected in the first reading frame of the sequences in each case. The payload is computed as the ratio of message to cover nucleotides in the stego-sequence. Notice that the results show an increase in the number of genes detected in the stego-sequence compared with those of the cover sequence. That was expected because the encoded message sequence will probably form some genes that will add to the detected ORFs in the resultant stego-sequence. For example, in the case of the AAEX03000038 sequence, the message was sliced into 343 segments. this means that only 342 genes out of the 364 cover genes are needed for hiding. However, during the extraction process, 657 genes were detected in the stego-sequence representing not only cover genes but also genes formed by the message content.

Furthermore, the embedding process was not successful for sequences AAEX03000001, AAEX03000010, and AAEX03000999 because none of them has enough ORFs to hide the message segments. For example, *AAEX03000999* is a sequence that is 22,099 bases long with only 48 ORFs. Since the message is sliced into 832 segments, we need at least 831 cover genes to infuse those segments into. It is also worth to notice that the number of message segments changes in each case. In fact, in our implementation, the randomness of the splicing process does not only depend on the secret key, but also on the number of bases in the longest ORF in the identified the cover sequence.

5.2. Comparisons

In this set of experiments, the performance of the proposed technique was compared with some existing methods in terms of capacity, blind extraction, and security against brute force attacks. With blind extraction we mean that the original cover sequence is not required during the extraction process to retrieve the embedded message. With non-blind methods, the cover sequence needs to be communicated in advance which can draw suspicion and affect the security of the channel.

The results listed in table 2, show that the insertion method proposed in [12] may be more robust to brute-forth attacks than the proposed method, but it is not blind. On the other hand, the proposed method achieves a higher hiding capacity than all the methods in [12] while maintaining the advantage of blind extraction. The same is true for the GCBC method, despite it is also a blind technique, its hiding capacity is less than that offered by the proposed method. The methods proposed in [12] were not evaluated in terms of robustness, so there is no way to compare them to the proposed method in that regard. However, it is obvious though that they did not succeed to offer a better hiding capacity. Finally, although the technique introduced in [21] offers the same hiding capacity, the details of the proposed method added more parameters to the hiding process that enhanced its security.

Table 1: Experimental results for hiding 30KB of text

Cover Sequence			Number of message segments	Stego-Sequence		
Accession number	Length (bp)	Number of detected ORFs		Length (bp)	Number of detected ORFs	Payload (*bpn*)
AL645637	207,629	588	222	147,239	525	1.69
AC168892	197,841	563	452	167,027	743	1.49
AAEX03000080	305,811	823	437	162,125	750	1.54
AAEX03000038	133,800	364	343	157,811	657	1.59
AC153526	200,117	521	281	151,259	592	1.65
AC168874	206,488	523	466	169,277	771	1.48
AL645625	226,754	553	490	178,616	790	1.40
AAEX03000001	24,025	59	526	--	--	--
AAEX03000010	44,186	98	403	--	--	--
AAEX03000999	22,099	48	832	--	--	--

Table 2: A comparison with some existing techniques

Author	Method	Capacity (bpn)	Security (P_{bf})	Blind?
[12], 2010	Insertion	0.58	$\frac{1}{1.63 \times 10^8} \times \frac{1}{n-1} \times \frac{1}{2^m-1} \times \frac{1}{2^{s-1}} \times \frac{1}{24}$	No
	Complementary	0.07	$\frac{1}{1.63 \times 10^8} \times \frac{1}{24^2}$	No
	Substitution	0.82	$\frac{1}{(2^{|S|}-1)^2} \times \frac{1}{6}$	No
[15], 2016	Generic Complementary Base Substitution (GCBS)	1.5	$\frac{1}{(2^{|S|}-1)^2} \times \frac{1}{6} \times \frac{1}{24}$	Yes
[16], 2018	Noncircular type (NHS)	1.243	NA	yes
	Circular type (CHS)	1.865	NA	yes
[21], 2020	Random Splicing	2	$\frac{1}{(2^{|C|}-1)^2} \times \frac{1}{24}$	yes
Proposed	ORF-guided Splicing	2	$\frac{1}{(2^{|C|}-1)} \times \frac{1}{24} \times \frac{1}{6} \times \frac{1}{3}$	yes

6. Conclusions

This paper describes a steganographic method that extends the work presented in [21] and uses DNA sequence data for data hiding purposes. The proposed technique consist of two processes: hiding and extraction. The hiding module starts with an encryption step that encodes the secret message as a DNA sequence. The cover sequence is then spliced into coding and non-coding segments in a given reading frame. The encrypted sequence is also spliced; but is a random fashion, and infused into the cover's gene-coding segments. The extraction module, on the other hand, reverses the hiding process starting from gene detection and ending with a decryption step.

The proposed method is blind, which means that parties of the communication don't need to exchange anything in advance other than the secret key. Experimental results showed a superior performance of the proposed technique in terms of capacity and security. The proposed method achieved a hiding capacity of 2 bit per nucleotide, which is the highest among all methods except [21]. However, the proposed technique succeeded to eliminate the need for embedding header information about the size of the hidden message in [21]. Furthermore, the proposed method showed strong robustness against attacks making it almost unbreakable. Not to mention the ciphering step that protects the contents of the secret message in case the steganographic shield was cracked.

This research can be extended in one of two directions. First, introducing randomness in the merging process of the message and cover segments. That is, message segments can be infused in a random order in between the cover ORFs. Secondly, encryption techniques other than the play-fair cipher can be explored as well.

Conflict of Interest

The authors declare no conflict of interest.

References

[1] Herodotus, Herodotus : The History, University of Chicago Press, 1987.
[2] G. Simmons, "The Prisoners' Problem and the Subliminal Channel," Advances in Cryptology, Springer, 51-67, 1984, doi:10.1007/978-1-4684-4730-9_5.
[3] A. Cheddad, J. Condell, K. Curran, and P. Mc Kevitt, "Digital Image Steganography: Survey and Analysis of Current Methods," Signal Processing, **90**, 727-752, 2010. doi: 10.1016/j.sigpro.2009.08.010.
[4] P. Balgurgi, S. Jagtap, "Audio Steganography used for Secure Data Transmission," in International Conference on Advances in Computing. Advances in Intelligent Systems and Computing, 2013, doi:10.1007/978-81-322-0740-5_83.
[5] M. Sadek, A. Khalifa, M. Gad-El Haaq, "Robust Video Steganography Algorithm using Adaptive Skin-tone Detection," Multimedia Tools and Applications, **76**(2), 2017, doi:10.1007/s11042-015-3170-8.
[6] Y. Tsai, I. Chi, C. Chan, "A Vertex-Based 3D Authentication Algorithm Based on Spatial Subdivision," Symmetry, **10**(10), 2018, doi:10.3390/sym10100422.
[7] J. MacLean, D. Dampier, J. Davis, "Methods of Information Hiding and Detection in File Systems," in Fifth International Workshop on Systematic Approaches to Digital Forensic Engineering (SADFE), 66-69, 2010, doi:10.1109/SADFE.2010.17.
[8] C. Clelland, R. Taylor, C. Bancroft, "Hiding Messages in DNA Microdots," Nature, **399**, 533-534, 1999, doi:10.1038/21092.
[9] S. Jiao, R. Goutte, "Hiding Data in DNA of Living Organisms," Natural Science, **1**(3), 181-184, 2009, doi:10.4236/ns.2009.13023.
[10] D. Heider, M. Pyka, A. Barnekow, "DNA Watermarks in Non-Coding Regulatory Sequences," BMC Research Notes, **2**(125), 2009, doi:10.1186/1756-0500-2-125

[11] D. Na, "DNA Steganography: Hiding Undetectable Secret Messages Within the Single Nucleotide Polymorphisms Of A Genome and Detecting Mutation-Induced Errors," Microb Cell Fact, **19**(128), 2020, doi:10.1186/s12934-020-01387-0
[12] H. Shiu, K. Ng, J. Fang, R. Lee, C. Huang, "Data Hiding Methods based upon DNA Sequences," Information Sciences., **180**(11), 2196-2208, 2010. doi: 10.1016/j.ins.2010.01.030.
[13] A. Khalifa, "LSBase: A Key Encapsulation Scheme to Improve Hybrid Crypto-Systems using DNA Steganography," in 8th International conference on Computer and Engineering, 105-110, 2013, doi:10.1109/ICCES.2013.6707182.
[14] S. Lee, "Reversible Data Hiding for DNA Sequence using Multilevel Histogram Shifting," Security and Communication Networks, 2018. doi:10.1155/2018/3530969.
[15] A. Khalifa, A. Elhadad, S. Hamad, "Secure Blind Data Hiding into Pseudo DNA Sequences Using Playfair Ciphering and Generic Complementary Substitution," Applied Mathematics & Information Sciences, **10**(4), 2016, doi:10.18576/amis/100427
[16] M. Sabry, M. Hashem, T. Nazmy, M. Khalifa, "A DNA and Amino Acids-Based Implementation of Playfair Cipher," (IJCSIS) International Journal of Computer Science and Information Security, **8**(3), 129-136, 2010.
[17] S. Hamad, "A Novel Implementation of an Extended 8x8 Playfair Cipher Using Interweaving on DNA-encoded Data," International Journal of Electrical and Computer Engineering, **4**(1), 93-100, 2014, doi:10.11591/ijece.v4i1.4969.
[18] M. Biswas, K. Alam, S. Tamura, Y. Morimoto, "A Technique for DNA Cryptography based on Dynamic Mechanisms," Journal of Information Security and Applications, **48**, 2019, doi: 10.1016/j.jisa.2019.102363.
[19] M. Cui, Y. Zhang, "Advancing DNA Steganography with Incorporation of Randomness," ChemBioChem, **21**(17), 2503-2511, 2020, doi:10.1002/cbic.202000149.
[20] D. Zebari, H. Haron, S. Zeebaree, "Security Issues in DNA Based on Data Hiding: A Review," International Journal of Applied Engineering Research, **12**(24), 15363-15377, 2017.
[21] A. Khalifa, "A Blind DNA-Steganography Approach using Ciphering and Random Sequence Splicing," in 10th International Conference on Information Science and Technology (ICIST), 86-90, 2020, doi:10.1109/ICIST49303.2020.9202036.
[22] A. Ghosh, M. Bansal, "A glossary of DNA structures from A to Z," ACTA Crystallography D, Biological Crystallography, **59**(4), 620-626, 2003, doi:10.1107/s0907444903003251.
[23] F. Crick, "Central Dogma of Molecular Biology," Nature, **227**, 561–563, 1970, doi:10.1038/227561a0.
[24] M. Adam, H. Ardinger, R. Pagon, et al, Gene Reviews, University of Washington, 1993-2021.

Activity-Based Cost Estimation Model for The Extrusion of Variant Aluminum Profiles

Mohammad AL-Tahat[*], Issam Jalham, Abbas Al-Refaie, Mohammed Fawzi Alhaj Yousef

Industrial engineering department, The University of Jordan, Amman, 11942, Jordan

A R T I C L E I N F O	A B S T R A C T
	A competitive manufacturing environment dictates to be conscious of the real cost of production to increase profitability, to have a precise cost estimation, and to avoid cost distortion. Activity-Based Costing (ABC) is one choice to achieve these objectives. This paper aims to build an ABC method, consequently, to explore its application for a local Aluminum extrusion factory that producing variant Aluminum profiles. The considered Aluminum extrusion factory is investigated carefully. Production resources, processes, and activities are identified for each product type, cost rates for each processing step are estimated, cost- estimating relationship model that mathematically describes the cost of the extruded product as a function of all consumable properties is created. Cost stream mapping through the production centers is analyzed then costs of existing resources are assigned, cost rates are obtained, accordingly results are discussed and presented. A comparison between the traditional costing method and the ABC is conducted, the comparison reveals that the ABC Estimates of the unit production costs are closer to reality than those obtained by the traditional costing method, contributing to the determination of realistic profit margins that are appropriate to the competitive market situation. Finally, recommendations and avenues for future works are suggested.

1. Introduction

Improvement of system performance plays an important role in many areas of research. For example, the Kanban methodology as an improvement approach is presented in [1], performance improvement of maintenance effectiveness in health care services was investigated by [2]. On the other hand, business performance using structural equation modeling was examined in [3], a problem of multiple criteria decision making (MCDM) for a pharmaceutical system was solved in [4]. In other studies:

- Improvement of pharmaceutical tablet production was investigated in [5].
- A model to improve the constant work-in-process (CONWIP) using the continuous-time Markov chain modeling approach was presented in [6].
- The implementation of Concurrent Engineering (CE) methodology for performance improvements of some Jordanian industrial sectors was described in [7].

- An Activity-Based Cost Estimation Model for steel foundry to improve cost estimation was explained in [8].

This paper aims to develop an activity-based cost estimation model to be suitable for use in aluminum profile extrusion plants of various shapes and types. The proposed model is expected to contribute to an estimate of manufacturing costs closer to reality with more accuracy and precision.

The use of accurate and precise costing methods has become a major need in all fields of manufacturing as it enables managers to take appropriate planning and control decisions. Generally, two costing methods may follow in manufacturing [9], the first is the traditional Costing (TC) method that implies job ordering and process costing, and the second one is the Activity Based Costing (ABC) method, which was conceived in the mid-'80s by [10]. ABC method was mainly used to correct misleading overhead allocations. Furthermore, the method is elaborated to solve the distortion problems of the traditional costing system [10,11]. The Chartered Institute of Management Accountants [12] defines ABC as an "approach to the costing and monitoring of activities which involves tracing resource consumption and costing final outputs. Resources are assigned to activities, and activities to cost

[*]Corresponding Author: Mohammad AL-Tahat, E-mail: altahat@ju.edu.jo

objects based on consumption estimates. The latter utilize cost drivers to attach activity costs to outputs" [12]. ABC has aroused considerable interest in the last forty years, it produced precise cost estimates and designed to solve many obstacles and distortion costs [13], which cannot be solved by the traditional costing approach. Therefore, ABC is used with medium- and long-term planning horizon which is known as a strategic cost system [13]. Unlike the TCS method, ABC traces the overhead to an activity related to the product, rather than to the product itself [14]. The ABC method provides relevant and useful information for the decision-making process in various domains, such as the definition of cost and sales prices of products, the identification of processes where greater effort is needed to improve or adapt them to the new realities and needs, and the restructuring of some areas of the industrial unit [15]. A method for overcoming the limitations of TC was presented in [16]. ABC has received its name because of the focus on the activities performed in the realization of a product it has become a mature cost estimation and accounting method [13]. Recently, the main research on the ABC costing system had been highlighted in [17], the developments in growth and future research opportunities, and the mutual contribution on the topic between foundations, and authors over time had been also highlighted in [17]. In [18] the ABC method was applied on the inductor element for better precision in an electronic manufacture located at Pahang, Malaysia. Managers of manufacturing systems facing the challenges of estimating accurate costs and of setting a realistic profitable selling price of their products, specifically in a multi-products multi-process manufacturing system, where there is a high overlapping between production activities, and when the overhead costs are high. Setting a realistic profitable selling price that considers all costs elements also constitutes a challenge for most manufacturers. Referring to [19,20], the advantages of ABC can be summarized as; (1) Provides accurate cost estimate, (2) Flexible, (3) effective for long term planning, (4) Offers significant financial and non-financial measures at an operational level. (5) Supports better pricing policy. (6) Helps to understand the cost behavior of products, (6) helps management to highlights costing problems, (7) Highlight's opportunities for improvements, and (8) assigning the overhead cost based on processes and activities.

These advantages have inspired the authors of this paper to investigate the methodology of employing ABC principles in one local Jordanian Aluminum extrusion factory. The selected extrusion factory produces variant Aluminum profiles that fit with the market's demand. In particular, the objective of this work is to: (1) Develop ACB model that fits the selected Aluminum extrusion factory in Jordan, moreover, it can be implemented also for any aluminum extrusion factory. (2) Estimate the manufacturing costs of producing Aluminum profiles using the developed ABC method for the Aluminum profiles that can be produced by the considered factory. (3) Revealing the advantages of the ABC approach over the Traditional costing system (TCS) by comparing them.

After investigating the literature referred to in this paper, other recently published scientific papers that examined the application of ABC to material extrusion processes in general and aluminum extrusion specifically were searched. The authors found that there are scientific papers close to the field of this

research, such as [21–23], at the same time the authors were unable to find published papers that deal with the current research scope. Consequently, this paper has contributed to a unique and qualitative scientific contribution, which is the application of ABC as a modern accounting method to a specific manufacturing process, which is the aluminum extrusion process, which enhances the novelty of this research, considering the continuous search of production managers and industrial cost analysts, to find the most accurate, and objective accounting methods, as is the case in the ABC method.

2. Modeling of Aluminum extrusion activities and resources consumption

This paper is considering an aluminum extrusion factory that produces seven types of Aluminum profiles namely, (1) mill finish profile, (2) powder coated profile, (3) wood finish profile, (4) silver matt profile, (5) Bright silver profile, (6) champagne profile, and (7) bronze profile. These products are produced through the following main processes; (a) extrusion, (b) powder coating, and (c) anodizing. In the Anodizing process, silver matt profile, bright silver profile, champagne profile, and bronze profile are produced. As shown in Figure 1, the extrusion of aluminum is the transformation of raw aluminum logs into variant profiles shape, aluminum logs are fed to the manufacturing system and flow through the production line according to the layout shown by Figure 2. Details of the typical extrusion process of aluminum profiles are depicted in Figure 3. As shown in Figure 3, the mill finish profile was produced after the extrusion process, then packed and shipped directly after finishing the heat treatment process at the aging furnace without any surface treatment.
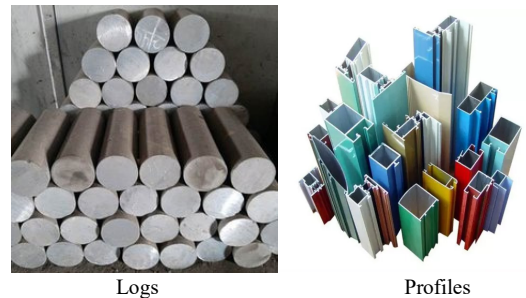
Logs   Profiles
Figure 1: Extrusion manufacturing system of aluminum profiles
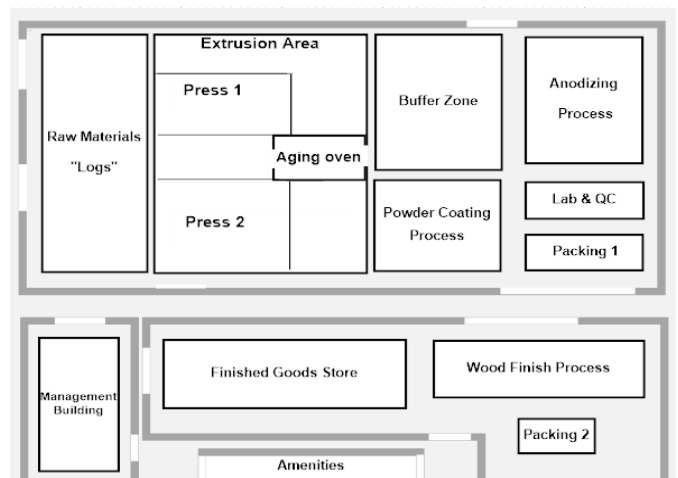
Figure 2: Layout of the proposed extrusion manufacturing system and its support departments
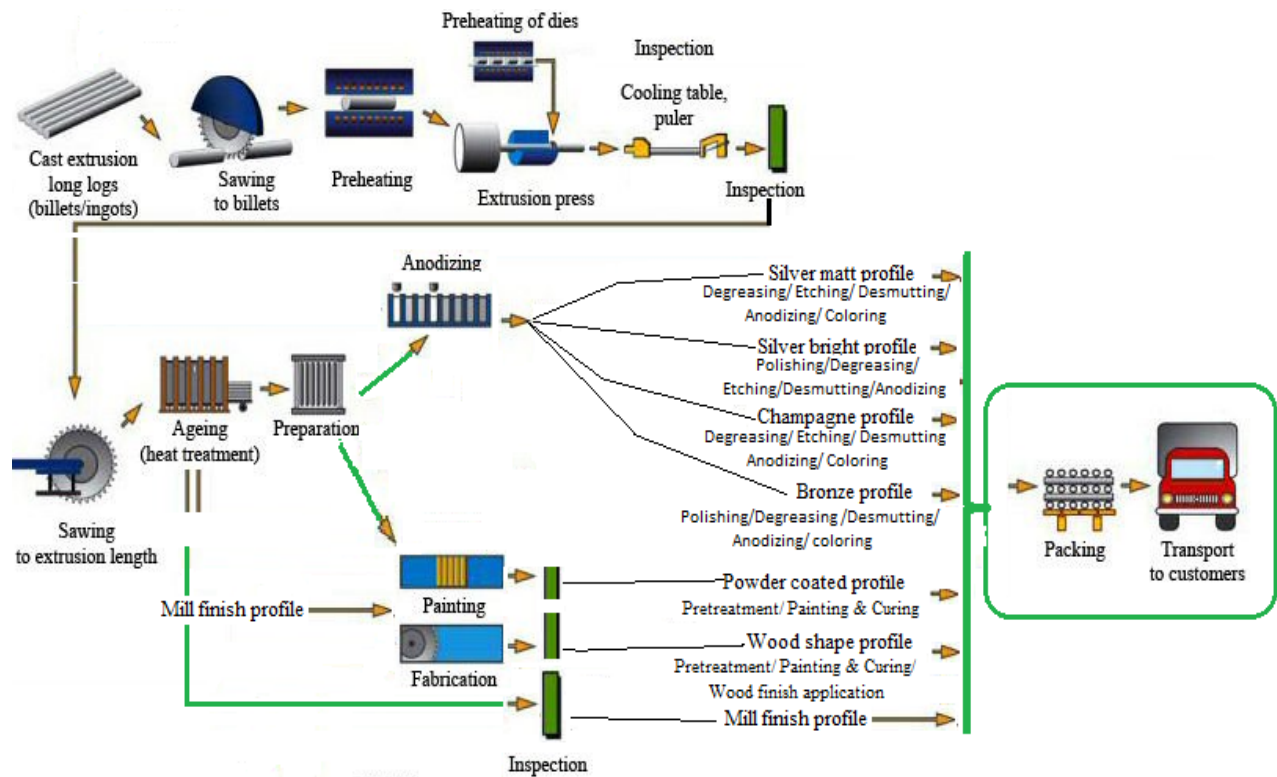
Mill finish profile may be transformed through the anodizing process into, silver matt profile, bright silver profile, champagne profile, or bronze profile upon request, the profile moves to a sequence of dipping stages of 18 baths. Mill finish profile may be transformed through the powder coating process to produce the powder-coated profile. Also, the mill finish profile may be transformed through the wood finish application process to produce the wood shape profile. Silver matt, silver bright, champagne matt, and bronze profiles are an anodized profile. Some Aluminum extrusion factories cost these four products as a unit one, although they have different processing sequences.

Extrusion Factor (EF) is the ratio of the average yearly production to the standard designed production capacity over a year. As in Figure 4, production of aluminum profile over the last ten years are investigated, yearly production is found to be 300 tons of different aluminum profiles, the average EF of a designed production capacity of a maximum of 600 tons is equal to (0.50).
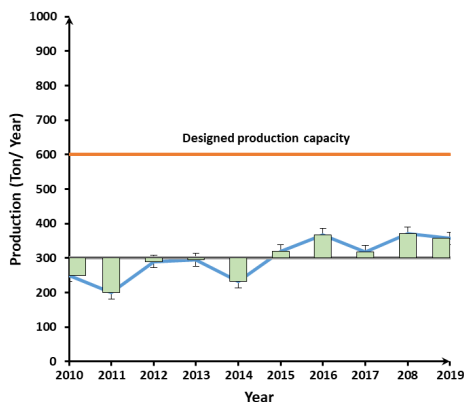
Figure 4: Actual capacity of Extrusion Factor (EF) over the past ten years

The monthly production is estimated by spreading the average of the actual yearly production over 12 working months, therefore the actual Monthly Production (AMP) production quantity is:

$$AMP = \frac{Average\ Yearly\ actual\ production}{Working\ months\ per\ year}$$

$$AMP = \frac{300}{12} = 25\ (Tons\ per\ Year)$$

2.1. Activities and activity centers

Cost allocation was defined in [20] as; "the process of assigning costs when a direct measure does not exist for the number of resources consumed by a particular cost object". Cost allocations in ABC consist of two stages [8], in the first stage the overhead costs are assigned to cost centers, while in the second stage, cost rate are assigned to the jobs according to activities required to accomplish the extrusion process, this stage needs to have an accurate cost set that accounts for how much it costs to create a product. Figure 5 illustrates the two stages of allocation.

As shown in Figure 3, many activities being carried out in the system. The main activities are; acquisition long logs, sawing long logs into billets, billets preheating, preparation of extrusion press, extrusion, the extruded products then pass through cooling and inspection stages, then cut to the required length, heat-treated, products may move to preparation or fabrication. Anodized items may go through; degreasing, etching, smutting, coloring, or polishing, and painting. Fabricated items move to, pre-treatment,

painting, curing, and wood finish application.   Finally, any final product will be inspected, packed, and shipped to external customers. Such activity centers are traced, resources needed to accomplish each activity are identified, it is assumed that these activity centers consume certain levels of resources. The resource consumption is calculated using utilization levels of these centers per Kilogram of final extruded profiles.
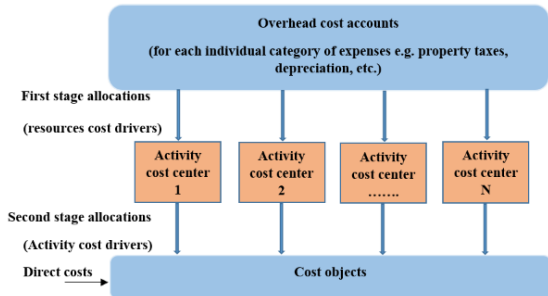
Figure 5: Two-stage allocation process for an activity-based costing system

2.2. Resources consumption

 UPC) is the summation of the costs of activities that go on to produce that product. For every activity, one should calculate how much the cost of the consumed resources. Costs of activities that go on to produce certain aluminum profile can be classified - as shown in Figure 6- into the following four categories: 1) Cost of resources related to the extrusion process (EPC), 2) Cost of resources related to the Manufacturing Overhead Cost (MOC), 3) Cost of resources related to Selling and Marketing (SMC), and 4)

cost of resources related to the Administrative Cost (ADC), these classes are explained briefly as follows;

I) Cost of resources related to the extrusion process (EPC). Represents values expenditures of direct labor and direct materials, EPC involved:

Item 1. Cost of direct material (CDM): costs of materials directly charged to the extruded profile during its passage through the plant. This cost element considers long logs charging materials cost, painting materials, release agent, consumed materials for fabrication, consumed materials during the anodizing operations, and consumed materials in packaging and inspection.

Item 2. Cost of direct labor, (CDL). Cost of employees directly involved in the extrusion of the aluminum profiles. Such as wages and salaries paid for the involved blue dress workers.

II) Cost of resources related to the Manufacturing Overhead Cost (MOC). MOC embraces all expenditures incurred in the production of the aluminum profiles that are not direct material or direct labor. MOC implies:

Item 3. Indirect material cost, (IDMC). Cost of materials that are not directly charged to the extrusion, such as; materials consumed in fabrication, aging, heat treatment, extrusion dies, tools, inspection devices, and supplies used include water, lighting, heating fuel, electric power, and maintenance supplies. Also, extrusion dies, consumed materials for cutting, painting, and heat treatment (heat treatment media, wooden materials, cutting off tools, etc.), lubricant, coolant, and painting materials. Engineering and planning cost, (EPC). Covers engineering department and technical, planning, quality engineering, Continual and agile improvements, maintenance, etc.
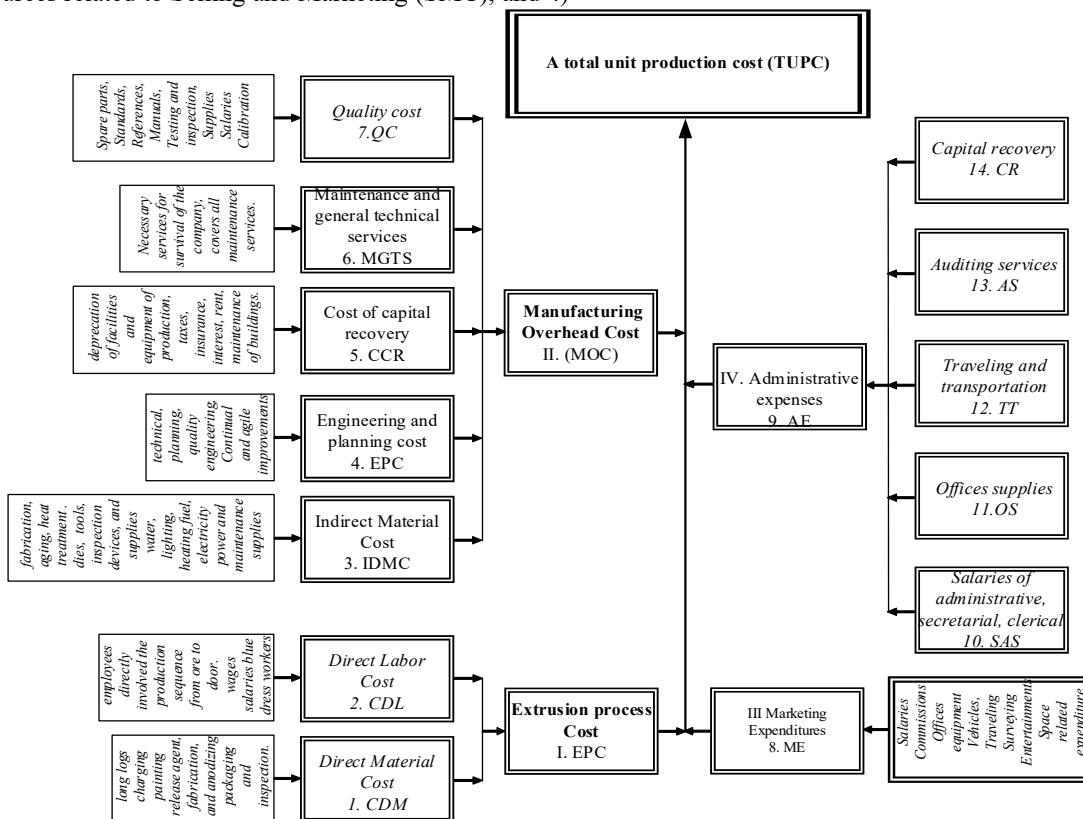
Figure 6: Main Components of the Developed ABC Structure

Item 5. Cost of capital recovery (CCR). Encompasses deprecation cost of facilities covering equipment and production facilities, taxes, insurance, interest, rent, maintenance of production buildings, and other related hidden costs.

Item 6. Maintenance and general technical services (MGTS), such as failure costs, prevention costs, surplus cost, and necessary maintenance services for the survival of the company.

Item 7. Quality cost (QC). The cost spent to buy spare parts, standards, references, manuals, testing and inspection, and other materials supplies needed for quality management activities. It also includes rework cost, significant costs related to quality, and salaries of operators and calibration costs.

III Marketing Expenditures (ME).

Item 8. ME includes salaries of sales and marketing personnel, commissions, cost of using office equipment and different vehicles, traveling cost, surveying cost, entertainment of customers, sales space, and other related expenditures.

IV) Administrative expenses (AE), which implies the followings:

Item 9. AE is related to such items as; (10) salaries of administrative, secretarial, and clerical personnel; (11) office supplies; (12) traveling and transportation, (13) auditing services that are necessary to direct the operation, and other related issues.

Item 14. Capital Recovery (CR). Represents the depreciation on such equipment as vehicles, cars, machines, land, offices, hardware and software systems, and other facilities belonging to the company but not related directly to the production.

It is worthy to mention in this regard that costs elements, such as hidden costs, surplus costs, rework cost, failure costs, prevention costs and other significant costs are present in every work center and are considered when estimating the cost rates within work centers.

3. Mapping cost of resources with activity centers

Twenty different activities are identified to produce the aluminum profiles, Figure 7, these are; (1) Long logs ordering, (2) Billets preparations, (3) Billets Preheating, (4) Preheating of dies, (5) Extrusion, (6) Cooling, (7) Inspection, (8) Billet-length fixing, (9) Aging (Heat treatment), (10), preparation for the production of non-standard profiles, (11) Anodizing, (12) Painting, (13) Fabrication, (14) Degreasing, (15) Etching, (16) Desmutting, (17) Coloring, (18) Polishing, (19) Wood application, (20) Packing. Consequently, resources are allocated, then the summation of costs of resources that are consumed by every activity center is calculated. Based on the cost structure model presented in the previous sections. The determination of which activity consumed which resource and how much of the resource is used by that activity is the key to cost calculation. Figure 7 demonstrates the relationship between resources and activities and how these relations contribute to the final production cost, the figure shows that the cost of the produced Aluminum profiles is estimated based on how starting components and raw materials physically flow within the activity centers through the deferent division of the factory. The production unit production cost (TUPC) of the produced profiles reflect the cost of resources and Work-In-Process (WIP) items account at each activity center.

4. ABC costing of total production unit production cost

Notations presented in Table 1 are used for mathematical representation of the model. Figure 3 is a general illustration of the flow of any type of aluminum profile. For a specific profile type, some modifications may be required. Some profiles are not pass through all the activity centers and hence the allocated cost for the non-passed centers will be zero. For example, the mill finish profile is finally produced after heat treatment, Anodizing, Painting, Fabrication, Degreasing, Etching, Desmutting, Coloring are not visited by this product.
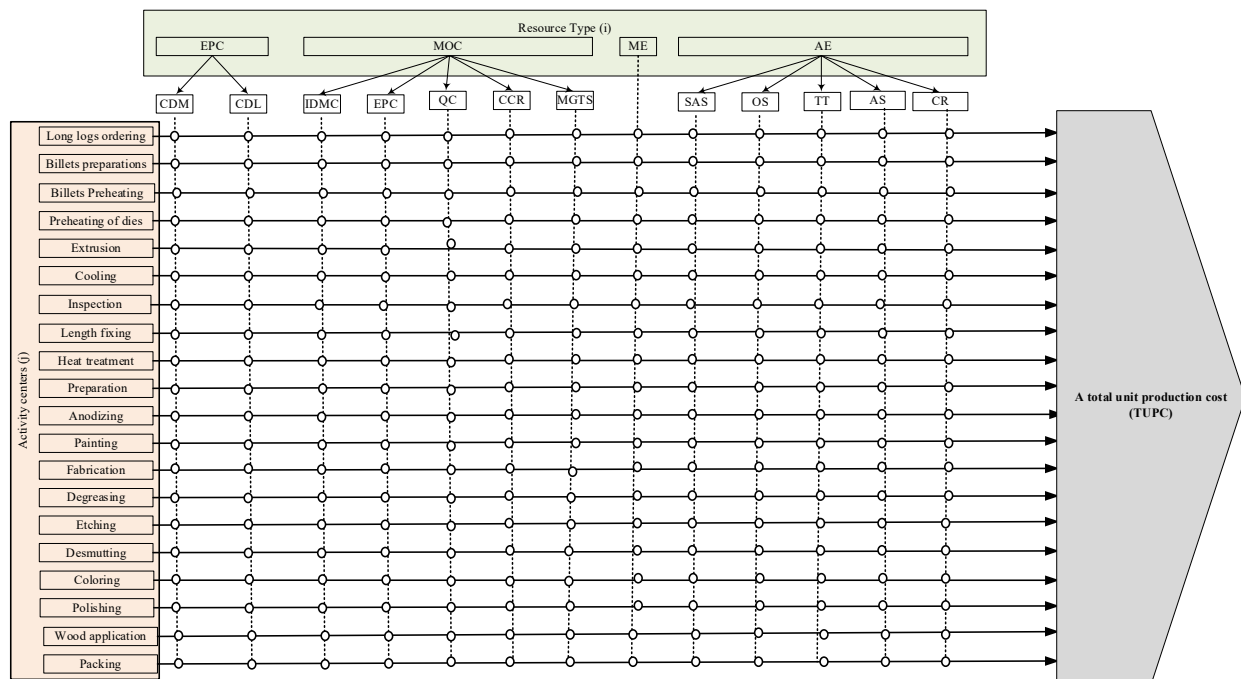
Figure 7: Contribution to final cost and relationship between resources and activity center

Table 1: Used Notations

Symbol	Description
TUPC	Total unit production cost, \$/1000 Kilogram
I	Total available number of resources
i	Resource index (*i* = 1, 2, ... I)
J	Total available number of activity centers
j	Center index *(j = 1, 2, ... J)*
R*ij*	Cost rate of consuming the ith resource at the jth activity center for producing a one-kilogram profile. (\$/1Kg)

$$TUPC = 1000\sum_{i=1}^{I}\sum_{j=1}^{J}R_{ij} \qquad (1)$$

4.1. ABC cost rates

The primal target of this paper is to present an ABC approach for estimation TPUC, this work will not consider the detailed derivation of how the rates (R$_{ij}$) are drawn. These cost rates represent the values of resources consumed by work centers. The computation of these rates is highly dependent on the skills and on the experience of the industrial engineers who computed them. As a result, cost rates are presented in Appendix 1. These cost rates cover the whole range of the profiles. Reference to the activity resource relationships shown in Figure 7, TPUC for any Aluminum profile type can be calculated using equation (1). The total production cost of any finished Aluminum profile is the sum of the allocated costs at each activity center the part undergoes during its journey of the production process.

4.2. ABC calculations

According to Figure 7, TUPC is the sum of the allocated costs for each activity center the part undergoes in its production process. TUPC for any profile type can be computed by equation (1) using the cost information given in Table 2.
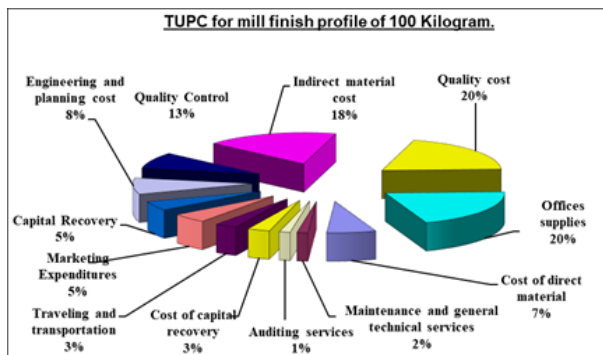
Figure 8: Cost-percentages allocation of mill finish profile.

Consider a mill finish Aluminum profile of 100 Kilogram. TUPC of this item is the summation of cost for all consumed resources (\$448). Cost-percentages allocation of the considered profile in terms of resource areas associated with its production processes is shown in Figure 8. Similarly, TPUC for all profiles are computed, then presented in Table 3.

4.3. Traditional costing system versus Activity-Based costing.

According to the Traditional Costing System (TCS) that is followed by the factory, the total costs of the considered profiles are shown in Table 4.

Based on ABC, the most expensive Aluminum profile is Mill Finish, while the lowest cost is for Powder Coated profile. Based on TCS, the most expensive profiles are Silver Bright, Champagne, and Bronze profile, while the lowest cost is for Mill Finish profile. ABC depicts the cost visibility that can be considered as a visual tool that shows how costs are contributed to total production unit production cost (TPUC) downstream the considered extrusion factory through the different production activities, Pareto chart in Figure 9 highlights how resources consumption contributes to TPUC through the different production activities for Mill Finish profile. ABC results can provide quantitative figures to how the costing process is appraised and the improved visibility of cost through the allocation of cost from resources to activities. ABC enables managers to recognize the hierarchy of all cost elements, not only the direct and indirect costs elements as in TCS. According to what had been presented in [23] a brief and purposeful, comparison between the benefits and the drawbacks of both the traditional and the ABC costing methods is presented in Table 5 where the critical characteristics of ABC versus TCS are examined. Figure 10 shows that the most important cost parameters are the cost of direct material (CDM), Cost of direct labor (CDL), Indirect material cost (IDMC), marketing expenditures (ME), salaries of administrative, secretarial, and clerical personnel (SAS) and cost of offices supplies. The final production cost is highly sensitive to such highlighted parameters. Verification of results is conducted by comparing results with those obtained by the traditional costing system TCS.

The methodology pursued in this work is valuable for Aluminum extrusion with more accuracy and precision when comparing with the TCS. That enables managers to estimate the cost of WIP at any time during the production sequence. ABC has some limitations, as the number of activities increases, the cost of estimation becomes higher., in addition to the difficulties of gathering activity data in service organizations and labor-intensive companies due to the variant and overlapped human activities.

5. Conclusions

The desired objectives of the research were successfully achieved, and the developed ABC model was suitable for use in estimating the costs of extruding aluminum profiles. Moreover, this costing model is used to compare the costs of extruding different profiles, which helps the management in ordering the consequent marketing and productivity priorities. It is concluded that the most expensive Aluminum profile is Mill finish, while the lowest cost is for Powder coated profile. ABC depicts the cost visibility that can be considered as a visual tool that shows how costs are contributed to total production unit production cost (TPUC). ABC enables managers to recognize the hierarchy of all cost elements, not only the direct and indirect costs elements as in TCS. The most important cost parameters are the cost of direct material (CDM), Cost of direct labor (CDL), Indirect material cost (IDMC), marketing expenditures (ME), salaries of administrative, secretarial, and clerical personnel (SAS), and cost of offices supplies.

Table 2: Computations of TUPC ($) for a mill finish Aluminium profile of 100 Kilogram weight.

Resource Type (i)	Profile type	J=1= Long logs ordering	J=2= Billet's preparations	J=3 Billets Preheating	J=4 Preheating of dies	J=5 Extrusion	J=6 Cooling	J=7 Inspection	J=8 Length fixing	J=9 Heat treatment	J=10 Preparation	J=11 Anodizing	J=12 Painting	J=13 Fabrication	j=14 Degreasing	j=15 Etching	j=16 Desmutting	j=17 Coloring	j=18 Polishing	j=19 Wood application	j=20 Packing	Sub-Total
CDM		0.025	0.023	0.016	0.000	0.001	0.004	0.000	0.002	0.000	0.016	0.000	0.000	0.004	0.021	0.000	0.009	0.004	0.000	0.000	0.000	0.13
CDL		0.240	0.020	0.020	0.000	0.000	0.000	0.000	0.000	0.000	2.240	0.000	0.000	0.003	0.000	0.000	0.000	0.051	0.000	0.000	0.000	2.57
IDMC		0.077	0.087	0.087	0.000	0.008	0.015	0.003	0.000	0.000	0.000	0.008	0.003	0.001	0.045	0.000	0.001	0.007	0.000	0.000	0.000	0.34
EPC		0.060	0.006	0.005	0.000	0.001	0.003	0.000	0.000	0.000	0.013	0.000	0.000	0.000	0.027	0.009	0.012	0.001	0.007	0.007	0.007	0.16
QC		0.087	0.080	0.010	0.000	0.004	0.015	0.010	0.019	0.000	0.007	0.001	0.001	0.002	0.007	0.000	0.000	0.030	0.007	0.007	0.093	0.38
CCR	Mill Finish	0.000	0.000	0.000	0.000	0.000	0.000	0.000	0.000	0.000	0.000	0.000	0.000	0.057	0.000	0.000	0.000	0.000	0.000	0.000	0.000	0.06
MGTS		0.013	0.001	0.001	0.000	0.000	0.001	0.000	0.000	0.000	0.003	0.000	0.000	0.010	0.000	0.000	0.000	0.000	0.000	0.000	0.000	0.03
ME		0.014	0.001	0.001	0.000	0.000	0.001	0.000	0.000	0.000	0.003	0.000	0.000	0.000	0.001	0.000	0.000	0.005	0.021	0.021	0.021	0.09
SAS		0.060	0.006	0.005	0.000	0.001	0.003	0.000	0.000	0.000	0.013	0.000	0.000	0.000	0.027	0.009	0.012	0.001	0.007	0.007	0.007	0.16
OS		0.087	0.080	0.010	0.000	0.004	0.015	0.010	0.019	0.000	0.007	0.001	0.001	0.002	0.007	0.000	0.000	0.030	0.007	0.007	0.093	0.38
TT		0.000	0.000	0.000	0.000	0.000	0.000	0.000	0.000	0.000	0.000	0.000	0.000	0.057	0.000	0.000	0.000	0.000	0.000	0.000	0.000	0.06
AS		0.013	0.001	0.001	0.000	0.000	0.001	0.000	0.000	0.000	0.003	0.000	0.000	0.010	0.000	0.000	0.000	0.000	0.000	0.000	0.000	0.03
CR		0.014	0.001	0.001	0.000	0.000	0.001	0.000	0.000	0.000	0.003	0.000	0.000	0.000	0.001	0.000	0.000	0.005	0.021	0.021	0.021	0.09

TUPC of Mill Finish$/Kg	4.48
TUPC of Mill Finish of 100 Kg Weight ($/Kg)	448.00

Table 3: TPUC of all Aluminum Profiles

Profile Type	TPUC ($/Kg)
Mill Finish	4.48
Powder Coated	2.03
Wood Finish	2.11
Silver Matt	2.04
Silver Bright	2.59
Champagne	2.95
Bronze	2.51

Table 4: Cost of all Aluminum Profiles based on traditional costing system

Profile Type	Cost ($/Kg)
Mill Finish	2.75
Powder Coated	3.18
Wood Finish	3.50
Silver Matt	3.89
Silver Bright	3.89
Champagne	3.89
Bronze	3.89

Table 5: Activity-Based Costing versus Traditional Costing

Traditional Costing	Activity-Based Costing
- Simpler and easier - Inexpensive. - Low overhead costs - With large production volume and low product's Varity - For external cost reporting	- Difficult to implement. - Costly - High overhead costs - With low production volume and high product's Varity - For internal cost reporting - Greater accuracy and precision.
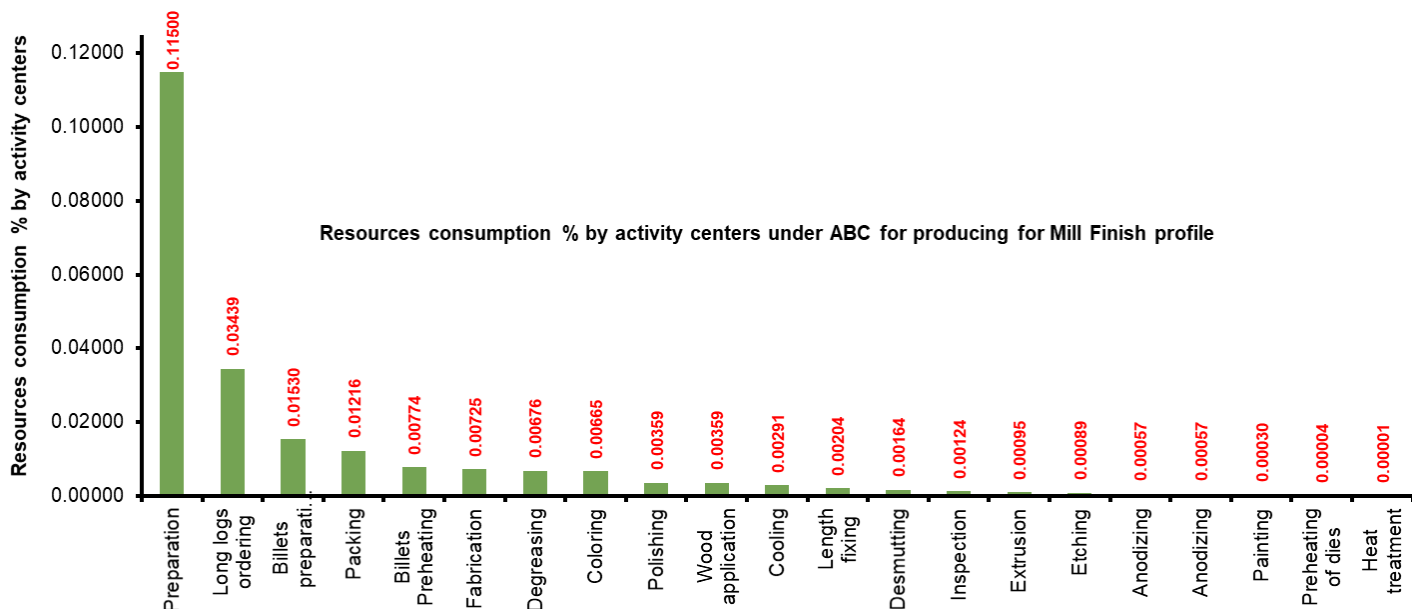
Figure 9: Resource consumption % by activity centers under ABC for Mill finish profile.
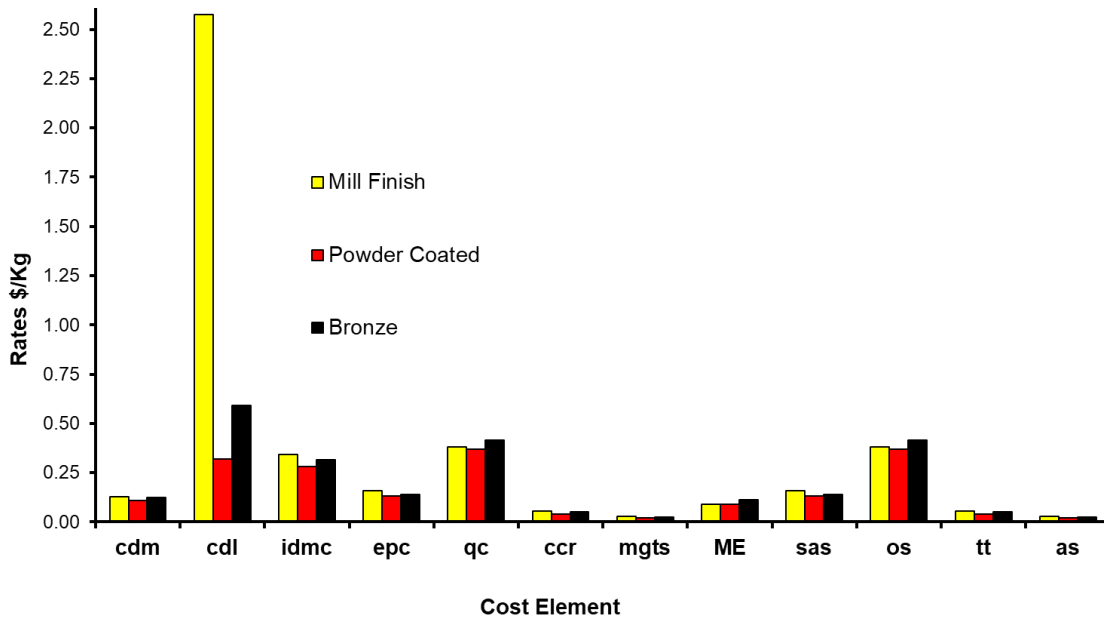
Figure 10: Comparison between Cost rate for every cost element for three profiles' type

Conflict of Interest

The authors declare no conflict of interest.

References

[1] M.D. Al-Tahat, "Optimizing of Work in Progress (WIP) in Kanban Controlled Production Lines," Dirasat: Engineering Sciences, **32**, 123–132, 2005.

[2] K.R. Al-Momani, M.D. Al-Tahat, E. Jarada, "Performance measures for improvement of maintenance effectiveness," in Proceedings - ICSSSM'06: 2006 International Conference on Service Systems and Service Management, 632–637, 2006, doi:10.1109/ICSSSM.2006.320535.

[3] A.-R. Abbas, M.D. Al-Tahat, "Effects of Knowledge Management and Organization Learning on Firms' Performance," The Journal of Nature Science and Sustainable Technology (JNSST), **8**, 369–390, 2014.

[4] D. Dalalah, M.D. Al-Tahat, K. Bataineh, "Mutually Dependent Multi-criteria Decision Making," Fuzzy Information and Engineering, **4**(2), 195–216, 2012, doi:10.1007/s12543-012-0111-3.

[5] M.D. AL-Tahat, A.K.M. Abdul Jawwad, Y.L. Abu Nahleh, "Ordinal Logistic Regression Model of Failure Mode and Effects Analysis (FMEA) in Pharmaceutical Tabletting Tools," Engineering Failure Analysis, **27**(January), 322–332, 2013, doi:10.1016/j.engfailanal.2012.08.017.

[6] M.D. Al-Tahat, I.A. Rawabdeh, "Stochastic analysis and design of CONWIP controlled production systems," Journal of Manufacturing Technology Management, **19**(2), 253–273, 2008, doi:10.1108/17410380810847945.

[7] M.D. Al-Tahat, A.M. Al-Habashneh, I.S. Jalham, "A Statistical Comparison of the Implementation of Concurrent Engineering in Jordanian Industry," Open Journal of Statistics, **09**(03), 361–372, 2019, doi:10.4236/ojs.2019.93025.

[8] M.D. Al-Tahat, A.R. Abbas, "Activity-based cost estimation model for foundry systems producing steel castings," Jordan Journal of Mechanical and Industrial Engineering, **6**(1), 75–86, 2012.

[9] C. Drury, "Management and Cost Accounting Eighth Edition Colin Drury," Management and Cost Accounting Eighth Edition Colin Drury, **7**(2), 1–16, 2012.

[10] R. Cooper, R.S. Kaplan, "Measure Costs Right: Make the Right Decision.," Harvard Business Review, **66**(5), 96–103, 1988.

[11] R. Cooper, R.S. Kaplan, "How Cost Accounting Systematically Distorts Product Costs," Accounting and Management Field Study Perspectives, 49–72, 1987.

[12] CIMA, Activity Based Costing Topic Gateway, 2008.

[13] C. Homburg, "Improving activity-based costing heuristics by higher-level cost drivers," European Journal of Operational Research, **157**(2), 332–343, 2004, doi:10.1016/S0377-2217(03)00220-0.

[14] L. Ronald, "Activity-based models for cost management systems," Choice Reviews Online, **33**(05), 33-2831-33–2831, 1996, doi:10.5860/choice.33-2831.

[15] L. Barreto, A. Amaral, T. Pereira, "The implementation of an Activity-Based Costing (ABC) system in a manufacturing company," Procedia Manufacturing, **13**, 1245–1252, 2017.

[16] I. Mahal, M. Akram Hossain, "Activity-Based Costing (ABC)-An Effective Tool for Better Management," Research Journal of Finance and Accounting Www.Iiste.Org ISSN, **6**(4), 66–74, 2015.

[17] P. Quesado, R. Silva, "Activity-based costing (ABC) and its implication for open innovation," Journal of Open Innovation: Technology, Market, and Complexity, **7**(1), 1–20, 2021, doi:10.3390/joitmc7010041.

[18] N.F. Zamrud, M.Y. Abu, "Comparative Study: Activity Based Costing and Time Driven Activity Based Costing in Electronic Industry," Journal of Modern Manufacturing Systems and Technology, **4**(1), 68–81, 2020, doi:10.15282/jmmst.v4i1.3840.

[19] R. Sreekantha, Cost Management 6th Sem Bcom Product Speci cations, 2021.

[20] W.N. Lanen, S.W. Anderson, M.W. Maher, D.T. Dearman, "Fundamentals of Cost Accounting," Issues in Accounting Education, **25**(4), 791–792, 2010, doi:10.2308/iace.2010.25.4.791.

[21] A. Kampker, P. Ayvaz, G. Lukas, S. Hohenstein, V. Kromer, "Activity-based Cost Model for Material Extrusion Processes Along the Additive Manufacturing Process Chain," in IEEE International Conference on Industrial Engineering and Engineering Management, 489–495, 2019, doi:10.1109/IEEM44572.2019.8978507.

[22] H. Gholami, N.S. Jiran, S. Mahmood, M.Z.M. Saman, N.M. Yusof, V. Draskovic, R. Jovovic, "Application of activity-based costing in estimating the costs of manufacturing process," Transformations in Business and Economics, **18**(2), 839–860, 2019.

[23] S. Bazrafshan, B. Karamshahi, "Examining the Disadvantages of Activity Based Costing (ABC) System and Introducing the Modern (Behavior Based Costing) (BBC) System," International Journal of Management, Accounting and Economics, **4**(2), 163–177, 2017.

Appendix 1: Cost rates of resources at each activity center R_{ij} ($/Kg)

Resource Type (i)	Profile type	Long logs order	Billets preparation	Billets Preheating	Preheating of die	Extrusion	Cooling	Inspection	Length fixing	Heat treatment	Preparation	Anodizing	Painting	Fabrication	Degreasing	Etching	Desmutting	Coloring	Polishing	Wood application	Packing	Sub-Total
CDM	Mill Finish	0.025	0.023	0.016	0.000	0.001	0.004	0.000	0.002	0.000	0.016	0.000	0.000	0.004	0.021	0.000	0.009	0.004	0.000	0.000	0.000	0.13
	Powder Coated	0.025	0.023	0.016	0.000	0.001	0.004	0.000	0.002	0.004	0.000	0.000	0.000	0.004	0.021	0.000	0.009	0.003	0.000	0.000	0.000	0.11
	Wood finish	0.025	0.023	0.016	0.000	0.001	0.004	0.000	0.002	0.004	0.000	0.000	0.000	0.004	0.021	0.000	0.009	0.003	0.000	0.000	0.000	0.11
	Silver Matt	0.025	0.023	0.016	0.000	0.001	0.004	0.000	0.002	0.004	0.000	0.000	0.000	0.004	0.021	0.000	0.009	0.002	0.000	0.000	0.000	0.11
	Silver Bright	0.025	0.023	0.016	0.000	0.001	0.004	0.000	0.002	0.020	0.000	0.000	0.000	0.004	0.021	0.000	0.009	0.003	0.000	0.000	0.000	0.13
	Champagne	0.025	0.023	0.016	0.000	0.001	0.004	0.000	0.002	0.016	0.000	0.000	0.000	0.004	0.021	0.000	0.009	0.003	0.000	0.000	0.000	0.13
	Bronze	0.025	0.023	0.016	0.000	0.001	0.004	0.000	0.002	0.016	0.000	0.000	0.000	0.004	0.021	0.000	0.009	0.003	0.000	0.000	0.000	0.13
CDL	Mill Finish	0.240	0.020	0.020	0.000	0.000	0.000	0.000	0.000	0.000	2.240	0.000	0.000	0.003	0.000	0.000	0.000	0.051	0.000	0.000	0.000	2.57
	Powder Coated	0.240	0.020	0.020	0.000	0.000	0.000	0.000	0.000	0.000	0.000	0.000	0.000	0.003	0.000	0.000	0.000	0.040	0.000	0.000	0.000	0.32
	Wood finish	0.240	0.020	0.020	0.000	0.000	0.000	0.000	0.000	0.067	0.000	0.000	0.000	0.003	0.000	0.000	0.000	0.036	0.000	0.000	0.000	0.39
	Silver Matt	0.240	0.020	0.020	0.000	0.000	0.000	0.000	0.000	0.067	0.000	0.000	0.000	0.003	0.000	0.000	0.000	0.031	0.000	0.000	0.000	0.38
	Silver Bright	0.240	0.020	0.020	0.000	0.000	0.000	0.000	0.000	0.335	0.000	0.000	0.000	0.003	0.000	0.000	0.000	0.036	0.000	0.000	0.000	0.65
	Champagne	0.240	0.020	0.020	0.000	0.000	0.000	0.000	0.000	0.268	0.000	0.000	0.000	0.003	0.000	0.000	0.000	0.040	0.000	0.000	0.000	0.59
	Bronze	0.240	0.020	0.020	0.000	0.000	0.000	0.000	0.000	0.268	0.000	0.000	0.000	0.003	0.000	0.000	0.000	0.040	0.000	0.000	0.000	0.59
IDMC	Mill Finish	0.077	0.087	0.087	0.000	0.008	0.015	0.003	0.000	0.000	0.000	0.008	0.003	0.001	0.045	0.000	0.001	0.007	0.000	0.000	0.000	0.34
	Powder Coated	0.060	0.068	0.068	0.000	0.006	0.012	0.003	0.000	0.000	0.000	0.008	0.003	0.001	0.045	0.000	0.001	0.005	0.000	0.000	0.000	0.28
	Wood finish	0.055	0.062	0.062	0.000	0.005	0.011	0.003	0.000	0.009	0.000	0.008	0.003	0.001	0.045	0.000	0.001	0.005	0.000	0.000	0.000	0.27
	Silver Matt	0.046	0.052	0.052	0.000	0.005	0.009	0.003	0.000	0.009	0.000	0.008	0.003	0.001	0.045	0.000	0.001	0.004	0.000	0.000	0.000	0.24
	Silver Bright	0.055	0.062	0.062	0.000	0.005	0.011	0.003	0.000	0.045	0.000	0.008	0.003	0.001	0.045	0.000	0.001	0.005	0.000	0.000	0.000	0.31
	Champagne	0.060	0.068	0.068	0.000	0.006	0.012	0.003	0.000	0.036	0.000	0.008	0.003	0.001	0.045	0.000	0.001	0.005	0.000	0.000	0.000	0.32
	Bronze	0.060	0.068	0.068	0.000	0.006	0.012	0.003	0.000	0.036	0.000	0.008	0.003	0.001	0.045	0.000	0.001	0.005	0.000	0.000	0.000	0.32
EPC	Mill Finish	0.060	0.006	0.005	0.000	0.001	0.003	0.000	0.000	0.000	0.013	0.000	0.000	0.000	0.027	0.009	0.012	0.001	0.007	0.007	0.007	0.16
	Powder Coated	0.047	0.006	0.004	0.000	0.001	0.003	0.000	0.000	0.000	0.000	0.000	0.000	0.000	0.027	0.009	0.012	0.001	0.007	0.007	0.007	0.13
	Wood finish	0.043	0.006	0.003	0.000	0.001	0.002	0.000	0.000	0.002	0.000	0.000	0.000	0.000	0.027	0.009	0.012	0.001	0.007	0.007	0.007	0.13
	Silver Matt	0.036	0.006	0.003	0.000	0.000	0.002	0.000	0.000	0.002	0.000	0.000	0.000	0.000	0.027	0.009	0.012	0.001	0.007	0.007	0.007	0.12
	Silver Bright	0.043	0.006	0.003	0.000	0.001	0.002	0.000	0.000	0.010	0.000	0.000	0.000	0.000	0.027	0.009	0.012	0.001	0.007	0.007	0.007	0.14
	Champagne	0.047	0.006	0.004	0.000	0.001	0.003	0.000	0.000	0.008	0.000	0.000	0.000	0.000	0.027	0.009	0.012	0.001	0.007	0.007	0.007	0.14
	Bronze	0.047	0.006	0.004	0.000	0.001	0.003	0.000	0.000	0.008	0.000	0.000	0.000	0.000	0.027	0.009	0.012	0.001	0.007	0.007	0.007	0.14
QC	Mill Finish	0.087	0.080	0.010	0.000	0.004	0.015	0.010	0.019	0.000	0.007	0.001	0.001	0.002	0.007	0.000	0.000	0.030	0.007	0.007	0.093	0.38
	Powder Coated	0.087	0.080	0.010	0.000	0.004	0.015	0.010	0.019	0.000	0.000	0.001	0.001	0.002	0.007	0.000	0.000	0.030	0.007	0.007	0.093	0.37
	Wood finish	0.087	0.080	0.010	0.000	0.004	0.015	0.010	0.019	0.010	0.000	0.001	0.001	0.002	0.007	0.000	0.000	0.030	0.007	0.007	0.093	0.38
	Silver Matt	0.087	0.080	0.010	0.000	0.004	0.015	0.010	0.019	0.010	0.000	0.001	0.001	0.002	0.007	0.000	0.000	0.030	0.007	0.007	0.093	0.38
	Silver Bright	0.087	0.080	0.010	0.000	0.004	0.015	0.010	0.019	0.050	0.000	0.001	0.001	0.002	0.007	0.000	0.000	0.030	0.007	0.007	0.093	0.42
	Champagne	0.087	0.080	0.010	0.000	0.004	0.015	0.010	0.019	0.040	0.000	0.001	0.001	0.002	0.007	0.000	0.000	0.030	0.007	0.007	0.093	0.41
	Bronze	0.087	0.080	0.010	0.000	0.004	0.015	0.010	0.019	0.040	0.000	0.001	0.001	0.002	0.007	0.000	0.000	0.030	0.007	0.007	0.093	0.41
CCR	Mill Finish	0.000	0.000	0.000	0.000	0.000	0.000	0.000	0.000	0.000	0.000	0.000	0.000	0.057	0.000	0.000	0.000	0.000	0.000	0.000	0.000	0.06
	Powder Coated	0.000	0.000	0.000	0.000	0.000	0.000	0.000	0.000	0.000	0.000	0.000	0.000	0.045	0.000	0.000	0.000	0.000	0.000	0.000	0.000	0.04
	Wood finish	0.000	0.000	0.000	0.000	0.000	0.000	0.000	0.000	0.002	0.000	0.000	0.000	0.041	0.000	0.000	0.000	0.000	0.000	0.000	0.000	0.04
	Silver Matt	0.000	0.000	0.000	0.000	0.000	0.000	0.000	0.000	0.002	0.000	0.000	0.000	0.034	0.000	0.000	0.000	0.000	0.000	0.000	0.000	0.04
	Silver Bright	0.000	0.000	0.000	0.000	0.000	0.000	0.000	0.000	0.010	0.000	0.000	0.000	0.041	0.000	0.000	0.000	0.000	0.000	0.000	0.000	0.05
	Champagne	0.000	0.000	0.000	0.000	0.000	0.000	0.000	0.000	0.008	0.000	0.000	0.000	0.045	0.000	0.000	0.000	0.000	0.000	0.000	0.000	0.05
	Bronze	0.000	0.000	0.000	0.000	0.000	0.000	0.000	0.000	0.008	0.000	0.000	0.000	0.045	0.000	0.000	0.000	0.000	0.000	0.000	0.000	0.05
MGTS	Mill Finish	0.013	0.001	0.001	0.000	0.000	0.001	0.000	0.000	0.000	0.003	0.000	0.000	0.010	0.000	0.000	0.000	0.000	0.000	0.000	0.000	0.03
	Powder Coated	0.010	0.006	0.001	0.000	0.000	0.001	0.000	0.000	0.000	0.000	0.000	0.000	0.007	0.000	0.000	0.000	0.000	0.000	0.000	0.000	0.02
	Wood finish	0.009	0.006	0.001	0.000	0.000	0.000	0.000	0.000	0.000	0.000	0.000	0.000	0.007	0.000	0.000	0.000	0.000	0.000	0.000	0.000	0.02
	Silver Matt	0.008	0.006	0.001	0.000	0.000	0.000	0.000	0.000	0.000	0.000	0.000	0.000	0.006	0.000	0.000	0.000	0.000	0.000	0.000	0.000	0.02
	Silver Bright	0.009	0.006	0.001	0.000	0.000	0.000	0.000	0.000	0.000	0.000	0.000	0.000	0.007	0.000	0.000	0.000	0.000	0.000	0.000	0.000	0.02
	Champagne	0.010	0.006	0.001	0.000	0.000	0.001	0.000	0.000	0.000	0.000	0.000	0.000	0.007	0.000	0.000	0.000	0.000	0.000	0.000	0.000	0.02
	Bronze	0.010	0.006	0.001	0.000	0.000	0.001	0.000	0.000	0.000	0.000	0.000	0.000	0.007	0.000	0.000	0.000	0.000	0.000	0.000	0.000	0.02
ME	Mill Finish	0.014	0.001	0.001	0.000	0.000	0.001	0.000	0.000	0.000	0.003	0.000	0.000	0.000	0.001	0.000	0.000	0.005	0.021	0.021	0.021	0.09
	Powder Coated	0.014	0.001	0.001	0.000	0.000	0.001	0.000	0.000	0.000	0.000	0.000	0.000	0.000	0.001	0.000	0.000	0.004	0.021	0.021	0.021	0.09
	Wood finish	0.014	0.001	0.001	0.000	0.000	0.001	0.000	0.000	0.006	0.000	0.000	0.000	0.000	0.001	0.000	0.000	0.003	0.021	0.021	0.021	0.09
	Silver Matt	0.014	0.001	0.001	0.000	0.000	0.001	0.000	0.000	0.006	0.000	0.000	0.000	0.000	0.001	0.000	0.000	0.003	0.021	0.021	0.021	0.09
	Silver Bright	0.014	0.001	0.001	0.000	0.000	0.001	0.000	0.000	0.030	0.000	0.000	0.000	0.000	0.001	0.000	0.000	0.003	0.021	0.021	0.021	0.12
	Champagne	0.014	0.001	0.001	0.000	0.000	0.001	0.000	0.000	0.240	0.000	0.000	0.000	0.000	0.001	0.000	0.000	0.004	0.021	0.021	0.021	0.33
	Bronze	0.014	0.001	0.001	0.000	0.000	0.001	0.000	0.000	0.024	0.000	0.000	0.000	0.000	0.001	0.000	0.000	0.004	0.021	0.021	0.021	0.11
SAS	Mill Finish	0.060	0.006	0.005	0.000	0.001	0.003	0.000	0.000	0.000	0.013	0.000	0.000	0.000	0.027	0.009	0.012	0.001	0.007	0.007	0.007	0.16
	Powder Coated	0.047	0.006	0.004	0.000	0.001	0.003	0.000	0.000	0.000	0.000	0.000	0.000	0.000	0.027	0.009	0.012	0.001	0.007	0.007	0.007	0.13
	Wood finish	0.043	0.006	0.003	0.000	0.001	0.002	0.000	0.000	0.002	0.000	0.000	0.000	0.000	0.027	0.009	0.012	0.001	0.007	0.007	0.007	0.13
	Silver Matt	0.036	0.006	0.003	0.000	0.000	0.002	0.000	0.000	0.002	0.000	0.000	0.000	0.000	0.027	0.009	0.012	0.001	0.007	0.007	0.007	0.12
	Silver Bright	0.043	0.006	0.003	0.000	0.001	0.002	0.000	0.000	0.010	0.000	0.000	0.000	0.000	0.027	0.009	0.012	0.001	0.007	0.007	0.007	0.14
	Champagne	0.047	0.006	0.004	0.000	0.001	0.003	0.000	0.000	0.008	0.000	0.000	0.000	0.000	0.027	0.009	0.012	0.001	0.007	0.007	0.007	0.14
	Bronze	0.047	0.006	0.004	0.000	0.001	0.003	0.000	0.000	0.008	0.000	0.000	0.000	0.000	0.027	0.009	0.012	0.001	0.007	0.007	0.007	0.14
OS	Mill Finish	0.087	0.080	0.010	0.000	0.004	0.015	0.010	0.019	0.000	0.007	0.001	0.001	0.002	0.007	0.000	0.000	0.030	0.007	0.007	0.093	0.38
	Powder Coated	0.087	0.080	0.010	0.000	0.004	0.015	0.010	0.019	0.000	0.000	0.001	0.001	0.002	0.007	0.000	0.000	0.030	0.007	0.007	0.093	0.37
	Wood finish	0.087	0.080	0.010	0.000	0.004	0.015	0.010	0.019	0.010	0.000	0.001	0.001	0.002	0.007	0.000	0.000	0.030	0.007	0.007	0.093	0.38
	Silver Matt	0.087	0.080	0.010	0.000	0.004	0.015	0.010	0.019	0.010	0.000	0.001	0.001	0.002	0.007	0.000	0.000	0.030	0.007	0.007	0.093	0.38
	Silver Bright	0.087	0.080	0.010	0.000	0.004	0.015	0.010	0.019	0.050	0.000	0.001	0.001	0.002	0.007	0.000	0.000	0.030	0.007	0.007	0.093	0.42
	Champagne	0.087	0.080	0.010	0.000	0.004	0.015	0.010	0.019	0.040	0.000	0.001	0.001	0.002	0.007	0.000	0.000	0.030	0.007	0.007	0.093	0.41
	Bronze	0.087	0.080	0.010	0.000	0.004	0.015	0.010	0.019	0.040	0.000	0.001	0.001	0.002	0.007	0.000	0.000	0.030	0.007	0.007	0.093	0.41
TT	Mill Finish	0.000	0.000	0.000	0.000	0.000	0.000	0.000	0.000	0.000	0.000	0.000	0.000	0.057	0.000	0.000	0.000	0.000	0.000	0.000	0.000	0.06
	Powder Coated	0.000	0.000	0.000	0.000	0.000	0.000	0.000	0.000	0.000	0.000	0.000	0.000	0.045	0.000	0.000	0.000	0.000	0.000	0.000	0.000	0.04
	Wood finish	0.000	0.000	0.000	0.000	0.000	0.000	0.000	0.000	0.002	0.000	0.000	0.000	0.041	0.000	0.000	0.000	0.000	0.000	0.000	0.000	0.04
	Silver Matt	0.000	0.000	0.000	0.000	0.000	0.000	0.000	0.000	0.002	0.000	0.000	0.000	0.034	0.000	0.000	0.000	0.000	0.000	0.000	0.000	0.04
	Silver Bright	0.000	0.000	0.000	0.000	0.000	0.000	0.000	0.000	0.010	0.000	0.000	0.000	0.041	0.000	0.000	0.000	0.000	0.000	0.000	0.000	0.05
	Champagne	0.000	0.000	0.000	0.000	0.000	0.000	0.000	0.000	0.008	0.000	0.000	0.000	0.045	0.000	0.000	0.000	0.000	0.000	0.000	0.000	0.05
	Bronze	0.000	0.000	0.000	0.000	0.000	0.000	0.000	0.000	0.008	0.000	0.000	0.000	0.045	0.000	0.000	0.000	0.000	0.000	0.000	0.000	0.05
AS	Mill Finish	0.013	0.001	0.001	0.000	0.000	0.001	0.000	0.000	0.000	0.003	0.000	0.000	0.010	0.000	0.000	0.000	0.000	0.000	0.000	0.000	0.03
	Powder Coated	0.010	0.006	0.001	0.000	0.000	0.001	0.000	0.000	0.000	0.000	0.000	0.000	0.007	0.000	0.000	0.000	0.000	0.000	0.000	0.000	0.02
	Wood finish	0.009	0.006	0.001	0.000	0.000	0.000	0.000	0.000	0.000	0.000	0.000	0.000	0.007	0.000	0.000	0.000	0.000	0.000	0.000	0.000	0.02
	Silver Matt	0.008	0.006	0.001	0.000	0.000	0.000	0.000	0.000	0.000	0.000	0.000	0.000	0.006	0.000	0.000	0.000	0.000	0.000	0.000	0.000	0.02
	Silver Bright	0.009	0.006	0.001	0.000	0.000	0.000	0.000	0.000	0.000	0.000	0.000	0.000	0.007	0.000	0.000	0.000	0.000	0.000	0.000	0.000	0.02
	Champagne	0.010	0.006	0.001	0.000	0.000	0.001	0.000	0.000	0.000	0.000	0.000	0.000	0.007	0.000	0.000	0.000	0.000	0.000	0.000	0.000	0.02
	Bronze	0.010	0.006	0.001	0.000	0.000	0.000	0.000	0.000	0.000	0.000	0.000	0.000	0.007	0.000	0.000	0.000	0.000	0.000	0.000	0.000	0.02
CR	Mill Finish	0.014	0.001	0.001	0.000	0.000	0.001	0.000	0.000	0.000	0.003	0.000	0.000	0.000	0.001	0.000	0.000	0.005	0.021	0.021	0.021	0.09
	Powder Coated	0.014	0.001	0.001	0.000	0.000	0.001	0.000	0.000	0.000	0.000	0.000	0.000	0.000	0.001	0.000	0.000	0.004	0.021	0.021	0.021	0.09
	Wood finish	0.014	0.001	0.001	0.000	0.000	0.001	0.000	0.000	0.006	0.000	0.000	0.000	0.000	0.001	0.000	0.000	0.003	0.021	0.021	0.021	0.09
	Silver Matt	0.014	0.001	0.001	0.000	0.000	0.001	0.000	0.000	0.006	0.000	0.000	0.000	0.000	0.001	0.000	0.000	0.003	0.021	0.021	0.021	0.09
	Silver Bright	0.014	0.001	0.001	0.000	0.000	0.001	0.000	0.000	0.030	0.000	0.000	0.000	0.000	0.001	0.000	0.000	0.003	0.021	0.021	0.021	0.12
	Champagne	0.014	0.001	0.001	0.000	0.000	0.001	0.000	0.000	0.240	0.000	0.000	0.000	0.000	0.001	0.000	0.000	0.004	0.021	0.021	0.021	0.33
	Bronze	0.014	0.001	0.001	0.000	0.000	0.001	0.000	0.000	0.024	0.000	0.000	0.000	0.000	0.001	0.000	0.000	0.004	0.021	0.021	0.021	0.11

Use of Unmanned Aerial Vehicles in Aircraft Inspection

Andrej Novák[*,1], Martin Bugaj[1], Alena Novák Sedláčková[1], Branislav Kandera[1], Anna Stelmach[2], Tomasz Lusiak[3]

[1]University of Žilina, Air Transport Department, Žilina, 010 26, Slovakia

[2]Warsaw University of Technology, Faculty of Transport, Warsaw, 00-662, Poland

[3]Lublin University of Technology, Faculty of Mechanical Engineering, Lublin, 20-618, Poland

ARTICLE INFO	ABSTRACT
	The article further extends the researched issue of the unmanned aircraft use in the pre-flight and post-flight visual check of aircraft. Procedures of pre-flight inspection are fulfilled by the aircraft maintenance certified staff or the crew member before flight. The process is similar for all categories of aircraft, but its implementation differs for individual specific types of aircraft. Therefore, the article will deal only with small training aircraft, which will be used to verify the use of UAV (Unmanned Aerial Vehicle) in normal operation. It identifies and defines the problem of using multiple UAV in swarms and their usage in standard activities in aircraft operation. The outcome should be a reduction of the number of possible failures cause by the human factor with impact on the safety in operations. Proportionately important fact is the desirable minimization in the time necessary to carry out a pre-flight inspection process, which will improve the final indicator of the efficiency in aeroplane operations.

1. Introduction

This article builds on the existing field of research by the authors on the use of UAV by maintenance and training organizations as well as commercial airlines. In this research field, the articles Use of Unmanned Aerial Vehicles in Aircraft Maintenance [1] and Unmanned Aerial Vehicles and Their Use for Aircraft Inspection [2] have been published. In aviation, defined legal regulations and standards are implemented and must be strictly applied. Procedures related to aircraft periodic inspections and checks are performed during aircraft operations by certified organizations, always supervised by the Continuing Airworthiness Management Organization (CAMO). According to Commission Regulation (EU) no. 965/2012 laying down technical requirements and administrative procedures related to air operations pursuant to Regulation of the European Parliament and Council Regulation (EC) No. 216/2008 are aircraft operators at the same time also holders of an Air Operator Certificate (AOC). Aviation companies are obliged to implement a management system in operation with working management of safety risks in whole process of operation (Safety Management System - SMS). On top of that airlines are prior to each flight expected to perform own routine pre-flight

inspections. An urge to utilize new technologies and equipment that reflect changing nature of industry was a result of these rapid changes. Similarly, as industry puts an emphasis on the new technologies in accordance with Industry 4.0 principles, so must certified maintenance organizations (MROs) and continuing airworthiness management organizations (CAMOs) follow suit and utilize "Smart Technologies" [3] The collective response of maintenance and aviation industry organisations led to the creation of the concept "Smart Hangar", which enables CAMOs and MROs to conduct their business with a higher degree of objective accountability in detecting human error.

The UAV operation worldwide is growing in numbers, as are the areas of human activity in which UAV are operated professionally. They are part of all areas of human life and are already an integral part of the equipment of law enforcements and rescue units, photogrammetry, transport, construction, industry, research, logistics, they can furthermore be used for youngsters to play with. [4]. Technology evolves and changes with their increasing use. At the same time a relevant legislation for a safe utilisation should be in line with technological progress. This field must be protected by European legislation and national in a manner that will not restrict freedom [5].

*Corresponding Author: University of Žilina, Air Transport Department, Univerzitná 8215/1, 010 26 Žilina, Slovakia, Email: Novak30@uniza.sk

Recently Intel and Airbus have started a cooperation in a bid to further improve this process. Intel delivers UAV equipped with video recording devices that enable recording images or data which can later be used to generate whole three-dimensional models of Airbus aircraft. Airbus Aerial a subsidiary established by Airbus S.A.S provides equipment inspection services in different aviation industry sectors [6]. There are also other similar companies that operate in this market, such as French Ubisense S.A.S, MRO Drone Ltd from Great Britain and Canard Drones from Spain. These have lately developed particular procedures to provide inspection solutions for airports as well as aeroplanes [7], [8].

The goal of our project is to demonstrate the possible use of UAV system for aircraft inspection by a small aviation organization.

2. Definition of Smart Hangar concept

Smart Hangar can be defined as a set of actions including digitization of analytical tools, automation of its environment, smart manufacturing and logistics. If we should specify the concept of "Smart Hangar" in detail, it is necessary for the maintenance organization to expand key areas as they are listed in Figure 1.
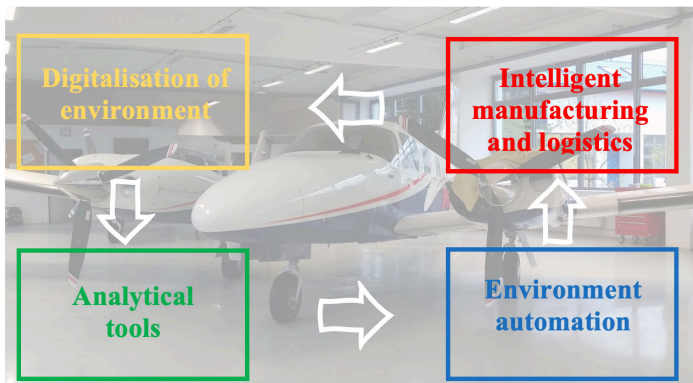
Figure 1: Concept of Smart Hangar for MRO. (Source: authors)

2.1. Digitization of environment and virtualization of tasks

In order to establish a functioning "Smart MRO" all work procedures and management systems that are effective at the moment need to be digitized to form a basic framework of the system. Maintenance organization, a continuing airworthiness management organization, hangar or even an airport that utilizes the electronic (paperless) system are able to achieve higher efficiency of operation. This can be done by online monitoring, assignment and approval of maintenance tasks. An MROs maintenance technician has access to the corporate network, therefore is able to work anytime from any location. Electronic handheld devices enable him to track, compare and record maintenance task [9].

2.2. Analytical tools of intelligent hangar

Digitization enables meaningful data analysis and improvement of internal processes. It also helps airlines optimize activities in cost planning, warehouse management and materials logistics. Employees can foresee errors in aircraft repair and maintenance and better plan their resources (both material and

human). This is possible through the advanced analysis that results from data collection. The use of interactive prediction software bots not only enables better control of material logistics and supplies, it also helps to reduce costs in MROs and the amount of supplies [10].

2.3. Robotization and automation of an environment

Introduction of collaborative robots brought increased productivity, work performance efficiency and directly increased work procedures and processes. Utilization of digitized end-to-end workflow monitoring resulted in higher level of safety and quality. After establishment of such innovative work environment unmanned aerial vehicles will be able to perform aircraft visual inspections prior, during or after the maintenance tasks are carried out. Further implementation of Automated Guided Vehicles (AGV) as well as Intelligent cabinet will help in search for and point-to-point transport of tools and aircraft parts from the storage to the place of the maintenance (point-to-use) in real time [9].

2.4. Intelligent manufacturing and logistics

3D printing, free-form fabrication or rapid prototyping are terms used to describe process of additive manufacturing (AM). It describes a process of merging materials in order to create any object/product from 3D model data. Manufacturing aircraft components using additive manufacturing method of 3D Printing (3DP) is eco-friendly and presents an opportunity to optimize the design of components at fraction of costs. Adaptive manufacturing provides range of advantages compared to regular manufacturing. Waiting time when replacing specific low-volume components that need to be replaced as soon as possible can be significantly reduced. It also uses less resources compared to standard manufacturing process. On the other hand, significant engineering and certification experience is required to fully utilize such technology to meet exact requirements of national aviation authorities (or EASA) in order for new parts to be approved for installation.

3. Research on pre-flight inspection process using UAV at University of Žilina (UNIZA)

Organisation and performance of aircraft maintenance at the University of Žilina conforms to the legislation of European Union. UNIZA is an Approved Maintenance Organization (AMO) with the appropriate permits and licence that conform to the requirements of Commission Regulation (EU) No. 1321/2014 under number SK.MF06. It sets out requirements for aircraft (EASA aircraft) that meet the requirements set out in Article 2 (1) of Regulation (EU) No.182/2011 of the European Parliament and of the Council No.1139/2018. Maintenance organizations have to meet the following requirements:

- for complex engine-powered aircraft and aircraft used by air carriers licensed in accordance with Regulation (EC) No 1008/2008 and their components (Part 145).

- for aircraft other than complex engine-powered airplanes and their components (Part-M Subpart F or Part-CAO).

Aircraft at University of Žilina are maintained in line with the certification and according to the latest regulations. Only trained

and certified personnel with corresponding technician's licence is authorized to release aircraft into the service.

Pre-flight aircraft inspection is always performed in line with the approved aircraft manual as well as the organization's operations manual.

3.1. Pre-flight inspection

PA34-220T SENECA V is a modern twin-engine aircraft used by University of Žilina for pilot trainings as well as aerial work. We have selected this aircraft for the research purposes. Inspection instructions listed in the following paragraph are extracted from the flight manual of the aircraft. In addition, procedures that are unique for the aircraft type have been also considered. First, it is required to inspect the general state of aircraft. It has to be inspected from outside as well as from inside. In case of winter weather conditions any build-up of snow or even icing on the flight and control surfaces has to be removed. Functionality of all lights and flashlight has to be ensured prior to the planned night flight. Operational manual section of Airplane Flight Manual offers in-depth clarification of information regarding the pre-flight inspection procedures [12]. Inspection process of PA34-220T SENECA V aircraft must be done in order depicted in figure 2. Aircraft cabin is first on the pre-flight inspection checklist (Figure 2, Point 1). According to the flight manual, correct operation of individual lightning, power supply, navigation and communication elements has to be ensured. In addition, all mechanical and safety elements together with correct fixation of luggage and flight documentation have to be inspected as well.
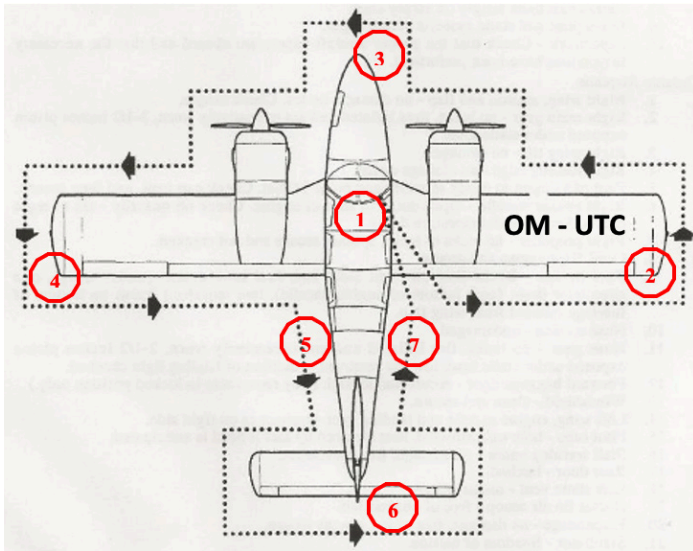
Figure 2: Inspection sequence of PA34-220T Seneca V aircraft. (Source: authors)

After this is completed an exterior inspection follows. Aircraft inspection starts with the check of the starboard wing following with a right engine in a counter clockwise direction. During this inspection every mechanical wing part such as flaps and ailerons are checked. Among other elements that are inspected are engine, propeller, amount of fuel, removal of fuel sludge as well as fuselage elements and chassis of the aircraft; at the front (Figure 2, point 3) we inspect windshield, tires, front landing gear leg, cargo compartment in the nose of aircraft together with landing reflector. While inspecting the top port wing (Figure 2 point 4), every

mechanical wing parts such as flaps and ailerons and flaps are checked together with an engine, propeller, fuel quantity, fuel sludge removal, icing indication, pitot tube, chassis control and fuselage parts. Inspection then continues with the fuselage on the left side (Figure 2, point 5). This segment consists of checks of fuselage for the presence of snow and ice, antenna, cargo bay, pitot-static system and side door. Similarly, the rear part of the aircraft is inspected for the presence of any snow or ice residues. It is followed by an inspection of elevator, rudders, air intake system. Moving to the right (Figure 2, point 7) it is required to check the fuselage for the presence of snow and ice. As on the left side of aircraft antennas and pitot-static system must be checked for any debris or dirt that may hamper their operation.

4. Use of UAV in pre-flight inspection

When inspecting an aircraft using a UAV this has to be performed outside. Movement and equipment of the UAV has to meet certain requirements when operating in the Control Zone (CTR) of particular airport. These include propeller cover, outdoor movement sensors and navigation including GNSS navigation. The decisive factor for the use of UAV in an aircraft monitoring and control system is the software and subsequent applications for data evaluation.

4.1. Methodology for aircraft object identification and changes

When performing pre-flight inspection, it is important to correctly recognize and identify the individual components and significant parts of the fuselage, engine and propeller blades to be inspected. Correct identification of individual components is a very important task. The recognition of any objects in general can be expressed by the following sequence of steps:

1. Image acquisition;

2. Pre-processing;

3. Segmentation;

4. Representation;

5. Classification.

After obtaining an image from a source (captured by a camera or from video), it is pre-processed, which means the image is prepared into such a form that it is possible to implement algorithms for further processing. This step can include converting a colour image into an image in shades of grey (see Figure 3), or using filters to remove, or suppress noise. Image processing algorithms are deployed in this step. The next step is segmentation, which extracts objects of interest, thus separating the foreground (what interests us) from the background (everything else). In the picture, the objects of interest are rivets on wings, but undesired objects (noise) also got there.

This is a general model, which means that not all blocks may always be followed. Their order may be changed, or the steps may be completely replaced by other procedures or combined into separate blocks. Formally, we can model the image as a continuous (image) function of two variables f(x,y), where f represents the value of brightness and (x,y) represent the coordinates on the surface. In the case of a dynamic image (video), we can also express the image as a function of three variables f(x,y,t), where t means time.
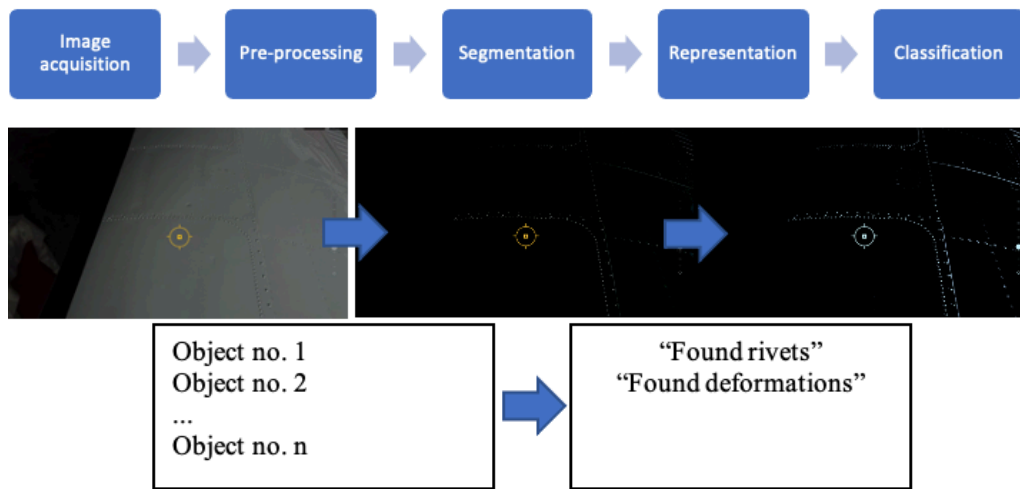
"Smart Hangar" solutions depend on partial systems and applications that safeguard the functioning of the whole system. Model - driven Software Development (MDSD) (see Figure 4) based on an automatic code generation of system requirements specification, it is typically used to providing specific properties to the whole system [13]. The module DeRoS safety specification DSL provides a simple and declarative syntax that makes the task of implementing the safety-related requirements accessible to robotics experts with less software engineering expertise. The risk of errors is reduced because the Declarative Robot Safety (DeRoS) declaration controls the automatic generation of all safety-related code. Our model approach directly enables implementation-independent reuse of the safety-relevant part of a robot controller between different versions, since the DeRoS declaration does not need to be changed when the underlying software changes (with the exception that names shared between DeRoS rules and component interfaces must be kept consistent) [14]. Such an approach can be utilized when enforcing safety regulations for unmanned systems or to state and improve system cross-sectional properties, as power unit energy balance, safety and timing or to supervise and organize the behaviour of number of UAV in a fleet system such as UAV swarm when inspecting more than one aircraft for example [15].

Figure 4: UAV Software platform for MDSD. (Source: authors)

PA34-220T Seneca V aircraft pre-flight inspection process has been detailed in chapter 3.1 of this article. If we are to carry out an aircraft pre-flight inspection, input variables and environmental properties, the core elements of the aircraft sensing model that identifies the state of the aircraft, need to be defined first. Next, the UAV flight and scanning trajectory, the time intervals of UAV movement relative to the defined trajectory, and the incremental termination of the scanning process must be defined and established. [16]. In the 3D-space of the proposed model, UAV will be characterised by a material point. We need to establish the start (and end) point of UAV take-off, then the altitude for individual reference points within specified trajectory, the total estimated period of its entire pre-flight inspection in the aircraft scanning phase [17, 18]. However, this describes the initial part of a complete aircraft pre-flight inspection. As soon as possible after the UAV inspection data are captured, they need to be processed and evaluated. Result of this operation should be a comprehensive information regarding the state of the aircraft which is then sent to the pilot. After inspecting the information, pilot decides whether an in-depth personal inspection of the aircraft or its parts that that deviate from the UAV sensing model is required. The pattern furthermore explains certain tasks included in the aircraft pre-flight examination, (see Figure 5) which must be carried out physically in accordance with the prescribed pre-flight inspections in the relevant aircraft documentation.

In order to create a functional model, it has to contain an information about the beginning point of UAV pre-flight inspection procedure. In the essence it surely is an exactly defined point at which the UAV take-off as well as the landing takes place. Such point is created during the planning of flight trajectory model by defining the default position. The flight route must respect the procedure of in-person pre-flight inspection carried out by a pilot as shown on the Figure 2. Model of pre-flight inspection can be seen on the Figure 6.

During the creation process of this functional model, based on the defined field of partial position points X1 to Xn; Y1 to Yn; Z1 to Zn. The initial take-off position of UAV is defined as:

$$X1 = 0; Y1 = 0; Z1 = 0 \qquad (1)$$

The UAV initial position at its start should be identical to its final position after its flight performance. In order to model the entire trajectory (see Figure 6), a sequence of position points must be defined. To ensure the safety of the scanning process and to obtain relevant data, a requirement for the constant altitude of the
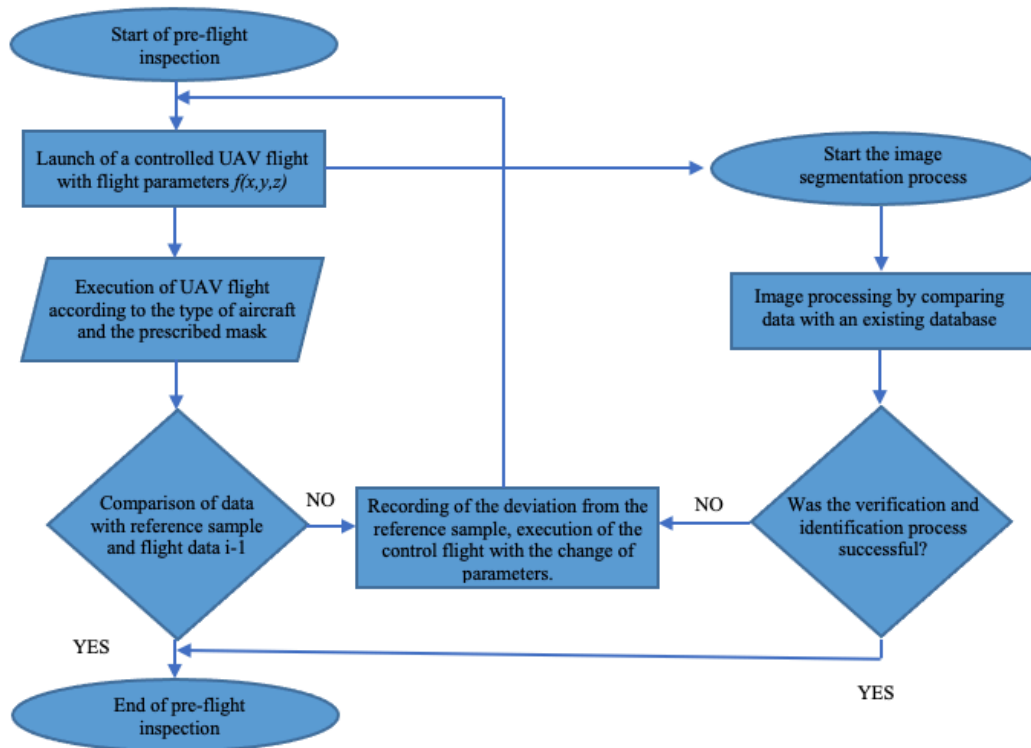
Figure 5: Aircraft inspection flowchart with image classification and evaluation (Source: authors)

UAV during the execution of the aircraft inspection was formulated. The determination of the constant altitude is based on several assumptions, namely:

- sufficient resolution value of the scanning device,
- security aspect,
- type of information obtained from the UAV.
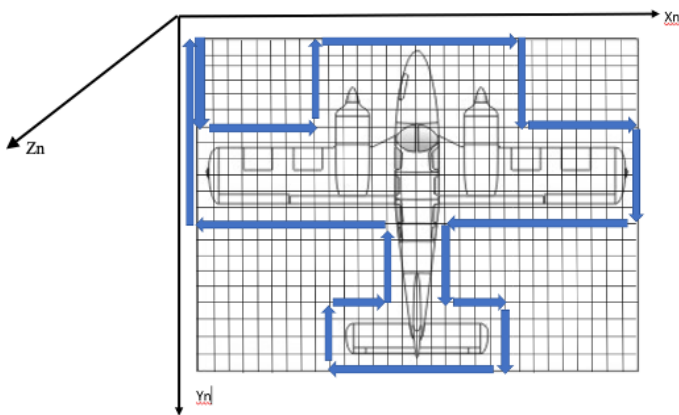
Figure 6: Model of UAV trajectory. (Source: authors)

In order to prevent potentially dangerous contacts with an aircraft it is of a paramount importance to design a so-called restricted no-go zone for UAV. Otherwise, the damage an aircraft may sustain can translate to considerable operational and financial consequences as a Figure 7. The minimum distance from any part of the aircraft has been set at:

$$\Delta l_{min}(Xn, Yn) = 0.5\text{m} \qquad (2)$$
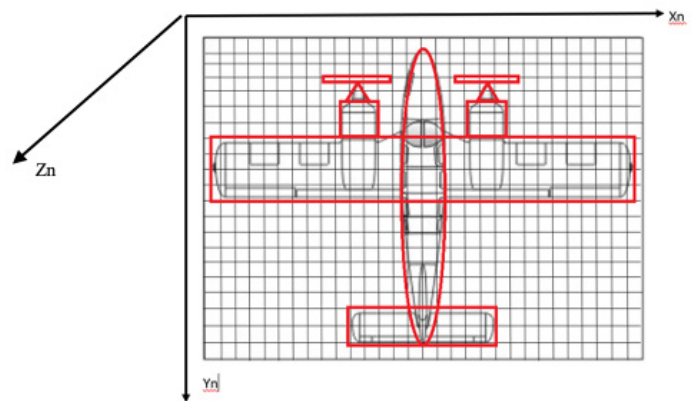
Figure 7: Restricted no-go zones for UAV. (Source: authors)

After the default starting position is defined, other reference points, meaning points where the flight trajectory has to be altered, are programmed. Each point is determined by its position:

$$B1\ (X_1, Y_1, Z_1);\ B2\ (X_2, Y_2, Z_2);\ ....\ Bn\ (Xn, Yn, Yn) \qquad (3)$$

$$D = D_{x,y} = \sqrt{(Xi - Xj)^2 + (Yi - Yj)^2} \qquad (4)$$

Where Xi and Yi determine the i-th point B, Xj and Yj coordinates present position of j-th point B of the set path of movement. The final trajectory is specified by reference coordinates and distances between determined UAV positions. The trajectory must be defined by data describing proposed restricted area around the aircraft. Suggested UAV flight trajectory model stands as:

$$D = D_{x,y} = \sqrt{(Xi - Xj)^2 + (Yi - Yj)^2}, (\forall B \nexists RZ(P \in Pi, Pj)) \quad (7)$$

The B points are belonging to red zone (RZ) is described by points with coordinates "Pi" and "Pj" in such form. Model which defines the final UAV trajectory around aircraft is relevant and in such form also applicable in the phase of programming the UAV. Significance of this step lays in the mitigation of the damage that may be caused by a possible clash between the inspected aircraft and the UAV. Data gathered by the UAV during the pre-flight inspection must be processed. The processing takes place in the form of a comparison of the obtained data with an aircraft reference model. The reference model must meet all requirements placed on real flight aircraft condition before each flight inspection begins.

4.3. Discussion

The use of UAV during pre-flight inspection brings benefits in several areas. By eliminating the influence of the human factor, which can reduce the level of safety of the aircraft, it is possible to achieve an increase in safety. The use UAV pre-flight inspection tour around the aircraft following the manufacturer's checklist. It's necessary pay special attention to lose or "smoking" rivets (which have a residue around them), the safety of all bolts and nuts, and safety-wired devices. At the same time, it is possible to increase efficiency by introducing automation. UAV application could support both aviation and airport operations, it would decrease the maintenance costs and aircraft inspection procedures. [19]. Like other technologies, UAV bring a wide range of benefits. But besides the benefits, the sad truth about UAV is that there are certain burning flaws like sudden crashes, risks from hacking, and security and privacy issues that plague this part of the technology. [20]

Another aspect of the UAV pre-flight inspection system is the development of a UAV communication system with a hardware-software platform, which will be designed to automate the processes of processing and transfer of information between involved parties so that there are no security risks associated with the transfer and processing of acquired information. Although the use of UAV in any process in air transport is a very complex and lengthy process, its potential benefits are undoubtedly clear.

5. Conclusion

Significant technological developments in the field of UAV have recently caused conditions to be created for their use in specific areas of civil aviation. There are ever more use cases in this area for use of UAV, despite being perceived as a threat to civil aviation. The philosophy of Smart Airport consists of several advanced concepts, one of which is the use of UAV in the process

of pre-flight inspections, this was also the subject of the presented article. Firstly, it was crucial to analyse and define technical and operational conditions for the UAV use in pre-flight inspection by detailed analysis of the environment, determining the nature of information that will form a set of input and output information and data and then creating a system to process and evaluate the data. The initial idea of creating this model of UAV application during a pre-flight inspection was to evaluate the overall aircraft condition. Potential threats were also described and a way of solving them was proposed. In the end, advantages of UAV application in the process of pre-flight inspections have been mentioned. Among the most important are the reduction of human factor influence in the performed pre-flight inspection, the time reduction allocated for this activity, which achieves a higher efficiency of the whole process. Further research actions would lead to a detailed definition of aircraft model reference samples for the purpose of obtained records comparison with the reference model. Furthermore, it will be required to develop a swarm model for UAV devices where several devices with diverse types of equipment (mechanical arm, laser scanner, digital camera, etc.) would cooperate with each other. Thanks to the use of modern digital and transmission technologies, it is possible to ensure real-time data comparison. However, it is always necessary to ensure the maximum level of safety of these processes when using UAV during the pre-flight inspection

Upcoming efforts will extend the experimental assessments to UAV simulations and actual flight tests to use probability numbers instead of frequencies which have been used in this case for demonstration purposes. In the author´s opinion and experience it is rather difficult to accomplish the certification and validation processes of safety functions as well as more efficient outcomes. For that reason, our strategy is to verify and validate already functioning safety system to guarantee that the safety system meets functional requirements and is suitable for risk mitigation. Besides, we will investigate how the UAV swarm can be implemented to monitor and ensure a safe flight operation of pre-flight inspection during this specific mission for example in aerodrome apron.

References

[1] A. Novák, A. Novák Sedlackova, M. Bugaj, B. Kandera, T. Lusiak, "Use of Unmanned Aerial Vehicles in Aircraft Maintenance", Transportation Research Procedia, **51**, 160-170, 2020, DOI 10.1016/j.trpro.2020.11.018

[2] M. Bugaj, A. Novák, A. Stelmach, T. Lusiak, "Unmanned Aerial Vehicles and Their Use for Aircraft Inspection," 2020 New Trends in Civil Aviation (NTCA), Prague, 45-50, 2020. doi: 10.23919/NTCA50409.2020.9290929

[3] J. Holl, "Hangar of the future Excelling in MRO", 6. December 2016, Airbus S.A.S Source: https://www.airbus.com/newsroom/news/en/2016/12/Hangar-of-the-future.html

[4] P. Kurdel, A.N. Sedláčková, J, Labun, "UAV flight safety close to the mountain massif",Transportation Research Procedia, **43**, 319-327 2019. doi:10.1016/j.trpro.2019.12.047

[5] A.N. Sedláčková, P. Kurdel, B. Mrekaj, "Synthesis criterion of ergatic base complex with focus on its reliability", INFORMATICS 2017 - Proceedings, 318-321, 2018. doi:10.1109/INFORMATICS.2017.8327267

[6] M. Fendt, "Airbus launches advanced indoor inspection drone to reduce

aircraft inspection times and enhance report quality, Commercial Aircraft", Airbus S.A.S , 2018. (Accessed: 10 April 2021)

[7]   A. Ward, "Ubisense and MRO Drone launch world's first 'Smart Hangar' solution", Ubisense 18.April 2018 Source: https://ubisense.com/ubisense-and-mro-drone-launch-worlds-first-smart-hangar-solution/

[8]   V. Ažaltovič, I. Škvareková, P. Pecho, B. Kandera, "Calculation of the ground casualty risk during aerial work of unmanned aerial vehicles in the urban environment", Transportation Research Procedia, **44**, 271-275, 2020. doi:10.1016/j.trpro.2020.02.043

[9]   A.N. Sedláčková, P. Kurdel, J. Labun, "Simulation of unmanned aircraft vehicle flight precision", Transportation Research Procedia, **44**, 313-320, 2020. doi:10.1016/j.trpro.2020.02.037

[10]   ST   Engenniering: Smart   MRO,   internet   1.7.2020 https://www.stengg.com/en/aerospace/capabilities/smart-mro/

[11]   Uniting Aviation, "The future of MRO: Emerging Technologies in Aircraft Maintenance", Uniting Aviation on August 1, 2019. (Source: https://www.unitingaviation.com/amp/news/capacity-efficiency/the-future-of-mro-emerging-technologies-in-aircraft-maintenance/) (Accessed: 2 April 2021).

[12]   Piper AIRCRAFT, "Airplane Maintenance Manual, Card 1 of 5, PA34-220T, SENECA III (ALL) and SENECA V (S/N's 3448038 THRU 3448079), Piper Aircraft Corporation, 2017, April 17, 2007.

[13]   M. Catlos, P. Kurdel, A.N. Sedlakova, J. Labun, M. Ceskovic, "Continual monitoring of precision of aerial transport objects", Paper presented at the NTAD 2018 - 13th International Scientific Conference - New Trends in Aviation   Development,   Proceedings,   76-81,   2018. doi:10.1109/NTAD.2018.8551683

[14]   A. Sorin, J. Kjeld, U.Schultz, "Towards Rule-Based Dynamic Safety Monitoring for Mobile Robots", Journal of Software Egnieering for Robotics, 2016. DOI: 10.6092/JOSER_2016_07_01_P120

[15]   F. Škultéty, B. Badánik, M. Bartoš, B. Kandera, "Design of controllable unmanned rescue parachute wing", Transportation Research Procedia, **35**, 220-229, 2018. doi:10.1016/j.trpro.2018.12.026

[16]   Min Xue "UAV Trajectory Modeling Using Neural Networks", 17th AIAA Aviation Technology, Integration, and Operations Conference. AIAA 2017-3072, 2017. doi: 10.2514/6.2017-3072

[17]   H. Zhou, H.L. Xiong, Y. Liu, N.D. Tan, L. Chen, "Trajectory Planning Algorithm of UAV Based on System Positioning Accuracy Constraints. Electronics **9**, 245-250, 2020. https://doi.org/10.3390/electronics9020250

[18]   L. Tan, J. Wu,X. Yang, S. Song, "Research on Optimal Landing Trajectory Planning Method between an UAV and a Moving Vessel", Appl. Sci. 2019, **9,** 3708, 2019. https://doi.org/10.3390/app9183708

[19]   F. Marcellin, "Positive uses of drones in aviation: UAV changing airports for   the   better",   Available   at: https://www.airport-technology.com/features/positive-uses-of-drones-in-aviation/ (Accessed: 4 April 2021).

[20]   A. Allouch, A. Koubâa, M. Khalgui, T. Abbes, "Qualitative and Quantitative Risk Analysis and Safety Assessment of Unmanned Aerial Vehicles Missions Over the Internet", IEEE Access, **7**, 53392-53410, 2019. doi: 10.1109/ACCESS.2019.2911980.

A Survey of Big Data Techniques for Extracting Information from Social Media Data

Carla Blank[1], Matthew McBurney[1], Maria Morgan[1], Raed Seetan[2,*]

[1]*Department of Mathematics and Statistics, Slippery Rock University, Slippery Rock, 16057, United States*

[2]*Department of Computer Science, Slippery Rock University, Slippery Rock, 16057, United States*

A R T I C L E I N F O	A B S T R A C T
	Data mined from social media can be used in a variety of methods. The goal of this paper is to explore some of the various methods of mining data from social media and the different areas of its applications. From the analysis of other studies, it was clear that methods such as text analysis, classification, clustering, mapping, testing/validity methods, regression, and research methods were the overarching themes of the previously done research. Pros, cons, and possible extensions were examined for the current research evaluated in the social media data mining area. At the conclusion of this survey, our research team found that text analysis, sentiment analysis, and support vector machine classifiers were among the most common themes of the research methods in this field. In most cases, multiple methods were attempted for each topic to be able to cross compare results.

1. Introduction

In this study, we examined the various techniques that have been used in data mining for social media data. With many social media platforms used by millions, such as Facebook, Twitter, Instagram, etc., all posts by users are collected and comprise the "big data" of social media. Social media data can be used in a variety of ways from predicting buying habits of users to generating information about emergency events.

The idea of using social media to make predictions about individuals is more relevant than ever. Across all types of individuals, social media usage has shown to be on the rise. For example, Figure 1a-c shows the social media growth over three variables (age, race and income). In all cases, more social media use is being experienced allowing us to collect data on a wide range of individuals for a variety of applications. Similarly, Figure 2 shows the frequency that these applications are being used. As seen, for the majority of the individuals, daily data is being obtained which can help better explain the behaviors showcased by people [1].

Selecting efficient methods in the task of social media data mining is a critical consideration for researchers because the methods used need to be executed efficiently when there is a large amount of data. Researchers must also consider the various types of data that are present when analyzing social media data.

A previous survey of data mining techniques in social media analyzed 66 reports on data mining in social media [2]. The authors of this paper mention the important fact that establishing successful data mining techniques in social media is difficult because of the amount of data and the velocity of that data; all social media data is collected in real time so there is constantly more data being added to the repositories where this data is stored. In this study, the authors identified 19 different data mining techniques that were used by researchers to analyze social media data and compared the effectiveness of these techniques. The authors noted that many of the researchers did not back up their methods with statistical significance testing, which presents an issue with the reliability of the methods used.

For the purpose of this research, we analyzed 12 previous studies that have been conducted on data mining social media data. While conducting this research, the following research questions were kept in mind to guide the focus of our analysis: what topics (or areas of interest) have been explored in regards to social media data mining, what methods have been used for data mining in social media data in these areas, are certain data mining methods applied to specific areas/topics, how do each of these data mining methods perform and can we make suggestions on how to approve future analysis projects on social media data mining.

*Corresponding Author: Raed Seetan, Computer Science Department, Slippery Rock University, 16057, USA, Email: raed.seetan@sru.edu Tel: 724-738-2940

www.astesj.com

https://dx.doi.org/10.25046/aj060322

189

Social Media Usage by Age
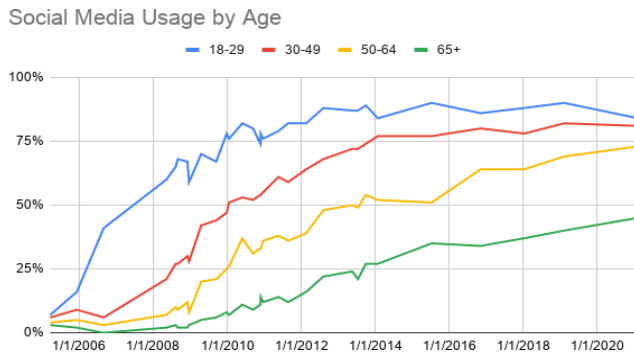
Figure 1a: Social Media Use by Age

Social Media Usage by Race
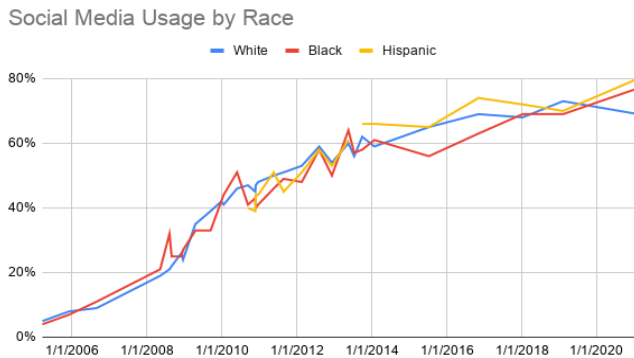
Figure 1b: Social Media Use by Race

Social Media Usage by Income
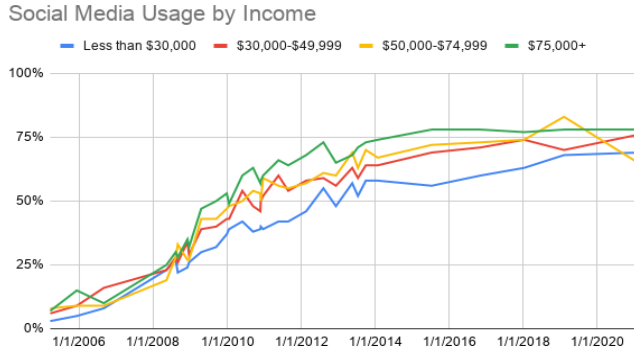
Figure 1c: Social Media Use by Income

The remainder of this paper will be structured as follows: we will first discuss the various methods that have been used in data mining social media data, we will then provide summaries on the 12 papers selected for this research followed by an overview of the findings from each paper, and finally we will provide a conclusion on the research that has been conducted for this paper.

2. Methods

There are many machine learning methods used in analyzing big data. The methods discussed below are used in the studies observed in this research paper.

2.1. Text Analysis

Text analysis is used to gather important information from unstructured text. Patterns of specific text can be collected, or

common words and phrases can be determined using text analysis. Many text analysis methods use natural language processing (NLP). Text analysis is frequently used in social media studies as users can post about anything they chose. Valuable insights can be derived from these data, such as companies collecting feedback about their brand or a specific product.

Figure 2: Frequency of platform usage

1) Latent Dirichlet Allocation (LDA): Latent Dirichlet Allocation (LDA) is a topic model in natural language processing. LDA allows sets of observations to be explained by unobserved groups that explain the similarity in some parts of the data. In LDA, both word distribution for each topic and topic proportion for each document are modeled using Dirichlet distributions [3]. Common topics and words within the text data can be ranked by their resulting probabilities to determine which occur most frequently.

2) Normalized Discounted Cumulative Gain: Normalized Discounted Cumulative Gain (NDCG) is a method for measuring the quality of a set of search results. The result of NDCG is a scaled ranking system which tells the user which results are relevant using a numbered ranking system. For example, a score of 0 meaning least relevant and a score of 2 meaning most relevant. In NDCG, very relevant results are more important than partly relevant or irrelevant results, which is called cumulative gain. Discounting is when relevant results are more important when they appear earlier in the search results. The ranking of the result should not depend on the query performed; this is normalization [4]. In discounted cumulative gain, results that appear lower are discounted, i.e., they are not as valuable as results that appear higher in the search results. Normalization scales the results to the best result seen.

3) Sentiment Analysis: Sentiment analysis is the classification of textual data to uncover classifications of emotions that can be seen in the text. The method is either rule based, governed by manually determined rules (like looking for specific words or phrases), automatic, governed by machine learning techniques, or a combination of the two. Naïve Bayes, Linear Regression, Support Vector Machines, and Deep Learning are commonly used classification algorithms to perform sentiment analysis [5]. Given the variety of machine learning techniques that can be used to perform sentiment analysis, the user is able to select which technique best suits their needs based on the type of data being used and the desired format of the result.

4) Text Analysis/Classification: Text analysis and classification have a primary goal of taking something which may be unstructured and trying to impose a structure on it. From a classification standpoint, this involves taking an unsorted list of items and attempting to assign them to appropriate groups. Text analysis, similarly, takes text and makes it understandable and easier to manage. This can be helpful while analyzing masses of text data such as social media, comments, and surveys [6]. Like sentiment analysis, the user has options to choose from when deciding how to perform text classification. Users can use a rule-based system, which classifies text into certain groups based on a set of linguistic rules that are pre-determined by the user. This method requires more work from the user to determine the rules to apply when classifying. Machine learning-based systems, such as Naive Bayes and Support Vector Machines, may also be used in text classification. It is up to the user to decide which method will perform best based on the size of their dataset and the result they wish to achieve.

5) TF-IDF: Term frequency - inverse document frequency (TF-IDF) serves as a statistical measure which determines the relevancy of a specific word in a defined collection of documents. TF-IDF is a widely accepted statistic because it not only accounts for how often a word appears, but also how many documents they appear in. Therefore, words such as "and" are not deemed inaccurately as relevant. This method is used for text vectorization (turning text into numbers) to further be processed by machine learning algorithms for various applications [7].

6) Twitter API Search: Twitter standard search API returns a set of tweets considered relevant by whatever the specified query was [8]. This method is used to gather results that can later be used in text analysis and sentiment analysis. An API search allows for "tweets" to be pulled from as early as 2006. This serves as helpful data when needing to examine text from a specific period of time (or comparison of times) for the analysis.

7) Active semi-supervised Clustering based Two-stage text classification (ACTC): ACTC is a method that turns text classification into a supervised problem [9]. This algorithm is done in two stages. The first stage is a clustering stage in which the data is clustered using a method called SemiCCAc; this algorithm was created to address that cluster-bias problem that often exists when clustering text data. The second step is a classification method using discriminative classifiers. In the first part of the algorithm, the unlabeled text data is clustered to create tentative labels for the clustered data. In the second part, the discriminative classifier is used to assign the final labels to each group of the text data. The resulting output after the classification stage is complete may require additional processing using supervised learning techniques. The idea behind the method of combining clustering with classification is to attempt to minimize the amount of text data that would be mis-labeled by using either clustering or classification alone; this combination should result in a reduction of the further processing of the output that would be needed when compared to only using one of the methods alone.

8) Example Adaption for Text categorization (EAT): Traditional text categorization algorithms work by categorizing text data based on negative and positive labels [10]. For example, if we have defined a category to gather all text related to plants and we wish to analyze a new set of text data to determine if this data is related to this category, the new data set may not be easily identified as either positive or negative because there are a variety of terms that may be used to identify text related to the plant category. The EAT algorithm works by teaching the classifier given the new dataset that is to be used. The authors who proposed this method gave the example of categorizing text data about an election. In analyzing a new text dataset, we also want to look out for terms such as "voters" to be associated with the election dataset. This new method works by identifying new terms that should be considered by the classifier in order to assign the text data a positive or negative label.

9) General Architecture for Text Engineering (GATE): GATE is a set of tools written in Java which can be used for analysis projects involving things like text mining and information extraction [11]. There are various tools that make up the GATE system, such as ANNIE, which is used for information extraction given a text dataset as input. Users of GATE can perform a wide variety of analytical tasks on text data, and there are various software that offer user-friendly versions of the system in a GUI environment. The GATE system accepts text datasets in various formats, such as txt, html, pdf, etc. The various inputs that are allowed in this system make it an ideal system in a field such as social media data mining because the text data associated with these tasks can often come in various formats. Because the user has the option of a GUI environment, results may be interpreted in a simpler manner as opposed to requiring additional processing.

2.2. Classification

Classification can be either supervised or unsupervised machine learning models, although they are commonly supervised learning. For unsupervised learning, the software determines the characteristics of the data to define classes. For supervised learning, a user can select the classes or use training sets with classes defined in order to train the software. These are used to predict the class of new data points.

1) Discriminant Analysis: Linear Discriminant Analysis (LDA) is both a classifier and a dimensionality reduction technique. LDA is the preferred method of analysis when there are more than two classes [12]. LDA is commonly used in the pre-processing step of machine learning and pattern classification projects. LDA uses Bayes' Theorem to estimate the probability that a new set of input values belongs to every class. The output class is the class with the highest probability. LDA assumes that the data are normally distributed and also assumes a common covariance matrix. Quadratic Discriminant Analysis (QDA) is a variant of LDA that allows for non-linear separation of data. There is not an assumption that the covariance of each of the classes is identical in QDA as with LDA [12].

2) Naïve Bayes: Naïve Bayes is a probabilistic classification method based on Bayes' theorem. It makes decisions using the Maximum A Posteriori decision rule in a Bayesian setting [2]. The goal is to determine the probability of the features occurring in each class and to return to the most likely class. The only thing that must be done before prediction is finding the parameters for the features' individual probability distributions. A naïve Bayes classifier assumes that the presence or absence of a particular feature of a class is unrelated to the presence or absence of other features. Naïve Bayes classifiers are popular for text classification. A classic use of naïve Bayes classifiers is spam filtering.

3) Support Vector Machines: Support Vector Machines are extremely popular supervised learning models. This method of classification creates a decision boundary which is designed by training points to then classify new data points based on which side of the boundary they fall on. Support vector machines offer a large advantage because they can create nonlinear boundaries easier than some other methods. This is done using a kernel trick which replaces its predictors with a kernel function [13].

4) Decision Trees: Decision trees are a way of performing classification on datasets [14]. Decision trees are popular in machine learning because they are easy to understand. The idea behind decision trees is that similar data points are grouped together in leaf nodes based on decisions that are made. These decisions are represented by the branches of the tree. Each lead node represents a label for a class. Data points are assigned to these classes by following the structure of the tree and going through the tests represented by each branch. Data points are assigned to a leaf node based on the result of the test at each branch that it goes through. So, for unlabeled text data, which is often what data sets consist of in social media data mining, the text data would go through the various tests along the tree structure in order to be assigned a class label.

5) K-Nearest Neighbor (KNN): KNN is a classification algorithm used in machine learning [15]. This algorithm works by analyzing the raw data points specifically by what other data points in the dataset are close to each other. A value K is selected by the researcher; this determines the number of "neighbors" each data point should have. The distance between a raw data point and it's neighbors is pre-determined by the researcher, meaning for a data point to be a neighbor it must be within a certain distance. Class labels are formed by the groups that are formed between each raw data point and its neighbors. This algorithm can be trained on a training dataset and tested on a test dataset in order to select the optimum distance and optimum value of K.

6) Logistic Regression: Logistic regression is a powerful classification algorithm; however, it is limited to two classes or binary classification problems [2]. While it can be extended for additional classes, it is rarely used this way. Logistic regression can be used to predict the likelihood of an outcome based on the input variables.

2.3. Clustering

Clustering is an unsupervised machine learning technique in which data are grouped together in order to make assumptions about the data. The data in each group, or cluster, are most similar to the other data in the same group as opposed to the other groups. It is useful in determining characteristics of data, such as clustering customer orders to determine which types of customers purchase certain products. Outliers are also more evident when using clustering. There are many types of clustering algorithms. Some of the more commonly used algorithms are K-means clustering, DBSCAN clustering, Affinity Propagation clustering, BIRCH clustering, and Mean-Shift clustering. The clustering methods discussed below are the methods used in the studies reviewed in this paper.

1) Positive examples and Negative examples Labeling Heuristics (PNLH): the purpose of Positive examples and Negative examples Labeling Heuristics (PNLH) is to extract reliable positive and negative examples [16]. Reliable negatives are extracted using features that occur more frequently in positive data. Then the sets of positives and negatives are enlarged by clustering the reliable negatives. If an example is close to a positive but not close to a negative example, it is added to the reliable positives. If an example is close to a negative example but not close to a positive example, it is added to the reliable negatives.

2) Similarity Matrix: a similarity matrix is a method of expressing the closeness of relationship between two data points. There are various methods of calculating a similarity score. A similarity matrix has many applications in clustering. Additionally, methods exist based on the similarity matrix such as the clustering-based similarity partitioning algorithm. This matrix provides a convenient way to showcase how points are related and showcase the clustering rationale [17].

3) Parallel Density-based Spatial Clustering with Noise (PDBSCAN): DBSCAN is a clustering method that utilizes a density method to cluster data points, it is highly used in the machine learning field [18]. For each data point within a cluster, there needs to be a minimum number of other data points within a predetermined radius of that data point. So, data points are grouped based on two predetermined parameters. The first parameter is "eps" which indicates how close the data points are to be to each other to be considered as being in the same cluster. The second is "minPoints" which tells the algorithm how many points must be within the radius of each data point. This traditional model of DBSCAN can be computationally expensive with large datasets, thus an updated version of this method called PDBSCAN has been proposed for big data mining, such as social media data mining [19]. This parallel version of this algorithm works by first creating local clusters within different pieces of the data. This is done in parallel, so the data is divided into sections and these local clusters are formed at the same time. Then, these local clusters for each section are combined to form the final clusters. Researchers have found that the parallel adjustment to the DBSCAN algorithm has greatly improved its performance with large datasets.

4) K-means Clustering: K-means clustering is an unsupervised learning algorithm that is used to cluster similar data points together [20]. The raw dataset is analyzed so that centroids are formed based on a given number K, K being the number of clusters that are to be formed from the data. Data points are assigned to clusters based on their similarity to the cluster's centroid. This algorithm will typically involve a lot of testing to determine the optimal value of the parameter K. K-means clustering is often performed by building the model on a subset of the raw data, called a training dataset, and then testing the algorithm on the remaining data, called the test dataset. Using this methodology of testing and training the algorithm allows researchers to more accurately cluster their data using the optimal value of K.

2.4. Mapping

Mapping is a machine learning technique in which input data is mapped to a category or class. It is a type of Artificial Neural Network (ANN) and can be either supervised or unsupervised.

1) Self Organizing Maps: Self organizing maps, while coming with a set of challenges, offer the great advantage of not needing humans to help them learn. This method is based on unsupervised learning and is a cooperative learning network. Self-organizing maps take high dimensional data and make it low dimensional. The map units are typically thought of as points on a two-dimensional lattice. Neighborhoods are created by identifying sets of points which can be classified into the same class, based on traits and attributes deemed best by the unsupervised learning technique [21].

2) Supervised Mapping: Supervised learning techniques require the use of training data as examples of input - output pairs. These examples allow the method to learn and appropriately classify new inputted data to the appropriate category. Such a technique uses a learning algorithm such as support vector machines, linear or logistic regression, naïve bayes, or linear discriminant analysis to name a few. The performance of the supervised learning technique can be very dependent on which algorithm is chosen to do the classification task [22].

2.5. Statistical Test/Model Validity Methods

Statistical tests use mathematics to determine the relationship between random and nonrandom variables. The random variables do not have a statistical influence on the dataset. Model validation shows the accuracy of the model. There are many methods that can measure the accuracy of a model, such as k-fold cross validation, Wilcoxon signed-rank test, and train/test split. The tests and methods used below were used in the studies observed for this paper.

1) Goodness of Fit: Goodness of fit is a measure between the observed values and the expected values of a model [23]. Goodness of fit describes how well a statistical model fits the dataset presented. It tells how well the sample data represents data in the actual population.

2) Kernel Density Estimation (KDE): The Kernel Density Estimation is a mathematical process of finding an estimated probability density function of a random variable [24]. KDE attempts to make inferences of a population based on a representative data set. The technique creates a smooth curve given a set of data. The estimation can also be used to generate points that look like they were from a dataset, which can help power simulations [24]. The KDE is created by plotting the data and creating a curve of the distribution. The curve is calculated by weighing points at a specific location. When more points are grouped at a location, the estimation is higher because the probability of a point being at that location is higher. The kernel function is used to weigh the points.

3) Precision at Rank k: Precision at k is the proportion of recommended items in the top k-set that are relevant to the number of recommended items [25]. A downfall of precision at k is that it fails to take the position of the recommended items in the top k into consideration.

4) Analysis of Variance (ANOVA): ANOVA is a statistical method that is used to examine differences among variables across two or more categories [26]. In simple terms, ANOVA allows analysts to identify the differences among different groups of variables at the same time. This is a very important technique in the field of social media data mining because it allows researchers to identify the unique relationships that may exist between certain social media users, for example. Furthermore, it allows researchers to then perform further analysis to find the reasonings behind these differences. The result of an ANOVA test is the F-statistic, which allows researchers to analyze the variance that exists among the various groups of data. Using the F-statistic, researchers can see if there is a real variance among groups of data, if true variance does not exist then the F-ratio resulting from the ANOVA test should be close to 1.

2.6. Regression

Regression is a statistical technique used to describe relationships between dependent and independent variables. There are various types of regression, including linear regression, logistic regression and multiple regression. The techniques described below are those used in the studies discussed in this paper.

1) Multiple Regression: Multiple regression is designed to create regression models based on multiple independent variables and a single dependent variable [27]. The model that is created provides the impact that the independent variables have on the dependent variable. It is important to keep the number of variables low because the model becomes more complex as variables are added.

2) Time Series Analysis: Time series analysis consists of taking time series data and trying to find the underlying pattern in the data to extract meaningful statistics or characteristics that would be helpful in forecasting or predicting future values. Various prediction methods exist, and many depend on the acknowledgement of cyclical, periodic, and seasonal behavior that exists in the data [28].

2.7. Research Methods

The research methods discussed in this section are methods used for analysis for various research projects. These methods did

not fit into the previous categories of methods defined. Only methods discussed in the observed studies are listed.

1) 5W Method (What, Where, When, Why, Who): The 5W method (What, Where, When, Why, Who) is a general model that can be used to approach a variety of analysis problems [29]. This method works by identifying the main themes related to the problem to be solved. In the field of data mining in social media, we can describe this model in general terms. The What aspect identifies what the problem is, what kind of data are we looking for? The Where aspect identifies where the data is located that we need for analysis. The When aspect identifies when the data of interest is to be collected. The Why aspect identifies why the event of interest occurred. The Who identifies who the social media data is being retrieved from (what users' posts are we interested in).

2) Inductive Content Analysis: Inductive content analysis is a technique used by researchers when the data of interest is not numeric, such as text data often seen in social media data mining tasks [30]. Researchers use inductive content analysis to identify features and develop theories about their data of interest. The process is inductive in that researchers analyze their dataset to come up with themes and conclusions by repeatedly analyzing their data of interest through a series of repeated steps. A process of inductive content analysis typically begins with the researchers organizing their data through some method such as classification and identifying the unique groups that are formed. These processes are then repeated until the researchers have come up with theories associated with their data that can either be further tested or explained for the purpose of the analysis task at hand.

3) Speeded-Up Robust Features (SURF): SURF is an advanced feature descriptor used to represent photo content [31]. It is a fast and robust algorithm used for feature extraction, feature description and feature matching.

3. Study Summaries

3.1. Crowdsourcing based Timeline Description of Urban Emergency Events using Social Media

A previous study utilized the 5W model in order to crowdsource information on urban emergency events from social media posts [29]. The 5W model consists of describing the what, where, when, who, and why information about the event. This study uses posts from Weibo users to test the effectiveness of their model in providing information on urban emergency events. Weibo is a social media platform, similar to Twitter, which has approximately 500 million users in China. The components of the 5W method are described and generated as follows:

1) What: What is the event that occurred? Generated by analyzing keywords from Weibo user posts, the authors refer to these keywords as "concepts". For example, if the event we are interested in is a fire, "fire" would be one of the concepts used to identify posts related to that event. Posts that contain these concepts are referred to as "positive samples".

2) Where: Once the positive samples are identified from the "what" element, spatial information can be extracted from those posts. For example, a post like "I see a fire on Huaihai Road" indicates that there is a fire and where that fire is located. Geographic Information System (GIS) based information from check-in locations can also be utilized to determine the "where". Two location-based service applications in China, Jiepang and Dianping, allow Weibo users to post their check-in location.

3) When: Determining when the event occurred can be done by determining the earliest time stamp for the posts in the positive sample and the latest time stamp. The first timestamp is referred to as the starting timestamp (ST) and the last timestamp is referred to as the ending timestamp (ET).

4) Who: Weibo posts can identify witnesses of the event and potentially the participator of the event. The witness would be the poster of the Weibo event, and the participator may be revealed from the witness' post.

5) Why: Posts by Weibo users may reveal why the event occurred, this will often come from posts by news outlets or police departments.

The authors present two case studies, a fire and a hijack situation, to test how the 5W model can be used to gain information on urban emergency events by crowdsourcing social media posts. The authors demonstrated that this model was beneficial in retrieving the needed information concerning each event from Weibo posts. The authors were able to identify relevant posts for each situation, which they called positive samples. These posts were retrieved by searching Weibo posts in the locations of the two events on the days in which the events occurred. From these positive samples, the authors were able to identify what happened (the event of interest), where the event occurred (from location information attached to the posts), when the even occurred (by looking at time stamps related to the posts in the positive samples), who the event affected, and why the event occurred.

The authors conclude that the 5W model was successful in extracting information about the urban emergency events presented in the two case studies. Future applications of this model may involve comparing the effectiveness when applying it to Weibo posts and posts from a different social media platform, such as Twitter or Facebook.

3.2. Mining Social Media Data for Understanding Students' Learning Experiences

In [32], the study conducted focused on analyzing Twitter posts from engineering students to understand the issues they face in regard to their educational experiences [32]. The model developed was then used to detect student issues in Twitter posts from students at Purdue university. The two main research goals of this study were to analyze social media data for educational purposes using various data mining techniques and qualitative analysis and to analyze Twitter posts from engineering students to understand the issues faced by these students in regard to their educational experience.

The authors began by collecting Twitter posts that used the hashtag "#engineeringProblems" over a time period of 14 months to create their first dataset. The second dataset was created by collecting all Twitter posts that are geo-tagged with the location

of Purdue University through a search of the Twitter search API. The Tweets gathered by searching for the hashtag showed that the problems faced by engineering students fall into distinct categories. The authors used a Naïve Bayes classifier to classify the Tweets into their categories. This classifier was then used to classify the Tweets collected from Purdue University to arrange the engineering students' Tweets into multiple categories based on the issues they were facing. The authors' multi-label classification model allowed for one Tweet to fall into multiple categories. The researchers found that the main issues faced by engineering students were things like sleep deprivation and lack of study-life balance.

Because the Twitter posts obtained from the hashtag search did not contain pre-defined categories, the authors used inductive content analysis to identify categories within the dataset. The authors were interested in developing categories based on the major issues faced by engineering students. From this inductive content analysis, the authors developed six major classes: heavy study load, lack of social engagement, negative emotion, sleep problems, diversity issues, and others. The authors used multi-label classification so that one Twitter post could fall into more than one of these classes, with the exception of the others class. The Twitter posts were organized into these classes by two researchers, and F1 scores were generated based on how each researcher labeled each post in order to decide on the finalized class assignments. The authors found that the Naïve Bayes classifier was the most effective classification method for their datasets. This classification method was then used to classify the Twitter posts from the Purdue University dataset into the six classes. The authors believe that the methods they have presented here can be applied to other social media platforms, such as Facebook, to further analyze issues faced by students.

3.3. Investigating the impact of social media advertising features on customer purchase intention

Social media ads have become increasingly popular, with companies investing a large amount of money for them. The biggest rationale of choosing social media ads is the idea that they can be customized to the specific individual. For example, based on what users post about, like, and share, advertisers can predict the most relevant ads for the user to see that will result in a sale or a click.

The study lists out two primary questions,

1) What is a suitable conceptual model that could be adopted to provide a clear picture covering the main aspects related to social media advertising?

2) What are the main factors associated with social media advertising that could predict the customer's purchase intention?

In order to figure out what data need mined, a variety of previous studies were analyzed looking at various factors such as attitude, irritation, informativeness, creativity, and privacy concerns were targeted using platforms such as Facebook, Twitter, and Myspace. Based on customer researchers, they found that there was a strong correlation between the performance expectancy of ads (how well they were geared to individuals) and people's views on social media advertising [33].

Structural equation modeling was the technique used for analyzing a proposed model based on Cronbach's alpha value. Some methods used in the analysis of the model was Goodness of Fit Index, the Adjusted Goodness of Fit Index, Normed-Fit Index, Comparative Fit Index, and Root Mean Square Error of Approximation.

A hypothesis test was run on each of the factors to see if they were significant in contributing to the prediction of proper advertisements leading to increased chance of a consumer purchasing using regression analysis. Multicollinearity tests ensured for the multiple regression that the variance inflation factors were not too high. Average variance extracted (AVE) and composite reliability (CR) were additionally tested to make sure they were in their recommended levels.

The research done in this study was able to confirm that being able to identify these characteristics can heavily improve the ability to target customers with appropriate ads. Hence, when mining social media posts in real time these factors are the important aspects to be able to filter out and utilize [33].

3.4. Corpus for Customer Purchase Behavior Prediction in Social Media

One application of making these models was done in a data mining study that analyzed how well iPhone sales could be predicted based on social media data. By analyzing tweet's such as "I bought an iPhone" and "Checking out the new iPhone", the corpus collected English tweets related to purchase behavior and then manually recorded if a user purchased a product [34]. After defining key phrases, extracting product details from eBay pages, and analyzing tweets. The proposed methodology by researchers in this type of situation would be to use machine learning to train a classifier on whether a phrasing results in a buy or not.

The corpus created for data mining tasks like this can be automated as much as possible. Examples of automated labeling tasks were provided such as finding the location of users, frequency, and past analysis of the same user. All of these items are believed to enhance a machine learning corpus to provide much more accurate and meaningful results [34].

3.5. Predicting Postpartum Changes in Emotion and Behavior via Social Media

As opposed to being able to help predict marketing and purchasing information, the researchers utilized user data from social media to predict the effect that giving birth would have on a mother. In order to accomplish this, tweets were analyzed for dimensions of social engagement, emotion, social network, and linguistic style [35].

In order to develop a predictive model and sort through the tweets, a two-stage approach was used to construct the sample of new mothers. Twitter being public presents a wide range of challenges because of the number of public posts and ones that may be irrelevant to the predictions being made. To condense the data set, the first strategy was to analyze tweets to find users that appeared to have a recent childbirth in their lives. These remaining individuals served as possible individuals for the sample.

The various factors of engagement, ego-network, emotion, and linguistic style were quantified so they could be rated based on the analysis of the tweets. Since Twitter maintains all of the Tweets from the user since the beginning of the account, the differences in these factors were able to be determined from before the child birth to after the child birth. With the calculations of these differences, groups were formed (extreme-changing mothers and standard-changing mothers) to use in supervised learning techniques.

To avoid overfitting the data, principal component analysis and randomized forest procedures were utilized. Methods such as linear, quadratic, discriminant classifiers, naïve Bayes, k-nearest neighbor, decision trees, and SVM with radial kernels were used in the classification process. Out of all of these, the SVM had the greatest accuracy with using a five-fold cross validation method. Using this methodology, there was a highest point of 80% accuracy on a testing data set of being able to classify new mothers who would experience postpartum depression after giving child birth [35].

3.6. Big data analytics for disaster response and recovery through sentiment T analysis

Big data from Twitter and other social media has been used for many applications, such as healthcare, multi-channel, finance, log analysis, traffic control, homeland security, telecommunications and retail marketing but is only in the early stages for disaster response and recovery [36]. Emergency help related requests during disaster situations rarely use social networks [36]. Because crisis situations are chaotic and disorganized, big data analysis of these data is a good fit for handling the environment. Typically, because of lack of information for the affected team, disaster management teams rely on incomplete or inaccurate information. Big data analytics can assist in getting the right information from large amounts of data, analyzing it and providing results to the disaster management or rescue teams to enable them to make the best course of action.

The authors of this study propose a method to identify a sentiment towards the philanthropic aids received by the people during and after a disaster [36]. While governments typically provide relief, the needs of people are not always met as the need is not always identified. This study uses tweets collected during three disasters to help build a model to meet the needs of those affected. First, the data are analyzed and categorized by the various needs of the people during and after the disaster. Second, various features, such as bag of words, parts of speech-based features, and various lexicon-based features are analyzed and the best performing algorithm in each category is identified [36]. Finally, a visualization method is proposed for the sentiment of the basic needs which would help the emergency responders. In order to provide help to emergency responders, a solution must be built that uses real-time data and analysis to determine the needs of the people during a disaster. The objective of this research is to build a conceptual model for disaster response and recovery by using the best features that classify the disaster data with highest accuracy [36].

The data obtained for this study were obtained for the following disasters: the India-Pakistan floods in September 2014, a seven cyclonic storm named HUDHUD in October 2014 and

another seven cyclonic storms named Nilofar. These data were collected from Twitter and contained 70,817 tweets. Part of these tweets were collected from Streaming Twitter API. This API only allows users to collect the past seven days' data. Since historical data cannot be obtained through this API, the rest of the data was collected using a third-party vendor 'Followthehashtag'. Keywords used to collect data are as follows: HUDHUD, Vizag flood, Nilofar, Kashmir floods, India-Pakstan floods, Pakistan floods [36]. The data collected for each disaster was collected for a specific time frame: HUHUD and Nilofar were collected from September 5, 2014 to November 15, 2014; Kashmir floods were collected from September 1, 2014 to October 15, 2014.

The preprocessing step is completed so that the machine learning algorithm can interpret the data. Since Twitter data contains Uniform Resource Locators (URLs), numbers, abbreviations, etc., it is important to remove these before performing further steps. The disaster area tweets are categorized by keyword filtering technique, which is common in Twitter analytics. The keywords are selected by identifying words that are used more than five times and also relevant to the category. Two steps are used in the text classification stage, the subjective sentences segregation and feature vector generation. The subjective sentences provide the sentiment related information, while features convert the subjective sentences to feature vectors to be used in the machine learning algorithm [36]. Text is separated into subjective and objective sentences based on the usage of words. The sentiment of people is identified in the subjective sentences. Since separating subjective and objectives is a manual task, tools can be used to automate the process. Publicly available sentiment-based lexicons are used to categorize the subjective sentences. To categorize disaster data, three lexicons were considered for the model, one from Twitter domain (AFINN) and the other lexicons which contain slang words, misspelled words, and morphological variants [36]. The disaster data is filtered with the list of positive and negative words from the lexicons. Anything not classified as positive or negative is removed. Parts of speech (POS) tagging is carried out to filter the adjectives and adverbs from entire streams of tweets. Bag of words (BOW) feature is where the entire text is represented as a list of words. The occurrence of each word is used as a feature in training a classifier [36]. Another feature is combining words. The adjacent two words are the bigram feature; the adjacent three words are the trigram feature. This is extended up to n numbers, so n-gram features to train the classifier. As n increases, the accuracy decreases. While training, the input is limited to the unigram model. Next a machine learning algorithm, support vector machine (SVM) is applied, as previous studies show SVM is the best algorithm for text classification. During preprocessing, the text is converted into a vector which consists of a set of features that represents the corresponding disaster related data [36]. The SVM algorithm then calculates and plots a hyperplane through supervised learning that divides positive and negative texts. The linear kernel was found to provide the best results. The results are evaluated by calculating the precision, recall and F-measure which are the three main metrics for measuring the performance of a classification system [36]. Precision is the percentage of classified text that is relevant. Recall is the fraction of classified text that is retrieved. F-measure is the ratio of the combination of precision and recall [36]. After the data has been

classified by the SVM algorithm, the positive and negative words are used to identify the opinion towards each category [36]. Sentiment strength is calculated from these results. In this study, the combination of the subjective phrase and machine learning algorithm with bigram feature presents the best classification accuracy of disaster related data [36].

This study used social media to determine the needs of the affected people and then using sentiment analysis determines if those needs are being met. Various visualizations were used in this paper, including box plots. The visualizations make it easier for emergency management personnel to understand the needs of those affected in order to provide the best assistance. The study also helps connect people who are willing to help with information regarding how they can help. Many times, an unaffected person will offer help, such as clothing or food, but is unsure how to get these to the affected people. The proposed method helps to bring those people together.

3.7. World Cup 2014 in the Twitter World: A big data analysis of sentiments in U.S. sports fans' tweets

It is indicated in recent social media research that sports fans use social media for a variety of reasons, including emotional response [37]. Present analysis uses big data analysis techniques to analyze sports fans' emotions and behaviors. The authors propose to use social media responses to measure the emotions and responses to sporting events or television shows [37]. If the results prove to be true, this would indicate that text-analysis is valid based on specific criteria. The authors also examine whether the tweets change with response to the gameplay. This study focused on Twitter data with a location stamp from the United States, although the World Cup took place in Brazil. This ensured the tweets were from users who were not in attendance at the World Cup.

The affective disposition toward a team can range from intense liking to intense disliking [37]. Typically, when a team is doing well, their fans are more likely to show joy or positive emotions. When a team is doing poorly, their fans are more likely to show negative emotions. If a viewer is not a fan of either team, they are typically not emotionally invested in the team and do not show the same emotions as a fan. Research in social media for emotional reasons is limited. Part of the literature review for this study found a survey method that analyzed the why sports fans used social media during sports and found a significant but weak relationship with sports fans' game enjoyment and their use of social media during mediated games [37]. Typically, emotion behaviors in data are coded by humans. Since social media data is so large, it would be impossible to analyze tweets manually for the number of fans watching a sporting event.

Sentiment analysis has increased over the last decade. Existing methods are based on linguistic resources or machine learning. The more common approach is to use linguistic resources, which uses lists of positive and negative words. This method counts the number of times a word appears which allows it to recognize words with positive polarity (favorable sentiment), negative polarity (unfavorable sentiment) or no polarity (neutral) [37].

This study used a natural experiment approach to monitor U.S. fans' emotions and reactions during the games when the U.S.

National Soccer team competed in the FIFA World Cup 2014. Sentiment analysis was used to examine the emotions manifested in the tweets [37]. Tweets were retrieved using Twitter's Search API during the 2014 FIFA World Cup. A web crawler was designed to collect and parse English tweets in real time using the following predefined hashtags: #FIFA, #Football, #WorldCup, or #Soccer, ignoring letter case.

Two analysis methods were used for sentiment analysis. First, NRC Word-Emotion Association lexicon was used to measure specific emotions, such as fear, anger, joy, sadness, disgust, surprise, trust and anticipation [37]. The authors used the lexicon words' frequency to measure the strength of the specific dimension [37]. An R application was used to extract the features from a tweet and create a score by counting the words that matched the eight categories or emotions listed above. Second, the tweets were then analyzed for emoticons expressing the mood with either a :(meaning sadness or :) meaning joy [37].

The findings of this study show that fanship of a team enhances one's worries and involvement in the game but being a fan of a sport is mainly tied to enjoyment and emotional release (anticipation). The use of big data analysis of the sentiments was as expected and can be reasonably explained [37].

3.8. A context-aware personalized travel recommendation system based on geotagged social media data mining

A previous study focused on using social media data to build a travel recommendation system [38]. The goal of this study was to build a system to recommend travel points of interest in different locations based on data obtained from social media posts previously made by users during previous travels. The idea being that the system can recommend a point of interest to a user in a new travel city, based on the previous points of interest they have visited in other cities. The authors built a system with a variety of functions in order to accomplish their goal of building this travel recommendation system. Their method was tested on the public API of the social media platform Flickr to collect the metadata of 736,383 photos that were taken between January 2001 and July 2011 in six different cities within China.

Geotag information available on the photos allowed the authors to cluster photos together based on location using the P-DBSCAN clustering algorithm. This method worked by clustering photos by location based on a predetermined maximum radius. Once the clusters were created, the authors used term frequency-inverse document frequency to score the location tag of each photo. The higher the score indicates a tag for a more distinctive location. Based on these results, the authors used Google Places to find points of interest associated with each location. The authors then used the timestamps of users' photos to determine the average time a visitor would spend at each point of interest. Matrices were built to examine the interests of users in each location. The Pearson correlation metric was then used to build a similarity matrix to find similarities among users' traveling patterns. The authors conclude that the method they have proposed was successful in examining user preferences and correctly suggesting travel points of interest in new cities based on their previous posts and their similarities to other users.

3.9. A Big Analytics Method for Tourist Behaviour Analysis

Big data analysis is lacking in the social media field in relation to decision making, specifically in Tourist Destination (TD) Management. This study focuses on supporting strategic decision-making in this sector because big data analytics has not provided use cases for strategic decision support [31]. TDs are areas of interest within a locality that tourists may visit or participate in sightseeing. Tourists share data via multiple sites: Flickr for photo sharing, YouTube for video sharing, Twitter for immediate response sharing, and Facebook for photo and comment sharing and discussion. These data could provide important information to tourism authorities, although they rarely collect the data. This study uses publicly available geotagged photo data on the photo-sharing site, Flickr.

This study evaluates a method based on unstructured data with meaningful content that is tourist focused. The method used in this study combines text processing, geographical data clustering, visual content processing and time series modeling to address the DMOs decision support needs. The results may provide DMOs with information in forecasting future and seasonal demands of tourism development, management and planning [31].

Textual metadata often contains keywords. These data are usually unstructured, which requires some pre-processing. The authors employed a text processing tool, General Architecture for Text Engineering (GATE). The geographical data clustering step is the next step in the process. Here, the authors aim to identify popular locations for each of the identified tourist interests. A clustering technique, P-DBSCAN, is used to identify popular areas of interest. It includes both the number of tourists that visit the location and the number of photos. This ensures that the identified locations have many visitors.

For each location, tourism managers are interested in the most representative photos for each tourist interest [32]. Representative photos identification was completed in two steps: Visual Content Representation and Kernel Density Estimation. For the visual content representation step, the authors adopted Speeded-Up Robust Features (SURF). A popular approach to represent photo content using local region descriptors is to represent each image as a visual bag of words. The descriptors are first extracted for a large set of local regions extracted from a set of random photos. K-means clustering is then applied to create a visual word vocabulary. Visual words are defined as the center of clusters and the value of k determines the number of visual words available [31]. Kernel Density Estimation (KDA) is then applied. The probability density function is calculated for each photo. The photos with the highest probability density function are considered the representative photos. The theme for each photo collection can be identified by examining the small selection of representative photos.

In order to determine how frequently and how many tourists can be expected to visit in certain months, a time series model is created. Popular fitting functions include linear, exponential, and quadratic types [31]. The mean absolute error (MAE) is used to select the most appropriate model for trend estimation rather than predict the actual value of the time series. A seasonal component is removed from the time series. The trend was modeled using a quadratic function and the seasonal means are calculated by the average of seasonal components for each month.

Those four techniques are combined in the solution artefact to process and analyze different types of data (textual, geographic, photos and time) in order to offer insight into tourist behavior and perceptions. The authors propose using the time-series model to predict tourism demand. The DMO will have insight into tourist interests but also time series trends, including any seasonal trends, which will help with strategic planning and decision-making.

The authors chose to use a representative sample of tourists' social media data for Melbourne, Australia. Geotagged data was extracted and processed using the techniques already described. These data were extracted from Flickr using its API using the coordinates of a bounding box around Melbourne, Australia (based on the longitude and latitude from Google maps).

Time series models were then built for forecasting future tourist demand in Melbourne. Seasonal mean models were created to determine seasonal patterns. These models help determine seasonal patterns of travel which can be used to determine tourist arrival. This will aid the tourism managers in strategic planning and decision making. These data showed no seasonal pattern for local Australian tourists. The pattern of tourists was different among the groups of data (Australia, Asia, Europe and North America), however was the same within the groups. For example, in North America, the high peak season was between January and March and in November; the low peak season was April through September.

This study automatically detects tourists interests in places and objects [31]. The authors were able to extract meaningful information from the geotagged photos, thus creating a solution that provides DMOs with information to make meaningful decisions based on key patterns and trends in tourist social media data. The full artefact in this study was presented to both academic and industry audiences, which helped improve the design [31]. The authors were also able to test the results of the artefact using not only the Melbourne data but data from other locations. Only data from Melbourne was presented in this study. If a sufficient number of photos are collected, this method proves to be effective for any city.

3.10. Network-Based Modeling and Intelligent Data Mining of Social Media for Improving Care

In [39], the study conducted aimed to analyze forum posts related to cancer treatment to identify positive and negative feedback to the treatments and side effects [39]. This study also aims to identify "influential users" within the forums of interest. Pharmaceutical companies have been tasking their IT departments with using social media data mining techniques to retrieve reviews from patients that have used their medication in order to easily retrieve feedback on their product. Social media data mining in reporting feedback of care can also be used by doctors and patients to improve care. Doctors may use such a system to recommend more effective treatment options and patients can use such a system to see previous feedback on treatment options that have been proposed by their doctors. This task is often completed using patient surveys; however, the authors indicate that social

media data mining for this purpose allows for access to more readily available information.

The authors of this study were interested in user feedback of the drug Erlotinib, which is used in the treatment of lung cancer. The authors began this experiment by searching the web for popular cancer forums, specifically those with a significant amount of posts related to lung cancer, four online forums were identified in this step. Within these forums identified, the authors searched for posts specifically related to lung cancer medication and noted that Erlotinib was the most frequently discussed drug. The authors then searched all of the forum posts for common terms related to positive and negative feedback, this was done using a Rapidminer data collection and processing process. The result of this step was a final list of words associated with negative and positive feedback; each word was given a term-frequency-inverse document frequency (TF-IDF) score. The words with the highest TF-IDF scores were tagged using a modified NLTK toolkit in order to add positive tags to negative words and vice versa. For example, for a post that says, "I do not feel great", a negative tag was added to the word "great". The authors then removed similar words and words that appeared less than 10 times, the result was a list of 110 words, half of which were positive and the other half being negative.

Another word list was created based on searching all forum posts related to side effects of Erlotinib. In order to identify terms associated with side effects, the authors referred to a vocabulary list from the National Library of Medicine's Medical Subject Heading. A list of the words related to side effects were then fed into the Radidminer processing tool in order to assign TF-IDF scores to each word. Words with the highest score, that appeared at least 10 times, were kept for the final list of words relating to side effects. The result of these two processes was a dataset of user forum posts which were each transformed into two vectors, one with 110 variables for the TF-IDF scores for the positive/negative terms and another with 10 variables containing the TF-IDF scores for the side effect terms. The vectors were then analyzed for clusters using Self Organizing Maps (SOM). The forum posts were first manually labeled as negative or positive before they were fed into the SOM. The purpose of the SOM step was to analyze the clusters formed, and the weights associated with those clusters, to see if there was a relationship between the clusters identified and the classification of the post being negative or positive.

The next step was to identify those users in the forums that are considered "influential." This was a topic of interest because these influential users can often drive the opinions of other users within the forum. This process was done using a combination of network-based analysis with a Markov chain modeling the various connections between nodes of the network. The opinions of these influential users were then analyzed to identify them as being negative or positive using a module average opinion (MAO) approach. This formula takes the sum of the TF-IDF scores associated with positive terms, minus the TF-IDF scores of the negative terms, and then divides this difference value by the sum of all TF-IDF scores. Lastly, forum posts related to side effects were identified using the list of side effect terms previously developed. The authors found that most feedback related to the drug was positive. The authors demonstrated that they were

successful in identifying "influential users" within the forums. These users were found to interact with other users on the forums very often and that users looked to these influential ones for further information. The authors used t-tests to score the posts associated with side effects, finding that rash and itching were the most frequent side effects reported. The authors summarize that methods similar to these can be used in the future to improve patient care and reduce costs.

3.11. Filtering big data from social media –Building an early warning system for adverse drug reactions

Adverse drug reactions (ADR) are unintended reactions or side effects for a medication. Usually, these are determined during clinical drug testing trials. The World Health Organization (WHO) uses "early warning" systems to monitor ADRs. Usually, the early warning systems are based on feedback from pharmacists and physicians rather than the patient. A growing number of pharmaceutical companies are now allowing consumers to report symptoms directly to them in order to ease legal and monetary implications [40]. Not all countries use consumer reports and even the ones that do have experience a delay in getting consumer reports of serious ADRs. Because of this, a different approach is needed.

Patients have taken to social media to discuss their medication use and experience. This information could be used for healthcare research. The user-generated content (UGC) is an emerging trend of data for early detection of adverse disease events [40]. Users tend to share their perceived risk of an ADR on a social media platform. These data provide an opportunity to mine the data for a relationship between drugs and their interactions. The challenge to this type of data is the messages are usually sparse and highly distributed. It is easy to obtain large amounts of unlabeled social media data, but it is costly and time consuming to manually classify and label the ADR messages to build an early warning system.

The objective of this study was to develop a process to scan large amounts of text-based posts collected from drug-related Web forms. The system will integrate both text and data-mining techniques to extract important text features from the posts and then classify the posts into positive/negative examples based on a few pre-identified ADR related posts. The classification process is based on a partially supervised learning method, which uses a small number of known positive posts to identify other posts of similar text features from a large corpus of unlabeled posts [40]. The results can be used to build an early warning system to assist the Food and Drug Administration and pharmaceutical companies.

Data collection consisted of crawling of Web forums to gather patient posts from social media. This study focused solely on discussion boards, in particular Medhelp, however the method could be expanded to include social media platforms such as Twitter and Facebook. The authors used domain experts to tag a large sample of posts related to the drugs in this study. If any ADR wordings were identified, it was labeled as a positive example; otherwise, it was a negative example.

The Latent Dirichlet allocation (LDA) is applied to construct a topic space over the corpus. It uses a small number of topics to

describe a collection of documents. The LDA model reduces the dimensions while maintaining the structure of the document. The authors then used the Gibbs sampling inference algorithm for approximation. During classifier construction, the authors selected reliable positive and negative examples to fit the distribution of the positive and negative classes, respectively.

In order to reduce the diversity of topics, the negative dataset is partitioned into smaller clusters. Here, they used the k-means clustering method. After the negative examples were extracted, they moved to the positive examples. The authors used Support Vector Machines as the text classifier.

Four benchmark methods, Example Adaptation for Text categorization (EAT), Positive examples and Negative examples Labeling Heuristics (PNLH), Active semi-supervised Clustering based Two-stage text Classification (ACTC) and Laplacian SVM, were compared with the method used in this study. The paired-sample Wilcox signed-rank test was applied to assess the statistical significance with respect to the best benchmark method. The approach in this study outperformed the benchmark techniques in most cases.

3.12. Helpfulness of user-generated reviews as a function of review sentiment, product type and information quality

In dealing with data mining, text analysis plays a vital role in filtering through reviews that people write for products to determine if they are useful or not. In this study, a method was developed to model the large amounts of reviews that people post on a daily basis (from sites such as Amazon) to determine which of those reviews are actually helpful.

In order to collect the data, reviews were collected and multiple regression was used to classify reviews as helpful or not. Text analysis revealed that extremely high and extremely low reviews were often over inflated, being based on very individualized experiences that would not help a wider audience. ANOVA served as a statistical measure to analyze the differences between the various categories of review (such as by star rating). Text analysis found that in the majority of cases, the most helpful and detailed information was being found in the 4-2 star rating [41].

Further filtering was able to be performed to determine truly useful features of reviews. Further modeling was performed to be able to factor in product type, which had different factors that impact what reviews are deemed to display quality information. Further considerations in this work can be to put important reviews more accessible to customers or identify fake reviews that are being posted simply to increase or decrease a specific product rating for an online site [41].

4. Overview of Findings

4.1. Social Media Studies

In the paper describing urban emergency event description through social media data mining, the authors developed a simple 5W model to describe the event of interest [29]. This method is very simple in that it only requires searching through public posts within a given location on a certain date range to describe an event that has already occurred. This paper showed how easily

information can be extracted from social media posts using basic words to search posts. While this paper develops a user-friendly way to search for social media posts of interest, there are some issues that could arise from this method. For example, if a researcher were to use this information to search for posts related to a fire that occurred in a certain area on a given date, searching for the word "fire" in Weibo posts may result in posts being returned that had this word but that were not related to the event that occurred. While this is still a good method to identify posts of interest, one should be aware that a method would need to be developed to filter-out posts that are irrelevant to the topic of interest. In the future, researchers should come up with an algorithm that can be employed to filter-out posts that are irrelevant to the current topic of interest. Future work involving these methods should also consider that size of the dataset that will need to be searched for relevant posts. In this example, the event was in a specific location. If this model were to be applied to future research that was concerned with a larger geographic location, for example an entire country, additional methods, such as programing, may need to be deployed to efficiently search through social media posts to find those that are of interest.

In the paper which described a system for identifying student experience, the authors used Twitter API search and Naïve Bayes classification to examine the problems faced by engineering students [32]. An easy method of searching for a relevant hashtag within Twitter was implemented. This approach works well for a system like Twitter in which users' posts very often include hashtags to identify the main themes in the post. The authors showed that the Naive Bayes classifier performed best with their dataset of interest. It is important to test multiple classification methods when analyzing datasets such as this one to find the best method. Future research that involves a similar dataset could use the methods described by these authors to compare if such methods would apply to all Twitter post datasets searching for hashtags of interest, or if the best classification method varies depending on what the resulting dataset is after a Twitter API search. One limitation to this specific approach was that the authors only searched for problems faced by engineering students but did not develop a method to identify positive feelings from engineering students. A collection of data like this may imply that only negative experiences were faced by engineering students. It would've been beneficial to compare positive posts from engineering students to learn more about the engineering student experience as a whole. In the future, this same algorithm could be applied to include other social media platforms, such as Facebook, because not all students actively use Twitter. An addition of this experiment should also involve coming up with positive hashtags or terms that would be used to identify posts of engineering students.

While studying "Investigating the impact of social media advertising features on customer purchase intention" it was clear that sites such as Facebook and Twitter performed well for the model [33]. However, the applications of this research were not tested in other social media environments to see if the same results would hold up. One argument for this is the reasoning of why certain personalities gravitate towards specific types of social media platforms. Since much time was devoted to model validity, it would have been worthwhile to explore how well the model did

analyzing photo captions on a site such as Twitter, or tying in photo analysis itself. As opposed to just text, video and images on social media could provide an unseen angle as to how customers look at products [33]. As viewed in the introductory section, with all social media platforms experiencing a rise in recent years, further work should be done to view correlations and associations between the various sites to see what behaviors can be seen as a commonality. As the data was collected from a survey of participants, it would be beneficial to anyone using this model to test it against a randomly selected group of individuals from other areas.

Corpus for Customer Purchase Behavior Prediction in Social Media provided insightful methodology of how social media posts could be used to determine if an individual would buy a product based on what they posted [34]. The downfall of this article was that it did not actually create a workable model that could be tested. Therefore, all proposed methodology were based off of other studies and what should theoretically" work and produce the best results (i.e., appropriate classifiers, sentiment analysis procedures, learning methods) without demonstrating that these claims were in fact true. This work does however provide an easy point for new researchers to build off of to help develop a working model. While the article mentions twitter extensively to obtain the data, no reference is mentioned as to how this would actually fully be implemented. Based on other studies, it seems reasonable that Twitter API searches could be implemented to gather tweets that could be fed into this proposed model once it is created [34].

The paper "Predicting Postpartum Changes in Emotion and Behavior via Social Media" provided several different methods of how to classify the data once text analysis was performed. This idea was an extremely highlighting feature of this paper since it involved linear and Quadratic discriminant classifiers, Naïve Bayes, k-nearest neighbor, decision trees, and support vector machines as tested methods. This allowed the reader to confirm the results of several other studies that SVM appeared to be the classification method which yielded the highest success and reliability rate [35]. The paper also shows social media can apply to make predictions about important aspects of people's lives. While the study focused primarily on Twitter, it would have been beneficial to see if the performance held up over other platforms as well [35]. Extensions in the research could also examine commonalities between the various social media platforms to make extensions on how a model for one social media platform may perform or be adjusted for any of the others. Based on the analysis performed and the more reliable results from the SVM classification method, this should form a good method choice for testing the analysis of text on sites that allow users to be more expansive with their word limits in posts. Additional analysis of the SVM method's reliability correlated with character length would provide great insight into if SVM is an overall choice for this type of analysis, or if it is the most effective when a stricter character limit is imposed on a user.

In the paper describing a system to perform sentiment analysis in response to disaster responses and recovery, sentiment analysis and SVM were used to create a classification system for social media. These results were presented to emergency responders in a visual form to help understand the needs of those affected [36].

The combination of both sentiment and SVM proved to be an effective method of classification. The method also included bag of words, where the entire text is shown as a list of words. The downfall to this is when taken out of context, the words may seem unimportant but in the full context of a sentence or tweet the word may be very important. Improvements to this study would be to include data from other sources, instead of only Twitter data, as well as considering sentences rather than individual words within tweets to ensure the context is captured properly. Also, particular keywords were provided to extract the appropriate data. Another improvement would be to create an algorithm that monitors Twitter data for an increase in use of a particular word or sentence, as is done with data that is trending in Twitter. The authors suggested future studies could include data from various disasters to improve the accuracy of the model. With multiple social media platforms, extracting data from multiple sources, while complex, could also improve the disaster response models.

In the paper describing a system to analyze sentiments of U.S. sports fans using tweets, sentiment analysis was performed using two methods: NRC Word-Emotion Association and analysis of tweets for emoticons expressing the mood. This study presented results that were expected: a fan's emotional state during a game is directly related to how well or how poorly their team is performing [37]. A limitation of this study is that a very specific group of fans was analyzed. The study used tweets from US fans that watched the World Cup 2014 from the United States, not in person. The authors assumed that when fans were happy it was because their team was doing well, so their assumption and hypothesis were essentially identical [37]. Data was collected only during the games. An improvement to this study would be to collect tweets from a longer time frame to determine if the users are truly fans of the team or only fans during the particular game evaluated. Additional statistical techniques could be applied, such as SVM, which works well with text classification. Individual words within the tweets were examined, rather than examining the context of a word within a tweet. To improve this method, future research could involve examining the entire tweet to ensure the proper context is examined.

4.2. Photo Sharing Studies

In the paper describing the creation of a travel recommendation system, the authors used a combination of P-DBSCAN clustering and TF-IDF to create a travel recommendation system based on the user's previous travel data [38]. This system was based on making recommendations for new travel locations based on previous locations the user has traveled to. The authors proved that their method of combining P-DBSCAN clustering and TF-IDF was efficient, and successful, in handling large datasets. With the size of the dataset that this method was tested on, one can assume that the same methods would be successful if an application of this kind were to be available to all social media users when traveling. It is likely these methods would be successful in other recommendation applications that used social media, such as an application to recommend restaurant options in a user's location. While the methods presented here provide a reliable system to follow to make future recommendations, there is some room for improvement in that the researchers only consider making

recommendations for users in which previous data has been supplied. A system such as this would not work for new users because there would be no previous data to go off of. A system such as this one should include an additional feature that new users can use to answer questions based on previous travel that has not been tracked in the travel recommendation system. A questionnaire which identifies previous places the user has traveled to and points of interest visited in those locations would improve the function of the travel system to be more beneficial to new users.

In the paper describing a system defining tourist behavior, the authors used Flickr's API to export photos and related metadata for analysis. The methods used were General Architecture for Text Engineering (GATE) for text processing, and P-DBSCAN for clustering [31]. P-DBSCAN is used to identify popular tourist areas. Speeded-Up Robust Features (SURF) and Kernel Density Estimation are applied. Time series models were used to determine the future tourist demand and seasonality demands. This system proved to be effective for not only the location analyzed in this study, Melbourne, Australia, but also for other locations if sufficient data is collected [31]. The strength of this study was that the authors incorporated tourist photos, which had not been done in previous studies. One limitation was the metadata for the photos. Complete metadata was not available for all photos extracted from Flickr. Another limitation was only one site was used to extract data. This limits the information to only photos and does not include emotional responses that may be found in other social media, such as tweets. A future recommendation would be to include data from some of the other social media platforms, such as Instagram, Snapchat, Facebook and Twitter to improve recommendations. Multiple types of data could also be analyzed, including photos, videos and status updates. Some users may tag themselves into a location without sharing a photo, making it valuable to collect other types of data. These additional data would likely require adjustments to the model; however, the model would provide a good foundation.

4.3. Medical Forum Studies

In the paper which described a system for improving medical care, the authors use a combination of TF-IDF and self-organizing maps to analyze forum posts within various medical forums [39]. The authors' model was careful to add negative and positive tags so that these posts were categorized correctly. The authors also identified influential users that could potentially sway the opinions of new users. As shown in the other papers mentioned here, TF-IDF is a common method used when analyzing social media posts, and it has shown to perform well for extracting information of interest. The authors show that the use of self-organizing maps is successful when the goal is not only to find social media posts relevant to your topic of interest, but also to find which users are considered to have influence over other users. One item that the authors did not consider was how long users of the forums may have been taking the drug of interest. It is well known that there is a period of time when a person begins taking a new drug in which their body is adapting to the drug, so some side-effects may be more intense for a period of time in the beginning. An improvement to this system may be to retrieve information on how a users' post may change over time after they

have been taking the drug of interest for a longer period. The same logic would apply to medical treatments that don't specifically involve drugs, such as a new kind of therapy that a patient is trying.

In the paper describing an early warning system for adverse drug reactions, the authors used Latent Dirichlet Allocation and Support Vector Machines to classify text from Medhelp [40]. Domain experts were used to tag sample posts related to the drugs in this study. If any ADRs were identified, the posts were marked as positive examples; otherwise, they were marked as negative examples. Support Vector Machines are particularly effective in text analysis. LDA performed well against the benchmarks from other studies that were presented in this paper. One limitation to this study is the need to use domain experts to classify posts. When human interaction is needed with big data, the sheer number of posts that can be evaluated is limited. In the future, an improvement could be creating an automated system to evaluate the social media posts rather than relying on a human to interact with the data. This would provide a larger sample of data, and allow the system to react in real-time, or close to real-time. As the authors discussed, an improvement to this model would be to collect from other sources, such as social media posts, rather than just web forums. While this method appeared successful compared with the benchmark methods, it is hard to imagine doing large scale analysis while relying on domain experts to manually review data in order to build a model. Other methods considered as well, since SVM and sentiment analysis were successful in several of the studies observed.

4.4. Product Review Studies

In the paper which described how to build a function to determine the helpfulness of user-generated reviews as a function of review sentiment, product type and information quality, text analysis was relied heavily on to be able to examine reviews [41]. Text analysis is a very big need when collecting data based on what people right. With the number of variables required to take into consideration, multiple regression was selected as the method of analysis with ANOVA being used to analyze the differences in the types of review classifications (such as 1-star, 2-star, etc.). In this text analysis situation, sentiment analysis did not appear. Since the text was already broken down into categories based on how a user rated them, it is interesting to wonder if this is the reason why sentiment analysis never made an appearance. From a classification standpoint, sentiment analysis would likely need to be used to classify them into their rating category, if this step was not already completed. Hence, it would have been an interesting extension if the researchers could have applied this to social media (as other papers) to analyze the mentions of products and then analyze if posts are useful [41]. As the authors only analyzed three product searches and three experience searches, the fact that the helpfulness and quality varied greatly over the review sentiment and product type raises questions of how this methodology would perform if used to model more diverse products.

5. Conclusion

In this paper, we evaluated twelve research papers that explored various data mining techniques for social media data.

While many methods were used for analysis, common themes were text analysis, SVM and sentiment analysis. The previous researchers used a variety of methods to extract data, such as using the API for the social media platform. Both the Twitter Search API and the Flickr API were used to extract data in some of the studies. Future recommendations were made for each individual study, sometimes recommending methods that worked particularly well in one of the other papers evaluated. Several of the studies evaluated were similar in theme but did not necessarily use the same types of analysis. All of the methods provided sufficient results for the studies, but it was interesting to look at different methods used for similar studies.

In the study that utilized social media posts to describe emergency events, the 5W method was used. Another study that also used social media for emergency events used sentiment analysis to determine the needs of the affected people. The authors used several algorithms, including SVM and sentiment analysis. Both of these studies had similar goals but very different and effective approaches. This may show that while a particular big data technique may work best in a situation, there are multiple research methods worth testing.

Two studies used proposed methods using Flickr data to provide recommendations to travelers and Travel Destination Management. Both of these studies used P-DBSCAN, but one expanded the recommendations further by analyzing seasonal timeframes of destinations. P-DBSCAN was effective in both of these studies.

The studies that used social media for improving medical care used different methods. The study monitoring feedback of the drug Erlotinib used a combination of TF-IDF and SOM. The study monitoring ADRs used LDA, k-means clustering and SVM as a classifier. Since the methods tested provided sufficient results, it would be worth further study to compare both methods to determine the best approach for using social media to analyze medical data.

Three studies evaluated social media for products. All three used different techniques in data mining. The Goodness of Fit, structured equation modeling and other similar models were used when investigating the impact on purchase intent. The study that focused on predicting iPhone sales proposed using machine learning to train a classifier based on phrasing in social media posts. The final product study focused on the helpfulness of product reviews. Multiple regression and text analysis were used in classifying reviews.

One study used Twitter data to evaluate students' learning experiences. Naïve Bayes was found to be the most effective classification method.

While all of these studies were based on social media data, they show there many diverse ways to effectively classify and analyze the data.

References

[1] Pew Research Center. (2021, April 26). Demographics of Social Media Users and Adoption in the United States. Pew Research Center: Internet, Science & Tech https://www.pewresearch.org/internet/fact-sheet/social-media/?menuItem=ad42e188-04e8-4a3c-87fb-e101714f1651

[2] M. N. Injadat, F. Salo, and A. B. Nassif, "Data mining techniques in social media: a survey." Neurocomputing, **214**, 2016, doi: 10.1016/j.neucom.2016.06.045.

[3] Data science & big data analytics: discovering, analyzing, visualizing and presenting data. Wiley, 2015.

[4] V. Mhaskar, "Measure Search Relevance using NDCG - Know More: T/DG Blog - Digital Thoughts," Measure Search Relevance using NDCG - Know More | T/DG Blog - Digital Thoughts, 28-Jun-2015. [Online]. Available: https://blog.thedigitalgroup.com/measuring-search-relevance-using-ndcg. [Accessed: 05-Apr-2020].

[5] S. Gupta, Sentiment Analysis: Concept, Analysis and Applications. 19-Jan-2018. [Online]. Available https://towardsdatascience.com/sentiment-analysis-concept-analysis-and-applications-6c94d6f58c17 . [Accessed: 15-Apr-2020].

[6] "Text Classification," MonkeyLearn, 27-Jan-2020. [Online]. Available: https://monkeylearn.com/text-classification/. [Accessed: 15-Apr-2020].

[7] H. C. Wu, R. W. P. Luk, K. F. Wong, and K. L. Kwok, "Interpreting TF-IDF term weights as making relevance decisions," ACM Transactions on Information Systems,. **26**(3), 1–37, 2008, doi: 10.1145/1361684.1361686..

[8] "Standard search API - Twitter Developers," Twitter. [Online]. Available: https://developer.twitter.com/en/docs/tweets/search/api-reference/get-search-tweets. [Accessed: 15-Apr-2020].

[9] X. Zhang and W.-X. Xiao, "Clustering based two-stage text classification requiring minimal training data," in 2012 International Conference on Systems and Informatics (ICSAI2012), 2012, doi: 10.1109/ICSAI.2012.6223496.

[10] S. Shimojo, Web and communication technologies and internet related social issues: proceedings, Springer, 2005.

[11] "Get Started with GATE (General Architecture for Text Engineering)," WhoIsHostingThis.com, 12-Dec-2018. [Online]. Available: https://www.whoishostingthis.com/resources/gate/. [Accessed: 20-Apr-2020].

[12] "Linear, Quadratic, and Regularized Discriminant Analysis," datascienceblog.net: R for Data Science, 30-Nov-2018. [Online]. Available: https://www.datascienceblog.net/post/machine-learning/linear-discriminant-analysis. [Accessed: 05-Apr-2020].

[13] R. Gandhi, "Support Vector Machine - Introduction to Machine Learning Algorithms," Medium, 05-Jul-2018. [Online]. Available: https://towardsdatascience.com/support-vector-machine-introduction-to-machine-learning-algorithms-934a444fca47. [Accessed: 15-Apr-2020].

[14] R. S. Brid, "Decision Trees - A simple way to visualize a decision," Medium, 26-Oct-2018. [Online]. Available: https://medium.com/greyatom/decision-trees-a-simple-way-to-visualize-a-decision-dc506a403aeb. [Accessed: 20-Apr-2020].

[15] O. Harrison, "Machine Learning Basics with the K-Nearest Neighbors Algorithm," Medium, 14-Jul-2019. [Online]. Available: https://towardsdatascience.com/machine-learning-basics-with-the-k-nearest-neighbors-algorithm-6a6e71d01761. [Accessed: 20-Apr-2020].

[16] J. Bekker and J. Davis, "Learning from positive and unlabeled data: a survey," Machine Learning, 109, 719-760, Apr. 2020, doi: 10.1007/s10994-020-05877-5.

[17] K. Baxter, "Similarity Matrix," Similarity Matrix - an overview | ScienceDirect Topics. [Online]. Available: https://www.sciencedirect.com/topics/computer-science/similarity-matrix. [Accessed: 15-Apr-2020].

[18] K. S. do Prado, "How DBSCAN works and why should we use it?," Medium, 03-Jun-2019. [Online]. Available: https://towardsdatascience.com/how-dbscan-works-and-why-should-i-use-it-443b4a191c80. [Accessed: 20-Apr-2020].

[19] M. M. A. Patwary, D. Palsetia, A. Agrawal, W.-K. Liao, F. Manne, and A. Choudhary, "A new scalable parallel DBSCAN algorithm using the disjoint-set data structure," 2012 International Conference fo1`r High Performance Computing, Networking, Storage and Analysis, 2012, doi: 10.1109/SC.2012.9.

[20] M. J. Garbade, "Understanding K-means Clustering in Machine Learning," Medium, 12-Sep-2018. [Online]. Available: https://towardsdatascience.com/understanding-k-means-clustering-in-machine-learning-6a6e67336aa1. [Accessed: 20-Apr-2020].

[21] J. Hollmen, Self-Organizing Map (SOM), 08-Mar-1996. [Online]. Available: https://users.ics.aalto.fi/jhollmen/dippa/node9.html. [Accessed: 15-Apr-2020].

[22] D. Soni, "Supervised vs. Unsupervised Learning," Medium, 16-Jul-2019. [Online]. Available: https://towardsdatascience.com/supervised-vs-unsupervised-learning-14f68e32ea8d. [Accessed: 15-Apr-2020].

[23] W. Kenton, "Goodness-Of-Fit Definition," Investopedia, 29-Jan-2020. [Online]. Available: https://www.investopedia.com/terms/g/goodness-of-

fit.asp. [Accessed: 05-Apr-2020].

[24] "Kernel Density Estimation," DeepAI, 17-May-2019. [Online]. Available: https://deepai.org/machine-learning-glossary-and-terms/kernel-density-estimation. [Accessed: 05-Apr-2020].

[25] M. Malaeb, "Recall and Precision at k for Recommender Systems," Medium, 04-Aug-2019. [Online]. Available: https://medium.com/@m_n_malaeb/recall-and-precision-at-k-for-recommender-systems-618483226c54. [Accessed: 05-Apr-2020].

[26] W. Kenton, "How Analysis of Variance (ANOVA) Works," Investopedia, 29-Jan-2020. [Online]. Available: https://www.investopedia.com/terms/a/anova.asp. [Accessed: 20-Apr-2020].

[27] P. Grant, "Understanding Multiple Regression," Medium, 23-Mar-2020. [Online]. Available: https://towardsdatascience.com/understanding-multiple-regression-249b16bde83e. [Accessed: 05-Apr-2020].

[28] "Time Series Analysis," Statistics Solutions. [Online]. Available: https://www.statisticssolutions.com/time-series-analysis/. [Accessed: 15-Apr-2020].

[29] Z. Xu et al, "Crowdsourcing based Timeline Description of Urban Emergency Events using Social Media," International Journal of Ad Hoc and Ubiquitous Computing, **25**(1/2), 1, 2017, doi: 10.1504/IJAHUC.2017.083481.

[30] S. Hall, "What Is Inductive Content Analysis?," Small Business - Chron.com, 26-Oct-2016. [Online]. Available: https://smallbusiness.chron.com/inductive-content-analysis-24666.html. [Accessed: 20-Apr-2020].

[31] S. J. Miah, H. Q. Vu, J. Gammack and M McGrath, "A Big Data Analytics Method for Tourist Behavior Analysis," Information & Management, **54**(6), 771-785, 2017, doi: 10.1016/j.im.2016.11.011.

[32] X. Chen, M. Vorvoreanu, and K. P. Madhavan, "Mining Social Media Data for Understanding Students' Learning Experiences," IEEE Transactions on Learning Technologies, **7**(3), 246–259, 2014, doi: 10.1109/TLT.2013.2296520.

[33] A. A. Alalwan, "Investigating the impact of social media advertising features on customer purchase intention," International Journal of Information Management, **42**, 65–77, 2018, doi: 10.1016/j.ijinfomgt.2018.06.001

[34] S. Sakaki, F. Chen, M. Korpusik, & Y.-Y. Chen, "Corpus for customer purchase behavior prediction in social media," in Proceedings of the Tenth International Conference on Language Resources and Evaluation (LREC'16), 2976–2980, 2016.

[35] M. D. Choudhury, S. Counts, and E. Horvitz, "Predicting postpartum changes in emotion and behavior via social media," in CHI '13: Proceedings of the SIGCHI Conference on Human Factors in Computing Systems, 3267-3276, 2013, doi: 10.1145/2470654.2466447

[36] J. R. Ragini, P. R. Anand and V. Bhaskar, "Big data analytics for disaster response and recovery through sentiment analysis," International Journal of Information Management, **2018**(42), 13-24, 2018, doi: 10.1016/j.ijinfomgt.2018.05.004.

[37] Y. Yu and X. Wang, "World cup 2014 in the Twitter world: a big data analysis of sentiments in U.S. sports fans' tweets," Computers in Human Behavior, **48**, 392-400, 2015, doi: 10.1016/j.chb.2015.01.075

[38] A. Majid, L. Chen, G. Chen, H. T. Mirza, I. Hussain, and J. Woodward, "A context-aware personalized travel recommendation system based on geotagged social media data mining," International Journal of Geographical Information Science, **27**(4), 662–684, 2013, doi: 10.1080/13658816.2012.696649.

[39] A. Akay, A. Dragomir, and B.-E. Erlandsson, "Network-Based Modeling and Intelligent Data Mining of Social Media for Improving Care," IEEE Journal of Biomedical and Health Informatics, **19**(1), 210–218, 2015, doi: 10.1109/JBHI.2014.2336251.

[40] M. Yang, M. Kiang and W. Shang, "Filtering big data from social media – Building an early warning system for adverse drug reactions," Journal of Biomedical Informatics, **54**, 230-240, 2015, doi: 10.1016/j.jbi.2015.01.011.

[41] A. Y. Chua, & S. Banerjee, "Helpfulness of user-generated reviews as a function of review sentiment, product type and information quality," Computers in Human Behavior, **54**, 547–554, 2016, doi: 10.1016/j.chb.2015.08.057.

Effectiveness and Suitability of the Automotive EHPS Software Reliability and Testing

Yanshuo Wang[1,*], Jim (Jinming) Yang[2], Ngandu M. Mbiye[2]

[1]*Department of Quality and Reliability, Dare Auto Inc., Plymouth, 48170, U.S.A.*

[2]*Department of Software Engineering, Dare Auto Inc., Plymouth, 48170, U.S.A.*

A B S T R A C T

The effectiveness and suitability for the reliability and test of the embedded software of the automotive EHPS (Electrical Hydraulic Power Steering) pump are extensively explored in this paper. The Crow-AMSAA analysis has been applied to evaluate the embedded software reliability growth based on the failure data collected in the prototype phase and in the field. The slope β of the Crow-AMSAA plot is smaller than 1 which indicates that the reliability of the embedded software is increasing and failure rate is decreasing. The field performance and reliability of the embedded software, which is the key indicator to evaluate the effectiveness and suitability of the reliability management and testing methods used in design and development, are also summarized in this paper. Using the real field and zero mileage data to evaluate the effectiveness and suitability of DFR (Design for Reliability) is also beneficial for the company to make the continuous improvement for the future embedded system/software design and development.

1. Introduction

This paper is an extension of work originally presented in paper entitled "An Automotive EHPS Software Reliability and Testing" that was published in 2020 Annual Reliability and Maintainability Symposium (RAMS) [1]. The previous paper was addressing the methodologies for Design for Reliability (DFR) and testing of the embedded software. This paper is using the data collected in the prototype build and in the field to address the reliability growth, the effectiveness and suitability of the reliability management and testing which were used in design and development. (Figure 1 shows the scopes of these two papers).

The vehicle steering system consists of steering wheel, column, EHPS pump, steering gear, pipes, and linkage etc.. EHPS pump has a hydraulic pump, BLDC (brushless direct current) motor, and ECU (electronic control unit). The hydraulic pump is driven by an electrical motor, and motor is controlled by ECU. EHPS pump provides the hydraulic flow to the steering gear in the power steering system. The control software is embedded in the MCU (Microcontroller Unit). (Figure 2 shows the EHPS pump and its interface).

1.1. Advantage of EHPS pump

Comparing to the conventional engine belt driven hydraulic power steering pump, the EHPS pump is powered by vehicle alternator and controlled on demand by the algorithm, the conventional engine belt driven hydraulic power steering pump operates continuously while the engine is powered. The EHPS pump provides *70%* energy saving over a comparable conventional power steering pump with constant displacement volume.

1.2 Control Software of EHPS pump

Control software quality is the key for providing reliable and safe power steering system operations. The application of systematic processes and techniques ensures software reliability. This includes the DFR (Design for Reliability), component and sub-system level reliability test, vehicle level test, and feedback from the field during development and the life of the product. The quality of the control software is also a concern for the OEMs (Original Equipment Manufacturer). In [2], the author illustrated the embedded software in crisis with examples from the automotive industry. In [3], the authors edited the Automotive Embedded Systems Handbook which provides an introduction and the scientific challenges to the automotive embedded system. The

dependability and performance of an embedded system is also depending on communication networks and protocols. Hence, certain characteristics on communication network have to be verified. In our case, the CAN (Controller Area Network) communication is used.

In addition to applying the DFR and testing methodologies in the software design and development, the effectiveness and suitability of DFR and testing of the embedded software need be evaluated [Figure 1].

1.3 Literature review

In [4], the author stated that software reliability is different from hardware reliability, it does not follow bathtub curve, it follows revised bathtub curve (shark teeth curve). This matched our experience when new features were added in earlier prototypes. During development, we placed a strong emphasis on regression testing. In [5], the authors described the enormous potential for defect prevention that can be achieved before the software is even tested. We saw that the quality difference between the concept prototypes and the production software which used different processes. Our evaluation is ongoing regarding the use of identical processes for concept prototypes and production software. The ASPICE process [6] matches [7] which proposed the software reliability assurance approach during its life cycle, and in [8] the authors is to address the software complexity. In [9], the authors presented a new embedded software reliability growth model. We are still evaluating the most practical calculations for future projects. In [10], the author proposed a verification strategy which enhances the effectiveness of integration testing of the distributed software functions. In [11], the author described the organization to adapt the standard classification scheme to and describes a methodology for comprehensively evaluating defect classification schemes. In [12], the authors describes the impact of strategical decisions on the software quality. In [13], the authors described the model based verification for embedded software. In [14], the authors introduced a method for constructing a software reliability evaluation framework based on historical data. They establish a software reliability evaluation model based on code metrics. In [15] proposed two approaches to use metric to analyze the large amount of measurement data generated during the software development process. In [16], the author proposed a technique to guide for the selection of an appropriate software reliability model for an ongoing software development project. In [17], the authors performed a review of currently available quantitative software reliability methods. In [18], the authors proposed a hazard-based effect analysis method to assess the distribution of the hazard degree of a remaining requirements fault. In [19], the authors described that the full automation of evolutionary testing method can improve the effectiveness and efficiency of the test process.

We apply the Crow-AMSAA (CA) model and field return data analysis methods to evaluate the effectiveness and suitability of the software reliability. The advantage of our methods is to use the system level or field failures on the vehicle to assess the component level embedded software reliability.

The CA and field data analysis methodologies are introduced in section 2. The data analysis of CA and field data is described in

section 3. The lessons learned and effectiveness of DFR methods are also summarized in section 3. In section 4, the lessons learned and effectiveness of the testing are summarized. Finally, the work of this paper is summarized in section 5.

2. Methodologies

2.1. Crow-AMSAA Reliability Growth

Dr. Crow proposed that the Duane model can be represented as non-homogeneous Poisson process (NHPP) model under Weibull intensity function ([20], [21], [22]).

When CA model applies, the cumulative failure *N(t)* can be calculated as following

$$N(t) = \lambda t^\beta \tag{1}$$

$$LnN(t) = Ln(\lambda) + \beta Ln(t) \tag{2}$$

The model intensity function $\rho(t) = \frac{dN(t)}{dt} = \lambda\beta t^{\beta-1}$ (3)

The cumulative event rate is to use the equation (1) divided by *t*. it is $C(t) = \lambda t^{\beta-1}$ (4)

Where *t* is the time in days, λ and β are constants, the scale parameter, λ, is the intercept on the y axis of *N(t)* when *t =1, (ln(1) =0)*; the slope β, is interpreted in a similar manner as a Weibull plot, If the slope $\beta > 1$, the failure rate is increasing, the failure rate is more rapid, if the slope $\beta < 1$, the failure rate is decreasing, the failure rate is slower, if the slope $\beta = 1$, the process is named the Homogenous Poisson Process (HPP), if the slope β is not equal *1*, the process is called Non Homogenous Poisson Process (NHPP). ([20], [21]). Weibull plot is for single failure mode, but CA model is for mixing failure modes.

IEC (International Electrotechnical Commission) MLE (Maximum Likelihood Estimation) solutions for interval or grouped data method is used for the fitting method in CA analysis ([23]). Using IEC 61164 methods, the Cramer-Von Mises statistic accepts the goodness of fit at a Fit-p% of 10% as indicated on the plots.

Based on the equation (1) and (2) above, the cumulative failures versus the cumulative days are used for CA analysis. We also apply the CA model to the cumulative quantities delivered in addition to the cumulative days for the failure event, the equation is as

$$N(t) = \lambda q(t)^\beta \tag{5}$$

here *q(t)* is the cumulative quantities delivered.

The cumulative reliability *R(t)* is calculated as following:

$$R(t) = 1 - F(t) \tag{6}$$

where *F(t)* is the failure rate,

$$F(t) = \frac{N(t)}{q(t)} \tag{7}$$

We also apply the CA plot to the cumulative reliability versus the cumulative days.

2.2. Field Data Approach

Not all the defects, faults and errors can be detected during software and system design and development. The field performance and reliability data has been collected and analyzed for this automotive EHPS pump. The product has been in the production for more than three years, we have sufficient data from the field (zero mileage [Table 1] and warranty [Figure 7,8,9,10]). The field complaints can be categorized to the following: supplier design manufacturing issue (SDMI), adjoining components' failure, and misdiagnosis by servicers [Figure 8]. The real root cause of the EHPS pump failures from warranty is listed in the Figure 10. Since the EHPS pump is an electrical mechanical/hydraulic component on the vehicle, we need determine the root cause by mechanical-hydraulic (pump), electrical-mechanical (BLDC motor), electronic and embedded software (ECU). The failure rate and reliability of embedded software are calculated by using the following formulas

$$WRR = \frac{NWPR}{NPS} * 100\% \tag{8}$$

$$SDMFR = WRR * \frac{NSDMI}{NWPR} * 100\% \tag{9}$$

$$SRFR = SDMFR * \frac{NSRI}{NSDMI} * 100\% \tag{10}$$

$$SR = 1\text{-} SRFR \tag{11}$$

where *WRR* is the warranty return rate. *NWPR* is the number of warranty parts replaced. *NPS* is the number of parts sold. *NSDMI* is the number of supplier design manufacturing issue. *SDMFR* is the supplier design manufacturing failure rate. *NSRI* is the number of software related issue. *SRFR* is the software related failure rate. *SR* is the software reliability.

The failures detected in the field can be traced back, and can be used to analyze the effectiveness and suitability for the reliability management and testing in design and development. The lessons learned is also beneficial for the future embedded software projects.

The aim of this paper is to assess the achievements, and to list all the anomalies found in the field, and to illustrate the effectiveness and suitability for all the methods listed in the previous 2020 RAMS paper [1].

3. Effectiveness and suitability for Design for Reliability

The CA software reliability growth is analyzed by using EHPS pump failure data. The following describes the embedded software reliability growth, the effectiveness and suitability by using ASPICE[6] design and development process.

3.1. Crow-AMSAA Data Analysis

The EHPS pump failure data has been collected since beginning of developing this project starting on 1/20/2014. There are four phases in this project: Phase I – Prototype, Phase II – Design Verification (DV) 1, Phase III –DV2 & Production Validation (PV), Phase IV – Production. The system failures and customer returns were counted at different phases. The root causes of the failures have been investigated and documented in the 8Ds

(8 Disciplines). The failures which caused by the embedded software were recorded separately. The time period of different phases, the cumulated days, the cumulative quantities delivered, the cumulative failures (due to software) and the cumulative reliability are summarized in the Table 2. The SuperSmith package (developed by Fulton Findings) was used for CA plots.

The CA analysis has been conducted for the cumulative failures (due to software) versus the cumulative days, and plotted in Figure 3. From the plot, the *β* value is *0.415* which is smaller than *1*. Thus the failure rate (due to embedded software) is decreasing, the embedded software reliability is growing as the timing cumulated.

The CA analysis has been conducted for the cumulative failures (due to software) versus the cumulative quantity delivered, and plotted in Figure 4. From the plot, the *β* value is *0.085* which is smaller than 1. Thus the failure rate (due to embedded software) is decreasing, the embedded software reliability is growing as large quantities delivered to customer.

The total software reliability versus the cumulative days was plotted in CA format in Figure 5 and 6. Figure 5 is normal plot without the log-log, but Figure 6 is the log-log plot. From the plots, the overall reliability change by time is demonstrated. The slope ($\beta_1 = 0.422$) indicates the embedded software reliability change rate while the timing cumulated.

3.2. The effectiveness of understanding the requirements

Based on the zero mileage, warranty data and frequent DCRs (Design Change Request), the following statements are applying to the effectiveness and suitability of understanding the requirements.

- Up to now, we have shipped roughly more than *600,000* EHPS pumps to our customers. The *WRR* is 0.1% (equation 8) (the *0.07%* is replaced after misdiagnosis by servicers, only *0.03%* (equation 9) is EHPS pump related issue, only about *0.0025%* (equation 10) may be embedded software related). From the warranty data, we can see the customer original requirements were well understood and implemented in EHPS pump system and software design and development. The misdiagnosis by servicers (about *71%*) is a big concern, this was caused by the vehicle system level issues, or the other adjoining components with EHPS pump [Figure 9,10]. For example, for the sake of the safety concern, if the EHPS does not receive CAN communication from the controlling stability and braking module, the EHPS must shut down. But this requirement would make the end driver with no power steering assist when losing CAN communication but no information on the instrument panel. Consequently, the EHPS pump had replaced unnecessarily in warranty, and EHPS pump reliability score had been decreased because of this requirement.

- There are dozens of power circuitry failures [Figure 9] (about *7.5%* of warranty returns) and majority of these cases were caused by the high current on the vehicle. This is a vehicle system issue, and the requirements were not clearly defined by the OEMs. That means the situation on the vehicle which could have the high current can damage the ECU of EHPS pump, and the EHPS control software needs protect the power

circuitry in EHPS ECU in that situation. But unfortunately the situation and condition is not clearly defined yet.

- The zero mileage issues: (a) Un-necessary ignition startup/run DTC (Diagnostics Trouble Code) issue implies that the customer requirement especially in the OEMs manufacturing site was not discussed and understood. This is a lessons learned for the future embedded software design and development. In addition to the requirement from different stakeholders, the OEMs vehicle assembly requirements must be understood and implemented; (b) As we found in the warranty, there are power circuitry failures in zero mileage as well. These may be related to the high current spike situation on the vehicle as well.

- Almost all the OEMs would request software changes, and we have received dozens of DCRs for all our supplied pumps after starting the productions. DCRs had significant impacts on the final software. They changed the pump speed maps and fan motor speeds. These reflect the differences between the real data collected in the field and the original customer requirements. The EHPS software was designed to adapt to changed requirements.

3.3. The effectiveness of developing the embedded software requirements & reliability goals

According to the field data, the requirements of the embedded software of the EHPS pump were carried over very well from vehicle and system requirements, but some of the vehicle system requirements (section 3.2) were not well defined which caused the lacking of the embedded software and system requirements of EHPS pump. The reliability of the embedded software of the EHPS pump *SR* is *1-0.0025%=99.9975%* (equation 11), this indicates the performance of the embedded software in the field is excellent.

3.4. The effectiveness of designing the system architecture

According to the field data, the DTCs such as ignition start up/run had not well defined in the system and software design. This was caused by the lacking of understanding of the vehicle requirements in OEMs and their assembly plants. Also the power circuitry issues (both zero mileage and warranty) were not well understood and calibrated between hardware and software. These issues need be considered further in future embedded software design and development.

3.5. The effectiveness of fault tree and design failure mode effect analysis (DFMEA)

According to the zero mileage and warranty issue, we realize we need a vehicle/system DFMEA and fault tree analysis to catch the potential failure modes at the vehicle/system level. In this way, it would prevent a lot of vehicle/system level zero mileage and warranty issues (CAN bus short, loss CAN communication etc.). This vehicles/system fault or failure modes analysis could be done by OEMs engineers. Dare Auto system engineers need contact OEMs engineers to prevent this kind of vehicle/system level issue. Because of the vehicle/system CAN bus issues, the EHPS pumps were replaced without any sympathy since the driver feels there is non-assist from power steering. The EHPS pump is the victim of

the "shut off the pump" requirement when the CAN is off (section 3.2).

Also the accuracy of the zero angle issues happened dozens of time during EHPS pump assembly. This caused the current and pump RPM were not accurate and out of the specification. The anomaly which we have experienced is to find the accurate zero-angle for the BLDC motor after motor assembly. This is caused by using a universal controller after motor assembly to find the zero angle, but after the whole EHPS assembly, the zero angle was changed since the new controller and motor are assembled together. In our software/system DFMEA and manufacturing PFMEA development, we need consider the accuracy of the parameters such as zero angle which could cause the performance degradant of EHPS pump. Hence we need require the motor/pump manufacturing to design and implement the correct processes in order to achieve the accurate parameters.

3.6. Software Reliability Growth & design change

We track the software reliability by using the software reliability growth matrix and four different levels of testing (Figure 11). The reliability performance of the embedded software in the zero mileage and warranty needs be updated in the reliability growth matrix. This will help us for future embedded software motor control project.

When we launched this product, the thorough reliability test had been performed in different design and development both in component and system level. Therefore, the software remained stable and without issues for a year. The software reliability is decreased when the OEMs requests a change. Generally, the software reliability after a change follows the shark teeth curve, not the bathtub curve [4]. After the first DCR, the software is considered suspect until its reliability is proven. For example, the OEMs requested a change in the DTC after the launch. Although, the DCR was successfully developed and validated according to our process, the requested change was found to be somewhat incompatible with the OEMs production line equipment. Under certain conditions at the factory, the DTC was set. The OEMs plant could not control the environment. This negatively impacted our reliability score. The lesson learned for the above issue is to certify the software only after the completion of the PER (Production Evaluation Run) at the OEMs factory.

Due to the customer requirements changes for the pump speed maps and fan motor speed requirements which mentioned in section 3.2, we had dozens of DCRs from customers for the software changes. One lessons learned is to cascade the customer CNs (change notice) to the cross functional team, the kickoff meeting is necessary to let every team members to understand the change request, and to implement it and validate it without any discrepancy.

4. Effectiveness and suitability of testing

4.1. Effectiveness of the component testing

As mentioned in section 3.2, some of the OEMs requirements were not clearly defined, this caused some of the system and software requirements were not well defined, hence the architecture design/coding and component testing were not well implemented.

4.2. Effectiveness of the SW integration testing

The comments of the effectiveness and suitability is the same as section 4.1.

4.3. The effectiveness of the sub-system level testing

The key output for the EHPS pump is to output the flow at a given pressure and pump speed. Each time we have the software release, we conduct the 5 points testing, the mapping test and pump bench testing (pressure vs. flow). The 5 points testing is described in the table below (Table 3). We also called the sub-system testing as "EHPS pump on the bench" test.

According to the zero mileage and warranty data, the simulated DTC code testing and the simulated CAN communication situation need be tested more at the system level. These need happen at EOL (end of line) test and system bench test. We have more work to do to define how we can simulated these testing without a vehicle in future.

4.4. The effectiveness of the vehicle level testing

A CAN bus is a robust vehicle bus standard designed to allow microcontrollers and devices to communicate with each other in applications without a host computer. It is a message-based protocol.

Without vehicle, it can only simulated the CAN message testing on the bench. But we do not have other electrical components on vehicle to communicate with. So the vehicle is needed in order to fully test the CAN network and communication timing. Some examples of tests include:

- CAN bus short

- Sleep/Wake up cycles

It is obvious that vehicle level CAN communication and electrical component harmony testing are needed according to the zero mileage and warranty data. *71%* EHPS pump replaced after warranty misdiagnosis by servicers is not acceptable due to the system or adjoining component related issues. The CAN and power mating connectors testing are needed before starting the production. In order to reduce the unnecessary cost of the warranty, the vehicle level test need be performed more by OEMs before starting the production.

5. Conclusion

The embedded software of the EHPS pump reliability growth has been modeled by using Crow-AMSAA method both in the cumulative timing and in the cumulative qualities delivered. The slope *β* value is *< 1* which means the failure rate is decreasing and the embedded software reliability is growing.

Based on zero mileage and warranty performance & reliability data of the EHPS pump, the effectiveness and suitability of the reliability and test of the embedded software have been discussed in this paper. This is an extension of the 2020 RAMS paper [1]. Using the real field data to evaluate the effectiveness and suitability of ASPICE DFR is beneficial for the future embedded software/system design and development. The lessons learned have been documented and evaluated to improve the software reliability management and test processes. The ASPICE processes

require the organization to collect the data to evaluate the effectiveness and suitability of each process. This paper summarizes the findings.

The main lesson is that the proper operations of the EHPS depend on the vehicle systems where it is installed. Our engineering staff need to involve the OEM's system engineering and service staff in order to prevent misdiagnosis of issues in the field that lead to unnecessary replacement of the properly operating units in the field.

As expected, the OEMs issue the change requests after the units have been in the field. The flexibility of the software and the regression testing reduce the occurrence of the shark tooth defects.

In summary, the paper is about the reliability of the EHPS pump software. Through multi-staged /multi-facet software testing procedures and methodologies, the zero-mileage failure rate of software has been significantly dropped. The rate has been dropped about *80%*. The zero-mileage issues are due to the failure of the process principally, (a) Incorrect software version loaded, (b) Incorrect calibration, (c) Incorrect process at the OEMs plant. The warranty issues are caused by mismatch of the specified behavior versus the real world conditions and the incorrect service instructions.

Table 1: List of zero mileage issues

Zero Mileage issues	Total
Unnecessary DTCs	10+
Power circuitry failures	2
Coupler broken	1
Inlet blockage	1
Residual oil	10+
Oil cap damaged	10+
Repeated bar code	4
Connector pin damaged	10+
Noise pump	2
Missing screws	2

Table 2: System failures due to software at different phases. The cumulative timing (total days), the cumulative quantities delivered, cumulative failures (due to the software) and cumulative reliability are documented in this table.

	Period		Cum Days	Cum Quant Delivers	Cum Fail.	Cum Reliability
	Starting	Ending				
I	1/20/2014	3/2/2015	406	168	32	0.809524
II	3/3/2015	4/29/2016	830	586	44	0.924915

| III | 4/30/2016 | 11/1/2017 | 1381 | 1964 | 49 | 0.975051 |
| IV | 11/2/2017 | 3/27/2021 | 2623 | 601964 | 69 | 0.999885 |

Table 3: 5 points test

Function and Performance 5 Points Test			
	T low (-40°C)	T normal (23°C)	T high (105°C)
V low (9V)	(5)		(5)
V normal (13.5V)		(5)	
V high (16V)	(5)		(5)

Figure 3: Crow-AMSAA Analysis (total failures vs. total days). The X axis is the total accumulative days since the project starting. The Y axis is the total accumulative occurrence of failures (due to software).
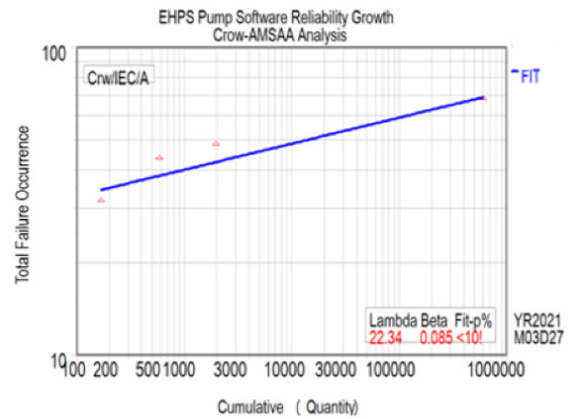
Figure 4: Crow-AMSAA Analysis (total failures vs. total quantities). The X axis is the total accumulative quantities delivered since the project starting. The Y axis is the total accumulative occurrence of failures (due to the software).

Figure 1: Flow chart of methods for automotive embedded software reliability. The DFR process and reliability testing were covered in previous RAMS paper. The evaluation of effectiveness is covered in current paper
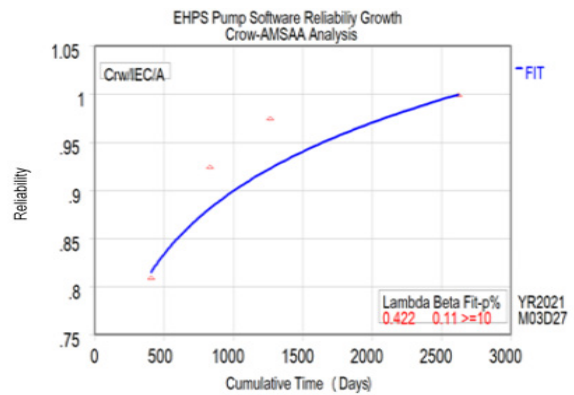
Figure 5: Crow-AMSAA Analysis (total reliability vs. total days). The X axis is the total accumulative days since the project starting. The Y axis is the total software reliability. (This is not the log to log plot).

Figure 2: EHPS pump and its interface
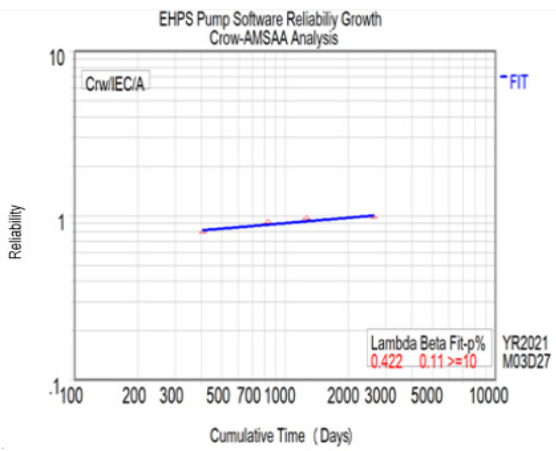
Figure 6: Crow-AMSAA Analysis (total reliability vs. total days). The X axis is the total accumulative days since the project starting. The Y axis is the total software reliability. (This is the log to log plot).

Figure 7: EHPS pump warranty complains by customer

Figure 8: EHPS pump warranty replacement categories

Figure 9: Warranty adjoining component faults

Figure 10: Total EHPS pump supplier design manufacturing issues
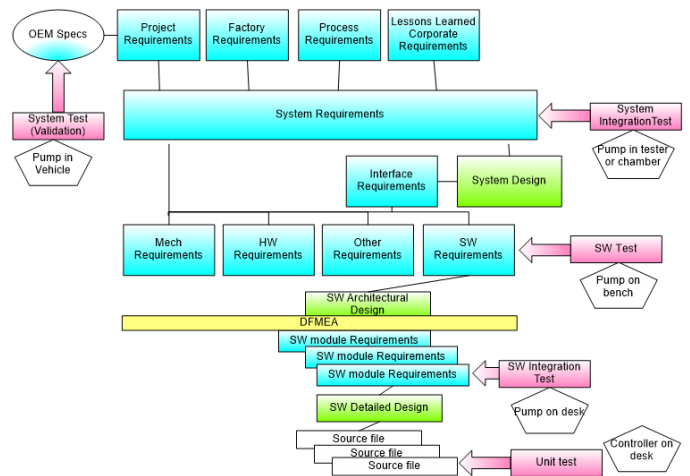
Figure 11: Requirements vs. test

Conflict of Interest

The authors declare no conflict of interest.

Acknowledgment

Thanks to the colleagues at Dare Auto Inc. in EHPS pump team for providing the data and implementing the embedded software, ECU, BLDC and pump. Also, thanks to the reviewers of the ASTES Journal for valuable advices for this paper.

References

[1] Y. Wang, J. J. Yang and N. M. Mbiye, "An Automotive EHPS Software Reliability and Testing," 2020 Annual Reliability and Maintainability Symposium (RAMS), Palm Springs, CA, USA, 2020, 1-6, doi: 10.1109/RAMS48030.2020.9153725.

[2] M. Wolf, "Embedded Software in Crisis," in Computer, vol. 49, no. 1, pp. 88-90, Jan. 2016, doi: 10.1109/MC.2016.18.

[3] N. Navet, F. Simonot-Lion, (Editors) "Automotive Embedded Systems Handbook, CRC Press , 2009 by Taylor & Francis Group, LLC.

[4] J. Pan, "Software Reliability," Carnegie Mellon University, 18-849 Dependable Embedded Systems, Spring 1999, https://users.ece.cmu.edu/~koopman/des_s99/sw_reliability/index.html

[5] M. Silverman,"Software Design for Reliability," George de La Fuente, Ops A La Carte LLC, 2008 Annual Reliability and Maintainability Symposium (RAMS).

[6] VDA QMC Working Group 13 / Automotive SIG, "Automotive SPICE Process Assessment / Reference Model", Version: 3.1, Date: 2017-11-01, Revision ID: 656, http://www.automotivespice.com/

[7] Y. Shi, P. Kalia, J. Evans, A. DiVenti, "An integrated life cycle-based software reliability assurance approach for NASA projects," 2010 Annual Reliability and Maintainability Symposium (RAMS).

[8] S. Saxena1, D. Agarwal, "A Systematic Literature Review on Software Reliability Estimation Model for Measuring the Effectiveness of Object Oriented Design," 2017 International Journal of Advanced Research in Computer and Communication Engineering, ISO 3297:2007, **6**(6), June 2017, doi:10.17148/IJARCCE.2017.6671
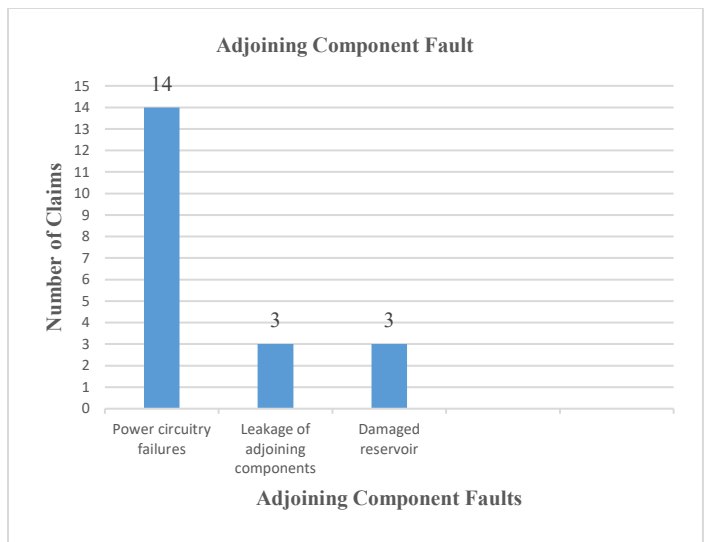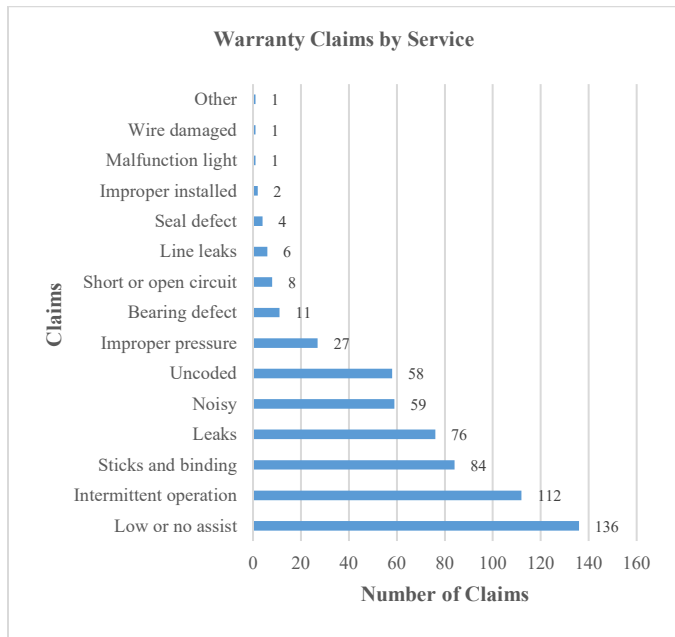
[9] R. K. Sharma, A. Kumar, "Analysis of Various Software Reliability Models and Proposing a New Model of Software Reliability for Embedded Systems," International Journal of Innovative Research in Computer Science & Technology (IJIRCST) ISSN: 2347-5552, **5**(3), May 2017 DOI: 10.21276/ijircst.2017.5.3.6

[10] A. Chunduri, "An Effective Verification Strategy for Testing Distributed Automotive Embedded Software Functions," Master of Science, Faculty of Computing Blekinge Institute of Technology, SE–371 79 Karlskrona, Sweden, 2016. Thesis no: MSSE-2016-08

[11] N. Mellegard, "Improving defect management in automotive software development," Ph.D thesis, Department of Computer Science and Engineering, Division of Software Engineering, Chalmers University of Technology | University of Gothenburg, Göteborg, Sweden 2013.

[12] C. Kugler, S. Kowalewski, J. Richenhagen, R. Maquet, A. Schloßer (2017) "Metrics-based strategies for quality assurance of automotive embedded software." In: Bargende M., Reuss HC., Wiedemann J. (eds) 17. Internationales Stuttgarter Symposium. Proceedings. Springer Vieweg, Wiesbaden. https://doi.org/10.1007/978-3-658-16988-6_56, First Online08 April 2017, DOIhttps://doi.org/10.1007/978-3-658-16988-6_56

[13] H. Shokry and M. Hinchey, "Model-based verification of embedded software," Lero—the Irish Software Engineering Research Centre, Published by the IEEE Computer Society APRIL 2009, DOI:10.1109/MC.2009.125, Corpus ID: 17393996

[14] Z. Song, Y. Wang, P. Zong, L. Wang, G. Feng, and W. Kang, "An Empirical Study of Comparison of Code Metric Aggregation Methods and Software Reliability Evaluation," 2020 Annual Reliability and Maintainability Symposium (RAMS), Palm Springs, CA, USA, 2020, DOI: 10.1109/RAMS48030.2020.9153606

[15] S. Dahab, E. Silva, S. Maag, A. S. Cavalli and W. Mallouli, "Enhancing Software Development Process Quality based on Metrics Correlation and Suggestion," In Proceedings of the 13th International Conference on Software Technologies (ICSOFT 2018), pages 120-131, DOI:10.5220/0006856501540165

[16] N. Miglani, "On the Choice of an Appropriate Software Reliability Growth Model," International Journal of Computer Applications (0975 – 8887), Volume 87 – No.9, February 2014, DOI:10.5120/15237-3772

[17] T. Chu, M. Yue, G. Martinez-Guridi, and J. Lehner, "Review of Quantitative Software Reliability Methods," Brookhaven National Laboratory Letter Report, Digital System Software PRA, JCN N-6725,September 2010

[18] B. Li, C. Smidts, "Effects Assessment for Requirements Faults of Safety Critical Software in Nuclear Industry," 2020 Annual Reliability and Maintainability Symposium (RAMS), Palm Springs, CA, USA, 2020. DOI: 10.1109/RAMS48030.2020.9153594

[19] H. Sthamer, J. Wegener and A, Baresel, "Using Evolutionary Testing to improve Efficiency and Quality in Software Testing," 2002 In Proceedings of the 2nd Asia-Pacific Conference on Software Testing Analysis and Review (AsiaSTAR)

[20] L. H. Crow, "Reliability Growth Planning, Analysis and Management," Tutorial, 2011 Annual Reliability and Maintainability Symposium

[21] R. B. Abernethy, "The New Weibull Handbook," Fifth Addition, , 2006

[22] D. E. Tananko, "Practical Guide to Reliability Growth Analysis,." Tutorial at 2020 Annual Reliability and Maintainability Symposium, Palm Springs, CA, USA, 2020,

[23] IEC 61164 Ed. 2.0 en:2004, "Reliability growth - Statistical test and estimation methods," International Electrotechnical Commission, 2004.

XMDD as Key Enabling Technology for Integration and Organizational Collaboration: Application to E-Learning Based on NRENs

Salim Saay *,1, Tiziana Margaria2

1*Department of Computer and Software Engineering, Engineering Faculty, Athlone Institute of Technology, Athlone, N37 HD68, Ireland*

2*Department Computer Science and Information System, Faculty of Engineering, University of Limerick, Limerick, V94 T9PX, Ireland and Lero, the SFI Research Centre on Software*

A R T I C L E   I N F O

A B S T R A C T

Collaborative E-learning is highly dependent on the well functioning of a complex socio-technical system that comprises information technology and various social processes. Large scale infrastructures like the National Research and Education Networks (NRENs) provide access to research and educational resources and provide collaboration between educational and research organizations, thus providing a set of essential services for e-learning. Currently, the lack of data integration between e-learning systems is still a problem in NREN domains, and a hurdle to collaborative e-learning. We address systematic cross-organizational collaboration and data integration between large-scale e-learning systems by designing an architecture for NREN e-learning systems to support open access education and learning. In particular, we design and provide a reference implementation for an e-learning broker that can provide the needed data integration and processes, and takes into consideration the strategies and policies for open access in education and training. We develop the architecture and reference implementation applying the eXtreme Model-Driven Development (XMDD) paradigm for software design and development, using the DIME low-code development environment for modelling data, processes, and user interface. We consider here two specific application settings: The national network of e-learning collaboration in AfgREN, centered on the Kabul University in Afghanistan, and the newly started collaboration between the Athlone Institute of Technology (AIT) and Limerick Institute of Technology (LIT) in Ireland, that are forming a new consortium under the newly introduced Technological University structure.

1   Introduction

Socio-Technical Systems are collaborative interacting systems where one or more social systems and a number of technical system work together to accomplish a goal meaningful for a community or user group. The technical part of the system is concerned with the processes, tasks, and technology needed to transform some inputs to corresponding outputs. The social part of the system is described by key attributes of people, such as people's skills, values, responsibilities, and their roles in the system [1]. In advanced collaborative e-learning, our application domain, the relationships among the administration of a university, the students, and lecturers are mediated by technical systems, as these people all cross-interact within individual and federated e-Learning systems. A large part of these interactions are mediated by the institutional e-learning platform(s), that act as a medium-to-large scale socio-technical system, and their underlying communication and federation infrastructure.

National Research and Educational Networks are a collaborative large scale scientific infrastructure that provides high quality and cost-effective services to academic and research organizations [2], providing cloud services such as Infrastructure as a Service (IAAS), Software as a Service (SAAS) and Platform as a Service (PAAS), that are new trends for NRENs [3]. Eduroam [4], EduGATE [5], eduGAIN [6] and Shibboleth [7] are widely adopted infrastructural building blocks used to provide a wide range of national services by NRENs and international services by so called regional NRENs. Specifically, Eduroam is a global wireless network that allows academics staff and researchers to access the services of their own institution with their roaming profile [4] from any participating institution. EduGATE is an identity manager used in GÉANT to provide participating users with access to the different applications with a Single-Sign-On technique, effectively providing a connection

---

*Corresponding Author: Dr. Salim Saay, Email: ssaay@ait.ie

between participating applications of the different NRENs that are members of GÉANT [5]. EduGAIN is also a national level identity management services provider, and it is used in the Irish Research and Education Network (HEAnet) [6]. Shibboleth supports collaboration and data integration between different learning management systems used in Internet2 and many NRENs [8]. Other platforms are directly or indirectly also service providers for collaboration, and provide widely adopted services for access and interoperability. For example, Office 365 provides a solution that integrates different applications, it uses Active Directory Federation Services (ADFS) and DirSync to provide a Single Sign-On password integration for a domain [9]. Similarly, the Security Assertion Markup Language (SAML) and Open Authentication (OAuth) [10] focus on providing and managing user Identities for SSO, so that the NREN users use the same Identity for all member applications. A secure SSO provides secured and uninterrupted services by keeping one authentication credential for each user so that, once authenticated, users do not need to provide their credentials again when accessing different web services that share the same SSO. Kamal et al. claim that Shibboleth is the most suitable SSO in the higher education domain. However, no global log-out, the infancy of the technology, implementation complexity, high reliability on assumptions that cause security risks are the main challenges of the Shibboleth technology [10]. The existence of duplicated data and duplicated profiles in the same domain is a serious problem for access, cost, and management. How to integrate the duplicated data requires further investigation. In this context, NREN infrastructures provide an opportunity to provide for uniform security, reliability, and reduction of the complexity for data integration across the participating e-learning system within the served NREN domain.

In this paper, that significantly extends work originally presented in ICALT 2020 [11], we focus on data integration in inter-institutional cross-organizational collaborations as well as in intra-institutional multi-campus collaboration, two challenging situations with which we have direct experience.

1.1 Data Integration of E-Learning Systems In Large Scale Cross-Organizational Collaborations

This is a challenge because they use different e-learning platforms that do not interoperate in a native way. For instance, Figure 1 shows that Moodle, eDX and the national Higher Education Management Information System (HEMIS) are implemented in a single domain at the Kabul University, Herat University and Balkh University in Afghanistan. The shortcomings of the current situation are due among other causes to the lack of support of Single Sign-On in the three running applications. Accordingly, the applications implemented in this national collaboration domain [12] do not currently exchange data and they reside on three different platforms. EdX is implemented at six universities across the Afghanistan Research and Education Network (AfgREN) for national collaboration and accessibility [13]. Moodle is the second popular e-Learning platform. It is widely implemented in universities of Afghanistan [14], and in fact lecturers and students used Moodle en masse during the recent

universities lockdowns. The Higher Education Management Information System (HEMIS) is a traditional students management system. It was introduced by the National Higher Education Strategic Plan (NHESP) of the Ministry of Higher Education of Afghanistan to support in a standardized way the decision-making process and control management tasks in the adopting organizations, which impact the organization's functions, performance, and productivity in all its aspects [15].

In our collaborative e-learning context, for example, the enrolment of students to universities is managed through this system. While it is mandatory for all universities to use HEMIS, also HEMIS does not support Single Sign On. As a consequence, each student has three profiles in three different e-Learning platforms, as shown in Figure 1. This distribution and partial data replication are challenging for the administration and maintenance of all these systems and their collaboration.
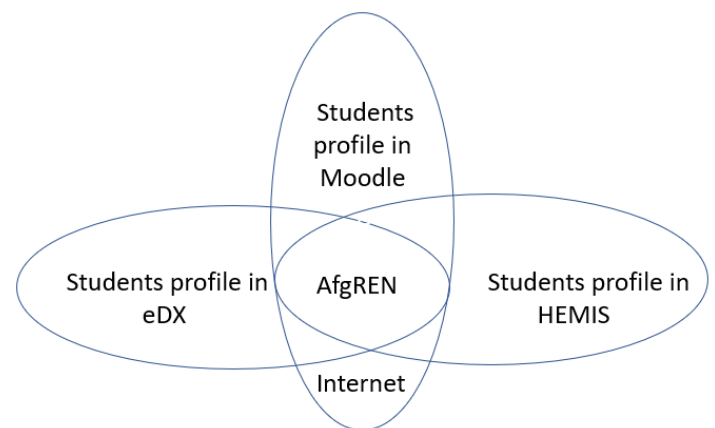
Figure 1: Student profiles in e-Learning systems of a single organization: The case of AfgREN

1.2 Data Integration of E-Learning Systems In Intra-Institutional Cross-Campuses

This second challenge is illustrated with an application in Ireland. Through the Technological Universities Act the Irish Department of Further and Higher Education, Research, Innovation (the Irish Ministry) established in 2018 a process whereby consortia of local Institutes of Technology[1] may submit an application for Technological University designation. De facto, this mechanism creates regional Technological Universities of larger size and diversity than the previous ITs. For example, in January 2019 the Technological University Dublin (TU Dublin) was formed by the amalgamation of three institutes of technology in the Dublin area (Dublin Institute of Technology, Institute of Technology Blanchardstown, and Institute of Technology Tallaght), yielding the second-largest university in Ireland based on the combined student population of 28,500. Other five TUs consortia have meanwhile applied, among which in 2021 the AIT-LIT consortium[2]. This consortium is now establishing a (technical) University for the Midlands and the Mid-West by combining the Athlone Institute of Technology (AIT) in Athlone (in the Midlands) and the Limerick Institute of Technology (LIT) in

---

[1]An Institute of Technology is similar to colleges/Universities of Applied Science in other countries
[2]https://aitlitconsortium.ie

Limerick (in the Mid-West). Accordingly, the new Technological University will be located in five different campuses across the Midlands and Mid-West of Ireland. In addition to the organizational and structural combination, many technical and infrastructural changes are also required: the data integration, resources sharing, and collaboration between technical systems of AIT and LIT need further investigation. To give an idea of the complexity of the challenge, of the six Working Groups established by the Professional Services Steering Group, five concern the socio-technical ecosystem of the e-learning platform[3].

Figure 2 shows the current state of the student profiles: they currently reside in different, independent e-learning systems of AIT and LIT, that need to be combined, and additionally also the financial system and many other information systems need data integration. The Higher Education Authority Network (HEANet) is the national research and education network (NREN) of Ireland: Similarly to AgfREN it provides a high speed secure and reliable backbone for the connection between these e-Learning systems, and users additionally also use public internet.
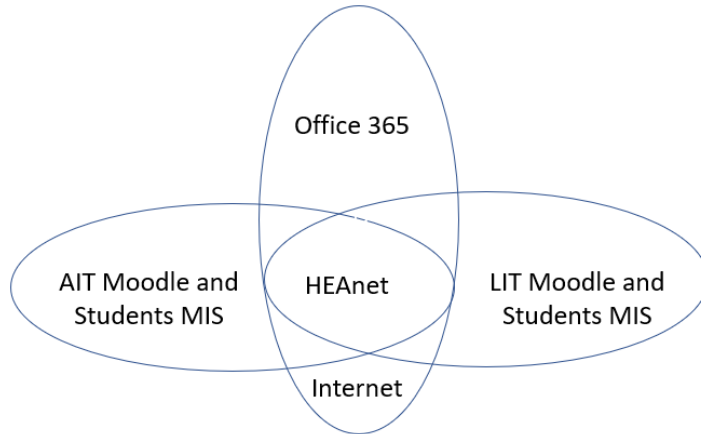
Figure 2: Currently interorganisational students profiles in the new AIT-LIT Technological University

In this paper, the contributions are

- to design an *e-learning architecture* based on NREN for the federated learning collaboration;

- in its pursuit, we apply the XMDD technology to design and implement a prototype of a *e-learning reference implementation* for data integration between different e-learning systems at three different levels: single organization, cross-organization and cross-nation.

- taking into consideration the *diverse organizational strategies, policies, law and procedures* of the collaborating parties.

Our solution and prototype go well beyond the SSO: we design a domain-specific e-learning broker for NRENs as a data integration application that focuses on an organization's reputation management, identity management, process management, service brokering, with a search engine to lead users to the services available in the NREN domain, like for example an NREN local course management

___
[3]https://aitlitconsortium.ie/our-journey/

system. The prototype is easily accessible to designers, managers, developers, customers, and users, and it can be used as a showcase of the concrete application [16]. In the prototype and later in the developed system, users of the e-learning system access the resources located in the NREN domain based on their role in their local organization. We define which type of data is accessible to students, and at which level and which types of data are accessible for the academic staff and admin staff of each university.

The architecture and the XMDD model-driven design are our methodological contributions. The practical realization of a service-based architecture on top of a variety of e-learning systems is the concrete proof of concept, that we applied to AfgREN as a case study.

Overall, we use advanced Information Technology and leading edge methods and tools for advanced Web application design and implementation, to produce computer software and applications that use the Internet and the World Wide Web to solve long term and large scale inter- and intra-institutional collaboration issues for e-learning.

The rest of the paper is organized as follows: Section 2 discusses the background of the domain technologies and the two case studies, Section 3 describes the methods and technologies adopted to produce the design and the solution, Section 4 illustrates the architecture design of the e-learning broker, Section 5 presents in detail the Model-driven design of the prototype reference system, in particular the Data model, Process models and GUI models, we explain our lesson learned in section 6, and the current status of the project explained in section 7, finally in Section 8 we conclude with a summary, some reflections and future work.

2 Background

Educational organizations need higher speed intranet and internet connections to access the heterogeneous traffic, and demand novel services [17]. Educational institutes at all levels suddenly closed in most countries worldwide due to the outbreak of COVID-19 early this year [18], and in many cases they have not yet returned to on-site education. According to the UNESCO report, due to the COVID-19 pandemic 850 million school children worldwide have been locked out of their schools, and have turned to online learning to continue their education, with added high pressure on e-learning systems and remote communication tools. While we hope the pandemic will soon pass, online education will always be needed for many aspects of high-quality education. Fortunately, over 120 countries [19] in the world established National Research and Education Networks (NRENs) to provide research and educational services, establishing a shared Information Technology infrastructure and providing it at a reduced cost with higher quality connection than regular and commercial Internet Service Providers (ISPs).

2.1 AfgREN

Concerning the background in the specific case studies considered in this paper, Figure 3 shows the current physical layout of the Afghanistan Research and Educational Network (AfgREN). Its Network Operation Center (NOC) is physically located at Kabul University and currently most of the AfgREN connectivity is provided by Afghan Telecom fiber optic links. Most public universities (in green) have a direct connection to the AfgREN NOC, but some like Herat University are connected indirectly by fiber. They use the same group of Internet Protocol (IP) address of AfgREN and its services, but the fiber network is from other ISPs. A group of provincial universities is connected to the AfgREN NOC via wireless WiMAX technology. Internationally, AfgREN is connected with the TEIN network by a 155 Mbps fiber optic link via Pakistan. TEIN covers mostly South Asian countries, with 21 NRENs of South Asian countries [3].

The services provided by federated members of TEIN include internet access, e-learning, tele-medicine, and support for research collaborations [2]. For the global connection, TEIN connects Asia to the European regional NREN GÉANT, which includes HEANet, the Irish Higher Education Authority net. GÉANT provides global identification via eduGAIN [6].

Various E-learning platforms such as Moodle, edX, Cisco Networking Academy, and many traditional applications including HEMIS are implemented in the AfgREN domain, providing a wealth of the most popular services [20]. The Higher Education Management Information System and the University entrance exam management information systems are specific purpose web-based applications developed by the Ministry of Higher Education of Afghanistan and they are used by all the public Universities in the country.
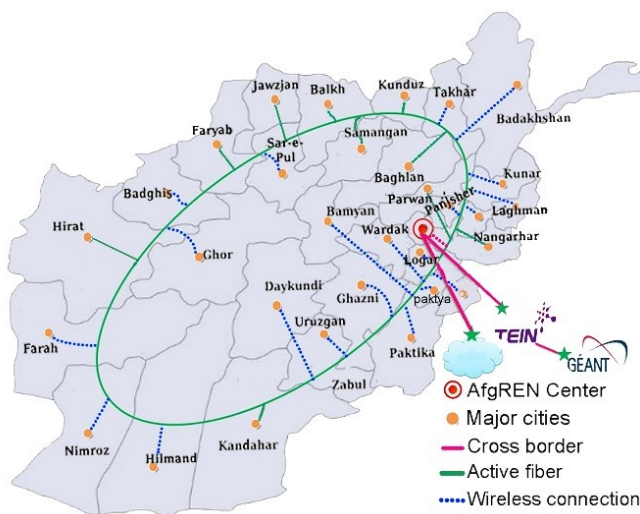
Figure 3: The AfgREN Layout and Connection Structure

Moodle [21] is an open-source e-learning platform that can be installed on a local server or accessed via the Internet. It provides a variety of communication facilities such as a discussion forum, message systems and wiki [21]. It is used for learning, assessment and management, and it provides various types of reports, courses, assignments and knowledge assessments.

edX [22] is also open-source, it was developed by the MIT and Harvard universities in the USA and it is mostly popular for MOOC courses and online certification. edX provides facilities for discussion between students and teachers, online video lectures, course materials, various online exams, and virtual libraries [23]. A comparison of edX with five other e-learning platforms in [21] (Coursera, Google Course Builder, Class2Go, Udemy, and Lernanta) shows that edX has more educational tools than the other four, each of these e-learning platforms has many good learning resources for the educational organization and avows that the integration of the platforms would provide many more learning opportunities for the students.

Cisco Networking Academy was the first e-learning system widely applied in Afghanistan universities. Kabul University is the main regional academy and trains instructors for other local academies [24]. The Cisco e-learning system is implemented in the Computer Science faculties in Afghanistan, providing course materials, laboratory tools, and an online examination system.

Moodle provides more features than edX and other e-learning systems used in the AfgREN domain. It offers more possibilities to customize and connect with other e-learning systems through its Learning Tool Interoperability [25] technology, and thus appears to be the most suitable platform for organizations that require a customized learning management system. However, there is a gap between these software applications and NRENs, and we endeavor to prototype an application to bridge the gap.

2.2 Technological University Consortium

The second case study in this paper concerns the new Technological University currently being established in Ireland from the combination of the Athlone Institute of Technology and the Limerick Institute of Technology.

AIT was established in 1970 under the structure of Regional Technical College (RTC) in Athlone, a city in the geographical centre of Ireland, to provide technician level courses. In 1993 AIT became an autonomous institution, in 1998 AIT was officially redesignated to Athlone Institute of Technology. Since then, AIT established itself as a center of academic excellence with an applied, industry-focused offering of engineering courses. AIT has more than 6,000 undergraduate, postgraduate and Ph.D. students from 84 nations around the world.

The Limerick Institute of Technology (LIT) is a multi-campus institute that was originally established in 1852 in the School of Ornamental Art and later restructured several times. Currently, LIT has three campuses located in Limerick, Tipperary, and Clare. LIT has more than 7,000 undergraduates, postgraduates, and Ph.D. students [26].

Based on the strategic plan of the Irish government [26] the new Technological University will start in September 2021 and operate in multiple campuses covering 4 counties (Limerick, Clare, Tipperary and Westmeath) as shown in Figure 4. The campuses will be connected by the HEAnet backbone. HEAnet [4] is the Irish national education and research network, providing e-infrastructure services

---

[4]https://www.heanet.ie/

for approximately 218,000 students and staff and connecting around 67 educational and research organizations at the national level. In total, around one million users in the research and academic organizations are using HEAnet. The main strategy of HEAnet [27] is to provide collaborative partners, trusted provider services, common, reparable and shareable solutions, innovative solutions, identity federation, brokerage, Key Advisor services, conduit to Europe services and make the country's institutions an excellent place to work.

Figure 4: The Technological University Multi-campuses (AIT-LIT), from [26]

The campuses will be connected by the HEAnet backbone. HEAnet [5] is the Irish national education and research network, providing e-infrastructure services for approximately 218,000 students and staff and connecting around 67 educational and research organizations at the national level. In total, around one million users in the research and academic organizations are using HEAnet. The main strategy of HEAnet [27] is to provide collaborative partners, trusted provider services, common, reparable and shareable solutions, innovative solutions, identity federation, brokerage, Key Advisor services, conduit to Europe services and make the country's institutions an excellent place to work.
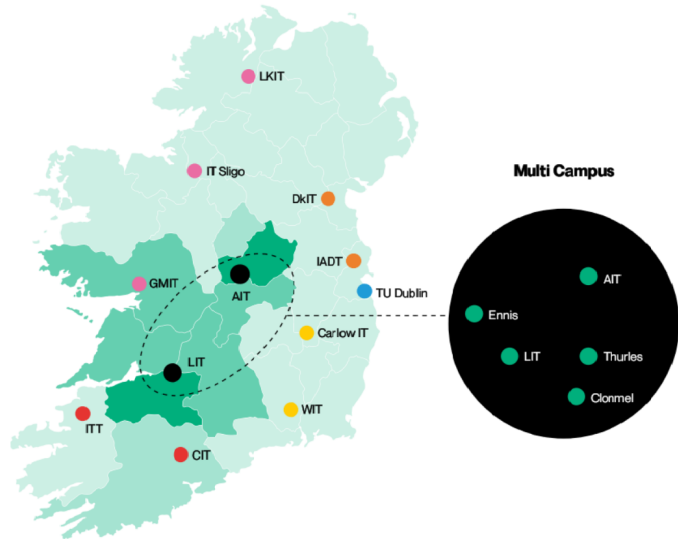
In this research, we target e-learning services brokerage in HEAnet as the means to provide collaboration between the multi-campuses of the new Technological University. Currently, HEAnet provides the served institutions with four types of brokerage including hardware and equipment, software and license, services and consultancy, and students and staff offers. However, e-learning brokerage is also very important for users. Instead of searching the websites of all institutes, users prefer to refer to the website of HEAnet and search there for their required courses[6].

3 Design and Implementation Method

For the analysis, design and implementation we adopted the eXtreme Model Driven Development paradigm (XMDD) [28]. This way we work primarily on models that are compiled to code and

automatically deployed, achieving an agile approach along the entire process and an extended DevOps technique for the prototype, that starts from models instead of code. Specifically, we used a three cycles scrum approach [29] to design the architecture [30] and the prototype of this e-Learning collaboration system. We used the Requirements Bazaar tool [31] to collect user stories and prioritize the requirements. Altogether, the applied design and development methodology is participative, agile, model-driven and low-code.

3.1 Participative Design

Collection of the user stories and the prioritization of the requirements are important steps in software development. We used the Requirements Bazaar concept and web-based tool [31] to collect, analyze, and then prioritize user stories. In addition to collecting the user stories, researchers and system developers can prioritize requirements based on the number of votes and comments provided by the users. Requirements Bazaar provides interaction facilities with the stakeholders from the beginning until the end of the project, facilitating the co-design and co-development approach we wished to adopt. We posted the list of elicited functional requirements and system/architecture features on the Requirements Bazaar portal as a project that we shared with the stakeholders. This enabled the various groups of contributors to Vote on requirements, Select requirements, add comments, add new requirements, and maintain continuous communication with the researchers. A vote means that this requirement is important and it has a high priority, a Select means that this item is required. Through comments, contributors can provide more detail to existing requirements, request changes to system features, and add sub-requirements for the system features. In this work, we combine votes and select in the same column because several stakeholders used them quite indifferently. When contributors selected both options we counted it only once [32].

We also distributed a questionnaire concerning the current state of the e-learning systems. Figure 5 shows that currently lecturers are using many different tools for online teaching and to share course materials. We also asked students about the same and their needs: data scattering is the main challenges that students and lecturers identified as a key problem for integration of the data between different applications.
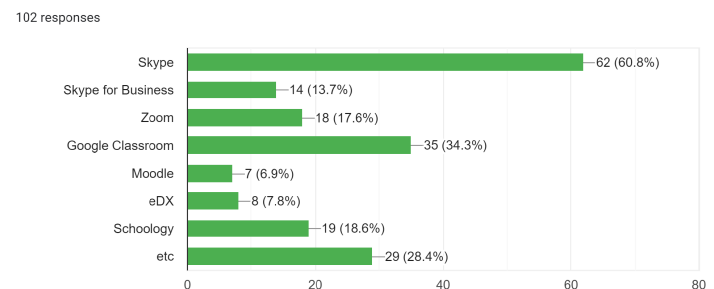

Figure 5: Applications in use for e-learning in the AfgREN domain

---

[5]https://www.heanet.ie/

[6]https://www.heanet.ie/

3.2 Agile Design and Development

Figure 6 summarizes the agile development of the application: the user stories and requirements are collected directly from the users by using Requirements Bazaar. After the planning we designed the prototype using DIME, an Integrated Modelling environment that supports a model driven development and a fast-turn around DevOps cycle adequate for rapid prototyping. Currently we have the first version of the functional prototype of the reference system.
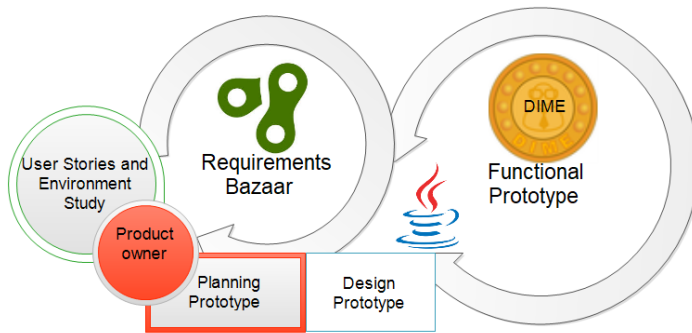

Figure 6: Methodology: the Agile development of the application and implementation tools

Figure 6 also shows the overall method from the tools perspective: we use Requirements Bazaar to collect the requirements, discuss with the users and collect the votes of the user and we prioritize the requirements based on the user's votes. We use DIME for modeling and prototyping. DIME automatically generates Java, JavaScript and DART code, so we export the generated code and proceed to the deployment to a Java EE server side and an Angular 2 Web execution environment. We use GitHub and Bitbucket for the version control and the technical review.

The fast turn-around time for a prototype release is enabled by the model driven approach combined with the adoption of low-code development.

3.3 Model Driven Development

XMDD [33] offers a fast, understandable and easily modifiable paradigm for the co-development of complex systems, and it supports the agile development of the project in a modern and efficient DevOps fashion. The quick and efficient design and deployment of a web application with the XMDD paradigm provides an opportunity for developers to get continuous feedback from the customers/users, and improve the application in agreement with the users until the end of the project life cycle. XMDD is an evolution of the traditional model-driven engineering method (MDE) [34] that in particular supports service-oriented integration, a platform- and feature-based construction and reuse, and continuous integration and evolution.

MDE is a domain-specific modeling methodology that formalizes via models the application structure, behavior and the requirements and properties of IT systems within a specific application domain. It also facilitates formally analyzing specific aspects of models, easing the correctness and performance checking on the models to detect errors early, before investing deep in the development life cycle.

XMDD focuses on **process models** as a primary artifact, understood as descriptions of what the system or application should do. It provides model-level artifacts that are executable even before the full application design and implementation, thus it is accessible also to people that are either less technically skilled, or even not interested at all in usual programming. The benefit for our application is that the adoption of XMDD reduces the time needed for the implementation of the application [34] by adding a coordination layer to the system architecture that describes and then implements the coordination logic between the different components of the architecture.

3.4 Low-code Development

Using DIME [35, 36] as a low-code development environment for the XMDD paradigm, we have a ready graphical modeling tool for the entire architecture, including the data model, control flow and data flow, GUI (interface model) and security/roles and rights model. These models are easier to understand than code, thus supporting the interaction and co-design between IT professionals, domain experts, business experts, and users better than at the code level or the traditional (more technical) modelling level as in a typical UML [37] approach. This approach is extensively validated: it has proven successful in the development of web applications, telecommunication systems, game development, robotics, and bioinformatics systems [34]. In particular, XMDD and DIME support Domain Specific Languages, intended as domain specific libraries of services that provide reusable functionalities [38] and features [39, 40].

4 E-Learning Broker Architecture Design

We designed a domain-specific service-oriented e-learning system for systematic data integration and service brokering between different e-learning systems in NRENs. We refer here to the specific case of AfgREN, but the architecture is general, as we aim at standardization for compatibility beyond specific regional consortia.

In the specific case study, AfgREN is established at Kabul University and it provides services to Afghanistan's public universities including Balkh University and Herat Universities. Figure 8 shows the architecture from the point of view of Kabul University: it has its own three layers (on the left) and it provides services to the external layer of the other universities (on the right) through the e-Learning Broker (center). The same layers and components exist for the other collaboration parties, which are symmetric.

In Afghanistan, the legal framework and procedures are the same for all the public Universities. This simplifies the collaboration because the three layers and several components in Kabul University's local architecture (shown in Figure 8 left) are also applicable to the other public Universities in Afghanistan. The second case study exemplifies how much of the architecture and the broker carries over to the Irish TU setting.

4.1 National, Cross-Organizational Collaboration

4.1.1 Requirements

Prior to the design of architecture, we performed an architectural requirements prioritization using Requirements Bazaar concept and tool with an expert group of stakeholders that comprised the e-learning committee of Kabul University and AfgREN network operation center engineers.

Figure 7 shows the functional requirements of system architecture together with the number of Votes/Select each attribute received in a Requirement Bazaar-supported session. We used Requirements Bazaar from the very early stages till the end of the development process to be in continuous contact with the remotely located expert groups, and negotiate and validate requirements and design decisions in each stage of the development.
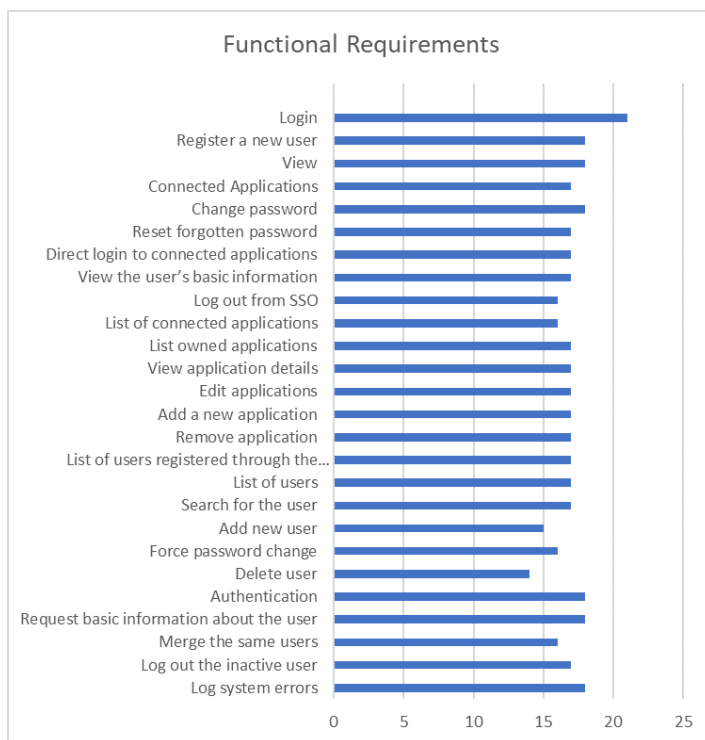

Figure 7: Functional Requirements of the System Architecture

4.1.2 Choosing the Architecture pattern

Different architecture patterns exist for different applications, such as Layered architecture, Event-Driven Architecture, Microkernel Architecture, Micro-services Architecture, and Space-Based Architecture [41]. We carefully analyzed the application domain and requirements to decide which architecture pattern is the most suitable for the target application.

Layered Architectures consists of several layers addressing individual concerns [42]. The required number of layers depends on the complexity of the application: some complex applications, such as the Internet of Vehicle (IoV), have five layers [43]. Most of the layered architectures have four layers: a presentation layer, a business logic layer, a persistence layer, and a database layer. Sometimes in sample architectures the architects combine the persistence

layer with the business logic layer. The process of passing data between layers needs to be very systematic. Layers need to be closed or open, only after having been processed by a specific layer the next layer is made accessible for its data processing. In a layered architecture, the components are accordingly also divided into these layers. The classification of components into different layers helps for easier separation of concerns in the development, test, and maintenance. Layers also provide better modifiability, offering a form of virtualization: if a component of one layer is changed, it does not affect components of the other layers. However, layers and tight coupling of components have a negative effect on the performance, agility, deployment and scalability of a system [41].

Event-Driven Architectures are used for highly scalable systems. Its two main typologies are the mediator topology and the broker topology.

A mediator topology is commonly used when the architect centralizes the events. The typical mediator topology has four main components (event queues, event mediator, event channel, and event processor) and two types of events: initial events and process events.

The broker topology is best used when the architect chains the events and does not need to centralize them. The broker topology has two main components: a broker component and an event processor component [45]. The Event-Driven Architecture pattern is a complex pattern, and the architect needs to consider the remote process availability issue, the lack of responsiveness and the broker reconnection logic in the broker event or face mediator failure [41].

Plug-in Architectures are used as a way of supporting relatively independent third party products. A Plug-in architecture pattern that is also called **Microkernel pattern** consists of two main components including the core system and one or more plugin modules. This architecture pattern is mostly used for product-based applications that have downloadable files.

Microservice Architectures are the oldest services-oriented pattern [50] and widely adopted in distributed and module-based systems. Currently, it is used as the predominant service-oriented architecture [50]. The microservice architecture pattern is a specialized alternative to a more general service-oriented architecture. It is a distributed architecture, where all components are separated and can be controlled with a remote access protocol. The distributed nature of this pattern provides more scalability and ease of deployment attributes [41]. However, microservice architectures have challenges of security [47].

The **Cloud Architecture** pattern is also called space-based architecture, and addresses the problem of scalability. An application that is accessible through a web interface is a suitable application for this pattern. However, the cloud architecture pattern is expensive and it is not suitable for a traditional database with a large number of operational services. The advantage of a cloud based architecture is that we can implement different architecture components in this pattern. The cloud-based patterns simplify the deployment of applications [48, 41].

Table 1 summarizes the comparative characterization of the described architecture patterns based on their quality attributes relevant to our application. We qualitatively indicate the extent to which each quality attributes is provided as Low (*), Medium (**) and High (***).

Table 1: Analysis of Architecture Patterns based on Quality Attributes [44, 42, 43, 41, 45, 46, 47, 48, 49]

Architecture Pattern	Agility	Deployment	Testability	Performance	Scalability
Layered Architecture	*	*	***	*	*
Event-Driven Architecture	***	***	*	***	***
Plug-in Architecture	***	***	***	***	*
Microservice Architecture	***	***	***	*	***
E-Learning Broker Architecture	**	***	***	***	***

4.1.3   The Hybrid NREN e-Learning Architecture

Given the needs of our applications, we adopted a layered, event-driven architecture with a broker technology that provides a high level of agility, ease of deployment, high level of performance and scalability [12, 49, 30, 20, 51]. In this system, the broker needs to publish events to different collaborative systems that are in different domains and follow different roles. Additionally, the XMDD paradigm automatically enforces a service-oriented approach [34] at the implementation level [52], so that we also reap the benefits of this paradigm in the application design and implementation. XMDD is compatible with the SCA service-oriented architectures standard [53], and is a service-oriented evoilution of the more traditional component based architectures in software design [54] and of the feature oriented architectures in early telecommunications services design [55]. It would even support higher order processes, allowing for full reconfigurability of the processes at runtime as shown in [56].

The NREN e-learning architecture shown in Figure 8 is composed of three layers: Internal Layer, Conceptual Layer, and External Layer (on the left). Each layer has several components and sub-components that provide the features identified as a core for any NREN e-learning system architecture.
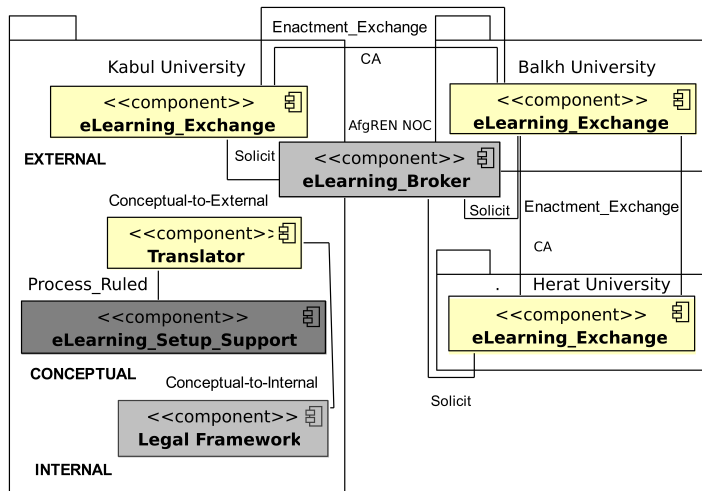
Figure 8: The Component diagram of eLearning System Architecture for a subset of AfgREN

Figure 8 is adapted from the reference architecture for managing dynamic inter-organizational business processes (eSRA) [57] and shows the abstract level of the AfgREN e-learning architecture [49].

- Looking at the structure in the main node, that in AfgREN is

at Kabul University (Figure 8 left), the e-learning platforms are located in the **External Layer**.

- The **Conceptual Layer** comprises an `e-learning_Setup_Support component` in which e-learning services are composed collaboratively in a crowdsourcing way. These e-learning services are process aware, have rules attached. Additionally, the Translator component converts heterogeneous data formats between the external and internal layers.

- The **Internal Layer** contains a Legal framework component in which local process enactment engines, legal process and orchestrate information technology infrastructure that is wrapped as a Web-service. Furthermore, in the Internal Layer local rules engines and local database systems capture the roles of the respective departments and user groups, including academic, administration and students. This structure and subdivision correspond to the essential features identified in various workshops with stakeholders of these groups.

4.1.4   The Broker Aspect: System-Level Features

The design of the e-Learning broker is based on the following elicited system-level features and requirements:

1. The NREN system supports the conceptual formulation of e-learning services between collaboration parties based on the accepted agreement and the established procedures.

2. Translation of the existing legal framework to a technical system, and the mapping of these between collaboration parties.

3. Projection of the e-learning services from the conceptual layer of each collaboration party to the external layer.

4. Brokering capability for the projected services. The broker needs to have access to all e-learning systems of the collaboration parties, the Broker provides an interface that users access different e-learning tools from a single interface, the Broker interface provide SSO services ad also integrate the data of used e-learning applications.

5. Verification of collaboration parties and exchangeable components is another task of Broker,

6. Announcement of the verified result to users, the new services, new members, and any possible issues also announce by the Broker component.

7. Stepwise and systematic construction of interoperable e-Learning architecture based on NRENs.

8. Technology independent e-Learning architecture based on NRENs, easy to port to more modern technologies.

9. Interfaces for the separation of heterogeneous data, to protect private information and to enable a separation of internal and external processes. Collaboration between systems by using Single-Sign-On technology

10. Loose coupling for the interoperability of the e-learning platforms.

11. No central role for any member of the collaboration parties, each collaborative party should act as a party.

12. The Broker application will be installed in the network operation center of the NREN.

4.1.5 Data Management

For **data management**, the NREN e-learning architecture adopts an abstract data repository. This style keeps e-learning service consumers and providers of shared data from knowing of each other's existence and the details of their respective internal implementations. The abstract data repository implements a layering style by interposing an intermediary 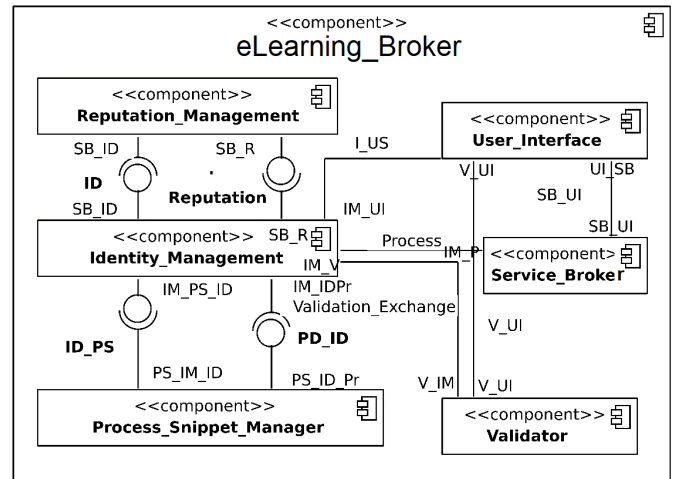protocol between the producer and consumers of the shared e-learning services. Its interface further reduces the coupling between data producers and consumers. Global and local process enactment and rules engines in the external- and internal layers are dedicated components for example for the technology translation, data mediation, and policy enforcement.

4.1.6 Broker-Based Service Mediation

The broker pattern in the AfgREN is implemented in the eLearning_Broker component, a separate component that mediates between collaboration parties within the architecture, facilitating the rapid and performant matching of e-learning needs with requests from users. Its purpose is the redirection and bundling of communication among the parties, preventing parties from finding, contacting, and investigating every potential collaborating party separately.

The service oriented architecture of the eLearning_Broker component is shown in Figure 9, and it is adapted from an NREN e-learning reference architecture [49]. The broker uses a publish/subscribe style in which publisher institutes submit new e-learning services, and all subscribers that are members of the NREN receive notifications automatically. The broker works as a notifier between the collaboration parties. The subscription contract between collaboration parties can be a collaboration contract with free cost or with a price. In this star-like topology the publishers and subscribers are the leaves. This style is advantageous in a multi-party collaboration environment with large numbers of potential e-learning service consumers and providers. It provides a good system performance because of the reduced communication overhead and it enhances the flexibility and ease of integration of additional (national) e-learning systems. In this type of topology, users can easily access the many types of e-learning services provided by collaboration parties in the NREN domain.

Figure 9: The e-Learning_Broker in Detail

4.1.7 The Core Services

The collaboration between organizations is based on the existing rules and procedures, and each party needs to specify their services and data. Conceptual patterns need to be set up in a technical system in such a way that collaborative parties access only the legal and correct exchangeable data.

Internally, the eLearning_Broker includes sub-components for Reputation_Management and Identity_Management, as well as a Process_Snippet_Manager, a Validator, the proper Service_Broker and a User_Interface.

The Reputation_Manager stores detailed information about collaboration parties including the list of exchangeable data/services and the level of service access. The Identity_Manager stores detailed information about the users, user groups, their access capabilities, and it exchanges information with all sub-components of the eLearning_Broker. The Process_Snippet_Manager stores the business processes and collaborates with the Service_Broker to provide the composed processes for the specific heterogeneous e-learning systems that each collaboration partner provides. There can be in fact various e-learning platforms, like Moodle or edX, that support different processes.

The Validator component consists of a Process_Communicator, a Verifier, a Translator, and an Interface_Checker. When this component receives a verification request, it processes it, verifies the legitimacy w.r.t the contractual sphere, the access to services via an interface, and sends back the results.
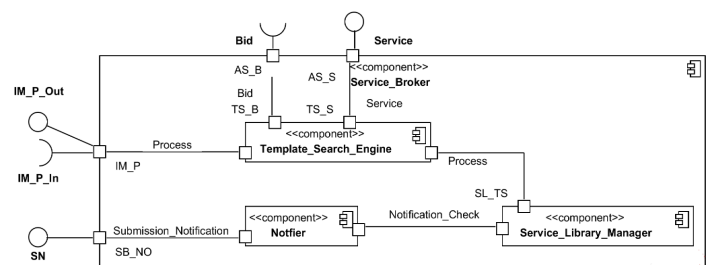

Figure 10: The e-Learning Service_Broker Details

The `Service_Broker_Manager` consists of three other sub-components: the `Service_Library_Manager`, a `Template_Search_Engine`, and a `Notifier`. The `Service_Library` stores the business processes of collaborative parties and provides information for the `Search_Engine` and `Notifier`. The business process specifications stored in the `Service_Library_Manager` works closely with the external layers of the collaboration parties. At the top-level users can search available services through the `Template_Search_Engine` interface of the `eLearning_Broker`. For instance in Figure 10 the `Search_Engine` exchanges data with the bid manager component for the brokering services. The `User_Interface` of the Broker provides access to all NREN e-Learning services through this search engine.

Finally, the `Interface` component provides the user access interface for the users, so that through SSO users can access many participating applications with a single login.

In Figure 8 the Balkh University and Herat University on the right side of the system architecture have the same components as Kabul University, they receive the services and data through their own `E-Learning_Exchange` components, and their internal architecture.

The `eLearning_Broker` component is an interface that facilitates the collaboration of e-learning systems through a rapid matching of e-learning needs with requests from users. Concretely, the broker works based on the collaboration agreement between the parties sharing e-learning services. Collaborating parties may have different agreements, e.g. Some exchangeable data may be offered for free while some services may need to be paid by the users or collaboration parties. The e-Learning broker also sends notifications to collaboration parties.

The central advantage of the broker in a multi-party collaboration environment with large numbers of potential e-learning service consumers and providers is high system performance, supporting efficient access to many e-learning services provided by collaboration parties. This is due to reduced communication overhead and enhanced flexibility and ease of integration of additional e-learning platforms, which were among the top quality attributes requested by the experts.
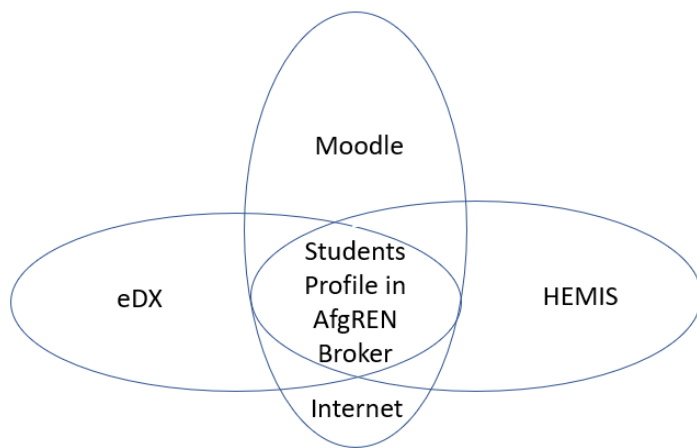
Figure 11: Successful Data Integration with the AfgREN Broker

The NREN e-learning architecture implements an abstract-data

repository style. This style shields e-learning service consumers and providers of shared data from the knowledge of each other's existence and the details of their respective internal implementations. Figure 11 shows the result of the solution provided by the new broker architecture; it solves the problem of data replication in a different system located in the same NREN domain shown in Figure 1.

Our proof of concept system in the reference implementation covers all the system features listed in Figure 7. These features were discussed with domain experts and prioritized. We prototyped the application Based on the designed system architecture, and shared it with the domain experts for further feedback and enhancement.

While the prototype is designed only for the AfgREN case, it is nicely applicable also for the Technological University.

4.2 Intra-Institutional Cross-Campus Collaboration

Cross-campuses collaboration within a federated institution requires to focus more on the resources sharing and data integration between different different applications: the e-learning setup must filter the exchangeable data based on the respective procedures and responsibilities of the collaboration units, which usually differ. In such a context, the legal framework and procedures, security and privacy are the top priorities.
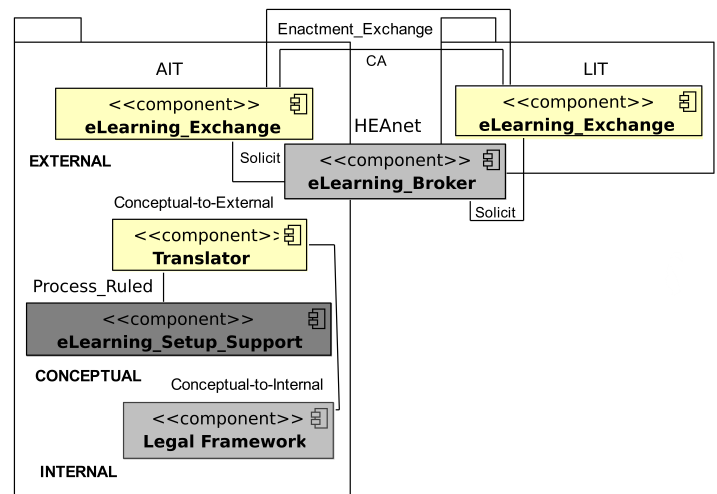
Figure 12: Intra-institutional cross-campuses collaboration Architecture

Considering that the various campuses in Figure 12 all connect through HEAnet, the collaboration setting of AIT and LIT under the new Technological University structure needs less filtering than other case studies, but still the sharing of the financial management systems and other resources sharing can be performed through the NREN Broker. The architecture proposed in Figure 12 shows that the three-layer NRENs cross-organization collaboration is applicable again. This time the focus of the translation and consistency check is between different units of the same (federated) organization and connects different e-learning applications that work in different campuses by considering the respective procedures, data security policies, and filters to apply to the exchangeable data.

The same three layers illustrated in AfgREN apply and are

replicated also for the cross-campuses collaboration. The formal move to the TU structure, with a start of operations as TU, will happen before the two ITs fully merge their policies and IT systems. The alignment of decisional and operational policies and regulations (that in Ireland are strongly local to each institution) and the de-duplication of IT systems to reach a single platform for every function will therefore happen gradually over time, if ever.

The TU will therefore face a transition time of likely several years where it will need to operate formally as one entity, but with regulations, policies and IT systems that start disjoint and will gradually converge, in some phased manner. The advantage of a broker based architecture as we propose is clear, due to the many components supporting the mapping of all these vital functions, it can evolve along the legal and operational changes, eliminating the need for costly point-to-point integration.

5 Model Driven Design of the E-learning Broker

Using DIME as a tool for prototyping and supporting XMDD and model-driven engineering method (MDE)[58] the web application development of the broker does not require extensive programming skills and it provides through the models an opportunity to involve a wide range of project stakeholders. This is a key factor for the success of a project.

We describe now the design of the AfgREN Collaboration Bridging Application, a web application that embodies the prototype for the AfgREN case study. We used the described XMDD approach and the DIME Integrated Modelling Environment as a MDD layer on top of the Eclipse IDE (integrated development environment).

For ease of understanding we describe the application design aspect by aspect, along the DIME model types: Data models for the data structures, Processes for the business logic, GUI for the web application presentation and interaction layer and Security for the Roles and rights management. We present the four aspects individually, but the prototype was developed in an agile and collaborative way, by co-designing and co-evolving the 4 types of models along the growth of the prototype in successive sprints.

5.1 Data Model

The data model in Figure 13 shows the structure of the e-Learning Broker that is an abstract model and organized elements of data that is relate to one another and to the properties of entities. The Base User, User, and Role were preexisting in DIME. We add the Broker component with its many sub-components: Thread, Category, SSO, Register, Search, Language, LegalFramwork, and detail of legal framework and many other sub components are required in the parts of the prototype. The Roles foreseen for the users of the application are a simple User group, an Admin group, a PowerUser group, and a GuestUser group. DIME creates a powerful data model for web applications with many advanced modeling features including AbstractType, ConcreteType, UserType, and EnumType, each of them have different attributes. The models are managed with bidirectional associations, association, and inheritance connection.

Three different Model Component Types are used in this data model: *Concrete types (C)* are used for the User, Broker, Thread, RegisterO, Category, SSO, Search LegalFramework, and Detail. The *User type (U)* is used for the Base User and the *Enum type (E)* is used for the Role and Language. We consider a User association connection between the User and BaseUser (in orange), a bidirectional connection between User and Thread (solid line), and an association connection between Broker and other components (arrows). In the associations as well as in the individual data types, we use square brackets to indicate lists or collections. For example, in Figure 13 the User association associates every User with the same BaseUser, but the BaseUser is associated to many concreteUsers, indicated as [concreteUser]. Similarly, a User can be associated to many Brokers and Threads.

The Model components have a rich set of typed attributes. For each attributes, the model shows whether they have no associations (yellow dot), unidirectional connection as the User.broker attribute with the Broker (yellow dot with one black dot), or bidirectional connection like the threads attribute of the User with another thread model component (yellow dot with two black dots).

All these model elements are formally defined, they are used by the DIME syntax and semantic checkers to ensure that the use of the components and data in the processes is syntactically and semantically correct. This integration of knowledge and checks across various model types is one of the advantages of XMDD as implemented in DIME in comparison with traditional model based approaches to software development, where these checks are not available, or not connected with a correct-by construction generation of code.

As we see, very little in this model is specific to a case study. While the languages will change (English and Persian in the AfgREN case, English and Irish in the TU case), as well as the specific Legal regulations (e.g., GDPR for privacy is mandatory in the EU but not in Afghanistan, which follows national laws instead) the vat majority of the fields is present and very similarly instantiated in both case studies. All the e-learning application fields for example are instantiated to Moodle in both cases, and the user categories and roles so far seem to be shareable as well.

In this sense, we think that a good part of the architecture, data model, implementation and ontology are domain specific to a federated collaboration architecture, thus widely reusable across various kinds of supervised and regulated collaboration, and that a good part of the domain specific aspects, like the e-learning applications and parts of the student management can also be shared at the platform level across all the deployment instances. Only a small part of the data model, processes, GUI etc will need to be customised to the specific collaboration and to the specific institution. For example, the fact that some institutions are connected through WiMax is taken care of at a lower layer (the underlying network and pure connectivity layer) and does not reflect itself on this architecture and models.
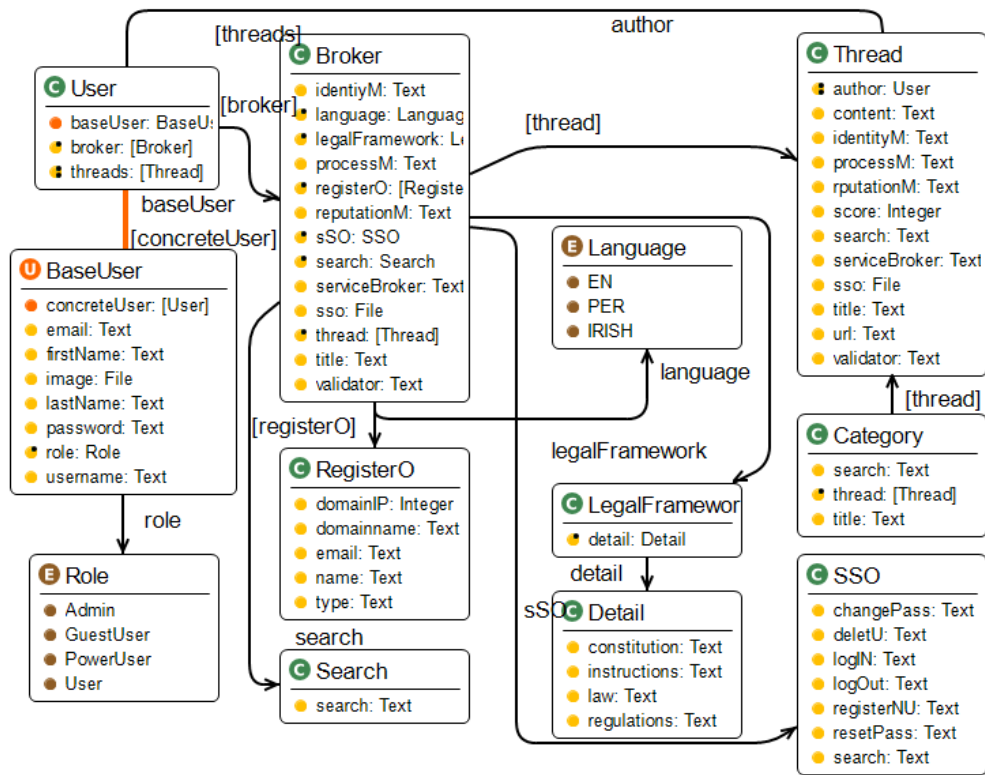
Figure 13: Data Model of the Broker Application (in DIME)
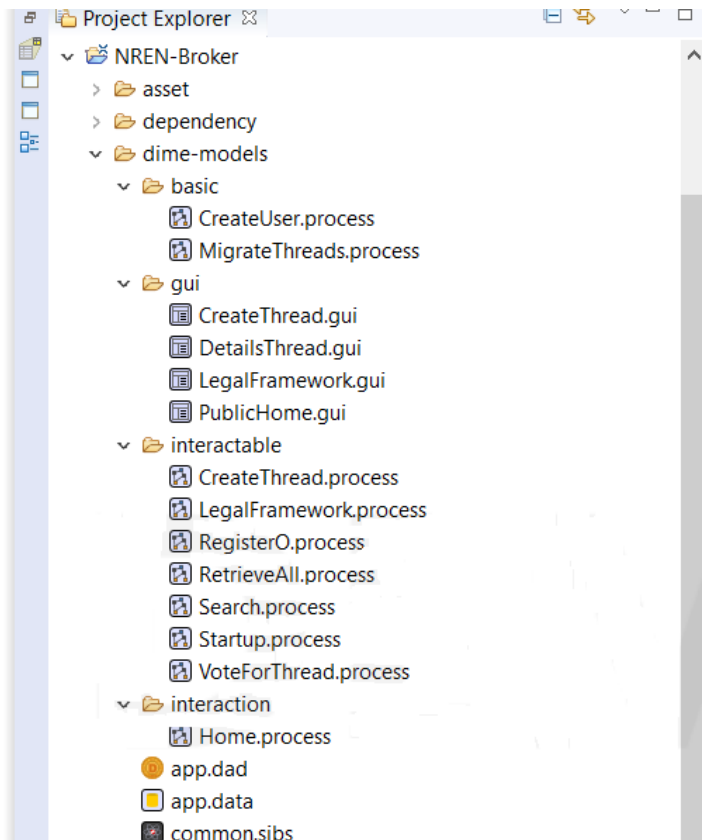
Figure 14: The e-Learning Broker Process Library (in DIME)

5.2 Process Models

The DIME process models support a complex business logic, with the usual patterns (sequential composition, alternative choice, parallel fork and join, and hierarchy), advanced dynamic access control and long-running processes. The process models are interdependently connected with the data model and the user interface models. A web application like the bridging application requires the collaboration of several model types. Figure 14 shows the palette of models we developed in this case study. We now describe some of them.

5.2.1 Home Process

The main process is the `Home process`. As shown in Figure 15, the Home Process model integrates the Public interface, Private interface and all required options for the Detail process of the e-Learning Broker application.

The process starts with the `RetrieveAllThreads` subprocess: it collects all the current learning materials including course title, learning support document, and library support materials, and then displays them on the `PublicHome` page. This is the public home page of the application, which is here represented by its GUI model. From the public home page, users can search for courses and materials. To do so, the system searches (`Search` process) the content metadata from all e-learning platforms registered in the NREN domain and collates the information in the `RetrieveAll` process. Filters can be successively applied.

Open-access material and courses that will be categorized by the Universities can be used publicly without system login and with no
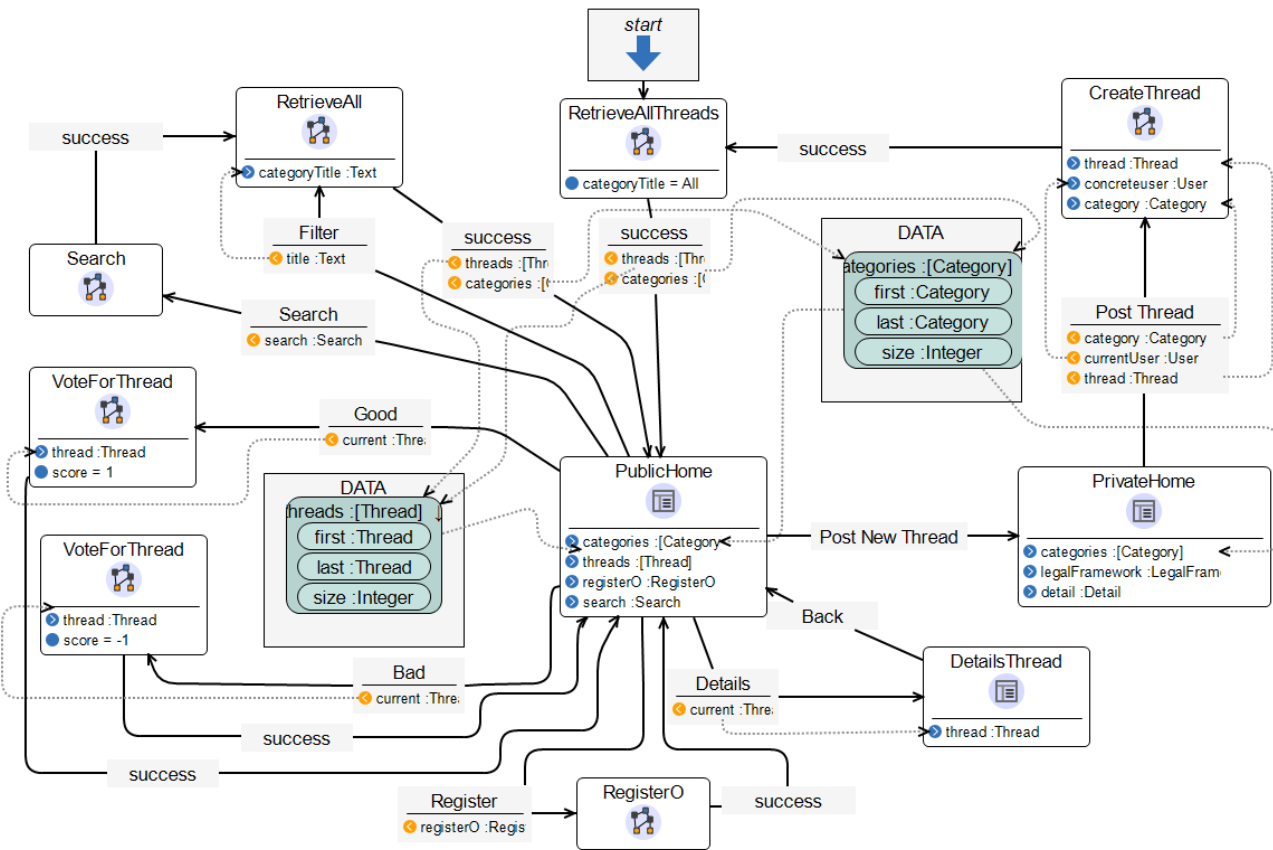
Figure 15: The e_Learning Broker Home Process: Control Flow and Data Flow in DIME

limitation. If a course requires login credential, the user is required to have a user account in the e-learning platform used for course management in their organization, and their e-learning platforms should be a member of the NREN SSO that is located in the Broker component. After logout, the user returns to the public page of the Broker application, and at the same time user logout from all collaboration e-Learning systems.

5.2.2 Startup Process

Figure 16 (left) shows the `Startup` process model that adds users and threads to the collaboration system in a role based fashion. The roles Admin and PowerUser can add threads. PowerUsers are involved in creating a course, learning content, and informative materials. The subjects are categorized by the name of the departments, and PowerUsers of the e-Learning application can add a list of subjects under the name of each department. The logic of this part of the process model leads the system users to a local bridging application server. The Moodle platform is also located on the same server. A title, a short description, and a URL are required for all threads (see the GUI model in Figure 17) (right). Then a category is selected and the thread is submitted. The system records the author and date of the thread creation, duplicate threads are notified to their author.

5.2.3 Register Organization Process

Registering new organizations to the list of collaboration parties is a core feature of the Broker, taken care of in the `Register0` process. Any user can add the reputation of the organization to the system, that needs approval by the Admin. The reputation of an organization is accessible through the registration button in the public interface. Figure 16(right) shows the process model for registering an organization on the basis of the name, type and official email of the organization, its domain name, and IP. This is a low-administration way to provide new facilities for the collaboration parties.

As evident from the Process Library in Figure 14, we defined and used more processes to perform other sub-tasks. From the process models briefly introduced we see that all the process models, the data model, and the interface models are integrated with each other and work together to generate a fully functional web application.

5.3 User Interface Models

The dynamic and responsive graphical user interface of the Collaboration Application is built by means of DIME's GUI process models, that are connected seamlessly to the business logic via hierarchical modeling. The Broker Web application has both a **public user interface** accessible to anyone, that shows a list of options and a list of subjects based on their category, and also a **private interface** accessible only to registered users. Figure 17(left) shows the top
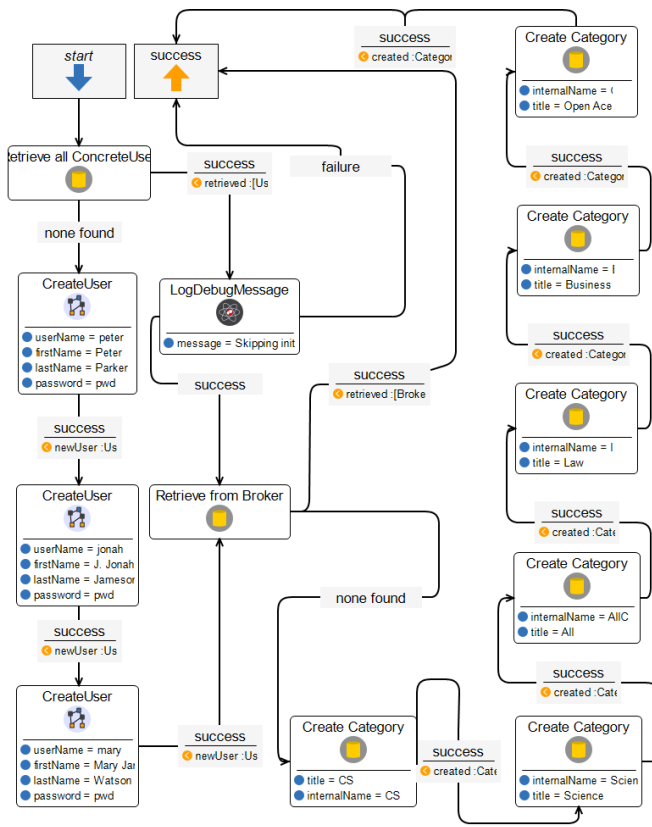
(a) Startup Process: Control Flow
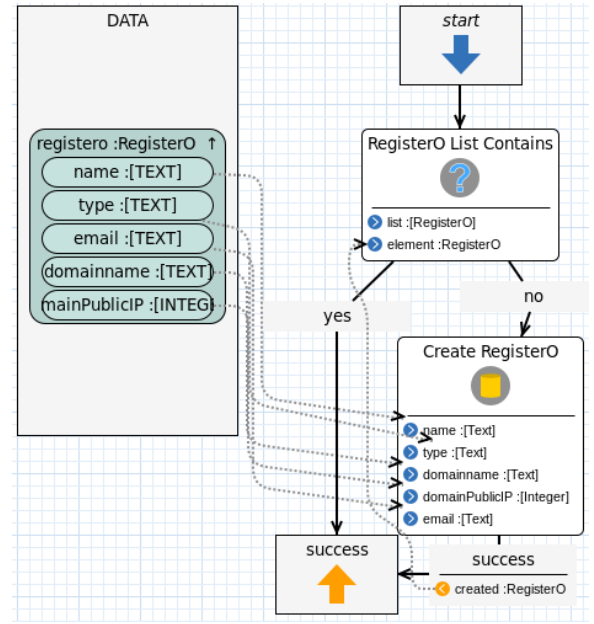
(b) RegisterO Process: Control and Data Flow

Figure 16: The e_Learning Broker Startup and Register Organization Processes in DIME

level DIME GUI model of the the public interface, and Figure 18 shows how the public interface of the deployed and running web application presents to the users.

The public user interface is intentionally kept simple. All the elements appearing on this interface (input fields, buttons, menus etc) are part of the GUI element library that comes with DIME, so there is no need to develop code for the GUI design, which is done in a purely zero-code drag and drop and configuration manner. This feature allows in particular a very efficient turn-around cycle for modifications of the look and feel of the web application.

The public interface also provides a good opportunity for the software developers to share with the reviewer team, product owner, and other stakeholders the prototype of the application, to get feedback and keep them committed to the project: these users can test and assess the application and give timely feedback, while most of them would not be able or willing to review the code.

Users of the participating institutions to the e-learning collaboration use the services of the NREN through the broker and the local e-learning systems in a secure way. They log in once to the server with their username and password, then to access other participating applications they are required at the first login a secure key. After the first login, they are enabled to use their applications without further formalities.

Once logged in, users reach their private user interface. From there they reach all the applications they are entitled to see in the NREN, and those where they can add new threads. Figure 17 shows the private interface model (right). The private interface is

role-specific, currently covering course developers, system administrators, auditors, and maintainers. The administrator role of the system can define different roles for the users.

For **security purposes**, we use the Elytron[59] technology contained in WildFly 14 to provide authentication, authorization, and data encryption.
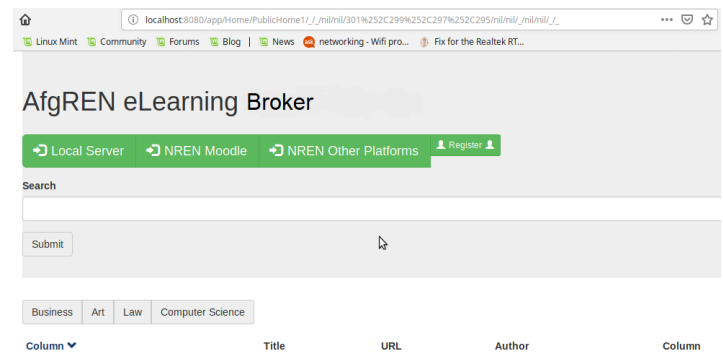
Figure 18: The e_Learning Broker Web Page

For the development of the current prototype, shown in Figure 18, we considered three options:

- In the first, a Moodle instance is installed on the server that runs the bridging application, and the Moodle application uses its Shibboleth instance to reach e-learning systems that support Shibboleth. In this case, the GUI model provides

(a) Public Interface: GUI Model

(b) Private Interface: GUI Model
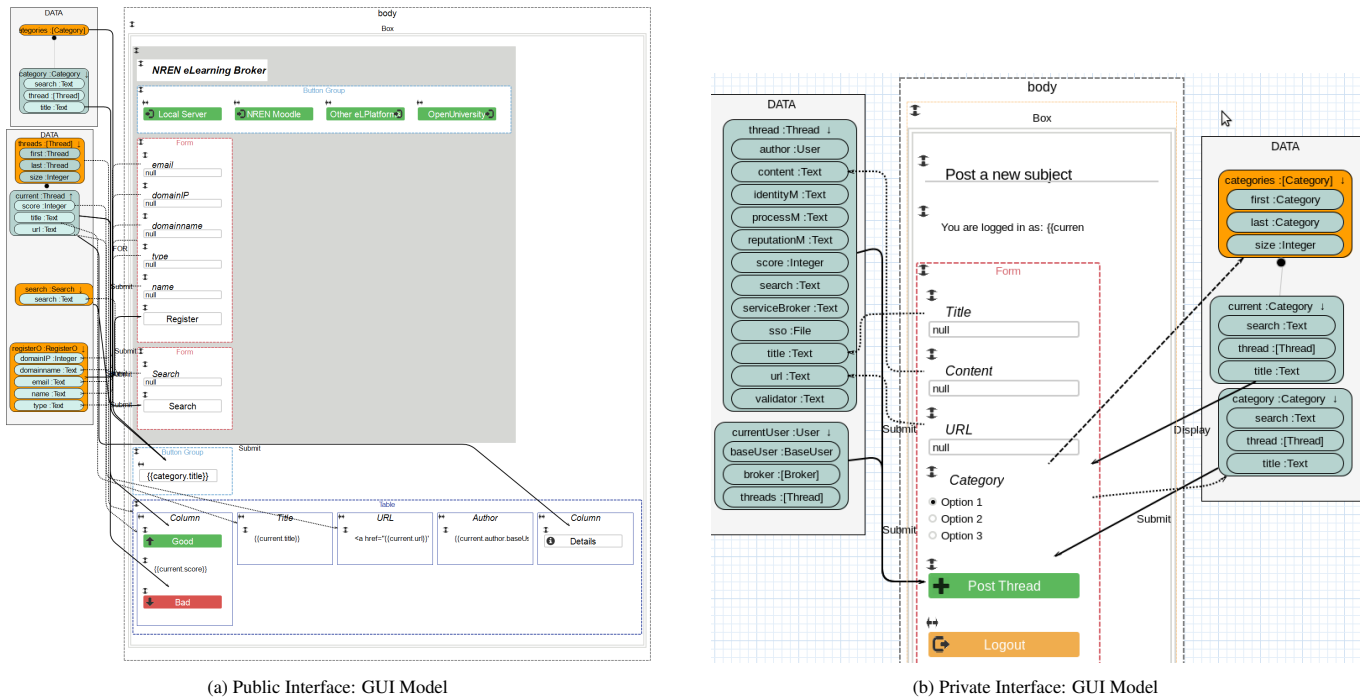
Figure 17: The e‑Learning Broker Public and Private Interface in DIME (GUI Models)

users with a button to login to Moodle. Once logged into this Moodle, users can access any other participating application that supports Shibboleth.

- A second option uses instead the Wildfly 14 contained in DIME. To configure the SSO, we replace the original DIME configuration with a modified ¡standalone-ha.xml¿. A key for using the SSO is created and shared with each member's application. We use this option for the applications that support wildfly Web Single Sign-On.

- Additionally, to access other e-learning platforms such as edX, and in-house developed applications, the GUI model of bridging application provides the third option for users. Currently, the button of the third option is linked to edX Afghanistan a customized e-learning application for Afghan public Universities. All three options are available in the public interface shown in figure 14 and users can select any option they required.

6 Lesson Learned

A central benefit of DIME and XMDD is that once a model is designed, due to the low-code approach to process development that reuses many preexisting components and a zero-code approach to the data design and GUI design, having the models is equivalent to having built a reference implementation. By code generation from the collection of models and components, as supported in DIME, we obtain a ready (prototype) application and this application is automatically deployed and fully functional for user testing or usage. This approach thus supports a more widely accessible collaborative

DevOps style of design and development that improves over the currently standard agile approaches, that are code-based.

This way, it is possible to share and reuse the generated (native Java, Javascript etc) code as-is, but also to change the models (in the DIME graphical editor, or alternatively in the standard Xpand Eclipse textual format) and re-generate and deploy a new version. This feature in particularly attractive in an environment that is still evolving, like for the TU intra-organisational collaboration. That collaboration is actually establishing an inter-organisational collaboration between two up to now independent institutions. It is likely to start as a very lightweight federation of distinct tools and systems, joined by a properly designed and managed access (SSO, security, and roles and rights), but it will over time substitute the 2 or more systems in place up to now for each aspect of the TU's e-learning and students management with potentially only one system - either one of the current locally adopted solutions or a new one. In this context, it is important to be able to quickly experiment with alternatives, for example in a staging configuration, with quick turn around of modifications and easy and immediate access to the successive versions of the various features and services.

We already assessed that the current reference prototype is portable with minor modifications also for the Technical University use case. The detailed design of the Technological University collaboration is still ongoing and the development of the full application is accordingly future work. Along the agile development style, a first beta-release will be followed by two more increments in the coming months.

Additionally, the prototype works as generic reference platform for collaborative e-learning and student management, including for example lighter-weight collaborations with associated institutions, for example for ERASMUS+ international programs or inter-institutional national courses of study as the Irish Higher Education

Authority increasingly promotes, for example in Digital Health Transformation. The central feature of the architecture, reference application and concrete Web Application is that we can evolve and extend them with ease, integrating more functionalities and features. Specifically, the DIME models are both intuitive and formal, and designing systems with these models does not require computer programming knowledge. This provides a real opportunity to have prototypes co-developed by real users, including student administration employees, for a true co-design by those who deeply know the requirements of the organization.

7 Current Status

From the list of features and the data model of Figure 7, the SSO, registration, search engine, user accounts, legal framework, thread, and categories are already actively working. The multilingual language option and the user role management will be active in the next version of the prototype. At this stage, validation has taken place technically in the developer test and continuous feedback has been gathered from representatives of the user groups addressed in the workshops.

In the specific AfgREN context, there is a higher uniformity than in general NRENs because the members are public Universities that follow the same policy, law, and procedures defined by the Ministry of Higher Education of Afghanistan, while international NRENs are more heterogeneous. The network infrastructures, e-learning systems, and other applications are the same as in other NRENs. We provided AfgREN with an SSO by configuring the AfgREN Broker application (designed and code-generated with DIME) to serve also as an SSO server. We installed Moodle and enabled Shibboleth on it in the same server. We have currently prototypes of the searching engine, identity manager and reputation manager. We are working to develop the remaining subcomponents of the broker (validator, translator) and to add an intelligent agent in the Broker that provides a fully transparent SSO service for the different e-learning platforms implemented in the NREN domain.

8 Conclusions

We provided a modular and extensible architecture for NRENs as a modification of a previous reference architecture for business collaboration, now ported and extended to the e-learning data integration, as well as a novel architecture of an e-Learning Broker that is technology independent and thus helps furthering open education and learning collaboration. We adopted a model-driven design paradigm for the development of a reference prototype of a Web-based Collaboration Application that supports open education collaboration and data integration between different e-learning systems co-existing in an NREN domain.

In particular, we adopted AfgREN as a case study, considering the specific policy and strategy legally in place in the AfgREN domain. Based on the proposed NREN e-Learning architecture, we designed the data model, several process models and the interface models of the NREN e-learning broker. These models and processes are going to be provided open source, both in a DIME-specific format and in export formats reusable independently of DIME.

The current prototype of the reference implementation is functional, and we have indeed made use of the rapid turn-around time of design and DevOps iterations enabled by the chosen XMDD and low-code development technologies.

References

[1] K. Upadhyaya, D. Mallik, "E-learning as a socio-technical system: An insight into factors influencing its effectiveness," Business Perspectives and Research, **2**(1), 1–12, 2013, doi:https://doi.org/10.1177/2278533720130101.

[2] A. C. Risdianto, P. M. Thet, A. Iqbal, N. A. M. Shaari, H. K. Atluri, G. N. Nurkahfi, A. Wantamanee, R. Hakimi, U. Javed, M. Ahmad, et al., "Deploying and Evaluating OF@ TEIN Access Center and Its Feasibility for Access Federation," Proceedings of the Asia-Pacific Advanced Network, **42**, 34–40, 2016.

[3] N. Suresh, J. Mbale, A. Terzoli, T. K. Mufeti, "Enhancing cloud connectivity among NRENs in the SADC region through a novel institution cloud infrastructure framework," in 2015 International Conference on Emerging Trends in Networks and Computer Communications (ETNCC), 179–184, IEEE, 2015, doi:10.1109/ETNCC.2015.7184830.

[4] L. Ssentongo, R. Kimera, B. Kakeeto, M. Mubiru, B. K. Moyer, M. Economou, C. J. Whalen, M. Tartakovsky, "Deploying Educational Roaming (eduroam) in a Rural Research Institution in Rakai, Uganda; Challenges and Lessons Learned," 2016.

[5] U. Pietrzyk, A. Zakhnini, M. Axer, S. Sauerzapf, D. Benoit, M. Gaens, "EduGATE–basic examples for educative purpose using the GATE simulation platform," Zeitschrift für Medizinische Physik, **23**(1), 65–70, 2013, doi:http://193.48.81.146/sites/default/files/dx.doi.org/10.1016/j.zemedi.2012.07.005.

[6] S. Michael, Z. J. Anna, "An Identity Provider as a Service platform for the eduGAIN research and education community," in 2019 IFIP/IEEE Symposium on Integrated Network and Service Management (IM), 739–740, IEEE, 2019, doi:978-3-903176-15-72019IFIP.

[7] M. Li, C.-H. Chi, C. Ding, R. Wong, Z. She, "A Multi-protocol Authentication Shibboleth Framework and Implementation for Identity Federation," in International Conference on Security and Privacy in Communication Systems, 81–101, Springer, 2018, doi:https://doi.org/10.1007/978-3-030-01704-0_5.

[8] N. Hamamoto, H. Ueda, M. Furukawa, M. Nakamura, T. Nishimura, S. Yokoyama, K. Yamaji, "Toward the Cross-Institutional Data Integration From Shibboleth Federated LMS," Procedia Computer Science, **159**, 1720–1729, 2019, doi:https://doi.org/10.1016/j.procs.2019.09.343.

[9] M. Katzer, D. Crawford, "Office 365 DirSync, ADFS, Single Sign On and Exchange Federation," in Office 365, 545–630, Springer, 2013, doi:https://doi.org/10.1007/978-1-4302-6527-6_11.

[10] P. Kamal, S. Mustafiz, F. M. A. Rahman, R. Taher, et al., "Evaluating the efficiency and effectiveness of a federated sso environment using shibboleth," Journal of Information Security, **6**(03), 166, 2015, doi:10.4236/jis.2015.63018.

[11] S. Saay, T. Margaria, "Xmdd as key enabling technology for integration of large scale elearning based on NREN," in 2020 IEEE 20th International Conference on Advanced Learning Technologies (ICALT), 45–46, IEEE, 2020, doi:10.1109/ICALT49669.2020.00020.

[12] S. Saay, A. Norta, "An architecture for e-learning infrastructures on a national level: a case study of the Afghanistan Research and Education Network," International Journal of Innovation and Learning, **23**(1), 54–75, 2018, doi: https://doi.org/10.1504/IJIL.2018.088790.

[13] U. K. Hazra, R. Das, S. Mukherjee, "e-Learning Platform in SAARC Countries," Library Philosophy and Practice, 1–9, 2019, doi:https://digitalcommons.unl.edu/libphilprac/2882.

[14] A. Khaliq, M. S. Shams, M. M. Niazi, "COVID-19 Pandemic: Challenges and Opportunities for Higher Education in the Afghanistan context," doi:https://kardan.edu.af/data/public/files/KJEMS-3.3-2020-03%2014102020083157.pdf.

[15] M. Z. Sana, "Common Distributed Data Storage for Higher Education Management Information System in Afghanistan," International Journal of Scientific Engineering and Science, 32–38, 2020, doi:http://ijses.com/wp-content/uploads/2020/05/120-IJSES-V4N4.pdf.

[16] M. Beer, M. C. Meier, B. Mosig, F. Probst, "A prototype for information-dense it project risk reporting: an action design research approach," in 2014 47th Hawaii International Conference on System Sciences, 3657–3666, IEEE, 2014, doi:10.1109/HICSS.2014.456.

[17] I. Turus, J. Kleist, A. M. Fagertun, "Evaluation of flex-grid architecture for NREN optical networks," in TERENA Networking Conference 2014, 2014, doi:https://orbit.dtu.dk/en/publications/evaluation-of-flex-grid-architecture-for-nren-optical-networks.

[18] S. Mahmood, "Instructional Strategies for Online Teaching in COVID-19 Pandemic," Human Behavior and Emerging Technologies, 2020, doi:https://doi.org/10.1002/hbe2.218.

[19] S. L. J. Villalón, C. C. L. Hermosa, "The Role of National Research and Education Networks Providing Connectivity and Advanced Network Services to Virtual Communities in Collaborative R&E Projects. CUDI: The Mexican Case," in International Conference on Supercomputing in Mexico, 24–47, Springer, 2015, doi:https://doi.org/10.1007/978-3-319-32243-8_3.

[20] S. Saay, M. Laanpere, A. Norta, "Requirements for e-testing services in the AfgREN cloud-based e-learning system," in International Computer Assisted Assessment Conference, 133–147, Springer, 2016, doi:https://doi.org/10.1007/978-3-319-57744-9_12.

[21] C. Costa, H. Alvelos, L. Teixeira, "The use of Moodle e-learning platform: a study in a Portuguese University," Procedia Technology, **5**, 334–343, 2012, doi:https://doi.org/10.1016/j.protcy.2012.09.037.

[22] D. Volchek, A. Romanov, D. Mouromtsev, "Towards the semantic MOOC: Extracting, enriching and interlinking e-learning data in open edX platform," in International Conference on Knowledge Engineering and the Semantic Web, 295–305, Springer, 2017, doi:https://doi.org/10.1007/978-3-319-69548-8_20.

[23] M. Blagojević, D. Milošević, "Massive open online courses: EdX vs Moodle MOOC," in Proc. 5th International Conference on Information Society and Technology, Kopaonik, Serbia, 346–351, 2015, doi:https://aosus.org/uploads/default/original/1X/97ba7ad9a50b2a3171ebaaa64d8cf2943af37807.pdf.

[24] H. Sokout, T. Usagawa, "Analyzing the Current Situation of E-learning at Kabul Polytechnic University," in Proceedings of the 2nd International Conference on Education and Multimedia Technology, 49–53, 2018, doi: https://doi.org/10.1145/3206129.3239428.

[25] A. Naim, M. R. Hussain, Q. N. Naveed, N. Ahmad, S. Qamar, N. Khan, T. A. Hweij, "Ensuring interoperability of e-learning and quality development in education," in 2019 IEEE Jordan International Joint Conference on Electrical Engineering and Information Technology (JEEIT), 736–741, IEEE, 2019, doi:doi:10.1109/JEEIT.2019.8717431.

[26] AIT – LIT Consortium, "The context for the new TU," in Application for designation as a technological university, 16–18, `https://www.aitlitconsortium.ie/`, 2020.

[27] A. Harding, "Design and Implementation of Service Level Agreements at HEAnet," www.heanet.ie, 2–14, 2007.

[28] T. Margaria, B. Steffen, "Agile IT: thinking in user-centric models," in International Symposium On Leveraging Applications of Formal Methods, Verification and Validation, 490–502, Springer, 2008, doi:https://doi.org/10.1007/978-3-540-88479-8_35.

[29] S. Sharma, N. Hasteer, "A comprehensive study on state of Scrum development," in 2016 International Conference on Computing, Communication and Automation (ICCCA), 867–872, IEEE, 2016, doi:10.1109/CCAA.2016.7813837.

[30] S. Saay, A. Norta, "Designing a Scalable Socio-Technical Method for Evaluating Large e-Governance Systems," in Advanced Computational and Communication Paradigms, 571–580, Springer, 2018, doi:https://doi.org/10.1007/978-981-10-8240-5_64.

[31] D. Renzel, M. Behrendt, R. Klamma, M. Jarke, "Requirements bazaar: Social requirements engineering for community-driven innovation," in 2013 21st IEEE International Requirements Engineering Conference (RE), 326–327, IEEE, 2013, doi:doi:10.1109/RE.2013.6636738.

[32] S. Saay, T. Margaria, "Model-Driven-Design of NREn Bridging Application: Case Study AfgREN," in 2020 IEEE 44th Annual Computers, Software, and Applications Conference (COMPSAC), 1522–1527, IEEE, 2020, doi:doi:10.1109/COMPSAC48688.2020.00-39.

[33] T. Margaria, B. Steffen, "eXtreme Model-Driven Development (XMDD) Technologies as a Hands-On Approach to Software Development Without Coding," Encyclopedia of Education and Information Technologies, 732–750, 2020, doi:https://doi.org/10.1007/978-3-030-10576-1.

[34] T. Margaria, B. Steffen, "Service-orientation: conquering complexity with XMDD," in Conquering Complexity, 217–236, Springer, 2012, doi:https://doi.org/10.1007/978-1-4471-2297-5_10.

[35] S. Boßelmann, M. Frohme, D. Kopetzki, M. Lybecait, S. Naujokat, J. Neubauer, D. Wirkner, P. Zweihoff, B. Steffen, "DIME: a programming-less modeling environment for web applications," in International Symposium on Leveraging Applications of Formal Methods, 809–832, Springer, 2016, doi: https://doi.org/10.1007.

[36] J. Neubauer, M. Frohme, B. Steffen, T. Margaria, "Prototype-driven development of web applications with DyWA," in International Symposium On Leveraging Applications of Formal Methods, Verification and Validation, 56–72, Springer, 2014, doi:https://doi.org/10.1007/978-3-662-45234-9_5.

[37] N. Moreno, P. Fraternali, A. Vallecillo, "WebML modelling in UML," IET software, **1**(3), 67–80, 2007, doi:10.1049/iet-sen:20060067.

[38] T. Margaria, A. Schieweck, "The Digital Thread in Industry 4.0," in International Conference on Integrated Formal Methods, 3–24, Springer, 2019, doi:https://doi.org/10.1007/978-3-030-34968-4_1.

[39] S. Jörges, A.-L. Lamprecht, T. Margaria, I. Schaefer, B. Steffen, "A constraint-based variability modeling framework," International Journal on Software Tools for Technology Transfer, **14**(5), 511–530, 2012, doi:https://doi.org/10.1007/s10009-012-0254-x.

[40] M. Karusseit, T. Margaria, "Feature-based modelling of a complex, online-reconfigurable decision support service," Electronic Notes in Theoretical Computer Science, **157**(2), 101–118, 2006, doi:https://doi.org/10.1016/j.entcs.2005.12.049.

[41] M. Kircher, P. Jain, Pattern-oriented software architecture, patterns for resource management, volume 3, John Wiley & Sons, 2013.

[42] A. Patwardhan, R. Patwardhan, S. Vartak, "Self-Contained Cross-Cutting Pipeline Software Architecture," arXiv preprint arXiv:1606.07991, 2016, doi: arXiv:1606.07991v1.

[43] O. Kaiwartya, A. H. Abdullah, Y. Cao, A. Altameem, M. Prasad, C.-T. Lin, X. Liu, "Internet of vehicles: Motivation, layered architecture, network model, challenges, and future aspects," IEEE Access, doi:doi:10.1109/ACCESS.2016.2603219.

[44] M. Richards, Software architecture patterns, volume 4, O'Reilly Media, Incorporated 1005 Gravenstein Highway North, Sebastopol, CA . . . , 2015.

[45] O.-A. Schipor, R.-D. Vatavu, J. Vanderdonckt, "Euphoria: A Scalable, event-driven architecture for designing interactions across heterogeneous devices in smart environments," Information and Software Technology, **109**, 43–59, 2019, doi:https://doi.org/10.1016/j.infsof.2019.01.006.

[46] A. Balalaie, A. Heydarnoori, P. Jamshidi, "Microservices architecture enables devops," London: Sharif University of Technology, 2014.

[47] N. Dragoni, S. Giallorenzo, A. L. Lafuente, M. Mazzara, F. Montesi, R. Mustafin, L. Safina, "Microservices: yesterday, today, and tomorrow," Present and ulterior software engineering, 195–216, 2017, doi:https://doi.org/10.1007/978-3-319-67425-4_12.

[48] F. J. García-Peñalvo, J. Cruz-Benito, C. Maderuelo, J. S. Pérez-Blanco, A. Martín-Suárez, "Usalpharma: A cloud-based architecture to support Quality Assurance training processes in health area using Virtual Worlds," The Scientific World Journal, **2014**, 2014, doi:https://doi.org/10.1155/2014/659364.

[49] S. Saay, "A Reference Architecture for A National E-Learning Infrastructure," in Ph.D Thesis, 20–80, Tallinn University, 2018.

[50] L. Chen, "Microservices: architecting for continuous delivery and DevOps," in 2018 IEEE International conference on software architecture (ICSA), 39–397, IEEE, 2018, doi:doi:10.1109/ICSA.2018.00013.

[51] S. Saay, A. Norta, M. Laanpere, "Towards an architecture for e-learning infrastructures on a national level: a case study of AfgREN," in International Conference on Web-Based Learning, 98–107, Springer, 2015, doi: https://doi.org/10.1007/978-3-319-32865-2_11.

[52] M. Karusseit, T. Margaria, "Feature-based modelling of a complex, online-reconfigurable decision support service," Electronic Notes in Theoretical Computer Science, **157**(2), 101–118, 2006, doi:https://doi.org/10.1016/j.entcs.2005.12.049.

[53] G. Jung, T. Margaria, R. Nagel, W. Schubert, B. Steffen, H. Voigt, "SCA and jABC: Bringing a service-oriented paradigm to web-service construction," in International Symposium On Leveraging Applications of Formal Methods, Verification and Validation, 139–154, Springer, 2008, doi:https://doi.org/10.1007/978-3-540-88479-8_11.

[54] T. Margaria, "Components, Features, and Agents in the ABC," in Objects, Agents, and Features, 154–174, Springer, 2004, doi:https://doi.org/10.1007/978-3-540-25930-5_10.

[55] T. Margaria, B. Steffen, M. Reitenspieß, "Service-oriented design: the roots," in International Conference on Service-Oriented Computing, 450–464, Springer, 2005, doi:https://doi.org/10.1007/11596141_34.

[56] J. Neubauer, B. Steffen, T. Margaria, "Higher-order process modeling: product-lining, variability modeling and beyond," arXiv preprint arXiv:1309.5143, 2013, doi:,doi:10.4204/EPTCS.129.1.

[57] A. Norta, P. Grefen, N. C. Narendra, "A reference architecture for managing dynamic inter-organizational business processes," Data & Knowledge Engineering, **91**, 52–89, 2014, doi:https://doi.org/10.1016/j.datak.2014.04.001.

[58] S. Boßelmann, A. Wickert, A.-L. Lamprecht, T. Margaria, "Modeling directly executable processes for healthcare professionals with xmdd," in Service Business Model Innovation in Healthcare and Hospital Management, 213–232, Springer, 2017, doi:https://doi.org/10.1007/978-3-319-46412-1_12.

[59] F. Marchioni, WildFly Administration Guide: The ultimate and most up-to-date guide to manage WildFly appication server, ITBuzzPress, 2020.

Effect of Smooth Transition and Hybrid Reality on Virtual Realism: A Case of Virtual Art Gallery

Ali Almutawa*

Kyushu University, Motooka Nishi-ku Fukuoka 819-0395, Japan

A R T I C L E I N F O	A B S T R A C T
	Virtual reality (VR) is finding applications in a wide range of industries; however, a significant number of users find VR experience considerably different from the real-world experience. To match the real-world experience, the VR experience should look real, should be immersive, and be in line with the users' anticipation. Achieving realism in the virtual representation of objects, however, presents several technical challenges. This study presents a new approach, "Smooth Transition and Hybrid Reality (STHR)," to easily enhance VR realism. In this approach, the participants are exposed to a mix of real-world objects (RWO) and virtual objects (VO), and a smooth transitioning from the real world to the VR space is obtained by making the real-space highly relevant to the VR space and vice-versa. To test the effectiveness of STHR, different experiments on spatial awareness were conducted, and finally, a virtual art gallery was created for the public. A total of 21 participants were included in the study and were randomized into experiment and control groups. The results indicated that the interaction with an RWO in the initial phase of VR significantly increases the task completion time and the attention (both, p<0.05). It was found that almost 50% of the participants relied on prior knowledge of the real space even when different visual information is delivered through VR. STHR based virtual art gallery (VAG) was created for the public, and the experience of random visitors was noted. In VAG, haptic feedback was provided by using an RWO (3D printed artwork), and the smooth transition from RW to VR was maintained. The average time spent in the VAG more than 5 minutes, and the feedback of visitors was highly positive.

1. Introduction

Technological advances make a significant impact on all forms of art and even create new art forms. Virtual reality (VR) and augmented reality (AR) are poised to make a remarkable shift in the way art is created, presented, and appreciated [1, 2]. However, in VR, replicating the effect that real artworks make on human perception presents several technical and psychological constraints [3-5].

The perceived quality of artwork usually differs from person to person, depending on their previous experiences and subjective interpretation of the visual information, and involves multi-process cognition and emotional associations [6, 7]. Typically, at art galleries and museums, observers view the artwork from a distance. The perception primarily relies on the processing of visual information of depth, distance, and angle. The ultimate goal of VR technology in art is to achieve digital art appreciation in the digital art space that is at least on par with its conventional counterpart. However, in the context of VR, as the viewers already

know they are observing a virtual object, comprehension of "reality" gets complicated and greatly depends on the immersion and presence rendered by the overall VR experience [8, 9].

The space setup and the method to transition into VR significantly influence the overall VR experience. It has been reported that creating a gentle transition from the real world into the virtual and back into the real environment could be an excellent solution to enhance the realism of VR. In a recent study, the effect of a gradual transition between the real world and VR was investigated by using a video feed from a stereo camera that gradually faded into the virtual content, creating a smooth transition, which significantly affected the participant's perception of virtual body ownership and presence [10]. The major issue with this smooth transition method is that a new 3D model must be provided for each different space. Constructing realistic 3D spaces is time-consuming, and, in several cases, the meant-to-be-shown virtual environment is entirely different from the real space. Furthermore, there can be differences in the scale of the space or in content [10-13]. However, despite all significant research in this

area, the factors that affect VR experience quality are not yet fully established.

In this work, we introduced the concept of Smooth Transition Coupled Hybrid Reality (STHR), wherein the participants were first deliberately introduced to a physical object, which was the replica of one of the virtual objects that the participant would see during VR. This step was expected to provide haptic feedback that matched the real world and the VR [14, 15]. Furthermore, the setup was designed to allow a smooth transition from the real world to the virtual world and vice-versa. This step involved making the real-world theme highly relevant to the virtual world and blocking all extraneous content to the maximum extent possible. The study also attempted to clarify the fundamental aspects of the impact of spatial awareness on the overall VR experience.

2. Methodology

The objective of this research was to find out approaches that can be utilized to enhance the VR experience. To that end, the concept of STHR was developed, which involved providing haptic feedback by a real-world object and enabling a smooth transition from a real-world environment to VR environment. To test the efficacy of STHR, we conducted different randomized experiments and examined anticipation, reality, immersion, and attention participants during their VR experience [8, 15, 16]. We have also monitored task-complication time and the number of collisions in different study groups. Finally, the validity of the STHR concept was demonstrated by creating a virtual art gallery for the common public and recording the realism experienced by random visitors [17].

2.1. Participants and questionnaire

There were 21 participants in the experiment. Before the experiments, all participants were asked to fill a questionnaire related to the basic information and previous VR experience. Each participant had to participate in all experiments. After each experiment, they were asked to fill a Presence and Reality judgment questionnaire [18]; the questionnaire had 25 questions that were to be scored on a scale of 1–10. Anticipation, reality, immersion, and attention during VR were analyzed from the questionnaire. At the end of all three experiments, we also conducted a survey and an interview with questions based on the participants' behavior.

2.2. Experiments

A total of three experiments were conducted in the same place in a specific sequence, one participant at a time. We chose a room that was unknown to all participants to eliminate any knowledge of the space. Before entering the experiment room (Figure S1), the participants were asked to wear an eye mask, close their eyes, and keep them closed until they entered the room and put on the head-mounted display (HMD). When the experiment was over, they were asked to close their eyes again until they left the room.

In the first experiment, we examined the effect of hybrid-reality on realism, i.e., we created the setup so that the participants interact with a real-world object (RWO) in the initial stage of the VR experiment. This approach provides haptic feedback that matched the real world and the VR gallery. The virtual space was a room with some furniture, a column offset from the center of the room creating a narrow passage, and some traffic cones to act as obstacles while walking in the room to perform the task (Figure 1, Figure 2). The participants were divided into two groups and randomly assigned to one of the two conditions. The first condition introduced some real-world objects (RWO) (a table and chair) with similar shape, size, and VR location as in the real environment. These objects were placed near the participant's starting point, which forced a natural interaction through either deliberate or accidental. These matching objects were the only things inside the experimental space. In the control group (CG), there were no real objects. For each group, we measured the time taken to complete the task of touching the red boxes, noted their routes of movement, and observed the distance traveled by the participants to avoid the obstacles, and compared them.
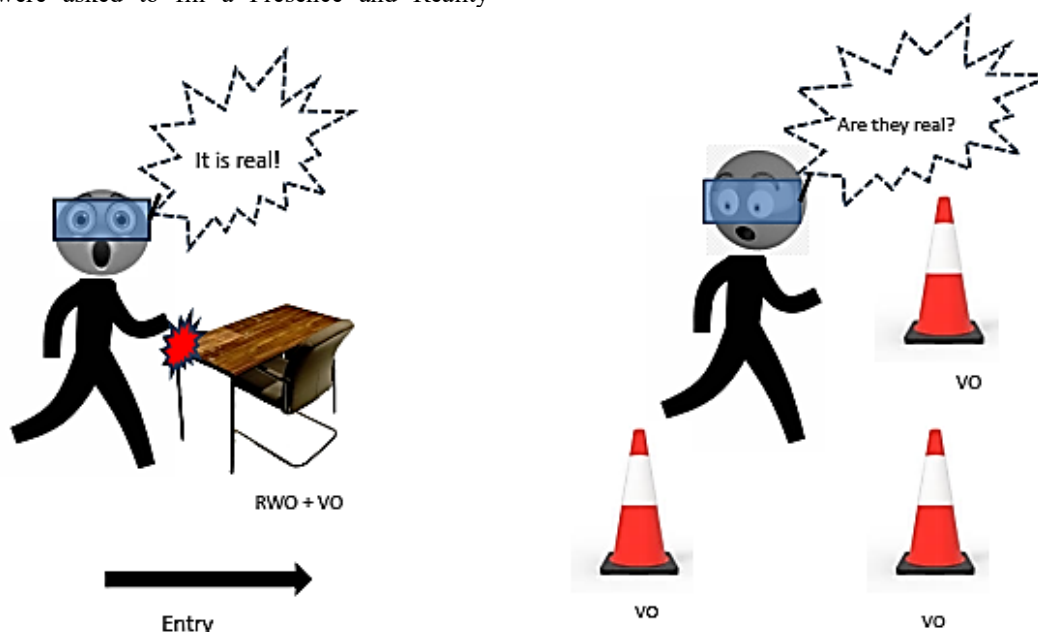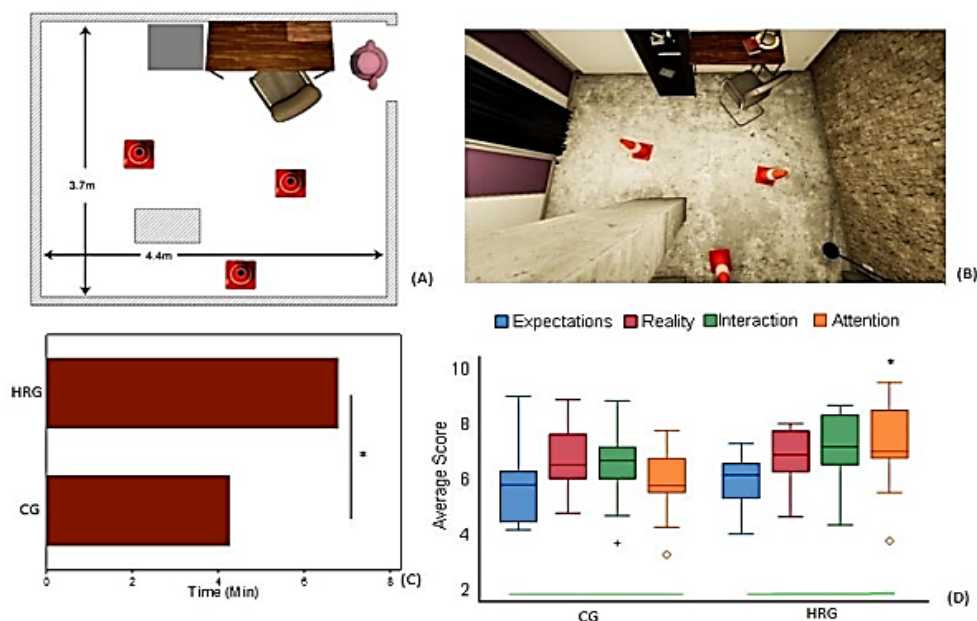
In the second experiment, we examined the difference in realism and task completion time when the participant is already aware of the real space. Essentially, it was a measure of the effect of spatial awareness of the real space on VR realism. The boundaries of the virtual and physical worlds were the same. Traffic cones were scattered around the virtual space that acted as obstacles when a participant walked into the room to perform the task of touching the red boxes (Figure 3). However, the experimental space did not have any physical object—it was empty. The experiment had two primary setup conditions: an environment where the participants can see the room set up to know it is empty (control group) and a group where the participants cannot see the actual space where the VR experiment was conducted. In this setup, a barrier (wall) blocked the participants' view of the real space. We compared the time taken to complete the tasks, the route of movement, and the distance traveled by the participants. In the last experiment, all the participants were allowed to see the room before wearing the VR headset; however, the VR setup was clearly different from the real space (Figure 4). We aimed to examine if the participant's memory of the real world would persist during the VR experience and how this knowledge affects their decision-making while experiencing VR.

This experiment focused on the route and actions taken by the participants. There was an obstacle (table) in the real environment that did not exist in the VR space. This obstacle blocked the path needed to reach the second red box. Thus, this was a bad environmental setup for VR.

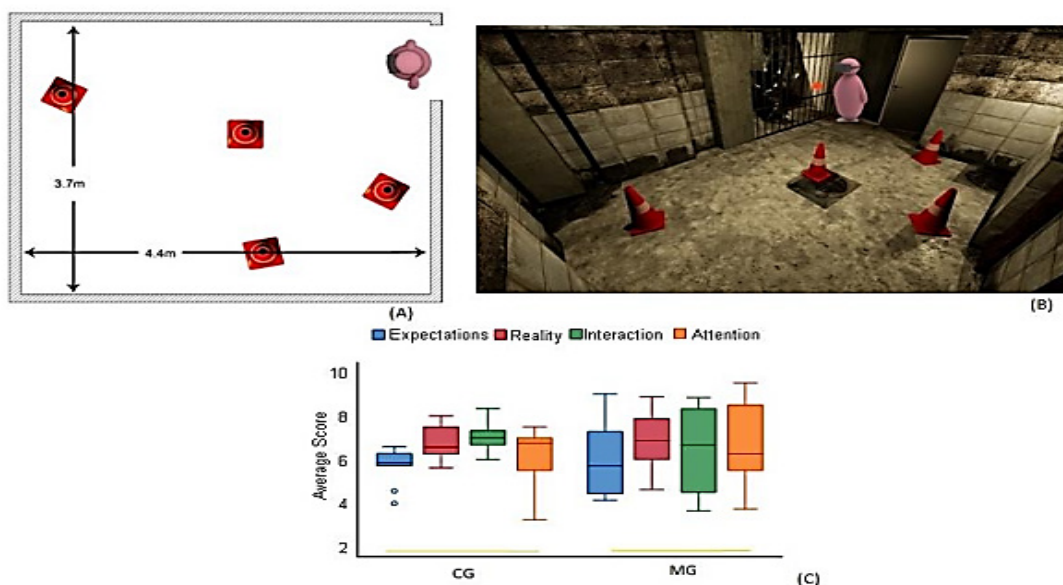Figure 3: VR space and dimensions of VR realism after Experiment 2 (spatial awareness). (A) Experimental space (B) Virtual-space (C) Assessment of different dimensions of VR realism. (MG: Mask group, CG: Control group)
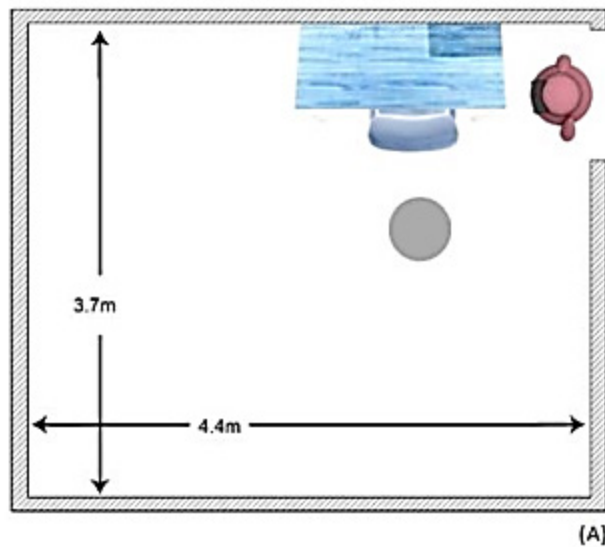
Figure 4: Effect of prior knowledge of real space on the decisions made in VR space (A) Experimental space (B) Virtual-space [Table chair (blue) were not a part of VR space but were present in the room and all participants have seen the room. The chair (gray) was introduced in between the VR experience]

However, this answers the following question: "how will the participants treat the real-life obstacles if they do not see them in VR? Will they remember them?" Besides, after touching the second-to-last box and on the way back to the starting point where the last box was, a new obstacle (chair) was rendered, which did not exist in the real world. This will answer the question that "How will the participants handle the newly spawned virtual obstacle? Will they prioritize their knowledge of the real space, or trust the visual information provided in VR?"

In the experiments, the participants were asked to perform a simple task of touching some red glowing boxes, which turned green when touched and then spawned a new red box in a new location in the virtual room. This task encouraged the participants to look and walk around the space while avoiding some room obstacles [19].

2.4. System

The system consisted of an HTC Vive headset with a Leap Motion sensor mounted on it for hand tracking and Vive motion controllers with 3D printed mounts fitted around the ankle to track the movement of feet. We tried to represent the use with a semi-realistic avatar in VR to help maintain the level of immersion [20-23]. The experiment space dimensions were 4.4 m x 3.7 m, with the HTC Vive lighthouses set on two opposite corners. We run VR content on an ASUS laptop (model GL502VS) equipped with Intel Core i7-6700HQ 2.60 GHz CPU, 16 GB RAM, and GTX 1070 graphics card. The content was created using Unreal Engine 4, which showed a 3D room modeled in Autodesk 3DS Max.

2.5. Virtual Art Gallery

To verify the validity of STHR in a real-life situation, we made a VR art gallery (VAG) that was open to the public for four days (Figure 5, Figure S2-S4). It was held in a multi-purpose space on the second floor of the designed common building of Kyushu University. The gallery showed four different 3D sculpted

artworks with themes based on Bonsai plants, which are an integral part of Japanese culture. The VR gallery design was based on conventional Japanese interior design. We used elements such as Tatami (Japanese flooring), Byoubu (Japanese folding partitions), and Shoji doors. STHR was defined as delivering a smooth transition from the real world to the virtual world and providing haptic feedback by creating a mix of real-world and virtual objects. In VAG, STHR involved four main concepts.

Most important among them is the haptic feedback that matched the real world and the VAG. It was introduced at the beginning of the VR experience by using a 3D printed replica of an artwork. Additionally, to assure a smooth transition from the real-world to VR, important features of the real space were maintained in VR as well. In our case, it was the windows of the building and the ceiling. Followed are more details on the public VAG.

The system used in the gallery was similar to the previous experiments. It consisted of an HTC Vive headset and a Leap Motion Controller mounted on it for hand tracking. Vive motion controllers to track the movement of feet were not used because collisions were not anticipated. The gallery space dimensions were 4 m × 6.5 m, with the HTC Vive lighthouses set on two opposite corners. The computer was equipped with Intel Core i7-6700HQ 2.60 GHz CPU, 24 GB RAM, GTX 980Ti graphics card, and Windows 10. The content was created using Unreal Engine 4, which showed a 3D room modeled in Autodesk 3DS Max and ran at 90 fps with 6 ms latency.

Before setting up the gallery, we made a poster informing visitors that the gallery was in a traditional Japanese style (Figure S2A). The poster showed a space with a Japanese scroll with calligraphy of the Bonsai kanji symbol, Tatami flooring, and Japanese sliding doors. The idea behind this was to set the expectations of the visitors regarding the content of the gallery. The gallery area was covered with black cloth on all sides to ensure that the visitors did not form a spatial image of the area of the gallery space (Figure S3A).
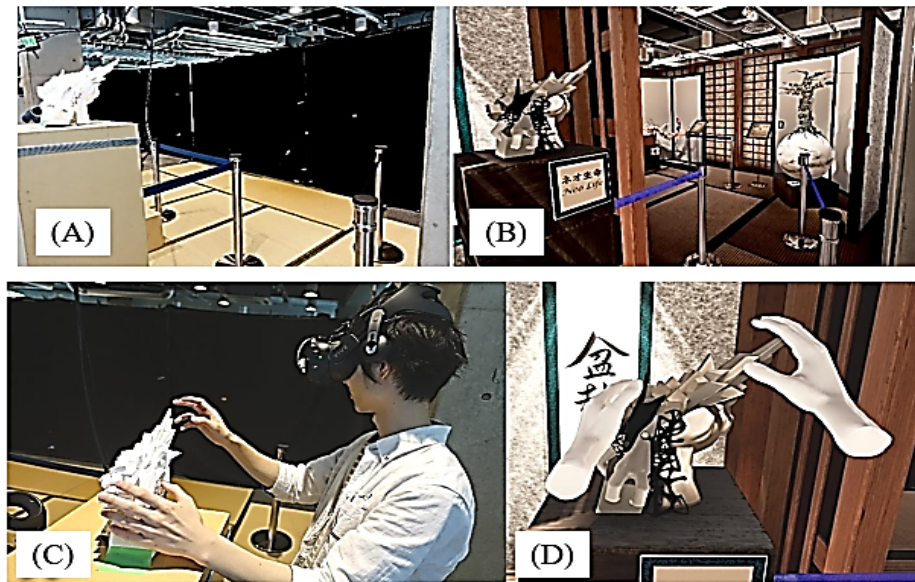
Figure 5: Virtual art gallery. (A) Gallery space in real life. (B) Gallery space in VR. (C) A visitor is interacting with the 3D printed replica of 1st artwork. (D) VR view of the interaction.

We created a small corridor between the wall and the covered space that led to the entry point so that visitors could not peek inside the content of the covered area through the entrance. Here, we indirectly introduced them to a simple common element (museum barriers) that they would encounter and interact with within the VR space. We used the barriers to mark the entry point and to stop anyone from entering the corridor. At the starting point outside the corridor, we asked the visitors to follow three instructions. First, to take their shoes off and wear slippers because it was a traditionally styled gallery and Tatami flooring had been used. This helped us provide constantly matching haptic feedback through the feet. Second, they had to close their eyes (we guided them through the corridor) and only open them after wearing the VR headset. Third, they could touch the first artwork but were not allowed to touch the other three artworks. The "do not touch" sign was clearly visible inside the VR gallery, similar to what is commonly seen in art galleries.

As soon as a visitor opened their eyes, they saw the first artwork. This first artwork, titled "Neo Life," was 3D printed and fixed on a display table (Figure 5C, Figure S4). Out of the four, it was the only artwork that existed in a physical form. In addition, we fixed a Vive tracking sensor on the backside of a display table to make sure that the table and the artwork are always in the correct position. The first thing the visitors did was step onto the Tatami flooring. This was the first matching and constant haptic feedback between the real world and the VR gallery throughout the whole experience. Then, we encouraged them to touch the first artwork, which provided a more detailed matching haptic feedback. A leap motion sensor was mounted on the Vive headset. It tracked and displayed the hands of the visitors while interacting with the physical objects. When they finished experiencing the first artwork, they entered the main gallery space on their right, passing between two pairs of museum barriers. We made the passage narrow to increase the chance of physical interaction with the barriers or its straps—these barriers matched with their real-world counters in shape and scale. However, there were no matching objects other than the Tatami floor; of course, the visitors did not know that the gallery was empty. The visitors freely looked at the artworks, and they were free to leave whenever they wanted to. We answered any questions and provided some verbal explanation regarding the concept of the artworks. When they finished, they went back to the starting point, closed their eyes, took off the VR headset, and were guided outside. In the end, we asked them to fill out a questionnaire to collect data about their VR gallery experience.

2.6. Statistical Analysis

3. Results

3.1. STHR

There were 21 participants (6 women). The mean age of participants was 29.0 ± 11.7 years, and there was no difference between men and women with respect to age ($p=0.934$). Overall, 9 (40.9%) participants had a previous VR experience. None of the participates had seen the real space before experiment 1. Nine (42.9%) participants had no video game experience, whereas 6 (28.6%) had significant video game exposure.

3.2. Effect of haptic feedback in hybrid reality on VR experience

In experiment one, there were 11 participants in the hybrid reality group (HRG) and 10 in the control group (CG) (Figure 2). There was no difference between the participants of these two groups with respect to gender, previous VR experience, or age (all $p>0.05$). The median time taken to complete the task was considerably longer in HRG than in CG [HRG:7.0 (6.4-7.6)vs. CG

4.0 (2.5-5.0); p=0.007]. The average number of collisions was not significantly different between the CG and HRG (p=0.888). The median value of anticipation, immersion, and reality were all slightly higher in the HRG; however, the difference was not statistically significant (all p>0.05). The median (IQR) attention score was 23.0 (22.0- 27.0) in the CG and 28.0 (27.0-34.0) in the HRG (p=0.045).In the interviews, 10 out of 11 of the HRG participants, who had an initial physical interaction with the objects in the real space, reported that they thought that all the furniture, columns, and cones shown in the VR did exist real. On the other hand, participants in the CG were not sure of the realism of the objects and used phrases such as "maybe there was," "might be there," and "avoiding it just in case" while talking about the objects in VR. The participants in the CG also moved closer to the obstacles. Participants thought that not avoiding collisions with the virtual objects is part of the experiment.

3.3. Effect of complete spatial awareness on VR experience

In the second experiment, we attempted to determine the effect of an unfamiliar environment on the actions of participants (Figure 3). There were 11 participants in the mask group (MG) and 10 in the CG. There was no difference between the participants of these two groups with respect to gender, previous virtual experience, or age (all p>0.05). The median time taken to complete the task was considerably longer in MG than in CG [MG:4.8 (4.2-5.8)Vs. CG: 43.4 (2.6-4.2); p=0.038]. The average number of collisions was not significantly different between the CG and MG (p=0.504). The anticipation, immersion reality, and attention were not different between the groups (all p>0.05). Upon observing the video capture, the completion time, and the discussion during interviews, we noticed that the people who saw the real space before wearing the headset had more freedom in their movement and were faster in completing the task. The participants in the MG were more cautious while moving around the obstacles, and 8 out of 11 used phrases such as "maybe there was," "might be there," and "avoiding it just in case" when talking about the existence of virtual objects. Two participants from this group attempted to touch and verify the presence of traffic cones.

3.4. Effect of hybrid reality on VR experience

Interestingly, 52.4% of the participants remembered the RWO (table) and avoided it without even seeing it. The participants who answered "no" had a physical interaction with the RWO. For the second question, which inquired whether the participants remembered the table at the end of the experiment, 66.7% of the participants voted "yes." However, a few people who voted "no" mentioned that they did remember the table but were unsure of its exact location. Notably, 8 of 10 participants who had a physical interaction with the table did not forget it. As for the VO (chair) present in the middle of the room, most participants tried to check if it was real. This experiment revealed that almost 50% of the participants relied on prior knowledge of the real space even when different visual information is delivered through VR. Moreover, the participants who did not remember the RWO became aware of it after the physical interaction, suggesting that physical interactions resulted in more vivid mental images. When we introduced an obstacle (a chair) at the end of experiment 3, for most, it was not as important as the table present in the real world, which was invisible in VR.

3.5. Virtual art gallery

There were 38 visitors to the VAG. The average time spent in the gallery was 5 min 57 s. As a percentage, 18.4% of the participants in this gallery participated in our previous three experiments. The age of visitors ranged17–70 years, with an average age of 31.26 years; out of the total, 58% were females. A total of 51.6% of the participants reported not having any previous experience with VR, while the rest had some prior experience with VR; however, none of them was a frequent user. Additionally, 46.4% mentioned that they did not play video games; however, most of them were interested in art. We asked the participants about the artwork they liked the most. The third artwork, titled "Distress," got the highest percentage with 47.4% of the votes. However, it received only 23% (77 s) of the view time, almost similar to the second artwork titled "Natural: Artificial" (76 s). The fourth artwork, titled "Incomplete Sculpt," recorded the longest observation time of 95 s (29%); however, it was liked by only 13% of the participants. The second and third artworks had similar sizes and viewing times. The first artwork received 78.5 s (24.5%) of the view time despite being the smallest in size. We believe this was due to the opportunity provided to visitors to touch and interact with it. We did not want to ask if the visitors thought there were physical artworks present in the VR gallery directly because we thought such a question might induce bias. Therefore, we asked them an indirect question: "Did you feel you wanted to touch the artworks?" 73.7% scored it with a five, which was the highest rating on our scale (Table S1).

4. Discussion

Realism in virtual reality has been a subject of great research interest. In this work, we examined whether spatial awareness of the real-world affects the overall VR experience. We have introduced a concept of STHR, wherein a mix of real-world objects and virtual objects are presented during VR experience, and a smooth transition from the RW space to VR space was made. Our results suggest that this approach significantly increases the time taken to complete the VR tasks and affects the participants' overall attention. Furthermore, in STHR based virtual art gallery made for the public, the visitors' overall feedback was highly positive.

To examine the impact of spatial awareness and haptic feedback, we first compared the VR experience of participants with and without STHR. For the STHR, the room was set up such that the participants interact with an RWO and experience haptic feedback. This interaction affected the perceived realism of VR, as was observed from increased task-completion time and change in the attention. It was also reported that by introducing minimal haptic feedback by felicitating physical matching interactions, the users' perception inside the VR environment could be altered [15]. Our results validate this hypothesis. Notably, the interviews conducted in the current work revealed that more than 90% of participants having initial physical interaction with the RWO thought that all the VO are RWO. Though in previous studies, different approaches have been tried to enhance VR realism, an analysis of different dimensions of VR realism is missing, and there is a lack of a simple and unified approach that can be used to enhance VR realism in different settings. In a notable development, a concept of substitutional reality (SR) by showing mixed footage of live scenes and recorded scenes was proposed

[24]. In another work on SR [25], furniture and other objects that already existed in the physical environment were replaced with similar-sized 3D models, providing the user with a similar spatial image of both real and VR spaces, thereby resulting in a better transition to the VR content. Haptic retargeting technique to enhance VR believability was also explored to enhance the VR experience [26].

Our study provided key insights on the effect of an unfamiliar environment on VR realism. By observing the video capture, the completion time, and the discussion during interviews, we noticed that the people who saw the real space before wearing the headset had more freedom in their movement and were faster in completing the task. We believe that adding a barrier/mask increased VR realism [27-31]. Regarding anticipation and hybrid reality, we surveyed the participants after introducing them to a VR environment where there is a mismatch between RWO and VRO, and an additional VR object was introduced during the experiment. The experiment revealed that almost half of the participants relied on the real space's prior knowledge even when different visual information is delivered through VR. Moreover, the participants who did not remember the real space during the experiment became aware of it after the physical interaction, suggesting that physical interactions resulted in a more intense experience [14, 32, 33].

The experiences of the visitors to VAG, which was based on the key concepts of STHR, i.e., providing haptic feedback in the initial phase of the VR experience and maintaining a smooth transition from RW space to VR space, corroborated the above-mentioned results. The average time spent in the gallery was good, suggesting a high level of engagement [34]. The feedback of visitors was generally positive, supporting the use of VAG. More than 80% of visitors rated the experience 4 or 5 on a scale of 5. Notably, there was no negative feedback. Interestingly, nine VAG visitors were curious about how the gallery looks like in real space. This part was not planned and happened naturally. Therefore, we asked them to fill the questionnaire first and then showed them how it looks. Surprisingly, all of them were shocked and did not expect that it was an empty space. Their response ranged from "I was tricked!", "It is an empty gallery," "No way!", "I fell into your plan!" to "There is nothing!" One person laughed and commented, "you are a good liar!" As mentioned before, we had used a 3D printed artwork to which visitors could interact. This 3D-printed artwork was made of plastic; however, the corresponding artwork in VR had some metal parts. The participant asked us how we made the art piece and, upon knowing that it was a 3D printed object, the visitor claimed that "…did not know you can 3D print with metal!" Notably, 12 visitors commented that it was an exciting experience to touch a sculptured artwork, which is usually not allowed in conventional galleries. These reactions suggest that the VAG successfully met its objectives. This supports our hypothesis that by enabling a smooth transition from real-space to virtual space and by providing relevant haptic feedback, realism in VR can be influenced [31, 35, 36].

STHR can be easily implemented in different settings; however, it is essential to understand our work's limitations before generalizing our findings. Though we have conducted controlled experiments and demonstrated the validity of STHR in VAG, more large-scale studies are needed to strengthen our conclusions'

generalizability. Our approach's main limitation is that the user needs to be unfamiliar with the real space before VR. This concept, therefore, is not feasible in an already familiar space such as VR experience at home. However, it may be an effective approach for VR in exhibitions or museums.

5. Conclusion

By blocking out the real space and through minimal haptic interactions, we were able to improve users' experience of VR. Prior information of real space has a profound effect on the decisions made by users during VR experience. This study suggests that by using STHR, VR experience can be improved. Our results also indicate that conflicting information between the real world and VR hinders VR experience. Creating the right setup for each VR experience is challenging; however, by implementing the method proposed in this work, a semi-unified covered space for various conditions can be created. Furthermore, the matching objects in many different experiences and locations can also be reused, such as fence barriers and glass boxes present in galleries, to enable physical interactions.

6. Future Outlook

The technological framework presented in this work offers many possibilities for enhancing the user's immersion in VR by carefully smoothening the transition to VR environment and using a perceptual stimulus. Future research should focus on the generalizability of this approach. As demonstrated in our work by the example of a real-world VR art gallery, STHR is particularly useful in museums and art galleries. We believe that the use of STHR in VR art galleries will have a significant impact on the way patrons connect with art, as the interaction with artworks involves advanced cognitive function and substantial processing of visual information. In future studies, we believe that by deliberately exposing the VR user to specific visual or auditory information while blocking the extraneous information, some targeted emotions can be amplified. Using this approach, the believability of VR can be further manipulated. As the use of VR is going to increase in the near future, STHR could play a pivotal role in enhancing the quality of the VR experience.

Conflict of Interest

The authors declare no conflict of interest.

Acknowledgment

References

[1] F.L. Schiavoni, L.L. Gonçalves, "From Virtual Reality to Digital Arts with Mosaicode," in 2017 19th Symposium on Virtual and Augmented Reality (SVR). 2017, doi:10.1109/SVR.2017.33.

[2] M. Langdon, "The work of art in a digital age: Art, technology and globalisation," 2014, Springer.

[3] S. Hall, R. Takahashi, "Augmented and virtual reality: the promise and peril of immersive technologies," in World Economic Forum, 2017.

[4] M. Barni, F. Bartolini, V. Cappellini, "Image processing for virtual restoration of artworks," IEEE Multimedia. **7**(2), 34-37, 2000, doi:10.1109/93.848424.

[5] M. Song, S. DiPaola, "Exploring different ways of navigating emotionally-responsive artwork in immersive virtual environments," in Proceedings of the Conference on Electronic Visualisation and the Arts. 2015, London, United Kingdom.doi:10.14236/ewic/eva2015.24.

[6] D.W. Zaidel, "Art and brain: insights from neuropsychology, biology and evolution," J Anat. **216**(2), 177-83, 2010, doi:10.1111/j.1469-7580.2009.01099.x.

[7] V. Aviv, "What does the brain tell us about abstract art?," Front Hum Neurosci. 8 85, 2014, doi:10.3389/fnhum.2014.00085.

[8] S. Poeschl, K. Wall, N. Doering, "Integration of spatial sound in immersive virtual environments an experimental study on effects of spatial sound on presence," in 2013 IEEE Virtual Reality (VR), 2013, doi:10.1109/VR.2013.6549396.

[9] M. Slater, M. Usoh, "Presence in immersive virtual environments," in Proceedings of IEEE Virtual Reality Annual International Symposium. 1993, doi:10.1109/VRAIS.1993.380793.

[10] S. Jung, P.J. Wisniewski, C.E. Hughes, "In limbo: The effect of gradual visual transition between real and virtual on virtual body ownership illusion and presence," in 2018 IEEE Conference on Virtual Reality and 3D User Interfaces (VR), 2018, IEEE.doi: 10.1109/VR.2018.8447562

[11] Q. Sun, A. Patney, L.-Y. Wei, O. Shapira, J. Lu, P. Asente, S. Zhu, M. McGuire, D. Luebke, G. Kaufman, "Towards virtual reality infinite walking: dynamic saccadic redirection," J ACM Trans. Graph. **37**(4), 1-13, 2018, doi:10.1145/3197517.3201294.

[12] D. Valkov, S. Flagge, "Smooth immersion: the benefits of making the transition to virtual environments a continuous process," in Proceedings of the 5th Symposium on Spatial User Interaction 2017, Brighton, United Kingdom: Association for Computing Machinery.doi:10.1145/3131277.3132183.

[13] B. Williams, G. Narasimham, B. Rump, T.P. McNamara, T.H. Carr, J. Rieser, B. Bodenheimer, "Exploring large virtual environments with an HMD when physical space is limited," in Proceedings of the 4th symposium on Applied perception in graphics and visualization. 2007, Tubingen, Germany: Association for Computing Machinery, doi:10.1145/12725 82.1272590.

[14] S.H. Lee, D.J. Kravitz, C.I. Baker, "Disentangling visual imagery and perception of real-world objects," Neuroimage, **59**(4), 4064-73, 2012, doi:10.1016/ j.neuroimage.2011.10.055.

[15] H.G. Hoffman, "Physically touching virtual objects using tactile augmentation enhances the realism of virtual environments," in Proceedings. IEEE 1998 Virtual Reality Annual International Symposium (Cat. No. 98CB36180), 1998, IEEE.doi:10.1109/VRAIS.1 998.658423.

[16] A. Gaggioli, "Transformative Experience Design," in Book "Transformative Experience Design." 2015, Sciendo Migration, 97-122, doi:10.1515/97831104711 37-006.

[17] A. Almutawa, R. Ueoka, "The Influence of Spatial Awareness on VR: Investigating the influence of the familiarity and awareness of content of the real space to the VR," in Proceedings of the 2019 3rd International Conference on Artificial Intelligence and Virtual Reality, 2019, Singapore, Singapore: Association for Computing Machinery.doi:10.1145/3348488.3348502.

[18] R.M. Baños, C. Botella, A. Garcia-Palacios, H. Villa, C. Perpiña, M. Alcañiz, "Presence and Reality Judgment in Virtual Environments: A Unitary Construct?," CyberPsychology & Behavior. **3**(3), 327-335, 2000, doi:10.1089/10949310050078760.

[19] P.W. Fink, P.S. Foo, W.H. Warren, "Obstacle avoidance during walking in real and virtual environments," J ACM Trans. Appl. Percept. 4 2–es, 2007, doi:10.1145/1227134.1227136.

[20] A. Steed, S. Frlston, M.M. Lopez, J. Drummond, Y. Pan, "An 'in the wild'experiment on presence and embodiment using consumer virtual reality equipment," **22**(4), 1406-1414, 2016, doi:10.1109/TVCG.2016.2518135.

[21] A. Steed, Y. Pan, F. Zisch, W. Steptoe, "The impact of a self-avatar on cognitive load in immersive virtual reality," in 2016 IEEE virtual reality (VR), 2016, IEEE.doi:10.1109/VR.2016.7504689.

[22] F. Argelaguet, L. Hoyet, M. Trico, A. Lécuyer, "The role of interaction in virtual embodiment: Effects of the virtual hand representation," in 2016 IEEE Virtual Reality (VR), 2016, IEEE.doi:10.1109/VR.201 6.7504682.

[23] C. Jay, R. Hubbold, "Amplifying head movements with head-mounted displays," Presence: Teleoperators & Virtual Environments, **12**(3), 268-276, 2003.

[24] K. Suzuki, S. Wakisaka, N. Fujii, "Substitutional reality system: a novel experimental platform for experiencing alternative reality," Sci Rep. **2**(1), 459, 2012, doi:10.1038/srep00459.

[25] A.L. Simeone, E. Velloso, H. Gellersen, "Substitutional reality: Using the physical environment to design virtual reality experiences," in Proceedings of the 33rd Annual ACM Conference on Human Factors in Computing Systems. 2015, doi:10.1145/2702123.2702389.

[26] M. Azmandian, M. Hancock, H. Benko, E. Ofek, A.D. Wilson, "Haptic retargeting: Dynamic repurposing of passive haptics for enhanced virtual reality experiences," in Proceedings of the 2016 chi conference on human factors in computing systems. 2016, doi:10.1145/2858036.2858226.

[27] P. Vuilleumier, "Anosognosia: the neurology of beliefs and uncertainties," Cortex. **40**(1), 9-17, 2004, doi:10.1016/s0010-9452(08)70918-3.

[28] J.A. Whitson, A.D. Galinsky, "Lacking control increases illusory pattern perception," Science. **322**(5898), 115-7, 2008, doi:10.1126/science.1159845.

[29] G. Riva, J.A. Waterworth, E.L. Waterworth, F. Mantovani, "From intention to action: The role of presence," New Ideas in Psychology, **29**(1), 24-37, 2011, doi:10.1016/j.newideapsych.2009.11.002.

[30] G. Herrera, R. Jordan, L. Vera, "Agency and presence: A common dependence on subjectivity?," Presence: Teleoperators and Virtual Environments. **15**(5), 539-552, 2006, doi:10.1162/pres.15.5.539.

[31] M. Slater, B. Lotto, M.M. Arnold, M.V. Sanchez-Vives, "How we experience immersive virtual environments: the concept of presence and its measurement," Anuario de psicología, **40**(2), 193-210, 2009.

[32] M. Thomas, C.G. Brown, N.G. Fajt, J.B. Kirschenbaum, "Virtual representations of real-world objects" 2017, U.S. Patent No. 9,728,010. Washington, DC: U.S. Patent and Trademark Office.

[33] A. Burns, T. Salter, B. Sugden, J. Sutherland, "Virtual reality environment with real world objects," 2018, U.S. Patent No. 9,865,089. Washington, DC: U.S. Patent and Trademark Office.

[34] J.K. Smith, L.F. Smith, "Spending time on art," Empirical Studies of the Arts. **19**(2), 229-236, 2001.

[35] M.V. Sanchez-Vives, M. Slater, "From presence to consciousness through virtual reality," Nature Reviews Neuroscience. **6**(4), 332-339, 2005.

[36] P. Johansson, L. Hall, S. Sikstrom, A. Olsson, "Failure to detect mismatches between intention and outcome in a simple decision task," Science. **310**(5745), 116-9, 2005, doi:10.1126/science.1111709.

Supplementary Data:

Table S1: Questionnaire response (VAG)

| Question	Response (Scale 1-5)				
	1	2	3	4	5
How often do you play video games?	13	2	5	5	3
Are you interested in art?	0	2	6	13	17
How real did the graphics look?	2	1	11	19	5
Do you think you were able to understand the materials of the objects around you?	1	5	6	17	9
Do you think you were able to understand the scale of the objects around you?	0	1	0	13	24
Do you think the scales of the real-world and VR were similar?	0	4	4	12	18
Did you feel you wanted to touch the Artworks?	0	2	1	7	28
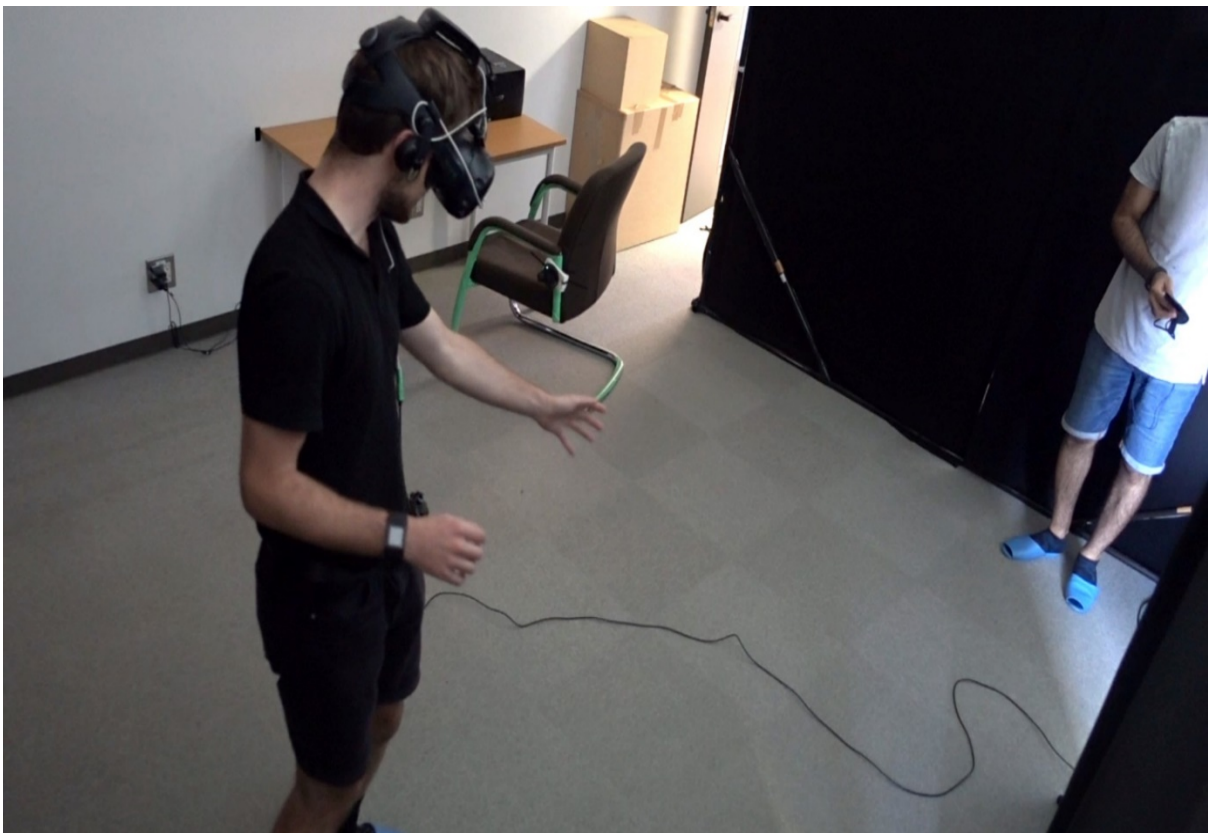
Figure S1. Actual photograph of the space used in experiment 1-3.

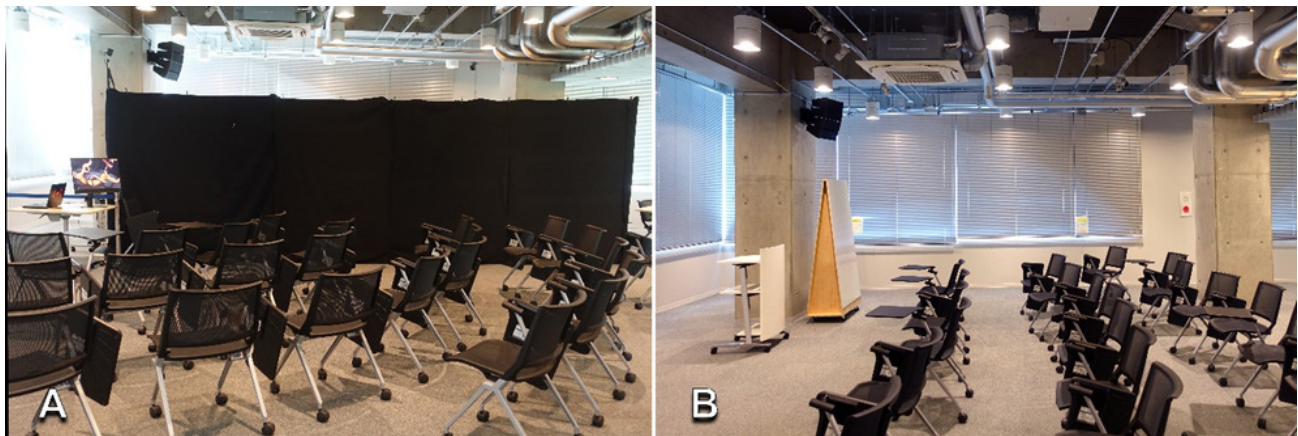Figure S2. (A) Gallery poster, (B) Entrance, and (C) Gallery plan.

Figure S3. (A) Gallery cover space. (B) Gallery space without the cover.
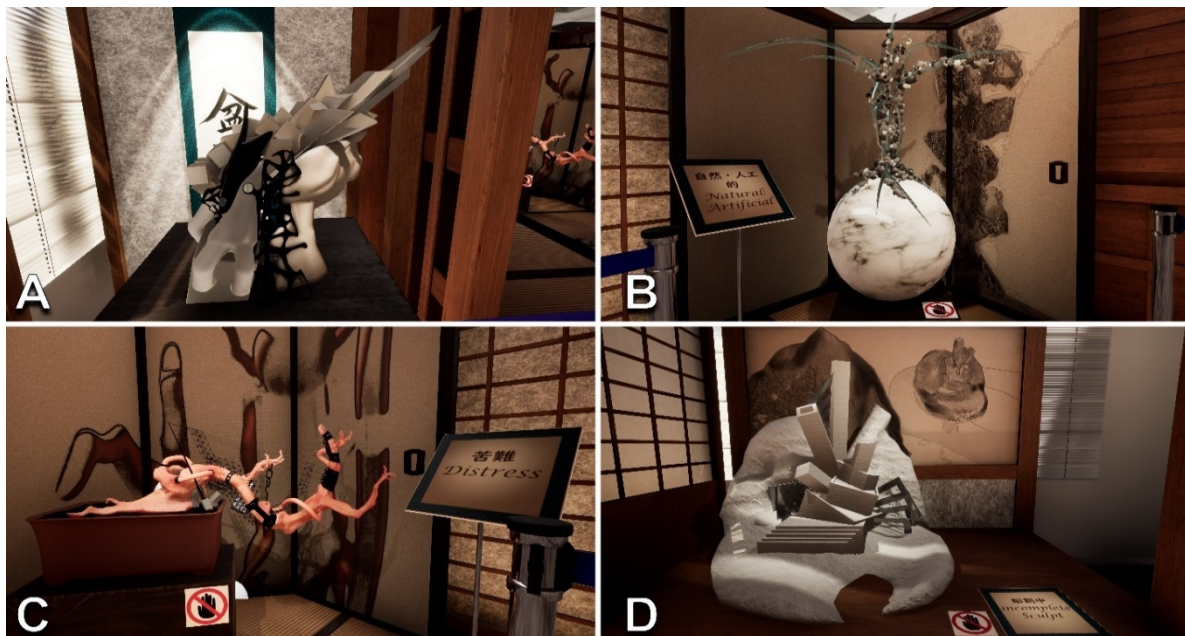
Figure S4. Artworks used in VAG.

Estimation of Land Degradation Loss by Water Erosion: Case of the Site of Biological and Ecological Interest of Ain Asmama (Western High Atlas, Morocco)

Adnane Labbaci[*,1], Said Moukrim[2], Said Lahssini[3], Said Laaribya[4], Hicham Mharzi Alaoui[5], Jamal Hallam[6,*]

[1]*Geoscience and Geoenvironment Laboratory, Department of Geology, Faculty of Sciences Ibn Zohr University, Agadir, 80000, Morocco*

[2]*BIOBIO Research Center, Faculty of Sciences, Mohammed V University, Rabat, 1000, Morocco*

[3]*Forest Inventory Department, National School of Forest Engineer, Salé, 10000, Morocco*

[4]*Department of Geography, Faculty of humanities and social sciences Chouaib Doukkali University, El Jadida, 24000, Morocco*

[5]*Fire Forest Service, High Commission on Water Forest and Combating Against Desertification, Rabat, 10000, Morocco*

[6]*National Institute of Agricultural Research of Morocco (INRA), Avenue des FAR B.P. 124 Inezgane, Agadir, 1000, Morocco*

A R T I C L E I N F O	A B S T R A C T
	Erosion affects large parts of Moroccan land, particularly in the mountains leading to soil quality deterioration and less vegetation cover. Located in the South-west of Morocco, the Site of Biological and Ecological Interest (SBEI) of Ain Asmama, where erosion threatens a major part of the region was investigated. The site has a terraced transitional bioclimate, between arid to sub-humid, of local conservation importance. The varied, dense, continuous, and well-preserved vegetation of the area is crucial to protect the soils against erosion. Qualitative observations show that soils are increasingly degraded, water erosion is developing, and sediments accumulate in dams and ponds. In this study we have used the Revised Universal Soil Loss Equation (RUSLE) to assess the erosion risk in this area. It helped to develop a synthetic map of erosion susceptibility. Our results show that the integration of the different parameters in the water erosion process estimated the loss of soil amounting 339,03 tons/ha/year over the whole site. This is equivalent to a value of soil lowering of 2,82 cm which is considered extremely high.

1. Introduction

Water erosion is an extremely complicated natural phenomenon. It has serious economic, human, and ecological consequences. Economic losses are estimated in millions of Dollars and are mainly associated to downslope damage to property, roads and other infrastructure, and destruction of plant cover trough grazing affecting the most productive agricultural and forest lands [1–3]. People, including women and youth, in the rural area whose livelihoods depend on natural resources for subsistence, are vulnerable to land degradation [4]. In this area, land degradation by water erosion leads to a persistent impoverishment of the populations, which causes their exodus towards cities.

Land degradation by water erosion impacts extend to ecosystems. It has significantly altered ecosystems functions and services, decreased the biological diversity of soils and forest, and reduced agricultural lands productivity [5].

Estimates of soil losses due to water erosion in Morocco, range from 500 to > 5,000 tons / km² / year depending on the region. Accumulation of sediments in natural and artificial waterbodies (siltation of dams and ponds) is estimated to average 75 million m³, equivalent to an annual reduction of 0.5% in the storage capacity of dams. In addition to the degradation of the quality of the mobilized drinking water, the storage capacity decline leads to a significant loss of water that would irrigate 10,000 ha / year [6]. In the Souss-Massa region, the cost of erosion has been estimated overall at 20.7 million DH; the core contributions to this cost are

---

associated to dam reservoirs (76.5%), upstream of the basin (22.4%), and to the Souss-Massa plain (1.12%) [7].

This study forms part of a larger project which evaluates land degradation at the Sites of Biological and Ecological Interest (SBEI) at national level. The aim of the study detailed here was to estimate loss of soil by water erosion in the SBEI of Ain Asmama, an important site for nature conservation in the Souss-Massa region. The outputs would provide useful data to assist in the design of adequate facilities based on multi-criteria analysis using GIS and remote sensing.

2. Study area

The SBEI of Ain Asmama is located at the western High Atlas of Morocco (between 9.03° and 9.33° East Longitude and 30.74° and 31° North Latitude) on the upper parts of the Ait Moussa river right bank. The total site area is 23 564 ha (Figure. 1).

Figure 1: Location map of the SBEI of Ain Asmama

Storied stands plateaus dominate the SBEI. They decrease gradually at altitude, from 1744 m to 780 m, toward the west and north. Argana corridor is a valley depression of the Issen river bordering the SBEI of Ain Asmama. The geological massif of the area contains deep valleys, canyons, sheer cliffs, and steep relief cut by short ravines and giving a rugged hilly feature with an eventful and picturesque appearance.

From the geological view, we have found the domination of the Jurassic and Permo-Triassic classes, with the presence of Quaternary terracing of local alluvium cones and colluvium deposits of the recent piedmonts (Figure. 2).

The climate of the area is dominated by the arid and the sub-humid [8]. The annual rainfall average varies from 240 mm to 470 mm and the highest recorded rainfall falls between November and February. The site is characterized by a diverse vegetation including endemic trees of the region such as Argan, Thuija, Holm oak and Juniper.

Figure 2: Geological classes' map of the Ain Asmama's SBEI

3. Materials and methods

Soil loss rates were estimated using the RUSLE factors were integrated into the GIS following the adjusted model to Moroccan conditions [9,10]:

$$A = R * K * LS * C * P \qquad (1)$$

where:

A = average soil loss (ton/ha/year)

R = rainfall-runoff erosivity factor (MJ.mm/ha.h.year)

K = soil erodibility factor (t.ha.h/ha.MJ.mm)

L = slope length factor (m)

S = slope steepness factor (degree)

C = cover-management factor

P = support practice factor.

3.1. Rainfall erosivity factor (R)

The erosive potential of raindrops impact is determined by the R factor. Several studies quantifying erosion in Morocco, to estimate the R factor we have used the Arnoldus model [11]:

$$R = 1.735*10*(11.5 * log \sum (pi2 /p) - 0.8188) \qquad (2)$$

where

R: Rainfall erosivity factor (MJ.mm/ha.h.year)

Pi: Average monthly (mm), and

P: mean annual precipitation (mm).

To allow comparison with previous studies, the R factor was estimated using the same model. Monthly and annual rainfall data

was computed for each weather station within the SBEI to calculate the R index using.

3.2. Soil erodibility factor (K)

The K factor is the intrinsic susceptibility of a soil to resist to climatic aggression. Given that the soil units map of SIBE does not exist, we developed a homogeneous distribution map of lithological units. the lithological map assumes that soil units are intricately linked to the parent material e of the underlying geological formations. The map of lithological formations was in turn assigned to different homogeneous soil units. A field survey was then carried out to collect soils samples within each homogeneous soil unit. The organic matter and soil textures were measured in the laboratory and the K factor was computed using the following formula:

$$100*K = 2.1*10-4*M1.14 (12-a) + 3.25 (b-2) + 2.5 (c-3) \quad (3)$$

where

K: soil erodibility factor (t.ha.MJ-1.mm-1)

M = (% sand + silt) * (100 -% clay)

a =% organic matter,

b = code of permeability,

c = code of the structure

3.3. Slope length (L) and steepness (S) factors

The slope length (L) and the slope steepness (S) factors give us an overview of the effect of topography on soil erosion. LS factor estimation was much easier and more accurate when using digital elevation model (DEM) in GIS. To evaluate the LS factor, we have used the following equation [12]:

$$LS= (L/22.15) m * (65.41*Sin^2(S) + 4.56 * Sin(S) + 0.065) \quad (4)$$

where

L = Slope length
S = Slope degree
m = factor dependent on the value of S:
m = 0.5 if S > 5.0%
m = 0.4 if 3.5<= S =< 4.5%
m = 0.3 if 1.0 <= S =< 3.0%
m = 0.2 if S = 1.0%

The slope length was determined using the Horton (1945) model that relates the slope steepness and length:

$$B = S/2L \quad (5)$$

where

B: The average of the watershed slope length (m);

S: The catchment area (m^2) and

L: The length of the river (m).

3.4. Land cover factor (C)

The estimation of the land cover factor takes in consideration the soil degradation's conditions, the nature of the land cover (presence of a different type of vegetation) allowed a slow runoff

and a better infiltration [13]. The C factor is of a significant importance in RUSEL equation and was estimated out of a developed land use map using Sentinel-2 satellite imagery, missions 2019 [14].

3.5. Support practice factor (P)

The (P) factor takes in consideration the different management related to the conservation measures on water and soil. In this study, we identified the cultivation practices at the SBEI for which the conservative value was assumed to be 0,50 [15].

4. Results and discussions

Erosion is a natural process that occurs worldwide and cannot be stopped [16]. The estimation of soil loss by erosion aims, however, to regulate human effects to maintain tolerable soil loss. For the very same purpose we mapped the water erosion of the Ain Asmama SBEI to help locate the impacts of the different influencing factors on the soil to manage them so that the erosion rate is within an acceptable range. In what follows, we present the results of each factor of the RUSLE equation and then the estimated soil loss of the watershed. Since there is no established threshold between acceptable and unacceptable erosion levels [16], we will convert our final estimation results to values of soil lowering [17] to verify the severity of erosion in the area. We will then discuss the loss of soil thickness relative to the literature.

4.1. Rainfall erosivity factor (R)

Rainfall data series from 1982 to 2019 (37 years) were collected for eight weather station within the SBEI. The data were used to estimate the Rainfall erosivity factor R following the Arnoldus method [11] (Table 1).

Table 1: Weather stations locations within the Ain Asmama SBEI's and the estimated Rainfall erosivity factor R

Station	X Easting (m)	Y Northing (m)	P (mm)	R
Argana	143 624	425 520	349.66	74.04
Ain Asmama	127 963	426 663	473.72	83.00
Imouzzer ida outanane	108 989	414 756	540.78	96.37
Amsoul	148 975	432 400	214.45	46.27
Aguenza	140 550	422 600	252.78	58.12
Bge Abdelmoumen	139 379	411 720	413.25	88.88
Tizguine	144 302	441 023	236.63	50.31
Iloudjane	175 648	469 482	332.15	54.89

The estimated R values (Table 1) within the SBEI range between 46,27 and 96,37 units / year. A linear interpolation model was built in ArcGIS to accurately differentiate between the climate zones around the area of a selected weather station. All the estimated Rainfall erosivity were then adjusted to the weather station altitude to account for elevations effect. Figure 3 shows the resulting R factor map.
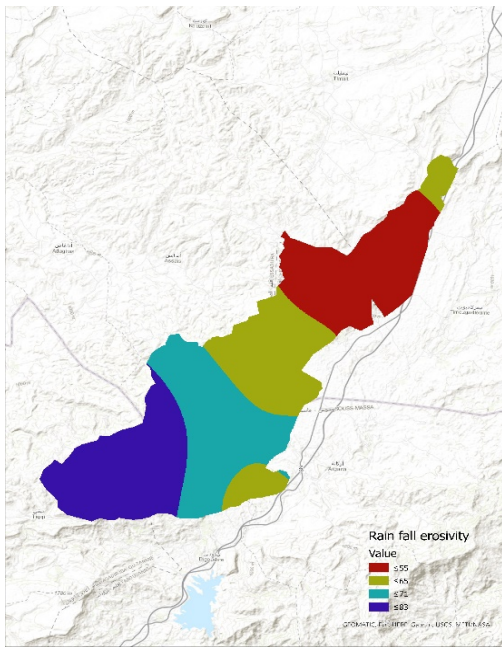
can increase the impact of the erosion in our study area which will in turn have an impact on the average soil loss downstream of the basin.

Table 2: Slope classes obtained from the reclassification of the Digital Elevation Model (DEM) of the SBEI of Ain Asmama

Slope in degree	Area (ha)	Percentage (%)
0 - 2	3 913.66	16.61
2 - 5	2 978.28	12.64
5 - 10	4 474.67	18.99
10 - 15	3 260.92	13.84
15 - 74	8 936.70	37.92
Total	**23 564,23**	**100.00**

Figure 5: Slope map of the SBEI of Ain Asmama (classes values are in degree)

Figure 6: Sub watersheds map of the SBEI of Ain Asmama

Figure 3: Rainfall erosivity factor (R) of the SBEI of Ain Asmama

4.2. Slope length (L) Slope and Slop steepness (S)

A topographic contour lines of a scanned and georeferenced standard topographic map of 1:50 000 were digitized to generate generated a digital elevation model (DEM). This resulted in an actual spot elevation of each selected point of the grid. The resulting data shows an elevation amplitude between 780 m to 1740 m.

Figure 4: Digital Elevation Model (DEM) map of the SBEI of Ain Asmama

The processing of the developed DEM showed a varying topography within the SBEI of Ain Asmama. The extracted slopes were between 0 and 74 degrees. The reclassification of the DEM resulted in 5 slope classes (Table 2). The slope classes, 0 to 5 degrees, suitable for agronomic land use were only 29.25% of the total area. Thirty eight percent of the area has a slope greater than 15 % suggesting an extremely high vulnerability to water erosion. Our results show the percentages of steep slopes are large and the

The Hydrology tools were applied in GIS to create a stream network of 40 sub-basins within the watershed. The slope length (L) was measured for each delineated sub basin using Horton method. The L values were between 45 and 183 m and the average length was101.95 m.

The estimated LS values were between 0 to 201 units 66% of which are higher than 30 units. This % coverage is in accordance with the classification of Manrique [18].

Table 3: LS factor classes and their %coverage in the Ain Asmama SBEI

LS classes	% coverage
0 - 5	20.01
5 - 15	07.05
15 - 20	02.70
20 - 30	04.52
> 30	65.71

Figure 7: Map of the combined slope steepness and Slope length factor (SL) of the SBEI of Ain Asmama

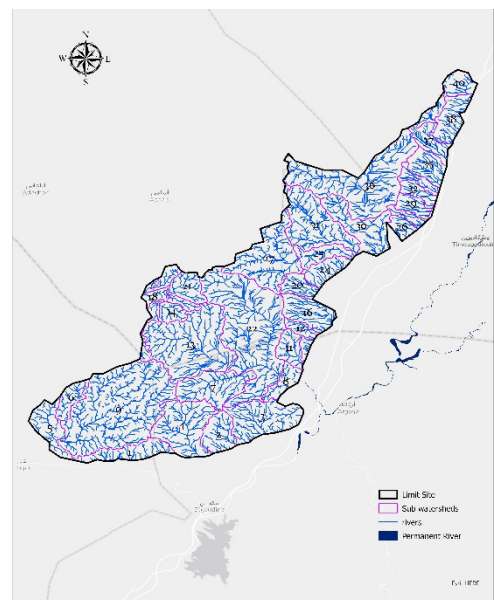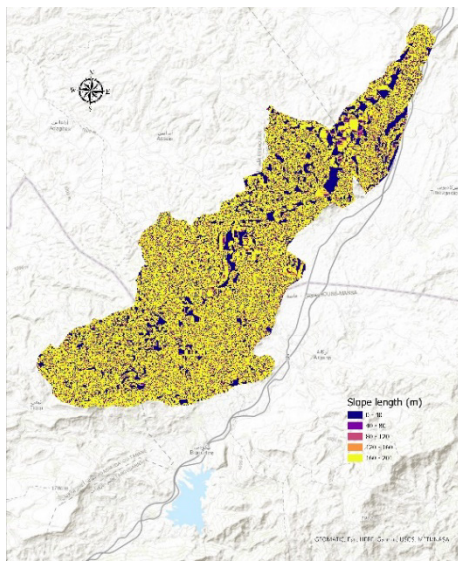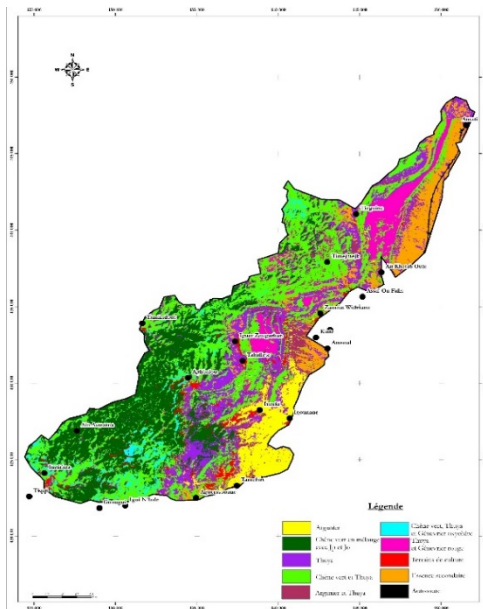Figure 8: Land cover map of the SBEI of Ain Asmama

4.3. Land cover factor (C)

Supervised classification of land cover using Sentinel-2 images brought out the following groupings: Crop lands, Matorral, Argan trees, Thuija, Juniper, Holm oakand Wasteland.

Uncovered soil (bare soil with low canopy and residue) is likely to be exposed to water erosion. Combining the NDVI map together with the 2019 land cover gives an estimation of density of vegetation. Using this outcome in addition to the land cover map (Figure 8) allowed identification of five land vegetation classes (Table 4) for which C factor values were assigned.

Table 4: Land cover classes and Values of land cover classes in the site of Ain Asmama

Vegetation classes	C factor value
Dense forest	0.01
Clear forest	0.10
Matorrals	0.16
Cultivated land	0.50
Wasteland	1.00
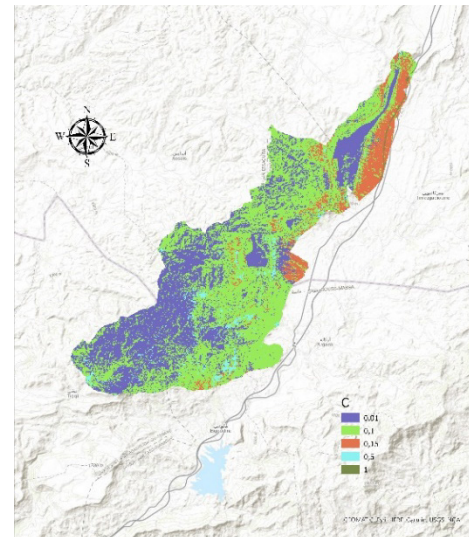
Figure 9: Land cover factor map of the SBEI of Ain Asmama

4.4. Soil erodibility factor (K)

Soil erodibility factor depends on several parameters such as cohesion strength between soil particles, soil and plant roots interaction, plants exudates, biological organisms (e.g., earthworms) and soil structure and its relation to soil moisture content [19]. Following the classification of Manrique [18] our results show that 95 % of the soils are highly to very highly erodible (Figure 10), in accordance.

Table 5: Soil erodibility factor (K) classes at Ain Asmama's site and the equivalent risk of erodibility following the classification of Manrique

K factor classes	Risk of erodibility	Area (ha)	Percentage coverage
K < 0.15	Very little erodible soils	0	0.00
0.15 < K < 0.25	Slightly erodible soils	474.29	02.01

0.25 < K < 0.35	Moderately erodible soils	762.98	03.24
0.35 <K < 0.45	Highly erodible soils	11 225.79	47.64
0.45 < K < 0.60	Very highly erodible soils	11 101.17	47.11
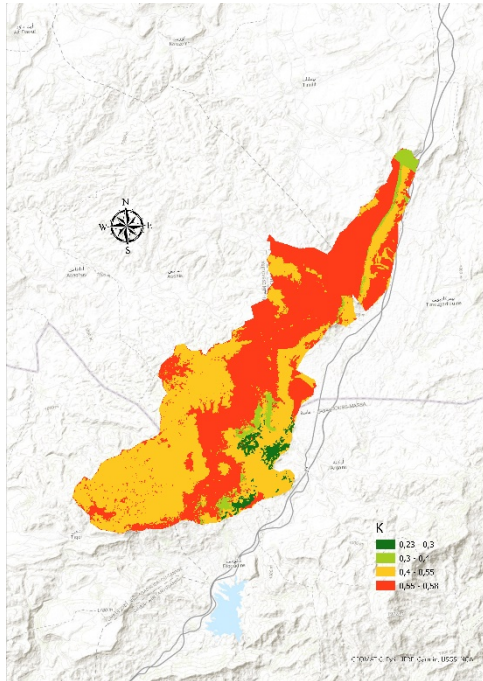
Figure 10: Soil erodibility factor (K) map of the SBEI of Ain Asmama

4.5. Support practice factor (P)

The factor P shows the effect of water and soil management and conservation measures on erosion. Qualitative observation made whilst identifying the land management practices of the SBEI indicate that 0.5 is the suitable P factor value to use for the soil loss assessment.

4.6. Soil loss rate estimation (A)

The overlapping of the thematic maps of RUSEL model factors, using GIS, has led to the establishment of the erosion map. This was in turn reclassified to produce the losses in soils by water erosion (tons / ha / year) (Figure. 11) of the SBEI of Ain Asmama: The estimated losses in soil regularly displaced downstream were between 0.1 and 339 tons/ha/year.

This range of rates of erosion alone is hard to interpret in terms of erosion severity and is meaningless because of the lack of an established threshold between acceptable and unacceptable. levels of erosion [16]. In the 1950s, the USDA considered values of soil-loss of ≈5 – 12 tons/ha/year as tolerance values to evaluate rates of soil erosion [20]. Researchers have expressed concern that the suggested values by USDA pose uncertainty on how to interpret the differences between modern and geological erosion rates [17]. The estimate of soil erosion in previous studies and its interpretation is very dependent on 1) the scale of the study (From laboratory measures, Field-plots compilation, sub-basins to catchments estimation), 2) the approaches adopted to generate the estimates (Rainfall simulation, Splash cups, Stereo photography,

RUSLE, USLE, etc), 3) and the aptitude of a soil to maintain its functions to provide ecosystem services [21].

To contrast the severity of erosion in the SBEI to previous studies using typical ranges of erosion, we converted our outputs to values of soil lowering [17]. For the conversion we used the standard soil bulk density of 1200 kg m^{-3} as suggested by Montgomery [17] in his widely cited paper. The results show that the soil in the SBEI is lowering by up to 2.82 cm per year, which is considered as an extremely high loss of soil. This soil lowering value is on average hundreds of orders of magnitude greater than the estimated soil lowering values in most of the previous literature summarized in [16], [17]. It is also several times greater than estimates of mean global soil production (from 0.06 to 0.08 mm per year) [22, 23].
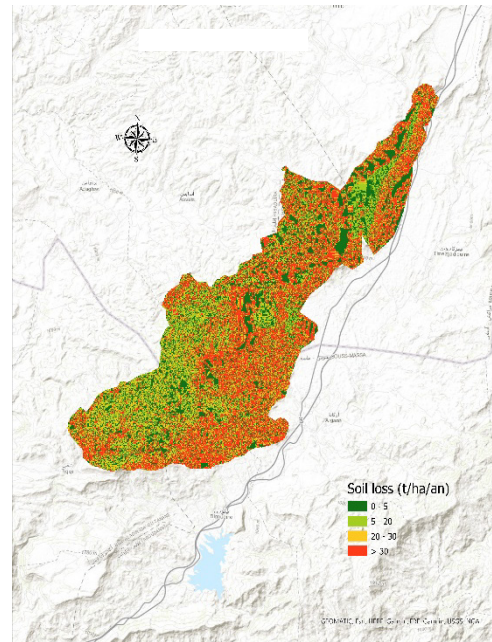
Figure 11: Soil loss map of the SBEI of Ain Asmama

5. Conclusion

This note presents the results of the hydric erosion assessment of the SBEI of Ain Asmama. We first established and implemented a cartographic database for each of the factors of the RUSLE model. which were in turn associated to thematic maps using GIS.

The outputs show that the rainfall an aggressiveness was up to 96.37 units / year. Most of the soils of the region are alluvium and colluvium depositions and weakly developed soils due to erosion on red clay. These soils are poorly permeable and prone to streaming development which in turn keeps the ravines actively widening. The estimated erodibility values were up to 0.58. The values of the slope length and steepness LS vary from 0 to 201. Land use map was established after a supervised classification of the Sentinel imagery associated to the field survey C factors were then assigned to each land cover class identified.

The thematic maps of each factor of the RUSLE equation; were overlapped to give the water erosion map [24]. The results show that the soil in the SBEI is lowering by up to 2.82 cm per

year, several times greater than estimates of average global soil production

References

[1] J. Boardman, "A short history of muddy floods," Land Degradation & Development, **21**(4), 303–309, 2010, doi:10.1002/ldr.1007.

[2] R. Evans, J. Boardman, "The new assessment of soil loss by water erosion in Europe. Panagos P. et al., 2015 Environmental Science & Policy 54, 438–447—A response," Environmental Science & Policy, **58**, 11–15, 2016, doi:10.1016/j.envsci.2015.12.013.

[3] P. Panagos, P. Borrelli, J. Poesen, C. Ballabio, E. Lugato, K. Meusburger, L. Montanarella, C. Alewell, "The new assessment of soil loss by water erosion in Europe," Environmental Science & Policy, **54**, 438–447, 2015, doi:10.1016/j.envsci.2015.08.012.

[4] L. Olsson, H. Barbosa, A. Cowie, K. Delusca, D. Flores-Renteria, K. Hermans, E. Jobbagy, W. Kurz, D. Li, D.J. Sonwa, L. Stringer, Land Degradation. In Climate Change and Land: an IPCC special report on climate change, desertification, land degradation, sustainable land management, food security, and greenhouse gas fluxes in terrestrial ecosystems, Intergovernmental Panel on Climate Change (IPCC), 2019.

[5] R. Parveen, U. Kumar, "Integrated approach of universal soil loss equation (USLE) and geographical information system (GIS) for soil loss risk assessment in Upper South Koel Basin, Jharkhand," **4**(6), 9, 2012, doi:10.4236/jgis.2012.46061.

[6] S. El Khatri, T. El hairech, "Drought conditions and management strategies in Morocco," Direction de La Météorologie Nationale, Casablanca, 7.

[7] F. Elame, M.R. Doukkali, A. Fadlaoui, "La gestion intégrée de l'eau à l'échelle du bassin de Souss-Massa: développement d'un modèle intégré de Bassin," Al Awamia127, 91–111, 2013.

[8] S. Moukrim, S. Lahssini, M. Rhazi, A.H. Mharzi, A. Benabou, I. Wahby, M. El Madihi, M. Arahou, L. Rhazi, "Climate change impacts on potential distribution of multipurpose agro-forestry species: Argania spinosa (L.) Skeels as case study," Agroforestry Systems, **93**(4), 1209–1219, 2019, doi:10.1007/s10457-018-0232-8.

[9] R. Kalman, The Climatic Factor of Erosion in the Sebou Watershed Morocco. Sebou Project, 32 p, 1967.

[10] S. Schmidt, C. Alewell, K. Meusburger, "Monthly RUSLE soil erosion risk of Swiss grasslands," Journal of Maps, **15**(2), 247–256, 2019, doi:10.1080/17445647.2019.1585980.

[11] H.M.J. Arnoldus, "Methodology used to determine the maximum potential average annual soil loss due to sheet and rill erosion in Morocco," 1977.

[12] W.H. Wischmeier, D.D. Smith, Predicting rainfall erosion losses: a guide to conservation planning, Department of Agriculture, Science and Education

[13] S. El Khatri, T. El hairech, "Drought conditions and management strategies in Morocco," Direction de La Météorologie Nationale, Casablanca, 7.

[14] A.Y. Yesuph, A.B. Dagnew, "Soil erosion mapping and severity analysis based on RUSLE model and local perception in the Beshillo Catchment of the Blue Nile Basin, Ethiopia," Environmental Systems Research, **8**(1), 17, 2019, doi:10.1186/s40068-019-0145-1.

[15] A. Gayen, S. Saha, H.R. Pourghasemi, "Soil erosion assessment using RUSLE model and its validation by FR probability model," Geocarto International, **35**(15), 1750–1768, 2019, doi:10.1080/10106049.2019.1581272.

[16] D.J. Pennock, Soil erosion: The greatest challenge for sustainable soil management, Food and Agriculture Organization of the United Nations, Rome, Italy, 2019.

[17] D.R. Montgomery, "Soil erosion and agricultural sustainability," Proceedings of the National Academy of Sciences, **104**(33), 13268–13272, 2007.

[18] L.A. Manrique, Land erodibility assessment methodology (LEAM): using soil survey data based on soil taxonomy, Editorial and Publication Shop, Honolulu, Hawaii, 1988.

[19] J. Hallam, M.E. Hodson, "Impact of different earthworm ecotypes on water stable aggregates and soil water holding capacity," Biology and Fertility of Soils, **56**(5), 607–617, 2020, doi:10.1007/s00374-020-01432-5.

[20] D.L. Schertz, "The basis for soil loss tolerances," Journal of Soil and Water Conservation, **38**(1), 10–14, 1983.

[21] FAO, Revised World Soil Charter, Rome, Italy, 2015.

[22] F.R. Troeh, J.A. Hobbs, R.L. Donahue, Soil and water conservation for productivity and environmental protection., Prentice-Hall, Inc., New jersey, USA, 1980.

[23] T. Wakatsuki, A. Rasyidin, "Rates of weathering and soil formation," Geoderma, **52**(3–4), 251–263, 1992, doi:10.1016/0016-7061(92)90040-E.

[24] V. Prasannakumar, H. Vijith, S. Abinod, N. Geetha, "Estimation of soil erosion risk within a small mountainous sub-watershed in Kerala, India, using Revised Universal Soil Loss Equation (RUSLE) and geo-information technology," Geoscience Frontiers, **3**(2), 209–215, 2012, doi:10.1016/j.gsf.2011.11.003.

Parametric Study for the Design of a Neutron Radiography Camera-Based Detector System

Evens Tebogo Moraba[*,1,2], Tranos Zuva[3], Chunling Du[2], Deon Marais[1]

[1]Department of Radiation sciences, The South African Nuclear Energy Corporation SOC. Limited, Pretoria, 0001, RSA

[2]Department of Computer Systems Engineering, Tshwane University of Technology, Pretoria, 0001, RSA

[3]Department of Information Technology, Vaal University of Technology, Vanderbijlpark, 1911, RSA

A R T I C L E   I N F O

A B S T R A C T

The field of view (FOV) and spatial resolution (SR) are the major image quality parameters which are being optimized in neutron radiography (NR) technique. This requires effective components selection during the design of NR detector systems. The selection is a discouraging task owing to often having conflicting experimental requirements and related constraints. In this work, models were developed to study the relationship between detector system components. These allow the simulation of detector system components whilst taking cognizance of specific experimental requirements and constraints in order to aid the design. Various commercial detector system components combinations were simulated to evaluate their performance. Results were benchmarked with the result from secondary data. 100% agreement between these data demonstrated the accuracy of the models, allowing purposeful selection. The ≈90% negative correlation between SR and FOV was identified as a tradeoff between these variables. Currently selected best combination offers a monotonic SR range of 25.5 – 170.92 μm pixel size, over FOV range of 52.3×52.3 mm^2 – 350×350 mm^2. The results also show that components can be selected for design of desired detector system within constraints to manage the field of view effectively; thereby optimizing the SR.

1. Introduction

The demand for high spatial resolution (SR) in neutron radiography (NR) facilities has grown with the need to investigate components comprising smaller features for scientific and industrial applications. This necessitates NR facilities to develop their detection methods as for maximal SR resulting in increased image quality. SR as a key parameter determines the imaging performance of detector systems[1, 2]. This describes the degree which two features of the object can be distinguished or separated in the acquired image [3], as well as the ratio of the image sensor size to that of the field-of-view (FOV) [4]. The availability of a simple and efficient method to manage the FOV in optimizing the SR is of high importance for NR, especially for camera-based detector systems (CBDS), as most NR installations incorporate a variable FOV using this type of the detector [1, 2, 5, 6]. The optimum combination of a large FOV and high SR is a great technical challenge for neutron detectors [1, 2, 7] due to the trade-offs between the two. Sophisticated high resolution detectors are

ideal for small specimens; however, they are not appropriate for experiments involving larger specimens owing to their small, fixed FOV [2, 8]. This is especially true where image stitching cannot be exploited for example in time dependent investigations such as liquid flow experiments. This requires detector development to meet the demands for various types of experiments that are performed using the NR technique [5, 9].

CBDS comprises a camera, lens and scintillator as basic components [2, 8]. They utilize prime lenses as part of the optics [4, 10]. These lenses are of great value in this type of detector system as their optical performance is usually much better than that of zoom lenses. Prime lenses are optimized for a single fixed FOV and most often have a wide maximum aperture setting which enable much faster shutter speeds and improved low-light functionality when compared to their zoom counterparts [4]. By employing a light tight detector box together with properly aligned components enables them to preserve the light illuminated from the back of the scintillator to yield high quality results [2, 5]**.** Prime lenses are significantly sharper than zoom lenses as they do not have additional internal elements that translate in order to enlarge

the image [11]. Diffraction increases with the number of internal lens elements as in the case of zoom lenses, resulting in degraded optical quality (N. Mansurov, Prime vs Zoom Lenses - A Beginners Guide, Photography Life, 2011). Finally, prime lenses cost relatively less [2] than zoom lenses for such reasons as having fewer internal components.

The use of prime lenses requires that the object distance (OD) be varied to increase or decrease the FOV size [4]. This can be achieved by either moving camera or the object plane (scintillator surface in this case) on a linear path corresponding to optical path. The latter is however not possible due to a fixed scintillator configuration in conventional CBDS. Translating the camera is therefore the only viable option to change the OD without exchanging components [4]. This technique enables a variable FOV[7] within a fixed range which is limited by factors such as space available in experimental area, scintillator size and neutron beam dimensions. The diagram in Figure 1 shows motorized CBDS intrinsic components to demonstrate the FOV management concept.
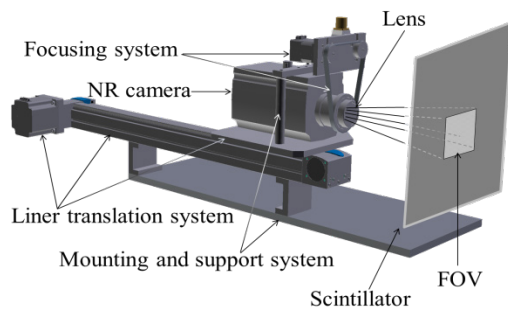

Figure 1: FOV management concept with a motorized camera translation

The other available method for consideration in changing the FOV is interchanging similar lenses of different focal lengths [5,12]. A different focal length will introduce a different angle-of-view (AOV) and therefore a different FOV. The number of achievable FOVs with this method is however limited by the number of lens units available and monotonic FOV variation across a desired range cannot be achieved. Methods such as these are expensive as they involve many components. The exchange process is time consuming and may also damage the fragile scientific components as a result of mishandling.

CBDS as used in NR requires careful selection of appropriate components during design based on established specific experimental requirements and constraints. Conventional component selection, configuration and calibration often lead to sub-optimal use with respect to the components maximum potential, limiting the ability to maximize SR.

The selection of components for design of CBDS can be a discouraging task, especially when constraints such as space available in the NR facility chamber and budget must be adhered to [13]. These together with experimental requirements involving investigations of specimens with various sizes and time dependent examinations, makes a choice of appropriate components combination for design of CBDS inevitable [2,4,12]. The detector system in NR facilities can be viewed as a portable instrument that can be employed at different NR facilities for experimental purposes [4]; therefore its technical requirements can be

formulated independently of characteristics of the beam and other external factors [4]. In this research, pragmatic mathematical models were developed to study parameters of the detector components and their relationship. Arbitrarily selected components combinations were used to evaluate the models. Combinations which ensure versatility with respect to investigations of specimens with various sizes, and still obtain the best possible SR, are presented. The trade-offs that must be considered when designing a CBDS under given constrains and experimental requirements are also described.

2. Material and Methods

The mathematical models were developed deriving from the detector system's optical system represented in Figure 2. Different inherent properties of similar detector system components results in different responses during experiments. The inherent properties are referred to as primary or independent parameters in this work and are defined by parameter values as specified by the manufacturer of the specific component. Selection of components allows these parameters to be varied to produce different results. Variables that are being manipulated using primary parameters are referred to in this work as secondary parameters. These performance-related variables are used in the design of the CBDS in order to satisfy specific requirements and are a function of the primary parameters. Their values are derived from mathematical models which were developed based on the CBDS's optical system and geometric arrangements of components. This allows parametric studies to be performed in order to establish relationships between parameters.
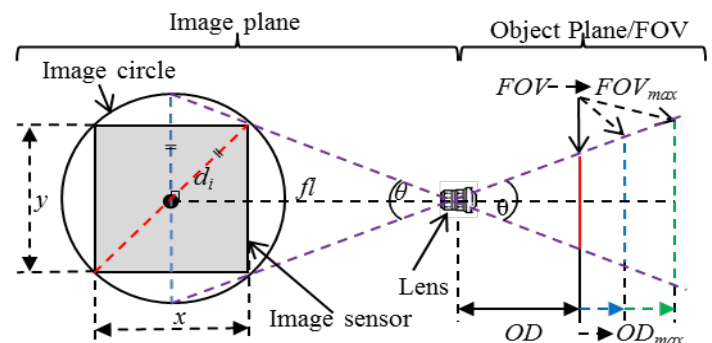
Figure 2: Schematic of the detector system's components geometrical arrangement and optical system

2.1 Material

Similar but different detector system components including scintillators, cameras and lenses were chosen arbitrarily to undertake a comparative parametric study through simulation in order to enable selection of components for the design of a suitable detector system based on requirements and constraints.

The following provides details for each category of components selected for simulation:

- *Cameras*

Three cameras with vastly different properties were selected from the Andor products range for comparison. Manufacturer's specifications show that connectivity is through a USB interface and all three feature a standard bayonet F-mount which enables lenses to be exchanged easily (Andor Technology, Belfast, Northern Ireland). The selected cameras are described below.

The Andor iKon-L 936 CCD-camera has a 2048 × 2048 array, aspect ratio of 1.0 and 13.5 μm pixel pitch which delivers a 27.6 × 27.6 mm² active image area. It features a 5-stage cooler which enables its large area sensor to be cooled down to -100 °C. This makes the iKon-L camera suitable for long exposure times and is ideal for low-light applications such as radiography

The Andor Zyla 5.5-HF front-illuminated CMOS-camera with a 2560 × 2160 array and 6.5 μm pixel pitch delivers a 21.8 mm diagonal FOV with a 16.6 × 14 mm² active image area giving an aspect ratio of 1.185. Its operating temperatures are from 0 ºC to 30 ºC ambient.

The Andor iKon-XL 230 model with back-illuminated CCD sensor offers a very large 61.4 × 61.4 mm² imaging area with a 4096 × 4108 array format, aspect ratio of 0.997 and 15 μm pixel size. The chip is thermoelectrically cooled down to -100 °C, and is ideal for applications such as Astronomy or X-ray/Neutron radiography.

- *Lenses*

Table 1 shows a summary of the four lenses selected from Nikon products and their properties from datasheets (Nikkor, Nikon Inc., Melville, NY, USA).

Table 1: Summary of Selected Lenses and their Properties

Lens	Focal Length	AOV	MFD
PC-E Micro NIKKOR f/2.8D ED	45 mm	51.4º	250 mm
Nikon AF-S NIKKOR f/1.4G	50 mm	46.8º	450 mm
Micro-NIKKOR f/2.8	55 mm	42.9º	250 mm
AF-S Micro NIKKOR F2.8G ED	60 mm	39.7º	185 mm

- *Scintillators*

Two, high light (blue emission) output, high resolution scintillators, namely a ^{6}LiF: ZnS Large Scintillator (LS) and a ZnS (Ag) -^{6}LiF Medium Scintillator (MS) were adopted for the object plane. The type, active size and the aspect ratio of these scintillators are shown in Table 2.

Table 2: Summary of Selected Scintillators for Simulation and their Properties

Scintillator	Type	Size	Aspect ratio
Larger	^{6}LiF: ZnS	400 × 400 mm²	1
Medium	ZnS(Ag)-^{6}LiF	350 × 350 mm²	1

3.1 Secondary Parameters Modeling

Figure 2 show that, the relationship between the image circle and the image sensor can be represented by the theorem of Pythagoras in equation (1).

$$d_i^2 = x^2 + y^2 \tag{1}$$

The sensor aspect ratio (δ) is the ratio of sensor width (x) to height (y) as given in the following equation as: height (y) as given in the following equation as:

$$\delta = x/y \tag{2}$$

Also in Figure 2, the focal length (fl) and AOV (θ) are fixed owing to the use of prime lenses. A change in FOV can therefore be achieved by varying the OD or by exchanging similar lens of different focal lengths; thus change in AOV. The latter cannot

easily achieve monotonic FOVs similar to when a single lens is in use with a motorized translation systems. This leaves the change in OD as the only appropriate method to change the FOV.

Calculation of the FOV is established by considering the similar triangles theorems, namely the vertical opposite angles and the angle-angle similarity theorem. These indicate that the object plane, as observed through a lens, has the same properties as the image plane of the optical system. As the OD can be changed, various FOVs can be achieved by varying the OD as shown in Figure 2, producing an instantaneous FOV (IFOV). This is calculated by the width (FOV_w) and the height (FOV_h) at a given OD and taking the aspect ratio of the image sensor into account. The length of the rectangle representing the IFOV's diagonal line is the actual FOV at the sensor position, and is calculated according to Pythagoras' theorem as in equation (3).

$$FOV = \sqrt{FOV_w{}^2 + FOV_h{}^2} \tag{3}$$

The physical size of the FOV is defined using the OD and the lens AOV using a trigonometric equation (4), as follows:

$$FOV = 2 \times tan(\theta/2) \times OD \tag{4}$$

The maximum FOV (FOV_{max}) is achieved at the position where the maximum OD (OD_{max}) is realized, and vice versa. OD_{max} is given by (5).

$$OD_{max} = FOV_{max}/2 \times tan(\theta/2) \tag{5}$$

The camera image sensor properties such as aspect ratio; play a major role in defining how the scintillator surface would be imaged, and to what extents the image can be captured and resolved. By disregarding the neutron beam size, the maximum FOV (FOV_{max}) the detector system can image is equal to the size of the maximum rectangle subjected to the sensor aspect ratio that can fit into the area of the scintillator defined by the width (W) and the height (H). The aspect ratios of both the scintillator and the image sensor must match, for the sensor to image the entire scintillator at FOV_{max} as shown in Figure 3(a).
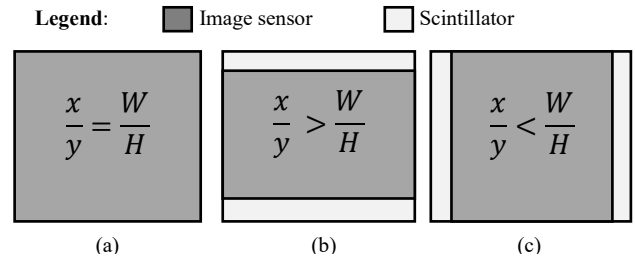
Figure 3: Effect of image sensor-scintillator aspect ratio matching at maximum FOV (a) Equal aspect ratios, (b) Large image sensor aspect ratio, causing vertical mismatch (c) Large scintillator aspect ratio, causing horizontal mismatch

If this is not the case, the mismatch in aspect ratios will result in the area of the scintillator not being imaged entirely at FOV_{max} [5], this phenomenon is illustrated in Figure 3 (b) and (c).

The mismatch as shown in the figures will cause either the horizontal side or vertical side to saturate first, curtailing any further increase in FOV, giving FOV_{max}. The following equations (6) – (8), based on Pythagoras' theorem were conditionally used to

calculate the FOV_{max}, given the scintillator and the image sensor aspect ratios:

$$FOV_{max} = \sqrt{W^2 + H^2} \quad ; \text{if } x/y = W/H \quad (6)$$

$$FOV_{max} = \sqrt{W^2 + (W/\delta)^2} \quad ; \text{if } x/y > W/H \quad (7)$$

$$FOV_{max} = \sqrt{(\delta H)^2 + H^2} \quad ; \text{if } x/y < W/H \quad (8)$$

The minimum focus distance (MFD) is a primary parameter which describes the minimum distance between the lens and the object plane, from which the lens is able to focus. This limits the extent to which the lens can be closest to the object plane, thereby defining the minimum OD (OD_{min}). The FOV_{min} the detector system can capture is calculated from this value by substituting the OD_{max} with OD_{min} and FOV_{max} with FOV_{min} in (5), as in (9).

$$FOV_{min} = 2 \times tan(\theta/2) \times OD_{min} \quad (9)$$

The FOV is changed primarily to achieve high level of SR. A change in FOV however changes the surface area of the object plane which the camera can image, thereby causing the area that the image sensor can resolve using a given lens to vary. This is equivalent to varying a SR. SR can be calculated either from the ratio of the sensor size to the FOV size, giving SR in line pairs per millimeter (*lp/mm*), or from the ratio of the FOV size to the sensor size, giving SR in micrometers (*μm*). This can be achieved using equations (10), and (11), respectively:

$$SR = FOV/CCD_{size} = FOV/d_i \ (lp/mm) \quad (10)$$

$$SR = d_i/FOV \ (\mu m) \quad (11)$$

3. Results and Discussion

This section discusses the benchmarking and evaluation of the results from simulation of models developed. To begin with, the Radiography Simulator software which is designed to simulate a radiograph of particular shape or type of material of the sample was used. Firstly, the simulation of radiographs with components combination selected from section 2.1 was carried out with Radiography Simulator in [14] to generate the evaluation datasets. The generated datset is then analysed for correctness of parameters representing the selected simulation setup. The results are presented to contrast with the results from models simulation.
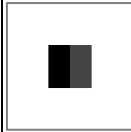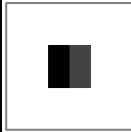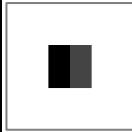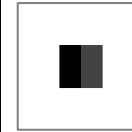
Secondly, the models are then simulated and the results are benchmarked against the Radiography Simulator results. The capability of the models to produce desirable results is then assessed, and lastly the results are used to select the best combination of components for a particular envisaged experimental requirement and constraint.

4.1 Models Benchmark Samples and Analysis Software

Secondary data were generated using Radiography Simulator to evaluate the success of the designed models. The dataset comprised of a simulated 12 cm × 1 cm × 12 cm (*l×b×h*) cube specimen made from two materials half each. The parameters used for simulation were from combination of the following detector system components specified in section 2.1: Andor iKon-L 936

CCD camera and MS in combination with the four lenses. Dataset of radiographs from MFD to the FOVmax were produced for each lens. Table 3 show a sample of data from each lens dataset. For each lens shown on the table, the first row consists of image at minimum OD with their respective OD position, second row consists of image at maximum OD also with position and the third row is the number of images generated per lens.

Table 3: Properties of images generated by Radiography Simulator

Lens	PC-E Micro NIKKOR f/2.8D ED 60mm	Nikon AF-S NIKKOR f/1.4G 55mm	Micro-NIKKOR f/2.8 50mm	AF-S Micro NIKKOR F2.8G ED 45mm
OD_{min}	185 mm	250 mm	450 mm	250 mm
OD_{max}	1238 mm	1135 mm	1032 mm	928 mm
Images	1053	885	582	678
Total Images		3198		

ImageJ open source imaging software, which is freely available to the scientific community [15] was used to analyse the simulated images and measure the sample size, FOV_{min}, FOV_{max} and SR in each of the dataset in Table 3 as shown in Figure 4.
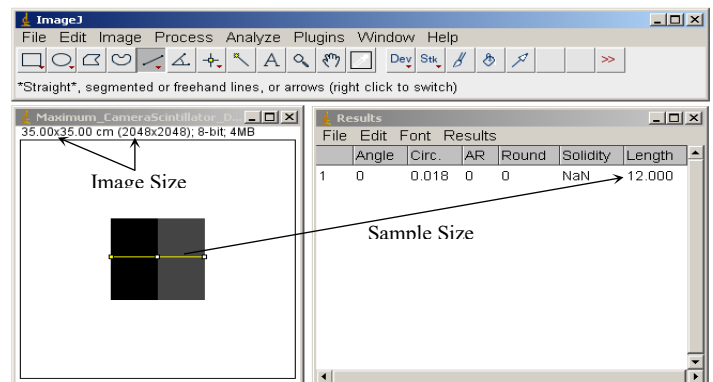
Figure 4: Radiograph measurement using ImageJ image analysis software

The results from ImageJ are tabled in Table 4, and they demonstrated that the simulated sample and components parameters selected are intrinsic to the simulated images.

Table 4: FOV range and SR range analyzed using ImageJ software

Lens	60mm PC-E Micro NIKKOR f/2.8D ED	55mm AF-S NIKKOR f/1.4G	50mm Micro-NIKKOR f/2.8	45mm AF-S Micro NIKKOR F2.8G ED
FOV range (mm)	73.9 – 495	109.0 – 495	216.1 – 495	133.5 – 495
SR range (μm)	25.5 – 170.9	37.6 – 70.9	74.6 – 170.9	46.1 – 170.9
SR range (lp/mm)	39.2 – 6.4	26.6 – 70.9	13.4 – 6.4	21.7 – 6.4

5.1 Simulation

Simulation of detector system components parameters for the design was undertaken using models developed in section 3.1. The results would aid in selecting the optimal combination of detector system components, constrained by experimental requirements. The data from physical detector system component listed in 2.1 were used in components combinations. The derived models were implemented in a spread sheet and the results are presented in the following subsections.

- *Field-of-View Area Saturation Determination*

To determine the FOV saturation (FOV_{max}) for a particular, the camera sensor and the scintillator aspect ratios were matched to determine the saturation size. This was realized using the aspect ratio matching for a camera sensor and scintillator. This was repeated the for combinations of the three Andor cameras and two scintillators. The aspect ratio matching was accomplished througt one of the fitting equation in (6) – (8) in each case. The results are given in Table 5. Column 1 shows the camera model; and column 2 and 4 indicate the match or type of mismatch for MS and LS respectively. The FOV_{max} with dimensions indicated in size by $W \times H$ for each combination is shown in column 3 and 5 for MS and LS respectively.

- *Object Distance Determination for a Variable Field-of-View*

The ODmax from which the FOV_{max} is derived is calculated from equation (5). The OD range data-points were simulated from zero (0) mm to OD_{max} with fixed predefined OD shift intervals of 1mm. In normalizing the data-points, the lens MFD was taken into account and all ODs below this point were discarded, staying on the useful OD range. The MFD and the resulting OD_{max}, are the OD range limits in each case shown in column 4 and 7 for MS and LS respectively.

Table 5: Aspect Ratio Matching for Sensor-Scintillator Combination with the Field-of-View Saturation

| Camera name; Aspect Ratio | Medium Scintillator (LS) - (400 x 400 mm²) | | Larger Scintillator (MS) - (350 x 350 mm²) | |
	Sensor Scintillat or Match	*FOV Size Saturation (W ×H) mm²*	*Sensor Scintillator Match*	*FOV Size Saturation (W×H)mm²*
Zyla 5.5 HF ;1.185	x/y > W/H	400 × 337	x/y > W/H	350 × 295
iKon-L 936 ;1.0	x/y = W/H	400 × 400	x/y = W/H	350 × 350
iKon-XL230 ;0.997	x/y < W/H	399 × 400	x/y < W/H	349 × 350

In evaluating the developed models, the parameters' values from benchmark dataset agree 100% with the Camera-Lens-Scintillator simulation using models in the result on Table 6 for Andor iKon-L 936 CCD camera and MS in combination with the four lenses.

The plots on Figure 5 show the OD range per camera using all lens-scintillator combinations. From the OD ranges determined, the variable FOV would then be realized by utilizing equation (4), and varying the *OD* within the OD range, resulting in a FOV ranging from the position of *MFD* where FOV_{min} is realized, to the position of OD_{max} were FOV_{max} is realized. Data points for FOV were simulated by ussuming a 1mm shift intervals for *OD*. The achieved FOV ranges for each combination are shown in Table 6 column 5 for MS and column 8 for LS. The evaluation dataset for Andor iKon-L 936 camera combined with the PC-E Micro NIKKOR f/2.8D ED 60mm lens match the result from models. The FOV change behavior was plotted over the OD range in Figure 5 for each lens-scintillator combination using different cameras shown in Table 6 column 1. MS was used in Figure 6 (a), (b), and (c) and LS in (d), (e) and (f).

Table 6: Simulation results for combinations of Camera-Lens-Scintillator

| Andor Camera; Aspect Ratio(δ) | Lens focal length | Maximum Spatial Resolution (lp/mm; μm) | Medium scintillator | | | Larger scintillator | | |
			Object Distance Range (mm)	*Field-of-View Range (mm)*	*Minimum Spatial Resolution (lp/mm; μm)*	*Object Distance Range (mm)*	*Field-of-View Range (mm)*	*Minimum Spatial Resolution (lp/mm; μm)*
Zyla 5.5 HF; 1.185	45 mm	22.9;43.7	250-782	146.4-458	5.85; 136.71	250-894	146.4-523	5.12;156.29
	50 mm	14.1;70,7	450-870	236.9-458	5.85; 136.71	450-994	236.9-523	5.12;156.29
	55 mm	28.0;35.6	250-958	119.5-458	5.85; 136.71	250-1094	119.5-523	5.12;156.29
	60 mm	41.3;24.2	185-1045	81.1- 458	5.85; 136.71	185-1194	81.1-523	5.12;156.29
iKon-L 936; 1.0	45 mm	21.7;46.1	250-927	133.5-495	7.31; 170.92	250-1059	133.5-566	6.40;195.26
	50 mm	13.4;74.6	450-1031	216.1-495	7.31; 170.92	450-1178	216.1-566	6.40;195.26
	55 mm	26.6;37.6	250-1135	109.0-495	7.31; 170.92	250-1297	109.0-566	6.40;195.26
	60 mm	39.2;25.5	185-1238	73.9-495	7.31; 170.92	185-1415	73.9-566	6.40;195.26
iKon-XL 230; 0.997	45 mm	23.0;43.5	250-927	133.3-494	11.74; 85.21	250-1059	133.3-565	10.27;97.35
	50 mm	37.2;26.9	45 -1031	215.8-494	11.74; 85.21	450-1178	215.8-565	10.27;97.35
	55 mm	18.8;53.3	250-1135	108.9-494	11.74; 85.21	250-1296	108.9-565	10.27;97.35
	60 mm	12.7;78.6	185-1238	73.8-494	11.74; 85.21	18 -1416	73.8-565	10.27; 97.35
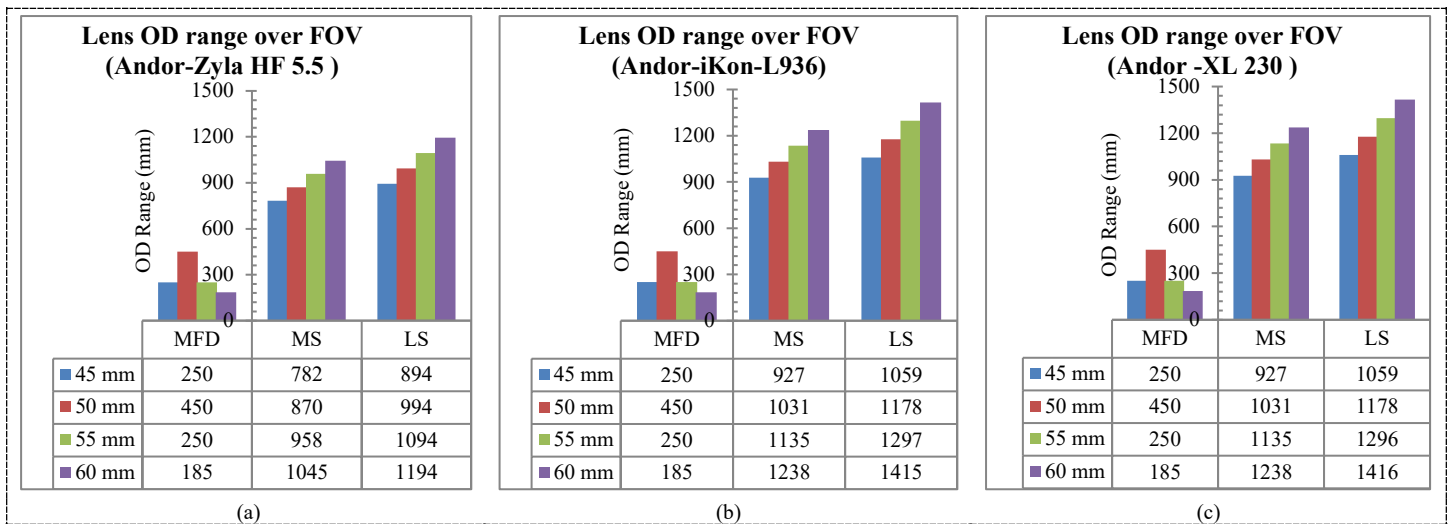
Figure 5: OD range per lens-scintillator combination for Andor cameras: (a) Zyla 5.5-HF, (b) and (c) iKon-L 936 and Andor iKon-XL 230
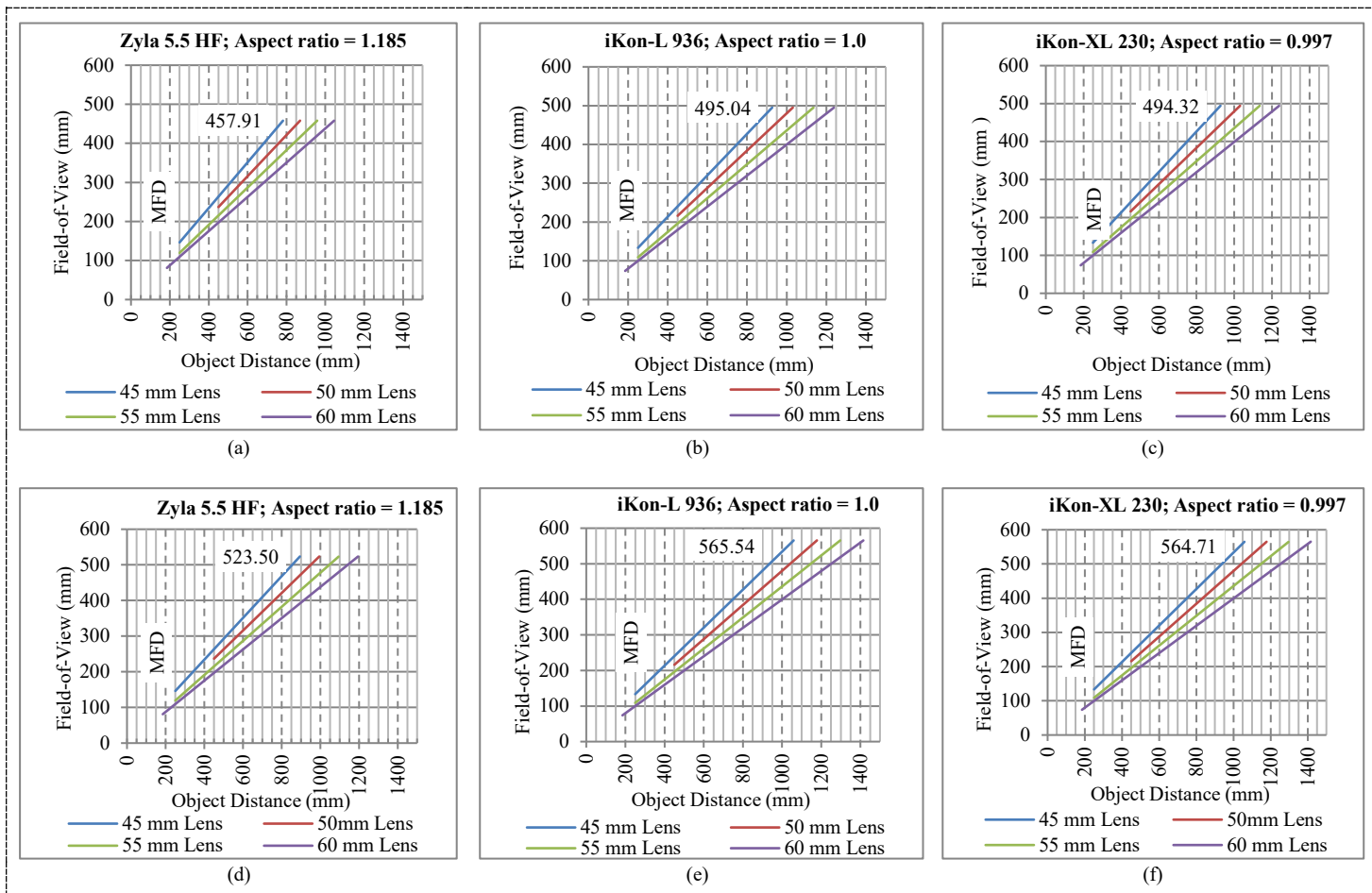
Figure 6: FOV range over OD for all camera-lens combination: First column (Zyla 5.5 HF), second column (iKon-L 936) and third column (iKon-XL 230)

- *Field-of-View Change for Variable Spatial Resolution*

As the FOV size changes (*IFOV*) with change in OD, SR also changes owing to a fixed sensor size. In simulating the SR each camera-lens-scintillator combination would produce at each FOV data point, equation (10), derived from the ratio of *FOV* to the d_i was used, giving results in *lp/mm* and vice versa, using equation (11), giving results in μm; both defines SR range. A 1mm shift interval for FOV data points was adopted over OD range. High SR range limit using both scintillators are shown in Table 6 column 3 and the low range limits in column 6 and 9 for MS and LS respectively. Figure 7 shows change in SR over the FOV size using various camera-lens combinations with the LS. Figure 7 (a), (b) and (c) shows the variation of SR in *lp/mm* whilst Figure 7 (d), (e) and (f) the same results shown in μm.
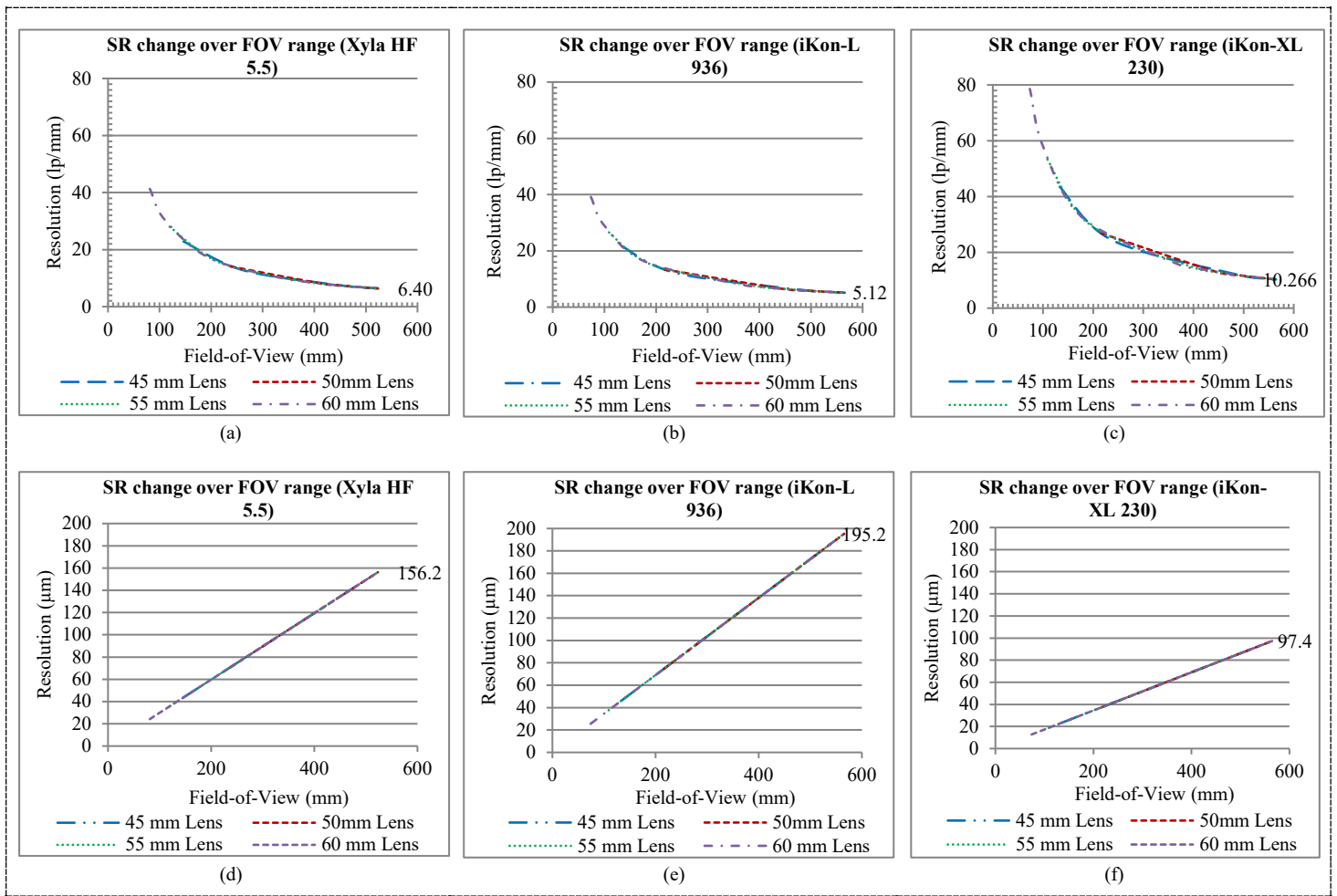
Figure 7: SR change over FOV range for all camera-lens combinations using LS: (a, b and c) in line pairs per mm and (d, e and f): in micrometers pixel size

- *Spatial Resolution and Object Distance*

As the length of OD is changed to vary the FOV, the SR also changes. The change in the SR as a function of OD is demonstrated for all camera-lens combinations and presented in Figure 8 (a), (b) and (c) for the MS and Fig. 8 (d), (e) and (f) for the LS.
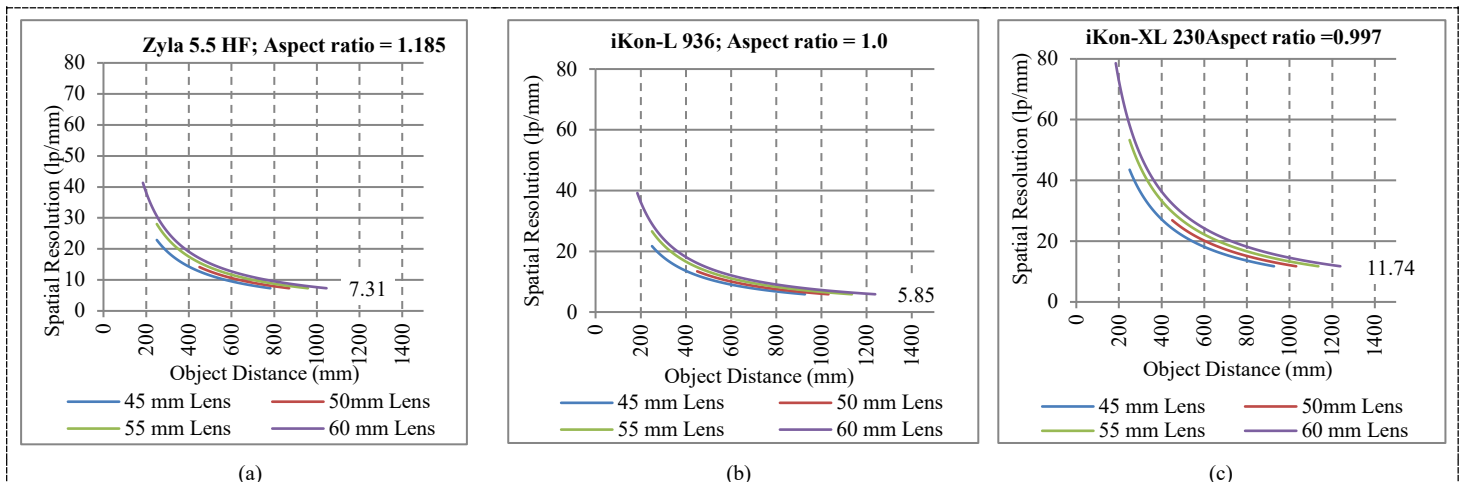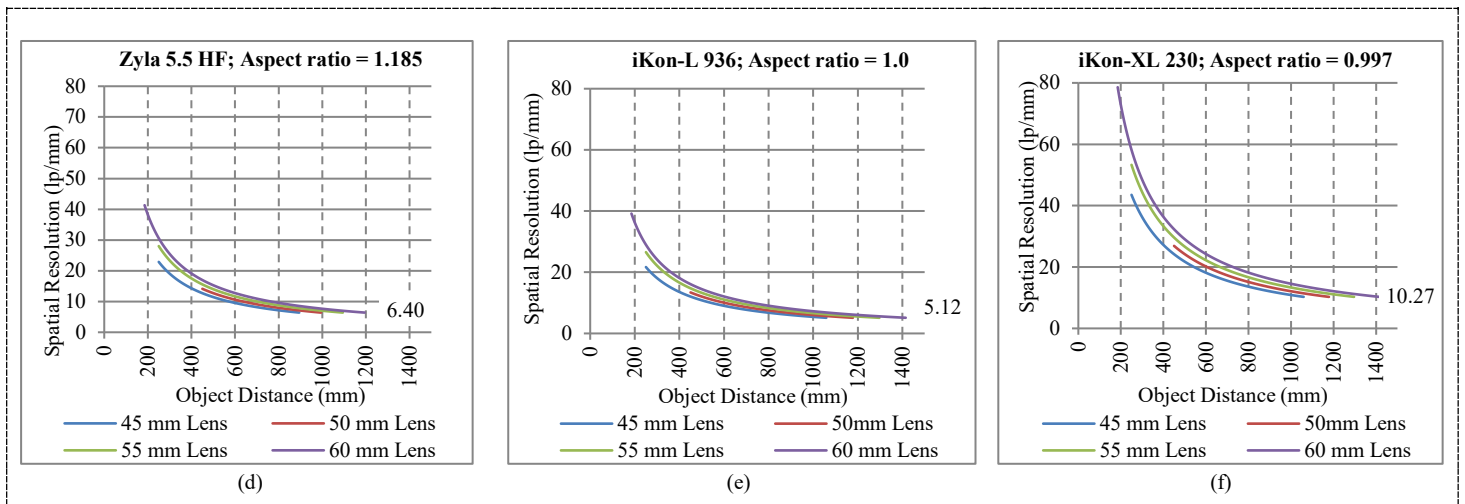
Figure 8: SR changes over OD range for all camera-lens combination using: MS in (a, b and c) and LS in (d, e and f)

The results in Figure 7 and Figure 8 show that the OD increases with increased FOV and OD decreases as SR increases. Figure 7 shows that the effective pixel size becomes bigger with larger FOV, indicating lower SR. The covariance due to the SR, FOV, and the correlation between OD and FOV, for the three cameras (each with a combination of four lenses over LS), were calculated using the covariance function (*Cov*) given in equation (12).

$$Cov(x,y) = \sum [(x_i - x_m) \times (y_i - y_m)]/(n - 1) \qquad (12)$$

where: x_i = a given x value in the dataset.
x_m = the mean, or average, of the x values.
y_i = the y value in the dataset that corresponds with x_i.
y_m = the mean, or average, of the y values.
n = the number of data points.

The strength of these relationships was calculated using Spearman's correlation coefficient (ρ), given by (13).

$$\rho = 1 - (6\sum d_i^2)/(n (n^2 - 1)) \qquad (13)$$

where: ρ = Spearman rank correlation coefficient
d_i = difference between the ranks of corresponding variables
n = number of observations

The results of this relationship are tabled in Table 7.

Table 7: Field-of-View, Spatial Resolution Covariance and Correlation per Camera-Lens Combination over LS

Lens	Zyla 5.5 HF *Covariance; Correlation*	iKon-L 936 *Covariance; Correlation*	iKon-XL 230 *Covariance; Correlation*
PC-E Micro NIKKOR 45 mm f/2.8D ED	-443.8; -0.947	-488.56; -0.934	-978.6; -0.934
Nikon AF-S NIKKOR 50 mm f/1.4G	-174.5; -0.979	-221.14; -.970	-442.9; -0.970
Micro-NIKKOR 55 mm f/2.8	-589.8; -0.930	-628.8; -0.915	-1258; -0.915
AF-S Micro NIKKOR 60 mm F2.8G ED	-922.4; -0.893	-939.67; -0.874	-1883; -0.874

The graphs in Figure 7 demonstrate an existing negative monotonic relationship between the SR and the FOV. Results also show that there is strong negative correlation between SR and the FOV (-90 %) as confirmed by the results in Table 7. Overall results show that, despite the trade-offs that accompanies each choice of combination. The selection lies in the balance between SR and a larger FOV range to accommodate specimens of different sizes.

Larger scintillators offer a large maximum FOV useful in the examination of large specimens without having to examine them in parts. However, the results given in Figure 6 show that, despite the lens or camera in use, larger scintillators demand longer ODs to cover the entire FOV. This contributes to the overall size of the detector system.

Smaller scintillators offering a small maximum FOV are good for a compact design. They are ideal when investigating small specimens. However, they complicate experiments involving large specimens, owing to specimens being scanned in sections. This requires increased time for examination and expert knowledge of image stitching during post-processing. While the camera chip size and the required SR should be the primary consideration in selecting the size of the scintillator, the underlying rationale should be based on the expected size of specimens and trade-offs.

Larger AOV lenses are ideal for a compact design where examinations involving large specimens and large FOVs are necessary; however, these lenses have long MFD and are unable to achieve a very small FOV. They produce small FOV ranges due to immediate FOV saturation. While it is useful to employ a larger FOV, it must be observed that the anti-correlation between the FOV and SR means the trade-off between the two is unavoidable. In contrast to larger AOV lenses, smaller AOV lenses have short MFDs which allow them to be placed very close to the object plane, thereby increasing the reproduction rate. These lenses are ideal in a design intended for smaller specimens necessitating a smaller FOV to maximize the SR; however, they demand a longer displacement for larger FOV applications, increasing the size of the detector system.

By assuming the sample sizes between 10 cm × 10 cm to 30 cm × 30 cm as a target size of samples envisaged, this suggests a FOV range as an experimental requirement. An adequate minimum FOV in the given range of components would be achieved by a 60mm PC-E Micro NIKKOR f/2.8D ED lens. This combined with the iKon-L 936 CCD camera and the 35mm × 35mm FOV scintillator would allow a SR range of 25.5 – 170.92 µm pixel size. In other work CBDS have previously reported a SR at the region of ≈ 100 to 500 µm and recently less than 50 µm [2]. If the budget as a constraint allows, with 1.3m space available at the position where the detector must be located. This detector system would make a bests combination for requirements stated.

4. Conclusion

In conclusion to the component selection strategy, the CBDS design should optimize the SR by managing the FOV. In pursuit to achieve this, the parametric study for the design of a CBDS was presented. We developed models to determine the maximize performance of the CBDS based on experimental requirements and given constraints. In particular, we tried to attain a balance between the FOV and the SR in order to provide a versatile detector system with respect to both variables through simulation. A clear understanding of the different constraints and experimental requirements would aid in the choice of components using the developed models.

To evaluate our models, we benchmarked the results with the secondary data and 100% agreement between the results demonstrated the desirable functionality of the models. The chosen scenario of experimental requirements and constraint has shown that these models are effective in guiding the development of the best detector system with given limitations.

In addition, we proposed a use of linear translation system for the changing the OD to achieve a monotonic FOV and SR. As future work, we plan to develop software for components combination selection. This software will take experimental requirements and constraints as input and return the best possible components combination that can be achieved.

Conflict of Interest

The authors declare no conflict of interest.

References

[1] A.P. Kaestner, Z. Kis, M.J. Radebe, D. Mannes, J. Hovind, C. Grünzweig, N. Kardjilov, E.H. Lehmann, "Samples to Determine the Resolution of Neutron Radiography and Tomography," Physics Procedia, **88**(September 2016), 258–265, 2017, doi:10.1016/j.phpro.2017.06.036.

[2] E.H. Lehmann, G. Frei, G. Kühne, P. Boillat, "The micro-setup for neutron imaging: A major step forward to improve the spatial resolution," Nuclear Instruments and Methods in Physics Research, Section A: Accelerators, Spectrometers, Detectors and Associated Equipment, **576**(2–3), 389–396, 2007, doi:10.1016/j.nima.2007.03.017.

[3] J. Rueckel, M. Stockmar, F. Pfeiffer, J. Herzen, "Spatial resolution characterization of a X-ray microCT system," Applied Radiation and Isotopes, **94**(September), 230–234, 2014, doi:10.1016/j.apradiso.2014.08.014.

[4] H. Pleinert, E. Lehmann, S. Körner, "Design of a new CCD-camera neutron radiography detector," Nuclear Instruments and Methods in Physics Research, Section A: Accelerators, Spectrometers, Detectors and Associated Equipment, **399**(2–3), 382–390, 1997, doi:10.1016/S0168-9002(97)00944-3.

[5] N. Kardjilov, M. Dawson, A. Hilger, I. Manke, M. Strobl, D. Penumadu, F.H. Kim, F. Garcia-Moreno, J. Banhart, "A highly adaptive detector system for high resolution neutron imaging," Nuclear Instruments and Methods in Physics Research Section A: Accelerators, Spectrometers, Detectors and Associated Equipment, **651**(1), 95–99, 2011, doi:10.1016/j.nima.2011.02.084.

[6] E. Lehmann, M. Raventos, R.P. Harti, P. Trtik, A. Kaestner, D. Mannes, C. Grünzweig, "Methodical Progress in Neutron Imaging at PSI," Physics Procedia, **88**(September 2016), 250–257, 2017, doi:10.1016/j.phpro.2017.06.035.

[7] D.S. Hussey, D.L. Jacobson, M. Arif, P.R. Huffman, R.E. Williams, J.C. Cook, "New neutron imaging facility at the NIST," Nuclear Instruments and Methods in Physics Research Section A: Accelerators, Spectrometers, Detectors and Associated Equipment, **542**(1–3), 9–15, 2005, doi:10.1016/j.nima.2005.01.004.

[8] C. Tötzke, I. Manke, A. Hilger, G. Choinka, N. Kardjilov, T. Arlt, H. Markötter, A. Schröder, K. Wippermann, D. Stolten, C. Hartnig, P. Krüger, R. Kuhn, J. Banhart, "Large area high resolution neutron imaging detector for fuel cell research," Journal of Power Sources, **196**(10), 4631–4637, 2011, doi:10.1016/j.jpowsour.2011.01.049.

[9] E.H. Lehmann, P. Vontobel, G. Frei, C. Brönnimann, "Neutron imaging—detector options and practical results," Nuclear Instruments and Methods in Physics Research Section A: Accelerators, Spectrometers, Detectors and Associated Equipment, **531**(1–2), 228–237, 2004, doi:10.1016/j.nima.2004.06.010.

[10] M. DINCA, "The implementation of a charge coupled device (CCD) camera in a neutron imaging system for real time and tomography investigations," Neutron Imaging:A Non-Destructive Tool for Materials Testing (IAEA-TECDOC Series), (September), 53–67, 2008, doi:978–92–0–110308–6.

[11] K. Eismann, S. Duggan, T. Grey, Real world digital photography, Pearson Education, 2010.

[12] N. Kardjilov, A. Hilger, I. Manke, M. Strobl, M. Dawson, S. Williams, J. Banhart, "Neutron tomography instrument CONRAD at HZB," Nuclear Instruments and Methods in Physics Research Section A: Accelerators, Spectrometers, Detectors and Associated Equipment, **651**(1), 47–52, 2011, doi:10.1016/j.nima.2011.01.067.

[13] E.H. Lehmann, P. Vontobel, G. Frei, G. Kuehne, A. Kaestner, "How to organize a neutron imaging user lab? 13 years of experience at PSI, CH," in Nuclear Instruments and Methods in Physics Research, Section A: Accelerators, Spectrometers, Detectors and Associated Equipment, 2011, doi:10.1016/j.nima.2010.12.135.

[14] R. Nshimirimana, A. Abraham, G. Nothnagel, A. Engelbrecht, "X-Ray and Neutron Radiography System Optimization by Means of a Multiobjective Approach and a Simplified Ray-Tracing Method," Nuclear Technology, 1–20, 2020, doi:10.1080/00295450.2020.1740562.

[15] C.A. Schneider, W.S. Rasband, K.W. Eliceiri, "NIH Image to ImageJ: 25 years of image analysis," Nature Methods, **9**(7), 671–675, 2012, doi:10.1038/nmeth.2089.

Microstrip Patch Antenna Designs with Quarter-Circular and Semi-Circular Slots in Patches for Wireless Communication Applications in Frequency Range of 1.2 GHz-4.6 GHz

Cihan Dogusgen Erbas[*]

Electrical and Electronics Engineering Department, Istanbul Yeni Yuzyil University, Istanbul, 34010, Turkey

A R T I C L E I N F O	A B S T R A C T
	In this study, 6 unique microstrip patch antennas with quarter-circular and semi-circular slots in patches are proposed. It is aimed to investigate the effect of these slots in the designed topologies. The antennas operate for wireless applications including Personal Communication Service (PCS), 3rd Generation (3G), The Standard for Wireless Fidelity (WiFi)/Wireless Local Area Network (WLAN)/Bluetooth, Long Term Evolution (LTE) and Global System for Mobile Communications at 1.8 GHz (GSM-1800). Simulation results for antenna performance parameters such as fractional bandwidth, gain, radiation pattern, radiation efficiency and total efficiency are presented.

1. Introduction

This paper is an extension of work originally presented at 11th International Conference of Electrical and Electronics Engineering [1]. Multi-band feature is often required in wireless communication systems because simultaneous operation of multiple technologies could be desirable. One antenna type that satisfies that feature is microstrip patch antennas. Microstrip patch antennas have been preferred in many wireless communication systems. [2, 3]. Operation in multiple frequency bands can be obtained by placing slots in patches and/or ground planes [4–6]. Various studies report on slotted microstrip patch antenna geometries: In one report [7], a microstrip patch antenna with a slotted rectangular radiating patch and a defected ground plane suitable for Bluetooth, LTE, Universal Mobile Telecommunications System Band II (UMTS-II), Industrial, Scientific and Medical band (ISM), WLAN, Worldwide Interoperability for Microwave Access (WiMAX), RFID, Wireless Broadband (WiBro) and WiFi is examined. In [8], the authors examine a microstrip patch antenna with an air-filled substrate and 3 open slots. The antenna operates between 1.77 GHz – 2.65 GHz. In [9], the authors focus on a dual-band microstrip patch antenna that consist of two layers separated by an air gap, and a triangular ground slot. The structure operates at 1.8 GHz and 2.4 GHz.

In this article, 6 microstrip patch antennas with quarter-circular and semi-circular slots in patches aimed for wireless operations are proposed. Geometry of the antennas are unique. It is intended to investigate the effect of patch truncations in these antenna topologies. The truncations are located symmetrically on the patches. Antenna performance parameters are simulated. Simulations as well as optimizations are carried out by utilizing ANSYS HFSS.

2. Antennas

2.1. Antenna 1

Antenna 1 has 2 identical quarter-circular slots in patch. These slots are located two diagonal patch corners. Radius of quarter-circles is given by r_1 (1.50 mm). The antenna is in square shape as all antennas in this article. Its operation range is 1.3905 GHz – 4.5739 GHz with a fractional bandwidth (FB) of 106.74%. Note that a simulation of the slotless configuration yields a resonance at 2.05 GHz using a coaxial probe as a feed located at (7, 9) mm. The frequency operation range is 1.365 GHz – 2.410 GHz with a fractional bandwidth of 55.36%. Operation frequency range is based on -10 dB impedance bandwidth ($|S_{11}|$<-10 dB). Height of the substrate is 4.30 mm. Its relative permittivity value is 15.5, and loss tangent value is 0.0001. Same substrate material and substrate height are used in all designed antennas. Length of the ground plane and patch without slots are 25 mm and 21.40 mm, respectively, which are the same as those of all designed antennas.

[*]Corresponding Author: Cihan Dogusgen Erbas, Email: cihan.dogusgen@yeniyuzyil.edu.tr

Antenna feed is a coaxial probe placed at (8, 8) mm in xy plane where center of the antenna is denoted as (0, 0) mm. All antennas in this article are fed by one coaxial probe. Antenna 1 is illustrated in Figure 1.
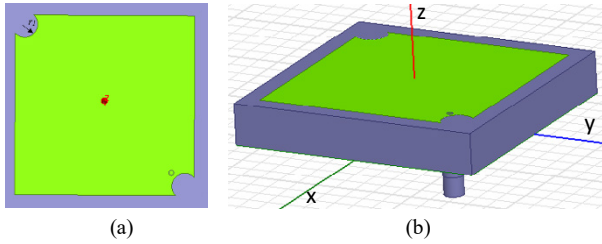
Figure 1: Antenna 1 (a) patch, (b) side view

2.2. Antenna 2

Antenna 2 has 4 identical quarter-circular slots in patch (see Figure 2). These slots are located at all patch corners. Radius of quarter-circles is given by r_1. The structure' s operation range is 1.4101 GHz – 4.5791 GHz (FB=105.82%). Antenna feed is placed at (8, 9) mm.
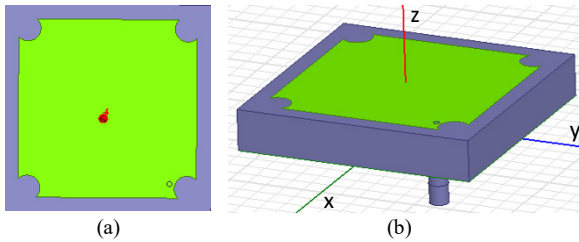
Figure 2: Antenna 2 (a) patch, (b) side view

2.3. Antenna 3

Antenna 3 has 2 identical semi-circular slots in the patch. These slots are located in the middle of two patch edges. The antenna is shown in Figure 3. Semi-circle radius is given by r_1. The structure' s operation range is 1.3287 GHz – 4.0406 GHz (FB=101.02%). Antenna feed is placed at (10, 6) mm.
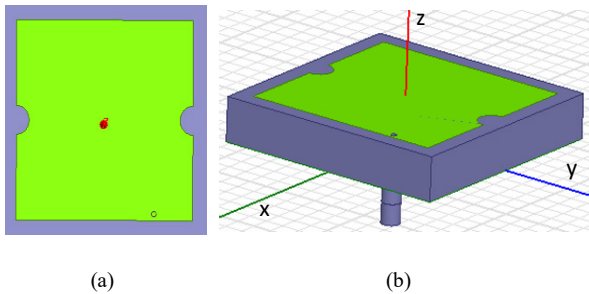
Figure 3: Antenna 3 (a) patch, (b) side view

2.4. Antenna 4

Antenna 4 has 4 identical semi-circular slots in the patch. These slots are located in the middle of all patch edges. The antenna is shown in Figure 4. Semi-circle radius is given by r_1. The structure' s operation ranges are 1.3543 GHz – 2.3231 GHz (FB=52.69%), and 2.8465 GHz – 4.1123 GHz (FB=36.38%). Antenna feed is placed at (7, 9) mm.
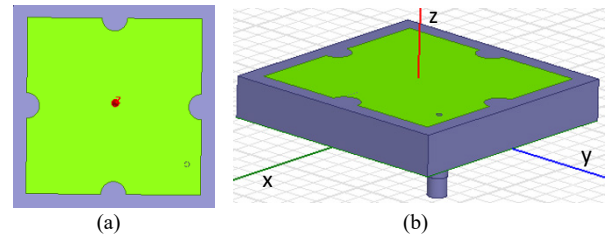
Figure 4: Antenna 4 (a) patch, (b) side view

2.5. Antenna 5

Antenna 5 has 2 identical semi-circular slots in the patch. These slots are located in the middle of two patch edges. The antenna is depicted in Figure 5. Semi-circle radius is given by r_2 (5 mm). The structure' s operation ranges are 1.2659 GHz – 2.1436 GHz (FB=51.49%), and 2.7428 – 4.6657 GHz (FB=51.91%). Antenna feed is placed at (7, 9) mm.
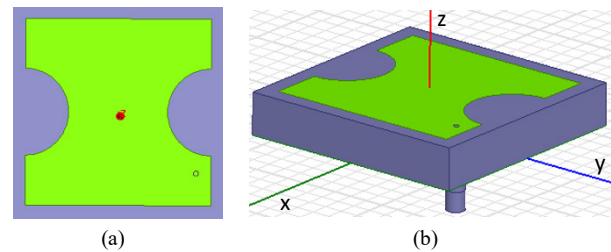
Figure 5: Antenna 5 (a) patch, (b) side view

2.6. Antenna 6

Antenna 6 has 4 identical semi-circular slots in the patch. These slots are located in the middle of all patch edges. The antenna is illustrated in Fig. 6. Semi-circle radius is given by r_2. The structure' s operation range is 1.3465 GHz – 1.8263 GHz (FB=30.24%). Antenna feed is placed at (5.7, 5.3) mm.
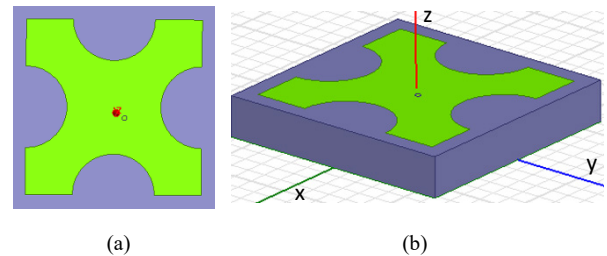
Figure 6: Antenna 6 (a) patch, (b) side view

3. Simulation Results

Simulation results regarding the antenna perormance parameters such as return loss, gain, and radiation pattern are presented for the designed antennas. The return loss and radiation pattern parameters are expressed in dB while the gain values are denoted in dBi. Radiation efficiency and total efficiency values are given in linear scale. Operation frequencies of interest are 1.9 GHz for PCS, 2.1 GHz for 3G, 2.45 GHz for WiFi/WLAN/Bluetooth, 2.6 GHz for LTE and 1.8 GHz for GSM-1800. Table 1 shows the the operations that the antennas are suitable for.

Table 1: Antennas and operations they are suitable for

Antenna	Operation
Antenna 1, 2, 3, 4	PCS, 3G, WiFi/WLAN/Bluetooth, LTE
Antenna 5	PCS, 3G
Antenna 6	GSM-1800

3.1. Results for Antenna 1

Return loss of antenna 1 is given in Figure 7. Maximum gains at 1.9 GHz, 2.1 GHz, 2.45 GHz and 2.6 GHz are 0.087 dBi, 0.055 dBi, 0.052 dBi and 0.058 dBi, respectively. Radiation efficieny values for the same frequencies (in order) are 0.982, 0.975, 0.964 and 0.967, respectively. Total efficiency values for the same frequencies (in order) are 0.923, 0.934, 0.882 and 0.871, respectively.

Figure 7: Return loss of antenna 1

Simulated radiation patterns for antenna 1 are shown in Figure 8. Note that radiation pattern plots represent the radiation intensity for all antennas.

3.2. Results for Antenna 2

Return loss of antenna 2 is given in Figure 9. Maximum gains at 1.9 GHz, 2.1 GHz, 2.45 GHz and 2.6 GHz are 0.097 dBi, 0.059 dBi, 0.044 dBi and 0.045 dBi, respectively. Radiation efficieny values for the same frequencies (in order) are 0.985, 0.981, 0.973 and 0.970, respectively. Total efficiency for the same frequencies (in order) are 0.924, 0.885, 0.842 and 0.856, respectively. Simulated radiation pattern plots are depicted in Figure 10.

3.3. Results for Antenna 3

Return loss of antenna 3 is given in Figure 11. Maximum gains at 1.9 GHz, 2.1 GHz, 2.45 GHz and 2.6 GHz are 0.085, 0.042, 0.047 and 0.066 dBi, respectively. Radiation efficieny values for the same frequencies (in order) are 0.968, 0.989, 0.982 and 0.974, respectively. Total efficiency values for the same frequencies (in order) are 0.911, 0.940, 0.881 and 0.872, respectively. Simulated radiation pattern plots are shown in Figure 12.

(a)

(b)

(c)

(d)
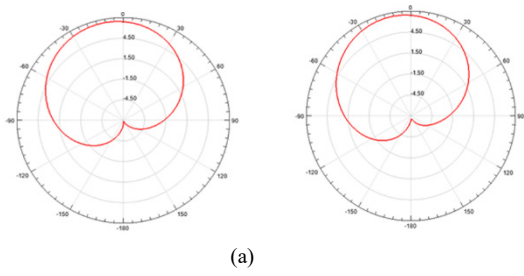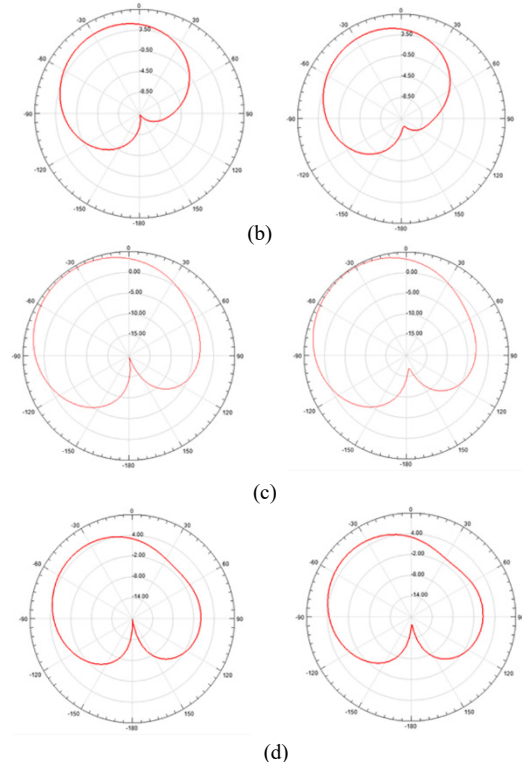
Figure 8: Antenna 1 radiation patterns of $\phi=0^{O}$ (left), and $\phi=90^{O}$ (right): (a) f=1.9 GHz, (b) f=2.1 GHz, (c) f=2.45 GHz, (d) f=2.6 GHz
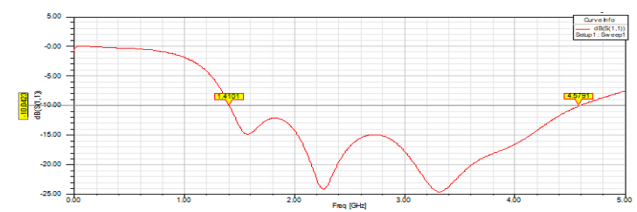
Figure 9: Return loss of antenna 2

(a)

(b)
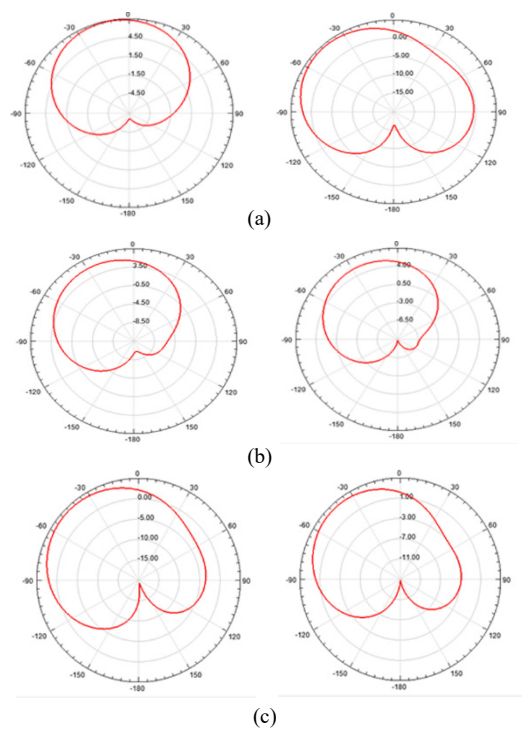
(c)
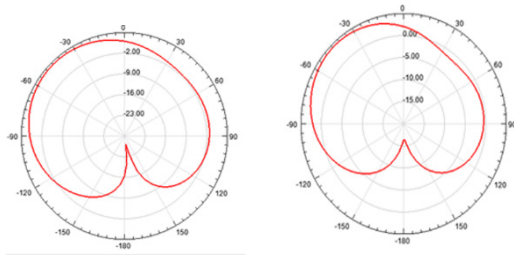
(d)

Figure 10: Antenna 2 radiation patterns of $\phi=0^O$ (left), and $\phi=90^O$ (right): (a) f=1.9 GHz, (b) f=2.1 GHz, (c) f=2.45 GHz, (d) f=2.6 GHz

Figure 11: Return loss of antenna 3

(d)

Figure 12: Antenna 3 radiation patterns of $\phi=0^O$ (left), and $\phi=90^O$ (right): (a) f=1.9 GHz, (b) f=2.1 GHz, (c) f=2.45 GHz, (d) f=2.6 GHz.
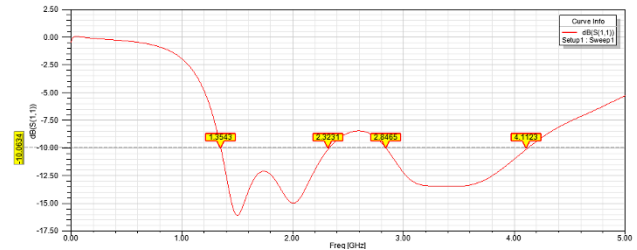
Figure 13: Return loss of antenna 4

3.4. Results for Antenna 4

Return loss of antenna 4 is given in Figure 13. Maximum gains at 1.9 GHz, 2.1 GHz, 2.45 GHz and 2.6 GHz are 0.074, 0.079, 0.082 and 0.087 dBi, respectively. Radiation efficiency values for the same frequencies (in order) are 0.978, 0.988, 0.974 and 0.982, respectively. Total efficiency values for the same frequencies (in order) are 0.935, 0.948, 0.847 and 0.841, respectively. Simulated radiation pattern plots are illustrated in Figure 14.

3.5. Results for Antenna 5

Return loss of antenna 5 is given in Fig. 15. Maximum gains at 1.9 GHz and 2.1 GHz are 0.053 and 0.062, respectively. Radiation efficiency values for the same frequencies (in order) are 0.984 and 0.997, respectively. Total efficiency values for the same frequencies (in order) are 0.958 and 0.910, respectively. Simulated radiation pattern plots are given in Fig. 16.
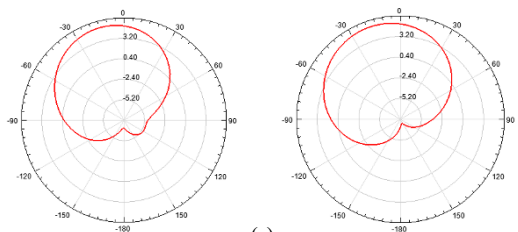
(a)
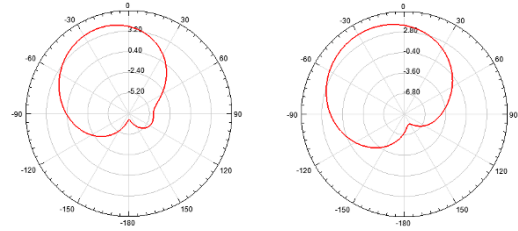
(b)
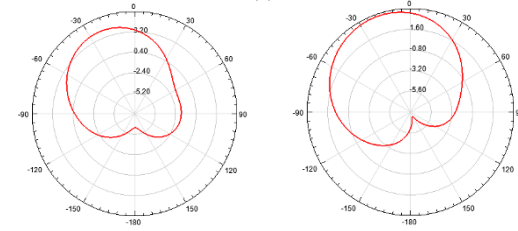
(c)
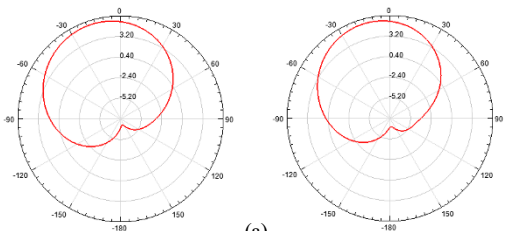
(a)
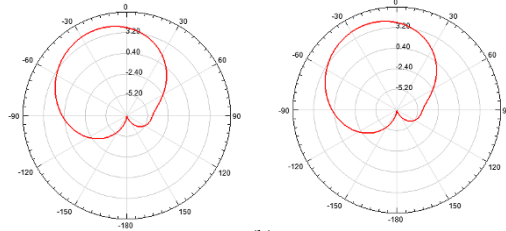
(b)
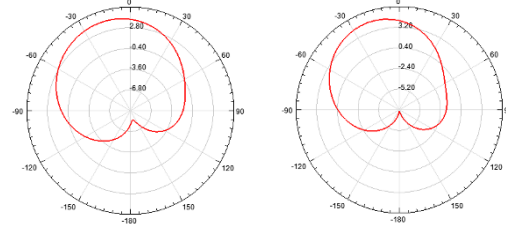
(c)
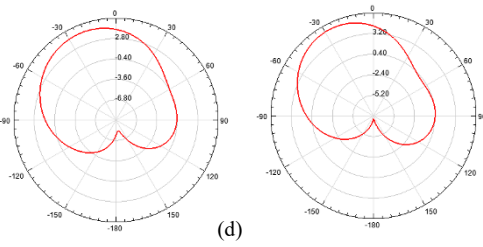
Figure 14: Antenna 4 radiation patterns of ϕ=0° (left), and ϕ=90° (right): (a) f=1.9 GHz, (b) f=2.1 GHz, (c) f=2.45 GHz, (d) f=2.6 GHz

Figure 15. Return loss of antenna 5

3.6. Results for Antenna 6

Return loss of antenna 6 is given in Figure 17. Radiation efficiency and total efficiency values at 1.8 GHz are 0.985 and 0.912, respectively. Simulated radiation pattern plots are illustrated in Figure 18.
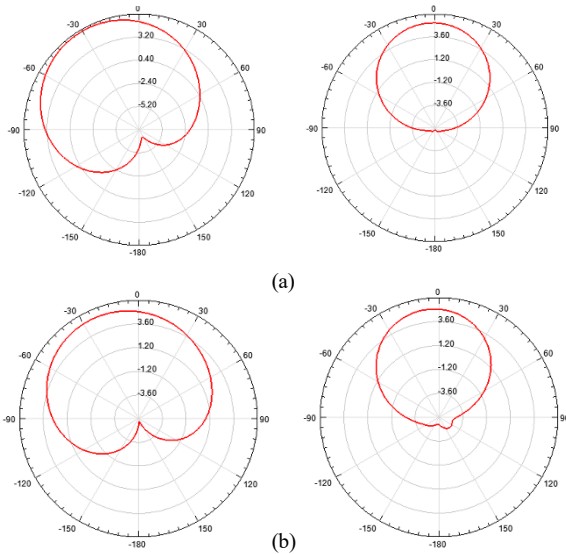
Figure 16: Antenna 5 radiation patterns of ϕ=0° (left), and ϕ=90° (right): (a) f=1.9 GHz, (b) f=2.1 GHz

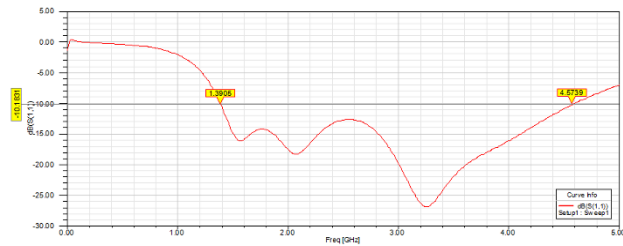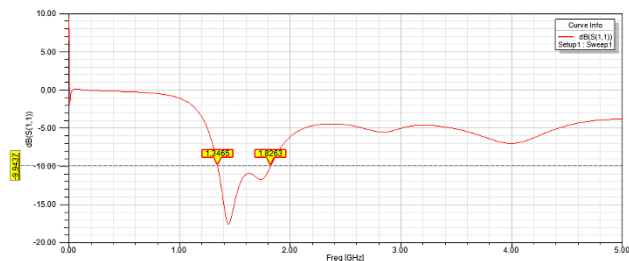
Figure 17: Return loss of antenna 6

Figure 18: Antenna 6 radiation patterns at f=1.8 GHz: ϕ=0° (left), and ϕ=90° (right)

4. Discussion

Considering the designed antennas, antenna 1, antenna 2, antenna 3 and antenna 4 are suitable for PCS, 3G, WiFi/WLAN/Bluetooth and LTE. Antenna 5 cannot be used for WiFi/WLAN/Bluetooth and LTE operations due to the related frequency bands. Likewise, antenna 6 is only suitable for GSM-1800 operation. Highest fractional bandwidth (106.74%) is obtained for antenna 1. Operation frequency band of antenna 2 is shifted upward compared to that of antenna 1. Similarly, an upward band shift is clear by taking into account the frequency band of antenna 3 as well as the lower and upper frequency ends of antenna 4. Also, an increase in the lower end of frequency band is clear by comparing antenna 5 and antenna 6 frequency values. This occurs because the antenna capacitance decreases as the slot dimension increases, which yields larger resonant frequencies. Note that as the antenna capacitance decreases, the resonant frequency increases. Maximum gains for all cases are similar. The case for PCS operation of antenna 2 has the highest maximum gain (0.097 dBi). Directional radiation patterns are obtained for all cases. Maximum radiation occurs in boresight for PCS operation of antenna 6. We have the highest radiation levels for PCS operation of antenna 2. Radiation efficiency and total efficiency values are relatively high indicating that the usage of a substrate with a high dielectric constant does not significantly lower the efficiencies. Simulations of surface current distribution on the antenna patches for different phase angles at all application frequencies reveal multiple current paths, which yield resonances. Note that the resonance occurs when the path length of the current equals to half of the resonant wavelength in the dielectric material. More information on current path length and resonant frequency analysis can be found in [10]. In order to verify the reliability of the simulation tool HFSS, following procedure is performed: Based on the theoretical calculations of patch width and patch length by using a resonant frequency [11], a reverse computation is carried out for the slotless microstrip patch antenna: The resonant frequency is analytically computed as 2.088 GHz by using the known values of the width and relative dielectric constant. Then, the length of the patch is computed as 15.48 mm by utilizing the calculations of effective length and extension length. Analytically computed values of the resonant frequency and the patch length are consistent with the simulated values. Note that a simulated resonant frequency for the slotless microstrip patch antenna is found to be 2.05 GHz.

5. Conclusion

Six square microstrip patch antennas with slots in patch are designed. Impact of quarter-circular and semi-circular patch truncations on the antenna performance parameters is examined. Results regarding the simulations of return loss, maximum gain, radiation pattern, radiation efficiency and total efficiency are presented. Optimizations are carried out in order to improve impedance matching.

References

[1] C. Dogusgen Erbas, B. Demirbas, C. Yaman and A. Okatan, "Design and comparison of microstrip patch antennas with different patch shapes for wireless communications" in 11th International Conference of Electrical and Electronics Engineering, 646-650, 2019, doi: 10.23919/ELECO47770.2019.8990499.

[2] M. Kumar, V. Nath, "Introducing multiband a wideband microstrip patch antennas using fractal geometries: development in last dacade", Wireless Pers. Commun., **98**, 2079-2105, 2018, doi: 10.1007/s11277-017-4965-x.

[3] C. A. Balanis, "Antenna theory: analysis and design", Wiley, 2012.

[4] G. Sami, M. Mohanna, M. L. Rabeh, "Tri-band microstrip antenna design for wireless communication applications", NRIAG Journal of Astronomy and Geophysics, **2**, 39-44, 2013, doi: 10.1016/j.nrjag.2013.06.007.

[5] M. R. Ahsan, M. T. Islam, M. H. Ullah "A microstrip-fed reformed rectangular shape slotted patch for simultaneous operation in GPS and WLAN bands", Microwave and Optical Technology Letters, **57**, 2204-2207, 2015, doi: 10.1002/mop.29290.

[6] C. Y. D. Sim, B. H. Yang, "A single layer dual-band CP microstrip antenna for GPS and DSRC applications", Journal of Electromagnetic Waves and Applications, **22**, 529-539, 2008, 10.1163/156939308784150308.

[7] J. Kaur, Nitika and R. Panwar, "Design and optimization of a dual-band slotted microstrip patch antenna using Differential Evolution Algorithm with improved cross polarization characteristics for wireless applications", Journal of Electromagnetic Waves and Applications, **33**, 1427-1442, 2019, doi: 10.1080/09205071.2019.1612283.

[8] W. W. Li, Q. H. Li, Y. Meng, J. Y. Wang, et. al. , "A broadband microstrip patch antenna with multiple open slots", Microw. Opt. Technol. Lett., **61**, 626-632, 2018, doi: 10.1002/mop.31646.

[9] N. Hassan, Z. Zakaria, W. Y. Sam, I. N. M. Hanapiah, "Design of dual-band microstrip patch antenna with right-angle triangular aperture slot for energy transfer application", International Journal of RF and Microwave Computer-Aided Engineering, **29**, 1-11, 2018, doi: 10.1002/mmce.21666.

[10] R. Varma, J. Ghosh and R. Bhattacharya, "A compact dual frequency double U-slot rectangular microstrip patch antenna for WiFi/WiMAX", **59**, 2174-2179, 2017, doi: 10.1002/mop.30705.

[11] C. A. Balanis, "Antenna Theory: Analysis and Design", Wiley, 2005.

ASTES

Dry Sliding Wear Behaviour of ZA27/ MoS2 Metal Matrix Composite

Mohamed Kafeel Delvi[1,*], Khazi Mohamed Kaleemulla[2]

[1]*Mechanical Engineering Department, Bearys Institute of Technology (Affilaited to VTU Belgavi) Mangalore, Karnataka, 5600, India*

[2]*Mechanical Engineering Department, University B.D.T. College of Engineering (Constituent College of VTU Belgavi) Davangere , Karnataka , 56000, India*

A R T I C L E   I N F O

A B S T R A C T

The Present work is to investigate effect of dry sliding wear behaviour of ZA27 base alloy, after reinforcing it with Molybdenum Di Sulphide (MoS_2) particles from 0% to 4% in five steps. To examine the wear behaviour of both reinforced and un-reinforced material, dry or unlubricated pin on disc tests were conducted. These tests were conducted at varying speeds and loads of 1.5m/s,3m/s, 4.6m/s, 6.15 m/s and 5N, 10N, 20N and 25Nrespectively with a constant sliding distance of 1000m. The results revealed that, MoS2 reinforced ZA27 alloy showed less wear loss as compared to base ZA27 alloy. Delamination, abrasion, and adhesive wear were observed at high speed and load. Worn surface of tested specimen were analysed and examined through Scanning Electron Microscope (SEM). To confirm presence of Molybdenum disulphide in prepared material, Energy Dispersion X-ray (EDX) test is carried out for 4% of Molybdenum disulphide reinforced ZA-27 material.

1. Introduction

From the last few decades, metal matrix composite has played a vital role in the improvement of physical and mechanical properties of traditional materials. Also, it plays a significant impact from an economic point of view due to its wide range of application in engineering material. It will always be a choice of many researchers to further improve its performance through changing or varying its composition[1]-[5]. Maximum work was done on the various Aluminium series in the field of non-ferrous metal. In comparison with aluminium less scope is given to other non-ferrous metal like brass, copper, magnesium, and zinc.

Pure zinc cannot compete with other non-ferrous material. But zinc when reinforced with the various proportion of aluminium, at certain composition, it can be observed that zinc properties improved to such level that it can be easily compete with other traditional non-ferrous material such as copper, brass, bronze, aluminium and also cast iron in the field of moderate load, medium speed and moderate operating temperature, generally ZA 27 applied for bearing and tribo material [6]-[9]. Many

researchers have experienced that 27% of aluminium reinforcement shows good mechanical and physical properties compared to other percentages. ZA27 stands for zinc containing 27 percentage of aluminium.ZA27 possesses tribo-mechanical properties, eco-friendly, excellent fluidity and foundry castability as well as low initial cost. Resistance to corrosion and high mechanical strength at room temperature are other admirable properties of ZA27 alloy [10]-[12]. These exceptional properties have motivated the researchers to further enhance its mechanical and tribological properties through reinforcing ZA 27alloy with a different metal, non-metal and ceramics with varying current alloy composition or changing method of casting. As a result, author [10],studied wearing of ZA 27 after Reinforcing with 2% graphite. In [13], reinforced graphite with ZA 27, varying its size and percentages to study it's mechanical properties. In [14], ZA 27is experimented with zircon by its varying percentage. Author [7] , reinforced small quantity of Manganese (Mn) with a weight range of 0.1% to 0.7% in ZA27 metal using the normal casting method. In paper [15], tribological test is conducted after reinforcing Mn content with ZA27 alloy. In paper [16], Za27 with 2% Magnesium (Mg) material is tested. Author [12], presented the paper on results of tribological investigations of composites with substrate made of the ZA-27 alloy reinforced by

*Corresponding Author: Mohamed Kafeel Delvi , Mechanical Engineering Department, Bearys Institute of Technology (Affilaited to VTU Belgavi) Mangalore, Karnataka , India, Contact No +91 9986347419 & rulerkafeel@yahoo.co.in

the Al_2O_3. Author [17], studied combined effect of reinforcement both 5% SiC and 1% Graphite particle in Za27 alloy. The combined effect of silicon, Silicon Carbide, graphite and copper with various percentage on ZA27 alloy is studied in another researcher [6] . Author [9], worked on reinforcing glass fibers of weight 1% to 5% in ZA27 alloy using the compo-casting method. In [18] ,examined the effect of various composition of titanium on ZA 27 alloy. Author [19], fabricated ZA27 alloy with 2% of TiB_2 particulates. In such a way, researchers have experimented with various reinforced materials and various method to improve the mechanical and tribological properties of ZA 27 alloy.

Molybdenum disulphide is an inorganic compound which is used as a solid lubricant, it is used in relatively high temperature when compared to graphite [20]. It has experimented with polymer and other organic material in the field of polymer matrix composite. It has also been observed that addition of Molybdenum disulphide has improved the tribological properties of high density poly ethylene and Polyetherether ketone (PEEK) composite in vacuum [21], it is also experimented with Phenolic resin to improve its mechanical and tribological properties [22], but rare literatures are found, in which Molybdenum disulphide was used as reinforcement material with Zinc Aluminium 27 (ZA -27) Metal Matrix composite. Since ZA 27 alloy is also applied in tribo material like bearing and bushing, which is subjected to frictional heat, MoS_2 is possess good lubricating property, generally it is used externally, to remove frictional heat between contact surface. Till now with mentioned composition of ZA 27 (Sn 1-2%,Cu 0.5%, 27% Al, balance zinc), no literature is found in which MoS_2 is used as reinforced material with ZA27 .

2. Experimentation

2.1. Material

The metal matrix selected for the present work is Zinc Aluminium alloy in which the proportion of Aluminium is 27%. The importance of ZA 27 alloy has already been discussed in the introduction. Composition of ZA27 is, Tin between 1% to 2%, Copper 0.5%, Aluminium 27% and remaining is zinc. Molybdenum disulphide (MoS_2) particle is used as reinforcement component which has particle size 40 micron with the average density of 5.6gm/mm3. MoS_2 fabricated with base ZA27 alloy with increasing proportion from 0 to 4% with an increment step of 1 %. Steel crucible is used in an electric heating furnace to melt alloy. A stirrer is attached with an adjustable speed motor which is used for stirring purpose. Skum powder or cleaning powder added to the molten metal in order to remove slag and flux.

2.2. Preparation of Specimen

Specimen for wear testing has prepared with the help of the stir casting method [23]. Based on the furnace's crucible size, a calculated amount of ZA 27 is weighed and placed in the crucible. Heating of crucible is carried out at a constant temperature of 600oC until the solid ZA27 is converted into a liquid phase. The

molten matrix is cooled to a mixing temperature of 490oC, at which stirring of molten metal was carried out with the help of a stirrer, which operates at the speed of 1 to 500 rpm. Based on the weight of molten ZA27, 1% MoS_2 particle was weighed and then poured in stirring liquid which is operated at speed of 200 rpm. Gradually speed of the stirrer is increased to a range of 320 to 350 rpm after mixing of reinforcement material. The Stirring of molten metal is continued for 5 minutes. Before pouring molten metal into a mould, a circular mould that is made of cast iron is heated. Heated molten metal is poured into the pre-heated mould. The same procedure is repeated for reinforcement of 2,3and 4 percentage of MoS2 particle. Mould is allowed to cool at room temperature, as a result, the molten metal inside the mould is solidified. Casted metal from the mould was removed and machined according to ASTM G99 standard size. Tested specimen of diameter (d) 10 mm and length of 1.5d to 2d is prepared. The end surface of the specimen is polished and flattened with the help of an emery sheet of 1000 size. Finally mirror polished surface at the end of the specimen is obtained for wear testing.

2.3. Wear testing of specimen.

Pin on disc apparatus (as shown in Figure 1:) is used to investigate the dry sliding wear behaviour of flatted end, mirror polished ZA27, ZA27/1%MoS2 ZA27/2%MoS2, ZA27/3%MoS2 and ZA27/4%MoS2 specimens. Load, sliding distance, and sliding speed are parameters considered for present wear testing. The selected value for loads is 5N, 10N, 20N and 25N. Sliding distance are 1.53m/s,3m/s, 4.6m/s and 6.15m/s with constant sliding distance of 1000m is maintained for both parameters. All tests is conducted at room temperature; details are shown in Table 2.1. During the test, the initial weight of the composite is measured using a weighing machine having the least count of 0.0001g. The testing pin is applied with a defined load, against the EN32 steel disc. The pin is pressed against the rotating disc at a track diameter of 98 mm at a specific speed, and a constant sliding distance of 1000m. The disc is rotated for prescribed speed, after running at a specific sliding distance, the rotating disc is stopped and tested specimen taken out from the setup. The final weight of the worn-out specimen is measured. The procedure is repeated to all specimen. Each specimen has experimented with three times and the average weight loss of each specimen is taken for wear analyse. Graph of the average wear loss of tested specimen vs. varying load and speed were plotted to examine the overall behaviour of all specimens. During testing, the specimen projected its particle on countersurface, as a result, a circular thin track of specimen is formed on the rotating disc due to the relative motion and difference of hardness between countersurface and specimen. As the specimen was softer than the rotating disc, the worn particles of a specimen are projected on the rotating disc. This analyses the counter-surface which is shown in Figure 2.

Table 1: Wear testing parameter

Pin material	ZA-27 with 0%, 1%, 2%, 3%and 4% MoS$_2$
Disc Material (rotating)	EN32 steel Disc usedas counter-body (65 HRC)
Track diameter	98mm
Sliding speed m/s	1.53, 3, 4..6,6.15
Load (N)	5,10,20 and 25
Sliding distance	1000m
Temperature	Room temperature

3. Experimental Results

3.1. Effect of Applied Load on Wear Loss

Prepared specimens of various compositions are tested at different loads of 5N, 10N, 20N and 25N at a constant sliding distance of 1000m and a constant sliding speed of 4.6m/s. The difference between the initial and final weight of each specimen was tabulated. Using obtained value graph of Wear loss in milligram (mg) versus various load in newton has generated as shown in Figure 3. It has been observed from the graph (Figure 3) that, as the load on the specimen is increased, the rate of wear is also increased for both molybdenum disulphide reinforced and unreinforced material. It has also been noticed from the above graph that unreinforced materials lost their maximum weight during the wear test when compared to reinforced material. At a lower load of 5N, mild wear was observed for reinforced material compared to a little high degree of wear was observed for unreinforced material. This trend of increasing weight loss due to wearing continues for the load of 10N and 15N, to mild weight loss to medium weight loss. The specimen was tested up to a load of 25 N, significant results have been seen at a higher load of 25N for the unreinforced material. Worn surface of specimen deformed. Worn material comes out and attached at the circular end of the specimen. Simultaneously when observed the behaviour of various reinforced materials, all reinforced composition showed the better results when compared to unreinforced specimen. Among composite specimen, 4% and 3% of the reinforced specimen showed good wear resistant compared to 1 % and 2% of the reinforced composite and also 3% and 4% of reinforced composite showed nearly repeated result and simultaneous experienced higher wear resistance as compared to unreinforced ZA27 and ZA27 contains lower composition MoS$_2$ like 1% and 2 %.From figure 3 it can be observed that there is an increase in wear-resistant as increased in the composition of MoS$_2$ in ZA 27, but There is slight breakage of trend that can be seen at an applied load of 25N, speed of 4.6 m/s and sliding distance of 1000m. The mixed result is observed for 3% and 4% reinforced composite at a higher load of 25N.

3.2. Effect of sliding speed on wear loss

After various load parameters, tests are conducted based on the sliding speed parameter. Prepared specimens of various compositions of 0%, 1%, 3% and 4% of molybdenum disulphide are tested at various sliding speed of 1.5m/s, 3m/s, 4.6 m/s 6.1m/s at constant sliding distance of 1000m and constant load of 20N. The difference between the initial and final weight of each specimen is tabulated. Using obtained value, the graph of wear loss in milligram versus various sliding speed in meter per second is generated as shown in Figure 4. It has been observed from the graph (Figure 4) that, as the sliding speed of the specimen is increased, the rate of wear is also increased for both molybdenum disulphide reinforced and unreinforced material. It has been noticed from the above graph that, unreinforced material lost its maximum weight during the wear test when compared to reinforced material up to a speed of 4.6m/s. But after 4.6m/s speed, remarkable results were noticed that 4% and unreinforced material was worn out much compared to both 3% and 1% of reinforced molybdenum disulphide materials at speed of 6.15m/s. From the above results and graphs of both varying speed and varying load, it can be concluded that addition of molybdenum disulphide is not more than 3 % percentage for higher speed of 6.15m/s and medium speed of 4.6m/s, 3 to 4 percentage of molybdenum disulphide can be used as reinforced material. Somewhat similar results have been found during varying load from 5N to 25 N. At low speed of 1.5m/s mild wear were observed for both molybdenum disulphide reinforced and unreinforced specimens. However, as the sliding speed increased proportionally wear rate has also increased and weight loss due to wear also increased. At a higher speed of 6.15m/s, the high degree of wear and tear is observed, as a result, the worn surface smeared and highly deformed than the actual dimension of the specimen. During the process, heavy vibration and noise noticed. Transfers of pin material on contact disc were also observed during testing of all specimens. It can be seen from both the graph of Figure 2 and Figure 3, 3% of percentage reinforced molybdenum disulphide has a more positive effect on the base metal ZA27 when compared with unreinforced as well as various reinforced material when tested for a parameter of varying load and varying speed.
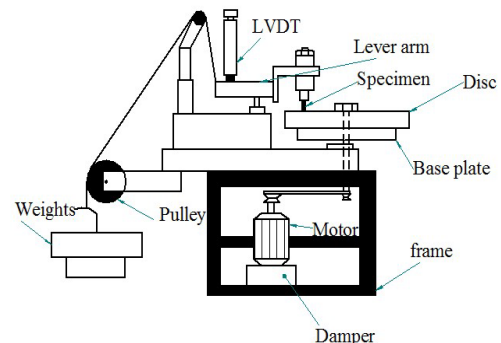
Figure 1: Schematic diagram of the dry sliding wear testing apparatus
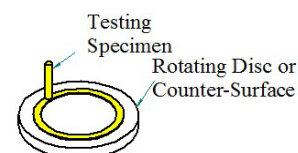
Figure 2: Analyses of countersurface during wear
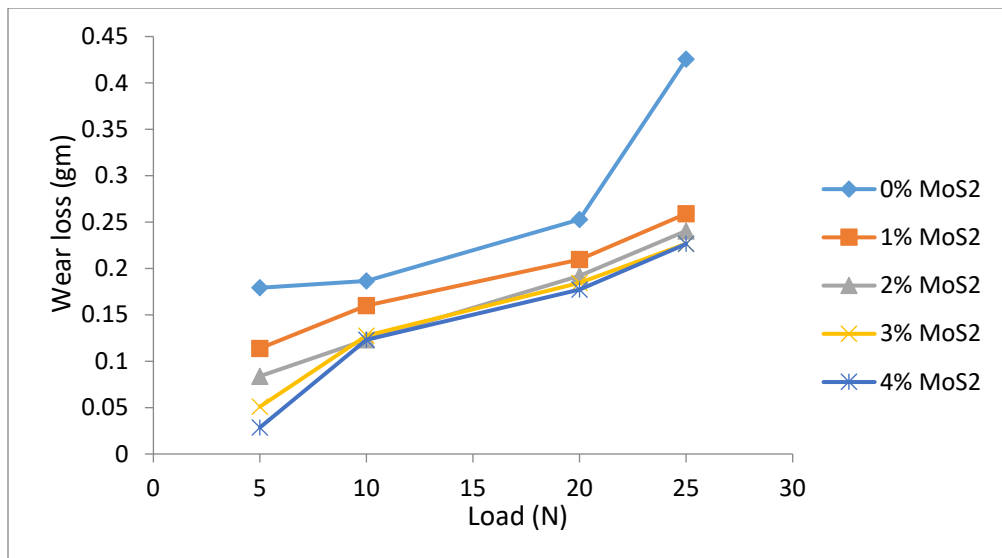
Figure 3: Variation of wear loss with varying applied Load for constant sliding of 1000m and sliding speed of 4.6m/s.
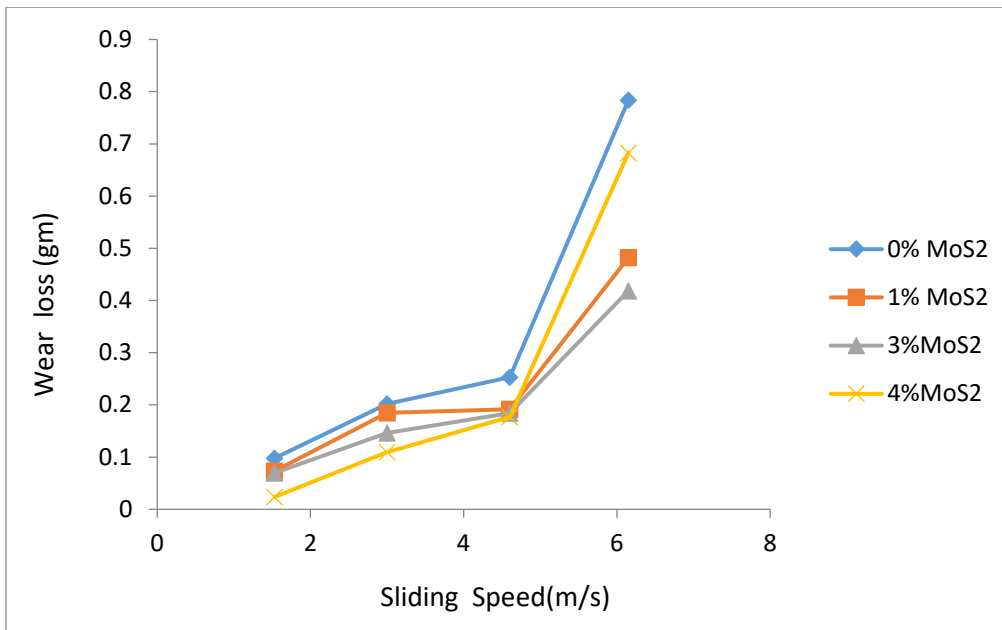
Figure 4: Variation of wear loss with varying Sliding speed for constant sliding distance of 1000m and load of 20N
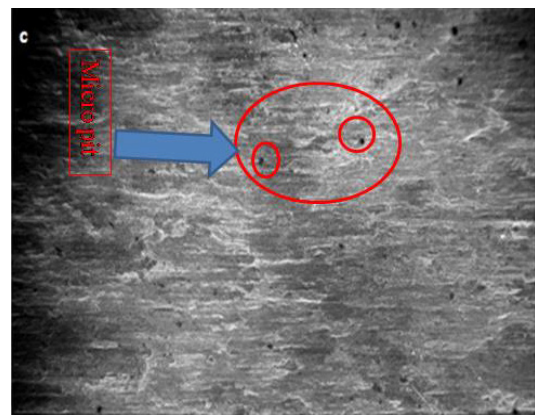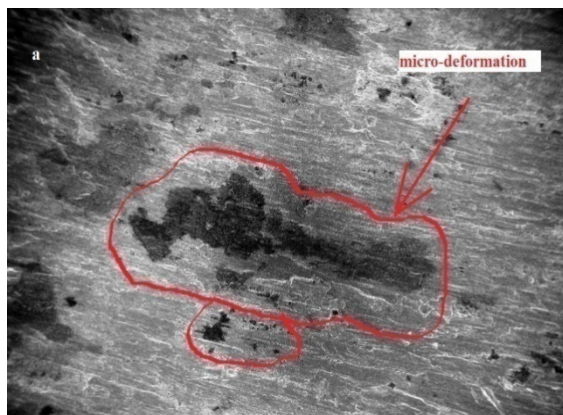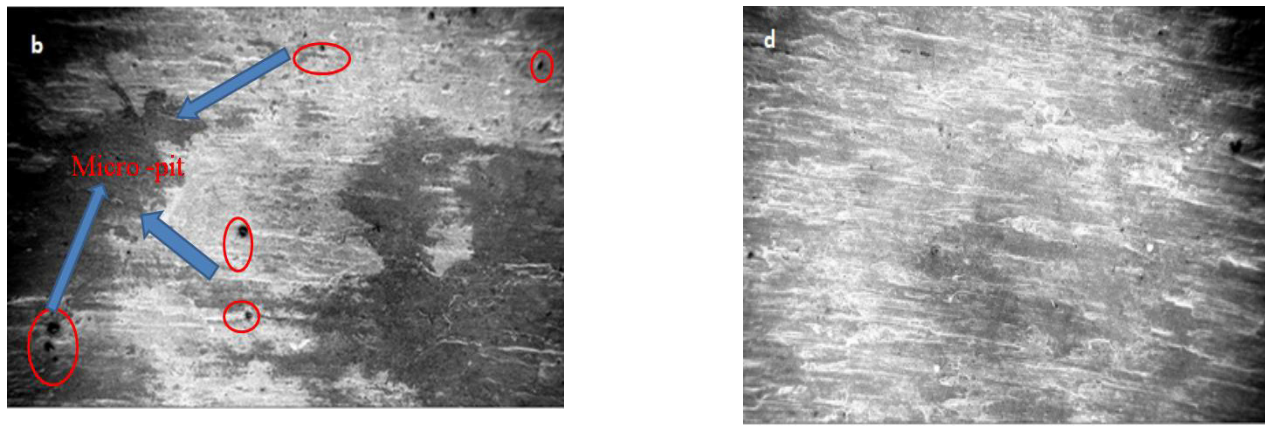
Figure 5: SEM image (100 µm size) of worn surface for the specimen for varying sliding speed of 4.6 m/s constant load of 20N and sliding distance of 1000m. a) 0% MoS$_2$ Figure b)1%MoS$_2$,Figure c)3%MoS$_2$Figure d)4%MoS$_2$

ElectronImage1

CKa1_

2OKa1

AlKa1

ZnKa1

SnLa1

MoLa1

SKa1
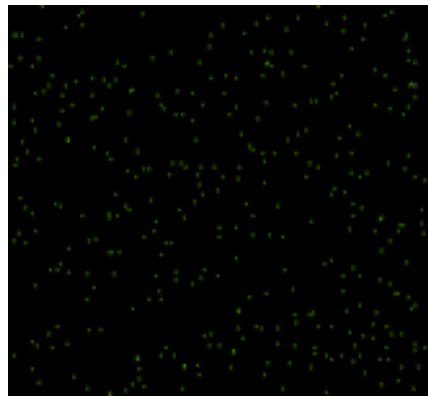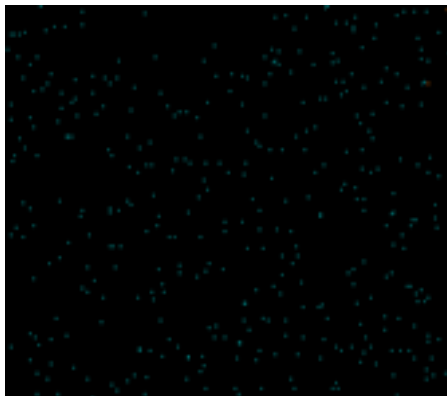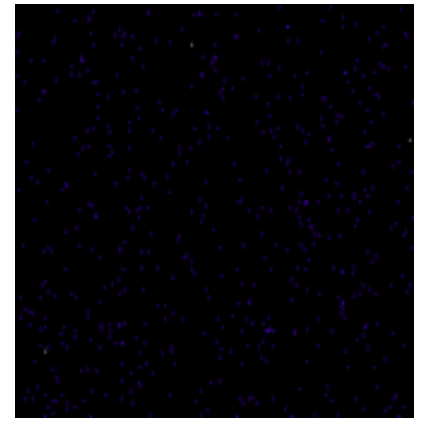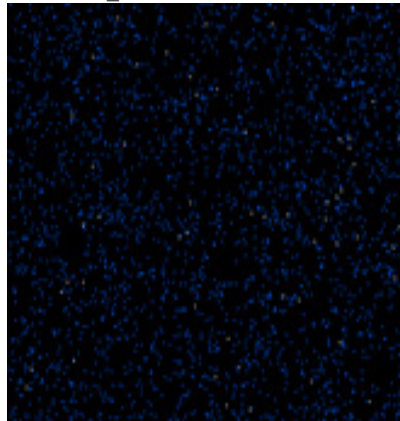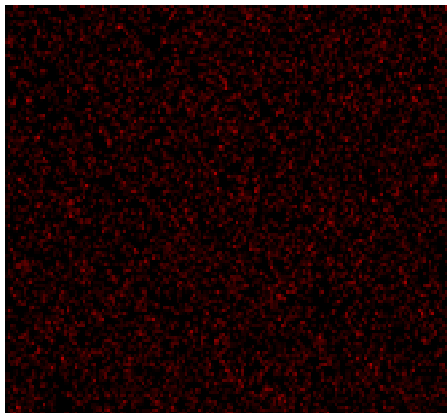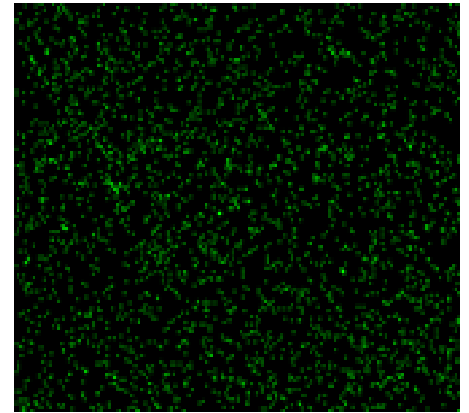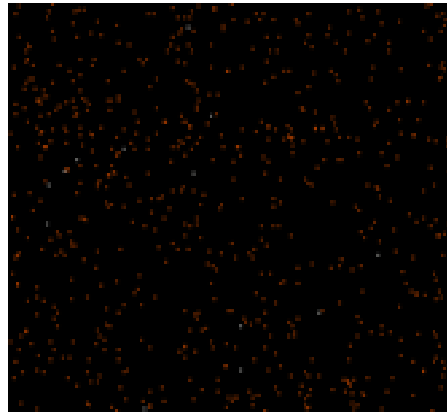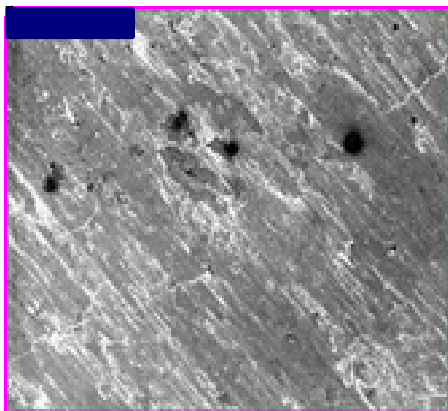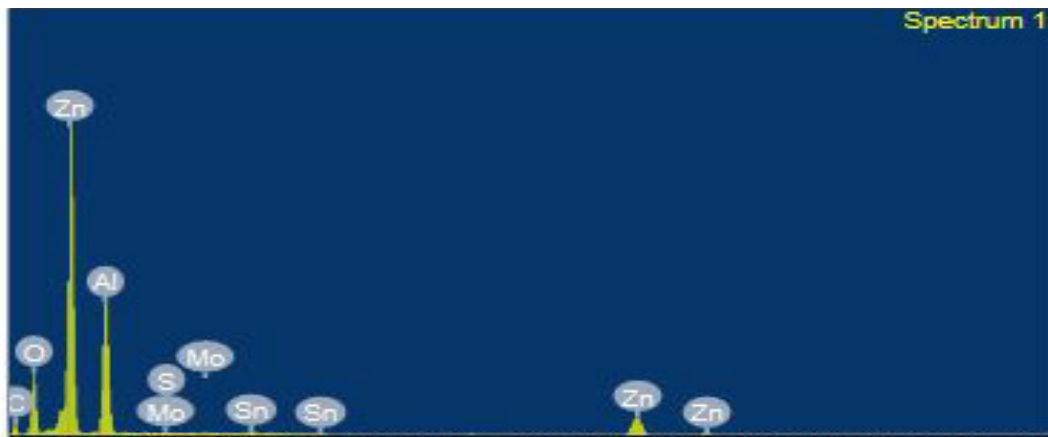
Figure 6: Energy Dispersion X-ray (EDX) report for 4% MoS$_2$ reinforced ZA-27 material

3.3. SEM Analyses of worn surface

Scanning electron microscope (SEM) image of the worn surface was taken for molybdenum disulphide reinforced and unreinforced ZA27 specimen, for a load of 20 N, speed of 4.6 m/s and distance of 1000 m. Interesting results are observed from Figure 3, for varying speed of 4.6m/s, at that speed, 4% MoS$_2$ reinforced specimen shows better results when compared to 3% MoS$_2$ and 1% MoS$_2$ reinforced material as well as unreinforced material. As a result, at that point, SEM analyses were carried out. As sliding speed increases wear rate also increases, this is already explained in the previous section. But after observing all four SEM images distinct changes can be seen between unreinforced and reinforced ZA27 base metal. From graph 2 and 3, it can be observed, unreinforced specimen exhibits poor wear performance compared to all reinforced specimen. Figure 5 a) shows SEM image of unreinforced material is not smooth. Micro debris appeared during operation between the rotating steel disc and tested specimen. During cyclic rotation of the disc, the micro-debris appeared between contact surface that leads to abrasive wear occur. As a result, due to brittle fracture, micro deformation can be seen in Figure 5(a), due to expelled of microchips from the worn surface and also minute damage was observed for the unreinforced specimen, from the SEM image shown in Figure 5(a). As the percentage of MoS$_2$ was increased in base metal, the level of damage is reduced which can be seen from SEM image of 1%MoS$_2$ in Figure 5(b), 3% MoS$_2$ in Figure 5(c) and 4% MoS$_2$ in Figure 4(d) for the speed of 4.6m/s. But crushed micro debris attached to the worn surface of both reinforced and unreinforced material during rotation of the disc. As the percentage of MoS$_2$ increased, wear rate in composite specimen up to load of 20 N, speed of 4.6 m/s and distance of 1000m decreased repeatedly for all MoS$_2$ reinforced specimens compared to the unreinforced specimen and each specimen was tested thrice to get repeatability of the result. This attributed to the presence of MoS$_2$ particle which acted as a lubricating agent which is projected out from worn specimen that reduces heating effect which occurred due to friction between pin and disc, similar findings were observed for Graphite from other researchers [24][10][1]. A similar observation can be seen from SEM image that, with the addition of reinforced material, comparatively more refined image, relatively lesser micro-deformation, and minimization of extraction micro-flake from the worn surface due to friction and heat can be observed. Comparing Figure 5(a) and Figure 5(b) , variation in size of damage in the form of micro-pit is observed at some portion of the surface as a result of the detachment of micro particles from the specimen during testing due to abrasive wear.Interestingly, the size of the micro-pit and the number of micro-pits is reduced for 1% MoS$_2$ reinforced specimen when compared to the unreinforced specimen as shown in the SEM image, which can be observed from Figure 5 (b) and 5(a). Both sizes of pits are marked with the help of a circle in Figure 5(a) and Figure 5(b). Further increase in the proportion of MoS$_2$, further reduced in size and the number of micro-pits that is shown in Figure 4 (c). When observed for 4% of MoS$_2$ reinforced image, a more refined surface can be seen in Figure 4(d) as compared to all remaining 3 images as shown in Figure 5(a), 5(b) and 5(c). The observed portion of the micro-deformed surface in Figure 5(a) and pits surface in Figure 5(b) and 5(c) are marked with the help of the ellipse in the SEM image.

3.4 EDX Analyses

To confirm, the presence of Molybdenum disulphide in ZA 27 based metal, energy dispersion X-ray (EDX) image taken for one of the reinforced specimens. For that 4%, Molybdenum disulphide reinforced ZA 27 used. The EDX image of 4 percentage of MoS$_2$ reinforced specimen can be seen in Figure 6. From the image, it can be seen that molybdenum and sulphide are distributed in the same orientation and location. It can also be concluded that there is no separation occur between Molybdenum particle and sulphur particle during casting due to high temperature. From electron image, it is observed that for 700 micro-meter sizes of worn surface more molybdenum was confirmed when compared to tin element.

4. Discussion

and sliding speed increases, the wear rate also increases. MoS_2 reinforced specimen shows a different level of wear rate depending upon the quantity of its reinforced alloy. However, interestingly, it has been observed that, up to some limit, at a sliding speed of 4.6m/s, reinforced material revealed less wear rate when compared to unreinforced material. Tests were conducted with increasing level of the parameter for applied load from 5N to 25N and sliding speed from 1.56 m/s to 6.15m/s. The end surface area of the stationary pin completely contacts with a rotating steel disc. Due to the difference in hardness and strength as well as relative motion between pin and disc, frictional heat generation was observed when a heated pin is taken out from the wearing machine after running it for a specific time. During operation, heavy noise and vibration were observed, which increased with increasing applied load and sliding speed of the pin for both molybdenum disulphide reinforced and unreinforced specimen. A similar situation was reported by other researchers [25]. During the low applied load of 5N and low sliding speed of 1.56 m/s, at a constant sliding distance of 1000m, the smooth polished surface of the pin turned to rough scratches. Micro or powder-like particles appeared from the pin during rotation of the disc, which are in contact with each other due to wear and friction. These particles are attached and smeared, abraded surface and spread over the track on which pin rotates during each cycle of revolution. Generally, abrasive type of wear occurred, as a result, weight of prepared specimen was reduced due to abrasive wear mechanism. But from both varying applied load and sliding speed graphs, composite material revealed better result when compared to unreinforced ZA 27 alloy for all parameter of speed and load. This can be attributed to the presence of Molybdenum disulphide particles. During operation, micro-particles were projected out from the specimen due to continuous shearing of surface on steel disc, simultaneously frictional heat was generated due to relative motion. In addition, it has observed that, at higher sliding speed and applied load, the material come out in the form of macro-debris and flakes faster rate than lower applied load and sliding speed, which caused a decrease in a final weight of the specimen. But the decrease in wear rate observed from the mentioned graph 3 and graph 4 for molybdenum disulphide reinforced ZA27 material compared to unreinforced ZA 27 material. During the testing, materials were projected out from the specimen, in the form of minute flakes or chips or small particles or debris depending upon the degree of applied load and sliding distance.

During the projection, in the case of a reinforced specimen, molybdenum disulphide was present, also come out from the specimen transform to the rotational track of the disc. As a result, molybdenum disulphide acts as a lubricating agent, which minimizes frictional heat, generated due to the relative motion between rotating disc and pin. Molybdenum disulphide smeared on the abraded surface, which projected out from the rotating pin, which is pressed against rotating disc due to applied load. It acts as a tribo-layer between rotating disc and pin, meaning the projected molybdenum disulphide will enter between stationary pin, which is compressed against the disc, which reduces the level of heat generation, which has not occurred for unreinforced ZA27

base alloy [27]. Similar findings are reported from other researchers regarding the reinforcement of graphite [10][1][26]. Similarly, it can also be seen from Scanning Electron Microscope (SEM) images from Figure 5 (a) to 5 (d). Where unreinforced specimen is shown in Figure 5 (a) observed more damage and cloud-like surface(marked in red colour), when compared to the other images that are shown in Figure 5 (b) for $1\%MoS_2$ reinforced ZA-27, Figure 5 (c) for 3% MoS_2 reinforced ZA-27,and Figure 5 (d) for 4% MoS_2reinforced ZA-27. After observing the images from Figure 5, it can be seen that, when the percentage of molybdenum disulphide increased, the size of the damage is reduced, fewer pits generated due to debris when compared to images shown in Figure 5(b), less uneven surface was observed in Figure 5 (c) and Figure 5(d) which was having reinforcement percentage 3% and 4% of molybdenum disulphide respectively compared to the unreinforced ZA-27 base alloy that is shown in Figure 5 (a) and 1% Molybdenum disulphide reinforced ZA 27 alloy shown in Figure 5(b). To confirm the presence of Molybdenum disulphide in reinforced ZA 27 alloy, one of the reinforced specimens was tested with Energy Dispersion X-ray (EDX) test. Energy Dispersion X-ray test was carried out for ZA27 alloy which was reinforced with 4% molybdenum disulphide. The image of the test as shown in Figure 6 confirmed the presence of MoS_2 in reinforced metal. It has also been observed that Molybdenum and sulphur are present at the same location. During operation, minute pits were generated due to interaction of specimen with projected debris which resulted in that shear stress will occur and that pit nucleates during rotation of the disc. Simultaneously, subsurface cracks are occurred in some specimen due to the removal layer in the form of flacks or chips as a result, severe abrasive wear was observed after the sliding speed of 4.6 m/s, at a constant sliding distance of 1000m and an applied load of 20N. Unambiguous results were observed after the speed of 4.6 m/s. Interestingly, at the speed of 6.15m/s, 3 % reinforced Molybdenum disulphide ZA 27 specimen showed the good result when compared to the unreinforced ZA 27 base alloy and similarly when the same composition is tested for varying load of 5N to 25N, 3% reinforced Molybdenum disulphide showed the better result at a higher applied load of 25N, when compared to unreinforced ZA 27 base alloy and some Molybdenum disulphide reinforced specimen for a constant sliding distance of 1000m and sliding speed of 4.6m/s. At a higher speed of 6.15m/s more noise and vibration occurred and more frictional heat was generated due to the relative motion between the pin and rotating steel disc. Due to frictional heat, applied pressure as well as surface contact area increases due to plastic deformation. As a result, attached debris and particles cluster are accumulated at the circular edge of the tested pin.

5. Conclusion

Present work, the investigation has been done on dry sliding wear behavior of ZA 27 base metal and ZA 27/MoS_2 reinforced metal under varying applied load and sliding speed conditions. It is also observed from the above-mentioned result that, MoS_2 reinforced ZA27 specimen having more wear resistant as

compared to the unreinforced ZA27 specimen in both varying load and speed. Up to 3% MoS_2 reinforced ZA 27 showed good wear resistant as compared to other percentages of reinforcement. But increasing in MoS_2 content beyond 4% for the higher load of 25N and the speed of 6.25m/s at a constant sliding distance of 1000m, there is a decrease in wear resistant is observed as compared to other reinforcement percentages, still better than unreinforced ZA27 alloy. Addition of molybdenum disulphide decrease wear rate of reinforced ZA 27 metal through smearing Molybdenum disulphide coat at the interface between the pin and the counter face. During medium load and speed, abrasion wear observed while at high speed, Delamination wear occurred due to nucleation of subsurface crack.

Acknowledgement

Conflict Of Interest

"On behalf of all authors, the corresponding author states that there is no conflict of interest"

Reference

[1] S. Basavarajappa, G. Chandramohan, K. Mukund, M. Ashwin, M. Prabu, "Dry Sliding Wear Behavior of Al 2219 / SiCp-Gr Hybrid Metal Matrix Composites," Journal of Materials Engineering and Performanc, **15**(December), 668–674, 2006, doi:10.1361/105994906X150803.

[2] F. Gul, M. Acilar, "Effect of the reinforcement volume fraction on the dry sliding wear behaviour of Al-10Si/SiCp composites produced by vacuum infiltration technique," Composites Science and Technology, **64**(13–14), 1959–1970, 2004, doi:10.1016/j.compscitech.2004.02.013.

[3] A.M. Davidson, D. Regener, "A comparison of aluminium-based metal-matrix composites reinforced with coated and uncoated particulate silicon carbide," Composites Science and Technology, **60**, 865–869, 2000, doi:10.1016/S0266-3538(99)00151-7.

[4] B. Venkataraman, G. Sundararajan, "Correlation between the characteristics of the mechanically mixed layer and wear behaviour of aluminium, Al-7075 alloy and Al-MMCs," Wear, **245**(1–2), 22–38, 2000, doi:10.1016/S0043-1648(00)00463-4.

[5] Y. Iwai, T. Honda, T. Miyajima, Y. Iwasaki, M.K. Surappa, "Dry sliding wear behavior of Al 2 O 3 Fiber reinforced aluminum composites," Composites Science and Technology, **60**, 1781–1789, 2000, doi:doi: org/10.1016/S0266-3538(00)00068-3.

[6] R. Auras, C. Schvezov, "Wear Behavior , Microstructure , and Dimensional Stability of As-Cast Zinc-Aluminum / SIC (Metal Matrix Composites) Alloys," **35**(May), 1579–1590, 2004.

[7] C. Domínguez, M. V. Moreno López, D. Ríos-Jara, "The influence of manganese on the microstructure and the strength of a ZA-27 alloy," Journal of Materials Science, **37**(23), 5123–5127, 2002, doi:10.1023/A:1021016522586.

[8] B.M.S. SC. Sharma , B.M. Girish, Rathnakar Kamath, "Graphite particles reinforced ZA-27 alloy composite materials for journal bearing application," Wear, **219**, 162–168, 1998, doi:org/10.1016/S0043-1648(98)00188-4.

[9] S.C. Sharma, B.M. Girish, B.M. Satish, R. Kamath, "Mechanical properties of as-cast and heat-treated ZA-27 alloy/short glass fiber composites," Journal of Materials Engineering and Performance, **7**(1), 93–99, 1998, doi:10.1361/105994998770348098.

[10] M. Babic, M. Slobodan, D. Džunic, B. Jeremic, B. Ilija, "Tribological behavior of composites based on ZA-27 alloy reinforced with graphite particles," Tribology Letters, **37**(2), 401–410, 2010, doi:10.1007/s11249-009-9535-2.

[11] M. Babić, S. Mitrović, R. Ninković, "Tribological potencial of zinc-

[12] S. Mitrović, M. Babić, I. Bobić, "ZA-27 alloy composites reinforced with Al2O3 particles," Tribology in Industry, **29**(3–4), 35–41, 2007.

[13] K.H.W. Seah, "Mechanical particulate properties composites of cast ZA 27 / graphite," **16**(5), 1–5, 1995.

[14] S.C. Sharma, B.M. Girish, D.R. Somashekar, B.M. Satish, R. Kamath, "Sliding wear behaviour of zircon particles reinforced ZA-27 alloy composite materials," Wear, **224**, 89–94, 1999.

[15] V. Algur, V.R. Kabadi, S.M. Ganechari, V. Rao, "Influence of Mn Content on Tribological Wear Behaviour of ZA-27 Alloy," Materials Today: Proceedings, **4**(10), 10927–10934, 2017, doi:10.1016/j.matpr.2017.08.048.

[16] T.J. Chen, Y. Hao, J. Sun, Y.D. Li, "Effects of Mg and RE additions on the semi-solid microstructure of a zinc alloy ZA27," Science and Technology of Advanced Materials, **4**(6), 495–502, 2003, doi:10.1016/j.stam.2004.01.002.

[17] K.H.W. Seah, S.C. Sharma, P.R. Rao, B.M. Girish, "Mechanical properties of as-cast and ZA-27 / silicon carbide particulate compositea," Materials & Design, **16**(5), 277–281, 1996, doi:org/10.1016/0261-3069(96)00008-8.

[18] W. Krajewski, "The Effect of Ti Addition on Properties of Selected Zn-Al Alloys," Phys. Stat. Sol, **145**, 389–399, 1995.

[19] Z.G. Li, "Fabrication of in situ TiB 2 particulates reinforced zinc alloy matrix composite," **121**, 1–4, 2014, doi:10.1016/j.matlet.2014.01.050.

[20] J.P.G. Farr, "Molybdenum disulphide in lubrication. a review," Wear, **35**, 1–22, 1975, doi:10.1016/0043-1648(75)90137-4.

[21] G. Theiler, T. Gradt, "Friction and wear of PEEK composites in vacuum environment," Wear, **269**, 278–284, 2010, doi:10.1016/j.wear.2010.04.007.

[22] G. Yi, F. Yan, "Mechanical and tribological properties of phenolic resin-based friction composites filled with several inorganic fillers," Wear, **262**, 121–129, 2007, doi:10.1016/j.wear.2006.04.004.

[23] S. Amirkhanlou, B. Niroumand, "Synthesis and characterization of 356-SiC p composites by stir casting and compocasting methods," Transactions of Nonferrous Metals Society of China, **20**, 788–793, 2010, doi:10.1016/S1003-6326(10)60582-1.

[24] B.K. Prasad, "Abrasive wear characteristics of a zinc-based alloy and zinc-alloy / SiC composite," Wear, **252**, 250–263, 2002, doi:org/10.1016/S0043-1648(01)00872-9.

[25] A.C. S. BASAVARAJAPPA, G. CHANDRAMOHAN, R. SUBRAMANIAN, "Dry sliding wear behaviour of Al 2219 / SiC metal matrix composites," Materials Science-Poland, **24**(2), 356–366, 2006.

[26] K.C. Wong, X. Lu, J. Cotter, D.T. Eadie, P.C. Wong, K.A.R. Mitchell, "Surface and friction characterization of MoS 2 and WS 2 third body thin films under simulated wheel / rail rolling – sliding contact," Wear, **264**, 526–534, 2008, doi:10.1016/j.wear.2007.04.004.

[27] P. Senthil Kumar, K. Manisekar, E. Subramanian, R. Narayanasamy, "Dry Sliding Friction and Wear Characteristics of Cu-Sn Alloy Containing Molybdenum Disulfide," Tribology Transactions, **56**(5), 857–866, 2013, doi:10.1080/10402004.2013.806685.

Evaluation of Radiological Health Risk Associated with Indian Tiles Available in Nigerian Markets

Adewoyin Olusegun Oladotun[1,*], Omeje Maxwell[1], Joel Emmanuel Sunday[1], Mojisola Rachael Usikalu[1], Zaidi Embong[2], Alam Saeed[3]

[1]*Department of Physics, College of Science and Technology, Covenant University, P.M.B 1023, Ota, Ogun State, 110253, Nigeria*

[2]*Faculty of Science, Technology and Human Development, Universiti Tun Hussein Onn Malaysia, Parit Raja, Batu Pahat, Johor, 86400 Malaysia*

[3]*Division of Science and Technology, University of Education Township Lahore, 42000, Pakistan*

ARTICLE INFO	ABSTRACT
	Seven imported Indian tiles available in the Nigerian markets were investigated in this study to determine their radiological health hazards on users. Gamma spectroscopy was used for the analysis. The calculated radiological variables such as the dose rate, radium equivalent, internal and external hazard indices, gamma index, annual effective dose and the corresponding alpha index were used to determine the potential health risks on people exposed to these building tiles. The average activity concentration of ^{226}Ra, ^{232}Th and ^{40}K were found to be 68.03, 84.79 and 620.89 Bq/kg respectively. These results were observed to be greater than the world recognized average safe boundary for building purposes. Similarly, the dose rate for all investigated tiles ranged between 59.14 and 154.65. This also revealed much higher values than the recommended standard except for GPI which recorded a lower result. However, the mean result of the radium activity equivalent in all the samples investigated was noted to be 237.09 Bq/kg. Both internal and external hazard indices reported much lower results than the recommended safe limit in all the tiles. Similarly, the gamma activity, the annual effective dose, and the alpha indices reported results that are within the safe limit. Therefore, it can be concluded that Indian tiles present in Nigerian market do not pose any health risk to users.

1. Introduction

One of the environmental challenges that is a concern in every part of the world is the exposure of man to radiation. The undue exposure of man to this radiation have been noted to result in adverse medical effect on human.[1]. Natural occurrences and man-made activities have had significant impacts on the level of radiation available in our environment. Therefore, satisfactory and acceptable information of the level of exposure from both man-made and natural radioactivity sources is very crucial. Researches have revealed that the earth crust is composed of different materials including materials that contain a relatively low concentration of naturally occurring radionuclides. It has also been noted in recent studies that water and soil polluted with radionuclides could be threats to the public health as well as the environment [2]. Further research revealed that the average

standard for indoor effective dose due to gamma rays from building materials is about 0.4 mSv per annum [1] and [3]. The major contributors identified for exposures to radiation of natural sources include radioactive nuclides present in the earth's crust, natural radionuclides present in human body (taken in through diets) and cosmic ray particles incident on the earth [1]. People are more prone to radiation exposure by staying indoors as the radioactive materials are more concentrated indoor than outdoor. This is because naturally occurring radioactive materials are present in the crust, ceilings, floors and concrete walls of schools, homes, offices and malls, where occupants spend a lot of time [4] and [5]. Moreover, the concentration of the radioactive materials is more in an indoor environment, when the ventilation is poor.

Generally, building materials are made from rocks and soil, which originate from the earth crust, while some are developed from a mixture of industrial by products[6] and [7]. Therefore,

they have very high tendency of containing more radioactive substances such as 238U and 232Th series and natural 40K, which are naturally part of the raw materials for building materials [3[, [5] and [8]. Also, every stage of construction of a building requires the use of soil or rocks and the land on which a building is sited constitute a major proportion of radioactive materials [9] and [10]. The foregone further established why the indoor concentration of these substances may be very high [9-11]. The availability of naturally occurring radioactive materials (NORMs) in building materials is the cause for the internal and external exposures of radiation to individuals staying in buildings [12-16]. Similarly plant cultivation and the introduction of various chemical fertilizers to aid the farming yield could expose consumers to more radiation. This is because the application of fertilizers to soil, used for farming purposes, may increase its radionuclide contents beyond proportion. Thus, man becomes unduly exposed when feeding on plants cultivated on these kind of lands because of exchange of nutrients between the soil and the plants [17]. Therefore, feeding on some of these plants, especially those that require more proportion of these chemical based fertilizers to germinate would expose man to radioactive substances.

Proper consideration of the above makes it clear that there is no escape for man from radiation exposure, the consolation is that adequate efforts must be made to control exposure so as to prevent the associated health risk. It is on this note that this research was conducted on the commonly purchased building tiles available in Nigeria so as to evaluate and ascertain the concentration of radionuclides in the tiles and also, to estimate the possible health risk of exposure to the people that are often in contact with them.

2. Materials and Methods

2.1. Preparation of Samples

Seven (7) different samples of tiles Indian branded tiles that are commonly available and purchased for building construction purposes in Nigerian markets were studied in this research (Table 1). The tiles were transported to the geological laboratory at Obafemi Awolowo University, Ile Ife in Osun State Nigeria for preparation. The tiles were prepared by first labelling and assigning sample identity to each pack. Second on the line of preparation involved breaking all the tile samples into smaller pieces for the next stage of processing using the Pascall Engineering Lab milling machine. The samples were crushed to size that would be easy for pulverization. One of the precautions observed at this stage was that, the crusher or lab milling machine was adequately cleaned using a pressure blower (Wolf power tools, made in London with serial and type and numbers 978 A and 8793 respectively) after each tile sample was crushed to prevent erroneous mixture of the samples. Furthermore, each sample of crushed tiles was pulverized by completely grinding them into fine powder using the disk "grinder/pulverizer" by Christy and Norris Limited. As done with the crusher, the pulverizer was thoroughly cleaned and blown by a pressure blower, after each sample was grinded in order to avoid cross

contamination of the samples. After this stage, a very fine powder of each sample was obtained, this was sieved using a 250 μm sieve size for the purpose of homogeneity. A measured quantity of 200 g of each sieved sample was first packaged in a high density polyethylene bottles (HDPB) before it was transferred to 500 mL size of Marinelli beakers for radioactivity study. The bottles had been earlier washed with detergent and thoroughly rinsed with ordinary water from borehole and finally rinsed with distilled water.

Table 1: Tables containing the list of tile samples imported from India

s/n	Sample Name	Sample ID
1	Rose Bite India	RBI
2	Tam Brown India	TBI
3	Goodwill Vitrified Tile	GVI
4	Green Pearl India	GPI
5	Goodwill Super Polish Porcelain Tiles	GSPPT
6	Black Galaxy India	BGI
7	Blue Pearl India	BPI

2.2. Gamma Spectrometric Analysis of the Selected Samples

The purchased samples of Indian tiles available in the Nigerian market were prepared in accordance to the IAEA TRS-295 [18]. The prepared samples were packaged in a plastic beaker container and were sealed for twenty-eight days for secular equilibrium, so that the parent radionuclide would be equal to the daughter. The samples were analyzed at the Nuclear laboratory of Universiti Malaysia with the use of High Purity Germanium detector using the approach engaged by [7] and [9-11].

3. Results and Discussion

3.1. Determination of Radioactivity Concentration

The radioactivity concentrations of ^{226}Ra, ^{232}Th, and ^{40}K for samples of produced in India and their corresponding average values are presented in Table 2.

The result of the activity concentrations of radionuclide contents in the samples of Indian tiles available in Nigeria ranged between 18.68 and 98.3 Bq/kg for ^{226}Ra, 42.1 and 104.28 Bq/kg for ^{232}Th and 181.4 and 871.0 Bq/kg for ^{40}K. For ^{226}Ra, TBI was observed to have the lowest activity concentration while GSPPT had the highest values. Similarly, for ^{232}Th, GPI recorded the lowest result while the highest value was recorded in RBI. Finally, BGI reported the highest activity concentration for ^{40}K, while the lowest result was noted in GPI. The mean results of the activity concentrations for ^{226}Ra, ^{232}Th and ^{40}K were estimated to be 68.03, 84.79 and 620.89 Bq/kg respectively. The mean values reported in this study were found to be much higher by 1.95, 2.83 and 1.55 times than the world average standard values of 35, 30 and 400 Bq/kg respectively, according to [19] findings. The results slightly compares with [10], this may be as a result of the similarity in the regional geology of the areas where the raw materials were sourced.

Table 2: Shows the activity concentration of ^{238}U, ^{232}Th and ^{40}K in the present study

s/n	Sample ID	Activity Concentration (Bq/kg)		
		^{226}Ra (Bq/kg)	^{232}Th(Bq/kg)	^{40}K (Bq/kg)
1	RBI	94.47 ± 0.5	104.28 ± 8.0	785.77 ± 15.0
2	TBI	18.68 ± 0.6	84.79 ± 8.0	670.45 ± 15.0
3	GVI	80.9 ± 0.5	88.2 ± 8.0	460.9 ± 15.0
4	GPI	41.9 ± 0.6	42.1 ± 9.0	181.4 ± 15.0
5	GSPPT	98.3 ± 0.5	92.2 ± 8.0	551.9 ± 15.0
6	BGI	81.51 ± 0.5	102.11 ± 8.0	871.0 ± 15.0
7	BPI	60.45 ± 0.5	79.86 ± 8.0	824.78 ± 15.0
	Mean	**68.03 ± 0.50**	**84.79 ± 8.0**	**620.89 ± 15.0**

3.2. Radiological Assessment

3.2.1. The Absorbed Dose Rate

Equation (1), recommended and used by [20] and [1] was used to determine the absorbed dose rates from the obtained activity concentrations and the estimated results are shown in Table 3.

$$D \text{ (nGyh}^{-1}) = 0.462C_{Ra} + 0.604C_{Th} + 0.0417C_k < 80\text{nGyh}^{-1} \qquad (1)$$

From the result presented in the Table below, it could be seen that all the results were far higher than the recommended standard of 80 nGy/h except for GPI which reported lower than the standard. The highest absorbed dose rate was reported in RBI while the lowest was noticed in GPI as presented in Table 3. The mean value of the absorbed dose rate was found to be 108.54 nGy/h. It could be seen that most of the Indian tiles available in Nigerian market have very high absorbed dose rate except for GPI, making the Indian tiles unsafe in this regard.

3.2.2. Determination of Radium equivalent (Ra_{eq})

The values of Ra_{eq} in the samples studied in this research were estimated using equation (2) according to [1], [12], [20].

$$Ra_{eq} = AC_{RA} + 1.43AC_{Th} + 0.077AC_K \qquad (2)$$

where AC_{RA}, AC_{Th} and AC_K are the activities concentration of ^{226}Ra, ^{232}Th and ^{40}K measured in Bq/kg respectively. The results of the radium equivalent activity obtained for the available Indian tiles in Nigeria varied between 116.15 and 304.09 Bq/kg (Table 3). The highest value of radium equivalent was noted in RBI while the lowest value was measured in GPI respectively. The average value of the activity concentration for radium equivalent was estimated to be 237.09 Bq/kg. In all, it was observed that for all the Indian tiles in Nigeria, their radium equivalent values were not above the accepted standard of 370 Bq/kg according to [12] and [20].

3.2.3. Calculation of External Hazard Index (H_{ex})

The radiation hazard index from gamma ray due to ^{226}Ra, ^{232}Th and ^{40}K could be estimated by equation (3) which is the equation foe calculating the external hazard index [1].

$$H_{ex} = (A_{Ra}/370) + (A_{Th}/259) + (A_K/4810) \leq 1 \qquad (3)$$

where,

A_{Ra}, A_{Th} and A_K are the average values of the activity concentrations of ^{226}Ra, ^{232}Th and ^{40}K in Bq/kg respectively. The standard recommended for the H_{ex} is a value less than 1 and at most equal to 1. From the result obtained, the H_{ex} varied between 0.31 and 0.82 for both GPI and RBI respectively. In this case, all the available Indian tiles considered for this parameter had values that are acceptable and within the allowable standard (Table 3). The estimated mean value of the H_{ex} obtained is 0.64. Thus, the Indian tiles are regarded to be safe for use in building construction purposes as far as this health parameter is concerned [1] and [14].

3.2.4. Internal Hazard Index Estimation (H_{in})

The internal hazard index is a measure of how much radiation an occupant of a confined setting is exposed to. This is represented by H_{in} and it can be calculated with equation (4) [21]:

$$H_{in} = (A_{Ra}/185) + (A_{Th}/259) + (A_K/4810) \leq 1 \qquad (4)$$

where A_{Ra}, A_{Th} and A_K are activity concentrations of ^{226}Ra, ^{232}Th and ^{40}K, respectively in Bq/kg. For a building construction material to be regarded as safe, the hazard index from the radiation emitted from such materials must be within a standard limit of less than or equal to 1. The observed values of H_{in} for the Indian tiles in Nigeria were noted to range between 0.25 and 1.08 (Table 3).

The lowest value of H_{in} was reported by TBI while the highest value was noticed in RBI. BGI and RBI were noticed to be greater than the recommended world safe value of 1 among the Indian tiles investigated, which might be considered unsafe for internal usage purposes. The average value of the H_{in} was estimated to be 0.78, which is within the recommended standard for use in building materials. The results presented in Table 3 agreed with [7] and [11].

Table 3: Presents the radium equivalent, dose rate, internal and external hazard indices

s/n	Sample ID	D_R	Ra_{eq}	H_{ex}	H_{in}
1	RBI	139.40	304.09	0.82	1.08
2	TBI	87.80	191.55	0.52	0.25
3	GVI	109.87	242.46	0.65	0.87
4	GPI	52.35	116.15	0.31	0.43
5	GSPPT	124.12	272.59	0.75	1.00
6	BGI	135.65	294.65	0.79	1.02
7	BPI	110.56	238.16	0.64	0.81
	Mean	**108.54**	**237.09**	**0.64**	**0.78**

3.2.5. *The Annual Effective Dose Rate (AEDR)*

Equation (5) was used to estimate the AEDE received by occupants from the indoor internal dose rate according to [1].

AEDR = (0.49CRa + 0.76CTh + 0.048CK) ×8.76×10⁻³   (5)

The values of the AEDE ranged between 0.18 and 0.67 mSvy⁻¹ with an average value of 0.50 mSvy⁻¹. The mean value from the Indian tiles being considered in this study was estimated to be lower than the world's recommended average value of 0.7 mSvy⁻¹ [11]. The values of AEDR for each sample are presented in Table 4. The result obtained for AEDR in this study was observed to be higher than [9]. This is suspected to be as a result of difference in the geological formations of the materials used in the production of the tiles.

3.2.6. *Gamma Index Estimation (Iγ)*

This index is engaged to calculate the hazrd of γ-radiation because of the presence of natural radionuclide in the samples being investigated. The gamma index (Iγ) is evaluated using Equation (6) according to [22].

Iγ = C_{Ra}/300 (Bq/kg) + C_{Th}/200 (Bq/kg) + C_K/3000 (Bq/kg)   (6)

The results obtained from the equation above for the Indian tile samples are presented below. A range of values between 0.29 and 1.10 were obtained from the calculation of the gamma index (Table 4). The results revealed RBI to have the highest result with a value of 1.10 while TBI was noted to have the lowest result. The recommended safe limit for gamma index varied between 0.3 and 1 mSvy⁻¹, which is the extra gamma dose to the ones received outside of the building [23]. The calculated average Iγ obtained is 0.80, which is less than the restricted limit by international standard. Thus, building materials such as tiles should not be considered for radioactivity if the excess gamma radiation emanating from them increases the annual effective dose of a member of the public by 0.3 mSv at the most. Based on the recommended standard for gamma index, most of the Indian tiles in Nigeria are below the safety limit of 1 mSv except RBI (1.10) and BGI (1.07).

3.2.7. *Determination of Alpha Index (Iα)*

The estimation of the alpha index is another essential part of hazard measurement that quantifies the amount of alpha radiation due to radon inhalation that has its source from building materials. The alpha index for the Indian tiles was determined using equation (7) [24] and [25] is:

Table 4: Presents the AEDR, gamma activity and alpha ray indices.

s/n	Sample ID	Annual Effective Dose AEDR (mSv/y)	Gamma activity Index (I_γ)	Alpha Index ($I_\propto$)
1	RBI	0.67	1.10	0.47
2	TBI	0.18	0.29	0.06
3	GVI	0.54	0.86	0.40
4	GPI	0.26	0.41	0.21
5	GSPPT	0.61	0.97	0.49
6	BGI	0.67	1.07	0.41
7	BPI	0.54	0.88	0.30
	Mean	**0.50**	**0.80**	**0.33**

$$I\alpha = C_{Ra}/200 \text{ (Bq/kg)} \qquad (7)$$

where C_{Ra} (Bq/kg) is defined according to [26], [25] and [21]. The Table above shows the values of the estimated alpha index from the Indian tiles that are available in Nigeria. It is observed that the upper boundary of the concentration of radon ($I\alpha$) is same as 1 [27], [28] and [26]. In the present study, the obtained results revealed that the radon concentration varied from 0.06 to 0.49 with a mean value of 0.33. TBI reported the lowest result while the highest value was noticed in GSPPT. The results obtained from the alpha index are far less than the recommended value. This implies that the exhalation of radon from all the investigated Indian tiles would amount in indoor concentration that is lower than 200 Bq/kg.

4. Conclusion

Seven imported Indian tiles available in Nigerian markets were investigated in this study to determine their radiological health hazards on users. The estimated radiological parameters such as the dose rate, radium equivalent, internal and external hazard indices, gamma index, annual effective dose and the corresponding alpha activity index were used to determine the potential health risks on people exposed to these tiles. The mean activity concentrations of ^{226}Ra, ^{232}Th and ^{40}K were discovered to be 68.03, 84.79 and 620.89 Bq/kg respectively. These values reported higher than the recommended safe limit for building purposes. Similarly, the dose rate for tiles investigated ranged between 59.14 and 154.65. This revealed much higher values than the recommended standard except for GPI which recorded a lower result. However, the mean result of the radium activity equivalent in all the samples investigated was observed to be 237.09 Bq/kg and it is much lower than the recommended safe limit. In the same way, the result of the external index varied between 0.31 and 0.82. Likewise, the result of the internal hazard index ranged between 0.25 and 1.08, with an average value of 0.78. Moreover, the results of the annual effective dose were between 0.18 and 0.67. Finally, the gamma activity and the alpha indices were estimated, their average values were found to be 0.80 and 0.33 respectively. All the above results are within the recommended safe limit for building tiles. Generally, the dose rate for Indian tiles are far higher than the recommended safe standard, but all other radiological parameters prove that the tiles are safe to be used for construction purposes in Nigeria. However, similar investigation is recommended to be conducted regularly in order to ascertain the safety of Nigerian consumers that depend largely on imported goods.

Acknowledgement

Conflict of Interest

There is no conflict of interest on this article.

References

[1] UNSCEAR. "Sources, Effects, and Risks of Ionizing Radiation," Report to the General Assembly, with Scientific Annexes, UN, New York, 2000.

[2] L. Yan, Q.V. Le, C. Sanne, et al. "Phytoremediation of radionuclides in soil, sediments and water," Journal of Hazardous Materials, **407**, 2021, doi.org/10.1016/j.jhazmat.2020.124771

[3] N. Sharma, J. Singh, S.C. Esakki, and R.M. Tripathi, "A study of the natural radioactivity and radon exhalation rate in some cement used in India and its

radiological significance," J Radiat Res Appl Sci., **9**(1), 47-56, 2016, doi.org/10.1016/j.jrras.2015.09.001

[4] IAEA, "Radiation in everyday life", www.iaea.org/publications/factsheets/english/radlife [accessed online on 15/12/2020].

[5] F.J. Maringer, A. Baumgartner, F. Rechberger, C.Siedel, M. Stietka, "Activity measurement and effective dose modelling of natural radionuclides in building material," Applied Radiation and Isotopes, **81**, 279-283, 2013, doi.org/10.1016/j.apradiso.2013.03.029

[6] H.H. Hussain, R.O. Hussain, R.M. Yousef, Q. Shamkhi, "Natural radioactivity of some local building materials in the middle Euphrates of Iraq," Journal of Radioanalytical and Nuclear Chemistry, **284**, 43-47, 2010, doi.org/10.1007/s10967-010-0464-1

[7] E.S. Joel, O. Maxwell, O.O. Adewoyin, et al., "Assessment of natural radioactivity in various commercial tiles used for building purposes in Nigeria," MethodsX, **5**, 18-19, 2018, doi.org/10.1016/j.mex.2017.12.002

[8] World Health Organization (WHO), "Handbook on indoor radon: a public health perspective," 2009.

[9] S. Elnobi, S. Harb, N.K. Ahmed, "Influence of grain size on radionuclide activity concentrations and radiological hazard of building material samples," Applied Radiation and Isotopes, **130**, 43-48, 2017, doi.org/10.1016/j.apradiso.2017.09.021

[10] S. Abdullahi, A.F. Ismail, S. Samat, "Determination of indoor doses and excess lifetime cancer risks caused by building materials containing natural radionuclides in Malaysia," Nuclear Engineering and Technology, **51**, 325-336, 2019, doi.org/10.1016/j.net.2018.09.017

[11] O. Maxwell, O.O. Adewoyin, E.S. Joel et al., "Radiation exposure to dwellers due to naturally occurring radionuclides found in selected commercial building materials sold in Nigeria," Journal of Radiation Research and Applied Sciences, **11**, 225-231, 2018, doi.org/10.1016/j.jrras.2018.01.007

[12] M. Gupta, R.P. Chauhan, "Estimation of Low-Level Radiation Dose from Some Building Materials Using Gamma Spectroscopy," Indoor Built Environ. **21**(3), 465-73, 2012, doi.org/10.1177%2F1420326X11414283

[13] S. Ali, M. Tufail, K. Jamil, A. Ahmad and H.A. Klian, "Gamma-ray activity and dose rate of brick samples from some areas of North West Frontier Province (NWFP), Pakistan," The Science of the Total Environment, **187**(3), 247-252, 1996, doi.org/10.1016/0048-9697(96)05109-1

[14] M. Faheem, S.A. Mujahid, Matiullah. "Assessment of radiological hazards due to the natural radioactivity in soil and building material samples collected from six districts of the Punjab province-Pakistan," Radiation Measurement, **43**, 1443–1447, 2008, doi.org/10.1016/j.radmeas.2008.02.014

[15] D. Ghosh, A. Deb, S. Bera, R. Sengupta and K.K. Patra "Assessment of alpha activity of building materials commonly used in West Bengal, India," Journal of Environmental Radioactivity, **99**(2), 316–321, 2008, doi.org/10.1016/j.jenvrad.2007.08.002

[16] S. Turhan, U.N. Baykan, K. Sen, "Measurement of the natural radioactivity in building materials used in Ankara and assessment of external doses," J. Radiol. Prot., **28** (1), 83–91, 2008, doi.org/10.1088/0952-4746/28/1/005

[17] P. Chauhan, R.P. Chauhan, M. Gupta, "Estimation of naturally occurring radionuclides in fertilizers using gamma spectrometry and elemental analysis by XRF and XRD techniques," Microchemical Journal, **106**, 73-78, 2013, doi.org/10.1016/j.microc.2012.05.007

[18] N. Damla, U. Cevik, A.I. Kobya, A. Celik, N. Celik, I. Yıldırım, "Assessment of natural radioactivity and mass attenuation coefficients of brick and roofing tile used in Turkey," Radiat. Meas., **46**, 701–708, 2011, doi.org/10.1016/j.radmeas.2011.06.004

[19] International Atomic Energy Agency (IAEA), "Construction and use of calibration facilities for Radiometric Field Equipment," Technical Reports Series No.309, IAEA,Vienna, 1989.

[20] International Atomic Energy Agency (IAEA), "Extent of Environmental Contamination by Naturally Occurring Radioactive Material (NORM) and Technological Options for Mitigation," Technical Reports Series No. 419, STI/DOC/010/419. 2003.

[21] UNSCEAR. Sources, Effects and Risks of Ionizing Radiations. United Nations, New York. 1998.

[22] J. Beretka, P.J. Mathew, "Natural radioactivity of Australian building materials, industrial waste sand by-products," Health Phys. **48**, 87–95, 1985, doi.org/10.1097/00004032-198501000-00007

[23] OECD (Organization for Economic Co-operation and Development), "Exposure to radiation from radioactivity in building materials,' Report by a group of experts of the OECD Nuclear Energy Agency, 1979.

[24] E.C., "Radiological protection principles concerning the natural radioactivity of building materials," Radiation Protection, 112. 1999.

[24] S. Righi, L. Bruzzi, "Natural radioactivity and radon exhalation in building materials used in Italian dwellings," J. Environ. Radioact. **88**, 158–170, 2006, doi.org/10.1016/j.jenvrad.2006.01.009

[25] L. Xinwei, W. Lingqing, J. Xiaodan, Y. Leipeng, D. Gelian, "Specific activity and hazards of Archeozoic–Cambrian rock samples collected from the Weibei area of Shaanxi, China," Radiat. Prot. Dosim. **118**, 352–359, 2006, doi.org/10.1093/rpd/nci339

[26] ICRP, "Protection against Rn-222 at home and at work," ICRP publication 65, Ann ICRP, **23** (2), 1-48,1994.

[27] M. Tufail, A. Nasim, J. Sabiha, H. Tehsin, "Natural radioactivity hazards of building bricks fabricated from soil of two districts of Pakistan," Journal of Radiological Protection, **27**, 481-492, 2007, doi.org/10.1088/0952-4746/27/4/009

The health Sector Between Innovation and Organizational Performance: Applied Research in Moroccan Hospitals

Abderrahmane Ouddasser, Anass Mellouki, Yassine Belyagou*, Kamal Yazzif

University Sidi Mohamed Ben Abdellah, Fez, 30000, Morocco

A R T I C L E I N F O	A B S T R A C T
	In the context of globalization and the crises that we are experiencing today, innovation becomes the engine of acceleration and resolution of all kinds of organizational dysfunctions. Different alternatives have been proposed by all researchers and practitioners. The role of this paper is to determine the peculiarities of innovation, including the role played by organizational, technological, and medical innovation in improving management practices within healthcare establishments. Although innovation is generally recognized as a vital point for the health sector, it is also crucial to study the place that these three forms of innovation can occupy in improving the quality of service and safety in care. This study assessed the impact of organizational, technological and medical innovations on the organizational performance of Moroccan health institutions. The data was collected using a structured questionnaire suitable for the Moroccan hospital environment, and 143 health professionals were managed at the Hassan II Hospital Center in Fez, Morocco. The broadcast data was analyzed using SPSS and structural partial least (PLS SEM). The results show that organizational innovation has a positive impact on hospital performance.

1. Introduction

If innovation is a concept widely used nowadays, it nevertheless refers to evolving definitions and plural approaches. Today, innovation is at the center of all concerns, since it consists of proposing new solutions and contributing to the success of the organization. Joseph Schumpeter an Austrian economist, proposed an epistemological reflection on the concept of innovation, showing that the types of innovation are appreciable elements to know the stages of growth [1].

Today the field of health is strongly linked to the ideology of progress and precisely to innovation. Although the subject of healthcare innovation is of striking topicality, it is, therefore, necessary to better understand the place occupied by this paradigm, which generally requires the active involvement of stakeholders in any strategic hospital decision, in the ultimate objective is to provide quality services for the benefit of users. The literature also reveals a space of conformity between the user and the hospital, and that this user must be considered as an actor in the recognition and creation of the value of healthcare establishments [2]. Let us note here that innovation is a priority

for any hospital organization whose objective is to face current challenges and an uncertain future.

Our paper will therefore look at the study of innovation through its various forms such as organizational innovation, technological innovation, and medical innovation to improve the performance of hospital activities. The central question that challenges us is the following: What role do organizational, technological, and medical innovation play in improving the organizational performance of healthcare establishments?

This present paper is composed of three essential parts, first, we devote to explaining innovation in its organizational form, then, we will propose to apprehend technological innovation, while the third part, will give place to a reading of medical innovation and its impact on organizational performance within healthcare establishments. Finally, we will carry out an empirical study that serves to measure the variables used and to test all the hypotheses from the literature.

This paper aims to study the classification of data within hospitals, then, we will study the contribution of pricing in improving the financial performance of healthcare establishments, and finally, we will carry out an empirical study.

*Corresponding Author: Yassine Belyagou : yassine.belyagou@usmba.ac.ma

Making it possible to measure and test all the hypotheses constituting the subject of our research question.

2. Literature review

Given the evolution of the health sector in recent years, it is clear that there are still dysfunctions in terms of innovation, as well as the good management of relations between health professionals. With this in mind, if we understand the perceptions and perspectives of healthcare professionals, it will lead to profound changes going forward. It is certainly possible to envisage a new space dedicated to completely modifying the traditional working methods in all sectors, more particularly at the level of the health system. Among these transformations, we retain here that the patient is a fundamental partner in any process of change. It is important to realize that the change can be envisaged primarily to understand that the organization is a space of exchange of ideas and values between the actors who think of remedying the problems of the sick people but on condition of leaving innovative traceability among all stakeholders [3].

In 2000, Dodgson and Hinze defined innovation as "*the scientific, technological, organizational, financial activities leading to the introduction of a new product, process or a new organization or even the improvement of these when they already exist*" [4]. The most commonly accepted idea about innovation is that it allows for the creation of a panoply of legislative reforms and thus allows for significant experiences in terms of sustainability and coordination [5].

2.1. Organizational innovation: a considerable evolution within healthcare establishments

Today, health establishments are very aware of strengthening the capacity of resources to face multiple obstacles, moreover, these establishments aim to provide care but also aim to promote innovation and manage risks [6]. Simply, human, technical and financial resources thus make it possible to increase the performance of hospitals [7]. It is necessary to understand that taking into account different tactics in favor of funds, therefore allow building a flexible, harmonious environment between the hospital, and its users. In recent years, organizational innovation has been considered to be a powerful lever for development, and sustainability for the health system, since it is currently suffering from a multitude of upheavals and constraints that hamper its development.

Currently, the health organization is working to promote the implementation of innovation projects in the organizational, technological, financial, and even institutional order. Also, hospitals must promote and value innovation from implementation through adoption and ownership across the industry to provide better performing and high-quality services for the benefit of patients. That said, several conclusions can be presented as follows :

- The collaborative work of all healthcare stakeholders (doctor, administrator, patient, etc.) in the adoption, appropriation and dissemination of innovation.
- Develop the creation and strengthening of innovation based on the technological aspect through fundamental scientific research, thus promoting public and private funding for research and development, and also creating public-private partnerships and knowledge exchange.
- Involve the perception of patients in the decision-making of any innovation.
- Highlight the advantages and benefits expected by the patients in order to recommend more adequate strategies in the realization.
- The establishment of training sessions for health professionals (administrators, executives, etc.) as well as the establishment of a control service.

Finally, this organizational innovation aims to increase transparency and improve the consistency of hospital actions carried out by healthcare professionals with the main objective of strengthening the patient-hospital relationship, but also strengthening the control of power over the hospital executive, and also to modernize health care facilities to provide quality and high-level services. It should be noted that organizational or even managerial innovation can generate significant results within specific timeframes. The advantages of innovation are also based on the design of new products as well as an optimization in terms of working methods, it should be noted that innovation makes it possible to change the subjective value of agents to an objective value allowing to increase well-being.

Given the results of the literature review, we underline that the first hypothesis essentially concerns the role that organizational innovation can play in the improvement of hospital structures.

H.1. Organizational innovation impacts organizational performance within healthcare facilities.

2.2. Technological innovation in health: a necessity for the future

The Today, the healthcare world faces several simultaneous challenges that are quite different from those that healthcare facilities usually face. The technology promised to reduce economic costs and promote a more sustainable and efficient health system [8]. In this regard, access to health information now transcends all geographic boundaries. The literature points out that public and private organizations are faced with a variety of issues that hinder their advancement, which prompts them to put in place innovative and highly developed strategies to deal with them. These strategies are technological innovations, especially when referring to the introduction of new technology into the organizational process or the launch of a new service. Whatever our attachment to the concept of technological innovation, we can deduce that it is one of the main windows of opening and modernization of hospital management practices. Otherwise, both tangible and intangible innovation can build rigorous models for maintaining well-being [9]. Although others like the OECD (2005) define innovation as: " […] *Implementation of a new or significantly improved product (good or service) or process, of a new marketing method or of a new organizational method in the practices of the company, the organization of the workplace or external relations* " [10].

Taking the example of the Organization for Economic Co-operation and Development, which emphasizes four types of innovation, namely: Innovation mainly concerns products and still processes, let us also add other types of innovation.

Innovations that influence marketing and internal and external communication methods, and ultimately organizational innovation and technological innovation. In the same context, notable advances have been made in the area of innovation, highlighting all types of innovations in the field of health.

Digital technologies have become omnipresent in professional activities [11], their deployment leads to profound changes in working methods, affecting the heart of activities and also affecting those carried out at its periphery on more relational and organizational dimensions, and managerial [12]. They also modify those that take place outside the traditional boundaries of the company, with teleworking [13]. Indeed, digital technology is an "accelerator of progress" in the field of medical research, it still makes it possible to study the evolution of a disease in many patients and further allows treatments to be better adapted to each individual particular case.

Given the results of the literature review, we underline that the second hypothesis essentially relates to the role that technology can play in improving hospital practices.

H.2. Technological innovation impacts organizational performance within healthcare establishments.

2.3. Medical innovation: a priority within healthcare establishments

The best way to deal with problems is to accept innovation as an underlying element in all actions. It is important to note that medical innovation has been able to generate several benefits, although these main missions continue to advance [14]. We underline that this type of innovation can take several forms, particularly when we are talking about innovation in pharmaceutical products (new drugs) or an invisible innovation that serves to renew care practices and therapeutic protocols in favor of patients users [15]. Also, a movement in medicine has emerged, today we can speak of collaborative medicine, personalized or even sustainable in terms of actions. But what gives birth to this sector is the aspect of innovation as well as the technology dedicated to this field. Of course, the patient and his family seek to benefit from agile information and quality service that will ensure their well-being.

Despite the advances made in medical innovation in the health sector, this innovation consists of restructuring traditional working methods, thus forging intimate links between health professionals and their patients. It is remarkable to indicate that this innovation occupies a preponderant place in the improvement of the care, in the progress of pharmaceutical products (drugs) as well as in the improvement of surgical techniques which have a positive impact on the speed of treatment the length of hospitalization, the minimization of stay, and the performance in terms of interventional radiology which calls into question the distribution of care between professionals. This innovation fundamentally changes the digital tools connected to the monitoring and treatment of medical cases for the benefit of patients. Moreover, the latter has a significant impact on the methods of care, on the duration of hospitalization (the stay), and also on the level of all the information related to the hospital [16].

However, to speak of the efforts of medical innovation, it is first to give importance to the institutional framework which plays in any hospital activity and thus supporting an improvement in the conditions. On the strength of its strengths, medical innovation has thus consolidated its position by creating a change in methods for economic practices. Several factors can push healthcare institutions to think globally towards the optics of medical innovation. That said, medical innovation, therefore, represents the progress expected from the healthcare establishment; it generally involves the introduction of new instruments for modernizing hospital practices as well as an improvement in priority strategies relating to patient pathology [17].

Given the results of the literature review, we underline that the second hypothesis essentially relates to the role that technology can play in improving hospital practices.

H.3. Medical innovation impacts organizational performance within healthcare establishments

3. Methodology

In this part, we are interested in explaining only our research approach which focuses mainly on our epistemological and methodological positioning, then, we will focus on operationalizing the dimensions of the independent variable and the dependent variable.

3.1. The research approaches

Following an in-depth reading of the literature on the field of innovation and the performance of hospital organizations, this work will attempt to answer the question of our research and to test the relationships that may exist between the different variables, we let's talk in particular about our research hypotheses.

This relationship is broadly part of the cause and effect between the independent variable (innovation) and the dependent variable (organizational performance). On the one hand, we will rely on carrying out an exploratory factor analysis to test the reliability and internal consistency of the measurement scales using the SPSS software, on the other hand, we will attempt to carry out the second analysis, said, confirmatory factor analysis which will lead us to confirm or refute all the hypotheses from our literature [18]. This logic is generally part of a positivist paradigm with a hypothetico-deductive approach and will be structured around a quantitative methodology [19].

3.2. Operationalization of the independent variable

The operationalization of the variables of our research work is a fundamental step insofar as it makes it possible to make the variables more concrete and readable in our field of research. Besides, this step will allow us to easily understand the different concepts used while drawing on previous studies thus promoting several clarifications around innovation and organizational performance.

Moreover, for the independent variable, we opted for the work of [20], [4] as well as the work carried out by [21]. These various previous works have led us to understand that innovation with its various forms, both organizational, technological, and medical, is intended to make the hospital context more efficient and adapted to the expectations of the population.

Clearly and precisely, it should be emphasized that innovation is a crucial element in the improvement of any hospital activity, that said, health establishments must strongly commit to the path of organizational innovation that is mainly based on the restructuring of working methods and the appropriation of a management style adapted to the hospital context. Likewise, technological innovation allows healthcare establishments to subscribe to the logic of digitizing the methods practiced within medico-technical services. Finally, the investment in medical innovation can further modify treatment protocols and will still allow the hospital's stocks of pharmaceutical products to be perfectly managed.

These three types of innovation are essential for the sustainability of hospital activities and make it possible to guarantee efficiency and high quality in terms of care and safety for patients and users. Table 1 clearly shows the three dimensions of the independent variables.

Table 1: Operationalization of the independent variable

The independent variable measurement scales			References
Organizational innovation	**Technological innovation**	**Medical innovation**	Cloutier (2003) Dodgson et Mark (2000) Eunika Mercier-Laurent (2008) [22]
continuous training	The proper use of connected tools	Drug inventory management	
Staff motivation	Integration of the information system	Improved treatment protocol	
Valuation of skills	Appropriation of management tools	Diagnostic and therapeutic strategies	
Career Management	Research and development	Digital pharmacy	

3.3. Operationalization of the dependent variable

For the dependent variable, we opted for the work of [23], [24]as well as the work carried out by [25], [26]. These various research works have enabled us to understand that organizational performance is a major concern for each healthcare establishment. Let us note here that the organizational performance within hospitals resides strongly on the sustainability and sustainability of health activities, in the same way, it depends more and more on providing quality care and services in favor of users, it also includes being part of the logic of efficiency to make the image of the healthcare establishment more attractive to patients.

Generally speaking, the inclusion of the health establishment in the perspective of organizational performance, therefore, makes it possible to promote and strengthen the relationship between the hospital and the patient, thus increasing the productivity of the staff care and services.

We emphasize that performance within a hospital is a major concern insofar as it enables managerial and hospital practices being changed, the objective of which is to provide care as quickly as possible. Specifically, we emphasize that quality will strengthen the interpersonal relationship and forge strong links between hospital and user [27], [28]. Table 2 clearly shows the three dimensions of the dependent variables.

Table 2: Operationalization of the dependent variable

The dependent variable measurement scales	References

Sustainability	Efficiency	Quality	
Adaptation	Achievement of goals	Yield	Shortell, Bennett, et Byck (1998) Piña-Garza et al. (2017) Sicotte and al., (1999)
Recognition	Productivity	User satisfaction	
Knowledge sharing	Work organization	Accessibility	

4. Analysis and discussion of the results

In the following paragraphs, we will rely on carrying out a descriptive analysis of our sample, then we will move on to exploratory factor analysis, and finally, confirmatory factor analysis will be carried out to test our developed hypotheses.

It is important to give an outline presentation of the University Hospital Center in Morocco, in particular of the Fez - Meknes region which is an integral part of our study. University Hospital Centers are understood to be public establishments with legal personality and financial autonomy. They play a capital role in the care of our national health system, they perform a variety of missions and are, moreover, centers of excellence in the provision of cutting-edge and high-tech care.

Our questionnaire is based beforehand on introducing simple and precise questions relating to the respondent's profile, then questions related to their professional context, and finally, a set of very relevant questions were addressed, the objective of which is to better understand our problem research.

As part of this empirical process, we will take into consideration the descriptive parameters of our sample of the Hospital - University Hassan II - Fez in Morocco knowing that 215 questionnaires were distributed, 167 questionnaires were returned completed, a response rate by 77.7%.

4.1. Collection of data

Before beginning the evaluation of the measurement scales and the test of the hypotheses, we will first present Center Hospital - Hassan II of Fez, Morocco, and a descriptive analysis of the sample.

Descriptive data analysis

Before proceeding with the development and analysis of the responses, it is necessary to first describe our sample as well as the respondents who will contribute to the success of this research work. Moreover, our respondents are generally health professionals whose function is to ensure the sustainability of the health establishment as well as to meet the expectations of the population in terms of care, and services. The distribution of our sample is generally oriented towards the description by gender, age, profile, a number of years of experience. Table 3 below illustrates all the responses received by health professionals.

The distribution of respondents

Before proceeding with the development of the analysis of the responses, it is necessary to first describe our sample as well as the respondents who will contribute to the success of this research work. Moreover, our respondents are generally health professionals whose function is to ensure the sustainability of the health establishment and to meet the expectations of the

population in terms of care and services. The distribution of our sample is generally oriented towards the description by sex, age, profile, number of years of experience.

➢ **By gender**

More than half of the respondents to the questionnaire sent to health professionals are men (55.1%). Women only represent 44.9% of respondents.

➢ **According to age**

Professionals aged between 36 and 44 and those aged between 45 and 54 are the players who have shown more involvement and profit-sharing in our problem and represent respectively 28.7% and 22.2% of the total number of respondents. On the other hand, respondents aged over 55 represent only 13.8%. While healthcare professionals aged 27 and 35, and 18 and 26, respectively, only represent a response rate of 19.1% and 16.1%.

➢ **According to years of experience**

We find that the majority of responses were conducted by respondents with more than 7 years of experience with a rate of 31.1%. So, for people with experience between 5 and 7 years and between 3 and 5 years only represent 29.3% and 22.2% respectively. In the end, health professionals who have experience between 1 and 3 years only represent 17.4% of the responses.

➢ **According to the position held**

Respondents exercising the administration service accounted for 31.7% of the responses. While doctors and technicians represent 28.7% and 16.2% respectively. For the case of nurses and pharmacists, represent only 13.1% and 10.2%.

Table 3: Description of our sample

Categorical classification	Membership	Frequency	%
Gender	Female	64	44,8
	Male	79	55,2
Professional category	Administrator	48	33,6
	Doctor	39	27,2
	Male nurse	19	13,2
	Technician	17	11,9
	Pharmacist	20	14
Age	18-26	11	7,7
	27-35	18	12,6
	36-44	45	31,4
	45-54	42	29,3
	55 and over	27	18,9
Region (Hassan II University Hospital Center - Fez)	Fez-Meknes	143	100
Number of years of experience	From 1 to 3 years	20	14
	3 to 5 years old	29	20,2
	From 5 to 7 years old	55	38,4
	From 7 years to older	39	27,3

4.2. Exploratory factor analysis

We note that the KMO[1] index of the independent variable, which is made up of three components, namely : organizational and technological innovation, and medical innovation displays values that respect the selected threshold (0.5). These different values are respectively as follows: 0.616; 0.709; 0.670. On the other hand, Bartlett's test displays a significant value close to 0 which makes it possible to reject the null hypothesis claiming that all the correlations are not significant [29], [30].

Concerning the quality of representation of the items, the latter display commonalities greater than 0.5 (threshold selected is 0.4), which attests to a good quality of representation, especially since all the factor contributions are significant because they exceed 0.5.

The clean measurement scales of "Organizational innovation" ; "Technological innovation" ; "Medical innovation" have respectively a very satisfactory Cronbach's Alpha value of 0.719; 0.746; 0.764 which demonstrates the reliability of the measurement scale.

We note that the KMO index of the dependent variable, which is made up of three components, namely: durability, efficiency, and quality displays values which respect the selected threshold (0.5). These different values are respectively as follows: 0.727; 0.680; 0.697. Also, Bartlett's test displays a significant value close to 0 which makes it possible to reject the null hypothesis claiming that all the correlations are not significant. Table 4 summarizes the exploratory factor analysis of the three dimensions of the independent variables.

About the quality of representation of the items, the latter display commonalities greater than 0.5 (threshold selected is 0.4), which attests to a good quality of representation, especially since all the factor contributions are significant because they exceed 0.5.

The clean measurement scales of "Sustainability"; "Efficiency"; "Quality" respectively have a very satisfactory Cronbach's Alpha of 0.910; 0.895; 0.821 which demonstrates the reliability of the measurement scale. Table 5 summarizes the exploratory factor analysis of the three dimensions of the dependent variables.

Table 4: Summary of the exploratory factor analysis of the independent variable

Independent variable	Organizational innovation	
Quality of representation	OI_1	,870
	OI_2	,731
	OI_3	,895
	OI_4	,765
KMO Test	,616	
Bartlett's Sphericity test	*Approximate chi-square*	190,041

	Signification	,000
Cronbach's alpha	,719	
Independent variable	**Technological innovation**	
Quality of representation	TI_1	,664
	TI_2	,478
	TI_3	,747
	TI_4	,415
KMO Test	,709	
Bartlett's Sphericity test	*Approximate chi-square*	173,227
	Signification	,000
Cronbach's alpha	,746	
Independent variable	**Medical innovation**	
Quality of representation	MI_1	,649
	MI_2	,552
	MI_3	,460
	MI_4	,709
KMO Test	,670	
Bartlett's Sphericity test	*Approximate chi-square*	206,269
	Signification	,000
Cronbach's alpha	,764	

Table 5: Summary of the exploratory factor analysis of the dependent variable

Dependent variable	**Sustainability**	
Quality of representation	SUST_1	,840
	SUST_2	,808
	SUST_3	,899
KMO Test	,727	
Bartlett's Sphericity test	*Approximate chi-square*	352,441
	Signification	,000
Cronbach's alpha	,910	
Dependent variable	**Efficiency**	
Quality of representation	EFF_1	,815
	EFF_2	,907
	EFF_3	,762
KMO Test	,680	

Bartlett's Sphericity test	*Approximate chi-square*	332,887
	Signification	,000
Cronbach's alpha	,895	
Dependent variable	**Quality**	
Quality of representation	QUAL_1	,802
	QUAL_2	,693
	QUAL_3	,719
KMO Test	,697	
Bartlett's Sphericity test	*Approximate chi-square*	183,674
	Signification	,000
Cronbach's alpha	,821	

4.1. Confirmatory factor analysis

Organizational innovation

The first confirmatory analysis with the four items of the "organizational innovation" variable shows unsatisfactory results on some criteria retained. First, the factorial contribution of items OI_1, OI_4 is less than 0.6, which shows that the AVE2 and CR3 are below the threshold used [31], [32].

To this end, we decided to delete these two items and to relaunch a second confirmatory factor analysis with the remaining items [33].

From the second confirmatory analysis, we find that the results are very satisfactory for all the criteria, this variable meets all the required conditions. Indeed, the composite reliability index (CR) is 0.817 (> 0.6) based on the work of [34];[35] . While the factorial contributions of the two items OI _2, OI _3 largely exceed the threshold we have used (> 0.6). For the extracted mean-variance (AVE) is greater than 0.5 (AVE = 0.695) therefore the convergent validity is checked.

Regarding the discriminant validity, table n° 10 shows that the conditions for verifying the discriminant validity are satisfied.

Table 6 below shows us that the variable "Organizational innovation" is reliable and valid.

Table 6: Test of composite reliability and validity of Organizational innovation

Variable	Items	Loadings		CR	AVE
		Before elimination	After elimination		
OI	OI_1	- 0,458	-	**0.817**	**0.695**
	OI_2	0,377	0,708		
	OI_3	0,871	0,943		
	OI_4	0,144	-		

---

[2] In statistics, the extracted mean variance is a measure of the amount of variance that is captured by a construct relative to the amount of variance due to measurement error.

[3] Composite reliability (CR) is a measure of internal consistency in scale

Technological innovation

The first confirmatory analysis with the four items of the "technological innovation" variable shows unsatisfactory results on some criteria retained. First, the factorial contribution of item TI_4 is less than 0.6, which shows that the AVE and CR are below the selected threshold.

To this end, we decided to delete these two items and relaunch a second confirmatory factor analysis with the remaining items.

From the second confirmatory analysis, we find that the results are very satisfactory for all the criteria, this variable meets all the required conditions. Indeed, the Composite Reliability Index (CR) is 0.829 (> 0.6). While the factorial contributions of the three items TI_1, TI_2, TI_3 largely exceed the threshold we have used (> 0.6). For the extracted mean-variance (AVE) is greater than 0.5 (AVE = 0.622) therefore the convergent validity is checked.

Regarding the discriminant validity, table n° 10 shows that the conditions for verifying the discriminant validity are satisfied.

Table 7 below shows us that the "Technological innovation" variable is reliable and valid.

Table 7: Test of composite reliability and validity of Technological innovation

Variable	Items	Loadings		CR	AVE
		Before elimination	After elimination		
TI	TI_1	0,843	0,848	0.829	0.622
	TI_2	0,864	0,867		
	TI_3	0,628	0,630		
	TI_4	0,233	-		

Medical innovation

The first confirmatory analysis with the four items of the "medical innovation" variable shows unsatisfactory results on some criteria retained. First, the factorial contribution of item MI_1 is less than 0.6, which shows that the AVE and CR are below the selected threshold.

To this end, we decided to delete these two items and relaunch a second confirmatory factor analysis with the remaining items.

From the second confirmatory analysis, we find that the results are very satisfactory for all the criteria, this variable meets all the required conditions. Indeed, the composite reliability index (CR) is 0.838 (> 0.6). While the factorial contributions of the three items MI_2, MI_3, MI_4 largely exceed the threshold we have used (> 0.6). For the extracted mean-variance (AVE) is greater than 0.5 (AVE = 0.638) therefore the convergent validity is checked.

Regarding the discriminant validity, table n° 10 shows that the conditions for verifying the discriminant validity are satisfied. Table 8 below shows us that the "Medical innovation" variable is reliable and valid.

Table 8: Test of composite reliability and validity of Medical innovation

Variable	Items	Loadings		CR	AVE
		Before elimination	After elimination		
MI	MI_1	0,342	-	0.838	0.638
	MI_2	0,783	0,839		
	MI_3	0,906	0,895		
	MI_4	0,689	0,639		

Organizational performance

The first confirmatory analysis with the four items of the "organizational performance" variable shows satisfactory results on all the criteria retained. First, the factorial contribution of all the items is greater than 0.6, which shows that the AVE and CR are greater than the threshold used and represent 0.725 and 0.929 respectively.

Regarding the discriminant validity, table n° 10 shows that the conditions for verifying the discriminant validity are satisfied.

Table 9 below shows us that the "Organizational performance" variable is reliable and valid.

Table 9: Test of composite reliability and validity of Organizational performance

Variable	Items	Loadings	CR	AVE
OP	OP_1	0,676	0.929	0.725
	OP_2	0,898		
	OP_3	0,871		
	OP_4	0,938		
	OP_5	0,863		

Discriminant validity of variables

Table 10: Discriminant validity of variables

	MI	OI	TI	OP
MI	**0.798**			
OI	-0.054	**0.834**		
TI	0.884	-0.121	**0.789**	
OP	0.121	-0.301	0.139	**0.852**

Testing research hypotheses and discussing the results

After having analyzed all the tests, we now move on to a major step that of testing the hypotheses as well as the discussion of all the results obtained.

As part of this modest work, we have relied on testing three hypotheses constituting the object of our research. These different assumptions make it possible to link all the variables of our model,

in particular, the independent variable "innovation", the dependent variable "organizational performance".

The calculation of the "P-Value" constitutes a fundamental step in our research work, moreover, a value of P-Value which does not exceed 5% ($P \leq 0.05$) means that the hypothesis is acceptable. Otherwise, where the P-value exceeds 5% ($P > 0.05$) means that the hypothesis is rejected. This test is performed based on the T - value (the value associated with the student test).

In this context, two hypotheses were rejected because they have a p-value that exceeds the threshold of 5%. So that the third hypothesis, that of the impact of organizational innovation on organizational performance, has been accepted because it has a p-value of less than 5%.

Table 11 shows all the relationships between independent and dependent variables.

Table 11: Research hypothesis test result

	Initial sample (O)	Sample mean (M)	Standard deviation (STDEV)	T value (| O / STDEV |)	P-values	Decision
MI → OP	0.063	0.092	0.244	0.258	0.797	*Rejected*
OI → OP	-0.291	-0.303	0.075	3.895	0.000	*Accepted*
TI → OP	0.048	0.035	0.245	0.198	0.843	*Rejected*

4.2. Discussion of results

Hypothesis n ° 1

First, we find that the construct "Organizational innovation" has a significant effect on "Organizational performance". Indeed, this construct positively influences organizational performance within the healthcare facility with a P-value of 0.000.

The results obtained at the Hassan II University Center - Fez in Morocco show a positive relationship between organizational innovation and organizational performance. In this context, we underline that the contribution of organizational innovation or innovation in its intangible form impacts and influences the performance of organizations, and therefore, this indicates that the implementation of innovation processes allowing reorganizing the way organizations operate is essential for the sustainability of their activities, and a very attractive overall quality. Following our review of the literature, we can underline that this relationship is recommended by various authors such as [20].
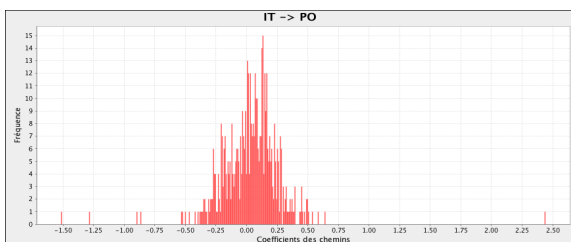
Figure 1 : The main relationships of the variables used in our model (OI --> OP)

Organizational innovation remains a necessity for the prosperity and growth of every healthcare establishment. Also, it is the bedrock of success for all other types of innovation. See the Figure 1 of hypothesis 1.

Therefore, hypothesis (H.1) is validated.

Hypothesis n ° 2

Second, we find that the construct "Technological innovation" has no significant effect on "Organizational performance". However, this construct negatively influences organizational performance within the healthcare facility with a P-value of 0.843.

Although technological innovation is theoretically essential to increase performance, field practice conceals that it does not have this influencing weight and therefore remains dependent on the context, culture, and values of each organization or establishment.

From the results obtained at the Hassan II University Hospital Center - Fez in Morocco, we note that technological innovation does not influence the relationship with organizational performance. That said, the enrollment of the health establishment towards the technology path strongly depends on investing previously in human resources including periodic training, apprenticeship, and improving working conditions. These various parameters are essential, and will lead to profound changes in the level of appropriation and dissemination of technological innovation. See the Figure 2 of hypothesis 2.

Therefore, the hypothesis (H.2) is not validated.
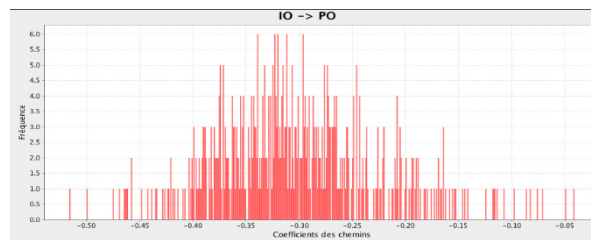
Figure 2 : The main relationships of the variables used in our model (TI --> OP)

Hypothesis n ° 3

Third, we find that the construct "medical innovation" has no significant effect on "organizational performance". However, this construct negatively influences Organizational performance within the healthcare facility with a P-value of 0.797.

According to the results obtained at the Hassan II University Hospital Center - Fez in Morocco, it should be noted that medical innovation is necessary to improve treatment protocols and better manage drug stocks. Despite its importance, this relationship is not significant within the Center Hospital Hassan II - Fez, because, according to the recommendations of health professionals, the health sector must be strongly involved in the establishment of all the mechanisms thus making it possible to make medical innovation relevant in the medium, and long term.

Despite the proven importance of medical innovation in improving treatment protocols, the reality of practice sometimes stems from constraints that slow down the achievement of this

end. These constraints are often linked to a lack of organizational agility of the establishment and the non-involvement of medical human resources in the path of innovative medicalization which requires much more investment in medical research. See the Figure 3 of hypothesis 3.

Therefore, the hypothesis (H.3) is not validated.

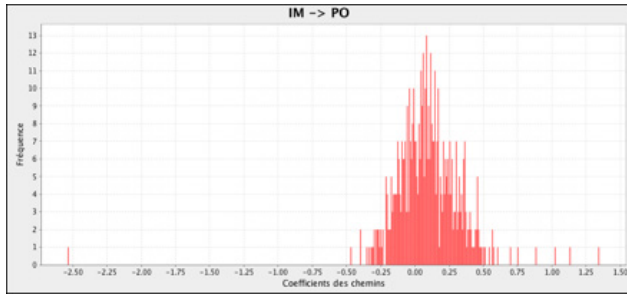Figure 3 : The main relationships of the variables used in our model (MI --> OP)

5. Conclusions

This present paper has tried to study the place that innovation can occupy with its various forms in the increase of organizational performance within health establishments. As a result, it emerges that innovation is a multidimensional notion that allows the health sector to seize opportunities to take into account measures for each context.

For the case of our research, we conducted a study on the contribution of organizational, technological, and medical innovations in improving the organizational performance of the Hassan II University Hospital Center - Fez, therefore, three hypotheses were tested based on exploratory factor analysis and confirmatory factor analysis. According to the results obtained, two hypotheses were rejected, those of technological innovation, and medical innovation, while the third hypothesis of the impact of organizational innovation was retained, which shows that this third form intangible is considered the basis of all form of innovation.

Moreover, for the Moroccan context, if hospitals tend to change, we will have to tackle this new paradigm now, based on international experiences. It is therefore essential to achieve this new logic without the involvement of all the stakeholders who exercise a crucial influence on the conduct of activities. In this regard, organizational, technological, and medical innovation today appear to be determining factors whose main mission is to achieve true hospital performance.

References

[1] G. Haberler, "Joseph Alois Schumpeter 1883–1950," The Quarterly Journal of Economics, **64**(3), 333–372, 1950.

[2] E.M. Castro, T. Van Regenmortel, K. Vanhaecht, W. Sermeus, A. Van Hecke, "Patient empowerment, patient participation and patient-centeredness in hospital care: a concept analysis based on a literature review," Patient Education and Counseling, **99**(12), 1923–1939, 2016.

[3] M. Hees, "Changements et résistances," Perspective Soignante, (7), 52–62, 2000.

[4] M. Dodgson, S. Hinze, "Indicators used to measure the innovation process: defects and possible remedies," Research Evaluation, **9**(2), 101–114, 2000.

[5] J. Hartley, "Innovation in governance and public services: Past and present," Public Money and Management, **25**(1), 27–34, 2005.

[6] J. Haderlein, "Unleashing the untapped potential of hospital philanthropy," Health Affairs, **25**(2), 541–545, 2006.

[7] H.E. Klarman, "Role of philanthropy in hospitals," American Journal of Public Health and the Nations Health, **52**(8), 1227–1237, 1962.

[8] A.U. Akeel, D. Mundy, "Re-thinking technology and its growing role in enabling patient empowerment," Health Informatics Journal, **25**(4), 1278–1289, 2019.

[9] P. McCann, R. Ortega-Argilés, "Modern regional innovation policy," Cambridge Journal of Regions, Economy and Society, **6**(2), 187–216, 2013.

[10] M. d'Oslo, "Principes directeurs proposés pour le recueil et l'interprétation des données sur l'innovation technologique," Paris: OCDE, 1997.

[11] G. Azar, F. Ciabuschi, "Organizational innovation, technological innovation, and export performance: The effects of innovation radicalness and extensiveness," International Business Review, **26**(2), 324–336, 2017.

[12] B. Kelly, D. Papanikolaou, A. Seru, M. Taddy, Measuring technological innovation over the long run, National Bureau of Economic Research, 2018.

[13] J. Vacherand-Revel, M. Ianeva, J. Guibourdenche, J.-F. Carlotti, "Les pratiques du télétravail pendulaire de cadres : reconfiguration des écosystèmes relationnels et d'activités," Psychologie Du Travail et Des Organisations, **22**(1), 54–73, 2016.

[14] C. Van den Bulte, G.L. Lilien, "Medical innovation revisited: Social contagion versus marketing effort," American Journal of Sociology, **106**(5), 1409–1435, 2001.

[15] A.M. Petersen, D. Rotolo, L. Leydesdorff, "A triple helix model of medical innovation: Supply, demand, and technological capabilities in terms of Medical Subject Headings," Research Policy, **45**(3), 666–681, 2016.

[16] V. Iacopino, D. Mascia, A. Cicchetti, "Professional networks and the alignment of individual perceptions about medical innovation," Health Care Management Review, **43**(2), 92–103, 2018.

[17] J. Gardner, Rethinking the clinical gaze: Patient-centred innovation in paediatric neurology, Springer, 2017.

[18] T.A. Brown, Confirmatory factor analysis for applied research, Guilford publications, 2015.

[19] C. Martini, "Hypothetico-Deductive Method," The Wiley-Blackwell Encyclopedia of Social Theory, 1–3, 2017.

[20] J. Cloutier, Qu'est-ce que l'innovation sociale ?, Crises Montréal, 2003.

[21] E. Mercier-Laurent, "Innovation organisationnelle vue comme une composante de l'innovation globale," Journée de Recherche Crest-Magellan Innovation Organisationnelle, **28**, 2015.

[22] S. Schrayer, Les technologies médicales : une industrie de la santé, Ed. Pradel, 1995.

[23] S.M. Shortell, C.L. Bennett, G.R. Byck, "Assessing the impact of continuous quality improvement on clinical practice: what it will take to accelerate progress," The Milbank Quarterly, **76**(4), 593–624, 1998.

[24] J.E. Piña-Garza, G.D. Montouris, F. Vekeman, W.Y. Cheng, E. Tuttle, P. Giguere-Duval, M.S. Duh, V. Shen, T.B. Saurer, J. Isojarvi, "Assessment of treatment patterns and healthcare costs associated with probable Lennox–Gastaut syndrome," Epilepsy & Behavior, **73**, 46–50, 2017.

[25] C. Sicotte, F. Champagne, A.P. Contandriopoulos, J. Barnsley, F. Beland, S.G. Leggat, J.L. Denis, H. Bilodeau, A. Langley, M. Bremond, G.R. Baker, "A Conceptual Framework for the Analysis of Health Care Organizations' Performance," Health Services Management Research, **11**(1), 24–41, 1998, doi:10.1177/095148489801100106.

[26] C. Sicotte, F. Champagne, A.-P. Contandriopoulos, C. TILQUIN, "La performance organisationnelle dans les organisations et les soins de santé," ruptures : Revue transdisciplinaire en sante, **6**(1), 34–101, 1999.

[27] T. Parsons, The social system., Free Press, Glencoe, Ill., 1951.

[28] T. Parsons, Social systems and the evolution of action theory, Free Press, 1977.

[29] H.F. Kaiser, "An index of factorial simplicity," Psychometrika, **39**(1), 31–36, 1974.

[30] H.F. Kaiser, "Image and anti-image covariance matrices from a correlation matrix that may be singular.," 1976.

[31] J.F. Hair Jr, M. Sarstedt, L. Hopkins, V.G. Kuppelwieser, "Partial least squares structural equation modeling (PLS-SEM): An emerging tool in business research," European Business Review, 2014.

[32] J.F. Hair, J.J. Risher, M. Sarstedt, C.M. Ringle, "When to use and how to report the results of PLS-SEM," European Business Review, 2019.

[33] T.R. Levine, "Confirmatory factor analysis," The International Encyclopedia of Interpersonal Communication, 1–5, 2015.

[34] R.P. Bagozzi, Y. Yi, "On the evaluation of structural equation models," Journal of the Academy of Marketing Science, **16**(1), 74–94, 1988.

[35] K. Wilson, E. Sandoz, J. Kitchens, M. Roberts, "The Valued Living Questionnaire: Defining and Measuring Valued Action within a Behavioral Framework," The Psychological Record, **60**, 249–272, 2010, doi:10.1007/BF03395706.

ASTES

Optimized Multi-Core Parallel Tracking for Big Data Streaming Applications

Doaa Ahmed Sayed[*], Sherine Rady, Mostafa Aref

Ain Shams University, Faculty of Computer and Information Sciences, Cairo, 11865, Egypt

A R T I C L E I N F O	A B S T R A C T
	Efficient real-time clustering is a relevant topic in big data streams. Data stream clustering needs necessarily a short time execution frame with bounded memory utilizing a one-scan process. Because of the massive volumes and dynamics of data streams, parallel clustering solutions are urgent. This paper presents a new approach for this trend, with advantages to overcome the main challenges of huge data streams, time, and memory resources. A framework is proposed reliant on a data clustering parallel implementation that divides most recent incoming data streams within a sliding window mechanism to distribute them across a multi-core structure for processing. Every core is responsible for the processing and generation of intermediate micro-clusters for one data partition. The resulting micro clusters are consolidated utilizing the additive property of the micro-cluster data structure to merge those parallel clusters and obtain the final clusters. The proposed approach has been tested on two sorts of datasets: KDD-CUP'99 and KDD-CUP'98. The results show that the proposed optimized parallel window-based clustering approach is efficient for online cluster generation for big data streaming with regard to the performance measures processing time and scheduling delay. The processing time is 1.5 times faster, and the scheduling delay is approximately between 1.3 to 1.7 times less than the sequential implementation. Most important is that the clustering quality is equal to that of the non-parallel implementation.

1. Introduction

Modern advances in ICT and its utilization in business and life sectors have prompted the quick development of huge volumes of data recognized as big data [1]. The basic attributes of huge data are its dynamics (speed), which indicates that data upon arrival needs prompt processing at varying speediness. While for certain applications, the appearance, and preparation of data can be achieved as offline batch processing, other applications need continuous analysis in real-time for the arriving data [2-4]. Data stream clustering is characterized as the data gathering, considering as often as possible the arrival of new data chunks, while seeking the understanding of examples that may modify after some time [5]. The amount of data coming at high and changeable velocities that assume ordinary clustering algorithms ineffective in terms of meeting real-time requirements, and hence considered incapable of dealing with the requests properly [6].

Data stream clustering includes several difficulties; to meet continuous necessities [7]. The clustering should be executed in a brief period of timeframe with bounded memory using a single-scan process. So, following clusters in the sliding window is possibly an effective way to deal with the restrictions in time and memory [8].

Windowing is one famous handling strategy that is utilized with the data streams. Windowing applied to split data streams into windows, reliant on the time measurement. Exist different sorts of window models for the following changing data streams [7]: 1) Landmark, 2) Damped, and 3) Sliding. In a Landmark window, the window is controlled by a certain time point defined as a landmark and the present. It is utilizing for mining over the whole history of the data streams. Landmark is not fitting for applications where up-to-date data is more significant than obsolete data. In the damping model, weights are determined to data, where higher weights are given to the latest data items and less weight is specified to the outdated data. This implies that the model expects the latest information as more critical than the older data. Sliding window models suppose that the new data is more valuable than outdated

[*]Corresponding Author: Doaa Ahmed Sayed, doaa.ahmed74@yahoo.com

data by utilizing a window. The latest occurrences falling inside the window of the data stream are preserved while dispensing with old data. The reason to utilize the sliding window instead of models is regularly basically desired for keeping time and memory resources.

Recently, distributed and parallel algorithms provide solutions for analyzing big data streams in actuality, which is apparent in the more current research works [9]. Parallel solutions and distributed offer various advantages, such as diminishing the time, expanded versatility of arrangements, and suitability for applications of the distributed kind. The currently available multi-core processor commodity computers at afforded costs assist the development of applications in a much easier and reliable way. A computer can contain up to 72 core processors giving high processing power. The inquiry then remains how these available processing onboard resources are utilized for providing optimized solutions for the different real-time in-demand applications.

Most existing parallelism strategies for clustering algorithms cannot give the same clustering quality as the sequential algorithm [1]. The change in clustering quality is impacted influenced by the methods utilized for the data distribution partitioning and results consolidating techniques for the results.

SCluStream [8] is a previously introduced efficient sliding window-based algorithm for clustering data streams considering pre-mentioned data stream difficulties. It works in three phases, wherein the online phase; the most recent data is continuously maintained. The second phase is an expiring phase, where the old data is discarded such that less memory is squandered. The last phase is offline, where the clustering k-means++ algorithm is utilized.

This paper proposes a parallel implementation of the SCluStream algorithm utilizing a multi-core parallel processing framework. The implementation makes the best utilize of the ready cores utilizing a stand-alone platform on a single machine. In the framework, the data set is split into several partitions. Every partition is processed in a separate core, with an equal workload assigned for every partition. Sequential k-means++ is executed next to generate intermediate results (i.e. micro-clusters) for each partition. Eventually, final clusters are consolidated by applying the additive property on micro-clusters, which utilizes the concept of merging the two nearest micro clusters; reliant on the Euclidean distance between micro-clusters.

The organization of this paper is as follows: Section 2 summarizes the related works and existing gaps. Section 3 the spark streaming architecture is explained as the preliminary basis to our big data implementation. Section 4 explains the parallel clustering data streams reliant on the sliding-window and k-means++ parallel algorithm. In section 5 the experimental study and assessments are discussed. In the final section conclusion and future work are clarified.

2. Related work

Clustering huge data volumes require long execution times, especially when talking about dynamic data streams. Many solutions are proposed to beat this issue. Some of them have been done as batch analysis [10-13], while others as streaming analysis [14-19]. Some research enhanced the processing of the algorithm

itself by tuning its parameters or modifying the principal framework for the algorithm. Whereas other research opted for the utilization of the parallelism concept, which is often executed utilizing two major strategies. While the first strategy utilizes a network of linked machines, where the clustering algorithm is implemented on a group of computers [10-16]. The second strategy utilizes a single machine with a multi-core processor [11, 18, 19]. In both strategies, the data is distributed among the computers or cores in the first step. Next, comes a consolidation step which should sum up for the correct execution of the clustering algorithm, and which should be roughly as exact as possible when compared to the algorithm executing on a single machine. In the distributed environments, these two aforementioned steps in respective order are commonly identified as the mapping and reducing operations that correspond to the mentioned two steps in respective order. MapReduce [20, 21] is the common framework for effectively writing applications, which process enormous amounts of data in a parallel way.

A new parallel manner for partitioned clustering algorithms reliant on MapReduce is proposed [1]. The target of this optimization is to enhance data distribution on connected nodes and select the best centroids got from every reducer utilizing a GA (genetic algorithm) based results consolidating methodology. In the map phase, the data is distributed by utilizing the maximum distance among the data points of the various partitions. Consolidating the intermediate results acquired from the reducers on a single node utilizing the genetic algorithm to acquire final accurate results.

A common approach for parallel version of DBSCAN is proposed for clustering massive amount of data [11, 13, 18]. A huge dataset is separated into numerous partitions' dependent on the data dimensions and localized DBSCANs are applied to each partition in parallel through a map phase. The results of each partition are next consolidated in a final reduce phase, which has been performed differently in the three works. A single node tree is at first created for every data point in the dataset by utilizing the disjoint set information structure. Intermediate trees are merged according to the tree-based bottom-up approach after investigating the eps-neighborhood for haphazardly chosen points [11]. A division method named Cost Balanced Partition is utilized to produce partitions with equal capacities and cost-based partitioning (CBP), which determine the partition's data reliant on the estimated calculation cost [13]. For the merging phase, a graph-based algorithm is used to generate global clusters form local clusters. Complex grid partitioning is used for dividing the data space into several partitions for each dimension to minimize the processing time of DBSCAN in parallel processing [12]. Local DBSCAN is applied on each partition to make local clusters. In the merging phase the overlapping clusters are extracted from spatial clusters in a grid and spatial clusters in grids adjacent to its grid. The taken overlapping spatial clusters are consolidated to create one spatial cluster. This parallel addition meets the prerequisites of scalable execution for managing huge data sets. However, this addition is not appropriate for clustering real-time data. It requires traversing the whole dataset for parallel clustering which infers that its execution time is as yet reliant on the dataset size. Thus, while has a great execution for batch-oriented mode, it isn't reasonable for high-speed datasets [12, 13].

A presented parallel implementation for clustering high-dimensional data streams in streaming analysis is proposed [14, 15, 17, 22]. pGrid splits the high-dimensional data space into grids that are clustered the grids rather than the raw data [14]. pGrid uses the MapReduce framework. In the mapping phase, the arriving data point is projected onto its matching grid to depend on its dimensions, and thereafter the grid density is varied. In the reducing phase, the grid cells are merged by each dimension and at the end combining overlapping grid cells are combined to generate the global clustering result. PPreDeConStream is proposed with its parallel implementation in that utilized the shared memory model and the online-offline framework [11, 22]. A new data partitioning technique, Fast Clustering (FC) partitioning is applied. The idea of FC is reliant on splitting two 2-dimensional spaces into four sub-cells until a threshold is obtained (i.e. a threshold on the point's number in a cell) [15]. Then, the cells containing the number of points that are less than this threshold are deleted. The merging phase is based on an overlapping area between cells. Clustering multiple data streams concurrently has been done using a ClusTree algorithm [16,17]. Synopses of different concurrent streams are kept up in an index structure depend on R-tree. Keeping up summary statistics of each data object leads to a larger workload. When new data comes, the algorithm looks for the closest micro-cluster by navigating the tree of which leaf nodes have all the micro-clusters. The greatest hindrances of this algorithm are squandering more memory [17]. The addition of the conventional clustering algorithms Neural Gas (NG) and the Self-Organizing Map (SOM) for clustering data streams are proposed [19]. The extension is reliant on a simple patch decomposition of the data set and only requires a fixed memory space.

For most of the existing clustering parallel implementations, the clustering quality is commonly less accurate than the sequential implementation [1]. This is because the clustering quality is affected by the methods utilized in the data partitioning and consolidating phase. A common problem as well is that algorithms can't cope efficiently with fast-evolving data streams and consume large memory for tracking the clusters. For most of the presented related works, the processing time has been regarded as the major performance measure to be tracked, with no additional measures, such as the clustering quality and the scheduling delay.

3. Spark Streaming architecture

The principle concept in spark streaming is a discretized stream (DStream) [22, 23] which is a consecutive sequence of distributed collections of elements describing a continuous stream of data, and which is called RDDs (Resilient Distributed Datasets). DStreams can be created in two ways; either from a source (e.g. data from a socket, Kafka, file stream, etc.) or by transforming current DStreams utilizing parallel operators (e.g. Map, Reduce, and Window). RDDs are usually, partitioned across multi-cores by Spark. In spark, all the data is represented as RDDs and all DStream operations as RDD operations [24,25, 26].

The number of RDDs partitions created can be specified. The stream processing model in spark is a micro-batch processing. Data received by Input DStreams are processed using DStream operations.

The Spark cluster is responsible for scheduling and dividing the resource in the machine. The main target of the cluster manager is to divide the applications across resources to run the application in parallel mode. Apache Spark has three kinds of cluster managers, standalone, Hadoop YARN, and Apache Mesos. In this work, a standalone cluster manager is utilized.

In the view of master-slave architecture, Apache Spark has one master process and enormous worker processes. These are the following: - the master process consists of a job tracker and a name node. The job tracker is responsible for scheduling jobs and assigning the jobs to the task tracker on the worker process, which is responsible for executing the map and reduce function. The name node is responsible for the storage and management of file metadata and file distribution across several data nodes on worker nodes, which contain the data contents of these files.

Spark gives a graphical UI (user interface) to following the performance of applications. The two important metrics in web UI are 1) Scheduling Delay - the time a batch remains in a queue for the processing of prior batches to end. 2) Processing Time - the utilized time to process every batch of data. The stream processing model in spark is micro-batch processing, processing one batch at a time, so batches wait in the queue until the prior batches finish. The mechanism for minimizing the processing time of each batch and scheduling delay is to increase the parallelism [24, 25].

4. Parallel clustering approach for data streams

Parallel processing provides an optimized solution for clustering huge data streams given that the accuracy of clustering is preserved. In this section, the proposed parallel design of the SCluStream algorithm is described.

4.1. SCluStream

SCluStream saves more time and memory by processing the most recent transactions that fall within window size and the old data are eliminated, so SCluStream overcomes the main obstacles in data streams: - time and memory resources. In the proposed approach, SClustream is implemented on parallel processing utilizing a multicore platform to increase the performance of handling the large volumes of data streams. Figure 1 shows the primary steps of SCluStream and the connections between these steps. The representation of sequence steps and processes is described by the flowchart shown in figure 2. SCluStream consists of three phases.

1) Online phase

- Toward the start of the algorithm implementation, the q initial micro-clusters are generated from the incoming real-time data by applying k-means++ within the time window w_t.
- The window time w_t is kept up for following the latest instances falling during the window size of the data stream and dispensing the outdated data.
- Keeping the statistical data instead of keeping all incoming data in micro-clusters.
- A micro-cluster comprises of the following components {N, LS, SS, LST, SST} where, N the data points number, LS the linear sum of the N, and SS the squared sum of the N. The two last LST and SST are the sum and the sum of the squares of the timestamps of the N.

- When data point arrival, a single of the subsequent two possibilities take place: -
i) The data point is consumed by one of the current micro-clusters. This assimilation is based on the nearness of the cluster to the data point; this is determined by applying a distance metric among the centroid of the micro-cluster and the data point. So, the data point is consumed to the closest micro cluster.
ii) The data point is put in its specific new micro-cluster, however with the restriction that the micro-clusters number stays fixed. Thus, the current clusters number should be decreased by one, which can be accomplished by merging the two nearest micro clusters jointly.

2) Expiring phase

The snapshots are used for storing micro-clusters at each time slot t within a time window w_t. The establishment time for those expiring snapshots doesn't lie among the current time and the window time subtracted from current time. Defining the expiring snapshots from $ts_s < T_s - w_t$ where ts_s is the establishment time of snapshot, T_c is the current clusters number time, w_t is the window time.
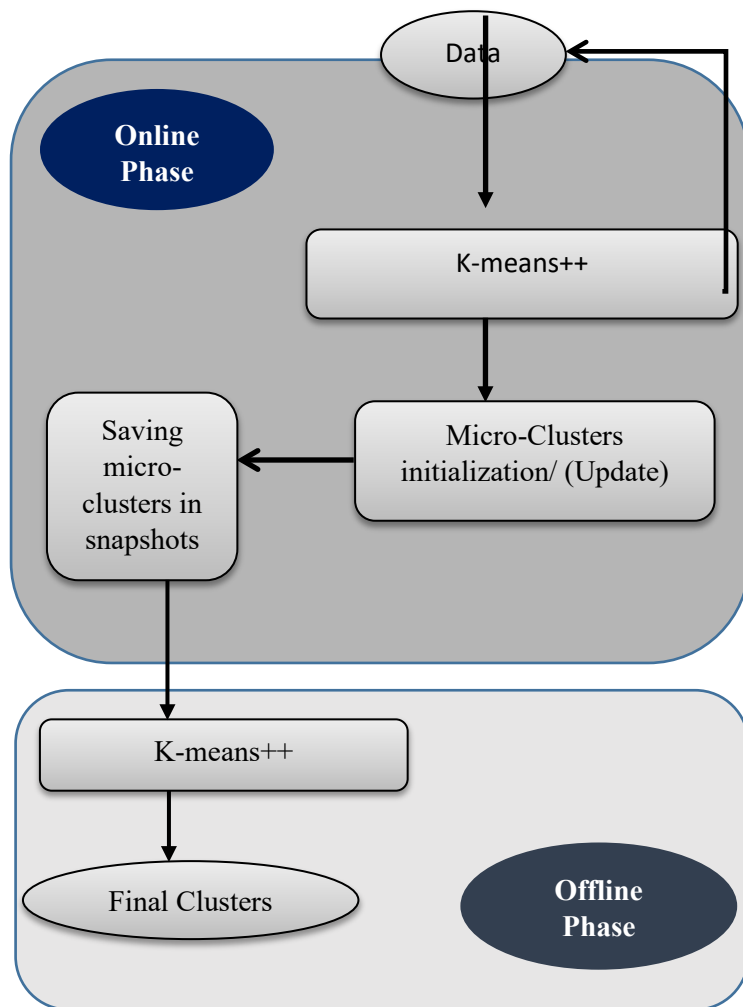
Figure 1: The primary steps of SCluStream [8]

3) Offline phase

The offline phase is consolidating the micro-clusters to deduce the final clusters. The offline phase obtains the micro clusters from kept snapshots during the time window wt. The final macro clusters are defined by utilizing k-means++ rather than conventional k-means to get more accurate results.

4.2. Parallel SCluStream processing

Partitioning the input data streams into a number of partitions. Perform Parallel processing of k-means++ algorithm in online phase on each partition to create micro clusters. Expanding the number of parallel tasks that one executor can execute by expanding the number of available cores to execute per executor. The number of partitions input data streams and operations are reliant on the existing number of cores. Each core is responsible for processing one partition. The steps in figure 3 show the primary steps of parallel-SCluStream and the connections among these steps.

The Steps of SCluStream algorithm involved in the parallel processing can be listed as follow:

1. In the initialization phase, the data is split into p partitions.
2. The online phase parallel processing can be described in the following steps.

    2.1 The distance calculation from every data point x to every centroid by utilizing Euclidean distance, the distance between every data point x and the c centroids.

$$D(\chi, \acute{c}) = \sqrt{\sum_{i=1}^{n}(\chi_i - \acute{c}_i)} \qquad (1)$$

    2.2 This step can be parallelized due to the volume of time used for parallelizing this step brings, an advantage by reducing the total processing time required for finishing this step as multiple cores will process some chunks of the complete dataset simultaneously.

    2.3 Assign data point x to the nearest centroid reliant on distance calculation in the previous step, this process requires a number of comparisons (reliant on the number of the clusters required to be obtained) for choosing the cluster where the data point x should be included. The comparison process will execute in multiple threads, every thread will assign only part of the records of the entire dataset to a single cluster.

    2.4 Compute a set of new partial centroids for each of the processed partitions. The distance between the new centroids is calculated.

    2.5 Compute new centroids for the whole data set and match the values of the new centroids, with the values of the centroids at the aforementioned iteration. If the new centroids are different from the previous iteration go to setp2; else continue to generate final clusters.

If the number of micro clusters is obtained then the final micro clusters is generated; else merging two nearest micro-clusters by using additive property of micro-cluster [7] data structure to generate the determined number of final clusters reliant on the distance calculated in step 3. The additive property means, the
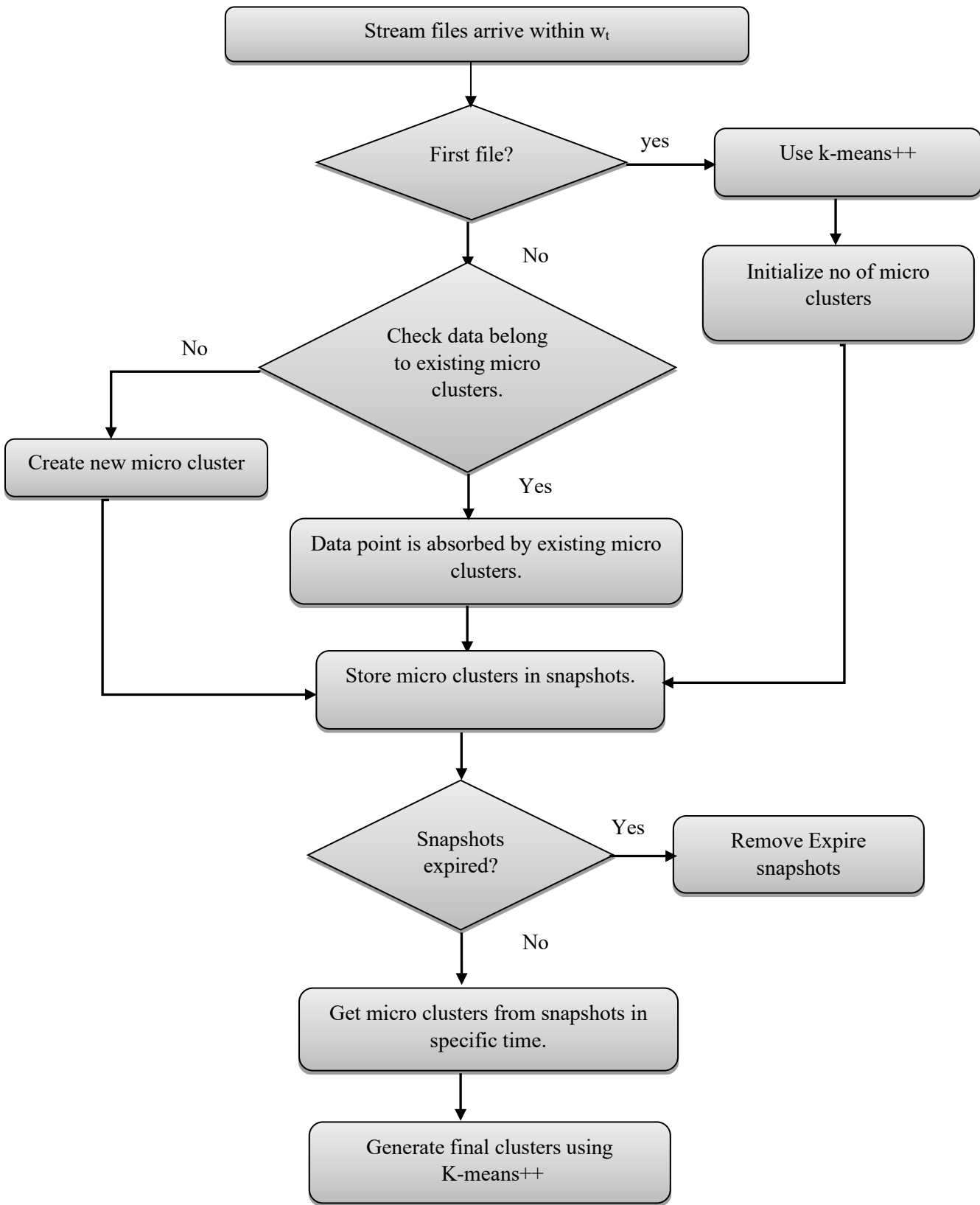
Figure2: SCluStream flowchart

nearest micro-clusters can be consolidated into a new micro-cluster by merging their components [7, 8]. The additive property for merging two nearest micro-clusters is declared in the following equations:

$$LS = LS_1 + LS_2 \quad (2)$$

$$SS = SS_1 + SS_2 \quad (3)$$

$$N = N_1 + N_2 \quad (4)$$

$$LST = LST_1 + LST_2 \tag{5}$$

$$SST = SST_1 + SST_2 \tag{6}$$

5. Experimental study

5.1. Experimental setup

All experiments have been implemented on a standalone implementation, where master process and worker processes all reside on a single machine. The machine used is a laptop with a processor core I5, 8G memory, and an Ubuntu 64-bit operating system. The cluster processing framework used is an apache spark using scale 2.10. The proposed approach has been tested on two datasets: one small and another large one. The results on both datasets show significant improvements in the efficiency of clustering in terms of processing time and scheduling delay without diminishing the clustering quality. The small and large datasets used for testing are respectively: 1) KDD-CUP'99, consisting of 494,021 rows and 43 attributes, and 2) KDD-CUP'98, consisting of 95,412 rows and 56 attributes. For the execution of the framework, configurations are set at first. The parameter settings identified in table 1 have been identified for experimentation.
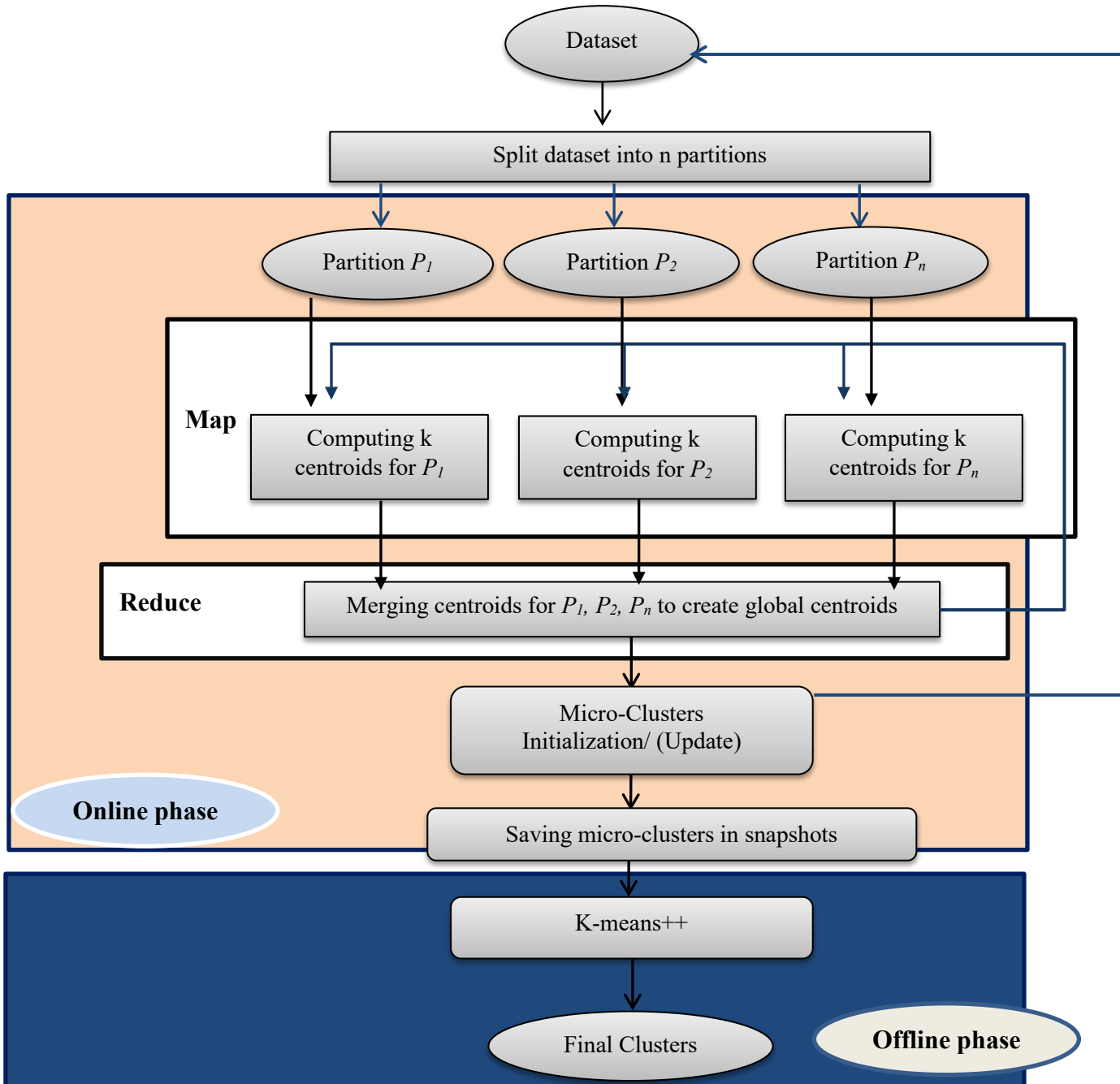
Figure 3: The primary steps of Parallel-SCluStream

Table 1: Parameter Settings Utilized in the Experimentation

Parameters	Value
The date points number n	2000
The micro clusters q number	50
The dimensions number in KDD-CUP'99 data set d	31
The dimensions number in KDD-CUP'98 data set d	56
Window size w_t	70s
The cores' number	3

In the settings, the cores' number is set to 3 cores because the laptop utilized in implementation consists of four cores, one core for the operating system and 3 cores for running the application. This setting is done in spark configuration to determine the maximum available cores for running applications on parallel processing. In the experimental study of the non-parallel SCluStream implementation, the clustering quality was tested with the different number of micro clusters and it was better when the number of the cluster was 50. Also, the clustering quality was tested at different window sizes of and it was better when the size of the window was equal to 70 [8]. Therefore, we used this number of micro clusters and the size of the window in the parameters setting for the parallel SCluStream implementation. The number of initial points can change (up or down), provided that it does not exceed the size of the streamed files.

For assessing the performance of the parallel architecture shown in figure 3, the following measures are recorded:

1) Scheduling Delay T_{SD} - the time a batch remains in a queue for the processing of prior batches to end.

2) Processing Time T_P - the utilized time to process no of the batches of data.

3) Clustering Quality (SSQ) - SSQ is measured for sequential processing and parallel processing. The distance D among data point x_i and the closest centroid C_{xi} is calculated $D(x_i, C_{xi})$. The SSQ is calculated as the sum of $D^2 = (x_i, C_{xi})$ for the whole points in current window. The smaller the value of SSQ, the superior the clustering quality.

$$SSQ = \sum_{i=0}^{n} Đ^2(\chi_i, Ç_{xi}) \qquad (7)$$

The dataset is divided into p partitions, where each partition has been processed in a separate core. The partitioning process is done in the initialization phase. In the map phase, every partition is processed in an isolated core to generate partial clusters. In the reduce phase merge partial clusters in one core to create final clusters.

5.2. The experimental results

1) Scheduling Delay

Figure 4 shows the scheduling delay of SCluStream for sequential and parallel processing for the different file sizes in the two real datasets. The average scheduling delay decrease with increment the level of parallelism by increment the number of partitions for input data and operations. But when the number of the partitions is bigger than the available cores number, the scheduling delay increment. When the number of partitions is five so 3 partitions are processing in parallel and the 4th, 5th partition

waits until one of three cores is workless. The results proved that the average scheduling delay decreases by increase the parallelism but with restriction to an available number of cores in the machine.

(a)   KDD-CUP'99 dataset

(b)   KDD-CUP'98 dataset
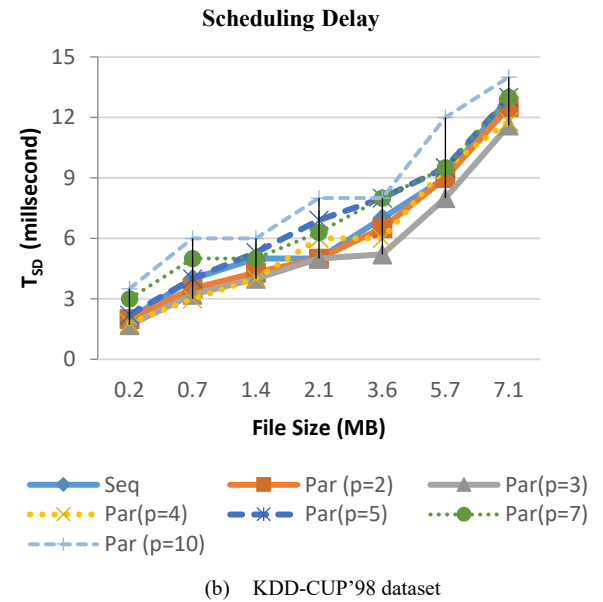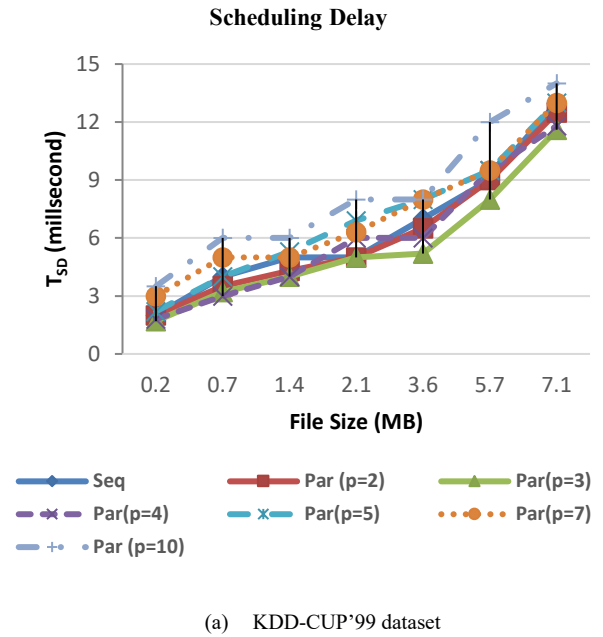
Figure 4: Scheduling delay of SCluStream for sequential and parallel processing for different file size

2) Processing time

Figure 5 illustrates the processing time for sequential and parallel processing of SCluStream versus different files size in the two real datasets. In figure 5-(a) sequential processing of 7.1MB file size which consists of 100000 records by SCluStream takes 13.2 seconds for KDD-CUP'99 data set. Processing 100000 points by parallel processing of SCluStream takes around 11 second when repartition the input data streams to 2 partitions, every partition being processed in a separate core simultaneously. Processing 100000 points takes around 9.6 second when repartition the input

data streams to 3 partitions. The processing time decrease when the number of partitions is less than or equal to the total number of cores as illustrated in figure 5 when repartition the input data streams to 2 or 3 partitions.

The 3 partition processes will execute in parallel reliant on available cores and the 4th partition process will process when one of the 3 cores, is workless. The average processing time for processing different bathes of data when repartition the input data to 5 partitions is nearly equal to the average processing time for sequence processing.

(a)   KDD-CUP'99 dataset

(b) KDD-CUP'99 dataset

Figure 5: Processing time of SCluStream for sequential and parallel processing for different file size.

In figure 5-(b) sequential processing 8.3MB file size which consists of 90000 records by SCluStream requires 15 seconds for KDD-CUP'98 data set. Processing 90000 points by parallel processing of SCluStream requires around 12.8 second when repartition the input data streams and to 2 partitions and takes around 11 second when repartition the input data streams and operations to 3 partitions. The processing time increase about 9.4 seconds from 4 partitions to 3 partitions and 3.4 seconds from the

4 partitions to 2 partitions because the 3 partition processes will run in parallel as there are three cores and the 4th partition process will process when one of the 3 cores, is workless. When the number of partitions is set to 5 partitions, the average processing time is nearly less than the average processing time for Sequential processing for different bathes of data in figure 5-(b) by 0.4 second. The average processing time for processing different bathes of data when repartition the input data to 7 and 10 is bigger than the average processing time for sequence processing. Assuming the dataset is part in numerous parts, not all parts will be handled in a similar time since the number of cores that will execute on a machine is bigger than the maximum number of cores that can be processed by that machine, implying that some of the cores will stand by till they have access to the CPU.

(a)   KDD-CUP'99 dataset

(b) KDD-CUP'98 dataset

Figure 6: Clustering Quality (SSQ) of sequential and parallel SCluStream for different file size

3) Clustering quality

Figure 6 illustrates the comparison among the clustering quality (SSQ) for sequence and parallel processing of SCluStream versus different files size at the same parameters in experimental configuration (points number 2000, micro clusters number (q=50),

window time (70 s)) in the two real datasets. Figure 6-(a) obviously shows that the average SSQ of sequential-SCluStream is approximately close or equal to the average SSQ of parallel SCluStream at a different level of parallelism, especially from partition 2 to partition 3 but from partition 4 to partition 10 the average SSQ is slightly affected from the average SSQ of sequential-SCluStream.

The average SSQ of parallel-SCluStream, especially from partition 2 to partition 4 is nearly close to the average SSQ of sequential-SCluStream in figure 6-(b) and the average SSQ of parallel-SCluStream from partition 5 to partition 10 is slightly affected from the average SSQ of sequential-SCluStream.

5.3. Results Discussion

The experimental results have presented that the parallel implementation for the SClustream managed to superiority the sequential SCluStream for the different parameter studied settings when testing on the two real datasets. Experiments for the processing time have shown that the parallel implementation for the SClustream is nearly 1.5 times quicker than the sequential SCluStream for both datasets. Experiments for the scheduling delay time have shown that the SClustream parallel implementation is approximately between 1.3 to 1.7 times less than the sequential SCluStream for both datasets. Scalability levels of the proposed approach were evaluated by varying the file sizes for the two datasets at the same number of cores, and results have shown the proposed approach succeeds to optimize the processing time and scheduling delay while remaining the clustering quality near or identical to the sequential SCluStream.

In the experimental setting, the number of cores is set to 3 cores according to the capability of the available computer. The data set has been divided the data set to 3 partitions suitable to the number of cores, making every core is responsible for processing one data partition. In this case, the proposed approach succeeded in decreasing the processing time of the dataset and decreasing the scheduling delay for every batch waiting for the previous batch. In case the dataset is divided into bigger than 3 partitions for the current implementation setup, then not all partitions would have been processed simultaneously, because the number of partitions running on a machine is bigger than the maximum number of cores for our used implementation. Hence, some of the partitions will need to wait until one of the cores become workless. In such case, the processing time and scheduling delay will probably bigger than the processing time and scheduling delay of the sequential execution. Running a cluster implementation, instead of the standalone implementation, is expected to provide a promising solution in regard to maintaining the clustering quality obtained, and with much more speed factor than the obtained in the standalone implementation. The conclusive setting for the standalone implementation is that for ensuring the best running parallel mechanism, it is recommended to set the number of partitions equal to the cores's number in the node so that all the partitions will process in parallel and the available resources will be utilized optimally.

6. Conclusion and future work

Recently, data stream clustering is becoming vital research. This problem needs a process capable of clustering continuous data while considering the constraints of memory and time and

generating clusters with high quality. In this paper, parallel clustering implementation on MapReduce and apache spark framework is for the clustering algorithm (SCluStream), which is an efficient algorithm for tracking clusters over sliding window mechanism, focusing on the latest transactions to speed up processing and execution. The implementation has been presented on a standalone cluster manager. The experimental study proved that the parallel standalone implementation with the multi-core processing is successful to take less processing time by approximately 1.5 times and between 1.3 to 1.7 times less scheduling delays than the non-parallel SCluStream implementation. Regarding the clustering quality, it is approximately equal to that of the non-parallel implementation. For obtaining much more clustering algorithm acceleration future work will consider the implementation in connected nodes by using a spark cluster, master nodes, and many worker nodes while making the best configuration and utilization of available executors and cores. Also, apply the best mechanisms for data partitioning and distribution. The automatic determination for all parameter settings will be applied in future work. In addition to comparing the parallel implementation of SCluStream with other data streaming parallel clustering algorithms such as pGrid with various real data sets to confirm the quality and performance for the parallel implementation of SCluStream compare to other algorithms.

References

[1] C.Liu, R.Ranjan, X.Zhang, C.Yang, D.Georgakopoulos, and J.Chen. "Public auditing for big data storage in cloud computing--a survey". Proceedings - 16th IEEE International Conference on Computational Science and Engineering, CSE 2013, 1128–1135. doi: 10.1109/CSE.2013.164.

[2] B.Val, Pablo, N.F.Garcia, L.S.Fernández, and J.A.Fisteus. "Patterns for distributed real-time stream processing". IEEE Transactions on Parallel and Distributed Systems, **28**(11), 3243–3257, 2017, doi.org/10.1109/TPDS.2017.2716929.

[3] N.Kaur, and S.K.Sood. "Efficient resource management system based on 4vs of big data streams". Big data research, **9**, 98-106, 2017, doi.org/10.1016/j.bdr.2017.02.002.

[4] T.S.Sliwinski, and S.L.Kang. "Applying parallel computing techniques to analyze terabyte atmospheric boundary layer model outputs". Big Data Research, **7**, 31–41, 2017, doi: 10.1016/j.bdr.2017.01.001.

[5] I.I.Yusuf, I.E. Thomas, M.Spichkova, and H.W. Schmidt. "Chiminey: Connecting scientists to hpc, cloud and big data". Big Data Research, **8**, 39–49., 2017, doi: 10.1016/j.bdr.2017.01.001.

[6] Z.Lv, H.Song, P.B.Val, A.Steed, and M.Jo. "Next-generation big data analytics: State of the art, challenges, and future research topics". IEEE Transactions on Industrial Informatics, **13**(4), 1891–1899, 2017, doi: 10.1109/TII.2017.2650204.

[7] J.A.Silva, E.R.Faria, R.C. Barros, E.R. Hruschka, A.C.d.Carvalho, and J.Gama. "Data stream clustering: A survey". ACM Computing Surveys (CSUR), **46**(1), 1–31, 2013, doi: 10.1145/2522968.2522981.

[8] D.Sayed, S.Rady, and M. Aref. "SCluStream: an efficient algorithm for tracking clusters over sliding window in big data streaming". International Journal of Intelligent Computing and Information Sciences, **19**(2), 1–19., 2019, doi:10.21608/IJICIS.2019.62592.

[9] C.C.Aggarwal. "Data streams: models and algorithms". Springer Science & Business Media, vol. 31, 2007, doi: 10.1007/978-0-387-47534-9.

[10] A. Bousbaci, and N.Kamel. "Efficient data distribution and results merging for parallel data clustering in map reduce environment". Applied Intelligence, **48**(8), 2408–2428.

[11] M.M.Patwary,A.D.Palsetia, A.Agrawal, W.k.Liao, F.Manne, and A.Choudhary. "A new scalable parallel DBSCAN algorithm using the disjoint-set data structure". SC'12: Proceedings of the International Conference on High Performance Computing, Networking, Storage and Analysis, 1–11, 2012, doi: 10.1109/SC.2012.9.

[12] T. Sakai, K.Tamura, K.Misaki, and H.Kitakami. "Parallel processing for density-based spatial clustering algorithm using complex grid partitioning and its performance evaluation". Proceedings of the International Conference on Parallel and Distributed Processing Techniques and Applications (PDPTA), **337**, 2016, doi:10.1109/TPDS.2019.2896143.

[13] Y. He, H.Tan, W.Luo, S.Feng, and J.Fan. "MR-DBSCAN: a scalable MapReduce-based DBSCAN algorithm for heavily skewed data". Frontiers of Computer Science, **8**(1), 83–99., 2014, doi: 10.1007/s11704-013-3158-3.

[14] X.Sun, and Y.C.Jiao. "pGrid: Parallel grid-based data stream clustering with mapreduce". Report. Oak Ridge National Laboratory. 2009.

[15] Y. Gong, R.O.Sinnott, and P.Rimba. "Rt-dbscan: Real-time parallel clustering of spatio-temporal data using spark-streaming". International Conference on Computational Science, 524–539, 2018, doi: 10.1007/978-3-319-93698-7.

[16] P.Kranen, I.Assent, C.Baldauf, and T.Seidl. "The ClusTree: indexing micro-clusters for anytime stream mining". Knowledge and Information Systems, **29**(2), 249–272, 2011, doi: 10.1007/s10115-010-0342-8.

[17] Z.R.Hesabi, T.Sellis, and X.Zhang. "Anytime concurrent clustering of multiple streams with an indexing tree". Workshop on Big Data, Streams and Heterogeneous Source Mining: Algorithms, Systems, Programming Models and Applications, 19–32, 2015, doi: 10.1.1.1080.3236.

[18] R.Tashvighi and A.Bagheri. "PPreDeConStream: A Parallel Version of PreDeConStream Algorithm". International Journal of Computer Applications, **975**, 8887, 2016, doi: 10.5120/ijca2016912235.

[19] N,Alex, A.Hasenfuss, and B.Hammer. "Patch clustering for massive data sets". Neurocomputing, **72**(7–9), 1455–1469, 2009, doi: 10.1016/j.neucom.2008.12.026.

[20] G.Mencagli, D.B.Heras, V.Cardellini, E.Casalicchio, E.Jeannot, F.Wolf, A.Salis. "Euro-Par 2018: Parallel Processing Workshops: Euro-Par 2018 International Workshops". In 24th International Conference on Parallel and Distributed Computing, Euro-Par 2018 Turin, Italy. Vol. 11339. Springer, 2018.

[21] I.D.Borlea, R.E.Precup, F.Dragan, A.B.Borlea. "Parallel Implementation of K-Means Algorithm Using MapReduce Approach". In IEEE 12th International Symposium on Applied Computational Intelligence and Informatics (SACI), 2018, doi: 10.1109/SACI.2018.8441018.

[22] M. Zaharia, M. Chowdhury, M. J. Franklin, S. Shenker, and I. Stoica. "Spark: Cluster computing with working sets". HotCloud, **10**(10–10), 95, 2010.

[23] Z.Yunquan, T.Cao, Shigang Li, Xinhui Tian, L.Yuan, H.Jia, and A.V. Vasilakos. "Parallel processing systems for big data: a survey". Proceedings of the IEEE, 104(11), 2114–2136, 2016, doi:10.1109/JPROC.2016.2591592.

[24] K.Holden, A.Konwinski, P.Wendell, and M.Zaharia. "Learning spark: lightning-fast big data analysis". O'Reilly Media, Inc., 2015.

[25] M. Zaharia, M. Chowdhury, M. J. Franklin, S. Shenker, and I. Stoica. "Spark: Cluster computing with working sets". HotCloud, **10**(10–10), 95, 2010.

[26] V.Sanz. Marco, B.Taylor, B.Porter, and Z.Wang. "Improving spark application throughput via memory aware task co-location: A mixture of experts approach". Proceedings of the 18th ACM/IFIP/USENIX Middleware Conference, 95–108. 2017, doi: 10.1145/3135974.3135984.

Driver Fatigue Tracking and Detection Method Based on OpenMV

Shiwei Zhou[1], Jiayuan Gong[*,1,2,3,4], Leipeng Qie[1], Zhuofei Xia[1], Haiying Zhou[1,5], Xin Jin[6]

[1]*Institute of Automotive Engineers, Hubei University of Automotive Technology, Shiyan City, 442000, China*

[2]*Acoustic Science and Technology Laboratory, Harbin Engineering University, Harbin 150001, China*

[3]*Key Laboratory of Marine Information Acquisition and Security (Harbin Engineering University), Ministry of Industry and Information Technology, Harbin 150001, China*

[4]*College of Underwater Acoustic Engineering, Harbin Engineering University, Harbin 150001, China*

[5]*Intelligent Power System Co., LTD, Wuhan 430000, China*

[6]*Shanghai Link-E Information and Technology Co. Ltd, Shanghai 200000, China*

A R T I C L E I N F O	A B S T R A C T
	Aiming at the problem of fatigue driving, this paper proposed a driver fatigue tracking and detection method combined with OpenMV. OpenMV is used for image acquisition, and the Dlib feature point model is used to locate the detected driver's face. The aspect ratio of eyes is calculated to judge the opening and closing of eyes, and then fatigue detection is performed by PERCLOS (Percentage of Eyelid Closure over the Pupil). The cradle head system is mounted for driver fatigue tracking and detection. The results show that the dynamic tracking system can improve the accuracy to 92.10% for relaxation and 85.20% for fatigue of driver fatigue detection. This system can be applied to the monitoring of fatigue driving very effectively.

1. Introduction

This paper is an extension of the work initially done in the conference OpenMV Based Cradle Head Mount Tracking System [1]. With the improvement of people's living standards, cars have entered thousands of households and become an irreplaceable means of transportation. At the same time, traffic accidents have become a serious social problem faced by countries all over the world, and have been recognized as the first major public harm to human life today. According to the statistics of China's Ministry of Transport, 48% of traffic accidents in China are caused by drivers' fatigue driving, with direct economic losses amounting to hundreds of thousands of dollars [2, 3]. Therefore, it is very necessary and urgent to study the fatigue driving detection system.

Fatigue driving detection techniques are divided into two categories. One is the subjective evaluation method. The other is the objective evaluation method. The subjective assessment method is recording sensory changes of drivers, and fill in the FS-

14 Fatigue Scale, Karolinska Sleep Scale, Pearson Fatigue Scale, and the Stanford Sleep Scale. However, too many subjective factors probably lead to inaccurate results. The objective evaluation methods are divided into three categories, namely, detection based on driver physiological parameters [4–8], detection based on vehicle behavior [9,10], and detection based on computer vision [11–20]. The detection based on driver physiological parameters, including electroencephalogram (EEG), electrocardiogram (ECG), electromyography (EMG), electrooculogram (EOG), and other parameters, can reflect the driver's physiological state. These detection methods have high accuracy, but the equipment is expensive and may disturb the driver's normal driving. The vehicle behavior-based detection is to monitor the driver's state through the judgment of the vehicle's movement track and the steering wheel's operating speed, etc. Such detection accuracy is general and is easily affected by the weather and other external environmental factors. The fatigue detection method based on computer vision uses the camera to extract features closely related to fatigue state, such as blink. Fatigue detection method based on computer vision as a non-contact

*Corresponding Author: Jiayuan Gong, rorypeck@126.com

detection method, it will not distract drivers. Thus, the driver's facial features and head posture are more precise, directly reflecting the driver's mental state. It has good practicability and accuracy, so it is a more suitable method to detect driver fatigue.

In this paper, it mainly proposes OpenMV based fatigue driving tracking and detection method. OpenMV is used as the camera to collect images, and the images are sent to PC through serial communication. Dlib feature point model is used to locate the detected driver's facial features, and the aspect ratio of eyes can identify whether the driver opens eyes or not. Fatigue detection is carried out by blinking frequency, and driver fatigue tracking detection is carried out by being combined with the cradle head system.

2. Materials and Method

Fatigue driving cradle head tracking and detection system is mainly composed of image acquisition and transmission module, cradle head tracking face module and fatigue detection module. Its system flow chart is shown in Figure 1.
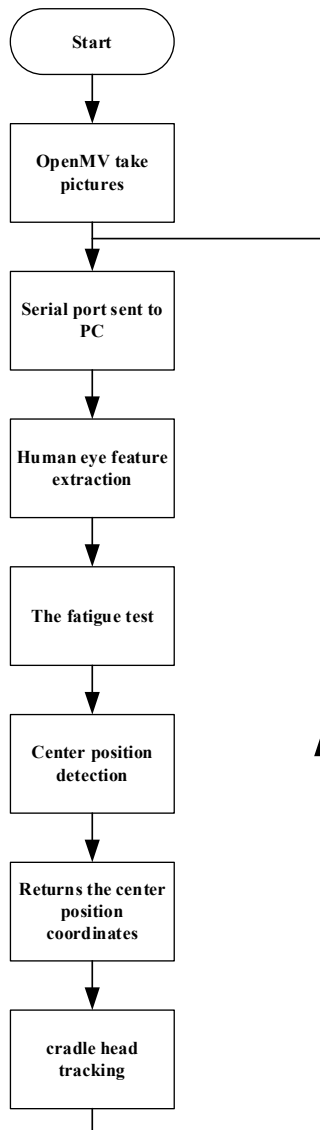
Figure 1: System Flow Chart

2.1. OpenMV Introduction

OpenMV is an open-source, low-cost and powerful machine vision module, as shown in Figure 2.

Figure 2: OpenMV Camera

It takes STM32F427CPU as the core and integrates the OV7725 camera chip. On small hardware modules, the core machine vision algorithm is efficiently implemented in C language, and the Python programming interface is supplied. Its programming language is MicroPython. MicroPython is a type of Python. Its syntax is as easy and practical as Python. By using MicroPython, we can program our own projects. It has built-in color recognition, shape recognition, face recognition, and eye recognition modules. Users can use machine vision functions provided by OpenMV to add unique competitiveness to their products and inventions.

2.2. Anaconda Introduction

Anaconda is a release version that contains 180+ scientific packages and their dependencies. Scientific packages include: Conda, Numpy, Scipy, etc. Anaconda is open-source and the installation is simple. It can use Python and R languages with high performance and has free community support. When we perform driver fatigue detection, we can directly import some corresponding libraries as shown in Figure 3.
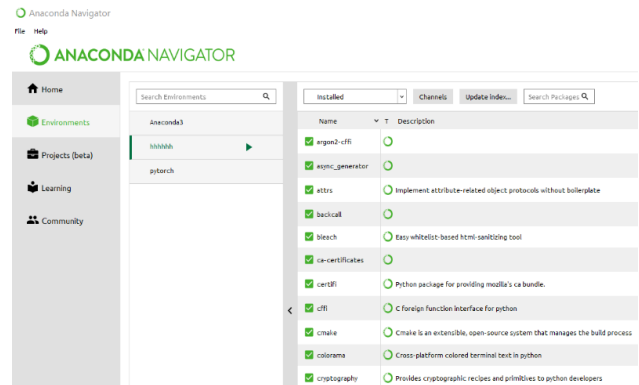
Figure 3: Anaconda Interface

2.3. Image Acquisition and Transmission

The fatigue tracking and detection system is mainly composed of OpenMV and PC.

Firstly, image collection is carried out at the OpenMV end. UART is asked to transmit image information to the Anaconda end, and the serial port is initialized. Then, reset the sensor and camera, set the size of the picture to 240*160, and perform a series of preprocessing on the picture, such as grayscale. When installing OpenMV, the camera is placed upside down in order to ensure

stability of the camera, so the flip function should be added to flip the picture. The OpenMV connection diagram is shown in Figure 4.
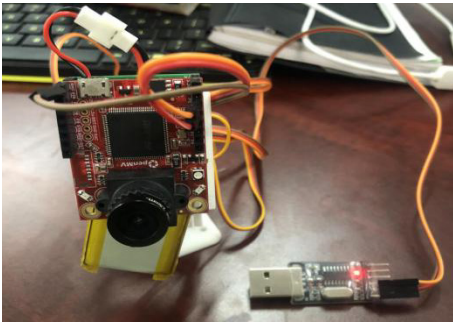
Figure 4: OpenMV Connection Diagram

After initialization, the pictures are transmitted, using the read function to read four bytes, and if it is "snap", a frame of image is sent.

In the anaconda side, first initialize the serial port, reset the input and output buffers, send the "snap" to get the image, and read the size and data of the image.

2.4. Feature Extraction and Fatigue Detection of Human Eyes

This paper is based primarily on the 68-feature point detection model of the Dlib library, and the feature point recognition test is carried out at first. Dlib is a face alignment algorithm based on regression tree. Firstly, import dependent libraries on the Anaconda side, such as OpenCV, Dlib, NumPy, etc. And import the Shape_Predictor_68_Face_Landmarks model. Read the image, import the rectangular face frame, and print out the 68 feature points in a circular manner, as shown in Figure 5.
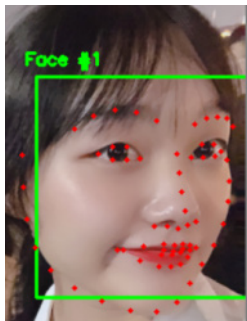
Figure 5: Feature Point Printing

The feature points used in this paper are that of both eyes, namely 36-48 points. Whether the driver is tired can be judged through the aspect ratio of eyes (EAR) [21–23]. There are 6 feature points for both left and right eyes, and the 6 feature points P1, P2, P3, P4, P5 and P6 are the points corresponding to the eyes in the facial feature points. This is shown in Figure 6.
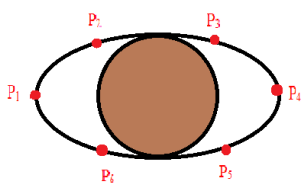
Figure 6: Eye Feature Points

When the state of eyes turns from open to close, the aspect ratio will change. The formula of EAR is as follows:

$$EAR = \frac{||P2-P6||+||P3-P5||}{2||P1-P4||} \tag{1}$$

In the formula, the numerator calculates the distance of the feature points of the eye in the vertical direction, and the denominator calculates the distance of the feature points of the eye in the horizontal direction. Since there is only one set of horizontal points and two sets of vertical points, the denominator is multiplied by 2 to ensure that both sets of feature points have the same weight.

Considering that the size of the eyes varies from person to person, the area of the eyes also changes dynamically due to the influence of the scene and the movement of the head, the degree of opening of the eyes is relative to its maximum open state. The detection results obtained after the average threshold [24–26] is set as 0.2 in the general algorithm are very inaccurate. Therefore, the average calculation method is adopted in fatigue detection in this paper: 30 times of data is collected first, and the average value is taken as the threshold, as showed in Table 1. The fatigue threshold of the driver is detected in advance, which significantly improves the reliability and accuracy of the algorithm.

Table 1: EAR Average

Number	EAR
1	0.23
2	0.26
3	0.27
4	0.30
5	0.32
6	0.33
average	0.28

By calculating the average aspect ratio of eyes, the threshold of eye fatigue is set as 0.28. If the EAR is bigger than it, the eyes are considered to be open. If the EAR is smaller than it, the eyes are considered to be close. See Figure 7.
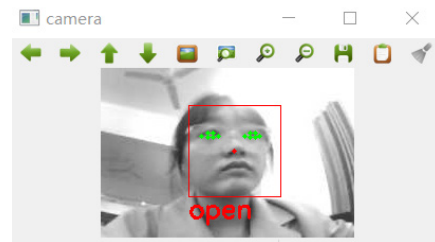
Figure 7: Eyes Open

PERCLOS (Percentage of Eyelid Closure over the Pupil) is defined as the percentage of time (70% or 80%) within a unit time (generally 1 minute or 30 seconds) that the eyes are closed. The driver is considered fatigue if the following formula is met:

The calculation formula of PERCLOS is as follows:

$$PERCLOS = \frac{Eye\ closure\ frames}{The\ total\ number\ of\ frames\ in\ the\ detection\ period} \times 100\% \tag{2}$$

Referring to relevant literature, the normal interval between two blinks is around 0.25 seconds, and people blink more than15 times per minute, so the PERCLOS value is about 6.25%. According to the literature[27, 28], general provisions PERCLOS is 20% for fatigue limit, when we apply this method in the human eye fatigue test, the goal of driver fatigue detection can be achieved.

We defined 100 frames of images as a cycle. If 20 frames of closed eyes are detected in 100 frames, it would be considered as fatigue and output tired, otherwise, output relaxed, as shown in Figure 8 and Figure 9, no detection is added shown in Figure 10.
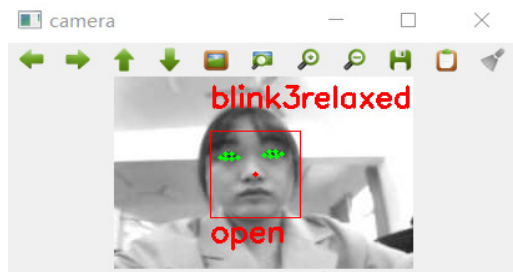
Figure 8: Relaxed
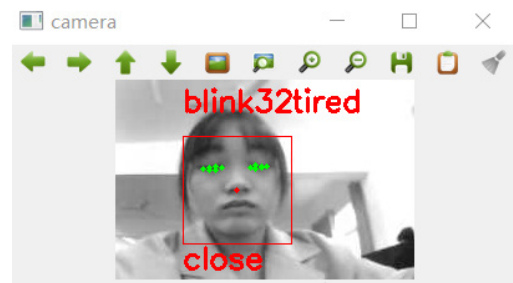
Figure 9: Tired
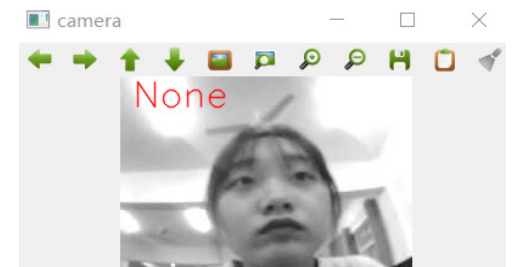
Figure 10: No Detection Added

The fatigue detection flow chart is shown in Figure 11.

2.5. Cradle Head Tracking System

The cradle head system is composed of OpenMV, 3D printing parts, PCB fixing plate, two Micro Steering Gears, and a lithium battery. The cradle head system is connected with OpenMV by welding pins. The tracking head of OpenMV firstly obtains the x and y coordinates of the center of the face, sends the coordinate information of the center to OpenMV through the serial port, and then controls the movement of the twosteering gears of the head by calculating the deviation between the coordinate of the center of the face and the center of the picture, to complete the driver's face tracking and detection.

PID control is proportional - integral - differential control, PID control is a correction method, that is, a control method defined in the principle of automatic control. Import PID and Servo control class, in which Servo(1) and Servo(2) are the upper and lower Servo, respectively. First, initialize the two parameters, set PID parameters as pan_pid = PID (p=0.25, I =0, Imax =90), tilt_pid = PID (p=0.25, I =0, Imax =90). When adjusting parameters, keep the values of I and Imax unchanged, and manually adjust the value of p. Face tracking is realized by controlling the pylon of the steering gear. The specific steps can be divided into the following steps:
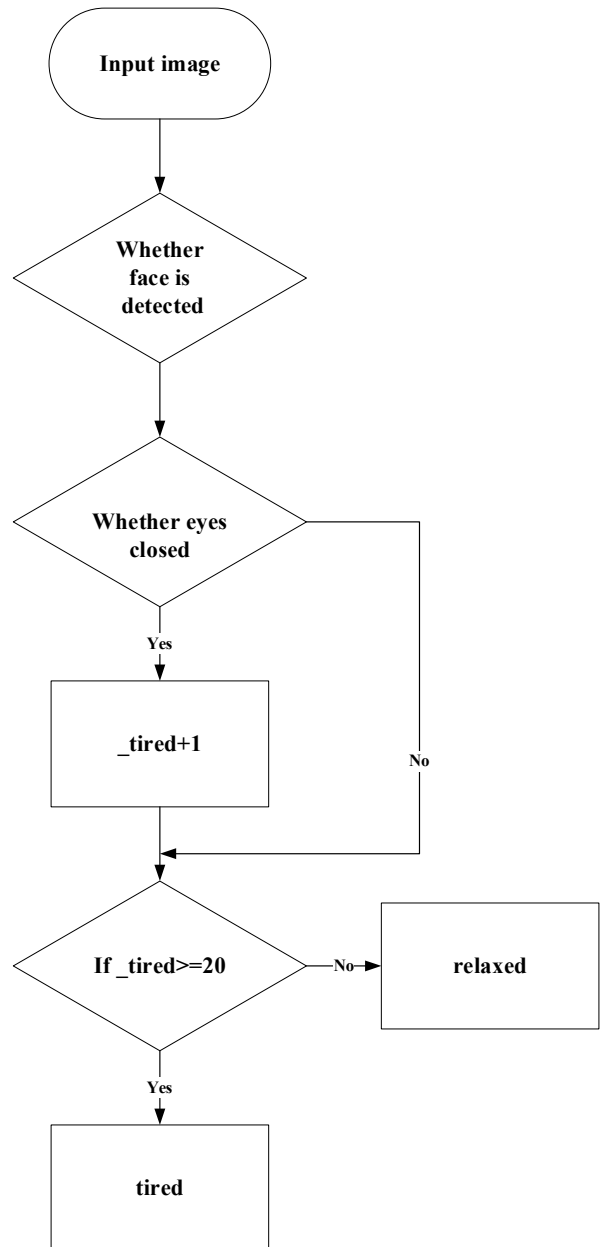
Figure 11: Fatigue Detection Flow Chart

- OpenMV for image acquisition.

- Obtain the coordinates of the center point of the face.

- Calculate the deviation between the face center coordinates and the picture center coordinates.

- The steering gear moves to realize cradle head tracking.

3. Experiment and Results analysis

3.1. Experiment

In order to test the effectiveness of the driver fatigue tracking and detection algorithm in this paper, and the influence of the dynamic tracking system after adding the cradle head on the driver fatigue detection effect. We conducted experiments on subjects and detected the driver fatigue detection system without the cradle head and the driver fatigue detection system with the cradle head respectively under the relaxed and fatigue states of the subjects. Figure 12 shows the driver fatigue detection system without the cradle head.
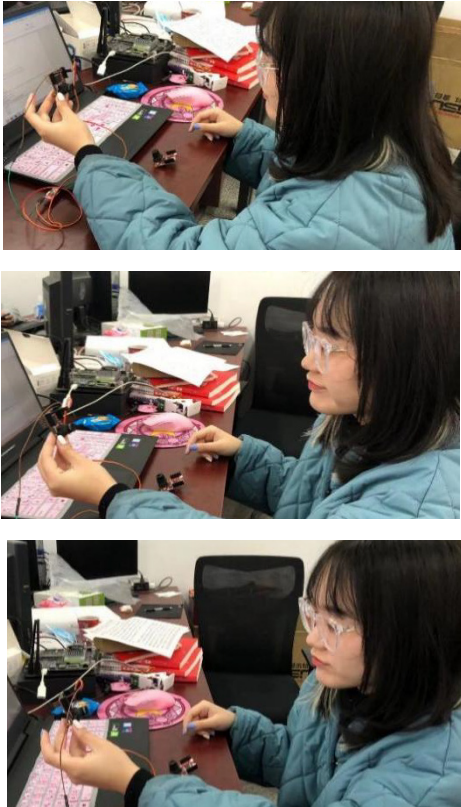
Figure 12: Face Tracking and Fatigue Detection without Cradle Head

Figure 13 shows the tracking process of the fatigue detection system after added the cradle head.
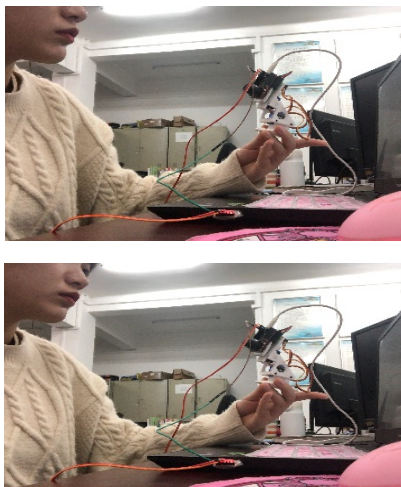
Figure 13: Face Tracking and Fatigue Detection with Cradle Head

It is found in the experimental process that the driver fatigue detection system with the cradle head can move up, down, left, and right with the driver's face to ensure that face recognition is always possible to monitor and distinguish the driver fatigue state in real-time.

3.2. Experimental Results

In order to test the effectiveness of the driver fatigue tracking detection algorithm in this paper, and the influence of the dynamic tracking system after adding the cradle head on the driver fatigue detection effect. We conducted experiments to identify and detect the driver fatigue detection system without the cradle head and the driver fatigue detection system with the cradle head respectively in two states of objects' relaxation and fatigue, identified and detected 4055 frames of images in each state, as shown in Table 2 and Table 3. With the same number of tests, we can clearly compare the accuracy of both.

Table 2: Fatigue Test Results without Cradle Head

State	Number of tests	Wrong number	Accuracy
relaxation	4055	405	90.01
fatigue	4055	790	80.52

Table 3: Fatigue Test Results with Cradle Head

State	Number of tests	Wrong number	Accuracy
relaxation	4055	320	92.10
fatigue	4055	600	85.20

3.3. Analysis of Experimental Results

When the cradle head system is not added, the test results of the driver fatigue detection are listed in Table 2. In the experiment, relaxed and fatigue states were respectively detected,the accuracy of the relaxed state reached 90.01% and the fatigue state only reached 80.52%. It can be seen from the results that there are still problems in the static fatigue detection system.

An image in error detection is extracted, as shown in Figure 14. Owing to the change of the driver's head position during the driving process, face recognition cannot be achieved, so the fatigue state of the driver cannot be detected, leading to low accuracy of fatigue detection results.
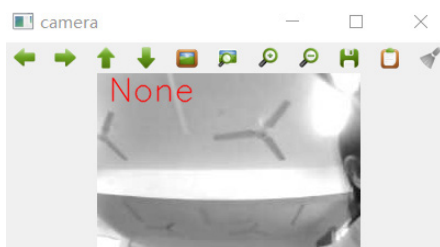
Figure 14: No Face Detected

After adding the cradle head system, the driver fatigue detection test results are listed in Table 3. It can be seen from the results that the detection accuracy of the driver in the relaxed state reached 92.1%, and the accuracy of the fatigue state also reached 85.2%. Comparing with the fatigue detection results without the cradle head, accuracy improved by 2.09% in the relaxed state and 4.68% in the fatigue state. The accuracy of fatigue detection and identification is improved obviously. At the same time, the dynamic tracking effect is also very good.

4. Conclusion

In this paper, OpenMV is used as a camera to collect driver images and transmit them to the PC through the serial port. The driver's face position was tracked by the cradle head system. The face key point detection algorithm based on integrated regression tree was adopted to locate 68-feature points in a small part of the face area, and the location information of human eye feature points was extracted from the key point information obtained. The open and closed states of human eyes were determined by EAR, the blink frequency is used to judge driver fatigue. And the detection method of open and closed eyes for the discrepancies of different drivers' eyes sizes was proposed. Then the center point of the face is transmitted back to the head so that the system can continuously track the face.

Through experiments, this paper proposes that the cradle head system can track well. The accuracy of the driver fatigue detection system with dynamic tracking can reach 92.1% and 85.2% respectively in relaxed and fatigue states, which effectively reduces the detection errors caused by the deviation of the driver's face position and improves the accuracy of the driver fatigue detection.

The driver fatigue detection system can detect the abnormal state of the driver as early as possible and effectively avoid the occurrence of traffic accidents.

Conflict of Interest

The authors declare no conflict of interest.

Acknowledgment

References

[1] S. Zhou, J. Gong, H. Zhou, Z. Zhu, C. He, K. Zhou, OpenMV Based Cradle Head Mount Tracking System, 501-502, 2020, doi:10.1109/DSA.2019.00085.

[2] S. Moslem, D. Farooq, O. Ghorbanzadeh, T. Blaschke, "Application of the AHP-BWM model for evaluating driver behavior factors related to road safety: A case study for Budapest," Symmetry, **12**(2), 2020, doi:10.3390/sym12020243.

[3] J. Cech, T. Soukupova, "Real-Time Eye Blink Detection using Facial Landmarks," Center for Machine Perception, Department of Cybernetics Faculty of Electrical Engineering, Czech Technical University in Prague, 1–8, 2016.

[4] F. Zhou, A. Alsaid, M. Blommer, R. Curry, R. Swaminathan, D. Kochhar, W. Talamonti, L. Tijerina, B. Lei, "Driver fatigue transition prediction in highly automated driving using physiological features," Expert Systems with Applications, **147**, 113204, 2020, doi:https://doi.org/10.1016/j.eswa.2020.113204.

[5] Individual Differential Driving Fatigue Detection Based on Non-Intrusive Measurement Index, 2016, doi:10.19721/j.cnki.1001-7372.2016.10.011.

[6] P. Shangguan, T. Qiu, T. Liu, S. Zou, Z. Liu, S. Zhang, "Feature extraction of {EEG} signals based on functional data analysis and its application to

recognition of driver fatigue state," Physiological Measurement, **41**(12), 125004, 2021, doi:10.1088/1361-6579/abc66e.

[7] J. Bai, L. Shen, H. Sun, B. Shen, Physiological Informatics: Collection and Analyses of Data from Wearable Sensors and Smartphone for Healthcare BT - Healthcare and Big Data Management, Springer Singapore, Singapore: 17–37, 2017, doi:10.1007/978-981-10-6041-0_2.

[8] D. de Waard, V. Studiecentrum, The Measurement of Drivers' Mental Workload, 1996.

[9] Z. Chen, "Study on Driver Fatigue Monitoring Based on BP Neural Network," 2005.

[10] D. Feng, M.Q. Feng, "Computer vision for SHM of civil infrastructure: From dynamic response measurement to damage detection – A review," Engineering Structures, **156**, 105–117, 2018, doi:https://doi.org/10.1016/j.engstruct.2017.11.018.

[11] X. Liang, Y. Shi, X. Zhan, Fatigue Driving Detection Based on Facial Features, 2018, doi:10.1145/3301551.3301555.

[12] J.I.A. Xiaoyun, Z. Lingyu, R.E.N. Jiang, Z. Nan, "Research on Fatigue Driving Detection Method of Facial Features Fusion AdaBoost," 2–7, 2016.

[13] S. Lee, M. Kim, H. Jung, D. Kwon, S. Choi, H. You, "Effects of a Motion Seat System on Driver's Passive Task-Related Fatigue: An On-Road Driving Study," Sensors, **20**, 2688, 2020, doi:10.3390/s20092688.

[14] C. Zheng, B. Xiaojuan, W. Yu, "Fatigue driving detection based on Haar feature and extreme learning machine," The Journal of China Universities of Posts and Telecommunications, **23**, 91–100, 2016, doi:10.1016/S1005-8885(16)60050-X.

[15] S. Computing, "An Improved Resnest Driver Head State Classification Algorithm," 2021.

[16] Q. Abbas, A. Alsheddy, Driver Fatigue Detection Systems Using Multi-Sensors, Smartphone, and Cloud-Based Computing Platforms: A Comparative Analysis, Sensors (Basel, Switzerland), **21**(1), 2020, doi:10.3390/s21010056.

[17] F. You, Y. Gong, H. Tu, J. Liang, H. Wang, "A Fatigue Driving Detection Algorithm Based on Facial Motion Information Entropy," Journal of Advanced Transportation, **2020**, 8851485, 2020, doi:10.1155/2020/8851485.

[18] H. Iridiastadi, "Fatigue in the Indonesian rail industry: A study examining passenger train drivers," Applied Ergonomics, **92**, 103332, 2021, doi:https://doi.org/10.1016/j.apergo.2020.103332.

[19] T. Zhang, Research on Multi-feature Fatigue Detection Based on Machine Vision.

[20] M. Zhang, Fatigue Driving Detection Based on Steering Wheel Grip Force.

[21] Z. Boulkenafet, Z. Akhtar, X. Feng, A. Hadid, Face Anti-spoofing in Biometric Systems BT - Biometric Security and Privacy: Opportunities & Challenges in The Big Data Era, Springer International Publishing, Cham: 299–321, 2017, doi:10.1007/978-3-319-47301-7_13.

[22] W.H. Tian, K.M. Zeng, Z.Q. Mo, B.Q. Lin, "Recognition of Unsafe Driving Behaviors Based on Convolutional Neural Network," Dianzi Keji Daxue Xuebao/Journal of the University of Electronic Science and Technology of China, **48**(3), 381–387, 2019, doi:10.3969/j.issn.1001-0548.2019.03.012.

[23] F. Yang, J. Huang, X. Yu, X. Cui, D. Metaxas, "University of Texas at Arlington," 561–564, 2012.

[24] K.S.C. Kumar, B. Bhowmick, "An Application for Driver Drowsiness Identification based on Pupil Detection using IR Camera BT - Proceedings of the First International Conference on Intelligent Human Computer Interaction," in: Tiwary, U. S., Siddiqui, T. J., Radhakrishna, M., and Tiwari, M. D., eds., Springer India, New Delhi: 73–82, 2009.

[25] V. Kazemi, J. Sullivan, "One millisecond face alignment with an ensemble of regression trees," Proceedings of the IEEE Computer Society Conference on Computer Vision and Pattern Recognition, 1867–1874, 2014, doi:10.1109/CVPR.2014.241.

[26] X. Wang, J. Wu, H. Zun, "Design of vision detection and early warning system for fatigue driving based on DSP," 68–70, 1377.

[27] F. Li, C.-H. Chen, G. Xu, L.P. Khoo, "Hierarchical Eye-Tracking Data Analytics for Human Fatigue Detection at a Traffic Control Center.," IEEE Trans. Hum. Mach. Syst., **50**(5), 465–474, 2020, doi:10.1109/THMS.2020.3016088.

[28] J. Ma, J. Zhang, Z. Gong, Y. Du, Study on Fatigue Driving Detection Model Based on Steering Operation Features and Eye Movement Features, 2018, doi:10.1109/CCSSE.2018.8724836.

Decision Support System for Testing and Evaluating Software in Organizations

Rotimi Adediran Ibitomi, Tefo Gordan Sekgweleo, Tiko Iyamu*

Department of Information technology, Cape Peninsula University of Technology, Cape Town, 8000, South Africa

A R T I C L E   I N F O

A B S T R A C T

Organizations make use of different tools and methods to test and evaluate software, for quality and appropriateness purposes. However, many organizations are unable to perform multiple testing activities (manual, automation and performance testing), using a single tool. As a result of limitation of some tools, some organizations are hampered in their attempt to test software, which affect productivities. This is a challenge that has for many years, caused severe problems for some organizations, affecting their time to respond to business change. The challenge is associated with the lack of framework to guide complementary use of multiple tools when carrying out software testing. This study employs the case study and the interpretivist approaches. From the findings, a decision support system (DSS) framework was developed, which can be used guide testing and evaluation of software in an organization. Also, the DSS is intended to support and assist software engineers, developers and managers in identifying the factors that influence their decisions from both, technical and non-technical perspectives, when testing software.

1. Introduction

The software process offers the flow of the software and expands the assurance of the software product under production [1]. This first step of test planning is the creation of the test plan which ensures that the testing activities are adhered to and determines precisely what the testing is meant to achieve. The test plan specifies the items to be tested, the level of testing, the sequence of testing, the manner in which the test strategy will be applied to each item, as well as the description of the test environment [2]. With such details the test plan establishes a clear indication to stakeholders, pertaining to the software testing.

Software testing methods are basically the approaches that can be adopted to test and evaluate software within the organization. It points out the direction to follow when conducting software testing. According to Mishra, the two most used types of testing methods are black box (functional) and white box (structural) testing [3]. Black box testing is also referred to as behavioral testing whereby the software is tested without the knowledge of the internal workings of the software [4]. White box testing is where the software tester knows the internal workings of the software [5]. In practice, when performing white box testing, the software tester is granted access to the code, to test the software [6].

At times, it can be surprisingly difficult for people to make decisions, especially when they do not understand the root cause of the problem. Thus, for the decision-makers to overcome limits and constraints encountered, they need *decision support systems* (DSS) to assist them in making difficult decisions for solving complex problems [7]. Decision-making is one of the essential activities of business management and forms a huge component of any process of implementation. Over the years, various DSSs were developed to support decision-makers at all levels in organizations including systems that could support problem structuring, operations, financial management and strategic decision-making, extending to support optimization and simulation [8]. In software testing and evaluation as well, DSSs can assist managers in making the correct decisions.

In assisting managers and software developers including engineers to make decisions and have support for their processes, this empirical study was conducted. The aim was to develop a DSS framework that can be used to test and evaluate software in an organization. Based on this, four research questions were formulated: (1) What are the tools that are used in testing software? (2) What are the methods involved in the testing of the software? (3) What factors influence the testing and evaluating of software in organizations? (4) How can a DSS framework be developed and used to address the challenges occurring during software testing and evaluation in organizations?

---

*Corresponding Author: Tiko Iyamu, Email: connectvilla@yahoo.com

The remainder of this paper is logically structured as follows: the review of literature related to the study is first presented, followed by the methodology that was applied in achieving the aim of the study. The data analysis and findings follow respectively. The DSS framework and discussion, which are based on the findings are presented before the conclusion.

2. Literature Review

The software automation tools enable software testers to create scripts that can run automatically to test the software. Software automation is valuable to enhance the tester by performing tasks that are tedious, if not impossible for a human, or are more cost effective to automate [9]. Automation testing is when the tester writes scripts for testing the software. Such scripts, running over and over again at no additional cost, are much faster than manual tests, and capable of reducing the time to run repetitive tests from days to hours. Manual testing is considered time consuming, resource intensive and allow some defects to remain uncovered [10]. Therefore, automation testing tools are there to help uncover defects.

Automated testing diminishes the cost of producing software while simultaneously increasing its reliability [11]. Due to the complexity and increasing size of the software, testing efforts are expected to increase. Therefore, automation testing arises as a practical necessity to reduce time and cost [12]. Furthermore, automation testing reduces the amount of manual work, increasing high coverage by executing more test cases and eliminating human errors especially when people tire after multiple repetitions [13]. Automation testing will also likely rectify some of the other problems, but it certainly is not a panacea for solving all problems [14]. In fact, it is always best to possess the skills for utilizing automation tools because without these skills, it is pointless possessing such tools.

The test process describes the test analysis and design as the activity of designing the test cases using the techniques selected during planning [15]. This can be successfully achieved if the software tester understands the user requirements. However, if the software tester fails to understand the user requirements and architecture software under test, it would not be possible to create test cases which will reveal more errors in a shorter amount of time [16]. A test case outlines the steps required to test any functionality of the software and contains the expected and actual results [1]. Such a comparison means the software tester can readily determine whether the software under test satisfies the requirements or functions properly. These test cases could be captured in a spreadsheet or a testing tool if the organization has one.

DSSs are designed to assist individuals or groups with decision-making and solving problems. DSS is described as "interactive computer-based systems that help people use computer communications, data, documents, knowledge and models, to solve problems and make decisions" [17]. Also, the DSS is considered to replace human decision-making as they assist humans to make informed decisions regarding problems they are facing, thereby enhancing the decision-making process. DSSs are not designed to automate decisions but to fairly support decision making because they are flexible enough to react to changing requirements [18]. Typically, most DSSs have three main components: a model system, a data system and user interface [19].

Each component fulfils its particular activity within the DSS. The data relating to the problem is stored in the knowledge base, the model generates decisions based on the content of the knowledge, and the user interface allows users to build models and attain decision support through the adjustment of input parameters [20]. DSSs are available to managers in support of decision-making processes for solving complex issues [21]. Therefore, decision makers can utilize these tools to compile useful information from documents, raw data, and personal knowledge to make decisions in solving problems. Some DSSs give structured information directly to managers and store knowledge which is availed to managers anytime deemed necessary [22].

3. Methodology

The qualitative approach enables researchers to capture the thoughts and feelings of the research participants, leading to an understanding of the meaning that people ascribe to their experiences [23]. As it provides rich descriptive accounts of the phenomenon under investigation [24], it is concerned with addressing the social aspects of the world and seeks to find answers regarding people's behavior, opinions, cultures and differences between social groups [25]. Qualitative research is effective in understanding and explaining complicated situations by obtaining daily knowledge to create theories [26].

A case study as "a contemporary phenomenon within its real-life context, especially when the boundaries between a phenomenon and context are not clear and the researcher has little control over the phenomenon and context" [27]. A high-quality case study puts emphasis on rigor, validity, and reliability [28]. In addition, a case study is suitable in an environment where there are large numbers of variables in a small number of applied units of analysis where the context is of great importance [29]. Three South African based organizations were used as cases in the study. Some details about the organizations are provided below. Twelve private and public organizations were identified, of which only seven had software testing units. From the seven, only three were prepared to participate in the study.

3.1. Mootledi Logistics

Mootledi Logistics is in Kempton Park, Gauteng province. It is a car rental organization that renders services locally and internationally. It relies on software it purchases from vendors as well as the software it develops in-house to serve its customers and perform day-to-day duties. However, such software requires testing and evaluating prior to its deployment into production to ensure that business continued as usual without interruptions. Participants who were involved for the purpose of this study were the employees of Mootledi Logistics. Initial interviews and follow-up interviews were conducted at the organization's premises in Kempton Park.

3.2. Mmuso Technologies

Mmuso Technologies is in Centurion, also in Gauteng province, with branches in various provinces around South Africa. Mmuso Technologies is responsible for providing government

departments with software solutions to fulfil their duties. Once the software is developed, tested, and evaluated it is then accepted by the government department that requested it, and adopted to perform day-to-day activities of that particular department. The software is used to render necessary services to the citizens of the Republic of South Africa. Participants who were involved for the purpose of this study are the employees of Mmuso Technologies.

3.3. Bokamoso Solutions

Bokamoso Solutions, situated in Illovo, Gauteng, is an organization which invests in research to ensure its convergence and relevance to the industry, thereby providing solutions that add value to its market base. Bokamoso Solutions employees are based at the client site to offer their specialized services. Those services include software development, infrastructure management, software testing and consulting.

The semi-structured interview technique was used to collect data from participants from the three organizations. As shown in Table 1, a total of thirty-nine people (technical x 28, business x 11) participated in the study. The interview was concluded at the point of saturation, which means that new information was not forthcoming.

Table 1: Participants in data collection

Case	Technical (IT)	Non-Technical (Bus.)
Mootledi Logistics	Project Managers x1	Business Managers x1
	Software Developers x2	Business Analysts x1
	Software Testers x2	Business Users x1
	Systems Analysts x1	
	Support Specialist x1	
	IT Managers x1	
Mmuso Technologies	Project Managers x1	Business Managers x1
	Software Developers x2	Business Analysts x1
	Software Testers x3	Business Users x1
	Systems Analysts x1	
	Support Specialist x1	
	IT Managers x1	
Bokamoso Solutions	Project Managers x2	Business Managers x2
	Software Developers x3	Business Analysts x1
	Software Testers x2	Business Users x2
	Systems Analysts x2	
	Support Specialist x1	
	IT Managers x1	
Total	28	11

In this study, data was analyzed using the hermeneutic technique from the interpretive approach. Hermeneutic was selected as it allows for a phenomenon to be studied subjectively. Hermeneutic focuses on reality as a human contrast, which can only be understood subjectively [30].

In conducting the analysis, the hermeneutic method of the interpretivist paradigm was applied. The Hermeneutic focuses on how humans construct meanings socially [31]. The method was applied to the following:

  i. the meanings which individuals give or associate to events and artefacts.
 ii. how those meanings manifest while providing health services.
iii. how the meanings were used to interact with the rules and regulations within the environment.

4. Data Analysis

The data from the three cases were combined. The analysis was conducted based on the research questions:

4.1. What are the tools that are used in testing software?

Software testing can be performed manually or with software testing tools, tools which are either free, open source or proprietary software. Open-source tools are often provided freely by those who developed them, free to be downloaded from the Internet. Proprietary tools, on the other hand, are commercialized, which means that they require licensing rights per user. The tools can be cost prohibitive, making affordability difficult for some organizations, from a purchase point of view. As a result, some organizations opt for using a Microsoft spreadsheet to capture test requirements, test cases and log defects. Other organizations though, can afford to invest larger amounts of money in software testing. This investment is used to set up independent software testing teams and purchase software testing tools that enable them to more readily perform various types of testing.

However, there is no single software testing tool that allows an organization to perform multiple testing activities such as manual, automation and performance testing. As a result of tool limitations, the organization fails to achieve its objectives in conducting end-to-end testing. Software testing needs to cover all requirements, both functional and non-functional. Therefore, the software testing team cannot claim to have produced quality software if they have only covered functional requirements or non-functional requirements as opposed to both. Consequently, organizations need to acquire these tools to cover the entire spectrum of software testing. For organizations it is costly, but for the companies producing these tools, it is profitable. The main reason for separating these tools is for the suppliers to make profits.

Having explored all three cases, one organization opted purely for open-source tools. However, they could not use Selenium effectively to perform automation testing because they relied on self-training. There was therefore not enough time for them to learn because they were also involved in the development, testing and evaluation of the software. As there was no independent software testing team, there was a lack of skill regarding software testing in this organization. As a result, poor quality software was produced.

The second organization purchased IBM rationale tools which enabled them to capture test requirements, test cases and log defects. Due to low budget, however, they adopted JMeter (open source) for performance testing. At least they had an independent software testing team, a manual testing tool and a performance testing tool. They had the advantage of producing quality software because they were able to cover both functional and non-functional testing. The only disadvantage was that they did not have an automation tool to accelerate the testing and evaluation of the software. Therefore, they required too many testers to perform manual and functional testing.

4.2. What are the methods involved in the testing of software?

Software testing methods are the approaches that can be adopted by the software testers to test and evaluate software

within the organization. Thus, software testers are trained and equipped with the necessary testing knowledge to assist with testing the software. These testing methods include black box and white box testing which have been discussed extensively in the introduction. Experienced software testers know which testing methods to follow and when. For example, black box testing is performed when the software tester does not know the internal workings of the software. Those who know the internal workings of the software and have programming knowledge perform white box testing. Software testers with limited knowledge of the software conduct grey box testing.

Not anyone is qualified to be a software tester. Software testing is a career field just like software development, project management and business analysis. There are international software testing standards approved by ISO which need to be adopted to produce quality software. Software testing is process-oriented; therefore, software testers must follow testing processes and frameworks to deliver quality software. It is an intense process which requires software testers to carefully follow a set of steps, instructions, guidelines and policies to produce quality software. The lack of framework, standards and procedures within the organization compromises the software quality. It is like picking up someone from the street who does not have a clue about software testing and simply instructing them to test the software.

4.3. What factors influence the testing and evaluating of software in organizations?

Software is a product and therefore, like every product released to the public or organization, needs to undergo testing. The software testing team needs to verify and validate whether the software behaves as expected. They need to test and evaluate both the functional and non-functional requirements of the software. Performing functional testing enables software testers to detect defects which could be fixed while the software is still undergoing testing. Detecting defects in production is risky because it hinders business, it taints the image of the organization and impacts negative customer reaction. Quality software that sustains and enables organizations to be competitive must be delivered to businesses. However, should the software work as expected, it does not necessarily mean it will automatically function, without testing the non-functional requirements. Performance testing is necessary to determine the response and stability of the software under countless workloads. It measures the quality attributes of the software such as scalability, reliability, and resource usage. Some public and private companies in Gauteng province encountered performance challenges whereby their software could not handle the load of users accessing their software. Therefore, it is vital for businesses to cover all the requirements when testing the software.

4.4. How can a DSS framework be developed and used to address the challenges occurring during software testing and evaluation in organizations?

The analysis and interpretation of the data indicate that if the challenges that occurs during software testing and evaluation are not addressed, they will continue to impact the quality of the software negatively. The consequences of not addressing these challenges will result in the software project not being implemented or perhaps worse, being implemented with defects. As a result, the organization's challenges will negatively impact business and customers.

From the analysis, certain factors were found to clearly influence the testing and evaluation of software. Based on the interpretation of these factors, a framework was developed. The DSS framework for testing and evaluating software was designed to assist with addressing the challenges occurring during the testing and evaluation of software in organizations.

4.5. How the objectives of the study were achieved

From the analysis of the data, interpretation was carried out. This was to further gain a deeper understanding of the factors that influence decisions that are made in software testing. The factors were used to develop a DSS. The interpretation is grouped into four categories to ease understanding as follows:

- Examine and understand the tools

This was primarily to examine and gain an understanding of how manual, automation and performance testing was carried out for software testing. There was an evident lack of management buy-in within the organization. It was evident that management was not willing to invest money in software testing. Firstly, there was no independent software testing team to test and evaluate the software in order to produce the quality of software within the organization. Employees who specialized in other fields such as business analysis and software development were tasked to do the software testing. As software testing is a specialized skill, the organization needed to utilize trained software testers to perform software testing. Secondly, free open-source software testing tools were adopted: instead of purchasing proprietary tools, the organization settled for free open-source software testing tools. Employees researched these tools, trained themselves on these tools and adopted those tools. However, they could not fully utilize the tools but used it only to perform automation testing. As a result, proper quality software could not be achieved, but this research objective.

- Explore and understand methods

The approaches adopted for testing software, white or black box was examined. The following factors indicated that quality was not taken seriously: process-oriented, lack of framework, lack of standards and procedures, software evaluation. Software testing is process-oriented. It is an intense process which requires software testers to follow a particular set of steps, instructions, guidelines and policies to produce quality software. Therefore, if the organization does not have a dedicated software testing team trained to perform software testing, they would not know how to test, what to test and when to test what. As software testing is procedural, software testers follow a particular sequence to execute their testing activities. Also, if there is no testing framework, no testing standards and no procedures, employees would not know how to test and evaluate the software. As a result, quality software cannot be delivered. This objective was also achieved.

- Examine the factors

We wanted to examine the factors that trigger software testing, which at the same time influences the testing and evaluating of software in an organization. Organizations rely on software for competitiveness and sustainability. Therefore, organizations must continue to develop software while also enhancing existing software. It is evident that this creates a need and influences the software testing and evaluation in organizations. However, in order for the software testing team to be able to test, they require documentation such as business requirement specifications and technical design specifications. They must follow testing standards and procedures when conducting software testing. Both functional and non-functional requirements must be integrated to achieve quality software. Various teams interact and work together to deliver quality software. Therefore, this objective was achieved.

- Based on the findings from the aim as stated above, a DSS framework is created

The aim of this DSS framework is to address the challenges that occur during software testing and evaluation in organizations. The DSS framework for testing and evaluating software in organizations was achieved based on the findings from the three selected organizations. Therefore, any organization either private, small to medium, or public may adopt this framework in testing and evaluating software. This framework, when followed, will guide the organization in delivering quality software.

5. DSS Framework for Testing and Evaluating Software

From the findings and interpretation thereof, seven factors were found to have a critical influence on the testing and evaluation of software within an organization: requirements, methodology, filtering, repository, governance, assessment, and institutionalization. Figure 1 depicts these factors and how they relate to each other. Each of the factors consist of phases (P1 . . .P^{+n}) in the sequential order of the activities. Some of the activities can be implemented in parallel. For example, policy, standard and principles within governance can be carried out concurrently. To understand the framework, the discussion should be read in conjunction with the factors mentioned in Figure 1 below.
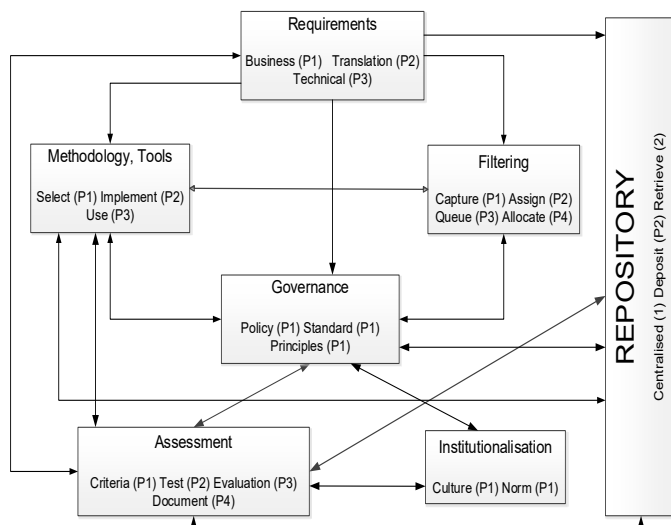
Figure 1: DSS framework for testing and evaluating software

5.1. Requirements

In an organization, software testing and evaluation requirements could be either functional or non-functional, in both business and technical units, respectively. The functional requirements basically describe what the software should do. Some of the typical functional requirements include factors such as business rules, authentication, external interfaces, reporting and administrative functions. The non-functional requirements describe how the software should technically behave within the environment. Non-functional requirements cover all the remaining requirements not covered by the functional requirements. The non-functional requirements specify the criteria used for the assessment of software in an organization. For example, the software should be able to coexist with other software in the environment. Also, the non-functional requirements elaborate a performance characteristic of the software. Some characteristics of non-functional requirements include response times, throughput and utilization of the software.

Manual software testers and automation testers extract the functional requirements from the business requirements they receive from the business analysis team. These functional requirements enable the creation of test requirements and test cases which are then captured in the software testing tools adopted by the organization. A test case outlines the steps required to test any functionality of the software and contains the expected and actual results [1]. Test cases are basically scenarios that have been identified from the requirement specification. These test cases can be automated by automation testers to assist the manual testers with regression testing. Therefore, organizations can purchase software testing tools or utilize open-source tools, depending on the investment the organization is willing to make in software testing.

Performance testers make use of non-functional requirements to test the performance of the software, monitoring the software's continuous load on the network. For example, potential leaks can be detected in memory utilization along with analysis of performance degradation and how the software copes under strenuous use. Performance testing is also performed through software testing tools adopted by the organization. Testing concurrent authentication, for example, means that a hall would be filled with a number of users that need to log in concurrently on the software tested. As it would be too expensive to get, for example, 1000 users in the same room to log into the particular software at the same time, a database nowadays locks input into the database for creating records per user. Therefore, it queues the input and creates individual records in the database.

Both functional and non-functional requirements get stored in the software testing tool used by the organization. Some organizations that do not have these tools, create test cases on spreadsheets and store them in a repository such as Microsoft SharePoint, Hyperaware, intranet or a shared drive. This storage enables any other team that might need that information to easily retrieve it.

5.2. Methodology

Software testing methodologies are the different ways of ensuring that the software under test is fully tested. Methodologies

and tools are selected and implemented based on organizational requirements. Software testing methodologies encompass functional and non-functional testing to validate the software under test. The testing methods include unit testing, integration testing, system testing and performance testing. As software increases in complexity and is enmeshed with the large number of different platforms and devices that need to be tested, it is more important than ever to have robust testing methodologies, ensuring that software being developed, has been carefully tested. This is to ensure that the software meets its specified requirements and can successfully operate in all anticipated environments with the required usability and security.

The software testing methodology has a definite test objective, test strategy and deliverables. Irrespective of which software development methodology (traditional or agile) has been adopted within the organization, the testing methodologies stated above can be applied in the testing and evaluation of software depending on the scope of the project. However, to successfully apply some of these methodologies, software testers require software testing tools. For example, performance testing is performed to determine the performance of the software or network in terms of response, speed and stability, under a particular workload.

Both human and non-human actors are dependent on each other to test and evaluate software. This is to ensure that quality software is delivered to those who requested it. Software testers, including manual, automation, and performance, require software testing tools to perform various types of software testing, as stated above. These tools could be proprietary or open source. LoadRunner is a tool that can be used in determining the performance and outcome of the software under load [32]. Software testing tools enable software testers to successfully perform their duties.

5.3. Filtering

Filtering in software testing and evaluation is a process of removing unwanted functionality or defects from the software, a process guided by requirements as illustrated in the framework (Figure 1). The main activities of the process are as follows: (1) capture the software into the systems; (2) thereafter the software is assigned to a domain; (3) this is put in a queue; (4) and then it is allocated to personnel for testing and evaluation. The fact is that human beings are prone to making mistakes. For example, the business analysts can incorrectly state the business rule in the requirement specification or specify a requirement ambiguously. If the mistake is not detected by the software developer, the business rule will be built into the code and the software will not behave as expected. When software testers are testing the software, the incorrect business rule would be detected as a defect because the software will not be functioning as expected. Therefore, detecting such defects filters unwanted functionality from the software. Regarding ambiguous requirements, the software tester will not be in a position to create some test cases due to unclear requirements. As a result, clarity regarding those requirements would be required from the business analyst. This, then, is the filtering process in terms of requirements.

When compiling test plans, the test managers can identify risks from the requirement specifications. Also, during execution of test cases, risks could be identified which might impact detrimentally on the quality of the software. These risks must be mitigated to produce quality software. Defects detected and logged during the testing and evaluation of software form part of the filtering process and it is the responsibility of the software testing team to filter all unwanted materials from the software under test in their efforts to deliver quality software.

5.4. Repository

A *repository* generally refers to a central place where information gets stored, accessed and maintained. The repository is defined by the organizational requirements. Activities of governance and assessment including the methodology and tools that are applied for testing and evaluation are stored in the repository, primarily to enable and support the ease of access to stock of organizational knowledge, which fosters quality testing and evaluation of software. Additionally, a repository enables control of organizational stock. Thus, those who wish to access the information that is stored in the repository must apply for access to retrieve whatever information they seek. All materials or information stored in the repository must be secured at all times to protect organizational information against attack and leakages.

There are other documents prepared by the software testing team which include statements of work, test plans and closure reports which must also be stored in the repository for audit purposes. Auditors require these documents during auditing to validate how the organization tested and evaluated their software. This information assists them in compiling their audit reports for the organization they are auditing. Also, the information that resides in the software testing tools such as test cases, execution of those test cases and defects logged and fixed for particular software, assists auditors in validating whether or not the software was tested and evaluated according to software testing standards. All these audit findings aid the organization in fixing their mistakes and improving how they test and evaluate software.

5.5. Governance

Governance plays a pivotal role in the process of evaluating the quality of the software. Governance includes policy, standards and principles which can be applied to the process of software testing and evaluation concurrently. Governance involves the definition of organizational test processes, test documentation and the derivation to testing techniques. The software testing process affords the organization with governance on ways to implement the adopted testing policy, standards and principles that aid the stakeholders to deliver quality software. Test governance enforces compliance to the organization's testing process. Governance also ensures that the testing processes are continually improved to ensure the constant, uninterrupted delivery of quality software.

Key documentation such as the test policy and the organizational test strategy requires management support as these documents form part of the organizational test processes. The testing processes can be broken into three parts: organizational and dynamic test processes, and test management processes [33]. All three test processes have key documentation that goes along with them for a successful testing organization. The test policy, for example, defines the overall principles that guide testing in the organization. This document is the primary testing document informing the entire testing organization of why software testing

is performed. All other testing documentation and processes are based on the test policy. It should include the test policy statement, policy principles and testing standards, as it is the foundation provided for the testing processes [33].

There are various standards available in the testing industry, IEEE's is common because it has a series of five standards [33]. The purpose of the standards is to provide generally acceptable methods of testing across the entire testing industry. Organizations can choose to comply fully with these standards or opt for partial compliance. The standards are not only limited to international standards, the organization can still produce and implement internal testing standards that can best fit the local context of their organization.

The principles of software testing, regarded as the beliefs of the testing organization, remind the software testers within the organization of the reason they test and how they test in the first place. The principles form the foundation of the software testing organization and are clearly articulated in the testing policy. These generally accepted testing principles are formulated by testing industry bodies like the International Software Testing Qualifications Board (ISTQB). These principles form part of the early training and development curriculum in software testing.

5.6. Assessment

Assessment promotes quality of software in an environment. Thus, many organizations find value in benchmarking their progress to improve their processes through assessment. Organizations that develop or enhance existing software have test processes in place to test and evaluate their software. The software testing processes begin with test planning, designing of test cases, preparing for execution and evaluating status till the test closure. During the test planning, the scope and risks, test approaches and testing objectives are identified, enabling the software testing team to identify how much testing needs to happen and what possible risks might be encountered.

The next stage is the analysis and design where software testers identify test conditions, evaluate the testability of requirements and the test environment is set up. During the test implementation, test cases are prioritized, and test data is created for those test cases and then executed. Once the execution is complete, the software testing team reports on the outcome of the testing and the closure report is compiled. Organizations that test and evaluate software have their own testing processes in place.

Therefore, organizations must assess their software testing process to improve the way in which they conduct software testing. It provides the opportunity for the organization to know itself and its competition better. As a result, the organization can strive to produce quality software that will enable it to out-compete its rivals. Through requirements, organizations are able to: identify testing objectives, determine the scope of testing, determine which testing approaches to employ and determine risks that might be incurred during testing. All these activities are documented and stored in the repository for future reference.

5.7. Institutionalization

Institutionalization is a state of stability that is required in software to guarantee quality. It is ways, such as continuous

assessment and adherence to governance, in which the software team performs their daily activities for testing and evaluation of software. Iyamu defines *institutionalization* as the process where practices are assimilated into the norm: the ways in which project stakeholders perform their testing and evaluation of software, finally becomes the organizational norm [34]. Those norms should match the internationally agreed set of standards for software testing applicable within any organization. By implementing these standards, the organization will be adopting the only internationally recognized and agreed standards for software testing, giving the organization a high-quality approach to testing software.

Such norms become the software testing culture that is adopted by software testers within the organization. The culture of software quality must be practiced in all parts of the organization because quality is essential for success. Software teams involve various stakeholders such as project managers, business analysts, software developers, software testers, designers, product owners and executive. All these stakeholders play a role in the quality of the final software. Due to this, they need to align their work and practices with agreed international standards, best practices and the test maturity levels in order to deliver quality software. Quality software enables the organization to compete locally and globally with other organizations.

Finally, institutionalization and norms manifest into the organization culture. Organizational culture is a combined means of regulating the behavior of employees within an organization which diffuses all activities as catalysts for the development and growth of the organization [35]. Should the foundation of this organizational culture hinge upon incorrect norms, then the organization would not be in a position to produce quality software. Thus, organizations need to align themselves with the best software testing practices, ISO testing processes as well as testing maturity models. In so doing, the best organizational culture will be practiced by employees. The organizational culture must be documented and stored in the repository so that new employees joining the organization can learn how quality software is produced within the organization. Moreover, existing employees can remind themselves of certain practices they may have forgotten.

6. Conclusion

Organizations are still facing the challenge of ensuring that software projects are tested and evaluated successfully so as not to disrupt business. However, organizations tend to invest in technology and place less emphasis on equipping software testers with software testing knowledge and skills. Hence the same challenges continue to repeat themselves over the years. The contribution of this study is mainly on empirical evidence, giving confidence to employers and employees in adjusting and managing the processes and activities in the testing and evaluation of software in their various organizations. The framework outlines the organizational activities, technologies and governance. The organizational activities include culture, people and operations. Technologies cover the dimensions of the systems, innovation and adoption. Governance includes transformation, awareness and collaboration. Therefore, IT decisions needed to be made to achieve the organizational strategy. This framework can be

adopted by any organization that intends to use technology to implement its organizational strategy.

References

[1] I. Hooda, R.S. Chhillar, "Software test process, testing types and techniques," International Journal of Computer Applications, **111**(13), 10-14, 2015, doi:10.5120/19597-1433.

[2] S. Agarwal, P. Sharma, K. Nikhil, 2012. "A review of the software testing process in SDLC," International Journal of Electronics Communication and Computer Engineering, **3**(1), 18-21, 2012.

[3] D. Mishra, S. Ostrovska, T. Hacaloglu, "Exploring and expanding students' success in software testing," Information Technology & People, **30**(4), 927-945, 2017, doi:10.1108/ITP-06-2016-0129.

[4.] T. Hussain, S. Singh, "A comparative study of software testing techniques viz. white box testing black box testing and grey box testing," International Journal Peer Reviewed Refereed, **2**(5), 1-8, 2015.

[5] M.A. Jamil, M. Arif, N.S.A. Abubakar, A. Ahmad, "Software testing techniques: A literature review," 6th International Conference on Information and Communication Technology for The Muslim World, 177-182, 2016, doi:10.1109/ICT4M.2016.045.

[6] S. Nidhra, J. Dondeti, "Black box and white box techniques - A literature review," International Journal of Embedded Systems and Applications, **2**(2), 29-50, 2012, doi:10.5121/ijesa.2012.2204.

[7] F.G. Filip, C.B. Zamfirescu, C. Ciurea, Computer-Supported Collaborative Decision-Making. Springer International Publishing, 2017.

[8] S. Liu, A. Duffy, R.I. Whitfield, I.M. Boyle, "Integration of decision support systems to improve decision support performance," Knowledge and Information Systems, **22**(3),261-286, 2010, doi.org/10.1007/s10115-009-0192-4.

[9] D. Hoffman, "Test Automation Architectures: Planning for Test Automation," International Quality Week, 37-45, 1999.

[10] M. Kaur, R. Kumari, "Comparative study of automated testing tools: TestComplete and QuickTest Pro," International Journal of Computer Applications, **24**(1):1-7, 2011, doi:10.1.1.259.4366.

[11] D. Shao, S. Khurshid, D.E. Perry, A Case for white-box testing using declarative specifications poster abstract. *Testing: Academic and Industrial Conference Practice and Research Techniques*, IEEE, 137-137), 2007, doi:10.1109/TAIC.PART.2007.36.

[12] G. Mandi, P. Kumar, "Reducing the size of test suite using a variant of non-dominated sorting genetic algorithm II,". International Journal of Advance Research in Computer Science and Management Studies, **1**(6), 66-75, 2013.

[13] A. Nawaz, K.M. Malik, Software Testing Process in Agile Development. Department of Computer Science School of Engineering, Blekinge Institute of Technology, 2008.

[14] J. Tretmans, "Testing concurrent systems: a formal approach," International Conference on Concurrency Theory, 46-66, 1999, doi.org/10.1007/3-540-48320-9_6.

[15] J. Kasurinen, "Software Organizations and Test Process Development," Advances in Computers, **85**,1-63, 2012, doi.org/10.1016/B978-0-12-396526-4.00001-1

[16] S.M.K. Quadri, S.U. Farooq, "Software testing – goals, principles, and limitations," International Journal of Computer Applications, **6**(9), 7-10, 2010, doi:10.5120/1343-1448.

[17] P. Hertz, S. Cavalieri, G.R. Finke, A. Duchi, P. Schönsleben, "A simulation-based decision support system for industrial field service network planning;" Simulation, **90**(1), 69-84, 2014, doi:10.1177/0037549713512685.

[18] P. Hertz, S. Cavalieri, G.R. Finke, A. Duchi, P. Schönsleben, "A simulation-based decision support system for industrial field service network planning," Simulation: Transactions of the Society for Modeling and Simulation International, 1-16, 2013, doi: 10.1177/0037549713512685

[19] B.A. Engel, J.Y. Choi, J. Harbor, S. Pandey, "Web-based DSS for hydrologic impact evaluation of small watershed land use changes," Computers and Electronics in Agriculture, **39**, 241-249, 2003, doi.org/10.1016/S0168-1699(03)00078-4

[20] S. Hosio, J. Goncalves, T. Anagnostopoulos, V. Kostakos, "Leveraging wisdom of the crowd for decision support," In Proceedings of the 30th International BCS Human Computer Interaction Conference: Fusion, 1-12, 2016, doi:10.14236/ewic/HCI2016.38.

[21] A. Athanasiadis, Z.S. Andreopoulou, "DSS applications in forest policy and management: Analysis of current trends," In International Conference on Information and Communication Technologies, 549-557, 2011, doi:10.13140/RG.2.1.4117.6404.

[22] A. Athanasiadis, Z. Andreopoulou, "A DSS for the identification of forest land types by the Greek Forest Service," International Journal of Sustainable Agricultural Management and Informatics, **1**(1), 76-88, 2015, doi: 10.1504/IJSAMI.2015.069053.

[23] J. Sutton, Z. Austin, "Qualitative research: Data collection, analysis, and management," The Canadian Journal of Hospital Pharmacy, **68**(3), 226–231, 2015, doi:10.4212/cjhp.v68i3.1456

[24] O. Gelo, D. Braakmann, G. Benetka, "Quantitative and Qualitative Research: Beyond the Debate," Integrative Psychological and Behavioral Science, **42**, 266–290, 2008, doi: 10.1007/s12124-008-9078-3

[25] J. Barker, P. Linsley, R. Kane, R. 2016. Evidence-based Practice for Nurses and Healthcare Professionals. 3rd ed. Sage Publications Inc, 2016.

[26] M. Petrescu, B. Lauer, "Qualitative Marketing Research: The State of Journal Publications," The Qualitative Report, **22**(9), 2248-2287, 2017, doi:10.46743/2160-3715/2017.2481.

[27] B. Yazan, "Three Approaches to Case Study Methods in Education: Yin, Merriam, and Stake," The Qualitative Report, **20**(2), 134-152, 2015, doi:10.46743/2160-3715/2015.2102.

[28] R.K. Yin, Case Study Research Design and Methods. 5th ed. Thousand Oaks, CA: Sage, 2014.

[29] S. Henderson, Research Methodology. International Journal of Sales, Retailing and Marketing, **4**(9),1-97, 2016,

[30] J. H. Kroeze, "Postmodernism, Interpretivism, and Formal Ontologies". Proceedings in: Research Methodologies, Innovations and Philosophies in Software Systems Engineering and Information Systems, British Cataloguing, 43-62, 2012, doi:10.4018/978-1-4666-0179-6.ch003.

[31] S. Robinson, R. Kerr, "Reflexive conversations: Constructing hermeneutic designs for qualitative management research," British Journal of Management, **26**(4), 777-790, 2015, doi.org/10.1111/1467-8551.12118.

[32] S. Sharmila, E. Ramadevi, "Analysis of performance testing on web applications," International Journal of Advanced Research in Computer and Communication Engineering, **3**(3),5258-5260, 2014.

[33] SO/IEC/IEEE International Standard. 2013. Software and systems engineering -- Software testing --Part 3: Test documentation. ISO/IEC/IEEE 29119-1:2013(E), 1-64. IEEE, 2013.

[34] T. Iyamu, "Institutionalisation of the enterprise architecture: The actor-network perspective," International Journal of Actor-Network Theory and Technological Innovation, **3**(1), 27-38, 201, doi:10.4018/978-1-4666-2166-4.ch012.

[35] G. Gavric, G. Sormaz, D. Ilic, "The Impact of Organizational Culture on the Ultimate Performance of a Company," International Review, **3**(4):25-30, Medimond Publishing Company, 2016,

Technique to Simulate an Oscillator Ensemble Represented by the Kuramoto Model

Mark Gourary*, Sergey Rusakov

CAD Department, Institute for Design Problems in Microelectronics of Russian Academy of Sciences, Moscow, 124365, Russia

A R T I C L E   I N F O

A B S T R A C T

The paper presents the technique for the user-friendly numerical simulation of coupled oscillators described by the Kuramoto model. Oscillators couplings are defined as arbitrary 2π-periodic functions given by the Fourier series. Matlab procedure was developed to generate netlist for the equivalent electrical circuit diagram of the Kuramoto model. The input data of the procedure include the natural frequencies of oscillators and the amplitudes of the couplings harmonics. Kirchhoff equations of the equivalent circuit coincide with the equations of the Kuramoto model. The generated netlists provide obtaining the simulation results using standard circuit simulator. These results numerically coincide with the transients computed using the original Kuramoto model. The presented examples confirm the convenience and effectiveness of the proposed approach.

1. Introduction

This paper is an extension of work originally presented at the 24th European Conference on Circuit Theory and Design, ECCTD 2020 [1] and this is refinement of work where we proposed simulation tool for analyzing ensembles of oscillators.

Studying the collective behavior of coupled oscillators is fundamental problem that has wide application in nature, science, and technology. Simulation of large networks of coupled oscillators is actual multidisciplinary problem due to high demand in various research areas of including biology, chemistry, physics, electronics etc. [2].

The relevance of this issue has been constantly increasing recently due to the growing interest in the study of oscillatory neural networks [3, 4], to the problem of mutual injection locking of oscillators under parasitic couplings in integrated circuits [5], and to various other applications.

The ensemble of physical oscillators is described by system of ordinary differential equations (ODE). Respectively, the analysis of the ensemble can be performed by numerical methods for ODE solving. This approach is effective for an ensemble with small number of simple oscillators [6]. Direct ODE solving of large oscillator ensembles requires too high computational effort. Therefore, simplified models are required for effective simulation of large oscillator systems [7].

The simplification techniques assume that the coupling strength between the oscillators is rather weak [8, 9]. In this case

the coupled oscillator waveform can be considered to coincide with the waveform of this oscillator in free running mode. Then the set of system variables includes only the phases of the oscillators.

The most widespread simplified model is the Kuramoto model (KM) [4, 9, 10] represented by ODE system with respect to phase variables. Kuramoto model describes each oscillator with a single phase variable. The oscillatory interconnections are described in Kuramoto model by 2π-periodic coupling functions.

The standard mathematical packages are usually used for the KM numerical solving. Most often Matlab software [11] is applied (see, for example, [12, 13]). Also, Python codes can be used for solving KM ODE system [14, 15].

However, using standard software packages leads in practice to some difficulties and does not provide effective simulation of an ensemble of oscillators in many applied cases. The user needs to think through the names of variables, repeatedly include the same operators in the code and describe the necessary operations for each specific task. This increases the amount of data preparation, takes a lot of time and leads to additional user errors.

For this reason, the development of universal approach and software tool to improve numerical efficiency of Kuramoto model applications and provide convenient analysis of the simulation results is the actual problem of simulation of ensemble of physical oscillators.

311

The above limitations are the motivation for the development of new numerical approaches that significantly increase the usability of applied tools.

The paper [16] is devoted to this topic. The paper is directed to reduce the arisen difficulties in process of the numerical solution while KM application. The approach [16] is based on representing the KM in the form of the state equations for an equivalent electrical circuit and applying an electrical simulation tool to this circuit. The obtained circuit simulation results are numerically equal to the results of KM simulation.

However, the implementation of the approach presented [16] has the following disadvantages:

- an equivalent circuit is constructed under the wave digital concept [17] which is run on digital signal processors and is not suitable for standard circuit simulators;

- coupling functions in KM can only be represented by sinusoids with the same amplitude, arbitrary functions are not allowed;

- considered sinusoidal coupling functions cannot include phase delay that leads to the impossibility to analyze some important types of coupled oscillators.

- The contribution of the presented paper is connected with new approach that allows to eliminate the limitations of [16]. We propose the following principles for constructing KM equivalent circuit:

- the equivalent circuit should be suitable to analyze by means of standard circuit simulators. Such a circuit consists of standard electrical components which can be described by input netlist;

- coupling functions of arbitrary 2π-periodic form can be considered in KM and specified by truncated Fourier series with the given harmonics amplitudes and phases;

- special-purpose technique to generate the equivalent circuit netlist should be applied.

In comparison with paper [1] the contribution involves additional simulation example to illustrate capabilities of the developed approach for analyzing oscillator ensembles.

The rest of the paper is organized as follows. Section 2 describes the known mathematical forms of the KM equations. Section 3 explains the forming the equivalent circuit for a given KM. Section 4 outlines the principles for the netlist generation procedure. Numerical experiments are presented in Section 5.

2. Kuramoto Model

2.1. Basic Model Equations

KM defines the behavior of a system of N weakly coupled oscillators. Each oscillator is characterized by its natural frequency (fundamental) ω_m and the time-varying instantaneous phase $\theta_m(t)$. In its simplest form, corresponding to the initial Kuramoto proposal (1) KM is represented as an ODE system [18, 19]:

$$\frac{d\theta_m}{dt} = \omega_m + \frac{K}{N}\sum_{n=1}^{N} sin(\theta_n - \theta_m), \qquad m = 1...N. \quad (1)$$

here K is the coupling strength assumed to be the same for all couplings. This form made it possible to obtain estimates of the behavior of the synchronized ensemble of oscillators. However, the assumption about the same couplings is not met in most cases, so more general form of KM was proposed [20, 21]

$$\frac{d\theta_m}{dt} = \omega_m + \sum_{n=1}^{N} A_{mn} sin(\theta_n - \theta_m), \qquad m = 1...N. \quad (2)$$

here A_{mn} is the individual coupling strength between m-th and n-th oscillators. Form (2) of KM is more flexible tool to represent real sets of coupled oscillators.

The natural extension of KM also considers the external periodic force [22, 23] as the excitation with a given phase θ_e applied to internal oscillators. In such case the Right-Hand Side of m-th equation (2) is supplemented by external coupling functions of the form $A_{m,e}(\theta_e - \theta_m)$.

In the simplest case when one oscillator is excited by a single stimulus, the KM equation has the form:

$$\frac{d\theta}{dt} = \omega + A_e sin(\theta - \theta_e). \quad (3)$$

The phase of the periodic excitation is $\theta_e = \omega_e t$ where ω_e is the excitation frequency that in the synchronized mode coincides with the oscillator frequency. The oscillator phase is $\theta = \omega_e t + \vartheta$ where φ is the initial phase of the synchronized oscillator. After substituting expressions for phases θ_e, θ into (3) we obtain the algebraic equation with respect to ϑ and the condition of its solution existence defining the locking range of the oscillator

$$\omega_e - \omega = A_e sin(\vartheta), |\omega_e - \omega| \le A_e. \quad (4)$$

In general case the locking range ω_{mn} of m-th oscillator under the excitation by n-th oscillator is equal to the coupling factor A_{mn}.

$$\omega_{mn} = A_{mn}. \quad (5)$$

System (2) with antisymmetric sinusoidal coupling functions always results in a synchronized behavior for a set of identical oscillators. However, starting from [24], it was found that some dynamical systems of identical oscillators can demonstrate unsynchronized states with quasiperiodic oscillations. Such states, defined as chimeras [25, 26], can be represented by KMs with additional phase shifts in sinusoidal arguments. Using notation (5), we can write:

$$\frac{d\theta_m}{dt} = \omega_m + \sum_{n=1}^{N} \omega_{mn} sin(\theta_n - \theta_m + \varphi_{mn}), \quad (6)$$

that can also be presented as the sum of sines and cosines due to $sin(\theta_n - \theta_m + \varphi_{mn}) = a sin(\theta_n - \theta_m) + b cos(\theta_n - \theta_m)$.

KM in the form (6) does not capture some of the effects inherent in coupled oscillators. E.g., superharmonic synchronization [27] of m-th oscillator under the excitation by k-th harmonic of n-th oscillator cannot be taken into account. Thus, more complicated coupling functions are needed, and the most general form of KM was defined as [10, 22]

$$\frac{d\theta_m}{dt} = \omega_m + \sum_{n=1}^{N} h_{mn}(\theta_n - \theta_m). \qquad (7)$$

Here $h_{mn}(\theta_n - \theta_m)$ are 2π-periodic coupling functions that are often approximated to desired accuracy using truncated Fourier series with sufficiently large number of terms:

$$h_{mn}(\theta_n - \theta_m) = \sum_{k=1}^{K_m} A_{mn}^{(k)} sin(k(\theta_n - \theta_m) + \varphi_{mn}^{(k)}). \quad (8)$$

Constant terms in the Fourier series (5) are zeroes ($A_{mn}^{(0)} = 0$) due to the compensation of nonzero terms by the change of fundamentals ω_m in (1). Similarly, diagonal entries are also assumed to be $A_{mm}^{(k)} = 0$ for all k.

Under notations (5) one can represent (8) as

$$\frac{d\theta_m}{dt} = \omega_m + \sum_{n=1}^{N} \sum_{k=1}^{K_m} \omega_{mn}^{(k)} sin(k(\theta_n - \theta_m) + \varphi_{mn}^{(k)}). (9)$$

Here $\omega_{mn}^{(k)}$ is equal to the locking range of superharmonic synchronization [13] of m-th oscillator under the excitation by k-th harmonic of n-th oscillator.

2.2. Modified Model Equations

To enhance the user-friendliness when simulating coupled oscillators, we have made some modifications to the KM (9).

Couplings activation moments were included in the model assuming all couplings were initially disabled.

The activation moment is defined by adding to the coupling function time-dependent multiplier $u(t − \tau_{mn})$ were $u(t)$ is the unit step function, τ_{mn} is the coupling activation moment. Then coupling function from KM (6) has the form:

$$g_{mn}(\theta_n - \theta_m, t) = u(t - \tau_{mn})\omega_{mn} sin(\theta_n - \theta_m + \varphi_{mn}). (10)$$

For the coupling functions defined by Fourier series (8), (9) we indicate the activation moment $\tau_{mn}^{(k)}$ for each k-th Fourier term.

Main results of KM simulations are presented by oscillator phases θ_m. However, the phase waveforms are often inconvenient for analyzing the simulation results due to include a linear component. More user-friendly data is represented by instantaneous frequency waveforms, that indicate the synchronization mode by their constant values. The instantaneous frequency in angular ($\omega_m^{\mathbf{inst}}$) or regular ($f_m^{\mathbf{inst}}$) forms is determined as following:

$$f_m^{inst} = \frac{\omega_m^{inst}}{2\pi} = \frac{1}{2\pi}\frac{d\theta_m}{dt}. \qquad (11)$$

Note that the angular form of the instantaneous frequency $\omega_m^{\mathbf{inst}}$ (7) is used in any KM form (1), (2), (6) and (9). This also corresponds to the Right-Hand Side of KM. But usually the user needs to analyze the frequency in the regular form $f_m^{\mathbf{inst}}$, so to avoid superfluous transforms one can convert KM to a form with respect to regular frequencies by dividing it by 2π. Then KM (9) is represented as

$$\frac{1}{2\pi}\frac{d\theta_m}{dt} =$$
$$= f_m + \sum_{n=1}^{N} \sum_{k=1}^{K_n} u(-\tau_{mn}^{(k)})f_{mn}^{(k)} sin(k(\theta_n - \theta_m) + \varphi_{mn}^{(k)}). \qquad (12)$$

where $f_m = \omega_m/2\pi$, $f_{mn}^{(k)} = \omega_{mn}^{(k)}/2\pi$.

3. Representation of Kuramoto Model by Equivalent Electrical Circuit

The behavior of the oscillator ensemble can be obtained by the simulation of the electrical circuit if state equations of the circuit coincide with the KM ODE system (12) of the ensemble. Thus, we proposed the following structure of the equivalent circuit.

Each m-th oscillator from KM corresponds to the node in the equivalent circuit with the same index m. The voltage of the node is equal to the phase of KM (12): $\theta_m(t) \equiv V_m(t)$.

The devices connected in parallel to m-th node include:

1. Capacitor $C_m=1/(2\pi)$ representing the phase differentiation in the left-hand side of (12). The capacitor current is numerically equal to the instantaneous frequency of m-th oscillator:

$$I_m^{inst}(t) = C_m \cdot dV_m/dt = 1/2\pi \, d\theta_m/dt = f_m^{inst}(t). \quad (13)$$

2. Independent current source numerically equal to the fundamental of m-th oscillator

$$I_m^{fund} = f_m. \qquad (14)$$

3. Nonlinear current sources correspond to Fourier terms in the Right-Hand Side of (9). Each source represents k-th Fourier harmonic of a coupling function from m-th to n-th oscillator:

$$I_{m,n,k}^{harm}(t, v_n, v_m) =$$
$$= (t - \tau_{mn}^{(k)})f_{mn}^{(k)} sin(k(V_n - V_m) + \varphi_{mn}^{(k)}). \qquad (15)$$

here parameters $f_m, \tau_{mn}^{(k)}, f_{mn}^{(k)}, \varphi_{mn}^{(k)}$ are defined in KM (12).

One can see that Kirchhoff Current Law (KCL) equations for the equivalent circuit with M nodes corresponding to all oscillators of KM represent the same ODE system as the initial KM:

- the KCL equation for the node of m-th capacitor coincides with m-th equation of KM (12),

- the voltage (V) of m-th node is numerically equal to the instantaneous phase (rad) of m-th oscillator,

- the current (A) through m-th capacitor is numerically equal to the instantaneous frequency (Hz) of m-th oscillator due to (11).

Note that m-th node in the equivalent circuit (13-15) is floating due to the capacitor connection to the current sources. Hence the initial capacitor voltage equal to the initial oscillator phase should be defined to provide transient simulation.

The example in Figure 1 represents the equivalent circuit for KM of the pair of coupled oscillators.
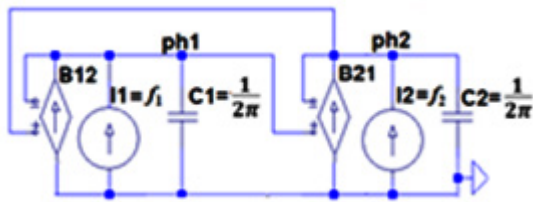
Figure 1: The equivalent circuit for KM of the pair of coupled oscillators.

Input netlist of the circuit in Figure 1 for oscillators' fundamentals f_1=100Hz, f_2=102Hz and couplings parameters, f_{12}=f_{21}=1Hz, τ_{12}=1sec., τ_{21}=5sec. has the form:

Input netlist for KM of the pair of coupled oscillators.

.params inv2pi=0.5/pi   *parameter to define constant $1/2\pi$

* oscillators (13)

C1 0 ph1 {$1/2\pi$}

C2 0 ph2 {$1/2\pi$}

* fundamentals (14)

I1 ph1 0 100

I2 ph2 0 102

* couplings (15)

B12 ph1 0 I = 1*sin(v(ph2,ph1))*u(time - 1)

B21 ph1 0 I = 1*sin(v(ph1,ph2))*u(time - 5)

* initial phases of oscillators

.IC v(ph1) = 0

.IC v(ph1) = 0

.end

After processing the netlist by LTspice circuit simulator [28] one can obtain instantaneous frequencies of oscillators as current waveforms of capacitors C1 and C2 (13). Examples of the waveforms I(C1), I(C2) are presented in Figure 2.

The waveforms in Figure 2a are obtained for parameters given in the presented netlist. While both couplings at t < 1sec are disabled the oscillators produce their natural frequencies f_1=100Hz and f_2=102Hz. At t=1sec coupling 1-2 is activated but the coupling factor f_{12}=1Hz is insufficient ($|f_1$- $f_2|$ =2 > f_{12}) to provide synchronization of the oscillator #2 by the oscillator #1. So, beats appear in the instantaneous frequency waveform at 1 < t < 5sec. After the activation of both couplings at t > 5sec the oscillators are mutually synchronized with common frequency 101Hz.
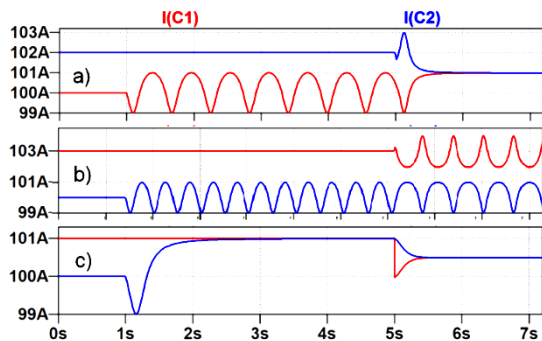
Figure 2: Simulated waveforms of instantaneous frequencies of capacitances currents obtained for f1=100Hz and a) f2=102Hz, b) f2=103Hz, c) f2=101Hz

Figure 2b demonstrates simulation results for an increased value of the second fundamental to f_2 = 103Hz. results for an increased value of the second fundamental to f_2 = 103Hz. The discrepancy of fundamentals is too large ($|f_1$-$f_2|$ = 3Hz) to provide synchronization even under the activation of both couplings.

The decrease of the second fundamental to f_2=101Hz (($|f_1$- $f_2|$ =1Hz) leads to waveforms in Figure 2c with synchronization under both unidirectional and bidirectional couplings.

4. Automatic Forming of Input netlist by Matlab Description of Kuramoto Model

For the convenience of forming a Input netlist of an equivalent electrical circuit, we introduce the naming rules for nodes and components of the circuit that is shown in Table 1.

Table 1: Netlist names corresponding to m-th oscillator.

m-th circuit components (KM variable)	Notation	Netlist name
m-th node (m-th oscillator)	m	ph*m*
Node voltage (oscillator phase)	v_m	v(ph*m*)
m-th capacitor	C_m	C*m*
Capacitor current (instantaneous frequency)	I_m^C	I(C*m*)
m-th DC current source (natural frequency)	I_m^{fund}	I*m*
Behavioral current source (coupling harmonic) k - harmonic index, *m,n* – oscillators indexes	$I_{m,n.k}^{harm}$	B*m*_*n*_*k*

C*m*   0   ph*m*   {$1/2\pi$};   differentiation operator

I*m*   ph*m*   0 f_m;   natural frequency

……………………………………………

B*m*_*n*_*k* ph*m* 0   *k*-th harmonic of *mn* coupling

$+ \ I = u(t - \tau_{mn}^{(k)}) f_{mn}^{(k)} \sin(k(v(ph n) - v(ph m)) + \varphi_{mn}^{(k)})$

………………………………………..

………………………………………..

.IC v(ph*m*) = PHm;   initial phase of m-th oscillator

One can see from this fragment that the netlist of the equivalent circuit contains significant amount of duplicate or redundant text data because the same oscillator indexes can be repeated in many component names. For example, the oscillator index *m* is included in the name of the node representing the oscillator phase and in the name of each component connected to the node.

Redundancy increases for the netlists with many Fourier harmonics (B*m*_*n*_*k*). In this case the same indexes of oscillators must be presented in each behavioral source (B*m*_*n*_*k*) both as the part of its name and names of reference nodal voltages v(ph*n*).

To eliminate the redundancy of the input data, we propose to generate the Input netlist using the procedure based on the description of interacting oscillators in compact form without data duplication. The form is convenient for filling out by the user.

When developing the procedure, we firstly changed the set of primary parameters in favor of relative values. Considering that KM is applicable to the ensemble of oscillators with close natural frequencies one can introduce the "base frequency" parameter f_b, which is close to average fundamentals of all oscillators.

Individual natural frequencies are set by defining its relative deviations (r_m) from the base frequency:

$$r_m = (f_m - f_b)/f_b \text{ or } f_m = (r_m + 1) \cdot f_b. \tag{16}$$

The coupling factors $f_{mn}^{(k)}$ in (10) are determined by relative values $r_{mn}^{(k)}$ with respect either to the base frequency:

$$r_{mn}^{(k)} = f_{mn}^{(k)}/f_b, \tag{17}$$

or to the natural frequency of the excited oscillator,

$$r_{mn}^{(k)} = f_{mn}^{(k)}/f_m = f_{mn}^{(k)}/((r_m + 1) \cdot f_b). \tag{18}$$

The choice between options (17), (18) depends on the control logical variable mr=0/1 that is set for all KM couplings.

Phases in (10) are set relatively to 2π: $\phi_m^k = \varphi_m^k/2\pi$.

$$\phi_m^k = \varphi_m^k/2\pi. \tag{19}$$

The procedure to generate an Input netlist is developed using Matlab software [7], so parameters (13) – (15) are grouped in the Matlab data types that include:

1. Simple numeric variables:

- **fb** – basic frequency.

- **mr** – type of relative parameter.

- **Tsim** – simulation time.

2. Cell array **osc** that contains oscillators' parameters. Each array element contains parameters of one (m-th) oscillator:

- the relative deviations of natural frequency r_m (16);

- the initial phase $\theta_m(0)$.

The oscillator parameters are set by assigning them to the array element with the oscillator index, e.g.

osc{n1} =[r_{n1} $\theta_{n1}(0)$];

osc{n2}=[r_{n2}];

……

osc{nL}=[r_{nL} $\theta_{nL}(0)$];

Oscillator indices (n1, n2, …nL) are arbitrary non-repeating integers. The value of zero initial phase can be omitted (see n2).

3. Cell matrix **coup** with parameters of couplings. Each matrix entry (m, n) defines cell array of parameters of harmonics $I_{m,n,k}^{harm}(t, v_n, v_m)$ (15) for given indexes of excited (m) and exciting (n) oscillators. The sequential number of the parameter vector presents the harmonic index k and components of the vector define coupling factor, phase shift and switching moment of the harmonic. Thus, the coupling function (m, n) with k harmonics is represented as matrix entry with parameters of all harmonics:

coup{m,n}={[$r_{mn}^{(1)}$ $\phi_{mn}^{(1)}$ $\tau_{mn}^{(1)}$][$r_{mn}^{(2)}$ $\phi_{mn}^{(2)}$ $\tau_{mn}^{(2)}$] … [$r_{mn}^{(k)}$ $\phi_{mn}^{(k)}$ $\tau_{mn}^{(k)}$] };

For example, the pair of coupled harmonic oscillators in Figure 1 is defined by the following description:

fb=100;

osc{1}=[0];

osc{2}=[0.06];

coup{1,2}={[0.01 0 1]};

coup{2,1}={[0.01 0 5]};

One can see that this description is more compact than presented above Input netlist of the equivalent circuit in Figure 1. More essential reducing of the size of input data can be achieved for KM containing many coupling functions with large number of Fourier harmonics.

Thus, to simulate the oscillator ensemble defined by the given KM one should perform the following operations:

- form Matlab description of the KM by filling-in cell array **osc** with parameters of oscillators and filling-in cell matrix **coup** with parameters of couplings;

- generate Input netlist by applying the developed procedure to the formed KM description;

- apply standard circuit simulator to the generated netlist;

- analyze time-domain dependences of phases and frequencies by applying the simulator waveform viewer to the corresponding nodal voltages and capacitances currents.

5. Numerical Examples

Here we present two numerical examples that illustrate the application of the developed approach to the analysis of ensembles of oscillators. To simulate the generated equivalent circuit, the LTspice circuit simulator [28] was used.

The first example presents 8 ensembles of 9 oscillators with natural frequencies evenly distributed in the interval [98 – 102] Hz:

$$f_n = 95 + n, n = 1 \dots 9. \tag{20}$$

The oscillators are sequentially coupled in forward direction and have one or two reverse couplings forming different versions of closed sequence that are shown in Figure 3.a1-a8. The figure 3aN represents the version with the index N of the intermediate oscillator between reverse couplings (Figure 3a1 is the version with one coupling).
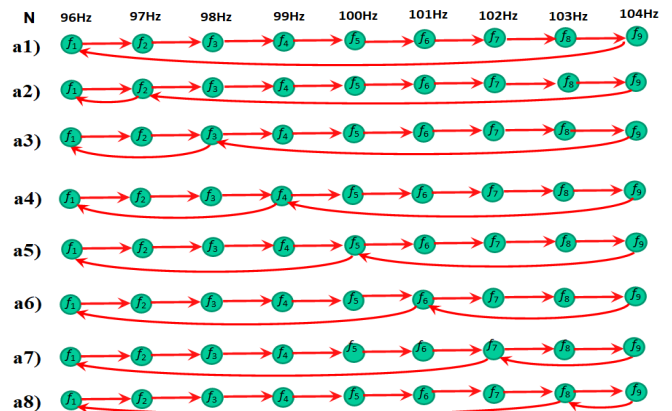
Figure 3: Series of oscillators 1-8 with reverse couplings through N-th oscillator: aN), N=1…8.

All couplings in each ensemble a1-a8 are defined by sine functions (2) with the same coupling factor $r_{mn}^{(1)} = \rho$ (for all m, n).

The aim of the experiments is to determine for each version the value of the common coupling factor providing the ensemble synchronization - ρ_{synch} and to compare obtained values for different versions. To obtain the results the ensembles in Figure a1-a8 must be simulated for a range of overall coupling factors.

To perform the simulation the developed procedure was applied. As an example we present below Matlab descriptions of KM for a1, a5 and corresponding simulation results.

% Matlab description for KM a1

fb = 100; mr = 0; Tsim=15;

osc{1}=[-0.08]; osc{2}=[-0.06]; osc{3}=[-0.04];

osc{4}=[-0.02]; osc{5}=[0.0]; osc{6}=[0.02];

osc{7}=[0.04]; osc{8}=[0.06]; osc{ 9}=[0.08];

coup{2,1}={[ρ 0 1]}; coup{3,2}={[ρ 0 1]};
coup{4,3}={[ρ 0 1]}; coup{5,4}={[ρ 0 1]};
coup{6,5}={[ρ 0 1]}; coup{7,6}={[ρ 0 1]};
coup{8,7}={[ρ 0 1]}; coup{9,8}={[ρ 0 1]};
coup{1,9}={[ρ 0 1]};

Simulation results are represented in Figure 4a-d, where the waveforms of the instantaneous frequencies $f_1(t)$ and $f_9(t)$ are shown for the different values of coupling factors:

1. Small value $\rho = 1.3$Hz $\approx 0.125\rho_{synch}$ (Figure 4a). The waveforms are close to sine curves.

2. Moderate value $\rho = 5.4$Hz $\approx 0.5\rho_{synch}$ (Figure 4b). The distortions of sinusoids increase.

3. The value approaching the synchronization value $\rho = 10.8$Hz $\approx 0.99\cdot\rho_{synch}$ (Figure 4c). The waveforms are represented by pulsed curves both for $f_1(t)$ and $f_9(t)$.

4. The minimal value for the synchronization $\rho = \rho_{synch} = 10.8$Hz (Figure 4d). Initial pulses disappear and after that both instantaneous frequencies are equal to the constant synchronization frequency $f_1(t) = f_9(t) = f_{synch}$
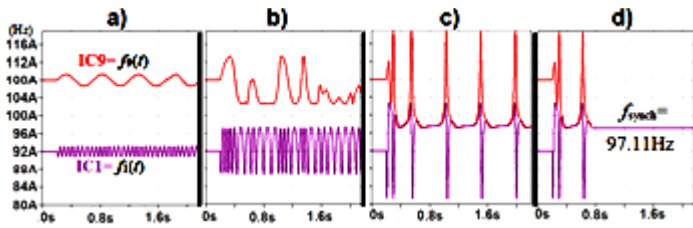
Figure 4: Simulation results for KM a1, The instantaneous frequencies $f_1(t)$ and $f_9(t)$ for the values of the common coupling factor ρ: a) ρ = 1.3Hz; b) ρ = 5Hz; c) ρ = 10.8Hz; d) ρ = ρ_{synch} = 10.8Hz.

Matlab description for KM a5 differ from KM a1 by replacing coupling coup{1,9}={[ρ 0 1]}; by 2 couplings:

coup{1,5}={[ρ 0 1]}; coup{5,9}={[ρ 0 1]};

Experimental waveforms of the instantaneous frequencies $f_1(t)$, $f_5(t)$ and $f_9(t)$ are shown in Figure 5, for the similar coupling factors: ρ = 1.05Hz, ρ = 4.2Hz, ρ = 8.35Hz, ρ_{synch} = 8.41Hz.
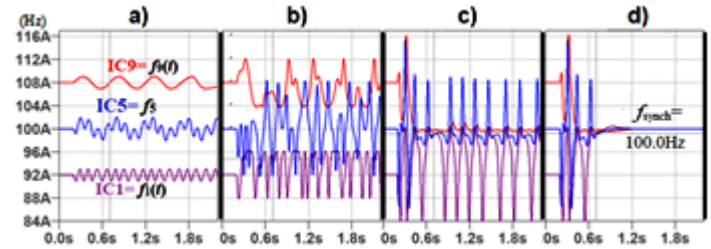
Figure 5: Simulation results for KM a5, The instantaneous frequencies $f_1(t)$ and $f_9(t)$ for the values of the coupling factor ρ: a) ρ = 1.05Hz; b) ρ = 4.2Hz; c) ρ = 8.4Hz; d) ρ = 8.41Hz.

Simulations like Figure 4, 5 were performed for all oscillator ensembles a1-a8 (Fig 3). The obtained numerical characteristics are presented in Table 2. Each column of the table contains:

- the name of the ensemble (N),

- the common coupling factor providing synchronizing (f_{ij}),

- the deviation of the synchronization frequency from the basic frequency (Δf_{syn}).

Table 2 Numerical characteristics of oscillator ensembles a1-a8

N	a1	a2	a3	a4	a5	a6	a7	a8
f_{ij}	10.86	16.49	8.01	14.36	8.411	13.97	9.15	12.41
f_s	97.11	99.79	100.0	99.23	100.0	100.0	100.3	97.08

The second example is a ring sequence (Figure 6a) of 5 oscillators with couplings, which are sequentially switched on with a delay of 5 seconds. The natural frequencies of the oscillators are evenly distributed in the interval [98 - 102] Hz (base frequency - 100 Hz). Each coupling function in an open loop 1–2–3–4–5 contains only the first harmonic with zero phase shift $\phi_{mn}^{(1)} = 0$ and coupling factors are $f_{mn}^{(1)}$=3Hz ($r_{mn}^{(1)}$=0.03).

The aim of the numerical experiments is to analyze the dependence of the synchronization process on the magnitude of the coupling function between the first and fifth oscillators ($g_{51}(\theta_{15})$).

The initial description of the ring ensemble is presented in Figure 6b for 5-1 coupling factor $r_{15}^{(1)} = 0.005$. Waveforms of instantaneous frequencies of oscillators obtained as simulation results are presented in Figure 7.
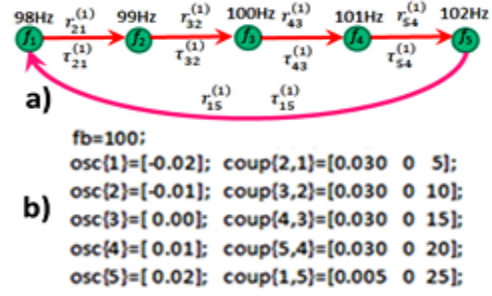
Figure 6: a) The ring of 5 coupled harmonic oscillators, b) matlab description of the ring.

At t < 5sec the instantaneous frequencies of all oscillators coincide with their natural frequencies because all couplings are disabled. After coupling 1-2 is switched on at t = 5sec the second oscillator is synchronized by the natural frequency of the first one. Similarly the synchronization of oscillators 3 , 4 occurs at t = 10sec

and at t = 15sec correspondingly. But enabling coupling 4-5 at t = 20sec does not lead to the synchronization of oscillator 5 because the discrepancy of frequencies $(f_5 - f_1 = 4Hz)$ exceeds the coupling factor $r_{54}^{(1)} = r_{54}^{(1)} \cdot f_b = 3Hz$. As a result, the oscillator 5 instantaneous frequency at 20 < t < 25sec is a periodic waveform. Enabling coupling 5-1 closes the ring and interrupts all synchronizations at t > 25 sec where instantaneous frequencies of all oscillators are time varying waveforms.
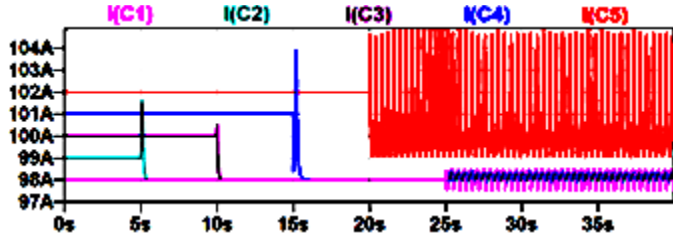
Figure 7: Simulation results obtained using matlab description in Figure 6b.

In more details the waveforms at t = 24-28 sec. can be seen in Figure 8a which is the first one of the plots in Figure 8a-e representing simulation results for some values of 5-1 coupling factor $r_{15}^{(1)}$. The unsynchronized behavior of the oscillators is seen in two intervals: $r_{15}^{(1)} \le 0.041$ (Figure 6a,b) and $r_{15}^{(1)} \ge 0.078$ (Figure 6e). In the interval $0.0042 \le r_{15}^{(1)} \le 0.077$ (Figure 6c-d) all oscillators are mutually synchronized.

Thus, two bifurcation points can be defined in the axis of values of the coupling factor. At $r_{15}^{(1)} = 0.00415$ the transition from unsynchronized (Figure 8b) to synchronized (Figure 8c) mode occurs. The inverse transition (from Figure 8d to Figure 8e) occurs at $r_{15}^{(1)} = 0.0775$.

A similar analysis of the impact of the coupling factor was performed for the 5-1coupling function with a non-zero phase shift ($\phi_{15}^{(1)} = \pi/2$). The results are shown in Figure 9.

The input description of the 5-1 coupling is presented as

coup{1,5}={[0.025 0.25 25]};
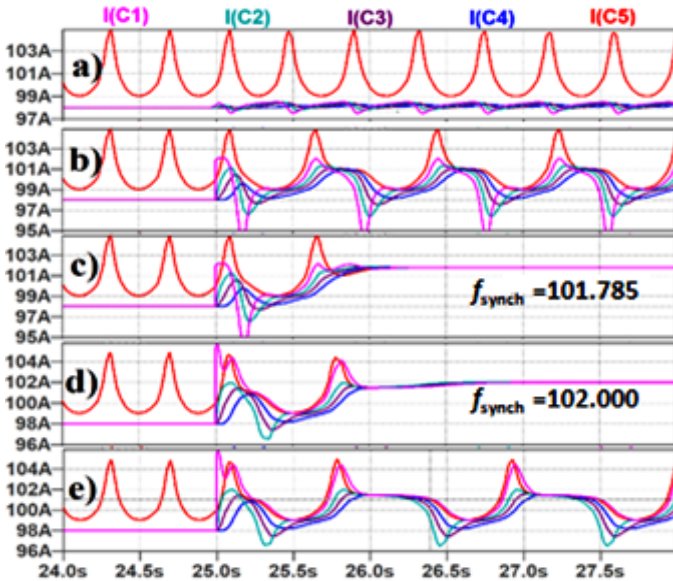
Figure 8: Simulation results for various 5-1 coupling factors a) $r_{15}^{(1)}$=0.005, b) $r_{15}^{(1)}$=0.041, c) $r_{15}^{(1)}$=0.042, d) $r_{15}^{(1)}$=0.077 e) $r_{15}^{(1)}$=0.078.
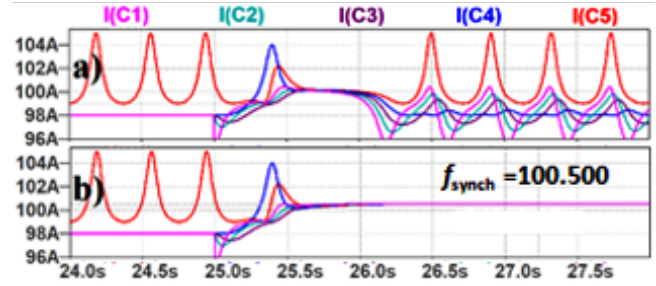
Figure 9: Simulation results for various 5-1 coupling factors under phase shift $\phi_{15}^{(1)} = \pi/2$: a) $r_{15}^{(1)}$=0.024, b) $r_{15}^{(1)}$=0.025.

Some obtained waveforms in Figure 9 demonstrate the transition from unsynchronized (Figure 9a) to synchronized (Figure 9b) mode in the single bifurcation point $r_{15}^{(1)} \approx 0.0245$.

The simulated waveforms in Figure 10 are obtained under varying the second harmonic magnitude ($r_{15}^{(2)}$) of 5-1 coupling function. The phase shift and all other harmonics of the coupling function are zeroes.

coup{1,5}={[ ] [0.014 0 25]};
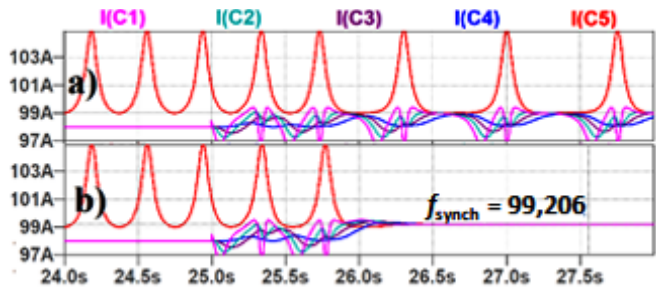
Figure 10: Simulation results for 5-1 for coupling function with the second harmonic only ($r_{15}^{(1)}$=0.0): a) $r_{15}^{(2)}$=0.014, b) $r_{15}^{(2)}$=0.015.

Here similarly to Figure 9 the domains of unsynchronized and synchronized modes are separated by the sole bifurcation point of the second harmonic $r_{15}^{(2)} \approx 0.0145$.

Thus, the presented experiments showed the useful application of the proposed approach to simulating coupled oscillators.

6. Conclusions

The paper presents the numerical approach to simulate ensembles of arbitrary oscillators. The principles of operation of the required software based on the circuit simulator and the Matlab system are developed.

The proposed approach for analyzing an ensemble of oscillators is based on the construction of model of electrical circuit. The Kirchhoff equations of this model coincide with the Kuramoto model equations of the considered ensemble. The unambiguous correspondence between the currents and voltages of the equivalent circuit and the phases and frequencies of the Kuramoto model is provided. As a result, simulating the equivalent electrical circuit performs the computation of the transients in the ensemble including computation of oscillatory phases and frequencies. The analysis of obtained transients is supported by plotting tools of modern electrical simulators.

The set of simple rules provides constructing of the equivalent circuit for coupling functions defined by their Fourier series. The numerical procedure has been developed to automatically create the input netlist. The routine generates netlist by processing the compact form of user-friendly ensemble description. The description includes lists of oscillator parameters and communication parameters represented as a Matlab structure.

The presented numerical examples have demonstrated the efficiency and convenience of the proposed approach.

Acknowledgment

References

[1] M.M. Gourary, S.G. Rusakov, "A Simulation Tool for Analysis of Oscillator Ensembles Defined by Kuramoto Model," 2020 European Conference on Circuit Theory and Design (ECCTD), Sofia, Bulgaria, 1-4, 2020, doi: 10.1109/ECCTD49232.2020.9218382.

[2] S.H. Strogatz, Nonlinear Dynamics and Chaos with Applications to Physics, Biology, Chemistry, and Engineering, Westview Press, 2015. 2, 528. ISBN 978-0-813-34910-7.

[3] M. Bonnin, F. Corinto, M. Gilli, "Periodic Oscillations in Weakly Connected Cellular Nonlinear Networks," IEEE Transactions on Circuits and Systems I: Regular Papers, **55**(6), 1671-1684, 2008, doi: 10.1109/TCSI.2008.916460.

[4] P. Ashwin, S. Coombes, R.J. Nicks, "Mathematical Frameworks for Oscillatory Network Dynamics in Neuroscience," Journal of Mathematical Neuroscience 6 (2), 1-92, 2016, doi: 10.1186/s13408-015-0033-6.

[5] P. Bhansali, J. Roychowdhury, "Injection Locking Analysis and Simulation of Weakly Coupled Oscillator Networks," in Simulation and Verification of Electronic and Biological Systems, 71-93, Springer Science+Business Media B.V., 2011, doi: 10.1007/978-94-007-0149-6_4.

[6] K.S.T. Alain, F.H. Bertrand, "A Secure Communication Scheme using Generalized Modified Projective Synchronization of Coupled Colpitts Oscillators," IJMSC, **4** (1), 56-70, 2018, doi: 10.5815/ijmsc.2018.01.04

[7] P. Maffezzoni, B. Bahr, Z. Zhang, L. Daniel, "Reducing Phase Noise in Multi-Phase Oscillators," IEEE Transactions on Circuits and Systems I: Regular Papers, **63**(3), 379-388, 2016, doi: 10.1109/TCSI.2016.2525078.

[8] C. Gong, A. Pikovsky, "Low-Dimensional Dynamics for Higher Order Harmonic Globally Coupled Phase Oscillator Ensemble", Physical Review E. **100** (6-1), 062210, 2019, doi: 10.1103/PhysRevE.100.062210.

[9] F. Dörfler, F. Bullo, "Synchronization in complex networks of phase oscillators: A survey," Automatica, **50**(6), 1539-1564, 2014. doi: 10.1016/j.automatica.2014.04.012.

[10] J.A. Acebron, L.L. Bonilla, C.J.P. Pérez Vicente, F. Ritort and R. Spigler, "The Kuramoto model: A simple paradigm for synchronization phenomena," Reviews of Modern Physics **77**(1), 137 – 185, 2005, doi: https://doi.org/10.1103/RevModPhys.77.137

[11] A. Gilat, Matlab: An Introduction with Applications, 7th Edition Pod for Student Choice, John Wiley & Sons, Incorporated, 2017.

[12] J. Kim, "Kuramoto model Numerical code (MATLAB)," in https://appmath.wordpress.com/2017/07/23/kuramoto-model-numerical-code-matlab

[13] "Cleve's Corner: Cleve Moler on Mathematics and Computing" in https://blogs.mathworks.com/cleve/2019/08/26/kuramoto-model-of-synchronized-oscillators/

[14] "Python implementation of the Kuramoto model on graphs" in https://github.com/fabridamicelli/kuramoto_model

[15] O'Keeffe, K.P., Hong, H. Strogatz, S.H. Oscillators that sync and swarm. Nat Commun 8, 1504 (2017). doi: 10.1038/s41467-017-01190-3

[16] K. Ochs, D. Michaelis and J. Roggendorf, "Circuit Synthesis and Electrical Interpretation of Synchronization in the Kuramoto Model," 2019 30th Irish Signals and Systems Conference (ISSC), Maynooth, Ireland, 1-5, 2019, doi: 10.1109/ISSC.2019.8904942.

[17] A. Fettweis, "Wave Digital Filters: Theory and Practice," Proceedings of the IEEE, **74**(2), 270–327, 1986, doi: 10.1109/PROC.1986.13458.

[18] Y. Kuramoto "Self-entrainment of a population of coupled non-linear oscillators," In: Araki H. (eds) International Symposium on Mathematical Problems in Theoretical Physics. Lecture Notes in Physics, **39**. Springer, Berlin, Heidelberg, 1975, doi: 10.1007/BFb0013365.

[19] S.N. Dorogovtsev, J.F.F. Mendes "Evolution of networks," Advances in Physics, **51**(4), 1079-1187, 2002, doi: 10.1080/00018730110112519

[20] F. A. Rodrigues, T.K.DM. Peron, P.Ji, "The Kuramoto model in complex networks," Physics Reports, **610**, 1-98 2016. doi: 10.1016/j.physrep.2015.10.008ted, 2017.

[21] A. Arenas, A. Díaz-Guilera, J. Kurths, Y. Moreno, C. Zhou, "Synchronization in complex networks," Physics Reports, **469**(3), 93-153, 2008, doi: 10.1016/j.physrep.2008.09.002.

[22] ben-Avraham, D.A. Barrát, M. Barthélemy, A. Vespignani, "Dynamical Processes on Complex Networks," Journal Statically Physics, **135,** 773–774, 2009, doi: 10.1007/s10955-009-9761-x

[23] A. Bohn, J. García-Ojalvo, "Synchronization of coupled biological oscillators under spatially heterogeneous environmental forcing," Journal of Theoretical Biology," **250**(1), 37-47, 2008, doi: 10.1016/j.jtbi.2007.09.036.

[24] Y. Kuramoto, D. Battogtokh, "Coexistence of Coherence and Incoherence in Nonlocally Coupled Phase Oscillators," Nonlinear Phenomena in Complex Systems, **5**(4), 380–385, 2002.

[25] P. Kumar, D. Verma, D.: Parmananda, P. "Partially synchronized states in an ensemble of chemo-mechanical oscillators," Physics Letters A. **381**(29), 2337-2343, 2017. doi: 10.1016/j.physleta.2017.05.032.

[26] M.J. Panaggi and D.M. Abrams, "Chimera states: coexistence of coherence and incoherence in networks of coupled oscillators," Nonlinearity, **28**(3), 2015, doi: 10.1088/0951-7715/28/3/R67.

[27] F. Yuan, Injection-locking in mixed-mode signal processing, Springer, New York, 2019.

[28] LTspice, in https://www.analog.com/en/design-center/design-tools-and-calculators/ltspice-simulator.html

Phase-Adjusted Microwave Oscillators Based on a Discriminator

Vladimir Mushegovich Gevorkyan[*], Yuri Alekseevich Kazantsev, Sergey Nikolaevich Mikhalin

Computing machines, systems and networks, National Research University "MPEI", Moscow, 111250, Russia

A R T I C L E   I N F O

A B S T R A C T

At the conference "System timing, shaping and signal processing" "SYNCHRONO-2020" there was report: "Simulation of steady state microwave oscillator with dielectric resonator" and "Microwave generators, driven by voltage-based microassemblies with dielectric resonators". An algorithm for calculating a generator with an open dielectric resonator is described. Based on the DesignLab 8.0 simulation environment, the analysis of the stationary mode of generators with electric control (voltage) of the oscillation frequency with parallel and serial feedback circuits is carried out. Analysis of the characteristics of the developed generators in the X-band of voltage-controlled oscillators (VCO) indicated the prospects for using a device with sequential feedback, characterized by a lower level of phase noise (depending on the frequency tuning range, having values from minus 85 to minus 95 dB/Hz when tuning from the generation frequency by 10 kHz). However, this noise level is significantly (by 15...20 dB) worse than world analogues in this frequency range (the C and X frequency ranges are considered). The purpose of creating the device is to use it in generators with analog phase frequency adjustment based on a frequency discriminator. This article describes the characteristics of the VCO and calculates the topology of the phase locked loop (PLL) circuit based on a discriminator formed by a high-quality open dielectric resonator. Such a technical solution is promising as stable generators alternative to highly stable free oscillator. The prototype of the generator under consideration described in the work of A.V. Gorevoy.

1. Introduction

The variant of constructing the topology of a generator with analog phase frequency adjustment (equivalent PLL) based on a frequency discriminator are considered in article. The device is constructed using an oscillator with electrical frequency tuning by changing the constant voltage on a varactor diode embedded in an oscillating system that includes an open dielectric resonator (DR).

The feature of the given design solution and the achieved electrical characteristics of the VCO is the use of the Russian element base: an active element, a varactor diode, a dielectric resonator, dielectric substrates, etc. Among the variants of the active elements of the VCO – complete hybrid-integrated microwave chips produced by Planeta-IRMIS LLC, St. Petersburg, and the hybrid-monolithic integrated circuit (HMIC) model M411154-1 produced by SRC «Istok» named after Shokin, Russia, Moscow region, Fryazino-town − the last one was selected. In this case, the oscillator is designed according to a scheme with

sequential (internal) feedback based on a field semiconductor structure, which pre-limits (from below) the expected spectral level of phase noise of the generators [1-3]. However, the advantage of this solution is a higher level of output power.

The PLL generator is based on a developed VCO with the use of oscillatory systems based on an open dielectric resonator, the resonant frequency (in the form of a coupling frequency) of which is controlled by changing the capacitance of a varactor diode (VD), electromagnetically coupling with the DR. The electromagnetic coupling is implemented using a segment of a microstrip line (MSL) − a microstrip resonator (MSR), electromagnetically coupled with the DR and galvanically connected to the VD [4]. The developed design of the VCO uses a varactor diode KA611A-5,B (in the configuration 026 (11) – "cot"). DR [5] with a Q-factor of ~4000 forms by ceramic disk with a relative permittivity of ~40, with a diameter of 5 mm and a thickness of 2 mm. Note that the phase noise of the VCO is not determined by the Q-factor DR, but is determined by the quality factor of the vibrating system of the generator which adjusted by insertion loss due to coupling with

[*]Corresponding Author: Vladimir Mushegovich Gevorkyan, Email: GevorkianVM@mpei.ru

varactor diode, the quality factor of which does not exceed a few hundred.

VCO is designed on the basis of a simulation algorithm using a combination of well known wave and our developed circuit representations of active and passive components of microwave circuits. This made it possible to implement the process of optimizing the generator parameters [6-8]. VCO was designed in a three-centimeter wavelength range based on the upper limit of the active element's working area.

The PLL circuit topology is based on the results of the studies given in [9], calculated using matrix representations [10] of microwave circuits with DR.

2. Main part

2.1. Voltage-controlled oscillator

The PLL generator is designed on the basis of a voltage-controlled generator, which, in turn, is built according to the scheme with sequential (internal) feedback according to the topology shown in Figure 1.
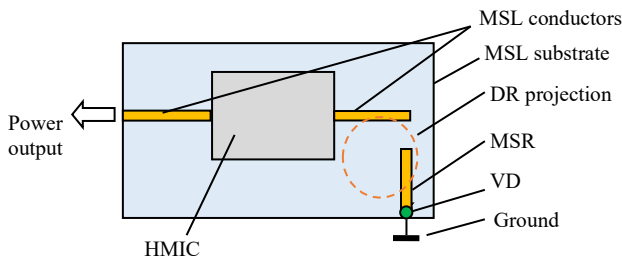
Figure 1: Topology of the VCO on the HMIC of model M411154 (power circuits are not shown)
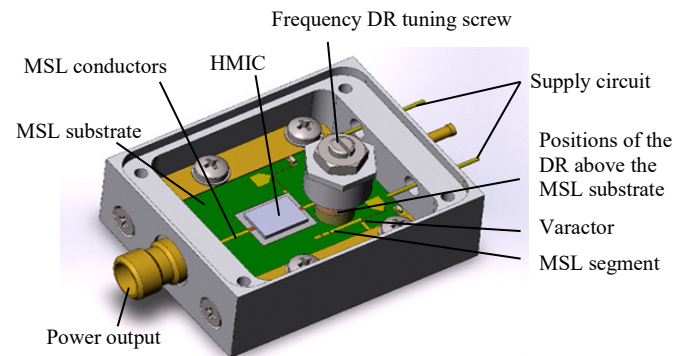
Figure 2: Oscillator with internal feedback (the cover is removed)
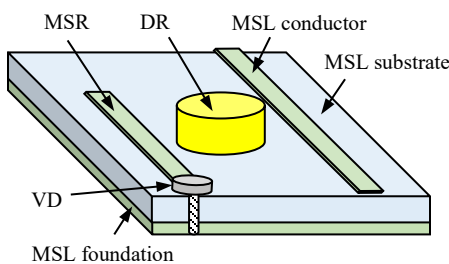
Figure 3: Oscillatory system DR-MSR-VD − frequency-tunable circuit

The design of the VCO is shown in Figure 2, and the circuit topology of the oscillatory system of such VCO coincide to the

standard technical solution [4], which is shown in Figure 3. However, as shown by the research, the direct application of such a topology, which is characterized by the presence of a direct (bypassing the DR) electromagnetic coupling between the VD and the MSL segment, worsens the spectral characteristics of the oscillator and limits the range of frequency tuning of the VCO. These characteristics can be improved using the topology shown in Figure 1. Here, the use of orthogonal placement of the MSL and MSR conductors excludes a direct coupling between the VD and the input of HMIS. Designed oscillator with the PLL is based on a block structure. Each block of a certain functional purpose represents an independent technical solution, and the combination forms a VCO with a PLL. The external appearance of the VCO is shown in Figure 4, and the internal structure of the device is shown in Figure 5.
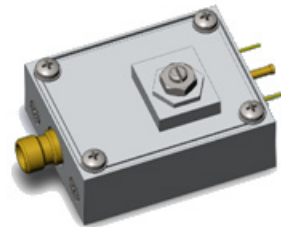
Figure 4: Appearance of the VCO with internal feedback
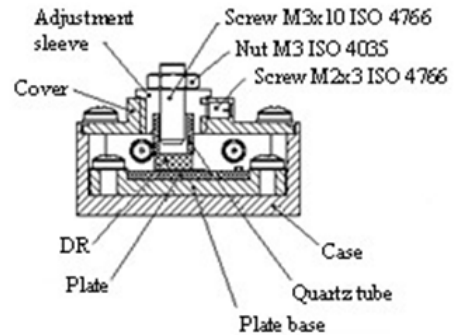
Figure 5: Internal structure of the voltage-controlled oscillator design
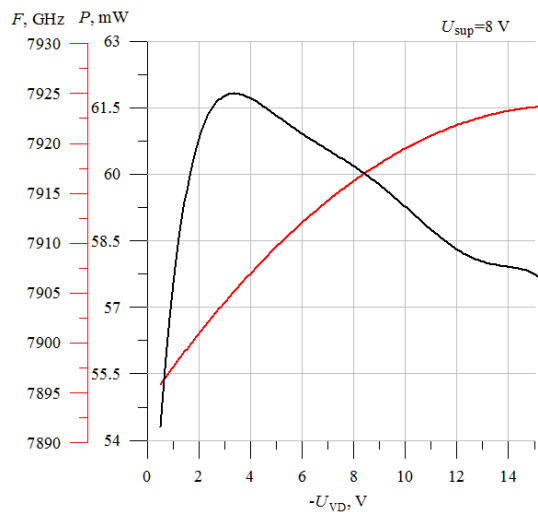
Figure 6: Dependences of frequency and output power of VCO on HMIC of M411154-1 model versus the voltage on the varactor U_{VD}

In the process of creating the device, we studied the VCO with sequential feedback for a number of central frequencies in the C-

and X- bands. Typical dependences of the VCO characteristics on the supply and control voltages, as well as the ambient temperature, typical for generators with DR on the chip on HMIC model M411154-1 at all frequency points, are shown in Figures 6-8.
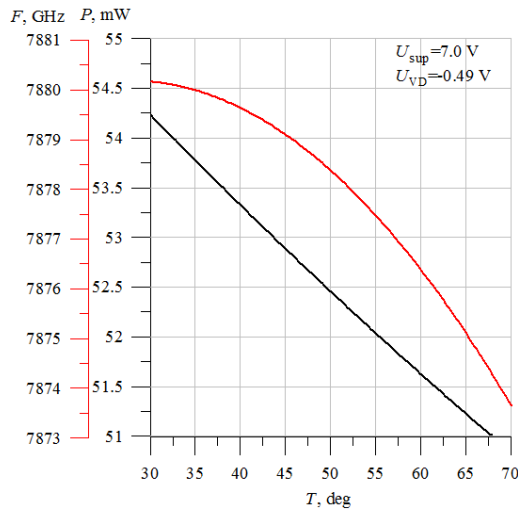
Figure 7: Dependences of frequency and output power of VCO on HMIC of M411154-1 model versus the environment temperature
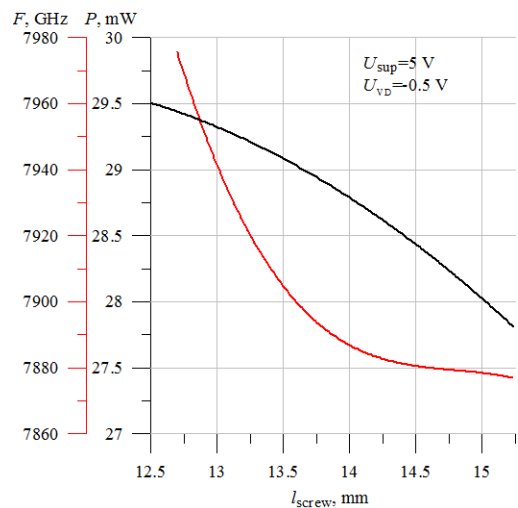
Figure 8: Dependence of frequency and output power of VCO on HMIC on the M411154-1 model versus the relative position of the screw for mechanical frequency tuning l_{screw}(voltages: of power supply U_{sup}=5.0 V; on varactor U_{VD}=−0.5 V)

Note that the dependence of the generation frequency on the voltage change on the varactor qualitatively repeats the form of the calculated curves. The change in the output voltage is not estimated by calculation, but does not exceed 10%. As can be seen from Figure 8, the output power level depends on the frequency of the DR (or the communication frequency of the DR - MSR system), that is, on the electrical length between the connection point of the DR and the output of the HMIC chip.

Different frequencies VCO have the same appearance Figure 4 and sizes. This VCO differ in the resonant frequency of the DR (and, accordingly, the frequency of the MSR). The same frequency letter of the VCO can operate at different supply voltage of the HMIC, the range of possible values of which is from 5 V to 10 V. A change in the supply voltage is accompanied by a change in the output power. Changing the voltage by 50% causes the output

power to double. At the same time, the VCO operates steadily at all voltage values in this range. The upper limit of the supply voltage of the VCO is limited to the maximum permissible value of the supply voltage of the HMIC and it is 10 V. The output power of the VCO varies from 25 to 60 mW in the frequency range from 7 to 11 GHz. The operating current of the VCO supply is from 45 to 50 mA, the efficiency is from 11% (at U_{sup}=5 V) up to 10% (at U_{sup}=10 V).

Confirmed according to the manufacturer property HMIC model M411154-1 decrease of the spectral density of phase noise with increasing voltage, amounting to about minus 2 dB/Hz with increasing the supply voltage at 1 V. The spectral density of phase noise VCO with internal feedback is almost independent of the frequency within the operating range of the chip. The observed deterioration of the spectral power density of phase noise in the VCO when the central frequency changes from 9.67 GHz (the level was minus 96 dB/Hz when tuning from the carrier at 10 kHz) to 10.045 GHz (the level was minus 90.5 dB/Hz when tuning from the carrier at 10 kHz) is determined by the properties of the oscillatory system at these frequencies (Figure 9).
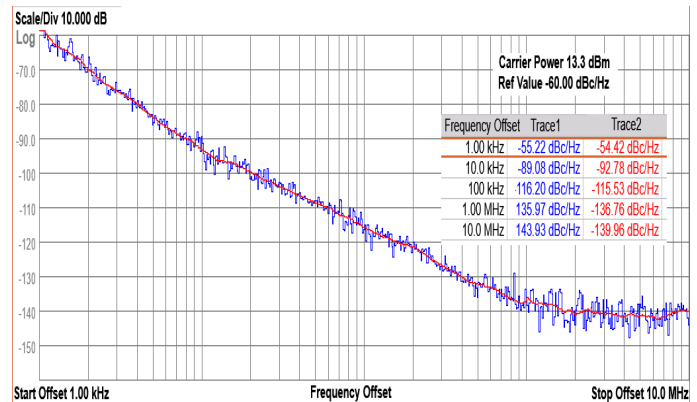
Figure 9: One-Way Phase noise, dB/Hz

From the point of view of the functional purpose of the created VCO, namely, the formation of a phase frequency adjustment system, such a change in the level of spectral density of phase noise is not critical. Note that the achieved values of the phase noise level correspond to a weak connection of the VD with the DR (small insertion loss), which corresponds to a small (0.1%...0.15%) range of adjustment of the "working" frequency of the oscillatory system. When the frequency tuning range (range of coupling and generation) is tripled, the phase noise level increases to minus 83...85 dB/Hz when the carrier frequency is tuned to 10 kHz.

2.2. VCO temperature characteristic

Focusing on the creation of an oscillator using PLL, the characteristics of the spectral density of phase noise of the VCO noted above should be evaluated in conjunction with the possible temperature shift of the generation frequency allowed for its development by the PLL ring. Therefore, an important characteristic for the VCO is the temperature frequency coefficient (TCF), which determines the necessary range of electrical adjustment of the generation frequency to maintain the operation of the automatic frequency adjustment ring.

It is obvious that with the growth of the TCF and, accordingly, the expansion of the necessary frequency range of the VCO

frequency adjustment, the phase noise of the VCO increases. The solution of the problem of thermal stabilization of the frequency of generation in VCO devices completely repeats the methods of thermal stabilization of free-oscillator with DR. The main action is to apply thermal compensation of frequency shifts formed by the entire set of frequency-dependent elements of the oscillator design, the opposite shift of the frequency of the DR (in the VCO − it is coupling frequency of the oscillatory system DR-MSR-VD). Thermal compensation can be provided by the correct choice of the TCF resonant frequency DR, that is the temperature coefficient of the relative permittivity of its ceramic material. However, this technique does not provide smooth adjustment of TCF DR and, accordingly, technology adjustment of TCF VCO in the process of regulating the resonance frequency of the DR. To adjust TCF DR (and VCO in General), you can use the dependence of the resonant frequency of the DR on the distance to the metal inclusion (for example, the end of the screw).

Unacceptable lack the engineering solution to the problem of thermal compensation of the frequency shifts of the oscillator with a DR (DRO), based on the influence of the position of the end face of the screw (frequency) at TCF DR (and the generator in General) is the simultaneous effect of the selected position adjusting screw at the resonant frequency of the PD and its temperature characteristics. This problem is solved in the design of the temperature compensator [11] (Fig. 10). Here, practically independent control of the parameters: TCF of the generator and its frequency – is achieved. In such a design, independent control of the parameters of the DR (Fig. 10, pos. 3) ensures its position on the dielectric substrate 1 (on the one of its side), which is located in a close metal cavity 2 (generator housing). DR 3 the electromagnetically-coupled with strip line segment 4 (not visible) which connected to the active element 5. The effect of independent control of the parameters of the DR 3 is provided by the below-cutoff waveguide 7. The segment of the circular waveguide 7 is mounted in cover 10 of the cavity 2 with a possibility to movement coaxially on the opposite to DR 3. There are moveable short-circuitor 8 is mounted on the one end of the waveguide 7. On another end of the waveguide 7 fixed installed the dielectric disk 9. The diameter, relative permittivity and thickness of dielectric disk 9 are determined by special calculated ratios taking into account the properties of DR 6. The second DR 6 is mounted of the disk 9 surface facing to DR 3, DR 6 TCF is opposite in sign to the TCF of DR 3**.** The control of TCF of DRO is provided by a variation of TCF of the coupling frequency of the system of two coupled DR 3 and 6.
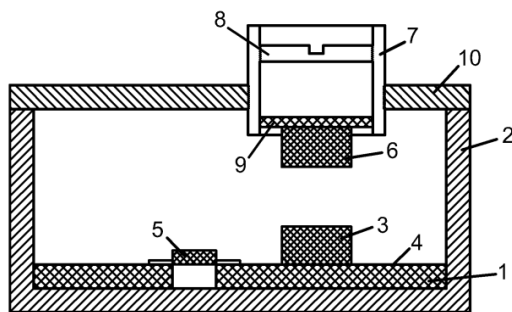
Figure 10: The thermal compensation system of DRO frequency shift

The frequency of the generator is adjusted through a series of adjustments and their combination.

The displacement of the movable short-circuitor 8 in the circular below-cutoff waveguide segment 7 causes a change of the own resonant frequency of DR 6. In this case, the following change of electromagnetic coupling of DR 6 with the first DR 3, and so and the change of the coupling resonant frequency, that's controls to the oscillation frequency, and the temperature coefficient of the frequency in our oscillator. In the similar manner, the variation of electromagnetic coupling between the first 3 and second 6 DR influences upon the oscillator parameters. The coupling change between DRs 3 and 6 is provided by the longitudinal displacement of the circular below-cutoff waveguide segment 7, on which the second DR 6 is mounted. The various influences of these two retuning elements upon the frequency of the generated oscillations and on its TCF permits to perform its independent adjustment. We would like to note that the TCF tuning of such an oscillatory system represents a regression process and requires a number of iterations provided in several stages.

Nevertheless, at reaching of the required result, the constructive relationships, which provide the required oscillator parameters, are enough confidently reproduced in the series of devices, for example, in the production of Figure 11.

Figure 11: X-band VCO with the thermal compensation system of DR

Our experience in developing such a generator with the described design of the oscillatory system shows the possibility of providing a TCF corresponding to temperature shifts of 20 kHz/°C in the temperature range from -40°C to +60°C at a frequency of 10 GHz. However, the described technical solution of the microwave generator has a design disadvantage with obvious advantages. Note, that with the application of the correctly selected TCF DR, it is perhaps to achieve satisfactory TCF VCO value. In the presented version, the temperature shift of the VCO frequency is less than 100 kHz/ºC, which is 10 MHz when the temperature changes by 100ºC. If the ambient temperature range is reduced to 10ºC, the frequency shift range is reduced to 1MHz.

With that said, in our device, the problem of thermal compensation of temperature shifts of the VCO frequency is solved in a complex with thermostating of PLL elements based on Peltier regulators. This made it possible to reduce the required range by varactor frequency tuning to about 3 MHz and thus reduce the level of phase noise by 10 dB.

The given data of the VCO with internal feedback show that it is possible to create generators on the domestic HMIS, the set of parameters of which corresponds to the world level [12].

2.3. Characteristics of the thermostat

Effective stabilization of frequency and the device of the oscillator with PLL as a whole is possible when placing the VCO

(or when the block structure of the generator − all its nodes) inside the thermos. Maintaining the set temperature is possible either by liquid cooling (heating), or using Peltier elements. The latter, although it has a lower efficiency, does not contain mechanical components (pump), does not pose a danger to electronic components (in case of media leakage), is absolutely resistant to mechanical influences, and also removes maintenance issues.

A Peltier element, which is a semiconductor wafer with dimensions of 34×30×8 mm, is used for temperature control of a PLL generator with overall dimensions of about 60×50×30 mm (volume V) in the range from +20 to +30°C when the ambient temperature changes from –20 to +60°C. The Peltier element surface is in direct contact with the temperature-controlled object. The radiator removes excess heat from the heating side of the Peltier plate.

The thermostat device, in addition to the Peltier element, contains a temperature sensor, a control circuit, and a power supply – Figure 12.
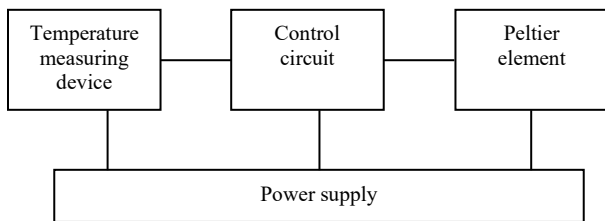
Figure 12: Structural diagram of the thermostat

The temperature sensor is implemented on the TMP01 Analog Devices chip, contains a precision semiconductor thermosensitive element with a reference voltage source (RVS) and two comparators in one 8-pin package and provides temperature measurement accuracy at 1°C in the temperature range from –55 to +125°C.

The control circuit is formed by an amplifier and two comparators that set two temperature thresholds, relative to which the control circuit includes heating or cooling the thermostatically controlled object. To create two reference temperature values, an RVS is used – Figure 13.
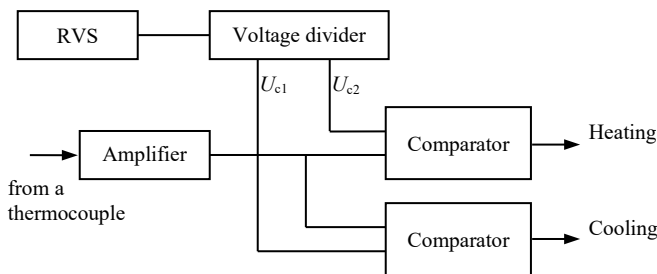
Figure 13: Functional diagram of the temperature control device

The temperature condition of the Peltier element plane is controlled by the current from units of amperes using power transistors, using bridge drivers (they provide current flow through a large load in the required direction, depending on the control signals "Heating" and "Cooling").

The heat stabilizer is based on integrated circuits TMP01 and L298 and Peltier element for 10 W (maximum current of 3.5 A), which provided temperature maintenance in the range from +20 to +30°C in a thermostatically controlled device with a power consumption of no more than 1 W (power consumption of the VCO ~0.5 W) with a volume V in a given range of ambient temperatures. For demand response to changes in temperature stabilized device power control exceeds the power that "excites" the system, i.e. leads to excessive heating or cooling.

The schematic diagram of the control device contains circuit solutions (Schmitt inverters) designed to increase the stability of the control path in the area of threshold temperatures and prevent multiple switching of the driver due to temperature measurement errors, instability of the reference voltage source, interference effects, etc.

Implementation of the thermos is made using rigid foam ("penoplex") and has a wall thickness of at least 20 mm (Figure 14).
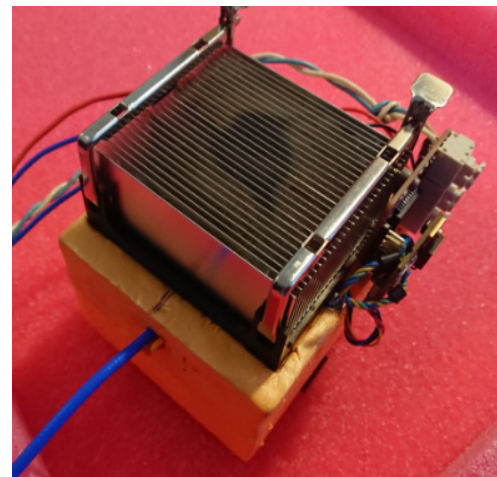
Figure 14: Thermostatic generator

The thermal stabilizer provided stability of the VCO generation frequency better than 1 MHz in the temperature range from –20 to +60°C, which simplifies the requirements for a sufficient range of tuning its frequency less than 2 MHz and thus the level of phase noise of the VCO is not worse than 90 dB/Hz when debugging from the central frequency at 10 kHz.

2.4. The topology of the phase-adjustment loop Calculation

We analyze the construction of the PLL loop based on the phase discriminator on the DR. The principle of constructing such a generator is known [9] (Figure 15), the characteristics are limited by the selective capabilities (the steepness of the phase characteristic) of acceptable design solutions of the DR and, according to A. Gorevoy, are mainly determined by the spectral characteristics of the PLL circuit, which, in turn, depends on the phase noise introduced by the LNA. Based on the estimation of the spectral density parameter of phase noise in the circuit Figure 15 at approximately 150 dB/Hz with a 10 kHz detuning from the generation frequency with the given characteristics of the circuit elements and with phase noise of the VCO of approximately 110 dB/Hz with a 10 kHz detuning from the generation frequency, it is of interest to use the scheme for phase stabilization of the frequency of the developed VCO.
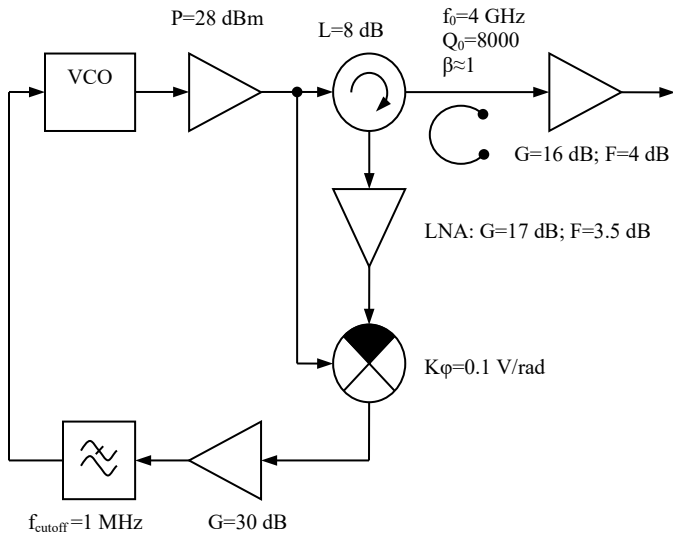
Figure 15: PLL generator with rejecting DR filter

We will evaluate the characteristics of PLL circuit elements when constructing a discriminator based on a DR made of modern ceramic materials with a lower $TE_{01\delta}$ oscillation mode, whose own Q-factor exceeds 1000 at a frequency of 10 GHz [5]. In this case, the PLL circuit is organized according to Figure 16.
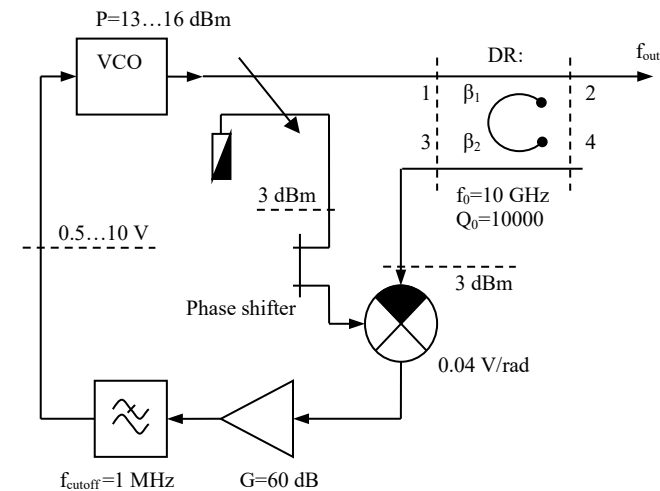
Figure 16: PLL generator with pass band DR filter

In contrast to the circuit of Figure 15, the phase discriminator is formed using a band-pass filter on the DR, represented by a four-pole with ports 1...4. The single-ended phase detector is formed by a hybrid bridge and a HSHS-8202TR1G diode Assembly. The required level of the input signal on the diodes, equal to 2.5 dBm, taking into account the losses in the hybrid bridge of 0.5 dB, is provided by the transmission coefficient of the directional coupler (in our case, minus 10...13 dB) and the transmission coefficient of the filter on the DR (four-pole with ports 1...4). The filter characteristic, i.e. the required coupling coefficients of DR β_1 with the input MSL (between ports 1 and 3) and β_2 with the output line (between ports 2 and 4) are determined using wave matrices of DR [10], which for the resonant frequency has the form:

$$(1 + \beta_1 + \beta_2)\begin{bmatrix} b_1 \\ b_2 \\ b_3 \\ b_4 \end{bmatrix} = \mathbf{M} \begin{bmatrix} a_1 \\ a_2 \\ a_3 \\ a_4 \end{bmatrix}$$

$$\mathbf{M} = \begin{bmatrix} \beta_1 & 1+\beta_2 & -\sqrt{\beta_1\beta_2} & \sqrt{\beta_1\beta_2} \\ 1+\beta_2 & \beta_1 & \sqrt{\beta_1\beta_2} & -\sqrt{\beta_1\beta_2} \\ -\sqrt{\beta_1\beta_2} & \sqrt{\beta_1\beta_2} & \beta_2 & 1+\beta_1 \\ \sqrt{\beta_1\beta_2} & -\sqrt{\beta_1\beta_2} & 1+\beta_1 & \beta_2 \end{bmatrix}$$

(1)

where a_i и b_i − incident and reflected waves at the entrances i equal 1...4, a a_1=13…16 dBm. Taking into account equality $a_1 = -b_4$, since to the port 4 a quarter-wave open segment of a long line is connected and, in the approximation, $a_2 \approx a_3 \approx 0$ «reflected» wave b_3 entrance 4 it is represented by the formula

$$b_3 = \left[-\frac{2\sqrt{\beta_1\beta_2}}{1+\beta_1+2\beta_2} \right]^2 a_1 \approx 2.5 \text{ dBm, from which the coupling}$$

coefficients β_1 and β_2 are determined, which are interconnected by the equation

$$\beta_2^2 + (1 - 4\beta_1)\beta_2 + \frac{(1+\beta_1)^2}{4} = 0$$

(2)

Given the requirement of the maximum loaded Q-factor of DR (minimization of the model coefficient) to the equation (2) satisfy the positive values of relationship coefficients β_1=0.05 and β_2=0.2. Thus the output device at the resonant frequency level of a wave decreases by 0.17 dB, and the loaded Q-factor will be 8000.
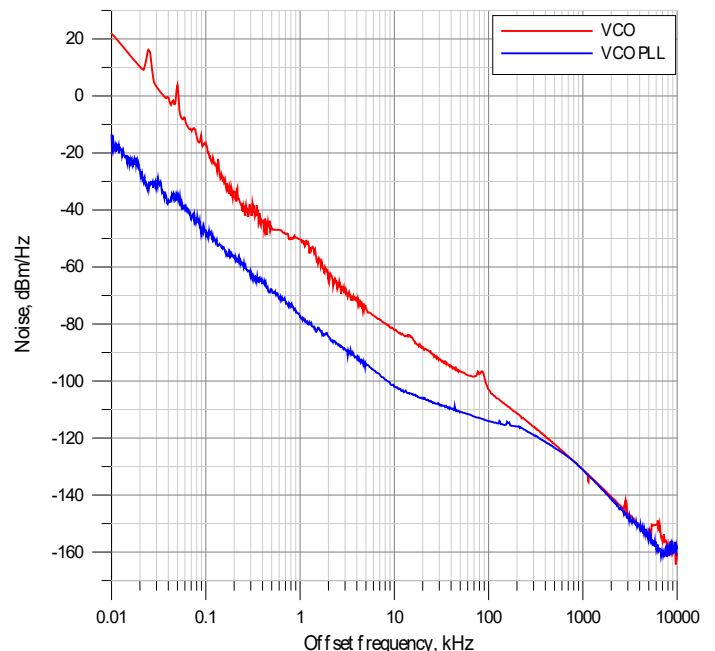
Figure 17: One-Way Phase noise, dB/Hz

Experimentally, it was possible to realize the value of the coupling coefficients, which provided a wave attenuation of 0.5 dB at the resonant frequency of the DR (with a loaded Q-factor of 5500). At the output of the 3 bandpass filter, the wave level was minus 11 dB relative to the level a_1. At the output of the phase detector, the voltage is 3...30 mV with a phase change of 45º, which corresponds to a transmission coefficient of 0.04 V/rad.

The obtained characteristics at the points of the phase control circuit correspond to the circuit parameters given in [9], which suggests the possibility of improving the level of phase noise of the developed VCO by 20...25 dB. However, the actual parameters of the PLL generator based on the frequency discriminator were slightly worse than expected, as illustrated in Figure 17. The reason lies in the insufficiently accurate setting of the electrical lengths of the MSL segments of the phase discriminator topology.

3. Conclusion

The results of creating a VCO representing the option of a PLL generator are presented. The properties of the VCO are studied and optimized to ensure phase adjustment of its frequency. There are designed the device for temperature control of the oscillation frequency of the VCO PLL circuit. The options considered for building a PLL circuit based frequency discriminator, educated DR. This method of constructing highly stable oscillators is well known [13], but requires the use of extremely high-quality resonators (Q-factor of about 100,000) to construct a frequency discriminator. But generators with such DR are not suitable for technical use due to poor thermal stability and vibration resistance. Nevertheless, modern ceramic resonators (Q-factor of about 15,000) allow us to achieve an acceptable level of phase noise of generators built on this principle. The algorithm for analytical calculation circuit PLL oscillator voltage controlled on the basis of the frequency discriminator is presented. Physical modeling of the phase discriminator performed based on the calculation results confirmed the reliability of the calculated data.

The process of creating PLL generators with electrical frequency adjustment (or controlled by constant voltage) showed the possibility of successful application of design algorithms for such devices, including phase correction circuits, when the obtained characteristics of the nodes (options) of PLL generators differ within the ranges of technological adjustments.

The Russian element base makes it possible to create devices with parameters at the level of foreign analogues based on palliative technical solutions.

Created on the basis of a domestic active element (produced by NPP «Istok» named after Shokin), a varactor diode (produced by NIIPP Tomsk) and open dielectric resonators (produced by LLC «Keramika», St. Petersburg), the VCO corresponds to the level of foreign analogues in terms of a set of parameters. The use of PLL assumes the possibility of reducing phase noise by 20...25 dB/Hz. In addition, the development involves further improvement of both the parameters of the VCO and the PLL chain based on improving the characteristics of the element base.

Conflict of Interest

The authors declare no conflict of interest.

References

[1] A.I. Afanas'ev, L.V. Alekseychik, I.I. Brodulenko, N.G. Gavrilyuk, V.A. Maltsev, "Technical condition, development trends and design of stable solid-state generators and low-power microwave filters Reviews on ET," Series 1, UHF Electronics, **2**(1698), 1993. doi: 10.1016/j.jfoodeng.2018.04.009

[2] V. Gevorkyan, V. Kochemasov and V. Shadsky,"Generators with the use of dielectric resonators. Part 1," Electronics. The science. Technology. Business, **2**, 114−128, 2020, doi:10.22184/1992-4178.2020.193.2.114.128.

[3] U. Güttich,"Active Elements Used in Microstrip Dielectric Resonator Oscillators", Microwave Journal, **4**, 92−96, 1996.

[4] T.N. Narytnik, V.I. Priymak, V.B. Fedorov, "Oscillatory microwave systems with miniature dielectric resonators in amplifying and converting devices," Electronic equipment, Series 1, **7**, Microwave Electronics, 15–21, 1985.

[5] "RF and UHF ceramic materials and microwave elements", The catalogue of products of JSC «Ceramica», Sankt-Peterburg, 2004.

[6] V.M. Gevorkyan and Yu.A. Kazantsev, "Analysis of scattering matrices of UHF devices with the help of equivalent circuits in the software DesignLab 8.0", Proceedings of MKEEE-2016, 254−256, 2016. DOI: 10.1109/SYNCHROINFO49631.2020.9166117

[7] V.M. Gevorkyan, Yu.A. Kazantsev and S.N. Mikhalin, "Analysis of UHF resonance circuit with electrical frequency control by utilization of the software DesignLab 8.0", Proceedings of MKEEE-2018, 382−386, 2018.

[8] Design Procedures for Series and Parallel Feedback Microwave DROs. Stellenbosch University, 2007. DOI: 10.1109/MKEEE49631.2018.9166117

[9] A. Gorevoy, "A Low Noise Oscillator Based on a Conventional Dielectric Resonator", Microwave Journal, **11**, 84−94, 2013.

[10] M.E. Ilchenko, V.F. Vzyatyshev, L.G. Gassanov, Yu.M. Bezborodov, M.N. Berger, V.S. Dobromyslov, B.Yu. Kopilevich, T.N. Narytnik, V.B. Fedorov, B.S. Chernii, "Dielectric resonators," M.: Radio and Communication, 1989

[11] A.I. Abramenkov, V.M. Gevorkyan and D.A. Kovtunov, "Generator", Certificate on USSR invention N1653125 dated 01.06.1989. Bull of invent N20 dated 30.05.1991.

[12] L. Belov, V. Khilkevich, "Generators with dielectric resonators for frequency stabilization," Electronics: Science, Technology, Business, **7**, 54–59, 2006.

[13] D.P. Zarapkin, "Application of dielectric resonators with waves of the "whispering gallery" type for frequency stabilization of ultrahigh frequency autogenerators," Radio Engineering, **2**, 28–35, 2002.

Optical Satellite Images Services for Precision Agricultural use: A Review

Asmae Dakir[*], Barramou Fatima Zahra, Alami Bachir Omar

Hassania School of Public Works, SGEO, Casablanca, 20230, Morocco

A R T I C L E I N F O	A B S T R A C T
	The recent advances in geoscience technologies and earth observation tools have evolved in recent years in a fast cadence. Since 1980 with the apparition of Landsat mission firstly named the Earth Resources Technology Satellite, with 80 m spatial resolution; the ability to capture finest details was limited. The emergence of new concepts in agriculture like digital agriculture and precision agriculture (PA) was challenging the capacity of satellite images to capture the variation within the field. The domain that was firstly more dedicated to aerial and handheld remote sensing is now accessible to satellite remote sensing thanks to recent advancements that had provided more satisfactory spatial resolution reaching 0.3 m in a daily revisit frequency. Different providers have launched commercial, very high-resolution nanosatellite constellations to respond to more precise needs, and increasing the availability of remotely sensed images expands the horizon of our choices of imagery sources. The present work intends to compare spatial, temporal, spectral, and radiometric resolution, considering the farmer's requirements and precision agriculture application's requirements nowadays available and the future generation satellite missions, and benchmark the major satellite images providers. It exposes the characteristics and future missions to facilitate adequate choice. The criterion of selecting the appropriate sensors among the considerable amount of providers was limited to optical data, with less than 10 m spatial resolution and frequent revisit time. The offer of imagery is majorly commercial missions; the available open and accessible alternative is limited in the sentinel mission with 10 m spatial resolution.

1. Introduction

In the context of general population growth and the challenge of sustainable development necessary to keep a general balance globally and respond to humankind's needs, the agricultural domain had exploited the technological progress to have efficient decision-making for sustainably using natural resources. Digital agriculture had then made farming sufficient and intelligent [1]. The key concept is to monitor and manage the variability within the field with smart technologies to improve productivity. Many techniques have been employed in digital agriculture, like big data, the Internet of Things (IoT), and remote sensing [2].

Recent studies have shown the advantage of proximal and handheld remote sensing, including aerial imagery to manage the agricultural sector in a finer centimetric spatial resolution [3, 4], advanced techniques have allowed monitoring the variability within the field so the intervention could be specific and punctual. The main application had permitted the detection of agricultural disease and its extent to establish the suitable way of intervention

and the adequate amount of pesticide to apply [5, 6]. Other applications concern the determination of water requirement at the plant scale for precision irrigation [3, 7, 8] as well as the determination of soil fertility [9], yield and biomass production [2, 10] and others.

As an alternative, satellite remote sensing provides optical and radar imagery and multiple spectral bands in NIR (Near Infrared) and visible spectrum and SWIR and thermal bands, which had allowed monitoring vegetation and soil characteristics due to vegetation indices and other processes. Several indices were deployed in the literature, with the more familiar Normalized Vegetation Index NDVI [11] as well as Enhanced Vegetation Index EVI [12] and the Modified Soil Vegetation Index MSAVI [13].

Recent advances in spatial resolution satellite remote sensing data made precision agriculture even more efficient and directed to proximal and handheld remote sensing [14]. Since the first LANDSAT mission launched in 1972 with 80 m spatial resolution (for VNIR bands), advancement had never ceased to capture finer

details, with higher revisit frequency and more acceptable radiometric resolution. Providers of satellite imagery have launched new missions with new technologies (nanosatellites) that had made satellites a considerable competitor to other technologies. Many countries have then opted for this solution to assure spatial independence as Italy, China, Europe, Canada, Japan, and others.

This work aims to give an overview of high and very high resolution updated satellite remote sensing imagery used in precision agriculture applications. High resolutions had allowed an equivalent of aerial imagery quality, and coming missions are ensuring the continuity and improvement of actual available data.

2. Spatial Resolution Requirement

According to the application, the scale and the objective of the study required spatial resolution differs. The spatial resolution presents the size of one pixel on the ground and defines the precision of captured details. The first satellite mission for earth observation Landsat had a spatial resolution of 80 m, and its application to resolve precision agriculture problems was limited. The evolution of technology has allowed a steady progression in spatial resolution. The next mission was SPOT 1 in 1986, with a resolution of 20 m for multispectral bands. The spatial resolution was finer to 4 m with IKONOS in 1999 and 1 m for the Panchromatic band. The primary constraint of having a finer spatial resolution was the high cost of the scene covering smaller areas with lower availability. The standard classification in the term of spatial resolution considers the following:

Low resolution $\geqslant$ 30 m and < 300 m

Medium resolution $\geqslant$ 5 m and < 30 m

High resolution $\geqslant$ 1.0 m and < 5 m

Very high resolution < 1.0 m. [15]

In precision agriculture, the spatial resolution requirement differs according to the application. Many applications are demanding a finer resolution compared to others as the study of phenotyping [14]. The work conducted in [16] had compared the applicability of satellite images for plan phenotyping with four satellite imagery with high spatial resolution Pleiades-1A (0.5m), Spot 6 (1.5m), Planet (3.0m), and Rapid Eye (5.0m). The average NDVI was extracted from each satellite image, and the data were correlated with seed yield and biomass. The results have shown that (3.0 m) and Rapid Eye (5.0 m) images were less related to biomass and seed yield and likely will require higher resolution for reliable prediction of crop performance. The correlation begins to decrease at 1.0 m image resolution. This study showed the potential of a resolution of 0.5 to 1 m to capture phenotypic differences.

In [16], the author had used three WorldView-3 and Sentinel-2A images covering the agricultural season to demonstrate the potential of extracting vegetation indices, particularly Normalised Difference Vegetation Index NDVI, Green Normalized Difference Vegetation Index GNDVI. Soil Adjusted Vegetation Index SAVI, from different dates to classify crop types. The results have shown the suitability of the chosen imagery that gives an overall accuracy of 91%.

The work conducted by [17] had used 55 scenes Landsat 8 Operational Land Imager (OLI) to provide optical indices accoupled with PALSAR-2, JERS-1, and Sentinel 1 data with final 200 scenes that have been used to monitor rice agriculture across Myanmar. The results showed that the combination between NDVI index, LSWI, and SATVI had the best overall map.

3. Very High-Resolution Satellite Imagery And Aerial Imagery

As technological development has changed satellite technology, imagery has reached a more spatial, temporal, and radiometric resolution. Digital agriculture had profited from this advancement and had exploited satellite imagery in precision agriculture that was more oriented using aerial and handheld remote sensing [4, 18].

Aerial and satellite imagery have been complementary for different studies [14]. The progress made in terms of spatial resolution had opened the perspective of replacing aerial imagery and proximal remote sensing with satellite remote sensing that have achieved a spatial resolution beyond 0.3 m.

Firstly, satellites present many advantages over aerial imagery, especially for large-scale projects that demand programming several flights; it is disadvantageous in terms of the budget and time to cover all the studied area, the logistics, and planning requirements. Aerial missions have many restrictions as airspace permits and planning for appropriate landing points having in mind the weather condition that can delay aerial missions. Then, satellite imagery can afford permanent focus in inaccessible areas with high frequency achieving several times per day. It presents a competitive alternative to aerial imagery with low cost and post-processing requirements.

4. Special Needs of Satellite Imagery In Precision Agriculture Applications

Remote sensing technology had been employed for classical crop inventory and large-scale yield prediction [19]. The employment of remote sensing in precision agriculture was recently due to diverse factors. Mainly, the concept was relatively recent and required daily images with a high spatial resolution to monitor vegetation throughout the agricultural season. Nevertheless, the availability of very high temporal and spatial resolution was only available in 2002, with the lunch of the SPOT mission, having 2-3 days revisit and 10 m spatial resolution.

The availability of required remote sensing imagery has then allowed employing them in precision farming issues. Table 1 presents examples of remote sensing imagery used in precision farming applications.

5. Potential Sources of High-Resolution Satellite Imagery

The choice of satellite imagery for precision agricultural use depends on the application; the first requirement is spatial resolution. The offer had progressed recently, reaching a centimetric commercially available data. Providers offer different products depending on the spectral bands, revisit time, and spatial resolution. Table 2 presents the main providers of satellite imagery suitable for precision agricultural use; the main decisive factor for selection is a spatial resolution equal or inferior to 10 m that allows

Table 1: Examples of remote sensing imagery used in precision farming applications

Imagery data	Application	Aim
Planet Scope imagery (3 m)	Yield prediction [5]	Developing a method to generate carrot yield maps using machine learning algorithms, satellite spectral data, and ground truth.
Landsat 8 OLI images	Detection, prediction, and evaluation of crop diseases [5]	Defining which methods of atmospheric correction combined with machine learning techniques can approximate evaluating the disease in the field data.
Pleiades-1A(0.5 m), SPOT 6(1.5 m), Planet Scope (3.0m), and Rapid Eye (5.0 m)+ Aerial data	phenotype crop performance and phenological traits using genotypes [18]	Evaluating and establishing remote sensing methods for high-throughput plant phenotyping in dry bean breeding nurseries
Chinese satellite Gaofen-1 images- Landsat imagery	Evaluation of expansion and suitability [20]	Evaluation of expansion and suitability of hickory crop (land-cover map with emphasis on young and mature hickory plantations)
RapidEye Imagery	Precision irrigation [7]	Determining the optimal time and depth of Soil Water Content SWC and its relationship to maize grain yield (2) to determine if satellite-derived vegetation indices coupled with SWC could further improve the relationship between maize grain yield and SWC.

Table 2: Satellite imagery for precision agricultural use

Sensor name	Number of multispectral bands	Spatial resolution	Revisit time	accessibility	Provider	Launched year	Radiometric resolution/bit
Dove	4 (RGB, NIR)	3 m	1 day	commercial	Planet Labs	2019	Visual: 8 bit / 16 bit analytic
RAPIDEYE	5 (RGB, red edge, NIR)	5 m	1 day	commercial		2008	12
SKYSAT 1/ 2	5 (RGB, NIR, pan)	0.9	1	commercial		2013/2014	Visual: 8 bit , 16 bit Pansharpened
WorldView-1	Pan	0.50 m	1.7	commercial	Digital Globe	2007	11
WorldView-2	Pan + 8 Multispectral	0.46	1.1 day	commercial		2009	11
WorldView-3	Pan + 8 Multispectral + 8 SWIR	0.31 m	1 day	commercial		2014	11 Ms/ 14 SWIR
WorldView-4	Pan + 4 Multispectral (R, G, B, NIR)	0.31	1 day	commercial		2016	11
GeoEye-1	Pan + 4 Multispectral	0.41 (0.46)[d]	< 3	commercial		2008	12
QuickBird	Pan + 4 Multispectral	0.55	2 - 12 days	commercial		2001	11
IKONOS	Pan + 4 Multispectral	0.82	3 days	commercial		1999	11
KOMPSAT 3, 3A (Arirang-3)	4 + pan	0,5 m / 0,4 m	1.4 days	commercial		2012	14
KOMPSAT-2	5 + PAN	1 m PAN / 4 m MS	1 day	commercial		2006	10
Deimos-2	4 + PAN	1 m PAN / 4 m MS	2 days	commercial		2014	10
Dubaisat-2	4 + PAN	1 m Pan / 4 m MS	8 days	commercial		2013	10
SuperView-1 or GaoJing-1 (01/02/03/04)	4+ pan	0.5m pan /2m MS	3 days	commercial	SpaceWill	launched in 2016 planned to be completed by 2022	stereo imaging, long strip, multiple strips collect, multiple-point targets collect

ZY-3 or (Zi-Yuan 3)	4 + Pan	5,8 MS	5 days	commercial		2012	10
Gaofen-1 / -6	4 + Pan	2 m PAN 8 m MS	4 days	commercial		2013	14
Gaofen-2	4 + pan	0.80 m PAN 3.24 m MS	5 days	commercial		2014	14
SJ-9A/B (Shi Jian-9)	5 + pan	2.5m PAN/ 10m MS	4/8 days	commercial		2012	-
Pléiades 1A, 1B	4	0,7 m PAN 2,8 MS	1 day	commercial		2012	12
SPOT 6, 7	04-janv	1,5 m Pan / 6m MS	twice daily	commercial	AIRBUS	2012-2014	12
Vision-1	4 + pan	0.9m Pan 3.5m MS	1 day	commercial		2018	12
TripleSat 1/2/3	4 + PAN	3.2 m and 0,8 m pan	1 day	commercial	21AT Asia	2015	10-bits
Cartosat-2C	4	2 PAN 0.65 MS	4 days	commercial	Indian Space Research Organisation (ISRO)	2016	11
Sentinel-2A	13	10	5 days	open, free	ESA	2015	12
Sentinel-2B	13	10	5 days	open, free		2017	12
VNREDSat-1	4 + PAN	2.5 m PAN and 10 MS	3 -8 days	commercial	VAST and Astrium	2013	12
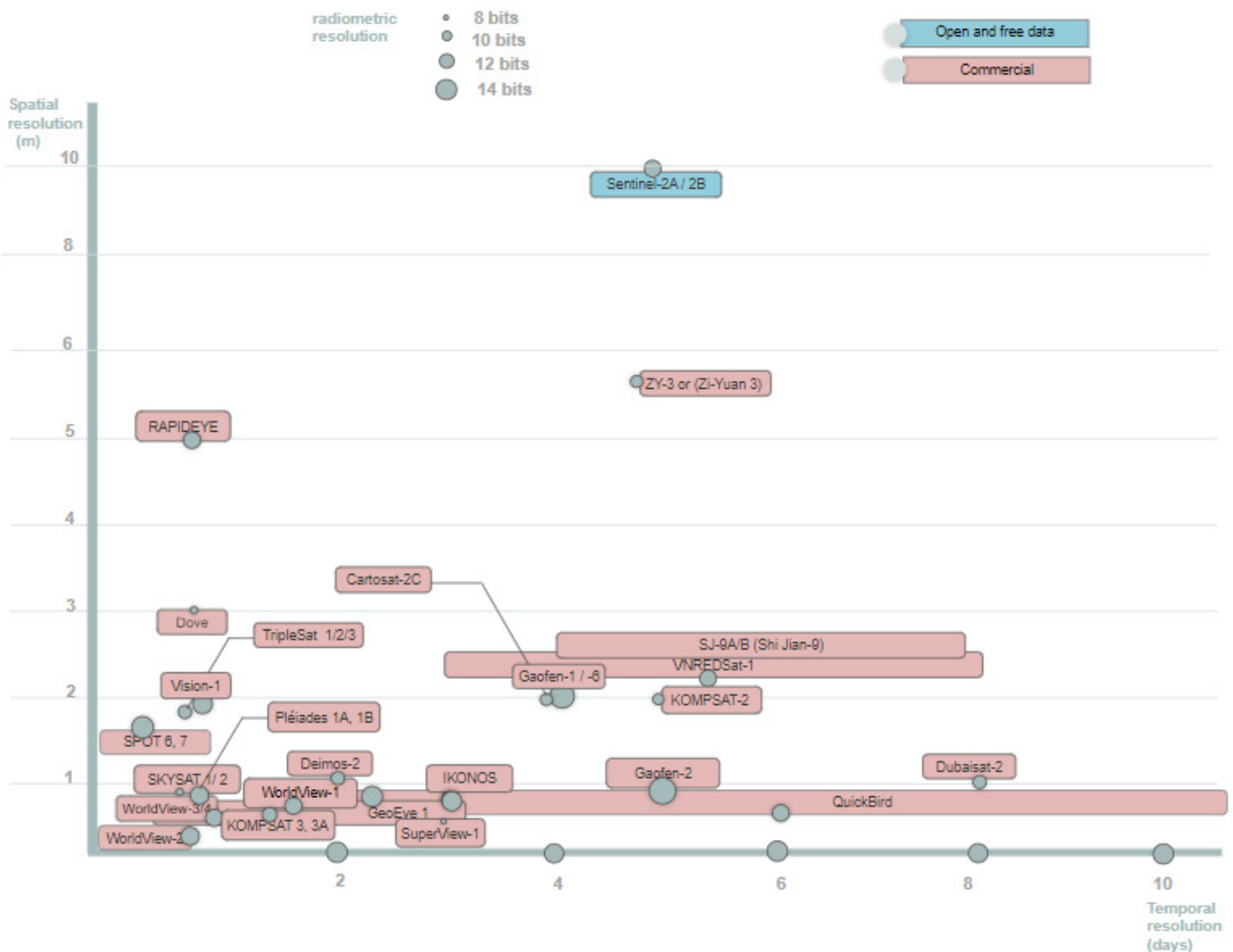
Figure 1: Comparison of imagery services for precision agricultural use

monitoring within field agriculture. The second factor is a high frequency lower than five days to supervise vegetation growth and repartition over time.

As with most other optical satellites, all very high-resolution optical satellites are operated in a sun-synchronous orbit, usually collecting data in the descending orbit.

The current offer of satellite imagery in 2021 has given multiple sensors for precision agriculture's applications, as shown in (figure 1). The WorldView2/3/4 mission seems to offer the more precise imagery in terms of spatial and temporal resolution daily and under 1 m, while the open and accessible data are minimal to the Sentinel mission with a spatial resolution of 10 m in 5 days. Nevertheless, the Sentinel mission can have limits for applications that demand precise spatial resolution, as shown in figure 2. (1) Presents the variability within the field using the NDVI index, the 10 m spatial resolution allows to limit the areas demanding intervention.

The sensors offer a general spectral resolution of 4 bands in visible and near-infrared (VNIR) spectrum for the most captors, while other sensors allow more advanced analysis using VNIR and SWIR bands for Sentinel 2 and WorldView2/3 missions. The SWIR bands allow the measurement of water content, leaf temperature photosynthesis, transpiration, stomatal conductance, and internal CO_2 content by extracting several vegetation indices like NDWI, NMDI, MSI to detect genotype effect and monitor drought [21], while the VNIR bands give information about chlorophyll absorption and monitor vegetation's health and productivity. VNIR permits the generation of yield maps, phenotype crop performance, evaluation of the disease in the field, evaluation of expansion and suitability, and precision irrigation use.

<div align="center">(1)   (2)</div>
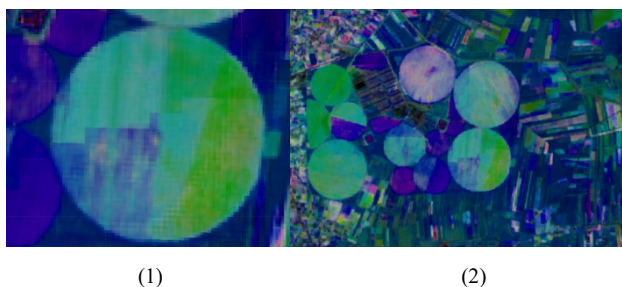
Figure 2. NDVI index extracted from Sentinel 2 imagery

6. Future Generation Satellite Missions

6.1. Pléiades Neo

Airbus will launch in early 2021 its most advanced constellation that will provide optical 100% available commercial imagery, with 0.3 m spatial resolution. Its constellation formed of 4 satellites operated in the same sun-synchronous orbit will allow a high revisit time twice daily at 46° off-Nadir and daily 30° off-Nadir. The radiometric resolution is planned for 12 bits and a spectral resolution of 6 multispectral bands (Blue, Blue, Green, Red, Red Edge, Near-infrared) and the panchromatic band. The mission is conceived for a lifetime of 10 years.

6.2. Blacksky Global

BlackSky Global, a startup company, founded in 2013, is a new "satellite imaging as a service" provider aimed at

commercializing access to high-performance satellite imagery. BlackSky constellation owned by Spaceflight Industries now includes six satellites. The company is on track to add ten more satellites to its constellation by the end of 2021.The company's long-term goals are to deploy 30 satellites by 2023 and possibly 60 years after, depending on the market demand. The constellation capabilities enable a unique revisit capacity of a few hours or less with a spatial resolution of up to 75 cm and low pricing [22].

6.3. URTHEDAILY

The constellation of UrtheDaily is planned to be launched in 2022. Its specification is its design to be compatible with Sentinel, RapidEye, and Landsat missions to ease cross-calibration with trusted references and to minimize the effects of atmospheric variations. UrtheDaily is designed to acquire high-quality, multispectral imagery at 5 m spatial resolution with daily revisit time. The constellation is initially designed with eight satellites to be launched in 2022.

6.4. Planet Imagery

Planet Labs is an American private Earth-imaging company. Founded in December 2010, Planet designs, builds and launches satellites by using lean, low-cost electronics. The Constellation of SuperDoves operates more than 150 satellites that together provide a dataset of Earth observation imagery with a unique combination of coverage, frequency, and resolution. It launches new satellites every three or four-month [23] . The constellation had added 48 SuperDoves to the constellation in January 2021

6.5. GAOFEN 14- 13 (GF-13, GF-14)

An optical stereo mapping satellite in a sun-synchronous orbit (GF-14) and a geostationary earth observation satellite (GF-13). The Gaofen satellites form a series of civilian Earth observation satellites that comprises more than 20 satellites. They are part of China's High-definition Earth Observation System (CHEOPS). GF-13and GF-14 are government-funded programs designed to provide real-time global surveillance data. They will be mainly used for land surveys, crop yield estimation, environmental management, meteorological early warning and forecast, and disaster prevention and reduction, providing information services to develop the national economy.

7. Conclusion

This paper presented the principle satellite services freely and commercially available for different precision agriculture applications. The results showed that recent PA applications are demanding more precise imagery. The recent technological advances have permitted a steady advance in spatial resolution attending 0.3 m and twice-daily revisit time with a sensibility reaching 14 bits. The current trends of satellite imagery are towards 100% commercially available imagery with lower costs and fast access that allows a large delivery to a community of users, especially for agricultural concerns. Future progress conduct trends towards using large nanosatellites constellation to satisfy a large demanding community with an extending lifetime reaching 15 years, leading to the prolongation of the longevity of the missions and consistent supply of highly calibrated data.

Conflict of Interest

The authors declare no conflict of interest.

References

[1] M. Shepherd, J.A. Turner, B. Small, D. Wheeler, "Priorities for science to overcome hurdles thwarting the full promise of the 'digital agriculture' revolution," Journal of the Science of Food and Agriculture, **100**(14), 5083–5092, 2020, doi:https://doi.org/10.1002/jsfa.9346.

[2] M.C.F. Wei, L.F. Maldaner, P.M.N. Ottoni, J.P. Molin, "Carrot Yield Mapping: A Precision Agriculture Approach Based on Machine Learning," AI, **1**(2), 229–241, 2020, doi:10.3390/ai1020015.

[3] A.H.E. Nahry, R.R. Ali, A.A.E. Baroudy, "An approach for precision farming under pivot irrigation system using remote sensing and GIS techniques," Agricultural Water Management, **98**(4), 517–531, 2011, doi:10.1016/j.agwat.2010.09.012.

[4] Y. Lan, Z. Huang, X. Deng, Z. Zhu, H. Huang, Z. Zheng, B. Lian, G. Zeng, Z. Tong, "Comparison of machine learning methods for citrus greening detection on UAV multispectral images," Computers and Electronics in Agriculture, **171**, 105234, 2020, doi:10.1016/j.compag.2020.105234.

[5] J. da R. Miranda, M. de C. Alves, E.A. Pozza, H. Santos Neto, "Detection of coffee berry necrosis by digital image processing of landsat 8 oli satellite imagery," International Journal of Applied Earth Observation and Geoinformation, **85**, 101983, 2020, doi:10.1016/j.jag.2019.101983.

[6] G. Sambasivam, G.D. Opiyo, "A predictive machine learning application in agriculture: Cassava disease detection and classification with imbalanced dataset using convolutional neural networks," Egyptian Informatics Journal, 2020, doi:10.1016/j.eij.2020.02.007.

[7] A. de Lara, L. Longchamps, R. Khosla, "Soil Water Content and High-Resolution Imagery for Precision Irrigation: Maize Yield," Agronomy, **9**(4), 174, 2019, doi:10.3390/agronomy9040174.

[8] L. Tao, J. Li, X. Chen, Y. Su, Y. Zhang, W. Wang, X. Shi, "Estimation of actual irrigation area using remote sensing monitoring method in Hetao Irrigation District," in 2014 IEEE Geoscience and Remote Sensing Symposium, 2367–2370, 2014, doi:10.1109/IGARSS.2014.6946947.

[9] T. Wu, J. Luo, W. Dong, Y. Sun, L. Xia, X. Zhang, "Geo-Object-Based Soil Organic Matter Mapping Using Machine Learning Algorithms With Multi-Source Geo-Spatial Data," IEEE Journal of Selected Topics in Applied Earth Observations and Remote Sensing, **12**(4), 1091–1106, 2019, doi:10.1109/JSTARS.2019.2902375.

[10] A. Ashapure, J. Jung, A. Chang, S. Oh, J. Yeom, M. Maeda, A. Maeda, N. Dube, J. Landivar, S. Hague, W. Smith, "Developing a machine learning based cotton yield estimation framework using multi-temporal UAS data," ISPRS Journal of Photogrammetry and Remote Sensing, **169**, 180–194, 2020, doi:10.1016/j.isprsjprs.2020.09.015.

[11] B. Zheng, S.W. Myint, P.S. Thenkabail, R.M. Aggarwal, "A support vector machine to identify irrigated crop types using time-series Landsat NDVI data," International Journal of Applied Earth Observation and Geoinformation, **34**, 103–112, 2015, doi:10.1016/j.jag.2014.07.002.

[12] D. Arvor, M. Jonathan, M. Simoes, V. Dubreuil, L. Durieux, "Classification of MODIS EVI time series for crop mapping in the state of Mato Grosso, Brazil," International Journal of Remote Sensing, **32**, 7847–7871, 2011, doi:10.1080/01431161.2010.531783.

[13] G. Rondeaux, M. Steven, F. Baret, "Optimization of soil-adjusted vegetation indices," Remote Sensing of Environment, **55**(2), 95–107, 1996, doi:10.1016/0034-4257(95)00186-7.

[14] S. Sankaran, J.J. Quirós, P.N. Miklas, "Unmanned aerial system and satellite-based high resolution imagery for high-throughput phenotyping in dry bean," Computers and Electronics in Agriculture, **165**, 104965, 2019, doi:10.1016/j.compag.2019.104965.

[15] I. Dowman, K. Jacobsen, G.S. Konecy, High Resolution Optical Satellite Imagery, Whittles Publishing, 2012.

[16] Y. Palchoudhuri, R. Valcarce-Diñeiro, P. King, M. Sanabria-Soto, "Classification of multi-temporal spectral indices for crop type mapping: a case study in Coalville, UK," The Journal of Agricultural Science, 1–13, 2018, doi:10.1017/S0021859617000879.

[17] N. Torbick, D. Chowdhury, W. Salas, J. Qi, "Monitoring Rice Agriculture across Myanmar Using Time Series Sentinel-1 Assisted by Landsat-8 and PALSAR-2," Remote Sensing, **9**(2), 119, 2017, doi:10.3390/rs9020119.

[18] L. Han, G. Yang, H. Dai, B. Xu, H. Yang, H. Feng, Z. Li, X. Yang, "Modeling maize above-ground biomass based on machine learning approaches using UAV remote-sensing data," Plant Methods, **15**(1), 10, 2019, doi:10.1186/s13007-019-0394-z.

[19] S.K. Seelan, S. Laguette, G.M. Casady, G.A. Seielstad, "Remote sensing applications for precision agriculture: A learning community approach," Remote Sensing of Environment, **88**(1), 157–169, 2003, doi:10.1016/j.rse.2003.04.007.

[20] G. Li, Z. Cheng, D. Lu, W. Lu, J. Huang, J. Zhi, S. Li, "Examining hickory plantation expansion and evaluating suitability for it using multitemporal satellite imagery and ancillary data," Applied Geography, **109**, 102035, 2019, doi:10.1016/j.apgeog.2019.102035.

[21] P. Braga, L.G.T. Crusiol, M.R. Nanni, A.L.H. Caranhato, M.B. Fuhrmann, A.L. Nepomuceno, N. Neumaier, J.R.B. Farias, A. Koltun, L.S.A. Gonçalves, L.M. Mertz-Henning, "Vegetation indices and NIR-SWIR spectral bands as a phenotyping tool for water status determination in soybean," Precision Agriculture, **22**(1), 249–266, 2021, doi:10.1007/s11119-020-09740-4.

[22] R. Nasini, T.G. LoB, A. Oddone, "BlackSky constellation: very high resolution optical data for multi-daily revisit," 7.

[23] C. Yang, C. Yang, "High resolution satellite imaging sensors for precision agriculture," Frontiers of Agricultural Science and Engineering, **5**(4), 393–405, 2018, doi:10.15302/J-FASE-2018226.

Smart Mobility: Opportunities and Challenges for Colombian Cities

Erika Quiroga[*], Karen Gutiérrez

Facultad Tecnológica, Universidad Distrital Francisco José de Caldas, Bogotá, 110111, Colombia

A R T I C L E I N F O	A B S T R A C T
	The following document analyzes the current situation in mobility and intelligent transportation in Colombia and in some cities around the world. Presenting several cases of success and implementation of technologies and protocols that seek to improve the problems with the greatest impact in today's cities, such as traffic congestion, environmental impact, accessibility, and road safety. The main objective of this research is to propose recommendations appropriate for transportation systems in Colombian cities, identifying the present challenges; therefore, through this article we will expand the panorama on ITS (Intelligent Transport System) that can be developed taking into account the needs of each territory; optimizing the strategies proposed and in turn considering the solutions that are being carried out; taking them as a guide for cities that are still in search of better mobility plans.

1. Introduction

A UN study, with demographic data shows a population growth in urban areas, where it is estimated that 68% of the inhabitants will be located in cities by 2050 [1], this will occur mainly in developing countries due to the poverty rate that exists and that presents a prolonged increase. In addition, due to the increase in population, cities have had to transform the way they use their resources and start looking for technological alternatives. This idea has made the government, industry and society adopt the term Smart Cities [2].

A smart city is one that is concerned with the integration of all the factors that make up society; combining technology and organizational work to plan, optimize and monitor the resources, services and infrastructure available, offering its citizens well-being, sustainability and quality of life [3]. At the same time, a city can be called smart as long as ingenious ideas are developed that allow the growth of certain elements or pillars such as economy-productivity and labor market, mobility-transportation and infrastructure, surroundings-environment, people-level of qualification, life-living conditions and, governance-city management [4]. According to the above, it is determined that for the study of this article only one of the pillars that make up the

smart cities, smart mobility, will be taken; since it is considered a crucial factor in the development of cities and requires an analysis in the current scenario.

Considering the above, a smart city must be connected and automated in such a way that all its basic elements can become a whole. The energy is the main source for such connection, being the center of connectivity, communication and information [2]. The International Electrotechnical Commission (IEC) is responsible for standardization in the field of electricity, energy and other electrical and electronic components, therefore, focusing on smart cities formed an IEC Systems Committee [5] of electrotechnical aspects called SYC (Systems Committee), which delves into the Sustainable Development Goal for cities, controlling the implementation of new technologies, in addition to monitoring compliance with current regulations.

Mobility has been a challenge for cities around the world due to the different problems present in this environment, traffic congestion, deterioration of road infrastructure, accidents, gas and noise generation [6] are just some examples. This is why developed cities have worked to find technological solutions such as the implementation of IoT, Big Data, automated, hybrid or electronic vehicles [7], converting conventional transport into intelligent transport, optimizing and improving the quality of service for citizens [8]. A specific case is the European Union,

[*]Corresponding Author: Erika Quiroga, Facultad Tecnológica, Universidad Distrital Francisco José de Caldas, Bogotá, Colombia, ejquirogac@correo.udistrital.edu.co

that is constantly working on investment projects for the construction of smart cities [9], in total they have developed 81 projects, 70 have already culminated and 11 are still ongoing, of which 33 have addressed issues in mobility and transport [10].

On the other hand, in Latin America, public transportation is one of the most used mobility alternatives, where trips can be short in distance, but long in time; so alternatives such as Bus Rapid Transit (BRT), train systems, subways or cable cars are sought [11]. It should also be mentioned that studies have been conducted in the region that show the dissatisfaction of citizens; in terms of quality, time, comfort, safety, and cleanliness of transportation services, which is why many people have decided to purchase their own vehicles. However, this increase has caused greater traffic jams and congestion in cities [12]. Thus, road infrastructures in this region are not adequate for the number of vehicles moving in them; traffic control systems in many cases fail or are non-existences in these cities.

The current situation in Colombia is no different from the current scenario in Latin America; the dissatisfaction with transportation services is evident and therefore solutions are being sought in the country to reduce the impact on mobility in different cities. However, these technologies have not been successful because the systems are not adapted to the real situation of the place; the integration of services and their compatibility is not feasible and their implementation is complex [13].

Therefore, the development of this article will focus on the approach of recommendations suitable for Colombian cities. Identifying and analyzing technologies and communication protocols; that are currently used in different cities around the world, who are working to bring their transportation systems within the framework of intelligent mobility. Added to this, it is intended to show the current situation in Colombia and the aspects that should be strengthened.

2. Methodology

In the research of this article, information will be taken from different academic, organizational, and state sources of the last years; that will allow to build a real vision of the intelligent mobility scenario, mentioning the technological trends and protocols that make more efficient the management and control of traffic. Therefore, in order to formulate the necessary recommendations, the following step-by-step is determined to be used in the analysis of the document; P1: Make a description of the classification of the best countries in the world in mobility and intelligent transportation; P2: Define the essential factors in the measurement of the performance of the chosen pillar; P3: Identification of current technologies and infrastructures that are being developed and implemented around the world, mentioning some examples; P4: Description of the situation in Colombia recognizing the technologies used; P5: Formulate the appropriate recommendations in the country.

3. Analysis and development

In the study conducted by the IESE Business School of the University of Navarra in its report Cities in Motion 2020, a ranking is made among 174 cities around the world where nine (9) dimensions are evaluated among which are the mobility and transportation, in the top 10 of mobility the city that ranks first is New York (United States), followed by Paris (France) and London (United Kingdom) as shown in Table 1 [14]. It is evident that the regions that occupy the first places in smart mobility in the world are cities belonging to developed countries; that are constantly working to improve their indicators and it is precisely these three cities that led the overall ranking, being considered the smartest cities in the world.

Table 1: Ranking of the world's best cities in Mobility and Transportation.

Position	City	Country
1	New York	United States
2	Paris	France
3	London	United Kingdom
4	Berlin	Germany
5	Madrid	Spain
6	Munich	Germany
7	Vienna	Austria
8	Beijing	China
9	Barcelona	Spain
10	Shanghai	China

Own elaboration - Data taken from [14].

In turn, the factors that are evaluated to measure the performance of smart mobility in a city are determinants, such elements are public transport, accessibility, connectivity and road network [15], as shown in Figure 1. In this graph, three categories are described that intend to deploy the thematic for a better understanding; in the first place, there is the *dimension or pillar* Mobility and Intelligent Transport that is the basis of the analysis; from this level arise some ramifications called *factors* that are the aspects where the main needs and demands of today's cities are found, which is why it is of utmost importance to have *indicators* that allow evaluating the growth or performance of those strategies implemented to improve transportation systems.
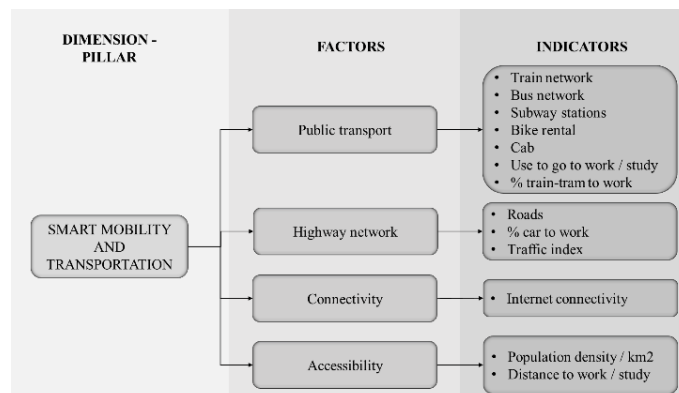
Figure 1: Intelligent mobility factors and indices [14], [15].

It is necessary to mention that the indicators may vary according to the population since cities have different needs and as a result their indexes also change; establishing unique objectives and measures to strengthen the transportation systems for each territory.

An example of these indexes is New York; a city that has implemented several transportation alternatives for its inhabitants, for this reason, some indicators have been defined, such as the following:

- # Of metro/bus passengers: 2.5 billion passengers/year. 7.5% increase since 2010.
- # Of bicycle trips (City Bike): 30,000 Trips/day (2016-2017 record).
- # Of passengers by Ferry: Grew, 4,000 trips/day (2016-2017 record).
- % Of trips per application: 90% increase since 2010.
- % Of vehicle registrations for rental: 22.7% increase (2016-2017 registration).
- % Of sustainable mode trips: 61.4% of total trips reported [16].

According to the above information, these indicators are related to the factors of public transportation and accessibility. The city government has focused its efforts on creating a diversified system; that facilitates the mobility of the population, while offering a portfolio of optimal possibilities that meet the needs of the user. Likewise, it can be observed that the results obtained in the last decade in NY were positive; since many of its indicators are in constant growth, allowing no means of transportation to collapse due to demand.

4. ITS- V2X Communications

A possible solution is found in ITS (Intelligent Transport Systems) which provide innovative alternatives through communication networks called V2X where all actors can exchange information with each other. These communications will allow better safety and traffic management; reducing accidents, gas emissions, improving vehicle flow at intersections or roads and in turn facilitating the use of autonomous and connected vehicles [17] which is the main means where this technology is applied.

In these networks there are four types of connection as shown in Figure 2, the first case, V2V (Vehicle-to-Vehicle) occurs in cars that being in motion communicate directly with other cars, in the case of V2I (Vehicle-to-Infrastructure) communication occurs when the vehicle is connected to the road infrastructure such as. In the case of V2P (Vehicle-to-Pedestrian) the connection is between cars and people who have a compatible device, and finally there is the case of V2N (Vehicle-to-Network) where the communication occurs when the car connects to the mobile network or available data networks [18].
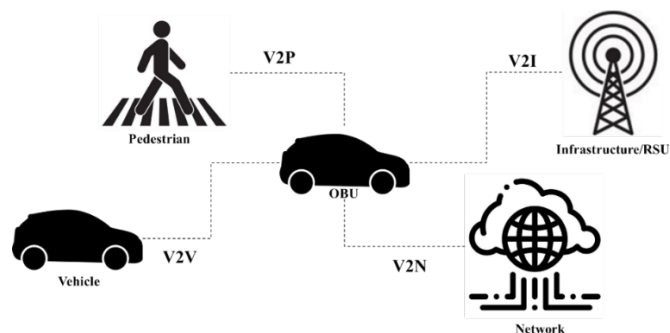
Figure 2: Connection types.

For these communications to be possible, two main technologies have been established, the first is DSRC (Dedicated Short Range Communications) defined for the United States and the second C-ITS or ITS-G5 specified for Europe, based on the first generation IEEE 802.11p standard, with which multiple tests have been performed in V2X communications [19]. However, with the scientific advances of recent years, better alternatives have been sought to develop different technologies, so a new standard called LTE-V2X was created, and its technology is called C-V2X, which is understood as cellular communication from vehicle to everything.

In DSRC and ITS-G5 technology, communication is possible by means of devices installed on the road that is responsible for exchanging information, among which are the so-called OBU (On Board Unit) devices that are located in vehicles and the RSU (Road Side Unit), which as its name suggests, are those devices that are located on the road [20]. Similarly, C-V2X technology is based on several technologies that have reached their maturity point, but will have greater difficulty in the transition to 5G networks, so using the current LTE standard enables communication between different users in mobility and can be executed in 5G mobile networks in the coming years [17].

For this reason, 5G networks are suitable for the creation of ITS through the use of small cells or macro cells; that will facilitate the exchange of information in a more agile way between existing types of communication; processing a large amount of data simultaneously coming from different devices avoiding background traffic [21]. This technology also has three key functions, the first is eMBB (enhanced Mobile Broadband) that offers a stable connection transmitting data at high-speed maintaining good communication in long periods of time, the second service URLLC (Ultra Reliable Low Latency Communications) data transmission is reliable. Finally, there is the mMTC (massive Machine Type Communications) case where a certain amount of data can be transmitted using fixed speed, connecting multiple IoT devices that are occasionally linked without collapsing the network [22].

4.1. Implementation cases.

Currently, projects or pilots based on the above-mentioned communication technologies, such as INFRAMIX [23], 5G

MOBIX, 5G CARMEN [24] and AUTO C-ITS, are being developed in several countries of the European Union.

- *INFRAMIX*

Project that seeks to improve the physical and digital road infrastructure of cities; through strategies that allow the analysis, road safety, traffic, and user satisfaction, monitoring and proper control of the system. Therefore, pilot tests have been launched in two countries, Spain, and Australia.

In both cases a 20 km segment of road was taken, equipped with different devices such as sensors, surveillance cameras, Bluetooth antennas, weather stations, using C-ITS-G5 and short range communications in which the V2I type predominates; at the same time traffic signs, RSU (control stations) and OBU (portable devices) were installed with which it was possible to exchange information throwing suggestions of lane or speed changes; the whole system was tested using 4G networks [25][26].

- *5G-MOBIX*

This is a project that seeks to test and develop the functionality of vehicles through technologies that focus on 5G networks, through the construction of cross-border corridors and tests in urban sites in different countries of the European Union, analyzing network coverage, demand for services and vehicular traffic.

Among the test sites are: (a) The Netherlands specifically in Brain port where combined road networks have been built, installing C-ITS technologies at intersections and at the same time fully equipping a six (6) km highway with surveillance cameras and C-ITS. These technologies when connected to 5G will manage to leverage the information collected on the road and in vehicles, renewing functions to prevention and automated driving [27]. (b) China-Jinan, this test site has two main roads equipped with LTE-V infrastructure and V2X-5G communications; suitable to prevention, automated overtaking, traffic efficiency and road safety evaluations [28].

- *5G CARMEN*

This project focuses on innovation to develop a hybrid network that integrates different types of communications such as long-range V2N, V2X and short-range V2I, through technologies such as C-V2X and 5G that can offer secure and cross-border services.

It is developed in the Bologna-Munich corridor with a section of 600 km distributed in three countries, its purpose is to take advantage of the progress made by 5G networks to improve the transport service making it safer, smarter and more environmentally friendly, thus offering a multi-tenant platform that can assist in mobility to this region [29].

- *AUTO C-ITS*

This project aims to improve the interoperability of transport services in Europe by means of C-ITS technology to promote

autonomous driving; therefore, it was decided to carry out three pilots in: Madrid, Paris, and Lisbon, strategically located in the so-called Atlantic corridor. Table 2 describes the different characteristics of the projects, such as their communication channels, current traffic conditions and C-ITS services in the cities. It is worth noting that the city in which there has been a greater development in C-ITS technology is in Madrid, covering a wider road segment and installing a greater number of RSUs. It is possible that this benefits the test since the defined traffic conditions are a little more detailed than in the other pilots; in addition to obtaining a greater amount of valuable information on vehicular traffic through constant monitoring [30].

Table 2: AUTO C-ITS pilot projects.

Pilot City.	Madrid - Spain.	Lisboan. - Portugal.	Paris - France.
Road.	A6 autovía del Noroeste, high occupancy reversible lane.	A9 CREL	Highway A13
Extension/ RSU	10 kms 15 RSU installed	7 kms Installed 5 RSUs	Installed 1 RSU
Traffic conditions.	-More than 20,000 vehicles/day. -Closed traffic: Controlled tests. -Open traffic: Private vehicles and collective public transport (bus).	-Open peri-urban traffic. -Controlled traffic conditions.	-Urban and peri-urban traffic.
Vehicles involved.	-Connected vehicles: 4 -Autonomous vehicles: 2	-Autonomous vehicles: 2 -Shuttle autonomous: 1 -Connected vehicles: 2	-Autonomous vehicles: 1 C1 Evie -Connected vehicles: 4 C3
Communication channel	ITS G5	ITS G5	ITS G5
Services C-ITS.	-Road Works information service. -Meteorological information service. -Traffic Service ahead.	-Notification of slow or stopped vehicles. -Meteorological information service. -Other dangerous notifications.	-Hazardous location notification. -Contextual speed adaptation. -Traffic scheduling assistant.

*Source: Own elaboration - Data taken from European Union [30].

- *VRUITS*

Similarly, there are some completed projects that have worked on ITS obtaining satisfactory results. One of these cases is the

VRUITS project that was developed with the support of the European Union in the Netherlands and Spain; its objective was to improve the mobility and safety of the vulnerable road user or VRU (cyclists or pedestrians) and in turn provide recommendations to intelligent transport systems based on evidence to achieve a complete integration with VRU [31]. The test conducted in the Netherlands consisted of improving safety at intersections by monitoring cyclists and car drivers and sending alerts about possible collisions; through the installation of RSUs, 80% of all cyclists were detected and confirmed the safety of the system.

The first evaluated whether the implementation of sensor-controlled traffic lights could optimize pedestrian mobility; the results showed that pedestrian waiting time was reduced by 20%. In the second case, the initiative sought to improve visibility at the crosswalk, reducing by 5% the number of pedestrians crossing at red lights, thereby increasing pedestrian safety.

5. Situation in Colombia

In Colombia, transportation has presented significant problems that deteriorate the mobility system in the different cities of the country, preventing its inhabitants from having a safe and quality service. Accident rate is one of these factors, only in 2019 there was a total of 6,826 deaths due to road accidents, of which 53.7% was motorcyclists, 25.6% pedestrians, 8.5% private vehicles and 6.3% cyclists [32]; the most affected departments were Antioquia, Valle del Cauca, Cundinamarca and Bogotá, in the latter it is estimated that every 5.6 minutes a simple collision or accident with injuries or death occurs [33].

Likewise, road congestion has become a critical point in mobility, according to the traffic index conducted by TomTom (company that annually monitors 57 countries, 416 cities in six (6) continents) Bogota was the third (3) most congested city in the world for 2019 with a congestion level of 68%; a 30 Min trip could increase to 58 Min in the morning and 63 Min at night during the rush hour. By 2020 this congestion level decreased to 53% due to the strict confinement that was presented by the sanitary emergency; however, the city remained in the third place in the world ranking becoming the most congested in Latin America [34].

Similarly, the number of automobiles greatly affects vehicular traffic, in recent years the vehicle fleet has increased considerably, according to the RUNT registry as of February 2021, a total of 16,176,803 vehicles were registered nationwide [35], including motorcycles, cars, vans, trucks, buses, among others; a number that continues to increase since it is optimal and convenient for citizens to purchase a vehicle rather than use public services.

Considering the above information, the government has devised some solutions to address part of the problems present in the transportation system of the country cities; for this reason, the Ministry of Transportation established a series of annual objectives to meet the ITS Project in the period 2015 – 2018. In this last year, the photodetection system was created and deployed throughout the country in order to monitor the speed of vehicles on the road and their violations [36]. Manual or automatic cameras are used to detect violations in image and video; operated by professionals from the control center to analyze the evidence obtained and validate it with the database of all cars registered in the cities [37].

Another of the ITS strategies was the implementation of the Vehicular Electronic Toll Collection systems, in this way electronic tolls were put into operation, managing to install 40 tolls in 2018. This system provides users with a unique onboard device, called TAG; which works with radiofrequency technology that allows them to make the relevant payments in an agile manner, avoiding lines and delays at the tolls [38]. Likewise, in 2019 in Bogota, smart traffic lights were installed at 21 intersections in the city to monitor and control vehicular traffic, obtaining real-time information on schedules and the number of vehicles transiting at these points, with the purpose of optimizing the light green time [39].

On the other hand, in 2020 there were already some fourth generation infrastructure projects (4G), including "safer tunnels" equipped with lighting, communication, fire detection and extinguishing systems; ventilation equipment, signaling and traffic light systems controlled from a command and control post [40]; these projects offer safety to the user, reduce environmental impact and ensure the stability of the work in the event of any catastrophe.

Finally, regarding communication networks, Colombia created the New Technologies Transition Plan, which aims to modernize the existing ones in the territory; Although in many urban areas 4G technologies have been successfully installed, there are still areas in the country where 2G and 3G communication networks are still in force, exactly 9.5 million Colombians and 34.3 million users do not have any mobile Internet connection [41], alarming figures for a country that discusses intelligent transportation systems; as a result of this, the aim is to achieve that before 2022 the whole country has access to a 4G network and can connect and communicate with the surrounding environment.

6. Recommendations

- It is evident that Colombia has failures in the deployment of mobile connections. Therefore, it is essential as a first step that 4G networks have a wide coverage throughout the territory providing secure and quality connectivity to the entire population. It is also necessary to create strategies that promote the use of these mobile networks in the cities; highlighting the variety of benefits that bring the connection to the mobile network.

- Likewise, it is necessary to carry out research and development on the technologies that are being implemented around the world; to create an adequate transportation system that is coherent with the particularities of the Colombian system. For this reason, the government plays a decisive role

in the development of ITS strategies since financing is fundamental so that the projects do not remain ideal or halfway through.

- Considering that some of the country's problems are traffic and road accidents; cities in Colombia could consider a scenario with autonomous and connected vehicles integrated to the public and private sector; allowing to build a technological environment through an infrastructure equipped with sensors, cameras, signaling, RSU, OBU and 5G network, leading the country to an intelligent mobility.

- A V2N, V2V or V2I communication pilot for cities in Colombia could be the beginning of a real digital transformation. Which would allow an evaluation of functionality and data analysis of traffic, accident, or weather conditions, in a real environment in real-time, progressively integrating autonomous vehicles to the conventional structure of the country.

7. Conclusions

Although ITS plans and projects have been created in the country since 2015, Colombian cities are not yet ready for the implementation of state-of-the-art technologies in this scenario, an example of this are their obsolete communication networks that would not allow a constant flow of large volumes of information without first collapsing. Therefore, talking about ITS is not only about sensors, cameras, or intelligent traffic lights, it is about building an interconnected environment where information is available to the user in real-time, allowing an efficient management of road resources to provide an appropriate service according to the needs of citizens.

In this way, countries such as Spain, France, the Netherlands, China, and Australia have made significant progress in intelligent mobility taking the lead in the implementation of V2X communication technologies, which for Colombia are still far away; however, this analysis was built to show the current panorama of these systems and identify the right way to build smart cities. Learning from the mentioned success cases, looking for a future implementation of ITS in the different cities of the country.

Colombia must continue working on the creation of intelligent transportation systems. Making incursions into the different available technologies mentioned in the article; building step-by-step strategies to build models like those seen today in the most developed countries in the world.

Conflict of Interest

The authors declare no conflict of interest.

References

[1] Z. Szabo, "The Effects of Globalization and Cyber Security on Smart Cities," Interdisciplinary Description of Complex Systems, **17**(3), 503–510, 2019, doi:10.7906/indecs.17.3.10.

[2] International Electrotechnical Commission, Smart Cities, 2020, doi:10.1109/jproc.2018.2812998.

[3] Z. Allam, P. Newman, "Redefining the Smart City: Culture, Metabolism and Governance," Smart Cities, **1**(1), 4–25, 2018, doi:10.3390/smartcities1010002.

[4] J. Winkowska, D. Szpilko, S. Pejić, "Smart city concept in the light of the literature review," Engineering Management in Production and Services, **11**(2), 70–86, 2019, doi:10.2478/emj-2019-0012.

[5] International Electrotechnical Commission, SyC Smart Cities Electrotechnical aspects of Smart Cities, 2019.

[6] F. Behrendt, "Cycling the Smart and Sustainable City: Analyzing EC Policy Documents on Internet of Things, Mobility and Transport, and Smart Cities," Sustainability, **11**(3), 763, 2019, doi:10.3390/su11030763.

[7] L. van Oers, E. de Hoop, E. Jolivet, S. Marvin, P. Späth, R. Raven, "The politics of smart expectations: Interrogating the knowledge claims of smart mobility," Futures, **122**, 102604, 2020, doi:10.1016/j.futures.2020.102604.

[8] D. Bamwesigye, P. Hlavackova, "Analysis of Sustainable Transport for Smart Cities," Sustainability, **11**(7), 2140, 2019, doi:10.3390/su11072140.

[9] A. Akande, P. Cabral, P. Gomes, S. Casteleyn, "The Lisbon ranking for smart sustainable cities in Europe," Sustainable Cities and Society, **44**, 475–487, 2019, doi:10.1016/j.scs.2018.10.009.

[10] European Commission, Projects | Smart Cities Marketplace.

[11] P. Yañez-Pagans, D. Martinez, O.A. Mitnik, L. Scholl, A. Vazquez, "Urban transport systems in Latin America and the Caribbean: lessons and challenges," Latin American Economic Review, **28**(15), 1–25, 2019, doi:10.1186/s40503-019-0079-z.

[12] M.E. Rivas, A. Suárez-Alemán, T. Serebrisky, Stylized Urban Transportation Facts in Latin America and the Caribbean, 2019, doi:10.18235/0001606.

[13] R. Salazar-Cabrera, A. Pachon, "Methodology for Design of an Intelligent Transport System (ITS) Architecture for Intermediate Colombian City," INGENIERÍA Y COMPETITIVIDAD, **21**(1), 49–62, 2019, doi:10.25100/iyc.v21i1.7654.

[14] IESE Businee School University of Navarra, IESE Cities in Motion Index 2020, 2020.

[15] M.A. Ur Rehman Tariq, A. Faumatu, M. Hussein, M.L. Ur Rahman Shahid, N. Muttil, "Smart city-ranking of major australian cities to achieve a smarter future," Sustainability (Switzerland), **12**(7), 2797, 2020, doi:10.3390/su12072797.

[16] NYC Department of Transportation, Mobility Report, 2019.

[17] A. Costandoiu, M. Leba, "Convergence of V2X communication systems and next generation networks," IOP Conference Series: Materials Science and Engineering, **477**(1), 012052, 2019, doi:10.1088/1757-899X/477/1/012052.

[18] GSMA, Espectro para Sistemas Inteligentes de Transporte Posición sobre políticas públicas de la GSMA, 2017.

[19] R. Molina-Masegosa, J. Gozalvez, M. Sepulcre, "Comparison of IEEE 802.11p and LTE-V2X: An Evaluation with Periodic and Aperiodic Messages of Constant and Variable Size," IEEE Access, **8**, 121526–121548, 2020, doi:10.1109/ACCESS.2020.3007115.

[20] K. Kiela, V. Barzdenas, M. Jurgo, V. Macaitis, J. Rafanavicius, A. Vasjanov, L. Kladovscikov, R. Navickas, "Review of V2X–IoT Standards and Frameworks for ITS Applications," Applied Sciences, **10**(12), 4314, 2020, doi:10.3390/app10124314.

[21] H. U. Mustakim, "5G Vehicular Network for Smart Vehicles in Smart City: A Review," Journal of Computer, Electronic, and Telecommunication, **1**(1), 2020, doi:10.52435/complete.v1i1.44.

[22] P. Popovski, K.F. Trillingsgaard, O. Simeone, G. Durisi, "5G wireless network slicing for eMBB, URLLC, and mMTC: A communication-theoretic view," IEEE Access, **6**, 55765–55779, 2018, doi:10.1109/ACCESS.2018.2872781.

[23] P. Lytrivis, E. Papanikolaou, A. Amditis, M. Dirnwöber, A. Froetscher, R. Protzmann, W. Rom, A. Kerschbaumer, "Advances in Road Infrastructure, both Physical and Digital, for Mixed Vehicle Traffic Flows.," Proceedings of 7th Transport Research Arena, Viena, Australia, 1–10, 2018.

[24] A. Kousaridas, A. Schimpe, S. Euler, X. Vilajosana, M. Fallgren, G. Landi, F. Moscatelli, S. Barmpounakis, F. Vázquez-Gallego, R. Sedar, R. Silva, L. Dizambourg, S. Wendt, M. Muehleisen, K. Eckert, J. Härri, J. Alonso-Zarate, "5G Cross-Border Operation for Connected and Automated Mobility: Challenges and Solutions," Future Internet, **12**(1), 5, 2019, doi:10.3390/fi12010005.

[25] INFRAMIX, Spanish test site – Inframix EU Project.

[26] INFRAMIX, Austrian test site – Inframix EU Project.

[27] European Commission, 5G-MOBIX - The Netherlands.

[28] European Commission, 5G-MOBIX - China.

[29] European Commission, About - 5G CARMEN.

[30] European Commission, AUTO C-ITS.

[31] European Commission, Moving in the right direction for the protection of

vulnerable road users | Results In Brief | CORDIS | European Commission.

[32] Agencia Nacional de Seguridad Vial, Histórico víctimas | ANSV.

[33] Bogotá, Análisis de accidentes viales en Bogotá en 2019 | Bogota.gov.co.

[34] TOMTOM, TomTom Traffic Index – Live congestion statistics and historical data.

[35] RUNT, Parque automotor registrado en RUNT | RUNT.

[36] Ministerio de Transporte, Proyectos ITS año 2018.

[37] Secretaria de Movilidad, CONOZCA LAS VÍAS DONDE SE UBICAN LAS CÁMARAS DE FOTODETECCIÓN DE INFRACCIONES QUE TIENE BOGOTÁ | Secretaría Distrital de Movilidad.

[38] Ministerio de Transporte, Peajes electrónicos - Ministerio de Transporte.

[39] Bogotá, Bogotá ya cuenta nuevos semáforos inteligentes | Bogota.gov.co.

[40] Agencia Nacional de Infraestructura, Túneles más seguros y eficientes en los proyectos 4G | Portal ANI.

[41] MinTIC, Colombia inicia transición de redes 2G y 3G hacia 4G.

Analyzing the Application of Two Main Microcontrollers in Engineering Education – A Case Study of three IEEE Conferences Focusing on Education

Arthur James Swart*

Central University of Technology, Bloemfontein, 9301, South Africa

A R T I C L E I N F O	A B S T R A C T
	Microcontrollers have revolutionized the field of Engineering Education. Their popularity and cost-effectiveness have opened a large door of activity for innovative projects at both the undergraduate and graduate levels. The purpose of this article is to review this activity in terms of where two of these microcontrollers have been used in Engineering Education so as to recommend further possible applications. Focus is limited to papers presented at three IEEE-based conferences over the past 10 years that mentioned the Arduino or Raspberry Pi. Documentary analysis is thus used where the abstracts of the conference papers were reviewed. Results indicate that EDUCON dominated the field of microcontroller education from 2013 to 2016, while the last three years have seen more papers dedicated to this topic being presented at the FIE series of conferences. A total of nine papers relating to microcontroller education has also been presented at TALE between 2012 and 2019. The main application of these microcontrollers has been in the field of Robotics, with general electronics and design-based learning following suit. At least 11 conference papers focusing on the use of these microcontrollers at school level were found. Overall, the Arduino outranks the Raspberry Pi by almost 4:1, with the most cited papers relating to Robotics education, to helping students at home to complete science and technology experiments and to programming. Further applications can extend to energy monitoring and academic development workshops.

1. Introduction

"When I was playing the game we never had the benefit of TV or video to analyze our techniques or look at faults, we depended on other cricketers to watch us and then tell us what they thought we were doing wrong." These words by a British athlete and cricket commentator, Sir Geoffrey Boycott, well highlight the importance of analyzing a technique in order to identify any possible faults or opportunities for further improvement. Of course, this would necessitate an adjustment of a current action in order to improve the given technique that can lead to greater success. Similarly, when it comes to Engineering Education, it is good to analyze what has been published over a period of time with regard to specific topics in order to identify any trends or opportunities for further research.

The surfacing of trends from data collections, such as user-generated content streams and news articles, is a popular and important data analysis activity, used in applications such as business intelligence, quantitative stock trading and social media exploration [1]. This has been extended to many different applications and fields of study, including Education. Identified trends in a specific field can be used to create awareness of what type of research has dominated a given topic over time and in formulating further recommendations with regard to that topic. For example, consider research on the trends relating to microcontroller education. A study noted the widespread dissemination of the Do-It-Yourself (DIY) culture and how modern-day microcontrollers have helped to fuel this culture [2]. Based on the trends identified in that study, a recommendation was made to use a multi-platform method using 8-bit microcontrollers and embedded C programming to maintain the effectiveness of microcontroller education. However, that study did not indicate how the number of publications relating to microcontroller education had increased over time, neither were the specific applications listed. This would help to identify further opportunities for the future application of microcontroller education.

Previous research has contrasted conference papers, journal articles and student dissertations to obtain bibliometric data [3-5]. However, the novelty of this study lies in its purpose, which is to contrast papers from three international IEEE conferences with regard to the application of microcontrollers in Engineering Education, so as to identify possible further applications. The use of citation analysis in this study is not for purposes of bibliometric analysis, but rather to determine which applications have attracted the most interest from fellow researchers around the globe. The article starts with a discussion on the rise of microcontrollers in Education. The context is then given along with the methodology. Results and conclusions follow at the end.

2. The rise of microcontrollers in Education

Microcontrollers were first considered at Intel in 1969 when a Japanese company approached Intel to build some integrated circuits for calculators [6]. Their history thus spans half a century, yet their impact has been extraordinary over the past two decades. They have indeed revolutionized electronic data acquisition systems [7], which is one of their primary applications.

Microcontrollers are used in many applications that require data acquisition, including industrial automation, control, measuring and consumer electronics [8]. They can be used in everything from relatively simple systems such as washing machines and vacuum cleaners, to much more advanced systems such as cars and robots [9]. In fact, they have become ubiquitous in our daily lives [10]. Its widespread adoption has necessitated changes to educational curricula, as institutions of higher learning move to make their programmes more relevant to the ever-changing technological landscape. These institutions seek to gain a competitive edge in the market of student recruitment, as they claim that their graduates will be better prepared to meet the demands of industry in the Fourth Industrial Revolution. Indeed, this revolution has been called "disruptive", as many changes have followed in its wake [11]. These changes led to the enhancement of new competence requirements (often termed "graduate attributes") and foster adjustments and the updating of qualifications. It also leads to the emergence and extinction of qualifications.

These changes are also evident in many school programmes, as governments seek to strengthen Science, Technology, Engineering and Mathematics (STEM) education among its youth. For example, in South Africa, President Cyril Ramaphosa has indicated in 2019 that government will introduce Coding and Robotics in primary schools (first years of schooling termed Grades R to 3) with a plan to implement it fully by 2022. This is one of the steps taken by government to improve education in the country. Indeed, in many western countries, Robotics is becoming increasingly common in primary and secondary education, both as a specific discipline and a tool to make STEM subjects more appealing to children [12].

3. Context of this study

The context of this study is limited to conference papers presented at three IEEE conferences that focused on Engineering Education. These conferences are [13]:

- EDUCON: This Global Engineering Education Conference provides a forum for academic, research and industrial collaboration on global Engineering Education. It is the flagship conference of the IEEE Education Society for Europe, the Middle East and North Africa (IEEE Region 8).

- FIE: Frontiers in Education has become the premiere conference for innovative curricula, Engineering Education and research excellence. This conference is usually held in various locations around the United States (IEEE Regions 1-6) and, occasionally, in international venues.

- TALE: This International Conference on Engineering, Technology and Education is the IEEE Education Society's flagship in the Asia-Pacific region (IEEE Region 10). It caters for researchers and practitioners with an interest in engineering, technology, and integrated STEM education, as well as those interested in the innovative use of digital technologies for learning, teaching, and assessment in any discipline.

The reason for focusing only on these conferences is the fact that they are rated by Microsoft Academic [14] under the top ten Engineering Education conferences in the world, and they focus on all fields of Engineering. Many of the top ten conferences on the Microsoft Academic list are field specific, such as Instrumentation, Cybernetics, Data Mining, Computer Science and Collaborative Learning.

The topic of interest is limited to the use of two microcontrollers, namely the Arduino and Raspberry Pi. The main reason for this is due to the dominance of conference papers on these two microcontrollers at the three conferences. Figure 1 highlights the total number of conference papers per year that included the word "microcontroller" for these three conferences, as found on the IEEE Xplore website.
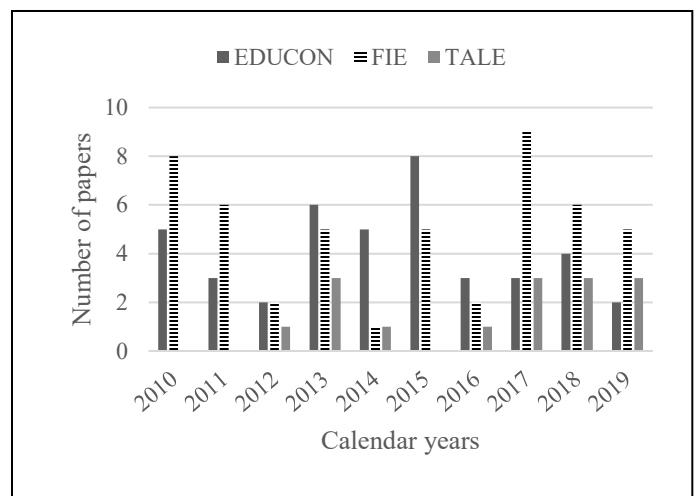
Figure 1: Conference papers using the word "microcontroller" from 2010 to 2019

More than 50% of these conference papers were related to the Arduino and Raspberry Pi. A secondary reason relates to the availability of communities of developers in which the participants share codes and experiences in projects relating to these platforms [14], which would make them easier to implement in Engineering Education.

It is noteworthy that EDUCON dominated the period of 2013 to 2016, while FIE dominated the last three years relating to the number of papers presented that mentioned the words "Arduino" and "Raspberry Pi". This fluctuation can negate forecasting in terms of which conference will dominate microcontroller education over the coming years. However, this "perceived" competition does bode well for the growth of microcontroller Education, especially within other fields of study or in other applications.

4. Methodology used

Documentary analysis were used where the abstracts of papers from the three conferences were reviewed. Documentary analysis is an important source of information, because it is non-relative, meaning that the information found in documents will remain the same over time [15]. These abstracts are retrieved from the IEEE Xplore database by limiting the search to three IEEE-based conferences, and by then searching within the results. For example, EDUCON is inserted into the search bar available on the home page. Conferences are then applied on the next page. Search within results is then used to first search for the word "Arduino" and then for the words "Raspberry Pi". The same procedure is then repeated for FIE and TALE. The search is limited to the time period of 2010 to 2019, as many conferences were impacted negatively in 2020 due to the global COVID-19 pandemic.

Abstracts are downloaded into a MS EXCEL sheet, where they are reviewed in terms of the field of application, number of authors, level of education and number of citations obtained since the publication. The citations can help to evaluate the impact of the publications [16], and also point to fields of application that are important to other researchers in Engineering Education. A large number of co-authors may indicate that more cross-disciplinary research is taking place. Within science, many studies have shown that papers with more co-authors tend to attract more citations [17].

5. Results

5.1. EDUCON results

Figure 2 contrasts the level of education where the microcontrollers have been applied. Arduino has dominated the discourse on the use of microcontrollers in Engineering Education as presented at EDUCON. A total of 15 papers were dedicated to it, with eight applied in Higher Education. It is encouraging to see that it has also been applied to STEM education at school level, where three papers were found in this regard. The Raspberry Pi has only been reported on in five papers relating to Higher Education. The generic column indicates that three papers reported on different levels of education where the Arduino has been implemented. Figure 3 indicates the various applications for the two microcontrollers that were presented since 2010 at EDUCON.

The main application relates to Robotics when considering the Arduino in Figure 3. This is not surprising, as Robotics research has increased at a rapid pace around the globe. More industries are searching for graduates with Robotics experience, and institutions of Higher Education are introducing new curriculums that include Robotics education. In fact, this is even being introduced at school level in South Africa, as mentioned earlier.

Electronics (A/D) feature second on the list of applications. Both basic analogue and digital electronics are covered in this number (three), indicating that the Arduino microcontroller has also been used to convey fundamental principles to Engineering students. Some principles may seem to be abstract to certain students. Seeing the "theory" in "practice", or in action, does indeed help students to grasp and retain key principles. This may also be applied to the application of design (two papers dedicated to this), where students need to understand various concepts that need to be synthesized to obtain a working model.
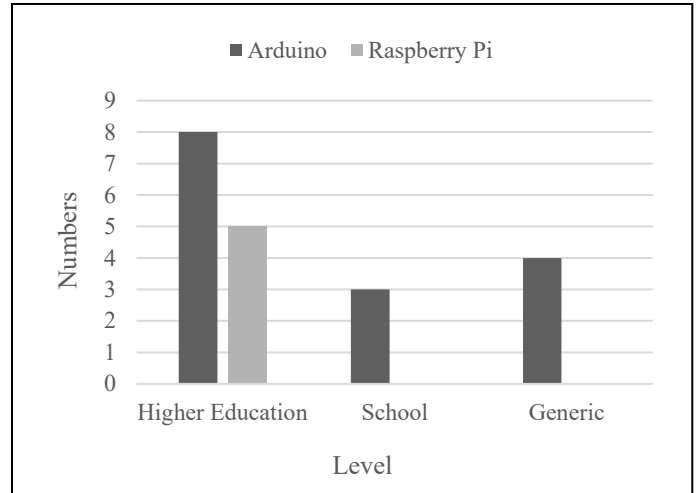
Figure 2: Level of education noted for papers presented at EDUCON
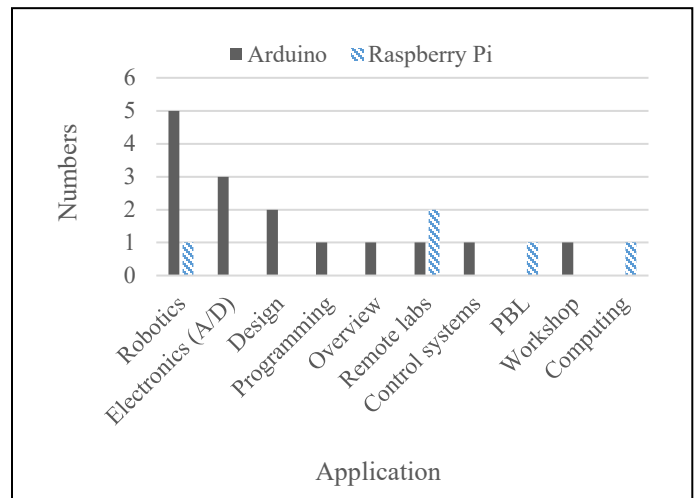
Figure 3: Applications discerned in EDUCON papers from 2010 onwards

The application "Design" covers the creation of an electronic circuit to fulfill specific requirements. "Programming" involves learning a new computer language, such as C++, while "Remote labs" involve online work were students can access an online remote laboratory from their place of residence to complete practical experiments. "Control systems" or "Control" require students to control electrical or mechanical equipment by using a microcontroller, while "PBL" (problem-based learning) requires students to make use of microcontrollers to solve an engineering-related problem. The "Workshop" application indicates a short course in which academics or students are trained in the basic use of a microcontroller, while "Computing" calls on students to

implement a microcontroller to perform mathematical or procedural tasks. The rest of the applications featured in only one paper each, with the dominant Raspberry Pi application being remote laboratories. This is expected, as the Raspberry Pi is a low-cost single-board computer that can function as a web server.

Figure 4 shows the number of authors for the 15 conference papers relating to Arduino as presented at EDUCON over the past ten years, along with their citation count. Figure 5 provides this same analysis for the Raspberry Pi.
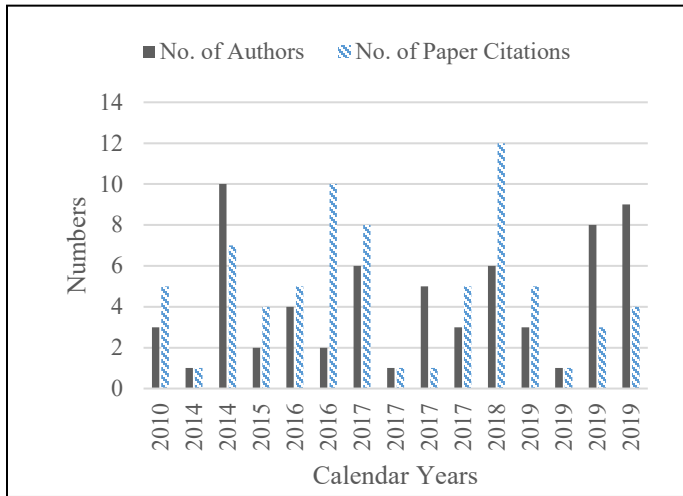
Figure 4: Number of authors versus their citations for EDUCON papers relating to Arduino as determined on 1 November 2020
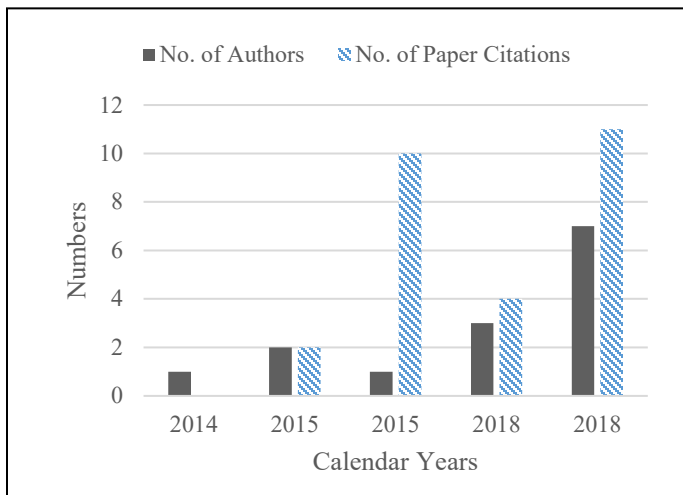
Figure 5: Number of authors versus their citations for EDUCON papers relating to the Raspberry Pi as determined on 1 November 2020

Two papers were presented in 2014 (see Figure 4), and four papers in 2019 (2 x 2014 and 4 x 2019). The maximum number of authors on a paper occurred in 2014, which was ten. That specific paper applied the Arduino microcontroller to the field of Robotics at school level. Two papers that have attracted the highest citation account were presented in 2016 (it focused on the design of electronic projects in Higher Education) and in 2018 (it focused on the use of Arduino in Robotics education at school level). Two papers were presented in 2015 (see Figure 5) and another two in 2018. The paper with the highest citation count was

published in 2018 and related to the field of Robotics education in Higher Education.

5.2. FIE results

Figure 6 contrasts the level of education, where the two microcontrollers have been applied in Engineering Education papers that were presented at FIE. Again, the Arduino dominated the discourse over the past ten years at this international conference, with the majority of papers reporting on its implementation in Higher Education. A higher number of papers have been published at FIE, compared to EDUCON. However, the trend seems to be similar between the two conferences, with the Arduino again dominating in Higher Education. Figure 7 highlights the main applications for the two microcontrollers in Engineering Education.
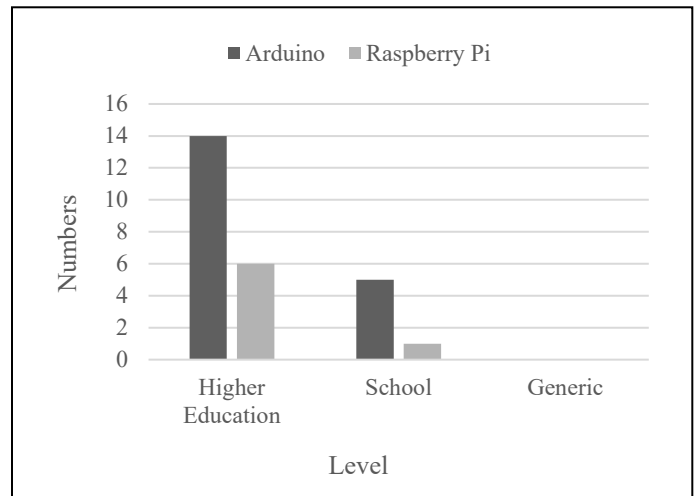
Figure 6: Level of education noted for papers presented at FIE
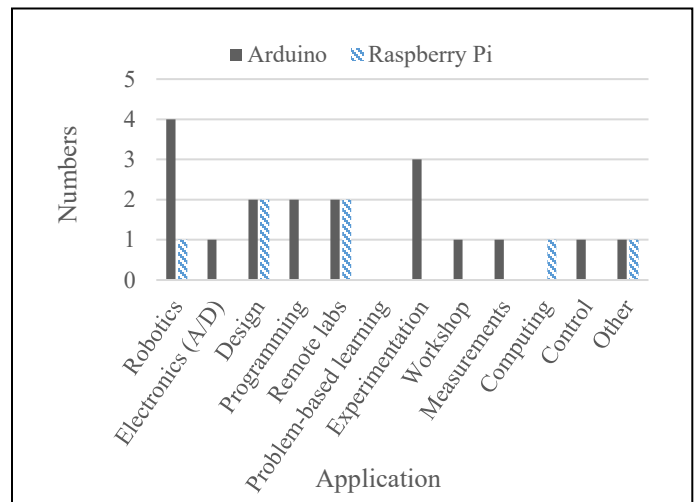
Figure 7: Applications discerned in FIE papers from 2010 onwards

Again, the field of Robotics education tops the list. However, the Arduino microcontroller has also been well applied in the field of experimentation, where two papers are focused on improving Science and Technology education at school level through laboratory experiments. The Raspberry Pi finds equal representation in the fields of design and remote laboratories.

"Experimentation" relates to the use of a microcontroller to complete a basic science experiment, while "Measurements" infer the measuring and recording of different parameters, such as temperature.

Figure 8 presents the number of authors for the papers along with their citation counts. An outstanding result is the citation of 2010. That particular conference paper reported on the use of an Arduino microcontroller to help students at home to complete science and technology experiments. This research would especially be applicable to 2020, where many students were forced to stay home due to the COVID-19 pandemic. Figure 9 provides this same analysis for the Raspberry Pi.
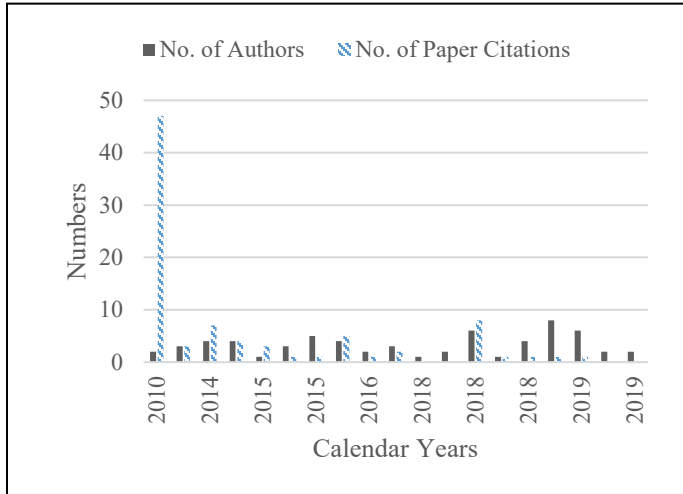
Figure 8: Number of authors versus their citations for FIE papers relating to Arduino as determined on 1 November 2020
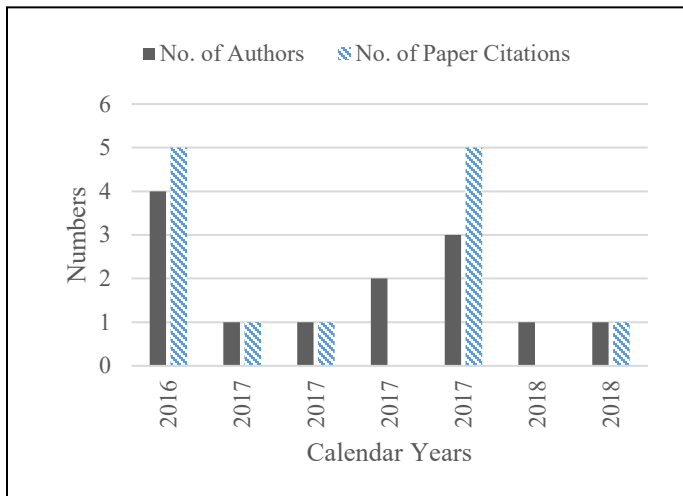
Figure 9: Number of authors versus their citations for FIE papers relating to the Raspberry Pi as determined on 1 November 2020

Four papers were presented in 2017 and another two in 2018 (see Figure 9). Two papers with the highest citation count were published in 2016 (related to the field of Robotics education in Higher Education) and in 2017 (related to remote laboratories).

Five papers were also found that reported on the use of both microcontrollers in the same course or module. All five papers reported on work done in Higher Education, where the fields of

application included project-based learning, design, modelling and programming. A paper presented in 2015 has a current citation count of 29, and reported on the use of a range of microcontrollers that were being used in a number of courses relating to project-based learning. Another paper presented in 2016 has a current citation count of 26, and reported on the use of multiple microcontrollers in design-based learning.

5.3. TALE results

Figure 10 contrasts the level of education, where the two microcontrollers have been applied in Engineering Education papers that were presented at TALE. Figure 11 shows the main applications for the two microcontrollers in Engineering Education, which include Robotics education, Design and Control.
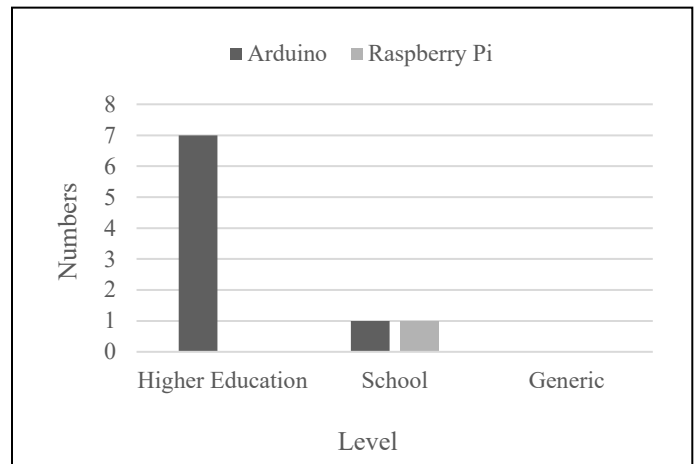
Figure 10: Level of education noted for papers presented at TALE
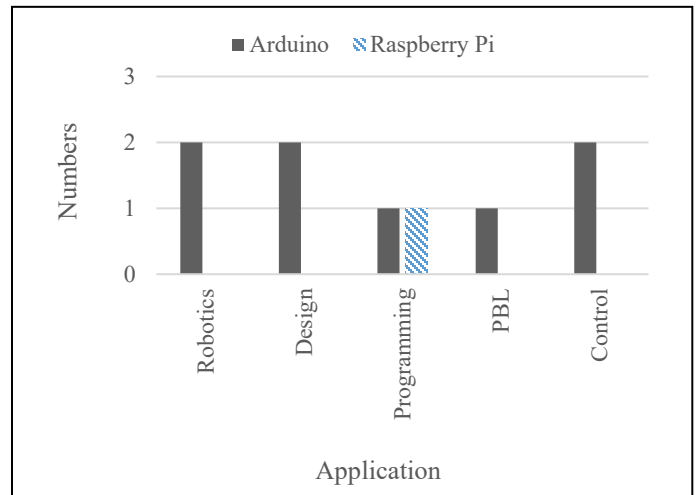
Figure 11: Applications discerned in TALE papers from 2010 onwards

Again, the use of Arduino has been well reported on in Higher Education (see Figure 10), with only two papers dedicated to this at school level for both the Arduino and Raspberry Pi. Nine papers have reported on the use of the Arduino or the Raspberry Pi over the past eight years of the TALE conference that was first held in 2012.

Figure 12 presents the number of authors for the papers along with their citation counts. Two papers were presented in 2014 and

three in 2018. One paper presented in 2014 has a current citation count of 9, and relates to project-based learning in Higher Education. Another paper presented in 2016 currently has an equal citation count, and relates to the use of Arduino in the field of Programming for freshmen Engineering students.

Only one paper relating to the use of the Raspberry Pi in the field of Programming at school level was found. Six authors contributed to this paper that was presented in 2019, and which has no citation count as yet. Table 1 contrasts the key results between the three international conferences.
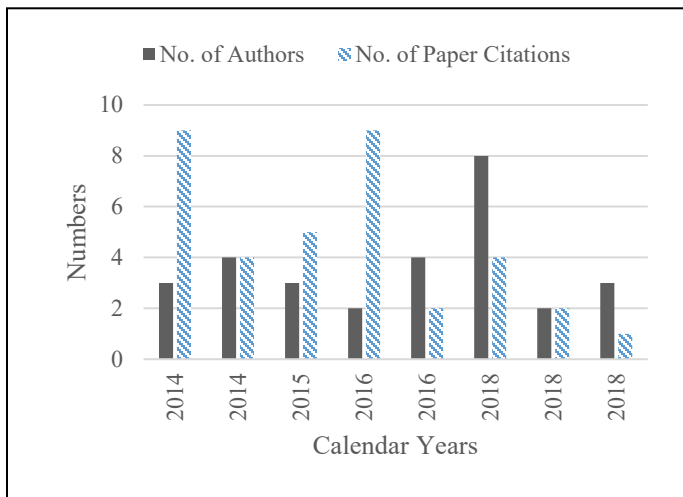
Figure 12: Number of authors versus their citations for TALE papers relating to the Arduino as determined on 1 November 2020

Table 1: Key results

| Conference	EDUCON		FIE		TALE	
Microcontroller	Arduino	Rasp-berry Pi	Arduino	Rasp-berry Pi	Arduino	Rasp-berry Pi
Dominant application	Robotics	Remote labs	Robotics	Remote labs	Robotics	Program-ming
No. Papers	15	5	19	7	8	1
Max. No. Authors on a paper	10	7	8	4	8	6
Ave. Authors	4,3	2,8	3,3	1,9	3,6	6,0
Ave. Citations	4,8	5,4	4,5	1,9	4,5	0,0
Dominant microcontroller	3,0		2,7		8,0	

FIE has a higher number of papers (19 + 7 = 26) than EDUCON or TALE. However, the ratio between papers related to the Arduino and to the Raspberry Pi is very similar, being 3:1 for EDUCON and 2.7:1 for FIE. TALE has a much higher ratio, being 8:1. All three conferences had papers with multiple authors, while the average citation count is the highest for EDUCON (4.8 and 5.4 respectively).

6. Possible difficulties in implementing microcontroller education at school/college/university level

Based on the results, it can be seen that more papers have reported on the use of microcontrollers in Higher Education as

opposed to school level. This may be due to a number of difficulties or challenges that are experienced at school level.

Firstly, it has been reported that schools have limited funding and resources [18] that would impact on the purchase of different technologies. Partnering with an institution of Higher Education could overcome this challenge, as many universities are mandated to engage in community development where they should make use of their resources to empower and uplift their communities.

Secondly, limited online resources to help learners or students to further their engagement with specific types of technology were noted [19]. Opting for open source software that is freely available to the public, and especially when it comes to programming that is required with microcontrollers, can help institutions or schools to decide on which option they wish to take. Both the Arduino and Raspberry Pi feature open source software. However, the Arduino is aimed at quick programming and circuit prototyping, while the Raspberry Pi acts as a learning tool for computer programming. The Arduino consumes less power than a Raspberry Pi [20], and is a cheaper board that also supports PWM and analog signals [21].

Thirdly, teaching programming is a challenge since the failure and dropout rate can be high in introductory programming courses [22]. Both teachers and learners could struggle to learn a new programming language. However, this can also be mitigated when numerous online resources and programming examples are available from which to learn. Partnering with an institution of Higher Education can also help in this regard, as academics proficient in programming can then volunteer their time to engage with learners at their schools.

7. Opportunities for further application in Engineering Education

Based on the EDUCON results, it can be forecasted that this international conference may see more papers in the future dedicated to using the Arduino microcontroller in Robotics education at school level. A rise in conference papers relating to its application in design-based modules may also be evident in the future. As regards the Raspberry Pi, more remote laboratories can be set up to help students complete practical experiments from their own home. However, further applications can be recommend with regard to the Arduino that can be presented at future conferences.

One of the past papers at FIE reported on the use of Arduino in the field of Measurements [23], in terms of educating students about remote environmental monitoring (e.g. temperature and humidity). However, the field of Energy Monitoring is also growing rapidly, as more countries seek to invest in renewable energy. Institutions should seek to incorporate energy monitoring techniques into their curriculum so as to better prepare graduates for this specific industry. An example of such a technique can relate to the use of an innovative jig to stimulate awareness among Engineering students about the principle of operation of solar panels. An Arduino can be used as part of that jig to help students visualize the results of their experiments on a personal computer.

A second application relates to the remote control of electronic or mechanical equipment. The advent of the Fourth Industrial revolution has enabled the rollout of many different sensors that

can now communicate with each other as part of the Internet of Things. One such application can focus on the remote control of garden plantation pumps using Arduino and mobile communications. Real-time monitoring of specific environmental conditions can help both academics and students to implement similar systems for other applications, such as an aquaponics system.

A third application relates to personal security. Globally, a drive exists to create awareness of gender-based violence and to empower communities to take a stand against domestic violence. Devices can be developed using microcontroller technology that can generate messages to a mobile number of a relative stipulating a victim's location and relevant surrounding information. This type of application may help students to not only think of engineering-related problems, but to also become aware of social problems that could be mitigated by the use of microcontroller technology.

A fourth application relates to workshops for academic staff. A workshop was reported on in a conference paper presented at FIE in 2019. This workshop was presented to school learners in an effort to stimulate awareness of engineering design principles [24]. Similar workshops could be designed to help promote academic development among lecturers at colleges or teachers in schools. This can form part of lifelong learning and enable individuals to remain registered with international bodies as part of their continuous professional development. An example of such a workshop can relate to helping lecturers from a technical and vocational college to improve their technical and programming skills by using the Arduino platform.

8. Conclusions

The purpose of this article was to analyze the application of two main microcontrollers in Engineering Education by reviewing what has been published over the past ten years at three international IEEE conferences that focus primarily on Engineering Education. Results indicate that EDUCON dominated the field of microcontroller education from 2013 to 2016, while more papers were dedicated to this topic being presented at the FIE series of conferences from 2017 to 2019.

Over the past ten years, 26 conference papers were presented at FIE relating to the Arduino and Raspberry Pi. Twenty conference papers were presented at EDUCON, while nine papers were presented at TALE. The main application of these microcontrollers has been in the field of Robotics, with general electronics and design-based learning following suit. At least eleven papers focusing on the use of these microcontrollers at school level were found. Overall, the Arduino outranks the Raspberry Pi by almost 4:1, with the most cited papers relating to Robotics education, to helping students at home to complete science and technology experiments, and to programming.

Further applications can extend to energy monitoring and academic development workshops. The importance of energy monitoring has increased with a global drive to install more renewable energy systems in the world. Continuous professional development is also of key importance, as professionals seek to

maintain their registration with official Engineering bodies around the world.

The future of using microcontrollers in Engineering Education is indeed bright, as more academics are seeking to promote student engagement by fusing theory and practice. Only time will tell to what heights academics will rise in their innovative use of these unique microcontrollers, as future analysis will reveal further trends and opportunities in this regard.

Conflict of interest

The authors declare no conflict of interest.

References

[1] N. Kamat, E. Wu, A. Nandi, "TrendQuery: a system for interactive exploration of trends," in Proceedings of the Workshop on Human-In-the-Loop Data Analytics, 1-4, 2016. doi.org/10.1145/2939502.2939514.

[2] D. E. Bolanakis, A. K. Rachioti, E. Glavas, "Nowadays trends in microcontroller education: Do we educate engineers or electronic hobbyists? Recommendation on a multi-platform method and system for lab training activities," in 2017 IEEE Global Engineering Education Conference (EDUCON), 73-77, 2017. doi.org/10.1109/EDUCON.2017.7942826.

[3] A. J. Swart, "Citation Analysis of Master Dissertations at the Central University of Technology, South Africa," AJLAIS, African Journal of Library, Archives and Information Sciences, **29**(2), 115-129, 2019. DOI not available.

[4] S. Van Herck, A. M. Fiscarelli, "Mind the Gap Gender and Computer Science Conferences," in IFIP International Conference on Human Choice and Computers, 232-249, 2018.

[5] P. Sebo, "General internal medicine and family medicine journals: Comparative study of published articles using bibliometric data," Medicine, **99**(24), 1-6, 2020. doi.org/10.1097/MD.0000000000020586.

[6] F. H. Siddig, "Designing and Implementing a Model for a Microcontroller Controlled Pick and Place," Masters in Engineering, Sudan University of Science and Technology, 2014.

[7] A. Busari Sherif, F. Dunmoye Abibat, F. Akingbade Kayode, "Development of Arduino-based Data Acquisition System for Environmental Monitoring using Zigbee Communication Protocol," APTIKOM Journal on Computer Science and Information Technologies, **1**(3), 109-118, 2016. doi.org/10.34306/csit.v1i3.56.

[8] D. R. da S. Medeiros, M. F. Torquato, M. A. Fernandes, "Embedded genetic algorithm for low-power, low-cost, and low-size-memory devices," Engineering Reports, **2**(9), 12231, 2020. doi.org/10.1002/eng2.12231.

[9] O. H. Graven, J. Bjørk, "The use of an Arduino pocket lab to increase motivation in Electrical engineering students for programming," in 2016 IEEE International Conference on Teaching, Assessment, and Learning for Engineering (TALE), 239-243, 2016. doi.org/10.1109/TALE.2016.7851800.

[10] W. Yu, O. Farook, J. P. Agrawal, A. Ahmed, "Board# 63: Teaching Microcontrollers with Emphasis on Control Applications in the Undergraduate Engineering Technology Program," in 2017 ASEE Annual Conference & Exposition2017. doi.org/10.18260/1-2--27895.

[11] G. Spoettl, V. Tūtlys, "Education and Training for the Fourth Industrial Revolution," Jurnal Pendidikan Teknologi dan Kejuruan, **26**(1), 1-6, 2020. doi.org/10.21831/jptk.v26i1.29848.

[12] J. Vega, J. M. Cañas, "PyBoKids: an innovative python-based educational framework using real and simulated arduino robots," Electronics, **8**(8), 899, 2019. doi.org/10.3390/electronics8080899.

[13] V. R. Paragarino, I. F. Silveira, M. Llamas-Nistal, "Open educational resources: A brief vision from IEEE topics," in 2018 IEEE Global Engineering Education Conference (EDUCON), 2076-2081, 2018. doi.org/10.1109/EDUCON.2018.8363495.

[14] J. Á. Ariza, "A proposal for teaching programming languages through open hardware tools," in 2016 IEEE 8th International conference on engineering education (ICEED), 202-207, 2016. doi.org/10.1109/ICEED.2016.7856072.

[15] F. E. A. Batista, G. S. Junior, I. F. Oliveira, "Precariousness, flexibility, and labor relations in the Fashion Industry," Research, Society and Development, **10**(1), e11510110841-e11510110841, 2021.

[16] Y. Xie, L. Ji, B. Zhang, G. Huang, "Evolution of the scientific literature on input–output analysis: A bibliometric analysis of 1990–2017," Sustainability, **10**(9), 3135, 2018. doi.org/10.3390/su10093135.

[17] J. M. Levitt, M. Thelwall, "Long term productivity and collaboration in information science," Scientometrics, **108**(3), 1103-1117, 2016. doi.org/10.1007/s11192-016-2061-8.

[18] S. A. Nadira, L. Shixiang, X. Chen, "SWOT Analysis of the Management and Operation of Secondary Education System in Dhaka City of Bangladesh," International Journal of Science, Technology and Society, **8**(4), 80, 2020. doi.org/10.11648/j.ijsts.20200804.11

[19] N. R. Hussein, Z. S. M Saleem, D. H. Musa, N. Ibrahim, I. A. Naqid, "Impact of COVID-19 on the medical education: experience from Kurdistan region of Iraq," Journal of Medical Education, **19**(1), 1, 2020. doi.org/10.5812/jme.106889.

[20] C. A. Okigbo, A. Seeam, S. P. Guness, X. Bellekens, G. Bekaroo, V. Ramsurrun, "Low cost air quality monitoring: comparing the energy consumption of an arduino against a raspberry Pi based system," in Proceedings of the 2nd International Conference on Intelligent and Innovative Computing Applications, 1-8, 2020.

[21] E. Lemos, A. Ghoshal, A. Aspat, "Hardware Architecture and Implementation of an AI Pet Robot," International Journal of Applied Sciences and Smart Technologies, **2**(2), 21-46, 2020. doi.org/10.24071/ijasst.v2i2.2792.

[22] Z. Mabni, N. Shamsudin, S. Aliman, R. A. Latif, "Factors Influencing Students' Performance in the First Computer Programming Course Taught Using Blended Learning Approach," Environment-Behaviour Proceedings Journal, 5(SI3), 181-186, 2020. doi.org/10.21834/ebpj.v5iSI3.2559.

[23] D. Călinoiu, R. Ionel, M. Lascu, A. Cioablă, "Arduino and LabVIEW in educational remote monitoring applications," in 2014 IEEE Frontiers in Education Conference (FIE) Proceedings, 1-5, 2014. doi.org/10.1109/FIE.2014.7044027.

[24] A. J. Penn, A. Baynes, "Exploring How Affinity toward Engineering Increases in Underserved Youth After Summer Physical Computing Workshop," in 2019 IEEE Frontiers in Education Conference (FIE), 1-5, 2019. doi.org/10.1109/FIE43999.2019.9028706.

Recognition of Emotion from Emoticon with Text in Microblog Using LSTM

Juyana Islam[1], M. A. H. Akhand[1,*], Md. Ahsan Habib[1], Md Abdus Samad Kamal[2], Nazmul Siddique[3]

[1]*Dept. of Computer Science and Engineering, Khulna University of Engineering & Technology, Khulna 9203, Bangladesh*

[2]*Graduate School of Science and Technology, Gunma University, Kiryu 376-8515, Japan*

[3]*School of Computing, Engineering and Intelligent Systems, Ulster University, Northern Ireland, UK*

A R T I C L E I N F O	A B S T R A C T
	With the advent of internet technology and social media, patterns of social communication in daily lives have changed whereby people use different social networking platforms. Microblog is a new platform for sharing opinions by means of emblematic expressions, which has become a resource for research on emotion analysis. Recognition of emotion from microblogs (REM) is an emerging research area in machine learning as the graphical emotional icons, known as emoticons, are becoming widespread with texts in microblogs. Studies hitherto have ignored emoticons for REM, which led to the current study where emoticons are translated into relevant emotional words and a REM method is proposed preserving the semantic relationship between texts and emoticons. The recognition is implemented using a Long-Short-Term Memory (LSTM) for the classification of emotions. The proposed REM method is verified on Twitter data and the recognition performances are compared with existing methods. The higher recognition accuracy unveils the potential of the emoticon-based REM for Microblogs applications.

1. Introduction

Expressions of emotion are fundamental features of intelligent beings, especially humans, that play important roles in social communication [1, 2]. In simple words, emotion represents a person's state of mind exposing into an expression such as happiness, sadness, anger, disgust, and fear. Humans express their emotions in verbal and nonverbal modes, such as speech [3], facial expression [4], body language [5], and expression using text [6]. Emotion has a strong correlation with mental health measured by positive and negative affect and plays a vital role in human social and personal life. With the advent of internet technology, people use various social networking platforms (e.g., Facebook, Twitter, Whatsapp) for social communication. People share their thoughts, feelings, and emotions on different socio-economic, politico-cultural issues using social media. Social media contents appear to emerge as a potential resource for research in human emotional and social behaviors.

Microblog is a common platform to share opinions; hence, it is an important source of emotion analysis of individuals. Microblog makes communication more convenient in our daily life. The most popular microblogs include Twitter [7], Facebook, Instagram,

LinkedIn, and Tumblr. A microblog-post can be reached a vast number of audiences within a short time through these platforms. Moreover, a post may reflect one's emotion or sentiment. Thus, sentiment analysis and emotion recognition are two critical tasks from microblog data [8–13]. Depression is the world's fourth major disease, which is deeply related to emotions [14] and often leads to suicidal tendencies. In the United States, suicide is the 10th major cause of death [15]. Social communications and microblog messages may reflect one's mental state. Thus, a potential application of microblog analysis is to take quick necessary actions against deeply depressed people (who might commit suicide) based on his microblog comments.

Analysis of social media contents, especially microblogs, has become very important in different prospects in the present internet era. Tracking and analyzing social media contents are advantageous for understanding public sentiment on any current socio, cultural, and political issue. Researchers have explored different techniques of extracting information from social media data, which have a direct impact on customer services, market research, public issues, and politics. Customer review analysis through such techniques plays an important role in improving the quality of the products and services for retaining customers and attract more [16]. The developed techniques are expected to play

*Corresponding Author: M. A. H. Akhand, Email: akhand@cse.kuet.ac.bd, and Tel.: +8801714087205

an essential role in the study of patients' psychology. Furthermore, emotion analysis is being considered as an emerging research domain for the assessment of mass opinion [17].

Automatic recognition of emotion from microblogs (REM) is a challenging task in the machine learning and computational intelligence domain. There are two main approaches to recognize emotions from microblogs: the knowledge-based approach and the machine learning (ML) approach [18]. In the knowledge-based approach, the task is to develop a set of rules analyzing the given data and then detect emotion using the rules [19]. In the ML approach, a dataset, which consists of patterns based on the features generated from the microblog data, is used to train an ML model, and then the model is used to predict the emotion for unseen data [20]. Typically, ML-based approaches are expected to perform better than knowledge-based approaches [29], [31]. Recently, deep learning (DL)-based methods, which work on the preprocessed data and do not require explicit features, are investigated for REM and found to be promising results [21], [22].

The existing REM methods ignored emoticons and other signs or symbols in the microblogs. These researches only considered texts for the recognition of emotion [23–25]. Nowadays, emoticons, the pictorial representations of facial expressions using characters and related symbols, are commonly used on social media sites. It is found that emoticons are becoming the most important features of online textual languages [26]. Among the few studies that dealt with emoticons is [22] using Convolutional Neural Network (CNN). In the study, words and emoticons from microblogs are processed separately in two different vectors and projected into the emotional space to classify using CNN. Emoticon consideration independent of the text seems not appropriate as emoticons embedded within the text fabricates a semantic or contextual meaning, which is important in emotion analysis. Placement of the emoticon within the text is also important as the different arrangement of emoticon within text may change the meaning. However, emoticon-based REM development is the motivation behind the present study.

This study aims to develop an improved REM method to keep the semantic links between emoticons and the relevant texts. Acknowledging emoticons as particular expressions of emotions, they are represented by suitable emotional words. The original sequence of emoticons in the microblog is unchanged since their sequence may have a vital role in expressing the appropriate emotion. With the necessary prepossessing of microblog data, a machine learning model suitable for examining the sequential or time-series information, known as the Long Short-Term Memory (LSTM), is employed to classify emotions. The recognition performances are compared with the existing method that uses only text expressions (i.e., ignores emoticons) in the recognition process. An initial version of the LSTM-based REM considering emoticons has been presented in a conference [1]; and, the present study is an extended version. The current REM presents the detailed theoretical analysis and experimental results. The higher recognition accuracy of the proposed REM justifies its use in emerging microblog applications.

The rest of the paper is organized as follows. Section 2 presents a brief survey of existing REM methods. Section 3 explains the proposed REM method. Section 4 provides detailed experimental results and analysis. Finally, the conclusion is presented in Section 5.

2. Related Works

Microblog analysis for REM is explored with the rapid growth of social media communication. Several studies were conducted in the last decade for REM from microblogs employing different ML methods, including Naive Bayes (NB) and Support Vector Machine (SVM). The DL-based techniques have also emerged remarkably in the recent REM studies.

Pre-processing of blog tests and distinguishable feature extraction with appropriate techniques are the two important tasks to apply any ML method for REM. Chaffar and Inkpen [18] extracted features from diary-like blog posts (called Aman's Dataset) using bags of words and N-grams. They used decision trees, NB, and SVM to recognize the six fundamental emotions (i.e., anger, disgust, fear, happiness, sadness, and surprise) using the features. The SVM is found best among the other classifiers. Silva and Haddela [27] also used Aman's data set and applied the SVM for REM purposes. But they investigated a concept called term weighting to enhance the conventional Term Frequency Inverse Document Frequency (TF-IDF) for feature extraction. Chirawichitchai [28] studied a feature selection technique by information gain and REM by SVM on Thai language blog texts from various social networking sites (e.g., Facebook).

In [29], the authors examined semi-supervised learning with SVM, called distant supervision, for REM from the Chinese tweets in Weibo using a large corpus with 1,027,853 Weibo statuses with emotion labels. Their proposed system predicted happiness emotion most accurately (90% accuracy rate) and worked well for anger. However, the system was less effective for detecting other emotions, e.g., fear, sadness, disgust, and surprise.

In [30], the authors used emoticons in their proposed REM method called the emoticon spaced model (ESM). The ESM learns a sentiment representation of words with the help of emoticons using a heuristic. Words with similar sentiments have similar coordinates in the emoticon space. The coordinates of words are fed into Multinomial naive Bayes (MNB) and SVM for classification. They applied their method on the Chinese microblog benchmark corpus NLP&CC2013 with 14,000 posts with the four most common emotion types (happiness, like, sadness, and disgust).

In [31], the authors performed REM from Twitter's data using NB; in preprocessing stage, they removed URL, special characters, stop-words, and few other things. In [32], the authors extracted features using different methods (e.g., Unigram, Bigram) on the collected 1200 Twitter emotional data and classified emotions using MNB. The large number of features combining Unigram and Bigram is shown to outperformed others with an accuracy of 95.3%.

In [14], the authors adapted emotional-related Chinese microblog (Sina Weibo) data for depression recognition adding "depression" as a new class and excluding the "surprise" class. They developed an emotion feature dictionary with seven types of emotions, namely depression, good, happiness, fear, sadness, disgust, and anger, for depression recognition using 1381 emotional words or phrases. In their study, Multi-kernel SVM is found better than KNN, NB, and standard SVM for depression

recognition from the combination of features from the user profile and user behavior and the features from blog texts.

Among different DL methods for REM, CNN and LSTM are the most well-known ones found in prominent studies recently. In [22], the authors proposed a CNN-based REM, called enhanced CNN (ECNN), that examines both texts and emoticons. Specifically, by placing the emoticons and words in two different vectors and projecting them into one emotional space, CNN is employed to classify emotion. They viewed emoticons as independent of the text, i.e., ignored the emoticon's order in the description. Such consideration might be misleading because emoticon placement or sequence in the text may have a specific meaning. ECNN applied on the Chinese Sina Weibo, NLPCC2013, and Twitter datasets (SEMEVAL). The experimental results on Chinese Sina Weibo, NLPCC2013, and Twitter microblog datasets showed that ECNN outperformed other methods, including SVM, bidirectional LSTM (BiLSTM).

On the other hand, in [21], the authors proposed a hybrid DL model, called Semantic-Emotion Neural Network (SENN), with BiLSTM and CNN for REM. BiLSTM is used to capture contextual information and focuses on the semantic relationship, and CNN is used to extract emotional features and focuses on the emotional connection between words. SENN was applied on Twitter and other social media data, but the use of emoticon is not clear in the decision process.

3. Recognition of Emotion from Microblog (REM) Managing Emoticon with Text

Recently, social media has become a dominant and popular platform for expressing and sharing emotion [3] using microblogs, photos, and videos. Remarkably, the microblog is the hot favorite choice, where one directly writes personal thoughts (e.g., own status, reactions to others, and opinions). Facebook and Twitter are examples of the most popular social media for expressing and communicating such personal thoughts in microblogs. Microblogs contain words, emoticons, hashtags, and various signs with distinct meanings. Since emoticons have become more popular elements besides the text than ever, they should be given proper attention in any microblog-based scheme of emotion recognition.

In this study, emphasis is given to emoticons and their association with texts in microblogs, considering that both are equally valuable to identify proper emotion. Some studies excluded emoticons in the preprocessing step considering those as noisy inputs [33]. But, in this study, emoticons are altered with emotional words and fused with texts for emotion recognition.

Algorithm 1: Recognition of emotion from microblogs (REM)

Input: Microblog M with W Words
Output: Emotion Category $EC \in$ (Happy, Sad, Angry, Love)

// Process 1: Emoticon alteration with textual meaning
For all $w \in W$ **do**
    If $M[w]$ is emoticon **then**
        $M[w]$ = Emoticon.meaning ($M[w]$)
    End If
End For

//Process 2: Tokenization with integer encoding
For all $w \in W$ **do**
    $IW[w]$ = Tokenizer ($M[w]$)
End For

// Process 3: Padding with 0 to render fixed S size
For all $w \in [S - W]$ **do**
    $P[w]$ = 0   // Consider 0 padding
End For
For all $w \in [S - W + 1 : S]$ **do**
    $P[w]$ = $IW[w]$ // Copy the rest values
End For

// Process 4: Emotion recognition using LSTM
//Embedding integer to 2D vector
For all $w \in S$ **do**
    $V[x, y]$ = Embedding ($P[w]$)
End For
EC = LSTM (V)

These interpreted emotional words and other texts presented in the proposed REM help the model perform improved emotion classification.

Figure 1 illustrates the framework of REM proposed in this study for a sample microblog containing an emoticon in the text. The REM consists of four sequential processes. In Process 1, emoticons are converted into relevant emotional words according to a predefined lookup table. The words are transformed into a sequence of integer numbers in Process 2. In Process 3, padding is conducted to form a vector containing the sequence of words with equal length. Finally, in Process 4, the LSTM is employed for classification of emotions into Happy, Sad, Angry, or Love.

Algorithm 1 shows the proposed REM where individual processes are marked. It takes microblog M with W words as input and provide emotion category EC. The whole method is broadly divided into two major parts: processing microblog data using processes 1, 2, and 3, and recognition with the LSTM network. The processes are briefly described in the following subsections.
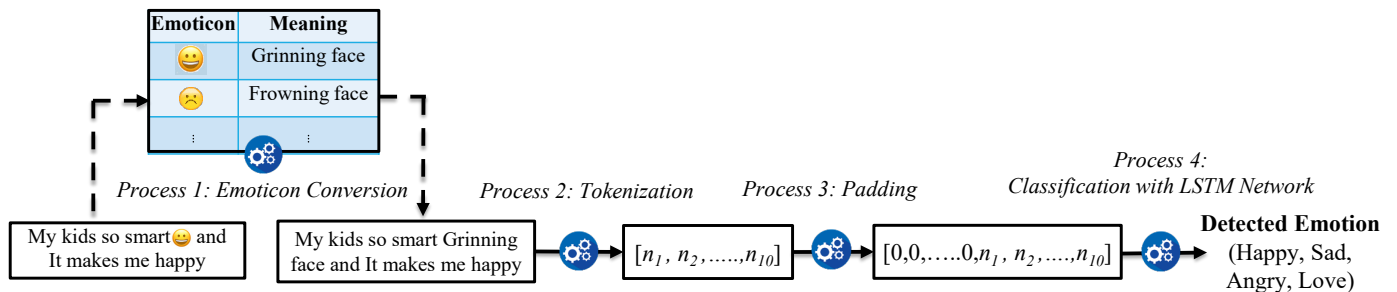
Figure 1: The proposed REM framework illustrating different processes for a sample microblog.
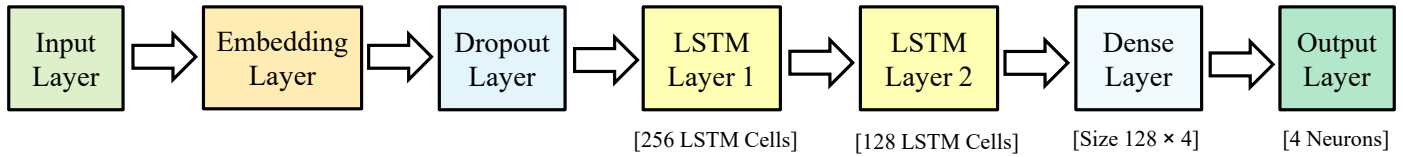
Figure 2: LSTM network architecture used in the proposed REM.

3.1. Microblogs Processing

Twitter is a popular microblog platform and it allows emoticons with texts. Thus, Twitter microblogs are collected and processed for REM in this study. Social media data contains noisy information that needs to be cleaned up to use in the system. Then the clean microblogs with emoticons and texts go through the Processes 1 to 3 (Fig. 1). In Process 1, each emoticon is replaced with corresponding text (i.e., equivalent word for the emoticon) using a function, called *Emoticon.meaning(),* with the help of a lookup table with equivalent words and emoticons. Process 2 is the Tokenization step: it removes unnecessary information and then, generates an integer vector sequence of words (*IW)* through integer encoding. Finally, Process 3 transforms *IW* to a defined fixed length size (say *S*) of words with zero initial paddings. If *IW* contains *W* integer values, the padding outcome *P* vector will contain zeros (i.e., 0) in initial *S-L* positions and the rest are *L* values from *IW*.

3.2. Emotion Recognition Using LSTM

The proposed structure of the LSTM network for the REM is shown in Figure 2. The network consists of an input layer, an embedding layer, a dropout layer, two LSTM layers, a dense layer, and finally, the output layer. The input in the LSTM network comprises a sequence of an integer number (defined fixed length *S*) with zero paddings in initial positions. The embedding layer simply transforms each integer word into a particular embedding vector. In the proposed architecture, the sizes of input integer words and embedding vectors are 78 and 128, respectively. Therefore, the output of the embedding for a microblog text is a 78×128 sized 2D vector. A dropout layer is placed just after the input layer, which randomly selects input features during training. The purpose of the dropout layer is to reduce overfitting and improve the generalization of the system.

There are two LSTM layers in the proposed architecture which are the main functional elements of the system. The first and second LSTM layers contain 256 and 128 hidden LSTM cells, respectively. Each LSTM cell in the first layer processes 128 sized embedding vectors and generates single output; therefore, the first LSTM layer produces 256 values which propagate to the input of each LSTM cell of the second layer. The second LSTM layer produces 128 values and the dense layer generates the emotional response from the values. Emotion recognition of this study is a multiclass (i.e., 4-class) classification problem to classify microblogs into four different emotion categories. Thus, it requires the dense layer to be of size 128×4. The output layer has to yield one of the four classes and therefore, the output layer comprises four neurons where each neuron represents a particular emotional state.

An LSTM cell is the heart of the LSTM network architecture illustrated in Fig. 3, which shows the basic building block of an
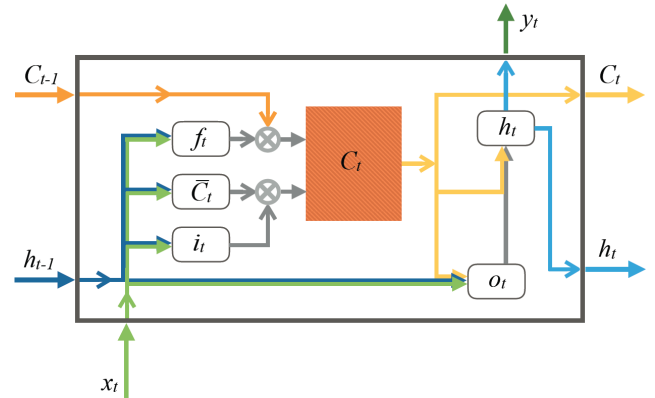
Figure 3: Basic building block of an LSTM cell.

LSTM cell. The LSTM cell consists of a forget gate (*f*), a memory cell (*C*), an input gate (*i*), and an output gate (*o*), At any state *t*, the memory block uses both the current input (x_t) and the previous hidden layer output (h_{t-1}) as inputs and generates new output (h_t) of the hidden layer. This memory block enables the LSTM network in forgetting and memorizing information as required. Hyperbolic tangent or *tanh (*symbol ϕ) and *sigmoidal* (symbol σ) functions are used as the gates. The memory unit calculates the candidate memory $\overline{C_t}$, f_t and input gate i_t at state *t* according to Eqs. (1-3).

$$\overline{C_t} = \phi \ (W_C * h_{t-1} + U_C * x_t + b_C) \tag{1}$$

$$f_t = \sigma \ (W_f * h_{t-1} + U_f * x_t + b_f) \tag{2}$$

$$i_t = \sigma \ (W_i * h_{t-1} + U_i * x_t + b_i) \tag{3}$$

Then, memory C_t is calculated using Eq. (4).

$$C_t = f_t * C_{t-1} + i_t + \overline{C_t} \tag{4}$$

h_t comes from C_t through the output gate o_t following Eqs. (5-6).

$$o_t = \sigma \ (W_o * h_{t-1} + U_o * x_t + b_o) \tag{5}$$

$$h_t = o_i * \phi(C_t) \tag{6}$$

In Eqs. (5-6), *W* and *U* denote the respective shared weights, and *b* denotes the bias vector. Finally, the output of an LSTM cell comes from h_t through the weight vector *V* defined as

$$y_t = V * h_t . \tag{7}$$

The LSTM is suitable for modeling complex time-series data since it can classify from any given sequence upon training. Therefore, the LSTM is chosen in the proposed REM to classify the processed microblogs. A detailed description of the LSTM is available in [34].

4. Experimental Studies

This section describes Twitter data preparation, experimental settings and experimental results of this study.

4.1. Dataset Preparation

To make the processed microblog data compatible with LSTM network, tokenization is performed using Keras open-source neural-network library [36] to convert the words to numerical values, and then padded with zeros for a fixed-sized vector. The

Table 1: Emoticons and corresponding word meanings

Sl.	Emoticon	Unicode	Textual Meaning	Emotion
1	😀	U+1F600	Grinning face	Happy
2	😄	U+1F604	Grinning face with smiling eyes	
3	😁	U+1F601	Beaming face with smiling eyes	
4	☺	U+263A	Smiling face	
5	😭	U+1F62D	Loudly crying face	Sad
6	😢	U+1F622	Crying face	
7	🥺	U+1F97A	Pleading face	
8	☹	U+2639	Frowning face	
9	😠	U+1F620	Angry face	Angry
10	😡	U+1F621	Pouting face	
11	😤	U+1F624	Face with steam from nose	
12	🤬	U+1F62C	Face with symbols on mouth	
13	😍	U+1F60D	Smiling face with heart-eyes	Love
14	🥰	U+1F970	Smiling face with hearts	
15	😘	U+1F618	Face blowing a kiss	
16	😚	U+1F617	Kissing face with closed eyes	

Table 2: Samples Twitter microblogs and emotion calabel

Microblog	Emotion Category
Yay! Very well deserved 😄	Happy
I'm so sorry 😭	Sad
😭 I just want the pain to go away	Sad
Apologies to him right now! 😡	Angry
😡 go follow right now	Angry
😍😍😍 Good night love	Love

size of the padded numeral blog was 78, whereas, it was 33 while emoticons were discarded.

4.2. Experimental Settings

Adam algorithm [37], a popular optimization algorithm in computer vision and natural language processing applications, is used to train LSTM. Softmax and categorical-cross entropy are considered as activation function and loss function, respectively. The dropout rate of the dropout layer is set to 0.3, and each LSTM layer contains 30% dropout and 20% recurrent dropout while training the model. Batch-wise training is common nowadays and LSTM training was performed for batch sizes 32, 64, and 128 which are commonly used in related studies. Among the collected 16012 tweets, 75% (i.e., 12009) were used to train LSTM, and the remaining 25% (i.e., 4003) were reserved for the test set to check the generalization ability of the system.

The proposed model was implemented in Python programming language. The experiments were performed using a jupyter notebook as well as Kaggle online environment. A PC with the following configuration is used for conducting the experiment model: HP ProBook 450 G4, processor: Intel(R) Core (TM) i5-5200U, CPU: 2.20 GHz, RAM: 8 GB, OS: Windows 10.

4.3. Experimental Results and Analysis

The emoticon consideration with text is the core significance of the proposed REM (with emoticons embedded in texts) from real-life Tweeter data. An experiment discarding emoticons (i.e., using texts only) is also carried out, it may be called REM without emoticon or text-only REM. The outcomes of text-only REM are compared with the proposed REM to observe the effect of emoticon.

In Figure 4, the accuracies of the LSTM for both the training and test sets are evaluated by varying the training epochs up to 200 for the different batch sizes (BSs). It is very clear from the graph that the accuracy of the proposed REM (as shown by the solid curves) is always better than the accuracy of the text-only REM (as shown by the dashed curve). Remarkably, the accuracy with the text-only case is compatible with the proposed REM while training. For example, at 100 epochs for BS=32 (in Fig. 4(a)), the achieved accuracies on the training set of the proposed REM and text-only REM are 0.994 and 0.957, respectively. However, regarding the test data, the accuracy of the proposed REM is much better than that of the method without emoticon (i.e., text-only REM). It is remarkable that the text-only REM test set accuracy is placed in a graph doubling its achieved value to make the graph better visualization. At a glance, the test set accuracy of the proposed REM is almost double that of the text-only REM with any BS values. As an example, at 100 epochs for BS=64 (in Fig. 4(b)), the achieved test set accuracy for proposed REM is 0.873; whereas, the value is only 0.424 for text-only REM. A similar observation is also visible for BS=128 in Fig. 4(c).

Figure 5 shows the best accuracies from individual experiments with different BS values. The training set accuracy for the text-only REM and the proposed REM are 0.963 and 0.994 for any BS value, respectively. Although performance on the
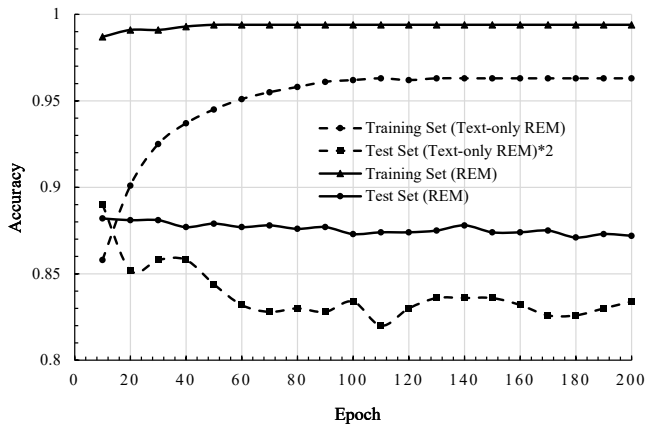
(a) BS= 32
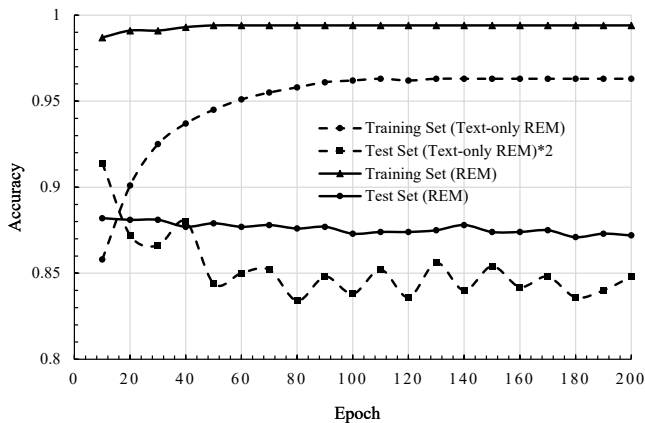
(b) BS= 64
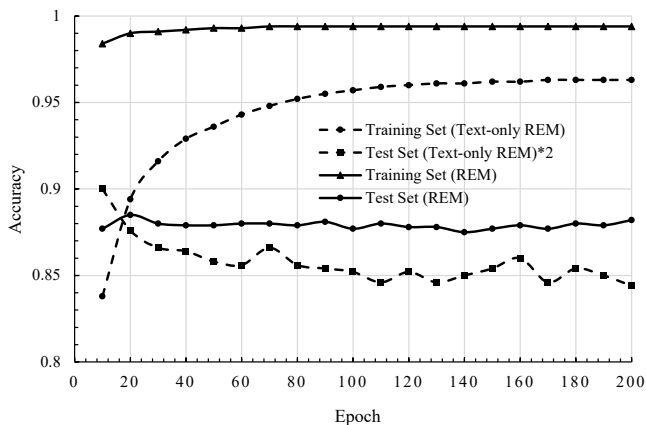
(c) BS= 128

Figure 4: Recognition accuracies of proposed REM (using both text and emoticon) and text-only REM varying training epochs for three different batch sizes (BSs) 32, 64 and 128.

training set is competitive with and without emoticon, it is remarkable on test set accuracy with emoticons. The best test set accuracies for the text-only REM are 0.445, 0.457, and 0.45 at BS values 32, 64, and 128, respectively. On the other hand, considering both emoticon and text, the proposed REM achieved much better test set accuracies and the values are 0.884, 0.882, and 0.885 at BS values 32, 64, and 128, respectively. Notably, training set accuracy indicates the memorization ability and test set accuracy indicates the generalization ability of a system to
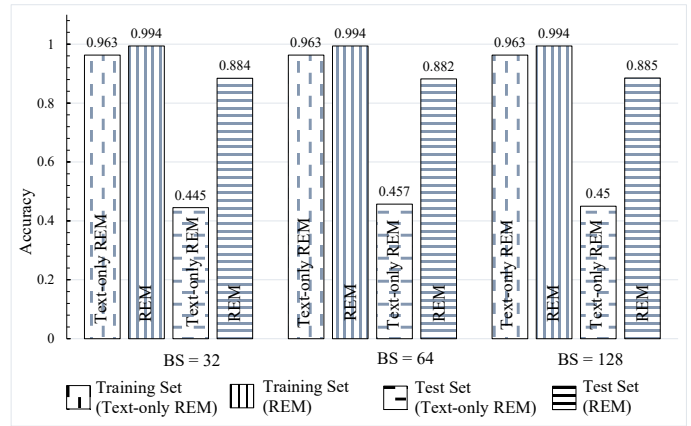
Figure 5: Best accuracies for training and test sets for proposed REM (text and emoticon) and text-only REM for training batch sizes (BSs) 32, 64 and 128.

work on unseen data. Test set accuracy is the key performance indicator for any machine learning system and it is a better score of proposed REM over text-only REM (i.e., without emoticon), which revealed that the use of emoticons enhances the ability of the proposed method in learning the emotion properly. However, the reason behind the worse performance with text-only REM is that the texts are limited in the selected tweet data and, in many cases, the text becomes meaningless without emotion, which has been explained in the data preparation section. Moreover, people do not care about meaning with text only when they use emoticon within it.

Table 3 and Table 4 show the emotion category-wise performance matrices of the proposed REM and text-only REM, respectively, for the best test accuracy cases shown in Fig. 4. The table shows the variation in actual and predicted emotions labeled for the individual emotion category. In the test set, 'Happy', 'Sad', 'Angry' and 'Love' emotion categories hold 1024, 956, 949, and 1074 tweet data consecutively. For the 'Happy' case in Table 3, for example, the proposed REM truly classified 914 cases, and the remaining 110 cases were misclassified into 'Sad', 'Angry' and 'Love' categories as 41, 33, and 36 cases, respectively. On the other hand, text-only REM truly classified only 442 cases as from Table 4. The proposed REM showed the best performance for the 'Angry' category by truly classifying 862 cases out of 949 cases

Table 3: Emotion category wise test set performance matrix for proposed REM method considering both emoticon and text.

Emotion Category	Total Sample	Detected Category			
		Happy	*Sad*	*Angry*	*Love*
Happy	1024	**914**	41	33	36
Sad	956	21	**857**	42	36
Angry	949	29	31	**862**	27
Love	1074	43	68	53	**910**

Table 4. Emotion category wise test set performance matrix for text-only REM.

Emotion Category	Total Sample	Detected Category			
		Happy	*Sad*	*Angry*	*Love*
Happy	1024	**442**	175	173	234
Sad	956	177	**419**	194	166
Angry	949	195	209	**434**	111
Love	1074	205	190	145	**534**

(i.e., 90.83% accuracy). On the other hand, the text-only method showed the best performance for the 'Love' category, truly classifying 534 cases out of 1074 cases (i.e., 49.72% accuracy). The performance comparison in the individual emotion category visualizes the proficiency of the proposed REM with emoticon and text.

On Twitter data, Table 5 compares the classification accuracy of the proposed method with other existing methods. The table also includes the methods used by various studies with a variety of dataset sizes. The existing methods considered Naive Bayes, CNN, and BiLSTM. The self-processed 16012 Twitter data used in the present study. The dataset used in [21] is larger than this study, but the authors did not mention how training and test sets are partitioned. Due to varying dataset sizes, the comparison with other methods may not be completely fair. However, the proposed method has outperformed any other methods showing a test set accuracy of 88.5%. The achieved accuracy is much better than the traditional machine learning with Naive Bayes [31] and deep learning methods with CNN and BiLSTM [21] [22]. It is already mentioned that study in [22] used emoticons but processed by separating them from the text. The main reason behind the outperforming ability of the proposed method is its emoticon management with text which is not appropriately handled in the existing methods. Finally, managing emoticons and texts simultaneously and classification with LSTM have been revealed as a promising emotion recognition method for microblogs.

Table 5: Performance comparison with existing methods on Twitter data.

Sl.	Author [Work Ref], Year	Sample Size (Training + Test)	Method Used	Test Set Accuracy
1	Wikarsa and Thahir [31], 2015	268 (116+152)	Naive Bayes	71.3%
2	Yang et al. [22], 2018	7200 (4600+2600)	CNN	72.6%
3	Batbaatar et al. [21], 2019	19678 (Not Mentioned)	BiLSTM + CNN	61.3%
4	Proposed Method	16012 (12009 + 4003)	LSTM	88.5%

5. Conclusions

Nowadays, people are very active on social media and frequently express their emotions using both texts and emoticons in microblogs. Emotion recognition from social media microblogs (i.e., REM) emerges as a promising and challenging research issue. It is essential to consider all necessary microblog information for comprehensive REM. Unlike many existing methods that only view the textual expressions for simplicity, this study has investigated REM utilizing both emoticons and texts simultaneously. Using the underlying LSTM technique, the proposed REM could interpret the emoticons in the context of text expressions in Twitter data to precisely classify the user emotions and outperformed the existing methods. The proposed REM method is expected to be an effective tool in emerging emotion

recognition-based applications and play a vital role in social communication.

This study has revealed the proficiency of REM managing emoticons, and at the same time, several research directions are opened from its motivational outcomes and gaps. REM is developed collecting Twitter data for only 16 selected emoticons related to the four emotions (Happy, Sad, Angry, and Love); and system including other emotional states (e.g., Disgust, Surprise) and more emoticons might be interesting. Another thing, the texts were limited in the selected blogs, information degraded due to emoticon removal in text-only REM, and finally, recognition performance with LSTM was poor without emoticons. It might be interesting research to investigate text and emoticon trade-off effects on REM performance. In addition, instead of LSTM, any other deep learning method (e.g., CNN) might also be investigated owing to achieve better classification performance. We wish to work in such directions for developing a more comprehensive REM in the future study.

References

[1] J. Islam, S. Ahmed, M.A.H. Akhand, N. Siddique, "Improved Emotion Recognition from Microblog Focusing on Both Emoticon and Text," in 2020 IEEE Region 10 Symposium (TENSYMP), IEEE: 778–782, 2020, doi:10.1109/TENSYMP50017.2020.9230725.

[2] L. Al-Shawaf, D. Conroy-Beam, K. Asao, D.M. Buss, "Human Emotions: An Evolutionary Psychological Perspective," Emotion Review, **8**(2), 173–186, 2016, doi:10.1177/1754073914565518.

[3] A.R. Avila, Z. Akhtar, J.F. Santos, D. OShaughnessy, T.H. Falk, "Feature Pooling of Modulation Spectrum Features for Improved Speech Emotion Recognition in the Wild," IEEE Transactions on Affective Computing, **12**(1), 177–188, 2021, doi:10.1109/TAFFC.2018.2858255.

[4] M.A.H. Akhand, S. Roy, N. Siddique, M.A.S. Kamal, T. Shimamura, "Facial Emotion Recognition Using Transfer Learning in the Deep CNN," Electronics, **10**(9), 1036, 2021, doi:10.3390/electronics10091036.

[5] G. Castellano, L. Kessous, G. Caridakis, Emotion Recognition through Multiple Modalities: Face, Body Gesture, Speech, Springer Berlin Heidelberg, Berlin, Heidelberg, Heidelberg: 92–103, 2008, doi:10.1007/978-3-540-85099-1_8.

[6] N. Alswaidan, M.E.B. Menai, "A survey of state-of-the-art approaches for emotion recognition in text," Knowledge and Information Systems, **62**(8), 2937–2987, 2020, doi:10.1007/s10115-020-01449-0.

[7] A. Java, X. Song, T. Finin, B. Tseng, "Why we twitter: understanding microblogging usage and communities," in Proceedings of the 9th WebKDD and 1st SNA-KDD 2007 workshop on Web mining and social network analysis - WebKDD/SNA-KDD '07, ACM Press, New York, New York, USA: 56–65, 2007, doi:10.1145/1348549.1348556.

[8] A. Ortigosa, J.M. Martín, R.M. Carro, "Sentiment analysis in Facebook and its application to e-learning," Computers in Human Behavior, **31**(1), 527–541, 2014, doi:10.1016/j.chb.2013.05.024.

[9] S. Gangrade, N. Shrivastava, J. Gangrade, "Instagram Sentiment Analysis: Opinion Mining," SSRN Electronic Journal, 2019, doi:10.2139/ssrn.3372757.

[10] M. Nam, E. Lee, J. Shin, "A Method for User Sentiment Classification using Instagram Hashtags," **18**(11), 1391–1399, 2015.

[11] M.Z. Naf'an, A.A. Bimantara, A. Larasati, E.M. Risondang, N.A.S. Nugraha, "Sentiment Analysis of Cyberbullying on Instagram User Comments," Journal of Data Science and Its Applications, **2**(1), 88–98, 2019, doi:10.21108/jdsa.2019.2.20.

[12] L. Huang, S. Li, G. Zhou, Emotion Corpus Construction on Microblog Text, 204–212, 2015, doi:10.1007/978-3-319-27194-1_21.

[13] R. Poonguzhali, V. Waldiya, S. Vinothini, K. Livisha, "Sentiment Analysis on LinkedIn Comments," International Journal of Engineering Research & Technology (IJERT), **6**(07), 2018.

[14] Z. Peng, Q. Hu, J. Dang, "Multi-kernel SVM based depression recognition using social media data," International Journal of Machine Learning and Cybernetics, **10**(1), 43–57, 2019, doi:10.1007/s13042-017-0697-1.

[15] S.R. Braithwaite, C. Giraud-Carrier, J. West, M.D. Barnes, C.L. Hanson, "Validating Machine Learning Algorithms for Twitter Data Against

Established Measures of Suicidality," JMIR Mental Health, **3**(2), e21, 2016, doi:10.2196/mental.4822.

[16] D. Gräbner, M. Zanker, G. Fliedl, M. Fuchs, Classification of Customer Reviews based on Sentiment Analysis, Springer Vienna, Vienna: 460–470, 2012, doi:10.1007/978-3-7091-1142-0_40.

[17] S. Shayaa, N.I. Jaafar, S. Bahri, A. Sulaiman, P. Seuk Wai, Y. Wai Chung, A.Z. Piprani, M.A. Al-Garadi, "Sentiment Analysis of Big Data: Methods, Applications, and Open Challenges," IEEE Access, **6**, 37807–37827, 2018, doi:10.1109/ACCESS.2018.2851311.

[18] S. Chaffar, D. Inkpen, Using a Heterogeneous Dataset for Emotion Analysis in Text, 62–67, 2011, doi:10.1007/978-3-642-21043-3_8.

[19] S. Nirenburg, K. Mahesh, Knowledge-Based Systems for Natural Language Processing., 1997.

[20] S.B. Kotsiantis, I.D. Zaharakis, P.E. Pintelas, "Machine learning: a review of classification and combining techniques," Artificial Intelligence Review, **26**(3), 159–190, 2006, doi:10.1007/s10462-007-9052-3.

[21] E. Batbaatar, M. Li, K.H. Ryu, "Semantic-Emotion Neural Network for Emotion Recognition from Text," IEEE Access, **7**, 111866–111878, 2019, doi:10.1109/ACCESS.2019.2934529.

[22] G. Yang, H. He, Q. Chen, "Emotion-semantic-enhanced neural network," IEEE/ACM Transactions on Audio Speech and Language Processing, **27**(3), 531–543, 2019, doi:10.1109/TASLP.2018.2885775.

[23] N. Colneric, J. Demsar, "Emotion Recognition on Twitter: Comparative Study and Training a Unison Model," IEEE Transactions on Affective Computing, **11**(3), 433–446, 2020, doi:10.1109/TAFFC.2018.2807817.

[24] A. Yousaf, M. Umer, S. Sadiq, S. Ullah, S. Mirjalili, V. Rupapara, M. Nappi, "Emotion Recognition by Textual Tweets Classification Using Voting Classifier (LR-SGD)," IEEE Access, **9**, 6286–6295, 2021, doi:10.1109/ACCESS.2020.3047831.

[25] K. Sailunaz, R. Alhajj, "Emotion and sentiment analysis from Twitter text," Journal of Computational Science, **36**, 101003, 2019, doi:10.1016/j.jocs.2019.05.009.

[26] M.S. Schlichtkrull, "Learning affective projections for emoticons on Twitter," in 2015 6th IEEE International Conference on Cognitive Infocommunications (CogInfoCom), IEEE: 539–543, 2015, doi:10.1109/CogInfoCom.2015.7390651.

[27] J. De Silva, P.S. Haddela, "A term weighting method for identifying emotions from text content," in 2013 IEEE 8th International Conference on Industrial and Information Systems, IEEE: 381–386, 2013, doi:10.1109/ICIInfS.2013.6732014.

[28] N. Chirawichitchai, "Emotion classification of Thai text based using term weighting and machine learning techniques," in 2014 11th International Joint Conference on Computer Science and Software Engineering (JCSSE), IEEE: 91–96, 2014, doi:10.1109/JCSSE.2014.6841848.

[29] Z. Yuan, M. Purver, "Predicting emotion labels for Chinese microblog texts," Studies in Computational Intelligence, **602**, 129–149, 2015, doi:10.1007/978-3-319-18458-6_7.

[30] F. Jiang, Y.-Q. Liu, H.-B. Luan, J.-S. Sun, X. Zhu, M. Zhang, S.-P. Ma, "Microblog Sentiment Analysis with Emoticon Space Model," Journal of Computer Science and Technology, **30**(5), 1120–1129, 2015, doi:10.1007/s11390-015-1587-1.

[31] L. Wikarsa, S.N. Thahir, "A text mining application of emotion classifications of Twitter's users using Naïve Bayes method," in 2015 1st International Conference on Wireless and Telematics (ICWT), IEEE: 1–6, 2015, doi:10.1109/ICWT.2015.7449218.

[32] J.K. Rout, K.K.R. Choo, A.K. Dash, S. Bakshi, S.K. Jena, K.L. Williams, "A model for sentiment and emotion analysis of unstructured social media text," Electronic Commerce Research, **18**(1), 181–199, 2018, doi:10.1007/s10660-017-9257-8.

[33] A. Hogenboom, D. Bal, F. Frasincar, M. Bal, F. de Jong, U. Kaymak, "Exploiting emoticons in sentiment analysis," in Proceedings of the 28th Annual ACM Symposium on Applied Computing - SAC '13, ACM Press, New York, New York, USA: 703, 2013, doi:10.1145/2480362.2480498.

[34] S. Hochreiter, J. Schmidhuber, "Long Short-Term Memory," Neural Computation, **9**(8), 1735–1780, 1997, doi:10.1162/neco.1997.9.8.1735.

[35] Full Emoji List, Available: https://unicode.org/emoji/charts/full-emoji-list.html, Accessed: March 31, 2021.

[36] Chollet François, Keras: The Python Deep Learning Library, 2015.

[37] D.P. Kingma, J. Ba, "Adam: A Method for Stochastic Optimization," 2014.

A S T E S

Performance of a Thermoelectric Cooler Box Powered Using Solar Panels with a Mini Pin Fin Heat Removal Unit

Mirmanto Mirmanto*, Syahrul Syahrul, Made Wirawan, Zulham Saputra

Mechanical Engineering Department, Engineering Faculty, University of Mataram, Mataram, 83125, Indonesia

A R T I C L E I N F O	A B S T R A C T
	Experiments to investigate the performance of a thermoelectric cooler box powered using a solar panel with a mini pin fin as the heat removal unit was conducted at the un-condition ambient temperature. Due to solar power, the power given to the thermoelectric on different days was different. However, the power on the day of the experiment was nearly stable because the solar panel was connected to a battery. The parameters tested were the cooler box temperatures and COP (coefficient of performance)and there were four Cases examined in this study: Case A (the cooler box was empty), Case B (the cooler box was filled with water of 3000 ml), Case C (the cooler box was charged with 6000 ml of water), and Case D (the cooler box was filled with 9000 ml of water). For these experimental conditions, the maximum COP was 0.51. This was obtained for the run with 9000 ml of water. Increasing the water volume raises the temperatures inside the cooler box and the optimum performance is discussed.

1. Introduction

This study was performed due to the goods transportation requirements. The transportation of goods, blood and vaccines needs portable refrigerators. Thermoelectric (TE) cooler boxes seem like becoming an option. This was owing to the reports presented by previous researchers, e.g. [1-5]. The authors elucidated that the TE cooler box was much lighter, compact, no leakages, durable and easier to maintain. However, there is a limitation of this cooler type, namely low COP, even its COP is always less than 1. This indicates that studies in this field are still wide open to increase the COP.

Several researchers have been trying some ways to increase the TE cooler performances. The COP can be raised by advancing the quality of TE materials, differing the application procedures, and wangling the unit of heat dissipation. The research on TE materials is devoted to increasing the COP. Nevertheless, in terms of material, the TE development is slow. Good material for TE is indicated by its figure of merit. Bismuth telluride (Bi_2Te_3) is widely employed in TE generators and coolers for low temperature. Bi_2Te_3 possess a maximum value of ZT~1 as reported in [6, 7]. According to the authors in [8], if the figure of merit can be increased to 2 or 3, the TE cooling can be cut-throat with compression systems. Furthermore, if the figure of merit is

as big as 6, then the TE cooling system can be used for cryogenic purposes. Due to the low development of TE material, increasing COP through applications has been becoming a choice. Some researches on the TE cooling application have been performed by several researchers, e.g. [1, 4, 5, 9]. However, the authors still obtained low COP (even less than 1). One parameter that can influence the COP of the TE cooling systems is the heat removal unit. In [10], the authors studied several heat removal units. They used heat removal units: a heat sink fin fan and a double fan heat pipe. Nevertheless, they still had a small COP.

Authors in [1] studied TE cooling using a mini channel and the power used to operate the TE cooling was a solar panel. They found that solar panel was promising power for the TE cooling system in the future. Furthermore, as electricity is expensive in several countries, e.g. Indonesia, renewable energy may be important to be applied. The good thing about using the solar panel is that this energy is free. Therefore, in this study, the energy used is generated using solar panels.

The theory of mini and microchannels has shown better heat transfer and more effectiveness. The studies of the micro and mini channels were conducted e.g. [11, 12]. The authors found that micro and mini channels could increase heat transfer. Nevertheless, again, in [1], the authors still obtained the COP of less than 1, although they already used a mini channel as the heat removal unit.

*Corresponding Author: M. Mirmanto, Jl. Majapahit, no. 62, Mataram, +6282111738971, m.mirmanto@unram.ac.id

Table 1: COP attained from available literatures related to the unit of heat dissipation

Referenses	Study	Heat removal unit	COP
[1]	TE cooler box powered using solar panels with a mini channel.	Mini channel	0.01-0.76
[10]	Experimental cooler box using two different heat dissipation units	Heat sink with fans Double fan heat pipe	0.002-0.02
[17]	Design and experimental solar TE refrigerator	Heat sink with fans	0.16
[18]	TE device for small scale space conditions	Heat sink with fans	0.43-0.45
[19]	TE refrigerator performance	Heat sink with fans	0.64
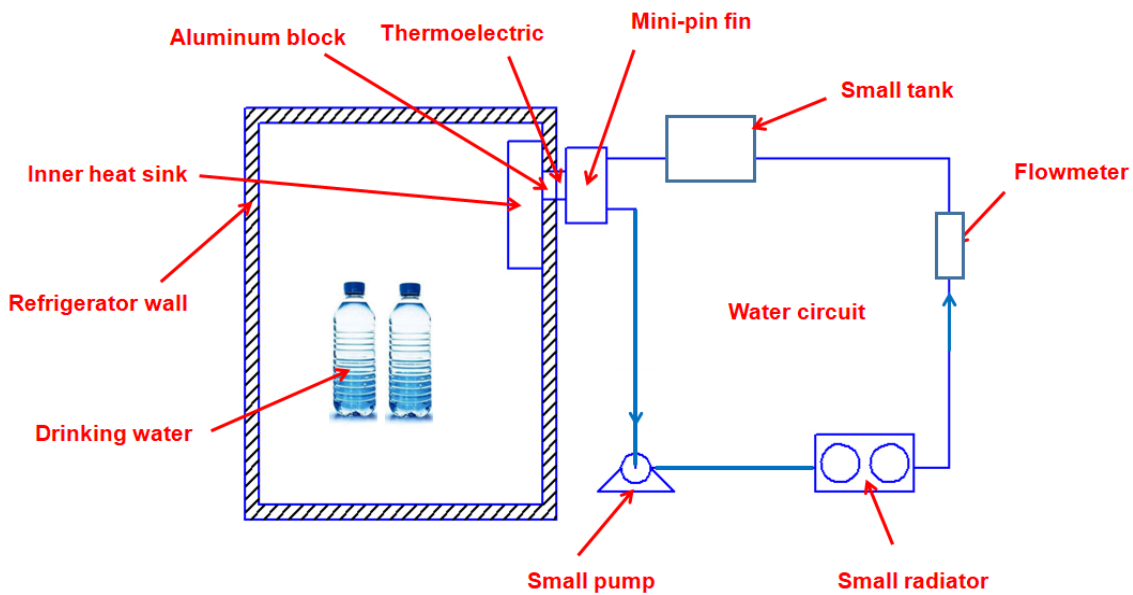
Figure 1: Schematic diagram of the apparatus

Because the COP gained in the previous study was still low, so this study tried using a mini pin fin. Studying mini or micro pin fin was ever conducted by several previous researchers, e.g. [13-15]. However, the authors in [16] stated that the mini pin fin could transfer high heat flux than conventional heat exchanger or mini channels. Owing to their encouragement, this current study used a mini pin fin as the heat removal unit. It was expected that the COP of the TE cooler box examined was higher than the COP obtained in the previous studies. This study was just to investigate the performance of the cooler box powered using solar panels with a mini pin fin as the heat removal unit. The study using a mini pin fin as a heat removal in a TE application has not been investigated yet. As shown in Table 1, none of the previous studies exposes the use of a mini pin fin as the heat removal unit at TE cooling systems. Hence, the novelty of this study is the heat removal unit that is constructed from a mini pin fin; it also contributes to the TE cooling system studies.

This study is a continuation of the previous study entitled performance of a large thermoelectric refrigerator power by a solar panel [1]. The difference in this study from the previous

study is the heat removal unit. In the previous study, the heat removal unit was constructed of a mini channel, while in this study the heat removal unit used was a mini pin fin.

2. Research Method

2.1. Experimental Set-up

This work is a part of TE cooling system studies using solar panels as power. This study is aimed to investigate the ability of a TE cooler run by solar panels with a mini pin fin as the heat dissipation unit, and to know the effect of water volume on the COP of the system. In the previous study, the heat removal unit was a minichannel, while in this recent study; the heat removal unit was a mini-pin fin. Nevertheless, the focus of this study was the performance of the TE cooler due to the heat removal unit. The study used a test rig shown in Figure 1. The test rig was also used in [1]. It consisted of a box, a TE, water, solar panels, a mini-pin fin, a pump, a radiator, a small tank, meter flow, a battery, a solar charger, and a data logger National Instrument (cDAQ-NI 9174). Similar to the previous study, all temperatures were measured utilizing thermocouples (K-type) that were calibrated in

an oil bath with an accuracy of ± 0.2°C, and the electrical power employed was assessed using a Vichy Vc8145 digital multimeter. The accuracy of ampere and volt measurement was 0.1% reading and 0.05% reading. Meanwhile, the water flow passing the mini-pin fin was calculated using FLR1000 flowmeter with an accuracy of ± 0.2 g/s.

As the electric current surges into the TE, the hot side temperature of the TE increased drastically. This increased temperature should be maintained so that it did not exceed 65°C, e.g. using water flow. If the hot side temperature was low, the cold side temperature was low too. That was why using TE as the cooler machine could be successful in cold countries because the environmental temperature was already low.
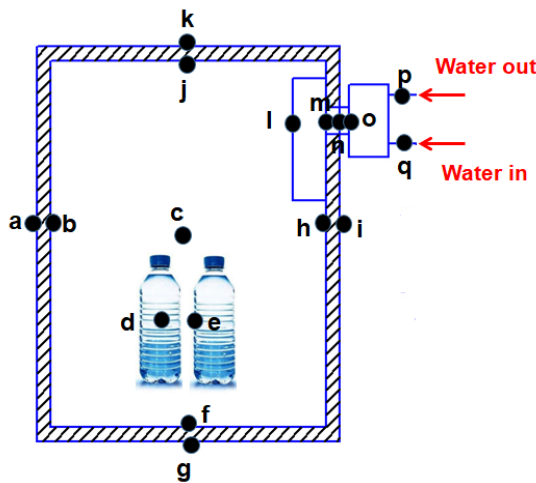
Figure 2: Thermocouple placements

Finally, the heat from the TE was taken away by the water flowing inside the mini pin fin towards the small radiator. The heat was then discharged from the small radiator into the ambient through a finned heat exchanger or radiator. Then the water came back to the small tank. The source of the electricity was solar panels; therefore, it fluctuated. When the sky was clear, the power

was large and vice versa. However, these fluctuations were eliminated by using a battery.

Thermocouple placements can be seen in Figure 2. Their locations are noted using the letters a-q. Meanwhile, the electrical flow diagram is presented in Figure 3. Two pieces of solar panels, each with 100WP power, were utilized and one free maintenance battery with a voltage of 12 V, and a current of 100 AH was employed. However, the analysis here was focused on the performance of the TE cooler only, while a depth analysis of the mini-pin fin and solar panel was not given in this study.

Parameters investigated were (1) heat absorbed by the TE (noted by Qc), (2) the power is given to the TE noted, P_T, and (3) COP. The heat absorbed by the TE (Qc) comprised of heat from the air, water and bottles inside the cooler box. The heat from the air can be predicted using equation (1). This equation can be found in [4, 10, 20]. The experimental uncertainties and conditions are listed in Table 2.

$$E_{a(i)} = m_a c_p \left(T_{(i-1)} - T_{(i)} \right) \tag{1}$$

E_a is the energy removed from the air inside the cooler box (J), m_a represents the air mass (kg), c_p is the specific heat (J/kg°C) and T is the temperature of the air. To change the energy into the heat rate, eq. (2) can be used, this equation can be obtained in [1, 4-5, 20-21].

The cooler box size used was 0.317 m x 0.235 m x 0.447 m. The mini-pin fin was bought from an online shop and this was usually used in the CPU for cooling the processor. The variations of investigated parameters are Case A (the cooler box is empty), Case B (the cooler box is filled with bottles containing 3000 ml of water), Case C (the cooler box is filled with bottles comprising 6000 ml of water) and the last is Case D (the cooler box is filled with bottles consisting 9000 ml of water).

$$Q_a = \frac{\sum_{1}^{n} E_{a(i)}}{t_{(n)}} \tag{2}$$
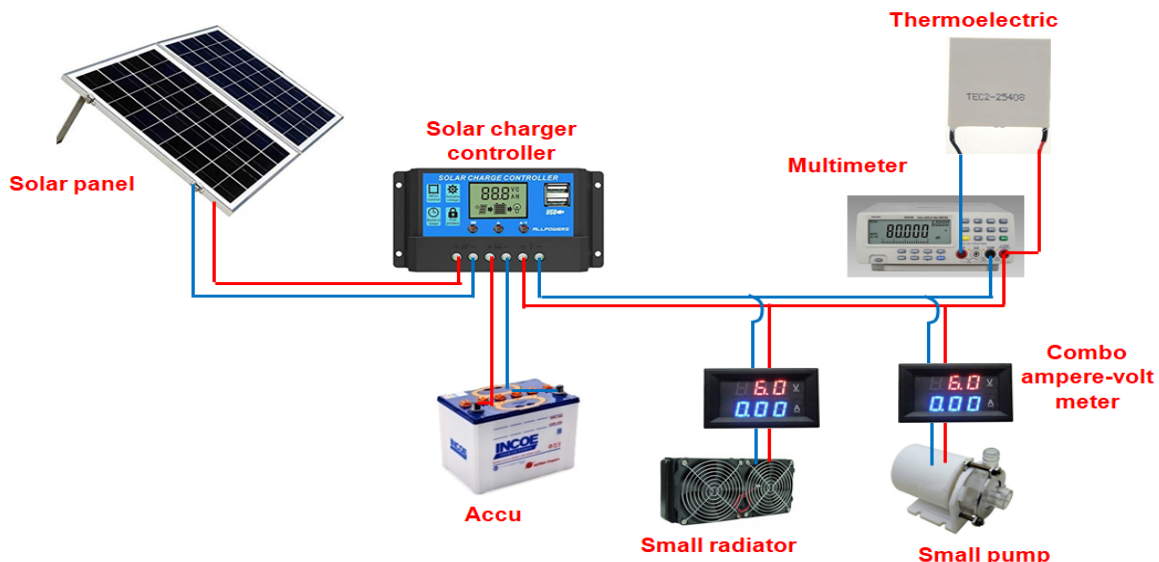
Figure 3: Electrical flow diagram

Table 2: Uncertainty and the operational conditions

No.	Parameter	Uncertainty	Range of measurements
1	Temperature (T)	± 0.2°C	9.42°C – 48.75°C
2	Cooling capacity (Q_c)	± 0.12 W	2.70 W – 20.63 W
3	Power input (P_T)	± 2 W	52.74 W – 85.68 W
4	Pump power (P_p)	± 0.21 W	4.86 W – 9.65 W
6	Power input for system (P_s)	± 2.8 W	65.9 W – 100.7 W
7	COP	± 0.01	0.041-0.34

Q_a is the heat rate taken from the air (W), t is the time of the running cooler box (s). The energy and the heat rates absorbed by the TE from the water and bottles also can be estimated using equations (1-2) by changing the subscript a to w and b. For water, the energy and the heat rate are noted as E_w and Q_w, while for the bottles, they are designated as E_b and Q_b. Despite Q from air, water and bottles, Q also came from the ambient through the cooler box walls. This type of heat rate is called the conduction heat rate.

$$Q_k = kA\frac{T_{wo} - T_{wi}}{L} \qquad (3)$$

where Q_k is the conduction heat (W), A is the heat transfer area (m²), L is the wall thickness (m), T_{wo} and T_{wi} are the outer and inner wall temperatures (°C). The total heat rate is noted by Q_c, it is the cooling capacity (W). Q_c is expressed in equation (4), which can be found in Changel and Boles [22].

$$Q_c = Q_a + Q_w + Q_b + Q_k \qquad (4)$$

Then the COP is the performance of the TE cooler box that can be expressed as

$$COP = \frac{Q_c}{P_T} \qquad (5)$$

$$COP_s = \frac{Q_c}{P_s} \qquad (6)$$

COP_s is the coefficient of performance based on all powers supplied to the experimental system. P_T is power flowed to the thermoelectric module (TEM) in watt, in the experiment it was measured directly using a multitester. P_s is the total power given

to the experimental system such as power for TEM, pump and heat exchanger. All powers required were measured directly. The TE specification used in this study is shown in Table 3.

Table 3: TEM specification

Model	TEC2-25408
Voltage	15.54V
Vmax (V)	15.4V
Imax (A)	8 A
Qmax (W)	65 W

3. Results and Discussion

Experimental results of a TE cooler box performance are presented in the form of graphs. Some recorded temperatures of air, water and bottle are reported in Figure 4. Figure 4 indicates that the ambient temperature increases for all Cases. This phenomenon was due to the time of experiments. The experiments were conducted from 9 o'clock until 12 o'clock local time. Therefore, the ambient temperature increased because the sun elevates with time. At the same time, the ambient temperature was not conditioned. However, the air temperature inside the cooler box for Cases A and B decreased with time, while for Cases C and D remained constant. For Cases C and D, the cooler box could no longer decrease the temperature inside. This was due to the performance of the cooler box. Increasing the volume of water inside the cooler box, the cooler box could not decrease the water temperature further. For Cases A and B, the phenomenon was also found in the previous studies, e.g. [1, 4-5, 19].
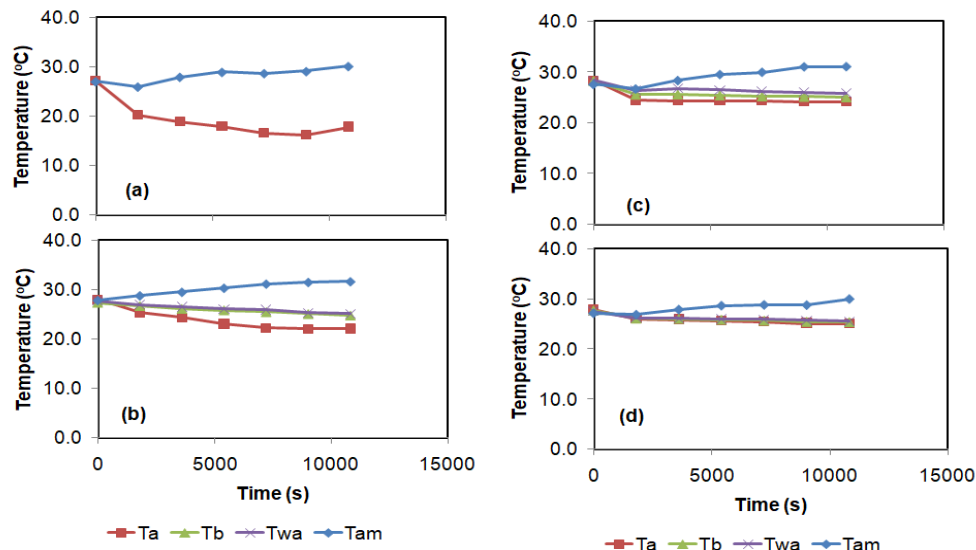
Figure 4: Recorded temperatures of air, water, and bottle inside the cooler box; (a) Case A, (b) Case B, (c) Case C, and (d) Case D

The increased ambient temperature affect greatly the cooling value. The estimated cooling value Q_c is presented in Figure 5. For all Cases, the Q_c increased with time. This was due to the presence of the conduction heat transfer from the ambient to the inner box through the cooler box walls. Increasing the ambient temperature levelled the difference temperature between the inside and ambient temperatures. Using equation (3) the obtained conduction heat rate increased. The increased conduction heat rate was also found in the previous studies [1, 4-5]. When Q_c was dominated by the conduction heat transfer rate, then it increased with time. Nevertheless, in this study, the experiments were run until noon local time, while in [4], the experiments were conducted for 7 hours. Therefore, they found that after the maximum value, the Q_c was constant. The problem in this current study was that in the afternoon the sun was covered by the building and trees so that the experiments were stopped. Nevertheless, Q_c could not be compared because that was obtained on different days as the cooler box was operated using solar panels. The reason for this was the power given to the system. It could be different on different days.

Another parameter investigated in this study was the COP. Although COP was obtained on different days, it could be compared because COP was cooling capacity per 1-watt power given to the TEC module, see equation (5). The relationship between COP and observation time is presented in Figure 6. The trend of the COP was different from that obtained by researchers in [4]. In [4], the ambient temperature remained constant, it did not increase and the COP increased and then after the peak, it decreased. In this study, the COP did not achieve the maximum value yet. However, Case D had the highest COP. The average COP of Case D was 0.51. Increasing the water volume elevated the COP. Comparing the COP of this study and the previous study indicated that using mini-pin fin got a lower COP than using a mini channel. This comparison did not agree with the results concerning mini and micro pin fins in [13-16]. Nevertheless, the problem, as explained above, was due to the imperfect placement of the mini pin fin. Also, in the previous study, the size of the mini channels was a bigger little bit.
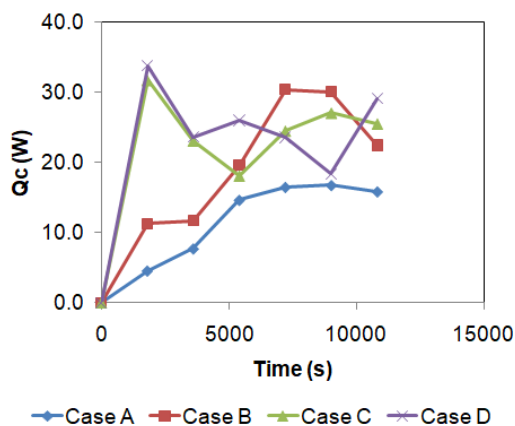
Figure 5: Relationship between Q_c and observation time

Additional data given in this study were the performance of the mini-pin fin, which was indicated by the mini pin fin efficiency. The experimental mini-pin fin efficiencies were found ranging from 82% - 93%. The efficiency was important to be

reported in this study to know the performance of the mini-pin fin. Those efficiencies were already good, however, the mini-pin fin installation was not perfect. It was difficult to instal the mini pin fin perfectly on the hot side surface of the TEC because between the mini pin fin and the hot side of the TEC, a thermocouple should be placed to measure the hot side temperature of the TEC.
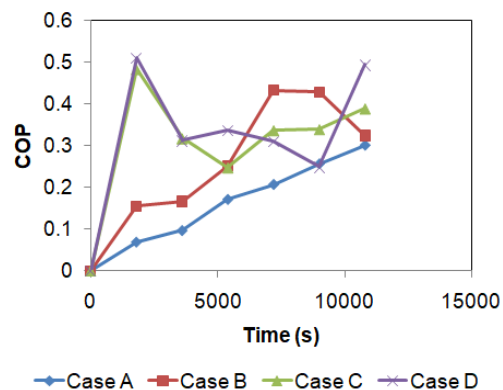
Figure 6: Relationship between COP and time

As the cooler box was run using solar panels, the recorded solar power was presented in Figure 8. Solar power, in general, increased with time. This was a similar trend to the Q_c and COP. This was due to the sun that rose along the time, especially in this study, the experiments were conducted from 09.00 to 12.00 local time. However, at midnight local time, all recorded solar powers decreased. This phenomenon was due to surrounding conditions. The solar panels were placed near the building and trees so that starting at 11.30 local time, the solar power panels were shaded. This was also the reason for the short time of running experiments. Due to the sun shaded, the experiments were stopped at 12 local time.
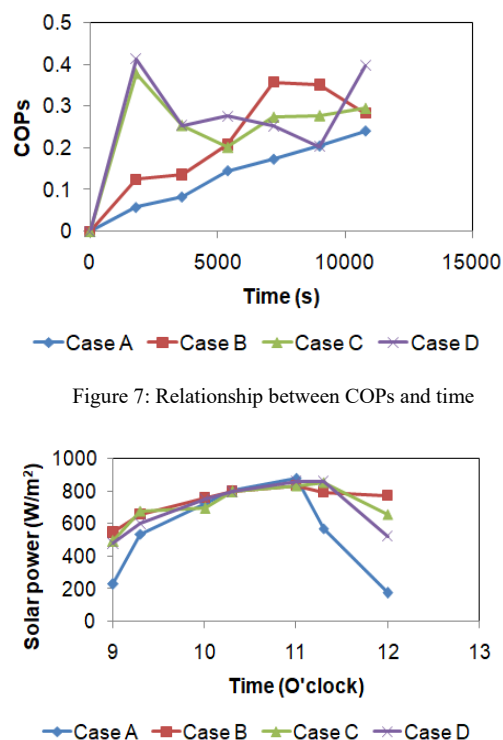
Figure 7: Relationship between COPs and time
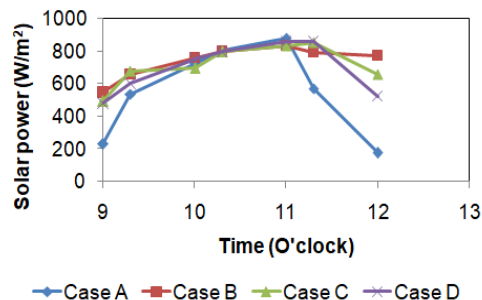
Figure 8: Relationship between solar power and observation time

4. Conclusion

A continuation study to assess the performances of a TE cooler box powered using solar panels with a mini pin fin as the heat removal unit was performed. Increasing the water volume raises the COP and the cooler temperatures. The optimal performance of the TE cooler box is Case B. COP increases with time for these experimental conditions. COP is lower than that obtained using the mini channel heat removal unit in the previous study. The maximum COP is 0.51 and the lower temperature obtained is 18°C. The lower COP is due to the imperfect placement of the heat removal unit. Further experiments need to be conducted to clarify the performance of the mini-pin fin in transferring heat. The parameter that can be compared is COP, but not the others. The solar panels are adequate to power the TE cooler box.

Acknowledgement

References

[1] M. Mirmanto, S. Syahrul, M. Wirawan, I.M.A. Sayoga, A.T. Wijayanta, I. Mahyudin. "Performance of a thermoelectric powered by solar panel for a large cooler box" Advances in Science, Technology and Engineering Systems Journal, **5**, 325-333, 2020. Doi: 10.25046/aj050141.

[2] M.K. Rawat, H. Chattopadhyay, S. Neogi, "A Review on developments of thermoelectric refrigeration and air conditioning systems: A novel potential green refrigeration and air conditioning technology," Int. J. Engineering Technology and Advanced Engineering, **3**, 362-367, 2013.

[3] B.V.K. Reddy, M. Barry, J. Li, M.K. Chyu, "Enhancement of thermoelectric device performance through integrated flow channels," Frontiers in Heat and Mass Transfer, **4**, 1-7, 2013. doi: 10.5098/hmt.v4.2.3001

[4] M. Mirmanto, S. Syahrul, Y. Wirdan, "Experimental performances of a thermoelectric cooler box with thermoelectric position variations," Engineering Science and Technology, An International Journal, **22**, 177-184, 2019. doi: 10.1016/j.jestch.2018.09.006

[5] Mirmanto, I.W. Joniarta, A.T. Wijayanta, Pranowo, M. Habiburrahman, Experimental performance of a cooler box with heat dissipation unit variations," International Journal of Heat and Technology, **37**, 991-998, 2019. doi: 10.18280/ijht.370408

[6] G. Min, D.M. Rowe, "An improved model for calculating the coefficient of performance of a peltier module," Energy Conversion and Management, **41**, 163–171, 2000. doi: 10.1016/S0196-8904(99)00102-8

[7] G. Min, D.M. Rowe, "Symbiotic application of thermoelectric conversion for fluid preheating/power generation," Energy Conversion and Management, **43**, 221–228, 2002.

[8] S.B. Riffat, X. Ma. "Improving The Coefficient of Performance of Thermoelectric Cooling Systems: A Review" Int. J. Energy Res **28**, 753–768, 2004. doi: 10.1002/er.991

[9] I. Bizzy, R. Apriansyah, "Kaji eksperimental kotak pendingin minuman kaleng dengan termoelektrik bersumber dari arus DC kendaraan dalam rangkaian seri dan paralel," Seminar Nasional Tahunan Teknik XII, Bandar Lampung, 2013.

[10] M. Mirmanto, I.B. Alit, I.M.A. Sayoga, R. Sutanto, N. Nurchayati, A. Mulyanto, "Experimental cooler box performance using two different heat removal units: A heat sink fin-fan, and a double fan heat pipe," Frontiers in Heat and Mass Transfer (FHMT) **10**, 1-7, 2018. Doi: 10.5098/hmt.10.34

[11] J. Hejcik, M. Jicha. "Single-phase Heat Transfer in Minichannels" EPJ Web of Conference, 67, 1-4, 2014. Doi: 10.1051/epjconf/20146702034

[12] T. Yeom, T. Simon, T. Zhang, M. Zhang, M. North, T. Cui, "Enhanced heat transfer of heat sink channels with micro pin fin roughened walls," Int. J. of Heat and Mass Transfer, **92**, 617–627, 2016. doi: 10.1016/j.ijheatmasstransfer.2015.09.014

[13] S.B. Chin, J.J. Foo, Y.L. Lai, T.K.Y. Yong. "Forced Convective Heat Transfer Enhancement with Perforated Pin Fins" Heat Mass Transfer, 49, 1447–1458, 2013. doi: 10.1007/s00231-013-1186-z

[14] Y. Peles, A. Kosar, C. Mishra, C.J. Kuo, B. Schneider, "Forced convective heat transfer across a pin fin micro heat sink," International Journal of Heat and Mass Transfer, **48**, 3615–3627, 2005. Doi: 10.1016/j.ijheatmasstransfer.2005.03.017

[15] O. Khonsue, "Enhancement of the forced convective heat transfer on mini-pin fin heat sinks with micro spiral fins," Heat Mass Transfer, 1-8, 2017. doi: 10.1007/s00231-017-2159-4

[16] A.S. Tijani, N.B. Jaffri, "Thermal analysis of perforated pin fin heat sink under forced convection condition," Procedia Manufacturing, **24**, 290-298, 2018. Doi: 10.1016/j.promfg.2018.06.025

[17] S.A. Abdul-Wahab, A. Elkamel, A.M. Al-Damkhi, I.A. Al-Habsi, H.S. Al-Rubai'ey', A.K. Al-Battashi, A.R. Al-Tamimi, K.H. Al-Mamari, M.U. Chutani, "Design and experimental investigation of portable solar thermoelectric refrigerator," Renewable Energy, **34**, 30-34, 2009. doi: 10.1016/j.renene.2008.04.026

[18] M. Gillott, L. Jiang, S. Riffat, "An investigation of thermoelectric cooling devices for small-scale space conditioning applications in buildings," International Journal of Energy Research, **34**, 776-786, 2010. Doi: 10.1002/er.1591

[19] S. Jugsujinda, A. Vora-ud, T. Seetawan, "Analysing of thermoelectric refrigerator performances," Procedia Engineering, **8**, 154-159, 2011. doi: 10.1016/j.proeng.2011.03.028

[20] J.P. Holman, Heat transfer, McGraw-Hill Education (India) Pvt Limited, 2002.

[21] F.P. Incropera, D.P. Dewitt, T.L. Bergman, A.S. Lavine, Fundamentals of heat and mass transfer, Sixth Edition, John Wiley and Sons, USA, 2006.

[22] Y.A. Cengel, Heat transfer a practical approach, 2nd Edition, Mcgraw-Hill (Tx), 2002.

Nomenclature

A	heat transfer area, m²
COP	coefficient of performance
c_p	heat capacity, $J.kg^{-1}.°C^{-1}$
E	energy, J
i	segment
n	end of segments
I	current, A
k	thermal conductivity, $W.m^{-1}.°C^{-1}$
L	wall thickness, m
P	power, W
Q	heat, W
t	time, s
T	temperature, ºC
TEC	thermoelectric cooler
V	voltage, V

Subscript:

a	air
am	ambient
b	bottle
c	cold side
wi	inner wall
wo	outer wall
k	conduction
p	plastic
s	system
T	power to TEM
w	water

ASTES

The Operational Performance of Mass Transportation Before Covid-19 and New Normal Life: Case Study BRT TransJateng, Central Java

Juanita Juanita[1,*], Titus Hari Setiawan[2], Anwar Ma'ruf [3]

[1]*Department of Civil Engineering, Universitas Muhammadiyah Purwokerto, Purwokerto, 53182, Indonesia*

[2]*School of Architecture, Planning, and Policy Development, Bandung Institute of Technology, Bandung, 40132, Indonesia*

[3]*Department of Chemical Engineering, Universitas Muhammadiyah Purwokerto, Purwokerto, 53182, Indonesia*

A R T I C L E I N F O	A B S T R A C T
	This article examines the operational performance of Bus Rapid Transit (BRT) before the pandemic and a new normal life. Overview of BRT operational performance in terms of the number of passengers transported, load factor and operating ratio. The method used is to compare the conditions before the pandemic and the new era of life. The findings of overall operations performance have decreased since the pandemic. However, BRT operations services are keep running by prioritizing health protocols. Efforts to control the spread of Covid-19 in BRT operations carried out by the policy steps presented. The government needs effort and consistency with BRT services in community services and strategies to prevent the spread of Covid-19.

1.   Introduction

The development of the city must be in line with the increase in good public transport. The role of the Government needed in improving public transport services. The operation of Bus Rapid Transit (BRT) in Indonesia regulated Law number 22 of 2009 concerning traffic. The BRT a public transport with economy class fares on routes subsidized by the Government or Local Government. Improving public transport performance requires attention to a harmonious subsystem and an increase in infrastructure development, service levels and policy support [1].

December 2019, the first time it identified that Covid-19 an impact on various sectors, especially the transportation sector. The transport sector affects service performance and health risks, financial sustainability, social equality and sustainable mobility [2]. The operational strengths and weaknesses of BRT contribute to overcoming and improving operations [3].

The purpose of the article is to reveal the operational performance of BRT before the pandemic and new normal life in terms of transported passengers, load factor and operating ratio. Implemented policies and efforts made by local government in preventing the spread of Covid-19 that expected to contribute to

the planning of BRT development in the adaptation of the new normal life in small and medium-sized cities.

2.   Study Context

BRT Trans Jateng is an integrated inter-city bus rapid service in the Central Java Province of Indonesia. BRT services operated under the Central Java Transportation Agency, where the operating system adopts Trans Jakarta and Trans Semarang services. Figure 1 describes the locations where the three BRT routes operate, namely in the province of Central Java. The routes studied here are the Purwokerto - Purbalingga route, the Semarang - Kendal route and the Semarang - Bawen route. The Purwokerto - Purbalingga route as corridor II is in Banyumas Regency which connects the city of Purwokerto to Purbalingga. The Semarang - Kendal route is corridor III continued to the Semarang - Bawen route. In general, the description of the three routes presented in Table 1. The total population of Central Java Province in 2020 is 36,516,035 people. The resident of the regency/city where the BRT operates is Kendal Regency 1,018,505 residents, Semarang Regency 1,053,094 residents, Purwokerto City 229,271 residents and Purbalingga Regency 998,561 residents [4], [5]. Referring to the criterion of small, medium and large cities [7], Purwokerto is in the small city category, while Purbalingga, Semarang and Kendal are in the medium city category.

*Corresponding Author Juanita Juanita, Department of Civil Engineering, juanitamstr@gmail.com

Population density over time series can assist policymakers in making adjustments to motivate policy effectiveness [6]. BRT operations affect urban development around systems that have high technical and performance characteristics [7]. The principle of developing the Trans Jateng BRT by the Regional Government focuses on the main corridors of two districts/cities so that connectivity built between the main path which can trigger changes in the behavior of private vehicle users to switch to public transportation through public transport services that are better than what was before (paratransit system).

Figure 1: Study area: Central Java Province

3. Methods

The paper examines the BRT system in Indonesia, especially in small and medium-sized cities in Central Java Province during the pandemic and the new normal life. The BRT route is in three corridors in three districts/cities which an empirical approach was carry in achieving the research objectives. The stages taken are data collection, data processing and analysis. Data on the number of passengers, load factor, vehicle operating costs and revenue are secondary data obtain from the Central Java Transportation Agency. Comparative data analysis carried to see the comparison between the pandemic era and the new normal, namely the number of passengers transported, load factor and operating ratio. The load factor shows the level of operational effectiveness of the BRT. The low load factor indicates less efficient operation. The operating ratio used to evaluate the impact of BRT operations as an economic indicator [8]. Also, the context of Government policy in providing BRT services during the pandemic and new normal is discussed here as the Government's efforts to control the spread of Covid-19.

4. Results

4.1. Corridor overview

In general, an overview of the three routes presented in Table 1. The longest operating route from the three corridors is Semarang - Bawen and the most recently operated is Semarang - Kendal. The tariff setting for the three corridors follows a flat-rate system, much closer to the same as IDR 2000 for students and IDR 4000 for public per trip. Moving or transit corridors are subject to applicable fees.

Especially for workers, the tariff is the same as for students. The requirements for passengers must show their employment card, clarified ID Card and work uniform when making payments.

Figure 2 shows the routes and shelters traversed by the Semarang - Bawen and Semarang Kendal routes. In Figure 2 The

Semarang - Bawen route (a) connects the city of Semarang from Tawang station to Bawen at the Bawen terminal via 71 shelters.

Table 1: Technical overview of the three BRT routes before the pandemic

	Corridor I	Corridor II	Corridor III
Route	Semarang – Bawen	Purwokerto – Purbalingga	Semarang – Kendal
Distance (km) round-trip	36,5	33,5	25,5
Rates (IDR)	Students: 2000 General: 4000	Students: 2000 General: 4000	Students: 2000 General: 4000
Shelter	71	32	47
Total fleet	26	14	14
launched operationally	07 July, 2017	13 August, 2018	15 October, 2020
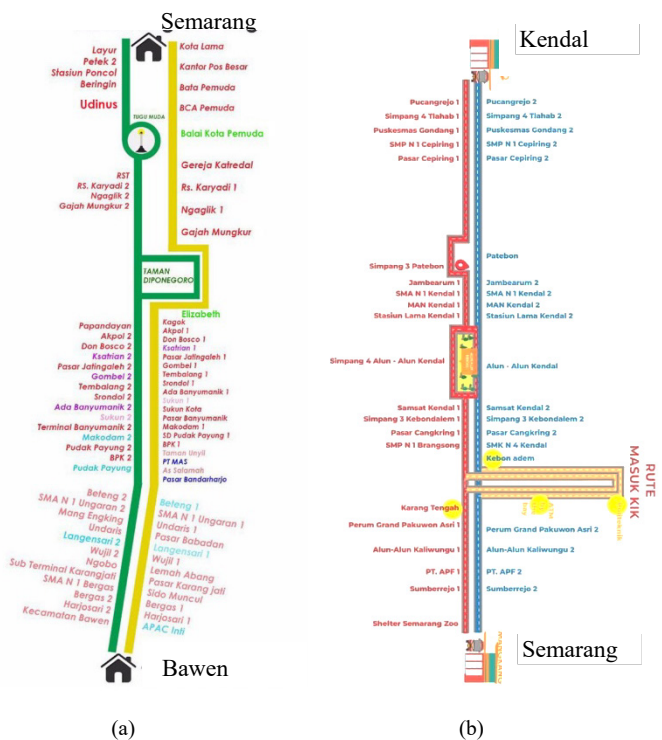
Figure 2: Semarang – Bawen (a) and Semarang - Kendal Routes (b)

The Semarang - Kendal route (b) starts / ends from Mangkang Terminal to Bahurekso Terminal. This route serves the Kendal industrial area with 47 bus-stop for boarding and boarding passengers. Meanwhile, Figure 3 the Purwokerto - Purbalingga route through 32 bus-stop. BRT operational performance is in the medium category when viewed from the condition shelters and the traffic space, especially the Purwokerto - Purbalingga corridor [9].

During the pandemic period, to prevent the spread of Covid-19, since April 2020, the Semarang - Bawen route has been changing, especially on Saturdays and Sundays. The closure of the protocol roads was carried out in the city of Semarang by the City Transportation Agency. Some of the bus stops are not active during the transfer, namely the "Balaikota" bus stops. The Semarang - Bawen route for boarding and disembarking passengers are carried out at several bus stops, purchasing tickets on the bus / on the bus stop by officers. Meanwhile, the Purwokerto - Purbalingga route

has diverted due to the closure of several roads. The impact is that two bus stops are not functioning. However, since February 27, 2021, all bus stops can functionalize to hop on and off passengers.

Figure 3: Purwokerto – Purbalingga route

4.2. BRT operational performance

Figure 4, Figure 5, Figure 6 shows the fluctuation of daily passenger in three corridors.
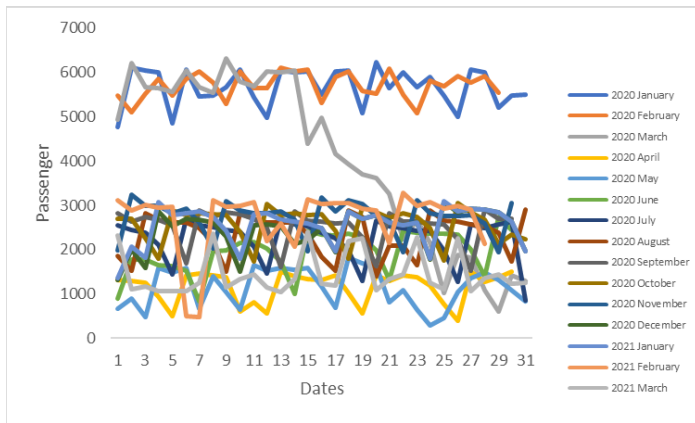
Figure 4: The daily travel in the Semarang – Bawen route

Figure 4 shows daily passenger fluctuations for the Semarang – Bawen route. In March 2020, since the announcement of the first case of Covid-19 in Indonesia, on March 9, the highest daily passengers were 6318 passengers, which decreased drastically to 607 passengers on March 29. But during 2020, the lowest number of passengers transported was 297 passengers on May 24. In 2021, February 24, since the Central Java "stay at home" program, passengers fell drastically and were the lowest on February 7 at 470 passengers, but rose again to reach the highest peak on February 22 at 3292 passengers.
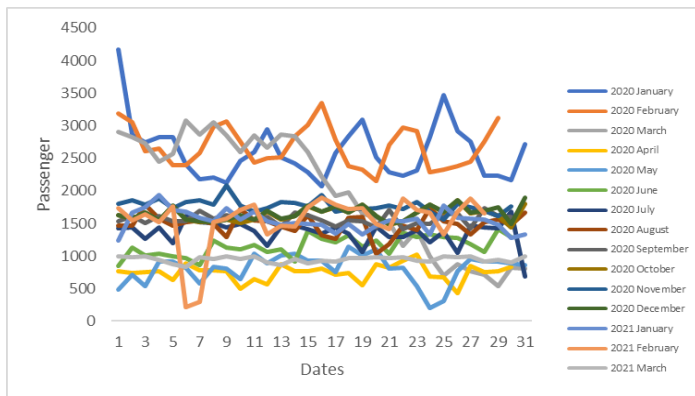
Figure 5: The daily travel in the Semarang – Kendal route

Figure 5 shows the daily passenger fluctuation of the Semarang – Kendal route. The highest number of daily passengers on the Semarang - Kendal route on January 1, 2020, were 4172 passengers. On March 29, 2020, daily passengers reached 539 passengers and reached the lowest position on May 24 at 203 passengers. In 2021, February 6, passengers dropped to 221 passengers but rose again on February 16, at 1902 passengers.
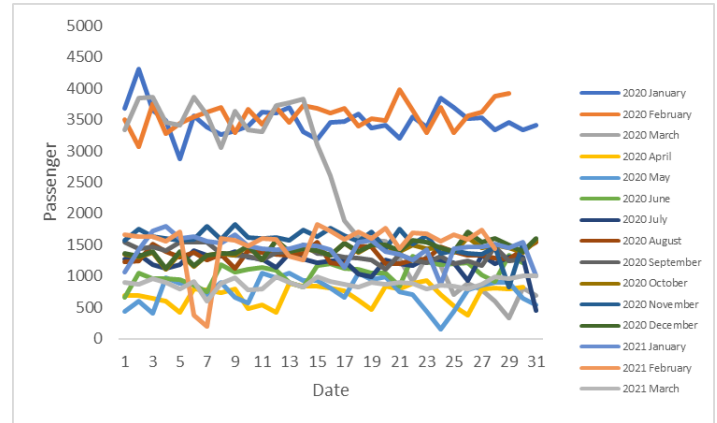
Figure 6: The daily travel in the Purwokerto –Purbalingga route

Figure 6 shows the daily passenger fluctuation of the Purwokerto - Purbalingga route. In 2020, the highest daily passenger on January 2 was 4304 passengers. On March 29, 2020, daily passengers reached 337 passengers. The lowest position on May 24 was 150 passengers. In 2021, daily passengers hit their lowest point on February 7 at 198 passengers but rose to their highest peak on February 15 at 1828 passengers.

Since the implementation of social distancing, of the three routes, that the lowest passengers, the Purwokerto - Purbalingga route was 150 passengers in May 2020.

Figure 7 shows the total passengers in the three corridors. In Indonesia, since March 2020, the first confirmed case of Covid-19, especially in the three corridors, has resulted in a decrease in the number of passengers. April 2020 saw was the lowest decrease in the number of passengers reaching 63% - 72%. Compared to other countries such as Budapest, Hungary, there is a decrease in demand for public transportation services by 80% [10]. In India, 5.3% of people switch to public transport during the transition period [11].
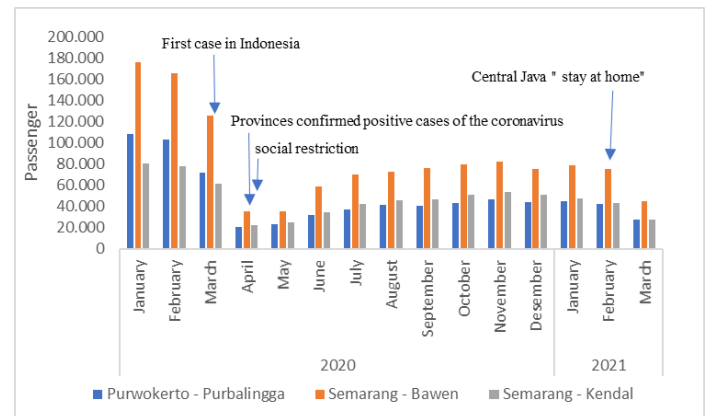
Figure 7: Total passengers

In 2020, the average demand growth for the Purwokerto - Purbalingga route (- 2%), the Semarang - Bawen route (- 1%) and the Semarang - Bawen route a constant demand trend (0%). The first quarter of 2021 the Purwokerto - Purbalingga route and the Semarang - Bawen route fell 13%, the Semarang - Bawen route fell 18%. The decrease caused by Government policies in controlling the spread of Covid-19 through large-scale social restrictions and preventing crowds. In February 2021, to further reduce the spread of Covid-19, the Central Java program implemented. Transportation services are not closed because they are part of public services. Trans Jateng BRT services both eras presented in Table 2. The policy to restrictions BRT operating hours enforced during the pandemic and the new normal. The restriction operation is from 6 AM to 9 AM and afternoon from 3 PM to 6 PM. Since the policy, there has a 35% decrease in passengers on the Purwokerto - Purbalingga route, a 40% reduction in passengers on the Semarang - Bawen route and a 36% for the Semarang - Kendal route. Headway during morning and evening peak hour around 5 - 10 minutes to anticipate the crowds at shelter and bus.

Table 2: Trans Jateng BRT services

Corridor	Pre-pandemic			New normal life		
	I	II	III	I	II	III
Headway	10-15	10-15	10-15	5-10	5-10	5-10
The shift in off-peak operating hours compacted at the peak	05.30 s/d 19.30	05.30 s/d 19.30	05.30 s/d 19.30	6-9 dan 15-18	6-9 dan 15-18	6-9 dan 15-18
Max pax	40	40	40	20	20	20
Round-trips	6	8	6	6	8	6

A decrease in demand for BRT services affects the load factor value. Load factor used in considering the optimal number of buses operating [12]. Early 2020, pre-pandemics is the high load factor, was almost 100% for the Semarang - Bawen route, 80% for the Purwokerto - Purbalingga route and 60% for the Semarang - Kendal route.
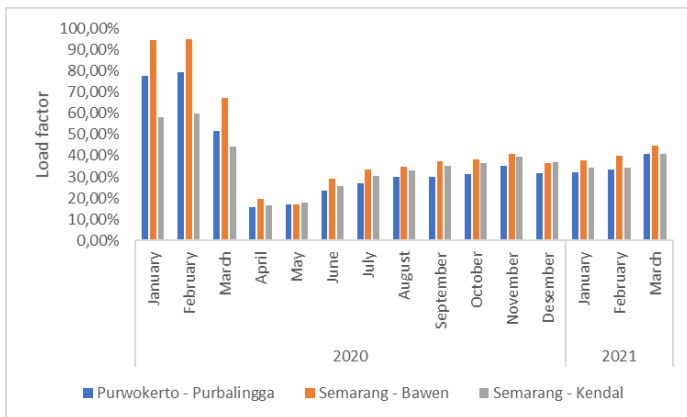
Figure 8: Load factor

In Figure 8, since the announcement of residents exposed to Covid-19 in April - May 2020, the load factor has dropped to less than 20% on three routes. To control the spread of Covid-19 in the Trans Central Java BRT, operators must provide bus operational services by paying attention to health protocols.

The implementation of this policy has an impact on increasing load factor starting June 2020. However, the load factor is less efficient from a commercial perspective, low load factor in providing base mobility services during the pandemic and the new era.

BRT revenue in both conditions presented in Figure 9. The highest incomes are in the Semarang - Bawen corridor. Income has fluctuated up and down this influenced by conditions, namely before the pandemic, upper revenues, but entering the pandemic period, it fell drastically while the new life period increased.
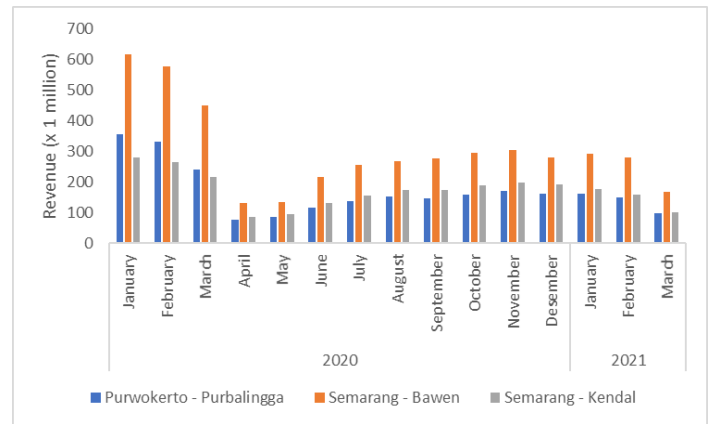
Figure 9: Revenue of BRT in three routes

The operational costs of the BRT before the pandemic until the new normal have not changed. Based on data from the Central Java Transportation Agency, the operational cost for the Purwokerto route is IDR 7,550 per bus kilometer, the Semarang - Bawen route is IDR 8,375 per bus kilometer and the Semarang - Kendal route is IDR 9,101 per bus kilometer. Therefore, with the route characteristics as in Table 1, the monthly operating charge for the three routes are Purwokerto - Purbalingga IDR 708 million, Semarang - Bawen IDR 1,192 million and Semarang - Bawen IDR 487 million.

BRT operating ratio derived from total revenue divided by operating expenses included depreciation. Cost-benefit analysis used to determine the frequency of bus services and the adequacy of the number of operating fleets [13]. The operating ratio presented in Figure 10. The operating ratio in early 2020 of the three routes highest on the Semarang - Kendal route is 0.58 others reached 0.5. April all routes have the lowest operating ratio. For the 2021 quarter, the operating ratio reached the highest value among other months. Overall, the average operating ratio in each quarter presented in Figure 11. The average operating ratio highest found in the Semarang - Kendal corridor. In 2020 the first quarter of before the pandemic, the average operating ratio was high, then in the second quarter since the pandemic decreased dramatically in the three routes. Since the third and fourth quarters of 2020, the operating ratio has started to increase again. However, since the beginning of 2021 and the implementation of the Central Java "stay at home" policy, the operating ratio decreased. The three

routes operating ratio values are less than expected, less than 1.05-1.08 [14].
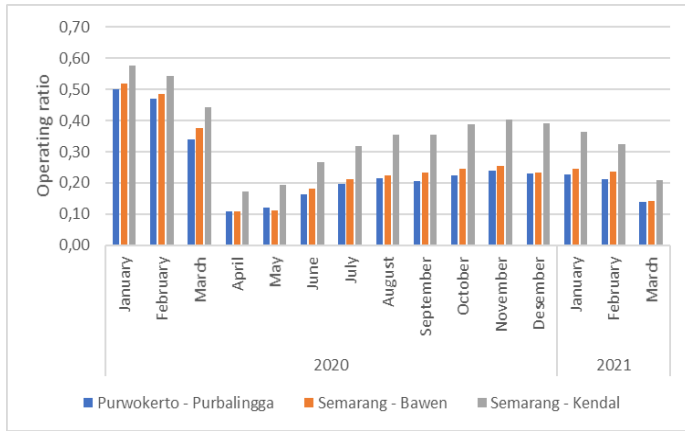
Figure 10: Operating ratio

The value of the three routes shows that the revenue earned has not been able to cover costs and has generated a sufficient surplus in the provision of investment and growth. According to some researchers, subsidized services will lose focus on cost-effectiveness and market orientation [15].
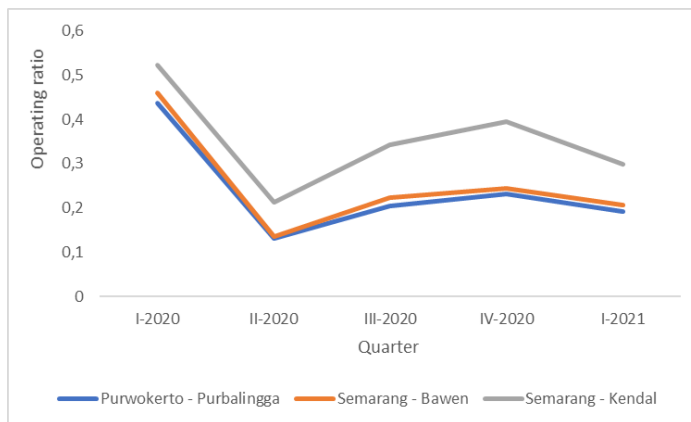
Figure 11: The average of operating ratio in each quarter

However, because BRT buses are a subsidized service, the focus is on fulfilling community services regardless of the advantages and disadvantages. Here, good public transport services stimulate community development on easy accessibility [16].

4.3. BRT Trans Jateng operational policy

Pandemics have broad social and economic impacts [17]. Control of the spread of Covid-19 carried out to provide healthy transportation services. Health-related safety perceptions of mode choice did not significantly influence modal choice decisions [11]. A pandemic is a test run of a future crisis and an opportunity to introduce discussions on the new green and public mobility paradigm [18]. The Indonesian government has launched various policies, enforced health protocols, and enforced sanctions. The impact of Covid-19 on public transport requires the need to adjust strategic, tactical and operational planning steps [19]. The enforcement of interventions at levels (border control measures, community transmission control measures and case-based control

measures are effective [20]. Control of passenger transportation carried out during travel preparation, during the trip and until the destination or arrival [21]. The Central Java Transportation Agency handles the control of the spread of Covid-19, including:

1. BRT operators maintain cleanliness and spray disinfectants on fleets at the first departure terminal minimum three time a day.
2. Operators are required to provide masks for the BRT crew.
3. The operator is obliged to provide tissue on the bus.
4. The operator must educate passengers about the dangers and ways of preventing the coronavirus.

Efforts to control the spread of Covid-19 in the provision of BRT services carried out in stages since it announced that residents were exposed to Covid-19, as shown in Figure 12. The handling of Covid-19 starting March 2020 will impose a maximum passenger restriction of 35 people as an effort of physical distancing policy. But starting March 21, the maximum passenger limit is 20 people. Physical distancing is carried out at bus stops and on buses by keeping a minimum distance of 1 meter. Efforts to comply with physical distancing and the make use of masks, especially in closed environments such as public transportation, significantly reduce the possibility of transmission [2]. Another health protocol is a body temperature of less than 37.5°.
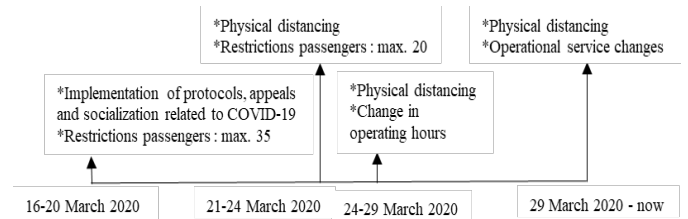
Figure 12: Preventive policy change

Beginning March 24, 2020, there will be a change in operating hours for the three Semarang - Bawen routes, namely early morning departures from 5:00 AM. to 9:00 AM., while going start at 3:00 PM. to 6:00 PM. from Tawang station and Bawen Terminal. The Semarang - Kendal route has an early departure at 5:30 AM and a late departure at 5:00 PM from Mangkang terminal and Bahurekso terminal, so the operational finish is at 6:00 PM. The Purwokerto - Purbalingga route departs early at 5:00 AM and late departures at 5:00 PM from the Bulupitu terminal and 4:45 PM from the Bukateja terminal so that operations completed at 6:00 PM until the Bulupitu terminal and Bukateja terminal. Even though there are changes in operating hours and loss in headway time, roundtrip trips per day remain. It is to anticipate restrictions on the number of passengers who not transported during peak hours. However, the business did not increase the operating ratio. March 29, 2020, operational service change services developed, especially e-payments. Notably, Semarang has implemented E-ticketing since 2019, while other routes are still under development in 2021. Especially for BRT Purwokerto - Purbalingga passengers, the factors of financing, convenience and traceability agree that the aspects applied in improving e-payment-based services [22].The policy stages carried out by paying attention to the relevant stakeholders. The roles and relationships of stakeholders must link public health and transport policymakers [23].

5. Conclusion

The operational performance of BRT before the pandemic for the Semarang - Bawen and Purwokerto-Purbalingga routes were already above 70 per cent, has the opportunity to increase the number of new fleets, while Semarang - Kendal at 60 per cent has no chance. The pandemic caused a drastic drop in the load factor and operating ratio as an economic indicator. The low operating ratio during the pandemic and new normal life causes BRT operations to be unsustainable. High operating costs are not worth the income received. It will be even heavier if the operator opens a new route. The efforts made by the BRT operator to control the transmission of Covid-19 through the implemented health protocol had an impact on increasing the value of the load factor and operating ratio, even though it was below the standard, should be appreciated. The government and BRT operator play a role in restoring the performance of a healthy transportation system competent to serve community mobility well, especially in small and medium-sized cities.

Acknowledgment

References

[1] X. Zhang, Q. Zhang, T. Sun, Y. Zou, H. Chen, "Evaluation of urban public transport priority performance based on the improved TOPSIS method: A case study of Wuhan," Sustainable Cities and Society, **43**, 357–365, 2018, doi:10.1016/j.scs.2018.08.013.

[2] A. Tirachini, O. Cats, "COVID-19 and public transportation: Current assessment, prospects, and research needs," Journal of Public Transportation, **22**(1), 1–34, 2020, doi:10.5038/2375-0901.22.1.1.

[3] N. Huy Nghia, T. Sy Sua, N. Minh Hieu, "Evaluating the maiden BRT corridor in Vietnam," Transport and Communications Science Journal, **71**(4), 336–346, 2020, doi:10.25073/tcsj.71.4.3.

[4] BPS Jawa Tengah, Provinsi Jawa Tengah dalam Angka 2021, BPS Jawa Tengah, Semarang, 2021.

[5] R.T. Sataloff, M.M. Johns, K.M. Kost, Kabupaten Banyumas dalam Angka 2021, BPS Banyumas, Banyumas, 2021.

[6] M. Arimura, T.V. Ha, K. Okumura, T. Asada, "Changes in urban mobility in Sapporo city, Japan due to the Covid-19 emergency declarations," Transportation Research Interdisciplinary Perspectives, **7**, 100212, 2020, doi:10.1016/j.trip.2020.100212.

[7] L. Prayogi, "Bus Rapid Transit system's influence on urban development: An inquiry to Boston and Seoul BRT systems' technical characteristics," IOP Conference Series: Earth and Environmental Science, **126**(1), 2018, doi:10.1088/1755-1315/126/1/012047.

[8] T. Satiennam, A. Fukuda, "A Study On The Introduction Of Bus Rapid Transit System In Asian Developing Cities," International Association of Traffic and Safety Sciences, **30**(2), 59–69, 2006, doi:10.1016/S0386-1112(14)60170-9.

[9] Juanita, B. Prastio, "Kajian Efektifitas Halte Bus BRT Transjateng Purwokerto," in Simposium Nasional Teknologi Infrastruktur Abad ke 21 UGM, 482–487, 2021.

[10] P. Bucsky, "Modal share changes due to COVID-19: The case of Budapest," Transportation Research Interdisciplinary Perspectives, **8**, 2020, doi:10.1016/j.trip.2020.100141.

[11] D.S. Pawar, A.K. Yadav, N. Akolekar, N.R. Velaga, "Impact of physical distancing due to novel coronavirus (SARS-CoV-2) on daily travel for work during transition to lockdown," Transportation Research Interdisciplinary Perspectives, **7**, 100203, 2020, doi:10.1016/j.trip.2020.100203.

[12] H. Kawaguchi, K. Kuromizu, S. Yagi, "A Minibus Supply Control Measure in Indonesia," in 13th WCTR, July 15-18, Rio de Janeiro: 1–15, 2013.

[13] Suwardo, "the Determination of Bus Service Frequency Using Cost-Benefit Approach," Jurnal Transportasi, **11**(1), 29–38, 2011.

[14] GTZ, Bus Regulation and Planning, 2004.

[15] N. Fearnley, "Free Fares Policies : Impact on Public Transport Mode Share and Other Transport Policy Goals," International Journal of Transportation, **1**(1), 75–90, 2013, doi:10.14257/ijt.2013. 1.1.05.

[16] T. Litman, Evaluating Public Transit As An Energy Conservation and Emission Reduction Strategy, Victoria Transport Policy Institute, 2012.

[17] A. Susilo, C.M. Rumende, C.W. Pitoyo, W.D. Santoso, M. Yulianti, H. Herikurniawan, R. Sinto, G. Singh, L. Nainggolan, E.J. Nelwan, L.K. Chen, A. Widhani, E. Wijaya, B. Wicaksana, M. Maksum, F. Annisa, C.O.M. Jasirwan, E. Yunihastuti, "Coronavirus Disease 2019: Tinjauan Literatur Terkini," Jurnal Penyakit Dalam Indonesia, **7**(1), 45, 2020, doi:10.7454/jpdi.v7i1.415.

[18] A. Tardivo, A. Carrillo Zanuy, C. Sánchez Martín, "COVID-19 Impact on Transport: A Paper from the Railways' Systems Research Perspective," Transportation Research Record: Journal of the Transportation Research Board, 036119812199067, 2021, doi:10.1177/0361198121990674.

[19] K. Gkiotsalitis, O. Cats, "Public transport planning adaption under the COVID-19 pandemic crisis: literature review of research needs and directions," Transport Reviews, **0**(0), 1–19, 2020, doi:10.1080/01441647.2020.1857886.

[20] D. Susanna, "When will the COVID-19 pandemic in indonesia end?," Kesmas, **15**(4), 160–162, 2020, doi:10.21109/KESMAS.V15I4.4361.

[21] Peraturan Menteri Perhubungan RI No PM 18, Pengendalian Transportasi Dalam Rangka Pencegahan Penyebaran Corona Virus Disease 2019 (COVID-19), **Nomor 9**(Pedoman Pembatasan Sosial Berskala Besar dalam Rangka Percepatan Penanganan Corona Virus DIsease 2019 (COVID-19)), 1–71, 2020.

[22] F. Romadlon, R.D. Lestari, F. Lestiana, N.A. Putri, "Kajian Pra-Implementasi Aplikasi Layanan pada Bus Rapid Transit Purwokerto-Purbalingga: Perspektif Penumpang Wanita," Warta Penelitian Perhubungan, **32**(2), 68–76, 2020, doi:10.25104/warlit.v32i2.1318.

[23] J. Zhang, "Transport policymaking that accounts for COVID-19 and future public health threats: A PASS approach," Transport Policy, **99**, 405–418, 2020, doi:10.1016/j.tranpol.2020.09.009.

Effect of Nano Clay and Marble Powder Waste as a Hybrid Addition on the Behavior of Normal and High Strength RC Columns Subjected to Axial Compressive Loading

Mostafa Ahmed Mahdi[*,1], Ahmed Hassan Ghallab [1], El-Saaid Ibrahim Zaki [2], Ahmed Sayed Elmannaey [3]

[1]*Ain Shams University, Structural Engineering Department, Faculty of Engineering, Cairo, 11865, Egypt*

[2]*Housing and Building National Research Center, Quality Control Institute, Giza, 8655, Egypt*

[3]*Construction Engineering Department, Faculty of Engineering, Misr University for Science and Technology, 6th of October City, 8655, Egypt*

A B S T R A C T

This paper studied the influence of using hybrid additives of Nano Clay (NC) and Marble Powder (MP) on the structural behavior of columns, in terms of ultimate capacity, axial strain, lateral strain, toughness, and failure pattern. For this purpose, ten column specimens were made from reinforced concrete (RC), either normal or high strength, and were tested under axial compressive loading. It was concluded that, regardless of the concrete strength of the RC columns, the presence of the optimum ratio of the hybrid additives (NC and MP) promotes more ductile behavior of the columns with enhancement in ultimate load capacity. Furthermore, it was found that NC particles act as additional ties on the micro scale level and increase the confinement in the RC columns. Also, the filling effect of MP particles, that strengthened the cement matrix, led to higher increment in the lateral strain and toughness. Briefly, Higher axial load capacity, better ductile performance, greater reduction in the ties ratio and larger dissipation of energy can be achieved by using the optimum hybrid additions of NC and MP in the RC columns.

1. Introduction

After many decades, concrete remains to be the most important construction material in the globe. Therefore, improving its properties, to make it more durable and eco-friendly material, is vital. So, adding pozzolanic and/or waste materials to concrete blends can play this role [1–6]. Also, using nanotechnology in processing these materials can add superior characteristics to them [7–11]. Pozzolanic materials such as slag, fly ash, metakaolin and silica fume, and waste (non-pozzolanic) materials such as, marble, granite and limestone powder can be utilized as a partial replacement of the cementing material in the concrete mix. For instance, kaolinite-based Nano Clay (NC) and Marble Powder (MP) are abundant in the Egyptian environment, which represents a motive for the Egyptian research community to use such materials in fabricating eco-friendly concrete [12,13].

NC possesses two major benefits -when properly added and dispersed- to concrete; its miniature size enhances its pozzolanic

activity and leads to consume more calcium hydroxide from the matrix producing calcium silicate hydrate gel. Moreover, its sheet-like form acts as a bridge in the hardened concrete, and consequently, prohibits crack propagation under loading. Both benefits boost the mechanical properties and durability of the concrete [13–22]. Also, MP can be used to replace part of the sand in concrete, thus, result in packing the cement matrix structure and producing denser and more durable concrete. In consequence, the reduction of cement amount and the use of waste material (MP) in concrete means less CO_2 emissions, and controlled disposal of waste materials to landfills [23–32].

Although the presence of nanoparticles in concrete mixtures enhances their performance, a few numbers of studies were concerned with its effect on the behavior of structural elements. In [33], the author tested eight beam–column joints under cyclic loading. These joints were casted from concrete with various amounts of fly ash and/or nano silica. It was concluded that the presence of additives, either separate or hybrid, enhanced flexural strength, maximum end deflection and maximum lateral load of the joints compared to control mix joint.

[*]Corresponding Author: Assistant Lecturer in Construction Engineering Department, Misr University for Science and Technology, 6 of October, Egypt. Email: mostafa.senosy@must.edu.eg, Contact: +201096800684

In [34], the author tested sixteen RC beams in flexure to investigate their bending and shear capacities. Group of beams was prepared by adding limestone filler as a partial replacement of cement with silica or alumina nanoparticles, while only nanoparticles were introduced in the second group. The first group experienced degradation in both shear and bending capacities, but on the other side, the second group showed enhancement in shear strength by about 7 to 9% and no significant enhancement in bending capacity.

In [35], the author casted seven RC beams to investigate their flexural behavior under the effect of using 10% of NC, effect of compression reinforcement ratios, flexural reinforcement ratios and characteristic strength of concrete. The addition of NC as cement replacement has a positive influence, compared to control beam, that led to an increase of 122, 107, 107 and 125% for initial crack load, ultimate load, maximum deflection and toughness, respectively, with minimum compression reinforcement ratio of 0.44 and minimum flexural reinforcement ratio of 1.29%.

In [36], the author prepared seven RC beams to investigate the effect of using 10% of NC and variation of characteristic concrete strength (f_{cu}) on the shear behavior of the beams. For f_{cu} equal 25 MPa, the addition of NC as cement replacement has a positive influence that led to an increase of 31.5%, 7.4% and 17.6% for initial crack load, ultimate load and toughness, respectively, compared to normal control beam. Moreover, the improved percentages for initial crack load, ultimate load and toughness of beam with 35 MPa concrete grade and with 10% NC were about 28%, 9.3% and 12.6%, respectively, compared to beam with 25 MPa concrete grade and with 10% NC.

In [37], the author prepared seven inverted T-section beams to investigate the effect of using 1% of Nano-Silica (NS) and the effect of flexural and shear reinforcement ratios on the flexural and shear behavior of the beams. Initial crack load, ultimate load and toughness of inverted T- beam with 1% NS as cement replacement improved by 31.4%, 6.6% and 16.65%, respectively, compared to control beam. In addition, the failure of the beam with 1% NS changed from flexure to flexure-shear mode and its cracks spacing were lesser compared to control beam.

In [38], the author tested four RC slabs which contained MP as replacement of cement with different ratios (0, 2.5, 5, and 7.5%). It was observed that, in all slabs containing different ratios of MP, the initial crack load and ultimate load increased compared to control slab. The best performance of RC slab was observed by using 5% MP with improved percentages of initial crack load, ultimate load and maximum deflection of about 20%, 10% and -4.6 %, respectively. In addition, using 5% of MP in RC slab decreased the number of cracks compared to the control slab, however, the number of cracks increased as the percentage of MP exceeded 5% in the mix increased.

Based on the available literature, the vast majority of research studies dealt with additives effect on concrete behavior from material point of view. On the other hand, the effect of additives on the performance of RC structural elements is still developing and needs to be under spotlight. The present study focuses on the behavior of either ordinary or high strength RC columns, with optimum ratios of NC and MP to take a wide step towards determining structural behavior/properties of concrete elements instead of only determining materials properties. Firstly, different concrete mixes were prepared with different ratios of NC and MP. Secondly, the optimum NC and MP ratios were elected to be used in casting the RC columns. Finally, the obtained test results were interpreted and compared to conventional concrete to reach an augmented comprehension of the behavior of this structural element.

2. Experimental Program

2.1. Overview

Based on an earlier research study conducted by the authors [39], Normal Strength Concrete (NSC) and High Strength Concrete (HSC) mixes were prepared with hybrid additions of various amounts of NC and MP. Also, many mixing techniques (sonicating, stirring and sprinkling after stirring) were adopted to guarantee the success of NC dispersion in the mix. After that, the mechanical performance of the mixes such as, compressive, flexure, splitting and bonding strengths were assessed at the age of 7 and 28 days. Additionally, permeability of the samples was determined, and microstructure of the mixes was captured. It was concluded that the best physical/mechanical performance of concrete mixes can be achieved by using nearly 3% NC and 10% MP additives ratios by weight of cement and sand, respectively. Also, sprinkling after stirring dispersion technique was an effective and practical mean of mixing to overcome NC agglomeration problem in concrete blends. The improvement in performance of concrete mixes can be attributed to three mechanisms; 1- the efficiency of NC in packing the voids by promoting pozzolanic reaction that formed additional C-S-H by consuming calcium hydroxide crystals, 2- the bridging effect of sheet-like NC particles which strengthened the cement matrix by preventing crack propagation, and 3- the filling effect of MP that strengthened cement matrix and the transition zone surrounding aggregates.

2.2. Concrete Mix Materials

The materials used in this study for concrete blends were Ordinary Portland Cement (OPC) (CEMI/52.5R) in accordance with ASTM C150 [40]. While, fine aggregates were natural siliceous sand with fineness modulus of 2.5, and coarse aggregates were crushed clean dolomite with nominal maximum size of 19.0 mm. Also, mineral additives of NC and MP were used for NSC, and Silica Fume (SF) was used in addition to NC and MP for HSC. For specimens' reinforcement, deformed high tensile steel was used for the longitudinal column reinforcement with actual grade 524/661 (yield stress/ultimate stress, MPa) whereas the transverse column reinforcement was formed from mild tensile steel with actual grade 358/517. The longitudinal and transverse column reinforcement conformed to ES 262-1/2009 [41] and ES 262-2/2009 [42], respectively.

The NC used in this study was amorphous nano-metakaolin with mean particle size distribution of 87.13 μm. The mean particle size distribution of MP was 7.25 μm. Silica Fume (SF) corresponds with the requirements of ASTM C 1240-03a [43]. High Performance Superplasticizer (SP), which is an aqueous solution of modified polycarboxylates, was used to obtain a required average slump within range of 100 to 200 mm. SP complied with EN 934-2 [44]. Tap water was used for both mixing and curing.

2.3. Concrete Mixture Proportions

Four mixes were prepared; two without NC and MP additives, while the other two mixes were supplied with additives. Table 1 shows the proportions of each concrete blend and the targeted compressive strength of each mix. The compressive strength test was conducted for the four mixes on standard cubes of size 150mm to obtain the f_{cu} according to BS EN 12390-3 [45].

2.4. Timber Formwork and Steel Reinforcement

Timber formworks were prepared and leveled horizontally for specimens casting. The steel reinforcement cages of specimens were aligned in the timber forms and adjust concrete clear cover to 20 mm. The longitudinal columns reinforcement was deformed steel bars of 10 mm, whereas, the transverse columns reinforcement was mild steel bars of 8 mm. The longitudinal reinforcement number and transverse reinforcement spacing are shown in Figure 1 and Table 2. At columns specimen ends, two precautions were adopted to prevent premature load failure occurrence at these locations that may result from stress concentration near points of load application as follows, a- the longitudinal bars were flexed horizontally to achieve full bond with concrete leading to resisting compression concentration at ends, b- additional ties were added to enhance confinement at ends of RC columns.

2.5. Concrete Proportions, Mixing and Curing Procedure

For concrete mixes with no additives, all the ingredients were added in the mixer and mixed for two minutes. On the other hand, mixes with additives were prepared by adding SP to mixing water and blended until obtaining homogenous solution. Then, 70% of this solution was utilized to stir and disperse NC using vane motor at about 2000 rpm speed for 2 min. At the same time, cement, aggregates, MP and SF (if added) were dry mixed in a rotary mixer for 1 min. After that, the remaining water-SP solution was added to the blend and mixed for additional 1 min. Finally, the ready stirred NC solution was manually sprinkled during mixing into rotary mixer for additional 3 min. to achieve the desired homogeneity. The fresh concrete was casted in the prepared column specimen forms. The concrete blends were consolidated using electrical vibrator to produce well compacted concrete without either voids or honeycomb. After one day from casting, specimens were de-molded from forms and cured by wrapping with wet burlap for 28 days at the laboratory conditions of 25 ºC temperature. At the end of curing process, RC columns were unwrapped to dry by keeping in the open lab environment into preparation for testing.

2.6. Columns Specimens

Ten square (150x150) RC columns with and without hybrid additions (NC and MP) tested under concentrated axial loading to determine their ultimate capacity, axial strain, lateral strain, toughness, and failure pattern. The parameters that were considered in this study were: material parameters; hybrid additives presence and concrete strength, and structural parameters; columns length (slenderness ratio), transverse and longitudinal steel bars ratio. Table 2 shows all the characteristics of the fabricated columns. As can be seen from Table 2, two target concrete strength were selected: 50 and 70 MPa, to represent NSC and HSC, respectively. The height of columns ranged from 1000mm to 2500mm to represent short or long columns, respectively. Also, the ratio of longitudinal reinforcement area to column cross sectional area (ρ%) had two values of about 1.4% to 2.8%, while the ratio of tie bars volume to column volume (ρv%) ranged between 0.5% to about 1%. Figure 1 depicts the concrete dimensions and steel reinforcement of the casted columns.

2.7. Testing Procedures and Instrumentation

Columns specimens were tested under concentric axial compression using hydraulic loading machine with a capacity of 2000 KN. The axial loading was applied via displacement control, at a rate of 0.5 mm/min, to monitor response of columns specimens beyond peak capacity. The monotonic axial loading was regulated to increase gradually till failure. Two rigid steel caps shown in Figure 2, 150 mm wide, were fabricated for confining the ends of the specimen to ensure preventing premature failure at these locations resulted from stress concentration near points of load application. Before testing, each specimen was aligned vertically until matching the centerline of the specimen with the line of axial load application. To measure axial and lateral strains of the tested specimen, three Linear Variable Differential Transformers (LVDTs) were used as shown in Figure 2. The L1 transducer was mounted at the bottom of the upper steel cap to measure axial displacement. The L2 and L3 transducers were mounted at mid height of the tested specimen on two perpendicular faces to measure lateral displacements. The average lateral deformation recorded using the L2 and L3 transducers was used to plot the lateral load-strain response of the columns.

Table 1: Mixing proportions of Concrete Blends

	NSC		HSC	
Mix No.	1(N)*	2(A)**	3(N)	4(A)
Target f_{cu} (MPa)	50	50	70	70
Cement (Kg/m³)	400	339.5	450	391.5
Sand (Kg/m³)	780	702	720	648
Agg. (Kg/m³)	1150	1150	1145	1145
Water (L/m³)	183	160	160	145
SP (L/m³)	5.8	6.13	10.8	11.25
NC (Kg/m³)	---	10.5	---	13.5
MP (Kg/m³)	---	78	---	72
SF (Kg/m³)	---	---	50	45
Water/binder	0.457	0.457	0.32	0.32

*N: No additives **A: Additives (3%NC and 10%MP)

Two electric resistance strain gauges (G1 and G2) were installed on one of the longitudinal and transverse reinforcement bars at the mid height of the tested specimen as shown in Figure 1. Load and displacement measurements were monitored and recorded using an automatic data acquisition software.

3. Parametric Study

Specimens were classified into groups to manage the collected test data. Thus, the parametric study incorporated hybrid materials presence, concrete strength, slenderness ratio, longitudinal and transverse reinforcement ratios. Table 3 clarifies the groups of column specimens and the studied parameters of each group.

4. Analysis and Discussion of Test Results

The effect of the studied factors on the behaviour of the tested columns is compared using three factors: ultimate strength, ductility and toughness. Figures 3 and 4 show the failure patterns of tested specimens.

Table 2: Scheme of the Tested Column Specimens

ID	Target f_{cu} (MPa)	Column Height H(mm)	Slenderness Ratio (λ)	L. Bars (fy=360MPa)	ρ %	Ties (fy=240MPa)	ρ_v %
				Long. Bars		**Trans. Bars**	
C1N*	50	1000	6.67	4Φ10	1.39	Ø8-200	0.5
C2N	50	1000	6.67	4Φ10	1.39	Ø8-160	0.65
C3A**	50	1000	6.67	4Φ10	1.39	Ø8-200	0.5
C4A	50	1000	6.67	4Φ10	1.39	Ø8-160	0.65
C5A	50	1000	6.67	4Φ10	1.39	Ø8-100	0.98
C6A	50	2000	13.33	4Φ10	1.39	Ø8-200	0.5
C7A	50	2500	16.67	4Φ10	1.39	Ø8-200	0.5
C8A	50	1000	6.67	8Φ10	2.78	Ø8-200	0.5
C9N	70	1000	6.67	4Φ10	1.39	Ø8-200	0.5
C10A	70	1000	6.67	4Φ10	1.39	Ø8-200	0.5

*N: No additives **A: Additives (3%NC and 10%MP)
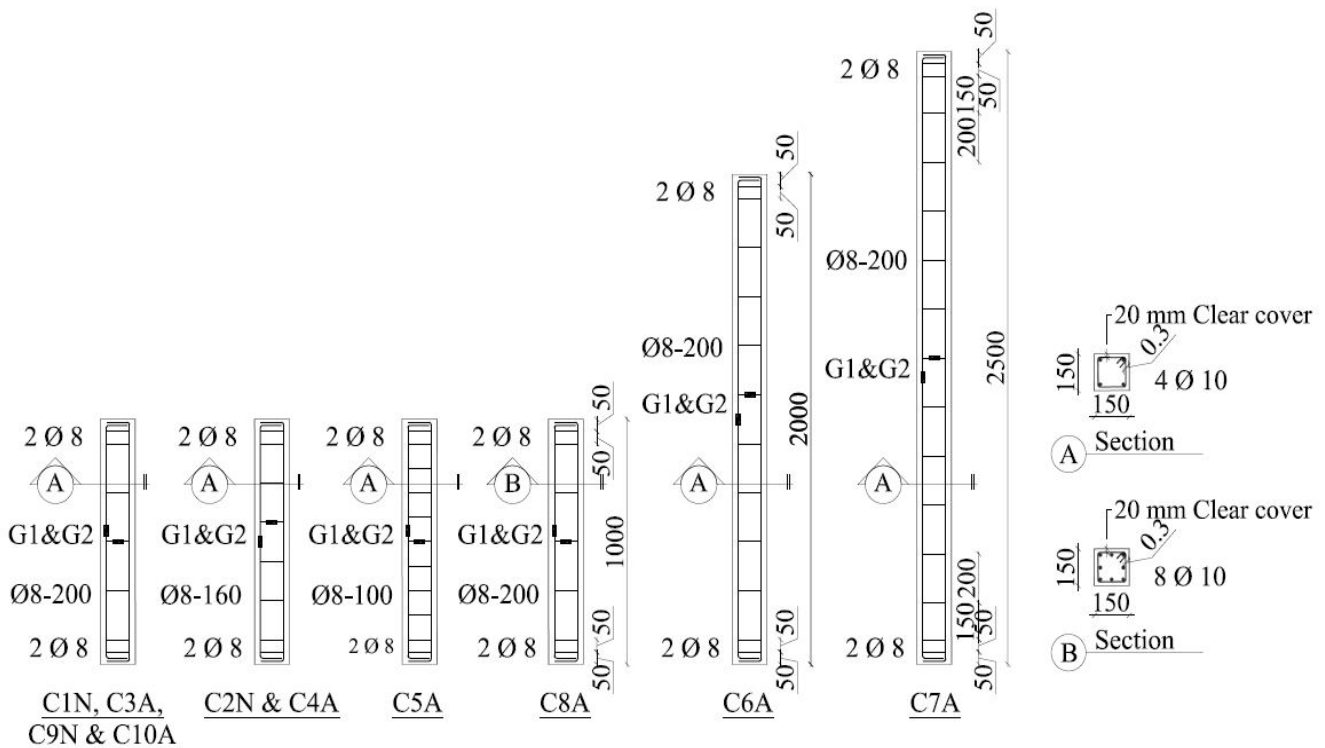
Figure 1: Dimensions and Steel Reinforcement Details of Tested Column Specimens.
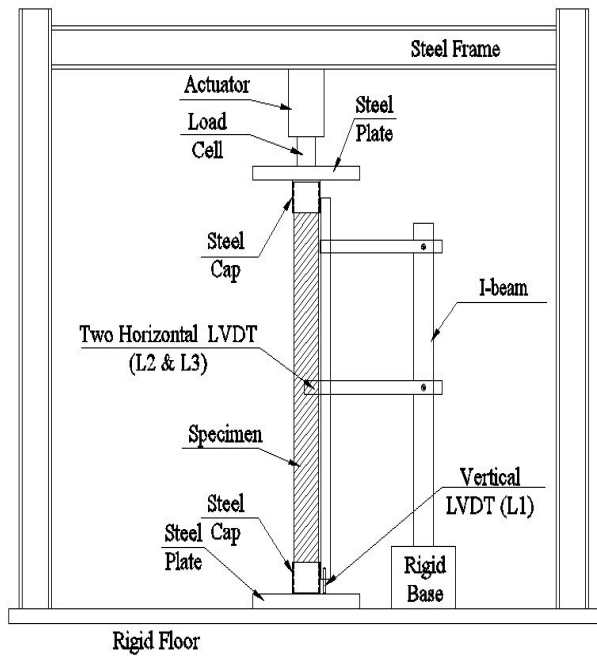
(a) Schematic.   (b) Laboratory.

Figure 2: Columns Instrumentation and Test Setup.

Table 4 summarizes the maximum axial load (Pc), the maximum axial strain (ε_c), the maximum lateral strain (ε_L) and toughness parameter (Au) for all tested columns.

In the following sections, the results of the experimental program were presented and the effect of each parameter in the parametric study is discussed.

4.1. Failure patterns

Failure locations of RC columns are presented in Figure 3. Failure occurred at two locations; the first is at the top or bottom end of the column specimen which indicating the stress concentration at the ends of the columns, while the second is at the mid third of the column height. Moreover, the bond failure (i.e. slip or separation) between concrete and steel bars could be one more reason for the appearance of end effect [46, 47].

The failure mechanisms of the tested columns were almost the same except for those columns made of HSC as they failed more suddenly in a higher brittle mode. The failure sequence for the columns was as follows: During increasing the applied load cracks occurred before the ultimate load was reached at the failure location, eventually, the concrete cover was spalled off. Finally, the tested columns were failed by crushing of concrete core in addition to yielding/buckling of longitudinal and/or transversal steel bars.

Most of the longitudinal steel bars were yielded and buckled as shown in Figure 4a. For the ties, some of them were yielded and broken due to necking, as shown in Figure 4b. The results of the tested columns in each group is presented and compared in Table 4.

4.2. Effect of Hybrid Additives Presence on RC columns (Group1)

The effect of hybrid additives on the behavior of RC columns was investigated in NSC columns with and without hybrid

additives (C1N compared to C3A and C2N compared to C4A) and HSC columns with and without hybrid additives (C9N compared to C10A). Due to the presence of hybrid additives in columns concrete mixtures, the strength and post-peak strains of the columns increased noticeably as observed from the comparison of the test data and the results shown in Table 4 and Figure 5.

As can be seen, the presence of hybrid additions in the column concrete mixture improved the maximum load compared to columns without hybrid additions. This can be attributed to the enhancement in the tensile strength property of the column concrete mixture resulting from NC particles in shape of sheets that act as bridge connecting both sides of the crack together preventing crack propagation which compatible with [15,39], subsequently, NC particles act as additional ties for the column but on the micro scale level. Moreover, the filling effect of MP that strengthened cement matrix and the transition zone surrounding aggregates has a role in this improvement.

For NSC columns with and without hybrid additives, in case of ties ratio = 0.5%, the maximum load of C3A compared to C1N increased from Pc=770KN to 834KN with an improvement of about 8%, while in case of ties ratio = 0.65%, the maximum load of C4A compared to C2N increased from Pc=835KN to 925KN with an improvement of about 11%. On the other hand, for HSC columns with and without hybrid additives, the maximum load of C10A compared to C9N increased from Pc=1261KN to 1372KN with an improvement of about 9% (see Table 4 and Figures 5 and 6).

For post-peak strains, for NSC columns with and without hybrid additives, the improvement in the axial strain of C3A slightly improved compared to C1N (about 4.5%), while the lateral strain of C3A significantly improved compared to C1N reaching about 16.7% indicating an important enhancement in post-peak ductility. In addition, the axial strain of C4A slightly improved compared to C2N reaching about 6%, while the lateral strain of C4A significantly improved compared to C2N reaching about 18%.

Table 3: Groups of column specimens and the studied parameters of each group.

Groups	Studied Parameter	Column ID	Hybrid Materials%	Column Sizes mm x mm	Column Height mm	Slenderness Ratio (λ)	Actual F_{cu} (Mpa)	Long bars L. Bars	ρ %	Lateral confinement Ties	ρv %
G1	Hybrid Materials Presence	C1N	---	150x150	1000	6.67	48.7	4Φ10	1.39	Ø8-200	0.5
		C3A	3%NC, 10%MP				51.2				
		C2N	---				48.7			Ø8-160	0.65
		C4A	3%NC, 10%MP				51.2				
		C9N	---				68.9			Ø8-200	0.5
		C10A	3%NC, 10%MP				72.1				
G2	Concrete Strength (F_{cu})	C1N	---		1000	6.67	48.7	4Φ10	1.39	Ø8-200	0.5
		C9N					68.9				
		C3A	3%NC, 10%MP				51.2				
		C10A					72.1				
G3	Ties Ratio (ρv %)	C1N	---		1000	6.67	48.7	4Φ10	1.39	Ø8-200	0.5
		C2N								Ø8-160	0.65
		C3A	3%NC, 10%MP				51.2			Ø8-200	0.5
		C4A								Ø8-160	0.65
		C5A								Ø8-100	0.98
G4	Slenderness (λ)	C1N	---		1000	6.67	48.7	4Φ10	1.39	Ø8-200	0.5
		C3A	3%NC, 10%MP				51.2				
		C3A	3%NC, 10%MP		1000	6.67	51.2				
		C6A			2000	13.33					
		C7A			2500	16.67					
G5	Longitudinal bars (ρ%)	C1N	---		1000	6.67	48.7	4Φ10	1.39	Ø8-200	0.5
		C3A	3%NC, 10%MP				51.2	4Φ10	1.39		
		C3A	3%NC, 10%MP				51.2	4Φ10	1.39		
		C8A	3%NC, 10%MP					8Φ10	2.78		

Also, for HSC columns with and without hybrid additives, the axial strain of C10A slightly improved compared to C9N reaching about 5%, while the lateral strain of C10A significantly improved compared to C9N reaching about 17% (see Table 4 and Figures 5 and 6). The higher increment in the lateral strain has been achieved with the aid of additional confinement offered by the presence of NC sheets that enhance the tensile property of concrete mixture as previously discussed.

The effect of hybrid additives on strength and ductility of RC columns with ties ratio = 0.65% (C4A compared to C2N) was more noticeable than columns with ties ratio = 0.5% (C3A compared to C1N). This resulted from the enhancement of the bond strength between steel reinforcement and concrete due to hybrid additives which is compatible with [15, 39]. As a result of the increase in the ties ratio and the obtained bond strength led to achieve more load capacity and enhanced post-peak strains.

a) C1N   b) C2N   c) C3A   d) C4A

e) C5A   f) C8A   g) C9N   h) C10A   i) C6A   j) C7A
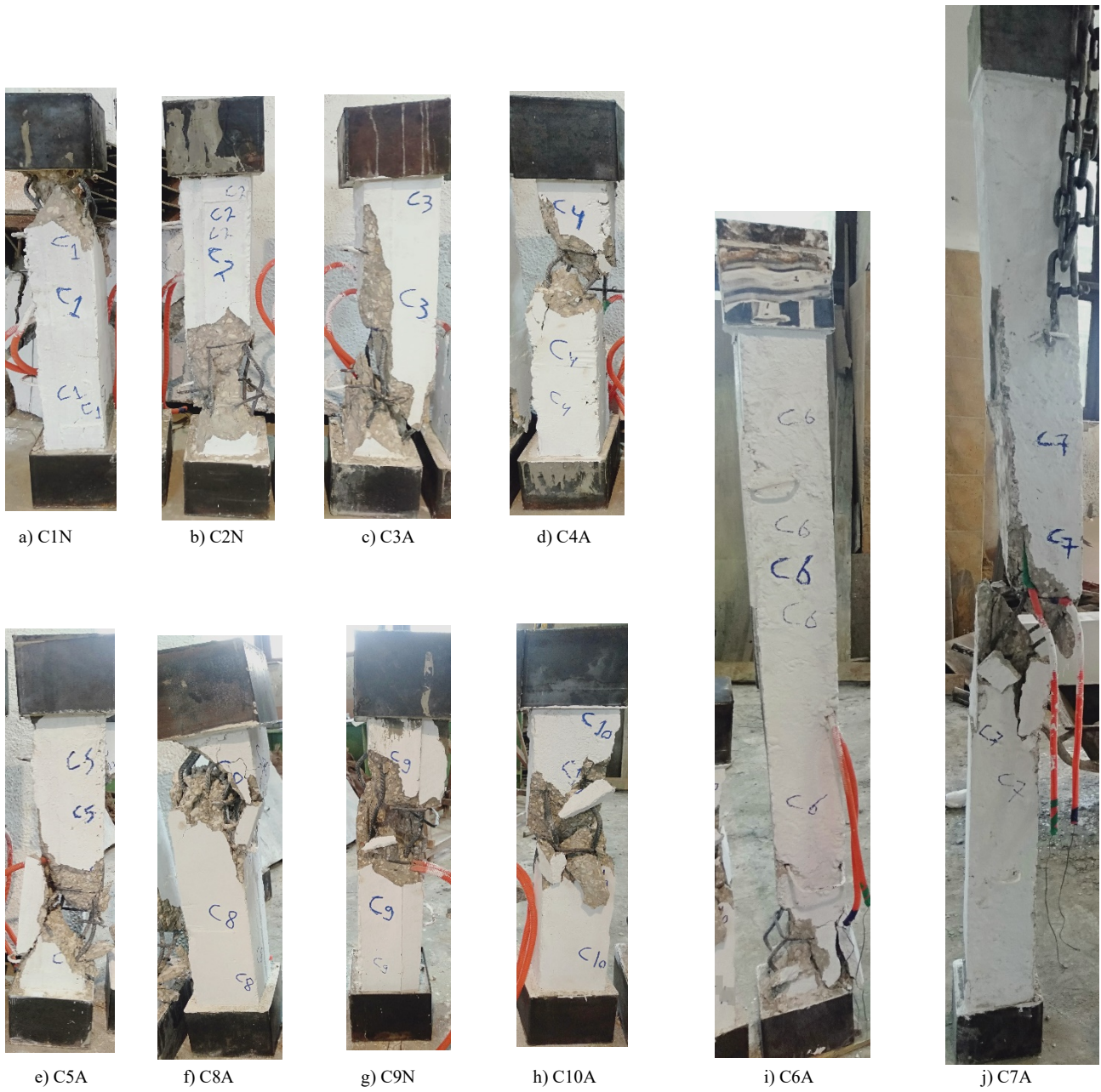
Figure 3: Failure Pattern for Each Column Specimen.
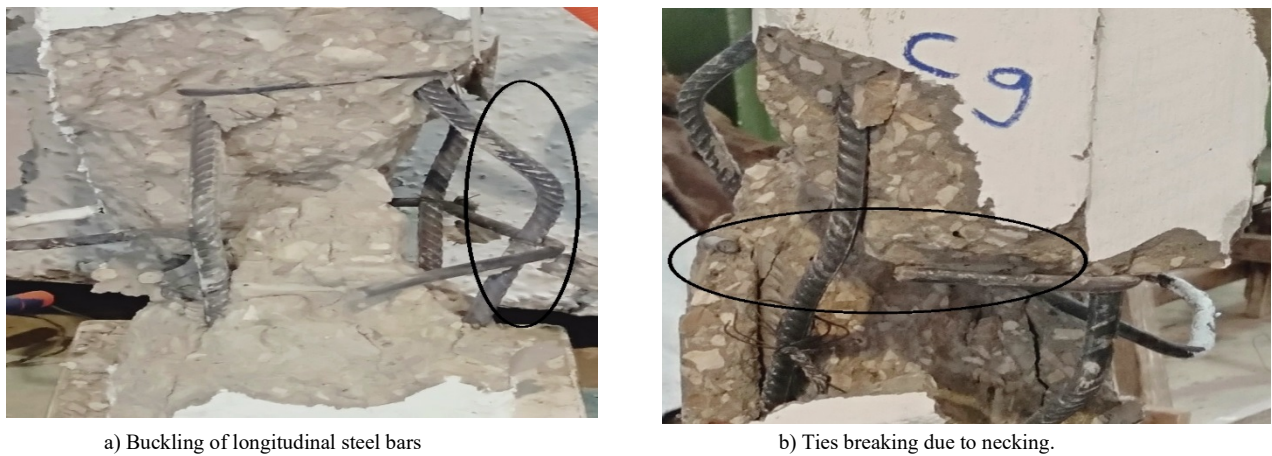
a) Buckling of longitudinal steel bars   b) Ties breaking due to necking.

Figure 4: Failure Pattern of the Steel Bars.

Table 4: Test Results of the Tested RC Columns

(Groups) & Parameters	Column ID	Actual F_{cu} (Mpa)	Maximum Axial Load		Axial Strain		Lateral Strain		Toughness	
			Pc (KN)	±%*	ε_cx10^{-3}	±%	ε_Lx10^{-3}	±%	Au (KN)	±%
(G1) Hybrid Additive Presence	C1N	48.7	770	--	5.50	--	8.0	--	3167	--
	C3A	51.2	834	+8.31	5.75	+4.55	9.33	+16.7	3606	+14
	C2N	48.7	835	--	5.80	--	10.0	--	3700	--
	C4A	51.2	925	+10.8	6.15	+6.03	11.8	+18.0	4581	+24
	C9N	68.9	1261	--	4.95	--	7.33	--	4641	--
	C10A	72.1	1372	+8.8	5.20	+5.05	8.60	+17.3	5228	+13
(G2) Concrete Strength (F_{cu})	C1N	48.7	770	--	5.50	--	8.0	--	3167	--
	C9N	68.9	1261	+63.8	4.95	-10.0	7.33	-8.33	4641	+46
	C3A	51.2	834	--	5.75	--	9.33	--	3606	--
	C10A	72.1	1372	+64.5	5.20	-9.57	8.60	-7.86	5300	+47
(G3) Ties Ratio (ρ_v%)	C1N	48.7	770	--	5.50	--	8.0	--	3167	--
	C2N		835	+8.44	5.80	+5.45	10.0	+25	3700	+17
	C3A		834	--	5.75	--	9.33	--	3606	--
	C4A	51.2	925	+10.9	6.15	+6.96	11.8	+26.4	4581	+27
	C5A		998	+19.7	6.50	+13.0	14.3	+53.6	5165	+43
(G4) Slenderness (λ)	C1N	48.7	770	--	5.50	--	8.0	--	3167	--
	C3A	51.2	834	+8.31	5.75	+4.55	9.33	+16.7	3606	+14
	C3A		834	--	5.75	--	9.33	--	3606	--
	C6A	51.2	733	-12.1	2.65	-53.9	27.3	+193	1463	-59
	C7A		690	-17.3	2.0	-65.2	30.7	+229	1036	-71
(G5) Long bars (ρ%)	C1N	48.7	770	--	5.50	--	8.0	--	3167	--
	C3A	51.2	834	+8.31	5.75	+4.55	9.33	+16.7	3606	+14
	C3A		834	--	5.75	--	9.33	--	3606	--
	C8A	51.2	717	-14.0	6.0	+4.35	9.67	+3.57	3257	-9.7

* ±%: Indicates percentage of increase/decrease in value relative to reference column which is the first column in each group.

For the toughness parameter in case of NSC columns with and without hybrid additives, the increment in toughness of C3A compared to C1N and C4A compared to C2N reached about 14% and 24%, respectively. Moreover, in case of HSC columns with and without hybrid additives, the gain in toughness for C10A reached 13% compared to C9N (see Table 4 and Figure 6).

In summary, the results for group1 columns indicated that the hybrid additives presence on the behavior of either NSC or HSC

RC columns led to enhanced strength and ductility of that columns. Also, it should be noted that columns with hybrid additives and with tie ratio 0.5% not only failed at almost the same axial load of column with higher tie ratio 0.65% and without additive (C3A and C2N) but also had higher ductility and toughness.

4.3. Effect of the Concrete strength Fcu (Group2)

The variation in concrete strength was investigated in NSC and HSC columns specimens without additives (C1N compared to

C9N) and with hybrid additives (C3A compared to C10A). Due to the increase in concrete strength and as expected, the maximum axial load of C9N increased noticeably compared to C1N as observed from the comparison of the test data and the curves shown in Table 4 and Figure 7. However, for similar columns but with hybrid additive, the increase in column strength was slightly higher compared to columns without hybrid additive.

For post-peak strains in case of increasing concrete strength, for NSC and HSC columns without hybrid additives, the declination in the axial and lateral strains of C9N compared to C1N reached 10% and 8.33%, respectively, while for columns made of NSC and HSC with hybrid additives the declination in the axial and lateral strains of C10A compared to C3A reached 9.57% and 7.86%, respectively. As can be seen, the enhancement in column post- peak ductility due to the hybrid additive was slightly higher in case of NSC and HSC (see Table 4 and Figures 7 and 8). Moreover, the decrease in the axial and lateral strains

have been obtained and expected due to the increase in the brittleness of concrete, resulted from the increased concrete strength which is compatible with [39,48].

For the toughness parameter in case of increasing concrete strength, the increment in toughness of C9N compared to C1N and C10A compared to C3A reached about 46% and 47%, respectively (see Table 4 and Figure 8).

In summary, the results for group2 columns indicated that increasing the concrete strength led to the enhancement of strength and toughness in columns, but the decrease of the post-peak strains was obtained. Also, it should be noted that columns with hybrid additives when casted of higher concrete strength blends, slight improvement in axial load, ductility and toughness was achieved in comparison to columns without additives.
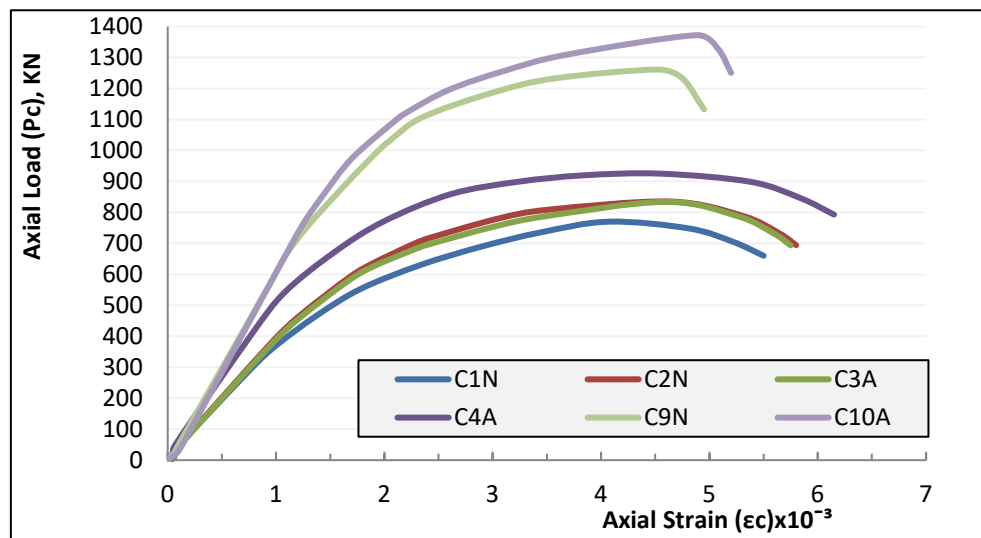
Figure 5: Load-Strain Curve for Group 1.
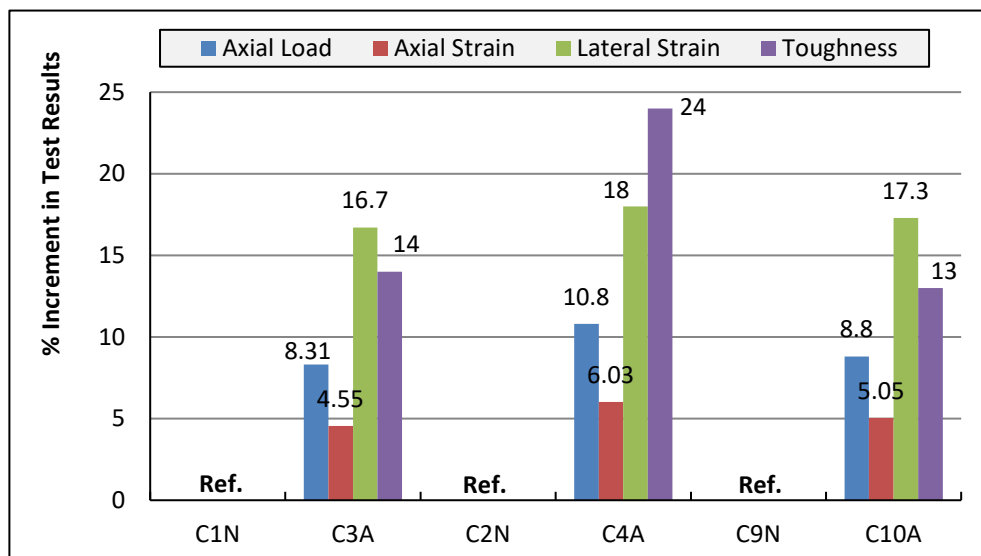
Figure 6: Percent Increment in Test Results for Group 1.

4.4. Effect of Ties Ratio ρv % (Group3)

The effect of increasing ties ratio (ρv %) of columns with hybrid additives was investigated in NSC columns (C3A compared to C4A and C5A), also, the behavior of these three columns and C2N was compared to column C1N to give an idea about how much the presence of additives did affect the response of these columns. Due to the presence of ties and under axial compressive loading the columns specimens turned out to be in a tri-axial compressive status. As the ties ratio increases, the confinement capacity on the RC columns increases significantly. This makes the strength and post-peak strains of the columns increase noticeably as observed from the comparison of the test data and the curves shown in Table 4 and Figure 9.

The effect of increasing ties ratio from 0.5% to 0.65% can be obtained by comparing C1N and C2N. As can be seen, the failure load of C2N increased by 8.44% (compared to C1N). For similar columns but with hybrid additives (C3A and C4A), the increase in strength of C4A was 10.9% compared to C3A (see Table 4 and Figures 9 and 10).

For post-peak strains in case of increasing ties ratio from 0.5% to 0.65%, for NSC columns without additives, the axial strain of

C2N slightly improved compared to C1N by about 5.5%, while the lateral strain of C2N significantly improved compared to C1N by about 25%, while for NSC columns with hybrid additives, the axial strain of C4A slightly improved compared to C3A with about 7%, while the lateral strain of C4A significantly improved compared to C3A with about 26.5% indicating obvious enhancement in post-peak ductility (see Table 4 and Figures 9 and 10). The high increment in the lateral strain has been achieved with the aid of additional confinement offered by increasing the ties ratio and the hybrid additives presence.

The other comparison of columns in this group was among columns C1N on one hand and columns C2N, C3A, C4A and C5A on the other hand. This comparison may help to give a clearer idea about the effect of additives presence in conjunction with the effect of ties ratio of columns on the response of these columns to axial loading. For instance, and when comparing the results of C4A (ρv=0.65%) to C1N (ρv=0.5%), a gain in the axial capacity has reached about 20%. This gain is about 2.4 that of C2N (ρv=0.65%) relative to C1N as shown in Figure 11. Also, the axial flexibility and toughness of C4A compared to C1N have experienced an incrementation of about 12 and 45%, respectively. Moreover, the obtained lateral strains have reached about 48%.
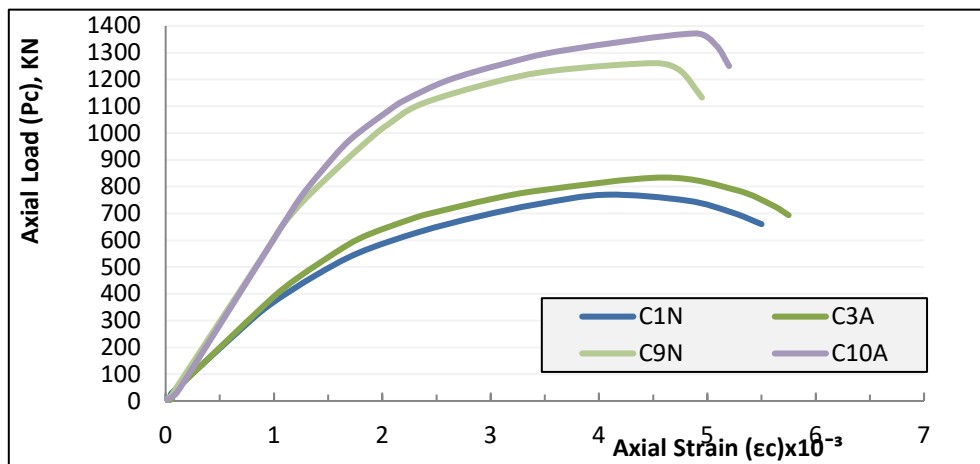
Figure 7: Load-Strain Curve for Group 2.
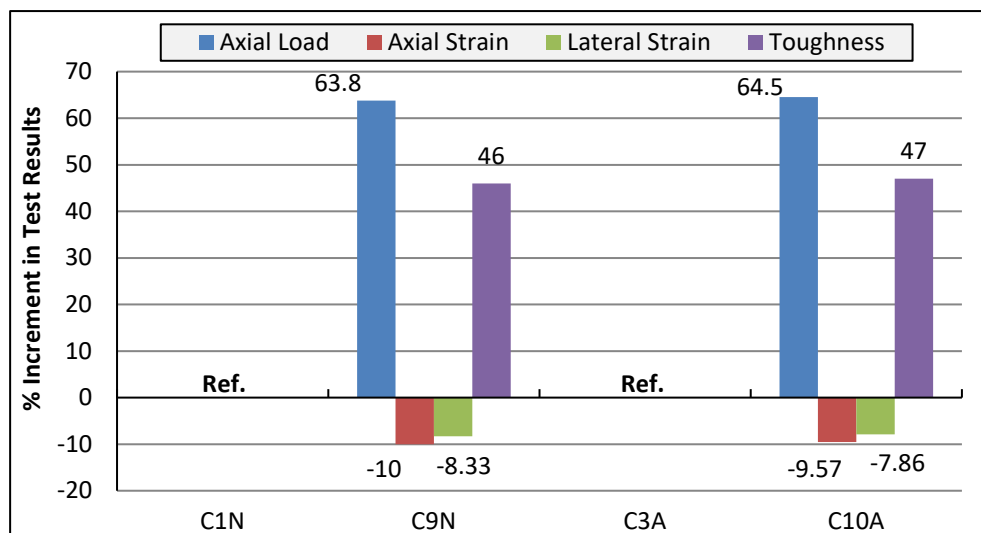
Figure 8: Percent Increment in Test Results for Group 2.

The presence of hybrid additives in RC columns (C4A compared to C3A) enhanced the column behavior in strength and ductility parameters in a higher pace than NSC columns (C2N compared to C1N). This can be attributed to the positive role of hybrid additives in boosting the tensile strength of concrete mixture as NC particles act as additional ties for the column but on the micro scale level. Moreover, the filling effect of MP that has strengthened cement matrix and the transition zone surrounding the aggregates.

Also, the more the ties ratio is (as for C5A compared to C3A), the more improvement in the maximum load was achieved 19.7% improvement ratio. And for post-peak strains, more improvement in the axial and lateral strains was achieved for C5A compared to C3A which reached 13% and 53.6%, respectively (see Table 4 and Figures 9 and 10).

Moreover, it was observed that the behavior of columns with hybrid additions (C3A with low ties ratio) almost resembles the behavior of columns of no additives (C2N with high ties ratio) with respect to strength and ductility. This emphasizes the significant effect of additives on the behavior of columns.

For the toughness parameter in case of increasing ties ratio from 0.5% to 0.65%, the increment in toughness of C2N compared to C1N, and C4A compared to C3A reached about 17% and 27%, respectively. Moreover, when raising the ties ratio from 0.5% to 0.98%, a gain in toughness for C5A reached 43% compared to C3A (see Table 4 and Figure 10).

In summary, the results for group3 columns indicated that increasing the amount of confinement through increasing of ties ratio led to strength and ductility enhancement in columns. Furthermore, it was noted that the hybrid additive presence offered additional confinement in RC columns.

4.5. Effect of the Slenderness Ratio of Columns (Group4)

The effect of increasing slenderness ratio (λ) of columns with hybrid additives was investigated in NSC columns (C3A compared to C6A and C7A), also, the behavior of these three columns was compared to column C1N to give an idea about how much the presence of additives did affect the response of these columns. As expected, the increase of slenderness ratio of
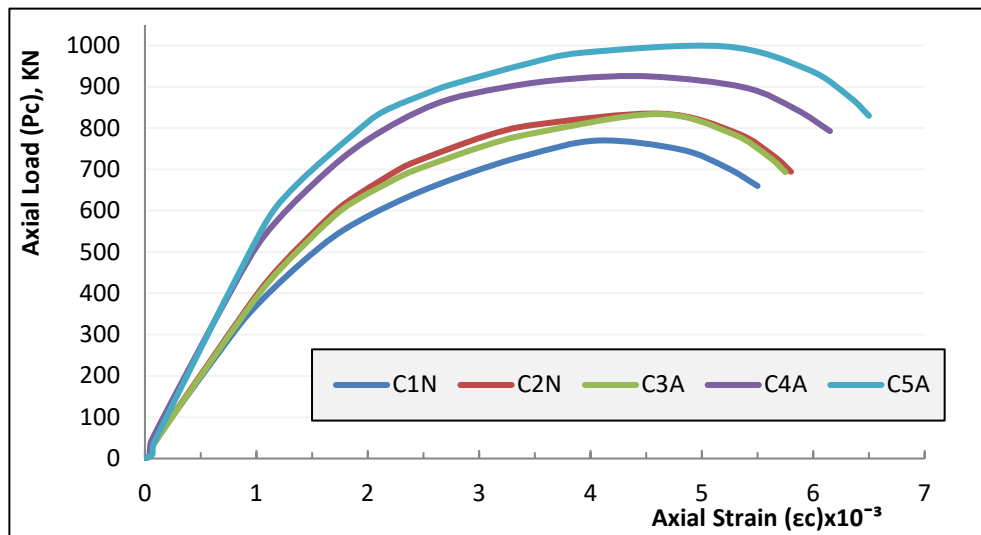
Figure 9: Load-Strain Curve for Group 3
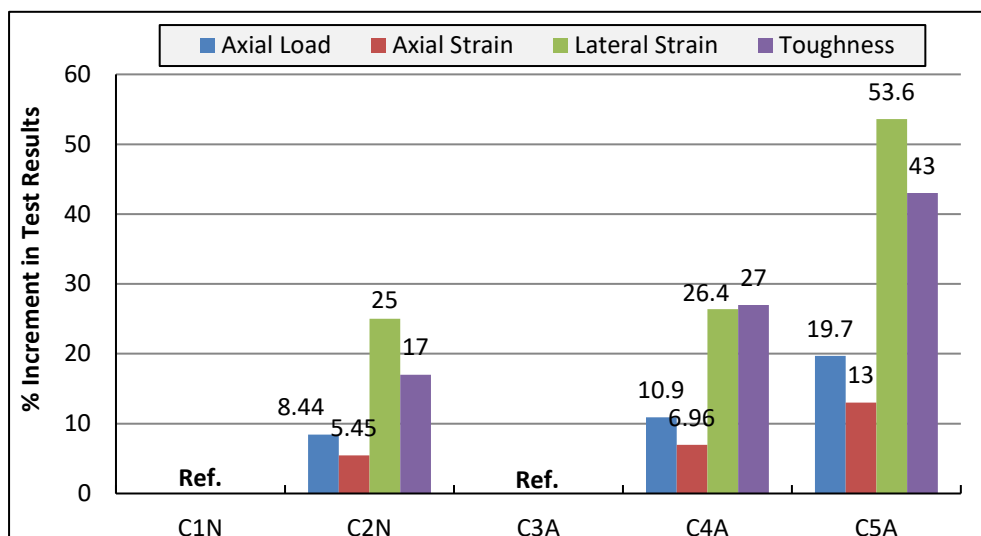
Figure 10: Percent Increment in Test Results for Group 3
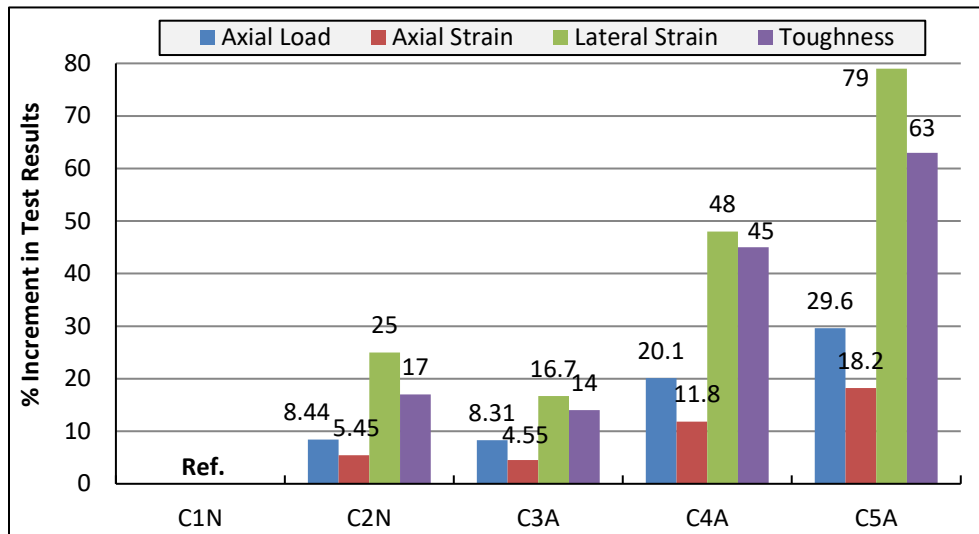
Figure 11: Percent Increment in Test Results for Group 3 Compared to Column C1N

columns led to a decrease in their maximum axial load. For instance, and when comparing the results of C7A to C3A, the reduction in the axial capacity has reached about 17%. Also, its axial flexibility and its toughness have experienced a degradation of about 65 and 70%, respectively. Moreover, the obtained lateral strains have exceeded the 200%, see Table 4 and Figure 12. Also, Figure 13 shows that the ultimate axial strain of column C7A, for example, is about one third that of column C3A. The results of C7A compared to C3A confirm that the higher slenderness ratio of columns gives the chance of higher lateral strains and consequently possibility of inelastic buckling appearance and loss of ductility and axial capacity of columns.

The second comparison was between the three columns (C3A, C6A and C7A) and column C1N. This comparison may help to give a clearer idea about the effect of additives presence in conjunction with the effect of slenderness ratio of columns on the response of these columns to axial loading. For instance, and when comparing the results of C7A to C1N, the reduction in the axial capacity has reached about 10% as shown in Figure 14. Also, its axial flexibility and its toughness have experienced a degradation of about 64 and 67%, respectively. Moreover, the obtained lateral strains have exceeded the 250%.

In summary, the results for group 4 columns indicated that the existence of inelastic buckling through increasing of slenderness ratio led to declining strength and ductility of RC columns.

4.6. Effect of the Longitudinal Steel Bars Ratio ρ% (Group5)

The effect of increasing long. bars ratio (ρ%) of columns with hybrid additives presence was investigated in NSC columns with hybrid additive and variable ρ% (C3A compared to C8A), also, both column test results were compared to NSC column C1N. unexpectedly, column C8A (which has twofold increase in reinforcement ratio of C3A) has shown less axial capacity and higher ductility than C3A, and this may be attributed to the higher load portion transferred to the longitudinal reinforcement. In consequence, local buckling of longitudinal bars has prematurely occurred, and column exhibited lower axial capacity and higher ductility, see Table 4 and Figures 15 and 16. By inspecting Figure 16, the comparison between columns C8A and C3A has shown loss of axial capacity and toughness of about 14% and 10%, respectively. On the other hand, the increase in axial and lateral strains has reached about 4% for both test results.
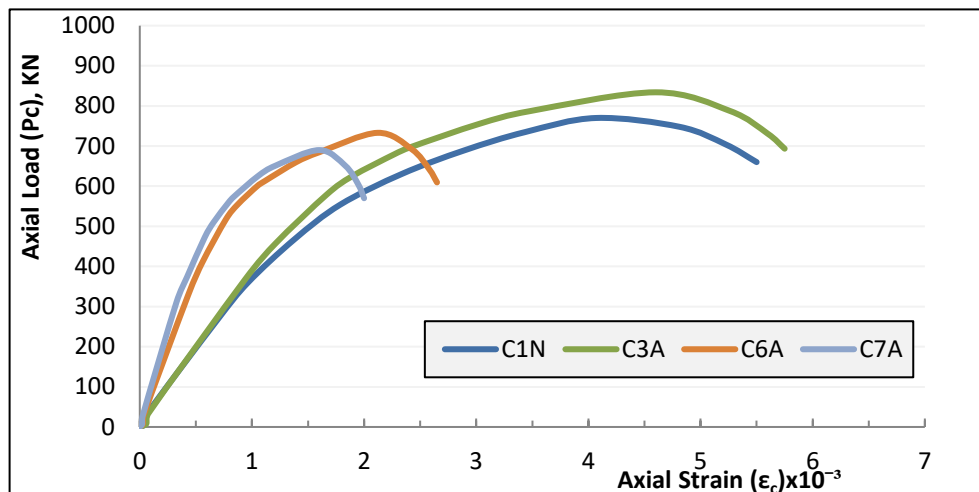
Figure 12: Load-Strain Curve for Group 4
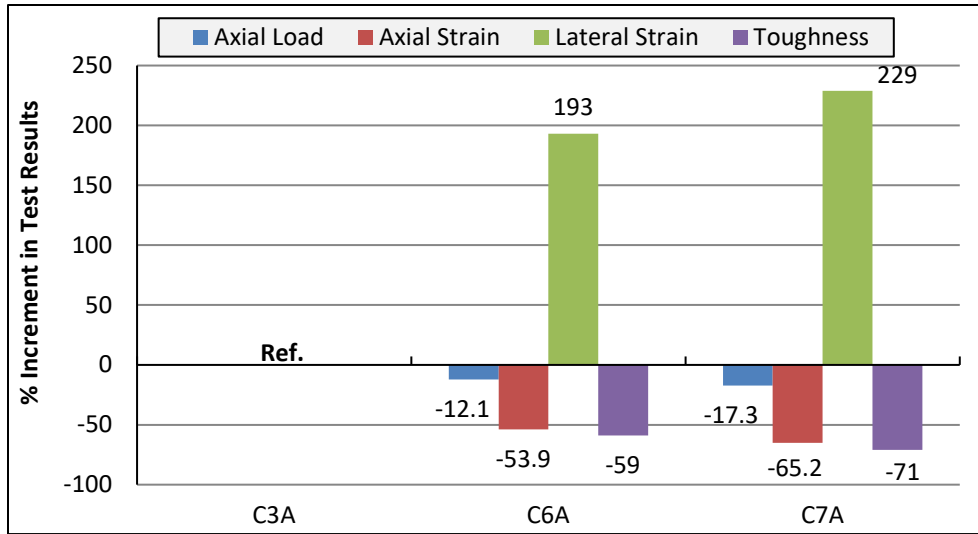
Figure 13: Percent Increment in Test Results for Group 4.
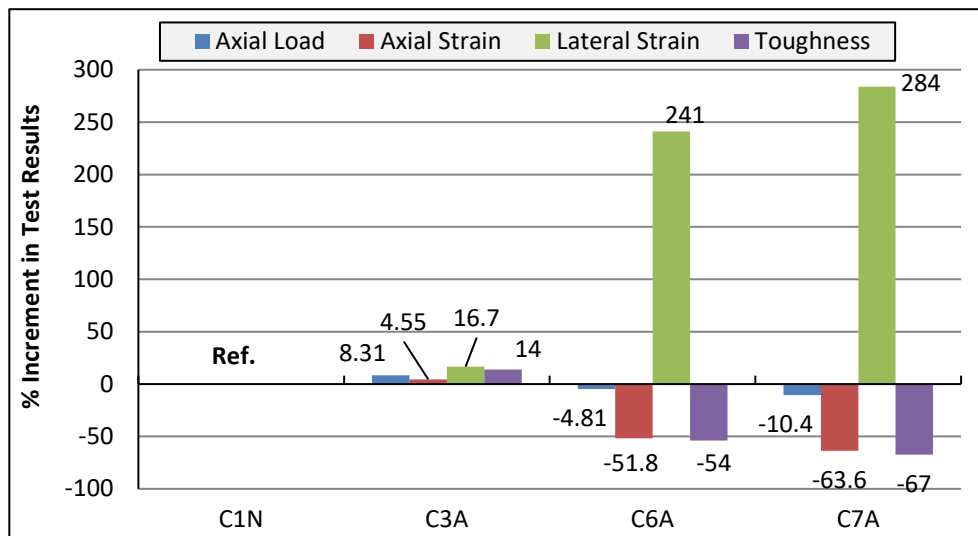
Figure 14: Percent Increment in Test Results for Group 4 Compared to Column C1N.

The other comparison of columns in this group was among columns C1N on one hand and columns C3A and C8A on the other hand. As can be seen from Figure 17, for instance, the comparison between columns C8A and C1N has shown loss of axial capacity of about 7%. On the other hand, the increase in axial strain, lateral strain and toughness has reached about 9%, 21% and 3%, respectively.

In summary, the results for group 5 columns indicated that increasing of long bars ratio led to declining strength and enhancing post-peak strains in columns.

4.7. Theoretical Evaluation of the Experimental Results

In this part, the experimentally evaluated ultimate axial compression load of the NSC/HSC columns with and without hybrid additive were compared with standard codes. Therefore, for each specimen, the calculated capacities according to different codes requirements [49–51]were determined and compared to the experimental results as shown in Table 5 and Figure 18. For each code method, all reduction factors of safety as materials and

resistances factors were used to give thorough and reliable comparison between the calculated and experimental capacities that design engineer can effectively use to design such elements. The standard equations used in this study are mentioned below for each code:

ACI 318-18:

$$Pu= 0.8 \; \emptyset \; (0.85 \; fc' \; (Ac\text{-}Ast) + Fy. \; Ast \qquad (1) \qquad [49]$$

Eurocode 2-2006:

$$Pu= 0.567. \; fc'. \; Ac + 0.87. \; Fy. \; Ast \qquad (2) \qquad [50]$$

ECP 203-2018:

$$Pu= 0.35. \; Fcu \; (Ac\text{-}Ast) + 0.67.Fy. \; Ast \qquad (3) \qquad [51]$$

Where, Fcu: Cube Concrete characteristics strength (MPa); fc': Cylinder Concrete characteristics strength (MPa); Ac: total cross sectional of column(mm2); Ast: total cross sectional of longitudinal bars (mm2); Fy: yield strength of longitudinal bars (MPa), Ø: Strength reduction factor.
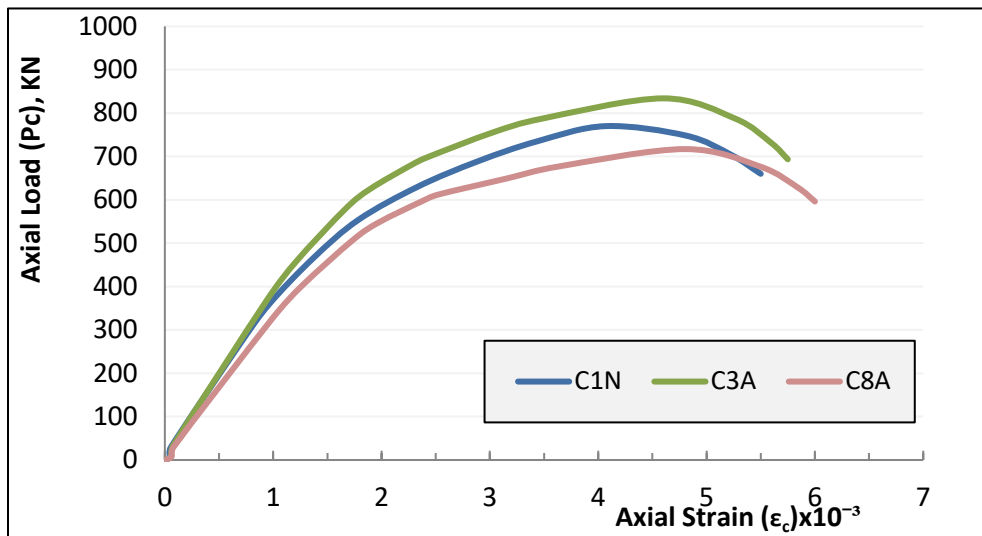
Figure 15: Load-Strain Curve for Group 5
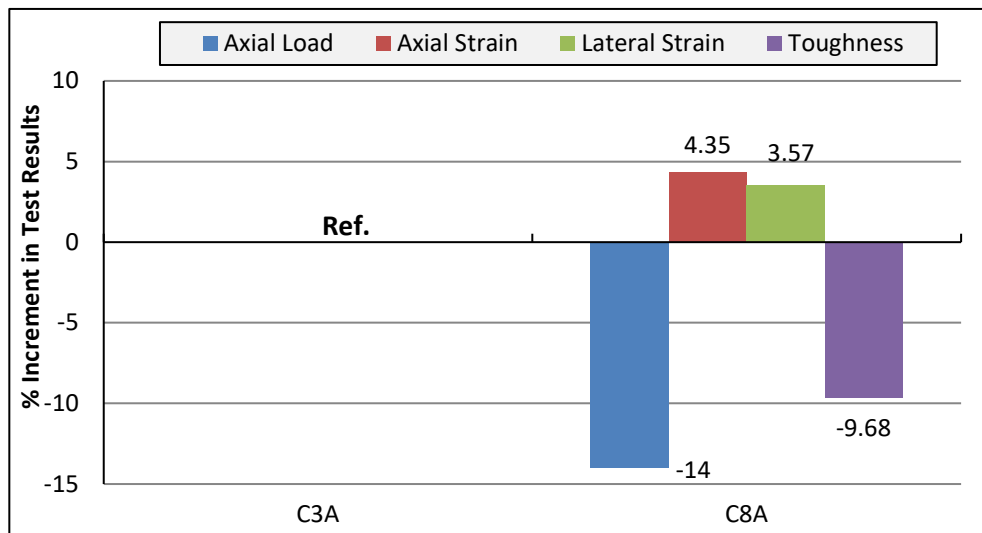
Figure 16: Percent Increment in Test Results for Group 5
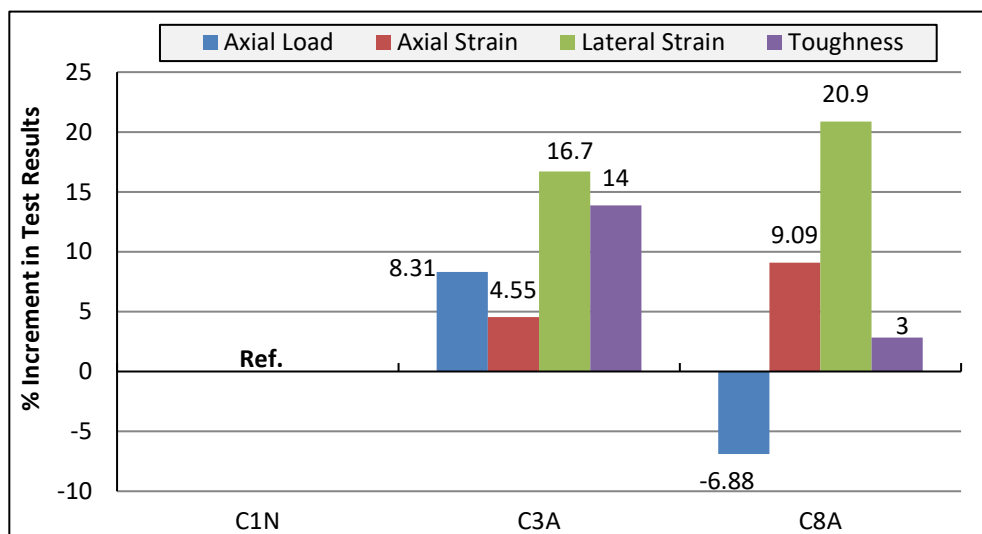
Figure 17: Percent Increment in Test Results for Group 5 Compared to Column C1N

Referring to Table 5 and Figure 18, it is observed that the calculated axial capacities of the NSC/HSC columns are almost the same as the used codes do not consider the confinement effect and mineral additives either has pozzolanic or filling effect as NC and MP for predicting the ultimate axial strength of the columns. As can be seen, the comparative studies (Pc compared to Pu) show that the calculated results are mostly lower than the experimental results which denotes that the calculated column capacities using the three preceding codes are almost on the conservative side.

For NSC columns, Eurocode 2-2006 [50] gives the closest estimate with an average of 21% lower than the experimental results, while ACI 318-18 [49] gives the greatest conservative results with an average of 66% lower than the test results, then it is followed by ECP 203-2018 [51] with an average of 59%. For HSC columns, Eurocode 2-2006 [50] gives an average estimate of about 53% lower than the experimental results, however ACI 318-18 [49] and ECP 203-2018 [51] gives an average estimate of capacity by about half the experimental results which indicates great conservative results.

It can be noted that, the ratio of experimental to calculated capacities (Pc/Pu) of RC columns with hybrid additive is bigger than columns without additive, an indicator of the enhanced bearing capacity of columns with hybrid additive when compared to conventional concrete.

It is clear that considerable contradictions exist between codes and the experimental results especially for HSC columns. It can be attributed to important parameters not adopted in these codes as neglecting of the ties confinement, increasing concrete strength and finally, regarding this study, effect of various mineral additives to concrete mixture that enhance its performance, thus affecting on the behavior of the columns.

4.8. Economic Feasibility Study of Using Nano Clay and the Marble Powder in Concrete Construction

Economic feasibility study for using the optimum ratios of NC and MP in concrete has been depicted herein. The cost of mixes of columns 1N and 3A were analyzed and presented in Table 6. It can be concluded from the feasibility study for the two mixes that the increase in cost was about 43%. On the other hand, the gains in axial capacity, axial strain, lateral strain and toughness were about 9, 5, 17 and 14%, respectively. These gains may seem unfeasible in comparison to the increase in the cost of concrete. But, combining these gains to the environmental benefits of reducing CO_2 emissions of cement production, which was reduced by about 15% in this mix, and using MP which represents a burden on landfills and waste management systems, gives the real feasibility of using such mixes. Moreover, these concrete mixes with hybrid additives are more durable as the filling effect of MP reduces its permeability and guarantees its resistance to any hazard attacks from the surrounding environment.

Table 5: Comparison Between Calculated Axial Capacities of Specimens by the Different Codes with the Experimental Results

ID	Exp. Axial Load	ACI 318-18 [49]		Eurocode 2-2006 [50]		ECP 203-2018 [51]	
	Pc (KN)	Pu (KN)	Pc/ Pu	Pu (KN)	Pc/ Pu	Pu (KN)	Pc/ Pu
C1N	770	467.6	1.65	640.2	1.20	488.4	1.58
C2N	835	467.6	1.79	640.2	1.30	488.4	1.71
C3A	834	487.2	1.71	665.7	1.25	507.8	1.64
C4A	925	487.2	1.90	665.7	1.39	507.8	1.82
C5A	998	487.2	2.05	665.7	1.50	507.8	1.97
C6A	733	487.2	1.50	665.7	1.10	507.8	1.44
C7A	690	487.2	1.42	665.7	1.04	507.8	1.36
C8A	717	567.1	1.26	808.8	0.89	612.4	1.17
Average for NSC Columns	….	….	1.66	….	1.21	…..	1.59
C9N	1261	626.1	2.01	846.3	1.49	645.3	1.95
C10A	1372	651.2	2.11	879.0	1.56	670.1	2.05
Average for HSC Columns	….	….	2.06	….	1.53	….	2.00
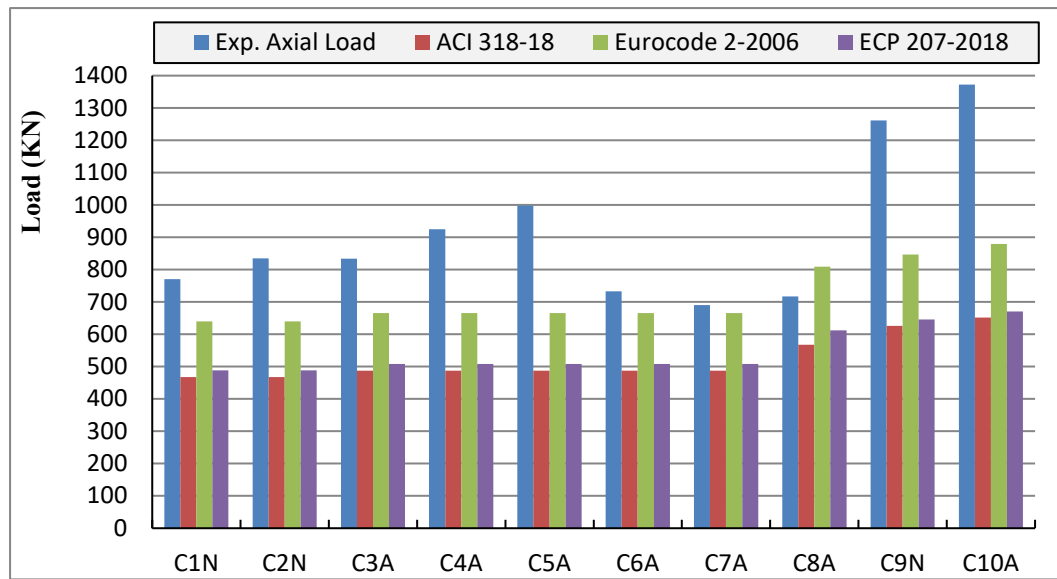
Figure 18: The Calculated Axial Capacities of Specimens by the Different Codes relative to the Experimental Results

Table 6: Economic feasibility of nano clay used in RC columns

Mix	Actual Fcu (Mpa)	Cement (Kg/m³)	Price of Cement (L.E)	NC (Kg/m³)	Price of NC (L.E)	Total Price of (Cement & NC) in the Mix (L.E)	% of Increment in the Cost	% of Increment in the Column Behavior (C3A compared to C1N)
1(N)*	48.7	400	360	---	---	360	Ref.	Ref.
2(A)**	51.2	339.5	305.5	10.5	210	515.5	43%	• 9% in Axial Load • 5% in Axial Strain • 17% in Lateral Strain • 14% in Toughness

*N: No additives **A: Additives (3%NC and 10%MP)

5. Summary and Conclusions

Ten reinforced concrete columns with and without the optimum ratio hybrid additives were tested under axial loading to determine their ultimate capacity, axial and lateral strains, ductility, and compared their failure pattern. The effect of presence of hybrid additives on concrete strength, ties ratio, slenderness ratio of columns and longitudinal steel bars ratio were studied. Based on the experimental results the following conclusions were obtained:

1. In both NSC and HSC RC columns, the presence of optimum ratios of the hybrid additive (NC and MP) has a positive effect on both strength and ductility of RC columns.

2. The presence of hybrid additives in RC columns with high ties ratio reasonably enhanced the column behavior in strength and ductility more than columns with low ties ratio.

3. The presence of NC sheets in the concrete mix added additional confinement in RC columns and improved the ductility of the tested columns and achieved highly increment in the lateral strain and toughness.

4. Increasing the concrete strength for column with hybrid additive led to slightly enhancing for axial load, ductility and toughness compared to columns without additive.

5. The behavior of RC column with hybrid additive and with low ties ratio (0.5%) almost approached the behavior of NSC column with high ties ratio (0.65%) in strength and ductility parameters. This emphasizes the significant effect of additives on the behavior of columns

6. Higher axial load capacity, better ductile performance, greater reduction in the ties ratio and larger dissipation of energy can be achieved by using hybrid additions in the RC columns.

7. Columns test results indicated that exhibition inelastic buckling through increasing of slenderness ratio led to declining strength and ductility in columns.

8. The high ratio of longitudinal steel bars leads to declining strength and enhancing post-peak strains in columns.

9. The failure mechanisms of the tested columns were almost the same unless RC columns made of HSC that failed more suddenly and its brittleness is notorious.

10. The presence of hybrid additions makes the RC columns less brittle compared to NSC/HSC columns. Generally, the RC columns with a higher concrete strength grade, a lower ties ratio, a higher slenderness ratio and a lower longitudinal reinforcement ratio exhibit a brittle failure behavior of RC columns.

11. Various coefficients should be adopted in the used codes as they have effect on the strength and ductility of columns such as confinement coefficient due to ties, increasing concrete strength for HSC and the effect of various mineral additives to concrete mixture.

12. The ratio of experimental to calculated capacities (Pc/Pu) of RC columns with hybrid additive is bigger than columns without additive, an indicator of the enhanced bearing capacity of columns with hybrid additive when compared to conventional concrete.

13. The calculated column capacities using the three preceding codes are mostly lower than the experimental results which denotes that design of columns strengths are almost on the conservative side. ACI 318-18 formula led to the greatest conservative estimate especially in HSC columns.

Conflict of Interest

The authors declare no conflict of interest.

References

[1] D. Le, Q. Wang, L. Galoisy, G. Renaudin, L. Izoret, G. Calas, "Greening effect in slag cement materials," Cement and Concrete Composites, **84**, 93–98, 2017, doi:10.1016/j.cemconcomp.2017.08.017.

[2] M.C. Bignozzia, "Sustainable cements for green buildings construction," Procedia Engineering, **21**, 915–921, 2011, doi:10.1016/j.proeng.2011.11.2094.

[3] K.M. Liew, A.O. Sojobi, L.W. Zhang, "Green concrete : Prospects and challenges," Construction and Building Materials, **156**, 1063–1095, 2017, doi:10.1016/j.conbuildmat.2017.09.008.

[4] M. Glavind, "Green concrete structures," Structural Concrete, **12**(1), 23–29, 2011, doi:10.1002/suco.201000022.

[5] J. David, M. Flower, J.G. Sanjayan, "Green House Gas Emissions due to Concrete Manufacture," Int J LCA, **12**(5), 282–288, 2007.

[6] S. Kubba, Green Building Materials and Products, Elsevier Inc: 227–311, 2012, doi:10.1016/B978-0-12-385128-4.00006-8.

[7] F. Sanchez, K. Sobolev, "Nanotechnology in concrete - A review," Construction and Building Materials, **24**(11), 2060–2071, 2010, doi:10.1016/j.conbuildmat.2010.03.014.

[8] K. Sobolev, M.F. Gutierrez, "How Nanotechnology Can Change the Concrete World," Construction and Manufacturing, 113–116, 2005.

[9] R. Olar, "Nanomaterials and Nanotechnologies for Civil Engineering," Technical University of Iasi Construction. Architecture, **4**, 109–117, 2011.

[10] V.K. Ganesh, "Nanotechnology in Civil Engineering," European Scientific Journal, **8**(27), 96–109, 2012.

[11] B. Birgisson, A.K. Mukhopadhyay, G. Geary, M. Khan, K. Sobolev, Nanotechnology in Concrete Materials, Transportation Research Circular, 2012.

[12] A.A. Aliabdo, A.M. AbdElmoaty, E.M. Auda, "Re-use of waste marble dust in the production of cement and concrete," Construction and Building Materials, **50**, 28–41, 2014, doi:10.1016/j.conbuildmat.2013.09.005.

[13] S.I. Zaki, O.A. Hodhod, F.E. Omar, "Comparison Between the Effect of Addition of Nano-Calcium Carbonate and Nano-Kaoline on Developing the Properties of Concrete," Интеллектуальные Системы в Производстве (Intelligent Systems in Production), **16**(3), 147–159, 2018, doi:10.22213/2410-9304-2018-3-147-159.

[14] M.A.. Langaroudi, Y. Mohammadi, "Effect of nano-clay on workability ,

[15] N. Hamed, M.S. El-feky, M. Kohail, E.A.R. Nasr, "Effect of nano-clay de-agglomeration on mechanical properties of concrete," Construction and Building Materials, **205**, 245–256, 2019, doi:10.1016/j.conbuildmat.2019.02.018.

[16] S.I. Zaki, H.A. Hodod, M.A. Mahdi, "The effect of using hybrid nano materials on drying shrinkage and strength of cement pastes," Nanotechnologies in Construction, **8**(2), 109–132, 2016, doi:DOI: dx.doi.org/10.15828/2075-8545-2016-8-2-109-134.

[17] S.I. Zaki, H.A. Hodhod, Y.A. Mosleh, "Assessing the Durability of Blended Concrete with Some Nanomaterials," in 9th International Conference on Nano Technology in Construction , Sharm El-Sheikh, Egypt, 2017.

[18] B. Sabir, S. Wild, J. Bai, "Metakaolin and calcined clays as pozzolans for concrete: A review," Cement and Concrete Composites, **23**(6), 441–454, 2001, doi:10.1016/S0958-9465(00)00092-5.

[19] M.S.M. Norhasri, M.S. Hamidah, A.M. Fadzil, O. Megawati, "Inclusion of nano metakaolin as additive in ultra high performance concrete (UHPC)," Construction and Building Materials, **127**, 167–175, 2016, doi:10.1016/j.conbuildmat.2016.09.127.

[20] A.M. Mohamed, "Influence of nano materials on flexural behavior and compressive strength of concrete," Housing and Building National Research Center, 2015, doi:10.1016/j.hbrcj.2014.11.006.

[21] A. Hakamy, F.U.A. Shaikh, I.M. Low, "Characteristics of nanoclay and calcined nanoclay-cement nanocomposites," Composites Part B, **78**, 174–184, 2015, doi:10.1016/j.compositesb.2015.03.074.

[22] P. Hosseini, A. Afshar, B. Vafaei, A. Booshehrian, E.M. Raisi, A. Esrafili, "Effects of nano-clay particles on the short-term properties of self-compacting concrete," European Journal of Environmental and Civil Engineering, 2015, doi:10.1080/19648189.2015.1096308.

[23] S. Chandrusha, S.R. Begum, G.M. Basha, "Utilization of Various Waste Materials in Concrete a Literature Review," International Journal of Engineering Science and Computing, **7**(11), 15386–15390, 2017.

[24] W.H. Khushefati, M.H. Swellam, M.I. Alattar, "Recycling granite and marble sludge as a construction material," International Journal of Current Research, **7**(08), 18982–18987, 2015.

[25] H. Elyamany, A.M. AbdElmoaty, B. Mohamed, "Effect of filler types on physical , mechanical and microstructure of self compacting concrete and Flow-able concrete," Alexandria Engineering Journal, 2014, doi:10.1016/j.aej.2014.03.010.

[26] R. Ciccu, R. Cosentino, C.C. Montani, A. El Kotb, H. Hamdy, "Strategic study on the Egyptian Marble and Granite Sector," Industrial Modernisation Centre, (August), 2005.

[27] S. Natarajan, P. Murugesan, "Synergistic Effect of Marble Powder and Green Sand on the Mechanical Properties of Concrete, Metakaolin-cement," Materials, **12**(476), 1–17, 2019, doi:10.3390/ma12030476.

[28] M.S. Hameed, A.S.S. Sekar, L. Balamurugan, V. Saraswathy, "Self-Compacting Concrete Using Marble Sludge Powder and Crushed Rock Dust," KSCE Journal of Civil Engineering, **16**(6), 980–988, 2012, doi:10.1007/s12205-012-1171-y.

[29] B. Rai, K. Naushad, A. Kr, T. Rushad, S.. Duggal, "Influence of Marble powder/ granules in Concrete mix," International Journal of Civil and Structural Engineering, **1**(4), 827–834, 2011.

[30] A.. Mashaly, B.. Shalaby, M.. El-Hefnawi, "Characterization of The Marble Sludge of The Shaq El Thoaban Industrial Zone , Egypt and Its Compatibility for Various Recycling Applications," Australian Journal of Basic and Applied Sciences, **6**(3), 153–161, 2012.

[31] O.M. Omar, G.D. AbdElhameed, M.A. Sherif, H.A. Mohamadien, "Influence of limestone waste as partial replacement material for sand and marble powder in concrete properties," Housing and Building National Research Center, **8**(3), 193–203, 2012, doi:10.1016/j.hbrcj.2012.10.005.

[32] S. Singh, A. Tiwari, R. Nagar, "Comparative Assessment of Effects of Sand & Cement Replacement in Concrete by Marble Dust & Inturn Deriving An Optimum Design Mix For Concrete Paver Blocks," in Global Stone Technology Forum (GSTF) December 17-18, Udaipur, 2015.

[33] Y. Shanmugasundaram, D. Nagarajan, S. Mohankumar, "Behavioural Investigation on the use of Nanosilica as An Additive in Concrete," ACEE Int. J. on Transportation and Urban Development, **3**(1), 2013.

[34] J. V Silva, R. Ismael, R.N.F. Carmo, C. Lourenço, E. Soldado, H. Costa, E. Júlio, "Influence of nano-SiO2 and nano-Al2O3 additions on the shear strength and the bending moment capacity of RC beams," Construction and Building Materials, **123**, 35–46, 2016, doi:10.1016/j.conbuildmat.2016.06.132.

[35] E.M. Lotfy, M. Abdelshakor, "Flexural Behavior of Reinforced Concrete

Beams With Nano-Metakaolin," International Journal of Latest Trends in Engineering and Technology, **8**(2), 231–240, 2019, doi:DOI: http://dx.doi.org/10.21172/1.82.031.

[36] M.A. Ahmed, E.M. Lotfy, "Structural Performance of Reinforced Concrete Beams with Nano- Meta-Kaolin in Shear," IOSR Journal of Mechanical and Civil Engineering (IOSR-JMCE), **14**(2), 88–96, 2017, doi:10.9790/1684-1402048896.

[37] W.A. Salman, I.H. El-kersh, E.M. Lotfy, M.A. Ahmed, "Behavior of reinforced concrete inverted T-section beams containing Nano-silica," IOSR Journal of Mechanical and Civil Engineering (IOSR-JMCE), **16**(5), 13–22, 2019, doi:10.9790/1684-1605041322.

[38] N. Soliman, "Effect of using Marble Powder in Concrete Mixes on the Behavior and Strength," International Journal of Current Engineering and Technology, **3**(5), 1863–1870, 2013.

[39] M.A. Mahdi, A.H. Ghallab, S.I. Zaki, A.S. Elmannaey, "Utilization of Nano Clay , Marble Powder and Silica Fume Waste as Hybrid Addition for Enhancing the Properties of Concrete," International Journal of Engineering Research & Technology (IJERT), **9**(12), 277–294, 2020.

[40] ASTM C150, Standard Specification for Portland Cement, Annual Book of ASTM Standards, doi:10.1520/C0150_C0150M-12.

[41] ES 262-1, Egyptian Standards – Ferrous Products Committee. Steel for the reinforcement of concrete Part1: – Plain bars; ES 262-1. Cairo (Egypt): Egyptian Organization for Standards and Quality, EOS, 2009.

[42] ES 262-2, "Egyptian Standards – Ferrous Products Committee. Steel for the reinforcement of concrete Part2: – Ribbed bars; ES 262-2. Cairo (Egypt): Egyptian Organization for Standards and Quality, EOS," 2009.

[43] ASTM C1240-03a, Standard Specification for Silica Fume Used in Cementitious Mixtures, 2003.

[44] BS EN 934-2:2001, "Admixtures for concrete , mortar and grout," British Standard,.

[45] BS EN 12390-3, Testing hardened concrete - Part 3 : Compressive strength of test specimens, 2009.

[46] T. Ichinose, Y. Kanayama, Y. Inoue, J.. Bolander, "Size effect on bond strength of deformed bars," Construction and Building Materials, **18**, 549–558, 2004, doi:10.1016/j.conbuildmat.2004.03.014.

[47] S. Sener, Z. Bazant, A. Fellow, E. Becq-Giraudon, "Size Effect on Failure of Bond Splices of Steel Bars in Concrete Beams," Journal of Structural Engineering, **125**, 653–660, 1999.

[48] X. Qian, Z. Li, "The relationships between stress and strain for high-performance concrete with metakaolin," Cement and Concrete Research, **31**, 1607–1611, 2001.

[49] ACI 318-19, Building Code Requirements for Structural Concrete, 2019.

[50] Eurocode 2, Manual for the design of concrete building structures to Eurocode 2, (September), 2006.

[51] ECP 203, Egyptian Code for Design and Construction of Reinforced Concrete Structures, 2018.

A Survey of FPGA Robotics Applications in the Period 2010 – 2019

Dimitris Ziouzios[1], Pavlos Kilintzis[2], Nikolaos Baras[1,*], Minas Dasygenis[1]

[1]*Department of Electrical and Computer Engineering, University of Western Macedonia, Kozani, 50100, Greece*

[2]*Department of Mechanical Engineering, University of Western Macedonia, Kozani, 50100, Greece*

A R T I C L E I N F O	A B S T R A C T
	FPGAs constitute a flexible and increasingly popular controlling solution for robotic applications. Their core advantages regarding high computational performance and software-like flexibility make them suitable controller platforms for robots. These robotic applications include localization / navigation, image processing, industrial or even more complex procedures such as operating on medical or human assistant tasks. This paper provides an overview of the publications regarding different robotic FPGA application fields as well as the most commonly-used robot types used for those applications for the 10-year period of 2010-2019. A short description of each paper reviewed is also included, providing a total view of FPGA technology trends in robotic applications over the last decade.

1. Introduction

Field programmable gate array (FPGA) devices are reconfigurable circuits composed of numerous interconnected logic cells. FPGAs contain an array of programmable logic blocks, and a hierarchy of "reconfigurable interconnects" that allow the blocks to be wired together. They are still used as a high-performance computing platform in multiple applications nowadays, despite their overshadowing by CPUs and GPUs. The general core advantages of FPGAs are that they can be easily connected to most types of circuits due to their protocol-independent serial links and they offer hard real-time computations and highly parallel effective programming with low power consumption, using algorithmic high-level synthesis [1]. FPGAs can be reconfigured and reprogrammed according to the user's requirements, unlike fixed hardware structures that CPUs have. This allows users to utilize them in a vast variety of applications.

Robots today are used for multiple tasks, for both industrial and consumer purposes that require high performance and low power consumption. They can be used for manufacturing or logistics purposes, while offering medical, educational, home, defense and other activities in the services' sector. So, the applications implemented on FPGAs in the robotics sector contain several multi-factorial tasks from multiple domains. Primarily those tasks include vision, sound or touch response systems and object tracing through processing of a high data flow coming from

sensor inputs. Furthermore, increased real-time requirements for controlling robotics' functionalities such as the movement of a robot, make FPGAs to be a more attractive processing solution since they can be reconfigured as many times as it is necessary, even during runtime, while they are utilized, until the required functionality is properly achieved. FPGAs can actually rewire their internal circuitry in order to allow configuration, after the control system is installed onto the field. Moreover, the high-power consumption of robotics applications indicates FPGAs as suitable computational systems in comparison to other solutions. In fact, the advantages of using reconfigurable dynamic systems do not exclusively lie on the increased adaptability to changing conditions, but also on reducing power consumption without affecting the robot's capabilities. Overall, the size and speed of an FPGA is similar to the application-specific integrated circuit (ASIC), but their shorter design cycle and reconfigurability capabilities make them more flexible for use in robotic applications [2].

FPGAs are a mature implementation technology, spanning over 35 years of technology improvements. At the same time, after 70 years of evolution in robotics the controlling complexity of them has reached a level that only high-end processing cores can handle. Investigating the blending between the robotics and the FPGAs in the related literature, we located a gap. In this paper, we aim to answer the research question: Given all the advantages in CPUs and GPUs, is it viable to use FPGAs in robotics applications, and if yes which are the areas that FPGAs excel in the robotics domain and what challenges loom ahead? Towards

---

*Corresponding Author: Nikolaos Baras, Email: nbaras@uowm.gr

this, we investigated IEEE listed scientific publications in the 10-year period between 2010 and 2019 in order to get an overall view of the typical application fields of FPGAs in robotic applications. Figure 1 shows the absolute quantity of the total publications regarding journals, conferences, early-access articles and magazines in the IEEE Xplore and ACM digital library depicting the actual publication tendency over the last 27 years, since the library includes publication data since 1993. The total publications count from 1993 to 2019 regarding FPGAs in robotics is 1174 publications, including the aforementioned four types of publications. The publication count for the testing period of 2010-2019 counts 815 publications in total, where 762 are conference papers, 49 journal papers, 2 early-access articles and 2 magazine articles. The average publication number over the 10 year investigation period is almost 80 publications per year. As accrued from Figure 1, from 1993 to 2001 the publication count remains relatively steady with less than 10 publications / year, while from 2002 to 2009 there is a yearly significant increase, reaching the top value of 81 publications in 2009. Since then, a fluctuating count is observed in the testing time period of 2010-2019, with the maximum value accomplished in 2019 with 102 publications. Figure 1 imprints the technological boom in the FPGA capabilities that started in the millennium (2000), allowing wide FPGA usage in robotic applications

This tendency lasted for almost a decade, until 2009 and since then the robotic FPGA applications - according to the publications count - remain relatively steady with fluctuating tendencies. Since the total publications for the tested time period are almost 800, the researchers choose to analyze 20 popular publications for each year, in order to imprint the latest scientific tendencies. The total number of publications tested for the 10-year period is 200.

The paper is structured as follows. First, a brief theoretical analysis of the modern robot types regarding their application fields and interaction mechanism is given, according to the latest literature trends. The description of the three main robot categories as classified in this survey, follows. The six main FPGA application fields, as uncovered in the survey analysis, are then quoted.

Figure 1: FPGA Robotics-related publications in IEEE Xplore and ACM digital library per year

The conclusion section sums up our findings, as indicated by the survey findings. All reviewed literature is quoted with application field and robot type categorization, a short description of each paper and the year of the publication.

2. Related Work

A shortlist of FPGA-related studies uncovering related application fields, architectures and technology trends has been revealed in the survey. The most detailed view for survey applications for a distinct period of time is included in [1]. 22 distinct technology applications of FPGAs (+ "other" quoted as distinct category) for a 15-year period are documented, investigating 815 publications in the IEEE Xplore and ACM digital library for the aforementioned duration. This survey offers a relatively indicative view of the FPGA technology trends until 2015, however it does not investigate the FPGA architectures designed specifically for robotics applications. Paper [3] highlights the availability of reconfigurable applications as platforms for digital controllers and quotes the most important factors for the technology trend of FPGAs utilization in comparison to other architectures, primarily due to the acceleration and flexibility of FPGAs, reduction of costs and reduced energy consumption. Study [4] quotes a general description of FPGAs, regarding their use as accelerators and simulator platforms, the usage of their integrated memory and their fault tolerance as well as the programming languages and computation methodologies. However, it does not quote applications per year or include a specific distinction of application fields The FPGA virtualization techniques are included in [5], separated into three categories - resource level, node level and multi-node level. The first level investigates whether FPGA's resources are reconfigurable or not. The node level explores the applications needed in both software and hardware terms regarding virtualization at a single FPGA. The existing architectures of how to connect multiple FPGAs are described in the multi-node level. The survey [6] investigates FPGA's routing architectures, dividing them into island-style routing and hierarchical routing. Furthermore, it quotes a brief description of the recent technology applications of FPGAs, distinguishing them into eight distinct categories. In conclusion, there are no specific surveys like this one and for this reason we believe our paper will play a pivotal role as a reference for researchers in the field of implementing robotic applications on FPGAs.

3. Application Fields of FPGAs in Robotics

In our survey, we categorized the papers into 6 major categories, according to the application. In order for an application field to be categorized as a distinct category, at least 5 publications had to be identified in the databases. Some application fields can be mixed, for instance, a robotic controller may use a regular FPGA algorithm and Fuzzy logic architecture or a navigation application can use SoC FPGA image processing systems. Distinct categories as well as mixed ones are referred to the Application Field column of Table 1, where the research overview is depicted. The Robot type column includes the type of robot which this publication's application is designed for. A short description of the publication's application regarding the algorithms used, the software or the type of the FPGA controller chips is included in the next column. The publication year and the reference number are depicted in the last two columns of Table 1.

3.1. Classification of Robots

While there is no strict classification of robots, most robotic applications can be either categorized according to their mechanism of interaction or according to their application field [7]. Figure 2 depicts the robot classification according to their mechanism of interaction [7]:
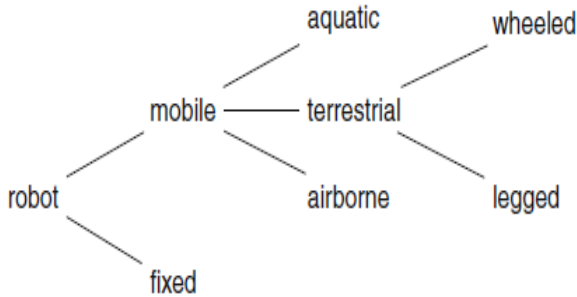
Figure 2: Robot classification by interaction mechanism [7]

The basic classification of robots according to their application field is shown on Figure 3. It has to be noted that the six sub-categories of Fig. 3 can also include variations. For instance, educational robots can either be wheeled or humanoid (legged) and industrial robots can be either articulated robots, cartesian robots, parallel, spherical, or SCARA, etc. [8]. The aforementioned categories are based on the primary means of navigation (for educational robots) or the robot's basic configuration (for industrial robots).

However, this survey includes the robotic applications that are FPGA-applied, so the classification of robots is done according to those categories that can use the application fields found in the survey publications and analyzed in the next chapter. The main robot categories of the FPGA-based robotic applications included in this survey are the following:

- Industrial Robots (A1)

- Autonomous Mobile Robots (A2)

- Humanoid Robots (A3)

For a robot type to be classified as a distinct category, at least 5 publications had to be found for the selected period. In other cases, this column is classified as "other", implying a different type of robot, described in the "description" column such as medical, defense, educational, etc.
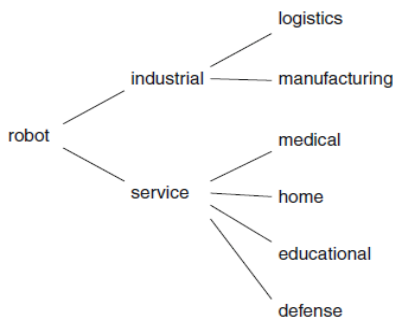
Figure 3: Classification of robots according to their application field [7]

3.1.1. Industrial Robots

Industrial robots constitute one of the major of the FPGA-related publications in this survey, as depicted in Fig. 4. The main subcategories of this main robot category are [10]:

- Articulated robots

- Cartesian robots

- Cylindrical robots

- SCARA robots

- Delta robots

- Polar robots

The articulated robot type is amongst the most common types of industrial robotics. It includes a mechanical arm conjoined to a stable base. Rotary joints connecting the arm associations may vary from two to ten joints although the most common robots are the ones with six joints. The joints give the robot additional freedom to its movement while the joints can be either orthogonal or parallel. Cartesian or Gantry robots are also amongst the most common robot types. They have a rectangular configuration with three prismatic joints (X, Y, Z) allowing linear motion, while some Gantry robots have an additional wrist allowing rotational motion. Cylindrical robots use a main arm making an up-and-down motion. This arm is internally embedded with a cylinder allowing the extension/reaction motion. Cylindrical robots use a 3-dimensional coordinated architecture using a specifically selected reference axis for selecting point positions. Cylindrical robots are mostly used in picking-placing materials operations. SCARA (Selective Compliance Assembly Robot Arm) robots use two parallel joints providing movement at a specifically selected track. The rotary tracks are placed vertically and the operating tooling attached to the arm moves horizontally, making SCARA robots most suitable for vertical assembly operations where efficient and quick pick and place operation is critical. The primary characteristic of the Delta robots is their parallel link configuration consisting of parallel joint connections linked to a common stable base. The positioning of the effector is controlled with the robotic arm making the robot type suitable for speedy pick-and-place applications. Polar (or spherical) robots use stationary arms with spherical work envelopes which can be placed in a polar-coordinated architecture. They use one linear and two rotary joints conjoining the links and a twisting joint conjoined to the arm.

3.1.2. Autonomous Mobile Robots

Autonomous Mobile Robots (AMR) have been classified as a distinct category because they can be used for industrial as well as domestic, medical, defense or educational purposes. An AMR is designed to move on wheels or with legs (human walking simulation is excluded from AMR category) across the ground floor to specified locations operating as a flexible assistant performing numerous tasks. The movement of an AMR is accomplished by using a total of advanced on-board sensors, FPGA-architectures and processors that allow it to comprehend and interpret its external environment. The aforementioned means offer the AMR the capability of combining the information from

multiple different sources such as video or GPS in order to navigate when there is a malfunction or full absence of data from one or more data sources. The core operation of an AMR is its control system, where FPGAs may constitute an implementation solution in many cases. While FPGA-based control systems are analytically explained in the next section, the design requirements of an effective AMR control system typically include:

- **Multiple sensor and processor integration:** As mentioned above, the possible malfunction, unreliability or inapplicability of any individual sensor or set of sensors must be coped with the integration and effective operation of the rest of AMR sensors. Furthermore, AMR must be able to accomplish all assigned tasks despite concurrent and often conflicting actions that need to be performed.

- **Reactivity to environment:** AMR should be capable of reacting to unscheduled sudden changes in the external environment by executing fast and efficient decisions in order to fulfill the assigned tasks. Software and architecture efficiency play a crucial role at that requirement, including the accuracy and usability of FPGA software algorithms.

- **Reprogrammability and Expandability:** An expandable architecture of an AMR allows the incremental build-up of the system and its continuous improvement and evolution. FPGA chips offer a significant advantage over other processing solutions in this case since they are reconfigurable and can be programmed to adopt a different behavior every time is required, changing the configuration of FPGA's internal circuitry.

3.1.3. Humanoid Robots

Humanoid robots are robotic applications that mimic human body structures in both behavioral and motion terms. They are considered a relatively complex robot type since it is necessary to consider their mechanical (musculoskeletal) structure, the computational and sensory nervous system, the applied methods of information processing in the robot's primary decision-making units and the applied software algorithms as a whole and for any given application that they have to perform. FPGA chips can be used for multiple humanoid robotic applications such as their motion control, communication modules between robots and users, visual sensing and processing that constitute the robot's total behavior in mimicking human functionality. However, the primary distinguishing element of humanoids in comparison to other robot types is their human mimetic motion and human-like robot reaction. The first element involves the robot's skeleton structure, the body proportions, the muscle arrangement and the joint performance [10]. Human-like robot reaction mainly represents the robot's responses for safety. This can be applied actively by using a feedback loop or passively by applying a suitable robot's mechanical design. Humanoids with high gains actuators tend to have a low performance on estimating correctly the forces applied by the human for specific functions, while the usage of integrated early-stage additional sensors shows better performance on that specific task [11]. FPGA chips constitute an efficient choice as a fused sensor architecture.

3.2. Application Fields

The sections analyzed below, will briefly introduce the primary application domains of FPGA-related technology components on robotics applications. These applications can be either mathematical and software algorithms, hardware FPGA-oriented architectures, mixed systems with FPGA components or combinations of all the above.

3.2.1. Robotic controllers

A robot constitutes an autonomous closed-loop control application because it is affected by the inputs from its sensors. Due to the highly effective integration of the intellectual properties of the embedded processors in the FPGA, the mathematical algorithms executing the demanding computations required by the robot controllers can be implemented by software in the FPGA. This application field mainly includes the coding of FPGA motion control systems of immobile robotic applications and industrial robots. Industrial immobile robots are widely used in order to solve tasks such as assembly, handling or welding.

Servo control is the most crucial part of robotic controller architecture since a possible failure to maintain a closed-loop behavior may delay the production process, damage the robot itself or even cause accidents and danger for human life. A servo-control solution based on FPGAs is considered amongst the most effective ones. Specifically, an FPGA-based control interface is responsible for multiple tasks in the robotic operation such as decoding feedback position data, processing communication signals and control outputs and transmitting the data to the actuators. The instructions provided to the robot used to perform specific actions are processed by the robotics control system. The programming language is actually used to describe all the variables that affect the robotics operation, primarily regarding movements on specifically set paths. There are several path types that a robot can operate under, depending on its purpose. The simplest type of robot motion is the movement from one point to the other, without having to perform any other parallel simultaneous actions. This motion can be executed as joint displacements and this type of control is called joint control [12]. The joint control motion expresses the interactions of position, acceleration and speed in the robot's language describing the necessary movements to perform the requested action. The main limitation of this control method is that the user needs joint dimensional information since he must comprehend the robot's joint displacements in order to drive the robot into the desired position. This limitation can be overcome by using the Cartesian space, which helps to interpret robot's movements by using Cartesian coordinates, based on the Jacobian Transpose matrix. This type of control is called Cartesian control. Due to this reason, the mathematical algorithms representing the kinematics of Cartesian control motion are significantly important in order to propose the most suitable control structures. The FPGA-based controller is then used to transform the trajectory created in the Cartesian space into a parallel robot's trajectory in joint space. This application field includes research undertaken for kinematics algorithms and software applications regarding the robotic controllers, mainly representing immobile robots executing industrial tasks.

3.2.2. Mapping – Navigation

This application field includes research regarding autonomous mobile robots, analyzing the usage of FPGA controllers in crucial operations, such as robot's localization, mapping and navigation. In general, the navigation of robots is divided into two parts: The 1st part is about the robot being capable of selecting the most suitable path between a starting and a finishing (goal) point. This path can be computed by either making calculations based on pre-loaded existing data or by processing incoming real-time data by GPS and other applications. The 2nd part includes the robot's real-time effectiveness on adapting its behavior to the external environment characteristics, such as avoiding obstacles, making turns and so on. FPGA applications can be used for both parts. Robot navigation is performed by using line following and obstacle avoiding algorithms that can operate with sensor data and probabilistic algorithms that study traffic and external environment patterns. The FPGA control unit is receiving and processing all incoming data from sensors and modules in order to choose the most suitable path.

Localization is another crucial process of mobile robotics as it is used in order to determine a robot's position in relation to an external reference point, called landmark. There are two localization methods: The first method calculates the distance from the landmark and its angle relative to the north, called the azimuth. The second method measures the angles to the object from two different positions, called triangulation. FPGA control units can process data and by applying the proper algorithms are capable of determining the right course. In recent years both localization techniques have been replaced by GPS location and navigation. FPGA receivers are often used to process GPS data and apply the proper navigation algorithms.

Simultaneous Localization and Mapping (SLAM) is the next-in-line step in robot mapping and navigation. A primary task of a mobile robot in an unknown environment is to create and frequently update a map of the environment and compute its current location within this map at the same time. This operation is called the SLAM operation. At normal conditions, the robot can use sensor or odometry measurements to gather information over its environment in order to perform localization and mapping. SLAM is used when these conditions are altered such as the localization at an underwater or space mission. Some researchers have proposed the use of probabilistic methods, such as Extended Kalman Filters [13]. The Extended Kaman Filters (EKF) algorithm simultaneously computes a model map of the environment and the current robot position based on odometric and exteroceptive sensor data. FPGA-based architectures usually implement the EKG algorithm. Alternative solutions avoiding the errors produced by odometry rely on scan-matching techniques that usually rely on range measurements acquired from robot sensors. Such an approach is the SMG algorithm [14]. This algorithm can perform SLAM by applying highly improved parameters which in turn considerably increase the algorithm's computational requirements. A considerable acceleration over software can be managed, by using the programmable resources of FPGA circuits and the parallelization properties of the algorithm.

3.2.3. Image Processing

FPGAs are widely used for the execution of digital image processing algorithms. They are used even more intensively, specifically in the case of real-time embedded applications, where latency and power are considered important issues. Typical topics in digital image processing are the evaluation of single images or numerous frames of a video signal for specifically set criteria such as movement information extraction or object tracking. For example, an FPGA embedded in a camera can execute image processing directly via the transmission of the image through the sensor. The camera provides a fully processed output stream that way, rather than just an image sequence.

The sector of robotics significantly benefits from the advantages provided by digital image processing on FPGAs. The image processing system of a robot is crucial for the enhancement of processing performance, since it includes the ability for spatial recognition and multiple detective algorithms to carry out the mission tasks. These tasks primarily include localization/navigation in the case of autonomous mobile robots. The primary reason for applying algorithms in FPGA robotics is the parallelism option which allows advantageous capabilities such as real-time image filtering for pre-processing purposes. Moreover, the local memory embedded in current FPGA architectures allows the buffering of pertinent image information to limit the communication with external memories, a situation that can potentially form a bottleneck [1].

Furthermore, FPGAs are more effective in comparison to CPUs in several aspects, regarding the ideal image processing system. CPUs execute their operations sequentially, so the first operation must process the entire image before the second operation starts. Since FPGAs are operating in parallel, every operation of the algorithm can operate on different pixels of the image simultaneously. This denotes that the time needed to receive the first processed pixel and process the whole image is much shorter, in comparison to an exclusive CPU application. Even if a combined co-processing FPGA-CPU architecture is used to transfer or receive images from the CPU, the total processing time is still shorter than an architecture that exclusively uses the CPU. Moreover, image processing architectures for robotics based both on USB and PC interface, are usually applied by multithread software solutions, so hard real-time response cannot be achieved for the proper integration of image and behavioral usage. Therefore, a robotic vision system that can perform image processing through an FPGA, which is directly connected to the CMOS sensor is more efficient.

3.2.3. Neural Networks

Artificial Neural Networks (ANNs) can be used in a variety of tasks performed by robots such as trajectory and image recognition, vehicle control, image processing, pattern and sequence recognition and medical diagnostics. They are statistical models destined to adapt and self-program, by applying learning algorithms that make them execute the aforementioned tasks. ANNs operate as parallel distributed computing networks and they operate correspondingly to the biological neural system. According to this, there are multiple input signals directed to neurons. Every input is assigned to a relative weight value which correspondingly influences the impact of that specific input. In

modelling, weight values are the adaptive coefficients within the network that calculate the magnitude of the input signal. The neuron output signal is then created by adding all the weighted inputs algebraically, simulating the biological cell body [15].

In order to perform properly, developers arrange ANN architectures in specific layers that are implemented in parallel. Since ANNs require significant computational power, they are better implemented using parallel hardware architecture [16]. ANNs can be implemented by using either software or hardware implementation. Software implementation is the favorite choice, supporting ANN training and simulation on sequential computers for imitating a large variety of neural network models, with significant flexibility. That is so since the developers do not need to know the internal operations of the neural network elements, but can be exclusively focused on the software application of the ANN. On the contrary, hardware FPGA-based architectures offer high applicability and the significant advantage of parallelism. The two basic characteristics of the FPGA-based reconfigurable computing architecture are its dynamic adoption and parallelism. These architectures are most suitable to apply ANNs as a developer can achieve concurrency and easily reconfigure in order to adjust the topology and the weights of an ANN. In total, FPGA-based architectures offer numerous advantages for neural implementations such as:

- Prototyping through reprogrammability: The neural FPGA-based architectures can be directly tested in order to find the most effective one, without any additional costs. Furthermore, an effective application architecture already developed and implemented can be later replaced by another one, without the need to design a new chip.

- Embedment: FPGA architectures can be used for all kinds of embedded applications, in order to take advantage of the effectiveness of neural calculations.

- On-chip leaning: Usually on-chip learning is avoided as it is considered a complicated process that can easily lead to loss of efficiency due to a number of reasons. On the contrary, off-chip learning is a more preferable choice when there are no requirements for dynamic learning. In the case of FPGAs, on-chip learning can be executed before the chosen implementation of the learned ANN on the same chip.

- Mapping: FPGA-based ANN architectures can be mapped onto more modern and effective FPGAs, whenever technology advancements indicate so. The basic prerequisite for ANN implementation is the scalability level of the implementation method.

3.4. Fuzzy Logic Control

Control algorithms for detailed dynamic models often require the exact specification of accurate target values. These equations may be complex and nonlinear, requiring longer "run-time" in order to get processed. An alternative approach to the usage of classical logic controllers described in section III subsection B.1 is the usage of Fuzzy logic control algorithms, which use imprecise specifications in order to reach the same goal. Fuzzy logic controllers are implemented to applications that are difficult by nature to model precisely. They are often considered more

robust algorithms in planning parameter value changes, in comparison to regular control algorithms, since they do not require high precision and high computational power.

In the sector of robotics, fuzzy logic controllers are often used for automatic navigation purposes. This is due to their capacity to process a high number of imprecise and incomplete input signals. In such a case, signal input processing may allow robots to navigate in uncertain environments. A robot is equipped with multiple sensors that allow it to sense and process the environmental information. Fuzzy controllers receive sensor outputs as inputs for processing according to the fuzzy rule database that dictates the robot's possible behaviors. The robot decision making mechanism implemented by the fuzzy controller consists of three basic steps in order to reach the final decision. First, during fuzzification a crisp input value is converted to a fuzzy value that is performed by the use of the information in the fuzzy rule database. Next, fuzzy inference (rule evaluation) formulates the mapping from a given input to an output using fuzzy logic, applying the rules to the fuzzy inputs. The mapping includes the rule framework under which robot's decision making will take place. Then, during the defuzzification step the values from the output variables are calculated from the fuzzy values resulting in the controller's final decision [17]. In total, fuzzy algorithms allow the robot to choose amongst various combinations of decisions the most effective one, rather than being forced to make a pre-designed single decision.

A fuzzy logic controller is capable of processing inputs from a wide range of sensors. For instance, ultrasonic navigation sensors can calculate the distance between a robot and the obstacles of the external environment. GPS applications can be used for localization purposes, detecting the robot's current position. Fuzzy algorithms constitute a suitable controller solution for navigation in 2D and 3D environments, industrial robot manipulators [18], image processing algorithms [19] and several other robotic domains that require high computational power.

3.2.5. Swarm Robotics

Swarm robotics is the task of using multiple robots to perform different activities simultaneously, rather than using one robotic application with enhanced capabilities. It is considered a distributed approach that aims at coordinating robot behaviour by copying natural decision mechanisms of the biological entities (humans, animals). These algorithmic mechanisms allow a group of robots to achieve performance levels that could never be achieved by a single or a few robotic applications. The usage of multiple robots may significantly shorten manufacturing time, performing different tasks with simpler, scalable and more robust robotic applications. The major issue in swarm robotics is the effectiveness and precision of the coordination algorithms, as they are usually performing on the same physical object or environment.

There are two main approaches of designing swarm robotics. The first approach is the centralized system, according to which a primary robot acts as a leader-coordinator for the rest of the robots of the swarm [20]. In FPGA robotic controllers, this is a relatively simple solution for navigation tasks. In this case, a master (leader) robot plans the path planning to traverse to the direction of a certain goal point, with the rest of the robots to follow. The

behavioral control mechanism creates a constant mutual communication between the leader and the followers, whose behaviour is checked and corrected at specific time periods, according to the leader's motion. The core advantage of this approach is that all follower or slave robots can be simple robotic applications compared to the master robotic unit. The main disadvantage is that if the leader robotic unit fails to perform as planned or properly communicate with the followers, then the whole swarm fails to complete the task.
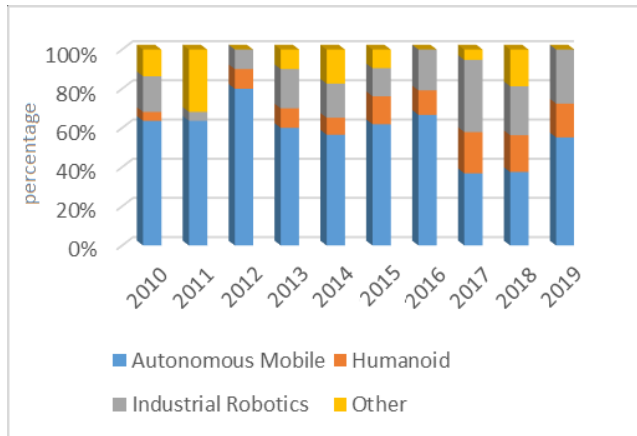
Figure 4: Robot types
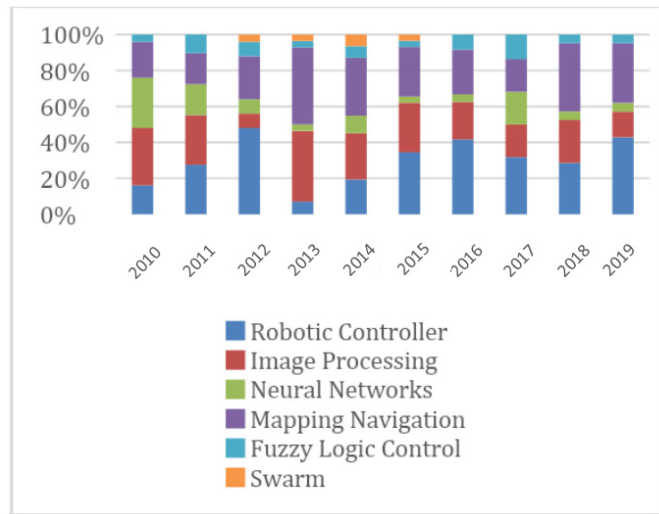
Figure 5: Distribution of FPGA applications for the period of 2010-2019

The second approach is the decentralized system that operates without a leader robotic unit and it is not affected by the cases of a single swarm unit failure or miscommunication amongst swarm members (agents). According to this approach, the motion of each robot is coordinated using local information exchange such as speed, obstacle existence or geographical coordinates, by the closest neighbor agents at a given time period. These motions are usually developed according to animal aggregations. Also, there is a physical decentralized system based on the physical interaction among agents. The communication amongst robots is either directional, by exerting forces to each other or in directional by manipulating or placing a common object. Directional communication may be applied by transmitting/receiving digital signals (WiFi, Bluetooth, etc), sound or light. In directional communication may be applied by either leaving optical markings

in the ground or placing/manipulating an object in the environment that will be used as a marking point by other agents [20]. In total, the centralized architectures are simpler and used primarily for navigation purposes while decentralized architectures are more complicated and can be used for performing activities such as simulations, biotechnology or military tasks.

In Figure 4 and Figure 5 the robot types and the distribution of FPGA applications found in this survey are depicted, according to the total count of 200 publications tested.

4. Reviewed Literature

In this section, we present and analyze the examined research publications of the IEEE & ACM database. For each application field, we present the publications by giving a short description for each publication. Only selected publications that utilized high performance, throughput and efficiency were selected. This description for each publication includes a summary of the publication, the key points and its specifications.

4.1. Application Field: Image Processing

In [161] we see an approach about a real time image processing patrol service robot. The robot consists of a CMOS camera module that sends data to the FPGA board. The genetic algorithm optimizes threshold values for the filtering operations according to various lighting environments. The visual navigation system has been developed for the linkage between flexible hardware circuits and real-time software applications for robot vision purposes. Experimental results show the feasibility of the proposed methodology.

In 2013, an FPGA algorithm used to detect corners in colored stereo images by implementing Harris corner detection technique [155]. The FPGA used is the XC5VLX50 and the architecture consists of 3 pipeline modules consisting of OmniVision image sensors in RGB555 format. Data is stored into a single DDR2 memory of Micron. By using less than 75% of FPGA resources and a 100MHz system clock, the authors achieved a corner detection rate of 0.33 pixels per clock cycle (ppcc) corresponding to a corner detection frequency of 54Hz for the stereo images. They highlighted the performance benefits of their methodology by conducting experiments.

A novel human-robot communication algorithm for both voice recognition and image processing embedded in an autonomous mobile robot [149] is proposed. The main controller is built on a Spartan FPGA processor, processing visual and voice information. The result of the research is a very flexible and powerful development tool for human-robot multimodal communication research and implementation. The hardware resources of this robot are wisely integrated by using the LabView graphical software toolkit, enabling a large amount of voice signals and image processing algorithms testing. The designed software drivers also allow various sensor modality including vision and speech signals analyzing. Endowed with these novel capabilities, the mobile robot displays intelligence and cooperativeness in its behavior, and becomes a versatile hardware system for human-robot multimodal communication implementation.

In 2014, researchers proposed a bio-inspired event-driven vision system using pseudo-simultaneous sensing [137]. The control system consists of a Spartan6 FPGA implementing a Convolutional Neural Network and a 3D construction algorithm. Experimental results demonstrate the application of this paradigm to implement Gabor filters and 3D stereo reconstruction systems. This architecture can be applied to real systems which need efficient and high-speed visual perception, like vehicle automatic driving, robotic applications in unstructured environments, or intelligent surveillance in security systems. Experimental results highlight the performance gains of the proposed methodology.

The authors of [147] published a research paper about a hexapod (6-legged spider like) robot using an FPGA-based robotic platform (Spartan 6). The system architecture involves an image sensor controller, a servo-motor controller and an AVR processor. Overall, the implementation of the servo motor controller in an FPGA has offered several advantages in terms of circuit design flexibility and simultaneous command executions when compared to conventional microcontroller-based system.

In 2014, researchers proposed an FPGA-based OV driver for VGA cameras [132]. For their implementation, they used an FPGA board (Cyclone EP2C5T144C8N) and optimized it using VHDL. The results from the conducted experiments suggest that the devised solution outperforms when compared to the coexisting implementations in terms of resources utilization.

Researchers published a research paper implementing a visual sensor unit for mapping and localization using a six-dimensional Micro Aerial Vehicle (MAR - drone) [126]. The sensor design is based on a XILINX FPGA System-on-Chip combining FPGA resources with an ARM A9 Dual-core processor

One year later, a group of researchers proposed a real-time machine vision system for an industrial robot that grasps items from an assembly line [119]. The items are in the same class, meaning that they have the same general shape but different details. The conducted experiments suggest that the machine parts can be located accurately under arbitrary in-plane rotations and can be classified correctly according to the details in their shapes. Guo's system can run with an industrial camera at a resolution of 640×480 and a speed of 50 fps (frames per second) or higher.

In 2015, the authors of an interesting research paper proposed a pragmatic incremental algorithm for achieving gain control and white balancing on an FPGA [112]. The proposed methodology significantly reduces the effects of the variations in lighting on the thresholds. In their paper, they propose a new color space which maximises the hue separation of the different coloured regions to improve the colour discrimination. All of the algorithms are designed to operate on data directly streamed from the camera, enabling a low latency FPGA implementation. The authors conducted real world experiments to evaluate the stability and performance of the proposed prototype.

In 2015, a group of researchers proposed a humanoid robot head with a vision system which has 22 degrees of freedom, including eyebrows sliding mechanism, the eye mechanism, jaw and neck mechanism [108]. The control system of the proposed prototype is an FPGA board. Facial movements are realized through driving traction mechanisms by controlling servos.The vision system of the robot S HFR-II Ihas a human-computer interaction interface with four kinds of work patterns,which includes facial expression recognitions and representations, face recognitions, gender recognitions and expression representations. The authors conducted experiments and the results suggest that the robot can recognize six basic expressions and vividly reproduce them.

Similarly to the aforementioned paper, in the same year, a group of researchers published an implementation of a face recognition system that captures facial images and recognizes a face and detects slight expressional changes of the test image [104]. In this paper, the authors read various facial images and store them. Then, images are compared bit by bit and any mismatch is detected. If the image is matched then a "Match found" message is displayed.

The author of [97] proposed a hardware accelerator to reduce the computation time of the scale-space analysis and the feature detection of the KAZE algorithm on Zynq-SoC family of FPGAs.

An interesting paper is proposed by [91] demonstrates an implementation of image mosaic algorithm on the Xilinx Zynq-7020 FPGA board. The system is able to process more than 60 frames per second (fps) and is capable of maintaining low power consumption. The authors verified the proposed methodology in a synthetic environment simulated using MATLAB.

A real time target tracking and positioning system based on FPGA is proposed by the authors of [89]. The hardware platform for the design is the development board by Xilinx´The system uses monocular camera to measure the orientation of target in real time. It acquires the video stream from a CMOS camera. The system realizes target tracking by extracting the color of the target as the feature, filtering˙detecting feature of the target and then displaying on the screen. The system realizes target positioning according to the centroid of the tracked target, then computing the orientation which can be used for the intelligent robot vision.

A group of researchers proposed a system that integrates different techniques to perform dimensional measurement of thick steel plate bevels using a DE0-Nano FPGA board [88]. The groove modeling is achieved through the use of line detection algorithms that look for straight lines and segments. The system level modeling and synthesis and the integration to the whole digital linear welding system, using only 28% of the FPGA's slices. Results Show the approach is a viable option to automate the process that is currently widely adopted in industry.

An interesting work about a high speed ball target tracking system based on FPGA (ZYNQ) [85] is proposed. With a CMOS sensor, the original frame can be transferred to the FPGA port. After the video streams go through the parallel image processing core, the color and corner features can be extracted. When compared to the predefined target's pattern, the target can be detected. The authors conducted real-world experiments to verify the feasibility of the proposed methodology.

In 2017, a group of researchers published their paper about an FPGA based real-time virtual blind cane system for the visually impaired, detecting obstacles in front of the user in real time [70]. Described three novel architectures of image segmentation, implemented on Virtex UltraScale XCVU190-2FLGC2104EES9847 FPGA. Working as a blind cane, the proposed system helps a blind person find the type of obstacle and the distance to it. The distance from the user to the obstacle is estimated by extracting the laser coordinate points on the obstacle, as well as tracking the system pointing angle. The paper provides a simple method to classify the obstacle's type by analyzing the laser intersection histogram. Real experimental results were also presented in the paper to highlight the validity and accuracy of the proposed system.

The same year, a group of researchers presented three novel architectures of image segmentation, implemented on Virtex UltraScale XCVU190-2FLGC2104EES9847 FPGA [69]. The sequential design which allows control over minute details of arithmetic design, The hybrid architecture provides a full fledged parallel and pipelined implementation of the algorithm and the hybrid architecture overall provides at least two times gain in acceleration.

One year later, a group of researchers propose a real time tracking hardware based on FPGA [60]. They converted a simulated and verified MATLAB code directly into HDL. The key point of their research is that the simulated and hardware outputs were consistent. Three types tracking algorithms (Kalman filter, extended Kalman filter and αβγ filter) were implemented to validate the proposed methodology.

In 2018, a research paper about a design approach of accelerating the execution of a robust algorithm based on Horn's quaternion solution [59] is proposed. The authors presented a HW architecture as well as its FPGA implementation. In their research paper, they also included results of the experiments they conducted.

Figure 6 depicts the total number of research papers that implemented FPGA Image Processing and the total Image Processing papers in robotics, from 2010 to 2019. It is evident that the popularity of FPGA and Image processing is steadily growing.

4.2. Application Field: Robotic Controller

A group of researchers propose an inverse kinematic algorithm for a parallel milling robot. The proposed robot consists of three robotic arms connected to a moving platform inside which there is a rotating spindle along a trajectory in the cartesian x, y, z space. The system is implemented using Altera Cyclone IV FPGA chip and it is evaluated by experimental results.

A group of researchers propose a robotic platform based on Lego Mindstorms in [162]. In their research, they included hardware, software and mechanical modules. A mathematical model for the motor and the PI controller are included. Experimental results highlight the performance gains of their implementation.

A system architecture controlling and monitoring household appliances through GSM. The system consists of an FPGA Xilinx

SP605 implemented in VHDL, the GSM circuit, the PIR sensor and the interface circuit that monitors the appliances

A connecting algorithm for interfacing the FPGA-based controllers to high level robotic software frameworks. The Unity-Link algorithm conjoins PC-processed architectures with nodes that provide demanding real-time control of distributed robotic systems

A group of researchers published their paper about an inverse kinematics FPGA algorithm for a biped robot, based on CORDIC operators of hyperbolic and circular vectoring. The speed of the proposed hardware FPGA application is compared to that of the Nios II CPU. The authors evaluated the proposed methodology by conducting experiments in a synthetic environment.

In 2019, the authors of [25] proposed an FPGA implementation of an adaptive neuro-fuzzy control for a teleoperation system. The controllers were developed in the MATLAB-Simulink environment and were implemented on FPGA using Simulink's fixed point tool and HDL Coder. The experimental results were very promising, as the latencies of these filters on the Field Programmable Gate Array (FPGA) platform were below 300ns with an average latency reduction of 188% (maximum of 570%) over the software versions running on a desktop PC CPU. This open-source event-based filter IP library for FPGA was tested on two different platforms and scenarios using different synthesis and implementation tools for Lattice and Xilinxvendors.
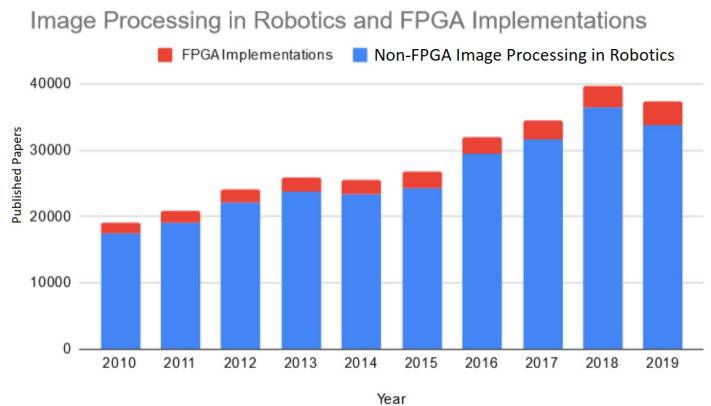
Figure 6. Research papers published about Image Processing using FPGA in Robotics compared to non-FPGA Image Processing papers in Robotics
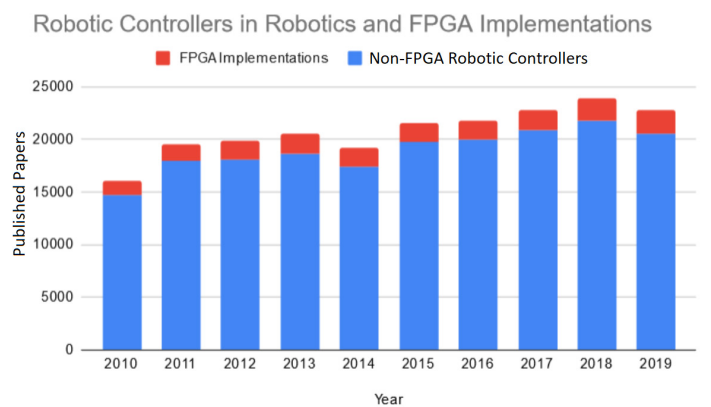
Figure 7. Research papers published about Robotic Controllers using FPGA compared to non-FPGA Robotic Controller papers

Figure 7 depicts the total number of research papers that implemented FPGA Robotic Controllers and the total Robotic Controllers papers in robotics, from 2010 to 2019. It is evident that the popularity of FPGA and Robotic Controllers is increasing.

4.3. Application Field: Neural Network

In 2012, the authors proposed an FPGA-based Neural Network algorithm for lane following of autonomous mobile robots [164]. The neural function consists of two main parts, the fixed points coding and the Sigmoïde function coding. The VHDL simulation is compiled in A Quartus II and implemented in Cyclone EP2C35F484C6 FPGA. The experimental results are promising and suggest high performance gains.

In [163], the authors publish their research paper about a stereo vision landing system architecture for an Unmanned Aerial Vehicle (UAV). The proposed FPGA-based Artificial Neural Network (ANN) algorithm is designed to apply real-time object tracking, 3D position computation via Visual Odometry methodology, Euclidean distance estimation from the landing target and horizontal displacement. The algorithm implementation was done on a Xilinx XC2V100 FPGA chip

In the same year, the authors proposed a Neural Processing Unit implementation [120] which reached a range from 6k to 90k iterations per second for the targeted neural map size. The authors propose a Neural Processing Unit designed as a programmable accelerator implementing recent equations close to self-organizing maps and neural fields. The proposed architecture is validated on FPGAdevices and compared to state of the art solutions. The trade-off proposed by this dedicated but programmable neural processing unit allows us to achieve significant improvements and makes our architecture adapted to many embedded systems.

An alternative architecture that exploits stochastic computation for doing classification with deep belief networks was proposed by the authors of [110] in 2015. The network was trained offline in MATLAB on the MNIST training dataset, and then implemented on an FPGA for classification at variable stochastic computation precision. Experimental results highlight the performance gains of the proposed methodology.
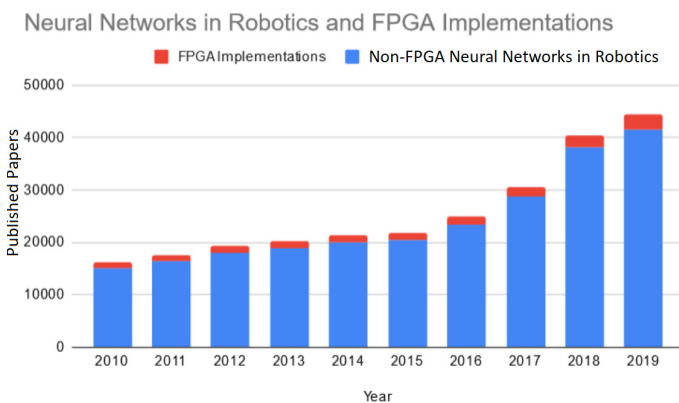
Figure 8. Research papers published about Neural Networks using FPGA in Robotics compared to non-FPGA Neural Network papers in Robotics

Figure 8 depicts the total number of research papers that implemented FPGA Neural Networks and the total Neural Network papers in robotics, from 2010 to 2019. The popularity of

FPGA and Networks is increasing steadily. Compared to the early 2010s, the Neural Networks using FPGA and the Neural Networks research papers in general have increased by a factor of 2.92.

4.4. Application Field: Mapping & Navigation

In [146], a color tracking algorithm was proposed for autonomous mobile robots, using a CMOS camera and an ultrasonic sensor. The design implementation was done on a Digilent Nexys2 FPGA. The video is captured and further processed by the FPGA board and displayed on a 3.2 inch screen. They conducted real world experiments to evaluate the stability and performance of their prototype.

A group of researchers proposed a processor embodying a Radio Frequency Identification Detection (RFID) algorithm and a CORDIC algorithm on a Kintex-7 FPGA platform [140]. The proposed system is used for navigation and anti-collision purposes. Experimental results highlight the performance gains of the proposed methodology.

In [135], a Micro Aerial Vehicle (MAV) architecture was proposed consisting of two subsystems: a) An image processing subsystem consisting of two VGA cameras and an Inertial Measurement Unit (IMU) and b) A control system using an Altera SoC FPGA. The interesting aspect of this research is that motion estimation and outlier rejection algorithms were included.

In the same year, an FPGA-based in-door flight localization/navigation system with a pan-tilt camera was proposed [129]. The FPGA (XC6SLX100) was used for image analysis and quad rotor control. The authors validated the proposed methodology by conducting real world experiments.

The authors of [119] proposed an improved ant colony system algorithm for path planning by establishing two new mechanisms for pheromone updating. They included partial pheromone updating and opposite pheromone updating. The authors evaluated the proposed methodology by conducting experiments in a synthetic environment.

[114] presents an effective data cache configuration where the number of active ways and hence its total capacity can be configured at run-time. When using the best data cache configuration, a reduction of 7% the power consumed at a 1% execution time penalty is suggested and it is the same result for the SLAM-EKF algorithm.

The authors of [113] present a novel methodology based entirely on the on-board approach. The obstacle avoidance system that is proposed is suitable for running on low-power embedded devices, leveraging a light-weight low power stereo vision system on FPGA used on Micro Aerial Vehicles (MAVs).

A group of researchers proposed a robot navigation system using a combination of sophisticated image processing algorithms [111]. Their system is used to generate a map and an extended A* algorithm to plan the path. A turtlebot localizes itself in an environment containing several obstacles and a destination. The authors evaluated the proposed methodology by conducting experiments in a synthetic environment.

[109] presents an FPGA-based hardware architecture of EKF Prediction Stage applied to the Mobile Robotics Localization Problem. It runs on an Altera Cyclone IV FPGA with a Nios II processor, adapted to the mobile platform Pioneer 3AT. The experimental results look very promising, as the execution time results point out that the hardware solution has a speed up factor greater than 2 in comparison with the embedded software implementations.

In 2015, a hardware structure for a vision-based autonomous vehicle navigation system was proposed [107]. Results showed that it is possible to implement the structure without consuming a high number of FPGA resources and achieve acceptable execution times. Analyzing the final hardware structure this goal was achieved with a considerably high frame-rate.

In the same year, an investigation was conducted [100]on the amount and sophistication of sensing and processing hardware needed by a mobile robot for performing high-level tasks in real time, such as azimuth calculation and dynamic obstacle tracing. The paper suggests that one ultrasonic sensor along with a coordinate rotation digital computer processor are adequate for azimuth calculation while one more ultrasonic sensor is required for dynamic obstacle tracing.

In [98], a hardware architecture is proposed to accelerate Rapidly-Exploring Random Trees (RRT) path planning algorithm using multiple Kd-trees to conduct the parallel search. The authors evaluated the proposed methodology by conducting experiments in a synthetic environment.

One year later, the authors of [78] propose a technique to evaluate sparse equations on an FPGA by restricting the maximum amount of items in the system. The implementation is done using CλaSH which allows a transformation from mathematical descriptions to a hardware design. The system uses a sparse data notation and puts constraints on the number of loop closures to restrict the amount of computations. Experimental results highlight the performance gains of the proposed methodology.

The first multilevel implementation of the Harris-Stephens corner detector and the Oriented FAST and rotated BRIEF (ORB) feature extractor running on FPGA hardware was published [74] in 2017. The Tarsier device performs excellently as it successfully generates descriptors for real images with sufficiently low latency for integration into a 1080p resolution 60 fps loop.

In the same year, the authors of [62] present their research about the development of a neuromorphic system on a Spartan 6 FPGA generating locomotion patterns (gaits) for three different legged robots (biped, quadruped, and hexapod). The authors validated the proposed methodology by conducting real world experiments. Moreover, the proposed spiking neuron model consumes less hardware resources and power than those based on coupled.

In 2019, an angular position tracking control was implemented using modified D channel PID algorithm [40]. It was developed in such a way that the reading of data, the calculation of the control signals, and the controlling of the motors are all implemented on FPGA. Experimental results highlight the performance gains of the proposed methodology.

Figure 9 depicts the total number of research papers that implemented FPGA Mapping & Navigation and the total Mapping & Navigation papers in robotics, from 2010 to 2019. It is evident that the popularity of FPGA and Mapping is increasing. This could possibly be caused by the general increased popularity of autonomous vehicles (Unmanned Aerial Vehicles, Unmanned Ground Vehicles and Unmanned Underwater Vehicles).
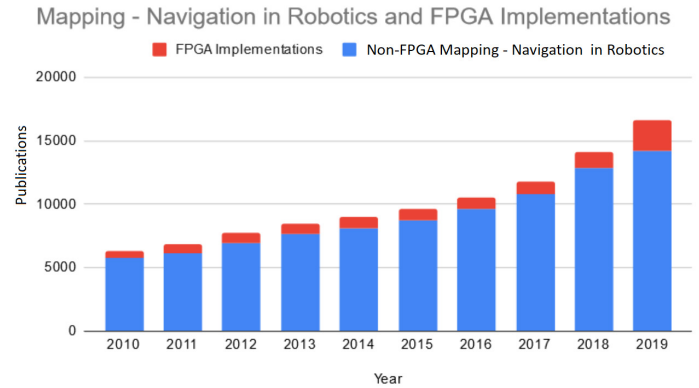
Figure 9. Research papers published about Mapping & Navigation using FPGA in Robotics compared to the non-FPGA Mapping & Navigation papers in Robotics

4.5. Application Field: Fuzzy Logic Control

In 2012 a fuzzy-logic controller [168] for an autonomous navigation robot was proposed. The controller is implemented using an Atmega16 microcontroller and tested using the whole robotic application. The FPGA implementation consists of the Fuzzy logic controller, the UART receiver (it translates data between serial to parallel form), the LCD controller (for controlling the LCD operations) and the ASCII to binary converter and binary to ASCII controllers.

In the same year, an interesting work is proposed about an autonomous parking FPGA-based system for a mobile robot [167]. The system scans the area for available parking space and performs the necessary maneuvers for parking. The whole system consists of three major parts, the car-like robot design, the development of a simulation model using MATLAB and Simulink and the fuzzy logic controller design. The evaluation of the paper was performed using a synthetic realistic environment.

A group of researchers published their research paper about an autonomous mobile robotic platform [165]. Their prototype is designed within the context of a robotic course. The system uses two separate FPGA-based controllers: A Proportional integral derivative (PID) controller and a fuzzy logic-based controller. Apart from the FPGA card, the robot's hardware design consists of two motors, eight sonar sensors, a radio frequency identification reader and a Basic Stamp microcontroller. For the modeling and implementation, they utilized MATLAB and Simulink.

Two fuzzy logic algorithms are developed: one for avoiding obstacles and another for avoiding obstacles / reaching a specific point. For the obstacle avoidance an ultrasonic sensor is used, while software is implemented using LabVIEW modules

In 2013, an interesting work is proposed about a fuzzy logic algorithm that is applied on an autonomous mobile robot for line tracking and obstacle avoidance tasks [145]. The software is

implemented by an Altera Quartus platform while Eclipse software is used to simulate the fuzzy rules. Several practical tests that were conducted by the authors reveal the effectiveness of the proposed fuzzy rules for which MRTQ was able to track the path more precisely and softly at different speeds and avoid the detected obstacle through the path readily.

In 2013, a paper was presented about a fuzzy-logic color extractor used on NI myRIO embedded system package [133]. In total, the fuzzy logic module, the real-time module, and the FPGA LabVIEW module are required for the implementation of the extractor on myRIO embedded device. The authors conducted multiple experiments and evaluated its effectiveness and performance gains.

In 2015, an interesting work is proposed about an omni-directional mobile platform control using the artificial intelligence technique of Fuzzy Logic; the control allows a practical and reliable driving control of 4 omni-directional wheels implemented on FPGA. The experimental results show increased performance and low power consumption.

Figure 10 depicts the total number of research papers that implemented FPGA Fuzzy Logic Control and the total Fuzzy Logic Control papers in robotics, from 2010 to 2019.
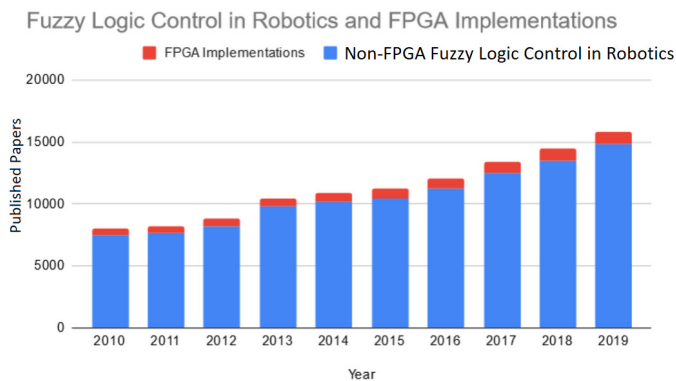
Figure 10. Research papers published about Fuzzy Logic Control using FPGA in Robotics compared to non-FPGA Fuzzy Logic Control papers in Robotics

4.6. Application Field: SWARM

In 2015, an interesting work is proposed about a behavioural control algorithm of a centralized swarm consisting of two robots [101]. In this paper, the authors present the challenges of multi robots and how the leader and follower robots can change their mode of behavioural control by switching between centralization and decentralization methods with a novel approach using implicit communication. According to the authors and their experimental results, the proposed implementation is very energy efficient. Robots are developed with minimal sensors (ultrasonic sensors, digital compass, RF Transceiver (PMOD-RF2)) and are implemented using a Spartan 3e FPGA board

Another interesting implementation was proposed by the authors of [84] in 2014. The heuristic approach based leader follower method is incorporated between robots for behavioural control. The robots were able to navigate in both static and dynamic conditions by using the modified M* based

obstacle avoidance mechanism with CORDIC module. The proposed methodology was validated by the implementation of the algorithm on Spartan 6 FPGAs (XC6SLX45 CSG324C).

In 2015, an interesting work is proposed about a pragmatic incremental algorithm for achieving gain control and white balancing on an FPGA [112]. The proposed methodology significantly reduces the effects of the variations in lighting on the thresholds. In their paper, they propose a new color space which maximises the hue separation of the different coloured regions to improve the colour discrimination. All of the algorithms are designed to operate on data directly streamed from the camera, enabling a low latency FPGA implementation.

Figure 11 depicts the total number of research papers that implemented FPGA SWARM and the total SWARM papers in robotics, from 2010 to 2019. Swarm and FPGA applications in robotics are not as popular as other fields, like mapping, image processing and controllers. However, SWARM and FPGA are still rising in popularity over the years.
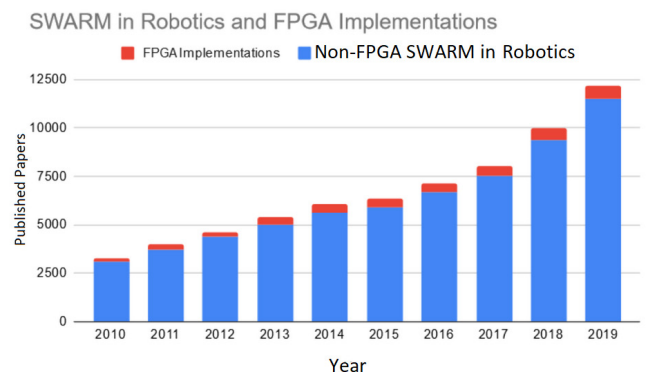
Figure 11. Research papers published about SWARM using FPGA in Robotics compared to non-FPGA SWARM papers in Robotics

5. Discussion

In the 2000s, FPGAs were seen as an inexpensive alternative to the traditional ASICs (Application Specific Integrated Circuit) for heavy computation tasks. Along with the decreased production cost and the technological advancements, this led to the increased popularity of FPGAs. This time period had significant improvements. Most importantly, they were software as well as hardware programmable. In boards released in the late 2000s, for the first time, the microprocessor was not the simple hardware block dropped into the FPGA as was done in older days, but included a full environment with caches, busses, Network-on-Chip and peripherals. Bundled software included operating systems, compilers and middleware: an entire ecosystem, rather than an integrated function block. The increased capabilities of FPGA boards of this era led to the increased usage in robotic applications, such as image processing, robotic controllers, mapping and navigation. In these fields, 10% of the published research papers utilize FPGA boards, presumably for the performance benefits they offer.

In the early and mid 2010s, FPGAs started to gain prominence in another field: neural networks, fuzzy logic control and swarm. Running neural network inference models takes significant

processing power. Graphics processing units (GPUs) are often used to accelerate inference processing, but in some cases, high-performance FPGAs might actually outperform GPUs in analyzing large amounts of data for machine learning.

Just as customers seeking custom integrated circuits 30 years ago were attracted to FPGAs over the complexity of ASICs, many are now attracted to multicore processors, graphic processing units (GPU) and software-programmable Application Specific Standard Products (ASSPs). These alternative solutions provide pre engineered systems with software to simplify mapping problems onto them. They sacrifice some of the flexibility, the performance and the power efficiency of programmable logic for ease-of-use. It is clear that, while there are many FPGA users who need to exploit the limits of FPGA technology, there are many others for whom the technological capability is adequate, but who are daunted by the complexity of using that technology.

The complexity and capability of devices have driven an increase in capability of design tools. Modern FPGA tool-sets include high-level synthesis compilation from C, Cuda and OpenCL to logic or to embedded microprocessors. Vendor-provided libraries of logic and processing functions meet design costs. Working operating systems and hypervisors control FPGA SoC operation. Team modules, including control, are built into FPGA design systems. Some capabilities are built by the vendors themselves, others are part of the growing FPGA ecosystem. Clearly, usability is critical to this next age of FPGAs and their adoption in robotics. If FPGA manufacturers focus on ease of use and solve the steep learning curve, FPGAs will be able to compete with GPUs and become dominant in high performance applications.

6. Conclusions

This survey revealed popular technological, research and industry trends of the past 10 years, regarding robot types used and processed in the research as well as application fields of the FPGAs. As depicted in Figure 4, the vast majority of robots for which applications are being developed are autonomous mobile robots especially when the algorithms developed for these robots are related to localization, mapping and navigation purposes.

In order to further increase the execution speed and efficiency of algorithms, developers utilize FPGA boards, as they offer an innovative solution. The popularity of FPGA boards has been steadily increasing over the last decades, as we can see in Figure 1. FPGAs offer significant advantages over software running on a CPU or GPU, including execution speed and energy efficiency. In a traditional local system, the FPGA board is typically located on-site, along with the other components of the device. However, in modern systems, FPGA boards can be found in the cloud, along with a high performance traditional server. As the server receives data from modern embedded IoT systems, images the server offloads the necessary information to be processed on the FPGA boards. Many boards support PCIe connectivity, with a maximum theoretical bandwidth of 15.75 GB/s in version 3.0. The main disadvantage of FPGA boards, however, is the increased engineering cost and complexity. The development process on FPGA boards includes the design of custom hardware circuits. Traditionally, these hardware circuits are described via Hardware Description Languages (HDL), such as VHDL and Verilog,

whereas software is programmed via one of a plethora of programming languages, such as Java, C and Python. An upcoming trend on FPGA is High Level Synthesis (HLS). HLS is allows the programming of FPGAs using regular programming languages such as OpenCL or C++, allowing for a much higher level of abstraction. However, even when using high level languages, programming FPGAs is still an order of magnitude more difficult than programming instruction based systems. Accelerating the computation process via FPGA boards is only efficient at larger scales, where the performance gain of the system outweighs the increased complexity and engineering cost.

The parallel architectures offered by the FPGAs easily offer the high computational power that continuous real-time localization and navigation tasks demand at a low cost, while mixed FPGA/DSP controllers offer flexibility over the process of complex image data that robotic visual systems include. This particular finding is in accordance with the high number of mapping / navigation application fields shown in Figure 5, for each consecutive year. As shown, the mapping and navigation application field is between half and one third of the total application fields for the 10-years tested period.

As depicted in Figure 4, the field of industrial robotics is the second most usually appearing robot field in the 2010-2019 publication search. FPGAs constitute a flexible solution in the implementation of kinematics algorithms that parallel multi-axis industrial robots often use, in comparison to DSP controllers. The example of the commonly used CORDIC algorithm implemented for rotation tasks in industrial robotics reveals the flexibility of FPGAs. That specific algorithm includes a significant extent of mathematical functions, so the development of a VLSI-based FPGA algorithm is often preferred as the implementation architecture of building a controller for multi-axis motion of robotic limbs. Figure 5 shows the high number of robotic controllers found in the survey, representing the flexibility of FPGAs in industrial robotic control.

Humanoid robots are the third most commonly appeared robot type in the survey. The multi-sensory humanoid robotic applications often demand multi-processor controllers based on mixed DSP/FPGA circuitry. The FPGA connectivity with DSP processors constitutes an effective solution of robotic applications that require multi-processing. The FPGA application fields applied to humanoid robots include regular robotic controllers for motion purposes, image processing applications for the process of visual data for pure image processing or mapping and navigation tasks, or neural network architectures for navigation or else. Swarm robotics also constitutes a wide FPGA application field. Complex behavioural algorithms which demand high computational power and high-levels of real-time communication between swarm members, can be easily implemented through FPGA architectures.

Conflict of Interest

The authors declare no conflict of interest.

Acknowledgment

Table 1: Other significant works that were reviewed

Field	Description	Year	Ref
4.1	A fast frame based on Block RAM reuse	2019	9
4.1	4.1 of a SoC FPGA using RGB-D sensor	2018	21
4.5 / 4.2	A hardware system for on-board support vector machine (SVM) model training for robotic transtibial prostheses locomotion recognition based on SoC-FPGA	2018	22
4.1	FPGA implement for multi-scale pedestrian detection using 4 different size histogram of oriented gradients (HOG) features	2018	23
4.2	An exemplary system for the calculation of the inverse kinematics of a robot arm, which is tailored for the implementation on a FPGA	2018	24
4.5 / 4.2	FPGA-based platform for integrated multi-axis motion control and motor drive	2018	26
4.2	A high-speed, high-accuracy fully pipelined architecture to solve inverse kinematics of a 3-DOF robot leg	2018	27
4.1 / 4.3 / 4.4	SqueezeNet DCNN is accelerated using an SoC FPGA in order for the offered object recognition resource to be employed in a robotic application	2018	28
4.3	A low cost and robust deep-learning based on gaze estimator is proposed to control surgical robots	2018	29
4.5 / 4.2	A novel robot control system based on EtherCAT In order to increase control frequency and expansibility for 7-degree-of-freedom (DoF) light-weight	2018	30
4.2	A control system architecture for knee joint surgery robot based on computer and motion (FPGA) control card	2018	31
4.4 - 4.3	An implementation of mechanical, electronics and software for a man-portable AUV with hybrid architecture	2018	32
4.1	A novel heterogeneous computer-on-module, integrating a Xilinx Zynq SoC and an Adapteva Epiphany multi-core processor	2018	33
4.3	A framework to integrate Deep Learning algorithms on the PYNQ-Z1 at the embedded system level	2018	34
4.2	An open-architecture controller with modularity	2018	35
4.1 - 4.4	A wireless panorama camera development specially for snake robot sensing	2018	36
4.2	A novel distributed SoC-based (PS + PL) impedance controller solution implemented in a robotic hand	2018	37
4.3	Implementation of the You only look once (YOLO) object detector on an FPGA	2018	38
4.1	A design approach of accelerating the execution of a robust algorithm based on Horn's quaternion solution and presents a HW architecture as well as its FPGA implementation	2018	39
4.4	Development of a Triangulation based Navigation Algorithm implemented on FPGA	2017	41

4.2	A mixed FPGA-microprocessor control architecture for a multi-axis industrial robot with vision-based behavior	2017	42
4.2	Robotic application performing auto-detection for high-voltage insulator inspection. The FPGA controller is used for step motor control, communication and signal acquisition	2017	43
4.2	A mixed FPGA-Microcontroller control architecture is included, using a Kawasaki RA10N robot body	2017	44
4.2	A high precision model of minimally invasive surgical robot	2017	45
4.2	A robotic system using a hard processor plus FPGA solution where the FPGA performs all real-time tasks, freeing the processor to run lower-frequency high level control and interface to other devices	2017	46
4.3	An FPGA implementation of Q-learning with Artificial 4.3 (ANN) reducing processing time	2017	47
4.2	A robust method based on a Dual-Core ARM Cortex-A9 System-on-Chip FPGA board that controls the motion of a Cartesian robot	2017	48
4.1 - 4.4	Three novel architectures of image segmentation, implemented on Virtex UltraScale XCVU190-2FLGC2104EES9847 FPGA. The sequential design which allowing control over minute details of arithmetic design, The hybrid architecture provides a full fledged parallel and pipelined implementation of the algorithm and the hybrid architecture overall provides at least 2X gain in acceleration	2017	49
4.1 - 4.4	An FPGA based real-time virtual blind cane system for the visually impaired, detecting obstacles in front of the user in real time. Described three novel architectures of image segmentation, implemented on Virtex UltraScale XCVU190-2FLGC2104EES9847 FPGA	2017	50
4.4	A novel approach of a robot navigation in smart indoor environment developed with the triangulation techniques using Coordinate Rotation Digital Computer (CORDIC) method	2017	51
4.2	Using inverse kinematics and zero moment point algorithmic program (IK-ZMP) to command robotic legs in parallel manner which algorithms were programmed in VHDL	2017	52
4.2	An overall design of the triple inverted pendulum on a cart model which can be used to illustrate various control design problems related to underactuated nonlinear mechanical systems	2017	53
4.4	The first multilevel implementation of the Harris-Stephens corner detector and the Oriented FAST and rotated BRIEF (ORB) feature extractor running on FPGA hardware, for computer vision and robotics applications. The Tarsier device performs excellently-it successfully generates descriptors for real images with sufficiently low latency for integration into a 1080p resolution 60 fps loop	2017	54
4.2	An open and high-performance industrial robot controller which consists of dual MCU + FPGA	2017	55
4.5 - 4.3	A swarm-based algorithm using spiking 4.3 (SNN) in order to simulate biological neuronal assemblies. The FPGA SNN system uses an FPGA Artix-7 chip executing mapping tasks	2017	56
4.3 - 4.2	A cerebellum-like spiking neural network model to be used as the short-range timing function for the talking robot's control system	2017	57
4.4	A technique to evaluate sparse equations on an FPGA by restricting the maximum amount of items in the system. The implementation is done using CλaSH which allows a transformation from mathematical descriptions to a hardware design. The system uses a sparse data notation and puts constraints on the number of loop closures to restrict the amount of computations	2017	58
4.5	A walking robot developed with the FPGA controller for investigating the robot's performance for moving in any direction and avoid obstacles. An FPGA Altera Max II microcontroller has been used, programmed with VHDL and fuzzy logic functions to control the walking robot	2016	61

4.4	An FPGA-based control unit is designed for a patrol robot, using a Spartan 3E board. Depth-first search (DFS) algorithm is used for visiting all the nodes in the patrolling path and this is implemented using black tags (RFID) and IR sensors	2016	63
4.4-4.6	A multi robots path planning like shortest path, behavioral control and obstacle avoidance using a Spartan 6 FPGA with modified M algorithm has resulted with less distance by that it consumes less power	2016	64
4.1	A high speed ball target tracking system based on FPGA (ZYNQ)	2016	65
4.4	A prototype for an autonomous robot using the FPGA DE0-Nano platform to implement. The system designed for having easier maintenance, control and, environmentally friendly	2016	66
4.2	Analyzing and accelerating the inverse Jacobian, pseudo inverse Jacobian, gradient descent, and the Newton method through an FPGA design using high-level synthesis (HLS). Implemented four numerical methods for solving the inverse kinematic problem of a 4 Degrees Of Freedom (DOF) robotic arm	2016	67
4.1	A system that integrates different techniques to perform dimensional measurement of thick steel plate bevels using a DE0-Nano FPGA board. The groove modeling is achieved through the use of line detection algorithms that look for straight lines and segments	2016	68
4.1	An implementation of image mosaic algorithm which is comprised of image registration and image fusion for better effect on the Xilinx Zynq-7020 FPGA board. The system is able to process more than 60 frames per second (fps) and maintaining a low power	2016	71
4.4 - 4.1	A processor-centric FPGA-based architecture for a latency reduction in the vision-based robotic navigation. Also, it can be used to other tasks like detection and tracking of image salient points	2016	72
4.4 - 4.1	A 6 Degree of Freedom (DoF) camera pose estimation algorithm using a monocular camera and non co-planar markers, design for robotics applications, and an implementation on a low cost CPU and the FPGA that can conduct precise 6-DoF estimations at 100Hz	2016	73
4.2	An effective method for calculating the onboard real-time path planning of large-scale space redundant manipulators	2016	75
4.4 - 4.1	A vision-based lane detection algorithm which requires no knowledge of any physical parameters like position and orientation of the camera and is hence very flexible. The algorithm is tested with 14 videos and demonstrate super fast speed, high accuracy, and super energy-efficient	2016	76
4.1	A hardware accelerator to reduces the computation time of the scale-space analysis and the feature detection of the KAZE algorithm on Zynq-SoC family of FPGAs	2016	77
4.3	A design automation tool, named Deep Burning, allowing the application developers to build from scratch learning accelerators that target their specific 4.3 models with custom configurations and optimized performance	2016	79
4.4-4.1	An investigation on the amount and sophistication of sensing and processing hardware needed by a mobile robot for performing high-level tasks in real time such as azimuth calculation and dynamic obstacle tracing which shown that one ultrasonic sensor along with a coordinate rotation digital computer processor are adequate for azimuth calculation while one more ultrasonic sensor is required for dynamic obstacle tracing	2016	80
4.4 - 4.6	Behavioural navigation control algorithm of a centralized swarm consisting of two robots, using FPGA Spartan 3e board	2015	81
4.4 - 4.1	A practical analysis of a SoC architecture that incorporates an FPGA with an embedded ARM processor for Visual SLAM applications	2015	82
4.2	A design and implementation of a novel system for robot-assisted fracture manipulation. The system was evaluated through positioning trials to measure its accuracy and repeatability	2015	83

4.4 - 4.1	A real-time image de-blurring by dynamics-based approach and parallel system architecture	2015	86
4.4 - 4.1	A hardware structure for a vision-based autonomous vehicle navigation system. Results showed that it is possible to implement the structure without consuming a high number of FPGA resources and achieve acceptable execution times. Analyzing the final hardware structure this goal was achieved with a considerably high frame-rate	2015	87
4.3	An alternative architecture that exploits stochastic computation for doing classification with deep belief networks. The network was trained offline in MATLAB on the MNIST training dataset, and then implemented on an FPGA for classification at variable stochastic computation precision	2015	90
4.1 – 4.6	Pragmatic incremental algorithms for achieving gain control and white balancing have been described and implemented on an FPGA	2015	92
4.4 - 4.1	A novel entirely on-board approach, obstacle avoidance system that is suitable for running on low-power embedded devices, leveraging a light-weight low power stereo vision system on FPGA used on Micro Aerial Vehicles (MAVs)	2015	93
4.4	An effective data cache configuration where the number of active ways and hence its total capacity can be configured at run-time. When using the best data cache configuration reveal a reduction of 7% the power consumed at a 1% execution time penalty and it is the same results for the SLAM-EKF algorithm	2015	94
4.2	A finger control for an anthropomorphic piano robot. The robot can play the right note and right rhythm, the punching force of the fingers are controlled just right while the robot is playing	2015	95
4.4	An improved ant colony system algorithm for path planning by establishing two new mechanisms for pheromone updating, including partial pheromone updating and opposite pheromone updating	2015	96
4.1	A real-time machine vision system for industrial robot to grasp from an assembly line a class of machine parts which are similar in the general shape but different in details using FPGA for acceleration	2015	99
4.4 - 4.1	Image-processing navigation algorithm using C language	2014	102
4.2	A dynamic (mathematical) model of a robot finger simulating human motion. An FPGA-based EtherCAT master-slave platform is developed in order to validate the model	2014	105
4.1 – 4.4	A visual sensor unit for mapping/localization used by a six-dimensional Micro Aerial Vehicle (MAR - drone). The sensor design is based on a XILINX FPGA System-on-Chip combining FPGA resources with an ARM A9	2014	106
4.4 - 4.1	A Micro Aerial Vehicle (MAV) architecture consisting of two subsystems: a) An 4.1 subsystem consisting of two VGA cameras and an Inertial Measurement Unit (IMU) and b) A control system using an Altera SoC FPGA. Motion estimation and outlier rejection algorithms are included	2014	115
4.2 - 4.1	A high-speed image visual servoing (VS) system is developed for a SCARA robot. VS is the procedure of the right positioning of the manipulator in order to mitigate the effects of disturbances. The proposed system uses a Cyclone III FPGA controller with a camera and a Position Sensitive Detector (PSD) for position computation	2014	116
4.1 - 4.3	A bio-inspired event-driven vision system not represented by frames, using pseudo-simultaneous sensing. The control system consists of a Spartan6 FPGA implementing a Convolutional Neural Network and a 3D construction algorithm	2014	117

4.2	An FPGA smart sensor interface remotely communicating the main controller with the sensors. An EP3CI6F484 FPGA controller interfaces with SDRAM controller, vibration sensors and a camera. The robot can be used for disaster affected areas and other fields where remote communication is demanded	2014	118
4.2	A Kinematics architecture is applied on an Altera FPGA-based parallel industrial 3-axis milling robot, using the CORDIC algorithm	2013	121
4.2	A Kinematics algorithm is applied on an Altera FPGA-based parallel industrial milling robot, using C language.	2013	122
4.4 - 4.1	An FPGA Based Platform for localization/navigation through a software/hardware solution	2013	123
4.2	A modular robot manipulator consisting of three modules with embedded FPGA controllers, for increased precision. The manipulator uses the Virtual Decomposition Control (VDC) technique where the host computer executes only kinematics calculations, and all the other control calculations are done by local decentralized embedded slave computers	2013	124
4.5	A fuzzy logic algorithm is applied on an autonomous mobile robot for line tracking and obstacle avoidance tasks. The software is implemented by an Altera QuantusII platform while Eclipse software is used to simulate the fuzzy rules	2013	125
4.2	A Spartan-3 FPGA chip is used as a controller for a servomotor control technique implemented for a hexapod robotic platform. The robot consists of 18 servomotors. The controller is programmed with VHDL and the simulation is done with a Xilinx ISE Simulator	2013	127
4.4 - 4.3	A multi-layer neural network perceptron application using a Spartan III FPGA chip designed to drive two servomotors of an autonomous mobile robot. FPGA has been described in VHDL	2013	128
4.2	An ARM + FPGA multi-axis motion controller is implemented on an industrial robotic platform (SCARA robot). The controller is adapted to independent real-time network communication in order to achieve real time servo control	2013	130
4.2	A smoothing robust control algorithm using the Manifold Deformation Design Scheme (MDDS) is implemented for a Delta robot. The controller is a combined Kernel FPGA and DSP. PFGA is used for computation of the feedback signals and synchronously control each joint while DSP performs MDDS calculations	2013	131
Other	A median filter based on Xilinx Spartan-3 FPGA. It is used to filter the output of the measurement module of a line sensor IP core by smoothing the signals, suppress impulse voice and preserve edge	2013	134
4.5	Two fuzzy logic algorithms are developed: one for avoiding obstacles and another for avoiding obstacles / reaching a specific point. For the obstacle avoidance an ultrasonic sensor is used, while software is implemented using LabVIEW modules	2013	136
4.1 - 4.4	A stereovision measurement algorithm based on (Scale Invariant Feature Transform) SIFT key points, implemented on an embedded 4.1 board based on DSP and FPGA. SIFT algorithm looks for key points in the image scale space and extracts invariant locations. The system uses two CCD cameras and an 4.1 board	2013	138
4.2	A connecting algorithm for interfacing the FPGA-based controllers to high level robotic software frameworks. The Unity-Link algorithm conjoins PC-processed architectures with nodes that provide demanding real-time control of distributed robotic systems	2013	139
4.1	A real time 4.1 patrol service robot consisting of a CMOS camera module sending data to the FPGA board	2012	141
4.2 - 4.4	A robotic platform - based on Lego Mindstorms - is presented, including hardware, software and mechanical modules. A mathematical model for the motor and the PI controller are included	2012	142

4.3	A stereo vision landing system architecture for an Unmanned Aerial Vehicle (UAV). The proposed FPGA-based Artificial Neural Network (ANN) algorithm is designed to apply real-time object tracking, 3D position computation via Visual Odometery methodology, Euclidian distance estimation from the landing target and horizontal displacement. The algorithm implementation was done on a Xilinx XC2V100 FPGA chip	2012	143
4.3	An FPGA-based Neural Network algorithm for lane following of autonomous mobile robots. The neural function consists of two main parts, the fixed points coding and the Sigmoïde function coding. The VHDL simulation is compiled in A Quartus II and implemented in Cyclone EP2C35F484C6 FPGA	2012	144
4.5	A fuzzy-logic controller for an autonomous navigation robot. The controller is implemented using an Atmega16 microcontroller and tested using the whole robotic application. The FPGA implementation consists of the 4.5ler, the UART receiver (it translates data between serial to parallel form), the LCD controller (for controlling the LCD operations) and the ASCII to binary converter and binary to ASCII controllers	2012	148
4.3	A hardware application of an FPGA-based controller using an artificial neural approach. The controller is capable of landscape learning, path planning, obstacle avoidance and sensory motor controlling. The controller is implemented as a SoC embedded on the robot, using a Virtex 6 VLX240T FPGA. The basic architecture of the controller consists of three basic layers: the pre-processing layer, the Self Organizing Map layers based on Kohonen maps and the computing layer	2012	150
4.4	A path planning / navigation algorithm for an autonomous mobile robot, using CORDIC architecture for implementing rotation. The robot's external interface includes an FPGA board consisting of Spartan XC2S50 FPGA and three ultrasonic sensors. The coding has been performed using VHDL and synthesized using Xilinx ISE	2012	151
4.1	A multi-resolution real-time dense stereo 4.1 algorithm is implemented. The algorithm's implementation is done on an Altera Stratix IV FPGA board with GigE vision cameras, using six levels of Gaussian Pyramids	2012	152
4.2	A hardware / software robotic application consisting of an operating software system that drives the FPGA controllers. The robotic (5 axe) system is an MK-2 industrial robotic arm and its controllers are operated by a XilinxVirtex II FPGA board and two PowerPC processors	2012	153
4.1	Digital image compression and decompression architecture applying M-JPEG2000 image compression standard, used for an UAV data link system. The two primary components of the system are an FPGA and an ADV212	2012	154
4.2	An FPGA-based speed controller for a DC motor designed for an autonomous mobile robot. The proportional integral (PI) controller used to achieve acceleration realized by the FPGA, while for decelerating control a braked deceleration circuit module is proposed. An additional motor protection circuit to avoid the motor driver IC damage is also included	2012	156
4.3	A 4.2 consisting of a multi-processor System on Chip implemented on a Spartan 3A FPGA, performing bio-inspired walking on a six-ledged robot (hexapod). The whole system consists of one soft processor used for high level decisions in motion decisions and six soft processors running independent control loops for the six legs respectively	2012	157
4.2	A hybrid architecture consisting of parallel FPGA (Spartan 6) and Advance RISC Machine microcontroller for visual trajectory-tracking. The system's framework consists of 3 main layers: The data layer where the FPGA performs input/output extension and hardware acceleration, the real-time layer where the microcontroller performs real-time control and the high performance layer where a computer executes complex tasks like navigation, map generating and artificial intelligence	2012	158
4.4	An FPGA-based algorithm for path planning and obstacle avoidance of autonomous mobile robots. The system consists of ultrasonic sensors and is implemented in a Xilinx FPGA Spartan II	2012	159
	A dexterous six-DOF, five-joint robotic arm for ping-pong is proposed. Each joint contains a motor position sensor, a current sensor and a temperature sensor and an FPGA for communication and control. More		

4.2	specifically, each joint contains four modules, the sensor signal processing, the joint servo control, the motor current control and the communication module	2012	160
4.4	An in-door navigation architecture implemented on FPGA based on impulse-based ultra-wideband (UWB) technology. The system consists of an UWB receiver installed on an autonomous mobile robot that utilizes time-difference on arrival (TDOA) between pairs of anchor nodes for localization purposes. These nodes transmit a coded repeated stream of ultra-short pulses	2011	166
4.5	A locomotion / visual information common function based on fuzzy logic is implemented on an FPGA.	2011	169

References

[1] R. Johannes, M. Porrmann, and U. Rückert. "Survey of FPGA applications in the period 2000–2015" Technical Report, Center of Excellence Cognitive Internaction Technology, Bielefeld University, Germany, 2017.

[2] M. Prado, "An FPGA-based open architecture industrial robot controller" IEEE Access 6, 13407--13417, 2018. .

[3] P. Carlos and M. Porrmann. 2007. The utilization of reconfigurable hardware to implement digital controllers: a review. In 2007 IEEE International Symposium on Industrial Electronics (ISIE'19). 2380--2385.

[4] T. Russell, K. Pocek, and A. DeHon "Reconfigurable computing architectures". In Proceedings of the IEEE. IEEE 103, **3** (2015), 332--354, 2015

[5] V. Anuj, K. Dang Pham, and D. Koch, "A survey on FPGA virtualization", 28th International Conference on Field Programmable Logic and Applications, 1310--1317, 2018..

[6] S. Gandhare and B. Karthikeyan "Survey on FPGA Architecture and Recent Applications" International Conference on Vision Towards Emerging Trends in Communication and Networking (ViTECoN'19), 1--4, 2019.

[7] B. Ari and F. Mondada, "Elements of robotics" Springer Nature, 2018.

[8] W. Mike. 2014. "Implementation of robot systems: an introduction to robotics, automation, and successful systems integration in manufacturing" Butterworth-Heinemann.

[9] H. Martin, "Industrial robotics", Springer handbook of robotics. Springer Nature, 2016

[10] A. Yuki, K. Okada, "Design principles of a human mimetic humanoid: Humanoid platform to study human intelligence and internal body systems". Science Robotics **2**, 13, 2017.

[11] S. Olivier and Thomas Flayols. 2019. An overview of humanoid robots technologies. In Biomechanics of Anthropomorphic Systems. Springer Cham, (2019), 281--310.

[12] S. Sánchez, R. Cortés, "Cartesian control for robot manipulators". In Robot manipulators trends and development, 165--212, 2010

[13] B. Vanderlei, E. Marques, and G. A. Constantinides, "A floating-point extended kalman filter implementation for autonomous mobile robots". Journal of Signal Processing Systems **56**, 1, 41--50, 2019.

[14] G. Mingas, Emmanouil Tsardoulias, and Loukas Petrou. 2012. An FPGA implementation of the SMG-SLAM algorithm. Microprocessors and Microsystems 36, 3, 190--204, 2012

[15] P. Young-seuk, S. Lek. "Artificial Neural Networks: Multilayer Perceptron for Ecological Modeling". Developments in environmental modelling, **28**, 123--140, 2016.

[16] Poliac, M. O., J. M. Zanetti, and D. M. Salerno. 1991. Performance measurements of seismocardiogram interpretation using neural networks. In 1991 Proceedings Computers in Cardiology (IEEE'91). 573--576.

[17] K. Erdal, M. Ahmadieh Khanesar "Fuzzy neural networks for real time control applications: concepts, modeling and algorithms for fast learning", Butterworth-Heinemann, 2016.

[18] P. Yanik, George Ford, and William McDaniel. 2010. An introduction and literature review of fuzzy logic applications for robot motion planning. In Proceedings of ASEE Southeast Section Conference (ASEE'10).

[19] I. Mario and M. Chacón. 2006. Fuzzy logic for image processing: definition and applications of a fuzzy image processing scheme. In Bai Y., Zhuang H., Wang D. (eds) Advanced Fuzzy Logic Technologies in Industrial Applications. 101--113.

[20] S. Giandomenico "Swarm Robotics". MDPI-Multidisciplinary Digital Publishing Institute, 2019

[21] A. Podlubne and D. Göhringer. FPGA-ROS: Methodology to Augment the Robot Operating System with FPGA Designs. In 2019 International Conference on ReConFigurable Computing and FPGAs (ReConFig'19). 1--5, 2019

[22] C. Fu and Y. Yu "FPGA-based Power Efficient Face Detection for Mobile Robots". In 2019 IEEE International Conference on Robotics and Biomimetics (ROBIO'19). 467--473, 2019

[23] T. Sun, Y. Liu, and Y. Wang "Design and implementation of a High-speed Lidar Data Reading System based on FPGA", In 2019 IEEE International Conference on Real-time Computing and Robotics (RCAR'19). 322--327, 2019

[24] K. Hocine, R. Mellah, and H. Talem, "Neuro-fuzzy Control of a Position-Position Teleoperation System Using FPGA". In 2019 24th International Conference on Methods and Models in Automation and Robotics (MMAR'19). 64--69., 2019

[25] L. Alejandro, "Low latency event-based filtering and feature extraction for dynamic vision sensors in real-time FPGA applications", IEEE Access 7, 134926--134942, 2019.

[26] C. Chien, and C. Hsu. HW/SW Co-design and FPGA Acceleration of a Feature-Based Visual Odometry. In 2019 4th International Conference on Robotics and Automation Engineering (ICRAE'19), 148--152, 2019.

[27] R. Martínez Peralta, E. Zamora Gómez, and J. Humberto Sossa Azuela "Efficient FPGA hardware implementation for robot manipulator kinematic modeling using rational trigonometry" IEEE Latin America Transactions, 1524--1536, 2019

[28] P. Christos, T. Nikos, and B. Michael. Design and Implementation of an APSoC-Based Robotic System with Motion Tracking Teleoperation. In 2019 8th International Conference on Modern Circuits and Systems Technologies (MOCAST'19). 1--4, doi: 10.1109/MOCAST.2019.8742037, 2019

[29] C. Zhengdong et al. 2019. Design of HEVC Intra Model Decision Based on Zynq. In 2019 IEEE International Conference on Real-time Computing and Robotics (RCAR'19). 311--315.

[30] A. Kyriakos et al. High Performance Accelerator for CNN Applications. In 2019 29th International Symposium on Power and Timing Modeling, Optimization and Simulation (PATMOS'19). 135--140. doi: 10.1109/PATMOS.2019.8862166.

[31] G. Ce et al. Customisable control policy learning for robotics. In 2019 IEEE 30th International Conference on Application-specific Systems, Architectures and Processors (ASAP'19). 91--98.

[32] B. G. Oliveira and Jorge Lobo. Interactive Demonstration of an Energy Efficient YOLOv3 Implementation in Reconfigurable Logic. In 2019 5th Experiment International Conference (exp. at'19). 235--236.

[33] Z. Chen et al. Eye-to-hand robotic visual tracking based on template matching on FPGAs. IEEE Access **7** (2019), 88870--88880.

[34] H. Chih-Lyang, H. Wu, and W. Hung. Software/Hardware-based hierarchical finite-time sliding-mode control with input saturation for an omnidirectional autonomous mobile robot. IEEE Access **7** (2019), 90254--90267, 2019

[35] D. , Zeyang and L Jing. Real-Time Attitude Estimation of Sigma-Point Kalman Filter via Matrix Operation Accelerator. In 2019 IEEE 13th International Symposium on Embedded Multicore/Many-core Systems-on-Chip (MCSoC). IEEE, 342--346, 2019

[36] D. Lee, C. Cheung, and Dan Pritsker. Radar-based Object Classification Using An Artificial Neural Network. In 2019 IEEE National Aerospace and Electronics Conference (NAECON'19). 305--310, 2019

[37] A. Kamaleldin et al. Modular memory system for RISC-V based MPSoCs on Xilinx FPGAs. In 2019 IEEE 13th International Symposium on Embedded Multicore/Many-core Systems-on-Chip (MCSoC'19). 68--73, 2019

[38] L. Ning et al. When Deep Learning Meets the Edge: Auto-Masking Deep Neural Networks for Efficient Machine Learning on Edge Devices. In 2019 IEEE 37th International Conference on Computer Design (ICCD'19). 506--514, 2019

[39] R. Tapiador Morales et al. "Spiking Row-by-Row FPGA Multi-Kernel and Multi-Layer Convolution Processor". In 29th International Conference on Field Programmable Logic and Applications (FPL'19). 248--249, 2019

[40] S. Zsolt, and S. Tihamér, Quadcopter control implemented on FPGA. In 2019 IEEE 19th International Symposium on Computational Intelligence and Informatics and 7th IEEE International Conference on Recent Achievements in Mechatronics, Automation, Computer Sciences and Robotics (CINTI-MACRo'19). 000049--000054, 2019

[41] C. Pedro-F et al. A proposal for a SoC FPGA-based image processing in RGB-D sensors for robotics applications. In 2018 IEEE 2nd Colombian Conference on Robotics and Automation (CCRA'18). 1--6, 2018

[42] M. Jingeng et al. Implementing a SoC-FPGA Based Acceleration System for On-Board SVM Training for Robotic Transtibial Prostheses. In 2018 IEEE International Conference on Real-time Computing and Robotics (RCAR'18). 150--155., 2018

[43] W. Ming-Shi and Zhe-Rong Zhang. FPGA implementation of HOG based multi-scale pedestrian detection. In 2018 IEEE International Conference on Applied System Invention (ICASI'18). 1099--1102.

[44] Koepper Alexander and Karsten Berns. Behavior-Based Approach for Calculation of a Robot Arm's Inverse Kinematics on a FPGA. In ISR 2018 50th International Symposium on Robotics (ISR'18). 1--8, 2018

[45] O. Rahnama, D. Frost, O. Miksik and P. Torr.. Real-Time Dense Stereo Matching With ELAS on FPGA-Accelerated Embedded Devices. In IEEE Robotics and Automation Letters **3**, 3 2018

[46] Y. Sun et al. "An SoC-based platform for integrated multi-axis motion control and motor drive" In 2018 International Power Electronics Conference (IPEC-Niigata 2018-ECCE Asia). 560--564

[47] G. Evangelista, Carlos Olaya, and Erick Rodríguez. Fully-pipelined CORDIC-based FPGA Realization for a 3-DOF Hexapod-Leg Inverse Kinematics Calculation. In 2018 WRC Symposium on Advanced Robotics and Automation (WRC SARA'18). 237--242.

[48] P. G. Mousouliotis et al. Expanding a robot's life: Low power object recognition via FPGA-based DCNN deployment. In 2018 7th International Conference on Modern Circuits and Systems Technologies (MOCAST'18). 1--4, 2018

[49] P. Li et al. Efficient and low-cost Deep-Learning based gaze estimator for surgical robot control. In 2018 IEEE International Conference on Real-time Computing and Robotics (RCAR'18). 58--63, 2018

[50] G. Zhang et al. A Control System Design for 7-DoF Light-weight Robot based on EtherCAT Bus. In 2018 IEEE International Conference on Mechatronics and Automation (ICMA'18). 2169--2174, 2018

[51] H. Sheng et al. Design of robot control system for minimally invasive surgery of knee joint. In 2018 IEEE 3rd Advanced Information Technology, Electronic and Automation Control Conference (IAEAC'18). 2583--2586.

[52] A. Cadena et al. Development of a hybrid autonomous underwater vehicle for benthic monitoring. In 2018 4th International Conference on Control, Automation and Robotics (ICCAR'18). 437--440.

[53] D. Klimeck et al. Resource-efficient Reconfigurable Computer-on-Module for Embedded Vision Applications. In 2018 IEEE 29th International Conference on Application-specific Systems, Architectures and Processors (ASAP'18). 1--4.

[54] L. Stornaiuolo, M. Santambrogio, and Donatella Sciuto. On how to efficiently implement deep learning algorithms on pynq platform. In 2018 IEEE Computer Society Annual Symposium on VLSI (ISVLSI'18). 587--590.

[55] M. Martínez-Prado et al. An FPGA-based open architecture industrial robot controller. IEEE Access 6 (2018), 13407--13417.

[56] L. Chen et al. Teleoperation Snake Robots with Panorama Vision. In 2018 11th International Workshop on Human Friendly Robotics (HFR'18). 54--59.

[57] S. A. Pertuz et al. A Modular and Distributed Impedance Control Architecture on a Chip for a Robotic Hand. In 2018 31st Symposium on Integrated Circuits and Systems Design (SBCCI'18). 1--6.

[58] H. Nakahara, A demonstration of FPGA-based you only look once version2 (YOLOv2). In 2018 28th International Conference on Field Programmable Logic and Applications (FPL'18). 4570--4571.

[59] N. Dimou et al. Parallel Robust Absolute Orientation on FPGA for Vision and Robotics. In 2018 25th IEEE International Conference on Electronics, Circuits and Systems (ICECS'18). 665--668.

[60] G. Haritha et al. Analysis of real-time tracking filters implementation in FPGA. In 2018 IEEE Distributed Computing, VLSI, Electrical Circuits and Robotics (DISCOVER). 158--162.

[61] S. , Yuhei, Acceleration of Publish/Subscribe Messaging in ROS-Compliant FPGA Component. In Proceedings of the 8th International Symposium on Highly Efficient Accelerators and Reconfigurable Technologies (HEART2017). Association for Computing Machinery, New York, NY, USA, Article 13, 1--6.

[62] Y. Z. Jing et al. Design of auto detection system for high-voltage insulator inspection robot. In 2017 International Conference on Robotics and Automation Sciences (ICRAS'17). 16--19, 2017

[63] L. Chen et al.. Development of an industrial robot controller with open architecture. In 2017 IEEE International Conference on Cybernetics and Intelligent Systems (CIS) and IEEE Conference on Robotics, Automation and Mechatronics (RAM'17). 754--756, 2017

[64] Z. Jiang et al. Kinematics calculation of minimally invasive surgical robot based on FPGA. In 2017 IEEE International Conference on Robotics and Biomimetics (ROBIO'17). 1726--1730, 2017

[65] Ben P. Jeppesen, et al. An FPGA-based controller for collaborative robotics. In 2017 IEEE 26th International Symposium on Industrial Electronics (ISIE'17). 1067--1072, 2017

[66] P. Reddy Gankidi and Jekan Thangavelautham. FPGA architecture for deep learning and its application to planetary robotics." In 2017 IEEE Aerospace Conference (AeroCon'17). 1--9.

[67] E. S. Fiestas and S. G. Prado, Motion control of a cartesian robot using a dual- core ARM cortex-A9 system-on-chip FPGA. In 2017 Latin American Robotics Symposium (LARS'17) and 2017 Brazilian Symposium on Robotics (SBR'17). 1--6, 2017

[68] R. Nahar, FPGA based parallelized architecture of efficient graph based image segmentation algorithm. In 2017 IEEE International Conference on Robotics and Biomimetics (ROBIO'17). 98--103, 2017

[69] K. Fan et al. Hardware implementation of a virtual blind cane on FPGA. In 2017 IEEE International Conference on Real-time Computing and Robotics (RCAR'17). 344--348, 2017

[70] M. C. Chinnaaiah et al. A versatile autonomous navigation algorithm for smart indoor environments using FPGA based robots. In 2017 International Conference on Intelligent Computing, Instrumentation and Control Technologies (ICICICT'17). 1196--1200.

[71] M. Yaqoob Javed et al. Implementation of FPGA based efficient gait controller for a biped robot. In 2017 2nd International Conference on Robotics and Automation Engineering (ICRAE'17). 42--47, 2017

[72] V. Šetka, R. Čečil, and M. Schlegel. Triple inverted pendulum system implementation using a new ARM/FPGA control platform. In 2017 18th International Carpathian Control Conference (ICCC'17). 321--326, 2017

[73] J. Weberruss et al. FPGA acceleration of multilevel ORB feature extraction for computer vision. In 2017 27th International Conference on Field Programmable Logic and Applications (FPL'17). 1--8.

[74] L. Chen, et al. Development of an industrial robot controller with open architecture. In 2017 IEEE International Conference on Cybernetics and Intelligent Systems (CIS) and IEEE Conference on Robotics, Automation and Mechatronics (RAM'17). 754--757.

[75] F. Palumbo et al. Feasibility study of real-time spiking neural network simulations on a swarm intelligence based digital architecture. In 2017 IEEE International Parallel and Distributed Processing Symposium Workshops (IPDPSW'17). 247--250.

[76] T. Vo Nhu, and Hideyuki Sawada. Cerebellum-like neural network for short-range timing function of a robotic speaking system. In 2017 3rd

International Conference on Control, Automation and Robotics (ICCAR'17). 184--187.

[77] R. Appel et al. Design-time improvement using a functional approach to specify GraphSLAM with deterministic performance on an FPGA. 2017 IEEE/RSJ International Conference on Intelligent Robots and Systems (IROS'17). 797--803.

[78] Z. Zhou et al. Mechatronic design of an ankle-foot rehabilitation robot for children with cerebral palsy and preliminary clinical trial. In 2017 IEEE International Conference on Industrial Technology (ICIT'17). 825--830.

[79] S. Chiang et al. 2017. The design of intelligent interactive service robots. In 2017 International Conference on Advanced Robotics and Intelligent Systems (ARIS'17). 100--103.

[80] S. Pullteap. Development of a walking robot by using FPGA controller. In 2016 11th France-Japan & 9th Europe-Asia Congress on Mechatronics (MECATRONICS)/17th International Conference on Research and Education in Mechatronics (REM'16). 054--057.

[81] J. Savage et al. Configurable Mobile Robot Behaviors Implemented on FPGA Based Architectures. In 2016 International Conference on Autonomous Robot Systems and Competitions (ICARSC'16). 317--322.

[82] M. C. Chinnaaiah, et al. A new approach: An FPGA based robot navigation for patrolling in a service environment. In 2016 International Conference on Research Advances in Integrated Navigation Systems (RAINS'16). 1--4.

[83] M. C. Chinnaaiah, et al. A versatile path planning algorithm with behavioural control using FPGA based robots. In 2016 10th International Conference on Intelligent Systems and Control (ISCO'16). 1--6.

[84] C. Lyu et al. High-speed target tracking base on FPGA. In 2016 IEEE International Conference on Real-time Computing and Robotics (RCAR'16). 272--276.

[85] T. Kho et al. Enhance implementation of embedded robot auto-navigation system using fpga for better performance. In 2016 3rd International Conference on Electronic Design (ICED'16). 309--314.

[86] F. Schwiegelshohn, Florian Kästner, and Michael Hübner. FPGA design of numerical methods for the robotic motion control task exploiting high-level synthesis. In 2016 IEEE International Conference on the Science of Electrical Engineering (ICSEE'16). 1--5.

[87] C. Rafael Steffens et al. FPGA Based Sensor Integration and Communication Protocols for Automated Robot Control in Linear Welding. In 2016 XIII Latin American Robotics Symposium and IV Brazilian Robotics Symposium (LARS/SBR'16). 115--120.

[88] C., Chen, et al. Real-time target tracking and positioning on FPGA. In 2016 IEEE International Conference on Real-time Computing and Robotics (RCAR'16). 448--453.

[89] Y. San Woo et al. 2016. Enhance implementation of flying robot auto-navigation system on FPGA for better performance. In 2016 3rd International Conference on Electronic Design (ICED'16). 315--320.

[90] W. Zhou et al. Real-time implementation of panoramic mosaic camera based on FPGA. In 2016 IEEE International Conference on Real-time Computing and Robotics (RCAR'16). 204--209.

[91] P. Čížek, J. Faigl, Low-latency image processing for vision-based navigation systems. In 2016 IEEE International Conference on Robotics and Automation (ICRA'16). 781--786.

[92] R. Konomura and K. Hori. FPGA-based 6-DoF pose estimation with a monocular camera using non co-planer marker and application on micro quadcopter. 2016 IEEE/RSJ International Conference on Intelligent Robots and Systems (IROS'16). 4250--4257.

[93] K. Boikos. Semi-dense SLAM on an FPGA SoC. In 2016 26th International Conference on Field Programmable Logic and Applications (FPL'16). 1—4, 2016.

[94] J. Yu et al. On-board real-time path planning design for large-scale 7-DOF space manipulator. In 2016 IEEE International Conference on Mechatronics and Automation, Harbin (ICMA'16). 1501--1506.

[95] K. Huang et al. 2016. A scalable lane detection algorithm on COTSs with OpenCL. In 2016 Design, Automation & Test in Europe Conference & Exhibition (DATE'16). 229--232.

[96] L. Kalms, A. Elhossini, and B. Juurlink. FPGA based hardware accelerator for KAZE feature extraction algorithm. In 2016 International Conference on Field-Programmable Technology (FPT'16). 281--284.

[97] S. Xiao, A. Postula, and N. Bergmann. Optimal random sampling based path planning on FPGAs. In 2016 26th International Conference on Field Programmable Logic and Applications (FPL'16). 1--2.

[98] Y. Wang et al. DeepBurning: automatic generation of FPGA-based learning accelerators for the neural network family. In 2016 53nd ACM/EDAC/IEEE Design Automation Conference (DAC'16).1--6.

[99] P. Vyas et al. Cordic-based azimuth calculation and obstacle tracing via optimal sensor placement on a mobile robot. In IEEE/ASME Transactions on Mechatronics 21, 5 (2015), 2317--2329.

[100] M. C. Chinnaiah, A novel approach in navigation of FPGA robots in robust indoor environment. In 2015 International Conference on Advanced Robotics and Intelligent Systems (ARIS'15). 1--6.

[101] V. Hugo Schulz, A SoC with FPGA Landmark Acquisition System for Binocular Visual SLAM. In 2015 12th Latin American Robotics Symposium and 2015 3rd Brazilian Symposium on Robotics (LARS-SBR'15). 336--341.

[102] G. Dagnino et al. Design and real-time control of a robotic system for fracture manipulation. In 2015 37th Annual International Conference of the IEEE Engineering in Medicine and Biology Society (EMBC'15). 4865--4868.

[103] R. Saumyarup et al. Face detection system using FPGA. In 2015 Online International Conference on Green Engineering and Technologies (IC-GET'15). 12--15.

[104] G. Quintal et al. Real-time FPGA decentralized inverse optimal neural control for a shrimp robot. In 2015 10th System of Systems Engineering Conference (SoSE'15). 250--255.

[105] M. D. Kim and Jun Ueda. 2015. Real-time image de-blurring and image processing for a robotic vision system. In 2015 IEEE International Conference on Robotics and Automation (ICRA'15). 1899--1904.

[106] M. A. Dias and Fernando S. Osório. 2015. Reconfigurable hardware architecture for vision-based driving systems. In 2015 12th Latin American Robotics Symposium and 2015 3rd Brazilian Symposium on Robotics (LARS-SBR'15). 97--102.

[107] X. Ke, Vision development of humanoid head robot SHFR-III. In 2015 IEEE International Conference on Robotics and Biomimetics (ROBIO'15). 1590--1595.

[108] L. Contreras et al.. Hardware architecture of the EKF prediction stage applied to mobile robot localization. In 2015 IEEE 6th Latin American Symposium on Circuits & Systems (LASCAS'15). 1--4.

[109] K. Sanni et al. Fpga implementation of a deep belief network architecture for character recognition using stochastic computation. In 2015 49th Annual Conference on Information Sciences and Systems (CISS'15). 1--5.

[110] J. Rettkowski, Robot navigation based on an efficient combination of an extended A∗ algorithm, bird's eye view and image stitching. In 2015 Conference on Design and Architectures for Signal and Image Processing (DASIP'15). 1--8.

[111] D. Bailey, Miguel Contreras, and Gourab Sen Gupta. Towards automatic colour segmentation for robot soccer. In 2015 6th International Conference on Automation, Robotics and Applications (ICARA'15). 478--483.

[112] H. Oleynikova, D. Honegger, and M. Pollefeys. Reactive avoidance using embedded stereo vision for MAV flight. In 2015 IEEE International Conference on Robotics and Automation (ICRA'15). 50--56.

[113] B. A. Silva et al. Run-time cache configuration for the LEON-3 embedded processor. In Proceedings of the 28th Symposium on Integrated Circuits and Systems Design (SBCCI'15). 1--6.

[114] Y. Li and C. Huang. Force control for the fingers of the piano playing robot—A gain switched approach. In 2015 IEEE 11th International Conference on Power Electronics and Drive Systems (PEDS'15) 265--270.

[115] C. Hsu et al. FPGA-based path planning using improved Ant Colony Optimization Algorithm. In 2015 IEEE 5th International Conference on Consumer Electronics-Berlin (ICCE-Berlin'15). 443--444.

[116] M. Pena et al . Fuzzy logic for omni directional mobile platform control displacement using FPGA and bluetooth. In IEEE Latin America Transactions 13, 6, 2015, 1907--1914.

[117] L. Zouari, M. Ben Ayed, and M. Abid. A hardware in the loop simulation for electrically driven robot manipulator. In 2015 IEEE 28th Canadian Conference on Electrical and Computer Engineering (CCECE'15). 1495--1501.

[118] H. Guo et al. Real-time detection and classification of machine parts with embedded system for industrial robot grasping. In 2015 IEEE International Conference on Mechatronics and Automation (ICMA'15). 1691--1696.

[119] L. Fiack, L. Rodriguez, and B. Miramond. 2015. Hardware design of a neural processing unit for bio-inspired computing. In 2015 IEEE 13th International New Circuits and Systems Conference (NEWCAS'15). 1--4.

[120] M. C. Chinnaaiah et al. 2014. A novel approach in implementation of rendezvous behavioral control between FPGA robots. In 2014 International Conference on Advanced Robotics and Intelligent Systems (ARIS'14). 97--102

[121] J. Heshmatpanah, S. Boroumand, and Mehdi Tale Masouleh. 2014. FPGA design and implementation for real time vision applications on NTACO mobile robot. In 2014 Second RSI/ISM International Conference on Robotics and Mechatronics (ICRoM'14). 172--177.

[122] A. M. Ashir, Atef A. Ata, and M. Shukri Salman. 2014. FPGA-based image processing system for Quality Control and Palletization applications. In 2014 IEEE International Conference on Autonomous Robot Systems and Competitions (ICARSC'14). 285--290.

[123] S. Agrawal and Ravi N. Prakash.. Implementation of WSN which can simultaneously monitor Temperature conditions and control robot for positional accuracy. In 2014 International Conference on Green Computing Communication and Electrical Engineering (ICGCCEE'14). 1--6.

[124] M. Hou et al. Analysis of the multi-finger dynamics for robot hand system based on EtherCAT. In 2014 10th International Conference on Natural Computation (ICNC'14). 1061--1065.

[125] J. Nikolic et al. A synchronized visual-inertial sensor system with FPGA pre-processing for accurate real-time SLAM. In 2014 IEEE international conference on robotics and automation (ICRA'14). 431--437.

[126] S. Seok et al. A highly parallelized control system platform architecture using multicore CPU and FPGA for multi-DoF robots. In 2014 IEEE International Conference on Robotics and Automation (ICRA'14). 5414--5419.

[127] F. Mota Muñoz, S. Martínez de la Piedra, and Karla C. Gómez. Development of a multi-DOF robotic controller for academic purposes. In 2014 International Conference on Mechatronics, Electronics and Automotive Engineering (ICMEAE'14). 104--109.

[128] R. Ladig and K. Shimonomura.. Fpga-based fast response image analysis for autonomous or semi-autonomous indoor flight. In Proceedings of the IEEE Conference on Computer Vision and Pattern Recognition Workshops (CVPRW'14). 668--673.

[129] C. Guo et al. Reconfigurable fault-tolerant joint control system for space robot. In Proceeding of the 11th World Congress on Intelligent Control and Automation (WCICA'14). 1899--1904.

[130] T. Zhang et al. Design and control of a multisensory five-finger prosthetic hand. In Proceeding of the 11th World Congress on Intelligent Control and Automation (WCICA'14). 3327--3332.

[131] E. Yusifli et al. An FPGA Based Resources Efficient Solution for the OmniVision Digital VGA Cameras Family. 2014 IEEE Intl Conf on High Performance Computing and Communications, 2014 IEEE 6th Intl Symp on Cyberspace Safety and Security, 2014 IEEE 11th Intl Conf on Embedded Software and Syst (HPCC'14, CSS'14, ICESS'14). 558--561.

[132] D. Oswald et al. Implementation of fuzzy color extractor on ni myrio embedded device. In 2014 International Conference on Multisensor Fusion and Information Integration for Intelligent Systems (MFI'14). 1--6.

[133] C. Andres Lara-Nino, Cesar Torres-Huitzil, and Jose Hugo Barron-Zambrano. Versatile educational and research robotic platform based on reconfigurable hardware. In 2014 International Conference on ReConFigurable Computing and FPGAs (ReConFig14). 1--6.

[134] G. Zhou et al. 2014. On-board inertial-assisted visual odometer on an embedded system. In 2014 IEEE International Conference on Robotics and Automation (ICRA'14). 2602--2608.

[135] M. H. Liyanage and N. Krouglicof . A single time scale visual servoing system for a high speed SCARA type robotic arm. In 2014 IEEE International Conference on Robotics and Automation (ICRA'14). 4153--4160.

[136] L. Alejandro, Teresa B. Linares-Barranco. Event-driven sensing and processing for high-speed robotic vision. In 2014 IEEE Biomedical Circuits and Systems Conference (BioCAS'14) Proceedings. 516--519.

[137] B. Y. Kumar and S. Ilaiyaraja. 2014. Smart interface for sensors in robot. In 2014 Sixth International Conference on Advanced Computing (ICoAC'14). 145--149.

[138] H. B. et al. Embedded FPGA controller for robot arm in material handling using reconfigurable nicompact RIO. In Second International Conference on Current Trends In Engineering and Technology (ICCTET'14). 125--131.

[139] S. Bhashis Roy, J. Bag, and S. Kumar Sarkar. Design and VLSI implementation of a robot navigation processor deploying CORDIC based anti-collision algorithm with RFID technology. In 2014 Annual IEEE India Conference (INDICON'14). 1--6.

[140] M. Petko et al. Acceleration of parallel robot trajectory generation in FPGA. 2013 IEEE 8th Conference on Industrial Electronics and Applications (ICIEA'13). 1123--1128.

[141] M. Petko et al. Acceleration of parallel robot trajectory generation in FPGA. In 2013 IEEE 8th Conference on Industrial Electronics and Applications (ICIEA'13). 1123--1128.

[142] A. Ghorbel et al. An FPGA based platform for real time robot localization. In 2013 International Conference on Individual and Collective Behaviors in Robotics (ICBR'13). 56--61.

[143] W. Zhu et al. Precision control of modular robot manipulators: The VDC approach with embedded FPGA. In IEEE Transactions on Robotics 29, 5 (2013), 1162--1179.

[144] S. Boroumand et al. Path tracking and obstacle avoidance of a FPGA-based mobile robot (MRTQ) via fuzzy algorithm. In 2013 13th Iranian Conference on Fuzzy Systems (IFSC'13). 1--5.

[145] S. Bold, Min A. Jeong, S. Min Jeon, and S. Ro Lee. FPGA based real time embedded color tracking mobile robot. In 2013 International Conference on IT Convergence and Security (ICITCS'13). 1--4.

[146] N. Alisa Ali et al. PWM controller design of a hexapod robot using FPGA. In 2013 IEEE International Conference on Control System, Computing and Engineering (ICCSCE'13). 310--314.

[147] B. Velasquez et al. Navigation control in FPGA for a differential-drive mobile robot. In 2013 16th International Conference on Advanced Robotics (ICAR'13). 1--6.

[148] C. Szász and G. Husi. Novel multimodal communication skills implementation on the NI-9631 robot. In IECON 2013-39th Annual Conference of the IEEE Industrial Electronics Society (IECON'13). 7837--7842.

[149] R. Li, Shiyao Lin, and Jian Chen. Embedded Motion Controller Design Based on RTEX Network. In 2013 5th International Conference on Intelligent Human-Machine Systems and Cybernetics (IHMSC'13). 326--329.

[150] H. Lin "The implementation of smoothing robust control for a delta robot" In 2013 Second International Conference on Robot, Vision and Signal Processing (RVSP'13). 208--213.

[151] Yen-Fang Li and L. Chuang. Controller design for music playing robot—Applied to the anthropomorphic piano robot. In 2013 IEEE 10th International Conference on Power Electronics and Drive Systems (PEDS'13). 968--973.

[152] C. C. Wong and C. C. Liu. FPGA realisation of inverse kinematics for biped robot based on CORDIC. Electronics letters 49, 5 (2013), 332--334.

[153] L. Mutauranwa and Magripa Nleya. 2013. An efficient median filter in a robot sensor soft ip-core. In 2013 Africon Pointe-Aux-Piments (Africon'13). 1--5.

[154] M. Fatih Aydogdu, M. Fatih Demirci, and C. Kasnakoglu. Pipelining Harris corner detection with a tiny FPGA for a mobile robot. In 2013 IEEE International Conference on Robotics and Biomimetics (ROBIO'13). 2177--2184.

[155] M. Mysorewala, et al. Design and implementation of fuzzy-logic based obstacle-avoidance and target-reaching algorithms on NI's embedded-FPGA robotic platform. In 2013 IEEE Symposium on Computational Intelligence in Control and Automation (CICA'13). 168--173.

[156] S. Cruz et al. FPGA implementation of a sequential extended Kalman filter algorithm applied to mobile robotics localization problems. In 2013 IEEE 4th Latin American Symposium on Circuits and Systems (LASCAS'13). 1--4.

[157] H. Song et al. A fast stereovision measurement algorithm based on SIFT keypoints for mobile robots. In 2013 IEEE International Conference on Mechatronics and Automation (ICMA'13). 1743--1748.

[158] A. Blaabjerg Lange, Ulrik Pagh Schultz, and Anders Stengaard Soerensen. Unity-link: A software-gateware interface for rapid prototyping of experimental robot controllers on fpgas. In 2013 IEEE/RSJ International Conference on Intelligent Robots and Systems (IROS'13). 3899--3906.

[159] B. Thanh Trung and N. Van Cuong. Monitoring and controlling devices system by GPRS on FPGA platform. In 2013 International Conference on Advanced Technologies for Communications (ATC'13). 713--717.

[160] K. Asami, H. Hagiwara, and M. Komori. Visual navigation system based on evolutionary computation on FPGA for patrol service robot. In The 1st IEEE Global Conference on Consumer Electronics 2012 (GCCE'12). 295--298.

[161] M. D.A. Siqueira, J. Conforto, and Marcos B.R. Vallim. An FPGA-Based Robotics Platform for Educational and Research Applications. In 2012 Brazilian Robotics Symposium and Latin American Robotics Symposium (SBR'12, LARS'12). 313--318.

[162] A. Din "Embedded low power controller for autonomous landing of UAV using artificial neural network" In 2012 10th International Conference on Frontiers of Information Technology (FIT'12). 196--203.

[163] A. Benjemmaa. Implementations approches of neural networks lane following system. In 2012 16th IEEE Mediterranean Electrotechnical Conference (MELECON'12). 515--518.

[164] R. Alba-Flores. Project-based learning approach in a senior level course in autonomous mobile robots. In 2012 Proceedings of IEEE Southeastcon (Southeastcon'12). 1--8.

[165] K. Gac. FPGA based hardware accelerator for calculations of the parallel robot inverse kinematics. In Proceedings of 2012 IEEE 17th International Conference on Emerging Technologies & Factory Automation (ETFA'12). 1--4.

[166] N. Scicluna et al. FPGA-based autonomous parking of a car-like robot using Fuzzy Logic Control. In 2012 19th IEEE International Conference on Electronics, Circuits, and Systems (ICECS'12). 229--232.

[167] T. Muthu et al. 2012. Fuzzy logic controller for autonomous navigation. In 2012 International Conference on Communication and Signal Processing (ICCSP'12). 81--92.

[168] H. Hagiwara, K. Asami, and Mochimitsu Komori. Real-time image processing system by using FPGA for service robots. In The 1st IEEE Global Conference on Consumer Electronics 2012 (GCCE'12). 720--723.

Factors Affecting the Decision of Selecting Banking to Save Money of Individual Customers - Experimental in Da Nang City

Le Anh Tuan[1,2,*], Mai Thi Quynh Nhu[1,2], Nguyen Le Nhan[1,2]

[1]*Faculty of Accounting, Duy Tan University, Da Nang, 550000, Vietnam*

[2]*Institute of Research and Development, Duy Tan University, Da Nang, 550000, Vietnam*

ARTICLE INFO	ABSTRACT
	The purpose of this study is to evaluate the factors affecting the decisions of factors affecting the decision of individual customers to choose a savings bank at commercial banks in Da Nang city. . Through the use of appropriate research methods, the authors have found that there are 5 factors with 5 groups of factors that greatly affect the decision of individual customers to choose a savings bank. Service quality, safety, stakeholder influence, financial benefit, convenience. Through this result, it will help opinions, orientations and solutions to improve individual customers' decisions on choosing a savings bank at joint stock commercial banks in Da Nang city.

1. Introduction

In today's competitive open economy, commercial banks always find ways to use many attractive and novel savings products to attract customers to their banks. On the part of customers using the service, they are also interested in factors related to the benefits of saving money at banks. This is also something that bank managers are interested in understanding, so identifying the factors that affect individual customers' choice of banks when saving money is a necessary job to help. Banks promote their strengths, enhance their image in the eyes of customers to attract more idle money from the population, contributing to improving business efficiency.

In 2018-2019, the macroeconomic situation and Da Nang continue to face many challenges. However, with the efforts of the whole political system, Da Nang has achieved many successes in the realization of local socio-economic development goals; in which, the banking sector has made an important contribution to the socio-economic development of Da Nang. Through general assessment of the banking performance of the city. In Da Nang in 2018-19, it is remarkable that the operations of the banking system in the area continue to grow compared to the previous years. By the end of 2018, the total mobilized capital in the province was about VND 125,994 billion, up 9.92% compared to the end of 2017, the highest growth rate in recent years (up 25.84%). In

which, 36/57 credit institutions have increased mobilized capital compared to the end of 2017, contributing greatly to the recovery and development of the business community in the city.

Each bank has its own capital mobilization policy, depending on the needs and purposes of its business. To have a large capital source requires commercial banks to have appropriate mobilization policies to attract the necessary amount of capital in the economy to serve their business and development. Although there is a high credit growth rate compared to the whole country (about 14%), the bad debt rate is low at 1.62%. At the same time, at the end of 2018, banks increased deposit and lending rates to stimulate demand, attract capital, and the impact of exchange rates and liquidity pressure. Techcombank raised interest rates for 12-36-month term from 6.4% a year to 6.8%. VIB applies 7.3% for the 24-month term. ACB also applies a new interest rate schedule for deposits with terms over 18 months, ranging from 7-7.2% a year, 0.1-0.3% higher than May.

2. Background Study

Up to now, there have been many practical studies on the adoption and use of e-banking services, including studies on the factors influencing the decision to use services. Typical electronic banking services. In [1], the author presented that intention is considered to include motivational factors that influence the behavior of each individual. These factors indicate the willingness or effort that each individual will put in the behavior. The above

definition explains behavior that is influenced by a person's confidence in his or her ability to perform the behavior. Therefore, behavior is affected by controlling cognitive and intent behaviors as well as attitudes, subjective criteria and perceptions of behavior controlling indirectly through intentions. In [2] the author expand the application of two Mobile banking service by adding the element of trust ("Feeling of trust") and 2 source factors ("Self-grasping ability" and "financial cost perception") into the model, and focus on the position of these factors in the existing structure of the TAM model. . In [3], the author define that behavioral intent is the ability of the consumer to use an innovation. With higher behavioral intentions, consumers will be more likely to use a new technology. There are a number of premises that can affect an individual's behavioral intentions. Applying the UTAUT model to study the behavior of 3G mobile telecommunications users in [4]. The author used the UTAUT model to conduct research surveys. The research results show that the factors that influence the "behavioral intent" include: "expectation of the effect", "social influence" and "favorable conditions", while the factor "expectations" in terms of effort " has no effect. In addition, three unrecognized relationships were discovered during the SEM analysis, modifying the UTAUT model for 3G telecommunications services. The biggest difference between this study and UTAUT theory is the issue of time of study and the significance of the determinant by external variables. Studying the factors affecting the intention to use online shopping services using the UTAUT model in [5]. The study identified 6 factors affecting the intention to use e-shopping services, including: (1) Expectation about price, (2) Perceived convenience, (3) Perception ease of use (4) Feel the pleasure, (5) Social influence, (6) Feel the risk of use. In addition, the model will also consider the influence on the intended use of three demographic variables: gender, income, and age. Inheriting the point of view of the above researchers, in [6], the author describes customers' savings deposit behavior expressed in choosing a bank and choosing a deposit period. Research on factors affecting the acceptability of Mobile Banking of individual customers applying the UTAUT model in [4]. Using the Unified Theory of Technology Acceptance and Use (UTAUT) to investigate the effects on people through Mobile banking, this study concludes that individuals' intentions on mobile services Banking is significantly affected by the following factors: (1) social influence, (2) perceived financial costs, (3) performance expectation, and (4) perceived trust in order of influence. Behaviors are significantly influenced by personal intentions and favorable conditions. This study found that gender controls the effect of performance expectations and financial cost perceptions on behavioral intent, age of adjustment, effects of favorable conditions, and perceived self-grasping. to real acceptance behavior.

Data were collected from 165 questionnaires and used regression to analyze relationships in [7]. The results have shown that all factors, except the "perceived cost" factor, have a significant impact on behavioral intent in using Mobile Banking. "Feeling useful" is the most influential factor in explaining the user's intent to accept. For users, "feel the ease of use" is the most important factor, while "feel efficient" significantly affects the intention of accepting the service. The results from these analyzes help banking organizations to have a suitable strategy for Mobile banking to expand their acceptability of this service. Background

theory related to rational action theory (TRA) developed in [8] and in [9] shows the inclusion and coordination of the components of attitudes in a structure. which are designed to better predict and explain consumer behavior in society based on two basic concepts: (i) consumer attitudes toward behavior and (ii) subjective standards of consumers. In addition, the intended behavioral theory (TPB) was developed in [9] by adding a cognitive element of behavior control to the TRA model. According to TPB, human behavior is guided by 3 factors: behavioral beliefs, normative beliefs and controlling beliefs. Thus, beliefs about behavior create an attitude of like or dislike about behavior; normative beliefs create subjective social or normative stress and controlling beliefs increase cognitive behavioral control.

Thus, most studies using TAM model are conducted based on the adoption and use of information / technology systems. In studies, the TAM model was found to be valuable in predicting the adoption of variables in the user system. However, in many areas, as mentioned earlier, the original TAM model does not fully explain behavioral intent towards technology adoption and adoption, and there is a need for research to add factors to improve predictability for this model. Up to now, there have been many studies on individual customer banking choices conducted in many different countries around the world, with many different survey subjects. This is a rich source of documents, the basis of orientation to conduct research on factors affecting the choice of banks of individual customers at joint stock commercial banks. Not to mention the research on the earliest bank selection criteria in the US, in [10], the author showed that the recommendation of friends is the most important factor, followed by reputation, reputation. of the bank and large loan capital. In the American university student article, in [11], the author presented that convenience is still the main reason most students choose their bank. In addition, family tradition and loyalty to the bank are also important factors for college students. In [12], the following factors are identified as the decisive attributes affecting the choice of banks: service fee collection policy, reputation, loan interest rate, disbursement time and friendly bank staff. In [13], it is reported that economic factors such as monthly costs and deposit interest play a decisive role in student's choice of bank. In [13], The author found fast and efficient service delivery, friendly, enthusiastic staff and a bank reputation are important factors in choosing select the student's bank. In [14], the author showed that the key factors influencing customer choice in Greece include: convenience, reputation of a bank, quality of products / services. , interest rates and fees, staff communication skills and qualifications, facilities, the environment of the points of sale, and satisfaction with after-sales service and services.

There have been many empirical studies at home and abroad on the factors affecting the decisions of individual customers to deposit money at banks in [15]-[19].The important factors affecting the deposit behavior of customers are financial interests, brand awareness, influence of relatives, fast and safe, marketing, service style of employees, delivery Convenient translation and safe feeling. In [20], the banking selection criteria of Business Administration students in Delhi, India concluded that convenience is an important determinant, Includes: parking, free delivery on demand, phonebanking, free home money transfer service because customers want to save time. In [21], the author conducted in Malaysia found three factors that most influence a

student's banking choice: sense of security, ATM service, and financial benefits. In [16], the author conducted a similar study to determine the factors influencing the choice of commercial banking of university students in South Africa. The study was based on a sample of 186 students from Fort Hare University (Alice campus). The researchers found that the important factors that determine a college student's choice of banking (ranked in diminishing importance) are: service, convenient location, attractiveness, gender referrals of others, marketing activities and prices. In [22], the author studied the factors affecting customer satisfaction in the banking industry in Pakistan to find the relationship between service quality, satisfaction and loyalty. customers. The research results show that 54% change in customer loyalty is due to service quality and customer satisfaction. The study concludes that, service quality affects customer satisfaction and customer satisfaction affects customer loyalty. In today's competitive marketplace, banks can gain a competitive edge by providing quality services that meet the needs of their customers.

For studies in this area in Vietnam, there has been a study on factors affecting the choice of banks of individual customers in [23] surveyed above. 350 individual customers in Da Lat city concluded that brand awareness has the strongest impact on the trend of choosing a bank, followed by factors: Convenience in terms of location, troubleshooting, photos enjoyment of a loved one, appearance and attitude toward marketing. Meanwhile, in [24], the author surveyed 200 customers using banking products and services showed that there is a positive relationship between customer satisfaction and reliability factors. feedback, accessibility, service capacity and quality of products and services. No correlation has been found between information and customer satisfaction. Based on the research results, a few recommendations have been proposed to improve the satisfaction of individual customers with Vietinbank East Hanoi branch in particular and other commercial banks in general. In [25], the author presented on the factors affecting the choice of savings banks of individual customers in Ho Chi Minh City, researched and surveyed over 500 customers. In [25], the author focused on testing the factors of service quality affecting satisfaction and loyalty. In which, testing a number of impacts that regulate the relationship of satisfaction - loyalty of customers for banking services in Hau Giang. Based on a survey sample from 333 customers, Cronbach's Alpha coefficients, exploratory factor analysis, confirmatory factor analysis and structural equation model were used for analysis. The results show that empathy and price are the factors that strongly impact on customer satisfaction. In [26], the author studied the factors affecting the satisfaction of customers with the savings deposit service at Agribank Binh Minh, Vinh Long. Research results show that, 4 main factors affecting customer satisfaction including responsiveness, facilities, service capacity and peace of mind. The relationship between the service quality and the satisfaction of customers participating in the transaction is very important to the operation of the retail bank.

The results of this study have identified 8 groups of factors that affect individual customers' banking choices, including: financial benefits, sense of security, referral, troubleshooting, service. Bank, brand, staff, convenience. At the same time also evaluate their importance. This is the guiding basis for commercial banks to take action measures that focus on key factors to influence customers' choice of banks and thereby attract more. customers using their

bank's retail products and services. Based on the research results, the author gives some suggestions to help banks maintain existing customers and attract new customers. From there, the leaders of banks can refer to make appropriate policies to increase the competitiveness of banks in the retail market. In [27], the author showed on the factors affecting the decision of individual customers to deposit savings - Research at Joint Stock Commercial Bank for Industry and Trade of Vietnam, Lam Dong province, based on into data collected from 184 observations processed by SPSS tool, with Cronbachs Alpha scale reliability testing techniques, factor analysis (EFA), correlation analysis and multiple regression analysis . Research results have identified 5 factors that directly affect individual customers' decisions to save money, including: brand awareness, influence of relatives, financial benefits, fast, safe and marketing. Based on the research results, governance implications have been proposed to better meet customer needs and expand markets to attract new customers. In [23], the author studied the factors affecting individual customer satisfaction with deposit products at Lien Viet Post Joint Stock Commercial Bank - Soc Trang Branch. Research results have found out 5 factors affecting the satisfaction of customers who save money at this bank are: Reliability; Tangible Media; guarantee; sympathy; Transaction office network. In which, tangible means, assurance, sympathy, and transaction office network are the factors that strongly affect the satisfaction of savings customers. As can be seen, the factor that is considered important by the customer when choosing banks varies from country to country and cultures due to differences in economic, cultural and banking systems.
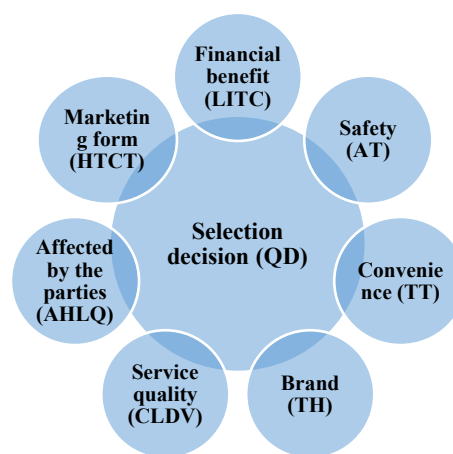
Figure 1: Proposed research model
(Source: Author compiled, 2020)

3. Research Methods

After consulting domestic and foreign research models, survey experts with the list and content as outlined in the discussion paper. The authors have formed a preliminary scale of factors affecting the decision of individual customers to choose a savings bank at commercial banks in Da Nang city to be used when surveying ideas. the experts. After synthesizing the answers of experts about the factors in the preliminary scale. The results of qualitative expert survey showed a high rate of agreement (over 80%) on 7 groups of factors and experts did not add any new groups of factors. After collecting information from the most knowledgeable and experienced staff about deposit services and customers who are conducting transactions at joint stock commercial banks who

have sent savings and intend to save money in the near future. With the model study on an overview of the research situation related to the factors that influence the decision to choose a bank to deposit a savings, we expect an analytical framework with 5 common factors affecting decide to choose a bank to save individual customers as follows:

Based on the research objectives, the survey and research model of the proposed factors influencing the decision to buy Korean facial care products by female university students in Da Nang city, based on the background theory presented above, the research hypotheses are determined as follows:

Hypothesis H1: Financial benefits (LITC) and decision to choose a savings bank of individual customers have positive relationship.

Financial benefits are assessed through two criteria: High saving interest rate and reasonable service fee. Savings deposit interest rate is an indispensable question of customers when looking for information about savings deposit service at a certain bank. Interest is the rate of interest a customer receives in addition to the principal, after a certain period of time at the bank. The bank uses a currency that customers commit to deposit with a fixed term to do business and seek profits, and pay interest on that deposit currency. Interest can be paid at the beginning of the term, paid periodically, or at the end of the term. In the banking sector in Vietnam, competition by savings interest rates is a traditional competitive measure to attract deposits. Interest rate is also the basic factor when customers choose a bank to save money.

Service fee is the cost that a customer has to pay to use banking products and services. When an individual customer comes to the bank not only to save money but also transact in many other areas such as proof of finance, transfer ... - maybe equal to the amount of money that has been saved. If products and services do not have big differences in characteristics and benefits, customers tend to choose products and services with lower costs. Therefore, service costs may also be a concern for customers when choosing a bank to save money.

Hypothesis H2: The safety (AT) and decision of individual customers to choose a savings bank have a positive relationship.

Transactions at banks are often sensitive because they are directly related to customers' financial resources, so a sense of security is a factor worth considering. In [15], the author pointed out that a sense of security reflects a desire of banking users to be stable and secure when making financial transactions. This means a sense of security that includes both security at banks and bank financial stability. Therefore, there are three criteria: Secure customer information, Strong banking financial foundation, Security conditions of transaction points are used to assess the sense of security of customers about the performing bank.

Hypothesis H3: Convenience (TT) and the individual customer's decision to choose a savings bank has a positive relationship.

Another characteristic of individual customers when conducting financial transactions is that they prioritize services that are provided quickly and can be done anywhere, at any time. This convenience is measured through 7 criteria: the large network

of transaction points, the location of convenient transaction points, having a transaction point near home / workplace, suitable bank transaction time, there is ample parking, e-banking available and free home deposit service. The network and location of transaction points provide customers with convenient mobility. Customers can deposit money in one city and withdraw money, transfer money ... in another city. In other words, individuals can perform transactions with the bank at any point in the system thanks to the development of information technology in the banking sector without spending much time and effort on going. again. Often times, the transaction points near home and work are arguably the most attractive. In addition, the spacious parking not only brings a sense of safety but also helps customers more convenient when dealing directly with the bank. Another factor that is considered is the bank's working time in accordance with the individual transaction schedule. Clients with flexible hours of work may not appreciate the fact that banks are open for transactions outside of office hours. On the contrary, for civil servants and office workers - who are often forced by strict working hours, the bank's acceptance of overtime will help them a lot in transactions.

Nowadays, when science and technology are developing rapidly, electronic transactions are expected to be one of the factors attracting customers for convenience. Individuals can perform transactions with the bank whether at home or on the street, with only one device with network connection such as laptop, desk phone, mobile phone ... Instead of having to directly go to bank transactions. Customers, individual customers can transfer, pay electricity and water bills, pay credit card bills or even save money, pay off loans, manage accounts at home, work with just few simple steps. Some other utilities such as free home deposit service should also be deployed for maximum convenience for customers.

Hypothesis H4: Brand (TH) and individual customers' decision to choose a savings bank has a positive relationship.

Combining a number of studies and factors Brand awareness is evaluated through the following observed variables: Recognition of the bank's brand name, logo, image, signature music, Community programs, activities Big sponsorship that the bank participates in and Promotions. In [28], the author showed that Brand awareness has a positive correlation with Brand Desire. Brand awareness is the first component of an attitude, an emotion. Consumers have a certain emotion towards a brand that is first and foremost about being aware of that brand among competing brands. Brand desire consists of two components: preference and preference. A consumer's interest in a brand is expressed through an emotion of interest. And when it comes to choosing between competing, interchangeable brands, consumers tend to choose the brand that causes the most emotion. The authors in [23] have shown that Brand awareness is a factor affecting the trend of choosing a bank, but the awareness aspect is only two points of view "brand is a system. identity "(AMA, 1960) and" brand is symbolic "(in [29]& In [30]), the level of brand awareness is limited only to recognizing the name, logo, image, music sign. characteristics of the brand, advertising and promotion programs of the bank ...Community programs, big sponsorships that the bank participates in and special, unique and attractive promotions contribute to helping consumers to identify banks among competing banks.

Hypothesis H5: Service quality (CLDV) and decision to choose a savings bank of individual customers have positive relationships.

The influence of the factor Products and services of the bank are assessed by easily opening a deposit account or a savings account, providing the service quickly and effectively to help customers not lose much. waiting in line for transactions and products and services are diversified and plentiful, meeting the different needs of consumers. In the era of industrialization and modernization, saving time is one of the criteria that customers are aiming for. Individual customers who come to the savings bank do not want to spend a lot of time on paperwork and procedures with a series of cumbersome and complicated processes. Therefore, the element of ease of opening an account and providing services quickly and efficiently can affect the choice of a bank.

Besides, as mentioned above, the service needs of individual customers are often diverse. A customer can both have a need for both short-term savings and long-term savings. In addition, customers come to certain banks first to save money, but later can use many other services such as wire transfer, payment for electricity and water bills, receiving remittances, borrowing money ... and vice versa. Therefore, diversified and diversified products and services with clear and accurate information are a factor worth considering when using a savings service at a bank.

Hypothesis H6: Related person influence (AHLQ) and decision to choose a savings bank of an individual customer with a positive relationship.

In [31], when people start to want to save money, they collect information about the brand and savings deposit products. of many different banks, thereby making decisions on choosing a bank to save money. Information about brands and product characteristics can be based on their own experiences, or on the recommendations or judgments of others. Therefore, the referral of a third party can be one of the factors influencing the decision-making process of choosing a bank to deposit a customer's savings. The recommendation of family members, friends and the bank staff who are transacting are 3 observed variables used to evaluate the Referral factor. Friends and relatives who have been using the bank's savings deposit service are a useful basis for new customers to choose which bank to save, based on practical experience, understanding and feeling.

In addition, the bank's employees who are transacting are also a valuable source of reference for customers. Usually, individual customers come to the bank not only to use the savings deposit service. They may have made transfers, withdraw money remittances, pay for goods ... before and have a rough feeling about the bank is transacting. At that time, the bank's staff was the bridge leading customers to their bank's savings service.

Hypothesis H7: The form of marketing promotion (HTCT) and the decision to choose a savings bank of individual customers have a positive relationship.

The role of marketing activities in the banking business is not much different from other business areas in conveying information from banks to customers and vice versa. In [24], the author has shown that attitude towards marketing has an influence on the brand desires of consumers. If they have a good attitude and are interested in the branding of a product or brand; distinguish it from competing products and brands; and when there is a demand, the ability to choose for that product or brand is very high.

Thus, the above factors have been tested in many previous studies. However, since most studies have been done in foreign countries, in many different territories, at different times, with separate observers, the results need to be checked for conformity. such as adjustments and supplements through pre-use research to determine the factors that actually affect the choice of banks to deposit money of individual customers.

Table 1: Summary of factors in the proposed research model

Factor	Encode	Hypothesis	Related studies
Financial benefits	LITC	+	[21]; [16]
The safety	AT	+	[31]; [14]
Convenience	TT	+	[20];[16];[14];[32]
Brand	TH	+	[23]; [14]
Service quality	CLDV	+	[14]
Related person influence	AHLQ	+	[16]; [32]
The form of marketing promotion	HTCT	+	[14]
Selection decision	QD		[16]; [14]; [32]

(Source: Author compiled, 2020)

3.1. Research model

The multivariate linear regression equation of this study has the form:

Overall regression function:

$$QD = \beta_0 + \beta_1 LI + \beta_2 AT + \beta_3 TT + \beta_4 TH + \beta_5 CLDV + \beta_6 AHLQ + \beta_7 HTCT + e_i$$

Inside:

- QD: Decided to choose individual customer's savings bank
- Financial benefits (LI)
- Safety (AT)
- Convenience (TT)
- Brand (TH)
- Quality of service (QoS)
- Affected person effects (AHLQ)
- Marketing form (HTCT)

The regression model will find out the independent factors that affect the dependent factor. At the same time, the model also describes the impact level, thereby helping us predict the value of the dependent factor.

4. Result

On the basis of influencing factors that were discovered in the research phase, the survey questionnaire was deployed to the identified survey subjects in the form of direct to individual customers. After giving out 400 surveys to individual customers in the form of live broadcast. Results of 305 votes were collected, processed again, of which 285 votes were met. Data used in the research of the topic are data obtained directly from the survey tables that have been cleaned to eliminate incomplete or inadequate survey responses to the research requirements.

4.1. Age

The results show that out of a total of 285 survey samples meeting the requirements, there are some couples 18-25 years old accounting for 5.3%, 25-40 years old accounting for 39.3%, the age from 40-60 accounts for 37.2% and Finally, the age over 60 accounts for 18.2%. The analysis results show that people aged 25-60 are often more interested in choosing a bank to save money, this is also a group of people with the ability to generate income and want to preserve their numbers. your money is safe and look for income from your savings.

4.2. Education level

Surveying 285 customers on factors affecting the decision to choose savings banks at commercial banks in Da Nang city, 1.1% of customers have high school education, 61.4% and 36.5% of clients have college / university degrees, 1.1% of customers have graduate degrees.

4.3. Income

Surveying 285 customers about factors affecting the choice of savings banks of individual customers at commercial banks in Da Nang city, customer groups with income from 5-10, customer groups goods with income from 10-50 million accounts and group of over 50 million accounts for the main proportion, this is also potential customers of the bank in mobilizing savings deposits.

4.4. Type of agency

Thus, there are 53% of customers working in state agencies, 18.9% of customers working in joint stock companies, 28.1% of customers working in joint ventures and the rest working in joint ventures. private companies and self-employed. Thus, the group of customers working at state agencies or joint ventures is the group most likely to deposit savings at banks.

After removing the unreliable observed variables, including: TH4, CLDV4, AHLQ2, CT1, CT2, CT3 according to the evaluation results above, re-test the Reliability of the scale with variables. The remaining results show as follows:

Table 2: Results of reliability analysis and factor analysis

No	Group variables		Number of observation variables	Cronbach's Alpha
1	Financial benefits	LITC	3	0.823
2	The safety	AT	4	0.835
3	Convenience	TT	4	0.782
4	Brand	TH	3	0.844
5	Service quality	CLDV	3	0.843
6	Selection decision	QD	3	0.939

(Source: Analysis results from SPSS 16.0 software)

Table 3: KMO coefficients and Bartlett's tests of independent factors

KMO coefficient		.800
Bartlett's test	**Approx. Chi-Square**	4250.315
	Df	171
	Sig.	.000

Rotated Component Matrix^a

	Component				
	1	2	3	4	5
CLDV2	.798				
CLDV1	.789				
CLDV3	.787				
TH2	.646				
TT3	.623				
TH1	.578				
TH3					
AT2		.832			
AT3		.791			
AT4		.679			
AT1		.649			
TT1		.593			
AH3			.827		
AH1			.788		
LITC1				.772	
LITC3				.771	
LITC2				.734	
TT2					.841
TT4					.638

Extraction Method: Principal Component Analysis.

Rotation Method: Varimax with Kaiser Normalization.

Rotation converged in 7 iterations.

(Source: Analysis results from SPSS 16.0 software)

The multivariate linear regression equation of this study has the form:

Overall regression function:

$$QD = \beta_0 + \beta_1 F1 + \beta_2 F2 + \beta_3 F3 + \beta_4 F4 + \beta_5 F5 + \beta_6 F6 + Ui$$

Sample regression function:

$$QD = \hat{\beta}_0 + \hat{\beta}_1 F1 + \hat{\beta}_2 F2 + \hat{\beta}_3 F3 + \hat{\beta}_4 F4 + \hat{\beta}_5 F5 + \hat{\beta}_6 F6 + ei$$

Inside:

QD: - Decided to choose the individual customer's savings bank

- F1 Service quality, includes variables CLDV2, CLDV1, CLDV3, TH2, TT3, TH1.

- F2 Safety, includes variables AT2, AT3, AT4, AT1, TT1.

- F3 Related effects, includes variables AH3, AH1.

- F4 Financial benefit, includes variables LITC1, LITC3, LITC2.

- F5 Convenience, includes variables TT2, TT4.

The regression model will find the independent factors that affect the dependent factor. At the same time, the model also describes the impact level, thereby helping us predict the value of the dependent factor.

The regression results in SPSS are as follows:

Table 4: Regression coefficients

Factor	Unstandardized Coefficients		Standardized Coefficients	T value	Sig.
	B	Standard error	Beta		
Constant	-1.905	.040		.000	1.000
F1 Service quality	.632	.040	.632	15.942	.000
F2 Safety	.314	.040	.314	7.915	.000
F3 Related effects	.218	.040	.218	5.509	.000
F4 Financial benefit	.092	.040	.092	2.324	.021
F5 Convenience	.085	.040	.085	2.146	.033

(Source: Analysis results from SPSS 16.0 software)

The regression results show that 5 independent factors from F1, F2, F3, F4, F5 are statistically significant, sig <0.05 is satisfactory, so they will be retained in the research model.

Table 5: Model Summary

Model	R	R Square	Adjusted R Square	Std. Error of the Estimate
1	.749[a]	.561	.554	.66814717

(Source: Analysis results from SPSS 16.0 software)

Based on the results in the table above, ANOVA has value Sig = 0.000 <0.05, so the hypothesis H0 is rejected, assuming the hypothesis H1. That means the model exists.

In other words, with 5% significance, it can be concluded that the decision to choose a savings bank of an individual customer is influenced by at least 1 of the remaining 5 factors:

The regression results showed that the Durbin-Watson Statistics was 2,182. Thus, the model exists and with d = 2,219 □ 2,0, we can conclude that the model does not exist negative or positive autocorrelation.

So, the regression estimation model would be:

$$QD = -1.905 + 0.632 F1 + 0.314 F2 + 0.218 F3 + 0.092 F4 + 0.085 F5$$

The standardized regression would be:

$$QD* = 0.632 F1* + 0.314 F2* + 0.218 F3* + 0.092 F4* + 0.08 F5*$$

And the model of quantitative research results takes the form:
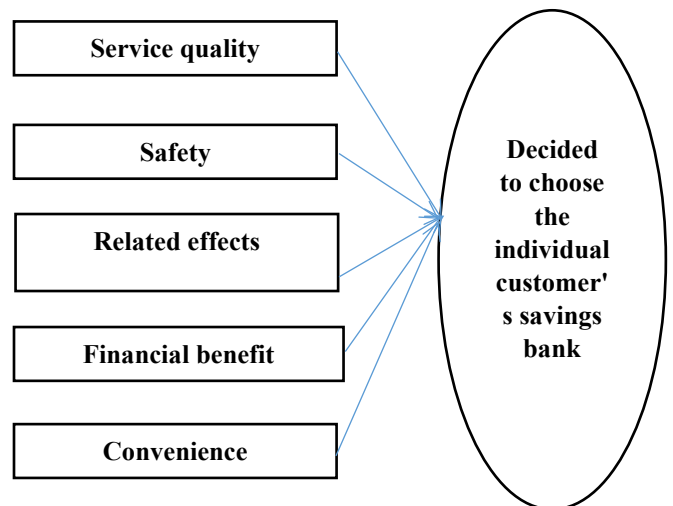
Figure 2: Research results

Linear regression model using Enter method is made with a number of assumptions and the model only really makes sense when these assumptions are guaranteed. Therefore, to ensure the reliability of the model, the topic must also evaluate the violation of necessary assumptions in linear regression. From the result in Figure 4.5, we have 1 <d = 2.219 <3 so we can conclude that the remainder are independent of each other and that the independence of the remainder is guaranteed. [33]

Finally, we will consider the multi-collinearity violation of the model. In the above correlation coefficient analysis, we have seen that the dependent variable has a fairly clear correlation with the independent variables, but we can also see that there is correlation between the independent variables. This will create the model's multicollinearity capability. Therefore, we have to detect multi-collinearity phenomenon by calculating the acceptability of the variable (Tolerance) and the variance inflation factor (VIF).

Thus, the linear regression model built according to the above equation does not violate the necessary assumptions in linear regression.

5. Conclusion

With the survey results including the number of samples of 285 for a regression model including 7 groups of factors affecting the decision of individual customers to choose a savings bank at commercial banks in Da Nang city. . The quantitative research results show that there are 5 groups of factors that greatly affect the decisions of individual customers to choose a savings bank: Service quality, Safety, Related effects, Benefits financial benefits, convenience

5.1. Improving the quality of banking services

Besides expanding the banking network, increasing investment in facilities and techniques, developing many convenient products to attract customers; Banks are constantly making efforts to perfect products, improve the quality of care and serve customers. Products and services are factors affecting customers' choice of banks to save savings. Because customers come to the bank, apart from the purpose of saving, have many other needs such as transferring money, paying bills ... Providing enough services according to customers' needs is also one of the attractive measures. Personal savings deposit. Therefore, the improvement of aspects related to the retail products and services that the bank offers to customers, including product variety, simplification of procedures, and time savings. , and there are different preferential policies depending on different subjects.

5.2. Increase safety for customers when sending money

With specific regulations on insured deposits, rights and obligations of the sender, payment limit, time of interest payment ... has shown the Bank's commitment and the State to ensure security. safety of depositors' deposits aims to best protect the legitimate rights and interests of depositors, ensure the safety and health of banking operations and handle financial crisis. In addition, the Bank needs to build support channels to help customers easily use smart services, tools and utilities to check their savings accounts at the Bank anytime, anywhere like channel. at the counter (account balance confirmation service), Internet Banking channel (for customers registered to use iPay service) or automatic answering switchboard channel (TPIN) ... As recommended by the Bank, customers Customers must also protect themselves when depositing money through the implementation of bank recommendations. Customers register SMS Banking with the Bank, enter the correct customer number or ID card to automatically look up the following information: Account balance, account number, last 5 transactions of the account account accounts, savings book balance, card status, exchange rate, savings interest rate, information on products, services, promotions….

5.3. Improve financial benefits for depositors

The research results show that among the factors individual customers will consider when choosing a bank to save money, financial benefits are the most important factor. In which, the observed variable "financial benefits" received a high consensus. It can be said that savings depositors appreciate the bank's financial capacity. Therefore, improving financial benefits is one of the conditions for banks to attract customers.

Financial benefits are shown through three aspects, including interest rates on savings deposits, fees applied to products and services and regular promotions. In general, this is one of the top concerns when customers use the bank's products and services. However, in Vietnam, issues related to interest rates are strictly managed by the State Bank of Vietnam through the ceiling deposit rate applicable to commercial banks. As more and more customers need convenience, the online savings channel becomes preeminent, especially for the group of 'digital customers'. Therefore, banks should encourage customers to deposit online savings with bonus interest rates, which is seen as a positive move proactively following customer needs and is a competitive factor in the market when The convenience of digital banking is becoming more and more popular in Vietnam. Both the Bank and the customers save translation time, and have established themselves in the retail industry with recognition from international organizations.

5.4. Increased convenience for customers to send money

Bank savings is always the first choice for unused idle money. However, many customers, when saving money, do not deposit all their idle money because they are afraid that they cannot withdraw their money when they need money, or they must withdraw their interest before their due date. Therefore, the bank needs to offer a solution for customers that should split the savings book instead of just depositing all the money in one book. Along with that, the bank needs to expand its network through increasing the number of transaction points, the banks also invest heavily in renovating the transaction space of the existing branches, providing a spacious transaction space. page, spacious, creating maximum comfort for customers. At the same time, banks also promote digital banking and gradually affirmed themselves with recognition from international organizations. On the digital banking platform, customers easily perform hundreds of types of services, from paying bills for electricity, water, telecommunications, monthly insurance to fast money transfers within 5 minutes for bank accounts. other goods

References

[1] I. Ajzen, "The theory of planned behavior." Organizational behavior and human decision processes, **50**(2), 179-211, 1991

[2] P. Luarnand and H.H. Lin, "Toward an understanding of the behavioral intention to use mobile banking." Computers in human behavior, **21**(6), 873-891, 2005.

[3] V. Venkatesh, S. M. Walton, and J. Y. L. Thong, "Consumer acceptance and use of information technology: extending the unified theory of acceptance and use of technology." MIS quarterly, 157-178, 2012

[4] C.-S. Yu, "Factors affecting individuals to adopt mobile banking: Empirical evidence from the UTAUT model." Journal of electronic commerce research **13**(2), 104, 2012

[5] H. Q. Cuong, Research on factors affecting the intention to use online shopping services (Nghiên cứu các yếu tố ảnh hưởng đến ý định sử dụng dịch vụ mua hàng điện tử qua mạng), National University of Ho Chi Minh City, 2020.

[6] L. T. T Hang, Research on bank savings behavior of individual customers in 2012 (Nghiên cứu hành vi gửi tiền tiết kiệm ngân hàng của khách hàng cá nhân năm 2012). Doctoral thesis, Academy of Social Sciences, 2012

[7] B. K. Jeong, M. Khouja, and K. Zhao, "The impacts of piracy and supply chain contracts on digital music channel performance." Decision Support Systems **52**(3), 590-603, 2012.

[8] M. Fishbein and I. Ajzen, "Belief, attitude, intention, and behavior: An introduction to theory and research.", 1977.

[9] I. Ajzen, "From intentions to actions: A theory of planned behavior." Action control. Springer, Berlin, Heidelberg, 11-39, 1985

[10] W. T. Anderson, E. P. Cox and D. G. Fulcher, "Bank Selection Decisions and Market Segmentation: Determinant attribute analysis reveals convenience- and sevice-oriented bank customers." Journal of Marketing, **40**(1): 40-4, 1976. DOI: 10.1177/002224297604000107

[11] D. D Schram, C. C. Darling Milloy, and W. E. Rowe, "Juvenile sex offenders: A follow-up study of reoffense behavior". Community Protection Research Project, Washington State Institute for Public Policy, 1991.

[12] K. Khazeh, and W. H. Decker, "How customers choose banks." Journal of Retail banking **14**(4), 41-45, 1992.

[13] D. H. Tootelian and R. M. Gaedeke, "Targeting the college market for banking services." Journal of Professional Services Marketing **14**(2), 161-172, 1996.

[14] E. Mylonakis, E. L. Hohmann, and S. B. Calderwood, "Central nervous system infection with Listeria monocytogenes. 33 years' experience at a general hospital and review of 776 episodes from the literature." Medicine **77**(5), 313-336, 1998.

[15] S. Mokhlis, N. Hazimah, N. Mat, and H. S. Salleh, "Commercial bank selection: the case of undergraduate students in Malaysia." International Review of Business Research Papers **4**(5), 258-270, 2008.

[16] C. Chigamba, and O. Fatoki, "Factors influencing the choice of commercial banks by university students in South Africa." International Journal of Business and Management, **6**(6), 66, 2011

[17] H H. Siddique, "Bank selection decision criteria employed by indian expatriates in sultanate of oman: an empirical analysis." International Journal of Business and Management Studies **4**(2), 55-64, 2012.

[18] S. S. Almejyesh and K. S. Rajha, "Behavioral determinants and their impact on customer savings deposits in Islamic banks in Saudi Arabia." Journal of Islamic Banking and Finance **2**(1), 163-186, 2014

[19] C. I. Enyinda, "Evaluation of relationship marketing in Islamic banks in the UAE: Empirical evidence based on sensitivity analysis algorithm." Journal of Economic & Financial Studies **2**(3), 01-12, 2014.

[20] A. Sajeevan Rao, and R. K. Sharma, "Bank selection criteria employed by MBA students in Delhi: An empirical analysis." Journal of business studies Quarterly **1**(2), 56-69, 2010.

[21] S. Mokhlis, H. S. Salleh, and N. H. N. Mat, "What do young intellectuals look for in a bank? An empirical analysis of attribute importance in retail bank selection." Journal of Management Research **3**(2), 1-15, 2011.

[22] R. I. Sabir, Ghafoor, O., Akhtar, N., Hafeez, I., and Rehman, A. U, "Factors affecting customer satisfaction in banking sector of Pakistan." International review of management and business research **3**(2), 1014, 2014

[23] P. T. Tam, and P. N. Thuy, Factors affecting individual customers' tendency to choose the Bank (Yếu tố ảnh hưởng đến xu hướng lựa chọn Ngân hàng của khách hàng cá nhân). Journal of Banking Science and Training, 103, April 2010.

[24] N. T. Gam, Research on factors affecting individual customer satisfaction for Joint Stock Commercial Bank for Industry and Trade East Hanoi Branch, (Nghiên cứu các yếu tố ảnh hưởng đến sự thỏa mãn của khách hàng cá nhân đối với ngân hàng thương mại cổ phần Công thương Chi nhánh Đông Hà Nội). Science & Technology Magazine, **81**, 33-40, 2011.

[25] L. M. Linh, Research on customer satisfaction and loyalty to banking services in Hau Giang province (Nghiên cứu sự hài lòng và trung thành của khách hàng đối với dịch vụ ngân hàng trên địa bàn tỉnh Hậu Giang), Journal of Social Sciences and Humanities, **12**, 34 – 41, 2014.

[26] P. D. Khoi, Factors affecting customer satisfaction with savings deposit services: The case of Agribank Binh Minh, Vinh Long (Các nhân tố ảnh hưởng đến mức độ hài lòng của khách hàng đối với dịch vụ tiền gửi tiết kiệm: Trường hợp Agribank Bình Minh,Vĩnh Long). Scientific Journal of Can Tho University, **40**, 50-57, 2015. Doi: 10.1263/03697854100265

[27] N. N. D. Phuong, Factors influencing individual customers' decisions to save money - Research at Joint Stock Commercial Bank for Industry and Trade of Vietnam (Các nhân tố ảnh hưởng đến quyết định gửi tiền tiết kiệm của khách hàng cá nhân - Nghiên cứu tại Ngân hàng Thương mại cổ phần Công Thương Việt Nam). Industry and Trade Magazine, No. 01, June 2014

[28] N. D. Tho, and N. T. M. Trang, Research the components of brand equity and measure them in the consumer goods market in Vietnam (Nghiên cứu các thành phần của giá trị thương hiệu và đo lường chúng trong thị trường hàng tiêu dùng tại Việt Nam). Ministry-MSB-level scientific research project, 22-33, 2002

[29] J. N. Kapferer, Die Marke, Kapital des Unternehmens. No. hal-00788645. 1992.

[30] D. A. Aaker, "Measuring brand equity across products and markets." California management review 38.3 1996.

[31] P. Gerrard and J. B. Cunningham, "Singapore's undergraduates: how they choose which bank to patronise." International Journal of Bank Marketing, 2001. Doi: 10.1108/02652320110388531

[32] J. Tank and K. Tyler, "UK student banking revisited: influences and the decision-making process." Journal of financial services marketing **10**(2), 152-164, 2005. Doi: 10.1177/002224297604068954

[33] H. Trong and C. N. M Ngoc, Research Data Analysis with SPSS (Phân tích dữ liệu nghiên cứu với SPSS (Tập 1)), Statistical Publishing House, Ho Chi Minh City, 2008

Identification of Genetic Variants for Prioritized miRNA-targeted Genes Associated with Complex Traits

Isabella He[1], Zhaohui Qin[2], Yongsheng Bai[*,3]

[1]*Pittsford Mendon High School, 472 Mendon Road, Pittsford, NY 14534, USA*

[2]*Department of Biostatistics and Bioinformatics, Emory University, Atlanta, GA 30322, USA*

[3]*Next-Gen Intelligent Science Training, Ann Arbor, MI 48105, USA*

A R T I C L E   I N F O

A B S T R A C T

Genome-wide association studies, or GWAS, have reported associations between SNPs and specific diseases/traits. GWAS results contain variants located in different genomic regions, including variants in the 3'UTR. MicroRNAs, or miRNAs, are small noncoding RNAs that bind to the 3'UTRs of genes to regulate gene expression. However, variant(s) that are located in the 3'UTR could impact miRNA binding, thus affecting expression of its targeted gene(s). To specifically elucidate miRNA targeting pairs and binding site variants associated with a specific trait, well-designed downstream analysis along with careful experimental design are necessary. Currently, there is no available state-of-the-art methodology for identifying miRNA targeting pairs and associated variants that could contribute to phenotypes using GWAS. Moreover, it is unrealistic to conduct experiments for elucidating all possible miRNA targeting pairs and binding site variants across the entire genome. In this project, we developed a bioinformatic pipeline to computationally identify genes and their targeting miRNA pairs that are enriched over the miRNA-gene tissue expression network for the studied genetic traits and examined the binding site variants' impact on Body Mass Index (BMI).

1. Introduction

GWAS is a powerful approach to identify common variants associated with common diseases/traits in studied populations [1, 2]. Traits may be activated due to genetics or changes in environment, or both.

MicroRNAs (miRNAs), noncoding RNAs with a length between 17-22 nucleotides, exert their impact on gene regulation through targeting mRNAs. To achieve their function, miRNAs bind to the 3' untranslated regions (3'UTRs) of target mRNAs which can often result in potential suppression of mRNA translation and/or gene expression.

Single-nucleotide polymorphisms (or SNPs) are the most common mutations found in the human genome [3, 4]. SNPs located in the 3'UTRs can potentially disrupt miRNA regulation [5]. A DNA motif is a conserved DNA sequence segment with biological consequences. The identification of a motif located in the 3'UTR could suggest how miRNAs potentially target genes in that region. Analysis of GWAS data by identifying genes or miRNAs that harbor genetic variants could elucidate trait-associated genetic variants [6].

In our experiment, we analyzed multiple traits compiled from GWAS and found BMI to be the most significant trait in the context of the miRNA-gene tissue expression target network. We further investigated several genes located within the region(s) associated with BMI, *FADS1* and *FADS2* due to their significant relevance to obesity and related conditions [7]. The overarching goal of this study is to identify how the interaction between genes and their targeting miRNAs change due to genetic variations and reveal any underlying biological mechanisms that contribute to the development of complex traits for humans.

2. Experimental Methods

To perform our experiment, we proposed the following approach:

---

[*]Corresponding Author: Yongsheng Bai, 2373 Foxway Drive, Ann Arbor, MI 48105, USA Contact No: (817)559-3448
Email: bioinformaticsresearchtomorrow@gmail.com
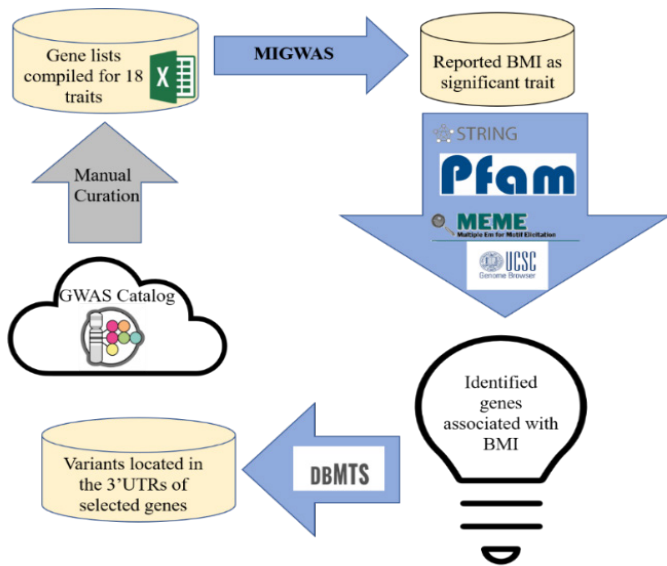
Figure 1: Workflow of variant identification for complex trait BMI

2.1. GWAS Traits Selection

We downloaded the annotation data of GWAS results from 18 traits, all of which had at least 100 associated genes as compiled by PheGenI [6]. All traits were previously described [8]. These traits ranged from autoimmune disorders such as Rheumatoid Arthritis and Asthma to behavior traits such as smoking.

2.2. Trait Relevant miRNA-gene Pairs Identification

We employed MIGWAS software [9, 10] using default running parameters (2018 Github version: https://github.com/saorisakaue/MIGWAS) to strengthen our analysis regarding all 18 traits and identify significant traits and miRNA-gene pair candidates over the gene tissue expression network. In order to run MIGWAS, we converted the variant genomic coordinate annotations (hg38) provided by PheGenI to the hg19 version. Figure 2 shows the Python pipeline of running MIGWAS.

```
Step 1:

python3    minimgnt.py    hg19_BMI.txt    --out
hg19_BMI_sumstats_trans --cpus 10 --not-remove-
HLA --remove-NA --no-rsid

Step 2:

python3      migwas.py         --phenotype
hg19_BMI_sumstats_trans           --out
miRA_hg19_BMI_sumstats_trans   --cpus  10  --
iterations 500 --output-candidate
```

Figure 2: Python code of running MIGWAS

2.3. Protein-Protein Interaction Examination and Domain Elucidation

We ran STRING database to look for evidence of interaction between the ten candidate genes associated with BMI at the protein level [11]. We also used Pfam to identify if there were any possible domains associated with BMI [12].

2.4. Motif Discovery for miRNA-targeted Genes Relevant to BMI Trait

We applied MEME software (version 5.3) to identify enriched motifs for the 3'UTR sequences retrieved from Ensembl Biomart Database [13, 14]. To run MEME, we stipulated the software parameter for the searched motif width to be between six and twenty base pairs. Also, the number of searched motifs was restricted to report the top six motifs. All other running parameters were kept as default.

2.5. Variant Identification for Selected Genes Associated with BMI

We checked the dbMTS database for reported candidate genes associated with BMI through MIGWAS and pinpointed SNPs located inside each gene's respective 3'UTRs [5].

3. Results

3.1. Selection of GWAS Results

We acquired the GWAS results of 18 traits with more than 100 associated genes that were reported in our recent study [8]. All selected traits are displayed in Table 1 below.

Table 1: Selected 18 traits as reported by PheGeni. All traits listed were associated with at least 100 genes.

Trait	# SNPs	# Genes
Alcoholism	802	657
Alzheimer's	873	1037
Arthritis, Rheumatoid	374	276
Asthma	712	818
Autistic Disorder	982	505
BMI	3601	1971
Coronary Artery Disease	493	471
Coronary Disease	440	345
Crohn's	633	403
T1D	309	235
T2D	542	416
Hypertension	314	270
NSCLC	129	131
Obesity	426	434
Osteoporosis	77	102
Psoriasis	425	292
Schizophrenia	1530	1453
Smoking	781	938

3.2. MIGWAS Analysis

We identified in particular that one out of the 18 traits, BMI, has a significant association with all tissues (p-value of .0313). There are only three traits which have a p-value reported for trait

and tissue association, including BMI, Crohn's, and Type 1 Diabetes (T1D) (Figure 3).

We have identified ten genes that are targeted by five miRNAs as candidate biomarkers in the BMI trait. For Crohn's, there was only one pair while T1D had two pairs (Table 2).
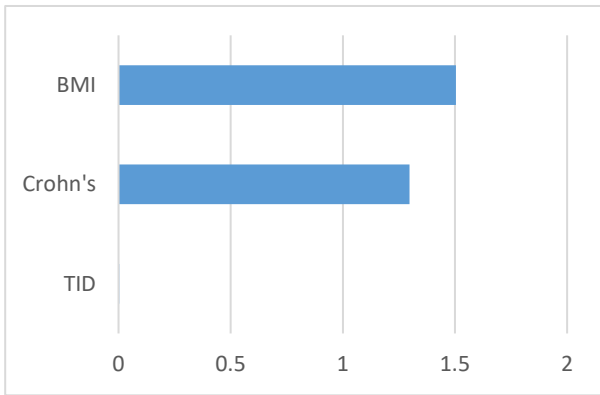
Figure 3: MIGWAS reported p-values (-log base 10 scale) for BMI, Crohn's disease, and Type 1 Diabetes.

Table 2: MIGWAS results for candidate genes/miRNAs identified for three traits

Trait name	Gene	miRNA
BMI	*ADAMTS9*	*hsa-mir-330*
BMI	*AMH*	*hsa-mir-615*
BMI	*CELSR2*	*hsa-mir-615*
BMI	*DNM3*	*hsa-mir-330*
BMI	*FADS1*	*hsa-mir-615*
BMI	*FADS2*	*hsa-mir-615*
BMI	*HOXC5*	*hsa-mir-615*
BMI	*MED17*	*hsa-mir-4531*
BMI	*NEGR1*	*hsa-mir-4721*
BMI	*OTUD7B*	*hsa-mir-642a*
Crohn's	*SYNGR1*	*hsa-mir-4728*
T1D	*HIPK1*	*hsa-mir-1236*
T1D	*TMEM116*	*hsa-mir-4646*

3.3. String Database Results

Out of the ten genes researched, there are three genes—*FADS2, FADS1*, and *AMH*—that interact with each other as reported by the STRING database, as shown in Figure 4. These three genes are also targeted by the same miRNA: *hsa-mir-615*. The STRING database also reported BMI's significant associations (FDR < .01) with fatty acid metabolism (hsa01212) and biosynthesis of unsaturated fatty acids (hsa01040) under KEGG pathways. Likewise, the BMI-related GO terms—linoleic acid metabolic process (GO:0043651), alpha-linolenic acid metabolic process (GO:0036109), and unsaturated fatty acid biosynthetic process (GO:0006636)—are also reported by the STRING database.

3.4. Pfam Database Results

The Pfam database reported two domains associated with BMI: Fatty Acid Desaturase (PF00487) and Cytochrome b5-like heme/steroid binding domain (PF00173), as shown in Figure 5.
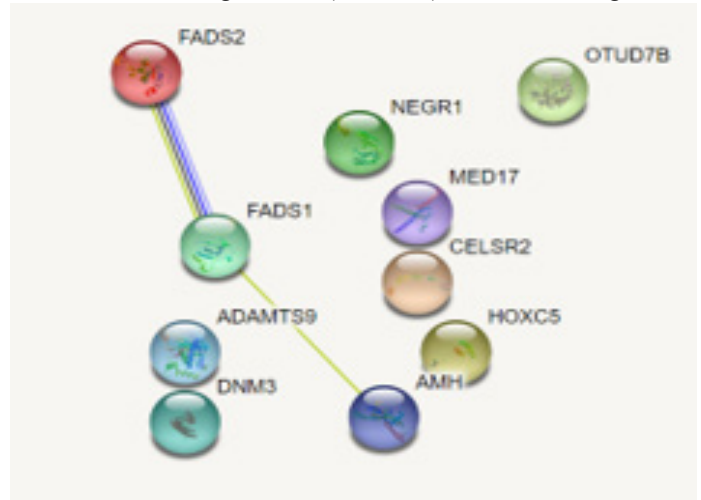
Figure 4: Protein-protein interaction results for all ten genes associated with BMI. Only three genes were found to have interactions with each other (*FADS1, FADS2, AMH*).

These results were consistent with the ones reported by the INTERPRO database.
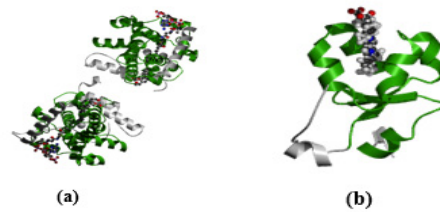
Figure 5: Protein structures of two BMI-associated domains. (a) displays the Fatty Acid Desaturase Domain. (b) displays the Cytochrome b5-like heme/steroid binding domain.

3.5. Motif Identification

Using MEME, we ran all ten of the genes associated with BMI. A motif was discovered containing nine out of these ten genes (*ADAMTS9, CELSR2, DNM3, FADS1, FADS2, HOXC5, MED17, NEGR1, OTUD7B*), with an e-value of .047 (Figure 6).

Figure 6: Motif conservation across nine (out of ten) genes associated with BMI

3.6. Variant Identification Results

To report known common variants contained in miRNA-targeted genes associated with BMI, we checked the UCSC Genome Browser [15]. This region contains multiple known variants (dbSNP 153 Track) that are located inside both *FADS1* and *FADS2* (see Figure 7 below). Interestingly, *FADS1*, *FADS2*, and *FEN1* (a neighboring gene) are highly expressed in the adrenal gland. As indicated by GTEx data, *CELSR2*, *FADS1*, and *FADS2* all are expressed with low amounts in both types of adipose tissue. Since all three genes are targeted by the same miRNA, *hsa-miR-615*, low expression of these genes in adipose tissues could be due to the repression effect of this miRNA.

Figure 7: UCSC Genome Browser view for variants located in the genomic regions of *FADS1/FADS2*. The orange vertical bars placed within the view pinpoint the general motif coordinates defined by MEME. The left bar represents the identified motif region for *FADS1* while the right bar represents *FADS2's* identified motif region.

3.7. dbMTS Results

To identify miRNA binding-site variants, we checked the dbMTS database [5]. Table 3 shows that multiple variants, which could alter the binding relationship of miRNAs and their targets, are often present in the 3'UTRs of miRNA-targeted genes associated with BMI.

4. Discussion and Interpretation

In this study, we applied cutting-edge bioinformatics tools and databases to select candidate genes/miRNAs associated with complex genetic trait(s), such as BMI.

Using MIGWAS, we analyzed three traits: BMI, Crohn's, and T1D. While both BMI and Crohn's had significant p-values in the gene expression network, Crohn's yielded only one gene/miRNA pair. On the contrary, T1D had a non-significant p-value but yielded 2 gene/miRNA pairs (see Figure 3 and Table 2). We concluded that a significant p-value does not necessarily indicate the existence of more miRNA-gene targeting pairs for specific traits. As a result of this MIGWAS analysis, we focused on investigating BMI as it had many gene/miRNA pairs in comparison to the other two traits mentioned. When performing

Table 3: Variant results reported in dbMTS

rs_dbSNP150	chr	pos	ref	alt	VEP_ensembl_Gene_Name
rs7528419	1	109274570	A	G	CELSR2
rs11102967	1	109274623	C	G	CELSR2
rs1277917	1	109274857	G	C	CELSR2
rs12740374	1	109274968	G	T	CELSR2
rs660240	1	109275216	T	C	CELSR2
rs57677983	1	109275536	C	A	CELSR2
rs658435	1	109275648	C	T	CELSR2
rs629301	1	109275684	G	T	CELSR2
rs10410	1	109279782	G	A	CELSR2
rs14000	1	109279887	T	C	CELSR2
rs1061955	1	149942458	G	A	OTUD7B
rs2757500	1	172309881	G	A	DNM3
rs2586422	1	172309937	A	G	DNM3
rs2586423	1	172310272	G	A	DNM3
rs2421994	1	172310769	G	A	DNM3
rs10489282	1	172407906	G	A	DNM3
rs4916255	1	172411735	C	A	DNM3
rs7528296	1	172412243	T	C	DNM3
rs11714364	3	64650182	C	A	ADAMTS9
rs9851598	3	64650452	G	A	ADAMTS9
rs4246215	11	61796827	G	T	FADS1, FADS2
rs174544	11	61800281	C	A	FADS1, FADS2
rs174545	11	61801834	C	A	FADS1, FADS2
rs174545	11	61801834	C	G	FADS1, FADS2
rs174546	11	61802358	C	T	FADS1
rs174568	11	61826344	C	T	FADS1, FADS2
rs482548	11	61865710	C	A	FADS2
rs17764288	11	61866264	G	A	FADS2
rs11539526	11	61866298	C	G	FADS2
rs77167250	11	61866475	C	T	FADS2
rs676586	11	93788239	C	T	MED17
rs606087	11	93789476	A	G	MED17
rs17652258	11	93814518	G	C	MED17
rs677019	11	93818291	T	C	MED17
rs654896	11	93818330	A	T	MED17
rs17573753	11	93818630	C	T	MED17
rs679241	11	93818748	A	G	MED17
rs585768	11	93819689	C	T	MED17
rs2071450	12	54034748	C	T	HOXC5
rs104894666	19	2250667	C	T	AMH

this study, we noticed that different tools/databases can analyze data with complementary results from different aspects.

For example, MIGWAS identified *CELSR2* containing 3'UTR variants also reported by the PheGenI database. MIGWAS identified two genes (out of nine)—*DNM3* and *FADS1*—that don't contain 3'UTR variants in the data provided by PheGenI. The other seven genes were not reported by PheGenI [6, 9].

After comparison, dbMTS reported results on nine genes total. Six genes (*OTUD7B, DNM3, ADAMTS9, MED17, FADS1,* and *FADS2*) contain 3'UTR variants also reported by MIGWAS. The remaining three genes (*CELSR2, HOXC5,* and *AMH*) do not contain 3'UTR variants as dbMTS states.

Using DIANA Tools, we identified two genes (*CELSR2* and *ADAMTS9*) that are targeted by *hsa-miR-615* [16]. Although MIGWAS stated that *ADAMTS9* was targeted by *hsa-miR-330*, this is likely due to this gene being targeted by multiple miRNAs. However, wet-lab experiments are needed to validate this conclusion. In addition, the targeting outcome of multiple genes associated with BMI by *hsa-miR-615* is significant. Studies show that increased levels of *hsa-miR-615* may help inhibit palmitate-induced hepatocyte apoptosis [17]. If saturation levels of palmitate, a type of fatty acid, are increased, this increases the likelihood of developing diseases such as non-alcoholic fatty liver disease, which is correlated with obesity (or a high BMI) [18]. Indeed, *CELSR2* was recently discovered to have significant high expression in cancerous tissue than normal tissue. Specifically, hepatocellular carcinoma, a primary liver cancer whose major risk factors include non-alcoholic fatty liver disease [19].

Current literature evidence supports that *FADS2* has been discovered to be a drug target gene as well as an miRNA-target gene for rheumatoid arthritis (RA) [10]. However, such evidence reports *hsa-miR-4728* as *FADS2's* target miRNA instead of *hsa-miR-615*. This suggests the involvement of both miRNAs in the development of BMI-related illnesses. In addition, multi-omics analysis proves *FADS2* is a potential biomarker for BMI. This is consistent with the conclusion that a high BMI leads to increased risk of developing RA, even though the biological mechanism responsible has yet to be identified [20, 21]. In addition, a recent study confirms that the *FADS1/2* cluster are significantly associated with fatty acid levels (see Figure 4). This study also reported *FADS1* alongside rs174546, matching our corresponding row in Table 3. Unlike our experiment, however, the mentioned study did not employ dbMTS to generate this match [22]. The conservation of both *FADS1* and *FADS2* in the identified motif (see Figures 6 and 7) further emphasizes the potential importance of these two genes in the association with BMI/development of obesity.

In a recent study, Kuryłowicz and colleagues report that two miRNAs—*hsa-miR-615* and *hsa-miR-330*—and their target genes (of which none are listed in Table 2) are involved in the oncogenesis pathway, otherwise known as the process where healthy cells become cancerous [23]. Shared target miRNAs between a genetic trait (BMI) and cancer suggests that the development of illness as a result of either share similar causal/biological factors. In addition, *hsa-miR-615* was found to be highly expressed in the subcutaneous adipose tissue (SAT) of obese patients after surgery-induced weight loss than the SAT of patients with a normal weight, suggesting that there is a difference in molecular pathways/miRNA expression between losing weight and consistently maintaining a healthy weight [23]. This is consistent with the finding that *hsa-miR-615* facilitates palmitate production which is correlated with a higher likelihood of developing obesity.

In our previous study, we found a statistically significant association between BMI and the PCDHA10 pathway [8]. PCDHA10 is a gene which codes for different protocadherins (Pcdhs), which play an important role in neural generation [24]. As neuronal development and brain structure have been linked to BMI through existing literature, this could be a reason why the PCDHA10 pathway is associated so strongly with BMI [25]. Although obesity is not identified by MIGWAS as a significant trait in our study, it has been reported to have been strongly associated with BMI and has some significant associations with body temperature [4, 26]. For future research, we would like to examine the popularity of variants located in the binding sites of 3'UTR for the miRNA-gene pairs of additional traits to further investigate the underlying biological mechanisms and causal factors of other genetic diseases, traits, and even cancers.

Conflict of Interest

The authors declare no conflict of interest.

Acknowledgment

References

[1] K. Norrgard, "Genetic variation and disease: GWAS," Nature Education **1**(1):87, 2008

[2] https://www.genome.gov/about-genomics/fact-sheets/Genome-Wide-Association-Studies-Fact-Sheet

[3] A. Auton, L.D. Brooks, R.M. Durbin, E.P. Garrison, H.M. Kang, J.O. Korbel, J.L. Marchini, S. McCarthy, G.A. McVean, G.R. Abecasis, "A global reference for human genetic variation," The 1000 Genomes Project Consortium, *Nature* 526**,** 68–74, 2015, https://doi.org/10.1038/nature15393

[4] D. Altshuler, P. Donnelly, "A haplotype map of the human genome," The International HapMap Consortium, *Nature* 437**,** 1299–1320, 2005, https://doi.org/10.1038/nature04226

[5] C. Li, M.D. Swartz, B. Yu, Y. Bai, X. Liu, "dbMTS: a comprehensive database of putative human microRNA target site SNVs and their functional predictions," bioRxiv. 2019, doi: https://doi.org/10.1101/554485

[6] E.M. Ramos, D. Hoffman, H.A. Junkins, D. Maglott, K. Ohan, S.T. Sherry, M. Feolo, L.A. Hindorff. "Phenotype-Genotype Integrator (PheGenI): synthesizing genome-wide association study (GWAS) data with existing genomic resources," European Journal of Human Genetics, **22**(1):144-147, 2014, doi:10.1038/ejhg.2013.96

[7] A. Maguolo, C. Zusi, A. Giontella, E.M.D.G. Miraglia, A. Tagetti, C. Fava, A. Morandi, C. Maffeis, "Influence of genetic variants in FADS2 and ELOVL2 genes on BMI and PUFAs homeostasis in children and adolescents with obesity," International Journal Observations (Lond). Aug 25, 2020, doi: 10.1038/s41366-020-00662-9. PMID: 32843713.

[8] I. He, T. Jiang, A. Thakur, Y. Bai, X. Qin, "Systematic and Comprehensive Survey of Genomic Loci Associated with Complex Diseases and Traits," Proc. of the 2020 14th IEEE International Conference on Bioinformatics and Biomedicine (BIBM), **1**, 1447-1452, 2020 doi: Bookmark: 10.1109/BIBM49941.2020.9313115

[9] S. Sakaue, J. Hirata, Y. Maeda, E. Kawakami, T. Nii, T. Kishikawa, K. Ishigaki, C. Terao, K. Suzuki, M. Akiyama, et al, "Integration of genetics and miRNA-target gene network identified disease biology implicated in tissue specificity," Nucleic Acids Reserves, **46**(22):11898-11909, 2018, doi: 10.1093/nar/gky1066

[10] Y. Okada, T. Muramatsu, N. Suita, M. Kanai, E. Kawakami, V. Iotchkova, N. Soranzo, J. Inazawa, T. Tanaka, "Significant impact of miRNA-target gene networks on genetics of human complex traits," Sci Rep, 6:22223, 2006.

[11] D. Szklarczyk, A.L. Gable, D. Lyon, A. Junge, S. Wyder, J. Huerta-Cepas, M. Simonovic, N.T. Doncheva, J.H. Morris, P. Bork, et al, "STRING v11: protein-protein association networks with increased coverage, supporting functional discovery in genome-wide experimental datasets," Nucleic Acids Res, Jan; **47**, 607-613, 2019, doi: 10.1093/nar/gky1131

[12] R.D. Finn, A. Bateman, J. Clements, P. Coggill, R.Y. Eberhardt, S. R. Eddy, A. Heger, K. Hetherington, L. Holm, J. Mistry, et at, "Pfam: the protein families database," Nucleic Acids Research, **42**(Database issue):D222-D230, 2014, doi:10.1093/nar/gkt1223

[13] T.L. Bailey, M. Bodén, F.A. Buske, M. Frith, C.E. Grant, L. Clementi, J. Ren, W.W. Li, W.S. Noble, "MEME SUITE: tools for motif discovery and

searching," Nucleic Acids Research, **37**, :W202-W208, 2009, doi: 10.1093/nar/gkp335

[14] A.D. Yates, P. Achuthan, W. Akanni, J. Allen, J. Allen, J. Alvarez-Jarreta, M.R. Amode, I.M. Armean, A.G. Azov, R. Bennett, et al. "Ensembl 2020," Nucleic Acids Research, **48**(D1), 08 January 2020, Pages D682-D688, https://doi.org/10.1093/nar/gkz966

[15] W.J. Kent, C.W. Sugnet, T.S. Furey, K.M. Roskin, T.H. Pringle, A.M. Zahler, D. Haussler, "The human genome browser at UCSC," Genome Res. **12**(6):996-1006, 2002, https://genome.ucsc.edu/index.html

[16] D. Karagkouni, M.D. Paraskevopoulou, S. Chatzopoulos, I.S. Vlachos, S. Tastsoglou, I. Kanellos, D. Papadimitriou, I. Kavakiotis, S. Maniou, G. Skoufos, et al, "DIANA-TarBase v8: a decade-long collection of experimentally supported miRNA-gene interactions," Nucleic Acids Res. 2018;**46**(D1):D239-D245, 2018, doi:10.1093/nar/gkx1141

[17] Y. Miyamoto, A.S. Mauer, S. Kumar, J.L. Mott, H. Malhi, "Mmu-miR-615-3p Regulates Lipoapoptosis by Inhibiting C/EBP Homologous Protein," PLoS ONE **9**(10), 2014: e109637. https://doi.org/10.1371/journal.pone.0109637

[18] E. Fabbrini, S. Sullivan, S. Klein, "Obesity and nonalcoholic fatty liver disease: biochemical, metabolic, and clinical implications," Hepatology. **51**(2):679-689, 2010 doi:10.1002/hep.23280

[19] M. Xu, S. Zhu, R. Xu, N. Lin, "Identification of CELSR2 as a novel prognostic biomarker for hepatocellular carcinoma," BMC Cancer **20**, 313, 2020, https://doi.org/10.1186/s12885-020-06813-5

[20] X. Feng, X. Xu, Y. Shi, X. Liu, H. Liu, H. Hou, L. Ji, Y. Li, W. Wang, Y. Wang, et al, "Body Mass Index and the Risk of Rheumatoid Arthritis: An Updated Dose-Response Meta-Analysis," Biomed Res Int, 2019:3579081, doi:10.1155/2019/3579081

[21] M.D. George, J.F. Baker, "The Obesity Epidemic and Consequences for Rheumatoid Arthritis Care," Curr Rheumatol Rep, **18**(1):6, 2016, doi:10.1007/s11926-015-0550-z

[22] Z. He, R. Zhang, F. Jiang, H. Zhang, A. Zhao, B. Xu, L. Jin, T. Wang, W. Jia, W. Jia, et al, "FADS1-FADS2 genetic polymorphisms are associated with fatty acid metabolism through changes in DNA methylation and gene expression," Clin Epigenet **10**, 113, 2018, https://doi.org/10.1186/s13148-018-0545-5

[23] A. Kuryłowicz, Z. Wicik, M. Owczarz, M.I. Jonas, M. Kotlarek, M. Swierniak, W. Lisik, M. Jonas, B. Noszczyk, M. Puzianowska-Kuznicka, "NGS Reveals Molecular Pathways Affected by Obesity and Weight Loss-Related Changes in miRNA Levels in Adipose Tissue," Int J Mol Sci, **19**(1):66. Published 2017 Dec 27, 2017, doi: 10.3390/ijms19010066

[24] K.M. Mah, J.A Weiner, "Regulation of WNT Signaling by Protocadherins," Seminars in Cell and Developmental Biology, August 2017, doi: 10.1016/j.semcdb.2017.07.043

[25] P. Vakli, R. Deak-Meszlenyi, T. Auer, Z. Vidnyanskzy, "Predicting Body Mass Index From Structural MRI Brain Images Using a Deep Convolutional Neural Network," Front. Neuriform, March 2020, https://doi.org/10.3389/fninf.2020.00010

[26] F. Bastardot, P. Marques-Vidal, P. Vollenweider, "Association of body temperature with obesity. The CoLaus study," International Journal of Obesity, **43**, 1026-1033, 2019